Virchows Arch (2003) 442:1–7
DOI 10.1007/s00428-002-0726-6

REVIEW ARTICLE

**Alfons Nadal · Antonio Cardesa**

# Molecular biology of laryngeal squamous cell carcinoma

Received: 4 June 2002 / Accepted: 6 September 2002 / Published online: 12 November 2002
© Springer-Verlag 2002

**Abstract** Some of the mechanisms involved in neoplastic transformation and progression of laryngeal squamous cell carcinoma (LSCC) are discussed. Although tumor suppressor inactivation of p53 and p16 is common in these tumors (about 50% each), oncogenic activation is less well characterized. Cyclin D1 and epidermal growth factor receptor amplification have been reported in one-third and one-quarter of LSCCs, respectively, both related to advanced stages, whereas *c-myc* could be amplified in 13% of cases although without associated overexpression. The role of *ras* in LSCC is, at most, exceptional, and the role of human papillomavirus infection in these neoplasms could have been largely overestimated. The *AIS* (amplified in squamous carcinoma) gene has been recently proposed as the main oncogenic target in head and neck squamous carcinomas and is a promising line of investigation. This, along with the link that exists between p53 and INK4 suppressor pathways through ARF and MDM-2, and the role of the universal cdk inhibitors (the Cip/Kip family) in these neoplasms deserve further investigation. Not forgotten are the mechanisms leading to cell immortalization and invasive capabilities acquisition, some of which are also briefly described.

**Keywords** *p53* gene · *p16* gene · Cyclin D1 · Collagenases · Telomerase

## Introduction

The scope of "molecular biology" encompasses a wide spectrum of techniques and concepts that are closely related to pathology. In fact, what pathologists look at when facing a slide of a neoplasm is the shape that results from changes in the molecular biology of normal cells. Over the years, the intimate mechanisms that underlie malignant transformation and progression are being uncovered. We are learning that some neoplasms share molecular pathways that others do not. Also, we are developing new approaches to determine precisely the mechanisms involved in particular neoplasms in order to develop new, more patient-specific therapeutic strategies since we are aware that not all patients with a given neoplasm will show the same behavior. Laryngeal carcinoma is the most frequent neoplasm in the head and neck region [29] and is notably prevalent in areas such as the Mediterranean basin [50]. However, the number of reports that deal with molecular biology of laryngeal carcinoma is clearly overwhelmed by those dealing with "head and neck" molecular pathology, which are not infrequently focused on oropharyngeal cancer [18].

The molecular biology of cancer can be separated into oncogene activation, tumor suppressor inactivation, immortalization, and activation of invasion and metastatic mechanisms. These compartments are not independent from each other and are arbitrarily defined. Some of them can be subdivided; there are two known ways of tumor suppressor inactivation: the tumor suppressor phenotype and the mutator phenotype [31].

### Oncogenes

#### c-myc

*c-myc* is a transcription factor that participates in the regulation of genes involved in normal cell proliferation and apoptosis [42]. *c-myc* overexpression related to *c-myc* gene rearrangement is a common oncogenic mechanism in B-cell lymphomas [65]. Dolcetti et al. reported *c-myc* amplification in 3 of 23 laryngeal squamous cell carcinomas (LSCCs), but without mRNA overexpression, suggesting that *c-myc* does not play a major role in laryngeal (and head and neck) neoplastic development [12]. Some other reports provide similar numbers for *c-myc* amplification but lack data on gene expression [10, 19, 27].

A. Nadal · A. Cardesa (✉)
Department of Anatomia Patologica, Hospital Clínic,
Universitat de Barcelona, Villarroel 170, 08036, Spain
e-mail: acardesa@clinic.ub.es
Tel.: +34-93-2275536, Fax: +34-93-2275717

*Epidermal growth factor receptor*

The epidermal growth factor receptor (EGFR) gene was amplified in 25% and its mRNA was overexpressed in 43% of LSCCs. Half of the overexpressed cases occurred in the absence of detectable gene amplification. Both phenomena occurred mainly in advanced tumors (stages 3 and 4) [32]. EGFR protein levels were higher in tumor than normal mucosa samples, and the highest levels were seen in high-grade tumors [57]. High levels of EGFR are meant to be associated with a high risk of lymph-node metastases [2].

ras

The role of *ras* in laryngeal carcinogenesis seems exceptional. Although a high incidence of *ras* mutations has been reported in laryngeal carcinomas [3], these results have not been confirmed lately [62, 19, 8]. *ras* mutations have been well characterized in oral cancers from betel chewers in India [55], but they seem to be very rare in laryngeal cancer. Overexpression of *ras* proteins has been reported in a series of head and neck squamous cell carcinomas including laryngeal tumors. This overexpression of H-, K-, and N-*ras* occurred in the absence of detectable mutations [69] and was independent of overexpression of EGFR [58].

*Cyclin D1*

Cyclin D1 is located in the 11q13 chromosome region, which has been shown to be amplified frequently in head and neck carcinomas [4, 64]. Some other putative oncogenes lie in this region, but only cyclin D1 has shown consistent overexpression. We demonstrated that cyclin D1 overexpression was closely correlated with cyclin D1 gene amplification, suggesting that this is the main mechanism of overexpression in laryngeal carcinomas [33]. Both phenomena were associated with an advanced stage of disease, which could indicate a more aggressive behavior for amplified/overexpressed cases. The main cyclin D1 partner in G1 is CDK4 [44]. Recent reports have also shown overexpression of CDK4. Simultaneous overexpression of both proteins resulted in the poorest survival in the series of patients [15].

*Cyclin E*

Cyclin E is also overexpressed in a significant fraction of laryngeal carcinomas, mainly in supraglottic tumors, and this overexpression is associated with poor histological differentiation, locally advanced tumors, presence of lymph node metastases, and an advanced stage. It also correlates with cell proliferation, measured by PCNA expression, and it constitutes a marker of poor prognosis, mainly in stages 1 and 2 [14].

Tumor suppressor genes

*Retinoblastoma*

The retinoblastoma susceptibility gene was the first tumor suppressor gene identified on the basis of differences between familial and sporadic retinoblastoma [38]. Allelic losses of 13q have been described frequently in head and neck cancer [60] but those losses of heterozygosity (LOH) are not related to immunohistochemical loss of retinoblastoma protein expression [70], which is an infrequent event [34] (Fig. 1a). This lack of correlation could indicate that other tumor suppressor genes may be near the retinoblastoma locus, and they could be the real targets for LOH [70].

*p53*

The first reports on p53 in laryngeal carcinomas came from 1992, when immunohistochemically detected p53 overexpression was related to the presence of genetic alterations. In a series of 58 LSCCs, 35 cases showed p53 overexpression. A short number of cases was analyzed for mutations and/or alterations in mRNA. All the immunohistochemically positive cases analyzed showed either mutations or aberrant transcripts, whereas only one of the negative cases analyzed showed an aberrant mRNA transcript [41]. Immunohistochemical analyses of p53 (Fig. 1b) overexpression do not find differences in stage, histological differentiation or prognosis, and p53 overexpression could be observed even in preinvasive lesions [13, 46]. Progression in the number of positive cases has been reported in relation to progression from normal epithelium to carcinoma in situ [9, 63, 46]. Dolcetti et al. found concordance in p53 expression between primary tumors and their lymph-node metastases [13]. Taken together, all these findings suggest that alterations in p53 occur in the early steps of neoplastic transformation in these tumors, but they do not provide additional advantages for neoplastic progression. However, p53 overexpression can be seen in tumors that lack apparent gene mutations [67], and there are a number of p53 mutants that produce a truncated protein that is undetectable by immunohistochemistry [47]. These facts have led to the conclusion that, in order to investigate p53 function abrogation, both DNA sequence analyses of exons 2 through 11 as well as immunohistochemical analyses are required to detect all known p53 alterations [7].

*p21$^{WAF1}$*

p21$^{WAF1}$ is a protein with cyclin-dependent kinase inhibitory activity [26] that is activated by wild-type, but not mutant, p53 [17]. We analyzed the expression of p21$^{WAF1}$ in LSCCs and saw that it was overexpressed in a significant fraction of carcinomas, both at mRNA and protein levels. This was a surprising finding that questioned its

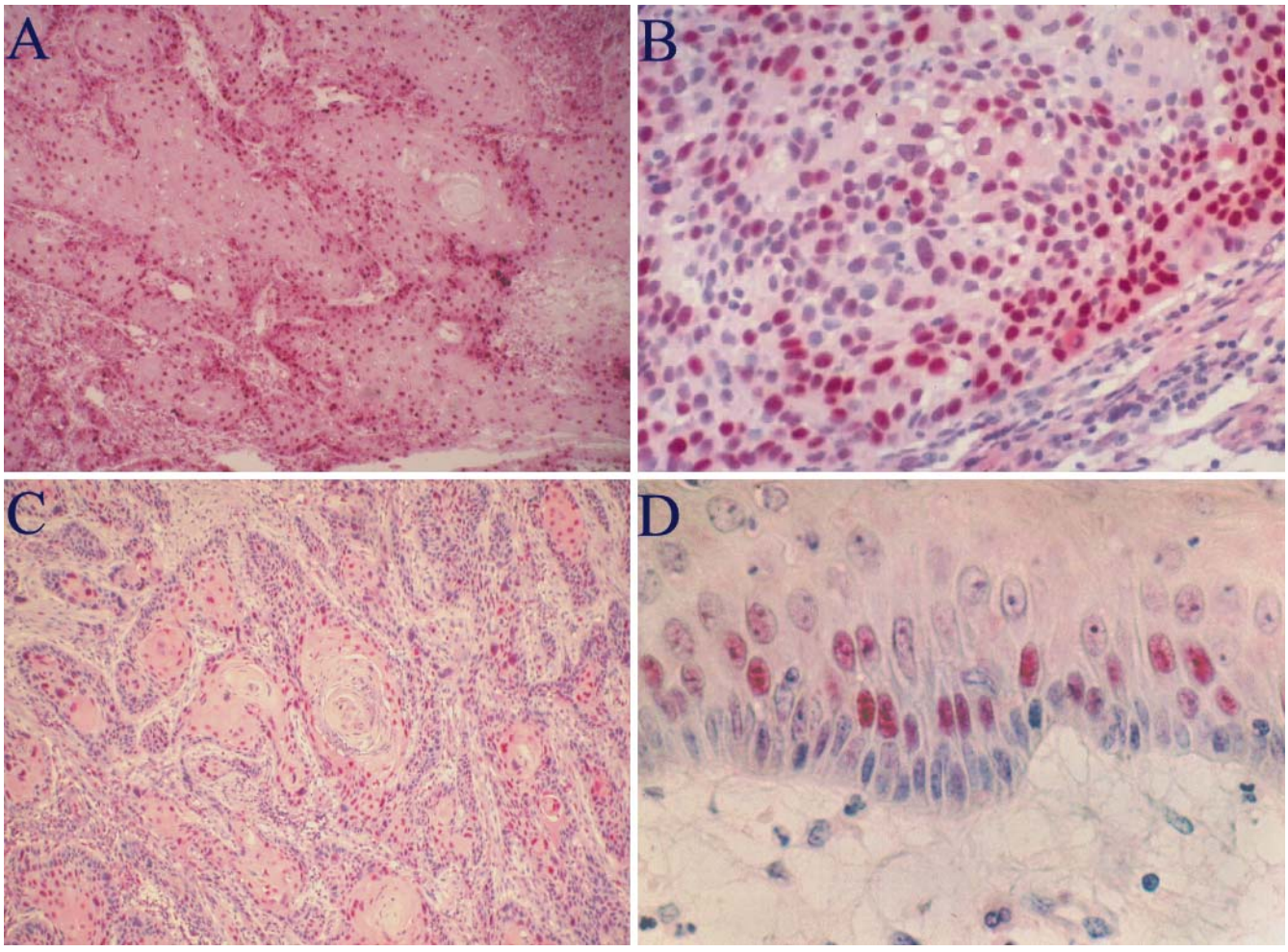



**Fig. 1** Immunohistochemical analysis of retinoblastoma, p53, and $p21^{WAF1}$ proteins in laryngeal squamous cell carcinoma (LSCC) and normal laryngeal squamous epithelium. **a** Retinoblastoma protein expression is detected in most LSCCs and shows an increase at the periphery of the nests, where proliferation occurs (original magnification ×10). **b** p53 protein expression is detected in more than half of the LSCCs and, as seen in retinoblastoma, many p53-positive cases show an increase in expression at the border of the tumor nest. However, p53 expression could be not enough to characterize p53 gene status in LSCC (original magnification ×20). **c** $p21^{WAF1}$ protein expression frequently shows a "target" pattern, resembling that seen in normal squamous cell epithelium (original magnification ×10). **d** $p21^{WAF1}$ protein expression in normal squamous cell epithelium is restricted to one or two cell layers, where proliferative activity ceases and squamous differentiation progresses (original magnification ×40)

role as a suppressor in LSCC. The levels of expression were independent of p53 gene status but were closely related to cell differentiation. Poorly differentiated carcinomas were immunohistochemically negative, and mRNA levels were lower than those of normal mucosa. Therefore, $p21^{WAF1}$ expression in LSCC is neither the result of p53 activation, nor is loss of $p21^{WAF1}$ expression a marker of p53 inactivation, but rather this cyclin-dependent kinase inhibitory protein participates in squamous differentiation in a similar way to that of normal epithelium [47] (Fig. 1c, d).

### *$p16^{INK4a}$*

$p16^{INK4a}$ is a member of the INK4 inhibitor kinase family that maps to the 9p21 region, which is frequently deleted in head and neck squamous cell carcinomas and cell lines. It binds to CDK4 and prevents it from binding to cyclin D1, thus inhibiting the catalytic activity of the CDK4/Cyclin D1 complexes [61]. $p16^{INK4a}$ can be inactivated by a variety of mechanisms such as mutation, homozygous deletion [36], and promoter hypermethylation that leads to gene silencing [45]. $p16^{INK4a}$ is inactivated in LSCC by mutation or homozygous deletion in 22% of cases each, and by hypermethylation in an additional 7%. Therefore, the results show that a little more than 50% of cases have inactivated $p16^{INK4a}$. Although expression analysis has been used to identify $p16^{INK4a}$ alterations with loss of expression as a marker for genetic alterations [66], we showed that a number of mutated cases (with concomitant loss of heterozygosity, therefore fully inactivated $p16^{INK4a}$) had normal or higher-than-normal expression levels [34, 35]. INK4A locus, where $p16^{INK4a}$ is located, is a complex locus that codifies two

different transcripts. $p16^{INK4a}$ and $p14^{ARF}$ share exons 2 and 3 but are structurally different proteins, because $p14^{ARF}$ is read in an alternative frame due to the structure of the alternative exons 1 (α and β) [37]. In our hands, both transcripts are coordinately expressed in LSCC [35].

*Transforming growth factor receptor*

Transforming growth factor-β (TGF-β) and TGF-β receptors (TGF-β-Rs) belong to a complex multifunctional pathway implicated in cell growth control and tissue remodeling [43]. Their role in laryngeal carcinogenesis is still debatable. Loss of expression associated with progression to invasive carcinoma has been reported in pre-malignant laryngeal lesions [20], whereas other authors report that there is neither a significant decrease in TGF-β-Rs in neoplastic laryngeal cells nor in TGF isoform production. This TGF-β production could explain some side effects, such as stromal desmoplasia, although the explanation for the loss of suppressor effect of TGF-β in laryngeal carcinoma is still lacking [25]. Interestingly, TGF-β-R inactivation is a phenomenon of the mutator phenotype that seems infrequent in head and neck carcinoma except for those cases with multiple primary tumors [56].

## Human papillomavirus

Human papillomavirus (HPV) infection is a well-known etiological factor for cervical squamous cell carcinoma. Viral oncoproteins E6 and E7 bind to and block activity of p53 and Rb, respectively [59, 16]. The participation of HPVs in laryngeal carcinogenesis is still under investigation. Southern-blot analysis showed low prevalence of HPV DNA in both neoplastic and non-neoplastic laryngeal tissues (only 5% and 4% each), in contrast with higher figures for other head and neck sites such as the tonsil (29%), tongue (18%), and pharynx (13%) [5]. Analyses of HPV DNA prevalence by PCR-based methods yield very different results [6, 51, 22, 39], and the use of this sensitive technique allows the detection of HPV DNA in normal mucosa in more than half of the cases, making the real meaning of HPV DNA detection in squamous carcinoma even more puzzling [51]. Our results agree with a low prevalence of HPV DNA in LSCC and point to other carcinogens as agents for the development of laryngeal carcinoma (unpublished observations).

## Telomerase

Telomerase activity is required for immortalization, a characteristic of neoplastic cells, whereas in normal tissues this is found only in germ and stem cells [11]. Most laryngeal carcinomas show either telomerase activity [30] or hTERT expression [40], which is thought to be related to telomerase activity. Telomerase activity has also been detected in adjacent normal-appearing mucosa, the closer to tumor, the higher the activity. Extracts from laryngeal carcinomas without telomerase activity can efficiently inhibit activity from telomerase-producing cells, suggesting the existence of a telomerase-inhibitory substance [30]. The presence of stem cells in regenerating epithelium could explain hTERT expression in non-neoplastic adult laryngeal tissues, whereas telomerase reactivation is responsible for hTERT expression in carcinomas [40].

## Adhesion molecules and extracellular matrix components

Changes in stromal and adhesion molecules have been reported in LSCC. Tenascin deposition is increased in invasive carcinomas compared with non-invasive lesions, and this deposition is associated with higher levels of CD44 and epithelial cathepsin D expression [23]. However, increases in deposition of both fibronectin and tenascin have also been reported related to increase with dysplasia in epithelial hyperplastic lesions [71]. In contrast, loss of CD44 expression is associated with metastatic disease in the form of nodal involvement [28]. Components of the basal membrane are also affected during invasive progression. In contrast to the general belief, the basal membrane does not disappear abruptly with the development of invasion, but rather shows a stepwise loss of components. Collagen VII is the first to show focal losses, whereas loss of collagen IV is associated with loss of squamous differentiation [24].

## Matrix metalloproteinases

The invasive and metastatic process requires the participation of proteolytic enzymes which facilitate detachment of individual cells from the primary tumor, degradation of basement membrane, and invasion of surrounding tissues. Collagenase activity in laryngeal and oral cavity carcinomas was described in 1975 [1]. Several proteinases have been involved since then in these processes in head and neck carcinomas.

Collagenase-3 (matrix metalloproteinase 13) was identified by Freije et al. in breast carcinoma, but not in non-neoplastic breast tissue [21]. Similarly, we found collagenase-3 expression in laryngeal squamous carcinomas but not in neighboring normal mucosa. Collagenase-3 expression was associated with advanced local invasion but not with nodal metastases or stage, suggesting that it collaborates in matrix degradation and local invasion but not in the metastatic process, and it was not found in the poorest differentiated tumors, indicating some relationship between collagenase-3 production and squamous differentiation. Interestingly, collagenase-3 expression was coordinated with the overexpression of two other members of the matrix metalloproteinase fami-

ly, gelatinase A (MMP-2) and membrane-type-1 matrix metalloproteinase (MT1-MMP), which can efficiently activate collagenase-3 by proteolysis of pro-collagenase-3 [8]. Whereas collagenase-3 appears to be produced by malignant epithelial cells, other members of the family have been found both in the neoplastic and in the stromal compartments. This is the case of collagenase-1 and stromelysin-2 [52].

Proteinases may also be involved in chemotherapy resistance. Drug resistant laryngeal cell lines have higher levels of cathepsin-D and urokinase-type plasminogen activator [48] and cathepsin B [49].

## Future perspectives

In summary, molecular events related to proto-oncogene activation, tumor suppressor inactivation, invasive capability acquisition, and cell immortalization have been described in laryngeal squamous cell carcinoma. Tumor suppressor inactivation has been largely proven and most of those neoplasms show inactivation of the p53 and $p16^{INK4a}$ pathways. However, recent knowledge that INK4a locus codifies two different genes, $p16^{INKa}$ and $p14^{ARF}$, introduces new insights for a possible coordinated role of p53 and $p16^{INK4a}$ suppressor pathways. $p14^{ARF}$ induces p53 stabilization by sequestering MDM-2 which, in turn, has been shown overexpressed in laryngeal carcinomas without evidence of gene amplification [53]. Although $p21^{WAF1}$ expression has not shown prognostic value, $p27^{Kip1}$ seems more promising [54]. However, oncogenic activation appears to be less elucidated. *ras* participation is, at most, exceptional, whereas the participation of cyclin D1 amplification and overexpression in a subset of cases is out of doubt, but there remains a pool of cases in which the oncogenic events are less than characterized. The recent description of AIS (Amplified In Squamous carcinoma), as a gene that encodes a number of different transcripts (p40, p51, p63) homologous to p53 but with a putative oncogenic potential, that could be amplified in a high number of head and neck carcinomas [68] would eventually fill the empty space in the oncogenic events involved in the development of laryngeal squamous cell carcinoma.

## References


1. Abramson M, Schiling RW, Huang CC, Salome RG (1975) Collagenase activity in epidermoid carcinoma of the oral cavity and larynx. Ann Otol Rhinol Laryngol 84:158–163
2. Almadori G, Cadoni G, Galli J, Ferrandina G, Scambia G, Exarchakos G, Paludetti G, Ottaviani F (1999) Epidermal growth factor receptor expression in primary laryngeal cancer: an independent prognostic factor of neck node relapse. Int J Cancer 20:188–191
3. Anwar K, Nakakuki K, Naiki H, Inuzuka M (1993) ras gene mutations and HPV infection are common in human laryngeal carcinoma. Int J Cancer 53:22–28
4. Berenson JR, Yan J, Micke RA (1989) Frequent amplification of the bcl-1 locus in head and neck squamous cell carcinomas. Oncogene 4:1111–1116
5. Brandsma JL, Abramson AL (1989) Association of papillomavirus with cancers of the head and neck. Arch Otolaryngol Head Neck Surg 115:621–625
6. Brandwein MS, Nuovo GJ, Biller H (1993) Analysis of prevalence of human papillomavirus in laryngeal carcinomas. Study of 40 cases using polymerase chain reaction and consensus primers. Ann Otol Rhinol Laryngol 102:309–313
7. Casey G, Lopez ME, Ramos JC, Plummer SJ, Arboleda MJ, Shaughnessy M, Karlan B, Slamon DJ (1996) DNA sequence analysis of exons 2 through 11 and immunohistochemical staining are required to detect all known p53 alterations in human malignancies. Oncogene 13:1971–1981
8. Cazorla M, Hernández L, Nadal A, Balbín M, López JM, Vizoso F, Fernández PL, Iwata K, Cardesa A, López-Otín C, Campo E (1998) Collagenase-3 expression is associated with advanced local invasion in human squamous cell carcinomas of the larynx. J Pathol 186:144–150
9. Coltrera MD, Zarbo RJ, Sakr WA, Gown AM (1992) Markers for dysplasia of the upper aerodigestive tract. Suprabasal expression of PCNA, p53, and CK19 in alcohol-fixed, embedded tissue. Am J Pathol 141:817–825
10. de la Guardia C, Casiano CA, Trinidad-Pinedo J, Báez A (2001) CENP-F gene amplification and overexpression in head and neck squamous cell carcinomas. Head Neck 23:104–112
11. Dhaene K, Van Marck E, Paerwaresch R (2000) Telomeres, telomerase and cancer: an up-date. Virchows Arch 437:1–16
12. Dolcetti R, Pelucchi R, Maestro S, Rizzo S, Pastore A, Boiocchi M (1991) Proto-oncogene allelic variations in human squamous cell carcinomas of the larynx. Eur Arch Otorhinolaryngol 248:279–285
13. Dolcetti R, Doglioni C, Maestro R, Gasparotto D, Barzan L, Pastore A, Romanelli M, Boiocchi M (1992) p53 overexpression is an early event in the development of human squamous-cell carcinomas of the larynx: genetic and prognostic implications. Int J Cancer 52:178–182
14. Dong Y, Sui L, Tai Y, Sugimoto K, Hirao T, Tokuda M (2000) Prognostic significance of cyclin E overexpression in laryngeal squamous cell carcinomas. Clin Cancer Res 6:4253–4258
15. Dong Y, Sui L, Sugimoto K, Tai Y, Tokuda M (2001) Cyclin D1-CDK4 complex, a possible critical factor for cell proliferation and prognosis in laryngeal squamous cell carcinomas. Int J Cancer (Pred Oncol) 95:209–215
16. Dyson N, Howley PM, Munger K, Harlow E (1989) The human papilloma virus-16 E7 oncoprotein is able to bind to the retinoblastoma gene product. Science 243:934–937
17. El-Deiry WS, Tokino T, Velculescu V, Levy DB, Parsons R, Trent JM, Lin D, Mercer WE, Kinzler KW, Vogelstein B (1993) WAF1, a potential mediator of p53 tumor suppression. Cell 75:817–825
18. Forastiere A, Koch W, Trotti A, Sidransky D (2001) Head and neck cancer. N Engl J Med 345:1890–1900
19. Fracchiolla NS, Pignataro L, Capaccio P, Trecca D, Boletini A, Ottaviani A, Polli E, Maiolo AT, Neri A (1995) Multiple genetic lesions in laryngeal squamous cell carcinomas. Cancer 75:1292–1301
20. Franchi A, Gallo O, Sardi I, Santucci M (2001) Downregulation of transforming growth factor beta type II receptor in laryngeal carcinogenesis. J Clin Pathol 54:201–204
21. Freije JM, Diez-Ita I, Balbin M, Sanchez LM, Blasco R, Tolivia J, Lopez-Otin C (1994) Molecular cloning and expression of collagenase-3, a novel human matrix metalloproteinase produced by breast carcinoma. J Biol Chem 269:16766–16773
22. Gorgoulis VG, Zacharatos P, Kotsinas A, Kyroudi A, Rassidakis AN, Ikonomopoulos JA, Barbatis C, Herrington CS, Kittas C (1999) Human papillomavirus (HPV) is possibly involved in laryngeal but not in lung carcinogenesis. Hum Pathol 30:274–283
23. Goussia AC, Ioachim EE, Peschos D, Assimakopoulos DA, Skevas A, Agnantis NJ (2000) Expression of the extracellular matrix protein tenascin in laryngeal epithelial lesions: correlation with fibronectin, CD44, cathepsin D and proliferation indices. Virchows Arch 436:579–584

24. Hagedorn H, Schreiner M, Wiest I, Tubel J, Schleicher ED, Nerlich AG (1998) Defective basement membrane in laryngeal carcinomas with heterogeneous loss of distinct components. Hum Pathol 29:447–454
25. Hagedorn H, Elbertzhagen A, Ruoss I, Sauer U, Nerlich AG (2001) Immunohistochemical analysis of major TGF-β isoforms and their receptors in laryngeal carcinomas. Virchows Arch 439:531–539
26. Harper JW, Adami GR, Wei N, Keyomarsi K, Elledge SJ (1993) The p21 cdk-interacting protein Cip1 is a potent inhibitor of G1 cyclin-dependent kinases. Cell 75:805–816
27. Haughey BH, von Hoff DD, Windle BE, Wahl GM, Mock PM (1992) c-myc oncogene copy number in squamous carcinoma of the head and neck. Am J Otolaryngol 13:168–171
28. Hirvikoski P, Tammi R, Kumpulainen E, Virtaniemi J, Parkkinen JJ, Tammi M, Johansson R, Agren U, Karhunen J, Kosma VM (1999) Irregular expression of hyaluronan and its CD44 receptor is associated with metastatic phenotype in laryngeal squamous cell carcinoma. Virchows Arch 434:37–44
29. Hoffman HT, Hynds Karnell L, Funk GF, Robinson RA, Menck HR (1998) The national cancer data base report on cancer of the head and neck. Arch Otolaryngol Head Neck Surg 124:951–962
30. Hohaus S, Cavallo S, Bellacosa Genuardi M, Galli J, Cadoni G, Almadori G, Lauriola L, Litwin S, Maurizi M, Neri G (1996) Telomerase activity in human laryngeal squamous cell carcinomas. Clin Cancer Res 2:1895–1900
31. Ionov Y, Peinado MA, Malkhosyan S, Shibata D, Perucho M (1993) Ubiquitous somatic mutations in simple repeated sequences reveal a new mechanism for colonic carcinogenesis. Nature 363:558–561
32. Irish JC, Bernstein A (1993) Oncogenes in head and neck cancer. Laryngoscope 103:42–52
33. Jares P, Fernández PL, Campo E, Nadal A, Bosch F, Aiza G, Nayach I, Traserra J, Cardesa A (1994) PRAD-1/Cyclin D1 gene amplification correlates with messenger RNA overexpression and tumor progression in human laryngeal carcinomas. Cancer Res 54:4813–4817
34. Jares P, Fernández PL, Nadal A, Cazorla M, Hernández L, Pinyol M, Hernández S, Traserra J, Cardesa A, Campo E (1997) $p16^{MTS1/CDK4I}$ mutations and concomitant loss of heterozygosity at 9p21–23 are frequent events in squamous cell carcinoma of the larynx. Oncogene 15:1445–1453
35. Jares P, Nadal A, Fernández PL, Pinyol M, Hernández L, Cazorla M, Hernández S, Beà S, Cardesa A, Campo E (1999) Disregulation of $p16^{MTS1/CDK4I}$ protein and mRNA expression is associated with gene alterations in squamous-cell carcinoma of the larynx. Int J Cancer 81:705–711
36. Kamb A, Gruis NA, Weaver-Feldhaus J, Liu Q, Harshman K, Tavtigian SV, Stockert E, Day RS 3rd, Johnson BE, Skolnick MH (1994) A cell cycle regulator potentially involved in genesis of many tumor types. Science 264:436–440
37. Kamijo T, Zindy F, Roussel MF, Quelle DE, Downing JR, Ashmum RA, Grosveld G, Sherr CJ (1997) Tumor suppression at the mouse INK4a locus mediated by alternative reading frame product $p19^{ARF}$. Cell 91:649–659
38. Knudson AG Jr (1971) Mutation and cancer: statistical study of retinoblastoma. Proc Natl Acad Sci U S A 68:820–823
39. Lindeberg H, Krogdahl A 1999 Laryngeal cancer and human papillomavirus: HPV is absent in the majority of laryngeal carcinomas. Cancer Lett 146:9–13
40. Luzar B, Poljak M, Marin IJ, Fischinger J, Gale N (2001) Quantitative measurement of telomerase catalytic subunit (hTERT) mRNA in laryngeal squamous cell carcinomas. Anticancer Res 21:4011–4015
41. Maestro R, Dolcetti R, Gasparotto D, Doglioni C, Pelucchi S, Barzan L, Grandi E, Boiocchi M (1992) High frequency of p53 gene alterations associated with protein overexpression in human squamous cell carcinoma of the larynx. Oncogene 7:1159–1166
42. Marcu KB, Bossone SA, Patel AJ (1992) Myc function and regulation. Annu Rev Biochem 61:809–860
43. Massagué J (1998) TGF-beta signal transduction. Annu Rev Biochem 67:753–791
44. Matsushime H, Ewen ME, Strom DK, Kato JY, Hanks SK, Roussel MF, Sherr CJ (1992) Identification and properties of an atypical catalytic subunit ($p34^{PSK-J3}$/cdk4) for mammalian D type G1 cyclins. Cell 71:323–334
45. Merlo A, Herman JG, Mao L, Lee DJ, Gabrielson E, Burger PC, Baylin SB, Sidransky D (1995) 5' CpG island methylation is associated with transcriptional silencing of the tumour supressor p16/CDKN2/MTS1 in human cancers. Nat Med 1:868–692
46. Nadal A, Campo E, Pinto J, Mallofré C, Palacín A, Arias C, Traserra J, Cardesa A (1995) p53 expression in normal, dysplastic, and neoplastic laryngeal epithelium. Absence of a correlation with prognostic factors. J Pathol 175:181–188
47. Nadal A, Jares P, Cazorla M, Fernández PL, Sanjuan X, Hernández L, Pinyol M, Aldea M, Mallofré C, Muntané J, Traserra J, Campo E, Cardesa A (1997) $p21^{WAF1/Cip1}$ expression is associated with cell differentiation but not with p53 mutations in squamous cell carcinomas of the larynx. J Pathol 183:156–163
48. Osmak M, Niksic D, Brozovic A, Ristov AA, Vrhovec I, Skrk J (1999) Drug resistant tumor cells have increased levels of tumor markers for invasion and metastasis. Anticancer Res 19:3193–3197
49. Osmak M, Svetic B, Gabrijelcic-Geiger D, Skrk J (2001) Drug-resistant human laryngeal carcinoma cells have increased levels of cathepsin B. Anticancer Res 21:481–483
50. Parkin DM, Pisani P, Ferlay J (1993) Estimates of the worldwide incidence of eighteen major cancers in 1985. Int J Cancer 54:594–606
51. Pérez-Ayala M, Ruiz-Cabello F, Esteban F, Concha A, Redondo M, Oliva MR, Cabrera T, Garrido F (1990) Presence of HPV 16 sequences in laryngeal carcinomas. Int J Cancer 46:8–11
52. Polette M, Clavel C, Muller D, Abecassis J, Binninger I, Birembaut P (1991) Detection of mRNAs encoding collagenase I and stromelysin 2 in carcinomas of the head and neck by in situ hybridization. Invasion Metastasis 11:76–83
53. Pruneri G, Pignataro L, Carboni N, Luminari S, Capaccio P, Neri A, Buffa R (1997) MDM-2 oncoprotein overexpression in laryngeal squamous cell carcinoma: association with wild-type p53 accumulation. Mod Pathol 10:785–792
54. Pruneri G, Pignataro L, Carboni N, BuffaR, Di Finizio D, Cesana BM, Neri A (1999) Clinical relevance of expression of the CIP/KIP cell-cycle inhibitors p21 and p27 in laryngeal cancer. J Clin Oncol 17:3150–3159
55. Saranath D, Chang SE, Bhoite LT, Panchal RG, Kerr IB, Mehta AR, Johnson NW, Deo MG (1991) High frequency mutations in codons 12 and 61 of H-*ras* oncogene in chewing tobacco-related human oral carcinoma in India. Br J Cancer 63:573–578
56. Sardi I, Franchi A, Bocciolini C, Mechi C, Frittelli A, Bruschini L, Gallo O (2001) Microsatellite instability as biomarker for risk of multiple primary malignancies of the upper aerodigestive tract. Oncol Rep 8:393–399
57. Scambia G, Benedetti Panici P, Battaglia F, Ferrandina G, Almadori G, Paludetti C, Maurizi M, Mancuso S (1991) Receptors for epidermal growth factor and steroid hormones in primary laryngeal tumors. Cancer 67:1347–1351
58. Scambia G, Catozzi L, Benedetti Panici P, Ferrandina G, Almadori G, Paludetti G, Cadoni G, Distefano M, Piffanelli A, Mancuso S (1994) Expression of ras oncogene p21 protein in normal and neoplastic laryngeal tissues: correlation with histopathological features and epidermal growth factor receptors. Br J Cancer 69:995–999
59. Scheffner M, Werness BA, Huibregtse JM, Levine AJ, Howley PM (1990) The E6 oncoprotein encoded by human papillomavirus types 16 and 18 promotes the degradation of p53. Cell 63:1129–1136
60. Scholnick SB, Sun PC, Shaw ME, Haughey BH, El-Mofty SK (1994) Frequent loss of heterozygosity for Rb, TP53, and

chromosome arm 3p, but not NME1 in squamous cell carcinomas of the supraglottic larynx. Cancer 73:2472–2480
61. Serrano M, Hannon GJ, Beach D (1993) A new regulatory motif in cell-cycle control causing specific inhibition of cyclin-D/CDK4. Nature 366:704–707
62. Shidara K, Suzuki T, Hara F, Nakajima T (1994) Lack of synergistic association between human papillomavirus and *ras* gene point mutation in laryngeal carcinomas. Laryngoscope 104:1008–1012
63. Shin DM, Kim J, Ro JY, Hittelman J, Roth JA, Hong WK, Hittelman WN (1994) Activation of p53 gene expression in premalignant lesions during head and neck tumorigenesis. Cancer Res 54:321–326
64. Somers KD, Cartwright SL, Schechter GL (1990) Amplification of the int-2 gene in human head and neck squamous cell carcinomas. Oncogene 5:915–920
65. Spencer CA, Groudine M (1991) Control of c-myc regulation in normal and neoplastic cells. Adv Cancer Res 68:1–48
66. Wing Yuen P, Man M, Yin Lam K, Lam Kwong Y (2002) Clinicopathological significance of p16 gene expression in the surgical treatment of head and neck squamous cell carcinomas. J Clin Pathol 55:58–60
67. Xu L, Chen YT, Huvos AG, Zlotolow IM, Retting WJ, Old LJ, Garin-Chesa P (1994) Overexpression of p53 protein in squamous cell carcinomas of the head and neck without apparent gene mutations Diagn Mol Pathol 3:83–92
68. Yamaguchi K, Wu L, Caballero OL, Hibi K, Trink B, Resto V, Cairns P, Okami K, Koch WM, Sidransky D, Jen J (2000) Frequent gain of the p40/p51/p63 gene locus in primary head and neck squamous cell carcinoma. Int J Cancer 86:684–689
69. Yarbrough WG, Shores C, Witsell DL, Weissler MC, Fidler ME, Gilmer TM (1994) *ras* mutations and expression in head and neck squamous cell carcinomas. Laryngoscope 104:1337–1347
70. Yoo GH, Xu H-J, Brennan JA, Westra W, Hruban RH, Koch W, Benedict WF, Sidransky D (1994) Infrequent inactivation of the retinoblastoma gene despite frequent loss of chromosome 13q in head and neck squamous cell carcinoma. Cancer Res 54:4603–4606
71. Zidar N, Gale N, Kambic V, Fischinger J (2001) Expression of tenascin and fibronectin in benign epithelial hyperplastic lesions and squamous carcinoma of the larynx. Anticancer Res 21:451–454

Virchows Arch (2003) 442:8–17
DOI 10.1007/s00428-002-0732-8

REVIEW ARTICLE

**Burkhard D. Bültmann · Karin Klingel · Karl Sotlar**
**C.-Thomas Bock · Reinhard Kandolf**

# Parvovirus B19: a pathogen responsible for more than hematologic disorders

Received: 5 September 2002 / Accepted: 26 September 2002 / Published online: 14 November 2002
© Springer-Verlag 2002

**Abstract** The clinical and pathomorphological patterns of parvovirus B19 (PVB19)-associated diseases is the result of a balance between virus, host target cells and immune response. It is a characteristic feature of PVB19 that in patients with various other preexisting diseases, e.g., many hemolytic anemias, immune complex-mediated vasculitic disorders, and primary or secondary immunodeficiencies, the underlying diseases can be triggered, aggravated or complicated by severe organ manifestations. Identification of PVB19 by means of routine histology and immunohistology is only given in lytic infections occurring in transient aplastic anemia or nonimmune hydrops fetalis by the detection of viral inclusion bodies in erythroid precursor cells. In all other PVB19-associated diseases, molecular pathological methods must be applied. In this report, quantitative real-time polymerase chain reaction was used to determine the viral load in formalin-fixed and paraffin-embedded tissues derived from various organs. Using in situ hybridization it was demonstrated that endothelial cells of the microcirculatory periphery of the heart and hepatobiliar system in lytic infections are PVB19-specific target cells in children and adults. Because treatment of lytic PVB19 infection has been successfully applied, the pathologist should be alerted to include PVB19 into the diagnostic spectrum of viral disease, especially in immunocompromised patients.

**Keywords** Parvovirus B19 · Endothelial cells · Microcirculation · Myocarditis · Molecular pathology

B.D. Bültmann (✉) · K. Klingel · K. Sotlar · C.-T. Bock
R. Kandolf
Institute of Pathology, University of Tübingen,
Liebermeisterstrasse 8, D-72076 Tübingen, Germany
e-mail: bdbueltm@med.uni-tuebingen.de
Tel.: +49-7071-2982266, Fax: +49-7071-292258

## Introduction

Yvonne Cossart, a virologist working in London in the mid-1970s, discovered B19 parvovirus (PVB 19) while investigating laboratory assays for hepatitis B [13]. The peculiar name of this virus, incidentally, derived from the blood bank code of one of the viremic blood bank donors, whose serum was number 19 in row B of the panel. PVB19 entered the medical curriculum as an agent of human disease when its association with erythema infectiosum (fifth disease, Ringelröteln), hydrops fetalis and transient aplastic anemia was demonstrated in the early 1980s [1, 2, 5, 27, 44, 46]. During the last few years a growing number of reports have been published demonstrating an association between PVB19 and many other clinical diseases [31, 37, 46, 58], for example arthritis [38, 55, 57], myocarditis [8, 16, 34, 40, 42, 43, 52], various vasculitic syndromes [12, 14, 18, 58], hepatitis [15, 24, 26, 54, 62], and neurological disorders [4, 61]. The study of the pathology of PVB19 infection has mostly been confined to the examination of the bone marrow in cases of anemia [19, 27, 32, 44, 51] and of fetal material tissues in cases of hydrops fetalis [5, 22, 39, 49].

For a better understanding of the pathogenesis of these seemingly unrelated diseases, in the present review, we will summarize the essential data about the viral structure, the cellular tropism of the virus, the natural course of the infection, the immunological host response and – as far as available – the histopathological, immunohistochemical and molecular pathological findings in different PVB19-related diseases. We present evidence that the pathogenesis and the clinical outcome of PVB19-related diseases involve two separate pathways: the first is due to lytic infection of susceptible dividing cells; the second is dependent on interaction with the immune response, mostly leading to a transient and self-limiting, rarely to persistent infection in immunocompetent persons. However, in patients with preexisting hematological and immunological disorders, severe complications can occur.

## Virus and cellular tropism

PVB19 belongs to the family of parvoviridiae which are among the smallest of the DNA viruses that infect eukaryotes [45, 63]. It is a small non-enveloped, single-stranded DNA virus containing a genome of 5600 bp. Under the electron microscope, it appears as a naked, spherical particle with a diameter varying from 18 nm to 26 nm. The individual virus particles possess an icosahedral symmetry. In PVB19 capsids, DNA molecules of both polarities are found in almost equal amounts. The genome appears to encode only for three proteins including the capsid proteins VP1 and VP2. The latter one, VP2 (molecular weight 58 kDa), is the smaller but more abundant structural protein and makes up approximately 96% of the viral capsid. It has been demonstrated to be important for antigen recognition by neutralizing antibodies. The larger capsid protein, VP1 (molecular weight 84 kDa), contains a domain that extends above the surface of the capsid and serves to interact with the cellular receptor. The third gene product, the nonstructural protein NS1, has been shown to be involved in DNA replication and in initiating apoptosis mediated by stimulation of cytokine production [30, 37]. Because of its limited genomic capacity, PVB19 requires mitotically active host cells for replication.

The cellular receptor has been identified as a globoside, a neutral glycosphingolipid that is present on erythroid precursor cells and erythrocytes, where it represents the blood group P antigen [7]. The presence of this receptor protein is necessary for viral infection. Individuals who lack the P phenotype are naturally immune against PVB19 infection [8]. The P antigen is also present on various other cells such as endothelial cells (ECs) and fetal myocardial cells [7].

## The PVB19 infection and immune response

Infection with PVB19 is common in most countries where it has been examined. In the USA and other regions with temperate climates, 60% or more adults are seropositive [30]. Infection occurs most commonly among school-aged children with a seasonal peak during late winter to early summer. PVB19 epidemics occur within a periodicity of 4–5 years. Infection is probably transmitted by droplets from respiratory secretions. Nosocomial outbreaks have been described. A recent report highlights the possibility of transmission from staff with rash illness to other personnel [36]. Transmission through blood and blood products is also possible given the high incidence of asymptomatic infection [48]. Recently, transmission through bone marrow transplantation has been reported [23].

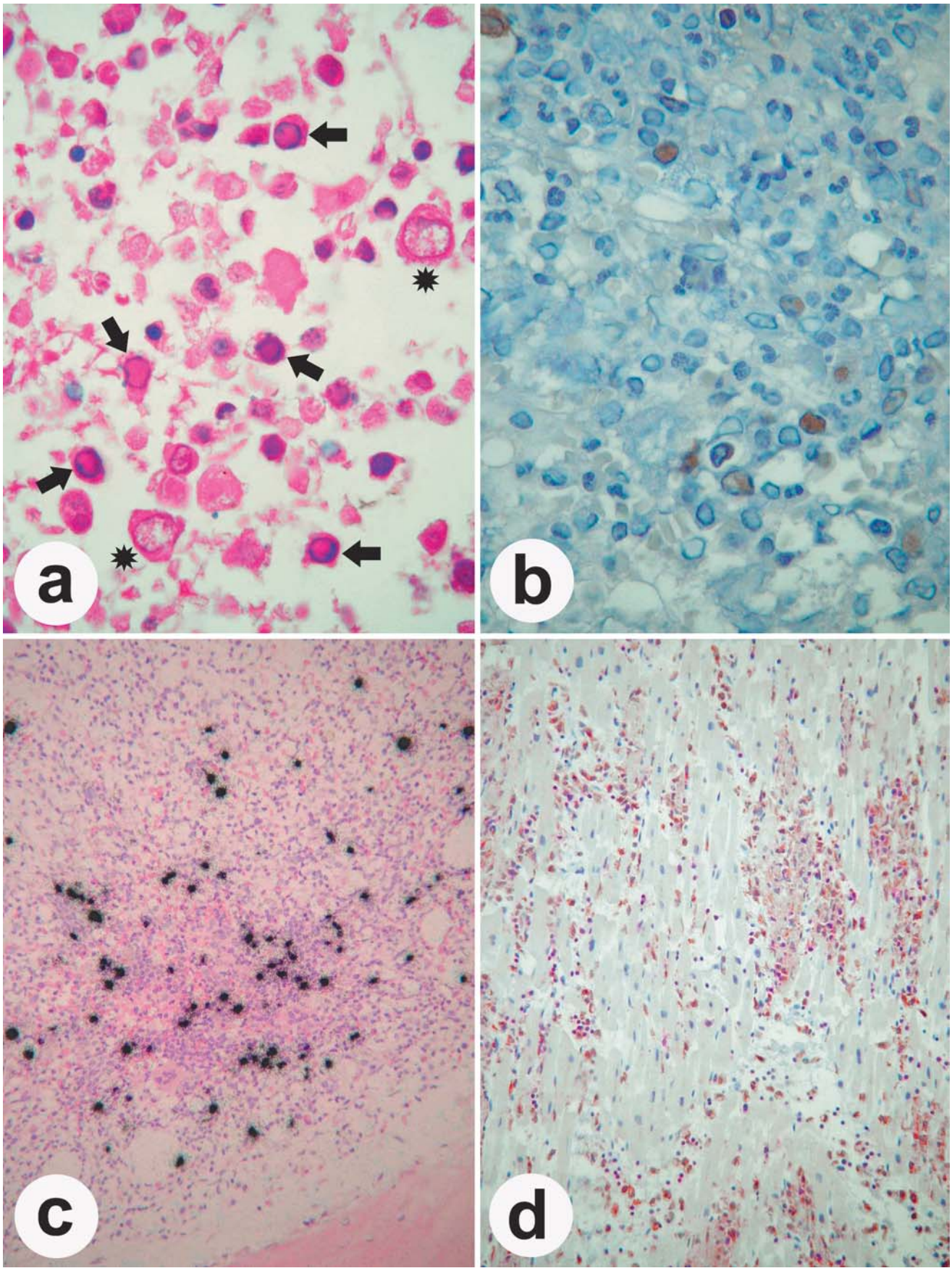
The sequence of events in natural or experimental infections [2] following intranasal inoculation of susceptible individuals is characterized by systemic infection with copious viremia ($10^{11}$–$10^{13}$ virus particles/ml blood) detectable for about 6 days, 1 week after inoculation. At the same time, virus sheds from the respiratory tract. As the titer of virus in blood falls, immunoglubulin (Ig)M antibodies begin to appear and are present for 2–3 months. PVB19–IgM immune complexes may be detected [45]. IgG antibodies cannot be observed until the third week after inoculation and persist per life. A T-cell immune response has not been reported. In the majority of patients, PVB19 is eliminated within a few weeks after infection. In about 20% of immunocompetent patients, however, the virus can persist for months, sometimes for years in the peripheral blood at a low rate, in synovial tissue and in the heart for hitherto unknown reasons [11, 42, 45]. Transfusion of blood or blood products of those clinically inapparent persons presents a source of PVB19 infection [48].

## Pathology-related diagnostic procedures

In lytic PVB19 infections (see: Transient aplastic anemia and nonimmune hydrops fetalis), in routinely stained histological sections so-called “Lantern” or “Lampion” cells can be detected that represent erythroid precursor cells (normoblasts) with intranuclear and/or intracytoplasmatic viral inclusions (Fig. 1a). In all other conditions an additional diagnostic armentarium has to be applied.

In PVB19-related cutaneous lesions, PVB19 viral particles have been detected in ECs by means of electron microscopy and immunohistology [56]. However, sensitivity of electron microscopy is very low and would only allow detection of PVB19 in biopsy specimen of cases with an extremely high viral load, e.g. in erythroid precursor cells in some bone marrow biopsies. Application of immunohistochemistry (IH) with commercially available monoclonal antibodies against VP1 and VP2 viral capsid proteins (clone R92 F6 Novocastra, Newcastle, UK) has been reported as a specific diagnostic procedure in formalin-fixed and paraffin-embedded tissues [39, 56]. However, divergent results regarding the sensitivity of these antibodies have been reported in the literature [32]. Molecular pathological methods such as dot-blot hybridization, polymerase chain reaction (PCR) and nested PCR have been successfully introduced in pathology to detect PVB19 genomes in formalin-fixed and paraffin-embedded tissues [9, 16, 42, 43, 44, 50, 55]. Recently, quantitative real-time PCR was applied to determine the viral load of PVB19 in different tissues [9, 40]. Besides greatly increasing the sensitivity of detection of viral DNA, however, gene-amplification techniques also carry a certain risk to produce false-positive results [63]. Critically, it has to be mentioned that the presence of PVB19 viral genomes in the tissue investigated might be due to viremia and not the result of real organ infection.

For pathologists, methods of great promise are isotopic and non-isotopic in situ hybridizations (ISHs), allowing the localization of PVB19 genomes in peculiar host target cells or perhaps immune cells secondarily involved in PVB19 infection [9, 22, 25, 32, 39, 50, 57].


a
b
c
d

Currently, we use the following molecular pathological techniques in our laboratories.

### Nested PCR

DNA and RNA are extracted simultaneously from deparaffinized tissue samples using proteinase K digestion followed by extraction with phenol/chloroform. For the detection of PVB19 DNA, nested PCR is performed using primers from the VP1/VP2 coding sequence (GenBank Acc. no. U38509 [17]; 35 cycles each at 94°C for 30 s, 56°C for 30 s, and 72°C for 45 s). First round is done with the 5′-primer PVB1: 5′-AGC ATG TGG AGT GAG GGG GC-3′ and 3′-primer PVB2: 5′-AAA GCA TCA GGA GCT ATA CTT CC-3′. Nested PCR primers are PVB3: 5′-GCT AAC TCT GTA ACT TGT AC-3′ and PVB4: 5′-AAA TAT CTC CAT GGG GTT GAG-3′. Specificity of PCR products is confirmed by automatic DNA sequencing [53].

### Quantitative real-time PCR

Primers and probe for quantitative PVB19 real-time PCR (Taqman 5700, Applied Biosystems, Foster City, Calif.) are derived from the PVB19 VP1/2 open reading frame (5′-primer PVB19-*Taq*1: 5′-TTT CAA AGT CAT GGA CAG TTA TCT GA-3′, 3′-primer PVB19-*Taq*2: 5′-TTG TGT AAG TCT TCA CTA GAT AAT ACT GCA TT-3′, *Taq*Man-probe FAM-5′-CCT TAT CAT CCA GTA GCA GTC ATG CAG AAC CT-3′-TAMRA). Reactions and cycling are performed using Universal *Taq*Man Master Mix and the PCR protocol as recommended by the manufacturer. PVB19 plasmid DNA in different dilutions ($2.5\times10^5$ to 250 genomes/ml are included to standardize the system. PVB19-infected bone marrow tissue derived from patients suffering on transient aplastic anemia or from non-immune hydrops fetalis serves as positive control. All samples are analyzed in minimum in duplets.

### In situ hybridization

In situ detection of PVB19 DNA is performed on dewaxed 5-µm tissue sections applying a protocol as described previously [9]. Hybridization mixture contains the $^{35}$S-labeled RNA antisense PVB19 probe [29]. After washing procedures, the tissue slide preparations are autoradiographed and stained with hematoxilin/eosin. Control RNA probes are synthesized from non-recombinant transcription vector Bluescript KS and from plasmid pCVB3-R1 providing enterovirus-specific RNA probes [6, 9, 29].

◀ **Fig. 1** **a** Bone marrow from a 3-month-old fetus suffering from non-immune hydrops fetalis with giant pronormoblasts (*) and many Lantern cells (*arrows*) Hematoxylin and eosin, ×400. **b**, **c** Comparison of immunohistochemistry (**b** ×250) and in situ hybridization (**c** ×100) demonstrating striking quantitative differences in the sensitivity to detect PVB19 positive normoblasts in the bone marrow of a patient suffering on pure red cell aplasia. **d** Multifocal areas of myocardial necrosis infiltrated by $PGM_1$-positive macrophages (*brown*) and CD3-positive lymphocytes (*red*) in a patient dying of fulminant PVB19 myocarditis. Immunohistochemical double-staining, ×50

## Clinical manifestations and disease-related pathology

### Transient aplastic anemia

As manifestation of PVB19-related lytic disease, temporary depression of erythropoiesis is probably a constant feature of all, even clinically inapparent or uncomplicated, acute PVB19 infections [2, 63]. Transient aplastic crisis occurs as a unique event in the life of patients with a variety of underlying forms of hemolysis including sickle cell anemia, congenital erythrocyte membrane defects, enzymopathies, thalassemias, acquired hemolytic anemias in adults, conditions of erythroid stress such as hemorrhage and iron deficiency, myelofibrosis and bone marrow transplantation [31, 37, 46, 63]. Anemia becomes symptomatic in the early viremic phase of infection [63]. The cessation of erythropoiesis after PVB19 infection lasts 5–7 days. Termination of the crisis is associated with a vigorous humoral immune response. Recovery is the rule and generally occurs within 1–2 months after disease onset [63].

Morphologically, PVB19 infection causes very distinctive abnormalities in the bone marrow. In addition to profound erythroid hypoplasia, two cells are characteristic of PVB19 infection of the erythroid lineage: giant pronormoblasts are typically seen in the bone marrow at the height of transient aplastic crisis (Fig. 1a). These cells probably reflect the cytopathic effect of the nonstructural viral protein NS-1 but they do not contain complete virus particles [45]. Later, erythroid precursors, the normoblasts, exhibit characteristic intranuclear eosinophilic inclusion bodies (so-called Lampion or Lantern cells) (Fig. 1a), which are packed with complete virions [5, 19, 63]. While PVB19 capsid proteins can be identified by immunohistology (Fig. 1b), PVB19 genomes are detected by ISH (Fig. 1c). Productive infection in these normoblasts is the only known source of the intensive viremia that is characteristic of lytic PVB19 infection [43]. Megakaryocytopoiesis may also be inhibited, however, in the absence of virus replication and most probably due to cytotoxic effects of NS1 [45].

### Pure red cell aplasia

Persistent PVB19 infection and pure red cell aplasia have been documented in four patient populations: congenital immunodeficiency (Nezelof's syndrome), children with lymphoblastic leukemia and other malignancies in remission after or during chemotherapy, recipi-

ents of solid organ transplantation and patients with acquired immunodeficiency syndrome [63]. The anemia may be intermittent, with periods of relapse associated with viremia and remissions with spontaneous disappearance of virus from the circulation, possibly due to depletion of the erythroid cell population. Dependent on the undulating course of disease, the bone marrow may contain giant pronormoblasts and/or Lantern cells. The diagnosis is established by detection of PVB19 genomes in the blood, serum or bone marrow by means of PCR and/or ISH (Fig. 1c), or, with lesser sensitivity, by IH [20, 32, 63]. It is important to identify PVB19 infection in these patients because intravenous immunoglobulin therapy (IVIG) may palliate their sometimes life-threatening anemia [3]. Human normal immunoglobulin preparations are a valuable source of neutralizing antibodies to PVB19, since at least half of the adult population have been exposed to the virus.

## PVB19 infection in pregnancy

The predilection of PVB19 for mitotically active tissue is dramatically illustrated by the severe consequences of fetal infections. Diaplacentar in-utero infection is a cause of non-immune hydrops fetalis in which the infant's death occurs as a result of severe anemia [28]. Pathologically, these hydropic infants show erythroblastosis, iron deposition in the liver and typical viral cytopathic alterations of normoblasts (Lantern cells) in the circulatory periphery of the liver and other organs [5]. PVB19 can be demonstrated by ISH, mainly in the liver or bone marrow. The risk of a fatal outcome for the fetus is highest with infection during the first and second trimester and was estimated to be less then 9% in a prospective study with a transplacental transmission rate of 33% [21, 30, 59]. In Germany, about half of the women in the reproductive age are PVB19 seronegative. In this regard PVB19 infection contributes – besides human cytomegalovirus infection – to the most frequent virus-related complications during pregnancy [37]. The pregnancy is lost most frequently 4–6 weeks after the onset of the rash illness of the mother. In the event of seroconversion during pregnancy, hydrops can be detected by ultrasound. Raised maternal α-fetoprotein levels are a marker of intrauterine PVB19 infection [10]. PVB19-related fetal teratogenicity has not been reported. The placenta represents a most fruitful source of nucleated red cells containing PVB19 inclusions and is worthy to be studied in all cases of non-immune hydrops fetalis. Macroscopically, the placenta is pale, friable, enlarged and edematous. Histologically, the villi are edematous. Fetal capillaries are filled with normoblasts and Lantern cells.

## Respiratory illness

Nonspecific respiratory tract illness is a common consequence of PVB19 infection, which can be mild or severe enough to mimic influenza. PVB19-related respiratory tract illness coincides with the viremic phase of the disease [2]. Information about pathomorphological changes are not available from the literature except from fetal lung tissue in which PVB19 was detected by ISH in some alveloar lining cells and in few capillary ECs but not in respiratory epithelia [39, 50].

## Rash illness
(fifth disease, erythema infectiosum, Ringelröteln)

Clinically, the exanthem occurs in three stages [33, 37]. The first begins around 18 days after the acquisition of the infection and is characterized by a fiery red rash on the cheeks – slapped-cheek appearance. At this stage the appearance may be suggestive of scarlet fever, drug sensitivity, other allergic reactions, or collagen vascular disorders. The second stage of the exanthem occurs 1–4 days after the facial involvement with the appearance of an erythematous maculopapular rash on the trunk and limbs. The third stage is highly variable in duration, lasting 1–3 weeks or more and is characterized by marked changes in the intensity of the rash, with periodic complete evanescence and recrudescence. In many cases, the illness is clinically indistinguishable from rubella. Reviewing the literature, there are only a few reports dealing with histopathological changes in PVB19-related rash illness [33, 56]. In the first erythematous stage, the leading morphological findings are dilated and slightly irregular shaped small veins and postcapillary venules in the papillary and reticular layers of the dermis, surrounded by a mild to moderate infiltrate of mononuclear cells and intermingled with sparse complement (C3) deposits. In some swollen ECs, viral capsid proteins or virus particles have been detected by means of immunohistology and/or electron microscopy [56]. Recently, Magro et al. published a more complex pattern of histopathological changes in cutaneous manifestation of PVB19 infection also dominated by a vascular injury pattern ranging from leukocytoclastic vasculitis with demonstrable immune complexes, interface dermatitis, eczematous alterations, granuloma annulare, and lesions with features of dermatomyositis or lupus erythematodes [33]. It is of special interest, that some of the patients with a complex dermatohistopathology were suffering from other preexisting diseases, e.g., tumors, chronic hepatitis C, allergic rhinitis, asthma bronchiale, and seronegative rheumatoid arthritis.

## Joint involvement

Another common complication of PVB19 infection is joint involvement [30, 37, 63]. It is relatively rare among children but in adult females it is commonplace occurring in 80% of infections with rash. In adults the most common presentation is with sudden onset of symmetrical arthritis affecting the small joints of the hand fol-

lowed by ankles, knees and elbows commencing 1–6 days after the onset of the rash. The clinical symptoms usually resolve within 2–4 weeks. In about 20% of patients symptoms persist for a few months or, rarely, for years with PVB19 being detectable in synovial tissue and peripheral blood [37]. Some longstanding cases of PVB19 arthropathy have been classified as benign rheumatoid arthritis. However, these cases are rheumatoid factor negative and other evidence indicates that PVB19 is not the cause of rheumatoid arthritis [11, 38, 54, 57]. Reviewing the literature, PVB19-specific histopathological findings in the synovia have not been reported. ISHs disclosed PVB19 genomes in immune cells, e.g. in macrophages and follicular dendritic cells of the inflammatory exudate, but not in synovial cells [25, 57]. Immune complexes which may be detected [63] can survive in phagocytic cells, likely explaining persistent infection in synovial membranes [45].

## Vasculitic syndromes

PVB19 has been linked to many systemic and local vasculitic syndromes like polyarteritis nodosa, Wegener's granulomatosis, Schönlein-Henoch purpura, systemic lupus erythematodes, and severe digital arterial occlusive disease [12, 14, 18, 58]. Evidence for PVB19 involvement is mainly based on serological or PCR data. In situ hybridization has not been performed in such cases. Reviewing the literature, there is convincing evidence that PVB19 is not aetiologically responsible for the development of these various forms of primary vasculitic syndromes, but can aggravate the underlying disease. The virus can induce endothelial injury with complement activation leading to inflammation and thrombosis. In addition, PVB19 IgM circulating immune complexes at the time of seroconversion may induce the exacerbation of the preexisting vascular disorder. Histopathological data for PVB19-associated modification of the morphology of the primary vasculitic syndromes are not available from the literature.

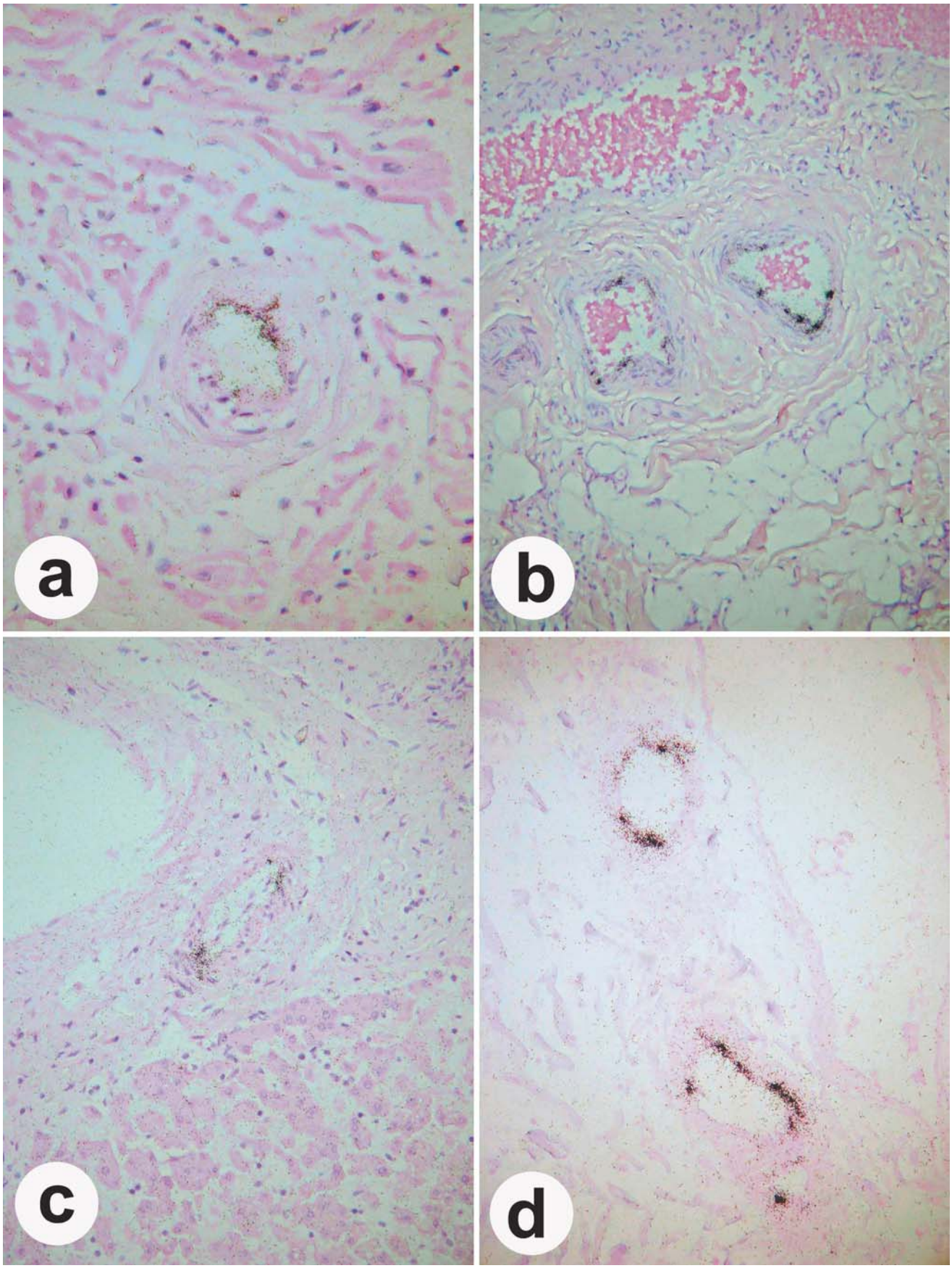
## Cardiac manifestations

A growing number of reports have suggested an association between PVB19 infection and acute or chronic cardiac diseases [9, 16, 34, 40, 42, 43, 47, 50, 52, 60]. The clinical presentation and the pathomorphological lesions depend on the age and the immunological state of the patient, as well as on the type (acute/lytic or chronic/persistent) of PVB19 infection.

Fetal myocardial cells express the cellular receptor (P antigen) for PVB19 [6]. In human fetuses suffering from PVB19-related non-immune hydrops fetalis, viral proteins and/or DNA can be demonstrated within cardiac myocytes (CMs) by means of IH or ISH [39, 47]. Fetal cardiac infection therefore seems plausible.

However, P antigen has not been demonstrated in CMs of older children or adults. In addition, given that PVB19 requires the host S-phase enzymes for viral replication, cytotoxic virus replication seems unlikely to occur in the post-partum heart, because human CMs are withdrawn from the cell cycle around the time of birth [40].

Summarizing the clinical, pathomorphological and molecular diagnostic data, it is of interest that most patients present with cardiac symptoms (acute congestive heart failure, arrhythmias, sudden cardiac arrest) 5–20 days after acute lytic PVB19 infection documented by viremia with $10^4$–$10^7$ viral genomes/ml blood or serum. Histopathological examination of heart tissue derived from endomyocardial biopsies (EMBs) or from autoptic material discloses active myocarditis with multifocal CM-necrosis or degeneration of CMs surrounded by a macrophage and T-lymphocyte containing mononuclear inflammatory exudate (Fig. 1d). Presence of PVB19 viral genomes within inflamed heart muscle tissue can be confirmed using PCR. We have had the possibility to investigate autopsy material derived from a 34-year-old female patient and a 16-year-old boy, both dying on fulminant PVB19 myocarditis. Application of quantitative real-time PCR revealed a viral load of $1.6\times10^3$–$4.3\times10^5$ PVB19 genome equivalents/µg extracted heart nucleic acid comparable to the viral load ($8\times10^5$ PVB19 genome equivalents/µg bone marrow nucleic acid) derived from a patient suffering from acute transient aplastic anemia (unpublished results). In our experience, formalin fixation and paraffin embedding reduces the number of detectable viral copies by factor of $10^2$–$10^3$, implying that in native heart tissue we could have expected $10^6$–$10^8$ viral genomes/µg extracted heart tissue DNA, possibly a critical mass to elicite virus-induced cell injury. Although the association between PVB19 infection and active myocarditis is clear, one must be cautious in interpreting the mechanisms through which myocarditis arises. Direct infection of CM in older children or adults has never been documented. We applied radioactive ISH in one patient dying of fulminant PVB19 myocarditis and in a 13-year-old girl suffering from PVB19-associated constrictive pericarditis. Heart tissues from both patients were characterized by a high viral load (>$10^4$ genome equivalents/µg extracted myocardial or pericardial nucleic acid). PVB19 DNA and RNA could be demonstrated in ECs lining small irregular dilated veins and small arteries within the myocardium and pericardium (Fig. 2a and b) indicating that ECs but not CMs are the PVB19-specific target cells in the postnatal perimyocardium. So far, PVB19-associated active perimyocarditis is different from enterovirus-induced inflammatory heart disease. In the latter, ECs are transiently used by the virus on its way to destroy CMs as the enterovirus-specific target cells by cytopathic effects [29]. Recently, high cytokine levels (interferon γ, tumor necrosis factor α, interleukins 6 and 8) have been described in PVB19-associated active and chronic myocarditis and were made responsible for induction of myocardial necrosis and inflammation [42]. Successful treatment of a patient with severe PVB19 perimyocarditis by IVIG has


a
b
c
d

been reported [42]. In life-threatening situations, cardiac transplantation has been performed [16].

In patients undergoing heart transplantation due to non-PVB19-related heart diseases, PVB19 infection in the postoperative phase can occur and may histologically not be discernable from mild to moderate rejection grade. Viral infection can be assumed if periods of cardiac rejection are difficult to control with the usual antirejection therapeutic regimens. In these cases PVB19 infection may immediately be diagnosed by application of molecular pathological methods, e.g., PCR, and, thus, lead to an improved treatment (i.e., IVIG therapy) that may serve to limit inflammatory damage to the transplanted heart [52].

From the presence of PVB19 genomes in the cardiac allografts without concomitant viremia it was concluded that PVB19 can persist in cardiac tissue [52]. Recently, PVB19 persistence in consecutive EMBs for more than 3 years has been described in a young immunocompetent girl clinically and histologically characterized by ongoing myocarditis [42]. Preliminary retrospective analysis of our files of EMBs disclosed PVB19 persistence in one or more consecutive EMBs of eight immunocompetent patients suffering from chronic myocarditis or dilated cardiomyopathy over a period of 6–18 months; PCR disclosed a low viral load ($<10^3$ PVB19 genome equivalents/µg extracted myocardial nucleic acid), the immunohistological hallmark was an increased number of $PGM_1$-positive macrophages within the interstitial cardiac tissue without concomitant myocyte necrosis (unpublished results). ISH detected PVB19 genomes in few interstitial cells but, hitherto, without identification of the target cell, e.g., macrophages or ECs, but not CMs (unpublished results).

The clinical significance and the mechanisms that mediate persistence of this viral infection in the heart muscle is unclear at this time.

### Hepatitis and other clinical manifestations

During the last few years, increasing numbers of reports are dealing with acute or fulminant hepatitis in children and adults in association with PVB19 infection [15, 24, 26, 54, 61, 62]. The diagnosis has been established on clinical data, laboratory findings and PCR data. Unfortunately, in no report has information about histopathological findings been presented. In one patient dying of fulminant PVB19-induced myocarditis, we had the chance to investigate liver and the gall bladder tissues. Clinically, an unusual hydrops of the gall bladder and unusual congestion of liver veins was detected at the time of hospital admission which could not be explained by congestive heart failure. We demonstrated by ISH that ECs of dilated small veins of the gall bladder and of small portal veins but not hepatocytes are the target cells for PVB19 in the liver (Fig. 2c and d). Quantitative real-time PCR detected a viral load of $8\times10^2$ and $1.2\times10^4$ viral genome equivalents/µg nucleic acid, respectively, from liver and gall bladder tissue.

Acute renal involvement in PVB19 infection has been described histologically, characterized by immune complex-mediated transient endocapillary proliferative glomerulonephritis at the time of IgM seroconversion [41]. Furthermore, association of PVB19 infection with transient disturbance of consciousness and acute meningoencephalitis have been reported [4, 61].

◀ **Fig. 2** **a**, **b** Detection of PVB19 positive endothelial cells (ECs) lining small intramyocardial [**a** in situ hybridization (ISH), ×150] and pericardial (**b** ISH, ×100) veins in two patients suffering from active myocarditis or constrictive pericarditis. **c**, **d** PVB19 viral genomes in ECs of small hepatic portal veins (**c** ISH, ×100) and submucosal blood vessels in gall bladder (**d** ISH, ×150)

## PVB19 infections in immunocompromised patients

In patients with primary or secondary immunodeficiencies (inborn errors, solid organ transplantation, HIV-infection, leukemia and other malignancies in remission after or during chemotherapy) chronic PVB19 infections have been described to count for severe, sometimes life-threatening diseases [20, 27, 31, 35, 44, 51]. Chronically infected patients have failed to mount a neutralizing antibody response to the virus and they lack the clinical symptoms of erythema infectiosum, fever, rash, and polyarthralgia/polyarthritis [2]. Besides hematological disorders (severe chronic anemias, pure red cell aplasia, reticulocytopenia and neutropenia) frequently myocarditis, pericarditis, acute heart and liver failure, meningitis and encephalitis have been reported. In patients with organ transplantation, PVB19-related mortality is about 7% [51].

## Conclusion

Infection with PVB19 is common when it has been examined. Pathologists are frequently involved in serious and potentially fatal conditions that occur in a minority of the population that is particularly predisposed, e.g., in immunocompromised patients. In transient or chronic aplastic anemia and in non-immune hydrops fetalis, the diagnosis can usually be established by application of histological routine stains. In all other conditions that may mimic other viral or immunologically mediated diseases, the armamentarium of molecular pathological methods must be extended: PCR can detect PVB19 genomes, quantitative real-time PCR gives information about the viral load in tissues investigated. IH and ISH allow the topographical identification of virus-specific target cells in histological sections. In this review, we have presented evidence that in children and adults with lytic PVB19 infection with high viral tissue load, ECs of the microcirculatory periphery of different organs are PVB19-specific target cells.

**Acknowledgements** The work presented was supported in part by the Federal Ministry of Education, Science, Research and Technology and the Interdisciplinary Center for Clinical Research of the Medical Faculty of the University of Tübingen (IZKF 01 KS 9602).

## References

1. Anderson MJ, Jones SE, FisherHoch SP, Lewis E, Hall SM, Bartlett CL, Cohen BJ, Mortimer PP, Pereira MS (1983) Human parvovirus, the cause of erythema infectiosum (fifth disease)? Lancet i:1378
2. Anderson MJ, Higgins PG, Davis LR, Willman JS, Jones SE, Kidd IM, Pattison JR, Tyrrell DA (1985) Experimental parvoviral infection in humans. J Infect Dis 152:257–265
3. Anderson LJ (1997) Treatment and prevention of human parvovirus B19 disease. In: Anderson LJ, Young NS (eds) Monographs in virology. Karger, Basel, pp. 137–148
4. Barah F, Vallely PJ, Chiswick ML, Cleator GM, Kerr JR (2001) Association of human parvovirus B19 infection with acute meningoencephalitis. Lancet 358:729–730
5. Benirschke K, Kaufmann P (2000) Erythroblastosis and hydrops fetalis. In: Benirschke K, Kaufmann P (eds) Pathology of the human placenta. Springer, Berlin Heidelberg New York, pp. 461–491
6. Blundell MC, Beard C, Astell CR (1987) Virology 157:534–538
7. Brown KE, Anderson SM, Young NS (1993) Erythrocyte P antigen: cellular receptor for B19 parvovirus. Science 262: 114–117
8. Brown KE, Hibbs JR, Gallinella G, Anderson SM, Lehman ED, McCarthy P, Young NS (1994) Resistance to parvovirus B19 infection due to lack of virus receptor (erythrocyte P antigen). N Engl J Med 330:1192–1196
9. Bültmann BD, Klingel K, Sotlar K, Bock CT, Baba HA, Sauter M, Kandolf R (2002) Fatal parvovirus B19 associated inflammatory cardiomyopathy: an endothelial cell mediated disease. Hum Pathol (in press)
10. Carrington D, Gilmore DH, Whittle MJ, Aitken D, Gibson AA, Patrick WJ, Brown T, Caul EO, Field AM, Clewley JP, Cohen, BJ (1987) Maternal serum α fetoprotein: a marker of fetal aplastic crises during intrauterine human parvovirus infection. Lancet i:433–435
11. Cassinotti P, Siegl G, Michel BA, Bruhlmann P (1998) Presence and significance of human parvovirus B19 DNA in synovial membranes and bone marrow from patients with arthritis of unknown origin. J Med Virol 56:199–204
12. Corman LC, Dolson DJ (1992) Polyarteritis nodosa and parvovirus B19 infection. Lancet 339:441
13. Cossart YE, Field AK, Cant B, Widdows D (1975) Parvoviruslike particles in human sera. Lancet i:72–73
14. Dingli D, Pfizenmaier DH, Arromdee E, Wennberg P, Spittell PC, ChangMiller A, Clarke BL (2000) Severe digital arterial occlusive disease and acute parvovirus B19 infection. Lancet 356:312–313
15. Drago F, Semino M, Rampini P, Rebora A (1999) Parvovirus B19 infection associated with acute hepatitis and a purpuric exanthem. Br J Dermatol 141:154–179
16. Enders G, Dotsch J, Bauer J, Nutzenadel W, Hengel H, Haffner D, Schalasta G, Searle K, Brown KE (1998) Life threatening parvovirus B19 associated myocarditis and cardiac transplantation as possible therapy: two case reports. Clin Infect Dis 26:355–358
17. Erdman DD, Durigon EL, Wang QY, Anderson LJ (1996) Genetic diversity of human parvovirus B19: sequence analysis of the VP1/VP2 gene from multiple isolates. J Gen Virol 77: 2767–2774
18. Finkel TH, Torok TJ, Ferguson PJ, Durigon EL, Zaki SR, Leung DY, Harbeck RJ, Gelfand EW, Saulsbury FT, Hollister JR, Anderson LJ (1994) Chronic parvovirus B19 infection and systemic necrotising vasculitis: Opportunistic infection or aetiological agent? Lancet 343:1255–1258
19. Foucar K (1995) Bone marrow pathology. ASCP Press, Chicago
20. Frickhofen N, Abkowitz JL, Safford M, Berry JM, Antunezde Mayolo J, Astrow A, Cohen R, Halperin I, King L, Mintzer D, et al (1990) Persistent B19 parvovirus infection in patients with human immunodeficiency virus type 1 (HIV1): a treatable cause of anemia in AIDS. Ann Intern Med 113:926–933
21. Hall SM (1990) Public Health Laboratory Service working in fifth disease. Prospective study of human parvovirus (B19) infection in pregnancy. Br Med J 300:1166–1170
22. Hassam S, Tratschin JD, Siegl G, Heitz PU (1990) In situ hybridization for the detection of human parvovirus B19 nucleic acid sequences in paraffin embedded specimens. Virchows Arch 59:257–261
23. Heegard ED, Laub Peterson B (2000) Parvovirus B19 transmitted by bone marrow. Br J Haematol 111:659–661
24. Hillingso J, Jensen JP, TomPetersen L (1998) Parvovirus B19 and acute hepatitis. Lancet 351:955–956
25. Kandolf R, Kirschner P, Hofschneider PH, Vischer TL (1989) Detection of parvovirus in a patient with "reactive arthritis" by in situ hybridization. Clin Rheumatol 8:398–401
26. Karetnyi YV, Beck PR, Markin RS, Langnas AN, Naides SJ (1999) Human parvovirus B19 infection in acute fulminant liver failure. Arch Virol 144:1713–1724
27. Kariyawasam HH, Gyi KN, Hodson ME (2000) Anemia in lung transplant patient caused by parvovirus B19. Thorax 55:619–620
28. Kinney JS, Anderson LJ, Farrar J, Strikas RA, Kumar ML, Kliegman RM, Sever JL, Hurwitz ES, Sikes RK (1988) Risk of adverse outcomes of pregnancy after human parvovirus B19 infection. J Infect Dis 157:662–667
29. Klingel K, Hohenadl C, Canu A, et al (1992) Ongoing enterovirus induced myocarditis is associated with persistent heart muscle infection. Proc Natl Acad Sci U S A 89:314–318
30. Koch WC (2001) Fifth (human parvovirus) and sixth (herpes virus 6) diseases. Curr Opin Infect Dis 14:343–356
31. Koch WC, Massey G, Russell CE, Adler SP (1990) Manifestations and treatment of human parvovirus infection in immunocompromised patients. J Pediatr 116:355–359
32. Liu W, Ittmann M, Liu J, Schoentag R, Tierno P, Greco MA, Sidhu G, Nierodzik M, Wieczorek R (1997) Human parvovirus B19 in bone marrows from adults with acquired immunodeficiency syndrome: a comparative study using in situ hybridization and immunohistochemistry. Hum Pathol 28:760–766
33. Magro CM, Dawood MR, Crowson AN (2000) The cutaneous manifestations of human parvovirus B19 infection. Hum Pathol 31:488–497
34. Malm C, Fridell E, Jansson K (1993) Heart failure after parvovirus B19 infection. Lancet 341:1408–1409
35. Marchand S, Tchernia G, Hiesse C, Tertian G, Cartron J, Kriaa F, Boubenider S, Goupy C, Lecointe D, Charpentier B (1999) Human parvovirus B19 infection in organ transplant recipients. Clin Transplant 13:17–24
36. Miyamoto K, Ogami M, Takahashi Y, Mori T, Akimoto S, Terashita H, Terashita T (2000) Outbreak of human parvovirus B19 in hospital workers. J Hosp Infect 45:238–241
37. Modrow S (2001) Parvovirus B19. Ein Infektionserreger mit vielen Erkrankungsbildern. Dt. Arztbl 98:A1620–A1624
38. Moore TL (2000) Parvovirus-associated arthritis. Curr Opin Rheumat 12:289–294
39. Morey AL, Porter HJ, Keeling JW, Fleming KA (1992) Non-isotopic in situ hybridization and immunophenotyping of infected cells in the investigation of human fetal parvovirus infection. J Clin Pathol 45:673–678
40. Murry CE, Keith RJ, Reichenbach DD (2001) Fatal parvovirus myocarditis in a 5 year-old girl. Hum Pathol 32:342–345
41. Nakazawa T, Tomosugi N, Sakamoto K, Asaka M, Yuri T, Ishikawa I, Kitagawa S (2000) Acute glomerulonephritis after human parvovirus B19 infection. Am J Kidney Dis 35:E31
42. Nigro G, Bastianon V, Colloridi V, Ventriglia F, Gallo P, D'Amati G, Koch WC, Adler SP (2000) Human parvovirus B19 infection in infancy associated with acute and chronic lymphocytic myocarditis and high cytokine levels: report of 3 cases and review. Clin Infect Dis 31:65–69

43. Orth T, Herr W, Spahn T, Voigtlander T, Michel D, Mertens T, Mayet WJ, Dippold W, MeyerzumBuschenfelde KH (1997) Human parvovirus B19 infection associated with severe acute perimyocarditis in a 34 year old man. Eur Heart J 18:524–525
44. Pamidi S, Friedman K, Kampalath B, Eshoa C, Hariharan S (2000) Human parvovirus B19 infection presenting as persistent anemia in renal transplant recipients. Transplantation 69: 2666–2669
45. Pattison JR (2000) Human parvoviruses. In: Zuckerman AJ, Banatvala JE, Pattison JR (eds) Principles and practice of clinical virology. John Wiley and Sons, Ltd. New York, pp. 645–658
46. Pattison JR, Jones SE, Hodgson J, Davis LR, White JM, Stroud CE, Murtaza L (1981) Parvovirus infections and hypoplastic crisis in sickle cell anemia. Lancet i:664–665
47. Porter HJ, Quantril AM, Fleming KA (1988) B19 parvovirus infection of myocardial cells. Lancet i:535–536
48. Robertson BH, Erdman DD (2000) Nonenveloped viruses transmitted by blood and blood products. Dev Biol Stand 102:29–35
49. Rodis JF, Borgida AF, Wilson M, Egan JF, Leo MV, Odibo AO, Campbell WA (1998) Management of parvovirus infection in pregnancy and outcomes of hydrops: a survey of members of the society of perinatal obstretricians. Am J Obstet Gynecol 179:985–989
50. Salimans MM, Rijke FM, Elsacker Niele AM (1989) Detection of parvovirus B19 DNA in fetal tissues by in situ hybridization and polymerase chain reaction. J Clin Pathol 42:525–530
51. Schleuning M, Jager G, Holler E, Hill W, Thomssen C, Denzlinger C, Lorenz T, Ledderose G, Wilmanns W, Kolb HJ (1999) Human parvovirus B19 associated disease in bone marrow transplantation. Infection 27:114–117
52. Schowengerdt KO, Ni J, Denfield SW, Gajarski RJ, Bowles NE, Rosenthal G, Kearney DL, Price JK, Rogers BB, Schauer GM, Chinnock RE, Towbin JA (1997) Association of parvovirus B19 genome in children with myocarditis and cardiac allograft rejection. Circulation 96:3549–3554
53. Smith LM, Sanders JZ, Kaiser RJ, Hughes P, Dodd C, Connell CR, Heiner C, Kent SB, Hood LE (1986) Fluorescence detection in automated DNA sequence analysis. Nature 321:674–679
54. Sokal EM, Melchior M, Cornu C, Vandenbroucke AT, Buts JP, Cohen BJ, Burtonboy G (1998) Acute parvovirus B19 infection associated with fulminant hepatitis of favourable prognosis in young children. Lancet 352:1739–1741
55. Stahl HD, Seidl B, Hubner B, Altrichter S, Pfeiffer R, Pustowoit B, Liebert UG, Hofmann J, vonSalisSoglio G, Emmrich F (2000) High incidence of parvovirus B19 DNA in synovial tissue of patients with undifferentiated mono and oligoarthritis. Clin Rheumatol 19:281–286
56. Takahashi M, Ito M, Sakamoto F, Shimizu N, Furukawa T, Takahashi M, Matsunaga Y (1995) Human parvovirus B19 infections: immunhistochemical and electronmicroscopic studies of skin lesions. J Cutan Pathol 22:168–172
57. Takahashi Y, Murai C, Shibata S, Munakata Y, Ishii T, Ishii K, Saitoh T, Sawai T, Sugamura K, Sasaki T (1998) Human parvovirus B19 as a causative agent for rheumatoid arthritis. Proc Natl Acad Sci U S A 95:8227–8232
58. Trapani S, Ermini M, Falcini F (1999) Human parvovirus B19 infection: its relationship with systemic lupus erythematosus. Semin Arthritis Rheum 28:319–325
59. Tolfvenstam T, Papadogiannakis N, Norbeck O, Petersson K, Broliden K (2001) Frequency of human parvovirus B19 infection in intrauterine fetal death. Lancet 357:1494–1497
60. Török TJ (1997) Unusual clinical manifestations reported in patients with parvovirus B19 infection. In: Anderson LJ, Young NS (eds) Monographs in virology: human parvovirus B19. Karger, Basel, pp. 61–97
61. Yoto Y, Kudoh T, Asanuma H, Numazaki K, Tsutsumi Y, Nakata S, Chiba S (1994) Transient disturbance of consciousness and hepatic dysfunction associated with human parvovirus B19 infection. Lancet 344:624–625
62. Yoto Y, Kudoh T, Haseyama K, Suzuki N, Chiba S (1996) Human parvovirus B19 infection associated with acute hepatitis. Lancet 347:868–869
63. Young NS (1996) Parvoviruses. In: Fields BN, Knipe DM, Howley PM, et al. (eds) Fields virology, Lippincott Raven, Philadelphia, pp. 2199–2236

Virchows Arch (2003) 442:18–24
DOI 10.1007/s00428-002-0674-1

ORIGINAL ARTICLE

**Denis Chatelain · Jean-François Fléjou**

# High-grade dysplasia and superficial adenocarcinoma in Barrett's esophagus: histological mapping and expression of p53, p21 and Bcl-2 oncoproteins

Received: 11 February 2002 / Accepted: 30 March 2002 / Published online: 24 September 2002
© Springer-Verlag 2002

**Abstract** In order to characterize the early morphological and molecular stages of the neoplastic progression of Barrett's mucosa, we performed the entire histological examination of ten specimens of resected Barrett's esophagus with high-grade dysplasia or superficial adenocarcinoma. The expression of p53, p21 and Bcl-2 proteins was assessed by immunohistochemistry. The surface of Barrett's mucosa ranged from 2.6 $cm^2$ to 31 $cm^2$. Dysplasia and adenocarcinoma always developed in specialized mucosa and often occupied small surfaces. High-grade dysplasia was multifocal in eight cases. There was no preferential site for neoplastic transformation into high-grade dysplasia or superficial adenocarcinoma in Barrett's mucosa. Three superficial adenocarcinomas and four high-grade dysplasias overexpressed p53 protein. p21 protein was focally expressed in nondysplastic mucosa and overexpressed in two superficial adenocarcinomas, one high-grade dysplasia and two low-grade dysplasias. In most cases, the expression of p21 and p53 proteins was unrelated. Bcl-2 protein was detected in only one area of low-grade dysplasia. In our study, high-grade dysplasia and superficial adenocarcinoma appeared as tiny lesions, often multifocal for high-grade dysplasia confirming the need for an extensive sampling of Barrett's mucosa in the endoscopic surveillance. p53 dysfunction plays a major role in the progression from dysplasia to carcinoma in Barrett's esophagus and appears unrelated to p21 and Bcl-2 expression.

**Keywords** Barrett's esophagus · Adenocarcinoma · Dysplasia · p53 protein · p21 protein

D. Chatelain · J.-F. Fléjou (✉)
Service d'anatomie pathologique, Hôpital Saint Antoine,
184 rue du Faubourg Saint-Antoine 75541, Paris Cedex 12, France
e-mail: jean-francois.flejou@sat.ap-hop-paris.fr
Tel.: +33-1-49283012, Fax: 33-1-49282878

## Introduction

Barrett's esophagus (BE) is an acquired condition in which the stratified squamous epithelium of the distal esophagus is replaced by a metaplastic columnar epithelium, the so-called specialized mucosa. It is a preneoplastic condition and the patients with specialized intestinal metaplasia of the distal esophagus are more likely to develop esophageal adenocarcinoma through a multistep morphological sequence with increasing grades of dysplasia [7]. The *p53* tumor suppressor gene is involved in the control of the cell cycle and the regulation of the programmed cell death (apoptosis). In response to cellular DNA damage, p53 protein can stop the cell cycle at phase G1, mainly by transactivating the *WAF1/CIP1* gene that encodes p21 protein, a potent inhibitor of cyclin-dependent kinases [3]. p53 protein may also induce apoptosis, particularly by inhibiting *Bcl-2* gene transduction [15]. It has been shown that most Barrett's adenocarcinomas show a *p53* gene mutation [8, 30]. However only limited and contradictory data have been published regarding the role of p21 and Bcl-2 proteins in Barrett's carcinogenesis [2, 6, 9, 13, 16, 19, 25, 31, 36]. In our study, we investigated the early stages of neoplasia in a series of ten resected BEs with high-grade dysplasias (HGD) (five cases) or superficial adenocarcinomas (five cases). We performed a detailed morphological study with a histological mapping of the whole BE and an immunohistochemical study of p53, p21 and Bcl-2 expression.

## Materials and methods

### Histological mapping

Ten specimens of esophagogastrectomy from patients with BE operated on consecutively in Beaujon hospital between 1994 and 1998 with the diagnosis of HGD or superficial adenocarcinoma were studied. The fresh surgical specimens were opened longitudinally, pinned out flat, photographed, both before and after lugol iodine staining, and fixed in 10% formalin. The entire Barrett

mucosa was submitted to histological examination through contiguous and regularly spaced (every 3 mm) slices of the esophageal wall extending from the squamo-columnar junction, defined as the junction between lugol iodine positive and negative esophageal mucosa, to the esophagogastric junction defined as the upper margin of the gastric folds. One lateral margin of each piece of tissue was marked with Indian ink so that each sample was correctly orientated. One hundred and ten sections were examined (from 5 to 33 sections by case). Sections (4-µm thick) from each case were stained with hematoxylin and eosin (H&E) and were reviewed independently by the two authors. In cases of disagreement, the slides were reviewed again simultaneously by both authors to achieve the same diagnosis.

Barrett's mucosa was confirmed by the presence of columnar-lined mucosa in the distal esophagus. Three types of mucosa were identified: fundic-type mucosa defined by the presence of glands lined with parietal and chief cells, junctional mucosa defined by the presence of glands lined with cylindrical mucous secreting cells, and specialized mucosa defined by the presence of goblet cells. According to Riddell et al., dysplasia was classified into mucosa negative for dysplasia, indefinite for dysplasia, low-grade dysplasia (LGD) and HGD [24]. Superficial adenocarcinoma was defined as adenocarcinoma limited to the mucosa or submucosa, irrespective of the lymph node status [18]. Intramucosal carcinoma differed from HGD by the invasion of the tumor through the basement membrane. The percentage of various histological types of mucosa was directly estimated on the slides, and was used to establish the areas of Barrett's metaplastic mucosa (fundic, junctional and specialized), dysplasia (low grade, high grade) and adenocarcinoma. These areas (in $mm^2$) were determined by multiplying the size of the lesion on the corresponding section, directly measured on the slide, by 3 mm (approximate thickness of embedded tissue). These values and the photographs of the specimens were used to draw Barrett's mucosa with all the various types of epithelium represented by a specific color (blue: squamous mucosa, dark brown: gastric mucosa, pink: junctional-type mucosa, light brown: fundic-type mucosa, yellow: specialized mucosa, green: low-grade dysplasia, red: high-grade dysplasia, black: superficial adenocarcinoma).

### Immunohistochemistry

Two paraffin blocks were selected in each case. The following lesions were present on the corresponding slides in all cases: HGD, LGD, nondysplastic Barrett's mucosa, esophageal squamous mucosa and gastric epithelium; superficial adenocarcinoma was present on the slides in five cases. For the immunohistochemical study, tissue sections (4-µm thick) were deparaffined in three changes of xylene for 10 minutes each. They were hydrated in decreasing concentrations of ethanol and rinsed in water. The slides were placed in 10 mmol/l sodium citrate buffer pH 6 (Sigma Chemical Co. St Louis, MO, USA) and microwaved at 2-min intervals for a total of 21 min at maximal power. Endogenous peroxidase was blocked with 1% $H_20_2$-methanol for 30 min at room temperature. The following primary antibodies were used: p53 protein (DO7, Dako, Glostrup, Denmark, 1/20), p21 protein (EA10, Oncogene Science, Cambridge, United Kingdom, 1/25) and Bcl-2 protein (124, Dako, Glostrup, 1/5). An indirect immunoperoxydase technique with DAB (Sigma) revelation was employed. In each run a slide was included with omission of the primary antibody for negative controls. An esophageal cancer with known abnormal p53 protein overexpression due to missense gene mutation, normal colon mucosa expressing p21 protein and reactive tonsil expressing Bcl-2 were used as positive controls. Omission of the primary antibody was used as a negative control for the corresponding antibody. The sections were reviewed independently by the authors and a consensus was achieved in divergent cases by common revision of the slides.

The cases were graded as positive or negative, according to the presence of a discrete or intense nuclear staining for p53 and p21 antibodies. In the adenocarcinomas 20% positive cells were considered as the lower limit for positivity. In Barrett's mucosa, either nondysplastic or dysplastic, the presence of contiguous positive cells occupying entirely or partially one gland was considered as the criterion for positivity, and the level of positivity in the gland (lower or upper half) was recorded. For Bcl-2 immunostaining the cases were graded as positive or negative according to the presence of a discrete or intense cytoplasmic staining of 20% of the cells.

## Results

### Clinical data and gross features

The patients were ten men aged between 28 years and 70 years (mean age 60 years). All of them had a hiatal hernia and gastroesophageal reflux disease which had been evolving for 1–30 years. In four cases, the diagnosis of BE and superficial adenocarcinoma or BE and HGD was made simultaneously. In the remaining six cases, BE was diagnosed from 1 year to 11 years before HGD or superficial adenocarcinoma. The length of BE on the surgical specimens varied from 0.5 cm to 10 cm. The gross appearance varied: irregular verrucous mucosa in two cases [1 HGD (Fig. 1b), one superficial adenocarcinoma (Fig. 1i)], nodules in two cases of superficial adenocarcinomas (Fig. 1f, h), ulceration in one case of superficial adenocarcinoma (Fig. 1j) and one case of HGD (Fig. 1d), and flat mucosa in five cases [two superficial adenocarcinomas (Fig. 1g, h) and three HGDs (Fig. 1a, c, e)].

### Histological mapping

The surface of Barrett's mucosa ranged from 2.6 $cm^2$ to 31 $cm^2$. In the ten cases, a large part of BE was mainly lined with specialized intestinal mucosa that represented from 18% to 90% of the total surface of Barrett's esophagus. Junctional mucosa was present at the proximal part of Barrett's mucosa in four cases (Fig. 1a, d, h, i). In two cases, there was fundic-type mucosa at the distal part of the esophagus, just above the gastroesophageal junction (Fig. 1d, f). In all the cases LGD was present associated with HGD and superficial adenocarcinoma (Fig. 1a–j). In the five cases of superficial adenocarcinoma, the cancer was surrounded by foci of HGD (Fig. 1a, g–j). Nondysplastic mucosa, dysplastic mucosa and superficial adenocarcinomas were always strongly intricated (Fig. 1a, g–j). The surface of HGD and/or superficial adenocarcinomas varied greatly from one case to another, ranging from 0.06 $cm^2$ to 8.6 $cm^2$ for HGD and from 0.3 $cm^2$ to 1.7 $cm^2$ for superficial adenocarcinomas (Table 1).

### Immunohistochemistry

In non-dysplastic mucosa and LGD, there was only focal and mild nuclear staining for p53 protein in 1–20% of the cells, usually located at the basal part of the gland.




**Fig. 1** **a** High-grade dysplasia at the gastroesophageal junction on flat Barrett's esophagus. **b** Low-grade dysplasia and high-grade dysplasia on verrucous Barrett's esophagus. **c** Low-grade dysplasia and high-grade dysplasia at the upper part of flat Barrett's esophagus. **d** Multifocal ulcerated high-grade dysplasia and low-grade dysplasia. **e** Multifocal low-grade dysplasia and high-grade dysplasia on flat Barrett's esophagus. **f** Nodular superficial adenocarcinoma surrounded by low-grade dysplasia and high-grade dysplasia at the middle part of Barrett's esophagus. **g** Small superficial adenocarcinoma arising on a short Barrett's esophagus. **h** Superficial adenocarcinoma surrounded by low-grade dysplasia and high-grade dysplasia. **i** Small verrucous superficial adenocarcinoma surrounded by high-grade dysplasia. **j** Ulcerated superficial adenocarcinoma surrounded by low-grade dysplasia and high-grade dysplasia

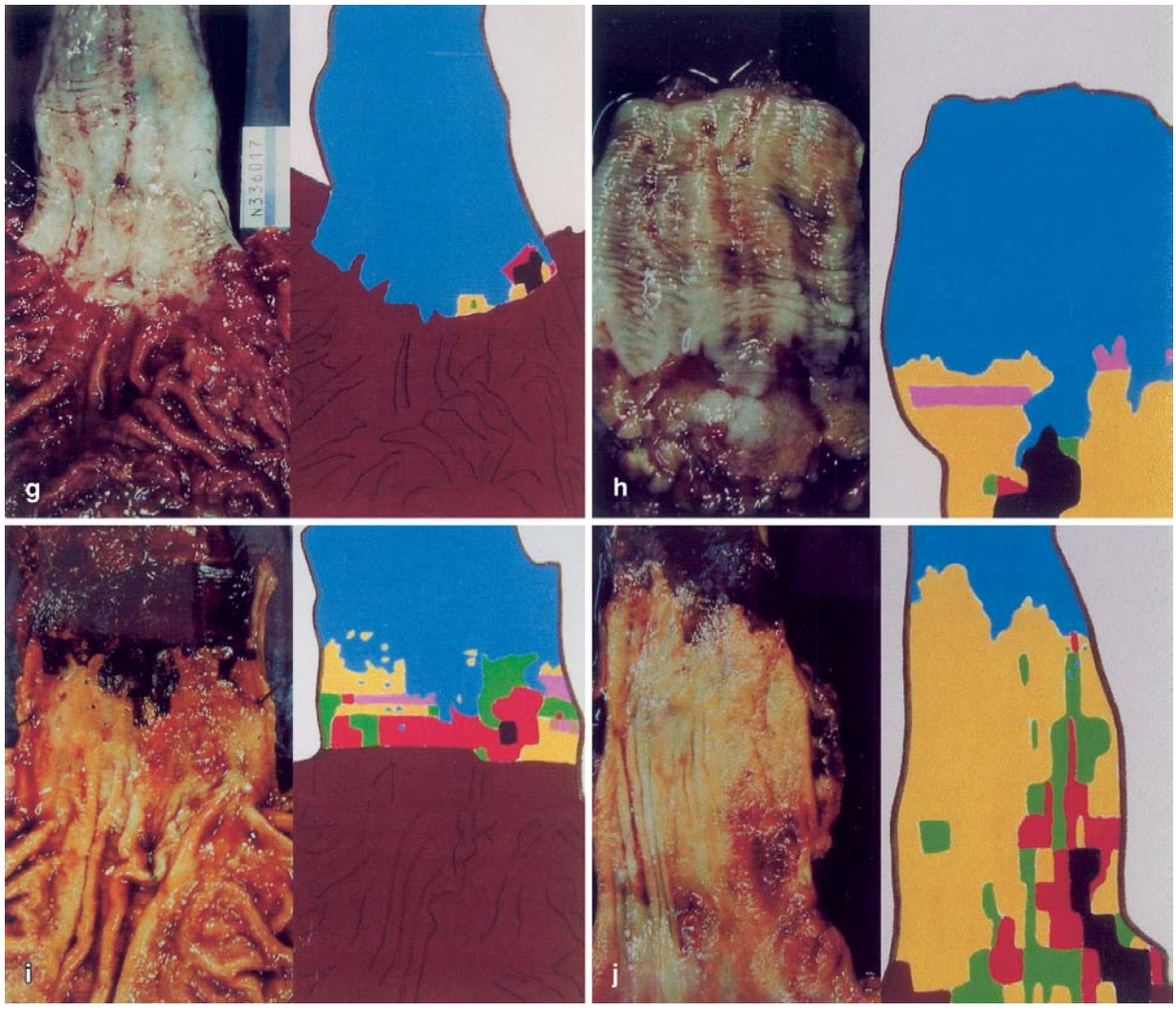



**Fig. 1** (continued)

**Table 1** Surface of the lesions in ten superficial adenocarcinomas and high-grade dysplasias (*HGD*) in Barrett's esophagus (*BE*). *LGD* low-grade dysplasia

| Patients | Surface of BE ($cm^2$) | Surface of junctional or fundic mucosa ($cm^2$) | Surface of specialized mucosa ($cm^2$) | Surface of LGD ($cm^2$) | Surface of HGD ($cm^2$) | Surface of superficial adenocarcinoma ($cm^2$) |
|---|---|---|---|---|---|---|
| Patient 1 | 2.66 | 0.2 (8%) | 2.4 (90%) | | 0.06 (2%) | |
| Patient 2 | 5.4 | | 2.1 (39%) | 0.5 (9%) | 2.8 (52%) | |
| Patient 3 | 5.4 | | 3.6 (67%) | 1.2 (22%) | 0.6 (11%) | |
| Patient 4 | 19.3 | 0.4 (2%) | 7.8 (40%) | 8.1 (42%) | 3 (16%) | |
| Patient 5 | 31 | 5.9 (19%) | 5.6 (18%) | 10.9(35%) | 8.6 (28%) | |
| Patient 6 | 11.2 | 2.3 (21%) | 3.9 (35%) | 2 (18%) | 1.3 (12%) | 1.7 (14%) |
| Patient 7 | 1.35 | | 0.6 (44%) | 0.05 (4%) | 0.3 (22%) | 0.4 (30%) |
| Patient 8 | 10 | 0.8 (8%) | 7.4 (74%) | 0.2 (2%) | 0.1 (1%) | 1.5 (15%) |
| Patient 9 | 9.4 | 0.6 (7%) | 3.1(33%) | 2 (23%) | 3.4 (37%) | 0.3 (3%) |
| Patient 10 | 19.6 | | 11.1 (57%) | 3.7 (19%) | 3.2 (16%) | 1.6 (8%) |
| Mean | 12.5 | 1.7 | 4.8 | 3.2 | 2.3 | 1.1 |

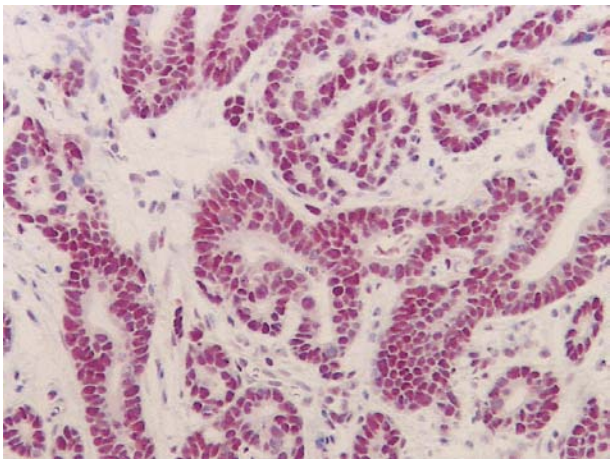


**Fig. 2** Diffuse nuclear staining with p53 antibody in one case of superficial adenocarcinoma

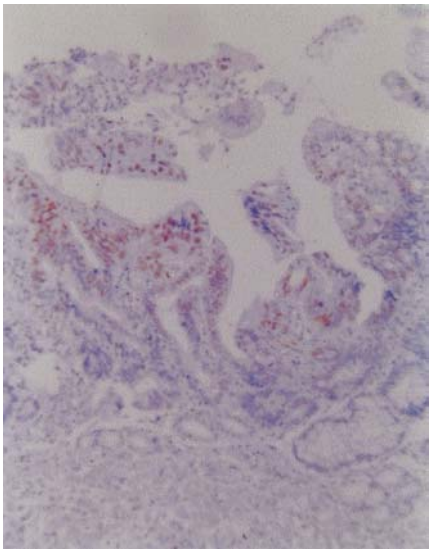


**Fig. 3** Nuclear staining with p21 antibody in one case of high-grade dysplasia

Diffuse nuclear staining in more than 50% of the cells was observed in three superficial adenocarcinoma (Fig. 2) and adjacent HGD and in four HGD. In HGD, p53 protein was expressed on the whole length of the epithelium especially at the mean part and the base of the glands.

In nondysplastic mucosa a mild nuclear staining with the p21 protein antibody was present in less than 20% of the surface epithelial cells. In two cases LGD showed positivity of more than 50% surface epithelial cells. Diffuse nuclear staining, in more than 50% of the cells, for the p21 protein was observed in two superficial adenocarcinomas and surrounding HGD. p21 protein was also expressed in one case of HGD without superficial adenocarcinoma (Fig. 3). p21 expression was associated with p53 nuclear expression in two cases (one superficial adenocarcinoma and one HGD).

No cells were immunoreactive for the Bcl-2 antibody in nondysplastic mucosa, dysplastic epithelium or superficial adenocarcinomas, except focally in one case of LGD where 30% of the cells of the base of the glands had cytoplasmic staining.

## Discussion

BE is a clinicopathologic entity initially described as a metaplastic columnar epithelium in the esophagus, lining more than 3 cm above the esophagogastric junction [30]. The definition of BE is now extended to short segments of specialized intestinal metaplasia in the distal esophagus [32]. BE is considered as the result of an abnormal healing of the esophageal mucosa secondarily to an aggression by the gastroesophageal acidic and/or alkaline reflux [33]. The main risk of BE is its malignant transformation into an adenocarcinoma of the esophagus. Although they have been studied extensively, the mechanisms of Barrett's carcinogenesis remain incompletely elucidated and the role of the gastroesophageal reflux, biliary salts, tobacco and alcohol consumption are still unclear.

Barrett's mucosa can be lined with three types of epithelium [20]. The fundic mucosa usually predominates at the distal part of BE [20]. Junctional mucosa and specialized mucosa are often intermixed at the mean and distal portions of BE [34, 35]. Except in children where it can be absent, specialized incomplete intestinal metaplasia is predominant, and is considered as the preneoplastic type of mucosa [7, 14, 26, 27].

In our study, a large part of BE was lined with specialized mucosa. Dysplasia (both low-grade and high-grade) and superficial adenocarcinomas developed exclusively on this type of mucosa. Metaplastic mucosa, dysplasia and adenocarcinoma were strongly intermixed confirming the metaplasia–dysplasia–carcinoma sequence in the neoplastic progression of BE. HGD and superficial adenocarcinoma were present both on long and short segments of BE, as it has already been reported [29]. Although it has been suggested that superficial adenocarcinoma develops most of the time close to the squamo-columnar junction [18], in our series as in other reports, adenocarcinomas occur in any part of BE including the lower part [14]. Dysplasia is often multifocal and appears on any part of the BE [1, 4, 14, 22]. Superficial adenocarcinoma can also be multifocal [12, 14]. The patchy irregular distribution of dysplastic and malignant areas in BE, without any endoscopically detectable lesion in many cases, strengthens the need for a systematic biopsic sampling of Barrett's mucosa during the endoscopy, even when no macroscopic lesion can be seen. It has been demonstrated that when an extensive sampling is performed it is possible to distinguish between HGD and early adenocarcinoma on biopsies [22].

Although some groups have obtained divergent results with a high proportion of adenocarcinomas in BE surgically resected for HGD [10], the preoperative diagnosis in our cases was always in keeping with the result of the examination of the surgical specimen (data not shown). In the few cases that have been studied extensively with histological examination of the entire Barrett mucosa, the areas of HGD and superficial adenocarcinomas are highly variable. In our series, HGD represents from 2% to 37% of the whole BE and superficial adenocarcinoma from 3% to 30% of the surface of BE. The average surface of HGD in BE is higher in our series (2.3 cm2) than in the series by Cameron et al. (1.3 $cm^2$) [1], but the surface of superficial adenocarcinomas are similar (1.1 $cm^2$ in our study and in the series by Cameron et al.) [1].

It must be emphasized that in most cases only a limited portion of Barrett's mucosa showed an unequivocal invasive superficial adenocarcinoma. This feature is important regarding the debate about the frequency of adenocarcinoma already present when only HGD is diagnosed on biopsies. This justifies again the need of repeated numerous biopsies of Barrett's mucosa when HGD is diagnosed, in case either a surveillance or a non surgical therapeutic attitude is decided, in order not to miss a small superficial adenocarcinoma.

On immunohistochemistry we observed a strong expression of p53 protein in most areas of HGD and superficial adenocarcinoma and no significant expression in nondysplastic metaplastic mucosa and LGD. *p53* gene mutation leads to the synthesis of a p53 mutated protein with an increased half-life that becomes detectable with anti-p53 antibodies while wild-type p53 is normally undetectable [21]. Immunostaining with p53 antibody is considered a good indicator of p53 gene mutation, and this mutation is detected in at least 50% of Barrett's adenocarcinomas [28]. Our study confirms the importance of *p53* gene in the progression of neoplastic lesion in BE [5]. As we only studied cases with HGD and superficial adenocarcinoma we cannot conjecture anything about the precise timing of *p53* gene alteration during Barrett's carcinogenesis. Basing on a number of mostly retrospective studies, some authors consider *p53* gene mutation an early event, occurring in metaplastic nondysplastic mucosa [17] while other studies have suggested it may be a crucial event at the transition between LGD and HGD [23].

p21 protein is an inhibitor of cyclin-dependent kinases which downregulates the G1/S-phase cell cycle transition [3]. In human cells p21 protein is considered a major effector of p53 that upregulates its nuclear expression [3]. The frequency of p21 protein expression has been diversely appreciated in numerous cancers including Barrett's adenocarcinomas [9, 16, 36]. In their immunohistochemical study of 88 Barrett's adenocarcinomas, Moskaluk et al. found a weak nuclear expression of p21 protein in 58 tumors (66%) and a strong expression in nine adenocarcinomas (10%) [16]. Hanas et al. showed an overexpression of p21 protein in a small series of 3 adenocarcinomas [14] and in their series of 32 esophageal adenocarcinomas, Woodward et al. showed an overexpression of p21 protein in 87.5% of the tumors [36]. Concerning the timing of p21 expression during the neoplastic progression of BE, Woodward et al. showed an overexpression of p21 protein in 25% of their cases of Barrett's metaplasia, in 30.8% of LGD and in 90.9% of HGD [36]. Hanas et al. found an overexpression of p21 protein most of the time in the surface epithelium of the metaplastic either dysplastic or nondysplastic mucosa. In only 7% of dysplastic mucosa, Moskaluk et al. observed an exclusive expression of p21 protein at the top of the glands, and of p53 protein at the lower part of the glands [16]. Woodward et al. showed a p21 immunostaining parallel to the staining pattern of p53 [36] and Hanas et al. found no correlation between the overexpression of p21 and p53 proteins [14]. In our study overexpression of p21 protein was relatively uncommon, present in areas of LGD (two cases), HGD (one case) and superficial adenocarcinoma (two cases). Moreover it was associated with the expression of p53 protein in only two cases. It seems that in BE, p21 protein expression is likely to be induced by a p53-independent pathway. The role of p21 in the neoplastic progression in BE and in the prognosis of Barrett's adenocarcinoma still has to be defined.

Bcl-2 protein is a major inhibitor of apoptosis [11]. The inhibition of apoptosis has been shown in many tumors to contribute to the molecular events leading to malignancy. Wild-type p53 protein can induce Bcl-2 inhibiting apoptosis [15]. As we did not observe any significant cytoplasmic expression of Bcl-2 in BE, we were unable to show a correlation between Bcl-2 and p53 expression. Divergent results have been published in the literature concerning the Bcl-2 protein expression in BE. The frequency reported varies from 8.3% to 72% of nondysplastic mucosa [2, 13, 31, 36], from 7.6% to 100% of LGD [2, 13, 25, 31, 36], from 9.5% to 55% of HGD [2, 13, 31, 36] and from 30% to 60% of adenocarcinomas [2, 13, 19, 31]; whereas other studies do not observe any expression of Bcl-2 in nondysplastic mucosa [6, 25], LGD [6], HGD [6, 25] and adenocarcinomas [6, 25, 36]. Although it is difficult to explain such discrepancies it seems unlikely that Bcl-2 protein plays an important role in the neoplastic progression of Barrett's mucosa.

In conclusion, our study shows that HGD and superficial adenocarcinoma can be localized in any part of BE. They often appear as multifocal lesions that can be very small. We confirm the need for an extensive sampling of Barrett's mucosa in the clinical surveillance of patients with BE and the frequency of p53 overexpression during the progression of Barrett's mucosa from dysplasia to adenocarcinoma. It seems that p53 abnormal expression occurs independently from p21 and Bcl-2 expression.

## References


1. Cameron AJ, Herschel A, Carpenter HC (1997) Barrett's esophagus, high grade dysplasia, and early adenocarcinoma: a pathological study. Am J Gastroenterol 92:586–591
2. Clarke MR, Chang KT, Stetler-Stevenson WG, Reynolds JC (1996) Barrett's metaplasia and Barrett's adenocarcinoma of the esophagus: MIB 1, bcl-2, type 4 collagen, type IV collagenase and cathepsin D expression (abstract). Mod Pathol 9:59A
3. El-Deiry WS, Tokino T, Velculescu VE, Levy DB, Parsons R, Trent JM, Lin D, Mercer WE, Kinzler KW, Volgenstein B (1993) WAF 1, a potential mediator of p53 tumor suppression. Cell 75:817–825
4. Elsen GM, Montgomery EA, Azumi N, Hartmann DP, Bhargava P, Lippman M, Benjamin SB (1999) Qualitative mapping of Barrett's metaplasia: a prerequisite for intervention trials. Gastrointest Endosc 50:814–818
5. Fléjou JF, Potet F, Muzeau F, Le Pelletier F, Fekete F, Henin D (1993) Overexpression of p53 protein in Barrett's syndrome with malignant transformation. J Clin Pathol 46:330–333
6. Goldblum JR, Rice TW (1995) Bcl-2 protein expression in the Barrett's metaplasia-dysplasia-carcinoma sequence. Mod Pathol 8:866–869
7. Hameeteman WGN, Tytgat NJ, Houthoff HJ, Van den Tweel JC (1989) Barrett's esophagus: development of dysplasia and adenocarcinoma. Gastroenterology 96:1249–1256
8. Hamelin R, Fléjou JF, Muzeau F, Potet F, Laurent-Puig P, Fekete F, Thomas G (1994) TP53 gene mutations and p53 protein immunoreactivity in malignant and premalignant Barrett's esophagus. Gastroenterology 107:1012–1018
9. Hanas JS, Lemer MR, Lightfoot SA, Raczkowski C, Kastens DJ, Brackett DJ, Postier RG (1999) Expression of the cyclin-dependent kinase inhibitor p21 (WAF1/CP1) and p53 tumor suppressor in dysplastic progression and adenocarcinoma in Barrett esophagus. Cancer 86:756–763
10. Heitmiller RF, Redmond M, Hamilton SR (1996) Barrett's esophagus with high grade dysplasia. An indication for prophylactic esophagectomy. Ann Surg 224:66–71
11. Hockenberry DM (1994) Bcl-2 in cancer, development and apoptosis. J Cell Sci 18:51–55
12. Itatsu T, Miwa H, Murai T, Terai T, Ohkura R, Sorimachi S, Wook Yang S, Ogihara T, Watanabe S, Hirai S, Sato N (1997) Multiple early esophageal cancers arising from Barrett's esophagus, and a review of cases of early adenocarinoma in Barrett's esophagus in Japan. J Gastroenterology 32:389–395
13. Katada N, Hinder RA, Smyrk TC, Hirabayashi N, Perdikis G, Lund RJ, Woodward T, Klingler PJ (1997) Apoptosis is inhibited early in the dysplasia-carcinoma sequence of Barrett esophagus. Arch Surg 132:728–733
14. Mc Ardle JE, Lewin KJ, Randall G, Weinstein W (1992) Distribution of dysplasia and early invasive carcinoma in Barrett's esophagus. Hum Pathol 23:479–482
15. Miyashita T, Krajewski S, Krajewska M (1994) Tumor suppressor gene p53 is a regulator of bcl-2 and bax gene expression in vitro and in vivo. Oncogene 9:1799–1805
16. Moskaluk CA, Heimiller R, Zahurak M, Schwab D, Sidransky D, Hamilton SR (1996) p53 and p21 WAF1/CIP1/SDI1 gene products in Barrett oesophagus and adenocarcinoma of the esophagus and esophagogastric junction. Hum Pathol 27: 1211–1220
17. Neshat K, Sanchez CA, Galipeau PC, Blount PL, Levine DS, Joslyn G, Reid B (1994) p53 mutations in Barrett's adenocarcinoma and high grade dysplasia. Gastroenterology 106: 1589–1595
18. Nishimaki T, Hölsher AH, Schuler M, Bollschweiler E, Becker K, Siewert JR (1991) Histopathologic characteristics of early adenocarcinoma in Barrett's esophagus. Cancer 68:1731–1736
19. Patel DD, Bhatavdekar IM, Chikhlikar PR, Patel YV, Shah NG, Ghosh N, Suthar TP, Balar DB (1997) Clinical significance of p53, nm23, and Bcl-2 in T3–4N1M0 oesophageal carcinoma: an immunohistochemical approach. J Surg Oncol 65:111–116
20. Paull A, Trier JS, Dalton MD, Camp RC, Loeb MP, Goyal RK (1976) The histologic spectrum of Barrett's esophagus. N Engl J Med 295:476–480
21. Reich NC, Oren M, Levine AJ (1983) Two distinct mechanisms regulate the levels of a cellular tumor antigen p53. Moll Cell Biol 3:2143–2150
22. Reid BJ, Weinstein WM, Lewin KJ, Haggitt RC, VanDeventer G, DenBesten L, Rubin CE (1988) Endoscopic biopsy can detect high-grade dysplasia or early adenocarcinoma in Barrett's esophagus without grossly recognizable neoplastic lesions. Gastroenterology 94:81–90
23. Riddell RH, Goldman H, Ransohoff DF, Appelman HD, Fenoglio CM, Haggitt RC (1983) Dysplasia in inflammatory bowel disease: standardized classification with provisional clinical applications. Hum Pathol 14:931–968
24. Rice TW, Goldblum JR, Falk GW, Tubbs RR, Kirby TJ, Casey G (1994) p53 immunoreactivity in Barrett's metaplasia, dysplasia and carcinoma. J Thorac Cardiovasc Surg 108:1132–1137
25. Rioux-Leclercq N, Turlin B, Sutherland F, Heresbach N, Launois B, Campion JP, Ramée MP (1999) Analysis of Ki-67, p53 and Bcl-2 expression in the dysplasia-carcinoma sequence of Barrett's esophagus. Oncol Rep 6:877–882
26. Rosenberg JC, Budev H, Edwards RC, Singal S, Steiger Z, Sundareson AS (1985) Analysis of adenocarcinoma in Barrett's esophagus utilising a staging system. Cancer 55:1353–1360
27. Schmidt HG, Riddell RH, Walter B, Skinner DB, Riemman JF (1985) Dysplasia in Barrett's esophagus. J Cancer Res Clin Oncol 110:145–152
28. Schneider PM, Casson AG, Levin B, Garewal HS, Hoelscher AF, Becker K, Dittler HJ, Cleary KR, Troster M, Siewert JR, Roth JA (1996) Mutations of p53 in Barrett's esophagus and Barrett's cancer: a prospective study of ninety-eight cases. J Thorac Cardiovasc Surg 111:323–333
29. Schnell TJ, Sontag SJ, Chejfec G (1992) Adenocarcinoma arising in tongues or short segments of Barrett's esophagus. Dig Dis Sci 37:137–143
30. Skinner DB, Walther BC, Riddell RH, Schmidt H, Iascone C, De Meester TR (1983) Barrett's esophagus: comparison of benign and malignant cases. Ann Surg 198:554–565
31. Soslow RA, Remotti H, Baergen RN, Altorki NK (1999) Suppression of apoptosis does not foster neoplastic growth in Barrett's esophagus. Mod Pathol 12:239–250
32. Spechler SJ, Zeroogian JM, Antonioli DA, Wang HH, Goyal RK (1994) Prevalence of metaplasia at the gastro-oesophageal junction. Lancet 344:1533–1536
33. Stein HJ, Barlow AP, de Meester TR, Hinder RA (1992) Complications in gastroesophageal reflux disease. Role of the lower esophageal sphincter, duodenogastric reflux and esophageal acid and alkaline exposure. Ann Surg 216:35–43
34. Thompson JJ, Zinsser KR, Enterline HAT (1983) Barrett's metaplasia and adenocarcinoma of the esophagus and gastroesophageal junction. Hum Pathol 14:42–61
35. Weinstein WM, Van Deventer G, Ippolitti A (1984) A histologic evaluation of Barrett's esophagus using a standardized endoscopic biopsy protocol. Gastroenterology 86:1296
36. Woodward TA, Klingler P, V-Genko P, T-Wolfe J (2000) Barrett's esophagus, apoptosis and cell cycle regulation: correlation of p53 with Bax, Bcl-2 and p21 protein expression. Anticancer Res 20:2427–2432

Virchows Arch (2003) 442:25–30
DOI 10.1007/s00428-002-0723-9

ORIGINAL ARTICLE

**Mika Sakaki · Mitsuyoshi Hirokawa
Shingo Wakatsuki · Toshiaki Sano · Kenji Endo
Yoshiyuki Fujii · Tatsuru Ikeda · Satoshi Kawaguchi
Takanori Hirose · Tadashi Hasegawa**

# Acral myxoinflammatory fibroblastic sarcoma: a report of five cases and review of the literature

Received: 15 July 2002 / Accepted: 9 September 2002 / Published online: 5 November 2002
© Springer-Verlag 2002

**Abstract** Five cases of acral myxoinflammatory fibroblastic sarcoma that occurred in the distal extremities within the subcutaneous tissue are described. In one case, recurrence and metastases were recognized rather rapidly, only 3 months after the first excision. There have been no reports of early recurrence or metastases, especially the latter. The predominant type of constituent cells, cellularity of the neoplastic cells and density of inflammatory cells varied microscopically among cases. However, characteristic ganglion-like cells, Reed-Sternberg-like cells, round mononuclear cells and myxoid stroma, sometimes only seen focally, were found in all cases. Positive immunoreaction for vimentin was present in all cases. There was no correlation between positivity of MIB-1 or p53 for the primary tumor and presence of recurrence or metastases. In conclusion, we should be more cautious about the possibility of recurrence or metastases in earlier phases of acral myxoinflammatory fibroblastic sarcoma. Identification of the atypical bizarre fibroblastic component as the manifestation of the malignant nature of this lesion is vital to correct diagnosis, and it is important to attend to the myxoid and hyalinized zones, the inflammatory infiltrate, the presence of ganglion-like cells and acral location as features of acral myxoinflammatory fibroblastic sarcoma.

**Keywords** Ganglion-like cell · Myxoid and hyalinized zones · Inflammatory infiltrate · Acral location

M. Sakaki (✉) · M. Hirokawa · S. Wakatsuki · T. Sano
Department of Pathology,
University of Tokushima School of Medicine,
3-18-15 Kuramoto-cho, Tokushima, 770-8503, Japan
e-mail: smika@basic.med.tokushima-u.ac.jp
Tel.: +81-88-6337064, Fax: +81-88-6339423

K. Endo
Department of Orthopedic Surgery,
University of Tokushima School of Medicine, Tokushima, Japan

Y. Fujii
Department of Pathology,
Tokushima Japanese Red Cross Hospital, Komatsushima, Japan

T. Ikeda
Department of Clinical Pathology, School of Medicine,
Sapporo Medical University, Sapporo, Japan

S. Kawaguchi
Department of Orthopedic Surgery, School of Medicine,
Sapporo Medical University, Sapporo, Japan

T. Hirose
Department of Pathology, Saitama Medical School,
Saitama, Japan

T. Hasegawa
Pathology Division, National Cancer Center Research Institute,
Tokyo, Japan

## Introduction

Meis-Kindblom et al. [2] in 1998 described the acral myxoinflammatory fibroblastic sarcoma, and Montgomery et al. [4] also named the tumor inflammatory myxohyaline tumor of distal extremities with virocyte or Reed-Sternberg-like cells at that time. It is a poorly circumscribed and typically multinodular tumor ranging from 1 cm to 8 cm in size. Clinically it develops in patients of all ages (range 4–91 years; median late 40s) and presents as a painless mass of the distal extremities, most frequently in the fingers and usually within the subcutaneous tissues [1, 2, 3, 4, 5]. Histologic features of this lesion are the presence of bizarre virocyte or Reed-Sternberg-like cells with enlarged vesicular nuclei and an often huge, inclusion-like nucleoli which are scattered among spindle to epithelioid neoplastic cells with a moderate degree of nuclear atypia in numerous inflammatory cells and a focal or prominent myxoid matrix [5]. Other constituent cells sometimes seen are multivacuolated lipoblast-like cells in a myxoid background, phagocytic cells that appear to engulf inflammatory cells and rounded mononuclear cells without atypia [5]. Acral myxoinflammatory fibroblastic sarcoma has been reported to be a unique low-grade tumor with a high rate of local recurrence and a low rate of metastases consisting of modified fibroblasts [2]. However, because this tumor has only recently been recognized, a variety of neoplastic or pseudotumorous lesions may be included in its differential diagnosis.

**Table 1** Clinical findings of five cases of acral myxoinflammatory fibroblastic sarcoma. *AMFS* acral myxoinflammatory fibroblastic sarcoma, *IMT* inflammatory myoblastic tumor, *NOS* not otherwise specified

| Case | Age (years)/sex | Site | Symptom | Symptom duration | Size (cm) | Treatment | Recurrence | Metastasis/site | Former diagnosis |
|---|---|---|---|---|---|---|---|---|---|
| 1 | 32/Female | Left dorsal foot | Swelling | 3 months | 2.5×2.5 | Local excision | – | – (1.5 years) | AMFS |
| 2 | 75/Male | Right palm | Swelling, hypesthesis | 5 months | 7×3 | Local excision | – | – (8 months) | AMFS |
| 3 | 37/Male | Right middle finger | Swelling | 1 month | 3×3 | Local excision | +, after 3 months | +, after 3 months/lymph nodes(1 year) | IMT for the primary Sarcoma, NOS for the recurrence |
| 4 | 15/Male | Right dorsal foot | Swelling | 5 months | 3×3 | Local excision | +, after 2 years | – (2.5 years) | Myxoid liposarcoma or fibrohistiocytic tumor for the primary Fibrohistiocytic tumor for the recurrence |
| 5 | 31/Male | Left hand | Swelling | 8 months | 3×3 | Local excision | – | – (4.8 years) | Low-grade spindle cell sarcoma |

We recently encountered five cases of acral myxoinflammatory fibroblastic sarcoma, of which one case presented with metastasis to the regional lymph nodes 3 months after the first excision. There have been approximately 100 cases of acral myxoinflammatory fibroblastic sarcoma reported so far [1, 2, 3, 4], most of which were identified in two articles [2, 4], but metastasis of acral myxoinflammatory fibroblastic sarcoma was rare and did not, to our knowledge, happen in such a short time. The aim of this report is to compare our cases with previous cases and to examine the histologic and immunohistochemical features associated with the metastatic potential of acral myxoinflammatory fibroblastic sarcoma.

## Materials and methods

### Case selection

Five cases described here were retrieved from the files of the Department of Pathology, University of Tokushima School of Medicine, Tokushima, Department of Pathology, Tokushima Japanese Red Cross Hospital, Komatsushima, Pathology Division, National Cancer Center Research Institute, Tokyo, and from the consultation files of two of the authors (Hirose and Hasegawa). Clinical details and follow-up information were obtained from hospital records (Table 1). Hematoxylin-eosin-stained slides were available for the primary tumors in all cases and for the recurrent tumors in cases 3 and 4.

### Immunohistochemical staining

Sections from paraffin blocks of the primary tumor and recurrence were used. Only a few sections from the recurrence in case 4 and the primary in case 5 were available. All the sections were examined by the labeled streptavidin-biotin method with appropriate use of positive and negative controls throughout. The primary antibodies used in this study and their details are listed in Table 2. Sections stained with antibodies against vimentin, desmin, calponin, CD68, Ki-67 and p53 were subjected to heat-induced epitope unmasking in a 10-mmol/l citrate buffer, pH 6.0, in an autoclave at 121ºC for 20 min. Proteolytic predigestion or trypsin treatment was also performed as required.

## Results

### Clinical findings

Clinical histories of the five patients are summarized in Table 1. The patients were four men and a woman aged from 15 years to 75 years old (mean 38 years). The tumors were located in the distal extremities in all cases and presented as painless swellings. One case (case 2) presented with hypoethesias of the affected site. The symptom durations were rather short, all within 8 months. The lesions were recognized as ill-defined masses with sizes from 2.5 cm to 7 cm (mean 3.7 cm) in the greatest diameter. Local excision was the primary treatment in all cases. Recurrence and metastases to the regional lymph nodes occurred 3 months after the treatment in case 3, and the recurrent and metastatic lesions were re-excised. Recurrence occurred 2 years after the treatment in case 4, and the recurrent lesion was re-excised. Magnetic resonance images of the foot in case 4 showed involvement of the recurrent tumor with the tendon sheath of the dorsal extensor muscle but no invasion of the bone (Fig. 1). The former diagnoses for the primary and recurrence were only inflammatory myoblastic tumor and sarcoma in case 3, myxoid liposarcoma or fibrohistiocytic tumor and fibrohistiocytic tumor in case 4 and low-grade spindle cell sarcoma in case 5. In the latest follow-up from 8 months to 4.8 years (mean 2 years, 1 month),

**Table 2** Immunohistochemical findings of five cases of acral myxoinflammatory fibroblastic sarcoma. *SMA* α-smooth muscle actin, *LCA* leukocyte common antigen, *ND* not determined. – negative, + <10% positivity, ++ 10–50% positivity, +++ >50% positivity

| Antigen (antibody) | Case 1 | Case 2 | Case 3 | | | Case 4 Recurrence | Case 5 |
|---|---|---|---|---|---|---|---|
| | | | Primary | Metastases | Recurrence | | |
| AE1/3 (AE1 and AE3), Dako, Glostrup, Denmark, 1:50 | + | – | – | | | – | – |
| Vimentin (V9), Dako, 1:50 | +++ | +++ | +++ | | | +++ | ++ |
| Desmin (D33), Dako, 1:50 | – | – | – | | | – | – |
| SMA (1A4), Sigma, Saint Louis, Mich., 1:400 | + | – | – | | | ++ | – |
| Calponin (CALP), Dako, 1:50 | + | – | – | | | – | – |
| CD68 (PG-M1), Dako, 1:100 | + | + | - | | | ND | ND |
| LCA (2B11+PD7/26), Dako, 1:200 | – | – | – | | | – | ND |
| CD34 (My10), Becton Dickinson, San Jose, Calif., 1:100 | + | – | – | | | + | + |
| S-100 protein, Dako, 1:400 | – | – | – | | | – | – |
| α1-antitripsin, Dako, 1:100 | ++ | +++ | +++ | | | ND | ND |
| Ki-67 (MIB-1), Dako, 1:100 | 15.4% | 6.5% | 12.1% | 5.1% | 11.2% | 7.2% | 5.0% |
| p53 (DO7), Dako, 1:100 | 5.3% | 0.5% | 1.1% | – | – | 20% | – |

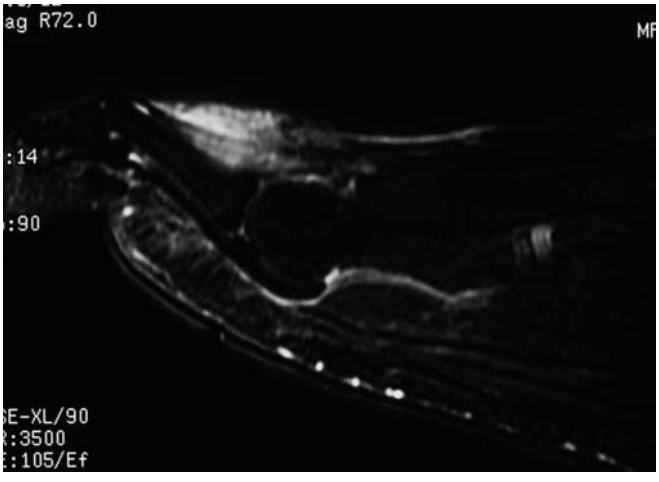



**Fig. 1** Sagittal T2-weighted magnetic resonance image of the foot shows involvement of the recurrent acral myxoinflammatory fibroblastic sarcoma in the tendon sheath of the dorsal extensor muscle but no invasion in the underlying phalanx (case 4)

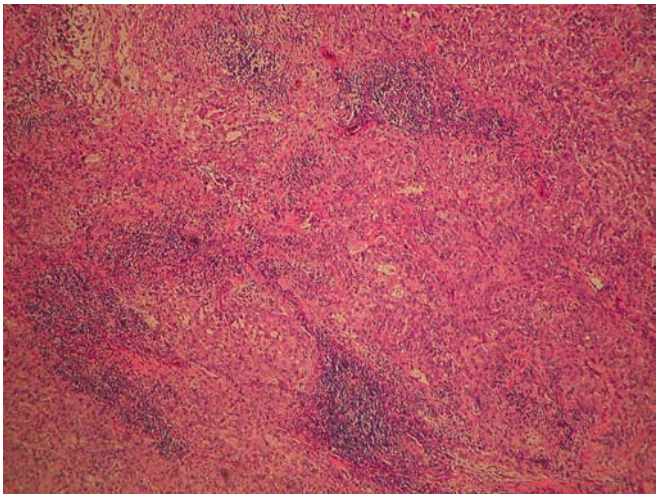


**Fig. 2** A vaguely multinodular growth pattern of an acral myxoinflammatory fibroblastic sarcoma (case 1) (×20)

there have been no further recurrences or metastases in these patients.

## Histologic findings

The architecture was vaguely multinodular in cases 1, 4 and 5 (Fig. 2) and rather diffuse in cases 2 and 3 (Fig. 3). This vague multinodularity was formed by the alternation of cellular areas with foci of hyalinized collagen fibers and hypocellular areas with a myxoid background. Various neoplastic cells including spindle and epithelioid cells with mild to moderate nuclear atypia (Fig. 4), ganglion-like cells (Fig. 5), Reed-Sternberg-like cells (Fig. 6), multivacuolated cells simulating lipoblasts (Fig. 7) and bland-looking rounded mononuclear cells were identified in all cases, except that there were no multivacuolated cells in cases 2, 3 and 5. Phagocytic cells, which seemed to engulf the inflammatory cells, were occasionally seen in cases 1 and 3. The cellularity was high in cases 1, 3 and 5. In case 1, the epithelioid cells were arranged in sheets (Fig. 8). The cellularity was lowest in case 2, and bland rounded mononuclear cells were the predominant type of the neoplastic cells. Spindle cells were most prominent in cases 4 and 5. Transitional cells from spindle or epithelioid cells to ganglion-like cells

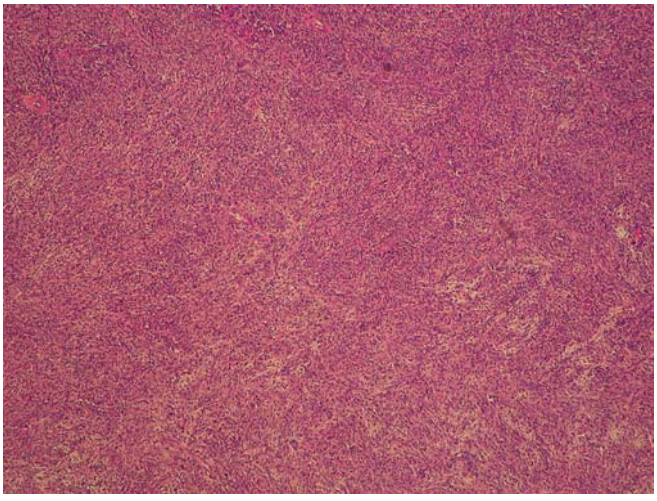


**Fig. 3** A rather diffuse growth pattern of an acral myxoinflammatory fibroblastic sarcoma (case 3) (×20)

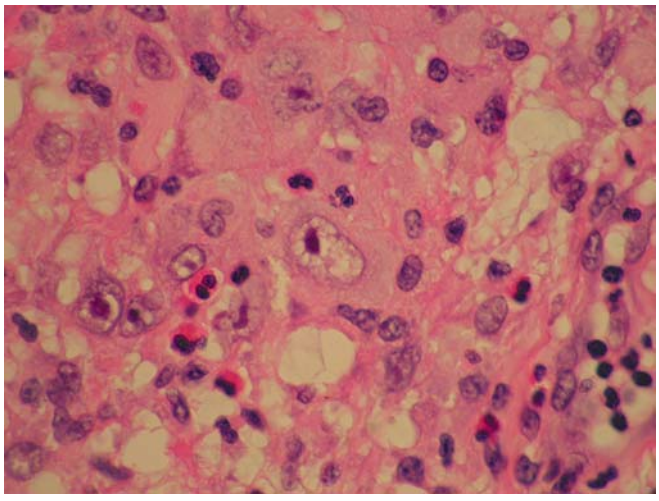


**Fig. 5** Large epithelioid cells with vesicular nuclei and enlarged eosinophilic nucleoli resembling the ganglion cells of an acral myxoinflammatory fibroblastic sarcoma (case 1) (×200)

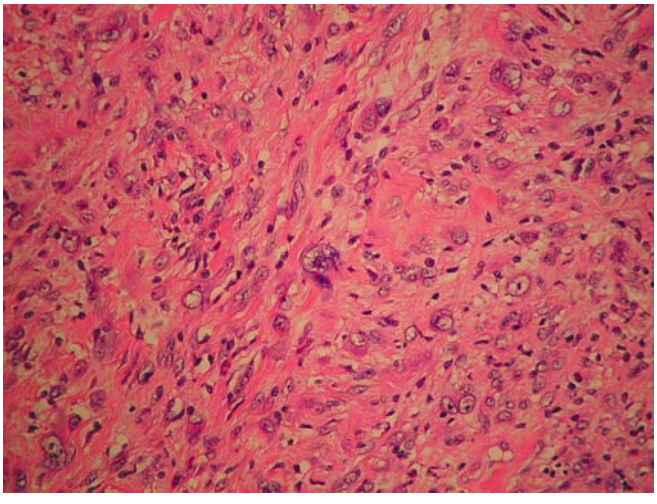


**Fig. 4** Spindle and epithelioid cells with mild to moderate nuclear atypia in a myxohyaline background are seen in an acral myxoinflammatory fibroblastic sarcoma (case 5) (×80)

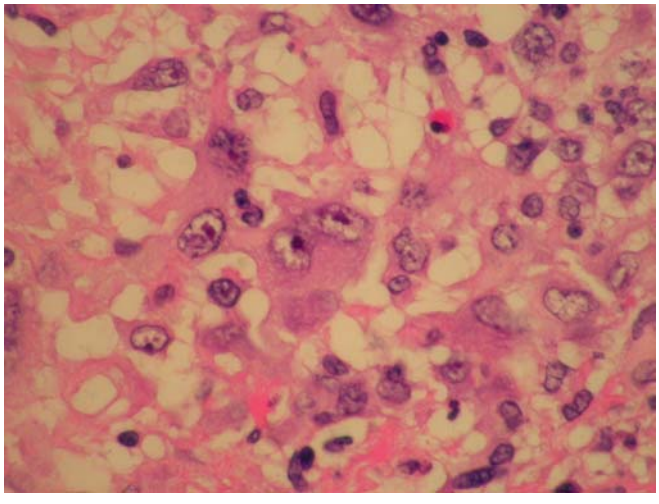


**Fig. 6** Binucleated cells mimicking Reed-Sternberg cells of an acral myxoinflammatory fibroblastic sarcoma (case 1) (×200)

were recognized in all cases. In five cases, mitotic figures were seen in 6 of 50 high-power fields (HPF), <1 of 50 HPF, 6 of 50 HPF, 4 of 50 HPF and <1 of 50 HPF.

Necrosis, only seen in case 2, comprised about 40% of the lesion. The density and type of inflammatory cells varied among the cases. In case 3, the inflammatory cells were diffusely dense and most of them were neutrophils, while scattered lymphocytes were the predominant type of inflammatory cell in cases 2, 4 and 5. Clusters of lymphocytes and their follicles were present, and eosinophils were as numerous as lymphocytes in case 1. Multinucleated giant cells including Touton-type giant cells were focally seen in case 2.

The recurrent and metastatic lymph-node lesions in case 3 showed a histologic appearance almost identical to the primary tumor. Mitosis was less than in the primary: 1–2 of 50 HPF. In the lymph node, metastases were multifocal and wedge-shaped in the cortex (Fig. 9). The non-neoplastic area of the lymph node showed follicular hyperplasia. Mitosis in the metastatic lymph nodes was difficult to evaluate because of intermingling lymphocytes. In the recurrent tumor of case 4, cellularity of the neoplastic cells became higher, and hypocellular areas were inconspicuous. Inflammatory cells also become denser, and the number of mitoses was slightly higher than that of the primary: 7 of 50 HPF.

## Immunohistochemical findings

Immunohistochemical findings are summarized in Table 2. Three types of tumor cells, atypical epithelioid cells in-

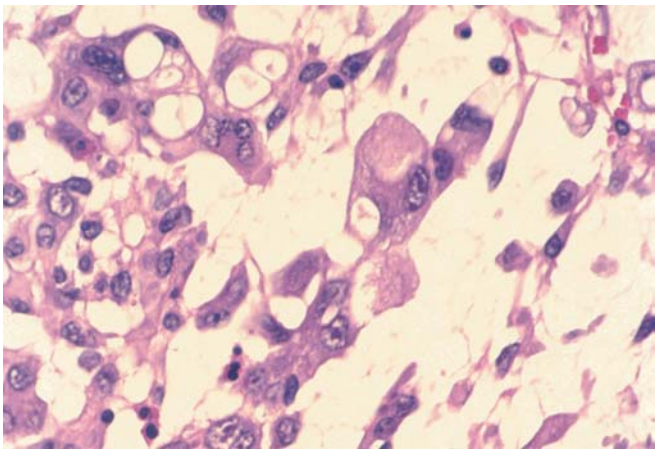


**Fig. 7** Lipoblast-like cells with intracytoplasmic vacuoles in a myxoid stroma of an acral myxoinflammatory fibroblastic sarcoma (case 1) (×200)

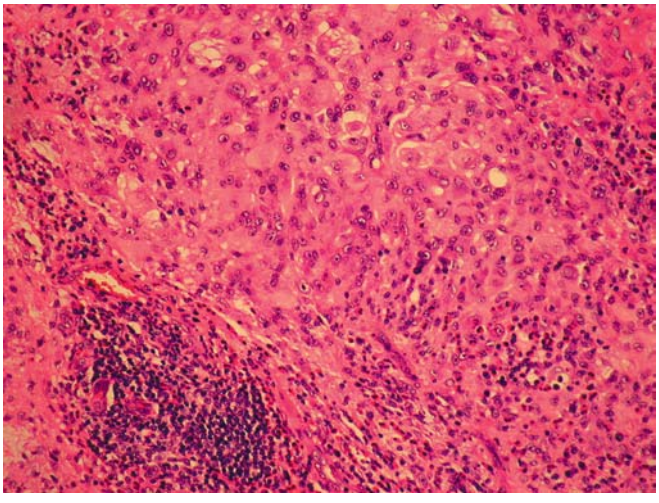


**Fig. 8** Epithelioid cells arranged in sheets with a lymphoid stroma of an acral myxoinflammatory fibroblastic sarcoma (case 1) (×50)

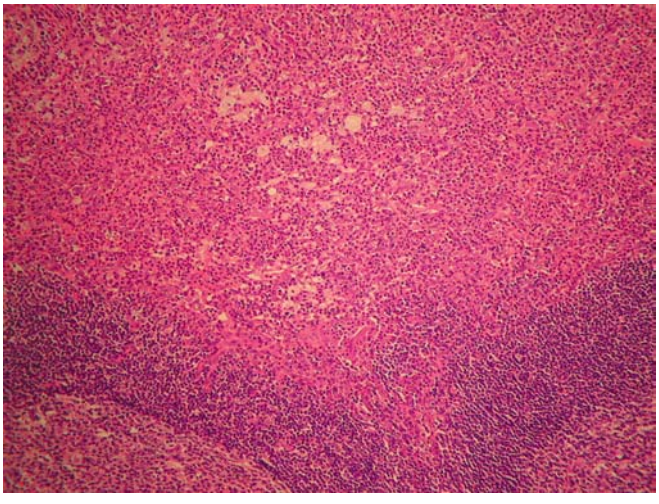


**Fig. 9** Wedge-shaped lymph-node metastasis in the cortex with two germinal centers in the right and left lower corners of an acral myxoinflammatory fibroblastic sarcoma (case 3) (×40)

cluding ganglion-like cells, Reed-Sternberg-like cells and multivacuolated cells, spindle cells and rounded mononuclear cells showed similar immunohistochemical staining in each case. They stained for vimentin in all cases and α1-antitripsin in three cases examined, with variable immunoreactivity for AE1/3, α-smooth muscle actin (SMA), calponin, CD68 and CD34. Sporadic positivity for SMA and calponin was present in case 1. Desmin, leukocyte common antigen and S-100 protein were negative. Ki-67 (MIB-1)-positivity in 4 cases of primary acral myxoinflammatory fibroblastic sarcoma (cases 1–3, 5) was 15.4%, 6.5%, 12.1% and 5.0%, respectively, and 7.2% for the recurrence in case 4. MIB-1-positivity of the recurrent and metastatic lymph-node lesions in case 3 was 5.1% and 11.2%, respectively. Similarly, p53-positivity in four cases of primary acral myxoinflammatory fibroblastic sarcoma (cases 1–3, 5) was 5.3%, 0.5%, 1.1% and 0%, respectively. The recurrent and metastatic lymph-node lesions of case 3 were negative for p53 while p53-positivity was identified as 20% in the recurrent lesion of case 4.

## Discussion

The clinical findings of five cases of acral myxoinflammatory fibroblastic sarcoma were similar to those in the literature; the tumors occurred as painless ill-defined masses in the subcutaneous tissue in the distal extremities of middle-aged individuals [1, 2, 3, 4, 5]. Although the tumors have been reported to be slow-growing masses [1, 2, 3, 4], the symptom duration of four cases was within the rather short period of 8 months. Furthermore, recurrence occurred in cases 3 and 4, 3 months and 2 years after the initial excisions, respectively. Follow-up information from a previous study showed that recurrences developed in 30 of 67 cases [1, 2, 3, 4], while their interval to the first recurrence ranged from 4 months to 11 years (median approximately 1 year). Compared with previous cases, recurrences occurred rather rapidly in case 3 where metastasis to the regional lymph nodes was recognized at the same time. Metastases have been previously reported to occur in only 2 of the 67 cases, in which metastases to the inguinal lymph node in 1 case and the lung in another case developed 1.5 years and 5 years after the primary surgery [2]. The interval between the initial excision and metastasis in case 3 was shorter than that in the previous cases. For this reason, we should be cautious about the possibility of early metastases, although the rate in acral myxoinflammatory fibroblastic sarcoma has been fairly low.

Histologically, most of the constituent cells in all the cases of acral myxoinflammatory fibroblastic sarcoma in this study had features as described by Weiss et al. [5]. However, the histologic findings of the present series varied from case to case. In cases 1, 3 and 5 cellularity of the neoplastic cells was higher than that in cases 2 and 4. Epithelioid cells were more prominent in cases 1 and 3. The most prominent type of inflammatory cell also

varied among cases. Necrosis, which was reported previously as an occasional finding, was seen only in case 2. While mitotic activity decreased from 6 of 50 HPF in the primary to 1–2 of 50 HPF in the recurrence of case 3, it increased from 4 of 50 HPF to 7 of 50 HPF in the recurrence of case 4 together with increased cellularity.

Immunohistochemical findings of the five cases were almost the same as those of the previous cases with the exception of positivity for α1-antitrypsin in three cases. The neoplastic cells diffusely stained for vimentin, with variable immunoreactivity for cytokeratin, smooth muscle markers, CD68 and CD34. Meis-Kindblom et al. [2] found that MIB-1-positivity was less than 1% in 20 of the 25 primary tumors and in three cases exceeded 10%. In the two recurrences, MIB-1-positivity was higher than in the primary. P53-reactivity in 18 of 25 primary tumors and in the two recurrences was negative, and more than 20% of the neoplastic cells were p53-positive in seven primary tumors [2]. In the present cases, all tumors including the recurrence and metastases showed more than 5% of MIB-1-positivity. However, the recurrence and metastases of case 3 did not show higher MIB-1-positivity than the primary. P53-positivity in the primary tumors was low, and p53 was negative in the recurrence and metastases in case 3. In another recurrent lesion (case 4), 20% of tumor cells were p53-positive. Thus, there seems to be no specific histologic and immunohistochemical finding associated with recurrence or metastasis within a short follow-up period.

The differential diagnosis is broad and varied depending on whether the inflammatory, myxoid, or bizarre atypical component predominates in the lesion as already described in detail [1, 2, 3, 4]. Most of the differential diagnoses mentioned so far were as follows: an infectious process, an inflammatory lesion such as tenosynovitis and proliferative or nodular fascitis, a neoplastic one such as giant cell tumor, inflammatory myofibroblastic tumor especially when inflammatory cells of lymphocytes and plasma cells predominated, liposarcoma, epithelioid sarcoma and myxoid malignant fibrous histiocytoma (MFH). For our cases as a whole, these diagnoses were all considered possible but could be distinguished. An inflammatory lesion, giant cell tumor, inflammatory myofibroblastic tumor, and inflammatory fibrosarcoma can be distinguished by recognizing the atypical spindle to epithelioid cells of acral myxoinflammatory fibroblastic sarcoma [5]. However, when acral myxoinflammatory fibroblastic sarcoma, as seen in case 1, shows an immunohistochemical feature of myofibroblast we should be more cautious about distinguishing the latter two neoplasms and leiomyosarcoma. Inflammatory myofibroblastic tumor and inflammatory fibrosarcoma are located most commonly in the abdomen or thorax [5] and leiomyosarcoma in the retroperitoneum or abdomen in contrast to the distal location of acral myxoinflammatory fibroblastic sarcoma. Recognizing that cytoplasmic vacuoles contain extracellular mucin rather than intracellular fat enables distinction from liposarcoma [2]. Myxoid MFH has been reported to be a difficult and important differential diagnosis [1, 2, 3, 4, 5]. Focal areas of high-grade pleomorphic, storiform MFH was found in myxoid MFH but not in acral myxoinflammatory fibroblastic sarcoma [5]. Like inflammatory myofibroblastic tumor and inflammatory fibrosarcoma, the proximal location favors myxoid MFH over acral myxoinflammatory fibroblastic sarcoma. When the lesion shows focal immunoreactivity for keratin as seen in case 1 or has necrosis as seen in case 2, epithelioid sarcoma should be distinguished. In case 1 desmoplastic response usually seen in epithelioid sarcoma was lacking, and immunoreactivity for keratin was just a focal weak reaction. In case 2, cellularity was too sparse for epithelioid sarcoma. In addition to the histologic distinction mentioned above, cytogenetic analysis can be of help. Lambert et al. [1] found a complex karyotype with reciprocal translocation t(1;10)(p22;q24) as well as the loss of chromosomes 3 and 13 in a case of acral myxoinflammatory fibroblastic sarcoma. The presence of these clonal chromosomal changes supports the neoplastic nature of the tumor and underscores that it represents a separate entity [1].

In conclusion, we should be more cautious about the possibility of the metastatic potential of this tumor. In addition to the findings mentioned above, familiarity with acral myxoinflammatory fibroblastic sarcoma was the most important factor in correct diagnosis. Distinction from other diseases is achieved by identifying the atypical bizarre fibroblastic component as the manifestation of the malignant nature of the lesion [2] and keeping in mind the myxoid and hyalinized zones, the inflammatory infiltrate, the presence of ganglion-like cells and the acral location as features of acral myxoinflammatory fibroblastic sarcoma.

## References


1. Lambert I, Debiec-Rychter M, Guelinckx P, Hagemeijer A, Sciot R (2001) Acral myxoinflammatory fibroblastic sarcoma with unique clonal chromosomal changes. Virchows Arch 438:509–512
2. Meis-Kindblom JM, Kindblom LG (1998) Acral myxoinflammatory fibroblastic sarcoma: a low-grade tumor of the hands and feet. Am J Surg Pathol 22:911–924
3. Michal M (1998) Inflammatory myxoid tumor of the soft parts with bizarre giant cells. Pathol Res Pract 194:529–533
4. Montgomery EA, Devaney KO, Giordano TJ, Weiss SW (1998) Inflammatory myxohyaline tumor of distal extremities with virocyte or Reed-Sternberg-like cells: a distinctive lesion with features simulating inflammatory conditions, Hodgkin's disease, and various sarcomas. Mod Pathol 11:384–391
5. Weiss SW, Goldblum JR (eds) (2001) Enzinger and Weiss's soft tissue tumors, 4th edn. Mosby, St. Louis, pp 1552–1571

Virchows Arch (2003) 442:31–38
DOI 10.1007/s00428-002-0728-4

ORIGINAL ARTICLE

**Sophie Clément · Augusto Orlandi · Leonardo Bocchi
Gianpaolo Pizzolato · Maria Pia Foschini
Vincenzo Eusebi · Giulio Gabbiani**

# Actin isoform pattern expression: a tool for the diagnosis and biological characterization of human rhabdomyosarcoma

Received: 30 April 2002 / Accepted: 19 September 2002 / Published online: 19 November 2002
© Springer-Verlag 2002

**Abstract** The diagnosis and characterization of rhabdomyosarcoma requires the use of combined histological and immunohistochemical criteria due to the variety of its histological patterns. The identification of actin isoform expression is accepted as a useful adjunct to the diagnosis and classification of soft tissue tumors. Using a new antibody specific for α-cardiac actin, obtained according to a recently described strategy for the production of polyclonal antibodies against actin isoforms [9], we have analyzed a series of 17 rhabdomyosarcomas, including all histological subtypes. In addition, we have evaluated the presence in these tumors of α-skeletal and α-smooth muscle actins. All specimens examined revealed a positive immunostaining for α-cardiac actin. Tumoral cells of eight cases also expressed α-smooth muscle actin and only three cases (all embryonal subtypes) were positive for α-skeletal actin. Our results indicate that immunohistochemical screening for α-cardiac actin expression is a useful tool for the diagnosis of rhabdomyosarcoma. They also suggest that the expression of α-skeletal actin is valuable in determining the subtype and possibly the state of differentiation of these tumors.

**Keywords** Cytoskeleton · Immunohistochemistry · Muscle development · Actin antibodies

S. Clément · L. Bocchi · G. Pizzolato · G. Gabbiani (✉)
Department of Pathology, University of Geneva,
1 rue Michel-Servet, 1211 Geneva 4, Switzerland
e-mail: giulio.gabbiani@medecine.unige.ch
Tel.: +41-22-7025742, Fax: +41-22-7025746

A. Orlandi
Institute of Anatomic Pathology,
Tor Vergata University of Rome, Italy

M.P. Foschini · V. Eusebi
Department of Oncology, Section of Anatomic Pathology,
University of Bologna, Bellaria Hospital, Bologna, Italy

## Introduction

In mammalians, actin isoforms are expressed in a tissue-specific pattern that is strictly conserved, although no specific functions have up to now been clearly defined for each of them [23]. Actin isoform sequence differences concern few amino acids, essentially located at the N-terminal portion of the molecule; this renders problematic the production of specific monoclonal and/or polyclonal antibodies. Despite these difficulties, few actin isoform-specific antibodies have been produced by different laboratories including ours [9, 17, 19, 35] and have proven useful for the study of biological features of different tissues [10, 21]; they have also been successfully utilized in the diagnosis of soft tissue tumors [32, 36]. We have recently developed a new strategy to purify polyclonal specific antibodies against actin isoforms [9]. Here, we describe the production of an α-cardiac actin-specific antibody (anti α-CA1) and its application to the diagnosis and characterization of rhabdomyosarcoma (RMS).

RMS, the most common soft-tissue malignancy of childhood and adolescence, is a highly heterogeneous group of tumors with respect to their clinical, morphological and differentiation features. The most accepted histological classification comprises botryoid, embryonal, alveolar and pleomorphic subtypes [14]; in addition a spindle cell variant has been described [6, 31]. Differences among subtypes are not only histological but also include clinical behavior and follow-up (for review see [14, 29]). The common feature of RMS is the propensity for the formation of neoplastic skeletal fibers; thus, the diagnosis is usually based, in addition to conventional histology, on immunohistochemical and ultrastructural investigations that identify this phenotype. Myoglobin, β-enolase and, more recently, myogenin and MyoD1 – two transcriptional regulatory proteins expressed early in skeletal muscle differentiation [38] – have been reported as myogenic markers [7, 13]. A strong immunostaining for myogenin has been associated with the alveolar subtype of RMS [13]; however, a negative staining in a pro-

portion of cases has been noted [7]. Although all RMSs revealed immunoreactive for MyoD1, the nuclear specificity often associated with a nonspecific background staining and reactivity of nonmyoid tissues as well as in other tumors, i.e., Wilms' tumor with myogenous differentiation, ectomesenchymomas [24] and small cell carcinoma with skeletal muscle differentiation [16], hinder its utility in paraffin-embedded routine diagnostic screening [7]. Antibodies against cytoskeletal proteins, actin and desmin in particular, have proven useful for the establishment of RMS diagnosis [2, 8, 11, 12, 15, 22, 28, 36]. We have previously reported that RMSs express transcripts for α-cardiac and α-smooth muscle actin but not α-skeletal actin mRNA [33]; however, results obtained from molecular biology studies are neither easily quantifiable nor routinely applicable during diagnostic procedures. Using anti α-CA1, in combination with two other antibodies specific respectively for α-smooth muscle actin [35] and α-skeletal actin [9] previously developed in our laboratory, we have investigated the differential expression of actin isoforms in 17 primary RMSs. Our results demonstrate that this approach facilitates the diagnosis of RMS and helps in the characterization of the principal subtypes of this tumor.

## Materials and methods

### Patient population

A total of 17 RMSs were obtained from the files of either the Division of Clinical Pathology, Geneva, Switzerland; the Institute of Anatomic Pathology, Tor Vergata University of Rome, Italy, or the Department of Oncology, University of Bologna, Italy. The main characteristics of patients are reported in Table 1. All tissue samples were fixed in 10% neutral buffered formalin and embedded in paraffin. For all tumors, the diagnosis of RMSs had been made on the basis of clinical and histological data using accepted classification criteria [14] and confirmed in some cases by immunohistochemical staining for established myogenic markers. Control tissues included: uterine leiomyoma (10); neuroblastoma (1); leiomyosarcoma (8), of which seven were uterine and one was from the skin; benign fibrous histiocytoma including dermato-fibroma (8) and lymphoma (1).

### Anti α-CA1 production and immunopurification

Anti α-CA1 was prepared following an experimental strategy adapted from the one previously used in order to prepare an antibody against α-skeletal actin (anti α-SKA1) [9]. Briefly, the $NH_2$-terminal decapeptide of α-cardiac actin (Ac-DEEDTTALVC-COOH) was coupled to maleimide activated keyhole limpet hemocyanin (KLH, Pierce, Rockford, Ill.) through its cysteine residue, according to the instructions of the manufacturer. The coupled peptide was used for antiserum production in a rabbit (performed by Biodesign International, Kennebunk, Me.). The antiserum was first affinity purified using Sulfolink beads (Pierce) coupled with the α-cardiac actin decapeptide. Elution fraction was dialyzed overnight against phosphate-buffered saline solution and then successively loaded on (1) a Sulfolink column coupled with the $NH_2$-terminal decapeptide of α-skeletal actin, (2) a column coupled with the $NH_2$-terminal decapeptide of β-cytoplasmic actin and (3) finally a column coupled with the $NH_2$-terminal decapeptide of γ-smooth muscle actin to remove the population of antibodies cross-reacting with these three isoforms. The antibodies present in the final flow-through were finally concentrated on the column coupled with the α-cardiac decapeptide, and the resulting elution fraction represented anti-αCA1.

### Electrophoretic and immunoblot analysis

Antibody specificity was determined by immunoblotting of the following whole-tissue homogenates: rat striated muscle, rat myocardium, human blood platelets, rat aorta and chicken gizzard

**Table 1** Clinicopathologic, morphological and immunohistochemical information of patients with rhabdomyosarcoma (RMS). *LTF* lost to follow-up, *DOD* died of disease, *NED* no evidence of disease, *AWD* alive with disease

| Case | Age (y) /sex | Localization | Morphological diagnosis | Status | α-Actin isoform expression in tumor cells | | | Desmin |
|---|---|---|---|---|---|---|---|---|
| | | | | | α-CARD | α-SK | α-SM | |
| 1 | 2.5/Male | Prostate | Embryonal | DOD (26 months) | +++ | +++ | – | +++ |
| 2 | 5/Female | Pelvic cavity | Embryonal | DOD (7 months) | +++ | + | – | +++ |
| 3 | 24/Male | Left jaw | Embryonal | DOD (3 months) | +++ | – | – | ++ |
| 4 | 15/Female | Anterior clinoid | Embryonal | LTF | ++ | – | ++ | + |
| 5 | 17/Female | Orbit | Embryonal | LTF | +++ | – | ++ | +++ |
| 6 | 2/Male | Right lung | Embryonal | DOD (10 months) | +++ | +++ | – | +++ |
| 7 | 22/Male | Orbit | Embryonal | NED (3 years) | +++ | – | – | +++ |
| 8 | 9/Male | Urethra/bladder | Embryonal, botryoid | LTF | +++ | – | – | + |
| 9 | 15/Male | Nasal cavity | Predominantly alveolar | AWD (2 years) | +++ | – | ++ | +++ |
| 10 | 6/Male | Para-testicular | Alveolar | AWD (3 years) | +++ | – | + | +++ |
| 11 | 23/Female | Pterygo-palatine pit | Alveolar | AWD (1 year) | +++ | – | – | + |
| 12 | 16/Male | Head-neck region | Alveolar | DOD (7 days) | +++ | – | – | +++ |
| 13 | 5/Male | Tongue | Mixed embryonal, alveolar | NED (6 years) | +++ | – | ++ | ++ |
| 14 | 49/Male | Striated muscle/ upper part of the back | Pleomorphic | LTF | +++ | – | + | +++ |
| 15 | 43/Male | Striated muscle/ lumbar region | Spindle cells | AWD (6 years) | + | – | – | + |
| 16 | 21/Female | Hand | Alveolar | DOD (2 years) | ++ | – | ++ | – |
| 17 | 25/Female | Shoulder | Alveolar | AWD (3 years) | ++ | – | ++ | ++ |

(40 µg per lane was loaded for Coomassie blue staining and 2 µg per lane for immunoblotting). Sodium dodecyl sulfate–polyacrylamide gel electrophoresis (SDS-PAGE) was carried out in 10% polyacrylamide gels [25] and the proteins were electroblotted to nitrocellulose according to Towbin et al. [39]. Nitrocellulose membranes were incubated with anti α-CA1 diluted in Tris-buffered saline solution containing 3% bovine serum albumin (BSA) and 0.1% Triton X-100 for 2 h at room temperature. After three washes with Tris-buffered saline, a second incubation was performed with peroxidase-conjugated affinity-purified goat anti-rabbit IgG (Jackson Immunoresearch Laboratories, West Grove, Pa.) at a dilution of 1:10,000 in Tris-buffered saline containing 0.1% BSA and 0.1% Triton X-100. Peroxidase activity was developed using the ECL Western-blotting system (Amersham, Rahn AG, Zürich, Switzerland), according to the instructions of the manufacturer.

### Light microscopy and immunohistochemistry

Four-micron sections of formalin-fixed and paraffin-embedded fragments of RMSs were either stained with hematoxylin-eosin or used for immunohistochemistry with anti α-SKA1 (1:40 dilution in Tris-buffered saline [9]), anti α-smooth muscle actin (α-sm1 [35]; 1:200 dilution in Tris-buffered saline), anti α-CA1 (1:20 dilution in Tris-buffered saline) and monoclonal antibody against human desmin (Clone 33, Dako, Glostrup, Denmark; 1:20 dilution in Tris-buffered saline). Immunoperoxidase staining was performed essentially as previously described [9]. After staining, sections were observed using a Zeiss Axiophot photomicroscope. Images were acquired with a high sensibility Axiocam color camera (Carl Zeiss, Oberkochen, Germany), stored on optical disks (Sony Corp, Tokyo, Japan) and printed with a digital Fujifilm Pictography 4000 printer (Fujifilm, Tokyo, Japan).

### Indirect immunofluorescence and confocal laser scanning microscopy

Rat hearts were embedded in OCT 4583 (Miles Scientific, Naperville, Ill.) and frozen in pre-cooled liquid isopentane. Three-micron cryostat sections were fixed in acetone at –20°C for 5 min and air-dried for 2 h at room temperature. Sections were double-stained with purified anti α-CA1 (1:20 dilution in phosphate-buffered saline solution) and monoclonal antibody against human desmin (Dako, 1:10 dilution). Subsequently, tissue sections were incubated with TRITC-conjugated anti-rabbit and fluorescein-labeled anti-mouse antibodies (both from Jackson ImmunoResearch Labs, Inc.), mounted in buffered polyvinyl alcohol [27] and observed with a confocal laser scan fluorescence inverted microscope (model LSM 510, Carl Zeiss). Images were stored on optical disks (Sony Corp) and printed with a digital Fujifilm Pictography 4000 printer (Fujifilm).

### Scoring of the staining

For each tumor specimen, the antibody-stained sections were carefully examined by two independent observers and staining was scored as follows: – all tumor cells negative, + 1–10% tumor cells positive, ++ 10–50% tumor cells positive, +++ 50–100% tumor cells positive.

## Results

### Purification and determination of the specificity of anti α-CA1

As shown previously for anti-SKA1 [9], immunization with hemocyanin-coupled α-cardiac actin $NH_2$-terminal decapeptide resulted in high titer antibodies showing an important cross-reactivity with all actin isoforms (data not shown). The first step of purification consisted of loading the immune serum on Sulfolink beads coupled with the decapeptide used for immunization. To test the cross-reactivity of the eluted antibodies with actin isoforms, we used extracts of rat striated muscle for α-skeletal actin; rat myocardium for α-cardiac actin; human blood platelets for β and γ cytoplasmic actins present at the ratio of 5 to 1 [26]; rat aorta for α-smooth muscle actin; and chicken gizzard for γ-smooth muscle actin. Sequences of actin isoforms are perfectly conserved in higher vertebrates [40], hence species differences did not interfere with our results. Western-blot analysis (Fig. 1A, panel b) showed that the antibody population eluted from the beads coupled with the α-cardiac decapeptide strongly reacted with α-cardiac actin but also with the other isoforms.

Following a strategy similar to one recently reported [9], antibody populations recognizing epitopes common to the other actin isoforms were then eliminated by sequential passages on columns coupled with $NH_2$-terminal decapeptide of actin isoforms sharing similar amino acid sequences with α-cardiac actin (see Materials and methods). Reactivity of the antibody following α-skeletal, β-cytoplasmic and γ-smooth muscle actin columns are presented in Fig. 1A, panels c, d and e, respectively. The resulting purified antibody population recognized the actin isoform present in the cardiac muscle extract but did not cross react with actin from platelets, aorta and gizzard (Fig. 1A, panel e). The antibody also recognized the skeletal muscle homogenate, albeit to a clearly lesser extent (Fig. 1A, panel c, lane 1).

α-Cardiac actin has been shown to be expressed in both skeletal and cardiac tissue during mouse development, to be detectable in adult skeletal muscle and to represent about 5% of the sarcomeric actin mRNA in adult mouse [18]. Therefore, because all extracts were blotted after loading with similar amounts of actin (Fig. 1A, panel a), it appeared likely that the reactivity of purified anti α-CA1 with the skeletal muscle extract is due to the fraction of muscle α-cardiac actin present in this tissue. To unequivocally test specificity, purified anti α-CA1 was incubated with synthetic peptides corresponding to the $NH_2$-terminal sequences of the six isoforms before immunoblotting analysis (Fig. 1B). The decapeptide of α-cardiac actin used for immunization completely blocked the reactivity of purified anti α-CA1; however, peptides corresponding to the $NH_2$-terminal sequence of the other actins including α-skeletal actin had no effect (Fig. 1B). Anti α-CA1 was then tested by means of immunofluorescence on rat cardiac muscle. Confocal microscopy demonstrated that, as expected, desmin and anti α-CA1 stainings are located in the Z-bands and I-bands of myocytes, respectively (Fig. 1C); no colocalization between these two antigens was observed. The staining distribution in the myocardium was uniform with the exception of areas in which, according to our previous results, α-skeletal actin was present instead of α-cardiac actin [9] (data not shown).

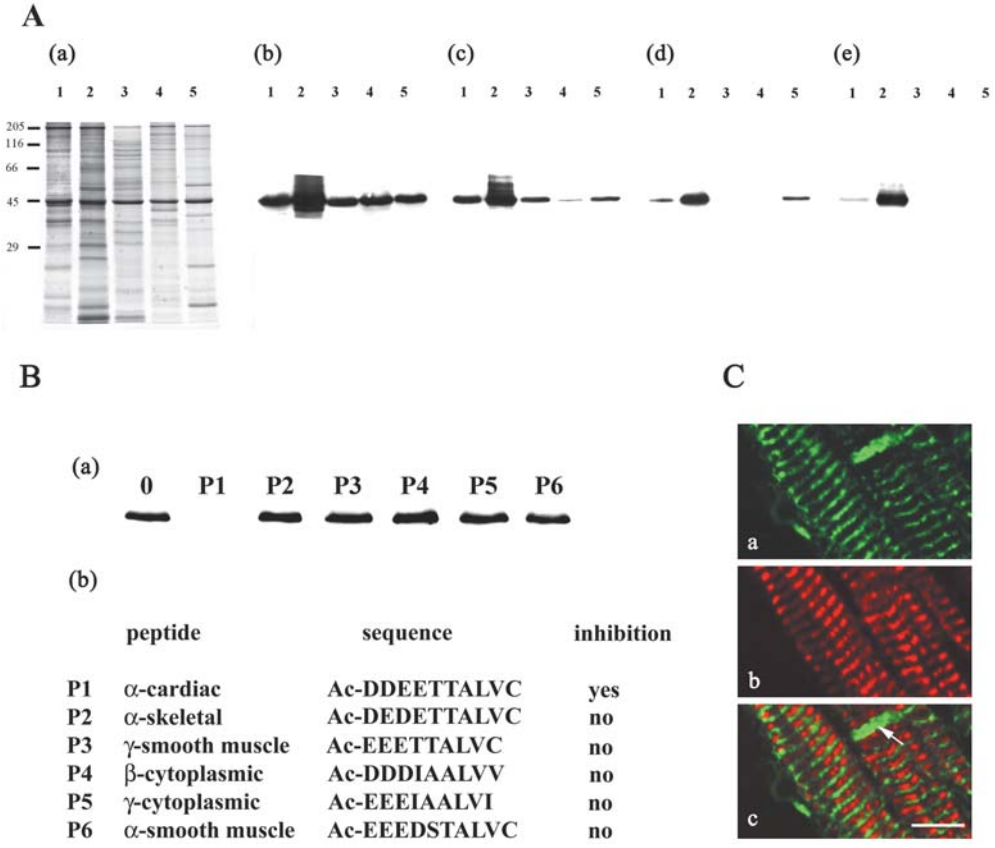



**Fig. 1** Characterization of anti α-CA1 specificity by Western-blot analysis and immunofluorescence. **A** Specificity of the antibody was assessed at different steps of purification by immunoblots on appropriate tissue or cell extracts. *a* Coomassie blue staining of a 10% gradient sodium dodecyl sulfate polyacrylamide gel electrophoresis (SDS-PAGE) of rat skeletal muscle (*lane 1*), rat myocardium (*lane 2*), human blood platelets (*lane 3*), rat aorta (*lane 4*) and chicken gizzard (*lane 5*) (40 μg per lane). *b–d* Western blots immunostained with anti α-CA1 at different purification steps. *b* The serum was run on beads coupled with the $NH_2$-terminal decapeptide of α-cardiac actin; then the fractions recovered from beads were further run on beads coupled with α-skeletal (*c*), β-cytoplasmic (*d*) and γ-smooth (*e*) $NH_2$-terminal decapeptides. The final antibody reacts strongly with cardiac and to a lesser extent with skeletal muscle homogenates (*e*). **B** Inhibitory effect of decapeptides corresponding to the $NH_2$-terminal sequence of actin isoforms on purified anti α-CA1 reactivity was tested by Western blot. Rat cardiac muscle homogenate was subjected to SDS-PAGE followed by Western blotting with purified anti α-CA1 alone (*lane 0*) or mixed with each of the peptides P1 to P6. Only P1 blocked the reactivity of anti α-CA1. **C** Adult rat cardiac muscle sections were double-labeled by indirect immunofluorescence with a monoclonal antibody against desmin (*a*) and the purified anti α-CA1 (*b*). Tissues were observed with a confocal laser scan fluorescence microscope. The overlay of images *a* and *b* presented in *c* shows no colocalization of these antigens. Anti α-CA1 is restricted to I-bands, while anti-desmin stains Z-lines and intercalated disks (*arrow*). *Scale bar* 5 μm

## Immunochemical staining of tumor specimens

Results of immunohistochemical investigation are summarized in Table 1. All RMSs tested except one revealed a positive staining for desmin but significant differences in the level of expression of this protein were observed: an important number of positive cells was present in nine cases, while in three others the number of positive cells was between 10% and 50%, and in four cases it was less than 10%.

We have previously shown by means of an antibody recognizing both α-skeletal and α-cardiac isoforms that a series of embryonal, alveolar and pleomorphic RMSs expressed α-sarcomeric actin [35]. The availability of specific anti α-SKA1 [9] and anti α-CA1 allowed us to investigate separately their expression in RMSs. As shown in Table 1, all tumors were positive for α-cardiac actin that was expressed in different proportions: 13 of 17 cases were strongly α-cardiac actin positive (between 50% and 100% of tumoral cells, see Fig. 2b, e). In only one case (spindle-cell RMS), the positivity was less than 10% (case 15, Fig. 3c); some vessels in this subtype were positive for this actin isoform (Fig. 3d see below). The majority of RMSs did not express α-skeletal actin. Figure 2 shows a typical example of an embryonal (*left column*) and an alveolar (*right column*) RMS stained with anti α-CA1 and anti α-SKA1. Both cases are strongly positive for α-cardiac actin (Fig. 2b, e) and negative for α-skeletal actin (Fig. 2c, f). In three RMSs (all embryonal), we found a coexpression of the two sarcomeric actin isoforms within the same area of the tumor (Fig. 3a and b). Tumoral cells positive for α-skeletal actin corresponded to differentiated rhabdomyoblasts with relatively abundant cytoplasm (Fig. 3b). The expression of α-smooth muscle actin was likewise investigated, as this actin isoform has been previously found in tumoral

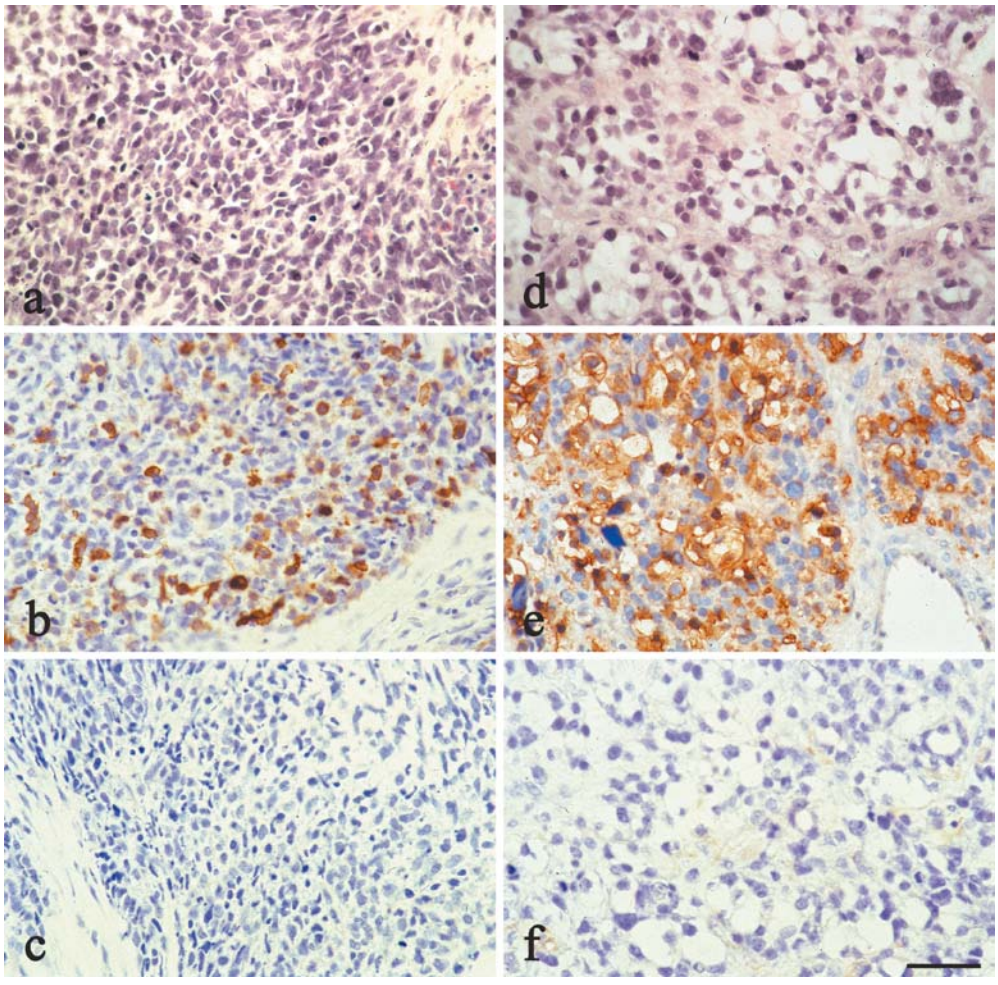



**Fig. 2.** Representative staining for α-cardiac and skeletal actins of alveolar and embryonal rhabdomyosarcoma (RMS). Serial sections of embryonal (case 5) and alveolar RMS (case 10) were stained with hematoxylin and eosin (**a** and **d**), anti α-CA1 (**b** and **e**) and anti α-SKA1 (**c** and **f**) antibodies. Both tumors are clearly positive for α-cardiac actin and negative for α-skeletal actin. *Scale bar* 200 μm

cells of some RMSs [35]. α-Smooth muscle actin was detectable in tumor cells of eight cases with levels of expression generally lower than those found for the other actin isoforms (Fig. 3e). It is interesting to note that the three cases of embryonal RMSs positive for α-skeletal actin were negative for α-smooth muscle actin (Table 1). No differences were present in the frequency of α-smooth muscle actin expression comparing alveolar and embryonal subtypes of RMSs. As expected, fibroblastic cells of the stroma reaction, when present in the tumor specimen, were strongly positive for α-smooth muscle actin (Fig. 3f). Staining for α-cardiac actin in control tumors was negative, with the exception of leiomyoma in which a slight positivity was seen in about 30% of cells in five cases and leiomyosarcoma in which a positivity was seen in about 20% of cells in two cases. In addition, in rare occasions, small arterial vessels were clearly positive both within the tumor and in adjacent apparently normal connective tissue.

## Discussion

During the last few years, antibodies specific for a single actin isoform have become progressively available [9], although some of them (e.g., against γ-smooth muscle or γ-cytoplasmic actins) are still lacking. The use of such antibodies has allowed exploration of the function of these slightly different but well-conserved and tissue-specific proteins; for example, evidence has been produced that α-smooth muscle actin plays a role in regulating the motility [30] and the contractility [3, 20] of myofibroblastic cells. The production of an antibody against α-cardiac actin has been previously described, but its specificity is dependent on the experimental conditions, with obvious difficulties in interpretation, particularly in routine diagnostic procedures [17]. We have recently developed a strategy, which has allowed us to produce antibodies strictly specific for α-skeletal [9] and α-cardiac (present paper) actins, despite the extremely small sequence difference distinguishing these two isoforms [40]. The success in producing such specific anti-actin antibodies suggests that this strategy may be attempted to obtain a complete panel of antibodies specific for each isoform.

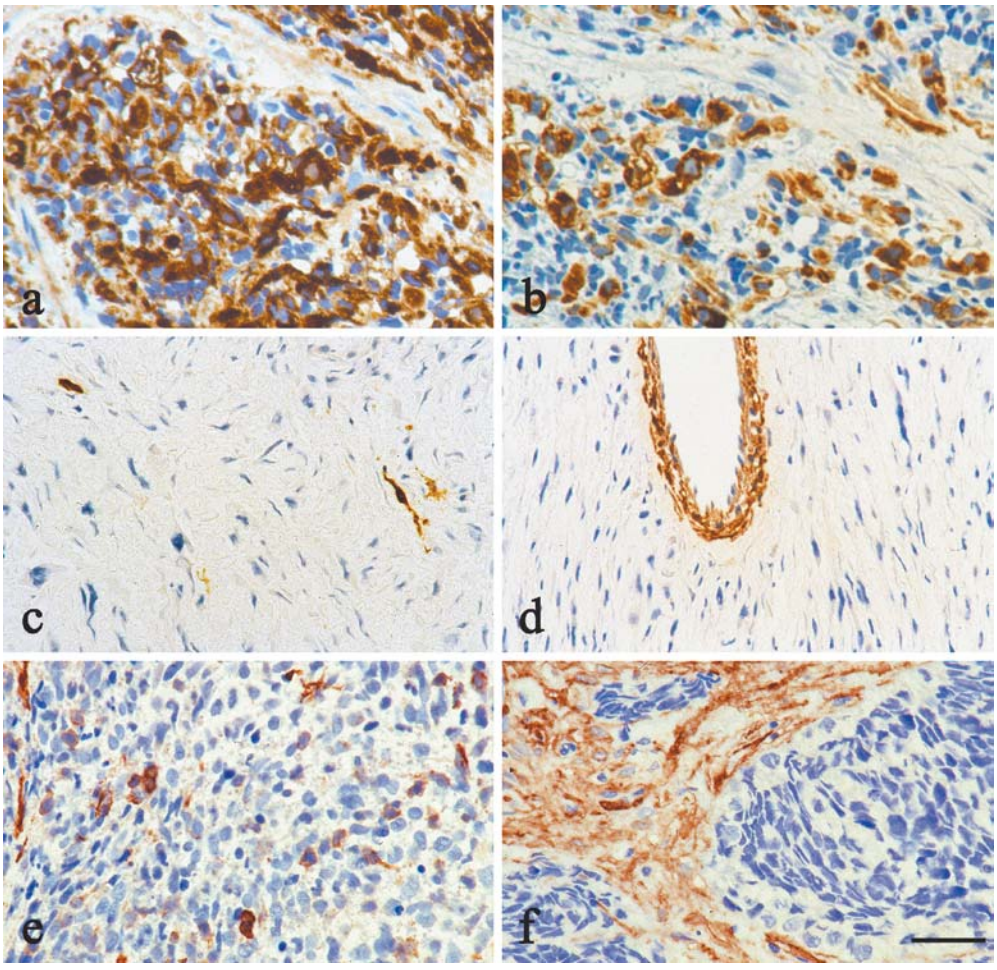



**Fig. 3** Actin isoforms distribution in different rhabdomyosarcomas (RMSs). **a**, **b** Representative pictures of a RMS positive for α-skeletal actin. Serial sections of case 1 were immunostained with anti α-CA1 (*a*) and anti α-SKA1 (*b*). Both antibodies strongly react with tumor cells. **c**, **d** α-Cardiac staining of spindle-cell RMS. A few cells of case 15 are positive throughout the tumor (*c*); interestingly, the wall of a small vessel reacts with anti α-CA1 (*d*). **e**, **f** α-Smooth muscle actin staining of RMS. Tumoral cells of case 5 reveal positive staining for α-smooth muscle actin (*e*). Stromal myofibroblasts of case 7 are positive for α-smooth muscle actin (*f*). *Scale bar* 200 μm

The antibodies against α-skeletal and α-smooth muscle actins have already proven their usefulness for the study of myocardial hypertrophy mechanisms in both experimental animals [9, 10] and humans [37]. The use of these antibodies in combination with anti α-CA1 should be of further help in order to precisely investigate skeletal and cardiac muscle development and disease.

In this work we have focused on a practical aspect of actin antibody utilization, i.e., the diagnosis of RMS, which remains difficult to establish without ambiguity. Immunohistochemical markers, in particular those recognizing cytoskeletal proteins, have improved the accuracy of the diagnosis of soft tissue tumors including RMS [2, 8, 11, 12, 15, 22, 28, 33, 36]. Traditionally, markers for myosin heavy chain or desmin have been used to distinguish RMS from other soft tissue sarcomas with similar histological patterns. However, these markers, in particular desmin, do not have optimal specificity for RMS and also present heterogeneous expression among RMSs [29]. Here we show that anti α-CA1 is a general marker of all subtypes of this tumor in accordance with previous results at the mRNA level [33]. All control soft tissue and small cell tumors examined were negative with the exception of most leiomyomas, few leiomyosarcomas and, in normal tissues, some arterial vessels. Hence, with these limitations, we confirm the specificity of α-cardiac actin positivity in the characterization of RMS. The presence of α-cardiac actin in arterial vessels has been previously reported [5]; further studies are needed in order to establish the role of this isoform in smooth muscle cells.

By means of an antibody recognizing both α-cardiac and α-skeletal actins, we have previously shown that sarcomeric actin expression is increased in well-differentiated relative to poorly differentiated RMSs [36]. In rat experimental RMS, it has also been shown, using biochemical techniques, that the pattern of actin isoform expression reflects the differentiation state of tumor cells [4]. Thus, the availability of specific antibodies will be important for the characterization of the degree of differentiation of RMS, including during the monitoring of therapeutic strategies [8]. The constant presence of α-cardiac actin and the fact that α-smooth muscle and α-skeletal actin isoforms are expressed in only some cases of our series of tumors raise the question of the relationship between actin isoform gene expression and biological behavior of tumoral cells. It is well established that α-cardiac and α-smooth muscle actin are transiently expressed during the development of skeletal muscle [34, 41], while α-skeletal actin represents the most differentiated isoform. Hence, the actin isoform ex-

pression pattern in RMSs mimics different developmental stages of skeletal muscle: RMSs positive for only α-cardiac and α-smooth muscle actins mimic an early developmental stage, whereas the positivity for α-skeletal actin in three embryonal cases reflects a higher differentiation of these tumors. This possibility is compatible with the histological features of RMS showing that rhabdomyoblasts with cross-striations are seen in 50–60% of embryonal RMS and more rarely in other subtypes [1].

In conclusion, we have produced a specific α-cardiac actin antibody that represents a useful adjunct for the diagnosis of RMS. Moreover it appears possible to use our panel of actin isoform specific antibodies, in addition to the already known markers of this tumor (for review see [29]), in order to characterize the different subtypes on the basis of their differentiation features; this may improve the understanding of the biology and evolution of RMS.

**Acknowledgements** We gratefully acknowledge Dr. I. Szalay and A. Ferlosio for providing some tumor samples; Mr. P. Henchoz for technical help, J.-C. Rumbeli and E. Denkinger for photographic work and Ms E. Homberg for secretarial work. Both Sophie Clément and Augusto Orlandi have equally contributed to this work. Grant and support sources: partially supported by the Swiss National Science Foundation (grants no. 31-61336.00 and 31-54048.98), the MURST (grant no. 995157119).

## References

1. Agamanolis DP, Dasu S, Krill CE (1986) Tumors of skeletal muscle. Hum Pathol 17:778–795
2. Altmannsberger M, Osborn M, Treuner J, Holscher A, Weber K, Shauer A (1982) Diagnosis of human childhood rhabdomyosarcoma of antibodies to desmin, the structural protein of muscle specific intermediate filaments. Virchows Arch 39: 203–215
3. Arora PD, Narani N, McCulloch CA (1999) The compliance of collagen gels regulates transforming growth factor-beta induction of alpha-smooth muscle actin in fibroblasts. Am J Pathol 154:871–882
4. Babai F, Skalli O, Schurch W, Seemayer TA, Gabbiani G (1988) Chemically induced rhabdomyosarcomas in rats. Ultrastructural, immunohistochemical, biochemical features and expression of alpha-actin isoforms. Virchows Arch 55:263–277
5. Bea F, Bar H, Watson L, Blessing E, Kubler W, Kreuzer J, Jahn L (2000) Cardiac alpha-actin in smooth muscle cells: detection in umbilical cord vessels and in atherosclerotic lesions. Basic Res Cardiol 95:106–113
6. Cavazzana AO, Schmidt D, Ninfo V, Harms D, Tollot M, Carli M, Treuner J, Betto R, Salviati G (1992) Spindle cell rhabdomyosarcoma. A prognostically favorable variant of rhabdomyosarcoma. Am J Surg Pathol 16:229–235
7. Cessna MH, Zhou H, Perkins SL, Tripp SR, Layfield L, Daines C, Coffin CM (2001) Are myogenin and myoD1 expression specific for rhabdomyosarcoma? A study of 150 cases, with emphasis on spindle cell mimics. Am J Surg Pathol 25:1150–1157
8. Cintorino M, Vindigni C, Del Vecchio MT, Tosi P, Frezzotti R, Hadjistilianou T, Leoncini P, Silvestri S, Skalli O, Gabbiani G (1989) Expression of actin isoforms and intermediate filament proteins in childhood orbital rhabdomyosarcomas. J Submicrosc Cytol Pathol 21:409–419
9. Clement S, Chaponnier C, Gabbiani G (1999) A subpopulation of cardiomyocytes expressing alpha-skeletal actin is identified by a specific polyclonal antibody. Circ Res 85:e51–e58
10. Clement S, Pellieux C, Chaponnier C, Pedrazzini T, Gabbiani G (2001) Angiotensin II stimulates alpha-skeletal actin expression in cadiomyocytes in vitro and in vivo in the absence of hypertension. Differentiation 69:66–74
11. de Jong A, van Kessel van Vark M, Albus Lutter C, van Raamsdonk W, Voûte P (1985) Skeletal muscle actin as tumor marker in the diagnosis of rhabdomyosarcoma in childhood. Am J Surg Pathol 9:467–474
12. Denk H, Krepler R, Artlieb U, Gabbiani G, Rungger-Brandle E, Leoncini P, Franke WW (1983) Proteins of intermediate filaments. An immunohistochemical and biochemical approach to the classification of soft tissue tumors. Am J Pathol 110:193–208
13. Dias P, Chen B, Dilday B, Palmer H, Hosoi H, Singh S, Wu C, Li X, Thompson J, Parham D, Qualman S, Houghton P (2000) Strong immunostaining for myogenin in rhabdomyosarcoma is significantly associated with tumors of the alveolar subclass. Am J Pathol 156:399–408
14. Enzinger FM, Weiss SW (2001) Rhabdomyosarcoma. In: Weiss SW, Goldblum JR (eds) Soft tissue tumors, 4th edn, Mosby, St Louis, pp 785–835
15. Eusebi V, Ceccarelli C, Gorza L, Schiaffino S, Bussolati G (1986) Immunocytochemistry of rhabdomyosarcoma. The use of four different markers. Am J Surg Pathol 10:293–299
16. Eusebi V, Damiani S, Pasquinelli G, Lorenzini P, Reuter VE, Rosai J (2000) Small cell neuroendocrine carcinoma with skeletal muscle differentiation: report of three cases. Am J Surg Pathol 24:223–230
17. Franke WW, Stehr S, Stumpp S, Kuhn C, Heid H, Rackwitz HR, Schnolzer M, Baumann R, Holzhausen HJ, Moll R (1996) Specific immunohistochemical detection of cardiac/fetal alpha-actin in human cardiomyocytes and regenerating skeletal muscle cells. Differentiation 60:245–250
18. Garner I, Sassoon D, Vandekerckhove J, Alonso S, Buckingham ME (1989) A developmental study of the abnormal expression of alpha-cardiac and alpha-skeletal actins in the striated muscle of a mutant mouse. Dev Biol 134:236–245
19. Gimona M, Vandekerckhove J, Goethals M, Herzog M, Lando Z, Small JV (1994) Beta-actin specific monoclonal antibody. Cell Motil Cytoskeleton 27:108–116
20. Hinz B, Celetta G, Tomasek JJ, Gabbiani G, Chaponnier C (2001) α-smooth muscle actin expression upregulates fibroblast contractile activity. Mol Biol Cell 12:2730–2741
21. Hinz B, Mastrangelo D, Iselin CE, Chaponnier C, Gabbiani G (2001) Mechanical tension controls granulation tissue contractile activity and myofibroblast differentiation. Am J Pathol 159:1009–1020
22. Jong AS, van Vark M, Albus-Lutter CE, van Raamsdonk W, Voute PA (1984) Myosin and myoglobin as tumor markers in the diagnosis of rhabdomyosarcoma. A comparative study. Am J Surg Pathol 8:521–528
23. Khaitlina SY (2001) Functional specificity of actin isoforms. Int Rev Cytol 202:35–98
24. Kumar S, Perlman E, Harris CA, Raffeld M, Tsokos M (2000) Myogenin is a specific marker for rhabdomyosarcoma: an immunohistochemical study in paraffin-embedded tissues. Mod Pathol 13:988–993
25. Laemmli UK (1970) Cleavage of structural proteins during the assembly of the head of bacteriophage T4. Nature 227:680–685
26. Landon F, Huc C, Thome F, Oriol C, Olomucki A (1977) Human platelet actin. Evidence of beta and gamma forms and similarity of properties with sarcomeric actin. Eur J Biochem 81:571–577
27. Lennette DA (1978) An improved mounting medium for immunofluorescence microscopy (letter). Am J Clin Pathol 69: 647–648
28. Miettinen M, Lehto VP, Badley RA, Virtanen I (1982) Expression of intermediate filaments in soft-tissue sarcomas. Int J Cancer 30:541–546
29. Parham DM (2001) Pathologic classification of rhabdomyosarcomas and correlations with molecular studies. Mod Pathol 14:506–514
30. Ronnov Jessen L, Petersen OW (1996) A function for filamentous alpha-smooth muscle actin: retardation of motility in fibroblasts. J Cell Biol 134:67–80

31. Rubin BP, Hasserjian RP, Singer S, Janecka I, Fletcher JA, Fletcher CD (1998) Spindle cell rhabdomyosarcoma (so-called) in adults: report of two cases with emphasis on differential diagnosis. Am J Surg Pathol 22:459–464
32. Schurch W, Skalli O, Seemayer TA, Gabbiani G (1987) Intermediate filament proteins and actin isoforms as markers for soft tissue tumor differentiation and origin. I. Smooth muscle tumors. Am J Pathol 128:91–103
33. Schurch W, Bochaton-Piallat ML, Geinoz A, d'Amore E, Laurini RN, Cintorino M, Begin LR, Boivin Y, Gabbiani G (1994) All histological types of primary human rhabdomyosarcoma express alpha-cardiac and not alpha-skeletal actin messenger RNA. Am J Pathol 144:836–846
34. Schwartz RJ, Rothblum KN (1981) Gene switching in myogenesis: differential expression of the chicken actin multigene family. Biochemistry 20:4122–4129
35. Skalli O, Ropraz P, Trzeciak A, Benzonana G, Gillessen D, Gabbiani G (1986) A monoclonal antibody against α-smooth muscle actin: a new probe for smooth muscle differentiation. J Cell Biol 103:2787–2796
36. Skalli O, Gabbiani G, Babai F, Seemayer TA, Pizzolato G, Schurch W (1988) Intermediate filament proteins and actin isoforms as markers for soft tissue tumor differentiation and origin. II. Rhabdomyosarcomas. Am J Pathol 130:515–531
37. Suurmeijer AJH, Clément S, Francesconi A, Bocchi L, Angelini A, Van Veldhuisen DJ, Spagnoli LG, Gabbiani G, Orlandi A (2002) Alpha actin isoform distribution in normal and failing human heart: a morphological, morphometrical and biochemical study. J Pathol (in press)
38. Tonin PN, Scrable H, Shimada H, Cavenee WK (1991) Muscle-specific gene expression in rhabdomyosarcomas and stages of human fetal skeletal muscle development. Cancer Res 51: 5100–5106
39. Towbin H, Staehelin T, Gordon J (1979) Electrophoretic transfer of proteins from polyacrylamide gels to nitrocellulose sheets: procedure and some applications. Proc Natl Acad Sci USA 76:4350–4354
40. Vandekerckhove J, Weber K (1979) The complete amino acid sequence of actins from bovine aorta, bovine heart, bovine fats skeletal muscle and rabbit slow skeletal muscle. Differentiation 14:123–133
41. Woodcock-Mitchell J, Mitchell JJ, Low RB, Kieny M, Sengel P, Rubbia L, Skalli O, Jackson B, Gabbiani G (1988) α-Smooth muscle actin is transiently expressed in embryonic rat cardiac and skeletal muscles. Differentiation 39:161–166

Virchows Arch (2003) 442:39–47
DOI 10.1007/s00428-002-0703-0

ORIGINAL ARTICLE

**Yu-Lan Jin · Hideaki Enzan · Naoto Kuroda**
**Yoshihiro Hayashi · Hirofumi Nakayama**
**Yan-Hu Zhang · Makoto Toi · Eriko Miyazaki**
**Makoto Hiroi · Li-Mei Guo · Toshiji Saibara**

# Tissue remodeling following submassive hemorrhagic necrosis in rat livers induced by an intraperitoneal injection of dimethylnitrosamine

Received: 5 March 2002 / Accepted: 12 June 2002 / Published online: 29 October 2002
© Springer-Verlag 2002

**Abstract** We examined regeneration and fibrosis in the necrotic areas of hepatic stellate cells (HSCs). Acute hepatic injury was induced in rats by administration of an intraperitoneal injection of high-dose dimethylnitrosamine (50 mg/kg body weight). Liver samples were obtained from rats 6, 12, 24, 36 h and 2, 3, 5, 7, 10, and 14 days after the injection. They were examined by light and electron microscopy and by immunohistochemical methods. Hemorrhagic necrosis became most prominent 36 h after treatment and extended into zones 3 and 2. In the submassive necrotic areas the sinusoidal structure was destroyed. No HSCs positive for α-smooth muscle actin or desmin were present. On day 5, when necrotic tissues were almost removed by infiltrating macrophages, HSCs strongly positive for α-smooth muscle actin and desmin appeared along the surface of the preserved parenchyma and migrated into the necrotic areas along the residual reticulin fibers. By day 14 most of the necrotic areas were almost completely replaced by the regeneration of hepatocytes and central to central (C-C) bridging fibrosis. Our results indicate that following submassive complete necrosis, HSCs in the preserved liver parenchyma have roles in the formation of sinusoidal wall for remodeling in necrotic areas via their activation, proliferation, and migration into the necrotic areas.

**Keywords** Hepatic stellate cell · Fibrosis · α-Smooth muscle actin · Dimethylnitrosamine · Rat

Y.-L. Jin (✉) · H. Enzan · N. Kuroda · Y. Hayashi · H. Nakayama
Y.-H. Zhang · M. Toi · E. Miyazaki · M. Hiroi · L.-M. Guo
First Department of Pathology, Kochi Medical School, Kohasu, Oko-cho, Nankoku City, Kochi, 783-8505, Japan
e-mail: jyl@kochi-ms.ac.jp
Tel.: +81-88-8802329, Fax: +81-88-8802332

T. Saibara
First Department of Internal Medicine, Kochi Medical School, Kohasu, Oko-cho, Nankoku City, Kochi, 783-8505, Japan

## Introduction

Hepatic stellate cells (HSCs, also referred to as Ito cells, fat-storing cells, and lipocytes) are liver-specific pericytes and play a critical role in tissue remodeling and the development of liver fibrosis [3, 10, 13, 15]. Previous studies indicate that the mechanism of fibrogenesis in early and advanced liver diseases is similar, regardless of the type of initial injuries, including viral, toxic, immune or metabolic [9, 10, 11, 22]. However, other studies demonstrate that there are subtle but distinctive differences in the manner of the HSC activation according to whether the liver injuries are viral or alcoholic [10, 11, 22].

Dimethylnitrosamine (DMN), the commonly detected N-nitrosamine in food, is metabolized in the liver. If a high dose of the chemical is administrated by one injection to experimental animals, it causes submassive necrosis that resembles human fulminant hepatitis [23]. On the other hand, it is well known that repeated injections of smaller dose DMN develop liver fibrosis or cirrhosis [1, 12, 17, 19, 20, 25]. In the latter treatment with DMN, the features of acute, subacute, and chronic injuries are admixed in the same liver after each injection [1, 12, 17, 19, 20, 25]. This may cause difficulty in the assessment of pathological findings. For these reasons we examined the sequential changes to fibrosis following submassive hepatic necrosis induced by only one injection of high dose DMN and showed the usefulness of this experimental model for the study of postnecrotic liver fibrosis and tissue remodeling. Furthermore, the present study demonstrates for the first time the process of HSCs recruitment in their necrotic areas.

## Materials and methods

### Animals

Forty male Wistar strain rats (7–10 weeks old) were used for DMN-induced liver injuries as well as five untreated rats and five saline-injected rats for normal controls. All animals were main-

tained under 12 h light/12h dark cycles in a day with food and water available ad libitum. Acute hepatic injury was induced by an intraperitoneal injection of DMN (Sigma, St. Louis, Mo., USA) in dose of 50 mg (diluted 1:100 with 0.15 M NaCl)/kg body weight, and four rats per each group were killed 6, 12, 24, 36 h and 2, 3, 5, 7, 10, and 14 days after the injection. The saline-injected rat group received only an equivalent amount of saline. Four rats in each time interval after treatment with DMN and three control rats received an intraperitoneal injection of 5-bromo-2-deoxyuridine (BrdU; 10 mg/kg body weight, at a concentration of 20 mg/ml in saline) 1 h before killing. All of the animals were anesthetized with diethylether before killing. Their livers were rapidly removed.

This study was approved by the Animal Care and Use Committee of Kochi Medical School and followed the National Institutes of Health guidelines for humane care and use of animals.

### Light microscopy and immunohistochemistry

Liver tissues from DMN-treated and control groups were fixed in 10% phosphate-buffered formalin for 2 days and then embedded in paraffin. The formalin-fixed and paraffin-embedded liver tissue sections about 3 μm thickness were dewaxed, rehydrated, and stained with hematoxylin and eosin, silver impregnation for reticulin fibers, and the Azan method for collagen fibers. Enzyme histochemistry for naphthol AS-D chloroacetate esterase was also performed. For immunohistochemical staining endogenous peroxidase was inhibited by 0.3% hydrogen peroxide in methanol for 15 min at room temperature and rinsed with 0.01 M phosphate-buffered saline (PBS; pH 7.2); (5 min, three times), and incubated in 10% normal rabbit serum (Dako) for 10 min. Subsequently they were incubated overnight at 4°C with each monoclonal antibody for α-smooth muscle actin (ASMA; 1A4, Dako, Glostrup, Denmark; 1:50), BrdU (Bu20a, Dako; 1:20), desmin (D33, Dako; 1: 50), and ED1 (Serotec, Oxford, UK; 1:500). After rinsing with PBS these sections were incubated for 60 min at room temperature with a 1:200 dilution of biotinylated rabbit anti-mouse IgG $F(ab')^2$ fragment (Dako) for all stainings. After rinsing with PBS these sections were incubated for 60 min at room temperature in an avidin-biotin-peroxidase complex solution. Finally, the sections were immersed in a substrate solution of 0.5% 3,3′-diaminobenzidine tetrahydrochloride (DAB; Sigma, St. Louis, Mo. USA) and 0.1% hydrogen peroxide in 0.05 M Tris buffer, pH 7.6 for three min at room temperature. The sections were lightly washed, counterstained with hematoxylin, dehydrated in ethanol, and mounted with Eukitt (Kindler, Freiburg, Germany). As a negative control for immunostaining, sections were incubated in normal mouse serum at the same concentration as that of the primary antibodies used in this study.

### Double immunohistochemical staining with anti-ASMA and anti-BrdU antibodies

To simultaneously detect cytoplasmic ASMA localization and nuclear BrdU incorporation in the same section sequential double immunohistochemical stainings were used. Briefly, sections were treated with methanol/peroxide as described above, and incubated with anti-BrdU for 60 min at room temperature. They were incubated with the avidin-biotin-peroxidase complex solution and immersed in 0.5% DAB and 0.1% hydrogen peroxide in 0.05 M Tris buffer as above. The nuclei of cells in the S-phase showed a brown color. Then the sections were incubated overnight with anti-ASMA antibody. After washing with PBS (pH 7.2) they were treated for 30 min with alkaline phosphatase conjugated rabbit anti-mouse IgG (Dako; diluted 1:50). To visualize the reaction for alkaline phosphatase the sections were stained with fast blue BB. The cytoplasmic reaction product for ASMA showed a blue color.

### Silver impregnation and immunohistochemical stain for ASMA

After silver impregnation the sections were incubated overnight with anti-ASMA antibody and visualized by DAB as described above.

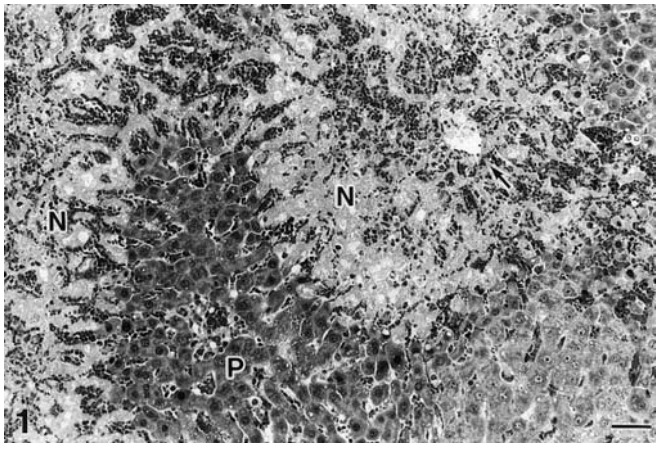



**Fig. 1** Submassive hemorrhagic necrosis with extension into zones 3 and 2 36 h after DMN injection. *N* Necrotic areas; *P* portal tract; *arrow* central vein. Hematoxylin and eosin; *bar* 40 μm

### Quantification for immunohistochemistry and double immunohistochemistry

The BrdU-positive hepatocytes and the ASMA-positive activated HSCs with a BrdU-labeled nucleus were counted in the rat liver parenchyma, excluding necrotic and fibrotic areas, at varying duration after DMN treatment. The mean number of these cells in 20 randomly selected fields under moderate magnification (x200) was calculated from four rat livers in every group. The data were expressed as the means ±standard error of the mean. The differences between two independent groups were tested by Student's paired *t*-test. The difference was considered significant when $P$ values were less than 0.05.

### Electron microscopy

Small pieces of liver tissues were prefixed in 2.5% glutaraldehyde in 0.1 M phosphate buffer (pH 7.4) for 24 h at 4°C and postfixed in 1% osmium tetroxide in phosphate buffer for 2 h at 4°C followed by dehydration and embedding in epoxy resin. For selecting optimal areas, semithin sections were stained with toluidine blue. Ultrathin sections stained with uranyl acetate and lead citrate were examined with a JEM 100S electron microscope (JEOL, Tokyo, Japan).

## Results

### Light microscopic and immunohistochemical observations

In control livers of untreated or saline-injected rats HSCs strongly positive for ASMA and desmin, i.e., HSCs with myofibroblastic transformation (activated HSCs), were not seen in the liver parenchyma. There were not any types of inflammatory cells present. All DMN-treated rats survived until they were killed. Liver tissues from rats in the same time interval after DMN treatment showed similar morphological changes. Six hours after DMN injection the centrilobular sinusoids were dilated. In addition, neutrophils positive for naphthol AS-D chloroacetate esterase were frequent in the sinusoidal lumen or with their adhesion to the sinusoidal wall. After 12 h small necrotic

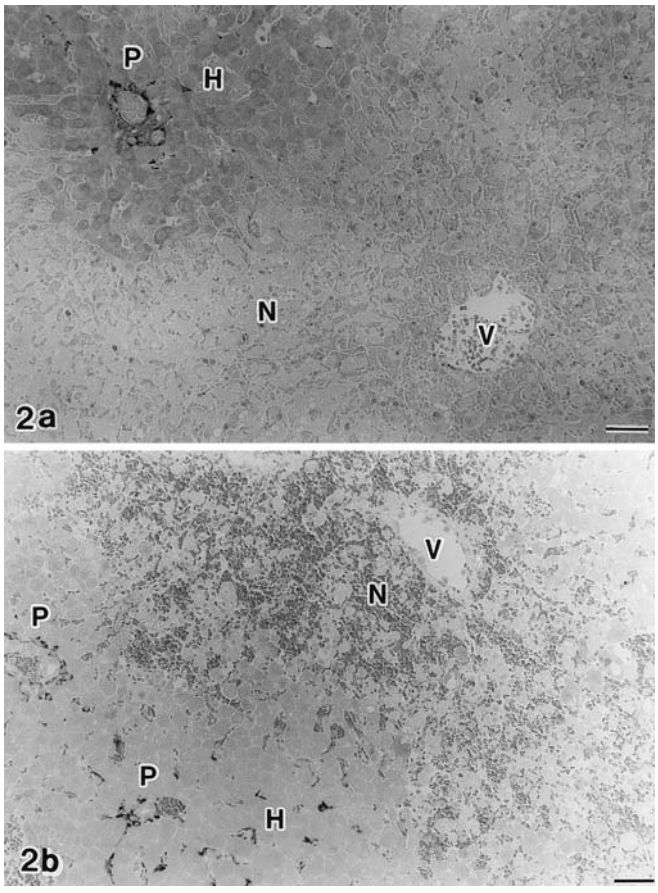



**Fig. 2a, b** At 36 h after DMN injection HSCs positive for ASMA and desmin are not seen in submassive necrotic areas (*N*). Vascular smooth muscle cells and pericytes in the portal tract (*P*) are positive for ASMA and desmin. Very few quiescent HSCs in the preserved parenchyma (*H*) are weakly positive for ASMA and desmin. *V* Central vein. Immunohistochemical stain for ASMA (**a**) and desmin (**b**); *bar* 40 μm

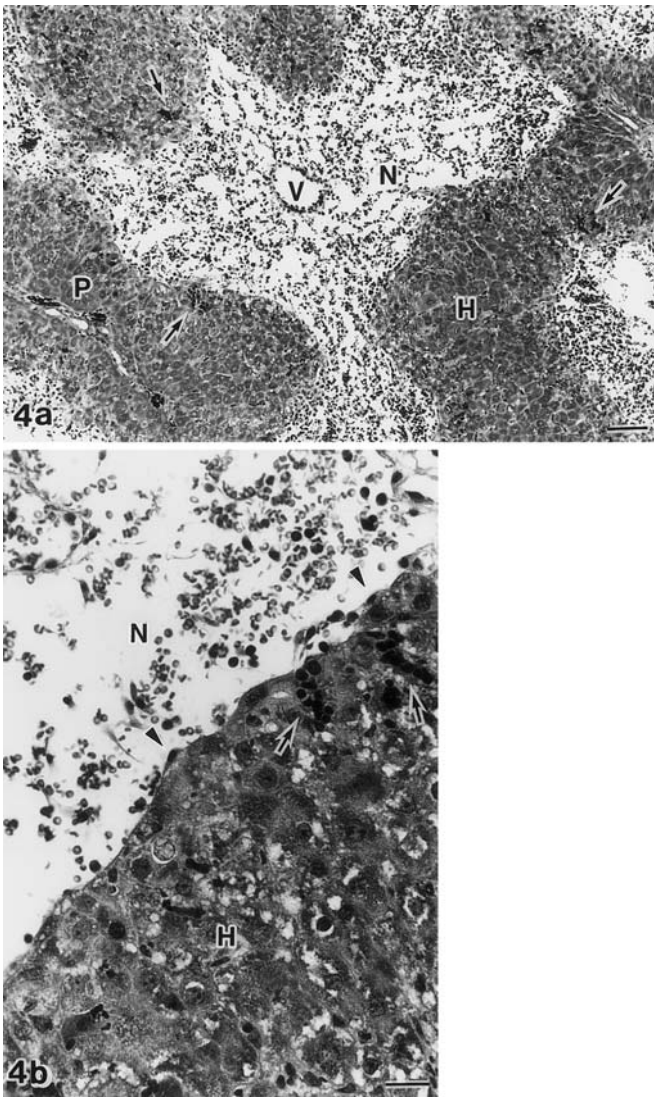



**Fig. 4 a** On day 5 after DMN injection the interface between the necrotic area and the preserved liver parenchyma is irregular. In the necrotic area erythrocytes and macrophages are scattered. Incomplete reticular structure is also present. *Bar* 80 μm. **b** Higher magnification of the interface. Spindle-shaped cells (*arrowheads*) are seen at the surface of liver parenchyma. *H* Liver parenchyma; *N* necrotic area; *P* portal tract; *V* central vein; *arrows* foci of erythropoiesis. Hematoxylin and eosin stain; *bar* 20 μm

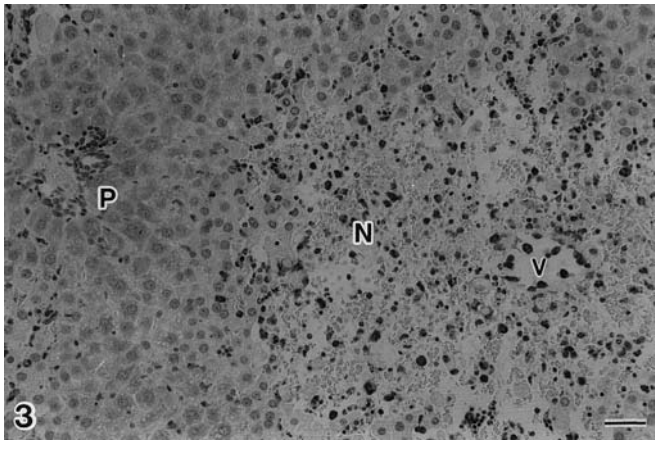



**Fig. 3** On day 3 after DMN injection numerous ED-1 positive macrophages infiltrate into the necrotic area (*N*) and some of them adhere to the wall of a central vein (*V*). *P* Portal tract. Immunohistochemical stain for ED-1; *bar* 40 μm

foci appeared in the centrilobular area, with infiltration of a few small macrophages and neutrophils. After 24 h the liver necrosis became more prominent and peaked at 36 h. The submassive hemorrhagic necrosis with extension into zones 3 and 2 developed, while the hepatic parenchyma around the portal tracts was preserved (Fig. 1). Neither ASMA-positive HSCs nor desmin-positive HSCs were observed in the necrotic areas (Fig. 2a, b), while a few HSCs weakly positive for ASMA or desmin were scattered within the preserved parenchyma. On days 2 and 3 after injection numerous ED-1 positive macrophages and other types of inflammatory cells infiltrated the necrotic areas (Fig. 3). On day 3 a few HSCs strongly

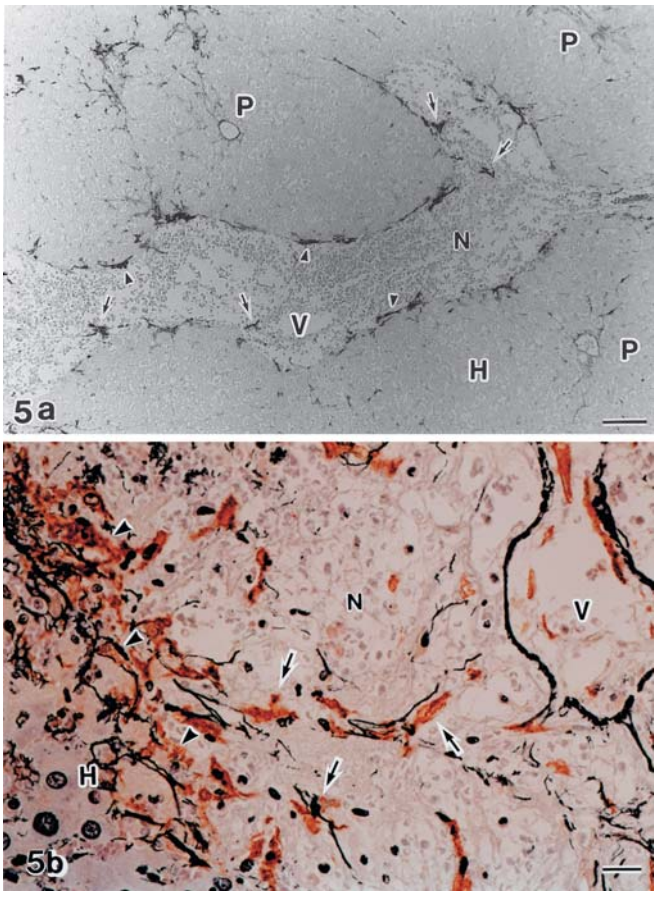



**Fig. 5** **a** On day 5 after DMN injection HSCs strongly positive for ASMA appear along the surface of the preserved liver parenchyma (*arrowheads*) and extend into the necrotic area (*arrows*). Immunohistochemical stain for ASMA; *bar* 80 μm. **b** ASMA in the cytoplasm is stained *brown*, while reticulin fibers are *black*. ASMA-positive activated HSCs are closely contacted with reticulin fibers along the margin of liver parenchyma (*arrowheads*) and in the necrotic area (*arrows*). Silver impregnation and immunohistochemical stain for ASMA; *bar* 20 μm. *H* Liver parenchyma; *N* necrotic area; *P* portal tract; *V* central vein

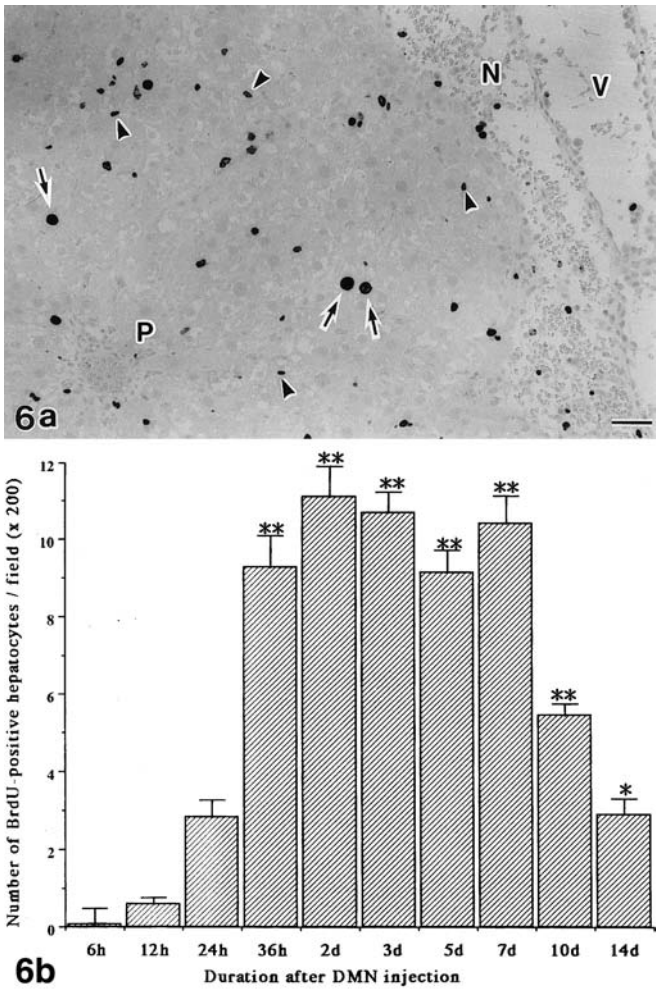
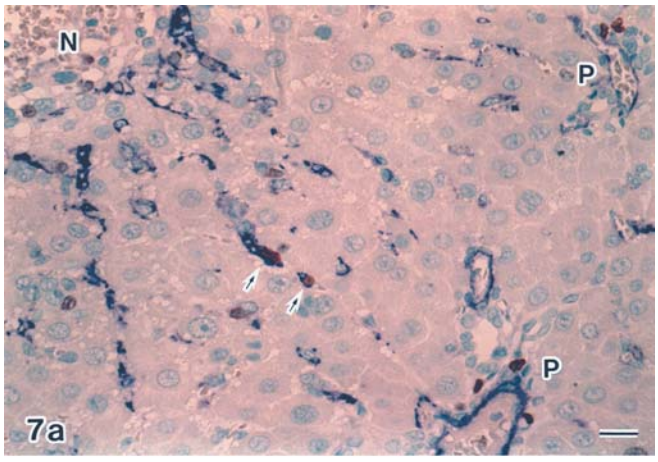



**Fig. 6** **a** On day 5 after DMN injection some hepatocytes (*arrows*) and perisinusoidal cells (*arrowheads*) in the parenchyma are positive for BrdU. *N* Necrotic area; *P* portal tract; *V* central vein; *bar* 40 μm. **b** Number of BrdU-positive hepatocytes in preserved liver parenchyma. Data were expressed as mean ±standard error of the mean. $*P<0.05$, $**P<0.001$ vs. 6 h after DMN injection

positive for ASMA and desmin appeared in the preserved parenchyma adjacent to necrotic areas.

With time necrotic tissues and erythrocytes were phagocytosed and digested by macrophages. After 5 days, with considerable removal of necrotic debris and decrease in inflammatory cell infiltration, the necrotic areas changed to irregularly shaped spaces containing residual reticulin fibers, some erythrocytes and macrophages (Fig. 4a). The interface between necrotic areas and preserved liver parenchyma was irregular but clear (Fig. 4b). In the liver parenchyma near the necrotic areas small foci of erythroblasts appeared from the 5th day. The erythroblastic islands had a peak in number and size on days 5–7 and almost disappeared on day 10 after DMN treatment. On day 5 activated HSCs strongly positive for ASMA and desmin were present on the surface of the preserved liver parenchyma, increased in number, and discontinuously rimmed the border between the liver parenchyma and necrotic areas (Fig. 5a). From the border the activated HSCs appeared to migrate into the necrotic areas along the residual reticular fibers (Fig. 5b). On day 5 BrdU-positive hepatocytes, perisinusoidal cells, and erythroblasts were frequent in the parenchyma (Fig. 6a). The hepatocytes positive for BrdU were absent in control rat livers and scattered in very few numbers 6 h after DMN injection but significantly increased in number from 24 h, with a peak on day 2, followed by a plateau until the seventh day after DMN injection (Fig. 6b). Some of the activated HSCs, which were strongly positive for ASMA, had a BrdU-positive nucleus (Fig. 7a). They increased in number from day 3 onwards and reached a peak on day 7 (Fig. 7b), thereafter falling toward control values on day 14. On day 7 the activated HSCs were most diffusely distributed along the sinusoids (Fig. 8) and the first histological signs of liver fibrosis were seen around the necrotic areas.



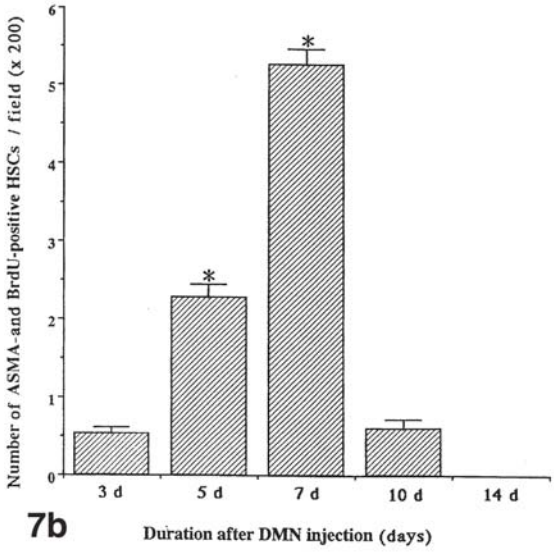




**Fig. 7 a** ASMA-positive HSCs having a BrdU-labeled nucleus (*arrows*) are identified in the preserved liver parenchyma on day 5 after DMN injection. BrdU is stained *brown* and ASMA *blue*. Unlabeled nuclei show a *pale blue*. P Portal tract; *N* necrotic area. Double immunohistochemical stain with anti-ASMA and anti-BrdU antibodies; *bar* 20 μm. **b** Number of ASMA-positive HSCs with a BrdU-positive nucleus in preserved liver parenchyma. Data were expressed as mean ±standard error of the mean. **P*<0.001 vs. 3 days after DMN injection

The postnecrotic irregularly shaped spaces were gradually replaced by regenerating hepatocytes and fibrosis. After 14 days thin fibrous tissue bands from adjoining centrilobular areas joined, forming the C-C bridging ibrosis (Fig. 9a). At this time almost all HSCs in the parenchyma became negative for ASMA again, although most of the spindle-shaped stromal cells in the areas of C-C bridging fibrosis stained positively with ASMA (Fig, 9b). The portal tracts were almost normal throughout the periods after DMN injection. Sequential histopathological changes in rat livers and in the number of BrdU-positive hepatocytes as well as activated HSCs in the preserved parenchyma after a single intraperitoneal injection of DMN are summarized in Table 1.

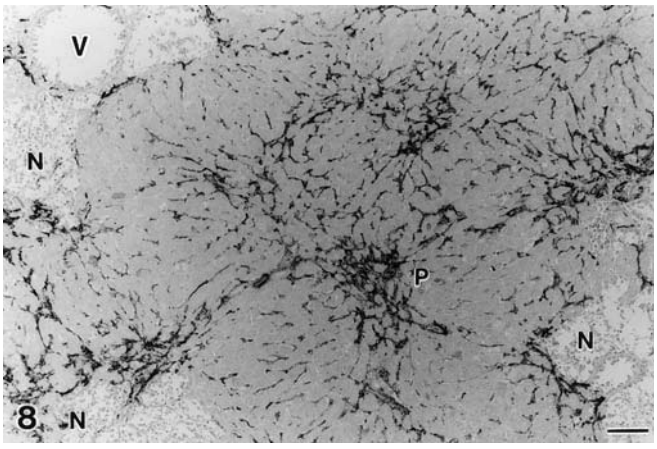
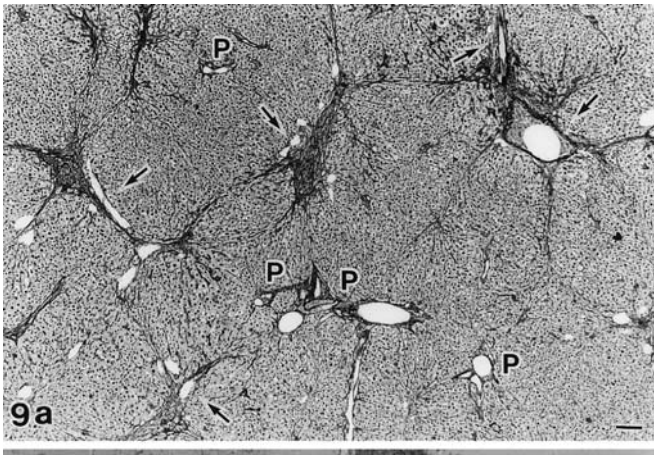



**Fig. 8** On the day 7 after DMN injection HSCs strongly positive for ASMA (activated HSCs) are increased in number and diffusely distributed in the liver parenchyma along the sinusoidal wall. *N* Necrotic area; *P* portal tract; *V* central vein. Immunohistochemical stain for ASMA; *bar* 80 μm



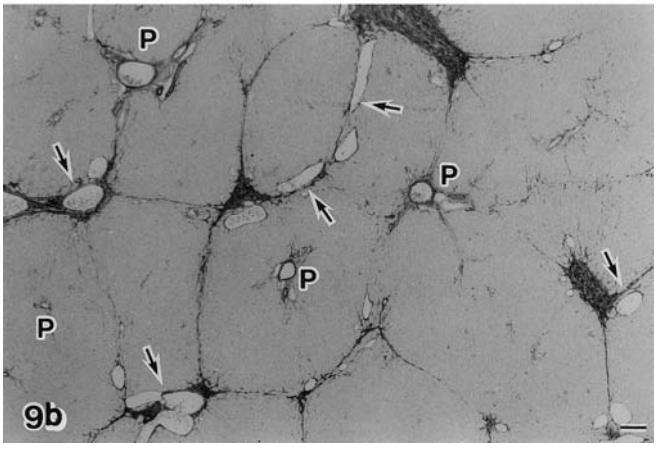




**Fig. 9a, b** On day 14 after DMN injection thin bundles of C-C bridging fibrosis binding adjacent centrilobular areas are seen. **a** Necrotic areas are replaced by regenerating hepatocytes and fibrosis. **b** No ASMA-positive HSCs are present in the parenchyma, but there are many stromal cells positive for ASMA in the area of C-C bridging fibrosis. *P* Portal tract; *arrows* central vein. Silver impregnation (**a**) and immunohistochemical stain for ASMA (**b**); *bar* 80 μm

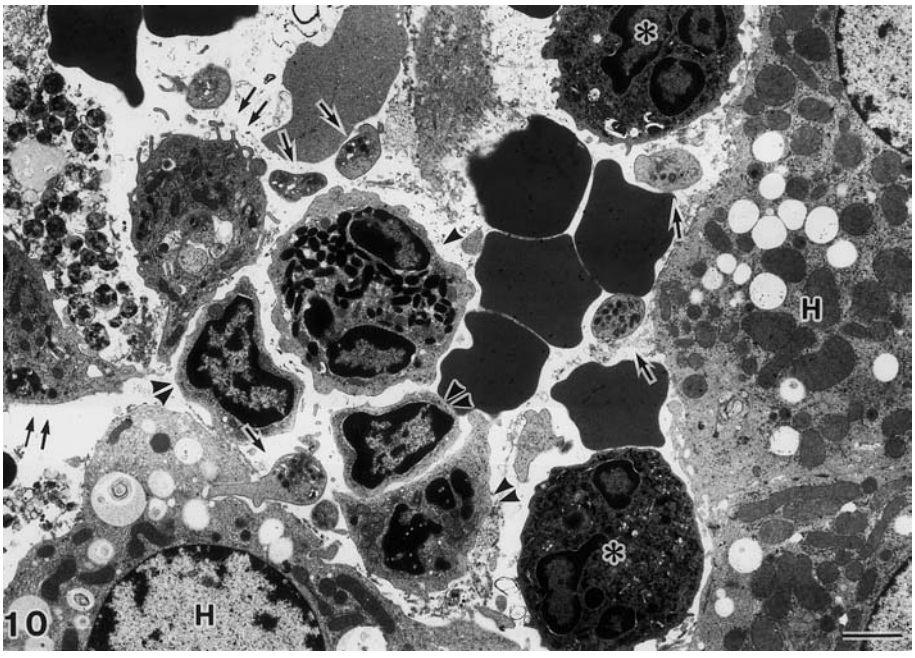



**Fig. 10** At 24 h after DMN injection platelets (*arrows*) and numerous inflammatory cells consisting of macrophages (*double arrows*), neutrophils (*asterisks*), an eosinophil *arrowhead*), and lymphocytes (*double arrowheads*) are identified in the necrotic area. The trabecular arrangement of liver cells and sinusoidal structure is completely lost. Endothelial cells and even HSCs are not present. *H* Hepatocyte; *bar* 2.5 μm

**Table 1** Sequential morphological changes in rat livers and number of BrdU$^+$ cells in preserved parenchyma after a single injection of high-dose DMN; the number of BrdU$^+$ cells is graded as –, +, ++, +++, and ++++, based on the results shown in Figs. 6b and 7b (*ASMA* α-smooth muscle actin, *HSC* hepatic stellate cell, *C-C* central-to-central)

| | Characteristic findings in liver parenchyma | Hepatocytes | ASMA$^+$ HSCs |
|---|---|---|---|
| 6 h | Dilatation of centrilobular sinusoids; frequent occurrence of neutrophils in sinusoids | ± | – |
| 12 h | Appearance of small necrotic foci with infiltration of small macrophages and neutrophils in the centrilobular areas | + | – |
| 24 | More prominent necrosis with more significant infiltration of inflammatory cells than at 12 h | ++ | – |
| 36 h | Development of submassive hemorrhagic necrosis with extension into zones 3 and 2 | ++++ | – |
| 2 days | Massive infiltration of inflammatory cells, predominantly macrophages, in necrotic areas | ++++ | ± |
| 3 days | Appearance of a few HSCs strongly positive ASMA and desmin in preserved parenchyma | ++++ | + |
| 5 days | Considerable removal of tissue debris from necrotic areas; rimming of preserved parenchyma by activated HSCs and their migration into necrotic areas along residual reticular fibers; formation of small erythroblastic islands in liver parenchyma adjacent to necrotic areas | ++++ | ++ |
| 7 days | Diffuse distribution of ASMA$^+$ HSCs along the sinusoids; first signs of fibrosis | ++++ | +++ |
| 10 days | Almost all replacement of postnecrotic space by regenerating hepatocytes and fibrosis; disappearance of erythropoiesis | +++ | ++ |
| 14 days | Formation of C-C bridging fibrosis | ++ | – |

### Ultrastructural finding

After 24 h platelets and various types of inflammatory cells including macrophages, neutrophils, eosinophils, and lymphocytes were seen in the necrotic areas of DMN-treated rat livers (Fig. 10). At 36 h, the most severe time point of necrosis, the sinusoidal structure was completely destroyed, resulting in the loss of the normal topographical relationship of sinusoidal cells. Neither HSCs containing fat droplets (quiescent HSCs) nor activated HSCs with myofibroblastic transformation were found in the necrotic areas. However, on day 5 occasional myofibroblasts originating from HSCs were observed in close association with macrophages, at the interface between the preserved liver parenchyma and the necrotic areas. They had well-developed rough endoplasmic reticulum and Golgi complexes in their cytoplasm. Microfilaments ran in bundles in the subplasmalemmal region (Fig. 11). On day 8 myofibroblasts with typical ultrastructural features were frequently seen in the fibrotic areas (Fig. 12).

## Discussion

It is well known that the activation of surviving HSCs in the hepatocyte necrotic areas, i.e., myofibroblastic transformation of HSCs, occurs promptly, irrespective of cause [10, 18]. It is an important initial event in the process of liver fibrosis [10, 18]. Immunohistochemically the quiescent and activated HSCs can be differentiated by the difference in their cytoplasmic staining intensity

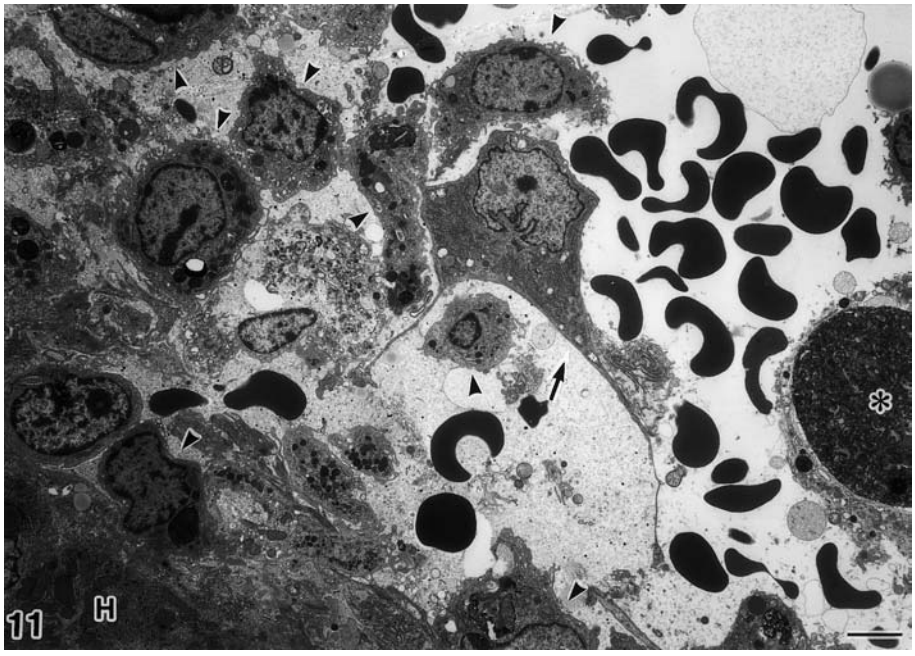



**Fig. 11** On day 5 after DMN injection an activated HSC (*arrow*) with long cytoplasmic processes is seen in the necrotic area adjacent to the preserved liver parenchyma, closely admixed with macrophages (*arrowheads*). A macrophage (*asterisk*) phagocytoses a necrotic liver cell. *H* Hepatocyte; *bar* 5 μm

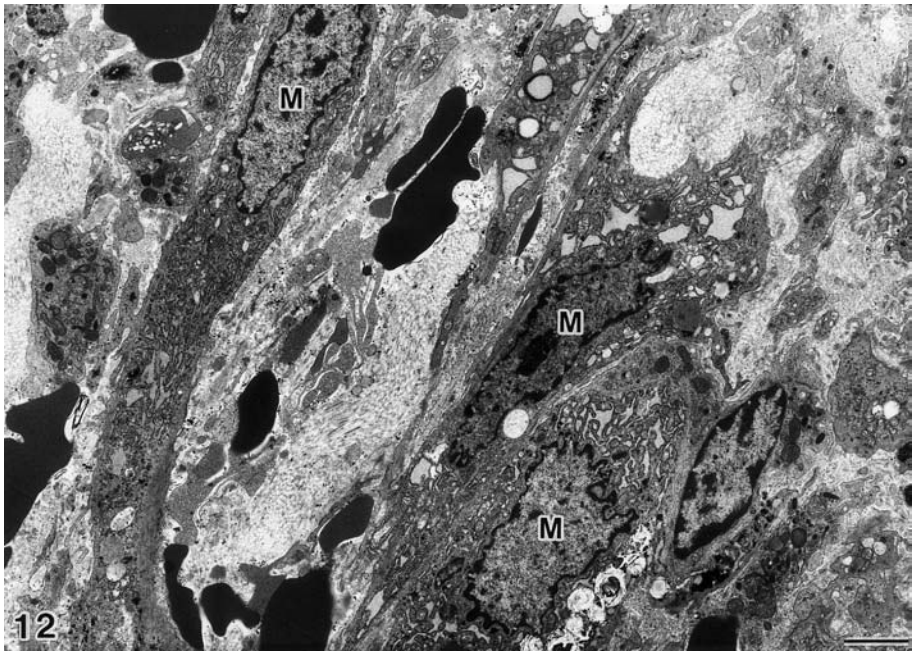



**Fig. 12** On day 8 after DMN injection typical myofibroblasts (*M*) are frequently seen in the fibrotic area; *bar* 2.5 μm

for desmin [2, 20] and ASMA [7, 15, 24]. When HSCs are activated, they become strongly positive for ASMA [7, 15, 24]. In the present study after a single injection of high-dose DMN, the quiescent and activated HSCs were not observed in the submassive hepatocellular necrotic areas. This finding is similar to that of our previous autopsy case of a patient with herpes simplex virus hepatitis [26]. However, it is different from those of human massive and submassive hepatic necrosis [8] and carbon tetrachloride-induced acute liver injury [5, 6] in which HSCs in hepatocyte necrotic areas survive and are promptly activated [5, 6, 8]. The reaction of HSCs in hepatocyte necrotic areas of human and animal livers may depend on the degree and mechanism of liver injuries. When the injury is moderate, HSCs adjacent to necrotic liver cells are rather activated and show a myofibroblastic transformation. However, if the liver injury is severe, HSCs may be destroyed, resulting in cell death. On the other hand, according to Hirata et al. [16], a high dose of DMN caused HSC apoptosis and subsequent endothelial sinusoidal cell degeneration with liver cell necrosis in rat livers, while in the $CCl_4$-induced liver cell necrosis, HSCs and sinusoidal endothelial cells were almost intact. Furthermore, if the metabolite, such as

acetaldehyde in alcohol metabolism, directly stimulates the HSCs, they may be activated without liver cell necrosis [11]. In this study a few HSCs strongly positive for ASMA and desmin occurred in the preserved liver parenchyma on day 3 after DMN treatment. Furthermore, the activated HSCs with a BrdU-positive nucleus are occasionally seen in the parenchyma. Then on day 5 the activated HSCs appeared at the border between the preserved liver parenchyma and necrotic areas. From the border they appeared to migrate into the necrotic area along the residual reticulin fibers. On day 7 after DMN treatment, when the activated HSCs became most numerous, the first sign of fibrosis occurred in the centrilobular areas. However, on day 14, almost all HSCs in the parenchyma became negative for ASMA again. These findings suggest that HSCs in the preserved liver parenchyma may be activated, proliferate, migrate into the necrotic areas, and play a major role in the postnecrotic liver regeneration and fibrosis. When the liver parenchyma regenerates, and the HSCs acquire the normal topographical relationships to liver cells and other types of sinusoidal cells, they may again show the morphological and phenotypical features for quiescent HSCs. Marked differences in the ASMA-immunostaining of HSCs in liver parenchyma between day 7 and day 14 after DMN injection, as shown in Figs. 8 and 9b , suggest the phenotype reversion of HSCs with regeneration. On the other hand, with the healing of liver injuries, the activated HSCs may be deleted by apoptosis [14], such as with the myofibroblasts in the experimental wound healing of the skin [4]

In experimental models of liver injuries induced by repeated injections of DMN [1, 12, 17, 19, 20, 25] or carbon tetrachloride [5, 6, 21], acute and chronic lesions are both present in the same liver. The pathological features are further modified with the adaptation of cells and tissues to repeated injections in the long duration. Our model with its use of a single shot of high-dose DMN, has merit in that we can examine the sequential changes from the necrosis of hepatocytes and HSCs to the regeneration of hepatocytes and the development of fibrosis by activated HSCs.

In conclusion, no HSCs survived in the submassive hemorrhagic necrotic areas after a single injection of high-dose DMN. Afterwards, HSCs in the preserved liver parenchyma were activated, proliferated, and migrated into the necrotic areas. Subsequent replacement of necrotic areas by regenerating hepatocytes and fibrosis may indicate that the activated HSCs play a significant role not only in the remodeling of sinusoidal wall necessary for the regeneration of hepatocytes but also in the formation of C-C bridging fibrosis at the site of the incomplete regeneration.

**Acknowledgements** We gratefully thank Dr. Ituro Ogata, First Department of Internal Medicine, University of Tokyo, for his advice and Mr. Daniel Ribble, Department of English, Kochi Medical School, for English correction of our manuscript. We are also grateful to Mr. Tadatoshi Tokaji, Ms. Hisayo Yamasaki, and Ms. Maya Yamamoto, First Department of Pathology, Kochi Medical School, for their excellent technical assistance. This study was supported in part by a Grant-in-Aid for Scientific Research from the Ministry of Education, Culture, Sports, Science, and Technology in Japan, grant C 13670176 and also supported by the Japan-China Medical Association.

## References

1. Baroni GS, Ambrosio LD, Curto P, Casini A, Mancini R, Jezequel AM, Benedetti A (1996) Interferon Gamma decreases hepatic stellate cell activation and extracellular matrix deposition in rat liver fibrosis. Hepatology 23:1189–1199
2. Burt AD, Bail BL, Balabaud C, Bioulac-Sage P (1993) Morphologic investigation of sinusoidal cells. Semin Liver Dis 13:21–38
3. Carloni V, Romanelli RG, Pinzani M, Laffi G, Gentilini P (1997) Focal adhesion kinase and phospholipase Cγ involvement in adhesion and migration of human hepatic stellate cells. Gastroenterology 112:522–531
4. Darby I, Skalli O, Gabbiani G (1990) α-smooth muscle actin is transiently expressed by myofibroblasts during experimental wound healing. Lab Invest 63:21–29
5. Enzan H (1985) Proliferation of Ito cells (fat-storing cells) in acute carbon tetrachloride liver injury. A light and electron microscopic autoradiographic study. Acta Pathol Jpn 35:1301–1308
6. Enzan H (1987) Protein synthesis in Ito cells (fat-storing cells) of cultured liver tissues from CCl4-treated mice. A light and electron microscopic autoradiographic study. Acta Pathol Jpn 37:225–230
7. Enzan H, Himeno H, Iwamura S, Saibara T, Onishi S, Yamamoto Y, Hara H (1994) Immunohistochemical identification of Ito cells and their myofibroblastic transformation in adult human liver. Virchows Arch 424:249–256
8. Enzan H, Himeno H, Iwamura S, Saibara T, Onishi S, Yamamoto Y, Miyazaki E, Hara H (1995) Sequential changes in human Ito cells and their relation to postnecrotic liver fibrosis in massive and submassive hepatic necrosis. Virchows Arch 426:95–101
9. Enzan H, Hayashi Y, Miyazaki E, Naruse K, Tao R, Kuroda N, Nakayama H, Kiyoku H, Hiroi M, Saibara T (1999) Morphological aspects of hepatic fibrosis and Ito cells (hepatic stellate cells), with special reference to their myofibroblastic transformation. In: Tanikawa K, Ueno T (eds) Liver diseases and hepatic sinusoidal cells. Springer, Berlin Heidelberg New York, pp 219–231
10. Friedman SL (1993) The cellular basis of hepatic fibrosis. Mechanisms and treatment strategies. N Engl J Med 328:1828–1835
11. Friedman SL (1999) Stellate cell activation in alcoholic fibrosis-an overview. Alcohol Clin Exp Res 23:904–910
12. George J, Chandrakasan G (1996) Molecular characteristics of dimethylnitrosamine induced fibrotic liver collagen. Biochim Biophys Acta 1292:215–222
13. Gressner AM (1994) Perisinusoidal lipocytes and fibrogenesis. Gut 35:1331–1333
14. Gressner AM (1998) The cell biology of liver fibrogenesis-an imbalance of proliferation, growth arrest and apoptosis of myofibroblasts. Cell Tissue Res 292:447–452
15. Hautekeete ML, Geerts A (1997) The hepatic stellate (Ito) cell: its role in human liver disease. Virchows Arch 430:195–207
16. Hirata K, Ogata I, Ohta Y, Fujuwara K (1989) Hepatic sinusoidal cell destruction in the development of intravascular coagulation in acute liver failure of rats. J Hepatol 158:157–165
17. Jezequel AM, Ballardini G, Mancini R, Paolucci F, Bianchi FB, Orlandi F (1990) Modulation of extracellular matrix components during dimethylnitrosamine-induced cirrhosis. J Hepatol 11:206–214

18. Maher JJ, McGuire RF (1990) Extracellular matrix gene expression increases preferentially in rat lipocytes and sinusoidal endothelial cells during hepatic fibrosis in vivo. J Clin Invest 86:1641–1648
19. Mancini R, Paolucci F, Baroni GS, Jezequel AM, Orlandi F (1991) Phenotypic analysis of inflammatory infiltrate in rats with dimethylnitrosamine-induced cirrhosis. Int J Exp Pathol 72:119–128
20. Mancini R, Jezequel AM, Benedetti A, Paolucci F, Trozzi L, Orlandi F (1992) Quantitative analysis of proliferating sinusoidal cells in dimethylnitrosamine-induced cirrhosis – an immunohistochemical study. J Hepatol 15:361–366
21. Milani S, Herbst H, Schuppan D, Hahn EG, Stein H (1989) In situ hybridization for procollagen types I, III, and IV mRNA in normal and fibrotic rat liver: evidence for predominant expression in nonparenchymal liver cells. Hepatology 10:84–92
22. Olaso E, Friedman SL (1998) Molecular regulation of hepatic fibrogenesis. J Hepatol 29:836–847
23. Oyaizu T, Shikata N, Senzaki H, Matsuzawa A, Tsubura A (1997) Studies on the mechanism of dimethylnitrosamine-induced acute liver injury in mice. Exp Toxicol Pathol 49:375–380
24. Pinzani M (1995) Novel insights into the biology and physiology of the Ito cell. Pharmacol Ther 66:387–412
25. Shimizu I, Ma Y-R, Mizobuchi Y, Liu F, Miura T, Nakai Y, Yasuda M, Shiba M, Horie T, Amagaya S, Kawada N, Hori H, Ito S (1999) Effects of sho-saiko-to, a Japanese herbal medicine, on hepatic fibrosis in rats. Hepatology 29:149–160
26. Toi M, Kuroda N, Tao L, Jin Y, Guo L, Miyazaki E, Hayashi Y, Hiroi M, Komatsu N, Nakata H, Ogata K, Enzan H (2001) Adult-onset herpes simplex virus hepatitis with diffuse myofibroblastic transformation of hepatic stellate cells (Ito cells) in non-necrotic areas. Pathol Int 51:288–292

Virchows Arch (2003) 442:48–55
DOI 10.1007/s00428-002-0715-9

ORIGINAL ARTICLE

**Alexander Klaus · Raimund Margreiter**
**Heinz Pernthaler · Günther Klima · Felix A. Offner**

# Diffuse mesenterial sclerosis: a characteristic feature of chronic small-bowel allograft rejection

Received: 5 June 2002 / Accepted: 4 September 2002 / Published online: 10 October 2002
© Springer-Verlag 2002

**Abstract** Chronic rejection is the major cause of late intestinal allograft dysfunction. The aim of this study was to analyze in detail the histopathological features of chronic rejection in the ACI-to-Lewis rat model of intestinal transplantation. Chronic rejection was achieved in orthotopic small-bowel allografts (ACI–Lewis) by limited immunosuppression with cyclosporin A (CyA). Isogeneic transplants (ACI–ACI) as well as native bowels (ACI) with and without immunosuppression served as controls. Bowels were removed together with the mesenteries 90 days postoperatively and analyzed using sections stained with hematoxylin and eosin as well as Masson's trichrome. The slides were coded, randomized and analyzed by grading of histological abnormalities. The most striking alterations of the allografts were noticed in the mesenteries exhibiting an extensive infiltration by mononuclear cells accompanied by a progressive diffuse fibrosis with shrinking of the mesenteries. These changes were most pronounced in the perivascular areas of the mesenteric arteriae and venae rectae. Three of five allografts showed vasculitis with myointimal proliferation of the arteriae rectae. Focally, there was spillover of the inflammatory cells onto the intestinal muscularis propria. The mucosa of the allografts showed mild blunting, lymphocytic infiltration of the crypt epithelium and increased crypt cell apoptoses. The submucosa was unaffected, and there were no detectable abnormalities of the enteric ganglion cells. The present data support the view that chronic rejection of intestinal allografts is characterized by a diffuse sclerosing mesenteritis which may significantly contribute to late graft dysfunction. The present model may be useful to study the pathomechanisms of this inflammatory fibrosing process.

**Keywords** Small-bowel transplantation · Chronic rejection · Mesenteritis

A. Klaus
Department of General Surgery, University of Innsbruck, Innsbruck, Austria

R. Margreiter (✉)
Department of Transplant Surgery, University of Innsbruck, Anichstrasse 35, 6020 Innsbruck, Austria
e-mail: raimund.margreiter@uibk.ac.at
Tel.: +43-0512-5042601, Fax: +43-0512-5042602

H. Pernthaler
Department of General Surgery, General Hospital of the Province of Bozen, Bozen, Italy

G. Klima
Department of Histology, University of Innsbruck, Innsbruck, Austria

F.A. Offner
Department of Pathology, Academic Teaching Hospital Feldkirch, Feldkirch, Austria

## Introduction

It is known from clinical experience that in most instances acute rejection episodes can be prevented or controlled by immunosuppressants currently in use. By contrast, chronic rejection processes have become the predominant cause of late dysfunction and eventual loss of allografts [1, 5, 20, 29]. Recent improvements in immunosuppression have renewed enthusiasm for intestinal transplantation. The application of new potent immunosuppressive drugs has made small-bowel transplantation clinically feasible for an increasing number of patients [1, 25]. Nevertheless, persistent postoperative alterations in gastrointestinal motility and chronic rejection remain major concerns [1, 5, 25].

Although the sequence of the histological changes of acute intestinal allograft rejection is well defined [7, 10, 15, 17, 18, 19, 31], comparatively little is known about the histopathology of chronic rejection of the small bowel [16, 24]. Heeckt and coworkers have shown that during chronic rejection, rat small-bowel allografts develop a significant hypertrophy of the muscularis externa [8].

Consequently, several other studies have focused on the abnormalities of the muscularis externa and more recently also on alterations of the intrinsic intestinal nervous system as potential causes of graft dysfunction [9, 26, 27]. However, much less attention has been paid to other changes, in particular, changes of the mesenteries.

We have recently used the rat ACI–Lewis model of chronic small–bowel allograft rejection to study rejection-associated alterations of the myoelectric activity [12]. In the present study we report on our observations of the histopathological alterations occurring in this model.

## Materials and methods

### Animals

Male ACI and Lewis rats weighing 200–220 g were used as donors and recipients and were purchased from Harlan-Sprague Dawley (Bochum, Germany). The animals were maintained on a 12-h/12-h light/dark cycle and were fed with commercially available rat-chow diet and tap water ad libitum conforming to the NIH guidelines as well as specific national laws.

### Operative procedure

Operations were performed under ether anesthesia as described previously [22]. One-step orthotopic small-bowel transplantation was carried out. Graft vessels were anastomosed to the infrarenal aorta and vena cava using microsurgical techniques. The graft was interposed in an end-to-end fashion below the ligament of Treitz after removal of the recipient's jejunoileum. The animal's general state of health (appearance, posture, feeding, and activity) was assessed daily. Body weight was measured daily for the first postoperative week and weekly thereafter.

### Experimental groups

- Group 1 ($n$=5): native gut of untreated male ACI rats.
- Group 2 ($n$=6): syngeneic orthotopic small-bowel transplantation (SBTx) was performed from ACI–ACI animals to evaluate the effect of the transplant procedure.
- Group 3 ($n$=5): ACI rats given cyclosporin A (CyA) at a dosage as described below.
- Group 4 ($n$=7): allogeneic orthotopic SBTx was carried out from ACI–Lewis rats to investigate the effects of chronic rejection.

All animals in groups 3 and 4 received CyA intramuscularly at a dosage of 15 mg/kg daily from day 0 to day 6 and every other day from day 7 to day 28. Thereafter, immunosuppression was discontinued. All animals were sacrificed on postoperative day 90 with an overdose of ether, and the grafts were removed together with the mesenteries for gross inspection and histology.

### Histopathological analyses

The entire graft including the mesentery was fixed in 4% buffered formalin for 2 days. Seven intestinal cross sections taken at 2- to 3-cm intervals together with the adherent mesentery were then embedded in paraffin. Three 4-μm serial sections per intestinal cross section were stained with hematoxylin and eosin as well as Masson's trichrome stain. All microscopic slides were examined by a gastrointestinal pathologist (F.A.O.), who was blinded to the grouping. All histopathological abnormalities were graded.

Infiltration of the mesentery by inflammatory cells was quantified: grade 0 was used for a normal mesentery; grade 1 was used for a mild increase in inflammatory cells; grade 2 indicated a pronounced and patchy infiltrate; and grade 3 a diffuse and dense infiltration of the entire mesentery. For each mesentery notation was also made of which cell types, mononuclear cells or granulocytes, were dominant in terms of total inflammatory infiltration. Fibrosis of the mesentery was assessed on trichrome-stained slides. Grade 0 was normal and grades 1 and 2 were used for a mild to moderate degree of fibrosis. Vasculitis of mesenterial arteries and veins was classified as either present (grade 1) or absent (grade 0). Spill-over of mononuclear cell infiltration of the muscularis externa was also graded as either present (grade 1) or absent (grade 0).

The mucosal architecture was graded as being preserved (grade 0) or disturbed (grade 1). Intraepithelial lymphocytes (IEL) were graded on a scale from 0 to 2. Grade 0 represented normal; grade 1 indicated a mild increase in IEL; and grade 2 was used for a dense infiltration of the epithelium by lymphocytes. For epithelial apoptoses, a grade 1 was used for a mild increase beyond what is normally present; grade 2 represented a significant increase in apoptotic bodies. The number of ganglion cells of the plexus myentericus was counted in three different cross sections per bowel and is expressed as the mean number of ganglion cells per cross section.

### Data analysis

Data were compiled as mean±standard error of the mean. Data were statistically analyzed with a coded Chi-square X test. A probability of $<0.05$ was accepted as significant.

## Results

### General observations

Three animals died because of bleeding or peritonitis due to a breakdown of the small-bowel anastomosis. These deaths (one animal from group 2 and two animals from group 4) were excluded from this study. All other animals appeared to be healthy throughout the study period. They ate normally, had regular bowel movements and were free of clinical signs of rejection. Native control animals (group 1) showed a continuous increase in body weight during the observation period. By contrast, animals undergoing syngeneic or allogeneic bowel transplantation (groups 2 and 4) as well as non-transplanted animals receiving CyA (group 3) showed an initial weight loss, which was most pronounced in the allogeneic group (Fig. 1). However, in allografted animals, a rapid recovery and increase in body weight was noted between day 14 and day 50. After this period the weight gain in this group of animals was less pronounced. Animals in groups 2 and 3 showed a continuous but slightly slower increase in body weight.

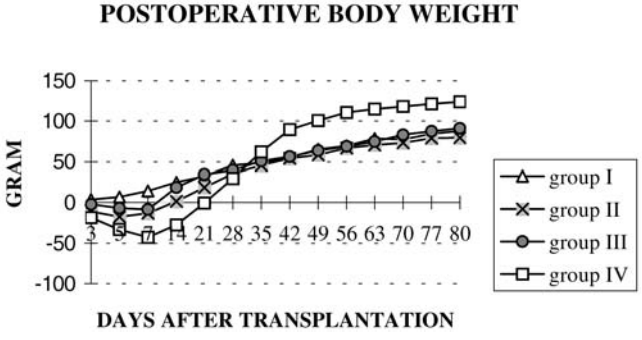



**Fig. 1** Summary of postoperative body weight. The body weights of the different experimental groups are depicted. The initial postoperative weight loss in allografted animals was followed by a rapid increase in body weight during postoperative days 14–50. Thereafter these animals showed a slight decline of their growth curve

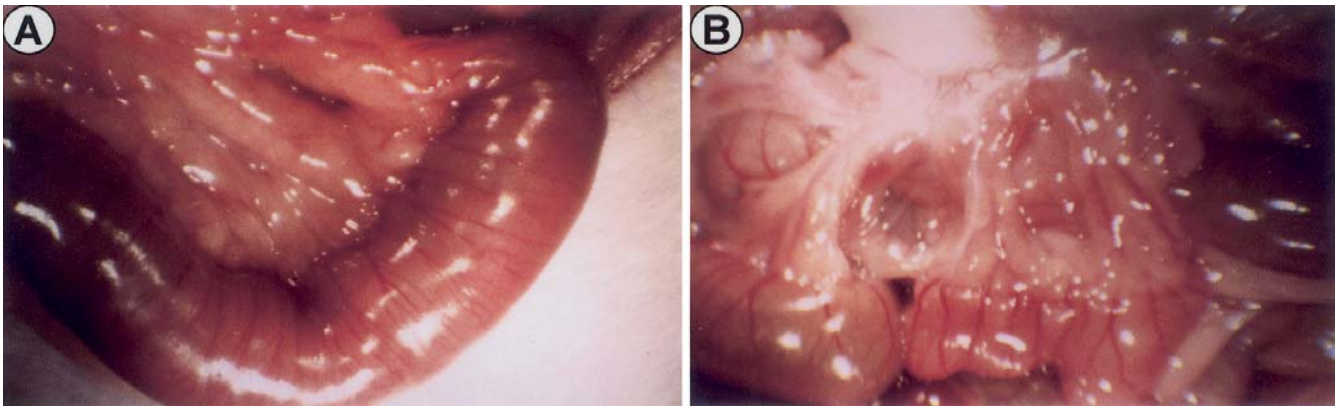



**Fig. 2** Macroscopy of chronically rejected grafts at sacrifice. **a** Allografts were frequently dilated and filled with feces. The bowel wall was thickened and stiff. **b** Grafts with an extensive mesenterial sclerosis showed a characteristic milky whitish mesenteric surface, and swollen lymph nodes of an allograft

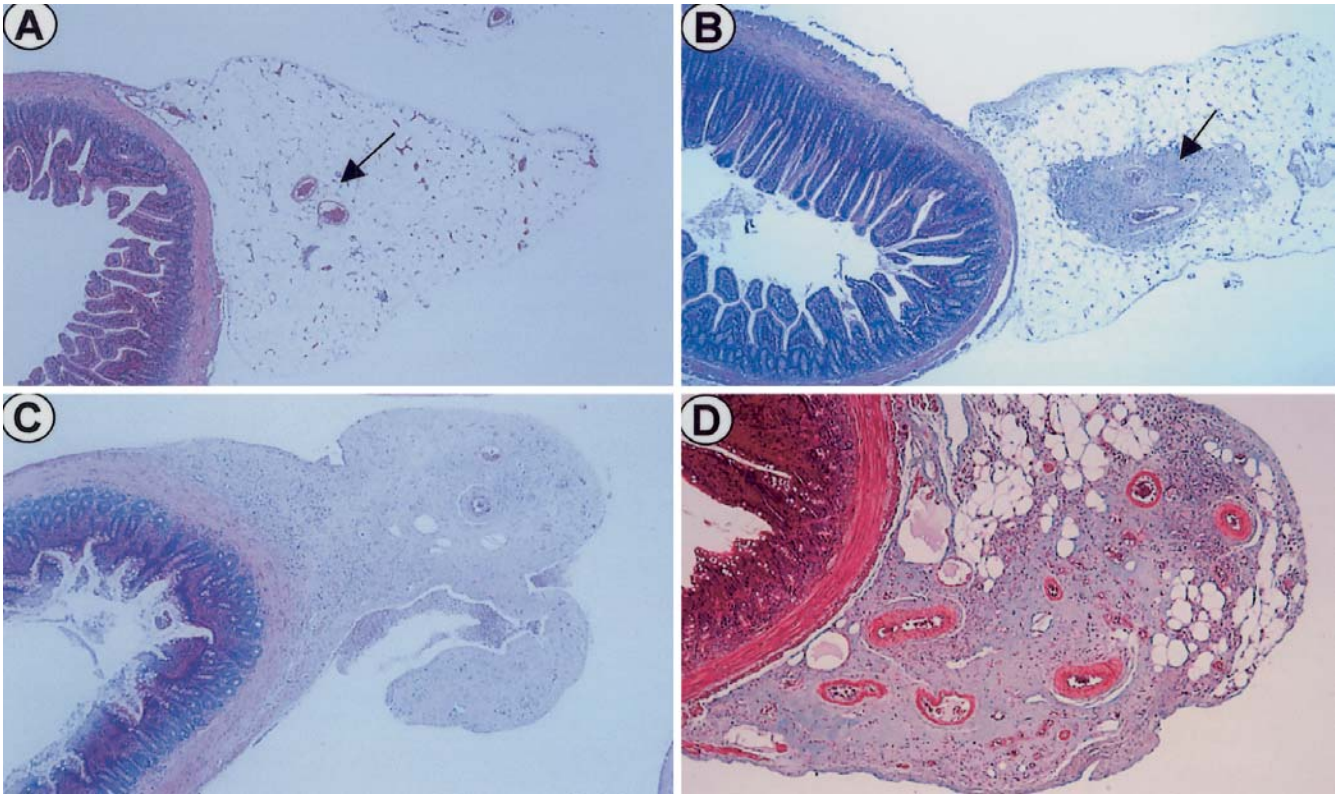



**Fig. 3** Mesenterial alterations in small-bowel allograft rejection-I (×20). **a** Low-power view of a mesenterial cross section of a control animal. Note the branch of an arteria recta with an accompanying vein. The vessels are embedded in normal fatty tissue. **b** Inflammatory cell infiltration of the immediate vicinity of the arteriae rectae and accompanying veins in a mesentery of an allograft (*arrow*). **c** Diffuse mononuclear cell infiltration of the whole diameter of the mesentery in chronic rejection. **d** Masson's trichrome stains revealed marked fibrosis of the allograft mesenteries

## Macroscopic abnormalities

On postoperative day 90, the grafts undergoing chronic rejection (group 4) showed grossly visible abnormalities. They were dilated, often entirely filled with feces and the bowel wall appeared thickened and stiff with some peritoneal adhesions. Marked abnormalities were noticed on inspection of the mesenteries. They showed a milky whitish surface, appeared fibrotic and there was a mild to moderate shortening when compared with control animals (Fig. 2a, b). The lymph nodes of these mesenteries were enlarged, whereas the Peyer's patches appeared scarred. Native bowels and isogeneic transplants had a normal appearance.

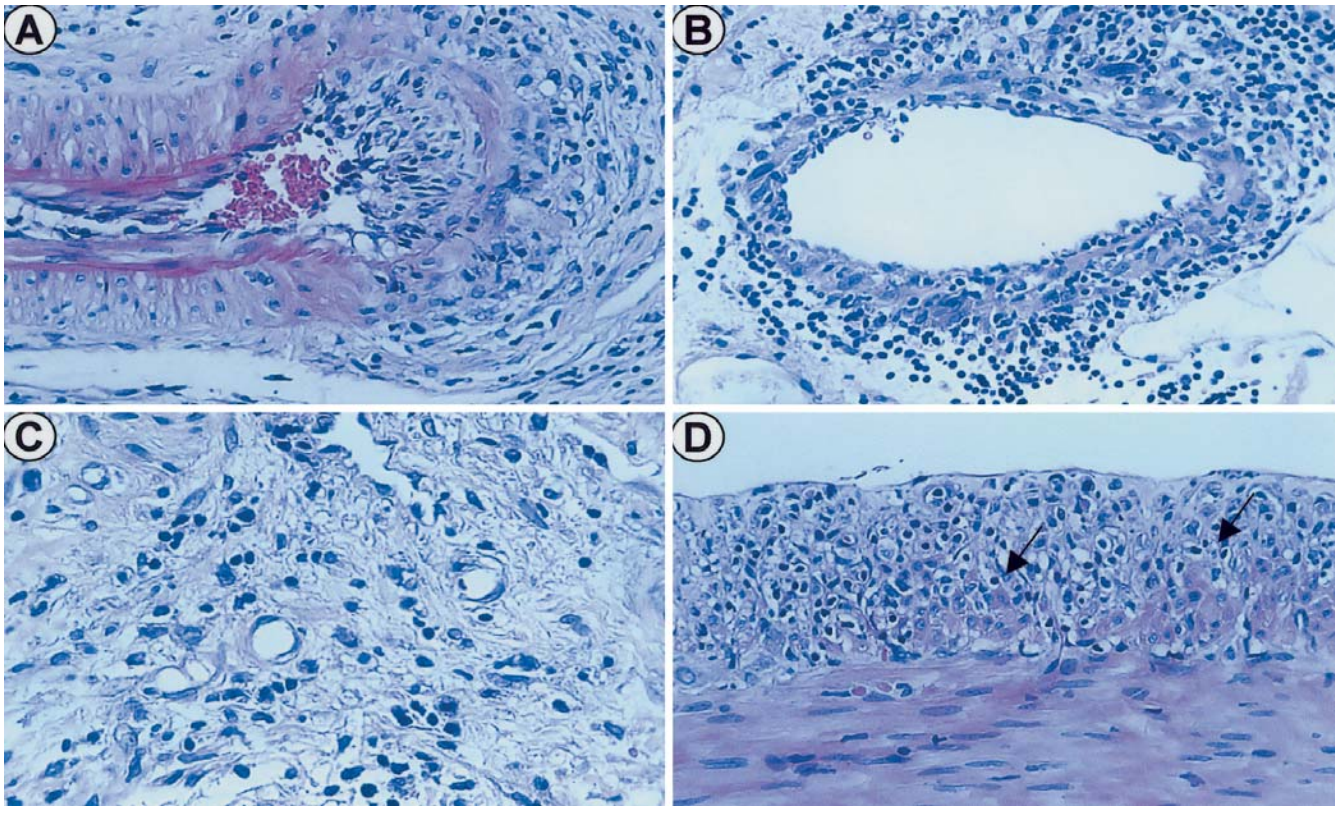



**Fig. 4** Mesenterial alterations in small-bowel allograft rejection-II (×200). **a** Vasculitis of an arteria recta with myointimal proliferation. Mononuclear cells invade the vascular wall. **b** Mild vasculitic abnormalities of mesenterial venous vessels. **c** High-power view of the mesenterial mononuclear cell infiltrate. **d** "Spill-over" of the mononuclear cellular infiltrate onto the outer layer of the muscularis propria. *Arrows* depict residual muscle cells

**Table 1** Scoring of histopathological alterations in chronic intestinal allograft rejection. The number (*n*) of animals with their respective histological grade are depicted. *SD* standard deviation, *NS* not significant, *CyA* cyclosporin A

| Group | *n* | Mesenterial inflammation *n*/grade | Mesenterial arterial vasculitis *n*/grade | Mesenterial venous vasculitis *n*/grade | Mesenterial fibrosis *n*/grade | Cellular infiltration of the muscularis propria *n*/grade | Myenteric ganglion cells mean±SD | Mucosal architecture *n*/grade | Intra-epithelial lymphocytes *n*/grade | Epithelial apoptotic bodies *n*/grade |
|---|---|---|---|---|---|---|---|---|---|---|
| 1 (Native controls) | 5 | 1/0<br>4/1* | 5/0 | 5/0 | 5/0 | 4/0<br>1/1 | 42.4±5.2 | 5/0 | 5/0 | 4/0<br>1/1 |
| 2 (Syngeneic SBTx) | 5 | 0/0<br>4/1*<br>1/2* | 5/0 | 5/0 | 5/0 | 3/0<br>2/1 | 42.5±5 | 5/0 | 5/0 | 5/0 |
| 3 (Native controls+CyA) | 5 | 0/0<br>5/1* | 5/0 | 5/0 | 5/0 | 4/0<br>1/1 | 43.6±4.4 | 5/0 | 5/0 | 5/0 |
| 4 (Allogeneic SBTx+CyA) | 5 | 0/0<br>0/1<br>5/2 | 2/0<br>1/1<br>2/2 | 2/0<br>1/2<br>2/2 | 0/0<br>3/1<br>2/2 | 0/0<br>5/1<br>0/2 | 44±5.3 | 0/0<br>5/1 | 0/0<br>2/1<br>3/2<br>0/3 | 0/0<br>0/1<br>3/2<br>2/2 |
| *P* value | | *P*<0.008 | *P*<0.003 | *P*<0.003 | *P*<0.003 | *P*<0.05 | NS | *P*<0.003 | *P*<0.003 | *P*<0.008 |

* Mixed predominantly granulocytic infiltration

## Histopathological findings

Histopathological analysis revealed distinctive abnormalities of the allografts. The detailed histological grading of the specimens is summarized in Table 1. The most pronounced changes were noticed within the mesenteries of the allografts. These were characterized by an infiltration by mononuclear cells and a progressive fibrosis with replacement of the mesenterial fat cells. In three animals the mesenteries seemed to be affected by this process in

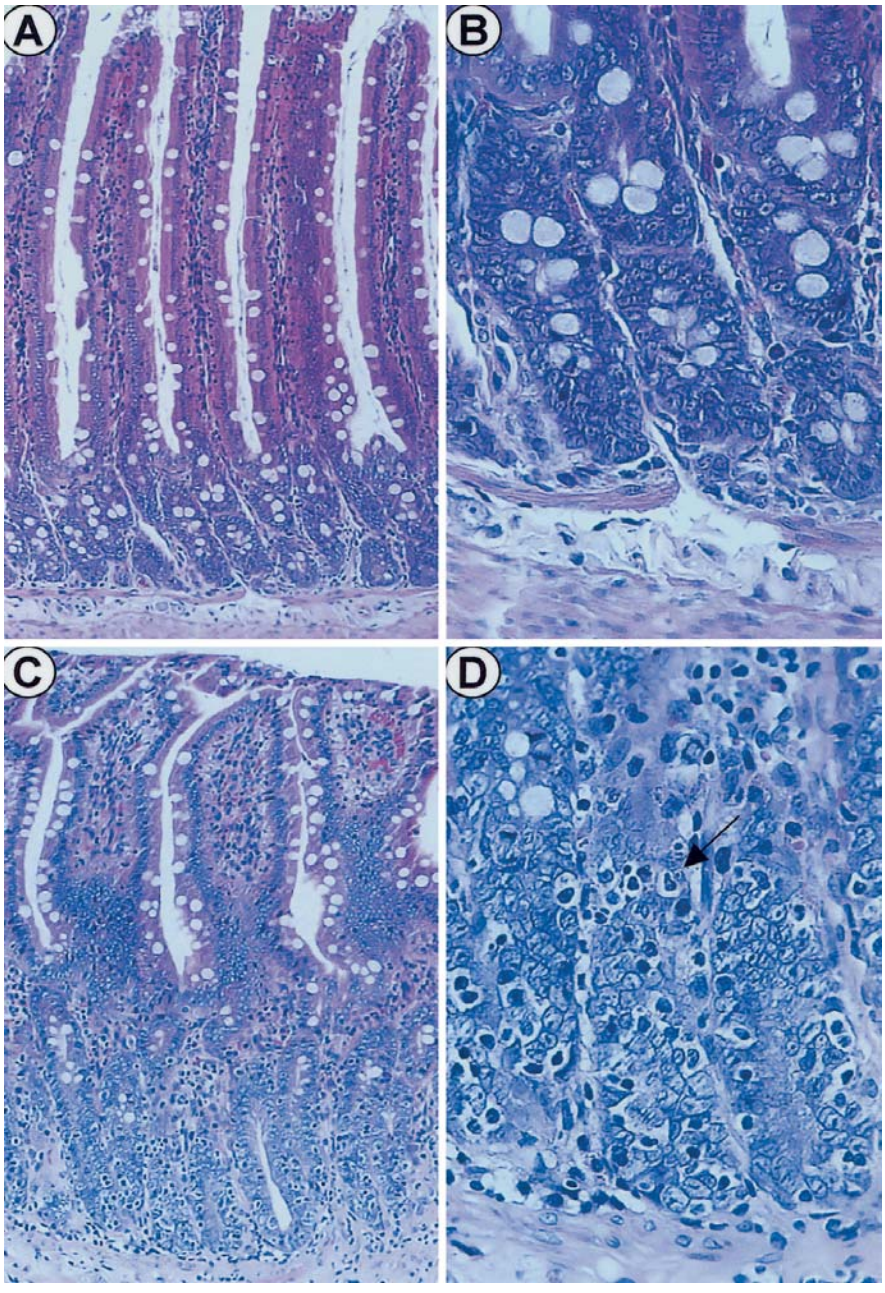



**Fig. 5** Mucosal alterations in small-bowel allograft rejection (×100). **a** Low-power view of the villous architecture in control animals (group 1, ×200). **b** The crypt epithelium of control animals showed only occasional intraepithelial lymphocytes (IEL) (×100). **c** Mild to moderate villous blunting of the mucosa in chronic allograft rejection (group 4). **d** There was an increase of IEL within the crypt epithelium and an increase of epithelial apoptoses (*arrow*) (×200)

a patchy fashion (grade 2: $n$=3). In some cross sections of these bowels, the mononuclear cell infiltration appeared to involve only the immediate vicinity of the major branches of the mesenteric vessels, i.e., the arteriae and venae rectae (Fig. 3a, b) but was more diffusely developed in other cross sections. In two allografts, however, we observed a diffuse infiltration by mononuclear cells which affected almost the whole mesentery (Fig. 3c). This mesenterial inflammation was closely associated with a progressive fibrosis. In some cross sections we noticed an almost complete replacement of the fat cells by collagenous tissue as highlighted by trichrome-stains (Fig. 3d). In three of the allografts there was also a focal intimal arteritis of the branches of the arteriae rectae (Fig. 4a). All of these arteries already showed myointimal proliferation. Three of the five allografts also exhibited mild inflammatory infiltration of venous vessels (Fig. 4b). In all allografted animals there was focal spill-over of mesenterial mononuclear inflammatory cells onto the lamina externa of the muscularis propria (Fig. 4c, d).

In the control groups the mesenteric tissue showed only patchy unspecific inflammation, predominantly by neutrophilic granulocytes. None of these control animals exhibited vasculitic changes or a fibrosis of the mesenterial tissue.

The mucosa was graded as being abnormal in all allografts showing mild to moderate villous blunting and a significant increase in IEL (grade 1 $n$=2; grade 2 $n$=3; Fig. 5c, d). Lymphocytic infiltration was exclusively no-

ticed within the epithelium of crypts with sparing of the epithelium of the villi. The increase in IEL was closely associated with epithelial injury, which became evident as a significant increase in epithelial apoptotic bodies (grade 1 $n$=2; grade 2 $n$=3; Fig. 5a–d). Adjacent epithelial cells showed reactive/regenerative changes with enlarged vesicular nuclei and loss of polarity. No abnormalities were detectable in the submucosal layer. Furthermore, there was no vasculitis of either mucosal or submucosal vessels.

In the control groups the architecture of the mucosa was normal in all animals (Fig. 5a, b). None of the control specimens exhibited an increase in IEL. One control animal (group 1) was graded as having a mild increase in apoptotic bodies.

Analysis of ganglion cells did not reveal significant numerical differences when comparing the plexus intermyentericus in allografts and controls (Table 1), and there were no morphological abnormalities of the ganglion cells.

## Discussion

Small-bowel transplantation has become an alternative to total parenteral nutrition for the treatment of intestinal failure. Although the surgical technique of small-bowel transplantation is well established, it is frequently complicated by rejection and/or sepsis, and the optimal immunosuppression protocol has not yet been identified [1, 6, 11, 20, 25]. During the past decade, experimental research has mainly focused on the control of acute rejection and graft-versus-host disease, the latter playing only a minor role in the clinical setting. Newer immunosuppressive agents have led to a remarkable improvement in short-term results. Chronic rejection, however, has remained a significant problem in the long-term success of clinical transplantation, not only of the bowel but also of all other organs [4, 5].

The model of orthotopic small-bowel transplantation using the ACI-to-Lewis rat strain combination was established by Heeckt et al. [8]. Using this strain combination they have shown that limited CyA immunosuppression leads to subclinical chronic rejection.

Indeed, also in our study the clinical condition of the animals at the time of sacrifice appeared to be good. However, chronic rejection altered the gross and microscopic aspect of the intestinal transplants. The graft intestines appeared thickened and rigid, and the mesenteries were shortened and fibrotic with a milky whitish surface. These findings correlated with histopathological abnormalities, and it is suggestive that these combined structural changes may have led to the functional impairment of the allografts. The latter was reflected by the dilatation of the grafts which were often filled with feces over the entire length as well as by our functional studies showing that the fasting motility of the rejected allografts revealed distinctive abnormalities [12].

Even though several studies vary with respect to the surgical technique, strain combination, and biopsy techniques used, a significant muscular hypertrophy was reported in various models of chronic intestinal allograft rejection [1, 4, 8, 16, 17, 24, 26, 28]. Indeed, also in our study the intestinal smooth muscle cells of the muscularis propria showed a tendency to hypertrophy. However, we did not evaluate this muscular thickening in detail because, in the present study, the intestinal muscle layers were not relaxed prior to fixation. Therefore, a considerable error due to different contractile states of the tissue was expected.

Recent studies have demonstrated that chronic rejection may also cause damage of the intrinsic nervous system with loss of enteric neurons and subsequent impairment of neuromuscular transmission [9, 26]. In contrast to these reports we could not find evidence of ganglion cell injury in our allografts. The reason for this discrepancy is currently not understood. One possible explanation may be that different stages of the process of chronic rejection were evaluated. However, interestingly in study of resected human intestinal allografts Noguchi and coworker did not find a loss of ganglion cells but a prominent hypertrophy of neural elements [21]. The significance of these discrepant observations requires further investigations.

Compared with descriptions of the structural alterations of the allograft intestines, much less attention has been paid to the allograft mesenteries in chronic rejection. The most striking changes in our study were observed within the mesenteries. They exhibited the features of a sclerosing mesenteritis with a diffuse inflammatory infiltration by mononuclear cells and a concomitant fibrosis with progressive replacement of the mesenterial fatty tissue. Interestingly, this inflammatory infiltration of the mesentery seems to begin in the immediate vicinity of the mesenteric arteriae rectae before spreading to the whole diameter of the mesentery. The cause for this remarkable zonal distribution is currently unclear but may be related to injury of the mesenteric vessels. Intimal arteritis and a mild vasculitis of mesenterial veins were in fact observed in our model and did primarily involve the mesenterial arteriae and venae rectae. All affected arteries showed myointimal proliferation as evidence of chronic injury. The mesenteric vasculitis may lead to ischemia-induced structural alterations of the intestinal wall with consecutive mucosal injury. Mucosal ischemia may therefore be an important marker to suspect vasculitis of the mesenterial vessels.

The progressive fibrosis of the mesenteries may be another important cause of consecutive injury to the allograft intestines. It is suggestive that shrinking and contraction of the mesenteries may lead to a compensatory hyperactivity of the intestinal musculature resulting in muscular hypertrophy. The underlying pathomechanisms of the mesenterial fibrosis are currently unclear but may involve the action of the inducers of fibrosis like transforming growth factor-β1 (TGF-β1) and basic fibroblast

growth factor (bFGF) [13, 14]. Interestingly, we have recently shown that the peritoneum may be a particularly rich source of both fibrogenic cytokines [3, 23]. An analysis of the expression of TGF-β1 and bFGF in the present model is currently under investigation.

In all allografts there was a patchy mononuclear infiltration of the lamina externa of the muscularis propria. It is likely that this represents spill-over of inflammatory cells from the mesentery and may possibly also contribute to the ultimate failure of bowel function.

Mucosal alterations associated with chronic rejection have been controversially discussed. Heeckt and coworkers did not describe alterations of the mucosa [8, 9]. Others found mucosal inflammation, apoptosis and cryptitis which is in accordance with our findings [30]. It may be possible that these changes are partly mediated by mild concurrent acute rejection episodes. Whether this mucosal injury may contribute to insufficient resorption and bowel dysfunction remains to be defined. However, these distinctive mucosal abnormalities may be helpful for the diagnosis for chronic rejection.

In summary, we have shown that chronic rejection in the ACI–Lewis model of intestinal transplantation causes significant morphological alterations of both the allograft intestines and mesenteries. The majority of publications about the histopathology of experimental chronic intestinal allograft rejection has focused on structural abnormalities of the intestinal wall and – with a few exceptions – neglected the alterations of the allograft mesenteries [8, 9, 16, 26, 27]. Up to now, a few more than 300 intestinal transplantations have been performed worldwide in humans, and there exists only limited information on the pathology of chronic rejection in resected graft specimens [2]. However, these few morphologic descriptions point to alterations of the mesenteries which are similar to the changes described in the present study [5, 17, 21]. The present model may thus be useful to discover new insights into the pathomechanisms of rejection-associated diffuse sclerosing mesenteritis.

## References


1. Abu-Elmagd K, Reyes J, Bond G, Mazariegos G, Wu T, Murase N, Sindhi R, Martin D, Colangelo J, Zak M, Janson D, Ezzelarab M, Dvorchik I, Parizhskaya M, Deutsch M, Demetris A, Fung J, Starzl TE (2001) Clinical intestinal transplantation: a decade of experience at a single center. Ann Surg 234:404–416
2. Beath SV (1999) Small bowel transplantation. Indian J Pediatr 66:71–74
3. Cronauer M, Stadlmann S, Klocker H, Abendstein B, Eder IE, Rogatsch H, Zeimet AG, Marth C, Offner FA (1999) Basic fibroblast growth factor synthesis by human peritoneal mesothelial cells-induction by interleukin-1. Am J Pathol 155:1977–1984
4. de Bruin RWF, Stein-Oakley AN, Kouwenhoven EA, Maguire JA, Jablonski P, Jin XJ, Doqling J, Thomson NM (2000) Functional, histological, and inflammatory changes in chronically rejecting small bowel transplants. Transpl Int 13:1–11
5. Demetris AJ, Murase N, Lee RG, Randhawa P, Zeevi A, Pham S, Duquesnoy R, Fung JJ, Starzl TE (1997) Chronic rejection. A general overview of histopathology and pathophysiology with emphasis on liver, heart and intestinal allografts. Ann Transplant 2:27–44
6. Finn L, Reyes J, Bueno J, Yunis E (1998) Epstein-Barr virus infections in children after tranplantation of the small intestine. Am J Surg Pathol 22:299–309
7. Gurakar A, Fagiuoli S, Hassanein T, Wright HI, Balkan M, Frezza E, Todo S, Starzl TE, Van Thiel DH (1994) Is rejection a diffuse or localized process in small bowel transplantation. Surg Endosc 8:762–764
8. Heeckt PF, Halfter WM, Schraut WH, Lee KKW, Bauer AJ (1993) Small bowel transplantation and chronic rejection alter rat smooth muscle structure and function. Surgery 114:449–457
9. Heeckt PF, Halfter W, Schraut WH, Bauer AJ (1997) Chronic rejection causes early destruction of the intrinsic nervous system in rat transplants. Am J Physiol 273:413–421
10. Hernandez M, Sanchez JJ, Jara J, Del Castillo D (1995) Small bowel transplantation: structural changes in absorption failure. Transplant Proc 27:2360–2362
11. Iyer KR, Srinath C, Horslen S, Fox IJ, Shaw BW, Sudan DL, Langnas AN (2002) Late graft loss and long-term outcome after isolated intestinal transplantation in children. J Pediatr Surg 37:151
12. Klaus A, Klima G, Margreiter R, Pernthaler H (2002) Myoelectric activity during chronic small bowel allograft rejection in rats. Dig Dis Sci (in press)
13. Kouwenhoven EA, Stein-Oakley AN, Jablonski P, de Bruin RW, Thomson NM (1999) EGF and TGF-beta-1 gene expression in chronically rejecting small bowel transplants. Dig Dis Sci 44:1117
14. Kouwenhoven EA, Stein-Oakley AN, Jablonski P, de Bruin RW, Thomson NM (1999) Upregulation of basic fibroblast growth factor during chronic intestinal rejection. Transplant Proc 31:590
15. Kuusanmaki P, Halttunen J, Paavonen T, Pakarinen M, Luukkonen P, Häry P (1994) Acute rejection of porcine small bowel allograft. Transplantation 58:757–763
16. Langrehr JM, Banner B, Lee KKW, Schraut WH (1993) Clinical course, morphology, and treatment of chronically rejecting small bowel allografts. Transplantation 55:242–250
17. Lee RG, Nakamura K, Tsamandas AC, Abu-elmagd K, Furukawa H, Hutson WR, Reyes J, Minguillan-Tabasco JS, Todo S, Demetris AJ (1996) Pathology of human intestinal transplantation. Gastroenterology 110:1820–1834
18. Monchik GJ, Russel PS (1971) Transplantation of small bowel in the rat: technical and immunological considerations. Surgery 70:693
19. Morrissey PE, Gollin G, Marks WH (1996) Small bowel allograft rejection detected by serum intestinal fatty acid-binding protein is reversible. Transplantation 61:1451–1455
20. Niv Y, Mor E, Tzakis AG (1999) Small bowel transplantation a clinical review. Am J Gastroenterol 94:3126–3130
21. Noguchi Si S, Reyes J, Mazariegos GV, Parizhskaya M, Jaffe R (2002) Pediatric intestinal transplantation: the resected allograft. Pediatr Dev Pathol 5:3–21
22. Pernthaler H, Kreczy A, Plattner R, Pfurtscheller G, Saltuari L, Schmid T, Öfner D, Klima G, Margreiter R (1994) Myoelectric activity during small bowel allograft rejection. Dig Dis Sci 39:1216–1221
23. Offner FA, Feichtinger H, Obrist P, Marth C, Klingler P, Grage B, Schmahl M, Knabbe C (1996) Transforming growth factor-β synthesis by human peritoneal mesothelial cells-induction by interleukin-1. Am J Pathol 148:1679–1688
24. Su GL, Walgenbach KJ, Heeckt PH, Wang Q, Halfter W, Whiteside TL, Bauer AJ (1996) Increased expression of interferon-γ in a rat model of chronic intestinal allograft rejection. Transplantation 62:242–248
25. Sudan DL, Kaufman SS, Shaw BWJr, Fox IJ, McCashland TM, Schafer DF, Radio SJ, Hinrichs SH, Vanderhoof JA, Langnas AN (2000) Isolated intestinal transplantation for intestinal failure. Am J Gastroenterol 95:1506–1515

26. Sugitani A, Reynolds JC, Nomoto M, Starzl TE, Todo S (1996) Intestinal neurons in acute and chronic rejection after small bowel transplantation in dogs. Transplant Proc 28:2543
27. Sugitani A, Bauer AJ, Reynolds JC, Halfter WM, Nomoto M, Starzl TE, Todo S (1997) The effect of small bowel transplantation on the morphology and physiology of intestinal muscle. Transplantation 63:186–194
28. Timmermann W, Gasser M, Meyer D, Kellersmann R, Gassel HJ, Ott C, Thiede A (1999) Progress in experimental intestinal transplantation in small animal models. Acta Gastroenterol Belg 62:216–220
29. Tinley NL, Whitley WD, Diamond JR, Kupiec-Weglinski JW, Adams DH (1991) Chronic rejection – an undefined conundrum. Transplantation 52:389–398
30. Vennarecci G, Berho M, Sommariva A, Neto AB, Misiakos EP, Inverardi L, Ruiz P, Ricordi C, Tzakis AG (2001) Apoptosis and rejection in rat intestinal transplantation: correlation with FK506 doses and donor specific bone marrow infusions. Transplantation 71:1718–1724
31. White FV, Reyes J, Jaffe R, Yunis EJ (1995) Pathology of intestinal transplantation in children. Am J Surg Pathol 19:687–698

Virchows Arch (2003) 442:56–65
DOI 10.1007/s00428-002-0720-z

ORIGINAL ARTICLE

**A. Schmiedl · H.-G. Hoymann · M. Ochs**
**A. Menke · A. Fehrenbach · N. Krug · T. Tschernig**
**J. M. Hohlfeld**

# Increase of inactive intra-alveolar surfactant subtypes in lungs of asthmatic Brown Norway rats

Received: 31 October 2001 / Accepted: 26 August 2002 / Published online: 22 November 2002
© Springer-Verlag 2002

**Abstract** We tested the hypothesis whether allergic airway inflammation in ovalbumin sensitized and challenged Brown Norway rats is associated with intrinsic surfactant alteration and dysfunction. The determination of intra-alveolar surfactant subtypes and alveolar edema within their original microenvironment is only possible using an ultrastructural stereological approach. Therefore both lungs of control and asthmatic rats were fixed by vascular perfusion. The volume fractions of surfactant subtypes and the epithelial surface fraction covered with alveolar edema were determined by point and intersection counting. Furthermore, lung resistance was measured by means of whole-body plethysmography. The surface activity of surfactant from bronchoalveolar lavage was determined as minimum surface tension at minimal bubble size with a pulsating bubble surfactometer. Compared with controls, in asthmatics (1) the fraction of inactive unilamellar forms was significantly increased from 56% to 66%, (2) the fraction of alveolar epithelium covered with alveolar edema visible by light microscopy was significantly increased from 0.7% to 5.0%, (3) the fraction of alveolar epithelium covered with fluid seen by electron microscopy expanded significantly from 5% to 21%, (4) lung resistance was significantly elevated from 14% to 86% and (5) surface tension was enhanced from 6 mN/m to 12 mN/m. Thus, the inflammatory process after allergen challenge of sensitized Brown Norway rats causes intra-alveolar surfactant alterations. These surfactant alterations might contribute to small airway dysfunction.

**Keywords** Rat · Lung · Asthma-induction · Surfactant · Stereology

A. Schmiedl (✉) · T. Tschernig
Department of Anatomy, Medical School of Hannover,
Carl-Neuberg-Straße 1, 30625 Hannover, Germany
e-mail: Schmiedl.Andreas@MH-Hannover.de

J.M. Hohlfeld
Department of Respiratory Medicine,
Medical School of Hannover, Carl-Neuberg-Straße 1,
30625 Hannover, Germany

H.-G. Hoymann · A. Menke · N. Krug · J.M. Hohlfeld
Fraunhofer Institute of Toxicology and Aerosol Research,
Drug Research and Clinical Inhalation, Nikolai-Fuchs-Straße 1,
30625 Hannover, Germany

A. Schmiedl · M. Ochs · A. Fehrenbach
Department of Anatomy, Division of Electron Microscopy,
University of Göttingen, Kreuzbergring 36, 37075 Göttingen,
Germany

## Introduction

Pulmonary surfactant covers the air–liquid interface inside the alveoli and small conducting airways [4, 12, 13, 14, 34]. This highly surface-active complex of phospholipids and proteins prevents alveolar collapse during exhalation and supports inspiratory opening and expansion of alveoli [8, 16, 34].

Alveolar surfactant harvested from the air spaces by bronchoalveolar lavage (BAL) consists of approximately 90% lipids, predominantly phospholipids, and 10% proteins including the surfactant apoproteins SP-A, SP-B, SP-C and SP-D [39]. From intra-alveolar surfactant collected by BAL, two subfractions can be obtained: surface-active heavy forms termed large aggregates (LAs) and surface-inactive light forms termed small aggregates (SAs) [36, 38]. Electron microscopic investigations revealed that the LAs mainly contain tubular myelin and lamellar body-like forms and that SAs consist of unilamellar vesicles [31, 38]. Alterations in surface activity are reflected by an increased SA/LA ratio [18, 25, 38].

The intracellular surfactant pool is represented by the lamellar bodies in the type-II pneumocytes of the alveolar epithelium which synthesize, secrete and recycle pulmonary surfactant [41]. The lamellar bodies of this cell type serve as storage organelles for the lipid components and particularly the hydrophobe surfactant proteins SP-B and SP-C [39, 41].

An intact pulmonary surfactant system is the prerequisite for normal respiratory functions [1, 6, 16, 34]. Surfactant abnormalities have been found in various diseases, such as acute respiratory distress syndrome (ARDS),

pneumonia, cardiogenic lung edema [16, 25] or after ischemia/reperfusion lung injury [10, 25, 30]. Furthermore, there is increasing evidence that surfactant dysfunction also occurs in asthmatics. Recent studies have shown that surface activity evaluated as minimum surface tension of surfactant isolated from BAL fluid was significantly reduced after allergen challenge both in animal models of asthma [26, 28] and in patients with asthma [20, 22]. Also, sputum of patients with acute asthma exhibited reduced surfactant activity [24].

Surfactant located in the small conducting airways is predominantly derived from alveolar sources [15, 16]. Because the conventional BAL studies provide no information about the original localization and microorganization of the intra-alveolar surfactant, we used an electron-microscopic and stereologic approach to determine the distribution of the different intra-alveolar surfactant subtypes in asthmatic lungs. We tested the hypothesis that surfactant dysfunctions are associated with intrinsic alveolar surfactant alterations in ovalbumin-sensitized and -challenged Brown Norway rats.

## Materials and methods

Thirty male Brown Norway rats (mean weight 260 g) were kept under specific pathogen-free conditions and had ad libitum access to food and water. The animals were separated into two groups. Fifteen rats served as controls without any sensitization for functional ($n$=12) and electron microscopic ($n$=3) studies. The other group was used for asthma induction.

### Asthma model

The rats were sensitized and challenged according to the asthma model for Brown Norway rats [33]. Briefly, sensitization was performed with 1 mg ovalbumin and 190 mg $Al(OH)_3$ in 1 ml 0.9% NaCl solution, applied subcutaneously, and with $5\times10^9$ heat-killed Bortedella pertussis bacilli (kindly donated by Chiron Behring, Marburg, Germany) in 0.4 ml 0.9% NaCl solution, given intraperitoneally (i.p.). The sensitization was repeated 6–7 days later. After another 6–7 days an airway challenge was carried out with an aerosol of 5% ovalbumin/saline solution (0.25 l/min). To this end, Brown Norway rats were placed in a Plexiglas tube for 15 min. A flexible latex mask was placed over the nose and connected to a nebulizer (Pariboy; Ritzau, Starnberg, Germany). Respiratory function variables were measured by means of whole-body plethysmography during challenge ($n$=12). Twenty-four hours later, the challenged rats were either used to obtain BAL fluid ($n$=12) or dissected for electron microscopic evaluation ($n$=3).

### In situ perfusion fixation

Brown Norway rats were anaesthetized with ether and i.p. pentobarbital-Na (Narcoren, 1 mg/kg body weight). After heparinization and intubation by tracheotomy, the rats were ventilated with a tidal volume of 5 ml and a respiration rate of 30–40 breaths per minute [10]. The positive-end expiratory pressure (PEEP) was adjusted using a liquid column to 3 cm $H_2O$ to prevent alveolar collapse during expiration. After thoracotomy, the pericardial cavity was opened, and a cannula was pushed forward into the pulmonal artery via the right ventricle. The cannula was connected to a reservoir containing perfusion solutions. Perfusion was started with Krebs-Henseleit buffer containing 0.25 g/100 ml procaine-HCl (19–25 ml in 30–60 s). The left atrium was opened for volume relief. Immediately after preperfusion, ventilation was stopped, the airway pressure was adjusted to 10 cm $H_2O$ and perfusion fixation was carried out with the fixation solution (1.5% glutaraldehyde and 1.5% paraformaldehyde in 0.15 M hydroxyethylpiperazine ethanesulfonic acid buffer; total osmolarity of 800 mosmol/l, vehicle osmolality of 300 mosmol/kg at pH 7.35). Perfusion of both solutions was carried out with hydrostatic pressure at 20 cm $H_2O$. The slightly hypertonic fixation solution prevents artificial development of edema [3]. After the end of perfusion fixation the trachea was tightened, and the heart-lung block was excised. The heart–lung block was immersed in cold fixative for 24 h before further processing. Before processing into tissue slices, absolute volumes of the fixed right and left single lung were determined by fluid displacement according to Scherle [32].

### Sampling

The standard sampling methods used were in accordance with those described by other authors [7, 9, 11, 17, 29]. After separation into the right and left single lung, each lung was embedded in 2% aqueous agar. Afterwards, the organ was cut from apical to caudal into parallel slices with a thickness of 3 mm using a tissue slicer. The position of the first cut was chosen at random between 0 mm and 3 mm [9]. Normally eight to ten slices were obtained per single lung. The organ slices were put in a processing tray with the apical section looking up. Starting with a random number, slices were alternately taken for light and for electron microscopy. Doing so, we normally obtained four to five slices for light and four to five slices for electron microscopy from each single lung. For systematic uniform random sampling of tissue blocks for electron microscopy, a transparent point grid with 11×11 points, each at a distance of 10 mm, was superimposed at random orientation over the collection of remaining slices [9]. Parts of the lung slices touched by a point were excised and cut into a tissue block with a size of 1–2 $mm^3$ [9]. Doing so, five to eight blocks were obtained from each single lung. This systematic uniform random sampling method guaranteed to obtain specimens which were representative of the whole organ [9, 10, 11, 30].

### Tissue processing

The further processing of specimens was carried out as described [9, 10, 30]. Briefly, after repeatedly rinsing in 0.1 M cacodylate buffer, tissue blocks were osmicated for 2 h in 1% $OsO_4$ in 0.1 M cacodylate buffer and rinsed again in 0.1 M cacodylate buffer repeatedly (six changes during 60 min). After twice rinsing in distilled water, specimens were stained en bloc overnight (12–18 h) at 4–8ºC with a mixture of equal portions of uranyl-acetate and water [(half-saturated aqueous uranyl acetate solution (1:1)]. After dehydration through an ascending series of alcohols (70%, 96%, 100%), whole tissue slices were embedded in a methacrylate resin (Technovit 7100; Kulzer, Heraeus, Germany). Sections of 1.5-µm thickness were stained with hematoxylin and eosin and used for quantitative light microscopic studies.

For ultrastructural analysis, specimens were dehydrated in an ascending series of acetone (70%, 90%, 100%) and embedded in araldite [9]. Ultra-thin sections (70 nm) were cut from five to eight blocks of each single lung and stained with lead citrate and uralyl acetetate in an ultrostainer (Leica, Bensheim, Germany). Qualitative and stereological analyses were carried out by means of a Leitz Laborlux 11 (Leitz, Wetzlar, Germany) and an EM 900 (Leo, Oberkochen, Germany).

### Stereological analysis

#### *Sampling*

*Light microscopy.* Systematic uniform random test-fields of view were obtained using the x- and y-axis of the microscope stage micrometers. Starting at a random position outside the section, e.g.

the upper left side, the microscope stage was moved at fixed intervals along both axes until the whole section was examined [9].

*Electron microscopy.* For scanning the ultra-thin sections we used the systematic quadrates subsampling method to generate test fields over the whole section [29]. Again, starting at a random position outside of the section, test fields were selected by moving the microscope stage at fixed intervals. Within the fluorescent screen, the square describing the dimensions for micrographs represents a potential quadrate. If the latter hit the regions of interest (septa, surfactant), then it was subsampled [29] Thus, each area of the section had the same chance of being evaluated [29].

## Stereological parameters

All stereologic parameters were determined by point and intersection counting [40]. Light microscopically, the fraction of lung parenchyma (Vv parenchyma/lung) and lung non-parenchyma (Vv non-parenchyma/lung) was determined by using an ocular integrated 100-point lattice test system (Integrationsplatte, Zeiss, Oberkochen, Germany). Furthermore, intra-alveolar edema was evaluated on-line (camera connected with a computer) at a final magnification of ×800.

Electron microscopic stereology for analysis of surfactant subtypes and intra-alveolar fluid accumulation was carried out on-line (CCD camera, CF 8, Kappa Messtechnik GmbH, Gleichen, Germany, connected with a computer) using an image analysis software package (AnalySIS 2.1; Soft Imaging System, Münster, Germany) at a final magnification of ×18,000.

### *Determination of alveolar fluid accumulation*

The preservation of intra-alveolar edematous fluid containing proteins in low concentrations is only possible during fixation by vascular perfusion provided that the protein concentration of the alveolar fluid is high enough to be fixed [2, 3]. To get information about increased fluid accumulation leading to intra-alveolar edema, we evaluated the epithelial surface covered with alveolar fluid ($I_I$epi-edema/epi-total) on-line by light and electron microscopy according to Velazquez et al. [37]. Therefore, we determined the surface fraction of alveolar epithelium covered with visible alveolar fluid using a coherent multipurpose test system with 48 test lines (Fig. 1b). The intersections with epithelium covered with fluid [I(epi-edema)] and without fluid [I(epi-without edema)] were counted. The intersections with epithelium covered with fluid [I(epi-edema)] were related to the total number of intersections with alveolar epithelium [I(epi-total)] composed of intersections with epithelium covered with fluid [I(epi-edema)] and without fluid [I(epi-without edema)].

The following formula was used:

$$I_I(\text{epi}-\text{edema}/\text{epi}-\text{total}) - \sum I(\text{epi}-\text{edema}) / I(\text{epi}-\text{edema}) + I(\text{epi}-\text{without edema}) \times 100$$

### *Determination of edema of the air–blood barrier*

To get information about edematous swelling of the air–blood barrier, the arithmetic mean barrier thickness ($\tau$) of the air–blood barrier was determined by point and intersection counting according to Weibel [40]. $\tau$ is defined as the distance from the superficial cell membrane of the alveolar epithelium to the luminal cell membrane of the capillary endothelium and is therefore a measure of barrier thickness [40]. $\tau$ was determined by counting the number of end points of the test lines lying on the air–blood barrier and the number of intersections of these lines with the internal and external boundaries of the barrier and computed by the following equation: $\tau = z \times p/2 \times (n_I + n_E)$, whereat z= length of the test line, p= number of endpoints falling onto the barrier, $n_I$=internal boundary, $n_E$= external boundary.

### *Determination of intra-alveolar surfactant*

The examination by electron microscopy revealed the different surfactant subtypes located in the hypophase (Fig. 1c). Tubular myelin, lamellar body-like forms and the surface film are regarded as active forms reducing the surface tension [31, 36]. Tubular myelin is a lattice-like arrangement of phospholipids (Fig. 1c). Lamellar body-like forms (lamellar body-like) with numerous more or less concentric, partly fused and not clearly separated lamellae resemble intracellular lamellar bodies (Fig. 1c). The surface layer is partly discontinuous or missing (Fig. 1c) because of disruption due to contact with aqueous solutions during fixation and rinsing [13]. Multilamellar vesicles (multilamellar, Fig. 1c) are characterized by several concentrically arranged phospholipid lamellae, which are clearly separated. The inactive surfactant forms are represented by unilamellar vesicles (unilamellar, Fig. 1c) which are surrounded by one phopholipid lamella and differ in size. The relative intra-alveolar surfactant composition was evaluated on-line by determination of the volume densities of the different surfactant subtypes related to total intra-alveolar surfactant ($V_V$ subtype/surf) [10, 30] using a multipurpose test system (Fig. 1d). The total intra-alveolar surfactant encompases points falling of all surfactant subtypes ($\Sigma P_{surf} = \Sigma P_{tubular\ myelin} + P_{lamellar\ body\ like} + P_{multilamellar} + P_{unilamellar}$). The relative subtype fractions were obtained using the following formula:

$$Vv\text{subtype}/\text{surf} = \sum P_{\text{subtype}} / \sum P_{\text{surf}} \times 100.$$

Doing so, the following volume densities were determined: $V_V$ tubular myelin/surf, $V_V$ lamellar body-like/surf, $V_V$ multilamellar/surf and $V_V$ unilamellar/surf.

The surface film at the air–liquid interphase could not be determined as volume density because of its two-dimensional nature. The total amount of intra-alveolar surfactant visible by transmission electron microscopy is very small. After careful perfusion fixation, not more than 13% of the epithelial surface fraction is covered with surfactant [30]. So, test fields exhibit a great variability of surfactant content. Therefore in a section of one tissue block, between 200 and 500 test fields with parenchyma were considered. From each single lung of one animal, four to eight tissue blocks were evaluated to guarantee that surfactant subtypes were hit by at least 200 points per animal [17]. In order to test the variability introduced by the stereological approach used for determination of surfactant, the coefficient of error (CE) for ratios was determined according to Kroustrup and Gundersen [23].

After determination of lung volume ($V_{lung}$) according to Scherle [32] and volume densities of lung parenchyma ($V_V$ parenchyma/lung), the absolute volumes for intra-alveolar surfactant were evaluated according to the following formula:

$$V_{\text{subtype}} = V_v\text{subtype}/\text{surf} \times V_v\ \text{parenchyma}/\text{lung} \times V_{\text{lung}}$$

## Pulmonary function

Lung resistance ($R_L$) was measured in intubated, spontaneously breathing rats. Brown Norway rats were anaesthetized with 2% halothane/30% oxygen and placed in a whole-body plethysmograph after oral intubation with a tracheal cannula (Cathlon; Jelco Raritan, N.J. USA; 52 mm, 1.78-mm inner diameter). Respiratory function variables were measured during spontaneous tidal breath-

**Fig. 1** **a** Light microscopy (resin section) of lung parenchyma of an asthmatic Brown Norway rat. Alveoli exhibit more or less pronounced liquid accumulation. The alveolar epithelium is partly covered with edematous fluid (*arrows*, primary magnification ×400). **b** Part of the multipurpose test-system (48 test lines with *circle*) used for determination of intra-alveolar fluid accumulation (×17,500.) **c** Different subtypes of intra-alveolar surfactant. *tm* tubular myelin, *lbl* lamellar body-like structure, *mlv* multilamellar vesicle, *ulv* unilamellar vesicle (×31,500). **d** Multipurpose test system (352 test points) used for determination of volume densities of intra-alveolar surfactant subtypes (×17,500)

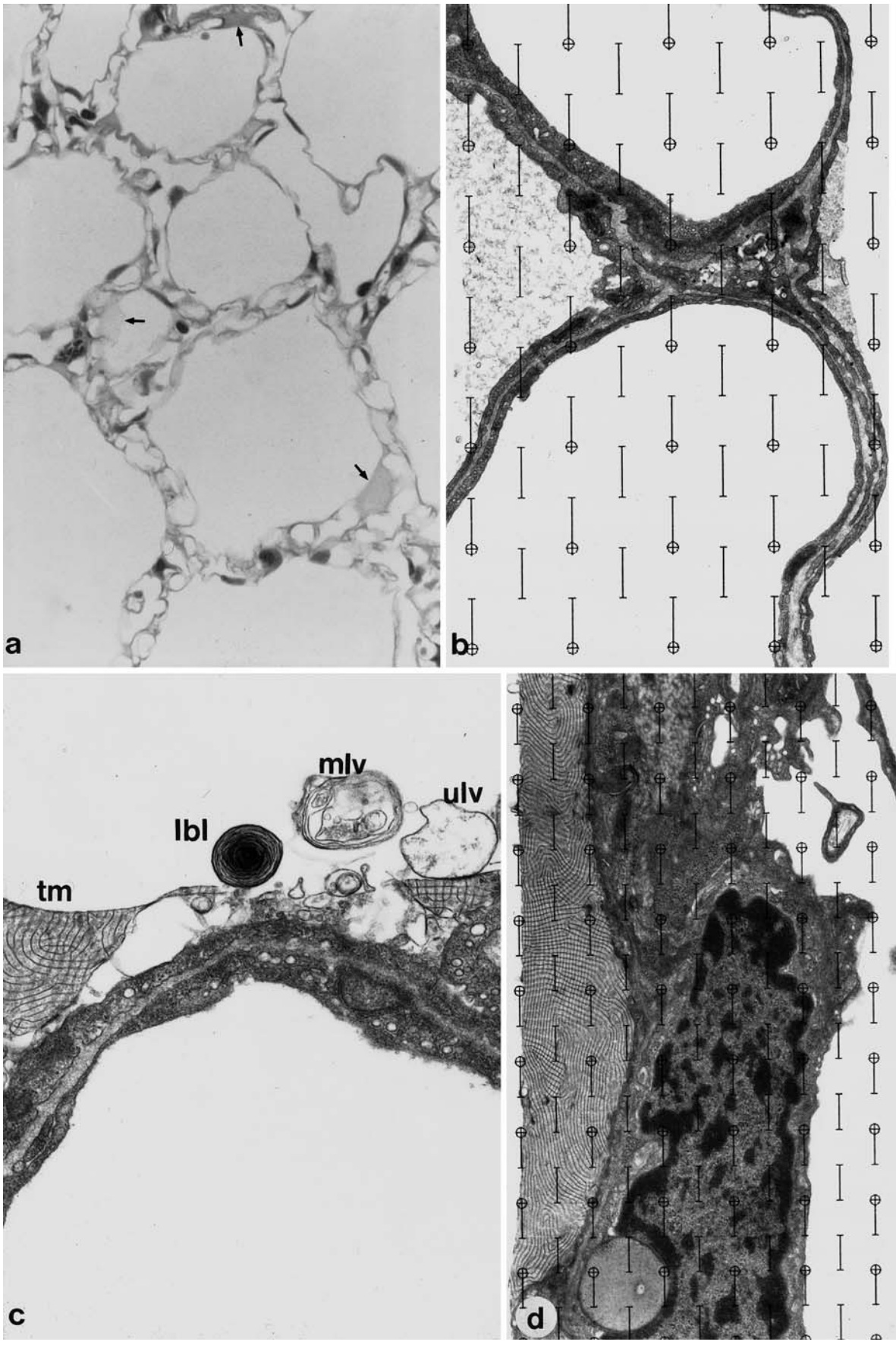

a
b
c
mlv
ulv
lbl
tm
d

**Table 1** Relative surface of alveolar epithelium associated with proteinaceous fluid and swelling of the air–blood barrier. In the asthmatic lungs, a significantly higher fraction of the alveolar epithelium is covered with proteinaceous fluid. The air–blood barrier (τ) shows no significant swelling. Values are given as means±SEM

| Experimental groups | Epithelial fraction covered with fluid [(Σ I(epi-edema)/I(epi-total) ×100)] [%] | | Barrier thickness (τ) [μm] |
|---|---|---|---|
| | Visible by light microscopy | Visible by electron microscopy | |
| Controls (*n*=3) | 0.7±0.1 | 5.0±1.8 | 1.21±0.06 |
| Asthmatics (*n*=3) | 5.0±0.9 | 20.9±2.0 | 1.32±0.08 |
| 1-Way ANOVA on ranks | *P*<0.04 | *P*<0.05 | n.s. |

**Table 2** Relative intra-alveolar surfactant composition in lungs of control and asthmatic rats. Volume fraction ($V_V$) of intra-alveolar surfactant subtypes as percentage of total intra-alveolar surfactant (surf).The fraction of inactive unilamellar forms is significantly higher in asthmatics than in controls. Values are given as means±SEM

| Experimental groups | $V_V$ lamellar body-like/surf (%) | $V_V$ tubular myelin/surf (%) | $V_V$ unilamellar/surf (%) | $V_V$ multilamellar/surf (%) |
|---|---|---|---|---|
| Controls (*n*=3) | 2.9±0.6 | 22.6±2.8 | 55.6±0.6 | 18.9±2.3 |
| Asthmatics (*n*=3) | 1.8±0.5 | 18.2±1.1 | 65.6±3.0 | 14.4±1.3 |
| 1-Way ANOVA on ranks | n.s. | n.s. | *P*<0.03 | n.s. |

ing throughout the allergen challenge. Total box pressure was measured with a differential pressure transducer, and airflow was determined with a pneumograph. $R_L$ was calculated as total box pressure divided by airflow. Results are presented as percentage changes in $R_L$ after challenge relative to baseline values.

### Surfactant activity measurements

BAL was carried out with warm saline solution in five 5-ml aliquots. After instillation, each aliquot was aspirated with gentle suction. The BAL fluid was pooled, and the recovered volume was recorded. The lavage fluid was filtered through sterile gauze and then centrifuged at 250×*g* for 10 min to get a cell-free supernatant. Subsequent high-speed centrifugation (48000×*g* for 60 min) was carried out to pellet the surfactant material which was then resuspended at 1 mg/ml.

The surface tension of the isolated surfactant was determined with a pulsating bubble surfactometer [8, 18]. Surface tension was calculated at minimal bubble size ($y_{min}$) registered after 5 min of pulsation at a rate of 20 cycles/min from the known pressure gradient across bubble surface and the bubble radius according to the law of Laplace [8]. Surface activity was stated as minimum surface tension.

The animal experiments were authorized by the local government and conformed to the Guide for the Care and Use of Laboratory Animals (NIH publication no. 85–23, revised 1996).

### Statistics

Differences of the stereological parameters between the two groups were tested for significance by the nonparametric Kruskal-Wallis 1-Way ANOVA on Ranks test. Differences in functional parameters were tested with the *t*-test. Mean values were given as ±SEM; *P*<0.05. All statistical analyses were performed using the Sigma Stat 2.0 and Sigma Plot 3.0 software programs (Jandel Scientific, Erkrath, Germany).

## Results

### Examination by light microscopy

In the hematoxylin and eosin stained methacrylate sections, edematous regions were recognized as pink-stained layers. While the lumina of the bronchi and bronchioli rarely exhibited edematous fluid in asthmatic and control lungs, peribronchovascular edema in the non-cartilaginous distal narrow airways was found more frequently in asthmatic lungs. In addition, alveolar epithelium of asthmatic lungs was more frequently covered with intra-alveolar edema fluid (Fig. 1a). Stereological examination showed a significant difference in the surface fraction covered with edematous fluid in controls and asthmatics (Table 1).

### Examination by electron microscopy

Pronounced proteinaceous fluid accumulation in the intra-alveolar hypophase was visible as flocculent electron scattering material. In asthmatics a significantly larger fraction of alveolar epithelium was covered with fluid (Fig. 3c, d; Table 1).

In both groups the lumina of some bronchioli contained different surfactant subtypes between the cilia of the ciliated bronchiolar epithelium (Fig. 2a, b). The alveolar region showed intact type-I and type-II pneumocytes without increased thickness of the air–blood barrier (Fig. 2c, Table 1). The lamellar bodies, intracellular surfactant storage

**Fig. 2** Ultrastructure of the epithelium of non-cartilaginous narrow airways and alveoli in the asthmatic lung (×12,600). **a** Tubular myelin (*arrowhead*) is visible between longitudinally and transversely sectioned cilia (×6000). **b** In some regions barely recognizable proteinaceous fluid is located in the hypophase (*arrow*) between the cilia. Inactive surfactant subtypes (*arrowhead*) and active tubular myelin (tm) are seen (×22,700). **c** Intact alveolar epithelium with type-I and type-II pneumocytes lines the alveoli in some areas. No alveolar edema is seen. Capillaries are free of plasma or blood as a result of perfusion fixation. The parts of the air–blood barrier are not thickened (×8100). **d** Intracellular and intra-alveolar surfactant pool. Lamellar bodies in type-II pneumocytes exhibit the typical lamellar structure. In the alveolar space different active and inactive subtypes of surfactant are distinguishable [(*tm* tubular myelin, *lbl* lamellar body-like structures, unilamellar vesicles (*arrowhead*)] (×12,600) ▶

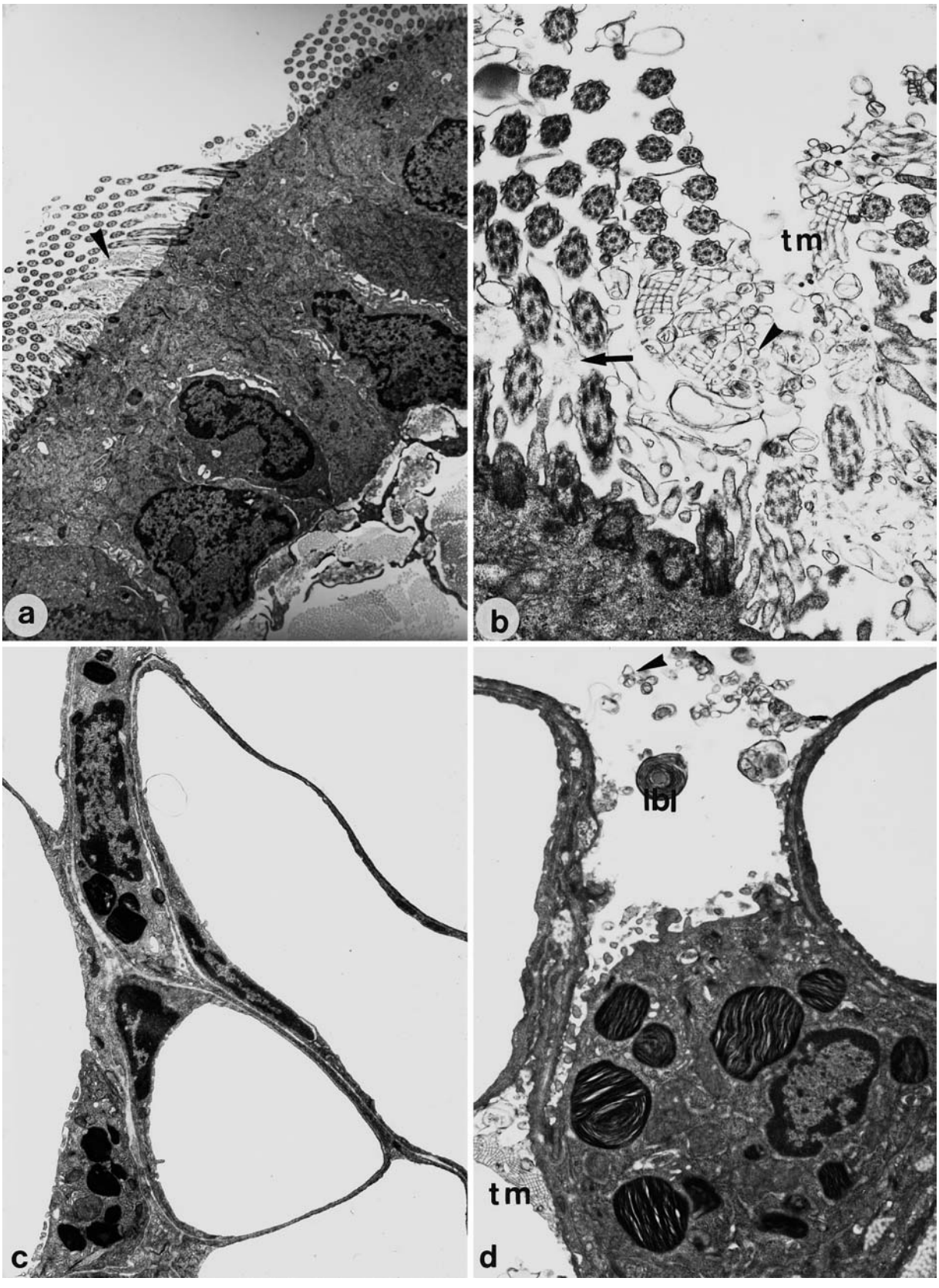

a
b
tm
c
lbl
tm
d

**Table 3** Total intra-alveolar surfactant and surfactant subtypes per lung volume. Absolute values of intra-alveolar surfactant. The relative portion of unilamellar vesicles as percentage of total intra-alveolar surfactant volume is with 65% in asthmatics significantly higher than controls (57%) ($P$<0.04). Values are given as means±SEM

| Experimental groups | $V_{surfactant}$ (µl) | $V_{lamellar\ body\text{-}like}$ (µl) | $V_{tubular\ myelin}$ (µl) | $V_{unilamellar}$ (µl) | $V_{multilamellar}$ (µl) | SA/LA |
|---|---|---|---|---|---|---|
| Controls ($n$=3) | 6.31±0.50 | 0.19±0.05 | 1.30±0.06 | 3.57±0.29 | 1.25±0.28 | 2.42±0.23 |
| Asthmatics ($n$=3) | 8.93±1.20 | 0.20±0.09 | 1.56±0.16 | 5.77±0.84 | 1.40±0.27 | 3.32±0.39 |

**Table 4** Minimum surface tension and lung resistance. In asthmatics, minimum surface tension is significantly higher and lung resistance is significantly elevated. Values are given as means±SEM

| Experimental groups | | Minimum surface tension ($y_{min}$) [mN/m] | Lung resistance ($R_L$) [delta %] |
|---|---|---|---|
| Controls | ($n$=7 or $n$=5) | 6.1±3.1 | 14.1±1.4 |
| Asthmatics | ($n$=12) | 11.9±2.2 | 86.4±16.8 |
| $t$-test | | $P$<0.05 | $P$<0.01 |

organelles located in type-II pneumocytes, qualitatively exhibited no conspicuous alterations (Fig. 2d). In both groups, parts of the alveolar epithelium were covered with active surfactant subtypes such as tubular myelin and inactive subtypes such as unilamellar vesicles located in the hypophase (Fig. 3a, b). The preservation of the alveolar surface film varied. Continuous and discontinuous covering of the hypophase was seen (Fig. 1c, Fig. 3a). In edematous regions, surfactant material seemed to be lifted off from the epithelial surface (Fig. 3c, d).

The relative and absolute intra-alveolar surfactant composition exhibited differences in asthmatic lungs compared to control lungs. The fractions of tubular myelin subtypes and the freshly secreted non-transformed lamellar body-like forms were moderately reduced (Table 2, Table 3). The fraction of inactive unilamellar forms was significantly increased (Table 2, Table 3). The CE introduced by the stereological sampling method for tubular myelin amounts to 19% in controls and 16% in asthmatics. The CE values for unilamellar vesicles are 10% in controls and 9% in asthmatics.

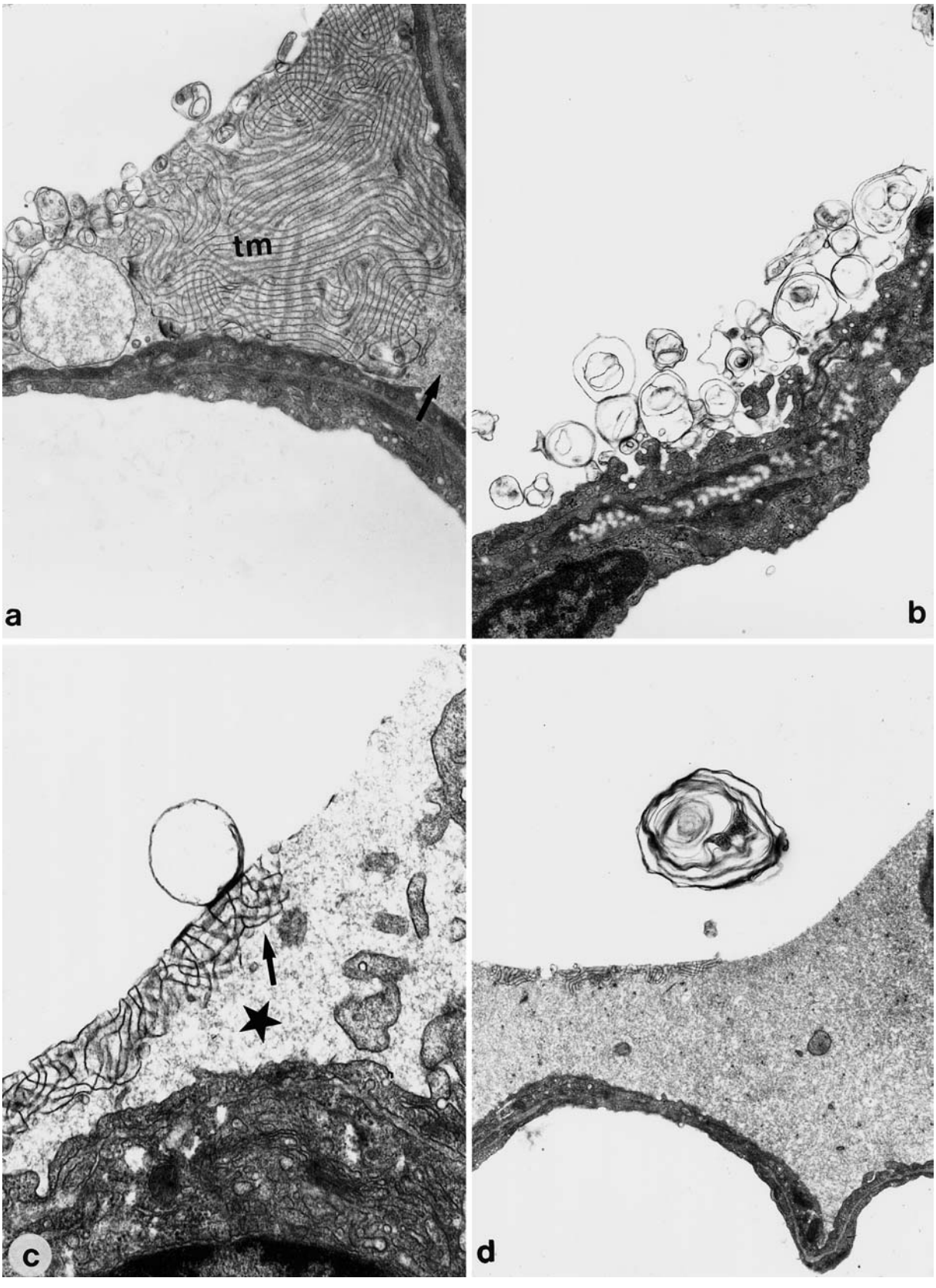
The electron microscopic data were supported by functional data (Table 4). In asthmatics, minimum surface tension was significantly higher, and lung resistance was significantly increased after allergen challenge (Table 4).

## Discussion

Our results show that asthmatic rats exhibit a significantly higher portion of inactive surfactant subtypes in the alveolar space of lung parenchyma than controls. The CE as an estimate for the variability introduced by stereological evaluation clearly stays in the limits validating reasonable precision of our estimations (<20%) [23]. The increase of inactive alveolar surfactant components occurs in combination with local intra-alveolar fluid accumulation as well as with the numerous eosinophils seen in the lung parenchyma of instillated asthmatic lungs. These findings support the suggestion of other authors that inflammation-dependent pathologic changes after allergen provocation occur not only in the small airways, but also in the alveolar areas [22, 28]. The small airways of the air-conducting system may be provided with alveolar surfactant components synthesized from type-II pneumocytes in the respiratory region because of alterations of the surface tension during the phase of inspiration and expiration. The tendency of surfactant to flow from areas of low surface tension such as in the alveoli to areas of higher surface tension such as in the conducting airways from the alveoli may reach the conducting airways at the end of expiration [15]. Therefore, every state of alveolar surfactant deficiency might involve adjacent air-conducting airways. The importance of surfactant for the stability of small airways was supported by other studies demonstrating the ability of intact surfactant to maintain patency and stability of small conducting airways [8, 15, 16, 20, 24]. The significant increase in inactive surfactant subtypes might be a cause of the higher SA/LA ratio of surfactant obtained from the BAL fluid of patients with asthma after allergen challenge [18].

The important role of pulmonary surfactant in the pathogenesis of asthma has been recognized in clinical and experimental studies [5, 24, 26, 27, 28]. Local allergen challenge in patients with asthma resulted in an inflammation of the air spaces with increased amounts of eosinophils and proteins combined with decreased surface activity of surfactant isolated from BAL fluid, measured as minimum surface tension in the pulsating bubble surfactometer and the capillary surfactometer [20]. Reduced surface activity of surfactant collected by BAL was also found in the guinea-pig asthma model [5, 26, 28].

**Fig. 3** Ultrastructure of parts of the air–blood barrier in asthmatic lungs. **a** Alveolar epithelium is covered with tubular myelin (tm) (×22,700). Local accumulation of proteinaceous fluid (*arrow*) with a unilamellar vesicle can be seen in the hypophase. The air–blood barrier exhibits no visible swelling. **b** Protrusions of type-I pneumocytes are covered with inactive unilamellar vesicles (×22,700). **c** Intra-alveolar fluid rich in proteins covers the alveolar epithelium (*asterisk*). The surfactant film and tubular myelin (*arrow*) is lifted off from the epithelium (×38,700). A unilamellar vesicle covers the surfactant film. **d** Pronounced proteinaceous fluid has accumulated between alveolar epithelium and tubular myelin. A large multilamellar vesicle can be seen above the surfactant film (×12,600)


tm
a
b
c
d

In previous clinical and experimental studies, pulmonary surfactant located in the alveolar space was harvested by means of lavage procedures, using a bronchoscope or a catheter and blind suction. Although BAL fluid is thought to be representative of both bronchial and alveolar areas, its origin is not clear [16, 22]. Additionally, lavage procedures separate surfactant from its microenvironment and disturb the pre-existing microstructural organization. Furthermore, BAL studies provide no information as to whether surfactant inactivation occurs already in the alveolar space, the place of its synthesis and secretion, or in the non-cartilaginous narrow airways. Therefore, for investigation of the intra-alveolar surfactant components within their natural microenvironment it was important to use an electron microscopic approach. In order to preserve intra-alveolar surfactant, we fixed lungs by perfusion "from behind" [3, 12].

Surfactant inactivation is caused by various mechanisms occurring during the inflammation process. A number of inflammatory stimuli modulate endothelial and epithelial permeability leading to extravasion of proteinaceous plasma fluid into the alveolar space and bronchial airways. Consistently, we were able to demonstrate a significantly higher portion of epithelial surface covered with precipitated plasma proteins outlining the dimensions of the edematous fluid in the alveolar space of asthmatic lungs. The plasma-derived proteins are inhibitors of surfactant functions as documented by numerous authors [19, 21, 35, 36]. Liu et al. ascertained a close correlation between decreases in surface tension of BAL fluid in the surfactometer and increase of the ratio of protein to phospholipids [26]. They concluded that surfactant was inhibited by proteins leaking into the airways. In vitro studies by Keough et al. showed that plasma proteins such as fibrinogen, globulin and albumin reduce the ability of surfactant suspension to minimize surface tension at the air–liquid interface and that the minimum attainable surface tension increases with increasing protein concentrations [21]. Holm et al. found that the inhibition of surface activity of calf lung surfactant extracts by albumin, hemoglobin or fibrinogen was abolished when protein was separated from surfactant by superspeed centrifugation [19]. Both authors suggested that inhibition of surfactant function by proteins is more likely to be caused by preventing surfactant lipids to adsorb at the air–liquid interphase than by direct molecular interactions between protein and surfactant [19, 21].

The higher portion of inactive unilamellar vesicles might also be the result of an accelerated conversion from active to inactive surfactant subtypes. Ueda et al. showed that the addition of serum proteins to heavy subtype surfactant increases the conversion rate from heavy to light subtypes [36]. The increased conversion rate might be due to interaction of proteins with convertase or to inhibition of SP-A, which is able to inhibit conversion [35, 38].

Increased alveolar surface tension subsequently reduces perimicrovascular interstitial hydrostatic pressure. The resulting increase of transvascular hydrostatic pressure gradient leads to additional forces towards the alveolar space amplifying intra-alveolar edema [3]. The additional plasma-protein dependent inactivation of surfactant could cause a vicious circle of potentiation of bronchoalveolar edema and bronchoconstriction.

Our findings of intra-alveolar edema and increase in inactive surfactant subtypes support the hypothesis that surfactant function is disturbed by proteinaceous fluid entering the alveoli. Thus, the inflammatory process after allergen challenge of sensitized Brown Norway rats causes intra-alveolar surfactant alterations. These surfactant alterations might contribute to small airway dysfunction.

**Acknowledgements** The authors gratefully acknowledge the expert technical assistance of Ms. A. Gerken, S. Freese, H. Hühn (Göttingen), M. Hanke (Hannover), M. Fathollahy (Hannover) and S. Elki (Hannover). The authors thank Prof. Dr. D. Grube (Hannover) for valuable discussions and Ms. S. Fryk (Hannover) for correction of the English text. Part of this work was supported by the Deutsche Forschungsgemeinschaft.

## References

1. Avery ME, Mead J (1959) Surface properties in relation to atelectasis and hyaline membrane disease. Am J Dis Child 97:517–523
2. Bachofen H, Schürch S, Michel RP, Weibel ER (1993) Experimental hydrostatic pulmonary edema in rabbit lungs. Morphology. Am Rev Respir Dis 147:989–996
3. Bachofen H, Bachofen M, Weibel ER (1988) Ultrastructural aspects of pulmonary edema. J Thorac Imag 3:1–7
4. Bastacky J, Lee CYC, Goerke J, Koushafar H, Yager D, Kenaga L, Speed TP, Chen Y, Clements JA (1995) Alveolar lining layer is thin and continuous: low-temperature scanning electron microscopy of rat lung. J Appl Physiol 79:1615–1628
5. Cheng G, Ueda T, Sugiyama K, Toda M, Fukuda T (2001) Compositional and functional changes of pulmonary surfactant in a guinea-pig model of chronic asthma. Respir Med 95: 180–186
6. Clements JA, Hustead RF, Johnson RP, Gribetz I (1961) Pulmonary surface tension and alveolar stability. J Appl Physiol 16:444–450
7. Cruz-Orive LM, Weibel ER (1981) Sampling designs for stereology. J Microsc 122:235–257
8. Enhorning G, Duffy LC, Welliver RC (1995) Pulmonary surfactant maintains patency of conducting airways in the rat. Am J Respir Crit Care Med 151:554–556
9. Fehrenbach H, Ochs M (1998) Studying lung ultrastructure. In: Uhlig S, Taylor AE (eds) Methods in pulmonary research. Birkhäuser, Basel, pp 429–454
10. Fehrenbach A, Ochs M, Warnecke T, Wahlers T, Wittwer T, Schmiedl A, Elki S, Meyer D, Richter J, Fehrenbach H (2000) Beneficial effect of lung preservation is related to ultrastructural integrity of tubular myelin after experimental ischemia and reperfusion. Am J Respir Crit Care Med 161:2058–2065
11. Gehr P, Geiser M, Stone KC, Crapo JD (1993) Morphometric analysis of the gas exchange region of the lung. In: Gardner DE, Crapo JD, McClellan RO (eds) Toxicology of the lung, 2nd edn. Raven Press, New York, pp 111–154
12. Gil J (1971) Ultrastructure of lung fixed under physiologically defined conditions. Arch Intern Med 27:896–902
13. Gil J, Weibel ER (1969/70) Improvements in demonstration of lining layer of lung alveoli by electron microscopy. Respir Physiol 8:13–36
14. Gil J, Weibel ER (1971) Extracellular lining of bronchiols after perfusion-fixation of rat lungs for electron microscopy. Anat Rec 169:185–200

15. Green FHY, Schürch S, Gehr P, Lee MM (2000) The role of surfactant in disease associated with particle exposure. In: Gehr P, Heyder J (eds) Particle-lung interactions. (Lung biology in health and disease, vol 143) Marcel Dekker, New York, pp 533–576
16. Griese M (1999) Pulmonary surfactant in health and human diseases: state of the art. Eur Respir J 13:1455–1476
17. Gundersen HJG, Jensen EB (1987) The efficiency of systematic sampling in stereology and its prediction. J Microsc 147: 229–263
18. Hohlfeld J, Hoymann HG, Molthan J, Fabel H, Heinrich U (1997) Aerosolized surfactant inhibits acetylcholine-induced airway obstruction in rats. Eur Respir J 10:2198–2203
19. Holm BA, Enhorning G, Notter RH (1988) A biophysical mechanism by which plasma proteins inhibit lung surfactant activity. Chem Phys Lipids 49:49–55
20. Jarjour NN, Enhorning G (1999) Antigen-induced airway inflammation in atopic subjects generates dysfunction of pulmonary surfactant. Am J Respir Crit Care Med 160:336–341
21. Keough KM, Parsons CS, Phang PT, Tweeddale MG (1988) Interactions between plasma proteins and pulmonary surfactant: surface balance studies. Can J Physiol Pharmacol 66: 1166–1173
22. Kraft M, Djukanovic R, Wilson S, Holgate ST, Martin RJ (1996) Alveolar tissue inflammation in asthma. Am J Respir Crit Care Med 154:1505–1510
23. Kroustrup JP, Gundersen H JG (1982) Sampling problems in an heterogeneous organ: quantitation of relative and total volume of pancreatic islets by light microscopy. J Microsc 132: 43–55
24. Kurashima K, Fujimura M, Matsuda T, Kobayashi T (1997) Surface activity of sputum from acute asthmatic patients. Am J Respir Crit Care Med 155:1254–1259
25. Lewis JF, Novick RJ, Veldhuizen RAW (1997) Surfactant in lung injury and lung transplantation. RG Landes Company, Austin, Texas, USA; International copyright, Springer, Berlin Heidelberg New York
26. Liu M, Wang L, Enhorning G (1995) Surfactant dysfunction develops when the immunized guinea-pig is challenged with ovalbumin aerosol. Clin Exp Allergy 25:1053–1060
27. Liu M, Wang E, Li E, Enhorning G (1996) Pulmonary surfactant given prophylactically alleviates an asthma attack in guinea-pigs. Clin Exp Allergy 26:270–275
28. Liu M, Wang L, Holm BA, Enhorning G (1997) Dysfunction of guinea-pig pulmonary surfactant and type II pneumocytes after repetitive challenge with aerosolized ovalbumin. Clin Exp Allergy 27:802–807
29. Müller AE, Cruz-Orive LM, Gehr P, Weibel ER (1991) Comparison of two subsampling methods for electron microscopic morphometry. J Microsc 123:35–49
30. Ochs M, Nenadic I, Fehrenbach A, Albes JM, Wahlers T, Richter J, Fehrenbach H (1999) Ultrastructural alterations in intraalveolar surfactant subtypes after experimental ischemia and reperfusion. Am J Respir Crit Care Med 160:718–724
31. Oulton M, MacDonald J, Janigan DT, Faulkner GT (1993) Mouse alveolar surfactant: characterization of subtypes prepared by differential centrifugation. Lipids 28:715–720
32. Scherle W (1970) A simple method for volumetry of organs in quantitative stereology. Mikroskopie 26:57–60
33. Schuster M, Tschernig T, Krug N, Pabst R (2000) Lymphocytes migrate from the blood into the bronchoalveolar lavage and lung parenchyma in the asthma model of the Brown Norway rat. Am J Respir Crit Care Med 161:558–566
34. Schürch S, Green FHY, Bachofen H (1998) Formation and structure of surface films: captive bubble surfactometry. Biochim Biophys Acta 1408:180–202
35. Strayer DS, Herting E, Sun B, Robertson B (1996) Antibody to surfactant protein A increases sensitivity of pulmonary surfactant to inactivation by fibrinogen in vivo. Am J Respir Crit Care Med 153:1116–1122
36. Ueda T, Ikegami M, Jobe A (1994) Surfactant subtypes. In vitro conversion, in vivo function, and effects of serum proteins. Am J Respir Crit Care Med 149:1254–1259
37. Velazquez M, Weibel ER, Kuhn C, Schuster DP (1991) PET evaluation of pulmonary vascular permeability: a structure–function correlation. J Appl Physiol 70:2206–2216
38. Veldhuizen RAW, Ito Y, Marcou J, Yao LY, McCaig L, Lewis JF (1997) Effects of lung injury on pulmonary surfactant aggregate conversion in vivo and in vitro. Am J Physiol 272:L872–L878
39. Weaver T, Whitsett JA (1991) Function and regulation of expression of pulmonary surfactant-associated proteins. Biochem J 273:249–264
40. Weibel ER (1979) Stereological methods. (Practical methods for biological morphometry, vol 1) Academic Press, New York
41. Wright JR (1994) Clearance and recycling of pulmonary surfactant. Am J Physiol 259:L1–L12

Virchows Arch (2003) 442:66–70
DOI 10.1007/s00428-002-0721-y

ORIGINAL ARTICLE

**Yousuke Akisawa · Isao Nishimori · Keisuke Taniuchi
Nobuto Okamoto · Tamotsu Takeuchi
Hiroshi Sonobe · Yuji Ohtsuki · Saburo Onishi**

# Expression of carbonic anhydrase-related protein CA-RP VIII in non-small cell lung cancer

Received: 24 May 2002 / Accepted: 9 September 2002 / Published online: 5 December 2002
© Springer-Verlag 2002

**Abstract** Carbonic anhydrase-related protein (CA-RP VIII) lacks a Zn-binding motif which is essential for carbonic anhydrase activity. Therefore, CA-RP VIII is believed to have a no catalytic activity and a new biological property. In the present study, CA-RP VIII expression in non-tumorous lung and non-small cell lung carcinomas was investigated. Little or no expression of CA-RP VIII was observed in human lungs by Northern-blot analysis. Reverse-transcription polymerase chain reaction analysis demonstrated CA-RP VIII mRNA in developing human lungs and, to a lesser extent, in normal lungs. Subsequent immunohistochemical staining revealed that CA-RP VIII was expressed in the pulmonary epithelium in developing lungs; however, CA-RP VIII expression was restricted in bronchial ciliated cells in adult lungs. Neither bronchial gland nor squamous metaplasia of interstitial pneumonia expressed CA-RP VIII. In contrast, CA-RP VIII was strongly expressed in almost all archival lung cancer specimens, which included 24 squamous cell carcinomas, 25 adenocarcinomas, and 6 adenosquamous cell carcinomas. Cancer cells at the front of tumor progression expressed CA-RP VIII in particular abundance. The present findings suggest that CA-RP VIII may play a role in non-small lung cell carcinomas.

**Keywords** CA-RP VIII · Lung cancer · Non-small · Oncofetal

Y. Akisawa · I. Nishimori · K. Taniuchi · N. Okamoto · S. Onishi
First Department of Internal Medicine, Kochi Medical School, Nankoku, Kochi 783-8505, Japan

T. Takeuchi (✉) · Y. Ohtsuki
Department of Pathology, Kochi Medical School, Nankoku, Kochi 783-8505, Japan
e-mail: takeutit@med.kochi-ms.ac.jp
Fax: +81-88-8802336

H. Sonobe
Department of Clinical Laboratory, National Fukuyama Hospital, Fukuyama, Japan

## Introduction

The carbonic anhydrases (CAs) are a family of zinc metal enzymes that catalyze the reversible hydration of $CO_2$ [11]. There are 11 human CA isozymes designated CA I–IV, VA,VB,VI,VII, IX, XII, and XIV. Moreover, recent studies discovered three CA-related proteins (CA-RP). CA-RP VIII is a CA-related protein that lacks critical amino acid residues at the active sites [5]. CA-RP VIII is therefore believed to be an enzymatically inactive isozyme; however, the amino acid motif of CA-RP VIII has been well conserved through evolution in vertebrates (approximately 98% amino acid homology is reported between humans and mice) [10]. This suggests that CA-RP VIII may play biologically significant roles in higher animals. Expression of murine CA-RP VIII mRNA is especially high in the brain, liver, lung, heart, gut, and thymus [8, 9, 10]. However, the detailed tissue distribution of CA-RP VIII protein still remains obscure. Very recently, we generated and characterized a novel monoclonal antibody which specifically reacted with human CA-RP VIII protein even in formalin-fixed and paraffin-embedded archival tissue sections [15].

In the present study, we examined CA-RP VIII expression in human non-tumorous tissue and lung carcinomas. Surprisingly, CA-RP VIII was strongly expressed at the front of cancer progression in non-small cell lung carcinomas and human developing lung tissues, but little expression was observed in non-tumorous lung tissues including the squamous metaplastic epithelium and bronchial gland.

## Materials and methods

### Northern-blot analysis

Northern-blot analysis was carried out as previously described [2]. Briefly, 620 bp cDNA probes of human CA-RP VIII were synthesized by means of polymerase chain reaction (PCR) using a specific primer pair, sense 5′-TCCTGATGCTAATGGGGAATACCAG-3′ and antisense 5′-CTAAGAGGCTGAGTGGGCCG-

AAAG-3′ and labeled with [α-32P] dCTP (ICN, Costa Mesa, Calif.) using a random primed DNA labeling kit (Roche Molecular Biochemicals, Mannheim, Germany). Multiple tissue Northern blots containing 2 μg poly(A)+ RNA from a panel of human tissues were purchased from Clontech Lab. Inc. (Palo Alto, Calif.). Membranes were prehybridized in the manufacturer's solution, and followed by incubation with a radiolabeled probe at 68°C for 1 h. After washing with 2× saline sodium citrate buffer/0.1% sodium dodecyl sulfate at room temperature, and then with 0.1× saline-sodium citrate buffer/0.1% sodium dodecyl sulfate at 42°C, the membranes were exposed to X-ray film (Fuji, Tokyo, Japan) at –80°C for 16 h.

### Detection of CA-RP VIII mRNA using reverse-transcription PCR analysis

Total cellular RNA was purchased from Chemicon International Inc. (Temecula, Calif.). We used total RNA as a substrate for cDNA synthesis with a reverse-transcription (RT) PCR kit (Life Technologies, Gaithesburg, Md.). The cDNA synthesis and subsequent PCR were performed according to the manufacturer's instructions. The primer sets used in this study were sense 5′-TCCTGATGCTAATGGGGAATACCAG-3′ and antisense 5′-CTAAGAGGCTGAGTGGGCCGAAAG-3′ for CA-RPVIII, and sense 5′-TCCACCACCCTGTTGCTGTA-3′ and antisense 5′-ACCACAGTCCATGCCATCAC-3′ for glyceraldehyde-3-phosphate dehydrogenase (G3PDH). The PCR reaction was carried out after a 3-min 94°C hot start, and consisted of 35 cycles of 94°C for 30 s, annealing at 58°C for 1 min, and elongation for 1 min. The PCR-amplified product was electrophoretically separated on a 2% agarose gel.

### Antibody, tissue sections, and immunohistochemical staining

Details of the procedures used to prepare a monoclonal antibody to human CA-RP VIII and immunohistochemical staining were described previously [15]. Briefly, a Balb/c mouse was repeatedly immunized with human CA-RP VIII peptide, NH2-CQLQIEEFRRLRTHVKGAE-COOH. Notably, this peptide is partially different to that of murine CA-RP VIII, although the amino acid homology between mouse and human is approximately 98%. The splenic lymphocytes from an immunized mouse were fused with partner myeloma cells, and hybridomas were selected according to the modified methods of Kohler and Milstein [6] as previously described [13]. One hybridoma secreting a monoclonal antibody which reacted with CA-RP VIII even in formalin-fixed and paraffin-embedded tissue sections was selected and established after limiting dilution. The specificity of the reaction of the antibody to human CA-RP VIII was confirmed by a preadsorption test using immunized peptide. Immunohistochemical staining of CA-RP VIII was performed as described previously [14, 15]. Briefly, archival tissues comprising 55 human non-small cell lung cancer and 5 interstitial pneumonia specimens were immunostained with a monoclonal antibody or control antibody using a streptavidin biotin complex peroxidase kit (DAKO LSAB Kit; Dakopatts, Kyoto, Japan). Fetal lung tissues were obtained from embryos and also used in the present study. The Committee of Kochi Medical School approved the protocol for this study. The immunohistochemical staining procedures were performed according to the manufacturer's protocol. Finally, the reaction was developed with diaminobenzidine, and the tissue sections were counterstained with hematoxylin. Anti-CA-RP VIII antibody was of IgM class, and we used isotype-matched monoclonal antibody to *Trichosporon beigelii*, a type of fungus [12]. Previous results demonstrated that this control antibody did not react to human tissues tested. The histology of lung cancer was classified using the World Health Organization system. Based on the number of stained lung cancer cells, immunohistochemical staining was semi-quantitatively scored as negative (less than 5%), weakly positive (5–20%), moderately positive (20–80%), or markedly positive (over 80%).

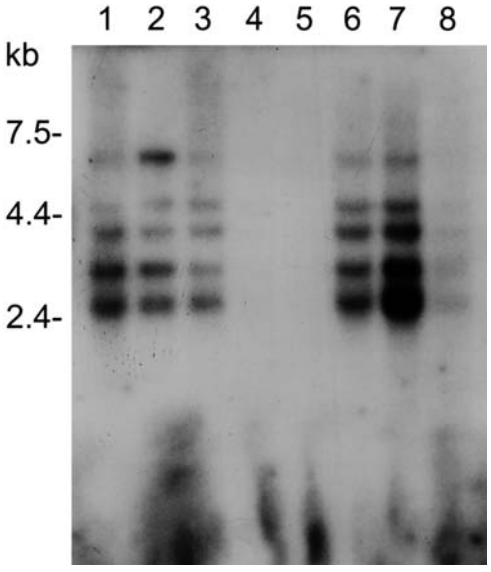



**Fig. 1** Northern blot analysis of CA8 mRNA in various human tissues. *1* heart, *2* brain, *3* placenta, *4* lung, *5* liver, *6* skeletal muscle, *7* kidney, *8* pancreas. Each lane contained ~2 μg poly(A)+ RNA

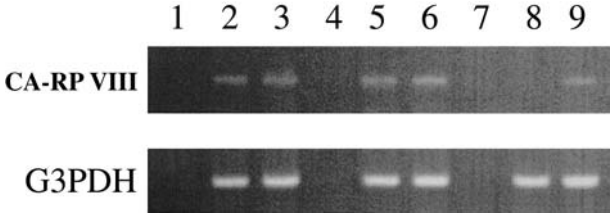



**Fig. 2** Detection of CA8 transcript by reverse transcriptase polymerase chain reaction (RT-PCR) analysis using specific primers. Total RNA from fetal lung tissues at 6 weeks (lanes 1–3), 12 weeks (lanes 4–6), and adult lung tissues (lanes 7–9) were subjected to RT-PCR [lanes 1, 4, and 7, (18 cycles); lanes 2, 5, and 8, (27 cycles); lanes 3,6, and 9 (35 cycles of PCR after RT reaction)] with CA-RP VIII and G3PDH primer sets. Note the even intensity of internal control bands for G3PDH

## Results

### mRNA expression in various human tissues

The results from Northern-blot analysis are demonstrated in Fig. 1. RNA species migrating at approximately 2.4, 3, 4, 4.5, and 7 kb were detected in the human heart, brain, placenta, skeletal muscle, kidney, and pancreas (lanes 1, 2, 3, 6, 7, and 8, respectively). However, less or no signals were observed in human lung and liver samples (lanes 4 and 5, respectively). The different sizes of RNA bands may reflect the multiple polyA signals found for CA-RP VIII mRNA. The results of subsequent RT-PCR analysis are shown in Fig. 2. RT-PCR demonstrated CA-RP VIII mRNA expression in developing and adult human lungs. Notably, CA-RP VIII expression in developing lungs was much higher than that in adult lungs.

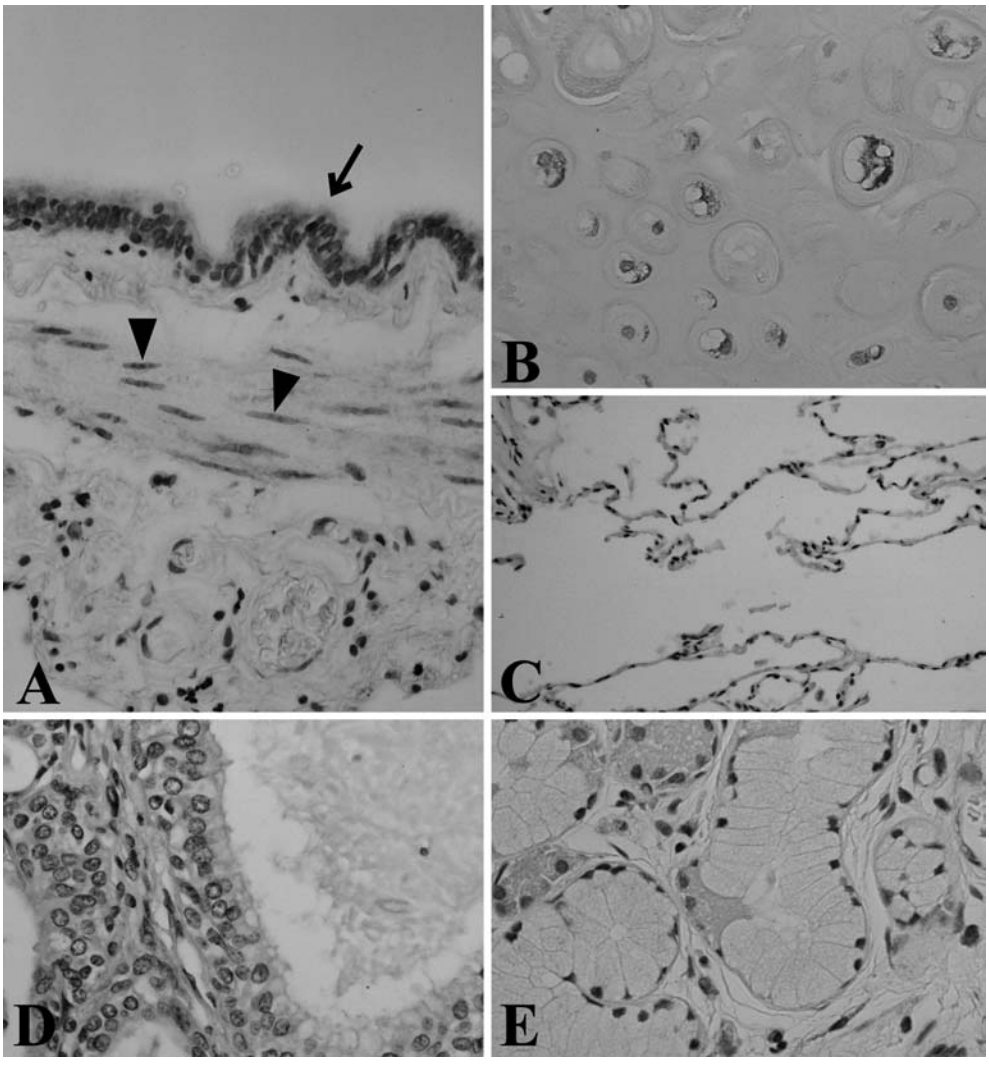



**Fig. 3** Immunohistochemical staining of non-tumorous lung tissue. CA-RP VIII was expressed in ciliated cells of bronchus (**A**, arrow), smooth muscle cells (**A**, arrowhead), and chondrocytes of bronchial cartilage (**B**). However, no significant staining was found in alveolar epithelial cells (**C**). Any significant CA-RP VIII expression was observed in neither metaplastic squamous epithelium of interstitial pneumonia nor bronchial gland (**D** and **E**, respectively). Original magnification was ×400 (**A**, **B**, **D**, **E**) and ×200 (**C**)

**Table 1** Summary of immunohistochemical staining of lung cancer specimens

| | Squamous cell carcinoma | Adenosquamous cell carcinoma | Adenocarcinoma |
|---|---|---|---|
| Markedly positive (>80%) | 18 | 4 | 17 |
| Moderately (20–80%) | 4 | 2 | 3 |
| Weakly (5–20%) | 1 | 0 | 5 |
| Negative | 1 | 0 | 0 |

Immunohistochemical staining

The bronchial ciliated cells were stained with monoclonal antibody to CA-RP VIII (Fig. 3A, arrow). CA-RP VIII expression was also demonstrated in smooth muscle cells and chondrocytes of bronchial cartilages (Fig. 3A, arrowhead and b, respectively). However, no significant staining was observed in alveolar epithelial cells, bronchial gland, and metaplastic squamous epithelium (Fig. 3C, D, E). In fetal tissues, CA-RP VIII was expressed in the developing pulmonary epithelium in the late canalicular phase (Fig. 4A, B). The results of immunohistochemical staining of lung cancer specimens are summarized in Table 1. As demonstrated in Fig. 4C and D, CA-RP VIII protein was immunohistochemically detected in 23 of 24 squamous cell carcinoma, all 25 adenocarcinoma, and all 6 adenosquamous cell carcinoma specimens tested. The CA-RP VIII expression in lung cancer was observed in the cytoplasm and was abundant at the front of tumor progression (Fig. 4C, arrow) rather that in the center of carcinomas (Fig. 4C, arrowhead). No significant staining was observed with the isotype-matched control antibody.

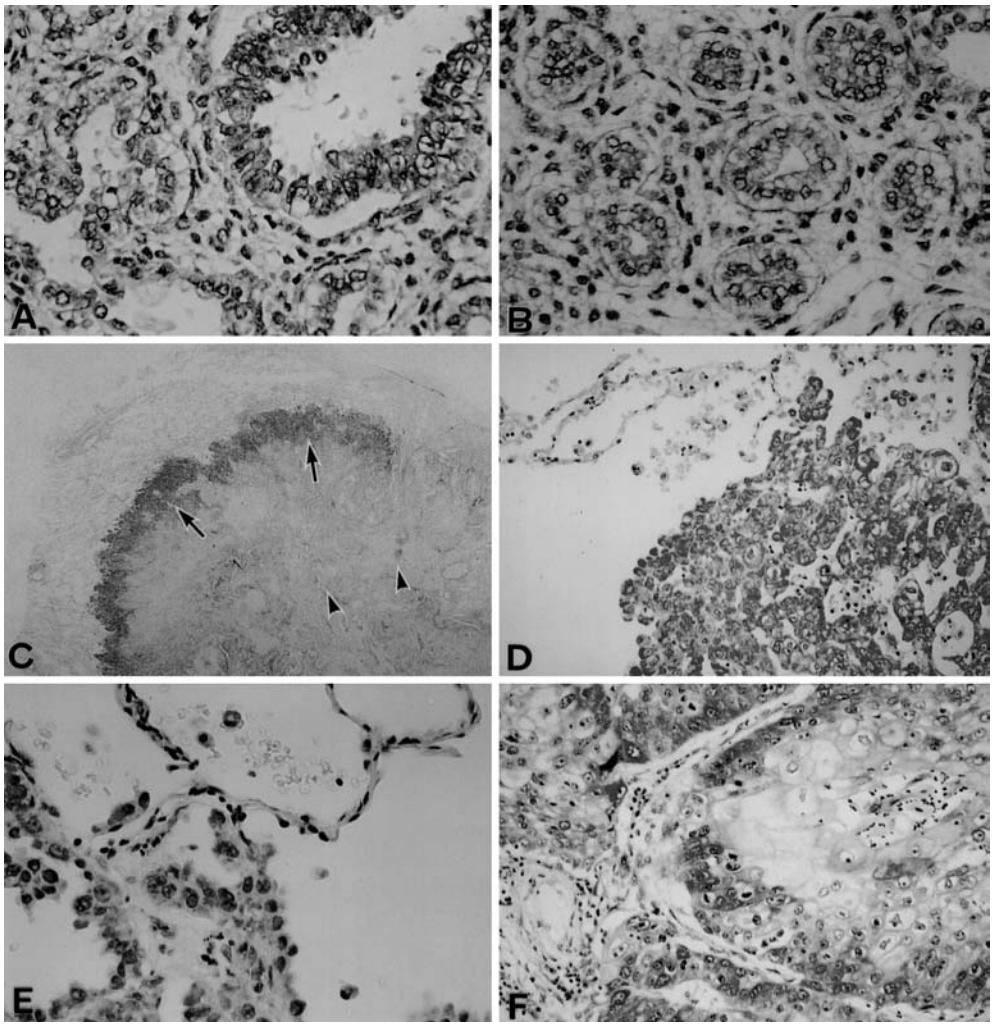



**Fig. 4** Immunohistochemical staining of fetal and non-small lung carcinoma tissue specimens. Strong CA-RP VIII expression was observed in 24-week fetal lung (**A**, **B**). CA-RP VIII was also strongly expressed at the front of tumor progression (**C**, arrow; **D**) rather than in the center of carcinoma (**C**, arrowhead). Alveolar bronchial cell carcinoma cells were also strongly stained at the tumor front (**E**). A representative case, a squamous cell carcinoma, is shown in **F**. Note the staining at the basal side of carcinoma (**F**). Original magnifications were ×1 (**C**), ×200 (**D**), and ×400 (**A**, **B**, **E**, **F**)

## Discussion

Lung cancer is one of the most frequent malignant neoplasms. To improve its poor prognosis, it is important to explore fundamental biological properties of lung cancer and design new approaches to therapy. CA8 (nomenclature for gene encoding CA-RP VIII protein) is a "non-classical" member of carbonic anhydrase gene family [1]. The fact that CA-RP VIII lacks critical amino acid residues at its enzymatically active site indicates that CA-RP VIII lacks $C0_2$-hydration activity. In contrast, carbonic anhydrase IV, which is known to be expressed in lung endothelial cells, is a high-activity isozyme [17]. Although the biological function of CA-RP VIII remains obscure, the high degree of conservation of amino acids between human and mouse indicates that CA-RP VIII has fundamental biological functions.

Previous reports noted the broad tissue distribution of CA-RP VIII in humans and mice [7, 8, 9]. CA-RP VIII mRNA was originally identified in the Purkinje cells of mouse cerebellum, and later in murine brain, liver, lung, heart, gut, and thymus. Skaggs et al. isolated a CA-RP VIII cDNA clone from human placenta and salivary gland cDNA libraries [10]. However, the precise tissue distribution of CA-RP VIII in human lung tissues had not previously been determined. Lakkis et al. reported that expression of Car8 (nomenclature for murine CA8 gene) mRNA was relatively high in lung [8]. We also confirmed CA-RP VIII mRNA expression in murine lung by Northern blotting (data not shown). However, CA-RP VIII mRNA was not detected in human adult lung by Northern-blot analysis (Fig. 1, lane 4). Although subsequent RT-PCR experiments detected CA-RP VIII mRNA in human lungs (Fig. 2), it is clear that human lung tissue did not express as much CA-RP VIII as previously described for mice.

RT-PCR experiments also demonstrated that CA-RPV III was strongly expressed in developing fetal lung (Fig. 2). The results of immunohistochemical staining were also consistent to the results of Northern blot and RT-PCR analysis (Fig. 3). Little CA-RP VIII expression was also observed in human adult non-tumorous lung tissues by immunohistochemical staining (Fig. 3). CA-RP VIII expression was restricted to bronchial ciliated cells, chondrocytes of bronchial cartilage, and smooth muscle cells in adult lung tissue (Fig. 3). In contrast, developing

pulmonary epithelium abundantly expressed CA-RP VIII protein (Fig. 4A, B). This pattern of expression led us to examine whether CA-RPVIII is an oncofetal antigen in human lungs. Immunohistochemical staining revealed that CA-RP VIII was strongly expressed in 54 of 55 pulmonary non-small carcinoma specimens (Fig. 4C–F, Table 1). Interestingly, intense staining was observed at the front of tumor progression (Fig. 4C, arrow). In contrast, CA-RP VIII expression was relatively weak in the center of carcinomas (Fig. 4C, arrow head). Marked expression (>80% positivity for total lung cancer cells) was observed in 18 of 24, 17 of 25, and 4 of 6 squamous cell carcinomas, adenocarcinomas, and adenosquamous cell carcinomas, respectively. Interestingly, CA-RP VIII expression was observed on the basal side of well-differentiated squamous cell carcinomas (Fig. 4F). This finding suggests that CA-RP VIII was strongly expressed in highly proliferative lung cancer cells. Notably, neither metaplastic squamous epithelium of interestial pneumonia specimens nor bronchial gland expressed CA-RP VIII (Fig. 3D, E). We further examined CA-RP VIII expression in other glands including intestinal gland; however, significant CA-RP VIII expression like normal adult bronchial epithelium was not observed (data not shown). Although the function of CA-RP VIII still remains obscure, CA-RP VIII has an extensive acidic region in its N-terminal region, like several transcriptional activators including GAL4, GCN4, and Herpesvirus VP16 [3, 4, 16]. Lakkis et al. thus speculated that CA-RP VIII may play a role in transcription or translation [8]. The present study supports their hypothesis, since tumor cells at the progressive front are likely to possess higher transcriptional or translational activity than cancer cells located in the tumor center. Combined together with the present study, it is likely that CA-RP VIII would have a feature of oncofetal antigen and have a role in non-small cell lung carcinomas.

## References


1. Bergenhem NC, Hallberg M, Wisen S (1998) Molecular characterization of the human carbonic anhydrase-related protein (HCA-RP VIII). Biochim Biophys Acta 1384:294–298
2. Fujikawa-Adachi K, Nishimori I, Taguchi T, Onishi S (1999) Human mitochondrial carbonic anhydrase VB. cDNA cloning, mRNA expression, subcellular localization, and mapping to chromosome X. J Biol Chem 274:21228–21233
3. Gill G, Sadowski I, Ptashne M (1990) Mutations that increase the activity of a transcriptional activator in yeast and mammalian cells. Proc Natl Acad Sci U S A 87:2127–2131
4. Hope IA, Struhl K (1986) Functional dissection of eukaryotic transcriptional activator protein, GCN4 of yeast. Cell 46:885–894
5. Kato K (1990) Sequence of a novel carbonic anhydrase-related polypeptide and its exclusive presence in the Purkinje cells. FEBS Lett 71:137–140
6. Kohler G, Milstein C (1975) Continuous cultures of fused cells secreting antibody of predefined specificity. Nature 256:495–497
7. Lakkis MM, Bergenhem NC, O'Shea KS, Tashian RE (1997) Expression of the acatalytic carbonic anhydrase VIII gene, Car8, during mouse embryonic development. Histochem J 29:135–141
8. Lakkis MM, O'Shea KS, Tashian RE (1997) Differential expression of the carbonic anhydrase genes for CA VII (Car7) and CA-RP VIII (Car8) in mouse brain. J Histochem Cytochem 45:657–662
9. Ling B, Bergenhem NCH, Dodgson SJ, Forster RE, Tashian RE (1994) Determination of mRNA levels for six carbonic anhydrase isozymes in rat lung. Isozyme Bull 27:47
10. Skaggs LA, Bergenhem NC, Venta PJ, Tashian RE (1993) The deduced amino acid sequence of human carbonic anhydrase-related protein (CARP) is 98% identical to the mouse homologue. Gene 126:291–292
11. Sly WS, Hu PY (1995) Human carbonic anhydrases and carbonic anhydrase deficiencies. Annu Rev Biochem 64:375–401
12. Takeuchi T, Kobayashi M, Moriki T, Miyoshi I (1988) Application of a monoclonal antibody for the detection of Trichosporon beigelii in paraffin-embedded tissue sections. J Pathol 156:23–27
13. Takeuchi T, Misaki A, Liang SB, Tachibana A, Hayashi N, Sonobe H, Ohtsuki Y (2000) Expression of T-cadherin (CDH13, H-Cadherin) in human brain and its characteristics as a negative growth regulator of epidermal growth factor in neuroblastoma cells. J Neurochem 74:1489–1497
14. Takeuchi T, Nicole S, Misaki A, Furihata M, Iwata J, Sonobe H, Ohtsuki Y (2001) Expression of SMARCF1, a truncated form of SWI1, in neuroblastoma. Am J Pathol 158:663–672
15. Taniuchi K, Nishimori I, Takeuchi T, Fujikawa-Adachi K, Ohtuski Y, Onishi S (2002) Developmental expression of carbonic anhydrase-related proteins VIII, X, XI in human brain. Neuroscience 112:93–99
16. Triezenberg S, Kingbury R, McKnight S (1988) Functional dissection of VP16, the trans-activator of Herpes simplex virus immediately early gene expression. Genes Dev 2:718–729
17. Zhu XL, Sly WS (1990) Carbonic anhydrase IV from human lung. J Biol Chem 265: 8795–8801

Virchows Arch (2003) 442:71–76
DOI 10.1007/s00428-002-0701-2

ORIGINAL ARTICLE

**Paola Collini · Giuseppe Sampietro · Juan Rosai**
**Silvana Pilotti**

# Minimally invasive (encapsulated) follicular carcinoma of the thyroid gland is the low-risk counterpart of widely invasive follicular carcinoma but not of insular carcinoma

Received: 28 February 2002 / Accepted: 5 July 2002 / Published online: 2 October 2002
© Springer-Verlag 2002

**Abstract** Minimally invasive (encapsulated) follicular carcinoma (MIFC), widely invasive follicular carcinoma (WIFC), and insular carcinoma (IC) are three distinct types of thyroid carcinomas composed of follicular cells, IC representing the poorly differentiated counterpart. Our aim was to test whether there is a time-dependent relationship among these three entities, in particular whether MIFC is the low-risk form of the entire group. We used overall survival analysis and multiple correspondence analysis (MCA), the latter exploring the clinicopathological characteristics at onset (sex, age, TNM/pTNM classification). The study included 18 MIFCs, 29 WIFCs, and 27 ICs. On the basis of both overall survival and MCA, WIFC emerged as the high-risk counterpart of MIFC, occurring in older age, with a larger size, a widespread growth into the thyroid parenchyma, and presenting with distant metastases. In both types of follicular carcinoma distant metastases involved only lung and bone, and there was no tendency for local spread beyond the thyroid capsule or nodal metastases. By contrast, IC confirmed to be a distinct high-risk lesion, showing both follicular and papillary-related biological behavior characteristics.

**Keywords** Follicular carcinoma · Minimally invasive follicular carcinoma · Widely invasive follicular carcinoma · Insular carcinoma · Multiple correspondence analysis

P. Collini (✉) · G. Sampietro · J. Rosai · S. Pilotti
Department of Pathology, Istituto Nazionale Tumori,
Via G. Venezian 1, 20133 Milan, Italy
e-mail: Paola.Collini@istitutotumori.mi.it
Tel.: +39-02-23903214, Fax: +39-02-23902756

*Present address:*
G. Sampietro, Servizio di Epidemiologia, ASL Citta' di Milano,
Corso Italia 19, Milan, Italy

## Introduction

Differentiated carcinomas deriving from the follicular epithelium of the thyroid gland can be divided into low-risk and high-risk forms on the basis of overall survival data. In general a poorly differentiated morphology entails a worse outcome, featuring high-risk forms which have been generically named "poorly differentiated carcinomas." This is true for papillary carcinoma, in which the presence of markers of poor differentiation such as the tall-cell and/or columnar-cell morphology have shown to be an independent high-risk factor [11, 13]. This seems also true for insular carcinoma (IC), a high-risk poorly differentiated tumor placed into the follicular-related group of thyroid carcinomas by the WHO classification [4, 12, 18], which is supported by the sharing of RAS gene family point mutations with the other members of this group [10]. However, while in IC the criteria of high risk depend upon the degree of differentiation, in usual follicular carcinomas (FCs) the division into low-risk and high-risk forms is based on their degree of invasiveness irrespective of differentiation grade. Two types are recognized: minimally invasive (MIFC) and widely invasive follicular carcinoma (WIFC). The former is an encapsulated neoplasm characterized by unequivocal vascular and/or capsular invasion, while the latter shows a widespread infiltration of blood vessels and/or into the adjacent thyroid parenchyma [14, 18]. In terms of outcome, while WIFC is a high-risk form, with an overall survival similar to that of IC [12, 14], MIFC shows a relatively uneventful course [14]. We compared the three forms of tumors to determine whether there is a time-dependent relationship among them and in particular whether MIFC is the low-risk form of the entire group.

## Materials and methods

Eighteen consecutive cases of MIFCs diagnosed and treated at the Istituto Nazionale Tumori of Milan between 1975 and 1993 were

matched with 29 consecutive cases of WIFCs and 27 consecutive cases of ICs retrieved during the same period and followed-up to the same date, which had been the object of a previous study [12]. To avoid possible bias we excluded from this study Hürthle cell FCs, claimed by some authors to have a different outcome [3, 6]. Only cases for which specimens from the primary tumors were available were included in this study. All the slides were reviewed and the original diagnosis confirmed by applying updated criteria [14, 18]. MIFC was defined as an encapsulated follicular neoplasm showing unequivocal capsular and/or vascular invasion [14, 18] (Figs. 1, 2). WIFC was defined as a follicular neoplasm showing widespread invasion into the thyroid parenchyma or into blood vessels [14, 18]. IC was defined as a widely invasive carcinoma with a prevalent poorly differentiated morphology, showing distinctive well-defined nests (insulae) of round or oval shape, formed by a uniform population of small cells with round nuclei and scant cytoplasm. In IC the pattern of growth is typically solid and microfollicular, but also trabecular, follicular and papillary featuring areas can be found. A variable mitotic activity, frequent necrotic foci, infiltrative margins, and vascular invasion are also present [4, 14, 18] (Fig. 3).

For each case the sex and the age of the patient at diagnosis, focality (single vs. multiple nodules in the thyroid gland), TNM/pTNM classification [16], and therapy were recorded. For WIFC and IC patients, the treatment of choice was total thyroidectomy with dissection of clinically enlarged lymph nodes, coupled with thyrotropin-suppressive therapy, and radioiodine therapy for inoperable persistent or relapsed disease. MIFC were subjected to total thyroidectomy or hemithyroidectomy, coupled with thyrotropin-suppressive therapy. Radioiodine therapy was applied to inoperable relapsed cases, after completion thyroidectomy when necessary. All patients were followed-up to June 1995 or to the time of death.

The relationship between clinicopathological characteristics at onset (sex, age, TNM/pTNM classification) of patients with the three histotypes under study (MIFC, WIFC, and IC) were explored by multiple correspondence analysis (MCA) [1, 7]. MCA has previously been used in clinicopathological investigations [15] to obtain a spatial visualization of the relationship among the variables under study, simplifying their interpretation. MCA was applied to the set of all possible two-way contingency tables obtained by cross-classification of the cases under study according to five structural variables (sex, age, pT, N/pN, M/pM classification), forming the multivariate structure of the sample under study. Histotype was analyzed as a supplementary variable, i.e., a variable which plays no role in the determination of the structure. The modalities of each structural variable were expressed as mutually exclusive binary dummy variables. Age categories were chosen based on the previous study [12]. Thus the original set of contingency tables was transformed into a complete disjunctive table with 74 rows, corresponding to the profiles of the 74 patients in the sample, and 12 columns, corresponding to the 12 modalities of the five structural variables. Profiles and modalities could be plotted as dots in a seven-dimensional space (12 modalities, five variables). The distance between points, defined according to a $\chi^2$ metrics, expressed the dissimilarities between modalities.

MCA aimed at supplying a low-dimensional image that well approximates the structure of the cloud of points defined in the original high dimensional space. Such an image was made up of the projections of the points in a subspace identified by the first two factorial axes, which were the axes of maximum dispersion (inertia) of the cloud. Moreover, from the MCA we obtained a measure of the contribution of each variable to any particular axis and the explanation of each category by each axis. This allowed the interpretation of the axes in terms of variables and modalities, and suggested which variables or modalities were closely related. In addition, it was possible to superimpose supplementary variables on the principal axes plots. This was particularly useful for studying histotypes and their relationship to the clinicopathological characteristics of the cases. The amount of information explained by each factorial axis was measured by an index suggested by Benzecrì [2]. This index allowed only for the axes with inertia greater than the value expected under the hypothesis of independence between structural variables.

Overall survival was calculated as the time elapsed from the date of surgery to the date of death (for all causes) or to the date of the last information. Overall survival patterns were estimated by

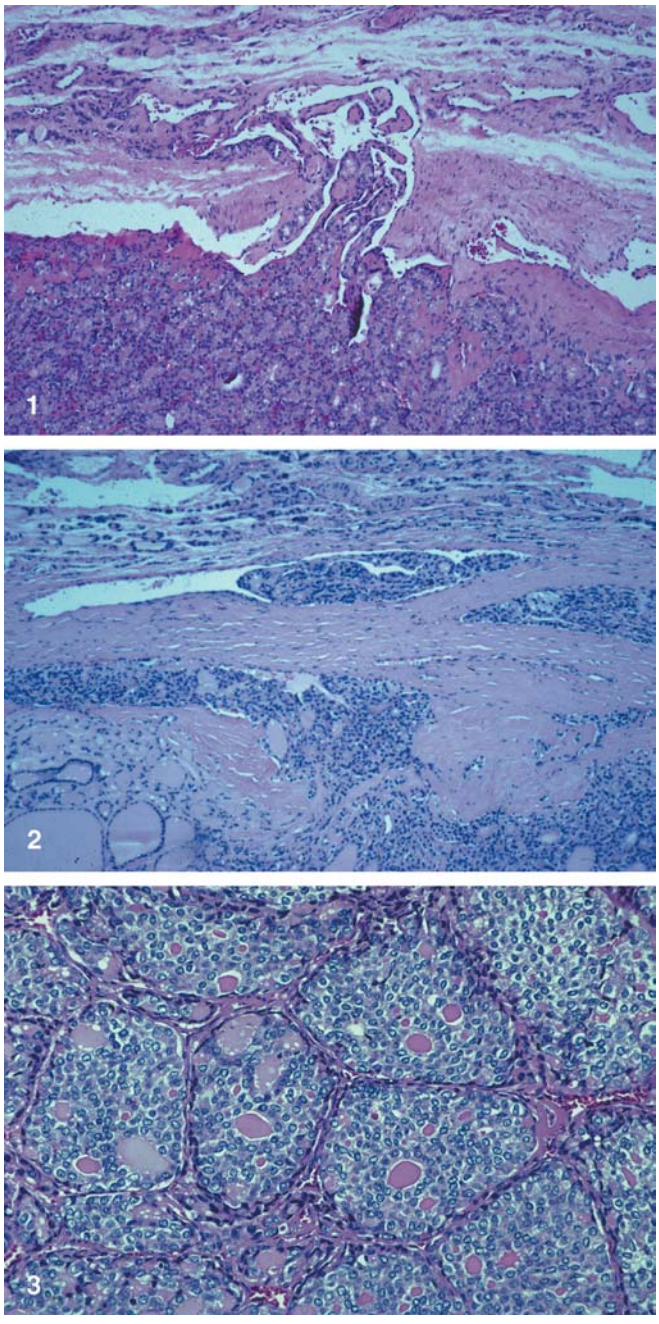



**Fig. 1** Evidence of capsular and vascular invasion in a minimally invasive follicular carcinoma of the thyroid gland; hematoxylin and eosin

**Fig. 2** Evidence of capsular and vascular invasion in a minimally invasive follicular carcinoma of the thyroid gland; hematoxylin and eosin

**Fig. 3** Distinctive "insulae" with a microfollicular pattern formed by small, uniform cells in a poorly differentiated insular carcinoma of the thyroid gland; hematoxylin and eosin

**Table 1** Frequency of distribution of the clinicopathological variables for each histotype (*MIFC* minimally invasive follicular carcinoma; *WIFC* widely invasive follicular carcinoma, *IC* insular carcinoma)

| | MIFC (*n*=18) | | WIFC (*n*=29) | | IC (*n*=27) | |
|---|---|---|---|---|---|---|
| | *n* | % | *n* | % | *n* | % |
| Sex | | | | | | |
| Female | 17 | | 17 | | 19 | |
| Male | 1 | 5.5 | 12 | 41 | 8 | 30 |
| Median age (years) | 39 | | 57 | | 53 | |
| Age at diagnosis (years) | | | | | | |
| ≤40 | 10 | | 4 | | 7 | |
| >40 | 8 | 44 | 25 | 86 | 20 | 74 |
| Multifocality | 0 | 0 | 7 | 24 | 14 | 52 |
| pT[a] | | | | | | |
| 2 | 13 | | 11 | | 7 | |
| 3 | 5 | | 16 | | 3 | |
| 4 | 0 | 0 | 2 | 7 | 16 | 62 |
| X | 0 | | 0 | | 1 | |
| N/pN[a] | | | | | | |
| 0 | 18 | | 27 | | 14 | |
| 1 | 0 | 0 | 2 | 7 | 13 | 48 |
| M/pM[a] | | | | | | |
| 0 | 18 | | 10 | | 15 | |
| 1 | 0 | 0 | 19 | 66 | 12 | 44 |
| Relapses[b] | 3 | 17 | 5 | 17 | 13 | 48 |
| Patients developing nodal metastases | 0 | 0 | 4 | 14 | 15 | 56 |
| Patients developing distant metastases | 3 | 17 | 20 | 69 | 19 | 70 |
| Sites of distant metastases | | | | | | |
| Lung | – | 17 | – | 31 | – | 41[c] |
| Bone | – | 11 | – | 59 | – | 33[c] |
| Overall survival | | | | | | |
| Dead | 0 | 0 | 10 | 34 | 14 | 52 |
| Dead of disease | 0 | 0 | 8 | 80 | 10 | 71 |
| Alive | 18 | 100 | 19 | 66 | 13 | 48 |
| Alive with disease | 1 | 5.5 | 11 | 58 | 2 | 15 |

[a] According to the TNM/pTNM classification [16]
[b] Clinically evident local relapses plus nodal relapses in N0/pN0 patients plus distant relapses in M0/pM0 patients and in M1/pM1 patients in sites different from those at diagnosis
[c] Also: liver, pleura, brain, soft tissues

means of the product-limit method. The *p* value was calculated by the log-rank method [9].

## Results

Table 1 compares the clinicopathological characteristics of the 18 cases of MIFCs, 29 WIFCs, and 27 ICs. Men were only 5.5% of the MIFC cases but 41% and 30% of the WIFCs and ICs, respectively. Median age was 39 years in MIFC, with 56% of the patients being younger than 40 years at diagnosis. By contrast, median age was 57 years (14% of the cases below 40 years) and 53 years (26% of the cases below 40 years) in WIFC and IC, respectively. Six MIFC patients underwent a total thyroidectomy, while in 12 cases a hemithyroidectomy was performed. In all IC and in 26 WIFC patients a total thyroidectomy was performed. In 3 cases of WIFC a hemithyroidectomy for tumor limited to one lobe of the thyroid gland, without nodal or distant metastases, was performed. Multifocality occurred in 24% and 52% of WIFCs and ICs, respectively, while it was absent in MIFCs. While in MIFC no cases were pT4 or N1/pN1or M1/pM1, 7% of WIFC and 62% of IC were pT4, 7% of WIFC and 48% of IC were N1/pN1, and 66% of WIFC and 44% of IC were M1/pM1. Relapses occurred in 17% of MIFCs, 17% of WIFCs and 48% of ICs. At the end of follow-up nodal metastases had occurred in 14% and 56% of WIFCs and ICs, respectively, but in no cases of MIFCs. Distant metastases had occurred in 17%, 69%, and 70% of MIFCs, WIFCs, and ICs, respectively. Metastases occurred only in bones and lung in both MIFC and WIFC, while in IC there was also involvement of liver, pleura, brain, and soft tissues. Distant metastases involved lung in 31% of WIFCs and in 41% of ICs, and bone in 59% of WIFCs and 33% of ICs, respectively. No association was found between extent of surgery and outcome. In particular, distant relapses occurred in a similar percentage (17%) in MIFC patients who underwent hemithyroidectomy or total thyroidectomy. No events occurred in the 3 hemithyroidectomized WIFC patients with tumors limited to one lobe of the thyroid gland. Radiotherapy was administered equally to WIFCs and ICs. Among alive patients there was evidence of disease in 5.5% of MIFCs, 58% of WIFCs, and 15% of ICs, mainly at bone, at the end of follow-up. No patient with MIFC died, while 34% of the WIFCs and 52% of the ICs did so.

The MCA (Fig. 4) was carried out on all 74 patients. As detailed in Table 2, 62.1% of variance was explained by the first factorial axis, while the second axis explained 36.3%. The remaining information (1.6%) was

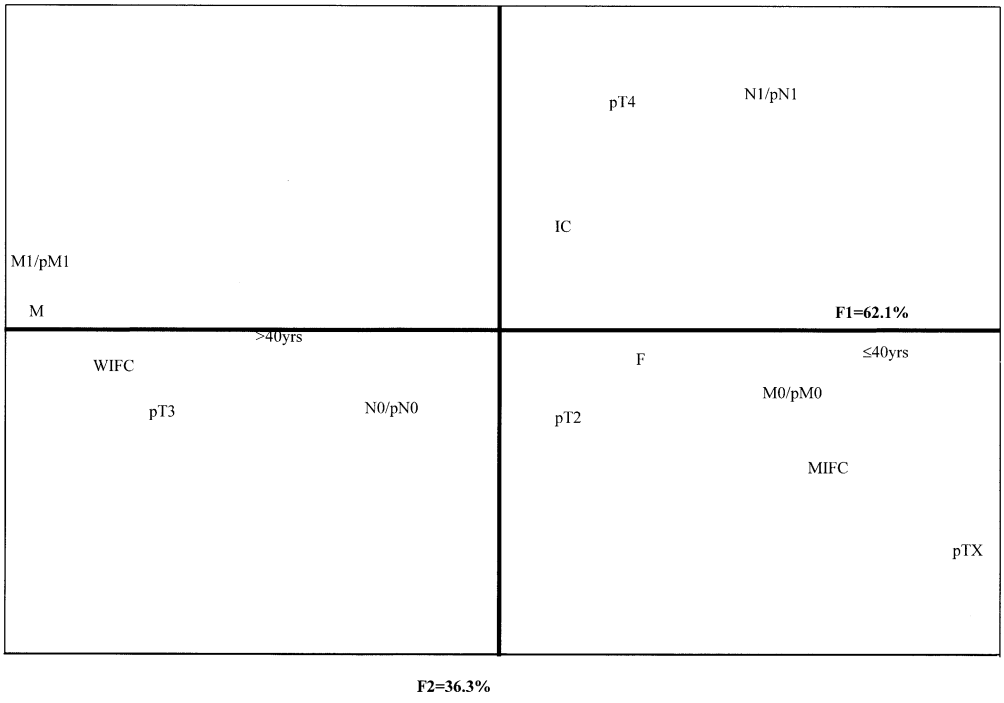



**Fig. 4** *F1* First factorial axis; *F2* second factorial axis; *≤40yrs* age at diagnosis 40 years or younger; *>40yrs* age at diagnosis over 40 years; *F* female; *M* male; *pTX*, *pT2*, *pT3*, *pT4*, *N0/pN0*, *N1/pN1*, *M0/pM0*, *M1/pM1* refer to the TNM/pTNM classification [16]; *MIFC* minimally invasive follicular carcinoma; *WIFC* widely invasive follicular carcinoma; *IC* insular carcinoma

**Table 2** Percentage contribution of the explanation of the first two axes of multiple correspondence analysis

| Variables | Axis 1 (62.1%) | Axis 2 (36.3%) | Number of categories |
|---|---|---|---|
| pT classification | 45.98 | 11.56 | 4 |
| N/pN classification | 43.40 | 6.68 | 2 |
| M/pM classification | 8.25 | 38.82 | 2 |
| Sex | 2.31 | 22.5 | 2 |
| Age at diagnosis (≤40/>40 years) | 0.06 | 20.40 | 2 |

explained by the other five axes. We considered principally the first two factorial axes, providing a plane on which both structural and supplementary variables were represented. Each category of the supplementary variable was projected as a point on this plane, giving a graphic representation of the profile of each histotype.

The first factorial axis was mainly determined by N/pN and pT variables. This axis contrasted N1/pN1 with N0/pN0, and pT4 with pT2 and pT3. The second factorial axis was mainly determined by M/pM, sex and age at diagnosis. This axis contrasted M1/pM1 with M0/pM0, men with women, and age over 40 with age of maximally 40 years. Plotting the histotypes as a supplementary variable, it was possible to see that the first factorial axis separated IC from both FCs, and in particular from MIFC, while the second factorial axis separated WIFC from MIFC.

The results obtained with the first axis of the MCA suggested a clearcut separation of IC from both FCs on the basis of the occurrence of pT4 and N1/pN1 classifications in the former. In particular, if taking account also of the other variables, the difference was much stronger between IC and MIFC: whereas M1/pM1, male sex and age over 40 years occurred similarly in ICs and WIFCs, this was not the case for MIFCs. These results were verified by the second axis that explained the differences between MIFCs and WIFCs on the basis of the occurrence of M1/pM1 classification, male sex, age at diagnosis over 40 years, and pT3 (vs pT2) classification in the latter group.

Median follow-up of all the patients of the three case series was 147 months (range 3–257 months), with 25% of the patients having a follow-up of over 165 months. Kaplan-Meier estimates (Fig. 5) were plotted for a 10-year period only because after this point the number of patients at risk was too low to yield a reliable survival curve. A statistically significant difference in overall survival was observed between the three histotypes ($P$=0.012, log-rank test, Fig. 5). None of the 18 MIFC patients (8 of whom had a follow-up above 10 years) died. Among the patients with a follow-up below 10 years, 9 of 23 WIFCs and 11 of 17 ICs died. Among the patients with a follow-up above 10 years, one of 6 WIFC and 3 of 10 ICs died.

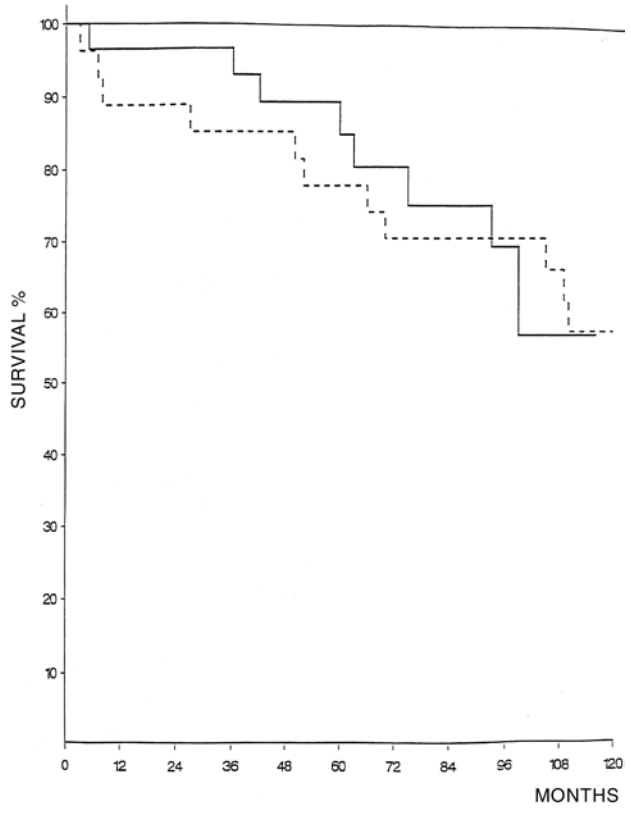



**Fig. 5** Overall survival curves of 18 minimally invasive follicular carcinomas (*thin solid line*), 29 widely invasive follicular carcinomas (*thick solid line*), and 27 insular carcinomas (*dashed line*)

## Discussion

The overall survival analysis showed a clearcut distinction between MIFC and both WIFC and IC ($P$=0.012). While the former was confirmed as a low-risk form (with no dead patients at the end of the observation period), the latter two histotypes represented high-risk forms with similar overall survival curves, in accordance with our previous data [11]. Thus the results confirm that both the presence of a poorly differentiated morphology (as in IC) and the degree of invasiveness into the surrounding thyroid parenchyma (as in WIFC) were effective in separating low-risk from high-risk forms of follicular-related carcinomas.

The main feature characterizing MIFC respect to both WIFC and IC is its lower degree of aggressiveness, which paralleled the minimal invasiveness into the thyroid parenchyma coupled with the low tendency to spread outside the thyroid gland. In addition, the presence of a complete, minimally invaded peritumoral capsule does represent a strong favorable prognostic factor in MIFCs. Consistently, we did not find a complete peritumoral capsule in WIFCs and ICs, both representing widely invasive carcinomas. A prognostic role of the presence of a peritumoral capsule was also suggested in poorly differentiated papillary carcinomas, where a favorable outcome was reported in a series of encapsulated columnar cell carcinomas [5].

Our MIFC series showed clinicopathological characteristics in keeping with the literature, apart from a higher percentage of distant relapses (i.e., 17% vs. about 5% [14]). This could be ascribable to the strict diagnostic criteria applied, that contributed to make smaller the number of MIFCs. In fact, our series did not encompass cases that showed only equivocal or incomplete capsular invasion. For such cases it was recently proposed the term of "follicular tumor of uncertain malignant potential," in keeping with their unremarkable outcome [17].

Finally, surgical approach did not affect the MIFC outcome, as the percentage of relapses was similar in hemithyroidectomized and totally thyroidectomized cases.

WIFC and IC shared a high degree of aggressiveness and an ominous outcome, with a similar high percentage of dead patients at the end of follow-up. In our previous analysis [12], histotype (WIFC vs. IC) did not result associated by itself with survival, but the presence of distant metastases did. At the end of follow-up the cumulative percentage of distant metastases in WIFCs was similar to ICs (69% vs. 70%), in keeping with their similar overall survival. Among alive WIFC and IC patients the higher percentage of WIFC patients with evidence of disease at the end of follow-up is likely to be related to the higher incidence in them of bone metastases (59% vs. 33%), less curable by radioiodine therapy respect to lung metastases [14].

Regarding the possible time-dependent course of a low-risk form into a high-risk form, the statistical analysis of the characteristics at onset through MCA highlighted the close relationship that exists between MIFC and WIFC and the segregation of either from IC. In fact, both the usual types of FC showed biological behavior characteristics typical of FCs (such as the lack of tendency to spread locally outside the thyroid capsule or to lymph nodes) and the occurrence of bone metastases in addition to those in the lungs. These results, when coupled with previous reports [8], strongly suggest that WIFC is the time-dependent high-risk form of MIFC. In fact, the former occurred in an older age group, featured a larger size and a widespread growth into the thyroid parenchyma, and often presented with distant metastases. Thus it retained the characteristics of local and distant spread that are typical of its minimally invasive counterpart, showing no tendency to spread beyond the thyroid capsule into the surrounding tissues and having distant metastases restricted to lungs and bone.

In keeping with what occurs in other types of "poorly differentiated carcinoma" of the thyroid gland and at variance with the two usual types of FC, IC showed papillary-related behavior features, i.e., tendency to extend beyond the thyroid capsule and presence of nodal metastases. In addition, metastases in sites other than lungs and bone occurred, such as liver, pleura, brain, and soft tissue, a finding also reported in poorly differentiated papillary carcinomas [11]. The present results make it very unlikely that MIFC is a direct precursor of IC, and

reinforce our previous suggestion that IC is a distinct entity among follicular cell-derived thyroid carcinomas [4, 12]. The role of age at onset and/or epigenetic factors, such as geographic variations, remains to be clarified. Further studies are also needed to test the possible influence on clinicopathological characteristics of the particular mutation at codon 61 of the N-RAS gene that seems to selectively affect IC [12].

In conclusion, MIFCs showed to be the low-risk counterpart of WIFCs on the basis of age at onset, size, TNM/pTNM classification, and biological behavior. By contrast, IC confirmed to be a distinct entity among follicular cell-derived thyroid carcinomas, sharing morphological features and outcome with both follicular and papillary-related carcinomas, despite bearing one molecular hallmark (RAS gene family point mutations) characteristic of follicular-related tumors of the thyroid gland [10, 12].

## References


1. Benzecrì JP (1973) Analyse des données. II. Analyse des correspondance. Dunod, Paris
2. Benzecrì JP (1979) Sur le calcul des taux d'inertie dans l'analyse d'un questionnaire. Cahiers Anal Donnees 4:377
3. Carcangiu ML (1997) Minimally invasive follicular carcinoma. Endocr Pathol 8:231–234
4. Carcangiu ML, Zampi G, Rosai J (1984) Poorly differentiated ("insular") thyroid carcinoma. A reinterpretation of Langhans' "wüchernde Struma." Am J Surg Pathol 8:655–668
5. Evans HL (1996) Encapsulated columnar-cell neoplasms of the thyroid. A report of four cases suggesting a favorable prognosis. Am J Surg Pathol 20:1205–1211
6. Evans HL, Vassilopoulou-Sellin R (1998) Follicular and Hürthle cell carcinomas of the thyroid. A comparative study. Am J Surg Pathol 22:1512–1520
7. Greenacre MJ (1996) Correspondence analysis in practice. Academic, London
8. Jorda M, Gonzales-Campora R, Mora J, Herrero-Zapatero A, Otal C, Galera H (1993) Prognostic factors in follicular carcinoma of the thyroid. Arch Pathol Lab Med 117:631–635
9. Kaplan EL, Meier P (1958) Nonparametric estimation from incomplete observation. J Am Stat Assoc 53:457–481
10. Oyama T, Suzuki T, Hara F, Iino Y, Ishida T, Sakamoto A, Nakajima T (1995) N-*ras* mutation of thyroid tumor with special reference to the follicular type. Pathol Int 45:45–50
11. Pilotti S, Collini P, Manzari A, Marubini E, Rilke F (1995) Poorly differentiated forms of papillary thyroid carcinomas: distinctive entities or morphological patterns? Semin Diagn Pathol 12:249–255
12. Pilotti S, Collini P, Mariani L, Placucci M, Bongarzone I, Vigneri P, Cipriani S, Falcetta F, Miceli R, Pierotti MA, Rilke F (1997) Insular carcinoma. A distinct de novo entity among follicular carcinomas of the thyroid gland. Am J Surg Pathol 21:1466–1473
13. Pilotti S, Collini P, Sampietro G, Manzari A, Marubini E, Rilke F (1998) Thyroid papillary carcinomas of columnar cell type. A clinicopathologic study of 16 cases. Cancer 83: 2421–2422 (Letter)
14. Rosai J, Carcangiu ML, De Lellis RA (1992) Tumors of the thyroid gland. In: Atlas of tumor pathology, 3rd series, fascicle 5. AFIP, Washington
15. Sampietro G, Tomasic G, Collini P, Biganzoli E, Boracchi P, Bidoli P, Pilotti S (2000) Gene product immunophenotyping of neuroendocrine lung tumors. No linking evidence between carcinoids and small-cell lung carcinomas suggested by multivariate statistical analysis. Appl Immunohistochem Mol Morphol 8:49–56
16. Sobin LH, Wittekind C (eds) (1997) UICC TNM Classification of malignant tumours, 5th edn. Wiley, New York
17. Williams ED (2000) Two proposal regarding the terminology of thyroid tumors. Int J Surg Pathol 8:181–183
18. World Health Organization (1988) International histological classification of tumours. Histological typing of thyroid tumors, 2nd edn. Springer, Berlin Heidelberg New York

Virchows Arch (2003) 442:77–81
DOI 10.1007/s00428-002-0725-7

CASE REPORT

**Kazuto Yamazaki**

# A gastric carcinosarcoma with neuroendocrine cell differentiation and undifferentiated spindle-shaped sarcoma component possibly progressing from the conventional tubular adenocarcinoma; an immunohistochemical and ultrastructural study

Received: 24 May 2002 / Accepted: 22 August 2002 / Published online: 14 November 2002
© Springer-Verlag 2002

**Abstract** A 56-year-old Japanese man underwent total gastrectomy with lymph-node dissection for a gastric tumor. In the oral rim of the excised large ulcerated tumor, a small nodular mass demonstrated a unique histology of a carcinosarcoma composed of more than three distinctive components. A major part of the large ulcerated tumor tissue consisted of conventional tubular adenocarcinoma, with the coincidental focal distribution of solid cell nests of poorly differentiated or neuroendocrine cell (small cell) carcinoma. Sarcoma cells were another of the constituents of the small nodular tumor with atypical spindle-shaped cells. All the excised lymph-node metastasis demonstrated the histology of tubular adenocarcinoma. In the sarcoma cells, many of the lineage-specific immunohistochemical markers were negative. Only vimentin was positive. Electron microscopy revealed that the neuroendocrine cell carcinoma contained cells with abundant small aggregations of neurosecretory-type granules in their cellular cytoplasm. Primitive cellular junctions and incomplete basal lamina were seen in the sarcoma cells. No transitional or hybrid-type cells were seen between carcinoma and sarcoma cells. The interfaces between the cancer cell nests and the proliferation of sarcoma cells are clearly discerned. It was speculated that the unique histology of carcinosarcoma might have progressed from the conventional type of pre-existing advanced tubular adenocarcinoma.

**Keywords** Composite tumor · Collision tumor · Histological progression · Cell-to-cell interaction · Small cell carcinoma

K. Yamazaki (✉)
Department of Pathology, Saiseikai Central Hospital,
1-4-17 Mita, Minatoku, Tokyo 108-0073, Japan
e-mail: KazutoYamazaki@aol.com
Tel.: +81-3-34518211, Fax: +81-3-34516102

## Introduction

Carcinosarcoma is a rare type of composite tumor consisting of carcinoma (epithelial malignancy) and sarcoma (mesenchymal malignancy) simultaneously in a single tumor. Hitherto, many pathological studies have reported on the variety of organs involved, including the stomach [1, 2, 3, 4, 5, 6, 7, 8, 9, 10, 11, 12, 13, 14, 15, 16, 17, 18, 19]. In the literature concerning conventional gastric mesenchymal tumors, the gastro-intestinal stromal tumor (GIST) is at present a very popular tumor entity, which could be characterized by the growth of immunohistochemically c-kit and/or CD34 positive tumor cells. Smooth muscle cell tumors are another popular tumor. However a composite tumor of the true carcinosarcoma type is very rarely found in the stomach, with less than 20 cases reported in the literature [1, 2, 3, 4, 5, 6, 7, 8, 9, 10, 11, 12, 13, 14, 15, 16, 17, 18, 19]. In the textbook of Fenoglio-Preiser et al. [7], gastric carcinosarcoma could arise in elderly men [4]. Among the gastric carcinosarcomas, rhabdomyosarcomatous differentiation [11, 14, 16, 19], neuroendocrine cell differentiation [5, 19], occurrence in the residual stomach [11, 12], formation of occasional polypoid or fungating mass [4, 8, 14, 15, 19] have been reported, and, in the advanced tumor, characteristic findings have been the association with a separate neuroendocrine cell tumor [2, 12, 14] and a worse prognosis [11].

The author encountered a patient with a rare case of gastric carcinosarcoma. Definitively more than three lineages of tumor cell differentiation were recognized in the tissue of the one tumor, namely not only conventional tubular adenocarcinoma, but also neuroendocrine cell carcinoma (small cell carcinoma) and a primitive spindle-shaped sarcoma component. It was speculated that the unique histology of carcinosarcoma might progress from a pre-existing advanced tubular adenocarcinoma of the conventional type.

## Clinical history

The patient was a 56-year-old Japanese man who complained of anorexia and disturbance of swallowing from 5 months before the admission for gastrectomy. He had rapidly lost body weight, approximately 5 kg over 3 months. He visited the hospital, and an infiltrating ulcerated gastric tumor was confirmed in the posterior wall of the gastric body by gastrointestinal tract roentogenography and endoscopy. In the abdominal computed tomography (CT) scan, swellings of para-abdominal aortic lymph nodes were revealed. The left subclavicular lymph node was also swollen. In the laboratory data, moderate anemia (Hb, 10.9 g/dl), and high serum levels of tumor markers were noted: carcinoembryonic antigen (CEA) 87.9 ng/ml, alpha feto-protein (AFP) 16 ng/ml, and CA19–9 1093 U/ml. He underwent total gastrectomy. The tumor was approximately 9×9 cm in size and penetrated directly into the anterior serosa of the pancreatic body, but did not invade the pancreatic parenchyma. The invaded tumor could not be completely excised. The perigastric lymph nodes were markedly swollen through the metastasis of the cancer. Liver metastasis was also seen intraoperatively. The patient died of esophageal obstruction by the local recurrence of the tumor and liver metastasis approximately 2 months after the operation.

## Materials and methods

### Light microscopy and immunohistochemistry

The excised stomach was fixed in 15% formalin, embedded in paraffin wax, sectioned, and stained in hematoxylin and eosin (H&E). For immunohistochemistry, the antigens of EMA, pankeratin (AE1+AE3; Dako, Denmark), keratins (CAM 5.2 and 34 beta E12), cytokeratin 7 (OV-TL 12/30; Dako, Denmark), cytokeratin 20 (Ks 20.8; Dako, Denmark), CEA, Leu7, chromogranin, synaptophysin, Desmin, Vimentin, CD34, c-kit, BerEP4, GFAP, NFP, alpha 1-antitrypsin, Kp-1 (CD68), LCA, alpha fetoprotein, alpha smooth muscle actin, and HMB45, Ki-67, p53, and PCNA, were examined using the Envision method (Envision kit; Dako, Denmark). Immunostaining was done with or without antigen-retrieval techniques (heating in autoclave or enzyme digestion methods).

### Electron microscopy

Small samples of tumor tissue were fixed in phosphate-buffered 2.5% glutaraldehyde and processed using conventional methods into epoxy resin. Ultrathin sections were stained with uranyl acetate and lead citrate, and examined under a JEOL-1200 EXII electron microscope.

## Results

On gross examination of the excised material from the patient's stomach, an ulcer-forming and infiltrating tumor was seen in the posterior wall of the gastric body. The mass measured 9×9×2 cm with a hole of approximately 3 cm in its diameter positioned in the center of the tumor, which was formed by the penetration of the tumor into the serosa of the pancreas body (Fig. 1a) but not invading the pancreatic parenchyma. An oral infiltrating rim of tumor tissue formed a nodular mass of approximately 2×2×2 cm (Fig. 1b). Lymph-node metastasis was observed in 28 of the total of 31 excised specimens.

The low-power microscopic view of the conventional histological examination revealed that the oral infiltrating nodular mass was composed of two components of carcinoma and sarcoma; that is, a carcinosarcoma (Fig. 2a, b). Many of the other tumor tissues consisted of the tubular adenocarcinoma typical of the conventional differentiated gastric adenocarcinoma. In the mucosa and part of the subserosal layer, the component of well to moderately differentiated tubular adenocarcinoma was observed among the coincidental distribution of solid

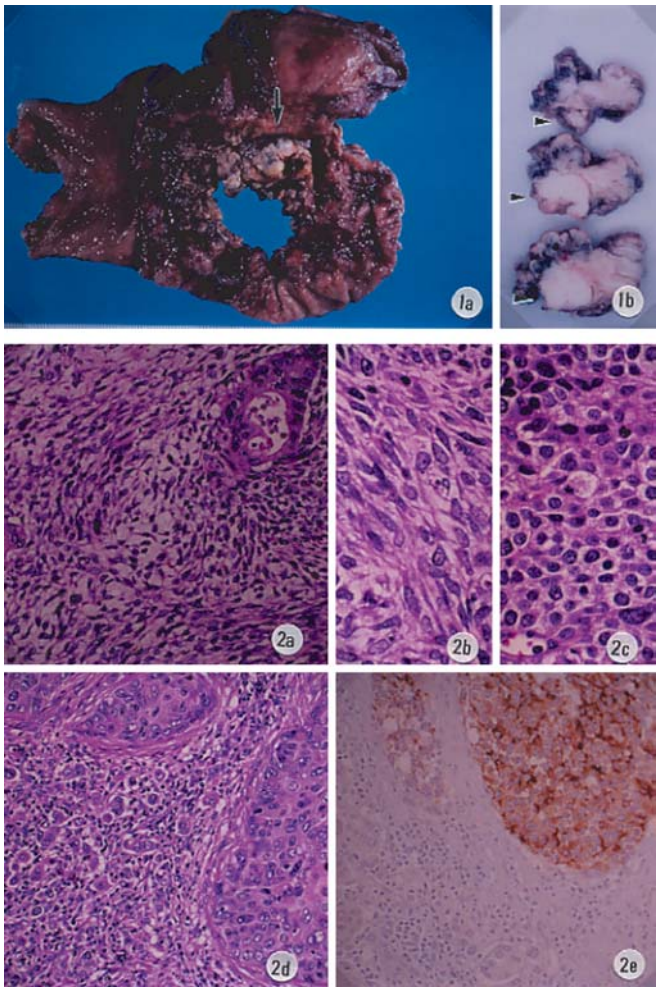



**Fig. 1** **a** Macroscopic view of the resected stomach. Right is the oral side. The stomach was opened along the great curvature. The *arrow* indicates the nodular tumor mass containing carcinosarcoma histology. **b** The excised surface of the nodular tumor mass (*arrow* in **a**). A yellow-white nodular mass (*arrowheads*) of approximately 2 cm in diameter. The overlying mucosa replaced by the conventional tubular adenocarcinoma.

**Fig. 2** Light microscopic and immunohistochemical observations of the tumor tissue. **a** Tubular adenocarcinoma forms irregular glands positioned among the sarcoma tissue [hematoxylin and eosin (H&E ×190)]. **b** Sarcoma component. Proliferation of undifferentiated spindle cells (H&E ×380). **c** Small cell carcinoma (neuroendocrine carcinoma) cells with a small amount of cytoplasm (H&E ×380). **d** Poorly differentiated or undifferentiated carcinoma with moderate amount of fibrous and lymphocytic stroma. Poorly differentiated carcinoma or squamoid carcinoma components are also seen (H&E ×190). **e** Small cell carcinoma (neuroendocrine carcinoma) cells labeled by anti-chromogranin A antibody. Adenocarcinoma nests were not labeled. Chromogranin A stain ×190

small cell nests of poorly differentiated or undifferentiated small cell carcinoma (Fig. 2c). The distribution of the adenocarcinoma was wide and constituted the major component within the tumor, while the sarcoma cells were another dominant constituent of the tumor with atypical spindle-shaped cells (Fig. 2a, b). The mixed tumor cells continuously invaded the subserosa and muscularis propria. In the tumor, an endocrine (small cell carcinoma) component was also observed (Fig. 2c, e). The three distinct components (tubular adenocarcinoma, sarcoma, and small cell carcinoma) were clearly recognizable without any definitive transitional areas among them (Fig. 2d, e). Occasionally small cell carcinoma cells and adenocarcinoma cells were distributed simultaneously. Both carcinoma components could be easily discerned. Even more poorly differentiated carcinoma or squamoid carcinoma components were also seen (Fig. 2d). The adenocarcinoma and small cell carcinoma cells showed marked lymphatic or venous invasion within the tumor tissue (Fig. 2d). All the excised lymph-node metastasis showed the histology of differentiated tubular adenocarcinoma.

The three components of the tumor showed distinctive immunoreactivities. Low molecular weight cytokeratin (CAM5.2), pankeratin (AE1+AE3), chromogranin A (Fig. 2e), and synaptophysin were positively stained in the small cell carcinoma (neuroendocrine cell carcinoma) component of the tumor. Cytokeratin 7 and cytokeratin 20, 34 beta E12 were all negative in the small cell carcinoma (neuroendocrine cell carcinoma) component. However, cytokeratin 7 and cytokeratin 20 were variably positive in well to moderately differentiated tubular carcinoma components. In the sarcoma cells, EMA, CEA, CAM5.2, 34 beta E12, AE1+AE3, cytokeratin 7, cytokeratin 20, chromogranin A, synaptophysin, alpha smooth muscle actin, c-kit, CD34, neurofilament protein, and S-100 protein were all negative. Only vimentin was positive in the sarcoma area. A minor population of the spindle sarcoma cells revealed some positive stains the by alpha smooth muscle actin and desmin. Ki-67, PCNA, and p-53 were positive in over 90% of the total tumor cells of three components (tubular adenocarcinoma, sarcoma, and small cell carcinoma). This rare case of carcinosarcoma of the stomach displaying three distinct components (well to moderately differentiated tubular carcinoma, neuroendocrine carcinoma and sarcoma). The percentage of the different components was evaluated. In the total area of the tumor tissue (total 100%), well to moderately differentiated tubular carcinoma occupied approximately 70%, neuroendocrine carcinoma occupied approximately 15%, and sarcoma occupied less than 15–20%.

Transmission electron microscopy revealed the adenocarcinoma cells and sarcoma cells mixed in the small area constituting the histology of the carcinosarcoma (Fig. 3a). Nodular aggregates of adenocarcinoma cells were seen with a tubular or small alveolar pattern. Short spindle-shaped and undifferentiated sarcoma cells with medium cytoplasmic densities were scattered in the loose extracellular matrix. Adenocarcinoma cells showed many apical microvilli surrounding the small tubular lumen (Fig. 3a). The apical junctional complex was rather well developed between adenocarcinoma cells (Fig. 3a). Ultrastructurally, the interfaces between cancer cell nests and the proliferation of sarcoma cells were clearly discerned. Neither transitional nor hybrid cells were recognized. Another area of the small cell carcinoma (neuroendocrine carcinoma) cells showed the abundant small aggregation of neurosecretory-type granules in their cytoplasm (Fig. 3b, c). Primitive cellular junctions forming between the adjacent tumor cells were also seen (Fig. 3c).

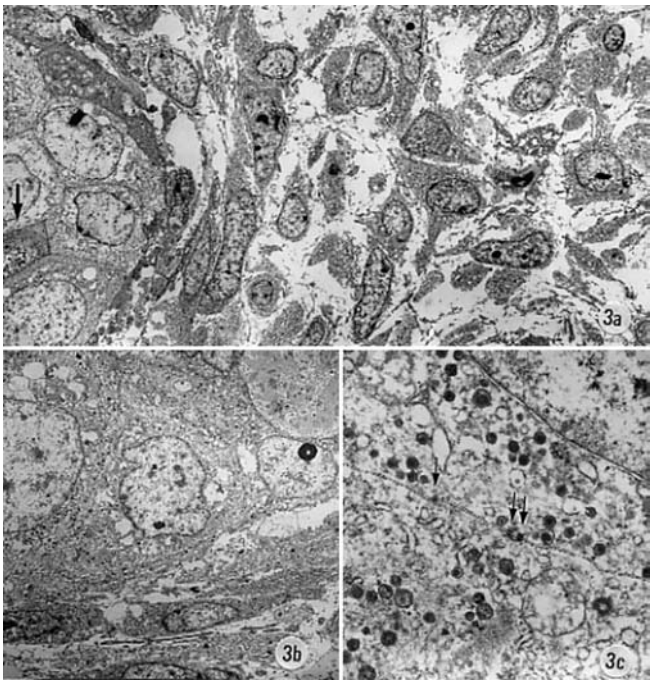



**Fig. 3** Transmission electron micrographs of adenocarcinoma cells and sarcoma cells. **a** Nodular aggregates of adenocarcinoma cells with a tubular or small alveolar pattern (*left*). Note the tubular small lumen (*arrow*) formed by the cancer cells with apical microvillous differentiation. On the *right*, short spindle-shaped sarcoma cells are scattered in the loose extracellular matrix (×1200). **b** Medium power view of the small cell carcinoma (neuroendocrine carcinoma) cells with neurosecretory-type granules (×2000). **c** High-power view of the small cell carcinoma (neuroendocrine carcinoma) cells with abundant small aggregations of neurosecretory-type granules. Primitive cellular junctions (*arrows*) are forming between the adjacent tumor cells (×12,000)

Transmission electron micrographs of sarcoma cells showed short spindle or satellite shaped sarcoma cells with a medium amount of cytoplasm and a well-developed rough endoplasmic reticulum (RER) scattered in the loose extracellular matrix (Fig. 4a). Some sarcoma cells were aggregated. The cytoplasm of sarcoma cells viewed at a higher magnification revealed a well-developed RER (Fig. 4b, c). Occasionally sarcoma cells formed primitive cellular junctions between the adjacent tumor cells (Fig. 4b, c). Incomplete basal lamina surrounding the sarcoma cells were also seen (Fig. 4c). Sarcoma cells were rather undifferentiated, and neither ul-

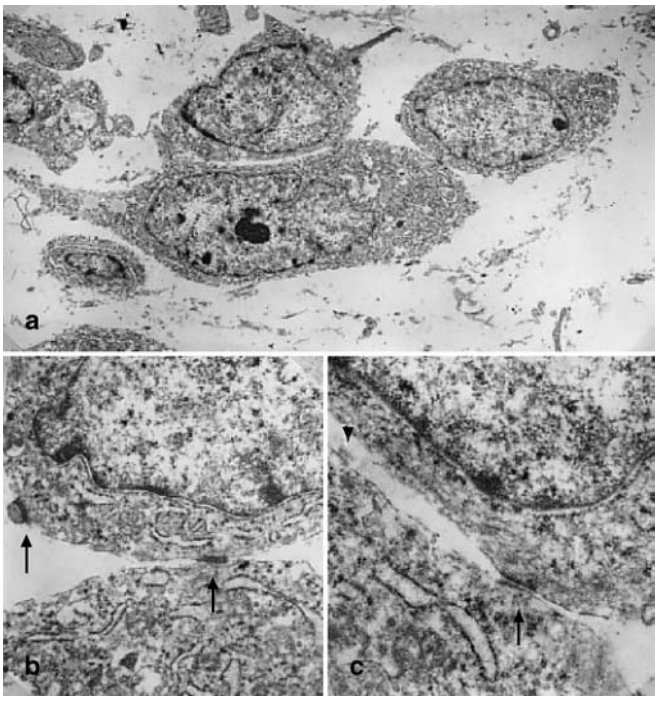



**Fig. 4** Transmission electron micrographs of sarcoma cells. **a** Short spindle-shaped sarcoma cells (×3600). **b** Higher power view of the cytoplasm of sarcoma cells with well-developed rough endoplasmic reticulum (RER). Primitive cellular junctions (*arrows*) are forming between the adjacent tumor cells (×12,000). **c** Higher power view of the cytoplasm of sarcoma cells. Primitive cellular junction (*arrow*) is forming between the adjacent tumor cells. Incomplete basal lamina surrounds the sarcoma cells (*arrowhead*) (×24,000)

trastructually differentiated structures of myofilaments, dense patches, nor Z-bands were seen.

## Discussion

Gastric carcinoma can have the spindle cell component [7, 8], termed sarcomatoid carcinoma or spindle cell carcinoma [7]. Fenoglio-Preiser et al. [7] described the existence of the sarcomatous component, sometimes stained with markers usually associated with epithelial cells [4, 12, 14, 19]. The present case, however, could be well distinguished from that sarcomatous carcinoma, since neither transitional nor hybrid cells were seen within the tumor and it was uniquely characterized by the rather well-mixed or composite nature of both components (carcinoma and sarcoma). In the present tumor, the sarcomatous area did not demonstrate the desmoplastic or non-tumorous growth associated with the benign stromal components of cancer, since cellular atypism, abnormal increase of mitosis, and a high labeling index of Ki-67, PCNA, and p-53 were seen in the tumor cells of all three components (tubular adenocarcinoma, sarcoma, and small cell carcinoma). However, definitive heterogeneous sarcomatous elements, such as cartilaginous [4], osteoblastic [14], fat, nerve, or rhabdomyoid features [11, 14, 16], could not be seen in the present tumor. In the present case, sarcoma cells showed quite undifferentiated characters. Moreover, a very small amount of sarcoma cells revealed immunohistochemical differentiation toward smooth muscle cells, such as alpha smooth muscle actin positive or desmin positive. The present carcinosarcoma could be distinguished from the collision tumor [18] since, in the carcinosarcomatous area, well-mixed histological components and a definitive composite histological nature were recognized. In the present case, composite histological nature of mixed endocrine-exocrine tumor in the cancer component was also interesting [3, 17].

Transmission electron microscopy showed that occasionally sarcoma cells formed primitive cellular junctions between the adjacent tumor cells. Incomplete basal lamina surrounding the sarcoma cells were also seen. Sarcoma cells revealed quite distinct cell-to-cell and cell-to-matrix interactions, which could be distinguished from those of cancer cells with definitive cellular junctions and polarity of basolateral and apical specificities. Ultrastructurally, the interface between cancer cell nests and the proliferation of sarcoma cells was clearly discerned. Neither transitional nor hybrid cells between cancer cells and sarcoma cells were recognized.

In the previous literature and among the many descriptions, formation of some polypoid masses is rather characteristic [8, 14, 15, 19]. In the present case, the oral infiltrating rim of the tumor tissue had formed a nodular mass of approximately 2×2×2 cm. Lewin and Appelman, in their AFIP fascicle [10], described rare tumors of gastric carcinosarcoma [2, 4, 6, 15]. They emphasized the high primary stage at the time of diagnosis. In the present case, similar to the literal description, the patient was in the advanced clinical stage at the time of diagnosis and excisional surgery. It might be interpreted from the histogenetic standpoint, just with the background of conventional ulcerated infiltrating tumor consisting of typical tubular adenocarcinoma, that the characteristic polypoid or nodular mass that contained the carcinosarcoma component could be newly generated. The unique histology of carcinosarcoma might progress from a pre-existing advanced tubular adenocarcinoma of the conventional type. In other words, as a first step, the cancer formed by the differentiated tubular adenocarcinoma might form a conventional ulcerated mass. Subsequently, at the second step, in the certain focus of well-differentiated tubular adenocarcinoma, the new unique histology of carcinosarcoma or neuroendocrine cell carcinoma might be generated from the accumulation of genetic defects along with the growth of the first conventional cancer. During the rather long period of tumor progression, the tumor might demonstrate one single histology of conventional tubular adenocarcinoma before the histological evolution to this carcinosarcoma, since, in the present case, all the excised lymph-node metastasis showed a single histology of differentiated tubular adenocarcinoma, but not carcinosarcoma histology. It was speculated that the unique carcinosarcoma histology might have progressed from a pre-existing advanced tubular adenocarcinoma of the conventional type.

**Acknowledgements** The authors acknowledge the assistance of T. Nagai and K. Fujita for their expertise in electron microscopy technique and Drs. K. Matuoka, H. Orikasa, K. Kato, and R. Oyama for their valuable discussion.

## References

1. Aiba M, Hirayama A, Suzuki T, et al (1991) Carcinosarcoma of the stomach: report of a case with review of the literature of gastrectomised patients. Surg Pathol 4:75–83
2. Bansal M, Kaneko M, Gordon RE (1982) Carcinosarcoma and separate carcinoid tumor of the stomach. A case report with light and electron microscopic studies. Cancer 50:1876–1881
3. Capella C, La Rosa S, Uccella et al (2000) Mixed endocrine-exocrine tumors of the gastrointestinal tract. Semin Diagn Pathol 17:91–103
4. Cho KJ, Myong MH, Choi DW, et al (1990) Carcinosarcoma of the stomach: a case report with light microscopic, immunohistochemical, and electron microscopic study. APMIS 98: 991–995
5. Cruz J, Paz JI, Cordero M, et al (1991) Carcinosarcoma of the stomach with endocrine differentiation. A case report. Tumori 77:355–357
6. Dundas SA, Slater DN, Wagner BE, et al (1988) Gastric adenocarcinoleiomyosarcoma: a light, electron microscopic and immunohistochemical study. Histopathology 13:347–353
7. Fenoglio-Preiser CM, Noffsinger AE, Stemmermann GN, et al (1998) The neoplastic stomach. In: Gastrointestinal Pathology: an atlas and text. Lippincot, Williams & Wilkins, Philadelphia, pp 237–274
8. Hanada M, Nakano K, Ii Y, et al (1985) Carcinosarcoma of the stomach. A case report with light microscopic, immunohistochemical, and electron microscopic study. Acta Pathol Jpn 35:951–959
9. Kallakury BV, Bui HX, deRosario A, et al (1992) Primary gastric adenosarcoma. Arch Pathol Lab Med 117:299–301
10. Lewin KJ, Appelman HD (1995) Miscellaneous tumors. In: Atlas of tumor pathology, Third series, Fascicle 18. Tumors of the esophagus and stomach. Armed Forces Institute of Pathology, Washington, DC, pp 457–462
11. Matsukuma S, Wada R, Hase K, et al (1997). Gastric stump carcinosarcoma with rhabdomyosarcomatous differentiation. Pathol Int 47:73–77
12. Melanto M, Bucconi S, Grillo BP, et al (1993) Carcinosarcoma and separate neuroendocrine malignant tumor of a malignancy promoter, the gastric stump. Anticancer Res 13:2485–2488
13. Miyauchi K, Yalano Y, Ohshima Y, et al (1994) A case of carcinosarcoma of the stomach. Nippon Shokakibyo Gakkai Zasshi 91:75–79
14. Nakayama Y, Murayama H, Iwasaki H, et al (1997) Gastric carcinosarcoma (sarcomatoid carcinoma) with rhabdomyoblastic and osteoblastic differentiation. Pathol Int 47:557–563
15. Robey-Caferty S, Grington DJ, Ro JY, et al (1990) Sarcomatoid carcinoma of the stomach. A report of three cases with immunohistochemical and ultrastructural observations. Cancer 65:1601–1606
16. Sato Y, Shimozono T, Kawano S, et al (2001) Gastric carcinosarcoma, coexistence of adenosquamous carcinoma and rhabdomyosarcoma: a case report. Histopathology 39:543–544
17. Solcia E, Kloppel G, Sobin LH (2000) Histological typing of endocrine tumours, 2nd edn. World Health Organization, International Histological Classification of Tumours, Springer, Berlin Heidelberg New York
18. Tokunaga O, Morimatsu M, Nakashima T (1979) Collision tumor of the stomach with carcinosarcoma and tubulo-papillary adenocarcinoma. Acta Pathol Jpn 29:819–824
19. Tsuneyama K, Sasaki M, Sabit A, et al (1999) A case report of gastric carcinosarcoma with rhabdomyosarcomatous and neuroendocrinal differentiation. Pathol Res Pract 165:93–97

Virchows Arch (2003) 442:82–85
DOI 10.1007/s00428-002-0727-5

CASE REPORT

**Paolo Giovanni Nuciforo · Laura Moneghini
Paola Braidotti · Laura Castoldi · Paolo De Rai
Silvano Bosari**

# Malakoplakia of the pancreas with diffuse lymph-node involvement

Received: 2 July 2002 / Accepted: 23 September 2002 / Published online: 12 November 2002
© Springer-Verlag 2002

**Abstract** We report a case of malakoplakia involving the pancreas in a 74-year-old man with associated regional lymphoadenopathy. Histological examination of both pancreas and lymph nodes revealed a diffuse histiocytic infiltrate containing numerous Michaelis-Gutmann bodies. Electron microscopy supported the diagnosis of malakoplakia and showed bacterial-like structures. Differential diagnosis includes myofibroblastic inflammatory tumor and histiocytic neoplasms. Lymph-node involvement during malakoplakia is extremely rare and it has never been documented microscopically. Lymphohematogenous spread of bacteria may be the cause of the nodal involvement, which, however, does not appear to influence the clinical course of the disease.

**Keywords** Malakoplakia · Pancreas · Lymph nodes

## Introduction

Malakoplakia is a distinct chronic granulomatous inflammation that usually involves the urinary bladder causing the formation of white-yellow plaques on the mucosal surface. The first case of this disease was reported by Michaelis and Gutmann in 1902 [8], and von Hansemann in 1903 coined the term of Malakoplakia (literally "soft plaque") [13]. Numerous other primary sites outside the urinary tract have been described, including the colon, gallbladder, genital tract, lung, breast and retroperitoneum [2, 3, 4, 10, 12]. The histological hallmark of malakoplakia is the large collection of periodic acid–Schiff (PAS)-positive macrophages (von Hansemann histiocytes), some containing characteristic Michaelis-Gutmann bodies. Although the pathogenetic mechanisms responsible for malakoplakia are not completely defined, a disorder involving the phagocytic digestion of specific microorganisms (*Escherichia coli*, *Klebsiella*, *Rhodococcus* species) mediated by lysosomal enzymes seems to play an important role [1]. An underlying systemic disease, such as immune deficiency or a neoplastic process, is frequently associated with malakoplakia. We describe here a patient presenting with malakoplakia of the pancreas, clinically mimicking a neoplastic process. Interestingly, it is the first case in which regional lymph-node involvement is documented histologically.

P.G. Nuciforo (✉) · L. Moneghini · P. Braidotti · S. Bosari
Università degli Studi di Milano,
Servizio di Anatomia Patologica. Azienda Ospedaliera S.Paolo
Via A. di Rudini 8, 20142 Milano, Italy
e-mail: paolonuciforo@hotmail.com
Tel.: +39-02-81844600, Fax: +39-02-89122032

L. Castoldi · P. De Rai
Department of Emergency Surgery, IRCCS Ospedale Maggiore,
Milan, Italy

## Clinical history

A 74-year-old man with systemic hypertension and diabetes mellitus presented at our institute with a 5-day-long history of low-grade fever and recurrent bouts of abdominal pain, which started 1 month before admission. Laboratory findings, including serum amylase, lipase, and tumor markers such as CEA, CA19-9 and α feto-protein (AFP), were normal. Computed tomography (CT) and magnetic resonance imaging (MRI) showed an ovoidal mass measuring 4×2 cm, involving the isthmus and the tail of the pancreas, suspicious for malignancy (Fig. 1). The remaining pancreatic parenchyma appeared unremarkable. Multiple celiac lymph nodes of less than 2 cm in diameter were also identified.

A laparotomy was performed and a frozen section of a peripancreatic lymph node displayed a fibroblastic proliferation mixed with multinucleated giant cells and inflammatory cells. Distal spleno-pancreatectomy with multiple lymph-node dissection was performed. The patient had an unremakable post-operative course and was discharged from the hospital without additional treatment. With a 13-month follow-up, the patient is currently well, displaying no evidence of recurrent disease.

## Materials and methods

For light microscopy, 3- to 5-μm paraffin sections of formalin-fixed tissue were stained with hematoxylin and eosin (H&E), PAS with diastase digestion (dPAS), von Kossa's, Perls' and Gram's stains. For immunohistochemistry, a standard avidin biotin complex (ABC) technique was applied. Antibodies used included those against smooth muscle actin (Dako, Golstrup, Denmark),

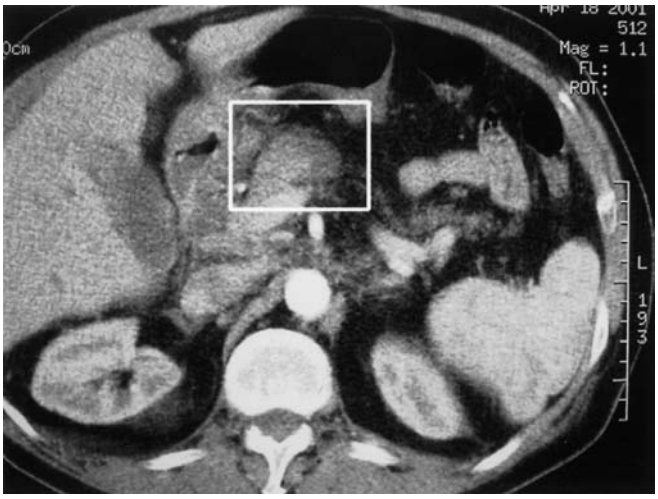



**Fig. 1** Computed tomography (CT) scan shows a heterogeneous, solid mass involving the pancreatic parenchyma

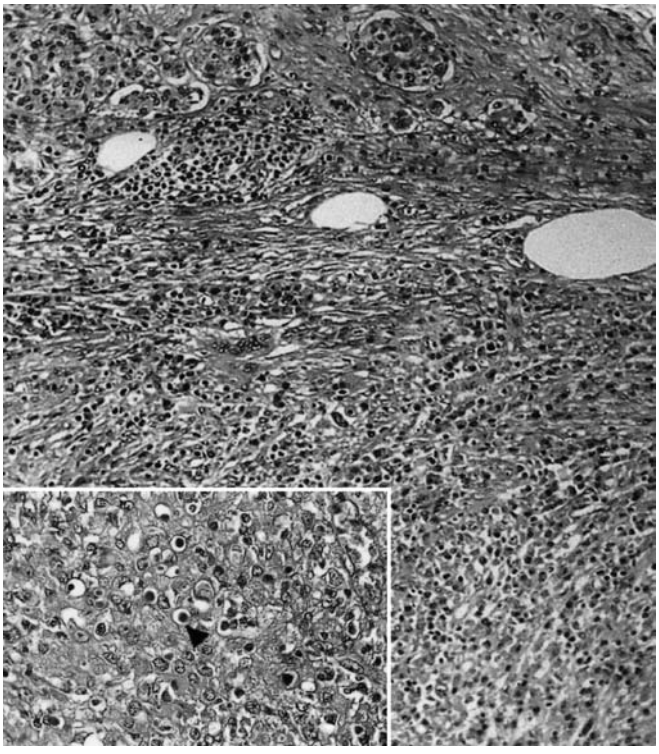


**Fig. 2** Pancreatic parenchyma is involved by a proliferation of inflammatory cells, multinucleated cells and macrophages containing numerous Michaelis-Gutmann bodies (hematoxylin-eosin, ×100). *Inset* A high magnification showing Michaelis-Gutmann bodies (*arrowhead* hematoxylin-eosin, ×400)

desmin (Dako), CD34 (Novocastra, Newcastle, UK), CD68 (Dako), cytokeratins AE1–AE3 (Biogenex, San Ramon, Calif.), kappa- and lamda immunoglobulin light chains (Dako), CD21 (Dako), CD23 (Novocastra, Newcastle, UK), and S-100 protein (Neomarker, Union City, Calif.).

For electron microscopy, small samples were retrieved from paraffin-embedded material, deparaffinized in xylene, rehydrated

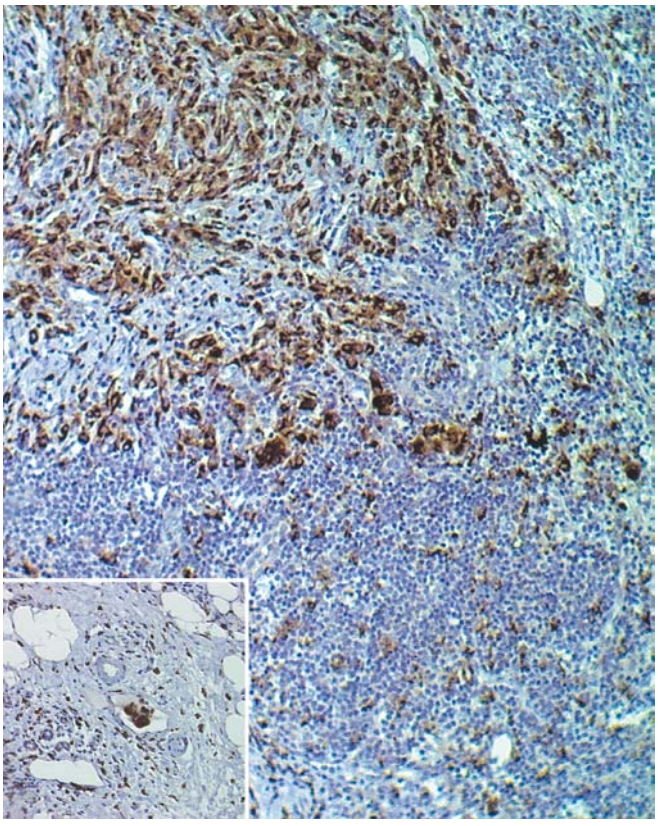


**Fig. 3** CD68 immunostain outlines the histiocytic proliferation inside lymph nodes. *Inset* Von Hansemann macrophages are detected inside lymphatic vessels at the periphery of the lesion (×200)

in ethanol, post-fixed in osmium tetroxyde (OsO4), dehydrated and embedded in epoxy resin. Ultrathin sections were counterstained in uranile acetate and lead citrate and observed in a Joel JEM 1010 (Tokio, Japan) electron microscope operating at 80 kV.

## Pathological results

The surgical resection specimen included the body and tail of the pancreas, measuring 11.5×5×2 cm, the spleen, measuring 9×7×4 cm and multiple regional nodes. Macroscopically, the body of the pancreas showed a well-circumscribed, not encapsulated, yellow-brown mass that measured 3.5 cm in greatest dimension. Histologically, the lesion was composed of multiple nodules of large PAS-positive histiocytes, separated by fibroblastic/myofibroblastic septa. Numerous small intracytoplasmic and interstitial targetoid spherules (Michaelis-Gutmann bodies) were easily identified (Fig. 2). These bodies were stained with von Kossa's and Perls' stains documenting their calcium and iron composition. Lymphatic vessels containing von Hansemann histiocytes were readily detected (Fig. 3, inset). Plasma cells, eosinophils, lymphocytes and multinucleated giant cells were also present. No mitoses nor necrosis were observed. Notably, 8 of 24 regional lymph nodes examined

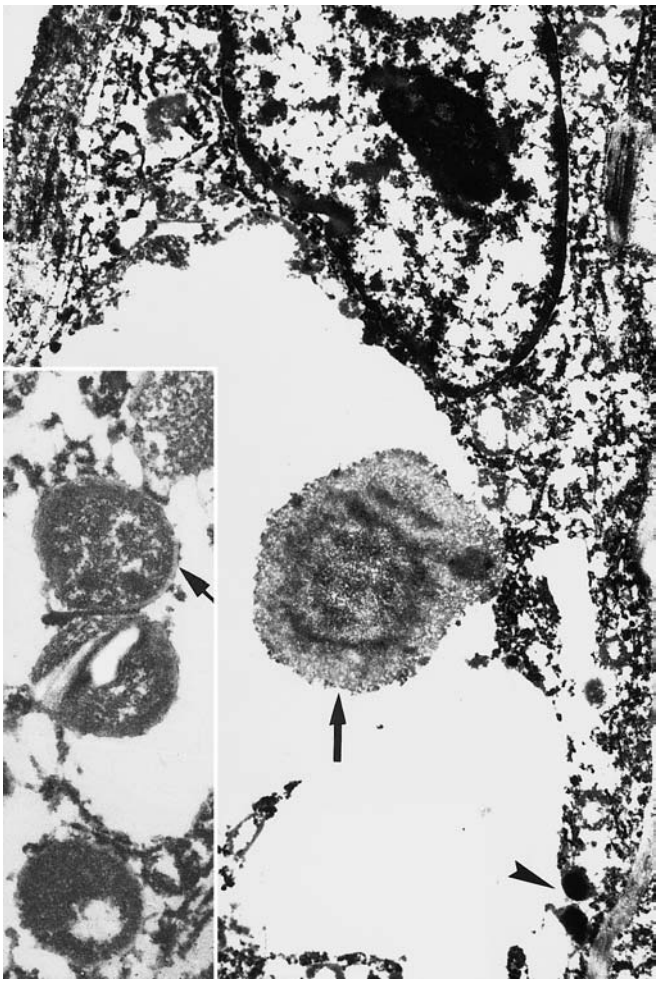


**Fig. 4** A macrophagic cell with a big vacuole containing a poorly calcified Michaelis-Gutmann body (*arrow*) and two electron-dense round structures (*arrowhead*; ×9200). *Inset* Other similar better-preserved round, bacterial-like structures with clear cell wall (*arrow*) and electron lucent internal zone (×23,000)

were partially and/or diffusely involved by the lesion (Fig. 3). The remaining pancreatic parenchyma showed features of chronic pancreatitis with prominent interlobular fibrosis, lymphoplasmacytic and histiocytic infiltrate without evidence of Michaelis-Gutmann bodies. We were not able to identify microorganisms with Gram stains. The spleen was normal. Immunohistochemically, CD68 was strongly positive in the histiocytic component. Desmin and smooth muscle actin were only weakly positive in the fibroblastic/myofibroblastic proliferation. CD34, cytokeratins, kappa and lamda immunoglobulin light chains, CD21, CD23, and S-100 protein were negative.

Ultrastructurally, numerous plasma cells and macrophages were clearly discernible; macrophages showed intracytoplasmatic vacuoles encircling Michaelis-Gutmann bodies at different stages of calcification. In some histiocytic-type cells, several phago-lysosomes were present containing bacterial-like structures (Fig. 4). The diagnosis of pancreatic malakoplakia with diffuse lymph-node involvement was rendered.

## Discussion

To date, only two cases of primary malakoplakia of the pancreas have been described. In one patient, the lesion was associated with chronic pancreatitis and adenocarcinoma [14]; in the other patient, a large lesion macroscopically mimicking a tumor was incidentally detected during elective colecystectomy for cholelithiasis [7]. In two other patients with immunodeficiency, secondary pancreatic involvement by adrenal/colonic and retroperitoneal malakoplakia has been described [5, 11]. These reports confirm that this lesion may have different predisposing factors including neoplasia, infective processes and chronic inflammatory diseases. Our patient reported a history of diabetes mellitus, frequently described in association with malakoplakia and presented with clinical signs and symptoms of chronic pancreatitis, later confirmed by histology. In this clinical setting, the pathogenesis of malakoplakia may be related to an abnormal, albeit localized, histiocytic response to chronic infection or inflammation associated with chronic pancreatitis. Ultrastructural features of bacteria were identified in our specimen whereas there was no clinical evidence of immunosuppression or neoplasia. The pancreatic localization of malakoplakia is a very uncommon event and lymph-node involvement is extremely rare. A recent report described a case of malakoplakia of the urinary bladder with involvement of nodes that appeared abnormal at CT and MRI [9]. The diagnosis of malakoplakia was confirmed by biopsy, but no histological evidence of lymph-node involvement was presented. Previously, Dervan et al. [6] reported a 59-year-old patient with generalized lymphadenopathy due to a proliferation of macrophages containing typical Michaelis-Gutmann bodies, confirmed by electron microscopy. Although the histological features were those of malakoplakia, the lesion behaved as a lymphoma, and the patient had a downhill clinical course with a fatal outcome.

The pathogenesis of lymph-nodal involvement in malakoplakia remains to be elucidated. It may be suggested that micro-organisms phagocytosed by the macrophages may either remain viable or partially digested in these cells, because of defective phagocytic digestion. These bacteria-laden histiocytes may remain at the site of implantation or enter into the lymphatic system, eventually localizing to regional lymph nodes. Therefore, the mechanism may be similar to lymph-node involvement in other infective processes such as tuberculosis and Whipple's disease.

Differential diagnosis should include other benign non-specific inflammatory lesions, myofibroblastic inflammatory tumor, and histiocytic neoplasms. Myofibroblastic inflammatory tumor typically occurs in patients younger than 20 years of age and consists of a spindle-

cell proliferation with mixed, variably prominent, lymphoid and plasma cell infiltrate. The histiocytic component, if present, is usually focal and lacks Michaelis-Gutmann bodies. Distinction is important since myofibroblastic inflammatory tumor, first considered a reactive process, is now considered by some authors a true neoplasm with the potential for recurrence and multifocality. With diffuse lymph-node involvement, histiocytic neoplasms such as malignant histiocytosis and follicular dendritic cell sarcoma have to be included in the differential diagnosis. Malignant histiocytosis is an extremely aggressive disease, characterized by the proliferation of pleomorphic histiocytes in expanded sinuses, with a grim prognosis. Follicular dendritic cell sarcoma is a rare low-grade malignant tumor composed of oval to spindled cells displaying a whorled or storiform growth pattern, characteristically mixed with small lymphocytes. In these cases, histiocytic neoplastic cells are immunoreactive for CD21, CD23 and CD35.

In conclusion, we describe in this report a rare case of malakoplakia localized in the pancreas, clinically mimicking a neoplastic process. Our case differs from the others previously reported in that our patient has a diffuse lymph-node involvement. However, the absence of local recurrence or distant spread suggests that node involvement does not influence the prognosis of malakoplakia.

**Acknowledgements** We thank Drs. Giuseppe Pietra and Antonio Nascimento for reviewing the case, Dr. Roberta Fasani for photographic assistance and Mrs. Anna Comi and Patrizia Doi for immunohistochemical studies.

## References

1. Abdou NI, Napomberjara C, Sagawa A, Ragland C, Stechschulte DJ, Nilsson U, Gourley W, Watanase I, Lindsey NJ, Allen MS (1977) Malakoplakia: evidence for monocyte lysosomal abnormality correctable by cholinergic agonist in vitro and in vivo. N Engl J Med 297:1413–1419
2. Boudny P, Kurrer MO, Stamm B, Laeng RH (2000) Malakoplakia of the colon in an infant with severe combined immunodeficiency (SCID) and charge association. Pathol Res Pract 196:577–582
3. Chalvardjian A, Picard L, Shaw R, Davey R, Cairns JD (1980) Malacoplakia of the female genital tract. Am J Obstet Gynecol 138:391–394
4. Charpentier P, Prade M, Bognel C, Gadenne C, Duvillard P (1983) Malakoplakia of the gallbladder. Hum Pathol 14:827–828
5. Colby TV (1978) Malakoplakia. Two unusual cases which presented with diagnostic problems. Am J Surg Pathol 2:377–382
6. Dervan PA, Teeling M, Dempsey J, Drury IM, O'Malley E, O'Connel D (1986) Lymphadenopathy due to fatal histiocytic proliferative disorder containing Michaelis-Gutmann bodies. Cancer 57:1337–1340
7. Kulatunga A, Kyllönen AP, Dammert K (1987) Malakoplakia of the pancreas. A case report. Acta Pathol Microbiol Immunol Scand 95:127–129
8. Michaelis L, Gutmann C (1902) Uber Einschlüsse in Blasentumoren. Z Klein Med 47:208–215
9. Ollier P, Bourrier P, Adil A, Anidjar M, Frija J (2000) Malakoplakie vèsicale et ganglionnaire: à propos d'un cas. J Radiol 81:158–160
10. Paquin ML, Davis JR, Weiner S (1986) Malacoplakia of Bartholin's gland. Arch Pathol Lab Med 110:757–758
11. Sinclair-Smith C, Kahn LB, Cywes S (1975) Malacoplakia in childhood: case report with ultrastructural observations and review of the literature. Arch Pathol Lab Med 99:198–203
12. Sughayer M, Ali SZ, Erozan YS, Dunsmore N, Hall GS (1997) Pulmonary malacoplakia associated with Rhodococcus equi infection in an AIDS patient. Report of a case with diagnosis by fine needle aspiration. Acta Cytol 41:507–512
13. von Hansemann D (1903) Uber Malakoplakia der Hornblase. Virchows Arch Pathol Anat 173:302–308
14. Zuk RJ, Neal JW, Baithun SI (1990) Malakoplakia of the pancreas. Virchows Arch Pathol Anat 417:181–184

Virchows Arch (2003) 442:86–87
DOI 10.1007/s00428-002-0708-8

LETTER TO THE EDITOR

**Helene Sjögren · Rigmor Dahlenfors**
**Göran Stenman · Joachim Mark**

# Observations by G-banding and multicolor spectral karyotyping in a salivary gland basal cell adenoma

Received: 2 May 2002 / Accepted: 2 May 2002 / Published online: 26 September 2002
© Springer-Verlag 2002

**Keywords** G-banding · Spectral karyotyping · Salivary gland · Basal cell adenoma

Sir,
During the past two decades, we have performed systematic cytogenetic studies of the most frequently occurring histological subtypes of benign and malignant salivary gland tumors [7, 10, 13]. In our total material, comprising more than 400 tumors, there is no case of benign salivary basal cell adenoma. This uncommonly diagnosed tumor type accounts for about 2–3% of all neoplasms in the salivary glands [4]. The basal cell adenoma was originally described by Kleinsasser and Klein in 1967 [3], who pointed out the resemblance of the tumor cells to the basal cells of ducts in salivary glands. Here, we present the karyotypic findings based on G-banding and spectral karyotyping (SKY) in such a tumor.

The patient was a 45-year-old woman who had been aware of a painless swelling in her left parotid gland for more than 10 years. During this period there had been no increase in size of the swelling. Clinical examination showed a well-demarcated, firm, non-tender and movable tumor in the lower and superficial part of the left parotid gland. A fine needle biopsy revealed sheets of monomorphic cells with a basaloid appearance, some of which formed tubular structures. A few small lumps of metachromatic substance were also observed. Based on the cytology, two diagnoses were considered: a basal cell adenoma versus an adenoid cystic carcinoma. Subsequently, a superficial parotidectomy was performed. The surgical specimen contained a completely removed, unencapsulated but well-demarcated, firm and lobular tumor. It measured approximately 0.9×0.9×1.0 cm. Histological examination revealed the typical picture of a basal cell adenoma (Fig. 1). There were no areas with signs of infiltrative growth.

Cytogenetic analysis was performed on short-term cultured tumor material [7]. Slides aged for 3 weeks were used for SKY analysis. The conditions for pretreatment, hybridization (Sky Paint probe), post-hybridization washes and detection were essentially as recommended by the manufacturer (ASI-Applied Spectral Imaging Ltd., Migdal Ha'Emek, Israel). Image acquisition was achieved using the SpectraCube system (ASI) mounted on a Zeiss Axioplan 2 Imaging microscope, and the analysis of spectral images was performed using the SkyView software (ASI) [12].

A total of 25 G-banded metaphase cells were karyotyped. Of these, three cells had a normal karyotype. Of the remaining cells, 20 had an abnormal stemline (mainline) karyotype with two marker chromosomes, a der(7) and a der(13). The other two cells were doubling products of the stemline cells. Detailed analysis of the G-banded metaphases and of seven metaphases analyzed using SKY allowed us to determine the composition of these markers and to precisely map the breakpoints. The stemline karyotype was 46, XX, der(7)t(7;13)(p15;q32), der(13)inv(13)(q12q32)t(7;13)(p15;q32) (Fig. 2a, b). No other structural changes were detected in any of the cells studied.

Only three cases of basal cell adenomas have previously been studied cytogenetically [2]. All of them originated from the parotid gland. One tumor had a normal karyotype, the second had a hyperdiploid karyotype with trisomy 8 as the sole anomaly, and the third case contained three closely related clones: 49, XX, +8, +8, +16 / 98, idem × 2, der(9)t(1;9)(q24;p24), +18, -22 / 98, idem × 2, i(1q), der(9)t(1;9)(q24;p24). The only common abnormality observed among these four tumors (the present case included) is one or two extra copies of chromosome 8 found in two of the tumors, suggesting that at least a subgroup of these tumors might be distinguished by trisomy 8. Whether or not the 7;13-translocation and/or inv(13) recorded in the present case are recurrent in basal cell adenomas is at present unknown.

H. Sjögren (✉) · G. Stenman
Lundberg Laboratory for Cancer Research,
Department of Pathology, Göteborg University,
Sahlgrenska University Hospital, 413 45 Göteborg, Sweden
e-mail: helene.sjogren@llcr.med.gu.se
Tel.: +46-31-3421957, Fax: +46-31-820525

R. Dahlenfors · J. Mark
Department of Pathology and Cytogenetics, Central Hospital,
Skövde, Sweden

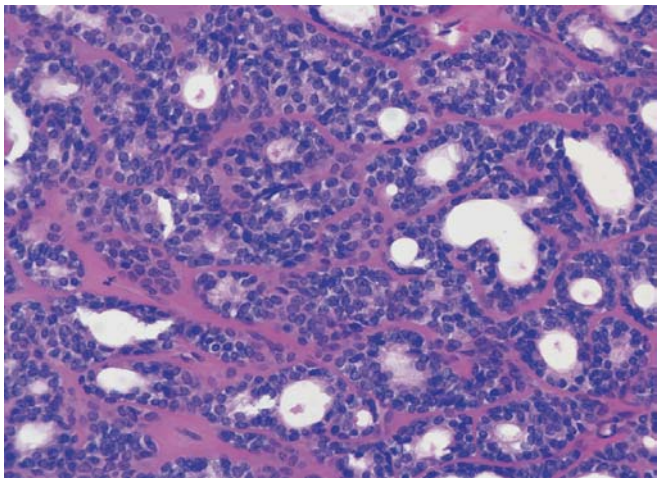


**Fig. 1** Typical histology of the basal cell adenoma with monomorphic, small, tumor cells sometimes forming tubular structures. Hematoxylin and eosin ×120

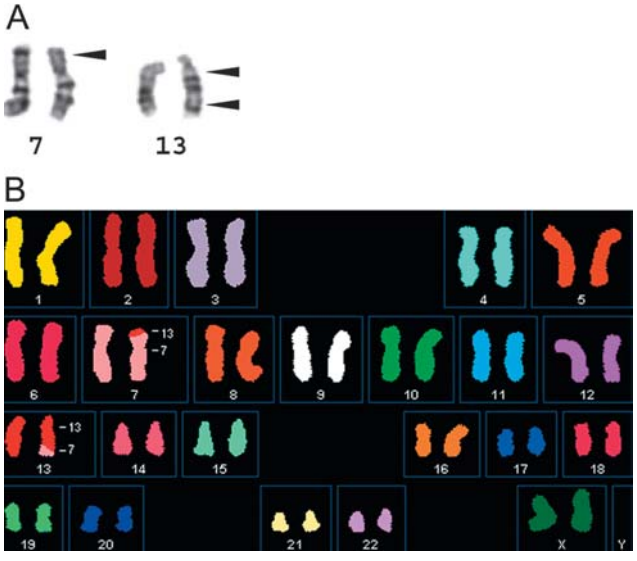



**Fig. 2** **a** G-banded partial karyotype showing the 7;13-translocation and the paracentric inversion of the der(13). Breakpoints are indicated by *arrowheads*. **b** Spectral karyotype (*SKY*) showing the absence of other rearrangements than those affecting one of the two chromosome 7 and 13 homologues. Translocated chromosome segments are indicated

When the karyotypic data for the basal cell adenomas are compared with those of the much more well-characterized pleomorphic adenomas [7] and Warthin's tumors [8], there seem to be certain obvious similarities. Thus, all three types of benign salivary gland neoplasms show one group of tumors characterized by a normal stemline. The other tumors are characterized by one or more abnormal stemlines which show recurrent structural and/or numerical deviations distinctive for each tumor type. The findings in a single case of a canalicular adenoma [1] and a single case of a sebaceous lymphadenoma [6], as well as in two cases of parotid oncocytomas [5] (Mark et al., unpublished observations) fit with these interpretations. It should be pointed out that in several of the above-discussed benign tumor types it has been possible from morphological studies of the in vitro outgrowing cells and from histochemical and molecular cytogenetic observations to conclude that the cells with normal karyotype mostly represent tumor cells and not outgrowing stromal cells [9, 11]. It should also be mentioned that, as a rule, the deviations found in the different benign tumor types have not been refound in any of the malignant salivary gland tumors so far analyzed. The only exception is the mucoepidermoid carcinoma where some cases show an 11;19-translocation [8] seemingly identical to that found in a subgroup of Warthin's tumor. Future molecular studies might provide an explanation for this enigmatic finding.

**Acknowledgements** This work was supported by grants from the Swedish Cancer Society and the IngaBritt and Arne Lundberg Research Foundation.

## References

1. Havel G, Dahlenfors R, Böckman P, Mark J (1996) Cytogenetical observations in a canalicular adenoma of the minor salivary glands. Hereditas 124:105–106
2. Hrynchak M, White V, Berean K, Horsman D (1994) Cytogenetic findings in seven lacrimal gland neoplasms. Cancer Genet Cytogenet 75:133–138
3. Kleinsasser O, Klein HJ (1967) Basalzelladenome der Speicheldrusen. Archiv Klin Exper Ohren- Nasen- und Kehlkopfheilk 189:302–316
4. Kratochvil FJ (1991) Canalicular adenoma and basal cell adenoma. In: Ellis GL, Auclair PL, Gnepp DR (eds) Surgical Pathology of the Salivary Glands. Saunders, Philadelphia, pp 202–224
5. Mark J, Dahlenfors R, Havel G, Böckman P (1991) Benign parotid oncocytoma with the chromosomal abnormality trisomi 7. Anticancer Res 11:1735–1737
6. Mark J, Dahlenfors R, Wedell B, Stenman G, Böckman P (1994) Cytogenetical and FISH analysis on a salivary sebaceous lymphadenoma. Oncol Rep 1:561–562
7. Mark J, Dahlenfors R, Wedell B (1997) Impact of the in vitro technique used on the cytogenetic pattern in pleomorphic adenomas. Cancer Genet Cytogenet 95:9–15
8. Nordkvist A, Mark J, Dahlenfors R, Bende M, Stenman G (1994) Cytogenetic observations in 13 cystadenolymphomas (Wartin's tumors). Cancer Genet Cytogenet 76:129–135
9. Rozell B, Stenman G, Hansson HA, Dahl D, Hansson G, Mark J (1985) Intermediate filaments in cultured human pleomorphic adenomas – an immunohistochemical study. Acta Pathol Microbiol Immunol Scand A 93:335–343
10. Röijer E, Dahlenfors R, Mark J, Stenman G (1997) Observations by chromosome banding, FISH and immunohistochemistry in an adenoid cystic carcinoma with del(17)(p13) as the sole deviation. Virchows Arch 430:339–342
11. Sahlin P, Mark J, Stenman G (1994) Interphase cytogenetic analysis of cultured pleomorphic adenomas with a normal karyotype. Int J Oncol 4:1225–1228
12. Schröck E, du Manoir S, Veldman T, Schoell B, Wienberg J, Fergusson-Smith MA, Ning Y, Lodbetter DH, Bar-AM I, Soenksen D, Garnini Y, Ried T (1996) Multicolor spectral karyotyping of human chromosomes. Science 273:494–497
13. Stenman G, Petursdottir V, Mellgren G, Mark J (1998) A child with a t(11;19)(q14–21;p12) in a pulmonary mucoepidermoid carcinoma. Virchows Arch 433:579–581

Virchows Arch (2003) 442:88
DOI 10.1007/s00428-002-0644-7

BOOK REVIEW

**H. Fox**

# Eytan R. Barnea, Eric Jauniaux, Peter E. Schwartz (eds): Cancer and pregnancy

## Springer, London, 2001 (ISBN 1-85233-374-X)

Received: 18 February 2002 / Accepted: 4 March 2002 / Published online: 26 November 2002
© Springer-Verlag 2002

This is a curious hybrid of a book. The first half of the text is a straightforward clinically based discussion of the diagnosis and management of malignant disease in the pregnant woman. Specific neoplasms, such as breast cancer and malignant melanoma, are discussed in detail as are the difficulties in the radiological diagnosis of cancer in pregnancy and the particular problems of chemotherapy and radiation during the gravid state. In this section of the book, virtually everything the obstetrician will want to know of oncology is covered as is all that the oncologist requires to know about obstetrics. Pathological input is minimal and there are occasional pathological solecisms.

The second half of the book is totally different and is largely concerned with a comparison of malignant tissues and trophoblast, with particular respect to immunomodulation, proliferation, angiogenic activity and invasiveness. Valid analogies are drawn and discussed but, nevertheless, differences are pointed out.

I found this a fascinating book but, being interested in both oncology and placentology, I belong to a very small minority group. I hope it receives a wider readership for it will broaden the horizons of all who are interested in either cancer or reproductive biology.

H. Fox (✉)
Department of Pathological Sciences, University of Manchester, Stopford Building, Manchester M 13 9PT, UK
Fax: +44-161-2755289

 © Springer-Verlag 2003

# ACKNOWLEDGEMENT TO REFEREES

The Managing Editors are grateful to the following colleagues for generously giving their time in careful evaluation of the manuscripts submitted to *Virchows Archiv* in 2002:

Adsay NV, Detroit (USA)
Aguzzi A, Zürich (CH)
Aigner T, Erlangen (D)
Amann K, Erlangen (D)
Ambrosch P, Kiel (D)
Andree C, Kiel (D)
Arbustini E, Pavia (IT)
Asa SL, Toronto (CAN)

Bannasch P, Heidelberg (D)
Barbareschi M, Trento (IT)
Baumann I, Erlangen (D)
Bedossa P, Kremlin-Bicêtre (F)
Berteau P, Paris (F)
Bioulac-Sage P, Bordeaux (F)
Blümcke I, Erlangen (D)
Bode B, Zürich (CH)
Böcking A, Düsseldorf (D)
Bordi C, Parma (IT)
Borisch B, Genf (CH)
Bosman FT, Lausanne (CH)
Bouwens L, Brussel (B)
Brabletz T, Erlangen (D)
Brandner S, London (UK)
Brousse N, Paris (F)
Bruneval P, Paris (F)
Bussolati G, Torino (IT)

Caduff R, Zürich (CH)
Capella C, Varese (IT)
Capron F, Clamart (F)
Carcangiu ML, Milano (IT)
Cardesa A, Barcelona (SP)
Carneiro MF, Porto (P)
Cathomas G, Liestal (CH)
Cazals D, Clichy (F)
Chott A, Wien (AU)
Couvelard A, Clichy (F)
Cuvelier C, Gent (B)

Damiani S, Bologna (IT)
Damjanov I, Kansas City (USA)
Deckert M, Köln (D)
Dei Tos AP, Treviso (IT)
Delling G, Hamburg (D)
De Mascarel A, Bordeaux (F)
Denk H, Graz (AU)
Derenzini M, Bologna (IT)
Desmet V, Leuven (B)
De Wolf-Peeters C, Leuven (B)
Diebold J, München (D)
Doglioni C, Belluno (IT)
Dombrowski F, Magdeburg (D)

Fahimi D, Heidelberg (D)
Fabiani B, Paris (F)
Faller G, Erlangen (D)
Feller AC, Lübeck (D)
Fend F, München (D)
Fisseler-Eckhoff A, Wiesbaden (D)
Fléjou JF, Paris (F)
Fletcher CDM, Boston (USA)
Foschini MP, Bologna (IT)
Foster CS, Liverpool (UK)
Füzesi L, Göttingen (D)

Gabbert H, Düsseldorf (D)
Gabbiani G, Genf (CH)
Gaulard P, Créteil (F)
Geboes K, Leuven (B)
Gerharz CD, Düsseldorf (D)
Gieseler F, Kiel (D)
Greiner A, Würzburg (D)
Gröne HJ, Heidelberg (D)
Guski H, Berlin (D)

Hansmann ML, Frankfurt (D)
Hauptmann S, Berlin (D)
Heilemariam S, Basel (CH)
Helpap B, Singen (D)
Herbay A.v., Heidelberg (D)
Höfler H, München (D)
Hofstädter F, Regensburg (D)
Horny HP, Lübeck (D)
Hummel M, Berlin (D)

Julie C, Paris (F)
Jundt G, Basel (CH)

Kalthoff H, Kiel (D)
Katenkamp D, Jena (D)
Kerjaschki D, Wien (AU)
Kikuchi M, Fukuoka (JP)
Kirchner T, Erlangen (D)
Klimpfinger M, Wien (AU)
Klimstra D, New York (USA)
Knüchel-Clarke R, Regensburg (D)
Koike M, Tokyo (JP)
Komminoth P, Baden (CH)
Kosmehl H, Erfurt (D)
Krenn V, Berlin (D)
Krismann M, Bochum (D)
Kurrer H, Zürich (CH)

Lamovec J, Ljubljana (SL)
Lax SF, Graz (AU)
Lehr A, Mainz (D)
Leoncini L, Siena (IT)
Leuschner I, Kiel (D)
Löhrs U, München (D)
Löning T, Hamburg (D)
Longnecker DS, Lebanon (USA)
Lüttges J, Kiel (D)
Lumb, PD, Manchester (UK)

Magrini E, Bologna (IT)
Magro G, Catania (IT)
Maingor F, Graz (AU)
Maiorano E, Bari (IT)
Martin A, Bobigny (F)
Marx A, Würzburg (D)
McNicol AM, Glasgow (UK)
Mechtersheimer G, Heidelberg (D)
Mentzel T, Friedrichshafen (D)
Michal M, Pilsen (CZ)
Miettinen M, Washington (USA)
Mihatsch MJ, Basel (CH)
Mihic D, Zürich (CH)
Mikuz G, Innsbruck (AU)
Mittermayer C, Aachen (D)
Moch H, Basel (CH)
Möller P, Ulm (D)
Mohr W, Ulm (D)
Moll R, Marburg (D)
Monges G, Marseille (F)
Montironi R, Ancona (IT)
Mrowietz U, Kiel (D)
Mueller JD, Boston (USA)
Müller JG, Würzburg (D)
Müller KM, Bochum (D)

Nesland JM, Oslo (N)
Niedobitek G, Erlangen (D)
Nizze H, Rostock (D)
Nogales F, Granada (SP)

Oberholzer M, Basel (CH)
Oberhuber G, Wien (AU)
Odenthal M, Köln (D)
Oehmichen M, Kiel (D)
Offerhaus GJA, Amsterdam (NL)

Papadopoulos T, Erlangen (D)
Paradis V, Clichy (F)
Paraf F, Limoges (F)
Parwaresch MR, Kiel (D)
Paulus W, Münster (D)
Pession A, Bologna (IT)
Peterse JL, Amsterdam (NL)
Petersen I, Berlin (D)
Peuchmaur M, Paris (F)
Pfaltz M, Zürich (CH)
Pfeifer U, Bonn (D)
Piard F, Dijon (F)
Pietsch T, Bonn (D)
Popper HH, Graz (AU)
Poremba C, Münster (D)
Praet M, Gent (B)
Prat J, Barcelona (SP)
Prevot S, Bondy (F)
Püschel K, Hamburg (D)

Röcken C, Magdeburg (D)
Roggendorf W, Würzburg (D)
Rosai J, Milano (IT)
Rose C, Würzburg (D)
Rosenbaum J, Bordaux (F)
Roth J, Zürich (CH)
Rudolph P, Kiel (D)
Rüschoff J, Kassel (D)

Sabourin JC, Villejuif (F)
Saeger W, Hamburg (D)
Sapino A, Torino (IT)
Sarbia M, Düsseldorf (D)
Sauter G, Basel (CH)
Scarpa A, Verona (IT)
Scheffer GL, Amsterdam (NL)
Schmid KW, Essen (D)
Schmidt D, Mannheim (D)
Schmitt-Gräff A, Freiburg (D)
Schnabel P, Heidelberg (D)
Schröder JM, Kiel (D)
Schultze-Werninghaus G, Bochum (D)
Schulz A, Giessen (D)
Schuppan D, Erlangen (D)
Schwechheimer K, Essen (D)
Sciot R, Leuven (B)
Scoazec JY, Lyon (F)
Sebagh M, Villejuif (F)
Selves J, Toulouse (F)
Simpson R, Exeter (UK)
Sipos B, Kiel (D)
Slootweg PJ, Utrecht (NL)
Sobrinho-Simões M, Porto (P)
Solcia E, Pavia (IT)
Stallmach T, Zürich (CH)
Stanta G, Triest (IT)
Stoerkel F, Wuppertal (D)
Stolte M, Bayreuth (D)
Tahara E, Hiroshima (JP)
Tallini G, Bologna (IT)
Tannapfel A, Leipzig (D)
Tavassoli FA, Washington (USA)
Tennstedt C, Berlin (D)
Terracciano L, Basel (CH)
Thiene G, Padova (IT)
Toma V, Zürich (CH)
Tot T, Falum (SW)
Turzynski A, Lübeck (D)

Van Damme B, Leuven (B)
van der Waal I, Amsterdam (NL)
van Marck E, Antwerpen (B)
Viale G, Milano (IT)
Vogt P, Zürich (CH)
Vollmer E, Borstel (D)

Wechsler J, Créteil (F)
Wells M, Sheffield (UK)
Wendum D, Paris (F)
Werner M, Freiburg (D)
Wiestler OD, Bonn (D)
Wittekind C, Leipzig (D)

Yagihashi S, Hirosaki (JP)

Zafrani ES, Créteil (F)
Zamboni G, Verona (IT)
Zatloukal K, Graz (AU)
Zeitz M, Berlin (D)
Zimmermann D, Zürich (CH)
Ziol M, Bondy (F)

 © Springer-Verlag 2003

# ANNOUNCEMENTS

9–11 May 2003
**6th International Course on Bone Marrow Biopsy Pathology**
Hanover, Germany

Under the auspices of the European Association for Hematopathology

Bone marrow histology has evolved into an integral part of modern haematological diagnostics. Moreover, it affords unique access to a biological understanding of important diseases affecting the haematopoietic system. The courses offered by the European Bone Marrow Working Group under the auspices of the European Association for Hematopathology are intended to provide high quality educational sessions in bone marrow histopathology and to bring together people who have a particular interest in this field. In addition to state-of-the-art lectures focusing on selected topics, there will be workshops where participants are invited to contribute their own interesting and instructive cases. Topics will be chronic myeloproliferative disorders, lymphoma, hypoplastic states and MDS, reactive and therapy-related changes.

Course fee: 300 €

*For further information* see http://www.mh-hannover.de/institute/pathologie/kongress or contact Institute of Pathology, Medizinische Hochschule Hannover, Carl-Neubergstr. 1, 30625 Hannover, Germany,
E-Mail: Laenger.Florian@MH-Hannover.de,
Tel.: 0049 511 532-4501; Fax: -5799

12–16 May 2003
**Diagnostic Histopathology of Breast Disease**
London, UK

May 12–16, 2003, at Hammersmith Hospital (Imperial College Faculty of Medicine), London, UK. A week-long course designed for pathologists at Consultant and Senior Trainee level. The course provides a comprehensive coverage of the Histopathology of Breast Disease, with special emphasis on areas that pose diagnostic difficulties. The participants will be given ample time to study histological preparations, followed by illustrated discussion of the cases. There will be special sessions dealing with the interpretation of core biopsies and fine needle aspirations. There will also be two daily talks dealing with specific topics, given by eminent breast pathologists and followed by discussion. The topics will include reporting breast biopsies, immunohistochemistry, receptor assessment, c-erbB-2, prognostic factors, proliferative lesions/ carcinoma in situ, problems in breast pathology, a practical approach to the diagnosis of breast lymphomas and molecular pathology. The faculty will include Ian Ellis, Christopher Elston, Andrew Hanby, Kristin Henry, Stephen Humphreys, Sunil Lakhani, Andrew Lee, Sarah Pinder, Sami Shousha, and Clive Wells.

*Further details from:* Wolfson Conference Centre, Hammersmith Hospital, Du Cane Road, London W12 ONN, UK. (Tel (44) 20 8383 3117/3227/3245; Fax (44) 20 8383 2428; e-mail wcc@ic.ac.uk)

12–23 May 2003
**International Course on Laboratory Animal Science**
Utrecht, The Netherlands

A two-week intensive course on laboratory animal science will be organized at the Department of Laboratory Animal Science – Utrecht, The Netherlands in May 2003. This course has been offered once a year since 1993.

The objective of this course is to present basic facts and principles that are essential for the humane use and care of animals and for the quality of research.

The contents of the course are in line with recommendations of the Federation of European Laboratory Animal Science Associations (FELASA) regarding the training of the young scientist whose research involves the use of vertebrate animals.

The course may also be of interest for those who intend to set up a similar course at their own institution. For this purpose, during the course the acquisition of teaching materials can be discussed with the course committee.

*For information and application forms please contact*:
Prof. Dr. L.F.M. van Zutphen or
Mr. Stephan van Meulebrouck
Department of Laboratory Animal Science
Faculty of Veterinary Medicine
P.O. Box 80.166
3508 TD Utrecht
The Netherlands
Phone: *31-30-2532033
Fax: *31-30-2537997
E-mail: pdk@las.vet.uu.nl
Internet: http://las.vet.uu.nl (click 'Education').

6 September 2003
**EUROPEAN BOARD OF PATHOLOGY**
**7th EXAMINATION 2003**
Ljubljana, Slovenia

The Seventh Examination of the European Board of Pathology will be held in Ljubljana, Slovenia, Saturday September 6, 2003. This Examination precedes the 19th Congress of the ESP.

*For information about the examination and application forms can be obtained from:*
Prod. Dr. J.G. van den Tweel
(chairman of The Examination Board)
Utrecht University Medical Center
Department of Pathology, H 04.312
P.O. Box 85500
3508 GA Utrecht
Fax: ++31-30-2544990
Tel.: ++31-30-2506565
e-mail: j.vandentweel@lab.azu.nl *or*
W.vanBragt@lab.azu.nl (secretary)
The same information is also available from Internet:
http:www.uems.be/pathol.htm, see index 2 and 3

Virchows Arch (2003) 442:93–94 © Springer-Verlag 2003

SOCIETY NEWS

# Invitation to the 19th European Congress of Pathology

On behalf of the European Society of Pathology (ESP) and the Organising Committee, we take great pleasure in inviting you to the 19th European Congress of Pathology, which will be held in Ljubljana, Slovenia, 6–11 September 2003.

Slovenia is not a large country, but at the hub of routes of trade and movement from east to west and north to south, it has always played a larger part in European events than its size would suggest. Slovenia is now an independent Central European state, on the sunny side of the Alps, bordering Italy, Austria, Hungary and Croatia. The landscape embraces rolling countryside leading to the Pannonian plain to the east, rugged Karst bordering the Adriatic Sea to the southwest, and the Alps to the north and west. The Slovenian nation of only two million today has survived mainly due to its culture, language and vitality. A bone flute, 30,000 years older than any other known in the world, and Europe's oldest bone needle, testify to the roots of culture here.

Its capital, Ljubljana, has a picturesque unity, composed of an architectural heritage spanning Roman Emona, through Renaissance and Baroque Ljubljana, to Secession Art Nouveau and Modern Ljubljana, so strongly marked by the influence of the world famous Slovenian architect, Jo e Plečnik. Ljubljana is an university city. The roots of the University go back to the seventeenth century with Academia Operosorum, the fourth Academy of Sciences in Europe. A Philharmonic Society dates back three centuries.

Ljubljana's congress tradition began in 1821, when the three emperors of the Holy Alliance met here to discuss the post-Napoleonic fate of Europe. These traditions have been brought together in the new Cultural and Congress Centre Cankarjev dom, with a capacity of 3,600, located in the heart of Ljubljana. Cankarjev dom is well equipped with all modern technical facilities and has an experienced in-house team to ensure the necessary high standards for scientific sessions and exhibitions. All Congress venues, and most hotels, are within walking distance of the centre of the city. Particular attention will be paid to stimulating the participation of trainees and young pathologists by securing as low a registration fee as possible, and inexpensive accommodations.

The European Society of Pathology has been succeeding in establishing its ever more continuous activity and influence. The old idea of a common programme of continuous education of pathologists has been realised through a number of courses organised each year by the European School of Pathology, at its headquarters in Turin and other centres throughout Europe. An increasing number of Working Groups within the European Society of Pathology, devoted to various fields, promote a continuous exchange of professional experiences and other information, the establishment of common diagnostic standards and collaboration on common research projects.

The biannual ESP Congresses retain a major role in fulfilling the main aims of the ESP in pathology education, exchange of the most recent research achievements and, particularly, in keeping together all branches of pathology, that otherwise tend to split according to organ systems, disease processes and the increasing number of techniques. The Congresses also keep together pathologists from the whole of Europe, irrespective of geographical and political borders.

We believe that the 19th European Congress of Pathology will continue the traditional approaches of previous Congresses and will serve to increase both links with European national and international pathology societies and intercontinental links, particularly with the International Academy of Pathology. The framework of the Congress Scientific Programme has been created with the strong impact and assistance of the ESP Working Groups, the ESP Executive/Scientific Committee and the Advisory Council as well as companion Societies. The programme covers all areas of pathology, provides information ranging from current diagnostic standards to recent advances in science and modern techniques, particularly those of molecular genetics, and includes a number of "hot" topics of today and tomorrow, which will be

presented by the best, internationally recognised experts at Keynote Lectures, Symposia, Special Presentations, Round Table Discussions, Short Courses and Slide Seminars. One evening is devoted to ESP Working Group Meetings, both business and scientific. Interesting Satellite Symposia will be organised by supporting companies, two by the main sponsor of the Congress Main Sponsor, Ventana Medical Systems S.A.

Furthermore, all practising pathologists and scientists are kindly invited to present their scientific achievements and exchange their professional experiences through Free Paper and Poster Sessions. The best Free Papers will be acknowledged by giving the authors the opportunity to present their achievements at the plenary session, at which the authors of the three best Poster Presentations will additionally receive special Awards.

All who are coming to Ljubljana are kindly invited to join us at two one-day Pre-Congress Meetings, prior to the Congress Opening Ceremony on Saturday: one on Pulmonary Pathology and the other devoted to non-neoplastic Nephropathology. There will also be a three-day Joint Meeting of the European and North American Society of Head and Neck Pathology. All Pre-Congress Meetings and a whole day Examination by the European Board of Pathology will be organised by using the facilities of the new building of the Faculty of Medicine, University of Ljubljana.

Culture kept the Slovenian national identity alive over the centuries and it still plays an important role in people's lives. The Congress will also highlight the traditional close connection between medicine and art. Some novel events are planned: an exhibition of the work of pathologists/painters and, especially, a Gala Concert on Monday evening in the main Gallus Concert Hall of the Congress Centre in Ljubljana, by pathologists/musicians from all over the world. A social programme is offered which reflects the warmth and hospitality of the Slovenian people.

The Second Millennium we have entered provides major challenges for all biomedical sciences, and the 19th European Congress of Pathology is a challenge for the Organisers. We sincerely hope that attendance at the Ljubljana Congress in 2003 will be a fruitful, enjoyable and memorable experience in every respect for all participants, and will give new impetus to our medical speciality in Slovenia.

We look forward to seeing you in September 2003 in Ljubljana.



Gianni Bussolati
President
European Society
of Pathology



Du an Ferluga
President
19th European Congress
of Pathology

Virchows Arch (2003) 442:95–98
DOI 10.1007/s00428-002-0742-6

REVIEW ARTICLE

**Paolo Scarani**

# Rudolf Virchow (1821–1902)

Received: 4 October 2002 / Accepted: 21 October 2002 / Published online: 19 December 2002
© Springer-Verlag 2002

**Abstract** Rudolf Virchow died 100 years ago. The author summarizes the multifaceted personality of this man who so profoundly influenced the shaping of contemporary surgical and experimental pathology and played an important role in designing the social structure of modern Germany. Goethe's influence in the development of 19th century morphology is also suggested.

**Keywords** Surgical pathology · History · Virchow · Goethe · Morphology

## Introduction: Goethe and morphology

Goethe was considered to be the founder of the term and the concept of morphology. Moreover, he perfectly understood that morphology was the only reliable tool available to interpret nature [3, 8, 9].

Virchow made a very similar statement at the start of his career [12]. As a young physician in Berlin, he perceived the poor quality of contemporary medicine. Clinical diagnostics in a modern sense was still shrouded in the mists of fiery controversies, and a consistent therapeutic practice was confined to a sort of dreamland. Therefore, the young Virchow stated that the only tool available to cross the quagmire of contemporary medicine consisted of morphology. Virchow wrote about Goethe's work concerning morphology (Goethe als Naturforscher und in besonderer Beziehung auf Schiller, 1861) [12]. Moreover, the influence Goethe played on prominent histologists such as Jan Purkinje [5] makes for sure that Virchow's early experience was triggered by that titanic polymath.

P. Scarani (✉)
Anatomy and anatomic pathology museum,
Istituto di anatomia umana normale,
University of Bologna,
Via Irnerio 48, 40126 Bologna, Italy
e-mail: scarani@biocfarm.unibo.it
Tel.: +39-051-390661, Fax: +39-051-390661

## The young Virchow: history, morphology and social commitment

Both Virchow's birthplace and family profoundly contributed to his mental shaping. He was born in 1821 in Schivelbein (Pommern), now Swidwin, a town now belonging to northern Poland. His parents inspired to him a profound love for nature and a deep sense of moral responsibility. Such an attitude to responsibility was the legacy of Martin Luther's moral teaching. The great achievements of modern Germany relied on the deep sense of moral responsibility of individuals to the community to which they belonged. Virchow was constantly committed to medical and social community. A philanthropic attitude is not quite rare in physicians. Virchow's exceptionality consisted of his belief that medical practice and political struggle were inseparable entities.

The fascination of Pommern's landscape, the trips to Rügen island to see the migration of cranes, left a constant imprinting in Virchow's soul: a burning desire to explore, to unravel, to scan meticulously every aspect of life.

The presence of Polish people in Pommern was also critical for Virchow's early experience. His ethnic ancestry is controversial. Doubtless, Virchow admired Slavic lore and culture profoundly, and also respected Polish people. Such an attitude was probably one of the primers for his political commitment.

His interest in history was also of major importance for his educational development. When Virchow started studying medicine in Berlin, he was particularly annoyed by the backwardness of the programs and of medical culture [12]. He was also an aggressive critic of the clumsy degree theses in Latin. Nevertheless, the presence of history in the medical core curriculum, was a decisive item for Virchow's cultural development because he was invited to write a history of his birthplace by his mentors (Zur Geschichte von Schivelbein, 1847) [12]. That was his first original work. Moreover, it elicited his interest in social themes. Once graduated, Virchow showed how morphology could be a fundamental tool in medicine by

performing autopsy in strict relation to his clinical practice.

His early great successes in demonstrating the etiopathogenesis of pulmonary embolism through an innovative application of experimental medicine to medical practice are well known. The same is for his early implementation of microscopy in pathology. The rapid emerging of the concept of cellular pathology was tarnished by the bitter and unfair competition with Robert Remak, the true inventor of cellular pathology and of the modern doctrine of neoplasia. Hans Peter Schmiedebach gathered a thorough documentation on that embarrassing episode [11].

Usually less appreciated is the attitude to the use of communication media present in Virchow's medical practice and research, clearly expressed by the foundation of the journal entitled Archiv für pathologische Anatomie und Physiologie und für klinische Medizin: the Virchow's Archiv.

Virchow was not yet 27 years old and had already evoked a stirring of curiosity in Europe. He knew a number of foreign languages – English, French, Italian, Greek, Latin – and a number of Slavish idioms and sentences. Therefore, he was quite able to communicate. He was also very aggressive. Carl Rokitansky was probably the first victim of Virchow's piercing criticism, because of his scarce interest for clinical correlations and microscopy.

1838 represented a milestone in Virchow's life. On behalf of the Prussian government, he performed a vast survey in Silesia to discover the causes of an epidemic (probably typhoid fever) afflicting that region. In his report, Virchow attributed the causes of the epidemic to the massive economic crisis encroaching northern Germany (cause of the emigration to Northern America in the first half of the 19th century). On that occasion, Virchow also exhibited his idiosyncrasy for infectious disease, the cause of his persistent hostility to Robert Koch in the years to follow [10].

While the Prussian government did not care for the report, Virchow achieved his political ripeness: he had become a radical, and when the revolution erupted in 1848, he was actively involved in Berlin's barricades attending the wounded at the Charité. Moreover, he had the bitter experience to fight against the royal Pommern regiment of Stettin at the barricade of Friedrichstrasse.

Virchow's rebel attitude caused a lot of trouble in his relatives, who supposed him to be a communist. Marx and Engels were just issuing their Manifesto. He justified himself with his father by writing that he wasn't [12]. Nevertheless, he was punished by the Prussian rulers and his activity at the Charité was severely limited.

In 1850, Virchow was invited to Würzburg (Bavaria) as a full professor. That was not just an exile. Albert Kölliker admired him sincerely and contributed to his nomination there. The period spent in Würzburg represented for Virchow an authentic triumph. Despite his cold and monotonous style, numerous fascinated students attended his lectures because he presented and discussed factual realities consistently and with stringent logic.

Virchow's coldness did not imply that he was unconcerned with teaching. The easiest demonstration of this is provided by his major works. They all show the typical structure of oral lectures, from which they probably originated.

The short period Virchow spent in Würzburg (1850–1856) represented the consolidation of his academic success and the start-up of a happy family life. Virchow married in 1850 to an adolescent girl (Rose Mayer), the daughter of a colleague, a professor of Obstetrics in Berlin. Rose begot him six children and presented to him an apparently quiet and serene family life.

The Bavarian government entrusted Virchow an enquiry on the health state in the Spessart. In his reports, Virchow expressed his disgust for the horrifying condition of life of the people, starving in dirty huts. Such a situation was commonplace in vast areas of Europe, and would be the primer of the social unrest of the 19th century and of the birth of the socialist movement. Nevertheless, Virchow perceived how backward the German states were with respect to England and France, despite the immense potentialities he envisaged in his country.

After the incendiary experience of 1848, he realized that a keener approach to political life was needed. The resurrected medicine had obtained the tools necessary to transform social reality in a positive sense, and Virchow established that an all-out commitment was needed. Just as in Italy, the unity of Germany was profoundly desired in progressive intellectual circles and was considered to be a fundamental condition to create a modern nation. The German federation with its parliament in Frankfurt am Main should have been the ideal prologue to a gradual and pacific unification of that huge country. However, a lethal enemy was rapidly recognized: the Prussian kingdom with its ruthless dynastic desire of hegemony. The parallel with Italy is still impressive: in both countries the unification was obtained via a dynastic war of conquest. The monarchs of the two young nations were never able to create a genuine consensus, and played an important role in generating the persistent unrest and the tragic common outcome we all know.

## Berlin: the climax

In 1856, Virchow was back in Berlin as full Professor of Anatomic Pathology and Physiology. His book *Die Cellular-Pathologie* was issued in 1858. Contemporarily, Virchow's political career was started with his nomination for the Council of Berlin. More significantly, he was among the founders of the German Party of progress (1861) and was admitted to the Prussian Parliament in 1862, just while Bismarck obtained the nomination for Prussian Prime Minister by King Wilhelm I: the clouds of a stormy political struggle were gathering.

The open-mindedness of Virchow was in sharp contrast with the profoundly anti-parliamentary feelings of Bismarck and of the King. Moreover, Bismarck wanted to obtain the financial support of a massive campaign for armaments as a prelude to the conquest of the supremacy of Prussia in Germany and in Europe, at variance with Virchow's request of social reforms. The aggressive opposition by Virchow and his party was a nuisance to Bismarck, who tried to circumvent the Parliament. A compromise between Virchow and Bismarck was practically impossible, because they represented two completely opposite ways to interpret politics. Bismarck saw in Virchow the incarnation of parliamentary democracy and an adversary able to gather a systematic opposition to his projects of military expansion. Therefore, his challenging Virchow to duel in 1865, although Bismarck had been publicly accused to be a liar, might rather appear as a cold plan to get rid of a man unable to trade with weapons than a reaction to a scorching offense. Many friends of Virchow thought like that. Fortunately, Virchow was not so crazy to accept the challenge [1, 12].

Despite the hostility of Bismarck, Virchow was able to obtain a major success: to transform Berlin in a splendid metropolis. That great city was very dirty, because the public sewers did not yet exist. Therefore, Virchow started studying the problem accurately, and, on invitation by Napoleon III, he visited the famous sewers of Paris in 1867. The ensuing project he submitted to the Berlin municipality was amply modified. Nevertheless, the city obtained its sewers (1873) and very soon assumed the solemn and elegant shape characteristic of the years before 1945 [6, 12].

Berlin is very close to the heart of Germans. It is very difficult to understand why Americans were convinced (apart from Kennedy) that it was a city of secondary importance and unworthy to struggle so much for apart from some hot episodes of the cold war. A meaningful witness of Virchow's affection to Berlin consists in his enthusiastic support to the creation and expansion of museums and art collections. In this field, the most prominent merit of Virchow consists of convincing Heinrich Schliemann to present to Berlin's museum a number of his archeological findings [12].

Schliemann had not been adequately appreciated for his merits in Germany; therefore, the splendid items from his archeological campaigns poured into the British Museum. Virchow met Schliemann in 1874, in coincidence with an impressive increase of Virchow's studies in old Germany and Poland. A profound interest in natural history, geology and folklore, ethnic peculiarities had always been a characteristic of Virchow's ordinary life. His travels, whatever the scope, had always some collateral 'adventures' in natural history, anthropology or geology, often involving Virchow's children. His interest in palaeo-anthropology, despite the famous blunder in interpreting the first finding of a Neanderthal man [7], permits to consider Virchow to be the first genuine palaeopathologist because of his skills in accurately dating with stratigraphy the corpses he studied and in correlating such findings with historic and folklore records. The friendship with Schliemann permitted to sharpen Virchow's palaeopathological skills during his visits to Troy and to the Nile valley (1888).

## Controversial items

While Virchow was visiting the Nile valley, Kaiser Friedrich III was dying, just after 3 months of rule. That death was considered to be a massive disgrace for Germany and Europe, because Friedrich, despite being a military hero (wars against Austria and France), appeared to be a wise and open-minded man, profoundly hostile to the aggressive and reactionary designs of Bismarck. Of course, there is no proof that Friedrich might have been able to avoid the increasing aggressive attitude of Germany and the first world war. However, Wilhelm II, his successor, was a very immature ruler, who immediately fired Bismarck and replaced him with a series of mediocre ministers, unable to counter him. Max Weber said that Wilhelm's Germany, the most advanced and civil nation in the world, appeared to be ruled by a patrol of crazy men. Many people gave Virchow the blame for that because he was wrong in diagnosing the laryngeal cancer of Friedrich III. A series of laryngeal biopsies were submitted to Virchow. He always diagnosed a benign process despite the progressive worsening of symptoms. The biopsy specimens have been reviewed and modern pathologists are convinced that Virchow had acquired sufficient knowledge and experience to identify that cancer correctly. While many modern pathologists stigmatized the error severely and judged it the first known example of malpractice in pathology, because the samples available were sufficient to formulate a correct diagnosis, recent studies appear to be more liable to absolve Virchow [2]. Virchow's contemporaries were not so severe and would specifically blame Virchow's lack of concern for the health of Friedrich III, a close friend to him. While the emperor was dying, Virchow was engaged in a ceaseless strolling in Egypt, Near East and Italy in search of anthropological and palaeopathologic findings [12]. Nevertheless, once back in Berlin, Virchow obtained the pardon of the imperial family.

Before examining other facets of the complex and fascinating personality of Virchow, it is appropriate to consider the intensive criticism this man is constantly undergoing. His misinterpretation of the Neanderthal skull as a modern case of microcephaly was discussed above. Of course, that was a blunder, although Virchow had correctly dated the geological layer where the skull had been found [12]. However, in other circumstances, Virchow produced interesting results as an antiquarian. Nevertheless, his influence on anthropology is considered a very pernicious one.

The dispute with Robert Koch about tuberculin as an effective therapeutic agent in tuberculosis has some very deep roots [10]. Virchow did not like Koch's studies in

infectious disease, because he did not immediately realize the importance of microorganisms in disease. Nevertheless, he was correct in criticizing the overestimated positive results obtained by Koch in his attempts to cure tuberculosis by tuberculin therapy. Autopsy demonstrated that the patients had died of active tuberculosis, despite the treatment with tuberculin. Nevertheless, Virchow is still represented as the villain in children's tales.

Such a judgment is probably severe. Virchow's ineptitude to understand Koch's and Cohnheim's discoveries appears to be a major cultural setback, however. Koch's discoveries were constantly considered with cold skepticism. Julius Cohnheim was probably the most prominent disciple of Virchow. Nevertheless, he never accepted the consistency of Cohnheim's splendid studies on acute inflammation and diapedesis. Because of the massive prestige Virchow enjoyed in medicine, such prejudices appeared to be very dangerous.

Another topic justifying some criticism to Virchow was his involvement in the Kulturkampf, the strife against the Catholic Church to limit its hegemony in Germany. Virchow himself apparently coined the term Kulturkampf (1873). During that unsuccessful struggle, he was aligned with Bismarck for the first and last time. On that occasion, Virchow did not appear like a fanatical anti-religious man. His point of view expressed the classic attitude of Lutherans and of democrats, their modern counterpart: a profound desire of independence of thought in every field of human life. Unfortunately, the struggle of Virchow and Bismarck was destined to failure. The last lethal blow to that project came from Hitler in 1933, with the signature of the concordat.

## Death. Virchow in our mind

25 January 1902: Virchow, in perfect health, fell along a tramway road and had a femur badly fractured. He never did recover completely until he died on 5 September [12].

Virchow was a good man, animated by sincere affection to mankind. We have already seen his intensive commitment to the poor condition of Poles, his aggressive parliamentary struggle against Bismarck and the conservative faction. During the war against France, Virchow organized a hospital train. After that war, he tried intensively to mitigate the bitter animosity of the French scientists against their German colleagues.

Therefore, in many circumstances, Virchow appears to be an honest democrat acting in perfect accord with his concept of medicine as a social and political practice. His struggle against Bismarck could neither avoid the wars nor the frightening adventure where Germans had been propelled by a myopic political establishment. Nevertheless, the commitment of Virchow and his democratic partners was effective in stimulating the social changes making Germany the most advanced country in social organization.

Virchow did not evoke human sympathy and affection because of his coldness and aggressive behavior. That was probably critical in producing a negative attitude in pathologists. In a famous inaugural speech issued in the Verhandlungen der deutschen pathologischen Gesellschaft in 1898, Virchow established a sort of supremacy of pathology and experimental medicine with respect to all other medical disciplines. That would create a sort of wall separating pathology from other medical disciplines and a series of difficulties never completely removed in the relationship between pathology and clinical practice. Nevertheless, I cannot blame Virchow for all that. His speech of 1898 expressed the pride of an old man celebrating a new successful discipline practically created by him and at the climax of its success.

In conclusion, the success of modern pathology in medicine was practically started at Virchow's return to Berlin (1856). Other Berlin luminaries, such as the surgeon Theodor Billroth (1829–1894), saw this resurrection of the pathological tradition as a way to inject both scientific culture and clinical utility into the medical milieu of Germany [4]. Billroth, in particular, concerned himself with placing surgery on solid scientific grounds, carefully tracking the work on the origins of tumor cells performed in the 1860s by Virchow and his successors. Billroth felt such work would be important in diagnosing and treating neoplastic disease. Indeed, it was in just that decade that pathological anatomy provided the tools by means of which inflammatory and malignant neoplasia could finally be differentiated. Thus, the ability of the surgeon was enhanced to distinguish between disease processes that, while appearing similar to gross inspection, actually bore critically dissimilar prognostic and management implications. Surgical pathology was born [4].

## References


1. Andree C (1995) Rudolf Virchow. Sämtliche Werke. Band 31 Abteilung II. Politik. Peter Lang, Bern
2. Feldmann H (2002) Diagnosis and therapy of diseases of the larynx in the history of medicine. Part III. After the invention of laryngoscopy. Laryngorhinootologie 81:596–604
3. Goethe JW (1988) Morphologie, Werke ausgewählt von Mathias Bertram. Digitale Bibliothek, Directmedia, Berlin
4. Harris H (2000) The birth of the cell. Yale U.P., New Haven
5. Jay V (2000) The extraordinary career of Dr Purkinje. Arch Pathol Lab Med 124:662–663
6. Richie A (1999) Faust's metropolis. A history of Berlin. Carroll & Graf, New York
7. Rosen G (1977) Rudolf Virchow and Neanderthal man. Am J Surg Pathol 1:183–187
8. Scarani P (2000) Johann Wolfgang Goethe (1749–1832): il creatore del termine e del concetto di morfologia. Pathologica 92:45–49
9. Scarani P (2001) Riflessi goethiani sui problemi della scienza contemporanea. Pathologica 93:71–73
10. Scarani P (2002) Robert Koch (1843–1910): una vita in trincea (contro i microbi, contro Virchow e contro tanti altri) ... ed un inaspettato parallelo con Golgi. Pathologica 94:44–57
11. Schmiedebach H (1995) Robert Remak (1815–1865) Ein Jüdischer Arzt im Spannungsfeld von Wissenschaft und Politik. Fischer, Stuttgart
12. Vasold M (1988) Rudolf Virchow. Der große Arzt und Politiker. Deutsche Verlags-Anstalt, Stuttgart

Virchows Arch (2003) 442:99–106
DOI 10.1007/s00428-002-0680-3

REVIEW ARTICLE

**Manfred Stolte**

# The new Vienna classification of epithelial neoplasia of the gastrointestinal tract: advantages and disadvantages

Received: 7 June 2002 / Accepted: 7 June 2002 / Published online: 13 December 2002
© Springer-Verlag 2002

**Abstract** A number of seminars have shown considerable differences between Japanese and Western pathologists in the diagnostic differentiation of reactive changes, dysplasia and well-differentiated adenocarcinoma in gastroenterological biopsy material. Lesions that most Western pathologists identify as "dysplasia" are often considered adenocarcinomas in Japan. A comparison of the biopsy-based diagnoses with those established in resected mucosa, however, reveals appreciable diagnostic inexperience on the part of Western pathologists, with significant discrepancies between their diagnoses based on biopsies and those based on resected material. Against this background, a new classification of epithelial neoplasia of the gastrointestinal tract was drafted on the occasion of the World Congress of Gastroenterology in Vienna in 1998. By collapsing the diagnoses "high-grade adenoma/dysplasia, noninvasive carcinoma (carcinoma in situ), and suspected invasive carcinoma" into a single category ("noninvasive high-grade neoplasia", category 4), this scheme should largely eliminate the diagnostic discrepancies between Western and Japanese pathologists. As with every classification, the Vienna classification has its advantages and disadvantages; these are discussed here. The most important advantage of the Vienna classification is that the various categories are associated with different recommendations for further diagnostic and therapeutic measures. This applies in particular to category 4, with the recommendation for only local treatment initially (endoscopic mucosal resection or surgical excision). Since the introduction of the Vienna classification, the new World Health Organization classification of neoplasia of the gastrointestinal tract has recently been published, in which the term dysplasia has been replaced by "intraepithelial neoplasia". This means that the Vienna classification needs to be modified accordingly.

M. Stolte (✉)
Institut für Pathologie, Klinikum Bayreuth,
Preuschwitzerstrasse 101, 95445 Bayreuth, Germany
e-mail: pathologie.klinikum-bayreuth@t-online.de

**Keywords** Dysplasia · Epithelial neoplasia · Adenocarcinoma

## Introduction

On the occasion of an American gastroenterological congress held in the middle of the 1990s, a Japanese gastroenterologist presented histological pictures of endoscopic mucosal resections purporting to show early gastric carcinoma limited to the mucosa. In the following discussion, an American pathologist dismissed the findings as merely "dysplasia", but not carcinoma. Prompted by this occurrence, Ronald Schlemper, a Dutch internist living and working in Japan, organized a 1-day slide seminar for Western and Japanese pathologists in Tokyo. The objective of this seminar, which was attended by four Western and four Japanese pathologists, was to establish whether there were indeed basic differences between Western and Japanese pathologists in the diagnosis of early carcinoma in the gastrointestinal mucosa – is a lesion merely dysplasia or already a carcinoma? This seminar concentrated solely on the borderline situations:

- Can a lesion still be considered a reactive change or is it already dysplasia?
- Is a lesion still dysplasia or adenoma, or already a well-differentiated tubular adenocarcinoma?

Only slides relevant to these questions were submitted to the eight pathologists for evaluation, but no unequivocally G3 carcinomas or signet ring cell carcinomas, and no "rarities". The results of the diagnostic evaluation of the gastric slides were subsequently published in Lancet [24] and those of colon slides in Cancer [25]; these results prompted a spate of commentaries in the literature [20, 22, 30] as well as a number of similar studies in the USA [14], Italy [18], Germany [27]. This international discussion of the classification of gastrointestinal epithelial neoplasias found a temporary end in a further study involving 32 prominent pathologists specializing in gastro-

**Table 1** Differences in the diagnostic work-up of biopsies obtained from 35 gastric mucosal lesions. *KL* K. Lewin, *RR* R. Riddell, *PS* P.Sipponen, *MS* M. Stolte, *MI* M. Itabashi, *YK* Y. Kato, *TS* T. Shimoda, *HW* H. Watanabe

| Diagnosis | "Western" | | | | "Japanese" | | | | | |
|---|---|---|---|---|---|---|---|---|---|---|
| | KL | RR | PS | Total (%) | MS | MI | YK | TS | HW | Total (%) |
| Regenerative epithelium | 2 | 3 | 1 | 6 | 1 | 2 | 3 | 3 | 2 | 6 |
| Low-grade dysplasia/adenoma | 3 | 8 | 9 | 19 | 1 | 1 | 1 | 1 | 1 | 3 |
| High-grade dysplasia/adenoma | 14 | 8 | 17 | 37 | 1 | 1 | 2 | 2 | 1 | 4 |
| Suspected carcinoma | 7 | 7 | 5 | 18 | 0 | 4 | 5 | 5 | 0 | 7 |
| Definite carcinoma | 9 | 9 | 3 | 20 | 32 | 27 | 24 | 24 | 31 | 80 |
| Agreement | 31.4%, kappa: 0.15 | | | | | | | | | |

enterological pathology from East and West. A discussion of the results of this study on the occasion of the World Congress of Gastroenterology held in Vienna in 1998 then led to the proposal to work out the new "Vienna classification" of epithelial neoplasias of the gastrointestinal tract [29].

## Japanese "fairy tales" or "Western deficiency"?

The considerable differences in the diagnostic evaluation of the gastric slides among the eight pathologists originally participating in the first seminar in Tokyo (Table 1) prompted a number of commentaries, some of which were highly critical. A German gastroenterologist, for example, entitled his commentary: "Early detection of gastric carcinoma: Japanese fairy tales?" [1]. He concluded that: "The high prevalence of gastric carcinoma in Japan, and the claimed successes in combating gastric carcinoma are possibly nothing but artefacts."

It must be pointed out, however, that this author overlooked the fact that the evaluations of one of the Western pathologists were virtually identical with those of his Japanese colleagues; furthermore, in comparison with the single Western pathologist and the four Japanese pathologists, there were relatively large differences among the three other Western pathologists in terms of the distribution of their diagnostic evaluations with regard to "regenerative changes", "adenoma/low-grade dysplasia", "adenoma/high-grade dysplasia", "suspicion of carcinoma", and "unequivocal carcinoma" (Table 1).

What the above-mentioned author also overlooked was the fact that considerable differences were also found between the three Western pathologists and the four Japanese pathologists and the single Western pathologist with regard to the evaluation of biopsies and endoscopically resected mucosa obtained from the same patients, which were evaluated separately and "blinded" (Table 2).

It might, of course, be speculated that these results were due merely to chance, since only eight pathologists were involved in the study. However, another slide seminar, again organized by Ronald Schlemper, which was evaluated and discussed on the occasion of the World Congress of Gastroenterology, clearly showed that this discrepancy between biopsy-based diagnosis and diagnosis based on resected material is the rule among the majority of Western pathologists. This remark, however, does not apply to all Western pathologists who participated in this seminar, since the results obtained in Vienna showed that five Western pathologists returned the same diagnoses as their Japanese colleagues.

**Table 2** Discrepancy and agreement of the diagnoses established by "Western" and "Japanese" pathologists in endoscopic mucosal specimens in comparison with forceps biopsy material obtained from the stomachs of the same patients (Results of the Tokyo Workshop). Comparison of the diagnoses established in biopsy and resected material

| | "Western" (%) | "Japanese" (%) |
|---|---|---|
| Discrepancy | 45 | 10 |
| Agreement | 55 | 90 |

A comparison of the diagnoses established in biopsy material with those made in resected mucosa (Table 3) shows that the pathologists adopting the "Western viewpoint" significantly more frequently changed their biopsy-based diagnosis of dysplasia to carcinoma in resected mucosa. This discrepancy between biopsy-based and resection-based diagnosis among Western pathologists is, indeed, so marked that an uncertainty in diagnosing biopsy material can be concluded. This is not particularly surprising, since far more early carcinomas are diagnosed in Japan than in the West, including more mucosal carcinomas. In Japan, 60–70% of early gastric carcinomas are currently removed via the endoscope. Experience in this area is therefore very much greater in Japan than in Western countries. It may thus well be that these differences (fewer examinations, less practice in the evaluation of such cases, and less experience) underlie the uncertainty of most Western pathologists. Against this background, it may be concluded that, rather than "Japanese fairy tales", "Western deficiency" is the more likely alternative [31]. This likelihood is supported by the results of my own inquiry conducted among the eight pathologists participating in the first Tokyo workshop, regarding the number of new gastric carcinomas they diagnosed in biopsy material at their institutes in 1998 (Table 4).

**Table 3** Frequency of revision of diagnoses made in endoscopically resected mucosa (EMR) vis-à-vis biopsy material established by pathologists with "Western" and "Japanese" viewpoints during the 1998 workshop in Vienna

| | "Western" (%) | "Japanese" (%) |
|---|---|---|
| Dysplasia–carcinoma | 27 | 5 |
| Carcinoma–dysplasia | 5 | 4 |

**Table 4** Number of gastric carcinomas newly diagnosed in biopsy material in 1998 by pathologists participating in the Tokyo seminar. *KL* K. Lewin, *RR* R. Riddell, *PS* P.Sipponen, *MS* M. Stolte, *MI* M. Itabashi, *YK* Y. Kato, *TS* T. Shimoda, *HW* H. Watanabe

| Gastric carcinoma: "Experience" | |
|---|---|
| Pathologist | Cases/1998 |
| KL | 27 |
| RR | 20 |
| PS | 19 |
| MS | 782 |
| MI | 97 |
| YK | ~400 |
| TS | 350 |
| HW | ~500 |

**Table 5** "Dysplasia" terminology collected from pathological reports (O. Stadelmann, personal communication)

| Dysplasia I–III |
|---|
| Metaplastic dysplasia |
| "Proper gastric type" of dysplasia |
| Hyperplastic dysplasia |
| Intestinal dysplasia |
| Adenomatous dysplasia |
| Microglandular dysplasia |
| Anaplastic dysplasia |
| Regenerative dysplasia |
| Diffuse dysplasia |
| Globoidal dysplasia |
| Strange dysplasia |

**Table 6** Literature reports of follow-up examinations in patients diagnosed as having "high-grade dysplasia" of the gastric mucosa

| First author | Year/Reference | *n* | HGD–Ca (%) | Time (months) |
|---|---|---|---|---|
| Saraga | 1987 [23] | 21 | 81 | 4 |
| Lansdown | 1990 [13] | 13 | 85 | 5 |
| Rugge | 1991 [18] | 8 | 75 | 4 |
| Fertita | 1993 [7] | 31 | 81 | 5 |
| Di Gregorio | 1993 [6] | 10 | 60 | 11 |
| Rugge | 1994 [19] | 18 | 78 | 9 |
| Kokkola | 1996 [12] | 3 | 67 | 18 |
| Median | | | 80 | 6 |

## Can we do without the term "dysplasia" in the evaluation of gastric biopsies?

If we take a critical look at the old definitions of dysplasia of the gastric mucosa:

- Structural changes in the surface epithelium [17]
- Atypical mucosa restricted to the epithelial layer [8]

it may be noted that these definitions are extremely vague and allow a great deal of scope for subjective interpretation. Nor did the first international definition bring about any appreciable change, since it contained a reference to a combination of "cellular atypia", "abnormal differentiation" and "disorganized mucosal architecture" [16]. It was at this time that Stadelmann made a collection of the terms used to diagnose dysplasia of the gastric mucosa (Table 5). Stadelmann's comment was a citation from The Acts of the Apostles 19, 32: "Some therefore cried one thing, and some another: for the assembly was confused; and the more part knew not wherefore they were come together" (Authorized King James Version).

Although the inflation in the diagnosis of dysplasia of the gastric mucosa that was observed in the 1970s did undergo a change after the introduction of the World Health Organization (WHO) definition of dysplasia: "unequivocal intra-epithelial neoplasia" [2], the significance of the dysplasia diagnosis as a precursor, concomitant or marginal lesion of a carcinoma continues to be both unclear and controversial. An analysis of follow-up studies investigating the question of high-grade dysplasia of the gastric mucosa published in the West (Table 6), reveals the striking fact that, in 80% of these cases, a carcinoma was subsequently diagnosed in the very short mean follow-up time of 6 months [6, 12, 13, 18, 19, 23]. In other words, at the time of its diagnosis, the high-grade dysplasia was with a high degree of probability, already a carcinoma. A prospective English study came to a similar conclusion [5].

In my experience as a consultant pathologist, more than 90% of the cases of "dysplasia" can be identified unequivocally as regenerative mucosa, adenoma or carcinoma. There remains only a relatively small percentage of cases in which, following Elster, we identify not "dysplasia", but "uncertain finding", and for which we recommend a careful endoscopy/biopsy follow-up as soon as possible.

Against this background, and despite the theoretically correct concept of the dysplasia–carcinoma sequence, the diagnosis of "dysplasia" in the gastric mucosa could be largely eliminated from our daily diagnostic routine. However, given the dominance of Western proponents of the dysplasia diagnosis in various international committees, this is currently not possible. In particular in the USA, for example, the diagnosis of dysplasia also has both legal and social aspects. Responding to my criticism of his "dysplasia cases", which I would have diagnosed as unequivocal carcinoma, an American patholo-

gist made the following remark: "By diagnosing dysplasia, I have, legally speaking, one foot in the boat and the other firmly on solid land, and am thus protected from possible litigation for malpractice should no carcinoma be found in the surgical specimen."

Furthermore, in the USA, many patients diagnosed as having carcinoma would lose their health insurance, or would have to pay higher premiums, which is not the case when the diagnosis made is "dysplasia". Thus it is that, in the USA; the diagnosis "dysplasia" is a "social" diagnosis (R. Haggitt, personal communication).

This makes it all the more surprising that the term "dysplasia" in the recently published new WHO classification has nevertheless now been replaced by that of "intra-epithelial neoplasia", which is categorized only into "low-grade" and "high-grade" [10].

## Does the Vienna classification put an end to diagnostic discrepancies?

The Vienna classification of gastrointestinal neoplasias was developed on the occasion of a pathological workshop held during the World Congress of Gastroenterology in Vienna (1988) (Table 7). The particular feature of this classification is the fact that the diagnoses which at previous international pathological seminars had led to considerable discrepancies, namely "high-grade adenoma/dysplasia", "noninvasive carcinoma" (carcinoma in situ) and "suspicion of invasive carcinoma", were collapsed into the category-4 "noninvasive high-grade neoplasia".

## Will these new categories make it possible to eliminate the discrepancies in the diagnosis of these lesions?

In terms of statistics, yes, since the differences between the pathologists adopting a "Western viewpoint" and those adopting a "Japanese viewpoint" are largely eliminated by this new classification, in particular as a result of the introduction of the synoptic category 4.This applies both to gastric (Fig. 1, Fig. 2) and to colorectal lesions (Fig. 3, Fig. 4), as also to esophageal lesions (Fig. 5, Fig. 6).

This is also demonstrated by a calculation of the percentage of agreement of the diagnoses and of kappa coefficients for the diagnoses in the stomach, colorectum and esophagus (Table 8).

## Vienna classification: advantages and critical points

It goes without saying that the Vienna classification represents merely a preliminary compromise that not only has advantages, but also contains a number of critical points. One of these critical points is the differentiation between noninvasive carcinomas, which is associated

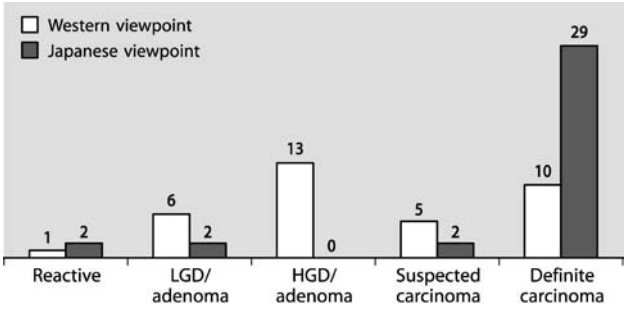



**Fig. 1** Diagnostic evaluation of 35 gastric lesions prior to the introduction of the Vienna classification of epithelial neoplasia (*LGD* low-grade dysplasia, *HGD* high-grade dysplasia)

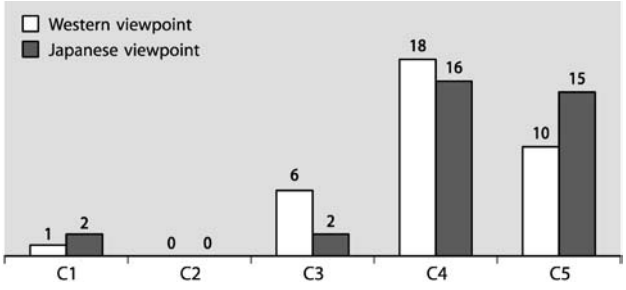



**Fig. 2** Diagnostic evaluation of 35 gastric lesions after the introduction of the Vienna classification of epithelial neoplasia (C1–C5 category 1–5 of the Vienna classification)

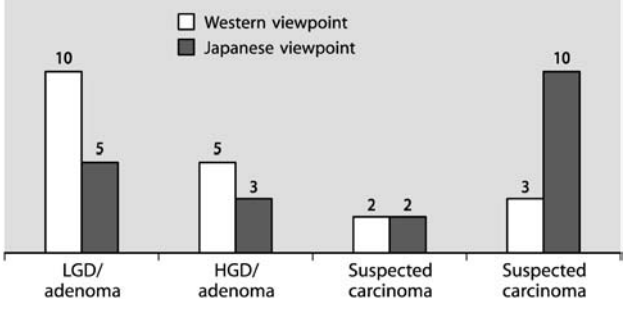



**Fig. 3** Diagnostic evaluation of colorectal lesions prior to the introduction of the Vienna classification of epithelial neoplasia (*LGD* low-grade dysplasia, *HGD* high-grade dysplasia)

**Table 7** Vienna classification of the gastrointestinal epithelial neoplasia [29]

| | |
|---|---|
| Category 1 | No neoplasia |
| Category 2 | Indefinite for neoplasia |
| Category 3 | Low-grade adenoma/dysplasia |
| Category 4 | Noninvasive high-grade neoplasia |
| 4.1. | High-grade adenoma/dysplasia |
| 4.2. | Noninvasive carcinoma (carcinoma in situ) |
| 4.3. | Suspicion for invasive carcinoma |
| Category 5 | Invasive neoplasia |
| 5.1. | Intramucosal carcinoma |
| 5.2. | Submucosal carcinoma (or deeper infiltration) |

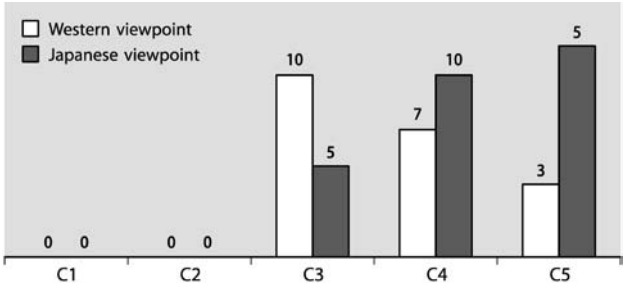



**Fig. 4** Diagnostic evaluation of colorectal lesions after the introduction of the Vienna classification of epithelial neoplasia (C1–C5 category 1–5 of the Vienna classification)

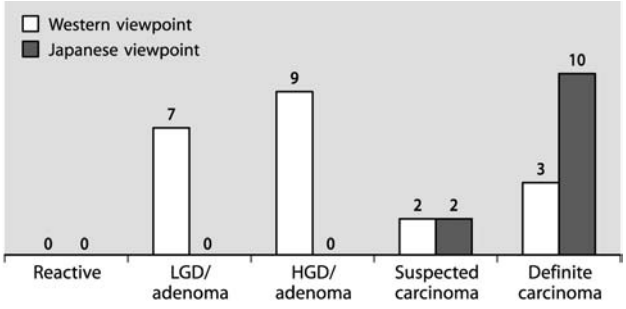



**Fig. 5** Diagnostic evaluation of 21 esophageal lesions prior to the introduction of the Vienna classification (*LGD* low-grade dysplasia, *HGD* high-grade dysplasia)

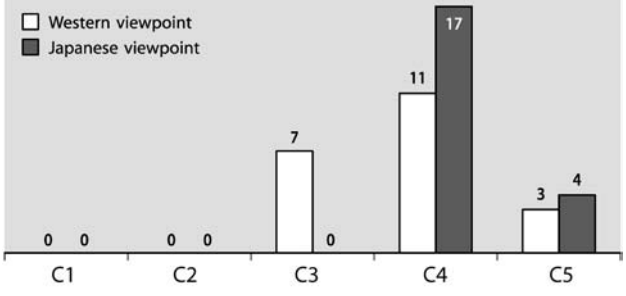



**Fig. 6** Diagnostic evaluation of 21 esophageal lesions after introduction of the Vienna classification (C1–C5 category 1–5 of the Vienna classification)

**Table 8** Agreement of the diagnoses and kappa coefficients for the diagnoses in biopsies obtained from the stomach, colorectum and esophagus in accordance with the former classification and the Vienna classification of gastrointestinal neoplasia

| | Agreement (%) | kappa (coefficient) |
|---|---|---|
| Former classification | | |
| Stomach | 37 | 0.16 |
| Colorectum | 45 | 0.27 |
| Esophagus | 14 | 0.01 |
| Vienna classification | | |
| Stomach | 71 | 0.55 |
| Colorectum | 65 | 0.47 |
| Esophagus | 62 | 0.31 |

with controversial discussion of the criteria for invasion into the lamina propria. For a diagnosis of carcinoma in the stomach, pathologists adopting the Western viewpoint require unequivocal invasion of the lamina propria or submucosa, and for colorectal carcinoma invasion of the submucosa as required by the WHO definition.

Pathologists adopting the "Japanese viewpoint" do not make this distinction between stomach and colorectum. For the diagnosis of a carcinoma, they require merely typical changes to the cell nuclei and the architecture of the neoplasia (Table 9). In contrast, pathologists taking the "Western viewpoint" require evidence of "solitary invading tumor cells" or "trabecular invasion of the lamina propria" for the unequivocal diagnosis of carcinoma. In the case of well-differentiated tubular adenocarcinomas, however, these criteria can hardly be expected to be met. This is shown by the example in Fig. 7 – when, in the mucosa, disrupted architecture with no solitary separate tumor cells invading the lamina propria is found, Western pathologists diagnose merely high-grade dysplasia. When, however, a neoplastic tubule is found in the submucosa (Fig. 8), these pathologists, too, diagnose carcinoma – even in the absence of separate individual tumor cells.

It is conceivable that, in the future, the molecular-pathological analysis of the processes necessary for invasion, namely dissolution of the intercellular connections, formation of matrix components, dissolution of matrix components, and migration through matricial components, might be an important diagnostic aid. One of the molecular markers for invasion may be the increased expression of beta catenin, which Brabletz et al. [3] showed to be present in the invasion front of colorectal carcinomas. Another potential marker for invasion might be MMP-7 – which is also known as matrilysin. Expression of this marker, namely, is found to be increased in high-grade dysplasia in colonic adenomas [15, 33], and its suppression in vitro leads to inhibition of invasion by colon carcinoma cells [34]. Of particular interest in this connection is the fact that a working group headed by Kirchner has recently demonstrated that beta-catenin regulates the expression of MMP-7 [4].

But, do we really have to wait for molecular markers to identify invasion? My own position is that the answer must be no. I go along with the convincing study published by Takahashi and Iwama in 1985 [32]. In their three-dimensional reconstructions of the micro-structure of well-differentiated tubular adenocarcinomas of the stomach, these authors were able to show that the carcinomatous tubules invade the lamina propria where they anastomose with neighboring tubules to give rise to a network of tubules. The discovery of this network shows that these well-differentiated adenocarcinomas arise by invasive growth throughout the lamina propria. The investigations of these authors show that separated groups of tumor cells in the lamina propria are to be found only in G2 and G3 adenocarcinomas. An analysis of the three-dimensional microstructure also showed clear differences between normal gastric mucosa, adenoma and G1

**Table 9** Major criteria for diagnosing carcinoma in the stomach and colorectum: "Western" and "Japanese" viewpoints

| Organ | Viewpoint | |
|---|---|---|
| | Western | Japanese |
| Stomach | Invasion of lamina propria or submucosa | Changes to nuclei/ glandular structure |
| Colorectum | Invasion of submucosa | |

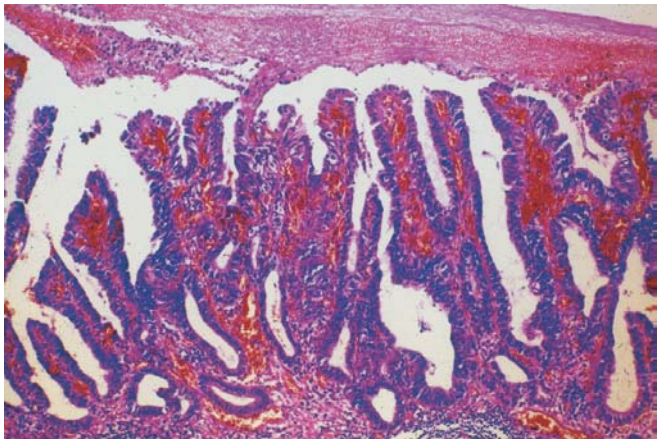


**Fig. 7** Intramucosal neoplasia that would be diagnosed by most Western pathologists as "high-grade dysplasia"

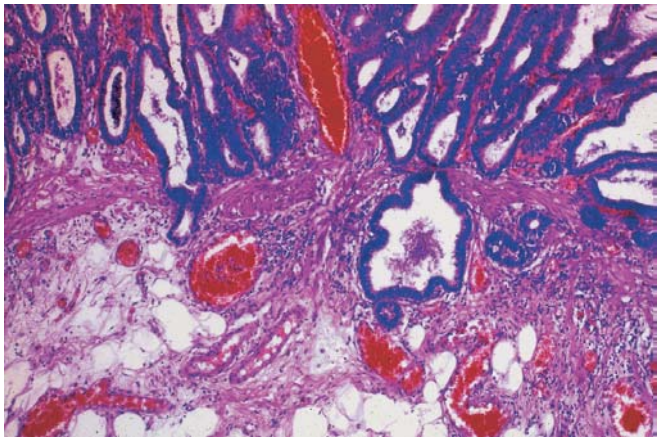


**Fig. 8** Neoplasia in the mucosa which, in the presence of an invasive tubule is diagnosed unequivocally as definite carcinoma even in the absence of separated tumor cells in the submucosa (same case as in Fig. 7)

adenocarcinomas. In combination with the cytological criteria of malignancy, this pattern-based diagnosis suffices for the diagnosis of a well-differentiated tubular adenocarcinoma [11].

**Table 10** Recommendations based on the categories of the Vienna classification

| Category | Consequence |
|---|---|
| 1. Negative | Optional surveillance |
| 2. Indefinite | Surveillance |
| 3. Noninvasive low-grade dysplasia | Surveillance/local treatment |
| 4. Noninvasive high-grade dysplasia | Local treatment |
| 5. Invasive carcinoma | Local/surgical treatment |

## The outstanding advantage: recommendations on how to proceed

The most important advantage of the Vienna classification is probably the fact that the various different categories provide a good basis for differentiated recommendations on how to proceed with further diagnostic and therapeutic measures (Table 10). This applies in particular to category 4, for which the recommendation is initially for only local treatment (endoscopic mucosectomy or laparoscopic excision). If the histological work-up of the locally resected specimen then confirms the diagnosis of adenoma, high-grade dysplasia or moderate to well-differentiated mucosal adenocarcinoma with a diameter of not more than 2 cm, no evidence of lymph-vessel invasion, and an adequate margin of safety, further surgical treatment is not absolutely necessary. The rationale for this is the fact that the risk of regional lymph-node metastasis is only approximately 2%, that is, less than the mortality and morbidity risk attendant on the surgical procedure. In western countries, this recommendation for local treatment might lead to a decrease in the use of gastrectomy, esophagectomy, etc., in cases of early carcinoma limited to the mucosa. Such an approach would be of benefit to these patients. In Japan, 50–60% of mucosal early carcinomas in the stomach are currently treated by local endoscopic resection of the tumor [9].

Admittedly, the recommendation for local therapy must be carefully and critically considered when the finding is "suspected carcinoma". In such a case, this always applies to the diagnostic work-up and treatment of early carcinoma of the gastrointestinal tract – the endoscopic finding in particular must be involved in the decision-taking process. After all, the diagnosis "suspected carcinoma" may be prompted by the finding of an non-steroidal anti-inflammatory (NSAID)/acetylsalicylic acid (ASA)-induced regenerative mucosa, which may often be associated with considerable nuclear atypia and

**Table 11** Modified Vienna classification of gastrointestinal epithelial neoplasia [26]

| | |
|---|---|
| Category 1 | No neoplasia |
| Category 2 | Indefinite for neoplasia |
| Category 3 | Low-grade adenoma/dysplasia |
| Category 4 | High-grade neoplasia |
| 4.1 | High-grade adenoma/dysplasia |
| 4.2 | Noninvasive carcinoma (carcinoma in situ) |
| 4.3 | Suspicion for invasive carcinoma |
| 4.4 | Intramucosal carcinoma |
| Category 5 | Submucosal invasive carcinoma (carcinoma with invasion of the submucosa or deeper) |

also with tumor-simulating architectural disruption. Since, however, NSAID/ASA-induced lesions are often multiple (erosions, shallow, and unsharply delimited ulcers at atypical locations), such findings should first prompt endoscopy/biopsy re-examination after discontinuation of the NSAID/ASA medication and appropriate treatment of the lesions, rather than a recommendation for immediate endoscopic resection.

Another critical point in the present Vienna classification is the recommendation "surveillance" or local treatment in the case of adenoma or low-grade dysplasia, for this is unequivocally a pre-cancerous lesion and should therefore always be completely removed endoscopically immediately after being diagnosed. This applies in particular to adenomas diagnosed in biopsy material, for, at the time of diagnosis, such adenomas may already contain a well-differentiated adenocarcinoma at some other site not included in the biopsy bite.

Yet another critical point is the diagnosis in the Vienna classification of "intramucosal colorectal carcinoma". Even if we were to recommend only local treatment for such a diagnosis, the danger of over-treatment by surgeons, that is unnecessary resection, is great. This is because of the fact that, although the mucosal carcinoma in the colorectum is justifiably a carcinoma on the basis of histology, cytology and molecular pathology, due to the absence of lymphatic vessels in the mucosa, it does not undergo lymphogenous metastasization, and, biologically speaking, is thus not a carcinoma. The Vienna classification places intramucosal carcinoma in category 5, consequently giving rise to the recommendation for local or surgical treatment. Japanese gastroenterologists have criticized the use of the word "or" in this recommendation as having the potential to justify superfluous major operations. This criticism has already led to the first modification of the Vienna classification with reassignment of the intramucosal carcinoma to category 4 (Table 11) [28, 26].

## Conclusion: pro or con

When we critically consider the question as to what is "really new" in the Vienna classification, the answer is very little:

1. The category "suspected invasive carcinoma" – this had not been contained in the WHO classification, although it had been known and used in our earlier daily routine diagnostic work, and also formed part of the Japanese classification.
2. Intramucosal carcinoma of the colorectum in the non-Japanese countries, and "non-invasive high-grade neoplasia".

This means that the Vienna classification, in fact, does not provide anything "really new", but merely a new categorization of the previous diagnoses. Despite the critical remarks, it must, however, be noted that the terminological consensus reflected in the Vienna classification represents an initial step toward resolving the diagnostic differences between pathologists. Furthermore, the Vienna classification might mark the start of an improvement in international comparisons of statistical data and provide a more sound basis for a comparison of the results of clinical research and research in the field of molecular biology.

The most important advantage of the Vienna classification is presumably the recommendations for the further diagnostic and therapeutic procedure, based on the new categorization. From this point of view, the "pros" predominate in the assessment of the Vienna classification of gastrointestinal epithelial neoplasia. This applies in particular to the collective nature of category 4 in this classification, since the recommendation for treatment derived from this categorization (initially merely endoscopic mucosectomy) will very likely now obviate a large number of major operative interventions with their associated relatively high mortality and morbidity rates, in non-Japanese countries too.

## Practical consequences

The Vienna classification of gastrointestinal epithelial neoplasia is a compromise between the "Japanese" and "Western" points of view of the diagnostic work-up. Although the new categorization of histological diagnoses does not produce anything "really new", it does have the advantage that the therapeutic consequences of the collective category 4 are in the first instance merely local treatment – also in non-Japanese countries – for neoplasias limited to the mucosa. In these defined cases, therefore, the "major" operative interventions – with their relatively high mortality and morbidity rates – that continue to predominate in Western countries, will in future largely be avoided – to the greater benefit of the patient.

## References

1. Anonymous (1997) Magenkarzinom-Früherkennung: japanische Märchen? Münch Med Wochenschr 139:21
2. Borchard F, Heilmann KL, Hermanek P et al (1991) Definition und klinische Bedeutung der Dysplasie im Verdauungstrakt. Pathologe 12:50–56

3. Brabletz T, Jung A, Hermann K, Günther K, Hohenberger W, Kirchner T (1998) Nuclear overexpression of the oncoprotein b-catenin in colorectal cancer is localized predominantly at the invasion front. Pathol Res Pract 194:701–704
4. Brabletz T, Jung A, Dag S, Hlubek F, Kirchner T (1999) Beta-catenin regulates the expression of the matrix metalloproteinase-7 in human colorectal cancer. Am J Pathol 155:1033–1038
5. De Dombal FT, Price AB, Thompson H et al (1990) The British society of gastroenterology early gastric cancer/dysplasia survey: an interim report. Gut 31:115–120
6. Di Gregorio C, Morandi P, Fante R, De Gaetani C (1993) Gastric dysplasia. A follow-up study. Am J Gastroenterol 88:1714–1719
7. Fertitta AM, Comin U, Terruzzi V, Minoli G, Zambeli G (1993) Clinical significance of gastric dysplasia: a multicenter follow-up study. Endoscopy 25:265–268
8. Grundmann E, Schlake W (1982) Histological classification of gastric cancer from initial to advanced stages. Pathol Res Pract 1973:260–274
9. Ida K, Okuda J, Katoh T, Katoh T, Kojima T, Ochiai J (1996) Recent advances and problems in the endoscopic treatment of early gastric cancer. Dig Endoscopy 8:46–52
10. Hamilton SR, Aalfonen LA (eds) (2000) Pathology and genetics of tumours of the digestive system. WHO classification of tumours. DARC Press, Lyon
11. Kirchner T, Brabletz T (2002) Tumour patterning: analogies of neoplastic morphogenesis with embryogenesis. Verh Dtsch Ges Pathol 84:22–27
12. Kokkola A, Haapiainen R, Laxen F, Puolakkainen P, Kivilaakso E, Virtamo J (1996) Risk of gastric carcinoma in patients with mucosal dysplasia associated with atrophic gastritis: a follow up study. J Clin Pathol 49:979–984
13. Lansdown M, Quirke P, Dixon MF, Axon ATR, Johnston D (1990) High grade dysplasia of the gastric mucosa: a marker for gastric carcinoma. Gut 31:977–983
14. Lauwers GY, Shimizu M, Correa P et al (1999) Evaluation of gastric biopsies for neoplasia: differences between Japanese and Western pathologists. Am J Surg Pathol 23:511–518
15. Mori M, Barnard GF, Mimori K, Ueo H, Akiyoshi T, Sugimachi K (1995) Overexpression of matrix metalloproteinase-7 mRNA in human colon carcinomas. Cancer 75[Suppl 6]: 1516–1519
16. Morson BC, Sobin LH, Grundmann E, Johansen A, Nagayo T, Serck-Hanssen A (1980) Precancerous conditions and epithelial dysplasia in the stomach. J Clin Pathol 33:711–721
17. Oehlert W, Keller P, Henke M, Strauch M (1979) Gastric mucosal dysplasia: what is its significance? Front Gastrointest Res 4:173–182
18. Rugge M, Farinati F, Di Mario F, Baffa R, Valiante F, Cardin F (1991) Gastric epithelial dysplasia: a prospective multicenter follow-up study from the interdisciplinary group on gastric epithelial dysplasia. Hum Pathol 22:1002–1008
19. Rugge M, Farinati F, Baffa R, Sonego F, Di Mario F, Leandro G (1994) Gastric epithelial dysplasia in the natural history of gastric cancer: a multicenter prospective follow-up study. Gastroenterology 107:1288–1296
20. Rugge M, Cassaro M. Farinati F (1997) Diagnosis of gastric carcinoma in Japan and Western countries. Lancet 350:448
21. Rugge M, Correa P, Dixon MF et al (2000) Gastric dysplasia: the Padova international classification. Am J Surg Pathol 24:167–176
22. Sakamoto J, Yasue M (1997) Do Japanese statistics on gastric carcinoma need to be revised? Lancet 349:1711–1712
23. Saraga EP, Gardiol D, Costa J (1987) Gastric dysplasia: a histological follow-up study. Am J Surg Pathol 11:788–796
24. Schlemper RJ, Itabashi M, Kato Y et al (1997) Differences and diagnostic criteria for gastric carcinoma between Japanese and western pathologists. Lancet 349:1725–1729
25. Schlemper RJ, Itabashi M, Kato Y et al. (1998) Differences and diagnostic criteria by Japanese and western pathologists to diagnosis colorectal carcinoma. Cancer 82:60–69
26. Schlemper RJ, Kato Y, Stolte M (1999) Well-differentiated adenocarcinoma or dysplasia of the gastric epithelium: rationale for a new classification system. Verh Dtsch Ges Pathol 83:62–70
27. Schlemper RJ, Borchard F, Dixon MF et al (2000) International comparability of the pathological diagnosis for early cancer of the digestive tract: Munich meeting. J Gastroenterol 35 [Suppl 12]:102–110
28. Schlemper RJ, Kato Y, Stolte M (2000) Diagnostic criteria for gastrointestinal carcinoma in Japan and Western countries: proposal for a new classification system of gastrointestinal epithelial neoplasia. J Gastroenterol Hepatol 15:C52–C60
29. Schlemper RJ, Riddell RH, Kato Y et al. (2000) The Vienna classification of gastrointestinal epithelial neoplasia. Gut 47:251–255
30. Stolte M (1997) Diagnosis of gastric carcinoma in Japan and western countries. Lancet 350:448
31. Stolte M (1999) Diagnosis of gastric carcinoma: Japanese fairy tales or Western deficiency? Virchows Arch 334:279–280
32. Takahashi T, Iwama N (1985) Three-dimensional microstructure of gastrointestinal tumors. Gland pattern and its diagnostic significance. Pathol Annu 200:419–440
33. Takeuchi N, Ichikawa Y, Ishikawa T et al (1997) Matrilysin gene expression in sporadic and familial colorectal adenomas. Mol Carcinog 19:225–229
34. Yamamoto H, Itoh F, Hinoda Y, Imai K (1995) Suppression of matrilysin inhibits colon cancer cell invasion in vitro. Int J Cancer 61:218–222

Virchows Arch (2003) 442:107–110
DOI 10.1007/s00428-002-0722-x

ORIGINAL ARTICLE

**Eugenio Maiorano · Giuseppe Renne**
**Nicoletta Tradati · Giuseppe Viale**

# Cytogical features of calcifying epithelial odontogenic tumor (Pindborg tumor) with abundant cementum-like material

Received: 26 April 2002 / Accepted: 6 September 2002 / Published online: 18 December 2002
© Springer-Verlag 2002

**Abstract** Calcifying epithelial odontogenic tumor (CEOT) is a rare tumor, most frequently occurring in the mandible and composed of large sheets of epithelial cells, sometimes showing nuclear pleomorphism. This paper was aimed at reporting of the cytological features of an unusual case of CEOT, affecting a 14-year-old female, with abundant deposition of intercellular calcified material. The cytological preparations were characterized by large clusters of scarcely cohesive, large polyhedral cells and abundant calcified material. The latter consisted of intensely basophilic substance either in large clusters or discrete concretions and, at high-power view, occasional tumor cells also contained calcified material. Histologically, the uncalcified stroma displayed focal Congo Red positivity with the typical birefringence under polarized light. The neoplastic cells were consistently immunoreactive for epithelial membrane antigen, vimentin and, to a lesser extent, for wide spectrum cytokeratins (AE1 AE3) and cytokeratins 8–18 and 19. The cytological features of CEOT are rather characteristic, and the detection of intra- and extracellular calcifications may help to differentiate this neoplasm from others that most commonly arise in this area.

**Keywords** Calcifying epithelial odontogenic tumor · Odontogenic tumors · Cytology · Calcified tissue · Cementum

E. Maiorano
Department of Pathological Anatomy and Genetics,
University of Bari, Bari, Italy

G. Renne · G. Viale (✉)
Division of Pathology and Laboratory Medicine,
European Institute of Oncology and University of Milan,
Via Ripamonti 435, 20100 Milan, Italy
e-mail: giuseppe.viale@ieo.it
Tel.: +39-02-57489419, Fax: +39-02-57489417

N. Tradati
Division of Head and Neck Surgery,
European Institute of Oncology, Milan, Italy

## Introduction

Calcifying epithelial odontogenic tumor (CEOT or Pindborg tumor) is a rare odontogenic neoplasm, first described by Jens Pindborg in 1955, that accounts for 1% of all odontogenic neoplasms and usually follows an indolent clinical course. It affects the mandible (posterior segments) more than the maxilla and is frequently associated with unerupted teeth or dentigerous cysts [5, 10, 14]. The age distribution is wide (15–75 years) with a peak in the fourth decade. CEOT has a mild tendency to recur, even after prolonged periods of time (more than 15 years) [4] and, very rarely, unequivocal malignant variants have been reported in elderly patients [2, 18].

It is composed of characteristic epithelial cells, growing in sheets, with prominent intercellular bridges, surrounded by variable amounts of amyloid substance and calcifications. Sometimes, the latter are arranged in concentric lamellae and interspersed within the epithelial cells (Liesegang rings). There is just one previous report dealing with the cytomorphology of typical CEOT, showing sheets of pleomorphic cells and amorphous material, surrounded by fibroblasts and occasional calcifications [6]. The current report was aimed at describing the cytological features of a rare variant of CEOT, characterized by abundant deposition of calcified material morphologically resembling cementum-like or osteoid-like substance.

## Case description

A 14-year-old female was admitted for progressive swelling of the posterior segment of the left hemi-mandible, of 4-months duration. Panoramic radiograms showed a radiolucent lesion with abundant intra-lesional calcifications and smooth margins (Fig. 1). The patient underwent a diagnostic biopsy that was submitted for intra-operative examination. The latter was carried out on touch preparations that were stained with hematoxylin and eosin (H&E) and Giemsa, and frozen tissue sections conventionally stained with H&E. Subsequently, the lesion was curetted, with removal of a rim of normal bone, and the patient has remained disease free 14 months after the original diagnosis.



**Fig. 1** Typical radiological appearance of calcifying epithelial odontogenic tumor (CEOT) of the posterior left hemi-mandible. The lesion is rather well circumscribed and shows an admixture of radiolucent and radioopaque areas

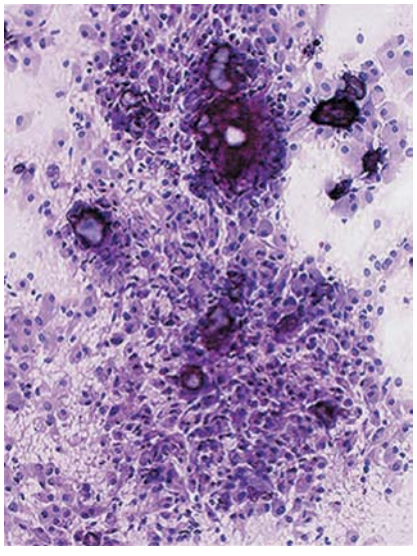


**Fig. 2** Panoramic view of calcifying epithelial odontogenic tumor (CEOT) with cementum-like particles in cytological preparations. Large clusters of heavily calcified material, stained blue with hematoxylin and eosin, are interspersed among sheets of polyhedral tumor cells (hematoxylin and eosin ×100)

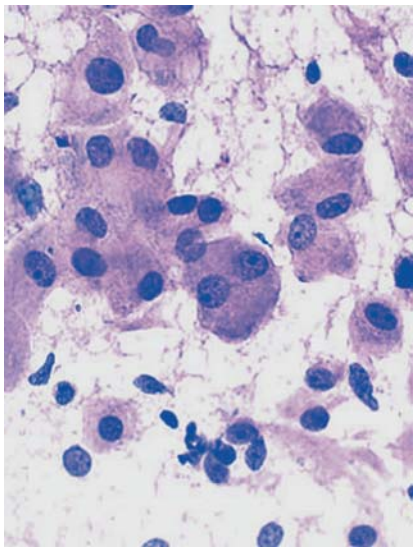


**Fig. 3** The tumor cells are large, with well-defined cytoplasmic borders, and show centrally placed nuclei with evident nucleoli (hematoxylin and eosin ×400)

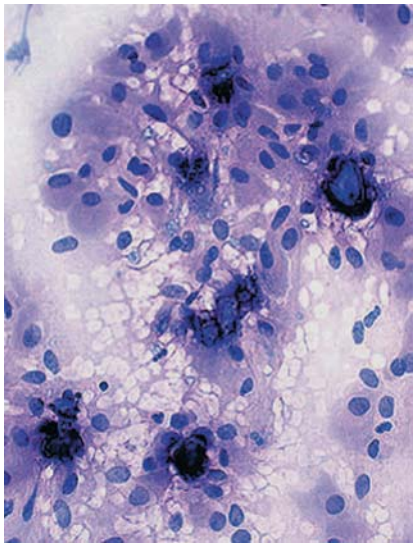


**Fig. 4** Occasionally, some tumor cells display intra-cytoplasmic calcifications that displace the nucleus toward the periphery (hematoxylin and eosin ×200)

## Cytopathology

The smears were characterized by sheets and large clusters of scarcely cohesive, polyhedral cells and abundant calcified material (Fig. 2). The tumor cells were large, with well-defined borders and intensely stained, eosinophilic cytoplasms. They possessed rounded to oval nuclei, showing mild polymorphism and evident nucleoli (Fig. 3).

The calcified material was present either as large clusters or as discrete concretions, both forms appearing intensely basophilic and with focal evidence of concentric lamination. At high-power view, occasional tumor cells also contained calcified material that seemed to push the nucleus peripherally (Fig. 4).

## Histopathology

Most of the tumor tissue was occupied by calcified material, morphologically resembling cementum-like particles (so-called "cementicles"), identical to those observed in the touch preparations. In addition, uncalcified and amorphous eosinophilic substance, resembling osteoid, was focally present. Intermingled with the above acellular substance, there were strands or tiny cords of polyhedral tumor cells (Fig. 5) very similar to those detected in the touch preparations. Focally, the tumor cells appeared evanescent, with poorly stained cytoplasms and almost invisible nuclei, resembling "ghost cells". Some of these also displayed intra-cytoplasmic calcification. Intercellular bridges were very seldom visible.

The uncalcified stroma displayed focal Congo Red positivity, showing the typical birefringence under polarized light (Fig. 5 – inset). Alcian blue and PAS were negative.

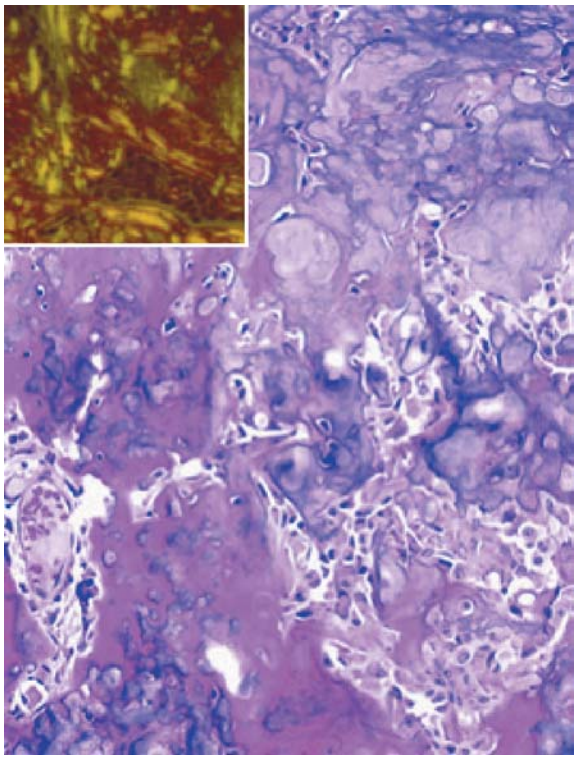


**Fig. 5** Histopathological features of calcifying epithelial odontogenic tumor (CEOT) with cementum-like material: the neoplastic cells are surrounded by large amounts of deeply calcified material (hematoxylin and eosin ×100). The latter displays typical green birefringence under polarized light after Congo Red stain (*inset*)

Immunohistochemistry

The neoplastic cells were consistently immunoreactive for epithelial membrane antigen (EMA), Vimentin and, to a lesser extent, for wide spectrum cytokeratins (AE1/AE3) and cytokeratins 8–18 and 19. Vimentin immunoreactivity was also detectable in the stromal component. Muscle-specific actin, S-100 protein, and melanoma antigen HMB 45 were negative.

## Discussion

Several histological variants of CEOT have been described, including: clear cell CEOT [7, 8, 14], peripheral (extra-osseous) CEOT, which frequently shows clear cell changes [9, 13], without calcifications [16], with myoepithelial cells [14], with Langerhans cells [1, 17], and CEOT with cementum-like component [3, 15]. The case reported herein fits into the latter category and was characterized by the presence of large amounts of acellular, basophilic particles, resembling cementum-like material, admixed with a minor calcified component morphologically resembling osteoid. Though less represented than in the corresponding histological slides, such features were already detectable in the touch preparations and represented a clue for a correct diagnosis. Particularly relevant for this purpose is the detection of very discrete amounts of intracellular calcification that were detected at high-power magnification.

The diagnosis surely is facilitated by adequate clinico-radiological information, such as the detection of intra-lesional calcifications on radiograms, but may be troublesome, especially when dealing with the clear cell variants. In such instances, the following neoplasms, usually not showing radiographically detectable calcifications, should be considered in the differential diagnosis [11, 12]:

- Clear cell odontogenic carcinoma (lacks amyloid and calcifications)
- Clear cell ameloblastoma (showing typical marginal palisading and columnar cells, at least focally)
- Intraosseous (mucoepidermoid) carcinoma (displaying Alcian blue /mucicarmine positivity)
- Salivary gland neoplasms, such as acinic cell carcinoma (intracytoplasmic PASd-positive granules) and epithelial-myoepithelial carcinoma (double-layered glandular structures with peripheral myoepithelial cells)
- Aggressive osteoblastoma (lacking of amyloid and cytokeratins-negative) [19]

Once correctly identified, mandibular CEOT can be adequately treated by conservative resection, such as enucleation or curettage, including a margin of intact bone, though prolonged follow-up of the patients is advised in view of possible recurrences even after prolonged time intervals. CEOT involving the maxillary bones or showing a prominent clear cell component should be treated more aggressively in consideration of their purported more aggressive potential [14].

## References


1. Asano M, Takahashi T, Kusama K, Iwase T, Hori M, Yamanoi H, Tanaka H, Moro A (1990) A variant of calcifying epithelial odontogenic tumor with Langerhans cells. J Oral Pathol Med 19:430–434
2. Basu MK, Matthews JB, Sear AJ, Browne RM (1984) Calcifying epithelial odontogenic tumor: a case showing features of malignancy. J Oral Pathol 13:310–319
3. el-Labban NG (1990) Cementum-like material in a case of Pindborg tumor. J Oral Pathol Med 19:166–169
4. Franklin CD, Hindle MO (1976) The calcifying epithelial odontogenic tumor – report of four cases; two with long-term follow-up. Br J Oral Maxillofac Surg 13:230–238
5. Ficarra G, Hansen LS, Stiesmeyer EH (1987) Intramural calcifying epithelial odontogenic tumor. Int J Oral Maxillofac Surg 16:217–221
6. Fulciniti F, Vetrani A, Zeppa P, Califano L, Palombini L (1995) Calcifying epithelial odontogenic tumor (Pindborg's tumor) on fine-needle aspiration biopsy smears: a case report. Diagn Cytopathol 12:71–75
7. Greer RO Jr, Richardson JF (1976) Clear-cell calcifying odontogenic tumor viewed relative to the Pindborg tumor. Oral Surg Oral Med Oral Pathol 42:775–779
8. Hicks MJ, Flaitz CM, Wong ME, McDaniel RK, Cagle PT (1994) Clear cell variant of calcifying epithelial odontogenic tumor: case report and review of the literature. Head Neck 16: 272–277
9. Houston GD, Fowler CB (1997) Extraosseous calcifying epithelial odontogenic tumor: report of two cases and review of the literature. Oral Surg Oral Med Oral Pathol Oral Radiol Endod 83:577–583

10. Ismail IM, Al-Talabani NG (1986) Calcifying epithelial odontogenic tumor associated with dentigerous cyst. Int J Oral Maxillofac Surg 15:108–111
11. Maiorano E, Altini M, Favia G (1997) Clear cell tumors of the salivary glands, jaws and oral mucosa. Semin Diagn Pathol 14:203–212
12. Maiorano E, Altini M, Viale G, Piattelli A, Favia G (2001) Clear cell odontogenic carcinoma. Report of two cases and review of the literature. Am J Clin Pathol 116:107–114
13. Orsini G, Favia G, Piattelli A (2000) Peripheral clear cell calcifying epithelial odontogenic tumor. Report of a case. J Periodontol 71:1177–1180
14. Philipsen HP, Reichart PA (2000) Calcifying epithelial odontogenic tumor: biological profile based on 181 cases from the literature. Oral Oncol 36:17–26
15. Slootweg PJ (1991) Bone and cementum as stromal features in Pindborg tumor. J Oral Pathol Med 20:93–95
16. Solomon MP, Vuletin JC, Pertschuk LP, Gormley MB, Rosen Y (1975) Calcifying epithelial odontogenic tumor. A histologic, histochemical, fluorescent, and ultrastructural study. Oral Surg Oral Med Oral Pathol 40:522–530
17. Takata T, Ogawa I, Miyauchi M, Ijuhin N, Nikai H, Fujita M (1993) Non-calcifying Pindborg tumor with Langerhans cells. J Oral Pathol Med 22:378–383
18. Veness MJ, Morgan G, Collins AP, Walker DM (2001) Calcifying epithelial odontogenic (Pindborg) tumor with malignant transformation and metastatic spread. Head Neck 23: 692–696
19. Vigneswaran N, Fernandes R, Rodu B, Baughman RA, Siegal GP (2001) Aggressive osteoblastoma of the mandible closely simulating calcifying epithelial odontogenic tumor. Report of two cases with unusual histopathologic findings. Pathol Res Pract 197:569–576

Virchows Arch (2003) 442:111–117
DOI 10.1007/s00428-002-0737-3

ORIGINAL ARTICLE

**Dominique Wendum · Pierre-Yves Boëlle
Valérie Rigau · Nicole Sebbagh
Sylviane Olschwang · Najat Mourra · Rolland Parc
Germain Trugnan · Joëlle Masliah
Jean-François Fléjou**

# Mucinous colon carcinomas with microsatellite instability have a lower microvessel density and lower vascular endothelial growth factor expression

Received: 18 June 2002 / Accepted: 7 October 2002 / Published online: 7 December 2002
© Springer-Verlag 2002

**Abstract** We determined the association between cyclooxygenase-2 (COX-2), vascular endothelial growth factor (VEGF) expression, microvessel density (MVD) and microsatellite instability (MSI) or the histological type in colon adenocarcinomas. Sixty-six cases were studied, 28 MSI+ and 38 MSI–. MSI phenotype was determined using polymerase chain reaction. MVD was assessed after CD31 staining in ten ×400 fields (0.96 $mm^2$) in the most vascularized areas. VEGF and COX-2 expression were studied by means of immunohistochemistry. MVD positively correlated with the levels of VEGF expression ($P=10^{-4}$) and also with the levels of COX-2 expression ($P=0.007$). MVD and VEGF expression were lower in MSI+ carcinomas ($P=0.002$ and $P=0.03$ respectively). When mucinous tumors were excluded from the statistical analysis, the association between low MVD, low VEGF and MSI status disappeared ($P=0.5$, $P=1$, respectively). MSI+ mucinous carcinomas had a lower MVD and VEGF expression than other MSI+ carcinomas ($P=0.008$ and $P=0.004$, respectively) and MSI– mucinous carcinomas ($P=0.01$ and $P=0.001$, respectively). COX-2 expression was lower in medullary carcinomas ($P=0.001$). In conclusion, mucinous MSI+ colon carcinomas represent a special group of colon adenocarcinomas relating to angiogenesis, with a lower MVD and VEGF expression than both MSI– mucinous carcinomas and MSI+ non-mucinous carcinomas. A low COX-2 expression could be related to the medullary phenotype. However, this has to be confirmed in a larger series. Finally, the low MVD of MSI+ mucinous colon adenocarcinomas could participate in their overall better prognosis.

**Keywords** Colon cancer · Microsatellite instability · Angiogenesis · VEGF · COX-2 · Mucinous adenocarcinoma

D. Wendum (✉) · V. Rigau · N. Sebbagh · N. Mourra · J.-F. Fléjou
Department of Pathology, Hôpital Saint-Antoine, AP-HP,
184 rue du faubourg Saint-Antoine, 75571 Paris Cedex 12, France
e-mail: dominique.wendum@sat.ap-hop-paris.fr
Tel.: +33-1-49282181, Fax: +33-1-49282878

D. Wendum · G. Trugnan · J. Masliah
INSERM U538, Faculté de médecine Saint-Antoine,
27 rue Chaligny, 75571 Paris Cedex 12, France

V. Rigau · S. Olschwang · J.-F. Fléjou
INSERM U434, Fondation Jean Dausset-CEPH,
27 rue Juliette Dodu, 75010 Paris, France

P.-Y. Boëlle
INSERM U444, Faculté de médecine Saint-Antoine,
27 rue Chaligny, 75571 Paris Cedex 12, France

R. Parc
Department of Digestive Surgery, Hôpital Saint-Antoine, AP-HP,
184 rue du faubourg Saint-Antoine, 75571 Paris Cedex 12, France

## Introduction

Tumor angiogenesis is defined as the formation of new blood vessels within and around a cancer. This neovascularization allows tumors to grow and metastasize and is induced by angiogenic factors. Among them, vascular endothelial growth factor (VEGF) is commonly found in tumors and is likely to play an important role in this process [9]. VEGF is overexpressed in colon cancer [18]. This overexpression correlates with vascular density [29], size of tumor, and stage of disease [18, 24]. Furthermore, intratumoral microvessel density (MVD) in colon cancer is also an important predictor of tumor recurrence and a prognostic factor [7, 10, 30].

Two types of colon cancer, distinct by their genetic alterations, have been clearly identified so far. One group is characterized by genetic instability at microsatellite loci and called MSI positive (MSI+ for "microsatellite instability"). The other group is characterized by hyperploidy and allelic losses and is called LOH positive (for

"loss of heterozygosity") or MSI– [3, 19]. MSI+ tumors often have distinctive features: proximal colonic location, mucinous or medullary histological type, and an improved prognosis compared with stage-matched MSI– controls [12, 14].

Cyclooxygenase-2 (COX-2) is an enzyme that converts arachidonic acid into prostaglandin H2. In contrast with COX-1, which is a constitutive enzyme, COX-2 is normally absent in most tissues and is expressed in response to growth factors and cytokines [5]. This key enzyme in prostaglandin synthesis is overexpressed in most colorectal adenocarcinomas [6], but MSI+ tumors have a reduced COX-2 expression compared with MSI– tumors [16, 28]. Moreover, overexpression of COX-2 has been shown to regulate angiogenesis in experimental models [27, 31].

Thus far, only one study has focused on angiogenesis in colon cancer with regard to the molecular phenotype of the tumor [32]. In that study, Wynter et al. showed a decrease in VEGF expression in MSI+ tumors but failed to find a lower MVD in the tumors.

We investigated MVD, VEGF, and COX-2 expression in MSI+ and MSI– colon adenocarcinomas. We hypothesized that the overall better prognosis of MSI+ cancers could be partially related to a lower MVD in relation to a lower VEGF expression. We also studied COX-2 expression in order to assess the relationship between COX-2 expression and angiogenesis in human tumor tissues.

## Methods

### Microsatellite instability

MSI was studied on paraffin-embedded tumor samples and on matching normal controls using polymerase chain reaction (PCR) and immunohistochemistry. Five to seven consecutive 20-µm tissue sections were cut and deparaffinized. DNA extraction was performed using the QIAamp DNA Mini Kit (Qiagen, Courtaboeuf, France). DNA samples were amplified using PCR at six microsatellite loci. Five loci belonged to the reference panel (BAT25, BAT26, D2S123, D5S346, D17S250), and the sixth locus was an alternative loci [transforming growth factor β receptor of type II (TGFβRII)], according to the National Cancer Institute Workshop on Microsatellite Instability [2]. Cancers showing electrophoretic shifts at two or more loci were designated MSI-H, cancers with only one locus positive MSI-L, and cancers with no band shift MSS. However, the distinction between MSI-L and MSS cancers is reliable only when a great number of microsatellite markers are studied [2]. We therefore joined the MSI-L cancers ($n$=6) to the MSS cancers ($n$=32) and called this group MSI–. MSI-H cancers ($n$=28) were called MSI+. We also assessed MSI by immunohistochemical evaluation of hMLH1 and hMSH2 protein expression, which was shown to be a sensible and specific method [21] (anti-human MLH1 monoclonal antibody, clone G168–728, 1/70, BD Pharmigen, and anti-human MSH2 monoclonal antibody, clone FE-11, 1/100, Oncogene Research Products). A loss of hMLH1 or hMSH2 protein expression was observed in all the MSI+ tumors and in none of the MSI–.

### Samples

The cases were selected from a series of 174 cases of colon cancers with a microsatellite phenotype that had previously been determined. We first selected the tumors with microsatellite instability (MSI+). The MSI– cases were chosen according to have similar stages between MSI+ and MSI– cases: for each MSI+ case selected, one or two MSI– cases were chosen matched on stage. Three cases were excluded due to immunostaining failure (VEGF staining failure $n$=1, VEGF and COX-2 staining failure $n$=2). Finally, 66 tumors obtained from 62 patients undergoing surgical resection were studied: 28 were MSI + and 38 were MSI–. Surgical specimens were fixed in 10% buffered formalin and embedded in paraffin. Pathological examination assessed histology of the tumor into three types [mucinous, medullary and "not otherwise specified" (NOS) adenocarcinomas] according to the World Health Organization (WHO) classification [13]. The stage was assessed according to the AJCC cancer staging system [8].

### Immunohistochemistry

Consecutive 4-µm tissue sections were cut from the same paraffin block that was used for MSI assessment. Immunolabelling was performed using an avidin-biotin-peroxidase technique (Vectastain ABC Kit, Vector, Burlingame, CA, USA) for VEGF and COX-2 or a three-step indirect method for CD31. The following antibodies were used: (i) VEGF (A-20) rabbit polyclonal IgG (Santa-Cruz Biotechnology, Santa-Cruz, CA, USA) at a dilution of 1/100, (ii) COX-2 mouse anti-human monoclonal antibody (N°160112, Cayman Chemical, Ann Arbor, MI, USA) at a dilution of 1/600, and (iii) CD31 mouse anti-human monoclonal antibody (M0823, Dako, Glostrup, Denmark) at a dilution of 1/30. Before immunostaining, endogenous peroxidase activity was inhibited with 0.1% hydrogen peroxide in methanol for 30 min. Microwave antigen retrieval was performed for COX-2 and CD31 (750 W for 15 min, then 150 W for 15 min) in citrate buffer (0.01 mol/l, pH 6). Color development was achieved with 3-amino-9-ethyl-carbazole, and sections were finally counterstained with hematoxylin. Negative control slides were obtained by omitting the primary antibody, and were all negative.

### Quantification of MVD

Vessel count was assessed by light microscopy on CD31 stained slides in tumor areas without necrosis and distant from an ulcerated surface. Slides were examined at low-power magnification (×50) to identify the areas with the highest MVD (the so-called "hot-spots"). In each case, the microvessels were counted in ten ×400 fields (0.96 $mm^2$) in the hot-spots. Consequently, in mucinous adenocarcinomas, MVD assessment was performed in fields containing only tumoral glands and stroma, excluding the areas composed predominantly of extracellular mucus. Any red-stained endothelial cell or endothelial cluster, with or without a lumen, clearly separated from adjacent microvessels was considered a single countable microvessel, as previously described [7]. Vascularity was expressed as the total count of microvessels in the ten fields.

### Assessment of stains

Labeled ganglion cells or smooth muscle cells of blood vessels were used as internal control for VEGF staining. Superficial positive interstitial cells were used as internal control for COX-2 staining. Tumors were divided into four equal surface areas. The staining for VEGF and COX-2 in tumor cells was scored semi-quantitatively in each area as follows: 0 no staining or staining in less than 10% of the tumor cells, 1 weak staining, 2 moderate staining, 3 strong staining. Representative examples are shown in Fig. 1. The final score (range from 0 to 12) was the sum of the four scores established for each subdivided area. When the final score was 0 or 1, we considered that there was no significant expression. A final score ranging from 2 to 5 defined a weak expression, a final score ranging from 6 or 9 defined a moderate expression, and a final score ranging from 10 to 12 defined a strong expression.

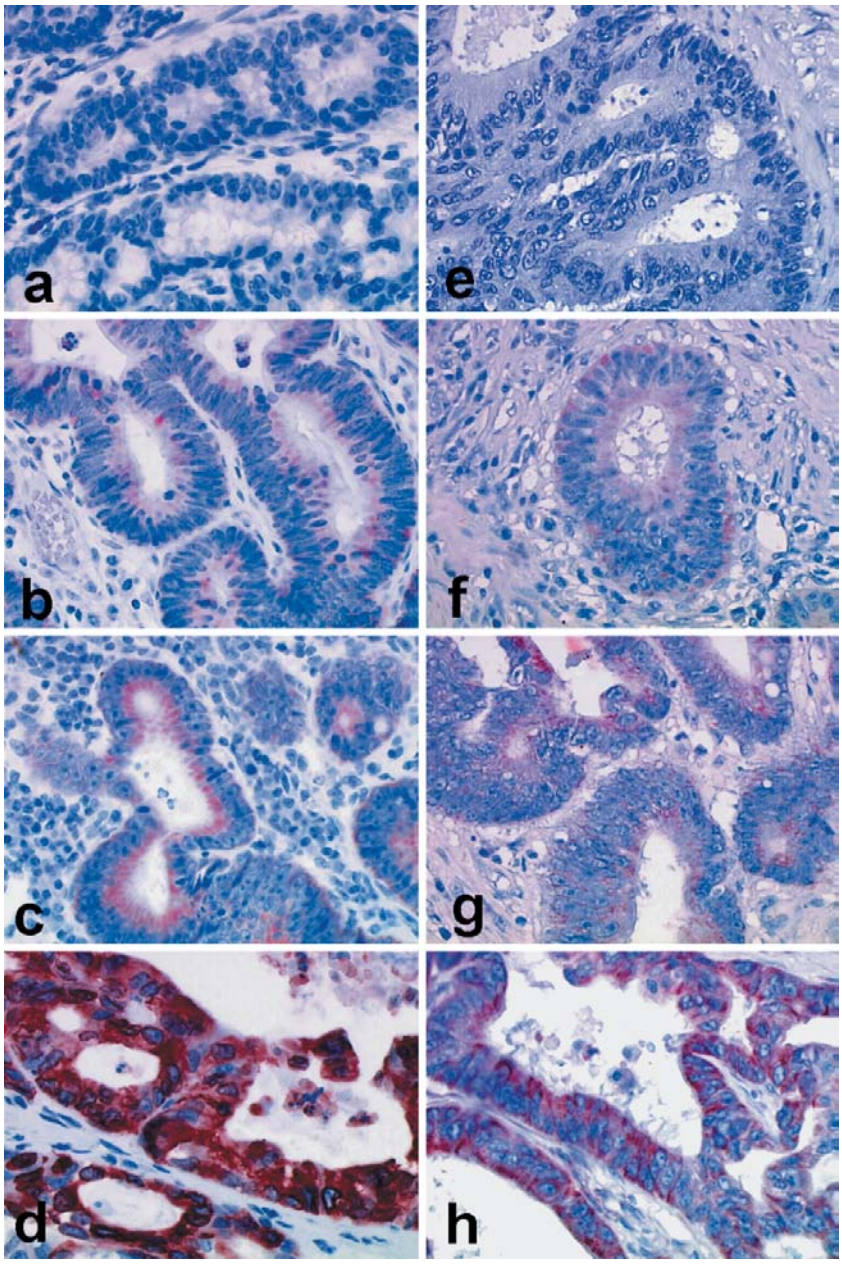



**Fig. 1** Semi-quantitative score of cyclooxygenase-2 (COX-2) and vascular endothelial growth factor (VEGF) immunostainings in colon cancer (×400). COX-2 immunostaining: negative (**a**), weak (**b**), moderate (**c**) and strong (**d**). VEGF imunostaining: negative (**e**), weak (**f**), moderate (**g**) and strong (**h**)

### Statistical analysis

The distribution of COX-2 and VEGF levels according to histological types or MSI phenotype were compared using Fisher's exact test. MVD was compared according to histological types or MSI phenotype using the Wilcoxon test. The comparison of MVD according to COX-2 and VEGF levels was carried out with the Jonckheere-Terpstra test since we were interested in the change of MVD with an increase in COX-2 or VEGF expression. All tests were carried out with the R software. Reported *P* values are two-sided and considered significant at the 5% level.

## Results

### Histological typing

Forty carcinomas were NOS and among them eleven were MSI+ (27.5%). Twenty tumors were mucinous and among them twelve were MSI+ (60%). Six tumors were medullary carcinomas and among them five (83.3%) were MSI+.

### Microvessel density

MVD was lower in MSI+ carcinomas ($P$=0.002, Table 1) and in medullary and mucinous carcinomas ($P$=0.003,

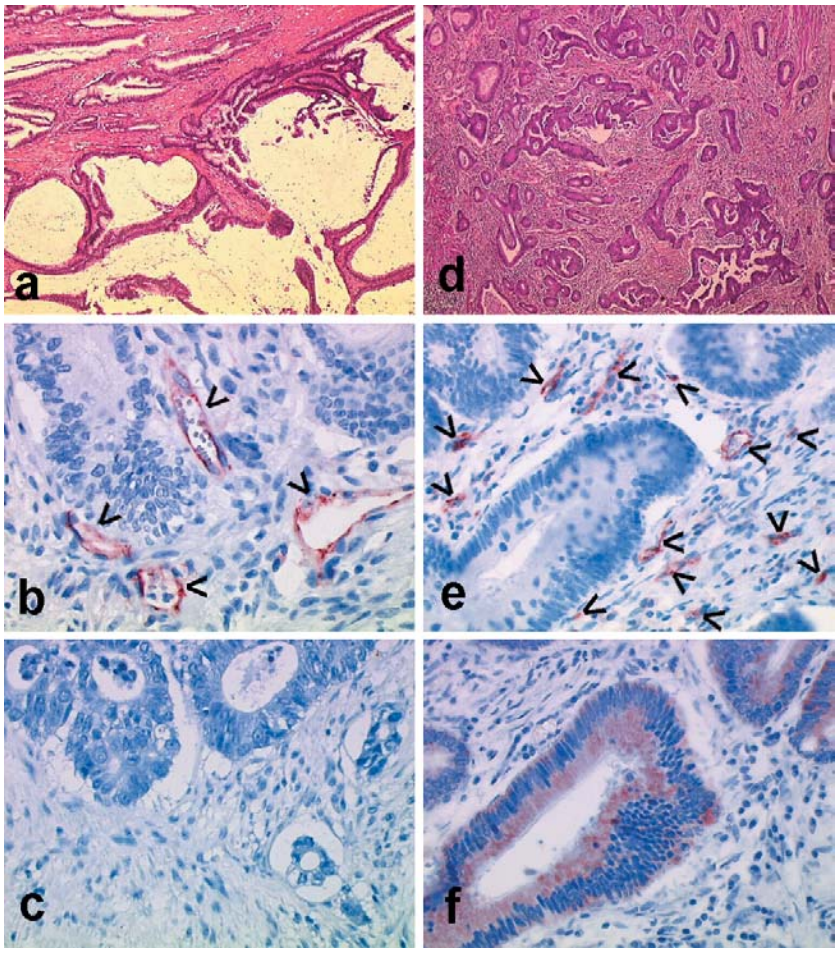



**Fig. 2** Histology, CD31 and vascular endothelial growth factor (VEGF) immunostainings in carcinomas with microsatellite instability (MSI). (**a**) MSI+ mucinous adenocarcinoma with (**b**) a low number of vessels (*arrowheads*) and (**c**) no VEGF staining in tumor cells. (**d**) A MSI+ "not otherwise specified" (NOS) adenocarcinoma with (**e**) a higher number of vessels (*arrowheads*) and (**e**) a moderate VEGF staining in tumor cells (HES ×100, immunostainings ×400)

**Table 1** Cyclooxygenase-2 (COX-2) expression, vascular endothelial growth factor (VEGF) expression and microvessel density (MVD; mean±SD) according to microsatellite instability (MSI). MSI phenotype was determined on paraffin-embedded tumor samples and on matching controls using polymerase chain reaction at six microsatellite loci. The tumors showing electrophoretic shifts at two or more loci were designated MSI+. COX-2 and VEGF expression were studied by means of immunohistochemistry. MVD was assessed in the most vascularized areas after CD31 staining in ten ×400 fields (0.96 $mm^2$). Staining for VEGF and COX-2 in tumor cells was scored semi-quantitatively

| | | MSI– | MSI+ | *P* value |
|---|---|---|---|---|
| COX-2 | Absent | 4 | 8 | 0.26 |
| | Weak | 13 | 10 | |
| | Moderate | 15 | 7 | |
| | Strong | 6 | 3 | |
| VEGF | Absent | 4 | 11 | 0.03 |
| | Weak | 17 | 10 | |
| | Moderate | 11 | 3 | |
| | Strong | 6 | 4 | |
| MVD | | 106.9±33.5 | 83.3±34.1 | 0.002 |

**Table 2** Cyclooxygenase-2 (COX-2) expression, vascular endothelial growth factor (VEGF) expression and microvessel density (MVD; mean±SD) according to tumor histology. COX-2 and VEGF expression were studied by means of immunohistochemistry. MVD was assessed in the most vascularized areas after CD31 staining in ten ×400 fields (0.96 $mm^2$). Staining for VEGF and COX-2 in tumor cells was scored semi-quantitatively. Pathological examination classified the histology of the tumors into three types [mucinous, medullary and "not otherwise specified" (NOS) adenocarcinomas] according to the World Health Organization classification

| | | NOS | Mucinous | Medullary | *P* value |
|---|---|---|---|---|---|
| COX-2 | Absent | 5 | 3 | 4 | 0.001 |
| | Weak | 14 | 7 | 2 | |
| | Moderate | 17 | 5 | 0 | |
| | Strong | 4 | 5 | 0 | |
| VEGF | Absent | 5 | 9 | 1 | 0.13 |
| | Weak | 17 | 6 | 4 | |
| | Moderate | 10 | 3 | 1 | |
| | Strong | 8 | 2 | 0 | |
| MVD | | 107±31.6 | 80.6±39.6 | 83.8±23.8 | 0.003 |

Table 2, Fig. 2). When mucinous tumors were excluded from the statistical analysis, there was no significant difference in MVD between MSI+ and MSI– carcinomas (*P*=0.5). MVD was lower in the MSI+ mucinous carcinomas than the MSI– mucinous carcinomas (*P*=0.01, Table 3). MVD was lower in the MSI+ mucinous carcinomas than the NOS MSI+ carcinomas (*P*=0.008, Table 3), whereas MVD was not different in the MSI–

**Table 3** Microvessel density (MVD) in "not otherwise specified" (NOS) and mucinous carcinomas according to microsatellite instability (MSI). MVD was assessed in the most vascularized areas after CD31 staining in ten ×400 fields (0.96 $mm^2$). Pathological examination classified the histology of the tumors into three types (mucinous, medullary and NOS adenocarcinomas) according to the World Health Organization classification. MSI phenotype was determined on paraffin-embedded tumor samples and on matching controls using polymerase chain reaction at six microsatellite loci. The tumors showing electrophoretic shifts at two or more loci were designated MSI+

| | NOS | Mucinous | *P* value* |
|---|---|---|---|
| MSI– | 105.9±30.2 | 110.5±47.8 | 0.78 |
| MSI+ | 109.9±36.6 | 60.7±13.4 | 0.008 |
| *P* value** | 0.56 | 0.01 | |

* Comparison between NOS and mucinous carcinomas
** Comparison between MSI– and MSI+ carcinomas

mucinous carcinomas than the NOS MSI– carcinomas (*P*=0.78, Table 3). There was a significant increase in MVD with COX-2 protein expression levels (*P*=0.007).

### VEGF expression

In tumors with VEGF immunoreactivity, staining was mainly observed in tumor cells. VEGF staining was also observed in smooth muscle cells of the muscularis propria and blood vessels, and in myenteric plexus ganglion cells. In some cases, a few cells within the stroma were stained. More often, some macrophages, fibroblasts, plasma cells, or endothelial cells were positive at the border of the tumor.

Of all the tumors, 15 showed no expression of VEGF, 27 a weak expression, 14 a moderate and 10 a strong expression. VEGF expression was lower in MSI+ carcinomas (*P*=0.03, Table 1). VEGF was lower in the MSI+ mucinous carcinomas than the MSI– mucinous carcinomas (*P*=0.001). VEGF expression was lower in the MSI+ mucinous carcinomas than the NOS MSI+ carcinomas (*P*=0.004) whereas it was not different in the MSI– mucinous carcinomas relative to the NOS MSI– carcinomas (*P*=0.75). There was a significant increase in MVD with VEGF protein expression levels ($P=10^{-4}$). There was no association between VEGF expression and COX-2 expression (*P*=0.12).

### COX-2 expression

COX-2 expression in tumor cells was always cytoplasmic. In some tumors, COX-2 staining was heterogeneous with scattered strongly positive tumor cells. Intense positive superficial interstitial cells were always present, even in tumors with no COX-2 expression in cancerous cells. Accordingly, these cells were used as positive internal control. Very rare isolated positive deep interstitial cells were identified in some cases. In the adjacent normal mucosa, there often was a weak COX-2 staining, which predominated in the superficial epithelial cells.

Twelve carcinomas had no significant COX-2 expression and 23 had a weak expression. Twenty-two carcinomas had a moderate and nine a strong COX-2 expression. There was an association between COX-2 expression and the histological type of the tumor (*P*=0.001, Table 2), medullary carcinomas having a lower expression. On the contrary, there was no difference in COX-2 expression between NOS and mucinous adenocarcinomas (*P*=0.8). There was no association between COX-2 expression and MSI status (*P*=0.26, Table 1).

## Discussion

In this study, we found a lower MVD in MSI+ colon carcinomas than MSI– (*P*=0.0008). As the prognosis of colon cancer is related, among other factors, to MVD [7, 10, 30], our results could participate to the better overall prognosis of MSI+ carcinomas [12]. This lower MVD is related to a lower VEGF expression. Indeed, we found a significant positive correlation between MVD and VEGF expression ($P=10^{-4}$), and a lower VEGF expression in MSI+ carcinomas (*P*=0.03). This confirms that VEGF has an important role in colon cancer angiogenesis.

This is the first study that clearly shows a lower MVD with a concomitant lower VEGF expression in MSI+ tumors relative to MSI–. Indeed, although Wynter et al. [32] found a lower VEGF expression in MSI+ tumors, they did not find a significant difference in MVD. Moreover, Losi et al. [20] found a lower MVD in hereditary non-polyposis colorectal cancer (HNPCC) tumors, defined according to the Amsterdam criteria, but they did not assess VEGF expression. Furthermore, although HNPCC tumors are mostly MSI+, there is no perfect overlap between these two tumor classifications, some HNPCC being MSI– and about 15% of sporadic colorectal cancers being MSI+ [11]. The different molecular pathways involved in MSI+ and MSI– tumorigenesis may contribute to different VEGF expression. For example, p53 and K-ras are differently involved according to the MSI status [15, 17] and both regulate VEGF expression [26, 33].

In our study, we also focused on the relationship between tumor histology and angiogenesis, which was never done before. We found that mucinous carcinomas had a lower MVD (*P*=0.003) than NOS adenocarcinomas. We assessed MVD in the most vascularized areas in the tumors. This method, used in most studies, led to exclude the large areas of mucus without cellular tissue in mucinous carcinomas. The hot spots in these tumors did not exhibit a mucinous histology at high magnification (Fig. 2b). Therefore, our MVD assessment reflects the vascularity of the tumoral tissue (tumor cells and stroma). Moreover, this method has already been used in ovarian mucinous tumors [25]. So, our results show that the neoplastic tissue in mucinous carcinomas has fewer vessels than NOS carcinomas. More precisely, when we

studied MVD and VEGF expression in the mucinous carcinomas, according to MSI, we found that only the MSI+ mucinous carcinomas had a lower MVD. Moreover, in accordance with this low vascularity, VEGF expression, which was assessed in the tumor cells, was also lower only in the MSI+ mucinous carcinomas. MSI+ mucinous carcinoma thus represents a special group of colon adenocarcinomas with regard to angiogenesis. In addition, Messerin et al. [23] showed that MSI+ mucinous carcinomas have a better prognosis than MSI– mucinous carcinomas. This better prognosis could be related to the low vascularity of these tumors that we show in our study.

Medullary carcinomas are characterized by uniform poorly differentiated tumor cells arranged in solid sheets with a prominent intratumoral lymphocytic infiltration [13]. Although only six medullary carcinomas were studied in our work, it was noteworthy that they had a low COX-2 expression relative to other types of carcinomas ($P$=0.001). Similarly, a low COX-2 expression was found associated with a solid/cribriform histologic pattern in a previous study [16]. However this result has to be confirmed in a larger series.

COX-2 is overexpressed in most colorectal adenocarcinomas [6], but MSI+ tumors have a reduced COX-2 expression relative to MSI– tumors [16, 28]. In our study we did not find a significant decrease of COX-2 expression in MSI+ ($P$=0.26). This could be related to the low number of medullary carcinomas in our series. Indeed, this type of carcinoma has a lower COX-2 expression and represents only 17.5% of the MSI+ carcinomas in our series, whereas they usually represent at least 25% in other series [1, 16].

In colorectal carcinomas, COX-2 stimulates angiogenesis by increasing angiogenic factor production [31]. In accordance with this experimental result and with other in vivo studies [4, 22, 27] we found a positive correlation between COX-2 expression and MVD ($P$=0.007). In contrast, we found no association between COX-2 and VEGF expression ($P$=0.12). Assessing an average COX-2 and VEGF expression on the whole slide could have concealed the association between VEGF and COX-2 expression in our study, as COX-2 induction of angiogenic factors seems to be a paracrine effect [31].

In conclusion, our study shows that mucinous carcinomas with microsatellite instability have a lower MVD and VEGF expression and represent a special group of colon carcinomas with regard to angiogenesis. Medullary carcinomas seem to have a lower COX-2 expression, but this has to be confirmed in a larger series. Finally, the low MVD in MSI+ mucinous colon carcinomas could participate in their better prognosis.

## References


1. Alexander J, Watanabe T, Wu TT, Rashid A, Li S, Hamilton SR (2001) Histopathological identification of colon cancer with microsatellite instability. Am J Pathol 158:527–535
2. Boland CR, Thibodeau SN, Hamilton SR, Sidransky D, Eshleman JR, Burt RW, Meltzer SJ, Rodriguez-Bigas MA, Fodde R, Ranzani GN, Srivastava S (1998) A National Cancer Institute Workshop on Microsatellite Instability for cancer detection and familial predisposition: development of international criteria for the determination of microsatellite instability in colorectal cancer. Cancer Res 58:5248–5257
3. Chung DC (2000) The genetic basis of colorectal cancer: insights into critical pathways of tumorigenesis. Gastroenterology 119:854–865
4. Cianchi F, Cortesini C, Bechi P, Fantappie O, Messerini L, Vannacci A, Sardi I, Baroni G, Boddi V, Mazzanti R, Masini E (2001) Up-regulation of cyclooxygenase 2 gene expression correlates with tumor angiogenesis in human colorectal cancer. Gastroenterology 121:1339–1347
5. Dubois RN, Abramson SB, Crofford L, Gupta RA, Simon LS, Van De Putte LB, Lipsky PE (1998) Cyclooxygenase in biology and disease. FASEB J 12:1063–1073
6. Eberhart CE, Coffey RJ, Radhika A, Giardiello FM, Ferrenbach S, DuBois RN (1994) Up-regulation of cyclooxygenase 2 gene expression in human colorectal adenomas and adenocarcinomas. Gastroenterology 107:1183–1188
7. Engel CJ, Bennett ST, Chambers AF, Doig GS, Kerkvliet N, O'Malley FP (1996) Tumor angiogenesis predicts recurrence in invasive colorectal cancer when controlled for Dukes staging. Am J Surg Pathol 20:1260–1265
8. Fleming ID, Cooper JS, Henson DE, Hutter RVP, Kennedy BP, Murphy GP, O'Sullivan B, Sobin LH, Yarbro JW (1997) AJCC cancer staging manual, 5th edn. JB Lippincott, Philadelphia
9. Folkman J (1995) Seminars in Medicine of the Beth Israel Hospital, Boston. Clinical applications of research on angiogenesis. N Engl J Med 333:1757–1763
10. Frank RE, Saclarides TJ, Leurgans S, Speziale NJ, Drab EA, Rubin DB (1995) Tumor angiogenesis as a predictor of recurrence and survival in patients with node-negative colon cancer. Ann Surg 222:695–699
11. Giardiello FM, Brensinger JD, Petersen GM (2001) AGA technical review on hereditary colorectal cancer and genetic testing. Gastroenterology 121:198–213
12. Gryfe R, Kim H, Hsieh ET, Aronson MD, Holowaty EJ, Bull SB, Redston M, Gallinger S (2000) Tumor microsatellite instability and clinical outcome in young patients with colorectal cancer. N Engl J Med 342:69–77
13. Hamilton SR, Aaltonen LA, (eds.) (2000) World Health Organization classification of tumours. Pathology and genetics of tumours of the digestive system. IARC Press, Lyon
14. Jass JR, Do KA, Simms LA, Iino H, Wynter C, Pillay SP, Searle J, Radford-Smith G, Young J, Leggett B (1998) Morphology of sporadic colorectal cancer with DNA replication errors. Gut 42:673–679
15. Kahlenberg MS, Stoler DL, Basik M, Petrelli NJ, Rodriguez-Bigas M, Anderson GR (1996) p53 tumor suppressor gene status and the degree of genomic instability in sporadic colorectal cancers. J Natl Cancer Inst 88:1665–1670
16. Karnes WE, Jr. Shattuck-Brandt R, Burgart LJ, DuBois RN, Tester DJ, Cunningham JM, Kim CY, McDonnell SK, Schaid DJ, Thibodeau SN (1998) Reduced COX-2 protein in colorectal cancer with defective mismatch repair. Cancer Res 58:5473–5477
17. Konishi M, Kikuchi-Yanoshita R, Tanaka K, Muraoka M, Onda A, Okumura Y, Kishi N, Iwama T, Mori T, Koike M, Ushio K, Chiba M, Nomizu S, Konishi F, Utsunomiya J, Miyaki M (1996) Molecular nature of colon tumors in hereditary nonpolyposis colon cancer, familial polyposis, and sporadic colon cancer. Gastroenterology 111:307–317
18. Landriscina M, Cassano A, Ratto C, Longo R, Ippoliti M, Palazzotti B, Crucitti F, Barone C (1998) Quantitative analysis of basic fibroblast growth factor and vascular endothelial growth factor in human colorectal cancer. Br J Cancer 78:765–770
19. Laurent-Puig P, Blons H, Cugnenc PH (1999) Sequence of molecular genetic events in colorectal tumorigenesis. Eur J Cancer Prev 8[Suppl 1]:S39–S47
20. Losi L, Fante R, Di Gregorio C, Aisoni ML, Lanza G, Maestri I, Roncucci L, Pedroni M, Ponz de Leon M (1995) Biologic

characterization of hereditary non-polyposis colorectal cancer. Nuclear ploidy, AgNOR count, microvessel distribution, oncogene expression, and grade-related parameters. Am J Clin Pathol 103:265–270
21. Marcus VA, Madlensky L, Gryfe R, Kim H, So K, Millar A, Temple LK, Hsieh E, Hiruki T, Narod S, Bapat BV, Gallinger S, Redston M (1999) Immunohistochemistry for hMLH1 and hMSH2: a practical test for DNA mismatch repair-deficient tumors. Am J Surg Pathol 23:1248–1255
22. Masunaga R, Kohno H, Dhar DK, Ohno S, Shibakita M, Kinugasa S, Yoshimura H, Tachibana M, Kubota H, Nagasue N (2000) Cyclooxygenase-2 expression correlates with tumor neovascularization and prognosis in human colorectal carcinoma patients. Clin Cancer Res 6:4064–4068
23. Messerini L, Ciantelli M, Baglioni S, Palomba A, Zampi G, Papi L (1999) Prognostic significance of microsatellite instability in sporadic mucinous colorectal cancers. Hum Pathol 30:629–634
24. Ono T, Miki C (2000) Factors influencing tissue concentration of vascular endothelial growth factor in colorectal carcinoma. Am J Gastroenterol 95:1062–1067
25. Orre M, Lotfi-Miri M, Mamers P, Rogers PA (1998) Increased microvessel density in mucinous compared with malignant serous and benign tumours of the ovary. Br J Cancer 77: 2204–2209
26. Ravi R, Mookerjee B, Bhujwalla ZM, Sutter CH, Artemov D, Zeng Q, Dillehay LE, Madan A, Semenza GL, Bedi A (2000) Regulation of tumor angiogenesis by p53-induced degradation of hypoxia-inducible factor 1alpha. Genes Dev 14:34–44
27. Sawaoka H, Tsuji S, Tsujii M, Gunawan ES, Sasaki Y, Kawano S, Hori M (1999) Cyclooxygenase inhibitors suppress angiogenesis and reduce tumor growth in vivo. Lab Invest 79: 1469–1477
28. Sinicrope FA, Lemoine M, Xi L, Lynch PM, Cleary KR, Shen Y, Frazier ML (1999) Reduced expression of cyclooxygenase 2 proteins in hereditary nonpolyposis colorectal cancers relative to sporadic cancers. Gastroenterology 117:350–358
29. Takahashi Y, Kitadai Y, Bucana CD, Cleary KR, Ellis LM (1995) Expression of vascular endothelial growth factor and its receptor, KDR, correlates with vascularity, metastasis, and proliferation of human colon cancer. Cancer Res 55:3964–3968
30. Takebayashi Y, Aklyama S, Yamada K, Akiba S, Aikou T (1996) Angiogenesis as an unfavorable prognostic factor in human colorectal carcinoma. Cancer 78:226–231
31. Tsujii M, Kawano S, Tsuji S, Sawaoka H, Hori M, DuBois RN (1998) Cyclooxygenase regulates angiogenesis induced by colon cancer cells. Cell 93:705–716
32. Wynter CV, Simms LA, Buttenshaw RL, Biden KG, Young J, Leggett BA, Conrad RJ, Schoch EM, Jass JR, Praga Pillay S (1999) Angiogenic factor VEGF is decreased in human colorectal neoplasms showing DNA microsatellite instability. J Pathol 189:319–325
33. Zhang X, Gaspard JP, Chung DC (2001) Regulation of vascular endothelial growth factor by the Wnt and K-ras pathways in colonic neoplasia. Cancer Res 61:6050–6054

Virchows Arch (2003) 442:118–123
DOI 10.1007/s00428-002-0718-6

ORIGINAL ARTICLE

**Reiko Ito · Naohide Oue · Xudong Zhu**
**Kazuhiro Yoshida · Hirofumi Nakayama**
**Hiroshi Yokozaki · Wataru Yasui**

# Expression of integrin-linked kinase is closely correlated with invasion and metastasis of gastric carcinoma

Received: 10 July 2002 / Accepted: 4 September 2002 / Published online: 14 December 2002
© Springer-Verlag 2002

**Abstract** Integrin-linked kinase (ILK), a serine/threonine protein kinase, implicates in cellular control of cell-matrix interactions and cell proliferation that is associated with a highly invasive phenotype of certain tumors. To study whether ILK is involved in the development and progression of gastric carcinoma, we examined the expression of ILK in gastric carcinoma cell lines, primary gastric carcinomas and corresponding non-neoplastic mucosa using reverse-transcription polymerase chain reaction (RT-PCR) and immunohistochemistry and analyzed the relationship with clinicopathological parameters. The expression of ILK mRNA was detected in 4 of 5 gastric carcinoma cell lines and 22 of 35 (63%) microdissected tumor samples of primary gastric carcinoma using RT-PCR. The incidence of cases with ILK mRNA expression was significantly higher in scirrhous and intermediate type (82%) than in medullary type (44%) ($P$=0.0204). Significant association was detected between ILK mRNA expression and presence of nodal metastasis ($P$=0.0388). Immunohistochemically, strong expression of ILK protein (over 50% of tumor cells were positive) was detected in 69% (84/122) of primary gastric carcinomas, whereas no ILK expression was found in non-neoplastic gastric epithelia. Strong expression of ILK protein was significantly associated with scirrhous and intermediate type ($P$=0.0217), deep invasion of tumor cells in gastric wall ($P$=0.0006), and presence of nodal metastasis ($P$=0.0176). These results strongly suggest that ILK may participate not only in stomach carcinogenesis especially of scirrhous and intermediate types but also in invasion and metastasis of gastric carcinoma. ILK might be a novel molecular marker for aggressive gastric cancer.

**Keywords** ILK · Gastric carcinoma · Invasion and metastasis · Immunohistochemistry

R. Ito · N. Oue · X. Zhu · H. Nakayama · W. Yasui (✉)
Department of Molecular Pathology,
Hiroshima University Graduate School of Biomedical Sciences,
1-2-3 Kasumi, Minami-ku, Hiroshima 734-8551, Japan
e-mail: wyasui@hiroshima-u.ac.jp
Tel.: +81-82-2575145, Fax: +81-82-2575149

K. Yoshida
Department of Surgery,
Research Institute for Nuclear Medicine and Biology,
Hiroshima University, 1-2-3 Kasumi, Minami-ku,
Hiroshima 734-8551, Japan

H. Yokozaki
Division of Surgical Pathology,
Kobe University Graduate School of Medicine Faculty
of Medical Sciences,
7-5-1 Kusunoki-cho, Chuo-ku, Kobe 650-0017, Japan

## Introduction

Integrins comprise a large family of cell-surface receptors that are found in many eukaryotic cellular membranes [8]. Integrins recognize several extracellular matrix proteins including individual matrix proteins such as fibronectin, collagen and vitronectin. Integrin-mediated interactions of cell with the extracellular matrix regulate a variety of cellular functions such as proliferation, differentiation, migration and survival. Integrins are important mediators of tumor invasion and metastasis through interaction with extracellular matrix [3, 22, 23, 30]. In gastric carcinomas, the expression of integrin β3 and β5 has been shown to correlate closely with scirrhous invasion (diffusely infiltrative pattern of growth with abundant fibrous stroma) [19]. Many studies using gastric carcinoma cell lines have indicated that integrin β1 is a crucial determinant of peritoneal dissemination, which is one of the characteristic behaviors of scirrhous-type gastric carcinoma [25, 26, 36]. We also previously reported that the expression of intergin β1 is closely associated with deep invasion and advanced stage of scirrhous-type gastric carcinoma [20]. However, while intergin β4 has been found to be a suppressor of peritoneal dissemination in animal model systems, the differential gene expression profile of scirrhous-type gastric cancer cell line revealed no correlation between downregulation of integrin β4 and invasion and metastasis [12, 15].

Integrin-linked kinase (ILK) is a 59-kDa serine/threonine protein kinase, which interacts directly with the cytoplasmic domain of integrin β1 and β3 [11]. ILK contains four ankyrin-like repeats [11] and a putative phosphoinositide phospholipid-binding motif [6]. ILK regulates integrin-mediated cell adhesion, E-cadherin expression, and extracellular fibronectin matrix assembly [4, 6]. Overexpression of ILK induces anchorage-independent cell growth in culture and tumor formation in vivo [4, 11, 27, 31]. Recent reports indicated that increased ILK expression is involved in prostate tumorigenesis and progression [9, 29]. Therefore, it is likely that ILK might be linked with invasion and metastasis of gastric carcinoma.

However, no study has been conducted to clarify the role of ILK in the stomach carcinogenesis and its progression. In the present study, we examined the expression of ILK in gastric carcinoma cell lines, primary gastric carcinoma tissues and corresponding non-neoplastic mucosa using immunohistochemistry and reverse-transcription polymerase chain reaction (RT-PCR), and analyzed the correlation of ILK expression with clinicopathological characteristics such as tumor stage, depth of tumor invasion, lymph-node metastasis and patient's prognosis.

## Materials and methods

### Tissue samples

A total of 122 gastric adenocarcinomas and corresponding non-neoplastic gastric mucosa were studied. For laser capture microdissection (LCM) and RNA extraction, tissue samples obtained at the time of surgery were immediately embedded in O.C.T. (optimal cutting temperature) compound (Sakura Finetechnical, Tokyo, Japan), frozen in liquid nitrogen, and stored at –80°C until use. For immunohistochemistry, tissues were fixed in 10% buffered formalin and embedded in paraffin.

We classified the gastric carcinomas according to the criteria of the Japanese Classification of Gastric Cancer [17]. Histological type was classified as follows: *pap* papillary adenocarcinoma, *tub1* well-differentiated tubular adenocarcinoma, *tub2* moderately differentiated tubular adenocarcinoma, *por1* solid-type poorly differentiated adenocarcinoma, *por2* non-solid type poorly differentiated adenocarcinoma, *sig* signet-ring cell carcinoma and *muc* mucinous adenocarcinoma. We regarded pap, tub1 and tub2 as well-differentiated type, and por1, por2, sig and muc as poorly differentiated type. Classification of the quantity of stroma was made as follows: scirrhous type (*sci*), stroma is abundant and fibrous; medullary type (*med*), stroma is scanty; intermediate type (*int*), the quantity of stroma is intermediate between sci and med. Depth of carcinoma invasion was classified as follows: *t1*, mucosa (m) and submucosa (sm); *t2*, muscularis propria (mp) and subserosa (ss); *t3*, serosa-exposed (se); *t4*, serosa-infiltrating (si).

### Cell line

Five human gastric carcinoma cell lines were studied. TMK-1 was established from a poorly differentiated adenocarcinoma in our laboratory [28]. Four cell lines of the MKN series (MKN-1, adenosquamous carcinoma; MKN-7 and MKN-28, well-differentiated adenocarcinoma; and MKN-45, poorly differentiated adenocarcinoma) were kindly provided by Dr. T. Suzuki (Fukushima Medical University, Fukushima Japan). All cell lines were routinely maintained in RPMI 1640 (Nissui Pharmaceutical Co. Ltd., Tokyo, Japan) containing 10% fetal bovine serum (FBS; Whittaker M. A. Bioproducts Inc., Walkersville, MD, USA) under conditions of 5% $CO_2$ in air at 37°C.

### Laser capture microdissection

The tissues in frozen blocks were cut into 5-μm-thick sections on a cryostat. The sections were fixed in 70% ethanol containing 5% acetic acid immediately after cutting and counter stained with hematoxylin shortly thereafter. We used the system of LCM-220, PixCell II. LCM allows isolation of tissue fragments that are as small in diameter as the area that a laser beam focuses on. The laser beam of this LCM system covers a circle of 30 μm or 60 μm in diameter. About 100 circles were dissected from one section and used for RT-PCR. In this step, we successfully collected carcinoma cells with minimal contamination of stromal components.

### RNA extraction and RT-PCR

Total RNA was extracted from the microdissected samples using the RNeasy mini kit (Qiagen Inc., Santa Clarita, CA), with the initial step being inversion of the LCM cap onto a microfuge tube and vortexing in a denaturation buffer containing guanidium isothiocyanate. Thereafter, the manufacturer's instructions were followed with the inclusion of 50 μg/ml carrier glycogen in all precipitation steps. Total RNA in 50-μl aliquots was stored at –80 C until use.

Each sample of total RNA was concentrated by vacuum evaporation from 50 μl to 4 μl for cDNA synthesis using the Super Script II (Gibco, Invitrogen Corp., Carlsbad, CA). A nested PCR approach was used to maximize the specificity of the reaction and to increase the product yield from microdissected minimal source material. The first PCR reaction was performed with sense primer-1 (5′-ATGGAC-GACATTTTCACTCAGTGC-3′) and anti-sense primer (5′-CTACTTGTCCTGCAT-CTTCTCAAG-3′). The nested step was performed using 1 μl of the initial 20-μl PCR products using sense primer-2 (5′-CTTGCACTGGGCCTGCC-GAG-3′) and the anti-sense primer for detection of 1.2 kb ILK PCR product. Each set of PCR reactions included a negative control with no template DNA. PCR conditions were 94°C for 5 min; 35 cycles of 94°C for 1 min, 55°C for 1 min and 72°C for 1 min and a final extension step of 72°C for 10 min. PCR products were visualized by ethidium bromide staining in agarose gels. RNA integrity was evaluated for each sample by amplification of β-actin sequences using the test cDNA. The reason why we utilized the nested PCR approach is that we detected only a faint band after the first PCR because total RNA was extracted from microdissected minimal source materials.

### Western blotting and immunohistochemistry

To confirm a specificity of anti-ILK antibody, Western blotting was carried out as described [37]. The cells were lysed in lysis buffer [50 mM Tris-HCl pH 7.4, 125 mM NaCl, 0.1%(v/v) NP-40, 5 mM ethylene diamine tetraacetic acid (EDTA), 50 mM NaF, 50 μg/ml phenylmethylsulfonyl fluoride (PMSF), 10 μg/ml leupeptin, 10 μg/ml soybean trypsin inhibitor, and 1 μg/ml aprotinin]. Protein (50 μg) was subjected to Western-blot analysis. Anti-ILK polyclonal antibody (Santa Cruz Biotechnology, CA) at a 1:100 dilution for ILK (C-19) was used in the primary reaction. As expected, a single band of 59 kDa was detected in representative two gastric cancer cell lines (Fig. 1).

Consecutive 4-μm tissue sections were prepared from paraffin blocks and immunostained for ILK. Immunohistochemical staining was performed using the immunoperoxidase technique with the Histofine Simple Stain Kit (Nichirei Biosciences, Tokyo, Japan). Anti-ILK antibody at a 1:200 dilution was used as primary antibody, while negative control staining was made using nonspecific IgG in the primary reaction. Stromal fibroblasts and smooth

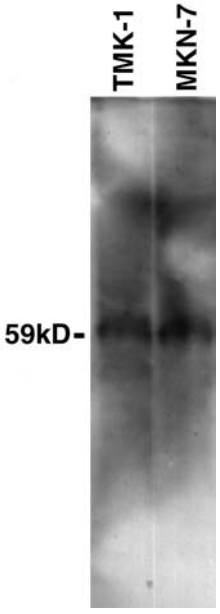



**Fig. 1** The specificity of integrin-linked kinase (ILK) antibody. Western-blot analysis was performed as described in Materials and methods. A single band of 59 kDa was detected in representative two gastric cancer cell lines




**Fig. 2** Integrin-linked kinase (ILK) mRNA expression in gastric carcinoma cell lines and gastric carcinoma tissues. Reverse transcription polymerase chain reaction was performed as described in Materials and methods. ILK mRNA expression was clearly detected in four gastric carcinoma cell lines (TMK-1, MKN-1, MKN-7 and MKN-45) and gastric carcinoma tissues (cases no. 3, 16, 21, 5, 32, and 6) (*N.C.* negative control)

muscle fibers were used for internal controls of positive immunoreaction.

Immunoreactivity was graded as – to +++, according to the number of cells stained. Grades were defined as follows: –, no positive cells; ±, less than 5% of tumor cells showed immunoreactivity; +, 5–50% of tumor cells showed immunoreactivity; ++, 50–80% of tumor cells showed immunoreactivity; +++, over 80% of tumor cells showed immunoreactivity. Grades ++ and +++ were regarded as strong expression, and grades ± and + were regarded as weak expression.

**Table 1** Expression of integrin-linked kinase (ILK) mRNA using reverse-transcription polymerase chain reaction in gastric carcinoma tissues

| | Case no. | Positive | Negative | *P* value[b] |
|---|---|---|---|---|
| Gastric carcinoma tissues | 35 | 22 (63%) | 13 (37%) | |
| Histology[a] | | | | |
| Well | 14 | 7 (50%) | 7 (50%) | 0.6777 |
| Poorly | 21 | 12 (57%) | 9 (43%) | |
| med | 18 | 8 (44%) | 10 (56%) | 0.0204 |
| sci and int | 17 | 14 (82%) | 3 (18%) | |
| Lymph-node metastasis | | | | |
| Negative | 19 | 9 (47%) | 10 (53%) | 0.0388 |
| Positive | 16 | 13 (81%) | 3 (19%) | |

[a] According to the criteria of the Japanese Classification of Gastric Carcinoma (*med* medulary type, *int* intermediate type, *sei* scirrhous type)

[b] Correlation was analyzed by chi-square for independence test and *P* values are shown. *P* values less than 0.05 are regarded as statistically significant

## Results

### Expression of ILK mRNA in gastric carcinomas detected using RT-PCR

We initially examined ILK mRNA expression in gastric carcinoma cell lines and microdissected primary gastric carcinoma tissues from 35 cases using RT-PCR. Representative pictures of RT-PCR analysis for ILK are shown in Fig. 2. Of the five cell lines, four constitutively expressed ILK mRNA. In the microdissected carcinoma tissues, ILK mRNA was clearly expressed in all cases of scirrhous type and intermediate type, whereas it was detected in one case of medullary type in Fig. 2. The results of RT-PCR in all the examined cases are summarized in Table 1. The expression of ILK mRNA was detected in 22 of 35 (63%) of microdissected tumor samples from 35 primary gastric carcinomas. ILK mRNA was expressed in 82% (14 of 17) of scirrhous and intermediate type and in 44% (8 of 18) of medullary type, respectively; the incidence was significantly different ($P$=0.0204). Furthermore, the incidence of cases with ILK mRNA expression was significantly higher in carcinomas with lymph-node metastasis (13 of 16; 81%) than in those without metastasis (9 of 19; 47%) ($P$=0.0388). The ILK mRNA expression was not detected in microdissected samples of non-neoplastic mucosa of gastric carcinoma patients or normal gastric mucosa (data not shown).

### Immunohistochemical detection of ILK protein in gastric carcinoma tissues and non-neoplastic mucosa

We next examined the expression and localization of ILK protein in 122 cases of gastric carcinomas and non-neoplastic mucosa immunohistochemically. Representative results of ILK staining are shown in Fig. 3. In non-neoplstic gastric mucosa, ILK was not detected in epithelial cells including foveolar epithelia, fundic glandular cells and pyloric glandular cells, which is consistent with the results of the aforementioned RT-PCR study, while ILK expression was found in many stromal cells including fibroblasts and infiltrating lymphocytes. However, tumor cells expressed ILK protein in most gastric carcinoma cases, and strong expression (staining grade ++ and +++; over 50% of tumor cells were positive) of ILK was detected in 69% (84 of 122) of the cases. ILK protein was localized in both cytoplasm and nuclei. Stro-

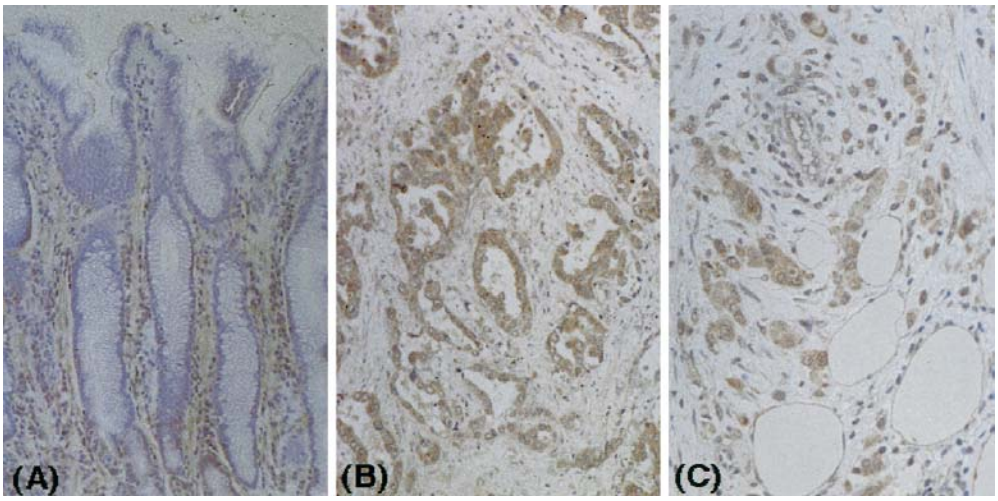



**Fig. 3** Immunostaining of integrin-linked kinase (ILK) in gastric carcinoma tissues and gastric non-neoplastic mucosa. **a** Non-neoplastic mucosa: ILK was not detected in epithelial cells including foveolar epithelia, fundic glandular cells and pyloric glandular cells, while ILK expression was found in many stromal cells. Moderately differentiated tubular adenocarcinoma (tub2) (**b**) and non-solid type poorly differentiated adenocarcinoma (por2) (**c**): tumor cells expressed ILK protein in most gastric carcinoma cells. ILK protein was localized in both cytoplasm and nuclei

**Table 2** Expression of integrin-linked kinase (ILK) in gastric carcinomas and its correlation with clinicopathological parameters

| | Case no. | ILK expression[a] | | *P* value[c] |
|---|---|---|---|---|
| | | Strong | Weak or none | |
| Gastric carcinomas | 122 | 84 (69%) | 38 (31%) | |
| Histology[b] | | | | |
| Well | 74 | 47 (63%) | 27 (37%) | 0.1139 |
| Poorly | 48 | 37 (77%) | 11 (23%) | |
| med | 48 | 25 (52%) | 23 (48%) | 0.0217 |
| sci and int | 74 | 59 (80%) | 15 (20%) | |
| Stage[b] | | | | |
| I and II | 75 | 47 (63%) | 28 (37%) | 0.0624 |
| III and IV | 47 | 37 (79%) | 10 (21%) | |
| Depth of invasion[b] | | | | |
| t1 | 43 | 20 (47%) | 23 (53%) | 0.0006 |
| t2 | 46 | 39 (85%) | 7 (15%) | |
| t3 | 19 | 13 (68%) | 6 (32%) | |
| t4 | 14 | 12 (86%) | 2 (14%) | |
| Lymph-node metastasis | | | | |
| Negative | 64 | 38 (61%) | 24 (39%) | 0.0176 |
| Positive | 58 | 46 (79%) | 12 (21%) | |

[a] Grades of ILK expression were classified as "strong" and "weak or none". *strong* over 50% of tumor cells showed immunoreactivity, *weak or none* less than 50% of tumor cells showed immunoreactivity or no staining

[b] According to the criteria of the Japanese Classification of Gastric Cancer

[c] Correlation was analyzed by chi-square for independence test and *P* values are shown. *P* values less than 0.05 are regarded as statistically significant

mal cells in cancer lesion were also positive to ILK, and rate of positive cells and intensity of the staining were not different from those in stromal components in non-neoplastic mucosa.

## Correlation between ILK expression and clinicopathological characteristics of gastric carcinoma

We then analyzed the relationship between the expression of ILK protein and clinicopathological parameters of gastric carcinoma. A summary is shown in Table 2. The incidence of cases with strong expression of ILK was significantly higher in scirrhous and intermediate type (59 of 74; 80%) than in medullary type (25 of 48; 52%) (*P*=0.0217), while the incidence did not differ by histological differentiation (well vs poorly). Strong expression of ILK was significantly associated with deep invasion of tumor cells in the gastric wall (*P*=0.0006). The incidence of strong expression of ILK tended to be higher in carcinomas of stages III and IV than those of stages I and II (*P*=0.0624). Furthermore, cases with strong ILK expression were significantly more frequent in carcinomas with lymph-node metastasis than in those without metastasis (*P*=0.0176).

## Survival rate of gastric carcinoma cases with or without ILK expression

Finally, we checked the survival rate of the gastric cancer patients after surgery. As shown in Fig. 4, the cases with strong expression of ILK showed a tendency to

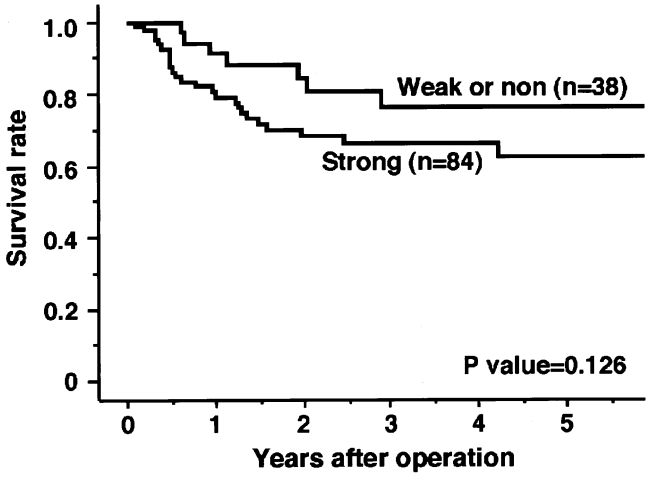



**Fig. 4** Survival rate of the gastric carcinoma patients compared with integrin-linked kinase (ILK) expression. The cases with strong expression of ILK showed tendency to have worse prognosis than the cases with weak expression of ILK or no expression, although it was not statistically significant

have a worse prognosis than the cases with weak expression of ILK or no expression, although it was not statistically significant ($P$=0.126).

## Discussion

Increased expression of the integrin β1 subunit has been reported to be responsible for the highly invasive and metastatic phenotype of gastric carcinoma especially of the scirrhous type [20, 26, 36]. Integrins not only mediate adhesion of cells to extracellular matrixes but also activate a number of intracellular signaling events [14, 33]. Integrin-mediated cell adhesion is known to regulate gene expression, such as FAK, β-catenin and cadherins, through the activation of transcription factors [8, 38]. Previous studies have revealed that these activations are mediated through ILK [2, 5, 38]. Recent reports have indicated that ILK is involved in prostate tumorigenesis and progression [9, 10, 29], suggesting that ILK might be a novel therapeutic target.

In the present study, we examined the expression of ILK in human gastric carcinoma cell lines and carcinoma tissues. Consistent with the elevated expression of ILK in other malignant tumors, including carcinoma of the breast [1], skin [16], prostate [9, 29] and colon [21], increased expression of ILK was detected in over 60% of gastric carcinomas, whereas non-neoplastic gastric epithelial cells did not express ILK. Therefore, increased ILK expression might be involved in the development of gastric carcinoma possibly through altered expression of cancer-related genes. Furthermore, ILK expression was significantly correlated with depth of invasion, nodal metastasis and amount of stromal tissue. Eventually, strong expression of ILK was significantly associated with scirrhous and intermediate types, deep invasion of tumor cells in gastric wall and the presence of nodal metastasis. These results are in accord with the previous reports of β1-integrin. It is conceivable that ILK is an important signal mediator of β1-integrin in invasion and metastasis of gastric carcinomas.

The kinase activity of ILK can be modulated by the interaction of cells with components of the extracellular matrix, by integrin clustering [35] and by growth factors [6]. The signal transduction from integrin and growth factor receptors through ILK to downstream regulates cell migration, cell cycle and cell survival [38]. It is well known that Akt, the glycogen synthase kinase-3 (GSK-3) and β-catenin are important mediators of signaling from ILK to downstream. AKT is known to induce angiogenesis and suppress apoptosis [38]. However, ILK inactivates GSK-3 and enhances the Wnt signaling [13]. Our present data suggest that ILK plays an important role in enhancement of invasion and metastasis of gastric carcinoma, resulting in high malignancy. It seems likely that the role of ILK in the progression of gastric carcinoma might include the pathway with stimulation of AKT and inactivation of GSK-3. It is necessary to study these mediators from the standpoint of invasion and metastasis of gastric carcinoma.

It has been reported that the *PTEN/MMAC1* tumor suppressor gene inhibits ILK activity [24]. ILK may be constitutively activated in certain tumors due to mutational inactivation of PTEN. There are some diverse reports about the role of *PTEN* in gastric and colorectal carcinomas [7, 18, 32, 34]. Mutational inactivation of the *PTEN* gene is extremely rare in gastrointestinal carcinomas. However, Kang et al. have described that epigenetic silencing of the *PTEN* by promoter methylation occurred frequently in gastric carcinoma, and the abnormalities of the *PTEN* gene were associated with tumor progression [18], whereas Sato et al. have reported that PTEN was rarely inactivated by promoter methylation in gastric carcinoma and did not participate in gastric carcinogenesis as a tumor suppressor gene [32]. To prove a correlation between ILK and PTEN, we should compare the status of PTEN inactivation with ILK activation in the cases used in this study.

In conclusion, the present results strongly suggest that ILK participates not only in the development but also in invasion and metastasis of gastric carcinoma. ILK might be a novel molecular target for diagnosis and therapeutics of aggressive gastric malignancy.

**Acknowledgements** This work was supported, in part, by Grants-in-Aid from the Ministry of Education, Culture, Sports, and Technology of Japan, and the Ministry of Health, Labor, and Welfare of Japan. The authors thank Masayoshi Takatani and Mutsumi Ueda for their skillful technical assistance. The authors are also grateful to Noriko Sagawa for her secretarial assistance.

## References

1. Attwell S, Roskelley C, Dedhar S (2000) The integrin-linked kinase (ILK) suppresses anoikis. Oncogene 19:3811–3815
2. Chen Q, Lin TH, Der CJ, Juliano RL (1996) Integrin-mediated activation of MEK and mitogen-activated protein kinase is independent of Ras. J Biol Chem 271:18122–18127

3. Dedhar S, Saulnier R, Nagle R, Overall CM (1993) Specific alterations in the expression of α3β1 and α6β4 integrins in highly invasive and metastatic variants of human prostate carcinoma cells selected by in vitro invasion through reconstituted basement membrane. Clin Exp Metastasis 11:391–400
4. Dedhar S (2000) Cell-substrate interactions and signaling through ILK. Curr Opin Cell Biol 12:250–256
5. Dedhar S, Hannigan GE (1996) Integrin cytoplasmic interactions and bidirectional transmembrane signalling. Curr Opin Cell Biol 8:657–669
6. Delcommenne M, Tan C, Gray V, Rue L, Woodgett J, Dedhar S (1998) Phosphoinositide-3-OH kinase-dependent regulation of glycogen synthase kinase 3 and protein kinase B/AKT by the integrin-linked kinase. Proc Natl Acad Sci USA 95:11211–11216
7. Fei G, Ebert MPA, Mawrin C, Leodolter A, Schmidt N, Dietzmann K, Malfertheiner P (2002) Reduced PTEN expression in gastric cancer and in the gastric mucosa of gastric cancer relatives. Eur J Gastroenterol Hepatol 14:297–303
8. Giancotti FG, Ruoslahti E (1999) Integrin signaling. Science 285:1028–1032
9. Graff JR, Deddens JA, Konicek BW, Colligan BM, Hurst BM, Carter HW, Carter JH (2001) Integrin-linked kinase expression increases with prostate tumor grade. Clin Cancer Res 7:1987–1991
10. Graff JR, Konicek BW, McNulty AM, Wang Z, Houck K, Allen S, Paul JD, Hbaiu A, Goode RG, Sandusky GE, Vessella RL, Neubauer BL (2000) Increased AKT activity contributes to prostate cancer progression by dramatically accelerating prostate tumor growth and diminishing $p27^{Kip1}$ expression. J Biol Chem 275:24500–24505
11. Hannigan GE, Leung Hagesteijn C, Fitz Gibbon L, Coppolino MG, Radeva G, Filmus J, Bell JC, Dedhar S (1996) Regulation of cell adhesion and anchorage-dependent growth by a new β1-integrin-linked protein kinase. Nature 379:91–96
12. Hippo Y, Yashiro M, Ishii M, Taniguchi H, Tsutsumi S, Hirakawa K, Kodama T, Aburatani H (2001) Differential gene expression profiles of scirrhous gastric cancer cells with high metastatic potential to peritoneum or lymph nodes. Cancer Res 61:889–895
13. Hoeflich KP, Luo J, Rubie EA, Tsao MS, Jin O, Woodgett JR (2000) Requirement for glycogen synthase kinase-3β in cell survival and NF-kappaB activation. Nature 406:86–90
14. Hynes R (1992) Integrins: versatility, modulation, and signaling in cell adhesion. Cell 69:11–25
15. Ishii Y, Ochiai A, Yamada T, Akimoto S, Yanagihara K, Kitajima M, Hirohashi S (2000) Integrin α6β4 as a suppressor and a predictive marker for peritoneal dissemination in human gastric cancer. Gastroenterology 118:497–506
16. Janji B, Melchior C, Gouon V, Vallar L, Kieffer N (1999) Autocrine TGF-β-regulated expression of adhesion receptors and integrin-linked kinase in HT-144 melanoma cells correlates with their metastatic phenotype. Int J Cancer 83:255–262
17. Japanese Research Society for Gastric Cancer (1995) Japanese classification of gastric carcinoma. Kanehara, Co. Ltd, Tokyo
18. Kang YH, Lee HS, Kim WH (2002) Prometer methylation and silencing of PTEN in gastric carcinoma. Lab Invest 82:285–291
19. Kawahara E, Ooi A, Nakanishi I (1995) Integrin distribution in gastric carcinoma: association of β3 and β 5 integrins with tumor invasiveness. Pathol Int 45:493–500
20. Kozako Y, Yasui W, Tahara E (1994) Expression of β1 integrin in human gastric carcinomas: correlation with histological type and tumor progression. Int J Oncol 5:225–230
21. Marotta A, Tan C, Gray V, Malik S, Gallinger S, Sanghera J, Dupuis B, Owen D, Dedhar S, Salh B (2001) Dysregulation of integrin-linked kinase (ILK) signaling in colonic polyposis. Oncogene 20:6250–6257
22. Matsumoto K, Ziober BL, Yao CC, Kramer RH (1995) Growth factor regulation of integrin-mediated cell motility. Cancer Metastasis Rev 14:205–217
23. Matsuura N, Puzon McLaughlin W, Irie A, Morikawa Y, Kakudo K, Takada Y (1996) Induction of experimental bone metastasis in mice by transfection of integrin α4β1 into tumor cells. Am J Pathol 148:55–61
24. Morimoto AM, Tomlinson MG, Nakatani K Bolen JB, Roth RA, Herbst R (2000) The MMAC1 tumor suppressor phosphatase inhibits phospholipase C and integrin-linked kinase activity. Oncogene 19:200–209
25. Nakashio T, Narita T, Akiyama S, Kasai Y, Kondo K, Ito K, Takagi H, Kannagi R (1997) Adhesion molecules and TGF-β1 are involved in the peritoneal dissemination of NUGC-4 human gastric cancer cells. Int J Cancer 70:612–618
26. Nishimura S, Chung YS, Yashiro M, Inoue T, Sowa M (1996) Role of α2 β1- and α3β1-integrin in the peritoneal implantation of scirrhous gastric carcinoma. Br J Cancer 74:1406–1412
27. Novak A, Hsu SC, Leung Hagesteijn C, Radeva G, Papkoff J, Montesano R, Roskelley C, Grosschedl R, Dedhar S (1998) Cell adhesion and the integrin-linked kinase regulate the LEF-1 and β-catenin signaling pathways. Proc Natl Acad Sci USA 95:4374–4379
28. Ochiai A, Yasui W, Tahara E (1985) Establishment and characterization of human signet ring cell gastric carcinoma cell lines with amplification of the c-myc oncogene. Cancer Res 57:3669–3671
29. Persad S, Attwell S, Gray V, Delcommenne M, Troussard A, Sanghera J, Dedhar S (2000) Inhibition of integrin-linked kinase (ILK) suppresses activation of protein kinase B/Akt and induces cell cycle arrest and apoptosis of PTEN-mutant prostate cancer cells. Proc Natl Acad Sci USA 97:3207–3212
30. Pullman WE, Bodmer WF (1992) Cloning and characterization of a gene that regulates cell adhesion. Nature 356:529–532
31. Radeva G, Petrocelli T, Behrend E, Leung Hagesteijn C, Filmus J, Slingerland J, Dedhar S (1997) Overexpression of the integrin-linked kinase promotes anchorage-independent cell cycle progression. J Biol Chem 272:13937–13944
32. Sato K, Tamura G, Tsuchiya T, Endoh Y, Sakata Y, Motoyama T, Usuba O, Kimura W, Terashima M, Nishizuka S, Zou T, Meltzer SJ (2002) Analysis of genetic and epigenetic alterations of the PTEN gene in gastric cancer. Virchows Arch 440:160–165
33. Schwartz MA (1993) Signaling by integrins: implications for tumorigenesis. Cancer Res 53:1503–1506
34. Taniyama K, Goodison S, Ito R, Bookstein R, Miyoshi N, Tahara E, Tarin D, Urquidi V (2001) PTEN expression is maintained in sporadic colorectail tumours. J Pathol 194:341–348
35. Wu C, Keightley SY, Leung Hagesteijn C, Radeva G, Coppolino M, Goicoechea S, McDonald JA, Dedhar S (1998) Integrin-linked protein kinase regulates fibronectin matrix assembly, E-cadherin expression, and tumorigenicity. J Biol Chem 273:528–536
36. Yasoshima T, Denno R, Kawaguchi S, Sato N, Okada Y, Ura H, Kikuchi K, Hirata K (1996) Establishment and characterization of human gastric carcinoma lines with high metastatic potential in the liver: changes in integrin expression associated with the ability to metastasize in the liver of nude mice. Jpn J Cancer Res 87:153–160
37. Yasui W, Ryoji M (1989) Presence of multiple species of polypeptides immunologically related to transcription factor TFIIIA in adult Xenopus tissues. Nucleic Acids Res 17:5597–5610
38. Yoganathan TN, Costello P, Chen X, Jabali M, Yan J, Leung D, Zhang Z, Yee A, Dedhar S, Sanghera J (2000) Integrin-linked kinase (ILK): a "hot" therapeutic target. Biochem Pharmacol 60:1115–1119

Virchows Arch (2003) 442:124–128
DOI 10.1007/s00428-002-0709-7

ORIGINAL ARTICLE

**Jos W. R. Meijer · Peter J. Wahab · Chris J. J. Mulder**

# Small intestinal biopsies in celiac disease: duodenal or jejunal?

Received: 14 February 2002 / Accepted: 21 June 2002 / Published online: 20 December 2002
© Springer-Verlag 2002

**Abstract** *Background:* For diagnosis and follow-up of celiac disease, pediatric societies advise that intestinal mucosal specimens should be obtained using suction capsule from the jejunum. This procedure is strenuous for patients, time-consuming, expensive and requires radiographic guidance. Mucosal biopsies from the distal duodenum can be obtained more easily under endoscopic vision using forceps. The aim of the present study was to compare biopsies taken from the duodenal mucosa by forceps and from the jejunal mucosa using suction capsule with respect to histological outcome. *Methods:* For this study, 171 paired biopsies were taken from 109 patients (1–75 years) from the distal duodenal mucosa using jumbo forceps and from the jejunal mucosa using Crosby suction capsule. Histological interpretation was performed according to a modified Marsh classification, including partial-, subtotal and total villous atrophy as Marsh IIIA, B, and C. *Results:* Fourteen suction capsule biopsies were of insufficient quality to be interpreted (8%). All duodenal forceps biopsies produced adequate material for histological scoring. No differences in histological scoring were seen in 145 of 157 compared biopsies (92%). Of 12 biopsies in which a discrepancy was present, 4 showed more severe lesions in the duodenum and 8 more severe lesions in the jejunum. The differences were of clinical significance, i.e., including the presence and absence of villous atrophy in 9 of 157 paired biopsies (6%). *Conclusion:* In the present study, we demonstrated that mucosal specimens taken from the distal duodenal and jejunal mucosa are strongly correlated. Clinically significant discrepancies were present in only 6% of paired biopsies. Therefore we suggest that, in diagnosis and follow-up of celiac disease, mucosal specimens may be taken from the duodenum using forceps to obtain adequate material for histological interpretation.

**Keywords** Celiac disease · Gluten-sensitive enteropathy · Small intestinal biopsy · Jejunal · Duodenal

J.W.R. Meijer
Department of Pathology, Rijnstate Hospital Arnhem, The Netherlands

P.J. Wahab (✉) · C.J.J. Mulder
Department of Gastroenterology and Hepatology, Rijnstate Hospital Arnhem, PO Box 9555, 6800 TA Arnhem, The Netherlands
e-mail: pwahab@rijnstate.nl
Tel.: +31-26-3787750, Fax: +31-26-3786737

## Introduction

Celiac disease is a chronic state of gluten-sensitive enteropathy, in which there are characteristic, but not specific, small intestinal mucosal abnormalities that impair absorption of nutrients. Per definition, mucosal histopathology normalizes after withdrawal of wheat gliadins and the equivalent barley and rye from the diet [9, 19]. Although the presence of antibodies to gliadin, endomysium and tissue transglutaminase as well as human leucocyte antigen (HLA)-DQ typing can support the diagnosis, the small intestinal biopsy (SIB) remains the hallmark of the diagnosis of celiac disease. Small intestinal mucosal pathology may be interpreted according to the modified Marsh criteria [8, 17, 18]. This spectrum consists of a progressive sequence of mucosal abnormalities of the small intestine, comprising infiltration of the epithelium with lymphocytes, hyperplasia of crypts, progressive loss of surface epithelial cells and, ultimately, villous atrophy. Celiac disease, i.e., gluten-sensitive enteropathy, affects the entire gastrointestinal tract but has its main manifestation in the proximal small bowel. Therefore, SIBs are traditionally taken from the jejunal mucosa as representative locus for diagnosing celiac disease. In fact, the European Society of Paediatric Gastroenterology and Nutrition (ESPGAN) criteria for celiac disease require jejunal biopsies be taken by capsule [9, 19]. Mucosal specimens can be obtained using radiographic guided suction capsules (Crosby, Quinton), which may or may not be introduced by endoscope [5, 11, 12, 15]. Unfortunately, this technique is strenuous for patients, requires radiographic support, is time consuming and is expensive. Alternatively, biopsies may be ob-

tained using jumbo forceps with a flexible endoscope introduced into the distal duodenum. Actually, since the mid-1990s the majority of gastroenterologists prefer the duodenal-forceps biopsies. The crucial point concerning the validity of such biopsies lies in the representative quality of the distal duodenal mucosa with respect to small intestinal pathology. Not only is there more natural irregularity of the proximal duodenal mucosa, but, specifically, the influence of nutrients mixed with gastric acid from the stomach and digestive fluids released into the duodenum in reaction to a meal may induce a chronic mild inflammatory response [13]. This may alter the appearance of mucosal inflammation and villous architectural changes and therefore disqualify duodenal biopsies for diagnostic use, especially when minor architectural changes and intraepithelial lymphocytosis must be considered. Furthermore, capsule-suction biopsy specimens have been reported to be inadequate for interpretation due to artifacts. Previous reports on the reliability of histological interpretation and success of obtaining adequate specimens of the capsule suction biopsies from the jejunum and the forceps biopsies from the duodenum are contradictory [1, 2, 3, 4, 6, 7, 10, 14, 16].

To investigate the validity of distal duodenal biopsies in diagnosis and follow-up of gluten-sensitive enteropathy, we performed the present study in which we took biopsies from both distal duodenum mucosa using endoscopic guided forceps and jejunal mucosa using endoscopically introduced, radiographic guided Crosby capsule. The objective was to compare the histological classification from the two biopsy sites in the same patient and, in extension, to evaluate the clinical consequences of possible discrepancies.

## Materials and methods

Between 1988 and 2000, 171 combined SIBs were taken at the endoscopy unit of our hospital for either diagnostic purposes or follow-up of celiac disease from both the duodenal and jejunal mucosa in 109 patients [34 men, 75 women; mean age 41 years (1–75 years)]. The patients were chosen sequentially, without selection. After informed consent, the patients were sedated with midazolam (0.05–0.20 mg/kg i.v.) and monitored by means of pulse-oxymetric and blood pressure control. A flexible endoscope (Olympus GIF 140, -IT100 or Fujinon 300 double lumen) was then introduced twice for obtaining mucosal specimens from the jejunum using Crosby capsule and four mucosal specimens from the distal duodenum (pars ascendens/flexura lienalis) using jumbo-forceps (MTW), respectively. The tissue samples were orientated and fixed in a formaldehyde solution. After processing in the pathology laboratory, the histological slices were interpreted by two of the authors (JWRM and PJW) according to the Marsh criteria. Marsh 0 comprises normal mucosal architecture without signs of inflammation. In a Marsh-I, lymphocytic enteritis, the small intestinal epithelium is infiltrated with lymphocytes; arbitrarily, the number that we consider as pathological is more than 30 lymphocytes per 100 enterocytes. Marsh-II, lymphocytic enteritis with crypthyperplasia is characterized by intraepithelial lymphocytosis and is accompanied by elongation and branching of crypts in which there is a (much) higher proliferation rate. In advanced mucosal pathology, Marsh-III, villous atrophy is present in the infiltrative-crypthyperplastic mucosa.

We introduced a modification of the original Marsh classification in interpreting advanced mucosal lesions and recognize three distinct stages of villous atrophy [17, 18]. In Marsh-IIIA lesions, partial villous atrophy, villi are shortened and blunt. Arbitrarily, we classify as Marsh IIIA if the villous:crypt ratio is below 1:1. Villi are clearly atrophic, but still recognizable in Marsh-IIIB lesions: subtotal villous atrophy. Finally, in Marsh III-C, total villous atrophy, the villi are absent or rudimentary, the mucosa resembling colonic mucosa (Fig. 1). For a representative interpretation of specimens, we considered an intact mucosa comprising at least five villi, or a length of at least 1000 μm to be obligatory. Discrepancies in the classification of mucosal abnormalities were considered to be of clinical significance, if they included the absence (Marsh 0,I,II) or presence of villous atrophy (Marsh IIIABC), as this criterion is mandatory for establishing the diagnosis of celiac disease as well as histological remission. In other words, discrepancies crossing the line between Marsh II and Marsh IIIA are clinically significant, as (1) the presence of villous atrophy in diagnostic biopsies is mandatory for the diagnosis of celiac disease justifying the installment of a gluten-free diet, (2) the absence of villous atrophy is mandatory for diagnosing histological remission in follow-up biopsies in patients on a gluten-free diet, and (3) persisting villous atrophy suggests the diagnosis of (diet) refractory celiac disease. Differences between duodenal and jejunal mucosal pathology remaining on either side of the line between Marsh II and Marsh IIIA do not differentiate in the diagnostic decision of whether celiac disease or celiac disease in histological remission is present.

## Results

The quality of 14 (8%) of the171 jejunal biopsies obtained using Crosby capsule was insufficient for interpretation. All duodenal biopsies were eligible for interpretation. Therefore, 157 paired duodenal/jejunal mucosal specimens were available for comparison (Table 1). Of these specimens, 51 paired biopsies were taken at diagnosis of gluten-sensitive enteropathy, 106 paired biopsies were taken as follow-up samples during a gluten-free diet. In 145 of 157 paired biopsies (92%) the histological scores were identical. In 12 paired biopsies (8%) a discrepancy was seen in the classification of mucosal pathology. Of 51 biopsies taken at the time of diagnosis of celiac disease, 4 showed a discrepancy, including 2 paired biopsies with more severe lesions in the proximal specimens (both Marsh IIIA in the duodenum and Marsh II in the jejunum) and 2 paired biopsies with more severe lesions in the distal specimens (respectively, duodenum Marsh I versus jejunum Marsh IIIB and duodenum Marsh I versus jejunum Marsh IIIA). In 8 of 106 paired biopsies taken during follow-up. we recognized a discrepancy in mucosal pathology. Two paired biopsies showed more severe lesions in the proximal specimens (respectively, duodenum Marsh II versus jejunum Marsh I and duodenum Marsh IIIA versus jejunum Marsh II). Six paired biopsies showed more severe lesions in the distal specimens (respectively, duodenum Marsh I versus jejunum Marsh II, three paired biopsies with duodenum Marsh II versus jejunum Marsh IIIA, duodenum Marsh II versus jejunum Marsh IIIB and duodenum Marsh IIIA versus jejunum Marsh IIIB).

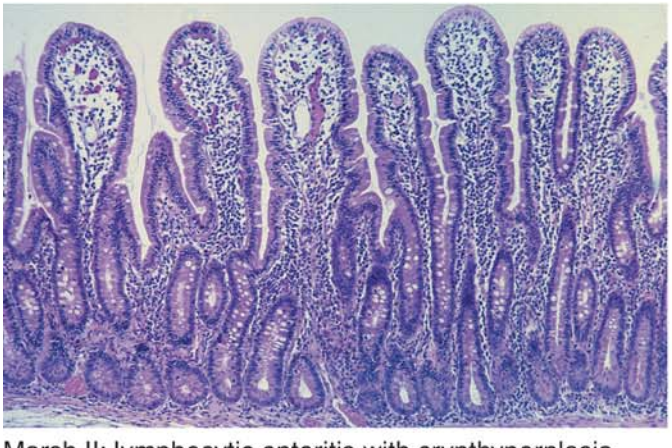
In 3 of these 12, the differences included Marsh I versus Marsh II, or Marsh IIIA versus Marsh IIIB, thereby not influencing clinical outcome. Therefore, a clinically



Marsh I: lymphocytic enteritis



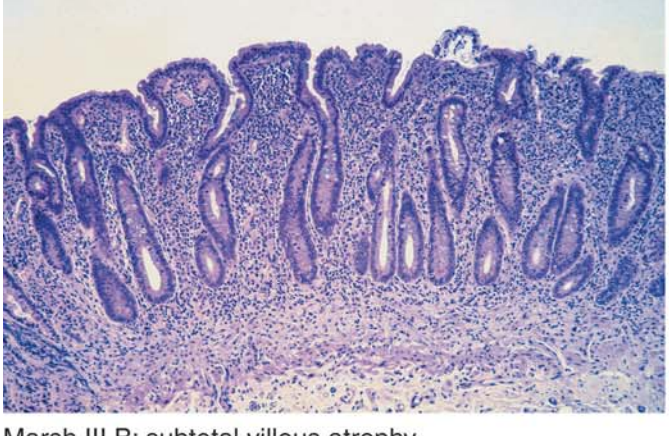
Intraepithelial lymphocytosis



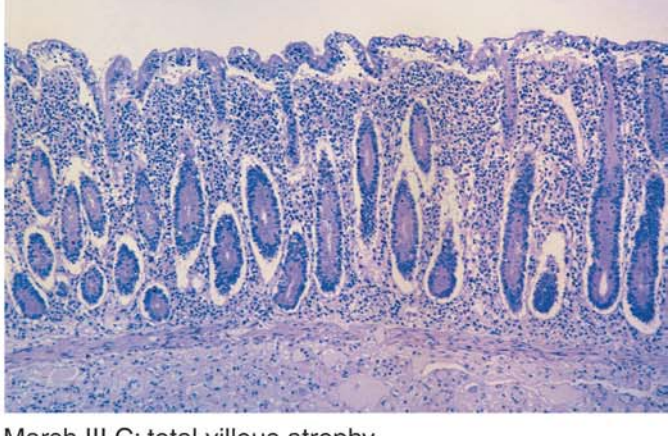
Marsh II: lymphocytic enteritis with crypthyperplasia



Marsh III A: partial villous atrophy



Marsh III B: subtotal villous atrophy



Marsh III C: total villous atrophy

**Table 1** Histological classification of 157 paired duodenal and jejunal biopsies

| | Jejunum | Marsh 0 | Marsh I | Marsh II | Marsh IIIA | Marsh IIIB | Marsh IIIC |
|---|---|---|---|---|---|---|---|
| Duodenum | | | | | | | |
| Marsh 0 | | 19[a] | | | | | |
| Marsh I | | | 28[a] | 1 | 1 | 1 | |
| Marsh II | | | 1 | 30[a] | 3 | 1 | |
| Marsh IIIA | | | | 3 | 37[a] | 1 | |
| Marsh IIIB | | | | | | 15[a] | |
| Marsh IIIC | | | | | | | 16[a] |

[a] Conformity of interpretation

significant discrepancy was seen in 9 of 157 paired biopsies (6%), 4 of 51 at diagnosis and 5 of 106 during follow-up. Three paired biopsies showed more severe lesions in the duodenal mucosa, and six paired biopsies showed more severe lesions in the jejunal mucosa. Differences including normal mucosa versus inflamed mucosa with or without villous atrophy were not seen.

## Discussion

In the present study we have demonstrated a strong correlation of mucosal pathology in gluten-sensitive enteropathy between specimens taken from the distal duodenal mucosa and the jejunal mucosa. In 145 of 157 paired biopsies (92%), the classification of mucosal pathology was identical and in 3 paired biopsies the differences were only gradual and did not influence clinical outcome (148/157: 94%). Only in nine paired biopsies (6%) did we see a clinically significant discrepancy between the duodenal and jejunal mucosal pathology. The severity of mucosal lesions was more aggravated in the duodenal mucosa in three paired biopsies (two at diagnosis and one during follow-up) and more aggravated in the jejunal mucosa in six paired biopsies (two at diagnosis and four during follow-up). This contradicts the assumption that duodenal mucosa is chronically irritated by gastric acid and digestive juices from the pancreas and liver thereby exaggerating the interpretation of mucosal inflammation [13]. If only the duodenal specimens would have been taken, this would have led to a missed diagnosis of villous atrophy in only 6 of 157 biopsies (4%) and a possible over-classification of mucosal pathology in 3 of 157 biopsies (2%). Furthermore, in 14 of 171 (8%) paired biopsies, the quality of the Crosby capsule suction specimens was insufficient for interpretation, whereas all duodenal forceps biopsies produced adequate material for interpretation.

The arbitrary interpretation of mucosal inflammation, with a cut-off point of 30 intra-epithelial lymphocytes per 100 enterocytes and/or a villous:crypt ratio of 1:1 for the classification of partial villous atrophy, is surely in part responsible for the discrepancies in interpreting mucosal pathology. Furthermore, mucosal abnormalities may be patchy and fluctuate around the arbitrary cut-off point.

In conclusion, we demonstrated that when comparing specimens taken from the distal duodenal and jejunal mucosa for diagnosis or follow-up of celiac disease, a clinically significant discrepancy is seen in a minority of 6% of paired biopsies. We assume a clinically significant discrepancy is present when the differences in mucosal pathology include crossing the line between Marsh II and Marsh IIIA because the presence or absence of villous atrophy determines whether or not the diagnosis of celiac disease or celiac disease in histological remission can be made. Furthermore, when taking specimens only from the distal duodenum, clinically important villous atrophy is missed in only 4% of biopsies. All paired biopsies with discrepancies included mucosal pathology, i.e., at least intraepithelial lymphocytosis. Therefore, we suggest that obtaining mucosal specimens from the distal duodenal mucosa in the diagnosis and follow-up of celiac disease can replace the procedure of taking SIBs from the jejunal mucosa. If the suspicion of celiac disease is strong, but biopsies show only Marsh-I or Marsh-II lesions, then jejunal biopsies should be taken, considering the small risk of duodenal biopsies being false-negative for villous atrophy.

◀ **Fig. 1** The histological spectrum of gluten-sensitive enteropathy (Marsh I–IIIC). **a** Marsh-I, lymphocytic enteritis; **b** intraepithelial lymphocytosis; **c** Marsh-II, lymphocytic enteritis with crypthyperplasia; **d** Marsh-IIIA, partial villous atrophy; **e** Marsh-IIIB, subtotal villous atrophy; **f** Marsh-IIIC, total villous atrophy

## References


1. Achkar E, Carey WD, Petras R, Sivak MV, Revta R (1986) Comparison of suction capsule and endoscopic biopsy of the small bowel mucosa. Gastrointest Endosc 32:278–281
2. Barakat M, Ali SM, Badani R et al (1983) Peroral endoscopic duodenal biopsy in infants and children. Acta Paediatr Scand 72:563–569
3. Branski D, Faber J, Shiner (1996) A comparison of small intestinal mucosal biopsies in children obtained by blind suction capsule with those obtained by endoscopy. J Paediatr Gastroenterol Nutr 22:194–196
4. Cellier C, Cuillerier E, Patey-Mariaud de Serre N, Marteau P, Verkarre V, Briere J, Brousse N, Barbier JP, Schmitz J, Landi B (1999) Push enteroscopy in celiac sprue and refractory sprue. Gastrointest Endosc 50:613–617
5. Crosby WH, Kugler HW (1957) Intraluminal biopsy of the small intestine. The intestinal biopsy capsule. Am J Digest Dis 2:236–241
6. Granot E, Goodman-Weil M, Pizov G, Sherman Y (1993) Histological comparison of suction capsule and endoscopic small intestinal mucosal biopsies in children. J Paediatr Gastroenterol Nutr 16:397–401

7. Kirberg A, Latorre, JJ, Hartard ME (1989) Endoscopic small intestinal biopsy in infants and children: its usefulness in the diagnosis of celiac disease and other enteropathies. J Paediatr Gastroenterol Nutr 9:178–181
8. Marsh MN (1992) Gluten, major histocompatibility complex and the small intestine: a molecular and immunobiologic approach to the spectrum of gluten sensitivity ('celiac sprue'). Gastroenterology 102:330–354
9. McNeish AS, Harms JK, Rey J et al (1979) The diagnosis of celiac disease. A commentary on the current practice of the European society for Paediatric Gastroenterology and Nutrition (ESPGAN). Arch Dis Child 54:629–637
10. Mee AS, Burke M, Vallon AG, Newman J, Cotton PB (1985) Small bowel biopsy for malabsorption comparison of the diagnostic adequacy of endoscopic forceps and capsule biopsy specimens. BMJ 291:769–772
11. Mulder CJJ, Simoons PP, van Nierop AJ, Meijer JWR (1992) Jejunal biopsy with an endoscopic guided capsule. Eur J Gastroenterol Hepatol 4:868–869
12. Prout BJ (1974) A rapid method of obtaining a jejunal biopsy using a Crosby capsule and a gastro-intestinal fibrescope. Gut 15:571–572
13. Schmitz-Moormann P, Schmidt-Siordahl R, Peter JH, Masarat S (1980) Morphometric studies of normal and inflamed duodenal mucosa. Path Res Pract 167:313–321
14. Scott BB, Jenkins D (1981) Endoscopic small intestinal biopsy. Gastrointest Endosc 27:162–167
15. Shiner M (1956) Jejunal biopsy. Lancet 1:85
16. Sullivan PB, Phillips MB, Neale G (1988) Endoscopic capsule biopsy of the small intestine. J Paediatr Gastroenterol Nutr 7: 544–547
17. Wahab PJ, Crusius JBA, Meijer JWR, Uil JJ, Mulder CJJ (2000) Cyclosporin in the treatment of adults with refractory coeliac disease – an open pilot study. Aliment Pharmacol Ther 14:767–774
18. Wahab PJ, Crusius BJA, Meijer JWR, Mulder CJJ (2001) Gluten challenge in borderline gluten sensitive enteropathy. Am J Gastroenterol 96:1464–1469
19. Walker-Smith JA, Guandalini S, Schmitz J, Shmerling DH, Visakorpe JK (1990) Revised criteria for diagnosis of coeliac disease. Report of the working group of the European Society of Paediatric Gastroenterology and Nutrition. Arch Dis Child 65:909–911

Virchows Arch (2003) 442:129–135
DOI 10.1007/s00428-002-0706-x

ORIGINAL ARTICLE

**Satoru Kase · Mitsuhiko Osaki · Soichiro Honjo**
**Hironobu Adachi · Shunichi Tsujitani**
**Nobuaki Kaibara · Hisao Ito**

# Expression of cyclo-oxygenase-2 is correlated with high intratumoral microvessel density and low apoptotic index in human esophageal squamous cell carcinomas

Received: 25 April 2002 / Accepted: 11 July 2002 / Published online: 7 December 2002
© Springer-Verlag 2002

**Abstract** Cyclo-oxygenase (COX) is a key enzyme in the conversion of arachidonic acid to prostanoids. COX-2 expression has been found in many malignancies. This study analyzed the correlation between COX-2 expression and angiogenesis or apoptosis in human esophageal carcinomas. The study examined the expression of COX-2 in six esophageal carcinoma cell lines and in 100 esophageal squamous cell carcinomas, comparing intratumoral microvessel density (IMVD) and apoptotic index (AI) by immunohistochemistry and TUNEL methods. COX-2 was variably expressed in all the cell lines examined. COX-2 immunoreactivity was observed mainly in the cytoplasm of carcinoma cells. Significantly higher mean IMVD and lower AI were noted in the 51 strong COX-2 expressing cases than in the 49 weak cases. IMVD and AI were negatively correlated. COX-2 expression was higher in the tumors with lymphatic invasion than in the others. These data indicate that COX-2 expression is associated with increased intratumoral microvessels and suppression of tumor cell apoptosis. Thus COX-2 might play an important role in the angiogenesis and regulation of apoptosis in esophageal squamous cell carcinomas.

**Keywords** Angiogenesis · Apoptosis · Cyclo-oxygenase-2, Esophagus · Squamous cell carcinoma

S. Kase (✉) · M. Osaki · S. Honjo · H. Adachi · H. Ito
First Department of Pathology, Faculty of Medicine,
Tottori University, 86, Nishi-cho, Yonago, Tottori 683-8503, Japan
e-mail: kaseron@grape.med.tottori-u.ac.jp
Fax: +81-859-348273

S. Tsujitani · N. Kaibara
First Department of Surgery, Faculty of Medicine,
Tottori University, 36-1 Nishi-cho, Yonago, Tottori, 683-8504,
Japan

## Introduction

Esophageal cancer is the ninth most common malignancy in the world, with areas encompassed by the Asian esophageal cancer belt having the highest incidence rates [29, 36]. Esophageal squamous cell carcinoma (SCC) is relatively common in Oriental countries [43] and is one of the most aggressive human diseases. Despite surgical treatment and adjuvant chemotherapy the overall 5-year survival rates ranges from 5% to 35% [40]. Recently, epidemiological studies have indicated an inverse association between decrease in the risk of colorectal cancer and intake of nonsteroidal anti-inflammatory drugs such as aspirin, indomethacin, and sulindac [12, 13, 14, 48]. Aspirin intake might also reduce the risk of death from esophageal cancer [6, 10, 49]. On the basis of these findings subsequent studies have addressed the role of the cyclo-oxygenase (COX) enzyme as a target molecule associated with carcinogenesis.

COX [prostaglandin (PG) H synthase] catalyzes the rate-limiting step in PG biosynthesis [4]. Two isoforms of COX have been identified: COX-1 is constitutively expressed in most mammalian tissues, and COX-2 is normally undetectable in most tissues but is rapidly induced by proinflammatory or mitogenic stimuli [20, 23, 58]. The enhanced expression of COX-2, but not of COX-1, has been found in a variety of human malignancies, including bronchial, pancreatic, breast, gastric, and colonic carcinomas [5, 16, 18, 19, 24, 32, 38, 39, 52].

Recent studies have demonstrated that COX-2 can affect carcinogenesis via several different mechanisms [3]. PGs, especially $PGE_2$, induced by COX-2 is higher in colon tumor tissues than in surrounding normal tissue [2], suggesting that PGs play a role in colonic tumorigenesis. COX-2 has also been reported to induce angiogenesis, which might be essential for tumor growth [51]. COX-2 expression is correlated with the density of CD34-positive microvascular endothelial cells in gastric carcinomas [53], implying that COX-2 overexpression is associated with angiogenesis. Moreover, previous studies

have indicated that COX-2 might be correlated with the regulation of apoptosis. The overexpression of COX-2 in rat intestinal epithelial cells was found to reduce the rate of apoptosis and increased the expression of the anti-apoptotic proto-oncogene *bcl-2* [50]. The treatment of OSC-2 cells derived from human esophageal SCC with selective COX-2 inhibitors induced apoptosis in a dose-dependent manner [60]. Although COX-2 expression has been reported in esophageal SCC and dysplasia [37, 44, 60], no studies have examined the correlation between COX-2 expression and angiogenesis or apoptosis in human esophageal carcinomas.

In the present study we focused on esophageal SCC, which shows poor patient prognosis and is relatively common in Asians, and analyzed the intratumoral microvessel density and percentage of apoptotic tumor cells in surgically removed esophageal SCCs. Then we compared these with the expression of COX-2 protein to assess the association with COX-2 expression and angiogenesis or apoptosis.

## Materials and methods

### Esophageal carcinoma cell lines

Six human esophageal carcinoma cell lines, TE-1, TE-2, TE-3, TE-7, TE-8, and TE-12, established by Nishihira et al. [31], were cultured in RPMI 1640 supplemented with 10% fetal calf serum, 100 U/ml penicillin, 100 μg/ml streptomycin, and 292 μg/ml L-glutamine. The TE-1 and TE-3 cell lines were derived from well differentiated SCCs, TE-2 from poorly differentiated SCCs, TE-7 from adenocarcinomas, and TE-8 and TE-12 from moderately differentiated SCCs.

### Operative specimens

One hundred esophageal SCCs were selected from the files of the First Department of Pathology, Faculty of Medicine, Tottori University. We obtained clinical information on age, gender, localization, and lymph node metastases from the clinical files of each patient. Table 1 shows the clinicopathological profiles and backgrounds of the 100 esophageal carcinoma patients (91 men, 9 women; mean age 64.2 years, range 45–84). None of the patients had received preoperative radio- and/or chemotherapy. All specimens were fixed in 10% buffered formalin and embedded in paraffin wax. Histological classification was established according to the WHO classification [54] into three categories; well, moderately, and poorly differentiated SCC. All the tumors were graded according to the TNM classification of the esophagus [47]. Briefly, SCC in situ is classified as Tis, tumor invasion to the lamina propria or submucosa as T1, muscularis propria as T2, and adventitia as T3. The pT category, the so-called pathological classification, corresponds to the T category. Tumor metastasis to the regional lymph nodes was noted in 62 (62.0%) cases, in none of the 3 Tis tumors, 5 (25.0%) of the 20 pT1 tumors, 5 (23.8%) of the 21 pT2 tumors and in 52 (92.8%) of the 56 pT3 tumors, the frequency being significantly higher in the pT3 tumors than in the other tumors.

**Table 1** Clinicopathological profiles of 100 human esophageal squamous cell carcinomas

| | Total ($n$=100) | COX-2 expression | | $P$ |
|---|---|---|---|---|
| | | Strong ($n$=51) | Weak ($n$=49) | |
| Differentiation | | | | 0.56 |
| Well | 8 | 4 | 4 | |
| Moderately | 42 | 24 | 18 | |
| Poorly | 50 | 23 | 27 | |
| Lymphatic metastases | | | | 0.16 |
| Positive | 62 | 35 | 27 | |
| Negative | 38 | 16 | 22 | |
| Location | | | | 0.59 |
| Upper | 28 | 12 | 16 | |
| Middle | 61 | 33 | 28 | |
| Lower | 11 | 6 | 5 | |
| pT category | | | | 0.06 |
| pTis | 3 | 0 | 3 | |
| pT1 | 20 | 8 | 12 | |
| pT2 | 21 | 15 | 6 | |
| pT3 | 56 | 28 | 28 | |
| Lymphatic invasion | | | | 0.03 |
| Positive | 60 | 36 | 24 | |
| Negative | 40 | 15 | 25 | |
| Venous invasion | | | | 0.56 |
| Positive | 22 | 10 | 12 | |
| Negative | 78 | 41 | 37 | |

### SDS-PAGE and western blot analysis

The subconfluent cells were rinsed in phosphate-buffered solution and solubilized in lysis buffer [150 mM NaCl, 20 mM Tris/HCl (pH7.4), 0.1% sodium dodecyl sulfate (SDS), 1% sodium deoxycholate, 1% Triton X-100, containing a mixture of proteinase inhibitors (5 μg/ml aprotinin, 1 μg/ml leupeptin, 1 mM phenylmethylsulfonyl fluoride, and 1 mg/ml trypsin inhibitor)] for 60 min on ice. The lysate was centrifuged at 2,500 *g* for 5 min. The protein concentration was determined by means of the Bradford protein assay (Bio-Rad, Richmond, Calif., USA) using bovine serum albumin as the standard protein. Of the protein 50 μg was separated by electrophoresis on SDS polyacrylamide gel electrophoresis (PAGE; 12% gel). Then the protein was electrotransferred onto polyvinylidene difluoride membranes (Immobilon, Millipore, Mass., USA). After 1 h incubation in blocking solution (5% nonfat dry milk in phosphate-buffered solution 0.5% Tween 20), the membrane was blotted with anti-COX-2 monoclonal antibody (1:500 dilution; 160112; Cayman, Ann Arbor, Mich, USA) and anti-β-actin monoclonal antibody (1:500 dilution; AC15, Sigma, St. Louis, Mo., USA). The blots were developed with peroxidase-labeled secondary antibodies. After extensive washing, specific bands were detected using an enhanced chemiluminescence system (ECL Detection System; Amersham, UK).

### Immunohistochemistry

Dewaxed paraffin sections were immunostained using the streptavidin-biotin-peroxidase complex (SAB) method [17]. The following primary antibodies were used: monoclonal antibody raised against COX-2 (dilution 1:100, 160112; Cayman) and monoclonal antibody raised against CD34 (no dilution; NU-4A1, Nichirei, Japan). As pretreatment, microwave-based antigen retrieval was performed in 10 mM citrate buffer (pH 6.0). Immunoreactions were visualized with diaminobenzidine, and the sections were counterstained with 3% methylgreen. To examine the specificity of immunostaining the primary antibody was replaced with mouse normal IgG or Tris-buffered saline. In this study initially the specimens were regarded

as COX-2 negative when less than 5% of the carcinoma cells showed positive signals. After determination of the true-negative cases we subdivided the positive tumors into those with weak expression (<50%) and strong expression (50% or more). For the determination of intratumoral microvessel density (IMVD) at least five of the most highly vascularized areas within a section were selected and counted under a light microscope with 200-fold magnification (i.e., ×20 objective lens and ×10 ocular lens; 0.7386 $mm^2$ per field), as described by Weidner et al. [56]. The average numbers were recorded as the IMVD for each case. The IMVD was counted by two authors (S.K. and M.O.) independently without knowledge of the clinical information, and then adjusted.

### TUNEL method

To detect DNA breaks in situ terminal deoxynucleotidyl transferase (TdT) mediated dUTP–digoxigenin nick-end labeling (TUNEL) was performed according to the method of Gavriel et al. [11], using an Apop Tag Plus in situ apoptosis detection kit (Intergen, N.Y., USA). Briefly, after deparaffinization and blocking of endogenous peroxidase with 2% hydrogen peroxidase ($H_2O_2$) in methanol for 30 min at room temperature the sections were incubated with 20 μg/ml proteinase K (Boehringer-Mannheim/Yamanouchi, Tokyo, Japan) for 40 min at 37°C. After prehybridization treatment, the sections were incubated with TdT, digoxigenin-11–dUTP and dATP in a moist chamber for 90 min at 37°C. Incubation with anti-digoxigenin antibody peroxidase for 30 min at room temperature was employed for the detection of digoxigenin-11–dUTP labeling, followed by color development with a solution containing 3,3′-diaminobenzidine and $H_2O_2$. Methyl-green was used for counterstaining. To examine the specificity of the TUNEL procedure slides were treated with TdT buffer solution not containing TdT or digoxigenin-11–dUTP as negative control. At the same time, the TUNEL procedure was also conducted with control slides of esophageal carcinoma, which were already known to show many apoptotic cells with TUNEL signals, to obtain consistent findings. The apoptotic index (AI; percentage of apoptotic cells) was obtained as the ratio of the number of TUNEL-positive cancer cells relative to counted tumor cells following cell counting in the well-labeled areas, as determined by scanning at low magnification. Actual counts were made at ×200 magnification in ten fields until more than 1,000 different tumor cells were counted.

### Statistical analysis

The correlation between IMVD and AI was analyzed using Spearman's rank correlation coefficient. The difference in the numerical data between the COX-2 expression and IMVD or AI was evaluated using the Mann-Whitney *U* test. Fisher's exact test were used to examine the association between COX-2 expression and clinicopathological parameters except for age. The $\chi^2$ test was used only for age. The level of significance was set at $P<0.05$.

## Results

### Expression of COX-2 in human esophageal carcinoma cell lines

We examined the expression levels of COX-2 protein by western blot analysis. As shown in Fig. 1, COX-2 protein in the esophageal carcinoma cell lines was variably detected as a clear single band at 72 kDa (Fig. 1). The expression level was highest in TE-12 and TE-7, followed by TE-3, TE-2, and TE-8, in this given. COX-2 was almost completely absent in TE-1.

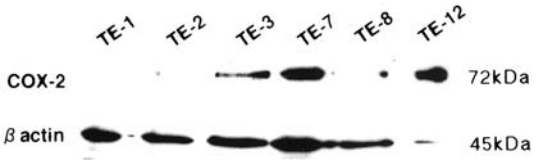



**Fig. 1** Western blot analysis of the expression of cyclo-oxygenase 2 (*COX-2*; 72 kDa) in six human esophageal carcinoma cell lines

**Table 2** Correlation between cyclo-oxygenase-2 (*COX-2*) expression and intratumoral microvessel density (*IMVD*), and apoptotic index (*AI*) in human esophageal squamous cell carcinomas

| | COX-2 negative area ($n$=49) | COX-2 positive area ($n$=51) | $P$ |
|---|---|---|---|
| IMVD | 96.0±4.20 | 120.9±3.95 | <0.0001 |
| AI | 3.18±0.21 | 2.19±0.21 | 0.0004 |

### COX-2 protein expression

COX-2 was not expressed in the normal squamous mucosa or stromal cells. In contrast, the expression was observed in a few inflammatory cells and smooth muscle cells. Several dysplastic cells adjacent to SCCs variably showed COX-2 immunoreactivity. The immunoreactivity was, however, clearly weaker than that of SCCs (data not shown). COX-2 immunoreactivity was observed mainly in the cytoplasm of esophageal carcinoma cells (Fig. 2A). The immunoreactivity was more predominant in the outer part of tumor nests than in the inner part. Strong COX-2 expression was noted in 51 (51.0%) of the 100 SCCs (Tables 1, 2). In demographic characteristics there were no significant relationships: strong expression was found in 48 men and 3 women, with a mean age of 64.1±1.39 years, and weak expression in 43 men and 6 women, with a mean age of 64.3±1.18 years.

### Relationship between COX-2 expression and clinicopathological findings in SCCs

Next we examined the relationships between COX-2 expression and clinicopathological profiles in the 100 esophageal SCCs (Table 1). COX-2 expression was not correlated with the parameters such as histological classification, metastasis to the regional lymph nodes, location, depth of the tumors, or venous invasion, except for lymphatic invasion which was significantly higher in the strong COX-2 expressing SCCs than in the weak SCCs ($P$=0.0268).

### Correlation between COX-2 expression, IMVD, and AI

We selected at least five areas containing cancer cells with COX-2 expression from the 51 COX-2-strong cases and the areas without COX-2 expression from the 49

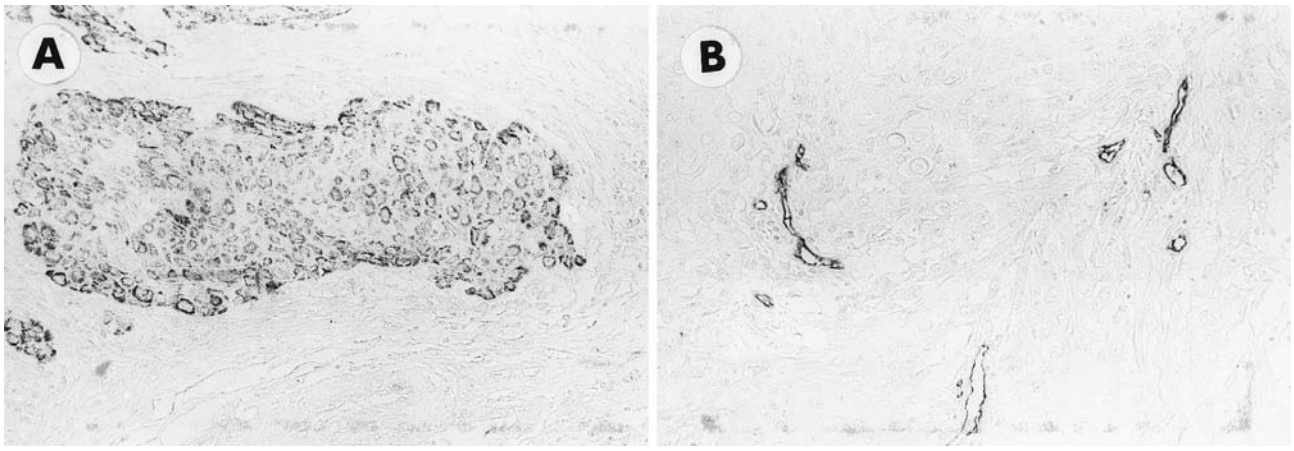



**Fig. 2** Immunohistochemistry of cyclo-oxygenase 2 (*COX-2*, **A**) and CD34 (**B**); original magnification ×50. **A** COX-2 immunoreactivity is noted in the cytoplasm in esophageal squamous cell carcinoma. **B** Endothelial cells of intratumoral microvessels are detected by CD34 immunoreactivity

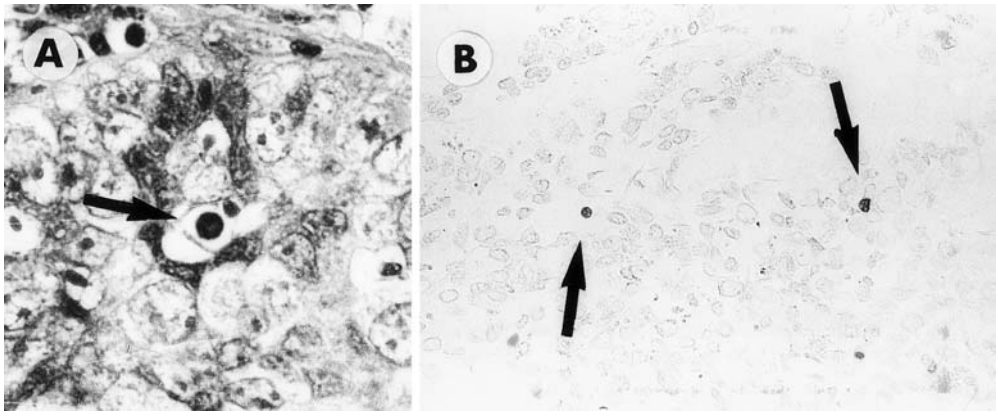



**Fig. 3** **A** Apoptotic cancer cells in hematoxylin-eosin stained sections. Apoptotic cell (*arrow*) is observed in cancer tissues; original magnification ×200. **B** Intense TUNEL signals (*arrows*) are visible in the nuclei of apoptotic cancer cells; original magnification ×100

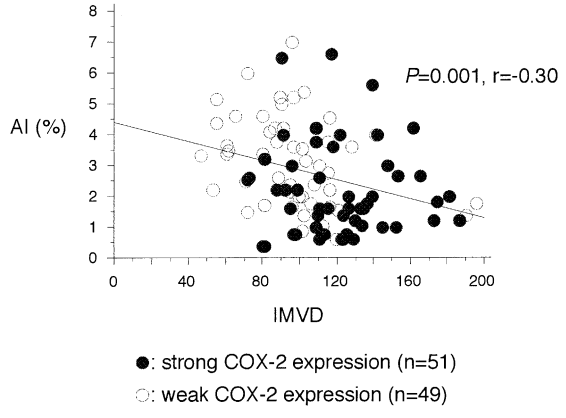



**Fig. 4** Spearman's rank correlation coefficient test for the correlation between apoptotic index (*AI*) and intratumoral microvessel density (*IMVD*). For all cases: $r$=–0.30, $P$=0.001

weak cases. Intratumoral microvessels were clearly demonstrated with CD34 immunostaining (Fig. 2B). Mean IMVD was 108.7±3.13 (range 46.0–195.0) in the 100 SCCs. Table 2 shows the correlation between COX-2 expression and IMVD. Mean IMVD was 120.9±3.95 in the 51 strong COX-2 expressing SCCs and 96.0±4.20 in the 49 weak SCCs, respectively, the frequency being significantly higher in the former than in the latter ($P$<0.0001).

Apoptotic cancer cells were clearly identified by brown nuclear TUNEL signals (Fig. 3B). Mean AI was 2.67±0.16 (range 0.40–7.00) in the 100 SCCs, 2.19±0.21 in the 51 strong COX-2 expressing SCCs and 3.18±0.21 in the 49 weak SCCs, the frequency being significantly higher in the weak SCCs than in the strong SCCs ($P$=0.0004).

Regression analysis of Spearman's rank correlation coefficient, on plots of IMVD vs. AI on a per case basis, showed a significant correlation between IMVD and AI in esophageal SCCs ($P$=0.001, $r$=–0.30, Fig. 4).

## Discussion

We clearly demonstrate the expression of COX-2 in human esophageal SCCs and esophageal carcinoma cell lines, in which specific bands were confirmed by western blot analysis, providing evidence of the specificity of the monoclonal antibody used in this study. Saukkonen et al. [41] also identified the specificity of this antibody

in gastric carcinoma. Here we also confirmed the expression of COX-2 in TE-7 derived from adenocarcinomas which are well known to overexpress COX-2 [57] as well as SCC cells using this antibody. In a previous study there was a significant correlation between COX-2 overexpression and lymphatic vessel invasion in gastric carcinoma [30]. Esophageal SCC also showed a correlation between strong COX-2 expression and lymphatic invasion of carcinoma cells in this study. Although there was no relationship between COX-2 expression and tumor differentiation in the present study, Ratnasinghe et al. [37] reported that COX-2 expression was more significant in well differentiated SCCs and was negative or weak in poorly differentiated SCCs. This discrepancy may be partly due to the number of specimens examined. They examined only 19 specimens, in contrast to 100 esophageal SCCs samples in the present study.

The regulation of apoptosis is cell type specific and dependent on the balance between pro- and antiapoptotic factors. A few experimental studies have demonstrated a clear positive correlation between COX-2 expression and resistance to apoptosis in human cells [46, 55]. Tsujii and DuBois [50] found that transfection of the *COX-2* gene resulted in the overexpression of antiapoptotic Bcl-2 protein and a reduction in susceptibility to apoptosis in rat intestinal epithelial cells. Despite these reports the exact role of COX-2 in the apoptotic mechanisms of human esophageal carcinoma remains unclear. Recently Katja et al. [60] demonstrated that treatment with a selective COX-2 inhibitor (NS398) induced apoptosis of a COX-2 expressing esophageal carcinoma cell line in a dose-dependent manner. NS398-induced apoptosis may occur via the cytochrome *c* pathway [25]. To our knowledge, this is the first report demonstrating that strong COX-2 expression is well correlated with the suppression of tumor cell apoptosis using a TUNEL method in human esophageal SCCs. Thus it is suggested that COX-2 expression plays an important role in escape from apoptosis in human esophageal SCCs even in vivo.

Angiogenesis is essential for tumor growth and the progression of various human tumors [7, 8]. Prevascular tumors less than 3 mm in diameter might remain dormant in situ for months to years [9]. Consequently a phenotypically transformed subclone of prevascular cells possessing angiogenic activity can show rapid growth, progression, and even metastasis [9, 15]. The process of intratumoral angiogenesis is regulated by the local balance of various growth factors or cytokines released by both tumor cells and normal cells [15]. We confirmed that strong COX-2 expression is correlated with an increase in intratumoral microvessel density. In a previous study COX-2 has been shown to stimulate angiogenesis by inducing such angiogenic factors as vascular endothelial growth factor (VEGF) and transforming growth factor β in colon cancer cell lines [51]. These mechanisms may also be involved in the association between COX-2 expression and angiogenesis in human esophageal SCCs.

It is well known that most tumor cells retain the ability to undergo apoptosis in response to hypoxic stress [1, 34, 45, 59]. Thus it is conceivable that there exists a close correlation between tumor angiogenesis and apoptosis. Little attention, however, has been paid to the relationship between angiogenesis and tumor cell apoptosis. The previous studies demonstrated a relationship between spontaneous tumor cell apoptosis and IMVD in human esophageal [33], gastric [27, 35], and colorectal carcinomas [28]. This study also confirmed a significant correlation between IMVD and AI in the 100 esophageal SCCs studied. Our results are consistent with previous reports in which the incidence of apoptosis was significantly influenced by the extent of neovascularization, suggesting that tumor angiogenesis contributes to a reduction in apoptosis in tumor cells. Recently it has been demonstrated that hypoxia induces COX-2 expression via the transcription factor nuclear factor (NF)-κB in human vascular endothelial cells [42]. NF-κB response elements exist in the promotor of the *COX-2* gene [26], indicating that the transcriptional factor NF-κB may control the COX-2 expression in terms of hypoxia-induced angiogenesis. In the present study we show that tumor cell apoptosis can be suppressed by strong COX-2 expression and induced by low IMVD, which might result in hypoxia of SCCs. To clarify the precise mechanisms of apoptosis in human esophageal SCCs further investigations are needed, especially regarding the relationship between hypoxia-induced apoptosis and COX-2 expression.

More recently cancer tissues with high COX-2 expression were found significantly more often in the middle and lower than in the cervical and upper esophagus. In addition, P53 expression was shown to be associated with the expression of COX-2 [21]. P53 expression is also correlated with the expression of VEGF in esophageal SCC [22]. Further studies are needed to clarify the relationship between COX-2 expression and apoptosis-related protein including P53, and angiogenic factors such as VEGF, thymidine phosphorylase, and angiopoietins.

In conclusion, our findings suggest that the strong expression of COX-2 leads to increased intratumoral microvessels and suppression of tumor cell apoptosis, which may be mechanisms involved in the contribution of COX-2 to the development of esophageal SCC and be of potential interest for clarification of the role of COX-2 in carcinogenesis. Since COX-2 expression, angiogenesis, and apoptosis constitute close networks, the COX-2 inhibitor might interfere with tumoral angiogenesis and progression. Thus, COX-2 could be an attractive target for the design of therapeutic and chemopreventive strategies in esophageal SCCs.

**Acknowledgements** This work was supported in part by a Grant-in-Aid for Scientific Research from the Ministry of Education, Culture, Sports, Science, and Technology (grant number: 11470050). The authors thank Mr. N. Itaki and Ms. M. Kajimura for their skillful technical assistance.

## References


1. Amellem O, Stokke T, Sandvik JA, Smedshammer L, Pettersen EO (1997) Hypoxia-induced apoptosis in human cells with normal p53 status and function, without any alteration in the nuclear protein level. Exp Cell Res 232:361–370
2. Bennett A, Del Tacca M, Stamford IF, Zebro T (1977) Prostaglandins from tumours of human large bowel. Br J Surg 35:882–884
3. Dempke W, Rie C, Grothey A, Schmoll HJ (2001) Cyclooxygenase-2: a novel target for cancer chemotherapy? J Cancer Res Clin Oncol 127:411–417
4. DeWitt DL (1991) Prostaglandin endoperoxyde synthase: regulation of enzyme expression. Biochim Biophys Acta 1083:121–134
5. Eberhart CE, Coffey RJ, Radhika A, Giardiello FM, Ferrenbach S, DuBois RN (1994) Up-regulation of cyclooxygenase-2 gene expression in human colorectal adenomas and adenocarcinomas. Gastroenterology 107:1183–1188
6. Farrow DC, Vaughan TL, Hansen PD, Stanford JL, Risch HA, Gammon MD, Chow WH, Dubrow R, Ahsan H, Mayne ST, Schoenberg JB, West AB, Rotterdam H, Fraumeni JF Jr, Blot WJ (1998) Use of aspirin and other nonsteroidal anti-inflammatory drugs and risk of esophageal and gastric cancer. Cancer Epidemiol Biomarkers Prev 7:97–102
7. Fidler IJ, Ellis LM (1990) The implications of angiogenesis for the biology and therapy of cancer metastasis. Cell 1990 79:185–188
8. Folkman J (1990) What is the evidence that tumors are angiogenesis dependent? J Natl Cancer Inst 82:4–6
9. Folkman J (1995) Seminars in Medicine of the Beth Israel Hospital, Boston. Clinical applications of research on angiogenesis. N Engl J Med 333:1757–1763
10. Funkhouser EM, Sharp GB (1995) Aspirin and reduced risk of esophageal carcinoma. Cancer 76:1116–1119
11. Gavrieli Y, Sherman Y, Ben-Sasson SA (1992) Identification of programmed cell death in situ via specific labeling of nuclear DNA fragmentation. J Cell Biol 119:493–501
12. Giardiello FM, Hamilton SR, Krush AJ, Piantadosi S, Hylind LM, Celano P, Booker SV, Robinson CR, Offerhaus GJ (1993) Treatment of colonic and rectal adenomas with sulindac in familial adenomatous polyposis. N Engl J Med 328:1313–1316
13. Giovannucci E, Egan KM, Hunter DJ, Stampfer MJ, Colditz GA, Willett WC, Speizer FE (1995) Aspirin and the risk of colorectal cancer in women. N Engl J Med 333:609–614
14. Greenberg ER, Baron JA, Freeman DHJ, Mandel JS, Haile R (1993) Reduced risk of large-bowel adenomas among aspirin users. J Natl Cancer Inst 85:912–916
15. Hanahan D, Folkman J (1996) Patterns and emerging mechanisms of the angiogenic switch during tumorigenesis. Cell 86:353–364
16. Hida T, Yatabe Y, Achiwa H, Muramatsu H, Kozaki K, Nakamura S, Ogawa M, Mitsudomi T, Sugiura T, Takahashi T (1998) Increased expression of cyclooxygenase-2 occurs frequently in human lung cancers, specifically in adenocarcinoma. Cancer Res 58:3761–3764
17. Hsu S-M, Raine L, Fanger H (1981) Use of avidin-biotin-peroxidase complex (ABC) in immunoperoxidase techniques: a comparison between ABC and unlabeled antibody (PAP) procedures. J Histochem Cytochem 29:577–580
18. Hwang D, Scollard D, Byrne J, Levine E (1998) Expression of cyclooxygenase-1 and cyclooxygenase-2 in human breast cancer. J Natl Cancer Inst 90:455–460
19. Kargman SL, O'Neil GP, Vickers PJ, Evans JF, Mancini JA, Jothy S (1995) Expression of prostaglandin G/H synthase-1 and -2 protein in human colon cancer. Cancer Res 55: 2556–2559
20. Kargman S, Charleson S, Cartwright M, Frank J, Riendeau D, Mancini J, Evans J, O'Neil G (1996) Characterization of prostaglandin G/H synthase 1 and 2 in rat, dog, monkey, and human gastrointestinal tracts. Gastroenterology 111:445–454
21. Kawabe A, Shimada Y, Uchida S, Maeda M, Sato F, Itami A, Imamura M (2002) Expression of cyclooxygenase-2 is associated with carcinogenesis of the lower part of thoracic esophageal squamous cell carcinoma and P53 expression. Oncology 62:46–54
22. Koida N, Nishio A, Hiraguri M, Hanazaki K, Adachi W, Amano J (2001) Coexpression of vascular endothelial growth factor and p53 protein in squamous cell carcinoma of the esophagus. Am J Gastroenterol 96:1733–1740
23. Kujubu DA, Reddy ST, Fletcher BS, Herschman HR (1993) Expression of the protein product of the prostaglandin synthase-2/*TIS10* gene in mitogen-stimulated Swiss 3T3 cells. J Biol Chem 268:5425–5430
24. Kutchera W, Jones DA, Matsunami N, Groden J, McIntyre TM, Zimmerman GA, White RL, Prescott SM (1996) Prostaglandin H synthase 2 is expressed abnormally in human colon cancer: evidence for a transcriptional effect. Proc Natl Acad Sci USA 93:4816–4820
25. Li M, Wu X, Xu XC (2001) Induction of apoptosis by cyclooxygenase-2 inhibitor NS398 through a cytochrome c-dependent pathway in esophageal cancer cells. Int J Cancer 93:218–223
26. Lim JW, Kim H, Kim KH (2001) Nuclear factor-kB regulates cyclooxygenase-2 expression and cell proliferation in human gastric cancer cells. Lab Invest 81:349–360
27. Lu C, Tanigawa N (1997) Spontaneous apoptosis is inversely related to intratumoral microvessel density in gastric carcinoma. Cancer Res 57:221–224
28. Matsuura T, Kuratate I, Teramachi K, Osaki M, Fukuda Y, Ito H (1999) Thymidine phosphorylase (dThdPase) expression is associated with both increase of intratumoral microvessels and decrease of apoptosis in human colorectal carcinomas. Cancer Res 59:5037–5040
29. Munoz N (1993) Epidemiological aspects of oesophageal cancer. Endoscopy 25:609–612
30. Murata H, Kawano S, Tsuji S, Tsuji M, Sawaoka H, Kimura Y, Shiozaki H, Hori M (1999) Cyclooxygenase-2 overexpression enhances lymphatic invasion and metastasis in human gastric carcinoma. Am J Gastroenterol 94:451–455
31. Nishihira T, Hashimoto Y, Katayama M, Mori S. Kuroki T (1993) Molecular and cellular features of esophageal cancer cells. J Cancer Res Clin Oncol 119:441–449
32. Okami J, Yamamoto H, Fujiwara Y, Tsujie M, Kondo M, Noura S, Oshima S, Nagano H, Dono K, Umeshita K, Ishikawa O, Sakon M, Matsuura N, Nakamori S, Monden M (1999) Overexpression of cyclooxygenase-2 in carcinoma of the pancreas. Clin Cancer Res 5:2018–2024
33. Okamoto E, Osaki M, Kase S, Adachi H, Ito H (2001) Thymidine phosphorylase expression causes both the increase of intratumoral microvessels and decrease of apoptosis in human esophageal carcinomas. Pathol Int 51:158–164
34. Oo TF, Henchcliffe C, Burke RE (1995) Apoptosis in substantia nigra following development hypoxic-ischemic injury. Neuroscience 69:893–901
35. Osaki M, Sakatani T, Okamoto E, Goto E, Adachi H, Ito H (2000) Thymidine phosphorylase expression results in a decrease in apoptosis and increase in intratumoral microvessel density in human gastric carcinomas. Virchows Arch 437:31–36
36. Parkin DM, Pisani P, Ferlay J (1993) Estimates of the worldwide incidence of eighteen major cancers in 1985. Int J Cancer 54:594–606
37. Ratnasinghe D, Tangrea J, Roth MJ, Dawsey S, Hu N, Anver M, Wang QH, Taylor PR (1999) Expression of cyclooxygenase-2 in human squamous cell carcinoma of the esophagus; an immunohistochemical survey. Anticancer Res 19: 171–174
38. Ristimaki A, Honkanen N, Jankala H, Sipponen P, Harkonen M (1997) Expression of cyclooxygenase-2 in human gastric carcinoma. Cancer Res 57:1276–1280
39. Sano H, Kawahito Y, Wilder RL, Hashiramoto A, Mukai S, Asai K, Kimura S, Kato H, Kondo M, Hla T (1995) Expression of cyclooxygenase-1 and -2 in human colorectal cancer. Cancer Res 55:3785–3789

40. Sarbia M, Verreet P, Bittinger F, Dutkowski P, Heep H, Willers R, Gabbert HE (1997) Basaloid squamous cell carcinoma of the esophagus: diagnosis and prognosis. Cancer 79:1871–1878
41. Saukkonen K, Nieminen O, Bastiaan R, Vilkki S, Harkonen M, Juhola M, Mecklin JP, Sipponen P, Ristimiaki A (2001) Expression of cyclooxygenase-2 in dysplasia of the stomach and in intestinal-type gastric adenocarcinoma. Clin Cancer Res 7:1923–1931
42. Schmedtje JF, Ji YS, Liu WL, DuBois RN, Runge MS (1997) Hypoxia induces cyclooxygenase-2 via NF-kappa B p65 transcription factor in human vascular endothelial cells. J Biol Chem 272:601–608
43. Schottenfeld D (1984) Epidemiology of cancer of esophagus. Semin Oncol 11:92–100
44. Shamma A, Yamamoto H, Doki Y, Okami J, Kondo M, Fujiwara Y, Yano M, Inoue M, Matsuura N, Shiozaki H, Monden M (2000) Up-reguration of cyclooxygenase-2 in squamous carcinogenesis of the esophagus. Clin Cancer Res 6:1229–1238
45. Shimizu S, Eguchi Y, Kamiike W, Itoh Y, Hasegawa J, Yamabe K, Otsuki Y, Matsuda H, Tsujimoto Y (1996) Induction of apoptosis as well as necrosis by hypoxia and predominant prevention of apoptosis by Bcl-2 and Bcl-XL. Cancer Res 56:2161–2166
46. Smith ML, Hawcroft G, Hull MA (2000) The effect of non-steroidal anti-inflammatory drugs on human colorectal cancer cells: evidence of different mechanisms of action. Eur J Cancer 36:664–674
47. Sobin LH, Wittekind C (ed) (1997) UICC TNM classification of malignant tumors, 5th edn. Wiley, New York
48. Thum MJ (1996) NSAID use and decreased risk of gastrointestinal cancers. Gastroenterol Clin North Am 25:333–348
49. Thun MJ, Namboodiri MM, Calle EE, Flanders WD, Heath CW Jr (1993) Aspirin use and risk of fatal cancer. Cancer Res 53:1322–1327
50. Tsujii M, DuBois RN (1995) Alteration in cellular adhesion and apoptosis in epithelial cells overexpressing prostaglandin endoperoxide synthase 2. Cell 83:493–501
51. Tsujii M, Kawano S, Tsuji S, Sawaoka H, Hori M, DuBois RN (1998) Cyclooxygenase regulates angiogenesis induced by colon cancer cells. Cell 93:705–716
52. Uefuji K, Ichikura T, Mochizuki H, Shinomiya N (1998) Expression of cyclooxygenase-2 protein in gastric adenocarcinoma. J Surg Oncol 69:168–172
53. Uefuji K, Ichikura T, Mochizuki H (2000) Cyclooxygenase-2 expression is related to prostaglandin biosynthesis and angiogenesis in human gastric cancer. Clin Cancer Res 6:135–138
54. Watanabe H, Jass JR, Sobin LH (eds) (1992) World Health Organization. International histological classification of the tumors; histological typing of oesophageal and gastric tumors, 2nd edn. Springer, Berlin Heidelberg New York
55. Watson AJ (1998) Chemopreventive effects of NSAIDs against colorectal cancer: regulation of apoptosis and mitosis by COX-1 and -2. Histol Histopathol 13:591–597
56. Weidner N, Semple JP, Welch WR, Folkman J (1991) Tumor angiogenesis and metastasis: correlation in invasive breast carcinoma. N Engl J Med 324:1–8
57. Wilson KT, Fu S, Ramanujam KS, Meltzer SJ (1998) Increased expression of inducible nitric oxide synthase and cyclooxygenase-2 in Barrett's esophagus and associated adenocarcinoma. Cancer Res 58:2929–2934
58. Vane J (1994) Towards a better aspirin. Nature 367:215–216
59. Yao KS, Clayton M, O'Dwyer PJ (1995) Apoptosis in human adenocarcinoma HT29 cells induced by exposure to hypoxia. J Natl Cancer Inst 87:117–122
60. Zimmermann KC, Sarbia M, Weber AA, Borchard F, Gabbert HE, Schror K (1999) Cyclooxygenase-2 expression in human esophageal carcinoma. Cancer Res 59:198–204

Virchows Arch (2003) 442:136–140
DOI 10.1007/s00428-002-0734-6

ORIGINAL ARTICLE

**Dušan Ferluga · Boštjan Luzar · Eldar M. Gadžijev**

# Follicular lymphoma of the gallbladder and extrahepatic bile ducts

Received: 19 July 2002 / Accepted: 16 October 2002 / Published online: 18 December 2002
© Springer-Verlag 2002

**Abstract** We report a case of a 63-year-old female, who presented with symptoms and signs of an acute biliary tract obstruction with jaundice and pain. Ultrasound together with intraoperative examination suggested a Klatskin tumour. Following radical resection, a tumour located predominantly in the wall of gallbladder, but infiltrating extensively also the walls of cystic, common hepatic and choledochus duct, was found. On the basis of cell morphology and the results of immunohistochemical analysis, the tumour was classified as an extranodal follicular lymphoma, grade II of the gallbladder, involving also hilar extrahepatic bile ducts. To the best of our knowledge, this is the first report of an extranodal follicular lymphoma in this location. A postoperative follow-up of more than 3 years has been completely uneventful without any symptoms or signs of disease recurrence.

**Keywords** Gallbladder · Extrahepatic biliary tract · Extranodal lymphoma · Follicular lymphoma

## Introduction

Extranodal lymphomas defined as being restricted to a solitary site, with or without the involvement of its contiguous lymph nodes, are particularly rare at some locations, including those of extrahepatic biliary tract, normally characterised by the absence or very limited amount of lymphatic tissue [13]. Nevertheless, gastrointestinal tract is the most common site for development of extranodal lymphomas [14, 25]. Among them, follicular lymphoma (FL) is infrequent, accounting for only 1–3% of cases [27]. Within the gastrointestinal tract, FLs occur most frequently in the small intestine, particularly in the terminal ileum, followed by the colo-rectum and stomach [25, 27, 31]. In addition, rare cases of FLs in the region of the ampulla of Vater have also been described [19, 22].

We report a case of FL involving predominantly the gallbladder and spreading into a cystic and common bile duct. To the best of our knowledge, primary FL of the gallbladder has not been described in the literature so far. The clinical presentation with jaundice together with ultrasound and intraoperative examination simulated a Klatskin tumour [15] – a carcinoma arising from the main hepatic duct or one of its lobar branches in the hilum of the liver. We believe that correct diagnosis in this situation is of therapeutic significance.

D. Ferluga (✉) · B. Luzar
Institute of Pathology, Faculty of Medicine University of Ljubljana, 1000 Ljubljana, Slovenia
e-mail: ferluga@mf.uni-lj.si
Tel.: +386-1-54377137, Fax: +386-1-54377101

E.M. Gadžijev
Clinical Department for Abdominal Surgery, Clinical Centre, Ljubljana, Slovenia

## Case history

A 63-year-old female was admitted to the hospital due to the symptoms and signs of acute extrahepatic biliary tract obstruction with jaundice and upper abdominal pain. Abdominal discomfort following fatty meals had already been present for 3 years. In the laboratory, pathological tests of liver function revealed a cholestatic pattern. Ultrasound examination demonstrated dilated intrahepatic bile ducts and a possible extrinsic compression of cystic and common bile ducts. The gallbladder wall was thickened up to 1 cm. There was no lymph-node enlargement in the abdominal cavity. Subsequent endoscopic retrograde cholangio-pancreatography revealed concentric stenosis of the cystic duct in the length of 15 mm as well as a dilatation of the intrahepatic bile ducts.

At operation, a firm bulky tumour mass was found infiltrating the wall of the shrunken gallbladder, surrounding and infiltrating the cystic duct, common hepatic duct and the choledochal duct (Fig. 1). A resection of the gallbladder and cystic and choledochal ducts with lymphadenectomy followed by biliodigestive anastomosis was performed. No dissemination of the disease within the abdominal cavity was observed during the surgical procedure.

A complete clinical work-up of the patient failed to detect the presence of any pre-existing inflammatory or autoimmune condition that might have induced the acquisition of MALT in and around the biliary tree. The patient received no additional treatment, and regular follow-up at 6-month intervals was performed. She was without signs of disease 3 years after surgery.

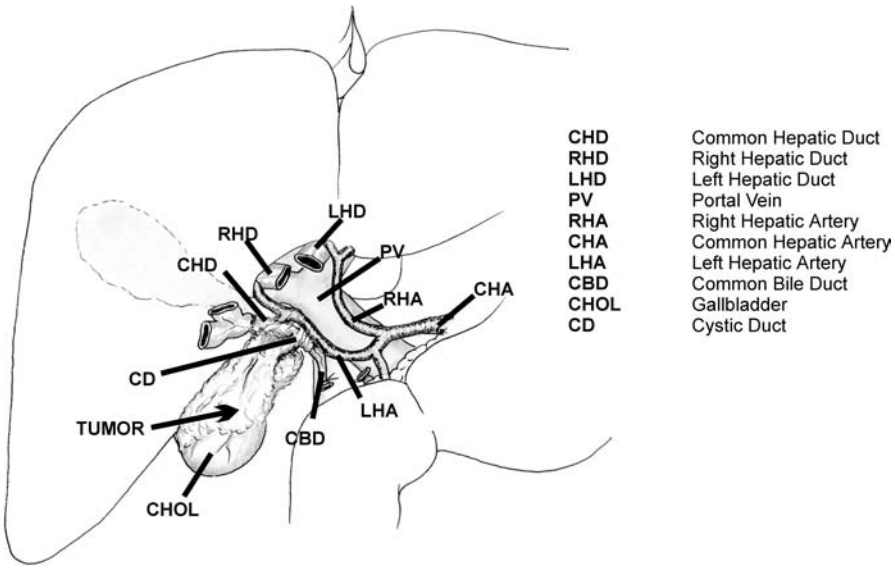



**Fig. 1** Intraoperative topographical view of the tumour

## Materials and methods

Tissue specimens were fixed in 4% formaldehyde solution phosphate buffered at pH 7.4, processed according to the standardised procedure and embedded in paraffin wax. Consecutive 4-μm sections were stained with haematoxylin and eosin. The lymphoma was classified according to the criteria proposed in the new World Health Organization (WHO) classification of haematopoietic neoplasms [23]. Selective tissue specimens were immunostained using the automatic immunostainer Dako TechMate TM 500 (Dako, Denmark) with the following commercially available primary antibodies: monoclonal mouse anti-human bcl-2 oncoprotein (Dako), monoclonal mouse anti-human B cell CD 20 and CD79a (Dako), polyclonal rabbit antibodies to CD 3 (Dako), monoclonal antibody to cyclin D1 (Novocastra, UK), monoclonal antibody to CD 5 (Dako), and monoclonal mouse antihuman antibody to Ki-67 antigen (clone MIB-1) (Dako). The polymerase chain reaction (PCR) assay for detection of t(14; 18) (q32; q21) chromosomal translocation was performed using primer complementary to the major breakpoint region of the bcl-2 gene and consensus primer for $J_H$ gene segment of the immunoglobulin heavy chain gene (IgH) as described elsewhere [2, 26].

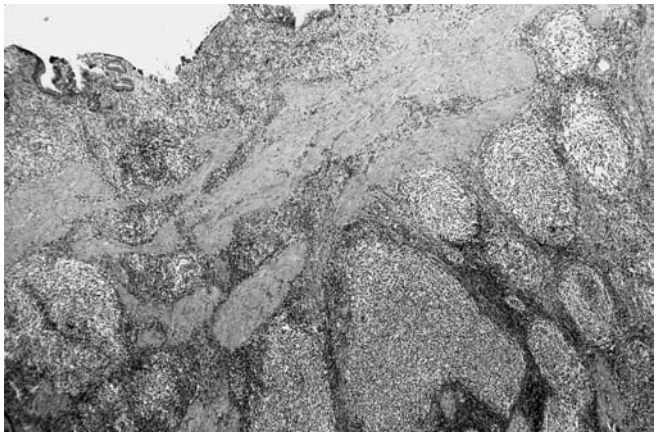


**Fig. 2** The gallbladder wall is diffusely infiltrated by neoplastic cells extending particularly prominently into the muscularis (hematoxylin and eosin stain, ×35)

## Results

The resected gallbladder was shrunken and measured 55×30×12 mm. Its wall was diffusely but unevenly thickened, measuring from 2 mm to 7 mm in diameter, and was grey-whitish to yellowish on the cut surface. Mucosa was finely granulated and uneven. The walls of cystic and choledochal duct were whitish-whitish, concentrically thickened with the lumen diameter focally narrowed up to 4 mm as well as dilated up to 12 mm, and unsharply demarcated from the surrounding tissue which included some apparently enlarged lymph nodes as well. There were no gallstones within the gallbladder or extrahepatic bile ducts.

On microscopy, the walls of the gallbladder as well as the neighbouring cystic, common bile and choledochal ducts were diffusely infiltrated by lymphoid cells extending into the muscularis and particularly prominently into the subserosal tissue (Fig. 2). The neoplastic infiltrate was composed predominantly of atypical small cleaved follicle centre-like cells (centrocytes) forming neoplastic follicles (Fig. 3). Additionally, up to 15 large atypical non-cleaved follicle centre-like cells (centroblasts) per high power field were found dispersed throughout the background of small cleaved tumour cells (Fig. 4). A moderate number of plasma cells were present beneath the surface epithelium. Immunohistochemically, neoplastic cells expressed markers of B-cell differentiation, and stained positively with CD20 and CD79a. The majority of neoplastic cells showed bcl-2 immunoreactivity (Fig. 5). Furthermore, they were CD5 and cyclin D1 negative. Semi-quantitative assessment of proliferative activity by Ki-67 antibody showed positive reaction in approximately 30% of tumour cells. Molecular

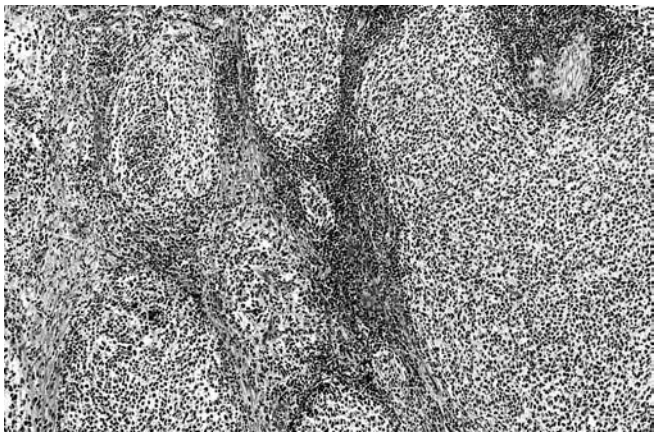


**Fig. 3** Neoplastic cells forming neoplastic follicles (hematoxylin and eosin stain, ×40)

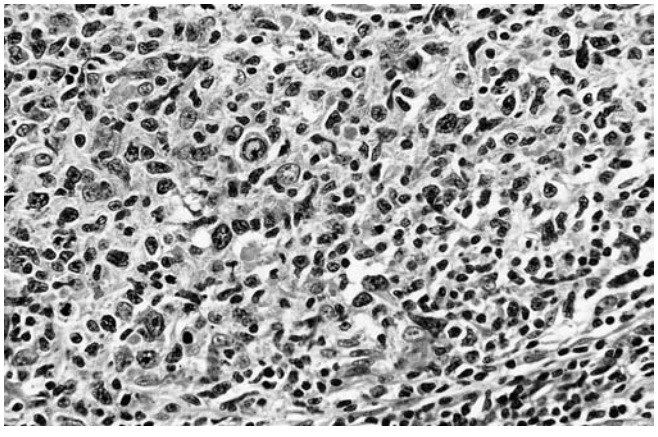


**Fig. 4** Several non-cleaved follicle centre-like cells (centroblasts) in the background of small cleaved follicle center-like cells (centrocytes) (hematoxylin and eosin stain, ×190)

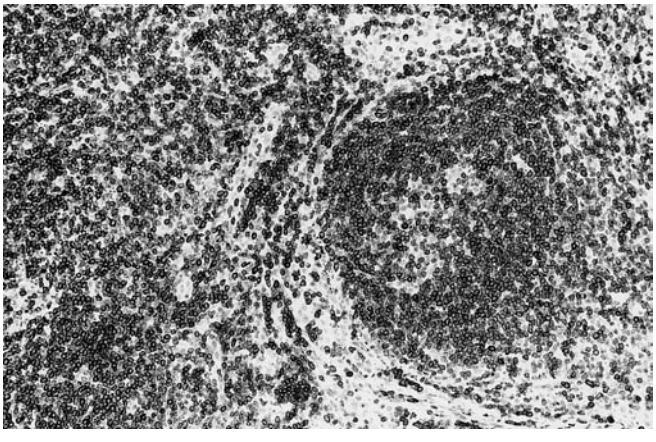


**Fig. 5** The majority of neoplastic cells express bcl-2 immunoreactivity (three-step immunoperoxidase staining for bcl-2, ×100)

pathology analysis using PCR assays failed to detect chromosome 18 breakpoint within the major breakpoint region of the bcl-2 gene. The analysis for breakpoints within a minor cluster region of the bcl-2 gene was not performed. Resected lymph nodes showed reactive changes only.

## Discussion

On the basis of cell morphology, follicular growth pattern, the presence of high levels of bcl-2 protein, and the absence of CD 5 and cyclin D1 positivity within the neoplastic cells, we classified the gallbladder lymphoma as FL, grade II.

To the best of our knowledge, FL of the gallbladder has not yet been reported in the English literature. In the review on the primary gallbladder lymphomas, Chatila et al. found reliable documentation for only nine cases (five lymphocytic lymphomas, one angiotropic lymphoma, one reticulum cell lymphoma and two MALT-omas) [6]. Most patients died shortly after surgery, although patients with MALT-oma reportedly had 'good outcome', but this was not defined any further [6]. Chatila et al. described another case of primary gallbladder MALT-oma with abdominal dissemination 18 months after cholecystectomy despite radiation and chemotherapy [6]. Since then, five additional cases of primary gallbladder MALT-omas were described, one associated with relapse in the gastric mucosa 5 years after initial diagnosis [7], one disseminated to the bone marrow [4], one associated with acute myeloid leukemia [1], while two patients remained free of disease at 1 year and 2 years after the diagnosis, respectively [18, 28]. Furthermore, a patient with primary T-cell lymphoblastic non-Hodgkin lymphoma of the gallbladder with 9-year disease-free follow-up after cholecystectomy and chemotherapy [20] and a patient with a primary lymphoblastic lymphoma of the pre-B type have also been reported recently [11].

FL is defined as a lymphoid neoplasm that reproduces most of the morphologic, immunophenotypic, and genetic features of lymphoid germinal centre [27]. The cytogenetic hallmark of FLs is translocation t(14;18)(q32;21), with rearrangement of the *BCL2* gene seen in up to 90% of cases [9]. However, it has recently been shown that the presence of this translocation is related to the grade of FL; being more frequent in FLs grade 1, 2 and 3a than in FLs grade 3b, with or without associated diffuse large B cell lymphoma (84%, 13%, respectively) [24]. The consequence of t(14;18) translocation is the presence of high levels of bcl-2 protein within the neoplastic cells, a 26-kDa protein that prolongs cell survival by inhibiting apoptosis [12].

Prognosis of FLs correlates with histological grade, with grades 1 and 2 being indolent and usually not curable, and grade 3 being more aggressive and having a potential for cure with aggressive therapy [23]. Our patient with FL grade II has been alive and well without signs of the disease 3 years after the operation. Differen-

tial diagnosis of FL primarily includes (a) reactive follicular hyperplasia, (b) marginal zone B cell lymphoma with prominent follicular colonisation (MALT lymphoma) and (c) mantle cell lymphoma [8, 16].

### Reactive follicular hyperplasia

Bcl-2 oncoprotein has been described to be particularly useful for distinguishing FL from reactive follicular hyperplasia [29, 30]. Immunohistochemical detection of bcl-2 oncoprotein shows rather diffuse and intense bcl-2 protein expression in the majority of FLs [29, 30], including the presently described case. Interestingly, we failed to detect chromosome 18 breakpoints within the major breakpoint region in the *BCL2* gene using PCR-based assays in FL of our patient. Nevertheless, breakpoints located outside major breakpoint region, not tested in our patient, have been reported in about 20% of FLs [5]. In addition, Buchonnet et al. could not locate breakpoints by PCR analysis in 8% of FLs, despite using a different set of primers [5]. Normal germinal centres have no bcl-2 immunoreactivity, which is however present in the mantle zone and also in interfollicular cells, although is less prominent [29, 30].

In FLs, neoplastic follicles are usually uniform in size, lack the well-formed mantle zone, are relatively monomorphous in appearance and contain few mitoses [8]. On the contrary, reactive follicles vary in size and shape, have a discrete mantle zone, lymphoid cells are of various types and mitoses are frequent [8].

Assessment of proliferative activity may also contribute in discrimination between FL and follicular hyperplasia. In our case approximately 30% Ki-67 positive tumour cells appear to be of a limited discrimination value. Ashton-Key at al. have shown that the proliferation fractions in the FL varied from 0.5% to 59% (mean 15.6%), with over 80% of FLs having proliferation fractions of less than 25% [3]. In contrast, proliferation fractions in reactive follicles ranged from 30.5% to 86.8% (mean 64.9%) [3]. They concluded that while a low proliferation fraction indicates a FL, a high proliferation fraction does not exclude the diagnosis of FL [3].

### MALT lymphoma

MALT lymphomas are characterised by diffuse infiltration of cells that resemble small cleaved follicular cells, numerous plasma cells, and epithelial invasion by lymphoma cells, a phenomenon described to be important in distinguishing MALT lymphomas from reactive lymphoid infiltrate [8]. Lymphoid follicles are often present and are regarded as reactive. In addition, translocation t(11;18) with the formation of *API2-MLT* fusion thought to occur almost exclusively in extranodal MALT lymphomas has been described recently [17].

### Mantle cell lymphoma

Mantle cell lymphoma is typically composed of small to medium sized lymphoid cells, which in many cases involve the mantle zone of some reactive follicles [16]. Contrary to FLs, neoplastic cells in mantle cell lymphoma show CD5 and cyclin D1 positivity [8]. However, they also express bcl-2 protein [8, 16].

### Conclusion

This is the first report on the primary follicular lymphoma of the gallbladder, presenting as an acute biliary tract obstruction, suggesting clinically and radiologically a Klatskin tumour – a bile duct carcinoma. The main importance of the present case is to draw the attention of pathologists to this unusual localisation and presentation of a follicular lymphoma, since the correct diagnosis is of therapeutic significance.

**Acknowledgements** The authors express sincere appreciation to Professor P.G. Isaacson, Department of Histopathology, Rockefeller Building, London, and Dr. G. Frizzera, Department of Immunopathology, New York Presbyterian Hospital, USA, for their confirmation of diagnosis and classification of malignant lymphoma of the gallbladder and extrahepatic bile ducts. Skilful assistance of mag. Ira Todorović, M.Sc., who performed molecular analysis studies, is also acknowledged.

## References

1. Abe Y, Takatsuki H, Okada Y, Saito A, Kimura T, Nishimura J (1999) Mucosa-associated lymphoid tissue type lymphoma of the gallbladder associated with acute myeloid leukemia. Intern Med 38:442–444
2. Aiello A, Delia D, Giardini R, Alasio L, Bartoli C, Pierotti MA, Pilotti S (1997) PCR analysis of IgH and BCL2 gene rearrangement in the diagnosis of follicular lymphoma in lymph node fine-needle aspiration. A critical appraisal. Diagn Mol Pathol 6:154–160
3. Ashton-Key M, Diss TC, Isaacson PG, Smith ME (1995) A comparative study of the value of immunohistochemistry and the polymerase chain reaction in the diagnosis of follicular lymphoma. Histopathology 27:501–508
4. Bickel A, Eitan A, Tsilman B, Cohen HI (1999) Low-grade B cell lymphoma of mucosa-associated lymphoid tissue (MALT) arising in the gallbladder. Hepatogastroenterology 46:1643–1646
5. Buchonnet G, Jardin F, Jean N, Bertrand P, Parmentier F, Tison S, Lepretre S, Contentin N, Lenain P, Stamatoullas-Bastard A, Tilly H, Bastard C (2002) Distribution of BCL2 breakpoints in follicular lymphoma and correlation with clinical features: specific subtypes or same disease? Leukemia 16:1852–1856
6. Chatila R, Fiedler PN, Vender RJ (1996) Primary lymphoma of the gallbladder: a case report and review of the literature. Am J Gastroenterol 91:2242–2244
7. Chim CS, Liang R, Loong F, Chung LP (2002) Primary mucosa-associated lymphoid tissue lymphoma of the gallbladder. Am J Med 112:505–507
8. Ferry JA, Harris NL (1997) Atlas of lymphoid hyperplasia and lymphoma. Saunders, Philadelphia
9. Freeman HJ, Anderson ME, Gascoyne RD (1997) Clinical, pathological and molecular genetic findings in small intestinal follicle center cell lymphoma. Can J Gastroenterol 11:31–34

10. Gaidano G, Pastore C, Capello D, Cilli V, Saglio G (1997) Molecular pathways in low grade B-cell lymphoma. Leuk Lymphoma 26:107–113
11. Gravel J, Lallier M, Garel L, Brochu P, Champagne J, Alvarez F (2001) Primary non-Hodgkin lymphoma of the extrahepatic biliary tract and gallbladder in a child. J Pediatr Gastroenterol Nutr 32:598–601
12. Hockenbery D, Nunez G, Milliman C, Schreiber RD, Korsmeyer SJ (1990) Bcl-2 is an inner mitochondrial membrane protein that blocks programmed cell death. Nature 348:334–336
13. Isaacson PG (1998) Primary gastric lymphoma. Adv Clin Pathol 2:3–13
14. Isaacson PG, Norton AJ (1994) Extranodal lymphomas. Churchill Livingstone, Edinburgh
15. Klatskin G (1965) Adenocarcinoma of the hepatic duct at its bifurcation within the porta hepatis. Am J Med 38:241–256
16. Loyson SAJ, de Boer CJ, Schuuring E, Kluin PM, van Krieken JHJM (1996) Mantle cell lymphoma. A morphological, immunohistochemical and molecular genetic study. Pathol Res Pract 192:781–789
17. Maes B, Baens M, Marynen P, De Wolf-Peeters CH (2000) The product of the t(11;18), an *API2-MLT* fusion, is an almost exclusive finding in the marginal zone cell lymphoma of extranodal MALT type. Ann Oncol 11:521–526
18. McCluggage WG, Mackel E, Mccusker G (1996) Primary low grade malignant lymphoma of mucosa-associated lymphoid tissue of gallbladder. Histopathology 29:285–287
19. Misdraji J, Castillo CF, Ferry JA (1997) Follicle center lymphoma of the ampulla of Vater presenting with jaundice. Am J Surg Pathol 21:484–488
20. Mitropoulos FA, Angelopoulou MK, Siakantaris MP, Rassidakis G, Vayiopoulos GA, Papalampros E, Kalovidouris A, Pangalis GA (2000) Primary non-Hodgkin's lymphoma of the gall bladder. Leuk Lymphoma 40:123–131
21. Mosnier JF, Brousse N, Sevestre C, Fléjou JF, Delteil C, Hénin D, Potet F (1992) Primary low-grade B-cell lymphoma of the mucosa-associated lymphoid tissue arising in the gallbladder. Histopathology 20:273–275
22. Nadal E, Martinez A, Jimenez M, Gines A, Campo E, Pique J, Lopez-Guillermo A (2002) Primary follicular lymphoma arising in the ampulla of Vater. Ann Hematol 81:228–231
23. Nathwani BN, Harris NL, Weisenburger D, Isaacson PG, Piris MA, Berger F, Müller-Hermelink HK, Swerdlow SH (2001) Follicular lymphoma. In: Jaffe ES, Harris NL, Stein H, Vardiman JW (eds) Pathology and genetics of tumours of the haematopoietic lymphoid tissues. IARC Press, Lyon, pp 162–167
24. Ott G, Katzenberger T, Lohr A, Kindelberger S, Rudiger T, Wilhelm M, Kalla J, Rosenwald A, Muller JG, Ott MM, Muller-Hermelink HK (2002) Cytomorphologic, immunohistochemical, and cytogenetic profiles of follicular lymphoma: 2 types of follicular lymphoma grade 3. Blood 99:3806–3812
25. Poggi MM, Cong PJ, Coleman CN, Jaffe ES (2002) Low-grade follicular lymphoma of the small intestine. J Clin Gastroenterol 34:155–159
26. Segal GH, Jorgensen T, Scott M, Braylan RC (1994) Optimal primer selection for clonality assessment by polymerase chain reaction analysis: II. Follicular lymphomas. Hum Pathol 25: 1276–1282
27. Shia J, Teruya-Feldstein J, Pan D, Hegde A, Klimstra D, Chaganti RSK, Qin J, Portlock CS, Filippa DA (2002) Primary follicular lymphoma of the gastrointestinal tract. A clinical and pathologic study of 26 cases. Am J Surg Pathol 26: 216–224
28. Tsuchiya T, Shimokawa I, Higami Y, Ohtani H, Shigeoka Y, Ohshima K, Tanaka K, Ayabe H (2001) Primary low-grade MALT lymphoma of the gallbladder. Pathol Int 51:965–969
29. Veloso JD, Rezuke WN, Cartun RW, Abernathy EC, Pastuszak WT (1995) Immunohistochemical distinction of follicular lymphoma from follicular hyperplasia in formalin-fixed tissues using monoclonal antibodies MT2 and bcl-2. Appl Immunohistochem 3:153–159
30. Wang T, Lasota J, Hanau CA, Miettinen M (1995) Bcl-2 oncoprotein is widespread in lymphoid tissue and lymphomas but its differential expression in benign versus malignant follicles and monocytoid B-cell proliferations is of diagnostic value. APMIS 103:655–662
31. Yoshino T, Miyake K, Ichimura K, Mannami T, Ohara N, Hamazaki S, Akagi T (2000) Increased incidence of follicular lymphoma in the duodenum. Am J Surg Pathol 24:688–693

Virchows Arch (2003) 442:141–150
DOI 10.1007/s00428-002-0716-8

ORIGINAL ARTICLE

**Maki Kawashima · Mika Ide · Masako Nakanishi**
**Mitsuru Kuwamura · Daijiro Kumagai · Jyoji Yamate**

# Immunophenotypical changes of neoplastic cells and tumor-associated macrophages in a rat dendritic cell sarcoma-derived transplantable tumor line (KB-D8)

Received: 19 July 2002 / Accepted: 19 August 2002 / Published online: 15 October 2002
© Springer-Verlag 2002

**Abstract** Basically, dendritic cell-derived sarcomas are characterized by expression of major histocompatibility complex class-II molecules, but the biological properties of the tumor cells remain to be elucidated. Recently, we established a novel transplantable cell line (KB-D8) from a dendritic cell sarcoma found in an F344 rat. In the present study, we investigated immunophenotypical changes of KB-D8 tumor cells and tumor-associated macrophages (TAMs) appearing in relation to tumor development in syngeneic F344 rats. A number of neoplastic cells in 0.5-cm-diameter KB-D8 tumors showed immunoreactions to OX6 (specific for rat antigen-presenting cells), ED1 (for rat exudate macrophages), and ED2 (for rat resident macrophages), and 72% and 11% of the OX6+ cells were double-immunostained with ED1 and ED2, respectively. Interestingly, the immunoreactions to these antibodies were gradually reduced with increasing size of KB-D8 tumors of 1-, 2-, and 3-cm diameter. These findings indicated that immunophenotypes of dendritic cell-derived sarcomas may be changeable depending on microenvironmental conditions in vivo. Many TAMs seen outside KB-D8 tumors reacted to OX6, ED1, and ED2; the numbers of TAMs immunopositive for these antibodies also decreased as the tumor grew. Similarly, the earlier temporary increase and subsequent gradual decrease in ED2+ and OX6+ cell numbers were observed in the spleen and liver of KB-D8-bearing rats. The reverse-transcription polymerase chain reaction showed mRNA expressions of granulocyte/macrophage-colony stimulating factor, monocyte-chemoattractant protein-1, and osteopontin in KB-D8 tumor tissues. Although the functional roles (biphasic roles: suppressing or promoting) of these factors should be investigated further in relation to tumor development, the factors might be partially responsible for the TAM reactions. KB-D8 would be a useful experimental model to investigate the biological characteristics of dendritic cell sarcomas and tumor immunology in the host.

**Keywords** Dendritic cell sarcoma · Immunohistochemistry · Major histocompatibility complex class-II molecule · Rat model · Tumor-associated macrophage

M. Kawashima · M. Ide · M. Nakanishi · M. Kuwamura
J. Yamate (✉)
Laboratory of Veterinary Pathology,
Graduate School of Agriculture and Biological Sciences,
Osaka Prefecture University, Gakuencho 1-1, Sakai,
Osaka 599-8531, Japan
e-mail: yamate@vet.osakafu-u.ac.jp
Tel.: +81-72-2549482, Fax: +81-72-2507208

D. Kumagai
Laboratory of Cell Pathobiology,
Graduate School of Agriculture and Biological Sciences,
Osaka Prefecture University, Gakuencho 1-1, Sakai,
Osaka 599-8531, Japan

## Introduction

Dendritic cells include interstitial dendritic cells in non-lymphoid tissues, follicular dendritic cells (FDCs) in the germinal center (B cell-rich areas) and interdigitating dendritic (reticulum) cells (IDCs) in the T cell-rich areas of lymphoid tissues [12]. In humans, dendritic cell sarcomas have been reported mainly in the lymph node, but the occurrence is exceedingly rare [11]. Dendritic cells play a central role in immune response as a potent antigen-presenting cell (APC) by expressing major histocompatibility complex (MHC) class-II molecules whose primary functions are to stimulate unprimed T cells. The expression of MHC class-II antigens depends on maturation or activation stages [26]. Ontogenetically, the dendritic cells are considered to develop from the hematopoietic stem cells, and the precursor cells at immature stage spread over the tissue; thus, the differentiation pathway of dendritic cells is distinct from that of monocytes and macrophages [32]. However, it was recently reported that monocytes/macrophages are able to transdifferentiate into dendritic cells under some conditions [6, 27]. More interestingly, a subset of B cells has been reported to give rise to dendritic morphology and func-

tions [4, 23]. Therefore, the histogenesis and cellular characteristics of dendritic cell-derived sarcomas appear to be heterogeneous and, thus, the biological properties remain to be investigated [11].

Recently, we succeeded in establishing a transplantable tumor line (KB) from a spontaneous dendritic cell sarcoma generated in the thymus of an old F344 rat, and an in vitro cloned cell line (KB-D8) was isolated from a KB-derived parent cell line (KB-P) [40]. KB tumors and tumors induced by inoculating KB-D8 cells were characterized by immunoreaction to OX6 [rat MHC class-II antigen (Ia)-recognizing antibody], ED5 (for rat FDCs), and RED-1 (for rat IDCs), and by the presence of tubulovesicular system consisting of numerous vesicles, sacs, and tubules in electron microcopy. Additionally, these neoplastic cells reacted to antibodies of ED1 (for rat exudate macrophages) and ED2 (for rat resident macrophages) in varying degrees. KB and KB-D8 may be useful experimental models for investigating the biological properties of dendritic cell sarcomas.

However, the immunolabeling with OX6 in KB-D8 tumor cells was various, and cultured KB-D8 cells did not react to OX6 [40]. Dendritic cells have an important function for the initiation of a tumor-induced immune system by expressing MHC class-II molecules [5]. Because KB-D8 cells are dendritic cell derived, we have speculated that microenvironmental conditions evoked in vivo by tumor–host interactions might be attributable to MHC class-II antigen expression in KB-D8 tumor cells. Thus, to shed some light on the nature of dendritic cell sarcomas, in the present study, we investigated immunophenotypical changes of KB-D8 tumor cells to OX6, as well as ED1 and ED2, in relation to tumor development. It is well known that tumor-associated macrophages (TAMs) [22], of which the recruitment may be mediated by monocyte/macrophage chemoattractant molecules such as granulocyte/macrophage-colony stimulating factor (GM-CSF), monocyte chemoattractant protein-1 (MCP-1) and osteopontin [7, 15, 36], appear at tumor site. To further characterize the dendritic cell-derived sarcoma, this study also investigated the appearance of TAMs in KB-D8 tumor-bearing rats by immunohistochemistry with ED1, ED2, and OX6, and mRNA expressions of such chemoattractants were analyzed in KB-D8 tumors and cultured KB-D8 cells using the reverse-transcription polymerase chain reaction (RT-PCR).

## Materials and methods

### Animals

Male F344/DuCrj rats (Charles River Japan, Shiga, Japan), aged 6 weeks, were used. During this experiment, they were housed in a barrier room at 22±4 C with a 12-h/12-h light/dark cycle and allowed free access to a standard commercial laboratory diet for rats (Oriental Yeast Co. Ltd., Tokyo, Japan). The experiment was in compliance with our institutional guidelines for animal care. All rats used in this study were euthanized under ether anesthesia.

### Induction of KB-D8 tumors and in vivo observations

The establishment and characteristics of KB-D8 cells have been described previously [40]. KB-D8 cells were serially passaged at 37 C in a humidified 5% $CO_2$ atmosphere. The growth medium used was Eagle's minimum essential medium (MEM; Nissui, Tokyo, Japan) containing 10% fetal bovine serum (Bioserum, UBI, Japan), 0.03% L-glutamine (Nissui), penicillin (100 U/ml), and streptomycin (100 μg/ml). KB-D8 tumors were easily induced in syngeneic F344 rats by inoculation of cultured KB-D8 cells; the tumors grew into nodules of 6-cm diameter 6 weeks after the inoculation [40]. In the present study, first, tumors were developed by subcutaneous inoculation of KB-D8 cells ($1\times10^6$). The developed tumors were aseptically removed and minced into small pieces (2 mm in diameter) with scissors. For in vivo observations, a tissue fragment was transplanted subcutaneously into each of the 12 F344 rats. These transplants were made through a trochar into the center of the interscapular region under light anesthesia with ether.

After the transplantation, the diameter of developing tumors was measured in millimeters with calipers twice a week. When tumors reached the size of 0.5, 1, 2, and 3 cm in diameter, three rats with tumors at each size point were examined. Three sham-operated, age-matched rats served as controls. Heparinized blood obtained from the abdominal aorta was smeared and stained with Giemsa for white blood cell differentiation of monocytes.

### Immunohistochemistry

Besides tumors, spleen and liver tissues were fixed in 10% neutral buffered formalin or Zamboni's solution (0.21% picric acid, 2% paraformaldehyde and 130 mM phosphate buffer, pH 7.4). The immunohistochemical analyses were performed by the indirect immunoperoxidase method with monoclonal antibodies of ED1 (Chemicon Int. Inc., Temecula, Calif., USA), ED2 (Serotec, Tokyo, Japan), and OX6 (Serotec). Formalin-fixed, deparaffinized sections were used for ED1 immunohistochemistry, and Zamboni's solution-fixed, deparaffinized sections for ED2 and OX6. The following pretreatments were made to quench endogenous peroxidase; sections applied for ED2 and OX6 were treated with 0.1% trypsin for 5–10 min at 37 C and then 3% $H_2O_2$ for 10 min; sections used for ED1 were treated by microwave for 5 min and then 3% $H_2O_2$ for 10 min. After the pretreatments, sections were incubated with 5% skimmed milk for 40 min at room temperature, and then incubated with each primary antibody for 14–24 h at 4°C. After washing three times in phosphate-buffered saline (PBS), HISTOFINE simple stain rat PO (Multi type Kit; Nichirei Corp., Tokyo, Japan), which involves amino acid polymer conjugated to anti-mouse Ig, was applied for 60 min at room temperature as the second step. Positive reactions were visualized with 3.3′-diaminobenzidine (DAB). Sections were counterstained lightly with hematoxylin.

In rat pathological lesions, ED1 is used for detection of exudate macrophages, and ED2 labels resident macrophages [36, 39]. OX6 stains cells expressing rat MHC class-II antigens [21, 29]. Cells reacting to ED1, ED2 or OX6 were counted within and around tumor textures, as well as in the red pulp of spleen and perilobular zone of hepatic lobules, at a magnification of ×400. Mean values±standard error (SEM) were calculated from the positive cell numbers in three to five randomly selected field (0.0625 $mm^2$ each) in each section. The counting methods at tumor sites were conducted, according to those described by Yamashiro et al. [36].

For morphology, formalin-fixed, deparaffinized sections were stained using hematoxylin and eosin (HE) stain.

### Immunohistochemical double staining

Zamboni's solution-fixed, deparaffinized tissue sections were stained by the Avidin-Biotin Complex (ABC) method (Vectastain ABC Kit; Vector Laboratories, Inc., Burlingame, Calif., USA)

with ED1 or OX6. After staining reaction (brown) with DAB, the sections were incubated in 10 mM citrate buffer to remove the antibodies used. Next, the same sections were incubated with primary antibodies for 14–24 h at 4 C; ED2 or OX6 was applied for ED1-immunostained sections, and ED1 or ED2 for OX6-immunostained sections. After washing three times in PBS, ENVISION/AP (Dako Corp., Carpinteria, Calif., USA), which includes goat anti-mouse Ig conjugated to alkaline phosphatase labeled-dextran polymer, was applied for 60 min; to visualize reaction for the second antibody, sections were stained red by Fuchsin substrate-chromogen system (Dako Corp.). Cells showing double immunreactions to ED2/ED1 or OX6/ED1 were counted in 300 ED1+ cells within tumor tissues or in 100 ED1+ cells around tumor tissues. Similarly, ED1+OX6+ or ED2+OX6+ cells were counted in OX6+ cells.

In addition, to see neoplastic proliferating activity of OX6+ cells, immunohistochemistry with a monoclonal antibody against proliferating cell nuclear antigen (PCNA; Dako) was performed on OX6-immunostained sections. The double immunohistochemical staining was similar to that described above; the positive reactions to OX6 were stained brown, and those to the anti-PCNA antibody were labeled red. Cells showing double reactions to OX6/anti-PCNA antibody were counted in 1000 anti-PCNA antibody-positive cells in 0.5-cm and 3-cm-diameter tumors.

### RNA isolation and RT-PCR

Total RNA was isolated from KB-D8 tumors and cultured KB-D8 cells by Trizol reagent (Gibco BRL, Gland Island, N.Y., USA). The RT-PCR method was conducted as described previously [34, 40]. From 5 μg of total RNA, the single-strand cDNA was synthesized with avian myeloblastosis virus transcriptase (Boehringer Mannheim Biochemica, Mannheim, Germany) and random hexamer oligonucleotide (Promega, Madison, Wis., USA). cDNA was amplified by PCR with *Taq* DNA polymerase (Takara Shuzou, Kyoto, Japan) and each of the specific primers (sense and antisense) for rat osteopontin, MCP-1, GM-CSF, or β-actin (control). The following conditions were used for the amplification: for osteopontin, 35 cycles of 45 s denaturation at 94 C, 45 s annealing at 50 C, 1.5 min synthesis at 72 C [15]; for MCP-1, 27 cycles of 15 s denaturation at 94 C, 30 s annealing at 55 C, 1 min synthesis at 72 C [14]; for GM-CSF, 40 cycles of 30 s denaturation at 94 C, 30 s annealing at 67 C, 30 s synthesis at 72 C [2, 30]. The oligonucleotides used were as follows: the osteopontin sense primer 5′-TCCAAGGAGTATAAGGAGAGGGCCA-3′ and antisense primer 5′-CTCTTAGGGTCTAGGACTAGCTTGT-3′; the MCP-1 sense primer 5′-ATGCAGGTCTCTCTGTCACG-3′ and antisense primer 5′-CTAGTTCTCTGTCATACT-3′; the GM-CSF sense primer 5′-ATGAAATCCTCAAAGGTGGTG-3′ and antisense primer 5′-GTAGATGCCATCAAAGAAGC-3′; for β-actin sense primer 5′-TAAAGACCTCTATGCCAACAC-3′ and antisense primer 5′-CTCCTGCTTGCTGATCCACAT-3′. The PCR products were electrophoresed in 2% agarose gel. DNA was stained with ethidium bromide on the gel. The size of the amplification band of osteopontin, MCP-1, GM-CSF, and β-actin was 350, 447, 275, and 214 bp, respectively. The bands were semi-quantitatively evaluated with image analysis software (NIH Image 1.61, Bethesda, Md., USA), and the intensity for osteopontin, MCP-1 or GM-CSF was normalized by that for β-actin [34, 40].

### Statistical evaluation

Paired samples were evaluated using the Student's *t*-test. Significance was accepted at $P<0.05$.

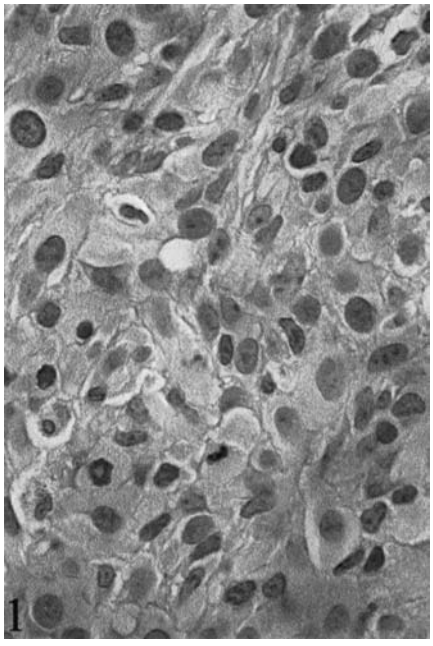


**Fig. 1** KB-D8 (a rat dendritic cell sarcoma-derived transplantable tumor line) tumor consisting of round, oval and spindle cells with abundant cytoplasm arranged in a compact sheet. Hematoxylin and eosin ×700

## Results

### Immunoexpressions for ED1, ED2, and OX6 within and around KB-D8 tumor tissues

Developed tumors were well encapsulated by thin fibrous tissues. Histologically, KB-D8 tumors were composed of round, oval and spindle cells with abundant cytoplasm arranged in a compact sheet (Fig. 1) and ill-defined bundle growth patterns. Cellular and nuclear atypism of the tumor cells progressed with tumor growth. These histological findings were in keeping with those in our previous report [40].

Immunohistochemically, cells reacting to ED1 (Fig. 2a), ED2 (Fig. 2b), and OX6 (Fig. 2c) were seen within tumor tissues. Among ED1+, ED2+, and OX6+ cells within 0.5-cm-diameter tumors, OX6+ cells showed the greatest number (Fig. 3a, b, c). Interestingly, the OX6+ cell number was dramatically decreased within 1-cm, 2-cm, and 3-cm-diameter tumors (Fig. 2d; Fig. 3c), in contrast to that within 0.5-cm-diameter tumors (Fig. 2c). The increased numbers of ED1+ and ED2+ cells seen within 0.5-cm and 1-cm-diameter tumors were gradually decreased within 2-cm and 3-cm-diameter tumors (Fig. 3a, b).

Around KB-D8 tumors of each size, ED2+ cells (Fig. 2b) were the most frequently seen cells among ED1+, ED2+, and OX6+ cells (Fig. 3a, b, c). The numbers of ED1+, ED2+, and OX6+ cells had already reached maximum around 0.5-cm-diameter tumors, and, thereafter, these numbers were gradually decreased with

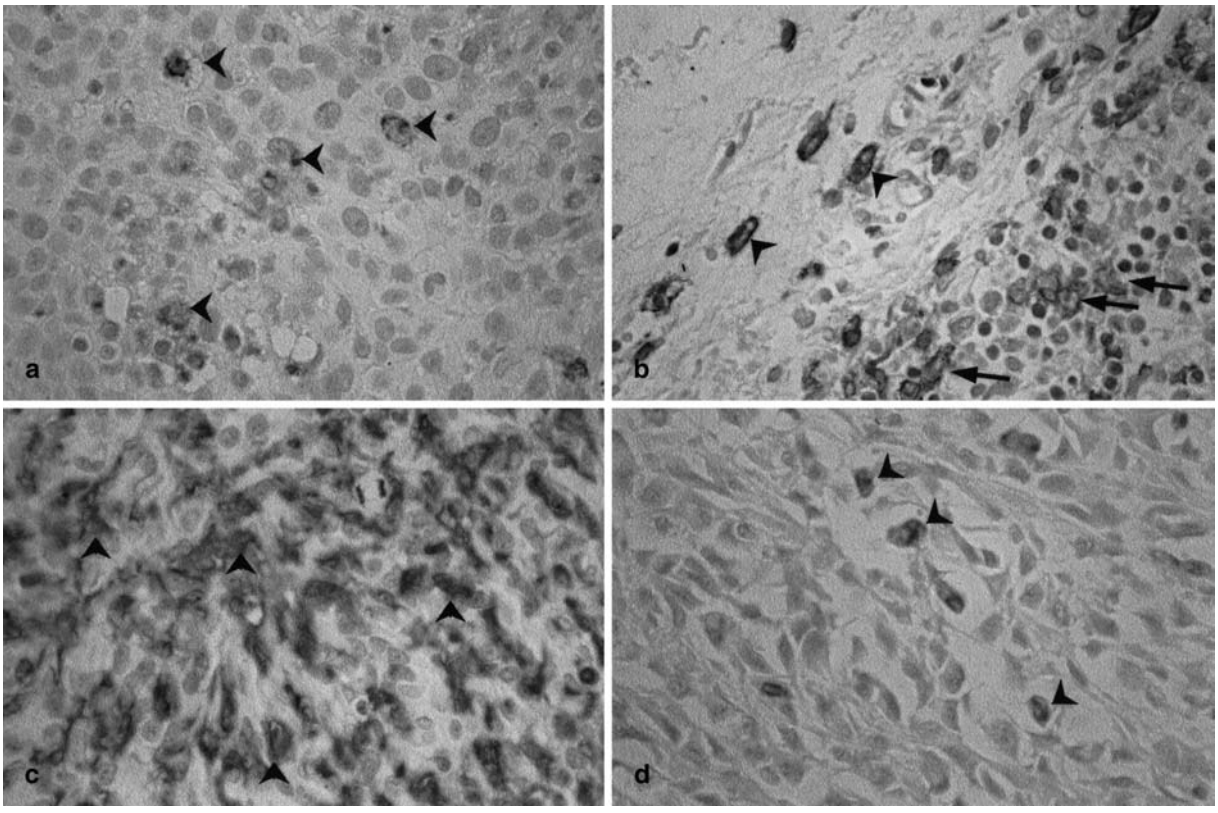



**Fig. 2** Immunohistochemistry for ED1 (**a**), ED2 (**b**), OX6 (**c**) in KB-D8 tumors of 0.5-cm diameter, as well as OX6 (**d**) in KB-D8 tumor of 3-cm diameter. Within tumor tissues, cells reacting to ED1 (**a**, *arrowheads*) and ED2 (**b**, *arrows*) are seen. The vast majority of cells within 0.5-cm-diameter tumor react to OX6 (**c**, *arrowheads*), whereas OX6-positive cells are infrequently seen within 3-cm-diameter tumor (**d**, *arrowheads*). Outside 0.5-cm-diameter tumor, there are some ED2-positive cells (**b**, *arrowheads*). All were counterstained with hematoxylin ×500

increasing size of the tumors (1 cm, 2 cm, and 3 cm in diameter).

To analyze the dual antigen expression, the double immunohistochemical stainings were carried out on 0.5-cm-diameter KB-D8 tumors. Of OX6+ cells within tumors, 72% showed ED1 immunoreaction (Fig. 4a), and 11% of the OX6+ cells reacted to ED2 (Fig. 4b); the percentage of OX6+ED1+ and ED2+ED1+ cells in ED1+ cells seen within tumors was 65% and 18%, respectively. In ED1+ cells seen around tumors, 71% and 34% showed double immunoreactions to OX6 and ED2, respectively, and the respective percentage of the double immunoreactions for ED1 and ED2 in OX6+ cells around tumors was 49% and 26%.

Of anti-PCNA antibody-positive cells in 0.5-cm-diameter tumors, 23% showed OX6 immunoreactivity (Fig. 4c), whereas the percentage of cells double-immunostained with OX6/anti-PCNA antibody in 3-cm-diameter tumors was less than 1%. Neither cells reacting to anti-PCNA antibody nor cells showing double-immunoreactions to OX6/anti-PCNA antibody were seen around tumors of 0.5-cm and 3-cm diameter.

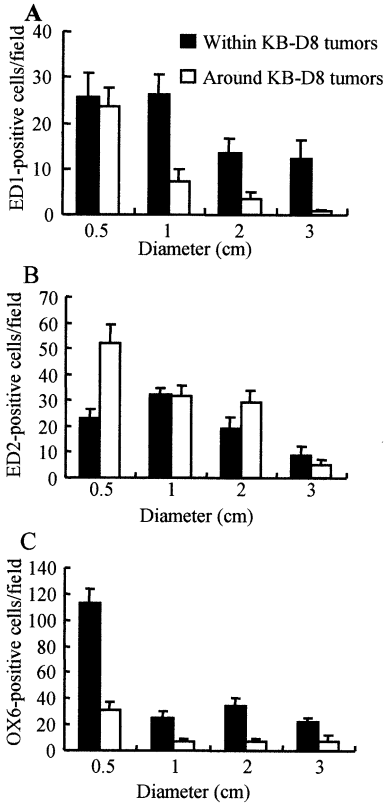



**Fig. 3** The numbers of ED1- (**a**), ED2- (**b**), and OX6- (**c**) positive cells within and around KB-D8 tumors of 0.5-cm, 1-cm, 2-cm, and 3-cm diameter. Values are mean ± standard error (SEM)

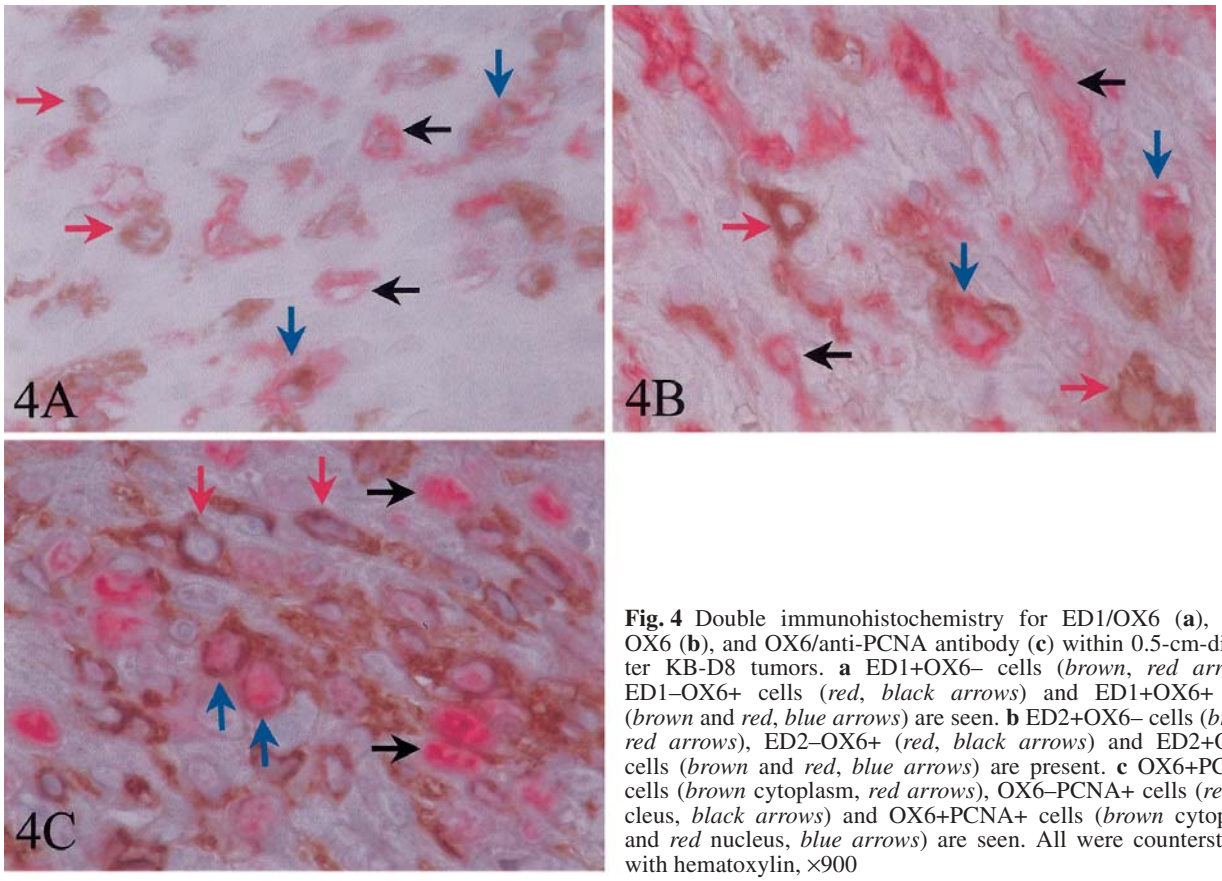



**Fig. 4** Double immunohistochemistry for ED1/OX6 (**a**), ED2/OX6 (**b**), and OX6/anti-PCNA antibody (**c**) within 0.5-cm-diameter KB-D8 tumors. **a** ED1+OX6– cells (*brown*, *red arrows*), ED1–OX6+ cells (*red*, *black arrows*) and ED1+OX6+ cells (*brown* and *red*, *blue arrows*) are seen. **b** ED2+OX6– cells (*brown*, *red arrows*), ED2–OX6+ (*red*, *black arrows*) and ED2+OX6+ cells (*brown* and *red*, *blue arrows*) are present. **c** OX6+PCNA– cells (*brown* cytoplasm, *red arrows*), OX6–PCNA+ cells (*red* nucleus, *black arrows*) and OX6+PCNA+ cells (*brown* cytoplasm and *red* nucleus, *blue arrows*) are seen. All were counterstained with hematoxylin, ×900

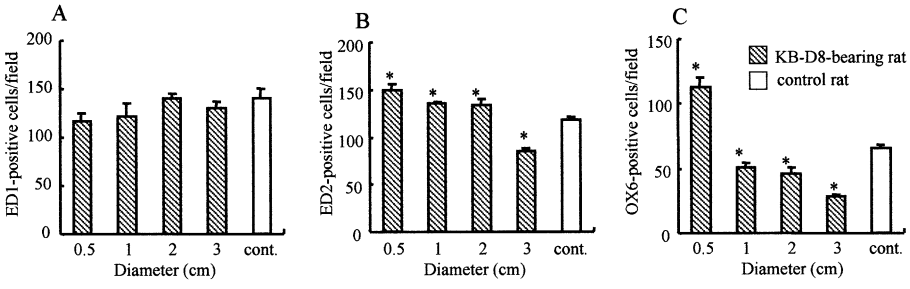



**Fig. 5** The numbers of ED1- (**a**), ED2- (**b**), and OX6- (**c**) positive cells in the red pulp of spleen in rats with KB-D8 tumors of 0.5-cm, 1-cm, 2-cm, and 3-cm diameter, and control rats (*cont.*). Values are means ±SEM. *Significantly different from controls at $P<0.05$

## Immunoexpressions for ED1, ED2, and OX6 in the spleen and liver, and blood monocytes

To examine the systematic alteration of macrophage populations in KB-D8-bearing rats, an immunohistochemical approach with ED1, ED2, and OX6 was preformed in the spleen and liver because of important roles of these organs in tumor immunology [16, 21, 33]. In the red pulp of spleen, there was no significant difference in ED1+ cell number between KB-D8 tumor-bearing and control rats (Fig. 5a; Fig. 6a). Compared with controls, the number of ED2+ cells in the spleen was significantly increased in rats with tumors of 0.5-, 1-, and 2-cm diameter, whereas it was significantly decreased in 3-cm-diameter tumor-bearing rats (Fig. 5b; Fig. 6b). OX6+ cell number showed a significant increase in the spleen of rats with 0.5-cm-diameter tumors, but the number was significantly decreased in rats with 1-cm, 2-cm, and 3-cm-diameter tumors (Fig. 5c; Fig. 6c).

In the perilobular zone of the liver, ED1+ cell number in rats with 1-cm and 3-cm-diameter tumors was significantly increased (Fig. 7a; Fig. 8a) and was particularly prominent in 3-cm-diameter tumors. There tended to be an increased number of hepatic ED2+ cells in 0.5-cm-diameter tumors, but this was significantly decreased in 2-cm and 3-cm-diameter tumors (Fig. 7b; Fig. 8b). Interestingly, cells reacting to OX6 showed a significant increase in rats with 0.5-cm-diameter tumors (Fig. 7c; Fig. 8c), but the number returned to control level in 1-cm-diameter tumors upward.

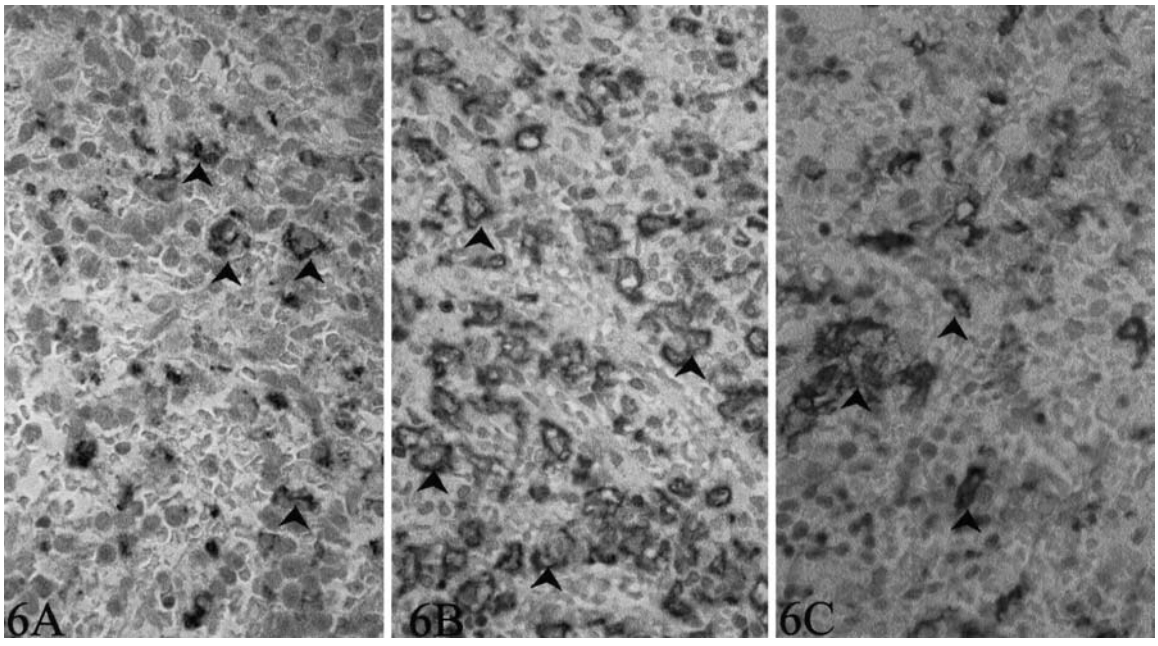



**Fig. 6** ED1- (**a**), ED2- (**b**), and OX6- (**c**) positive cells (*arrowheads*) seen in the red pulp of spleen in a rat with 0.5-cm-diameter tumor. All were counterstained with hematoxylin ×600

The ratio of blood monocytes in white blood cell count was significantly increased in rats with 0.5-cm-diameter tumors, but there was no difference in rats with tumors of 1-cm, 2-cm, and 3-cm-diameter (Fig. 9).

### mRNA expressions of GM-CSF, MCP-1, and osteopontin by RT-PCR

mRNA expressions of GM-CSF, MCP-1, and osteopontin were seen in KB-D8 tumors (Fig. 10). The semiquantitative analysis revealed that there were no marked differences in the mRNA expressions of GM-CSF and osteopontin between 1-cm and 3-cm-diameter tumors (Fig. 10a, c). On the contrary, mRNA expression of MCP-1 in 3-cm-diameter tumors was about twofold greater than that in 1-cm-diameter tumors (Fig. 10b).

KB-D8 cells also expressed mRNAs of GM-CSF and osteopontin, but MCP-1 mRNA expression could not be detected in the cultured cells (Fig. 10).

## Discussion

The majority of human dendritic cell sarcomas are derived from FDCs and IDCs [11, 13, 20]. Neoplastic cells in these sarcomas are usually characterized by immunoreactivity with an antibody against HLA-DR; according to a review article by Fonseca et al. [11]; however, 3 of 7 FDC sarcomas and 1 of 12 IDC sarcomas were negative for the antibody. KB-D8 tumor cells showed the immunoreaction to OX6, but the reactivity was not always consistent [40]. The OX6 has been widely used to detect APCs in rat pathological lesions [36, 41]. Intriguingly, the present study showed that OX6-immunopositive cells were greatest in number in 0.5-cm-diameter KB-D8 tumors, and with increasing tumor size, the positive cell number was reduced. In addition, 23% of anti-PCNA antibody-positive cells in 0.5-cm-diameter tumors exhibited immunoreactions to OX6, whereas the number of the double-immunopositive cells was decreased in 3-cm-diameter tumors. These findings indicated that as KB-D8 tumors grew, OX6-positive cells showing neoplastic proliferating activity decreased the antigens recognized by OX6. This implies that MHC class-II expression in dendritic cell-derived sarcomas

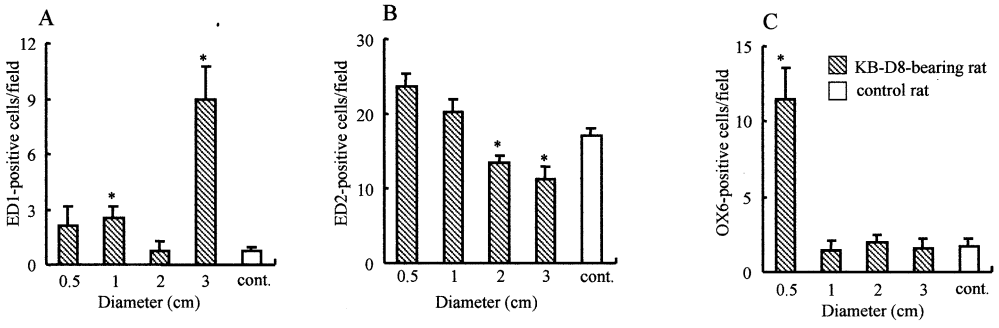



**Fig. 7** The numbers of ED1- (**a**), ED2- (**b**), and OX6- (**c**) positive cells in the perilobular zone of liver in rats with KB-D8 tumors of 0.5-cm, 1-cm, 2-cm, and 3-cm diameter, and control rats (*cont.*). Values are means ±SEM. *Significantly different from controls at $P<0.05$

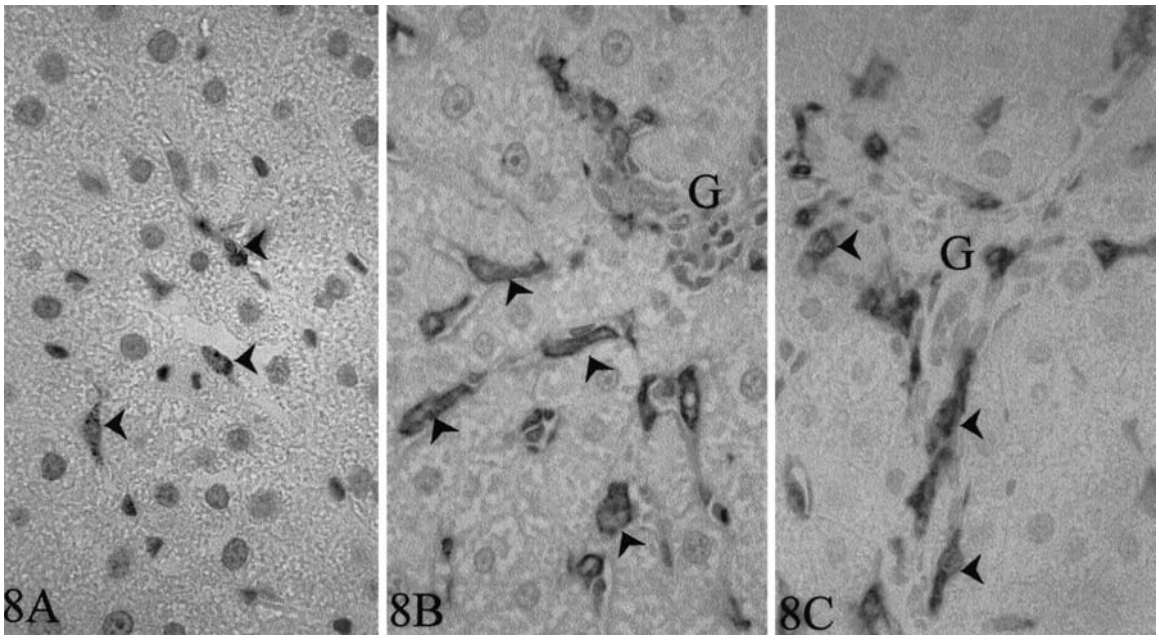



**Fig. 8** ED1- (**a**), ED2- (**b**), and OX6- (**c**) positive cells (*arrowheads*) seen in the perilobular zone of liver in a rat with 0.5-cm-diameter tumor. *G* Glisson's sheath. All were counterstained with hematoxylin ×600

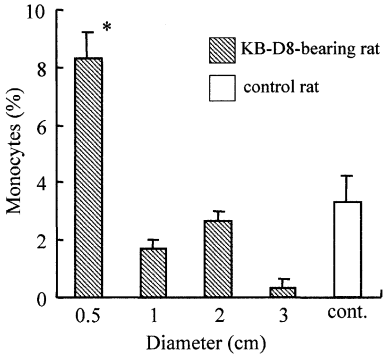



**Fig. 9** Blood monocyte ratio in white blood cell count in rats with KB-D8 tumors of 0.5-cm, 1-cm, 2-cm, and 3-cm diameter, and control rats (*cont.*). Values are mean±SEM. *Significantly different from controls $P<0.05$

may be changeable, depending on microenvironmental conditions in vivo. In the maturation process, dendritic cells originally develop from MHC class-II-negative precursors, and then give rise to low MHC class-II-positive cells (immature type); finally, immature dendritic cells can further upregulate the expression of MHC class-II molecules under stimulated conditions [17, 26]. Depending on tumor growth, neoplastic cells in KB-D8 tumors might become more immature (or dedifferentiated) in functions through losing the activity to express MHC class II. Because KB-D8 tumors are derived from APCs, this immunophenotypical alteration might be related to the balance between tumor growth and host immune system, indicating a unique biological nature of dendritic cell-derived sarcomas.

More interestingly, the double immunohistochemistry on 0.5-cm-diameter tumors showed that 72% and 11% of OX6+ cells were also positive for ED1 and ED2, respectively, indicating that KB-D8 cells expressing MHC class II could exhibit macrophage-like and histiocytic immuno-

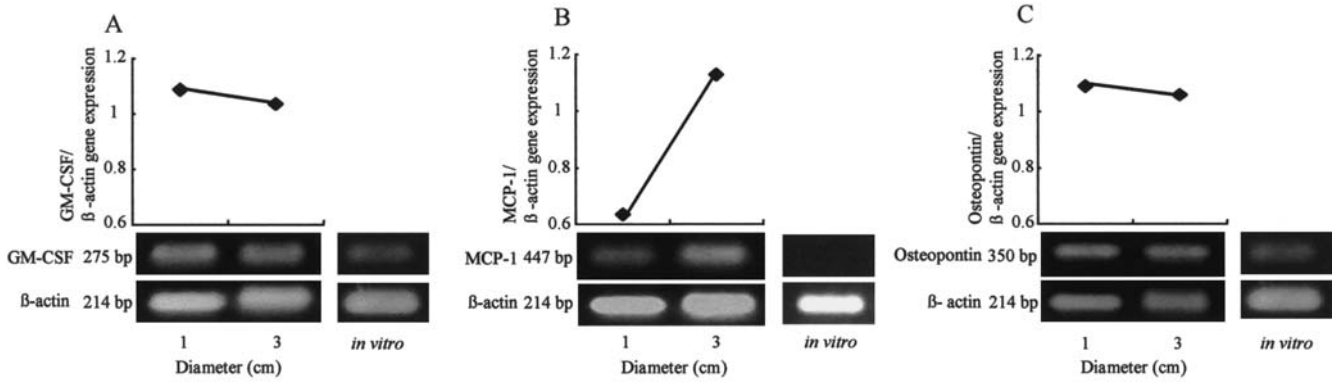



**Fig. 10** Reverse-transcription polymerase chain reaction analyses for mRNA expressions of granulocyte/macrophage colony stimulating factor (GM-CSF) (**a**), monocyte-chemoattractant protein-1 (MCP-1) (**b**), osteopontin (**c**), and β-actin (control) in KB-D8 tumors of 1-cm and 3-cm diameter (in vivo), and cultured KB-D8 cells (in vitro). The expression levels of GM-CSF, MCP-1, and osteopontin are normalized semi-quantitatively by the band of β-actin

phenotypes. ED1-recognizing antigens are on the membrane of cytoplasmic granules, especially phagolysosomes in rat exudate macrophages, and the degree of ED1 expression depends on the phagocytic activity [8, 9]. The functional roles of ED2-recognizing antigens are still undetermined, but ED2 reacts with cell membrane antigens of rat resident macrophages (Kupffer cells in the liver) [9, 35]. The present double immunohistochemistry also showed that 65% and 18% of ED1+ cells reacted to OX6 and ED2, respectively. Human dendritic cell sarcomas have been reported to react to CD14 and CD68 (both specific for human monocytes/macrophages) [11, 20]. Recently, it has been considered that monocytes/macrophage and dendritic cells have a common origin evolving from hematopoietic stem cells in the bone marrow and, thus, they can transdifferentiate in functions and phenotypes between them [6, 26, 27]. It is likely that there is a close relationship between dendritic cells and macrophages/histiocytes. Actually, it has been reported in rats that immature dendritic cells in the adrenal and pituitary glands, and interstitial dendritic cells in the liver reacted to ED1 [22, 28, 29]. In agreement with decreased number of OX6+ cells, ED1+ and ED2+ cell numbers within tumors were reduced with increasing size of KB-D8 tumors. The immunophenotypes of dendritic cell-derived sarcomas seem to be easily changed, depending on microenvironmental conditions evoked by the host-tumor relationship; this phenomenon should be examined closely for the immunohistochemical diagnosis of this tumor type.

TAMs play important roles in tumor immunology, because they may serve as both positive and negative mediators for tumor development [10]. To our knowledge, there have been no experimental data on the participation of TAMs in rat dendritic cell sarcomas. The present study revealed that outside KB-D8 tumors, there were cells reacting to ED1, ED2, and OX6, indicating that macrophage populations showing different immunophenotypes appeared as TAMs [19]. Among ED1+, ED2+, and OX6+ cells, the ED2+ cell number was greatest on 0.5-cm, 1-cm, and 2-cm-diameter tumors. This may imply that resident macrophages were quickly recruited against tumor growth. However, of the OX6+ cells seen around 0.5-cm-diameter tumors, 49% and 26% showed double immunostaining to ED1 and ED2, respectively; 71% and 34% of ED1+ cells revealed positive reactions to OX6 and ED2, respectively. Along with dendritic cells, activated macrophages, which may be derived from exudate and resident macrophages, might act as APCs in the immune system. It is interesting to note that the numbers of ED1+, ED2+, and OX6+ cells were decreased with the increasing size of KB-D8 tumors. TAMs play a suppressive role working against the generation and early growth of tumors by cytotoxicity, phagocytosis and MHC class-II expression, but developing tumors gradually change function, phenotype and number of TAMs, leading to tumor-induced immune suppression that may be related partly to immune tolerance [1, 5, 10]. Therefore, the decreased numbers of TAMs in developing KB-D8 tumors should reflect the alteration of the immune system of the tumor-bearing host. TAMs can prime and induce Th cells as an APC, and produce chemoattractant molecules to induce further TAMs within and around tumors [3, 5, 10, 12, 16, 18, 25, 42]. The vast majority of neoplastic cells in 0.5-cm-diameter KB-D8 tumors expressed MHC class-II molecules, demonstrable by OX6 immunohistochemistry. It is interesting to further pursue the tumor-derived antigenic components and the relationship between KB-D8 tumors and lymphocytes or TAMs.

The regulation of TAMs is related in part to soluble factors produced by TAMs themselves or by tumor cells [19]. The RT-PCR methods revealed that mRNAs of GM-CSF, MCP-1, and osteopontin were expressed in KB-D8 tumor tissues. These factors are known as effective macrophage chemoattractants in various pathological conditions [7, 15, 18, 36]. Among these factors, MCP-1 is the most potent factor responsible for the induction of TAMs, in particular for monocyte-derived exudate macrophages [36]. However, no mRNA expression was seen in cultured KB-D8 cells. Other host-derived cellular components such as endothelial cells, fibroblasts or infiltrated macrophages might release MCP-1 in KB-D8 tumors. These findings at least suggested possible contributions of these factors to reactions of TAMs at KB-D8 tumor sites.

Despite the decreased number of TAMs with KB-D8 tumor growth (Fig. 3), however, there were no marked differences in mRNA expressions of GM-CSF and osteopontin between 1-cm and 3-cm-diameter tumors, and rather MCP-1 mRNA expression was greater in 3-cm than 1-cm-diameter tumors (Fig. 10). Therefore, we investigated the systemic appearance of macrophage populations. Coinciding with the kinetics of TAMs around KB-D8 tumors, the numbers of ED2+ and OX6+ cells in the spleen and liver were increased in 0.5-cm-diameter tumors, and then tended to be decreased with increasing size of tumors (Fig. 5; Fig. 7); additionally, in rats with 0.5-cm-diameter tumors, blood monocyte ratio was markedly increased, and thereafter returned to control level. There was no positive correlation between TAM kinetics and mRNA expressions of chemoattractants examined. It was recently reported that some chemoattractants, which are produced by tumor cells, TAMs or host cells, may have biphasic functions (suppressing or promoting) to tumor development and TAM reactions [7, 16, 31]. Functional roles of chemoattractants produced in KB-D8 tumor tissues remains to be investigated with regard to tumor immunology and immunophenotypical changes of neoplastic cells and TAMs.

In conclusion, the present study demonstrated that immunophenotypes for ED1, ED2, and OX6 in KB-D8 tumor cells were changeable depending on tumor growth. In addition, TAMs, which took part in tumor immunity of KB-D8 tumors, consisted of heterogeneous macrophage populations reacting to ED1, ED2, and OX6. Basically, these immunoexpressions in neoplastic cells or TAMs were greatest at the early growth of KB-D8 tumors and, then, gradually reduced as the tumors grew. This phenomenon might be regulated partly by soluble

factors, such as GM-CSF, osteopontin and MCP-1, produced in tumor tissues. Similarly, we investigated TAMs in rat transplantable malignant fibrous histiocytomas (MFH), which were established in F344 rats [37]; cells reacting to OX6 and ED1 were rarely seen at the tumor site, although there were a moderate number of ED2+ cells (unpublished data). KB-D8 is a newly established cell line in F344 rats and may exhibit unique biological properties of dendritic cell-derived sarcomas in relation to tumor and host immunology, as shown in this study. The F344 rats have complete immune system, differing from nude mice or nude rats with xenotransplantation of human tumor lines. To further clarify the biological properties of dendritic cell-derived sarcomas, investigations are in progress in comparison with those of different transplantable tumor lines such as MFH, fibrosarcoma and pulmonary carcinoma, all lines which have been established in F344 rats in our laboratory [24, 37, 38].

**Acknowledgements** This work was supported in part by a Grant-in-Aid (no. 12660287 to J. Yamate) for Scientific Research C, the Ministry of Education, Sciences, Sports and Culture, Japan.

## References

1. Albert ML, Sauter B, Bhardwaj N (1998) Dendritic cells acquire antigen from apoptotic cells and induce class I-restricted CTLs. Nature 392:86–89
2. Andreutti D, Gabbiani G, Neuville P (1998) Early granulocyte-macrophage colony-stimulating factor expression by alveolar inflammatory cells during bleomycin-induced rat lung fibrosis. Lab Invest 78:1493–1502
3. Askew D, Burger CJ, Elgert KD (1993) Tumor-induced modulation of macrophage class II MHC molecule mRNA expression. Mol Immunol 30:911–920
4. Bjorck P, Kincade PW (1998) CD19+ pro-B cells can give rise to dendritic cells in vitro. J Immunol 161:5795–5799
5. Boczkowski D, Nair SK, Nam J-H, Lyerly HK Gilboa E (2000) Induction of tumor immunity and cytotoxic T lymphocyte responses using dendritic cells transfected with messenger RNA amplified from tumor cells. Cancer Res 60: 1028–1034
6. Cavanagh LL, Saal RJ, Grimmett KL, Thomas R (1998) Proliferation in monocyte-derived dendritic cell cultures is caused by progenitor cells capable at myeloid differentiation. Blood 92:1598–1607
7. Crawford HC, Matrisian LM, Liaw L (1998) Distinct roles of osteopontin in host defense activity and tumor survival during squamous cell carcinoma progression in vivo. Cancer Res 58: 5206–5215
8. Damoisaux JG, Döpp EA, Calame W, Chao D, Mac-Pherson GG, Dijkstra CD (1994) Rat macrophage lysosomal membrane antigen recognized by monoclonal antibody ED1. Immunology 83:140–147
9. Dijkstra CD, Döpp EA, Joling P, Kraal G (1985) The heterogeneity of mononuclear phagocytes in lymphoid organs: distinct macrophage subpopulations in rat recognized by monoclonal antibodies ED1, ED2 and ED3. Immunology 54:589–599
10. Elgert KD, Alleva DG, Mullins DW (1998) Tumor-induced immune dysfunction: the macrophage connection. J Leukoc Biol 64:275–290
11. Fonseca R, Yamakawa M, Nakamura S, van Heerde P, Miettinen M, Shek TWH, Myhre Jensen O, Rousselet MC, Tefferi A (1998) Follicular dendritic cell sarcoma and interdigitating reticulum cell sarcoma: a review. Am J Hematol 59: 161–167
12. Inaba K, Turley S, Iyoda T, Yamaide F, Shimoyama S, Reis e Sousa D, Germain RN, Mellman I, Steinman RM (2000) The formation of immunogenic major histocompatibility complex class II-peptide ligands in lysosomal compartments of dendritic cells is regulated by inflammatory stimuli. J Exp Med 191: 927–936
13. Katano H, Kaneko K, Shimizu S, Saito T, Irié T, Mori S (1997) Follicular dendritic cell sarcoma complicated by hyaline-vascular type Castleman's disease in a schizophrenic patient. Pathol Int 47:703–706
14. Kato S, Luyckx VA, Ots M, Lee K-W, Ziai F, Troy JL, Brenner BM Mackenzie HS (1999) Renin-angiotensin blockade lowers MCP-1 expression in diabetic rats. Kidney Int 56: 1037–1048
15. Kawashima R, Mochida S, Matsui A, YouLuTuZ Y, Ishikawa K, Toshima K, Yamanobe F, Inao M, Ikeda H, Ohno A, Nagoshi S, Uede T, Fujiwara K (1999) Expression of osteopontin in Kupffer cells and hepatic macrophages and stellate cells in rat liver after carbon tetrachloride intoxication: a possible factor for macrophage migration into hepatic necrotic areas. Biochem Biophys Res Commun 256:527–531
16. Kudo S, Matsuno K, Ezaki T, Ogawa M (1997) A novel migration pathway for rat dendritic cells from the blood: hepatic sinusoids-lymph translocation. J Exp Med 185:777–784
17. Lutz MB, Assmann CU, Girolomoni G, Ricciardi-Castagnoli P (1996) Different cytokines regulate antigen uptake and presentation of a precursor dendritic cell line. Eur J Immunol 26: 586–594
18. Mantovani A, Bottazzi B, Colotta F, Sozzani S, Ruco L (1992) The origin and function of tumor-associated macrophages. Immunol Today 13:265–270
19. Mantovani A, Ming WJ, Balotta C, Abdeljalil B, Bottazzi B (1986) Origin and regulation of tumor-associated macrophages: the role of tumor-derived chemotactic factor. Biochim Biophys Acta 865:59–67
20. Masunaga A, Nakamura H, Katata T, Furubayashi T, Kanayama Y, Yamada A, Shiroko Y, Itoyama S (1997) Follicular dendritic cell tumor with histiocytic characteristics and fibroblastic antigen. Pathol Int 47:707–712
21. Matsuno K, Ezaki T, Kudo S, Uehara Y (1996) A life stage of particle-laden rat dendritic cells in vivo: their terminal division, active phagocytosis, and translocation from the liver to the draining lymph. J Exp Med 183:1865–1878
22. McBride WH (1986) Phenotype and functions of intratumoral macrophages. Biochim Biophys Acta 865:27–41
23. Nagasaki M, Morikawa S, Torii I, Zhang J, Morikawa K (2000) A human B-lineage dendritic cell line, HBM-noda and its potential role in human T-cell leukemia/lymphoma virus type I infection. Pathol Int 50:280–290
24. Nakanishi M, Yamate J, Nakatsuji S, Ide M, Sawamoto O, Kuwamura M, Kotani T, Sakuma S (2002) Establishment of a transplantable tumor line (IP) derived from rat pulmonary carcinoma, developing humoral hypercalcemia of malignancy in IP-bearing rats. Virchows Arch 440:195–204
25. Peri G, Rossi V, Taraboletti G, Erroi A, Mantovani A (1986) Ia antigen expression and IL-1 activity in murine tumour-associated macrophages. Immunology 59:527–533
26. Rescigno M, Winzler C, Delia D, Mutini C, Lutz M, Ricciardi-Castagnoli P (1997) Dendritic cell maturation is required for initiation of the immune response. J Leukoc Biol 61:415–421
27. Romani N, Gruner S, Brang D, Kampgen E, Lenz A, Trochenbacher N, Konwalinka G, Fritsch PO, Steinman RM, Schuler G (1994) Proliferating dendritc cell progenitors in human blood. J Exp Med 180:83–93
28. Sato T (1998) Class II MHC-expressing cells in the rat adrenal gland defined by monoclonal antibodies. Histochem Cell Biol 109:359–367
29. Sato T, Inoue K (2000) Dendritic cells in the rat pituitary gland evaluated by the use of monoclonal antibodies and electron microscopy. Arch Histol Cytol 63:291–303
30. Smith LR, Lundeen KA, Dively JP, Carlo DJ, Brostoff SW (1994) Nucleotide sequence of the Lewis rat granulocyte–macrphage colony stimulating factor. Immunogenetics 39:80

31. Sotomayor EM, Fu Y-X Lopez-Cepero M, Herbert L, Jimenez JJ, Albarracin C, Lopez DM (1991) Role of tumor-derived cytokines on the immune system of mice bearing a mammary adenocarcinoma. J Immunol 147:2816–2823
32. Takahashi K, Naito M, Takeya M (1996) Development and heterogeneity of macrophages and their related cells through their differentiation pathways. Pathol Int 46:473–485
33. Thomson AW Lu L (1999) Are dendritic cells the key to liver transplant tolerance? Immunol Today 20:27–32
34. Tsujino K, Yamate J, Tsukamoto Y, Kumagai D, Kannan Y, Jippo T, Kuwamura M, Kotani T, Takeya M, Sakuma S (1997) Establishment and characterization of cell lines derived from a transplantable rat malignant meningioma: morphological heterogeneity and production of nerve growth factor. Acta Neuropathol 93:461–470
35. Whiteland JL, Nicholls SM, Shimeld C, Easty DL, Williams NA, Hill TJ (1995) Immunohistochemical detection of T-cell subsets and other leukocytes in paraffin-embedded rat and mouse tissues with monoclonal antibodies. J Histochem Cytochem 43:313–320
36. Yamashiro S, Takeya M, Nishi T, Kuratsu J, Yoshimura T, Ushio Y, Takahashi K (1994) Tumor-derived monocyte chemoattractant protein-1 induces intratumoral infiltration of monocyte-derived macrophage subpopulation in transplanted rat tumors. Am J Pathol 145:856–867
37. Yamate J, Tajima M, Togo M, Shibuya K, Ihara M, Kudow S (1991) Heterogeneity of cloned cell lines established from a transplantable rat malignant fibrous histiocytoma. Jpn J Cancer Res 82:298–307
38. Yamate J, Iwaki M, Kumagai D, Tsukamoto Y, Kuwamura M, Nakatsuji S, Tsunenari I, Kotani T, Sakuma S (1997) Characteristics of a rat fibrosarcoma-derived transplantable tumour line (SS) and cultured cell lines (SS-P and SS-A3–1) showing myofibroblastic and histiocytic phenotypes. Virchows Arch 431:431–440
39. Yamate J, Kumagai D, Tsujino K, Nakatsuji S, Kuwamura M, Kotani T, Sakuma S, LaMarre J (1999) Macrophage populations and apoptotic cells in the liver before spontaneous hepatitis in Long-Evans Cinnamon (LEC) rats. J Comp Pathol 120:333–346
40. Yamate J, Kuriyama T, Kawashima M, Nakanishi M, Ide M, Kuwamura M, Tsukamoto Y, Kotani T, Nakatsuji S (2002) Establishment and characterization of transplantable tumor line (KB) and cell lines (KB-P and KB-D8) from a rat thymus-derived dendritic cell sarcoma. Virchows Arch 440:616–626
41. Yamate J, Sato K, Ide M, Nakanishi M, Kuwamura M, Sakuma S, Nakatsuji S (2002) Participation of different macrophage populations and myofibroblastic cells in chronically developed renal interstitial fibrosis after cisplatin-induced renal injury in rats. Vet Pathol 39:322–333
42. Yurochko AD, Burger CJ, Elgert KD (1990) Two-color flow cytometric analysis of the expression of MAC and MHC class II antigens on macrophages during tumor growth. Cytometry 11:725–735

Virchows Arch (2003) 442:151–158
DOI 10.1007/s00428-002-0698-6

ORIGINAL ARTICLE

**Mitsue Sogawa · Takayuki Matsumoto
Hirokazu Yamagami · Tamaki Yamada
Yuriko Ozeki · Ikuya Yano · Yuji Nakajima
Tetsuo Arakawa · Kenji Kaneda**

# A murine model of granulomatous colitis with mesenteric lymphadenitis induced by mycobacterial cord factor

Received: 5 November 2001 / Accepted: 18 June 2002 / Published online: 17 August 2002
© Springer-Verlag 2002

**Abstract** Granulomatous colitis is a major entity of human intestinal diseases. We previously reported that intravenous injection of mycobacterial cord factor (CF), a potent macrophage activator, induced pulmonary granulomas in mice with enhanced production of Th1 cytokines and chemokines. In this study we made a murine model of granulomatous colitis by intramural injection of CF. A single dose of 300 μg CF was injected into the wall of the rat and mouse colon in the form of liposomes. After 1 week granulomas developed at the injection site, extending from the subserosa to the lamina propria, and persisted for longer than 6 weeks. They were composed mainly of ED1-positive macrophages, which often underwent apoptosis, and $CD4^+$ and $CD8^+$ lymphocytes, which preferentially infiltrated around the macrophage accumulation. Myofibroblast proliferation was not prominent, and no appreciable fibrosis resulted after the decline of granulomas. Although the intestinal epithelium was involved in inflammation, tissue injuries such as mucosal erosion or ulceration were not induced. When granulomas were formed near the Peyer's patches, they invaded deeply into the lymphoid tissue, producing many small islands. The mesenteric lymph nodes also had many granulomatous islands in the cortex and medulla, but the liver and spleen displayed no granulomatous changes, suggesting that liposomal CF spreads via the lymphatic vessels from the injection site. The CF-induced colonic granulomas associated with mesenteric lymphadenitis will be useful for investigating human granulomatous colitis.

**Keywords** Granulomatous colitis · Lymphadenitis · Cord factor · Rodents

M. Sogawa (✉) · Y. Ozeki · Y. Nakajima · K. Kaneda
Department of Anatomy,
Osaka City University Graduate School of Medicine,
1-4-3 Asahimachi, Abeno-ku, Osaka 545-8585, Japan
e-mail:.mitsue-s@med.osaka-cu.ac.jp
Tel.: +81-6-66453706, Fax: +81-6-66463603

M. Sogawa · T. Matsumoto · H. Yamagami · T. Arakawa
Department of Gastroenterology,
Osaka City University Graduate School of Medicine,
1-4-3 Asahimachi, Abeno-ku, Osaka 545-8585, Japan

H. Yamagami
Department of Host Defense,
Osaka City University Graduate School of Medicine,
1-4-3 Asahimachi, Abeno-ku, Osaka 545-8585, Japan

T. Yamada
Department of Internal Medicine,
Nagoya City University Graduate School of Medicine,
Nagoya 467-8601, Japan

I. Yano
Institute of BCG, Kiyose-shi, Tokyo 204-0022, Japan

## Introduction

Among human chronic inflammatory disorders in the colon, granulomatous colitis including Crohn's disease and intestinal tuberculosis are especially important because their incidence is increasing in both industrialized and developing countries [10, 17]. These two diseases have common pathological features, i.e., granuloma formation, prominent lymphoid aggregation extending into the submucosa, neutrophil polymorphs infiltration in the pericrypt and lumen, occasional ulcer formation, and association with mesenteric lymphadenitis [8, 17], and they are therefore often difficult to distinguish from each other by endoscopy, radiology, and histology [3, 28, 30] even with some differences in the number and size of granulomas and distribution of chronic inflammation [31]. Although the pathogenesis is not yet fully elucidated, several studies have demonstrated a causal relationship between Crohn's disease and mycobacterial infection [6, 11, 12, 15], suggesting that a common mechanism of granuloma formation is present. To investigate experimentally the pathogenesis of colonic granulomatous inflammation, two useful murine models have been developed, i.e., one induced with trinitrobenzene sulfonic acid (TNBS) [22] and the other with peptidoglycan/polysaccharide (PG/PS) polymers of group A streptococcal cell walls [34, 39]. In addition to these induc-

tive models, spontaneous models including senescence-accelerated mouse (SAM) P1/Yit [18] are known.

In a series of our previous studies we demonstrated that mycolic acid containing glycolipids, a cell wall component characteristic of mycobacteria and related taxa, are capable of inducing granuloma formation [14, 27, 40, 41] with enhanced production of Th1-differentiation cytokines such as interleukin (IL)-12 [26, 40], Th1 cytokines including IL-1β [40, 42], interferon (IFN)-γ [9, 40], granulocyte-macrophage colony-stimulating factor [42], and tumor necrosis factor (TNF)-α [40], chemokines such as monocyte chemotactic protein-1 [40] and macrophage inflammatory protein-1α, and vascular endothelial growth factor [33] through activation of macrophages and neutrophils, being associated with induction of accelerated T-cell apoptosis in the thymus [27]. They also function as antigens that evoke both humoral [7, 29] and cell-mediated immune responses [40]. Mycobacterial trehalose 6,6′-dimycolate, or cord factor (CF), is the most potent agent among these and transiently induces extensive granulomatous inflammation in the murine lung, liver, and spleen with the peak at 1 week, 3 weeks, and 3 weeks, respectively, after an intravenous injection via the tail vein in the form of micelles or liposomes [27, 40]. Granulomas, however, are not formed in the colon by this procedure probably because micelles or liposomes of the sizes small enough to pass through the pulmonary capillaries are unlikely to be entrapped by the intestinal capillaries, different from the hepatic sinusoids and splenic red pulp, both of which contain macrophages within them.

In this study, for the purpose of making a new murine model of granulomatous colitis, we intramurally injected purified mycobacterial CF in the rat and mouse colon, and investigated the pathological characteristics of the granulomas generated in the colon and mesenteric lymph nodes.

## Materials and methods

### Animals

Twenty-six, specific pathogen-free male Wistar rats (6 weeks) and eighteen, specific pathogen-free female BALB/c mice (8 weeks) were purchased from SLC (Shizuoka, Japan). They were housed under constant conditions and fed of standard chow pellet and water ad libitum. Experiments were performed in accordance with the standard guidelines for animal experiments of the Osaka City University Graduate School of Medicine.

### Preparation of CF

Mycobacterial CF was isolated and purified from *Mycobacterium tuberculosis* Aoyama B as previously described [40]. Briefly, mycobacteria were cultivated in Sauton medium for 5–6 weeks at 38°C. Bacteria were autoclaved at 121°C for 30 min and harvested. Lipids were serially extracted with chloroform-methanol (4:1 vol/vol), chloroform-methanol (3:1 vol/vol) and chloroform-methanol (2:1 vol/vol). A fraction of CF was purified by developing the lipids on a thin-layer plate of silica gel with chloroform-methanol-acetone-acetic acid (90:10:6:1 vol/vol/vol/vol) and subsequently with chloroform-methanol-water (90:10:1 vol/vol/vol). This procedure was repeated until a single spot was ultimately obtained on a thin-layer plate.

### Preparation of liposomes

Liposomes were prepared as previously described [27]. The mixture of CF, dipalmitoyl phosphatidylcholine, and dicetyl phosphate (Sigma, St. Louis, Mo., USA) (1:9:0.1 mol/mol/mol) were dissolved in chloroform, and evaporated and dried overnight. After phosphate-buffered saline was added, the suspension was sonicated for 4 min at 60°C. For the control CF-free liposomes were prepared.

### Treatment of animals

Under ether anesthesia the distal colon was exposed by laparotomy. With the procedure previously described [39], 300 μg CF in the form of liposomes or liposomes alone as the control was intramurally injected into the distal colon of rats and mice, using a 29-gauge needle. Ten rats and six mice were used for each CF-treated and control groups. Each five rats and three mice were killed 1 and 3 weeks after administration. Three untreated rats and three untreated mice were also killed at the same time intervals.

### Organ weight

At 1 and 3 weeks after injection, distal colons were taken out and weighed. The colon weight per unit length (g/cm) was then calculated. The liver and spleen were also weighed and their organ indices were calculated as follows: organ index=organ weight (g)/body weight (g) ×100.

### Histology

A part of the colon and the mesenteric lymph node were fixed in 10% formalin, dehydrated, and embedded in paraffin. Sections were stained with hematoxylin and eosin (H-E) and observed by light microscopy. For immunohistochemistry rat colons were used. As previously described [23], another part of the colon was immersion-fixed in a periodate-lysine 2% paraformaldehyde solution overnight at 4°C. After the successive transfer in 8–20% sucrose in 0.1 M phosphate buffer, pH 7.4, tissues were frozen in liquid nitrogen. Cryosections were cut by a CM3050 cryostat (Leica Instruments, Nussloch, Germany). To block endogenous peroxidase activity they were treated with 0.3% hydrogen peroxide in methanol. After washing with phosphate-buffered solution, they were treated with 5% fetal bovine serum for 1 h at room temperature to block nonspecific reactions. They were then incubated with mouse anti-rat ED-1 monoclonal antibody (mAb; 1:300 dilution; Phar Mingen, SanDiego, Calif., USA), mouse anti-rat CD4 mAb (1:1,000 dilution, Serotec, Oxford, UK), mouse anti-rat CD8 mAb (1:1,000 dilution, Serotec), and mouse anti-human α-smooth muscle actin (α-SMA) mAb (1:750 dilution; Dako, Carpinteria, Calif., USA), which cross-reacts with rat antigens, overnight at room temperature. After washing the sections were incubated with biotinylated rabbit anti-mouse immunoglobulin G antibody (1:500 dilution; Dako) for 1 h at room temperature, followed by incubation with horseradish peroxidase-labeled streptoavidin (LSAB kit, Dako) for 1 h at room temperature. Reaction products were visualized by treating sections with 0.2 mg/ml 3,3′-diaminobenzidine tetrahydrochloride in 0.05 M Tris-buffered saline, pH 7.4, in the presence of 0.003% hydrogen peroxide for 3–5 min. Counterstaining for nuclei was performed with methyl green.

### Statistic analysis

Data were expressed as the mean ±standard deviation and analyzed with a Power Macintosh G3 using Stat View 5.0 (SAS Institute, Cary, N.C., USA). The data which appeared to be statistically significant were compared by the analysis of variance for comparing the means of multiple groups and were considered significant if $P$ values were less than 0.05.

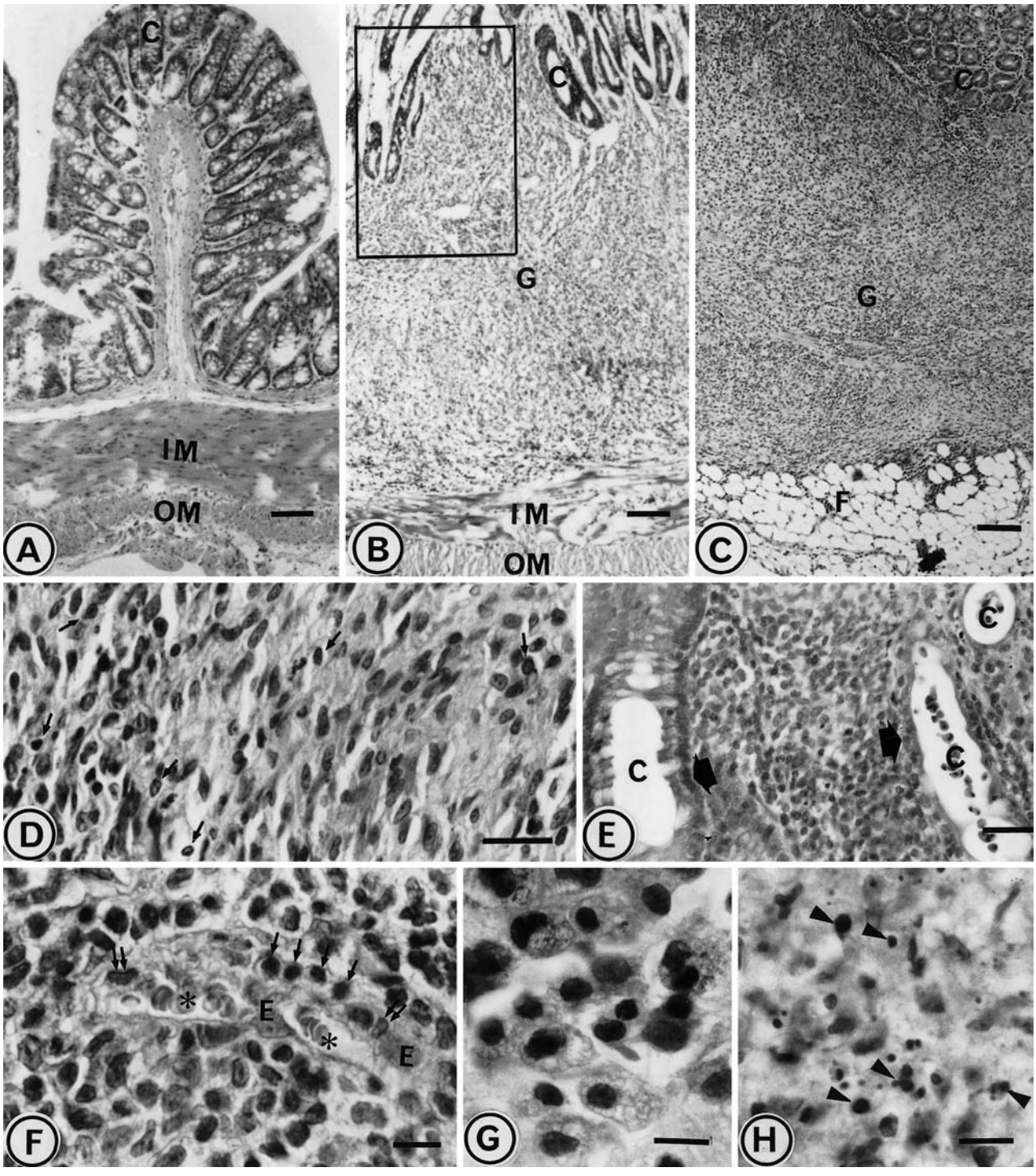



**Fig. 1A–H** **A** The rat colon 3 weeks after an intramural injection of liposomes alone. Histology is almost normal. *IM* Inner muscular layer; *OM* outer muscular layer; *C* crypts. **B** The rat colon 3 weeks after an intramural injection of liposomal CF. The granuloma (*G*) occupies the submucosa, and further extends toward the lamina propria around the crypts (*C*). *IM* Inner muscular layer; *OM* outer muscular layer. **C** The mouse colon 3 weeks after an injection of liposomal CF. The granuloma (*G*) develops in the submucosa and lamina propria. The muscular layer is obscure due to a prominent cell infiltration among muscle cells. Fatty deposits (*F*) are seen beneath the serosa. *C* Crypts. **D**–H The rat colon 1 week after an injection of liposomal CF. **D** Higher magnification of the granuloma. The granuloma is mainly consisted of macrophages and lymphocytes (*small arrows*). **E** The right crypt (*C*) adjacent to the granuloma contains the neutrophil remnants in the lumen. The epithelium (*large arrow*) of the right crypt became thinner than that (*large arrow*) of the left crypt (*C*). **F** A venule involved within the granuloma displays some lymphocytes (*double arrows*) adhering to the endothelium (*E*). Some lymphocytes (*small arrows*) migrate out of the vessel. *Asterisks* Lumen of the venule. **G** Macrophages in the central portion of the granuloma exhibit a foamy appearance probably by incorporating liposomes. **H** In the granuloma, apoptotic bodies (*arrowheads*) are frequently seen among infiltrating macrophages. **A** ×70; *bar* 100 μm. **B** ×70; *bar* 100 μm. **C** ×70; *bar* 100 μm. **D** ×530; *bar* 20 μm. **E** ×260; *bar* 30 μm. **F** ×700; *bar* 10 μm. **G** ×830; *bar* 10 μm. **H** ×830; *bar* 10 μm. H-E staining

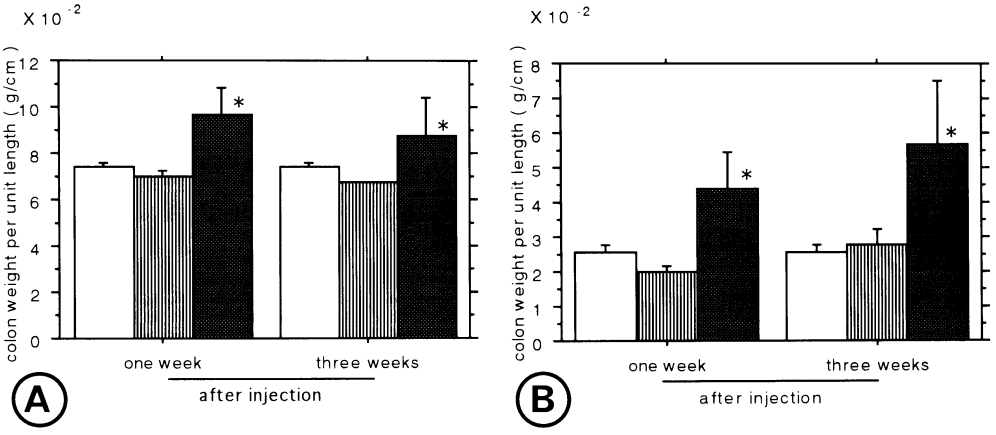



**Fig. 2A, B** The colon weight per unit length (g/cm) in untreated (*open column*), liposome alone-treated (*shaded column*) and liposomal CF-treated *(solid column*) animals 1 and 3 weeks after intramural injection. **A** Rats. **B** Mice. The value represents the mean ±SD. $n$=3–5 animals. *$P$<0.05 vs. the value of liposome alone-treated animals

## Results

At 1 and 3 weeks after intramural injection, the abdomen was opened under anesthesia. Due to extensive adhesion of the serosa to the surrounding tissue the outer surface of the treated colon was often difficult to be discerned macroscopically. By touching, however, the colonic wall was obviously thickened. The typical appearance of the "fat wrapping" previously described as the characteristic feature of human Crohn's disease [35] was not detected, although small fat deposits were sometimes seen. The mucosal surface showed no appreciable changes of ulcer and cobble-stone appearance.

In H-E stained sections granulomas were formed in the colonic wall after 1 and 3 weeks with no differences in architecture between these two times. Granuloma formation was induced in 10/10 (100%) CF-treated rats (Fig. 1B) and 6/6 (100%) CF-treated mice (Fig. 1C) but was in 0/10 (0%) control rats (Fig. 1A) and 0/6 (0%) control mice. Granulomas extended from the subserosa to the lamina propria in CF-treated rats and mice. They then gradually decreased in size, persisting until at 6 weeks to some extent. Fibrotic changes were not obvious after the regression of granulomas at 4 months. Consistent with these histological results, the colon weights per unit length in CF-treated rats (Fig. 2A) and mice (Fig. 2B) were significantly larger than those in control animals after both 1 and 3 weeks. In the liver and spleen, on the other hand, no significant increases in the organ index were found both after either 1 or 3 weeks. Histology confirmed that no granulomatous changes were induced in these organs (data not shown).

At higher magnifications, granulomas were seen to be composed mainly of macrophages and lymphocytes (Fig. 1D). Multinucleated giant cells were rarely seen. Neutrophils were scattered throughout the granuloma. The epithelium of the crypts adjacent to the granuloma was considerably attenuated and further infiltrated of neutrophil polymorphs (Fig. 1E). Neutrophils penetrated the epithelium and accumulated in the lumen of the crypt, indicating that the inflammation involved the epithelium. Lymphocytes were distributed among the macrophages. In the venules of the granuloma they were attached to the endothelial cells and subsequently migrated into the subendothelial spaces (Fig. 1F). Macrophages located in the central portion of the granuloma often gave a foamlike appearance probably due to incorporation of liposomes (Fig. 1G), while those in the periphery did not. Apoptotic bodies were frequently found among the macrophage infiltrate (Fig. 1H).

By immunohistochemistry many ED-1-positive macrophages were seen to be aggregated to constitute a major part of the granuloma (Fig. 3C). $CD4^+$ (Fig. 3A) and $CD8^+$ (Fig. 3B) lymphocytes representative of helper T (Th) cells and cytotoxic T (Tc) cells, respectively, were also abundant, being preferentially located around the macrophage accumulation. $\alpha$-$SMA^+$ cells representative of myofibroblasts and perivascular smooth muscle cells were less frequent within the macrophage accumulation than in the periphery (Fig. 3D).

When the granuloma was formed near the Peyer's patches, it extended deeply into the lymphoid tissue, generating many small islands (Fig. 4A, B), which consisted mainly of macrophages and lymphocytes (Fig. 4D). The mesenteric lymph nodes were macroscopically swollen and included many small granulomatous islands which were distributed both in the cortex and the medulla (Fig. 4C). The profile of the granuloma in the lymph nodes (Fig. 4E) was similar to that seen in the Peyer's patches.

## Discussion

This study demonstrates that an intramural injection of mycobacterial CF in the form of liposomes is capable of inducing granulomatous colitis in the rats and mice. Different from the granuloma formation in the lung, liver, and spleen after intravenous injection of CF [14, 27, 40, 41], the present colonic granulomas were formed only at the injection site due to the procedure of intramural injection. Colonic granulomas developed 1–3 weeks after injection in a kinetics similar to that of CF-induced hepatic and splenic granulomas in previous studies [27,

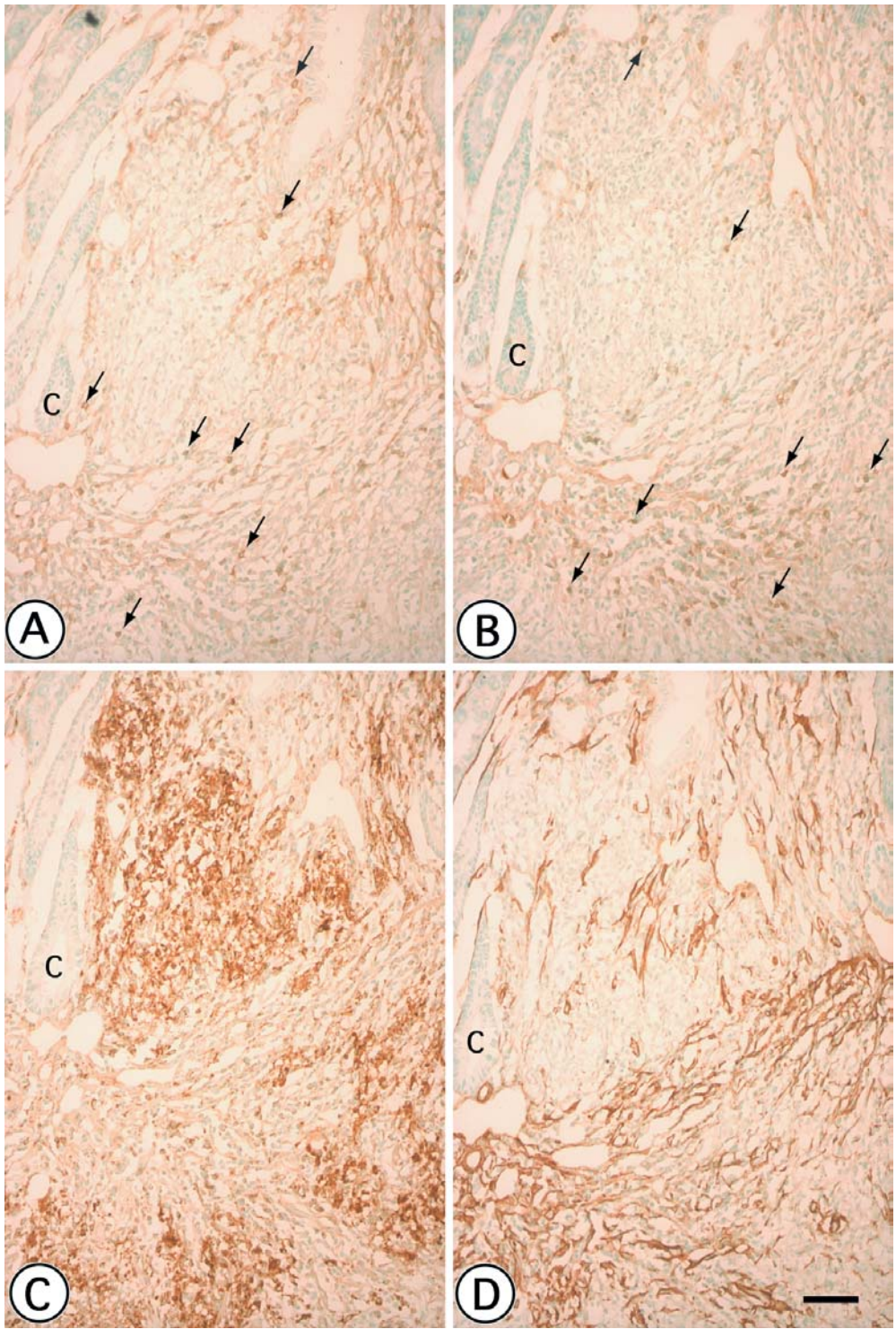



**Fig. 3** Serial sections of CF-induced granulomas in the rat colon at 3 weeks were immunohistochemically stained for CD4 (**A**), CD8 (**B**), ED-1 (**C**), and αSMA (**D**). This is the same portion as indicated by a *rectangle* in Fig. 1B. Many $CD4^+$ and $CD8^+$ cells (*arrows*) are found around the accumulation of ED-1 positive cells. $\alpha SMA^+$ cells representative of pericytes or myofibroblasts were not frequent in the macrophage accumulation. *C* Crypts. **A–D** ×180; *bar* 40 μm

40]. The fact that colonic granulomas were formed as early as at 1 week and persisted as long as 6 weeks suggests that they might develop as a foreign body type of granuloma in an initial stage, but that immune reactions might be involved at later stages [7, 29, 40].

As revealed in H-E stained and immunostained sections, granulomas consisted mainly of macrophages and lymphocytes. The macrophages located in the central portion of the granulomas contained abundant liposomes in the cytoplasm, as represented by foamy appearance, while those accumulated around the foamy cells were not vacuolated, indicating that, after resident macrophages phagocytosed liposomal CF and accumulated at the injection site, newly recruited macrophages from the circulation were added around them. Apoptotic figures were frequently observed in infiltrating macrophages

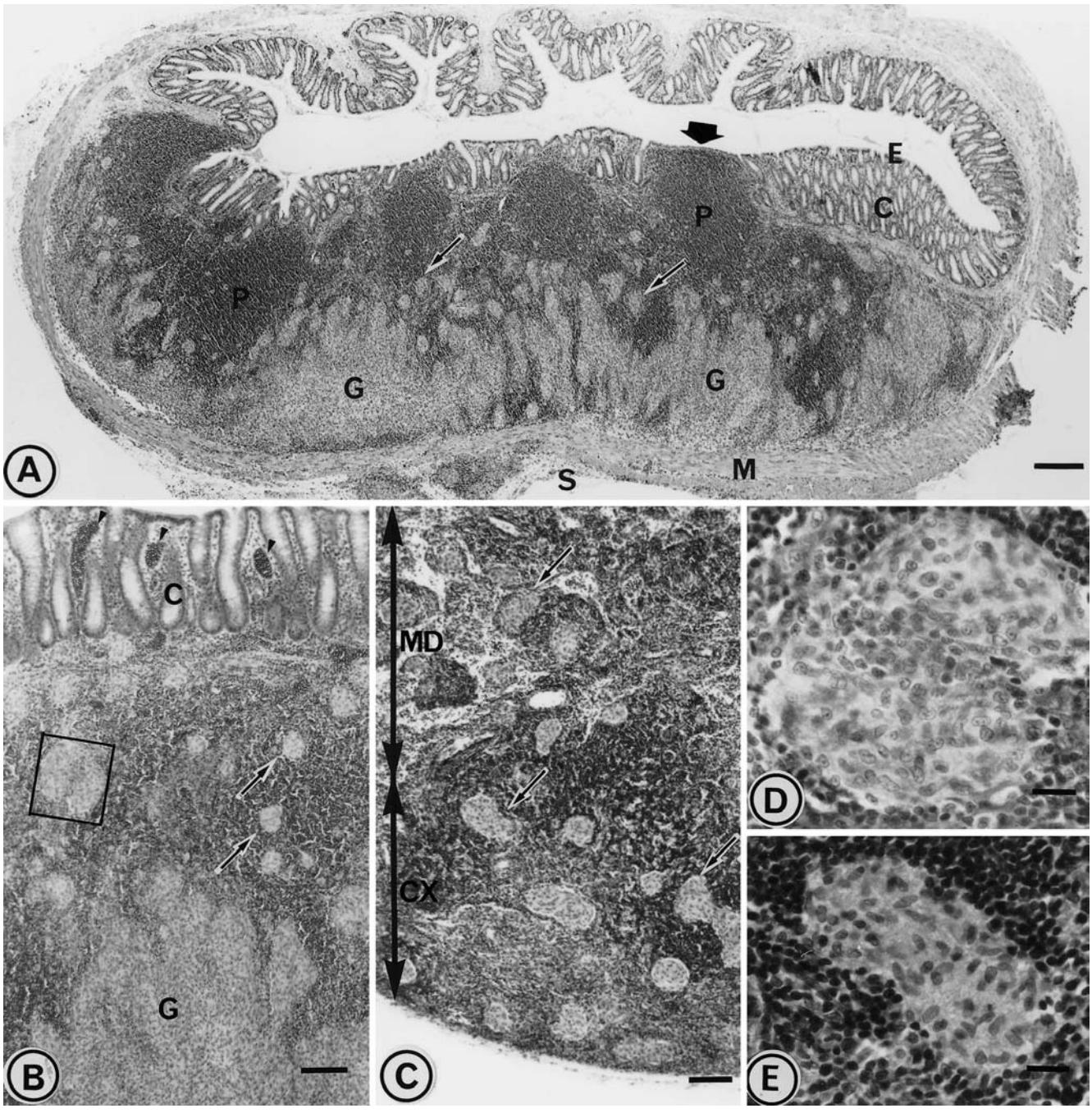



**Fig. 4A–E** **A** Granulomas (*G*) developing near the Peyer's patches (*P*) in the rat colon at 3 weeks after liposomal CF injection. They extend into the lymphoid tissues, forming small islands (*small arrows*). *Large arrow* Follicle-associated epithelium; *S* serosa; *M* muscular layer; *C* crypts; *E* epithelium. **B** Higher magnification of the granulomas (*G*) in the lymphoid tissue of the Peyer's patches. *Small arrows* Small granulomatous islands. The lymphatic vessels in the lamina propria include many lymphocytes (*arrowheads*). *C* Crypts. **C** Granuloma formation in the mesenteric lymph nodes. Granulomatous islands (*arrows*) are distributed both in the cortex (*CX*) and the medulla (*MD*). **D** Higher magnification of a rectangular portion of **B**. The granuloma in the Peyer's patches mainly consists of macrophages and lymphocytes. **E** Higher magnification of the granuloma in the mesenteric lymph nodes. Macrophages and lymphocytes are the predominant populations of the granuloma. **A** ×35; *bar* 200 μm. **B** ×70; *bar* 100 μm. **C** ×70; *bar* 100 μm. **D** ×330; *bar* 20 μm. **E** ×330; *bar* 20 μm. H-E staining

consistent with a previous report on bacille Calmette-Guérin induced hepatic granulomas [19]. This event seems to represent a balance between the influx of newly recruited macrophages and apoptotic elimination of granuloma macrophages in the maintenance and resolution of granulomas [19]. Many $CD4^+$ cells (Th cells) and $CD8^+$ cells (Tc cells) were also distributed in the granulomas, preferentially in the periphery of them. It has been demonstrated that IL-12, which induces the differentiation of Th1 cells from naive Th cells, and several Th1 cytokines such as IL-1β, TNF-α, and IFN-γ are generated by CF-induced pulmonary granulomas in both nonimmunized and CF-immunized mice, indicating that CF-induced granulomas are formed based on Th1 re-

sponses [40]. In Crohn's disease mucosal Th cells are involved in the progression of inflammation [37], and granuloma formation is related to Th1 responses [4, 13]. CF-induced colonic garnulomas are thus likely to be useful for analyzing the pathogenesis of Crohn's disease. Activation of myofibroblasts as represented by α-SMA expression was not appreciable within the granuloma, and in accordance with this finding fibrotic changes did not occur after the regression of granuloma. Similar results have been reported in *Propionibacterium acnes* induced hepatic granuloma, which transiently developed and diminished without leaving fibrosis [36].

Tissue damages such as mucosal erosion and ulceration are often encountered in human granulomatous colitis. Such figures, however, were not detected in the present model. This finding is consistent with the previous observation that CF-induced pulmonary and hepatic granulomas does not cause any parenchymal or epithelial destruction [14]. Although CF has both TNF-α priming [24] and TNF-α inducing [40] functions, it produces much less TNF-α than lipopolysaccharide (LPS) [27]. It has been suspected that an impairment of innate immune response to LPS is involved in the development of Crohn's disease from the association of NOD2, a gene product which activates nuclear factor κB with this disease [25]. This view is supported by the fact that LPS derived from the enterobacterium enhances the production of proinflammatory cytokines which induce increased permeability of the mucosa, as has been reported in Crohn's disease [38]. On the hypothesis that concomitant LPS would induce mucosal erosion in the present model, we intravenously injected 10 μg LPS into the rats bearing CF-induced colonic granulomas. However, no mucosal erosion was induced in the colon (data not shown).

Several murine models for enterocolitis have been developed. These are divided into two categories: (a) inductive models: TNBS-induced [22] and PG/PS-induced [34, 39] models, and (b) spontaneous models: a SAMP1/Yit model [18] and gene-targeted disruption of IL-2 [32], IL-10 [16], class II major histocompatibility complex [1], or T cell receptor α and β [20]. The present model is a new inductive model for granulomatous colitis, having several differences from previous two models; a TNBS model needs intraluminal ethanol application for the break of the epithelial barrier and does not require IFN-γ for the development of colitis [5]; a PG/PS model includes prominent neutrophil accumulation in the central portion of the granulomas in addition to macrophage infiltration and induces systemic inflammation involving splenic and hepatic granuloma formation, lymphadenitis, and arthritis [39]. In the present model granulomas were formed in the colon and mesenteric lymph nodes but not in the liver and spleen, indicating that CF-induced granulomatous inflammation is restricted to the injection site of the colon and the regional lymph nodes. Furthermore, colonic granulomas formed near the Peyer's patches extended deeply into the lymphoid tissues, making many small granulomatous islands within them. Since the lymphatic vessels are closely associated with colonic granulomas [21], lipophilic substances such as CF may easily enter the lymphatic vessels and spread in the lymphoid tissue of the Peyer's patches and regional lymph nodes. Lymphadenitis is a common feature seen in patients with intestinal tuberculosis [2] and Crohn's disease [8], and therefore the present model has good resemblance to these human granulomatous colonic diseases.

In conclusion, CF-induced granulomatous inflammation in the colon presumably as a Th1 murine model will be useful for investigating the pathogenesis of human granulomatous colitis.

## References


1. Aiko S, Grisham MB (1995) Spontaneous intestinal inflammation and nitric oxide metabolism in HLA-B27 transgenic rats. Gastroenterology 109:142–150
2. Akinoglu A, Bilgin I (1988) Tuberculous enteritis and peritonitis. Can J Surg 31:55–58
3. Arnold C, Moradpour D, Blum HE (1998) Tuberculous colitis mimicking Crohn's disease. Am J Gastroenterol 93:2294–2296
4. Berrebi D, Banerjee A, Paris R, Potet F, Aigrain Y, Emilie D, Cezard JP, Hugot JP, Navarro J, Peuchmaur M (1997) In situ Rantes and interferon-gamma gene expression in pediatric small bowel Crohn's disease. J Pediatr Gastroenterol Nutr 25:371–376
5. Camoglio L, te Velde AA, de Boer A, ten Kate FJ, Kopf M, van Deventer SJ (2000) Hapten-induced colitis associated with maintained Th1 and inflammatory responses in IFN-gamma receptor-deficient mice. Eur J Immunol 30:1486–1495
6. Cohavy O, Harth G, Horwitz M, Eggena M, Landers C, Sutton C, Targan SR, Braun J (1999) Identification of a novel mycobacterial histone H1 homologue (HupB) as an antigenic target of pANCA monoclonal antibody and serum immunoglobulin A from patients with Crohn's disease. Infect Immun 67:6510–6517
7. Fujiwara N, Pan J, Enomoto K, Terano Y, Honda T, Yano I (1999) Production and partial characterization of anti-cord factor (trehalose-6:6'-dimycolate) IgG antibody in rabbits recognizing mycolic acid subclasses of *Mycobacterium tuberculosis* or *Mycobacterium avium*. FEMS Immunol Med Microbiol 24:141–149
8. Geboes K, van den Oord J, De Wolf-Peeters C, Desmet V, Rutgeerts P, Janssens J, Vantrappen G, Penninckx F, Kerremans R (1986) The cellular composition of granulomas in mesenteric lymph nodes from patients with Crohn's disease. Virchows Arch A Pathol Anat Histopathol 409:679–692
9. Guillemard E, Geniteau-Legendre M, Kergot G, Lemaire G, Gessani S, Labarre C, Quero AM (1998) Simultaneous production of IFN-gamma, IFN-alpha/beta and nitric oxide in peritoneal macrophages from TDM-treated mice. J Biol Regul Homeost Agents 12:106–111
10. Horvath KD, Whelan RL (1998) Intestinal tuberculosis: return of an old disease. Am J Gastroenterol 93:692–696
11. Hubbard J, Surawics CM (1999) Etiological role of mycobacterium in Crohn's disease: an assessment of the literature. Dig Dis 17:6–13
12. Hulten K, Almashhrawi A, El-Zaatari FA, Graham DY (2000) Antibacterial therapy for Crohn's disease: a review emphasizing therapy directed against mycobacteria. Dig Dis Sci 45:445–456
13. Kakazu T, Hara J, Matsumoto T, Nakamura S, Oshitani N, Arakawa T, Kitano A, Nakatani K, Kinjo F, Kuroki T (1999) Type 1 T-helper cell predominance in granulomas of Crohn's disease. Am J Gastroenterol 94:2149–2155

14. Kaneda K, Sumi Y, Kurano F, Kato Y, Yano I (1986) Granuloma formation and hemopoiesis induced by C36–48-mycolic acid-containing glycolipids from *Nocardia rubra*. Infect Immun 54:869–875
15. Kobayashi K, Brown WR, Brennan PJ, Blaser MJ (1988) Serum antibodies to mycobacterial antigens in active Crohn's disease. Gastroenterology 94:1404–1411
16. Kühn R, Löhler J, Rennick D, Rajewsky K, Müller W (1993) Interleukin 10-deficient mice develop chronic enterocolitits. Cell 75:263–274
17. Mathan MM, Gilmour HM, Whitehead R (1995) The large intestine. In: Whitehead R (ed) Gastrointestinal and oesophageal pathology, 2nd edn. Churchill Livingstone, Edinburgh. pp 589–632
18. Matsumoto S, Okabe Y, Setoyama H, Takayama K, Ohtsuka J, Funahashi H, Imaoke A, Okada Y, Umesaki Y (1998) Inflammatory bowel disease-like enteritis and caecitis in a senescence accelerated mouse P1/Yit strain. Gut 43:71–78
19. Matsunaga K, Ito M (2000) Quantitative analysis of apoptotic cell death in granulomatous inflammation induced by intravenous challenge with *Cryptococcus neoformans* and bacillus Calmette-Guérin vaccine. Pathol Int 50:206–218
20. Mombaerts P, Mizoguchi E, Grusby MJ, Glimcher LH, Bhan AK, Tonegawa S (1993) Spontaneous development of inflammatory bowel disease in T cell receptor mutant mice. Cell 75:275–282
21. Mooney EE, Walker J, Hourihane DO (1995) Relation of granulomas to lymphatic vessels in Crohn's disease. J Clin Pathol 48:335–338
22. Morris GP, Beck PL, Herridge MS, Depew WT, Szewczuk MR, Wallace JL (1989) Hapten-induced model of chronic inflammation and ulceration in the rat colon. Gastroenterology 96:795–803
23. Nakatani K, Seki S, Kawada N, Kaneda K (2002) Expression of SPARC (secreted protein, acidic and rich in cysteine osteonectin) by activated hepatic stellate cells and its correlation with the stages of fibrogenesis in human chronic hepatitis. Virchows Arch (in press)
24. Natsuhara Y, Oka S, Kaneda K, Kato Y, Yano I (1990) Parallel antitumor, granuloma-forming and tumor-necrosis-factor-priming activities of mycoloyl glycolipids from *Nocardia rubra* that differ in carbohydrate moiety: structure-activity relationships. Cancer Immunol Immunother 31:99–106
25. Ogura Y, Bonnen DK, Hanauer SB, Nunez G, Cho JH (2001) A frameshift mutation in NOD2 associated with susceptibility to Crohn's disease. Nature 31:603–606
26. Oswald IP, Dozois CM, Petit J-F, Lemaire G (1997) Interleukin-12 synthesis is a required step in trehalose dimycolate-induced activation of mouse peritoneal macrophages. Infect Immun 65:1364–1369
27. Ozeki Y, Kaneda K, Fujiwara N, Morimoto M, Oka S, Yano I (1997) In vivo induction of apoptosis in the thymus by administration of mycobacterial cord factor (trehalose 6:6'-dimycolate). Infect Immun 65:1793–1799
28. Palnaes-Hanson C, Hegnhoj J, Moller A, Brauer C, Hage E, Jarnum S (1990) Ulcerative colitis and Crohn's disease of the colon: is there a macroscopic difference? Ann Chir Gynaecol 79:78–81
29. Pan J, Fujiwara N, Oka S, Maekura R, Ogura T, Yano I (1999) Anti-cord factor (trehalose 6:6'-dimycolate) IgG antibody in tuberculosis patients recognizes mycolic acid subclasses. Microbiol Immunol 43:863–869
30. Price AB (1978) Overlap in the spectrum of non-specific inflammatory bowel disease – 'colitis indeterminate'. J Clin Pathol 31:567–577
31. Pulimood AB, Ramakrishna BS, Kurian G, Peter S, Patra S, Mathan VI, Mathan MM (1999) Endoscopic mucosal biopsies are useful in distinguishing granulomatous colitis due to Crohn's disease from tuberculosis. Gut 45:537–541
32. Sadlack B, Merz H, Schorle H, Schimpl A, Feller AC, Horak I (1993) Ulcerative colitis-like disease in mice with a disrupted interleukin-2 gene. Cell 75:253–261
33. Sakaguchi I, Ikeda N, Nakayama M, Kato Y, Yano I, Kaneda K (2000) Trehalose 6:6'-dimycolate (cord factor) enhances neovascularization through vascular endothelial growth factor production by neutrophils and macrophages. Infect Immun 68:2043–2052
34. Sartor RB, Cromartie WJ, Powell DW, Schwab JH (1985) Granulomatous enterocolitis induced in rats by purified bacterial cell wall fragments. Gastroenterology 89:587–595
35. Sheehan AL, Warren BF, Gear MWL, Shepherd NA (1992) Fat-wrapping in Crohn's disease: pathological basis and relevance to surgical practice. Br J Surg 79:955–958
36. Tsuji H, Mukaida N, Harada A, Kaneko S, Matsushita E, Nakanuma Y. Tsutsui H, Okamura H, Nakanishi K, Tagawa Y, Iwakura Y, Kobayashi K, Matsushima T (1999) Alleviation of lipopolysaccharide-induced acute liver injury in *Propionibacterium acnes*-primed IFN-gamma-deficient mice by a concomitant reduction of TNF-alpha, IL-12, and IL-18 production. J Immunol 162:1049–1055
37. Watanabe M, Takaishi H, Hosoda Y, Ezaki T, Yajima T, Inoue N, Ueno Y, Iwao Y, Ishii H, Ishikawa H, et al (1995) CD4+ intestinal mucosal lymphocytes in the pathogenesis of Crohn's disease. J Gastroenterol 30 Suppl8:73–75
38. Wyatt J, Oberhuber G, Pongratz S, Puspok A, Moser G, Novacek G, Lochs H, Vogelsang H (1997) Increased gastric and intestinal permeability in patients with Crohn's disease. Am J Gastroenterol 92:1891–1896
39. Yamada T, Sartor RB, Marshall S, Specian RD, Grisham MB (1993) Mucosal injury and inflammation in a model of chronic granulomatous colitis in rats. Gastroenterology 104:759–771
40. Yamagami H, Matsumoto T, Fujiwara N, Arakawa T, Kaneda K, Yano I, Kobayashi K (2001) Trehalose 6:6'-dimycolate (cord factor) of *Mycobacterium tuberculosis* induces foreign-body- and hypersensitivity-type granulomas in mice. Infect Immun 69:810–815
41. Yano I, Tomiyasu I, Kitabatake S, Kaneda K (1984) Granuloma forming activity of mycolic acid-containing glycolipids in nocardia and related taxa. Acta Leprol 2:341–349
42. Yano I, Oka S, Natsuhara Y, Kato Y, Tomiyasu I, Kaneda K (1988) Molecular structure and immunopharmacological activities of the new glycolipids containing mycolic acids in actinomycetales. In: Okami Y, Beppu T, Ogawara H (eds) Biology of actinomycetes. Japan Scientific Societies, Tokyo, pp 469–477

Virchows Arch (2003) 442:159–162
DOI 10.1007/s00428-002-0719-5

TECHNICAL REPORT

**Kaoru Inoue · Yosuke Sakurada · Masaru Murakami
Mariko Shirota · Kinji Shirota**

# Detection of gene expression of vascular endothelial growth factor and flk-1 in the renal glomeruli of the normal rat kidney using the laser microdissection system

Received: 25 June 2002 / Accepted: 4 September 2002 / Published online: 29 October 2002
© Springer-Verlag 2002

**Abstract** The recent development of the laser microdissection (LMD) technique enables one to target particular tissues or cells for gene or protein analyses. The purpose of this study was to detect local mRNA expression of vascular endothelial growth factor (VEGF) and its receptor, flk-1, in the glomeruli of normal rat kidneys using the LMD system. Frozen sections of the kidney of 8-week-old male Wistar rats were made. The glomeruli were dissected from the frozen sections with the LMD system, and total RNA was extracted from 200 glomeruli in each kidney. Reverse-transcription polymerase chain reaction (RT-PCR) revealed the local mRNA expression of three isoforms of VEGF, flk-1 and GAPDH in the glomeruli. Moreover, the real-time PCR was performed to evaluate the experimental condition for quantification of VEGF and flk-1 mRNA expression using this system, and the results showed that at least 10 glomeruli might be needed for quantifying local VEGF mRNA expression. However, cDNA from 200 glomeruli was not enough for quantitative evaluation of flk-1 mRNA with this system. These results demonstrate the reproducibility of the analysis of mRNA expression in the renal glomeruli using the LMD system and also suggest that the application of the LMD technique will provide information to further our understanding of the mechanisms involved in kidney diseases.

**Keywords** VEGF · flk-1 · Glomeruli · Laser · Microdissection

K. Inoue · Y. Sakurada · K. Shirota (✉)
Research Institute of Biosciences, Azabu University,
1-17-71 Fuchinobe, Sagamihara, Kanagawa, 229-8501, Japan
e-mail: shirota@azabu-u.ac.jp
Tel.: +81-42-7692093, Fax: +81-42-7692093

M. Murakami
Laboratory of Molecular Biology, School of Veterinary Medicine,
Azabu University, Sagamihara, Japan

M. Shirota
Hatano Research Institute of Food and Drug Safety Center,
Hadano, Kanagawa, Japan

## Introduction

Vascular endothelial growth factor (VEGF) is a growth factor that has significant roles in angiogenesis, tumor growth and development [3]. It is composed of a group of at least five different molecular species in humans, designated as follows: $VEGF_{121}$, $VEGF_{145}$, $VEGF_{165}$, $VEGF_{189}$ and $VEGF_{206}$ [3]. In rats, VEGF is also composed of a group of three isoforms, designated $VEGF_{120}$, $VEGF_{164}$ and $VEGF_{188}$, which are equivalent to $VEGF_{121}$, $VEGF_{165}$ and $VEGF_{189}$ in humans, respectively [11]. There are two specific high-affinity VEGF receptors, flt-1 and KDR/flk-1, which are located on vascular endothelial cells, induce endothelial cell proliferation and increase vascular permeability to macromolecules [3]. In the renal glomeruli, VEGF is produced by podocytes in normal and diseased kidneys, activated mesangial cells, infiltrating leukocytes [2, 4, 5, 14, 15, 17] and endothelial cells in vitro [18]. The receptor flk-1 is expressed on normal, damaged and regenerating glomerular endothelial cells [10] as well as mesangial cells [17].

The analysis of the gene expression of the VEGF and its receptors in the glomeruli is important for understanding the mechanisms of glomerular diseases and for establishing the new therapeutic strategies. With the in situ hybridization technique, specific gene expression can be localized in tissues with high resolution, but the quantitative evaluation of the gene expression is difficult. However, the sieving method has been used to isolate the renal glomeruli; although, other renal tissues, especially cortical tubules sometimes contaminate the isolated specimens, and degradation of the RNA of the glomeruli may occur during the procedures.

The recent development of the laser microdissection (LMD) system enables one to collect pure single cells or specific parts from tissue sections for RNA analysis [6, 7, 12]. The mRNA expression of some factors such as transforming growth factor-β (TGF-β) in the renal glomeruli from experimental animals and human patients has been examined using some LMD systems [6, 12]. The combination of the LMD technique and quantitative reverse-

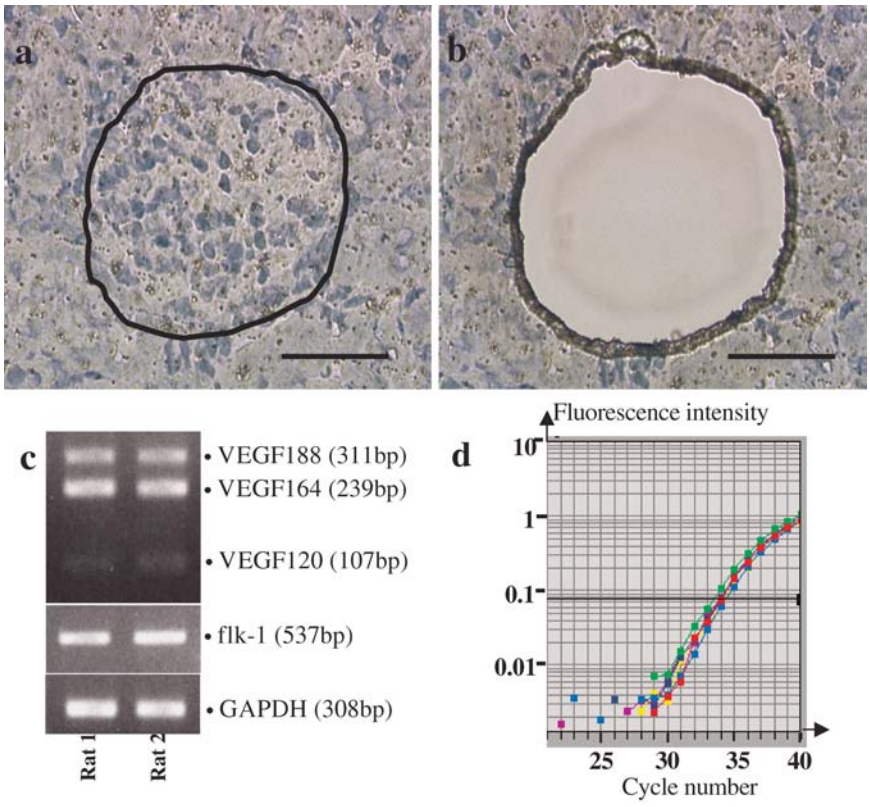



**Fig. 1** Collection of the renal glomeruli using a laser microdissection (LMD) system. The renal glomerulus in the frozen section stained with toluidine blue solution was exactly traced on the monitor with the computer mouse as indicated by the line (**a**). Then it was dissected with the ultraviolet laser (**b**), and the dissected glomeruli were directly dropped into microcentrifuge tube cap filled with a reagent for RNA extraction immediately after each dissection in the LMD system used in this study. The mRNA expression of rat $VEGF_{120}$, $VEGF_{164}$, $VEGF_{188}$, flk-1 and GAPDH in the normal rat glomeruli were collected using the LMD system. Most intense signal among VEGF isoforms was of $VEGF_{164}$ (**c**). The exponential amplification of VEGF cDNA derived from 200 glomeruli by real-time polymerase chain reaction. The amplification curves expressed by six different colors are of duplicated samples from three normal rats (**d**). Bars 50 μm (**a**, **b**)

transcription polymerase chain reaction (RT-PCR) should be very useful for analyzing gene expression in the glomeruli.

The purpose of this study was to detect the local mRNA expression of VEGF and flk-1 by RT-PCR in the glomeruli from normal rat kidney frozen sections using the LMD system in order to show the usefulness of this system for further applications to renal pathological research.

## Materials and methods

Two normal 8-week-old male Wistar rats (Charles River Japan, Inc., Yokohama, Japan) were sacrificed by bleeding under anesthesia, and their kidneys were collected. A part of the renal cortex was quickly frozen in liquid nitrogen and stored at –80ºC until use. Frozen sections (5 μm) of the kidneys were made and mounted on glass slides covered with PEN foil (2.5-μm thick; Leica Microsystems, Wetzlar, Germany) for the microdissection system used in this study. They were fixed with 70% ethanol at –20ºC for 10 s, gently washed twice with diethylpyrocarbonate (DEPC)-treated water, and thoroughly air dried. After that, the sections were stained with 0.05% toluidine blue (TB) solution, pH 4.1, (Wako Pure Chemical Industries, Ltd., Osaka, Japan) for 10 s, and then the TB solution was rinsed out with DEPC-treated water, and the sections were air dried. Then the renal glomeruli were dissected from the frozen sections with the LMD system using a 337-nm nitrogen ultraviolet (UV) laser (Leica Laser Microdissection System, Leica Microsystems) (Fig. 1a, b). The glomeruli were dissected from a section and dropped immediately into a microcentrifuge tube cap filled with 30 μl TRIzol reagent (Life Technologies, Rockville, Md., USA). Two-hundred glomeruli were collected into a 0.5-ml tube, and then the total RNA was extracted with TRIzol reagent according to the manufacturer's instructions, using ethachinmate (Wako Pure Chemical Industries, Ltd.) for general PCR analysis. First-strand cDNA was made from total RNA using the SuperScript First-strand Synthesis System for RT-PCR (Invitrogen Life Technologies, Carlsbad, Calif., USA) with oligo $(dT)_{12–18}$ primers. PCR was performed with a Takara PCR Thermal Cycler MP (Takara Shuzo, Ohtsu, Japan) with the following oligonucleotide primers: for VEGF (sense: 5′-CCGAATTCACCAAAGAAAGATAGAACAAAG-3′ and antisense: 5′-GGTGAGAGGTCTAGTTCCCGA-3′), for flk-1 (sense: 5′-GCCAATGAAGGGGAACTGAAGAC-3′ and antisense: 5′-TCTGACTGCTGGTGATGCTGTC-3′) and for GAPDH (sense: 5′-TCCCTCAAGATTGTCAGCAA-3′ and antisense: 5′-AGATCCACAACGGATACATT-3′) [9, 16, 19]. The PCR reaction was performed with Takara *Taq* (Takara Shuzo) under the following conditions: denaturation at 94ºC for 5 min; and then 35 cycles of denaturation at 94ºC for 45 s; hybridization at 50ºC for 30 s; extension at 72ºC for 30 s; and final extension at 72ºC for 5 min. Four microliters of the PCR products were separated by electrophoresis in a 2% agarose gel and stained with ethidium bromide. The signal intensity of each band on the gel was evaluated using NIH-image, and the ratios of the levels of the mRNA for the three isoforms of VEGF relative to the level of GAPDH mRNA were calculated.

For real-time PCR analysis, 10 or 200 glomeruli were taken from another three normal Wister rats using the LMD system, and the total RNA was extracted with RNeasy Mini Kit (Qiagen, Valencia, Calif., USA) and DNase digestion was performed with RNase-free DNase set (Qiagen). First-strand cDNA was made from total RNA using Sensiscript (Qiagen) with oligo $(dT)_{15}$ primer (Promega, Madison, Wis., USA). Real-time PCR was performed using the ABI Prism 7700 Sequence Detection System (Applied Biosystems, Foster City, Calif., USA). The TaqMan probe and primer pairs of VEGF and flk-1 were designed using Primer Express version 1.5 (Applied Biosystems) based on their sequence. The VEGF TaqMan probe was 5′-TGAAGTTCATGGACGTCTACCAGCGCA-3′. The VEGF forward primer sequence was 5'GAGCAGAAAGCCCATGAAGTG3', and its reverse sequence was 5′-GGTCTCAATTGGACGGCAAT-3′. The flk-1 TaqMan probe was 5′-TCTCCGTAGACCTGAAGCGGC-

GC-3′. The flk-1 forward primer sequence was 5′-AATTCGT-GCCCTATAAGAGCAAA-3′, and its reverse primer sequence was 5′-ACTGCTGGTGATGCTGTCCA-3′. GAPDH TaqMan probe, forward and reverse primers, were obtained from TaqMan Rodent GAPDH Control Reagents (Applied Biosystems). The PCR reaction mixture consisted of distilled water, TaqMan probes and primers of GAPDH and VEGF or flk-1, TaqMan Universal PCR Master Mix (Applied Biosystems) and the cDNA from the dissected glomeruli. PCR conditions were as follows: 2 min at 50ºC for uracil-N-glycosylase incubation, 10 min at 95ºC for the activation of AmpliTaq Gold DNA polymerase, and then 40 cycles of 95ºC for 15 s and 60ºC for 1 min. The amplification plots of VEGF, flk-1 and GAPDH in each sample was analyzed on the point of threshold cycle number and amplification curve to obtain stable quantitative results for the experiments afterwards.

## Results

Local expression of rat $VEGF_{120}$, $VEGF_{164}$, $VEGF_{188}$, flk-1 and GAPDH mRNAs was detected in the normal rat renal glomeruli from two normal rats, as shown by production of RT-PCR bands of the expected sizes (Fig. 1c). Among the three isoforms of rat VEGF, $VEGF_{164}$ and $VEGF_{120}$ had the strongest and weakest mRNA signals, respectively. The ratio of the level of the mRNA of each VEGF isoform to the level of GAPDH mRNA was almost the same in the glomeruli of the two normal rats ($VEGF_{120}$: 0.07 and 0.11, $VEGF_{164}$: 0.61and 0.66, and $VEGF_{188}$: 0.47 and 0.49).

The cDNA of VEGF and GAPDH derived from 200 glomeruli began amplifying at 29 and 27 cycles of PCR, respectively, and their plots showed exponential amplification by real-time PCR (Fig. 1d). It was also possible to detect exponential amplification of these cDNA derived from 10 glomeruli which began amplifying at 32 and 31 cycles, respectively. The cDNA of flk-1 derived from 200 glomeruli was also amplified using the same system. However, they began amplifying at over 35 cycles.

## Discussion

The LMD technique is very useful for mRNA analysis in the specific cells or tissues. With the LMD system used in this study, we can precisely trace the outlines of cells or functional units in the tissues and cut them using the UV laser with little tissue damage. We collected the dissected tissues into microcentrifuge tube caps filled with RNA extraction reagent immediately after each cutting, and thus reduced the loss and denaturation of biological materials [7]. Modification of the techniques for RNA extraction and transcription after microdissection may increase the sensitivity.

The expression of the mRNAs of rat VEGF isoforms $VEGF_{120}$, $VEGF_{164}$ and $VEGF_{188}$ were detected in the normal renal glomeruli, and that of $VEGF_{164}$ was the most abundant among the isoforms [11]. $VEGF_{164}$ is also the most abundant isoform in mouse glomeruli, whereas $VEGF_{188}$ is the least abundant [8]. Moreover, the relative amounts of the mRNA of the VEGF isoforms vary from organ to organ or tissue to tissue in developing and mature mice [13]. In the adult mouse kidney, the percentages of the mRNAs of $VEGF_{120}$, $VEGF_{164}$ and $VEGF_{188}$ were reported to be 20%, 63% and 17%, respectively [13]. Each VEGF isoform has unique characteristics or capacities of receptor binding, heparin binding, localization and activity [3]. Therefore, it is important to evaluate their different roles in glomerular diseases. We did not determine the ratios of the mRNA expression of the isoforms because the primer pair for real-time PCR was designed to detect all VEGF isoforms; however, the mRNA of $VEGF_{164}$ was most abundant. The ratio of each VEGF isoform mRNA to GAPDH mRNA was almost the same in the renal glomeruli of two normal rats in this study. This indicates the reproducibility of the analysis of mRNA expression in the renal glomeruli using the LMD system.

For the real-time PCR, we used 200 glomeruli and performed the RNA extraction and reverse transcription reaction using different reagents from those that were used for standard PCR as indicated by Boylan et al. [1]. The amplification plots of cDNA of VEGF and GAPDH revealed that cDNA derived from 200 glomeruli will be sufficient, and at least 10 glomeruli might be needed for quantitative analysis of these genes. As to flk-1, we could not obtain sufficient results for quantification of mRNA in this study. It might be due to the construction of primers and TaqMan probe used in this study or little expression of flk-1 mRNA in the normal glomeruli.

**Acknowledgements** This work was supported in part by a Grant-in-Aid for Exploratory Research (no. 14656125) from the Ministry of Education, Culture, Sports, Science and Technology of Japan.

## References

1. Boylan S, Honda S, Hjelmeland LM, Handa JT (2001) An optimized protocol for first strand cDNA synthesis from laser capture microdissected tissue. Lab Invest 81:1167–1169
2. Brown LF, Berse B, Tognazzi K, Manseau EJ, Van De Water L, Senger DR, Dvorak HF, Rosen S (1992) Vascular permeability factor mRNA and protein expression in human kidney. Kidney Int 42:1457–1461
3. Ferrara N (1999) Molecular and biological properties of vascular endothelial growth factor. J Mol Med 77:527–543
4. Gruden G, Thomas S, Burt D, Lane S, Chusney G, Sacks S, Viberti GC (1997) Mechanical stretch induces vascular permeability factor in human mesangial cells: mechanisms of signal transduction. Proc Natl Acad Sci U S A 94:12112–12116
5. Iijima K, Yoshikawa N, Connolly DT, Nakamura H (1993) Human mesangial cells and peripheral blood mononuclear cells produce vascular permeability factor. Kidney Int 44:959–966
6. Kohda Y, Murakami H, Moe OW, Star RA (2000) Analysis of segmental renal gene expression by laser capture microdissection. Kidney Int 57:321–331
7. Kolble K (2000) The LEICA microdissection system: design and applications. J Mol Med 78:B24–B25
8. Kretzler M, Schroppel B, Merkle M, Huber S, Mundel P, Horster M, Schlondorff D (1998) Detection of multiple vascular endothelial growth factor splice isoforms in single glomerular podocytes. Kidney Int 54[Suppl]67: S159–S161
9. Levy AP, Levy NS, Loscalzo J, Calderone A, Takahashi N, Yeo K-T, Koren G, Colucci WS, Goldberg MA (1995) Regulation of vascular endothelial growth factor in cardiac myocytes. Circ Res 76:758–766

10. Masuda Y, Shimizu, A, Mori T, Ishikawa T, Kitamura H, Ohashi R, Ishizaki M, Asano G, Sugisaki Y, Yamanaka N (2001) Vascular endothelial growth factor enhances glomerular capillary repair and accelerates resolution of experimentally induced glomerulonephritis. Am J Pathol 159:599–608
11. Merrill MJ, Bacic M, Edwards EA (1995) Differential expression of vascular endothelial growth factor (vascular permeability factor) forms in rat tissues. Growth Factors 12:11–15
12. Nagasawa Y, Takenaka M, Matsuoka Y, Imai E, Hori M (2000) Quantitation of mRNA expression in glomeruli using laser manipulated microdissection and laser pressure catapulting. Kidney Int 57:717–723
13. Ng Y-S, Rohan R, Sunday ME, Demello DE, D'amore PA (2000) Differential expression of VEGF isoforms in mouse during development and in the adult. Dev Dyn 220:112–121
14. Noguchi K, Yoshikawa N, Ito-Kariya S, Inoue Y, Hatashi Y, Ito H, Nakamura H, Iijima K (1998) Activated mesangial cells produce vascular permeability factor in early-stage mesangial proliferative glomerulonephritis. J Am Soc Nephrol 9:1815–1825
15. Shulman K, Rosen S, Tognazzi K, Manseau EJ, Brown LF (1996) Expression of vascular permeability factor (VPF/VEGF) is altered in many glomerular diseases. J Am Soc Nephrol 7:661–666
16. Terada Y, Tomita K, Nonoguchi H, Marumo F (1992) Different localization of two types of endothelium receptor mRNA in microdissected rat nephron segments using reverse transcription and polymerase chain reaction assay. J Clin Invest 90:107–112
17. Thomas S, Vanuystel J, Gruden G, Rodriguez V, Burt D, Gnudi L, Hartley B, Viberti GC (2000) Vascular endothelial growth factor receptors in human mesangium in vitro and in glomerular disease. J Am Soc Nephrol 11:1236–1243
18. Uchida K, Uchida S, Nitta K, Yumura W, Marumo F, Nihei H (1994) Glomerular endothelial cells in culture express and secrete vascular endothelial growth factor. Am J Physiol 266:F81–F88
19. Wen Y, Edelman JL, Kang T, Zeng N, Sachs G (1998) Two functional forms of vascular endothelial growth factor receptor-2/Flk-1 mRNA are expressed in normal rat retina. J Biol Chem 273:2090–2097

Virchows Arch (2003) 442:163–168
DOI 10.1007/s00428-002-0738-2

CASE REPORT

**Hiroyuki Morita · Takeshi Hasegawa
Toshinari Minamoto · Yoshio Oda · Kiyoko Inui
Hironori Tayama · Naoyuki Nakao
Yasushi Nakamoto · Terukuni Ideura
Ashio Yoshimura**

# Collagenofibrotic glomerulopathy with a widespread expression of type-V collagen

Received: 14 August 2002 / Accepted: 16 October 2002 / Published online: 13 December 2002
© Springer-Verlag 2002

**Abstract** Collagenofibrotic glomerulopathy is considered as a form of glomerulopathy in which organized collagen type III progressively deposits. We report a case of this disease with widespread expression of collagen type V. A 65-year-old woman was admitted to our hospital for further evaluation of nephrotic-range proteinuria. The patient had had anemia and hypertension for 9 years, and proteinuria for 3 years. A renal biopsy specimen showed a remarkable mesangial expansion with Congo red-negative and periodic acid-Schiff-positive deposits. At the ultrastructural level, two forms of bundling fibers were found in the mesangium and subendothelial side of the glomerular basement membranes (GBM). The GBM itself appeared normal. Immunohistochemical investigation showed that the glomerular lesions were strongly reactive with both anti-collagen type-III and -V antibodies. Immunoelectron microscopy demonstrated collagen type V in both forms of bundling fibers. Despite therapy, her renal function declined. The clinical course and renal pathology of this case were in accordance with collagenofibrotic glomerulopathy except for the widespread expression of collagen type V. Collagen type V is a fibrillar collagen capable of forming banding fibrils. This report poses the question whether collagen type V accumulates only in this particular case or whether it is a normal component in collagenofibrotic glomerulopathy.

**Keywords** Kidney disease · Collagenofibrotic glomerulopathy · Collagen type III · Collagen type V · Heterotypic collagen fibrils

H. Morita · T. Hasegawa · K. Inui · H. Tayama · N. Nakao
T. Ideura · A. Yoshimura (✉)
Division of Nephrology, Department of Medicine,
Showa University Fujigaoka Hospital, 1-30 Fujigaoka, Aoba-ku,
Yokohama, Japan
e-mail: yoshimura@showa-university-fujigaoka.gr.jp
Tel.: +81-45-9746388, Fax: +81-45-9733010

T. Minamoto
Division of Diagnostic Molecular Oncology,
Cancer Research Institute, Kanazawa University
Graduate School of Medical Science, 13-1 Takaramachi,
Kanazawa, Japan

Y. Oda
Department of Molecular Cell Pathology,
Kanazawa University Graduate School of Medical Science,
13-1 Takaramachi, Kanazawa, Japan

Y. Nakamoto
Department of Medicine, Kichijyoji Asahi Hospital, Tokyo, Japan

## Introduction

It is rare for the kidney glomerulus to have a bundle of collagen fibers. The nail-patella syndrome is an autosomal dominant hereditary disorder characterized by nail hypoplasia and bone abnormalities. Renal involvement of this syndrome is quite unique in that collagen bundles accumulate mainly in the glomerular basement membranes (GBM). Late in the 1970s, Arakawa et al. described two cases with fibrillar collagen accumulation mainly in the mesangium and proposed that they should belong to a new disease entity due to the absence of nail and bone abnormalities [8]. Eary in the 1980s, Dombros and Katz referred to the possibility that a similar case they had was either a variant of the nail-patella syndrome or a new genetic disease [13]. In 1990, Ikeda et al. reported a glomerulopathy with collagen type-III deposits in the absence of clinical pictures of the nail-patella syndrome [17]. In 1991, Arakawa and Yamanaka analyzed ten such cases and proposed the term "collagenofibrotic glomerulopathy" [7]. In the same year, Imbasciati et al. described their case, reviewed previous reports, and proposed the term "collagen type III glomerulopathy" [18]. It has now been accepted that the major collagen accumulating in this glomerulopathy is collagen type III [15, 18, 27].

Using well-characterized antibodies, we now describe a case of collagenofibrotic glomerulopathy that is dis-

tinct from previously reported cases due to the widespread deposition in glomeruli of collagen type V in addition to collagen type III.

## Case report

A 65-year-old woman was admitted to our hospital for evaluation of nephrotic-range proteinuria. Family history of the patient is unremarkable. She visited the division of hematology of our institute because of normocytic normochromatic anemia and hypertension 8 years prior to admission. The cause of anemia remained unknown despite bone marrow aspiration. Her anemia partially resolved without treatment 6 years prior to admission. Proteinuria appeared 3 years prior to admission and gradually progressed. One month before admission, urinary protein excretion was 6.3 g/day. On admission the blood pressure was 140/70 mmHg. Physical examination showed no abnormalities of the patellas or nails. Urinary protein excretion was 3.6 g/day without occult blood. In brief, laboratory data were as follows: white blood cells were 5100/μl, hemoglobin 9.3 g/dl, total protein 5.4 g/dl, albumin 3.3 g/dl, serum creatinine 1.0 mg/dl, creatinine clearance 55.1 ml/min, and total cholesterol 256 mg/dl. CH50 and serum levels of C3 and C4 were 39.9 U/ml, 117 mg/dl, and 31.3 mg/dl, respectively. Renal biopsy was performed on the 8th hospital day. She was discharged on the 18th hospital day and was followed as an outpatient. Despite blood pressure control with an angiotensin converting-enzyme inhibitor (captopril 37.5 mg/day) and an angiotensin receptor blocker (losartan 50 mg/day), nephrotic-range proteinuria persisted and her renal function gradually declined. Serum creatinine 6 months after discharge was 1.3 mg/dl.

## Materials and methods

### Anti-collagen type-V antibodies

Preparation and type specificity of the antibodies are described elsewhere [28]. In brief, collagen type V was isolated by differential salt precipitation from pepsin digests of human placenta. The purity of collagen type V was analyzed using sodium dodecylsulfate polyacrylamide gel electrophoresis (SDS-PAGE). Sprague-Dawley rats were immunized with gel-purified human collagen type V. Crude antisera were subjected initially to cross-adsorption on affinity columns consisting of human collagen types I, III, IV, and VI coupled with activated CH-Sepharose 4B, and then to immunoabsorption on an affinity column prepared from collagen type V. Furthermore, the specificity of the anti-type-V collagen antibodies was confirmed by the inhibition test using enzyme-linked immunosorbent assay (ELISA) [26, 28].

### Anti-collagen type-III antibodies

Monoclonal antibody against collagen type III was purchased from Daiichi Fine Chemicals (Tokyo, Japan). Type specificity is biochemically confirmed (private communication).

### Anti-collagen type-I, -IV, -V, and -VI antibodies

Monoclonal antibody against collagen type IV was purchased from Shiseido (Tokyo, Japan). Type specificity is confirmed by the inhibition test using ELISA [20]. Preparation and type specificities of the anti-collagen type-I, -V, and -VI antibodies are described elsewhere [28].

### Immunohistochemical procedures

Formalin-fixed and paraffin-embedded sections of renal biopsy specimens were processed for immunohistochemistry with antibodies against collagen types I, III, IV, V, and VI. As a secondary reagent, ENVISION+/peroxidase-conjugated anti-mouse immunoglobulins and ENVISION+/peroxidase-conjugated anti-rabbit immunoglobulins (Dako Japan Co., Kyoto Japan) were used for anti-type-III and -IV and anti-type-VI antibodies, respectively. For anti-type-I and -V antibodies, peroxidase-conjugated anti-rat immunoglobulins (Dako) were used. Control stainings were performed by replacing the primary antibodies with non-immunized goat serum.

### Immunoelectron microscopic procedures

Immunoelectron microscopy was performed with anti-type-V collagen antibodies on ultrathin epon-embedded sections of renal biopsy specimen. Briefly, pieces of biopsy were fixed in freshly prepared 0.1% glutaldehyde in 100 mM phosphate buffer, pH 7.2, for 48 h at 4°C. Ultrathin sections were processed for indirect immunogold labeling, as described elsewhere [11]. In control experiments, incubation with primary antibodies was replaced by irrelevant rat serum of the same dilution.

## Pathological findings

Renal biopsy specimen for light microscopy contained seven glomeruli. There were no globally sclerosed glomeruli. Tubulointerstitial and vascular changes were non-specific. Each glomerulus was filled with homogeneous and periodic acid-Schiff (PAS)-positive deposits (Fig. 1A). The deposits were Congo red-negative (data not shown) and mainly observed in the expanded mesangium and subendothelial areas (Fig. 1A). Hypercellularity of the mesangium was not prominent. The staining of the deposits was weaker than that of the GBM. Most of the capillary lumens were reduced in size. On periodic acid-Schiff silver methenamine (PASM) stains, a double-contour appearance of the GBM was occasionally observed (data not shown).

Immunofluorescence of the three glomeruli examined was negative for immunoglobulin G (IgG), immunoglobulin A (IgA), immunoglobulin M (IgM), C3, C4, and C1q complement components (data not shown).

Conventional electron microscopic examination showed that the mesangial matrix and the subendothelial side of the GBM were enlarged with mottled material (asterisks in Fig. 1B). Thickening, irregularity and electron-lucent areas within the GBM were not found (Fig. 1B). Tannic acid staining of the sections disclosed two forms of banding fibers (Fig. 2A) mainly in the expanded mesangium and subendothelial areas. One was a bundle of spiraled and frayed fibers. A typical periodicity of banding pattern in longitudinal sections was observed (Fig. 2B). Of note was a considerable variation in the diameter of the fibers. The other consisted of thinner fibers always located near the GBM (Fig. 2A). Each fiber had a diameter of about 30 nm (Fig. 2C), and the variation in fiber diameter was not remarkable.

The immunohistochemical and immunoelectron microscopic analyses were performed. The specificity of

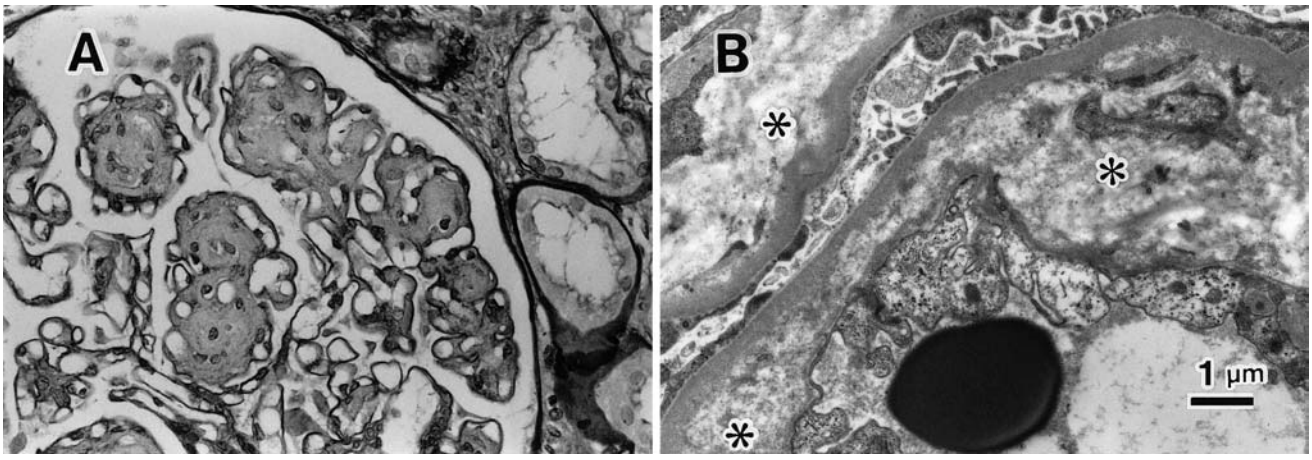



**Fig. 1** Light and electron microscopic findings. **A** Enlargement of the glomerular tuft due to the deposition of periodic acid-Schiff (PAS)-weakly-positive material is noted. Lobular architecture is seen. PAS stain. ×400. **B** Electron micrograph double-stained with uranyl acetate and lead citrate. The mesangium and endothelial sides of the glomerular basement membranes are filled with mottled materials, ×16,500

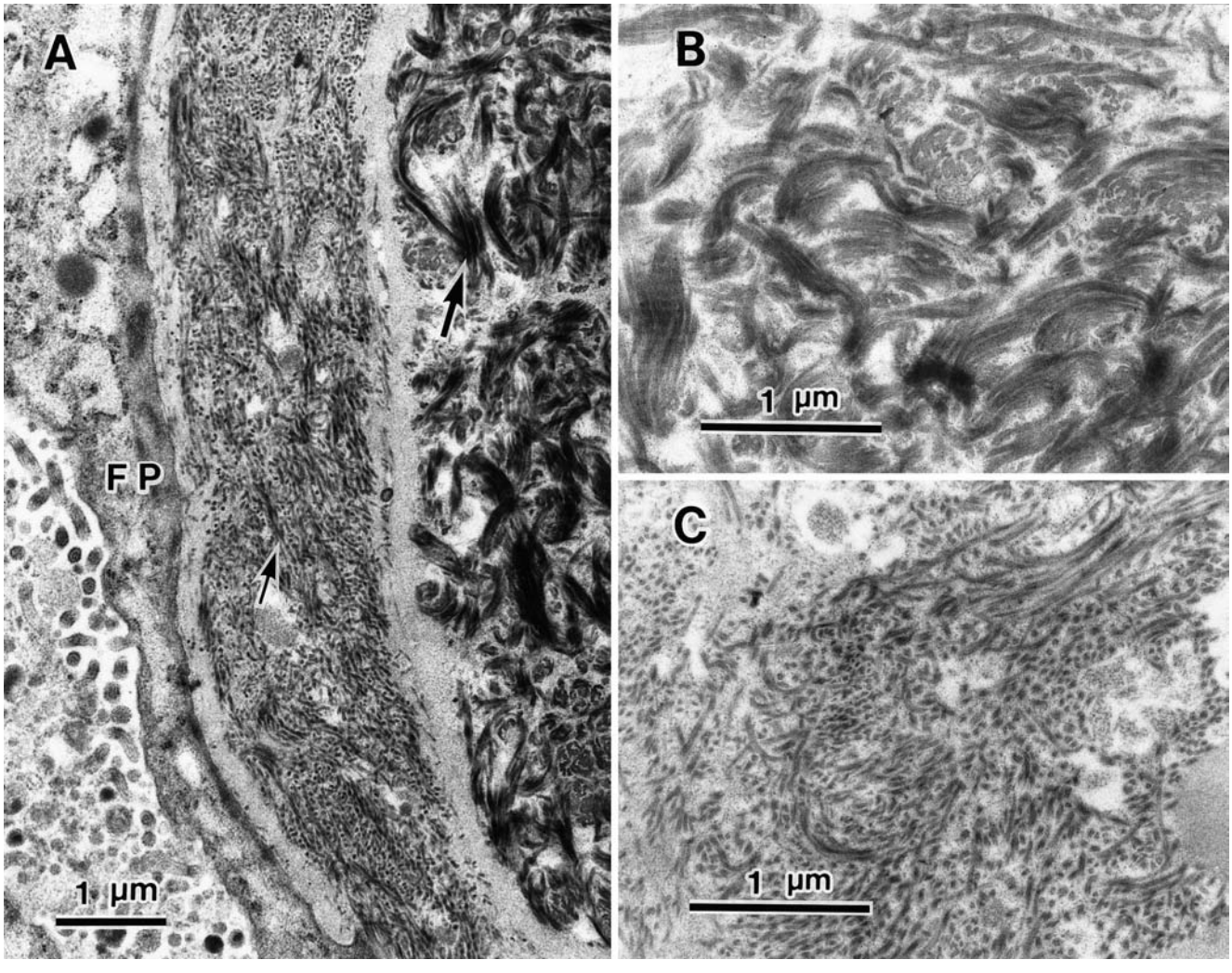



**Fig. 2** Electron micrograph of a tannic acid-stained section. Two forms of banding fibers are shown. **B**, **C** Each of the banding fibers indicated in **A** shown with big and small *arrows*, respectively, by higher magnification. **A** ×15,000, **B**, **C** ×24,500

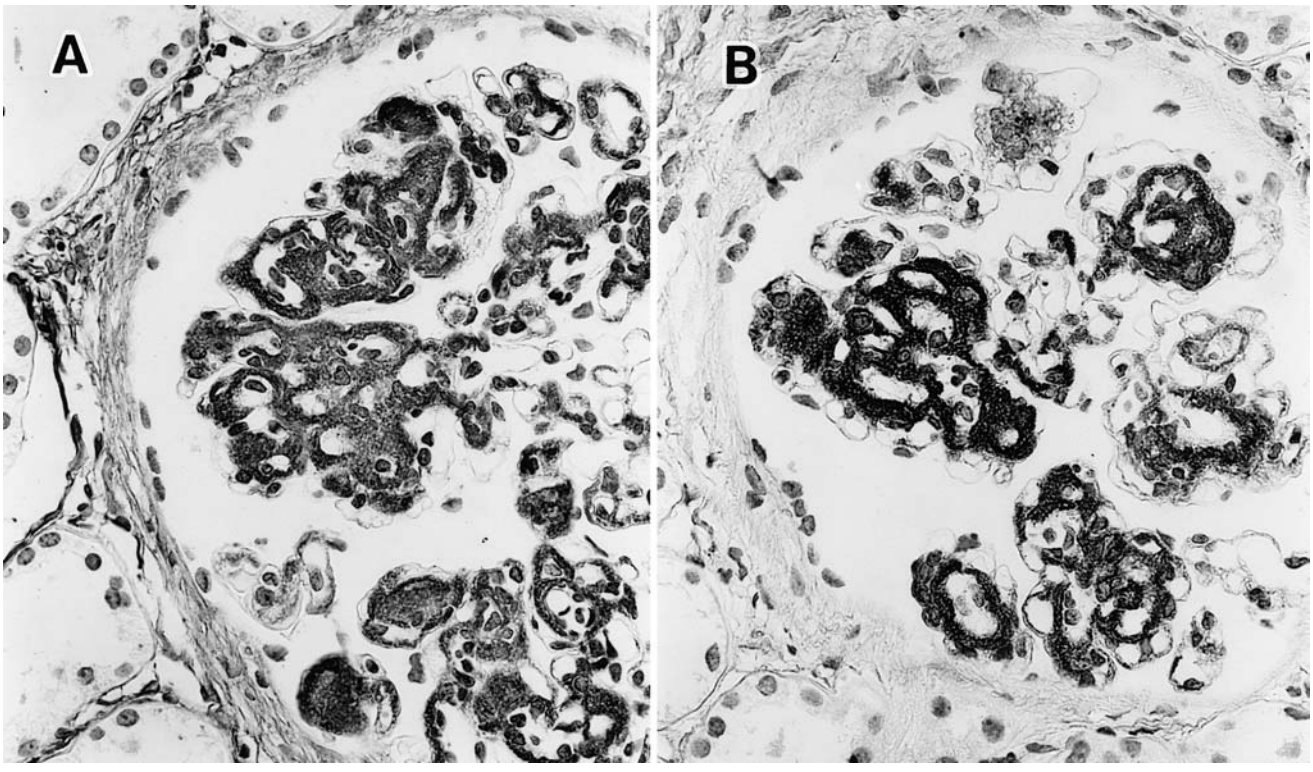



**Fig. 3** Immunohistochemical analysis for collagen types III and V. **A** Anti-collagen type-III antibody was used as described in the text. Glomerular lesions are strongly stained. Tubular basement membranes (TBM) are moderately stained. **B** Anti-collagen type-V antibody was used as described in the text. Staining pattern of the glomerular lesions is very similar, whereas TBM are not stained. **A**, **B** ×400

the antibodies to collagen types III and V is described in the Materials and methods. Glomerular deposits were not stained by immunofluorescent and immunohistochemical examinations using anti-human collagen antibodies specific for collagen types I, II, IV, and VI (data not shown). Glomerular staining was strong with anti-collagen type-III antibody (Fig. 3A). The staining appeared to be mainly in the mesangium and subendothelial areas (Fig. 3A). The GBM was not stained (Fig. 3A). The staining pattern of anti-human collagen type V antibodies was very similar to that of anti-human collagen type-III antibody (Fig. 3B). It appeared that the sites that were positive with anti-collagen type-III and -V antibodies corresponded well to the PAS- and PASM-positive material present in the mesangium and subendothelial areas of the GBM. When the antibodies against collagen types III and V were omitted during the staining procedure, the tissue was negative by immunohistochemistry (data not shown). Immunoelectron microscopy of epon-embedded renal biopsy revealed specific immunogold labeling with anti-human collagen type-V antibodies on the two forms of phosphotungstic acid stained collagen fibrils (Fig. 4A, B). No labeling was obtained on collagen fibrils when the first antibody was replaced by irrelevant rat serum of the same dilution (data not shown).

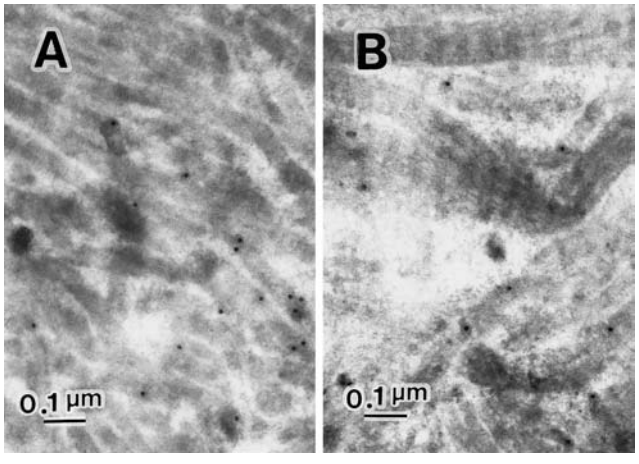



**Fig. 4** Localization of collagen type V by immunogold labeling on ultrathin sections counterstained with phosphotungstic acid. **A** Collagen type V is distributed on the 30-nm fibers in a dispersed pattern. **B** Collagen type V is also distributed on some of the spiraled and frayed fibers. Diameter of the fibers varies. It appears thinner fibers are specifically labeled. **A**, **B** ×52,500

## Discussion

Clinical findings and glomerular morphology at the light and electron microscopic levels of the present case are in accordance with collagenofibrotic glomerulopathy or collagen type-III glomerulopathy [1, 14]. The negative family history for kidney disease suggests the present case was sporadic, consistent with some reports [15, 18, 31, 32]. Due to the absence of a large pedigree, however, the possibility cannot completely be ruled out that the

disease occurred in an autosomal recessive fashion. In any case, glomerular deposition of collagen type III is a distinctive hallmark of this disease as its name signifies. According to previous reports, accumulation of collagen type I could be massive [32] and collagen type V might be shown as a minor collagen [31]. To our knowledge, we present the first case in which a widespread glomerular expression of collagen type V is seen. Using well-characterized antibodies, it should be re-examined whether our case is an extremely rare one or whether there are other such cases.

Our immunohistochemical examination strongly indicated that glomerular deposits of the present case contained collagen types III and V. Our electron microscopic study demonstrated the presence of spiraled and frayed collagen fibrils within the deposits. On morphologic grounds, similar collagen fibrils are seen in a genetic connective tissue disease, dermatosparaxis (meaning "tearing of skin") of animals [16, 29] and man [23]. In this disorder, pNcollagen (an intermediate in the processing of procollagen to collagen containing the N-propeptides but not the C-propeptides) accumulates. In a form of human dermatosparaxis, also known as Ehlers-Danlos syndrome type VII C, gene mutations for procollagen N-proteinase were identified [12]. Since electron-microscopic features of abnormal collagen in collagenofibrotic glomerulopathy and dermatosparaxis are similar, it may be worthy to examine whether pNcollagen is found in this glomerulopathy. Another interesting observation was that the diameter of the spiraled and frayed fibers varied. It has been proposed that collagen fibrils with varying size are composed of more than one collagen type. This idea is exemplified in collagen fibrils of various tissues such as the skin [22], placenta [3], embryonic cornea [9], and cartilage [25], where individual collagens, stained with type-specific anti-collagen antibodies, associate to form bundle architecture. It is possible that a bundle of spiraled and frayed collagen observed in the present case consists of heterotypic collagen fibrils containing at least collagen types III and V.

Electron microscopic examination demonstrated thinner tannic acid-positive fibers (about 30 nm in diameter) located near the GBM, while our immunoelectron microscopic examination showed specific immunogold labeling with type-V collagen antibody. It has been reported that collagen type V is widely distributed in a peri-basement membrane area in all connective tissues other than cartilage and bone [5]. It has also been reported in immunoelectron microscopic studies that collagen type V is distributed on fibrils less than 40 nm in diameter in the spleen [4], liver [6], and cornea [10]. Although the possibility still remains that thinner fibers are heterotypic collagens, our studies suggest collagen type V is a major component.

Collagen type V is a member of the fibrillary collagen family and capable of forming banding fibrils [2, 30]. Collagen type V is considered a minor collagen component of glomerular extracellular matrix (ECM) in humans. Widespread expression of collagen type V as seen in the present case is definitely pathological. Increased expression of collagen type V has been reported in other human glomerular diseases, such as the late stages of type-2 diabetes [21, 24] and in membranoproliferative glomerulonephritis type I [19]. The relationship between the thinner collagen fibers of 30 nm in diameter and the spiraled collagen fibrils observed in the present case remains to be investigated.

**Acknowledgements** The authors are profoundly grateful to Prof. Richard Johnson from Baylor Collage of Medicine for his critical review of the manuscript and Prof. Eijiro Adachi from Kitasato University for his valuable comments on collagen fibers. Ms. Kiyoko Nakano and Mr. Hiroaki Oniki from Showa University Fujigaoka Hospital are greatly acknowledged for their professional assistance in electron microscopic studies.

## References

1. Abt AB, Cohen AH (1996) Newer glomerular diseases. Semin Nephrol 16:501–510
2. Adachi E, Hayashi T (1985) In vitro formation of fine fibrils with a D-periodic banding pattern from type V collagen. Collagen Relat Res 5:225–232
3. Adachi E, Hayashi T (1986) In vitro formation of hybrid fibrils of type V collagen and type I collagen. Limited growth of type I collagen into thick fibrils by type V collagen. Connect Tissue Res 14:257–266
4. Adachi E, Hayashi T (1987) Comparison of axial banding patterns in fibrils of type V collagen and type I collagen. Collagen Relat Res 7:27–38
5. Adachi E, Hayashi T (1994) Anchoring of epithelia to underlying connective tissue: Evidence of frayed ends of collagen fibrils directly merging with meshwork of lamina densa. J Electron Microsc 43:264–271
6. Adachi E, Hayashi T, Hashimoto PH (1991) A comparison of the immunofluorescent localization of collagen types I, III, and V with the distribution of reticular fibers on the same liver sections of the snow monkey (Macaca fuscata). Cell Tissue Res 264:1–8
7. Arakawa M, Yamanaka N (eds) (1991) Collagenofibrotic glomerulopathy: A new type of primary glomerulopathy revealing massive collagen deposits in the renal glomerulus. In: Collagenofibrotic glomerulopathy. Nishimura Co Ltd, Nigata, Japan, pp 3–8
8. Arakawa M, Fueki H, Hirano H, Sato M, Yamaguchi T, Masuda H, Uemura S, Suzuki M, Yamagishi Y, Yamashita K, Nakazawa S (1979) Idiopathic mesangio-degenerative glomerulopathy: a proposal of new disease entity. Nichi-Jin-Shi (in Japanese) 21:914–915
9. Birk DE, Fitch JM, Linsenmayer TF (1986) Organization of collagen types I and V in the embryonic chicken cornea. Invest Ophthalmol Vis Sci 27:1470–1477
10. Birk DE, Fitch JM, Babiarz JP, Linsenmayer TF (1988) Collagen type I and type V are present in the same fibril in the avian corneal stroma. J Cell Biol 106:999–1008
11. Breiteneder-Geleff S, Matsui K, Soleiman A, Meraner P, Poczewski H, Kalt R, Schaffner G, Kerjaschki D. Podoplanin (1997) A novel 43-kD membrane protein of glomerular epithelial cells, is down-regulated in puromycin nephrosis. Am J Pathol 151:1141–1152
12. Colige A, Sieron AL, Li SW, Schwarze U, Petty E, Weertelecki W, Wilcox W, Krakow D, Cohn DH, Reardon W, Byers PH, Lapiere CM, Prockop DJ, Nusgens BV (1999) Human Ehlers-Danlos syndrome type VII C and bovine dermatosparaxis are caused by mutations in the procollagen I N-proteinase gene. Am J Hum Genet 65:308–317
13. Dombros N, Katz A (1982) Nail patella-like renal lesions in the absence of skeletal abnormalities. Am J Kidney Dis 1: 237–240

14. Gibson IW, More IAR (1998) Glomerular pathology: recent advances. J Pathol 184:123–129
15. Gubler MC, Dommergues JP, Foulard M, Bensman A, Leroy JP, Broyer M, Habis R (1993) Collagen type III glomerulopathy: a new type of hereditary nephropathy. Pediatr Nephrol 7:354–360
16. Holbrook KA, Byers PH, Counts DF, Hegreberg GA (1980) Dermatosparaxis in a Himalayan cat: II. Ultrastructual studies of dermal collagen. J Invest Dermatol 74:100–104
17. Ikeda K, Yokoyama H, Tomosugi N, Kida H, Oshima A, Kobayashi K (1990) Primary glomerular fibrosis: a new nephropathy caused by diffuse intra-glomerular increase in atypical type III collagen fibers. Clin Nephrol 33:155–159
18. Imbasciati E, Gherardi G, Morozumi K et al. (1991) Collagen type III glomerulopathy: a new idiopathic glomerular disease. Am J Nephrol 11:422–429
19. Inaba S, Tanizawa T, Takahashi T, Ishihara S, Arai M, Sakai Y, Kurose KK, Matsukura H, Okada T (1996) Decrease of mesangial matrix after immunosuppressive therapy in children with reversible membranoproliferative glomerulonephritis type I. Clin Nephrol 45:217–225
20. Kino J, Adachi E, Yoshida T, Nakajima K, Hayashi T (1988) Characterization of a monoclonal antibody against human placentatype IV collagen by immunoelectroblotting, antibody-coupled affinity chromatography and immunohistochemical localization. J Biochem 103:829–835
21. Kiryu K, Morita H, Fujita Y, Kawasumi M, Shinzato T, Tsuruta Y, Nakai S, Maeda K (1994) Phenotypic expression of type I, III, V, and VI collagens in patients with diabetic nephropathy: lmmunohistochemical comparison between HD and non-HD patients. Jpn J Nephrol 36:365–373
22. Lapiere CM, Nusgens B, Pierard GE (1977) Interaction between collagen type I and III in conditioning bundles organization. Connect Tissue Res 5:21–29
23. Lapiere CM, Nusgens BV (1993) Ehlers-Danlos type VII-C, or human dermatosparaxis. The offspring of a union between basic and clinical research. Arch Dermatol 129:1316–1319
24. Makino H, Shikata K, Wieslander J, Wada J, Kashihara N, Yoshioka K, Ota Z (1994) Localization of fibril/microfibril and basement membrane collagens in diabetic glomerulosclerosis in type 2 diabetes. Diabet Med 11:304–311
25. Mendler M, Eich-Bender SG, Vaughan L, Winterhalter KH, Bruckner P (1989) Cartilage contains mixed fibrils of collagen types II, IX, and XI. J Cell Biol 108:191–197
26. Minamoto T, Ooi A, Okada Y, Mai M, Nagai Y, Nakanishi I (1988) Desmoplastic reaction of gastric carcinoma: A light- and electron-microscopic immunohistochemical analysis using collagen type-specific antibodies. Hum Pathol 19:815–821
27. Mizuiri S, Hasegawa A, Kiuchi A, Amagasaki Y, Nakamura N, Sakaguchi H (1993) A case of collagenofibrotic glomerulopathy associated with hepatic perisinusoidal fibrosis. Nephron 63:183–187
28. Oda Y, Kawahara E, Minamoto T, Ueda Y, Ikeda K, Nagai Y, Nakanishi I (1988) Immunohistochemical studies on the tissue localization of collagen type I, III, IV, V and VI in schwannomas. Correlation with ultrastructual features of the extracellular matrix. Virchows Arch 56:153–163
29. Pierard GE, Le T, Hermanns JF, Nusgens BV, Lapiere CM (1987) Morphometric study of califlower collagen fibrils in dermatosparaxis of the calves. Coll Relat Res 6:481–492
30. Van der Rest M, Garrone R (1991) Collagen family of proteins. FASEB J 5:2814–2823
31. Yasuda T, Imai H, Nakamoto Y, Ohtani H, Komatsuda A, Wakui H, Miura A (1999) Collagenofibrotic glomerulopathy: a systemic disease. Am J Kidney Dis 33:123–127
32. Yoshida F, Yuzawa Y, Shigematsu H, Ito A, Yamazaki C, Yoshioka K, Ooshima A, Matsuo S (1993) Nephrotic syndrome with massive accumulation of type I and III collagen in the glomeruli. Int Med 32:171–176

Virchows Arch (2003) 442:169–172
DOI 10.1007/s00428-002-0730-x

CASE REPORT

**Keith E. Volmar · Tom C. Nguyen**
**Cynthia J. Holcroft · Karin J. Blakemore**
**Grover M. Hutchins**

# Phimosis as a cause of the prune belly syndrome: comparison to a more common pattern of proximal penile urethra obstruction

Received: 4 June 2002 / Accepted: 1 October 2002 / Published online: 30 November 2002
© Springer-Verlag 2002

**Abstract** The pathogenesis of the prune belly syndrome (PBS) remains controversial, but two theories predominate. The first theory supports an obstructive phenomenon early in gestation leading to irreversible damage to the genitourinary tract and abdominal wall. The second theory suggests mesodermal injury between the 6th and 10th weeks of gestation as the primary abnormality. This paper reports of two fetuses with the PBS phenotype that were examined postmortem at our institution. Thorough examination of the lower urinary tract allowed demonstration of anatomic obstruction of the urethra in both cases. One case illustrated a relatively common pattern of proximal penile urethral obstruction, a flap-like obstruction between the prostatic and penile urethra. The other case provided what we believe to be the first description of PBS caused by severe phimosis.

**Keywords** Fetus · Phimosis · Prune belly syndrome · Urethral obstruction

## Introduction

The prune belly syndrome (PBS) is so named for the wrinkled, prune-like appearance of the affected child's abdomen. The condition is also known as Eagle-Barrett syndrome, triad syndrome, or urethral obstruction malformation complex. Parker first attributed changes consistent with PBS to a syndrome in 1895 [4]. In 1950, Eagle and Barrett defined the syndrome as a triad of deficient abdominal wall musculature, undescended testes, and urinary tract abnormalities, including megacystis, megaloureter, hydronephrosis, and renal dysplasia [1]. Studies of the lower urinary tracts in these cases have shown varying incidence of urethral obstruction and a wide range of prostatic development. A recent study showed several patterns of urinary tract obstruction in PBS, including a flap-like obstruction at the junction of the prostatic and penile portions of the urethra [8]. The following two previously unreported cases compare the pattern of flap-like obstruction at the proximal penile urethra to obstruction caused by phimosis, a finding not previously described in relation to PBS.

K.E. Volmar · T.C. Nguyen · G.M. Hutchins (✉)
The Department of Pathology,
The Johns Hopkins Medical Institutions, 600 North Wolfe Street,
Baltimore, MD 21287, USA
e-mail: ghutchi@jhmi.edu
Tel.: +410-955-3765, Fax: +410-614-2243

C.J. Holcroft · K.J. Blakemore
The Department of Gynecology and Obstetrics,
The Johns Hopkins Medical Institutions, 600 North Wolfe Street,
Baltimore, MD 21287, USA

## Case reports

Case 1 – distal obstruction by phimosis

A healthy 30-year-old primigravida was referred to The Johns Hopkins Hospital secondary to an abnormal sonogram. A repeat ultrasound at 19 weeks and 6 days (Fig. 1) revealed a fetus with a markedly enlarged abdominal circumference (27.9 cm, equivalent to 31 weeks and 6 days), massive ascites, pericardial effusion, severe hydronephrosis, and anhydramnios. Maternal serology for human immunodeficiency virus (HIV), hepatitis B, and syphilis was negative, and there was no history of sexually transmitted disease. The patient's sister had given birth to a child with Down syndrome; there was no other family history of congenital malformation. The patient declined further intervention until several weeks later when she developed pre-eclampsia with hypertension and pedal edema at 23 weeks and 3 days. The patient's fundal height was 36 cm, equivalent to 36 weeks in size. An obstetrical sonogram showed further distention of the fetal abdomen to a circumference of 45 cm. In order to allow for vaginal delivery, fetal paracentesis was performed and yielded approximately 1900 ml clear yellow fluid. Labor was induced secondary to maternal pre-eclampsia and a nonviable fetus was delivered. The karyotype was 46, XY.

*Gross findings*

Postmortem examination revealed a male fetus with lax and wrinkled abdominal skin, the so-called "prune belly". The estimated anatomic age was 23–24 weeks (800 g, crown–rump 25 cm, heel–toe 4.0 cm), while the abdominal circumference was that expected of a full-term fetus. The fetus also had Potter facies, clubbed feet, and bilateral clinodactyly of the fifth finger. Internal exam showed 120 ml residual ascites, massive distention of the urinary bladder, bilateral

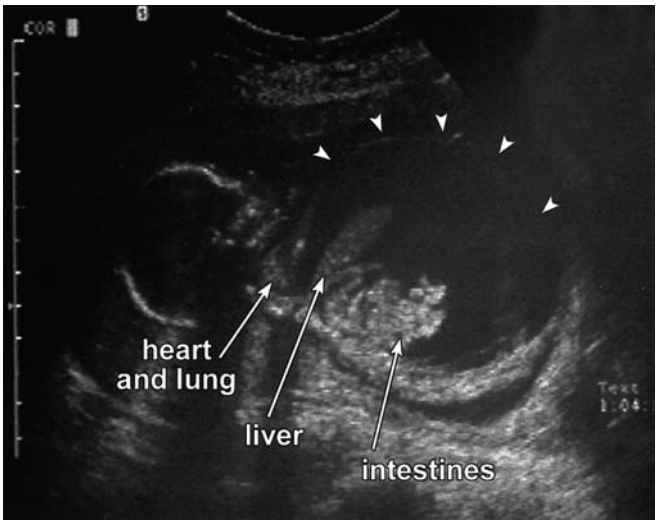



**Fig. 1** Case-1 sonogram at 19 weeks gestation showing marked distention of the fetal abdomen (*arrowheads*). The diaphragm is markedly elevated and the thoracic cavity is compressed

hydroureter, and bilateral hydronephrosis. The rib cage was flared and the heart and lungs were hypoplastic. The heart, lungs, and intestinal tract showed normal configuration, as did the nervous system.

*Histological findings*

To further define the pathology of the genitourinary system, the penis, bladder, and ureters were removed en bloc and injected with a water-soluble contrast medium. Subsequent postmortem cystourethrography delineated a filling defect in the most distal portion of the urethra indicating a possible obstruction (Fig. 2a). After formalin fixation in distention, the lower urinary tract was submitted for histological evaluation; the distal penis was submitted intact for complete serial sectioning. Hematoxylin and eosin sections from the penile bulb, midshaft and glans revealed marked urethral dilatation (Fig. 2b). Sections distal to the glans taken through the elongated prepuce revealed severe phimosis with the opening of the prepuce blocked by squamous epithelium (Fig. 2c). The corpora of the penis were normal, and megaurethra was not present. The bladder wall was thickened and prostatic gland development was less than expected for gestational age. The kidneys showed moderate renal dysplasia, with cystic dilatation of glomeruli, distortion and fibrosis of pyramids, distorted collecting ducts, and a reduced to absent nephrogenic zone. There was increased fibrous tissue in the abdominal wall with disruption and loss of muscle fibers.

Case 2 – proximal flap-like obstruction

A 29-year-old primigravida was referred to The Johns Hopkins Hospital secondary to an abnormal obstetrical sonogram. Ultraso-

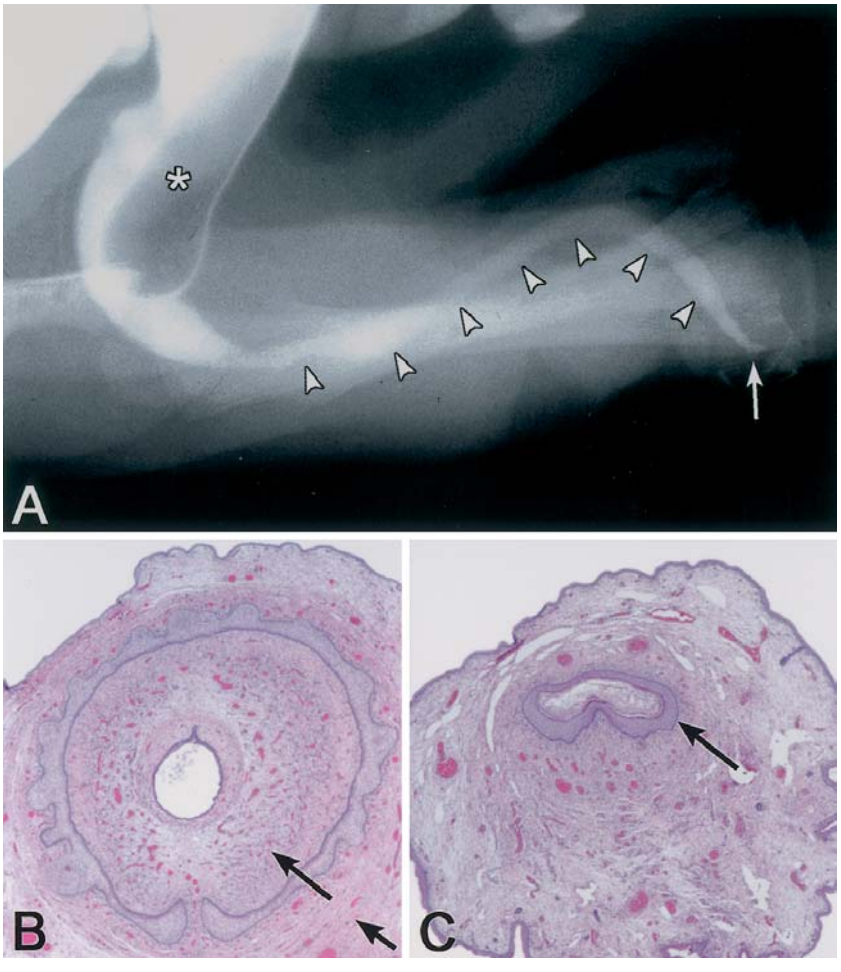



**Fig. 2** Case-1 pathology. **a** Postmortem cystourethrogram shows the urethra to be dilated in the prostatic (*) and penile (*arrowheads*) portions, but the lumen is lost in the region of the distal penis (*arrow*). **b** Proximal cross section in the region of the glans (*long arrow*) shows a markedly dilated urethra and surrounding prepuce (*short arrow*; medium power H&E). **c** Distal cross section of the prepuce beyond the tip of the glans showing occlusion of the opening of the prepuce by squamous epithelium (*arrow*; medium power H&E)

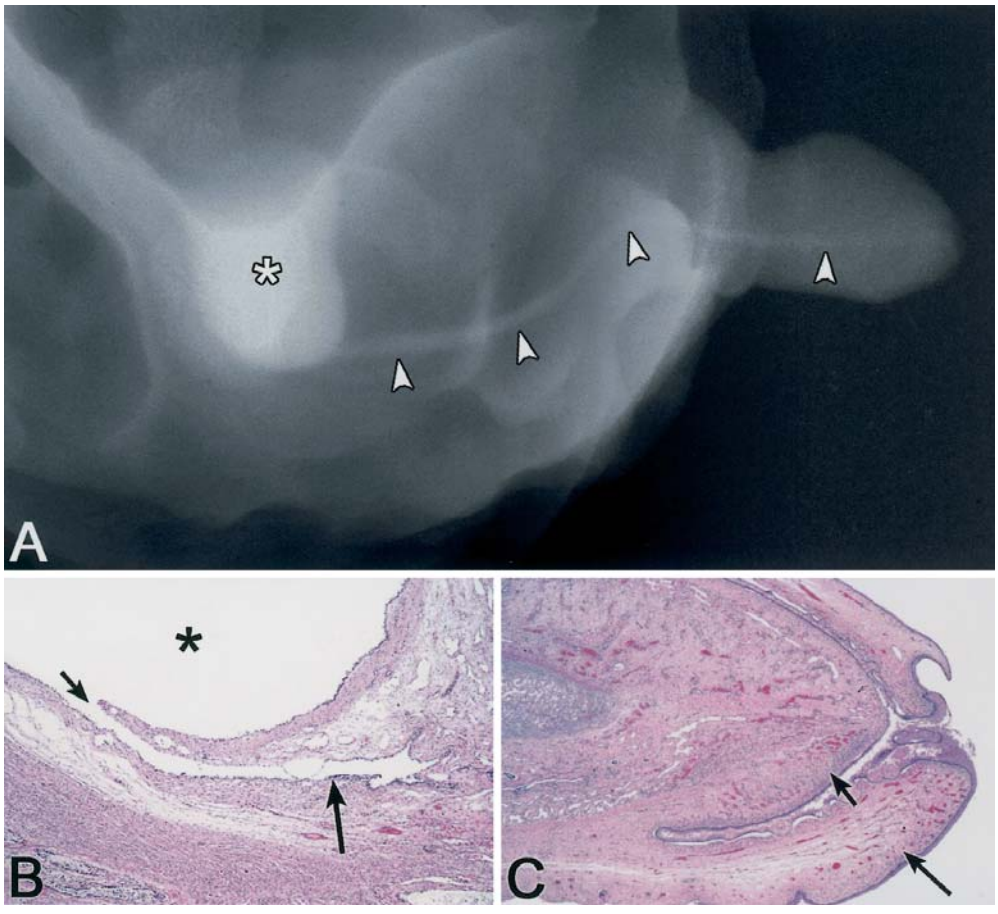



**Fig. 3** Case-2 pathology. **a** Postmortem cystourethrogram shows the prostatic urethra (*) bulging anteriorly and compressing the more distal penile urethra (*arrowheads*). **b** Longitudinal section through the midline demonstrating the prostatic (*) and penile (*long arrow*) portions of the urethra. A flap-like obstruction is evident with a small, narrow opening (*short arrow*; medium power H&E). **c** Longitudinal section through the distal penis demonstrating the normal relationship between the glans (*short arrow*) and the prepuce (*long arrow*; medium power H&E)

nography at our institution at 20 weeks and 4 days revealed oligohydramnios and multiple fetal abnormalities including a markedly enlarged bladder and dysplastic kidneys. The abdominal circumference was 21.6 cm, equivalent to an anatomic age of 26 weeks. Cytogenetic analysis of fetal urine revealed a karyotype of 46, XY with a balanced reciprocal translocation between 7p13 and 9q22; the same abnormality was detected in maternal blood. Maternal serology was negative for hepatitis B, and syphilis and there was no history of sexually transmitted disease. There was no family history of congenital malformation. The patient elected to terminate the pregnancy, and a prostaglandin induction of labor was performed at 23 weeks and 3 days.

*Gross findings*

External examination revealed a male fetus with an anatomic age consistent with 24–25 weeks gestation (812 g, crown–rump 23 cm, toe–heel 4.5 cm). The abdomen was enlarged and flaccid, exhibiting the prune belly appearance, and had a circumference of 23 cm (consistent with 27 weeks gestation). The fetus had Potter facies. The urinary bladder was massively enlarged, as were the ureters. The left kidney was significantly enlarged and cystic, while the right was only mildly enlarged. The heart and lungs were hypoplastic and confined within a small thoracic cavity. The heart, lungs, and intestinal tract showed normal configuration, as did the nervous system.

*Histological findings*

The lower urinary tract was removed en bloc and fixed in formalin distention. A water-soluble contrast medium was used for cystourethrography and revealed obstruction at the junction of the prostatic and penile portions of the urethra (Fig. 3a). The urethra and bladder were bisected in the midline and submitted for serial histological sectioning. The sections revealed an abnormally acute angle between the prostatic and penile portions of the urethra, with a very narrow connection (Fig. 3b). Sections of the penis showed no evidence of phimosis or other distal obstruction (Fig. 3c). The penis had a normal corpora, normal glans, normal prepuce, and normal caliber urethra in contrast to case 1 (Fig. 4). The bladder wall was thickened and the kidneys were dysplastic. No prostatic glands were seen.

## Comment

The etiology of the PBS has long been a source of great confusion and controversy. While many investigators initially embraced the theory of a primary urinary tract obstruction, set forth by Stumme in 1903 [1], others have pointed out difficulty in finding concrete proof of anatomic obstruction [3, 7, 9]. This has led to more recent work concluding that a primary mesenchymal defect leads to abnormalities in the lower urinary tract and abdominal wall [6, 7, 8, 9, 10]. A few investigators have conducted a thorough search for obstruction utilizing the en bloc serial sectioning technique. Such techniques have detected anatomic obstruction in the majority of cases [2, 5, 8].

In a recent study, serial sectioning and correlation with cystourethrography delineated multiple patterns of anatomic obstruction [8]. The most common pattern was that of a flap-like formation at the junction of the pros-

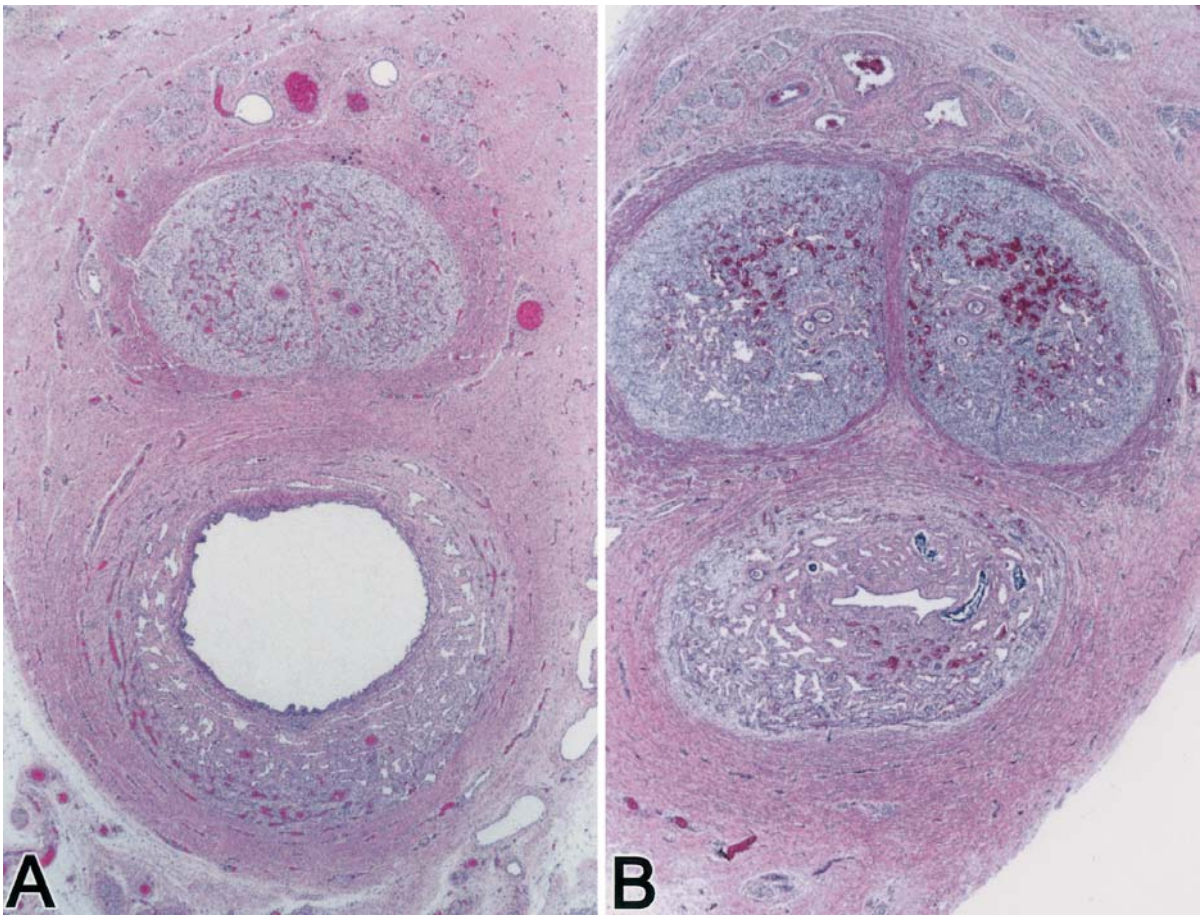



**Fig. 4** Comparison of urethra caliber. Cross-sections at level of the base of the penis show a markedly dilated urethra in case 1 (**a**) relative to case 2 (**b**) (medium power H&E)

tatic urethra with the proximal penile urethra. This was caused by a large dilated, saccular prostatic urethra folding over and pinching off the proximal penile urethra. Case 2 provides yet another example of this phenomenon. It is less common to find anatomic obstruction in the penile urethra itself. Case 1 details what we believe to be the first report of phimosis causing PBS.

In addition to the prune belly phenotype, the fetuses reported here had massively dilated bladders and ureters, with moderate to severe renal dysplasia. While the prostates lacked glandular development, each did demonstrate mesenchymal development to some degree, suggesting that the prostate did indeed form at some point. These findings suggest that the abnormal urinary tract and abdominal wall development in PBS is a pressure-induced dysplasia rather than a primary maldevelopment.

In summary, the cases presented here compare obstruction caused by phimosis to the more common flap-like malformation of the more proximal urethra in PBS. These cases re-emphasize the importance of a thorough search for anatomic obstruction in the examination of PBS cases. With the aid of postmortem cystourethrography, appropriate areas were identified for serial sectioning. These findings suggest that the phenotype of PBS and the abnormalities of prostatic development are secondary manifestations of anatomic or functional urethral obstruction.

## References

1. Eagle JF, Barrett GS (1950) Congenital deficiency of abdominal musculature with associated genitourinary abnormalities: a syndrome. Report of 9 cases. Pediatrics 6:721–736
2. Moerman P, Fryns J, Goddeeris P, Lauweryns JM (1984) Pathogenesis of the prune-belly syndrome: a functional urethral obstruction caused by prostatic hypoplasia. Pediatrics 73:470–475
3. Nunn IN, Stephens FD (1961) The triad syndrome: a composite anomaly of the abdominal wall, urinary system and testes. J Urol 86:782–794
4. Popek EJ, Tyson RW, Miller GJ, Caldwell S (1991) Prostate development in prune belly syndrome (PBS) and posterior urethral valves (PUV): etiology of PBS – lower urinary tract obstruction or primary mesenchymal defect? Pediatr Pathol 11:1–29
5. Poucell-Hatton S, Huang M, Bannykh S, Benirschke K, Masliah E (2000) Fetal obstructive uropathy: patterns of renal pathology. Pediatr Dev Pathol 3:223–231
6. Stephens FD, Gupta D (1994) Pathogenesis of the prune belly syndrome. J Urol 152:2328–2331
7. Straub E, Spranger J (1981) Etiology and pathogenesis of the prune belly syndrome. Kidney Int 20:695–699
8. Volmar KE, Fritsch MK, Perlman EJ, Hutchins GM (2001) Patterns of congenital lower urinary tract obstructive uropathy: relation to abnormal prostate and bladder development and the prune belly syndrome. Pediatr Dev Pathol 4:467–472
9. Wigger HJ, Blanc WA (1977) The prune belly syndrome. Pathol Annu 12:17–39
10. Williams DI, Burkholder GV (1967) The prune belly syndrome. J Urol 98:244–251

Virchows Arch (2003) 442:173–178
DOI 10.1007/s00428-002-0731-9

CASE REPORT

**Yukitoshi Satoh · Yuichi Ishikawa · Tatsu Miyoshi
Hiroyuki Mukai · Sakae Okumura · Ken Nakagawa**

# Pulmonary metastases from a low-grade endometrial stromal sarcoma confirmed by chromosome aberration and fluorescence in-situ hybridization approaches: a case of recurrence 13 years after hysterectomy

Received: 10 June 2002 / Accepted: 26 September 2002 / Published online: 26 November 2002
© Springer-Verlag 2002

**Abstract** Pulmonary metastasis from low-grade endometrial stromal sarcomas (ESSs) occasionally are found after long, disease-free periods, mostly as incidental histological or radiological discoveries. We describe a case of low-grade ESS presenting as nodular pulmonary metastases finally diagnosed by estrogen-receptor staining, cytogenetic and fluorescence in situ hybridization (FISH) analyses, and perusal of the histology of hysterectomy material. An abnormal nodule in the lung field was discovered by means of chest X-ray of a 47-year-old woman. She had been disease free for 13 years after hysterectomy for an alleged leiomyoma. A computed tomographic scan revealed nodules, with fluctuation in size over the 2-year period, in both lungs. Finally the lesion in the left lung was resected, and pulmonary endometriosis was suspected because of the lack of stromal cell nuclear atypia and positive immunohistochemical reactions for estrogen and progesterone receptors. However, a characteristic karyotype was identified cytogenetically: 46, XX, t(7;17)(p15;q11), the translocation of which, specific to ESS, was confirmed by FISH analysis. A final diagnosis of pulmonary metastases from an ESS could be made by reviewing the histology of the previous uterine tumor. In this case, metastatic lesions from an ESS showed a decrease as well as an increase in size, despite the malignant potential. Immunostaining for estrogen and progesterone receptors and cytogenetic and FISH analyses, together with clinical information on the past gynecological history, are valuable diagnostic keys.

Y. Satoh (✉) · Y. Ishikawa · T. Miyoshi · H. Mukai
Department of Pathology, the JFCR Cancer Institute,
1-37-1 Kami-ikebukuro, Toshima-ku, Tokyo 170-8455, Japan
e-mail: ysatoh@jfcr.or.jp
Tel.: +81-3-39180111, Fax: +81-3-53943889

Y. Satoh · T. Miyoshi · S. Okumura · K. Nakagawa
Department of Chest Surgery, the JFCR Cancer Institute Hospital,
1-37-1 Kami-ikebukuro, Toshima-ku, Tokyo 170-8455, Japan

**Keywords** Estrogen and progesterone receptors · Cytogenetics · Pulmonary metastases · Endometrial stromal sarcomas

## Introduction

The endometrial stromal sarcoma (ESS) is a rare neoplasm comprising only 0.2% of all uterine malignancies and approximately 15–26% of primary uterine sarcomas [1, 5, 8, 13, 14, 18]. It is subdivided into two distinct subtypes, low-grade and high-grade, based on differences in morphological atypia and proliferative activity [17]. The high-grade ESS has an aggressive nature, whereas low-grade lesions, known as endolymphatic stromal myosis, occasionally recur locally in the pelvic cavity or show distant metastasis, sometimes long after (for example, more than 10 years) the initial diagnosis [12, 21]. With such low-grade ESSs, diagnostic difficulties may arise, because neoplastic cells usually show slight or even no nuclear atypia as well as lacking any specific structural pattern on histological assessment.

We experienced an unusual case of pulmonary metastases from a low-grade ESS, in which asymptomatic nodules in both lungs were discovered by imaging procedures in a patient who had been disease free for 13 years after hysterectomy for a suspected leiomyoma. Since the nodules were composed of cells resembling those of the normal endometrial stroma and showed peculiar growth characteristics, they were the initially diagnosed as reflecting pulmonary endometriosis because of the lack of detailed information on the actual nature of the uterine tumor. Here, we describe the entire features of the case, of which a final diagnosis could be made based on immunohistological, cytogenetic and fluorescence in situ hybridization (FISH) analyses.

**Table 1** Changes in sizes of the bilateral lung nodules during follow-up. *CT* computed tomographic, – no record

| Date | Left lower lobe | | Right lower lobe | |
|---|---|---|---|---|
| | Roentgenogram | CT scan | Roentgenogram | CT scan |
| 10/04/1997 | 15 mm | – | 6 mm | – |
| 10/19/1998 | 25 mm | – | 8 mm | – |
| 11/07/1998 | – | 25 m | – | 9 mm |
| 12/08/1998 | 26 mm | – | – | – |
| 01/16/1999 | – | 26 mm | – | – |
| 03/24/1999 | 20 mm | – | – | – |
| 04/19/1999 | – | 20 mm | – | – |
| 08/07/1999 | 28 mm | – | – | – |
| 09/09/1999 | 20 mm | – | 4 mm | – |
| 09/21/1999 | – | 23 mm | – | – |
| 11/11/1999 | 32 mm | – | – | 7 mm |
| 11/19/1999 | Resected | Resected | 6 mm | – |

## Case report

A 47-year-old Japanese woman was admitted to the Cancer Institute Hospital for further examination of nodules existing in both lungs. These had been found at a regular health check-up on a chest X-ray film 2 years previously and followed up at another hospital. They had decreased in size, then increased again during the course of observations (Table 1). The patient had a history of simple hysterectomy under the clinical diagnosis of leiomyoma uteri at a local hospital 13 years previously (at the age of 34 years in 1986). She was followed up at the same hospital for several months after the operation, then ceased showing up because she felt well. Thereafter, she remained healthy and had no pulmonary symptoms, now or in the past. She had never used any hormonal medications and had always been in good health.

A computed tomographic (CT) scan revealed one 23-mm, well-circumscribed nodule in the left lower lung field and one 7-mm, well-circumscribed nodule in the right lower lung field. Considering the patient's history of hysterectomy for "myoma uteri", differential diagnosis included a "benign" metastasizing leiomyoma derived from the leiomyoma uteri as well as other benign and malignant lesions.

Transbronchial biopsy failed to access the tumors, so video-assisted thoracoscopic surgery for the nodule in the left lung was performed. As intra-operative frozen sections showed proliferation of monotonous small-sized oval to spindle-shaped cells without atypia, a benign nonepithelial neoplastic lesion was highly suspected.

Hormonal treatment was not administered after surgery. There were no new pulmonary nodules and the right one showed a gradual decrease in size during 1 year of follow-up. She is now alive and well after 2 years of follow-up.

## Materials and methods

For light microscopy, material from the surgical specimen was fixed in 15% buffered formalin and embedded in paraffin. Sections, 4 μm thick, were stained with hematoxylin and eosin. For immunohistochemistry, paraffin sections were stained using the SBC peroxidase method, with antibodies against the vimentin, actin (HHF35), desmin, S-100 protein, neuron-specific enolase (NSE), chromogranin A, synaptophysin, epithelial membrane antigen (EMA), cytokeratin AE1/AE3, estrogen and progesterone receptors (Nichirei), thyroid transcription factor-1 (TTF-1; Neomarkers) and surfactant apoprotein (PE-10; Dako).

Chromosome analysis was performed on fresh surgical material. Without collagenase dissociation, a cell suspension was seeded into tissue culture containing RPMI-1640 medium and antibiotics, supplemented with 10% fetal bovine serum, and incubated at 37°C in a 5% $CO_2$ atmosphere. When cultures entered exponential growth, they were harvested after Colcemid (0.01–0.05 μg/ml) treatment. Slides were prepared using conventional techniques and, after air drying, underwent quinaklin mustard staining. The standard International System of Human Cytogenetic Nomenclature (ISCN, 1995) was used to identify chromosomal abnormalities [16].

For FISH analysis, slides were prepared according to previously described protocols. FISH experiments were carried out using whole chromosome painting probes for chromosomes 7 and 17 labeled with Cy3 and FITC (fluorescein isothiocyanate), respectively (Cambio, Cambridge, UK), and chromosomes were counterstained with 4'-6'-diamidino-2-phenylindole (DAPI). Analyses were carried out using a fluorescence microscope with a charged-coupled device (CCD) camera. At least ten metaphase spreads were analyzed. Comparison of FISH signals and Q-banding was used to determine the composition of the derivative chromosomes.

## Results

### Histological findings

The resected material was an intra-parenchymal single, pale and soft nodule, 20 mm in diameter, found in the peripheral portion of the lower lobe. The nodule bulged above the covering pleura with rounded contours.

Microscopically, the nodule had an expansive non-infiltrative margin and was composed of cells identical to, or closely resembling, those of the normal endometrial stroma (Fig. 1a). The cells were uniform in appearance, size, shape and staining qualities. They were arranged in vaguely concentric patterns around vessels (Fig. 1b). Glandular structures were not evident within the lesion, and the proliferating cells had small amounts of eosinophilic cytoplasm, and the nuclei, with an oval to spindle shape, had finely granular chromatin with a thin nuclear membrane. Nucleoli were not easily identified. Mitotic activity was moderate (from 5 to 9 counts per 10 high-power fields), but no necrotic foci were identified. Some gland-like structures, thought to be residual alveoli with hyperplastic type-II pneumocytes, were embedded in the periphery of the tumor nest. No hemosiderin granules were observed within the lesion. No abnormalities were noted in the uninvolved pulmonary parenchyma around the lesion.

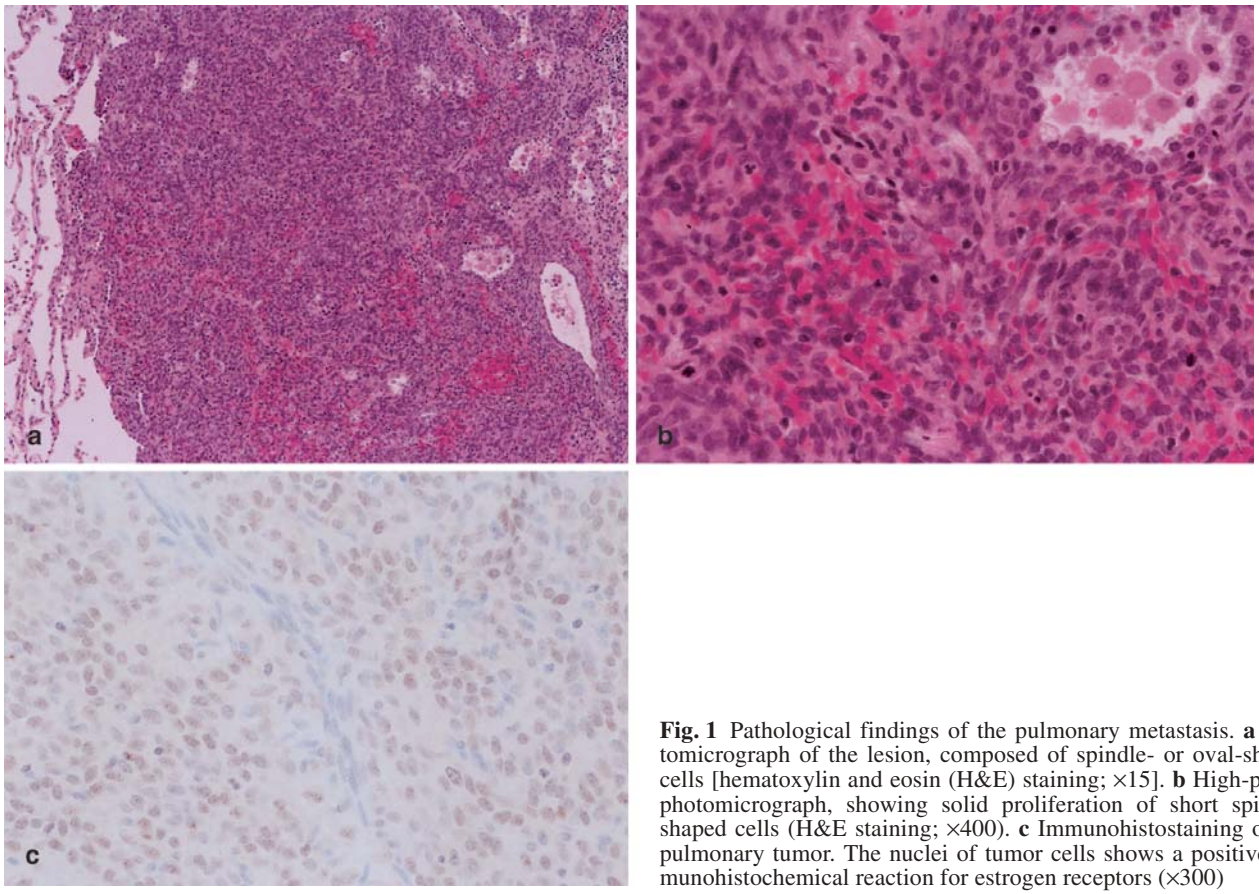



**Fig. 1** Pathological findings of the pulmonary metastasis. **a** Photomicrograph of the lesion, composed of spindle- or oval-shaped cells [hematoxylin and eosin (H&E) staining; ×15]. **b** High-power photomicrograph, showing solid proliferation of short spindle-shaped cells (H&E staining; ×400). **c** Immunohistostaining of the pulmonary tumor. The nuclei of tumor cells shows a positive immunohistochemical reaction for estrogen receptors (×300)

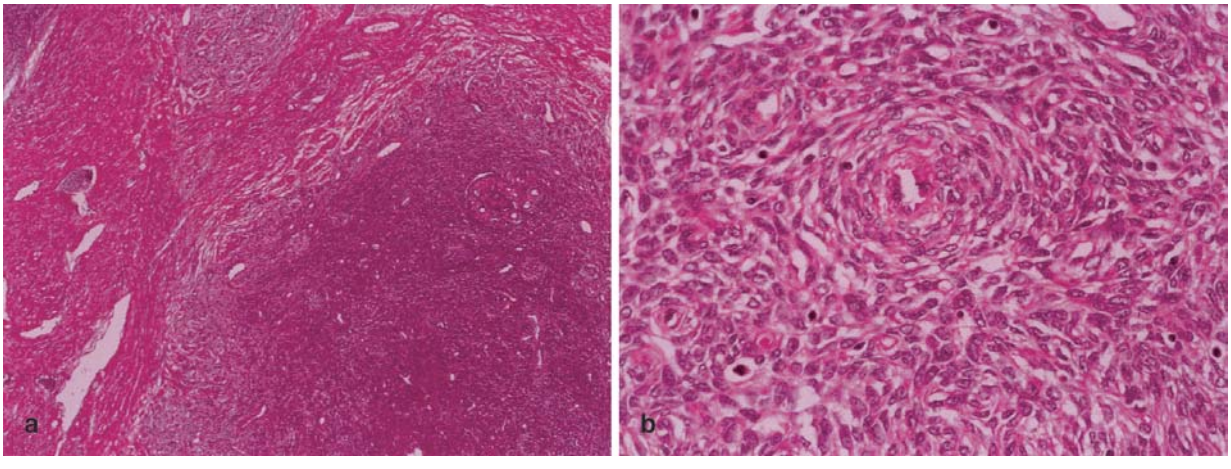



**Fig. 2** Histology of the uterine tumor resected 13 years previously. **a** Neoplastic cells resembling endometrial stromal cells with dense proliferation [hematoxylin and eosin (H&E) staining; ×15]. **b** No mitotic figures are apparent, but nuclear atypia are evident (H&E staining; ×400)

Immunohistochemistry demonstrated the tumor cells to be positive for vimentin and highly positive for estrogen and progesterone receptors (more than 90%, Fig. 1c); they were negative for cytokeratin, actin (HHF35), NSE, EMA, desmin, S-100 protein, chromogranin A, surfactant apoprotein (PE-10), TTF-1 and synaptophysin. These findings are compatible with an endometrial stromal nature [2, 4, 6, 15, 18]. Therefore, the tentative diagnosis at this stage was pulmonary stromal endometriosis [11].

Fortunately, it was possible to review the corpus uterine tumor, resected in 1986, retrospectively. According to the pathology report made 13 years ago, the tumor was a solid mass, sized 100×70×50 mm, whitish to yellowish in color, and showing expansive growth with a partly irregular border. The histological findings were

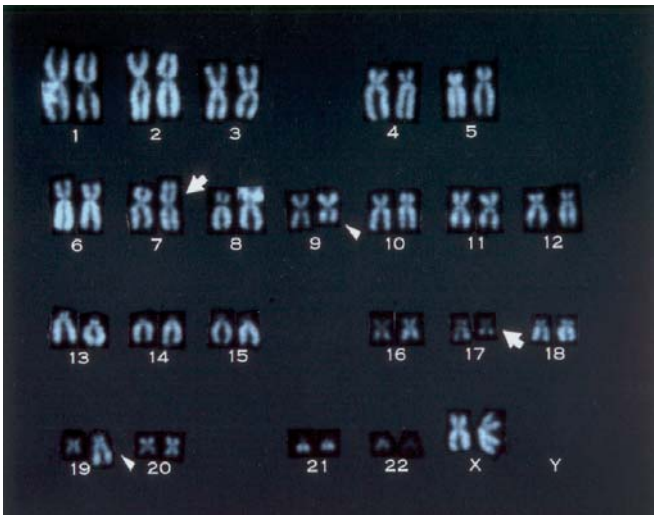



**Fig. 3** Q-banded karyotype of the pulmonary tumor cells. *Arrowheads* indicate the del(9)(q22) and add(19)(q13). *Arrows* indicate the two derivative chromosomes, der(7) and der(17), resulting from a 7;17 translocation

fundamentally the same as those for the lung nodule except for nuclear atypia. The tumor was composed of sheets of densely packed, uniform, small to medium-sized cells with slight nuclear atypia, and there were sparse mitotic figures (about 0–1 cell per 10 HPFs, Fig. 2). Venous infiltration was evident at the periphery, but no serosal involvement was seen. Based on these findings, the uterine neoplasm was diagnosed as a low-grade ESS with low proliferative activity in 1986.

### Chromosome analysis

For Q-banded analysis, ten metaphases were examined. The tumor cells were pseudo-diploid and showed monoclonal abnormalities, resulting in the following karyotype: 46,XX,t(7;17)(p15;q11),del(9)(q22), add(19)(q13) (Fig. 3). The translocation t(7;17) was confirmed by FISH analysis (Fig. 4).

### Clinical course, hormonal examination and basal body temperature

Hormonal parameters, including serum estradiol levels over 8 weeks, showed irregularities. Clinical tests, including gynecological examination and pelvic and abdominal ultrasonography, revealed no abnormalities. A CT scan of the abdomen performed after application of contrast medium also demonstrated no adnexal or peritoneal abnormalities. The basal body temperature chart recorded over 8 weeks showed no regular cycle.

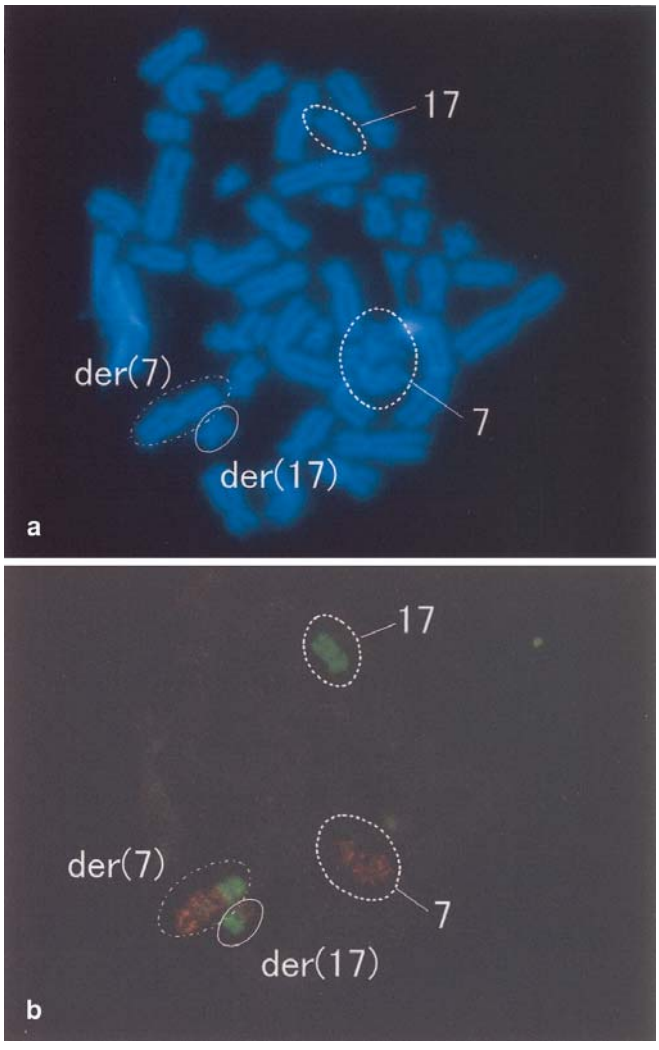



**Fig. 4** Fluorescence in-situ hybridization (FISH) analysis. **a** 4'-6'-diamidino-2-phenylindole-stained metaphase cell. **b** The same chromosome spread hybridized with whole chromosome probes for chromosomes 7(red) and 17(green). Green/red fusion signals are present on both der(7) and der(17)

## Discussion

When tumors or tumor-like conditions are found in the lungs of women who have a history of hysterectomy, even many years previously, clinicians and pathologists need to make a careful differential diagnosis [12]. Usually, the cases feature leiomyomatous lesions such as metastasizing leiomyomas of the uterus. In this report, we presented a case of multiple lesions composed of short spindle cells with little nuclear atypia and no other pathognomonic features in histology. Since the histology of the resected uterine tumor was unknown to either the surgeon or the pathologist at the time of the thoracotomy, the obvious question was whether these lesions were benign or malignant. Based on findings obtained from immunohistochemistry for estrogen and progesterone receptors and the characteristic fluctuation of size,

we diagnosed pulmonary endometriosis [1, 2, 4, 5, 14, 17, 18]. Further examinations, however, including chromosome analysis and FISH techniques, strongly suggested the lesions to be metastases from a low-grade ESS [4, 8, 9, 10, 20]. Subsequent examination of microscopic slides of the original uterine tumor confirmed this final diagnosis.

Low-grade ESS has been considered to be a hormone-sensitive neoplasm, as suggested by mRNA detection as well as by immunohistochemical evidence of estrogen and progesterone receptors [12, 19]. If sensitivity to hormones is identical to such immunohistochemical positivity to estrogen and progesterone receptors, the tumors in our case might have been dependent on serum concentration for growth. However, there was no apparent relationship between the tumor size and changes in serum gonadotropin levels or basal body temperature.

Cytogenetic analyses of pulmonary metastases of ESS have been limited, although several studies have demonstrated that primary lesions showed clonal structural abnormalities [4, 8, 9, 10, 20]. Rearrangements of chromosomes 6, 7 and 17 are the most consistent features [4, 8, 9, 10, 20]. In our case, a deletion of chromosome 9 at q22 band and rearrangement of chromosome 19 with material of unknown origin transferred to q13 with a t(7;17)(p15;q11) were present. A t(7;17) translocation seems to be a primary specific cytogenetic abnormality in the low-grade ESS [8]. The q13 band of chromosome 19 is often altered in malignant mixed mesodermal tumors of the uterus, arising mostly through the addition of material of unknown origin [7]. Aberrations of chromosome 19 have already been demonstrated in other low-grade ESSs, even if with different chromosomal change, so that such lesions, therefore, have relatively simple karyotypes, generally with rearrangements of two or three chromosomes. In contrast, multiple numerical and structural aberrations are typical of the high-grade ESS [8]. Therefore, application of cytogenetic techniques can provide useful evidence for diagnosis and subdivision of this type of lesion.

It is true that the lesion in our case metastasized from the uterus to the lungs, but the grade of malignancy was clearly very low. Although some mitotic figures were evident, stromal cell nuclear atypia such as enlargement, increased and/or coarse chromatin, and conspicuous nucleoli were absent in the pulmonary lesion. Furthermore, there were no hyaline sclerotic areas and no sex cord-like structures or cystic changes, strongly suggesting very low malignant potential [3, 4, 5]. The findings are thus in line with the well-differentiated nature, with fluctuation in size, presumably due to variation in response to female hormones.

When nonepithelial neoplastic lesions are found in the lungs of women with a history of gynecological disease, careful distinction between pulmonary metastases of ESS and other neoplasms is necessary. In such cases, it is suggested that immunostaining for estrogen or progesterone receptors and cytogenetic approaches for the pulmonary lesion, as well as the detailed investigation of history of gynecological disease, are very useful tools. Moreover, these could be applied for confirmation of the histomorphological diagnosis in our case for which pathological diagnosis of ESS was difficult due to the absence of stromal cell nuclear atypia.

**Acknowledgements** The authors wish to thank Dr. Hitoshi Satoh, Ph.D., Department of Cancer Research, Division of Pathology, The Institute of Medical Science, The University of Tokyo, for his technical expertise. This study is supported by Grants-in-aid from the Ministry of Education, Sports, Culture, Science and Technology, grants from the Ministry of Health, Labor and Welfare, the Smoking Research Foundation, and the Vehicles Racing Commemorative Foundation.

## References

1. Aaro LA, Symmonds RE, Dockerty MB (1966) Sarcoma of the uterus: a clinical and pathologic study of 177 cases. Am J Obstet Gynecol 94:101–109
2. Abrams J, Talcott J, Corson JM (1989) Pulmonary metastases in patients with low-grade endometrial stromal sarcoma. Cliniopathologic findings with immunohistochemical characterization. Am J Surg Pathol 13:133–140
3. Chang KL, Crabtree GS, Lim-Tan SK, Kempson RL, Hendrickson MR (1990) Primary uterine endometrial stromal neoplasms. A clinicopathologic study of 117 cases. Am J Surg Pathol 14:415–438
4. Cheung ANY, Ng WF, Chung LP, Khoo US (1996) Mixed low grade and high grade endometrial stromal sarcoma of uterus: differences on immunohistochemistry and chromosomal in situ hybridization. J Clin Pathol 49:604–607
5. Farhood AI, Abrams J (1991) Immunohistochemistry of endometrial stromal sarcoma. Hum Pathol 22:224–230
6. Fujishita A, Nakane PK, Koji T, Masuzaki H, Chavez RO, Yamabe T, Ishimaru T (1997) Expression of estrogen and progesterone receptors in endometrium and peritoneal endometriosis: an immunohistochemical and in situ hybridization study. Fertil Steril 67:856–864
7. Gil-Benso R, Lopez-Gines C, Carda-Batalla C, Monteagudo-Castro C, Torres JV, Llombart-Bosch A (1997) Cytogenetic findings in malignant mixed mesodermal tumours of the uterus. Cancer Genet Cytogenet 99:121–125
8. Gil-Benso R, Lopez-Gines C, Navarro S, Carda C, Llombart-Bosch A (1999) Endometrial stromal sarcomas: immunohistochemical, electron microscopical and cytogenetic findings in two cases. Virchows Arch 434:307–314
9. Hennig Y, Caselitz J, Bartnitzke S, Bullerdiek J (1997) A third case of a low-grade endometrial stromal sarcoma with a t(7;17)(p14 approximately 21; q11.2 approximately 21). Cancer Genet Cytogenet 98:84–86
10. Hrynchak M, Horsman D, Salski C, Berean K, Benedet JL (1994) Complex karyotypic alterations in an endometrial stromal sarcoma. Cancer Genet Cytogenet 77:45–49
11. Huber M, Wierrani F, Bohm G, Hauck H, Lintner F, Grunberger W (1999) Multiple endometrial stromal nodules with sparse cysts and glands in the lung – a nodular variation of endometriosis that may mimic metastases of sarcoma. Pathol Res Pract 195:59–64
12. Inayama Y, Shoji A, Odagiri S, Hirahara F, Ito T, Kawano N, Nakatani Y (2000) Detection of pulmonary metastasis of low-grade endometrial stromal sarcoma 25 years after hysterectomy. Pathol Res Pract 196:129–134
13. Kempson RL, Bari W (1970) Uterine sarcomas: classification, diagnosis and prognosis. Hum Pathol 1:331–349
14. Koss LG, Spiro RH, Brunschwig A (1965) Endometrial stromal sarcoma. Surg Gynecol Obstet 121:531–537

15. Mai KT, Yazdi HM, Perkins DG, Parks W (1997) Pathogenetic role of the stromal cells in endometriosis and adenomyosis. Histopathology 30:430–442
16. Mitelman F (1995) Guidelines for cancer cytogenetics. Supplement to an international system for human cytogenetic nomenclature. Karger for ISCN, Basel
17. Norris HJ, Taylor HB (1966) Mesenchymal tumors of the uterus. Cancer 19:755–766
18. Sabini G, Chumas JC, Mann WJ (1992) Steroid hormone receptors in endometrial stromal sarcomas. A biochemistry and immunohistochemical study. Am J Clin Pathol 97:381–386
19. Sakamoto H, Nakayama Y, Ohtani K, Seiki M, Satoh K (1997) Pulmonary metastatic lesion of endolymphatic stromal myosis expresses metastasis-related genes but not invasion-related matrix type metalloproteinase. Cancer Lett 112:245–249
20. Streekantaiah C, Li FP, Weidner N, Sandberg AA (1991) An endometrial stromal sarcoma with clonal cytogenetic abnormalities. Cancer Genet Cytogenet 55:163–166
21. Tabata T, Takeshima N, Hirai Y, Hasumi K (1999) Low-grade endometrial stromal sarcoma with cardiovascular involvement: a report of three cases. Gynecol Oncol 75:495–498

Virchows Arch (2003) 442:179–182
DOI 10.1007/s00428-002-0739-1

LETTER TO THE EDITOR

**Ida Münster Ikonomou · Jahn M. Nesland**
**Svein Arve Schjølseth · Sverre Heim · Jan Delabie**

# Mantle cell lymphoma with Homer-Wright rosettes

Received: 25 September 2002 / Accepted: 16 October 2002 / Published online: 19 December 2002
© Springer-Verlag 2002

**Keywords** Lymphoma · Mantle cell · Rosette formation

## Introduction

Homer-Wright-type rosettes are an important morphologic finding in small round cell neoplasms as they may point to the diagnosis of neural tumors such as neuroblastoma, medulloblastoma, retinoblastoma and PNET/Ewing sarcoma [2, 5]. However, Homer-Wright type rosettes can exceptionally be seen in other types of neoplasia as well such as synovial sarcoma and, notably, lymphoma [2]. Several types of lymphoma have been reported to display rosettes [3, 6, 7, 8, 9, 10]. We report here the first case of a mantle cell lymphoma displaying Homer-Wright rosettes.

## Case report

A 65-year-old man presented with a solitary enlarged cervical lymph node. He had no previous history of illness or lymphoma. The lymph node was sent for pathological examination. A diagnosis of mantle cell lymphoma was made. Subsequent staging did not reveal disease in any other locations. The patient was treated with eight cycles of cyclophosphamide, doxorubicin, vincristine and prednisone (CHOP) followed by local irradiation. Complete remission was obtained. However, 2 years later the tumor recurred in contralateral cervical lymph nodes and the mediastinum. Subsequently, the patient was treated with three cycles of etoposide, mitoxantrone, cytarabine and prednisone (ENAP), followed by radiation therapy to the cervical region and mediastinum. A complete second remission was obtained, but the tumor recurred 1 year later in the inguinal lymph nodes, the left axillae and the right parotic region. The patient was first treated with trophosphamide, then with rituximab. Palliative local radiotherapy was also given. Partial remission was obtained. A half year later the tumor relapsed in the retroperitoneal lymph nodes. Partial response was achieved with chemotherapy (bleomycine and vincristine). Some months later the patient succumbed to *pneumocystis carinii* pneumonia. An autopsi was not performed.

I. M. Ikonomou (✉) · J. M. Nesland · J. Delabie
Department of Pathology, The Norwegian Radium Hospital, University of Oslo, Norway
e-mail: i.m.m.ikonomu@labmed.uio.no
Tel.: +47-229-34151, Fax: +47-229-35426

S. A. Schjølseth
Department of Oncology, Oppland Sentral Hospital, Lillehammer, Norway

S. Heim
Department of Cancer Genetics, The Norwegian Radium Hospital, Oslo, Norway

## Results

The histology of all lymph-node samples was similar. The normal architecture was replaced by a partly diffuse, partly vaguely nodular proliferation of lymphoid cells. The lymphoid cells had medium-sized, hyperchromatic nuclei without conspicuous nucleoli. A moderate degree of polymorphism was noted. Rosettes and trabeculae consisting of a pallisade of cells around central eosinophilic fibrillary material were diffusely present (Fig. 1a).

Immunohistochemically, the tumor cells expressed CD45, CD20 and CD5 on their membrane and cyclinD1 in their nuclei (Fig. 1c and d). No CD3 or CD23 expression was noted. The fibrillary center of the rosettes stained strongly for CD45 and CD20 (Fig. 1e), weakly for actin and partly for vimentin, but not for desmin or alpha smooth muscle actin.

Ultrastructural studies showed that the center of the rosettes consisted of cytoplasmic projections of the surrounding cells. These projections contained mitochondria, rough endoplasmic reticulum, ribosomes and polyribosomes. No obvious filaments were seen. No membranous junctions nor external lamina were observed (Fig. 2).

Cytogenetic analysis was performed at diagnosis and at second recurrence. Largely the same clonal chromosomal aberrations were found on both occasions corresponding to a hypertetraploid karyotype 93~94, XXYY, t(1;5)(q1;q33), −7,del(7)(q22)x2,add(9)(p22)x2,t(11;14)(q13;q32)x2,+21,+21,+1–4mar. The primary aberration is the 11;14-translocation that is specific for mantle cell lymphoma; whereas, the other aberrations presumably

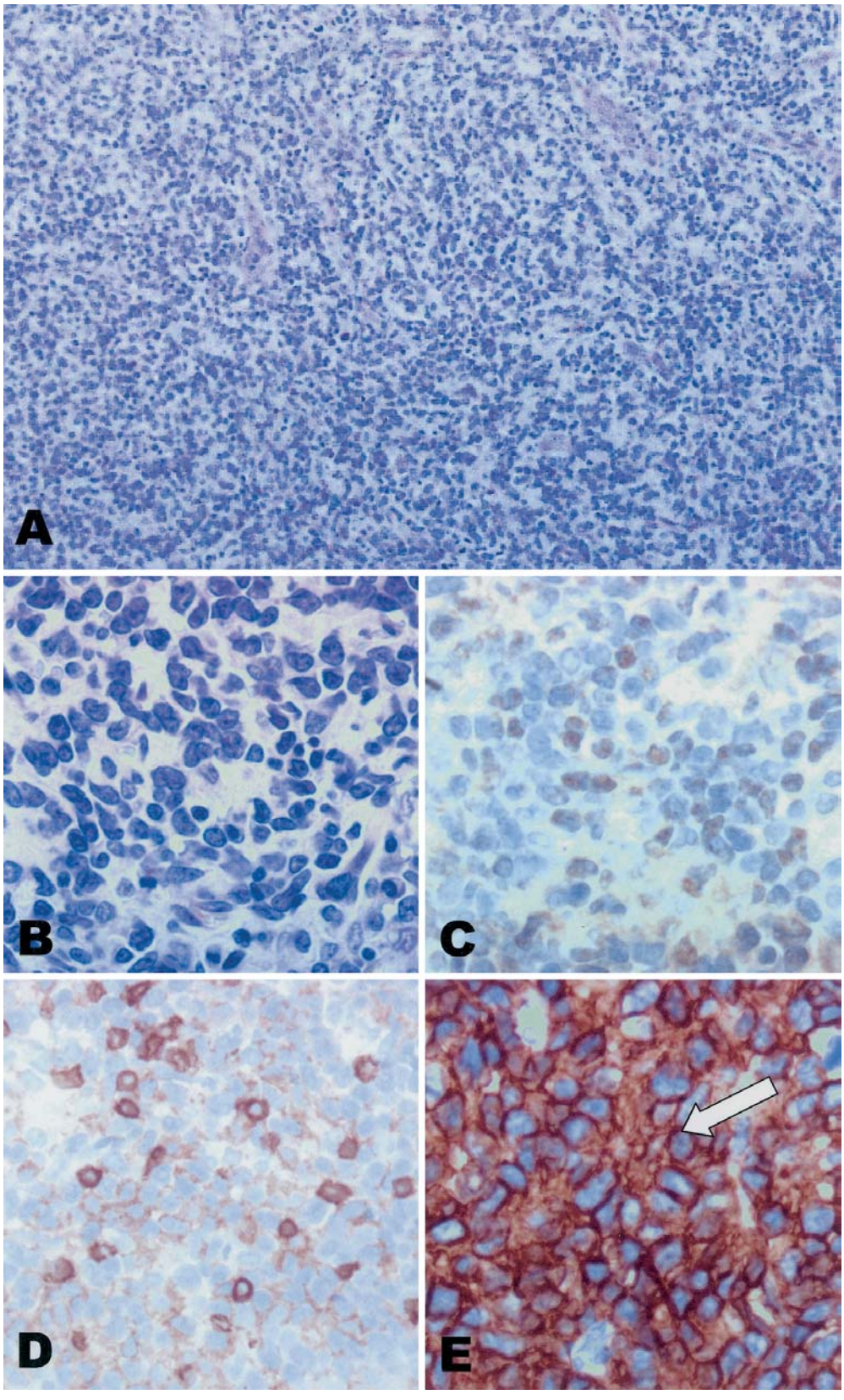



**Fig. 1** Histological and immunohistochemical features of the mantle cell lymphoma. **a** Morphological overview of the tumor reveals a proliferation of lymphoid cells with the formation of rosettes and trabeculae diffusely present. **b** The rosettes and trabeculae consist of a pallisade of cells around central eosinophilic fibrillary material. The tumor cells express nuclear cyclin D1 (**c**) and membranous CD5 (**d**), characteristic of mantle cell lymphoma. Immunohistochemical staining for CD20 highlights both the tumor cells and the central fibrillary material (*arrow*; **e**). *Original magnification* **a** ×60; **b–e** ×400

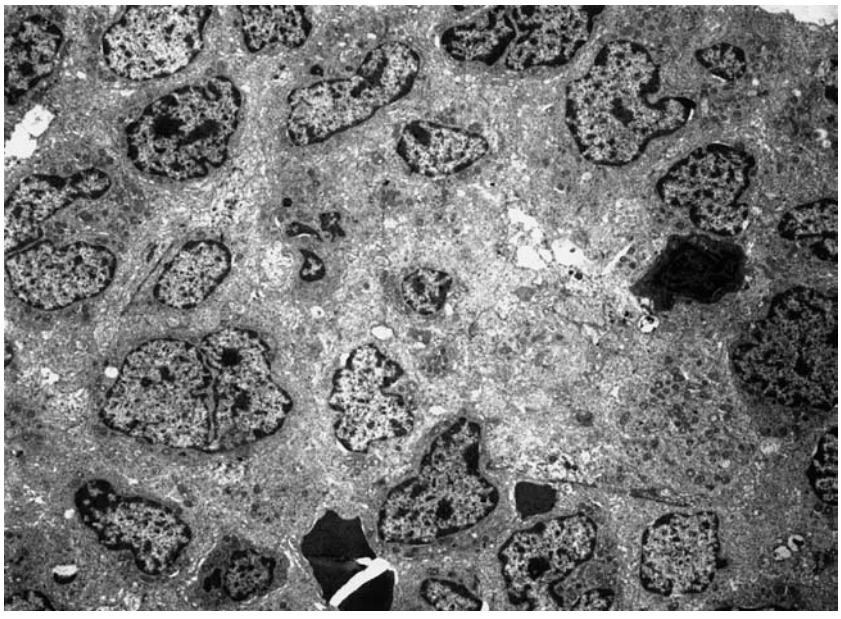


**Fig. 2** The central area of a rosette consisted of cytoplasmic projections of the lymphoma cells containing mitochondria, rough endoplasmic reticulum, ribosomes and polyribosomes. No obvious filaments were seen. No membranous specializations and no external lamina were present. Uranyl acetate-lead citrate; original magnification ×2300

are secondary, having developed as part of a clonal evolution within the lymphoma cell population [4].

Although Homer-Wright rosettes are typical of neural and neuroepithelial tumors and therefore of diagnostic importance, there have been several reports of their occurrence in lymphoma [2, 3, 5, 6, 7, 8, 9, 10]. Here we describe the occurrence of Homer-Wright rosettes in a case of mantle cell lymphoma. Homer-Wright rosettes have not been reported previously in mantle cell lymphoma, but have been reported in other lymphoma types.

Previously, Frizzera et al. described a case of follicular lymphoma with Homer-Wright rosettes [3]. As in the present case, rosettes in their case had a similar light microscopic and electron microscopic morphology (Fig. 1 and Fig. 2). The rosettes consisted of cytoplasmic projections of the surrounding cells. However, the cytoplasmic projections in the case of Frizzera et al. were more narrow and complex and rich in thin and intermediate filaments, whereas the projections in our case displayed more organelles such as mitochondria and rough endoplasmic reticulum. Koo et al. described three non-Hodgkin lymphoma cases with rosettes, one T-cell lymphoma, one small lymphocytic lymphoma and one diffuse large B-cell lymphoma [7]. The latter two cases contained rosettes with a central macrophage in addition to rosettes showing only cytoplasmic projections. Interestingly, ultrastructural examination revealed that the cytoplasmic projections forming the center of the rosettes derived from both tumor cells and macrophages. As in our case, their cases did not show any filaments in these cytoplasmic projections. Tsang et al. reported one case of diffuse large B-cell lymphoma with abundant fibrillary matrix and occasional rosettes [10]. The matrix consisted entirely of cytoplasmic projections upon ultrastructural examination. Ko et al. and Ozdemirli et al. reported a case of blastic NK-cell lymphoma and a case of lymphoblastic lymphoma, respectively, with Homer-Wright-type rosettes [6, 8]. The light microscopic findings of the rosettes were similar to those in our case.

The common theme in the few cases of non-Hodgkin lymphoma with rosettes is the presence of abundant cytoplasmic projections. The latter is also focally observed in follicular lymphoma, although no rosettes are formed [1]. Cytoplasmic projections without rosette formation are also typical in the so-called microvillous variant of diffuse large B-cell lymphoma [9]. Therefore, it seems clear that the formation of cytoplasmic projections or microvilli in non-Hodgkin lymphoma is not associated with any specific lymphoma type and that rosette-formation, although rare, is probably one end of the spectrum of microvilli formation. What causes lymphoma cells to form microvilli is not known.

In conclusion, we report a first case of mantle cell lymphoma with rosette formation. As other authors also have stressed, it is important for the diagnostic surgical pathologist to know that rosette formation is not specific to neural or neuro-epithelial tumors but also can be observed in lymphoma.

## References


1. Chittal SM, Caveriviere P, Voigt JJ, Dumont J, Benevent B, Faure P, Bordessoule GD, Delsol G (1987) Follicular lymphoma with abundant PAS-positive extracellular material. Immunohistochemical and ultrastructural observations. Am J Surg Pathol 11:618–624
2. Enzinger FM, Weiss SW (1995) Soft tissue tumors. 3rd edn. Mosby, St. Louis, Missouri
3. Frizzera G, Gajl-Peczalska K, Sibley RK, Rosai J, Cherwitz D, Hurd DD (1985) Rosette formation in malignant lymphoma. Am J Pathol 119:351–356
4. Jaffe ES, Harris NL, Stein H, Vardiman JW (eds) (2001) Pathology and genetics of tumours of haematopoietic and lymphoid tissues. World Health Organization classification of tumours. IARCPress, Lyon, France

5. Kleihues P, Cavenee WK (eds) (2000) Pathology and genetics of tumours of the nervous system. World Health Organization classification of tumours. IARCPress, Lyon, France
6. Ko YH, Kim SH, Ree HJ (1998) Blastic NK-cell lymphoma expressing terminal deoxynucleotidyl transferase with Homer-Wright type pseudorosettes formation. Histopathology 33: 547–555
7. Koo CH, Shin SS, Bracho F, Johnston WH, Rappaport H (1996) Rosette-forming non-Hodgkin's lymphomas. Histopathology 29:557–563
8. Ozdemirli M, Fanburg-Smith JC, Hartmann D-P, Azumi N, Miettinen M (2001) Differentiating lymphoblastic lymphoma and Ewing's sarcoma: lymphocyte markers and gene rearrangement. Mod Pathol 14:1175–1182
9. Rosai J (ed) (1995) Tumors of the lymph nodes and spleen. Atlas of tumor Pathology. 3rd series, fascicle no. 14. Armed Forces Institute of Pathology, Washington DC, pp 176–184
10. Tsang WYW, Chan JKC, Tang SK, Tse CCH, Cheung MMC (1992) Large cell lymphoma with fibrillary matrix. Histopathology 20:80–82

Virchows Arch (2003) 442:183–185
DOI 10.1007/s00428-002-0700-3

LETTER TO THE EDITOR

**Masato Nakamura · Yoshiyuki Abe**
**Hiroyuki Hatanaka · Yutaka Tsutsumi**
**Hiroshi Kijima · Yoshito Ueyama · Hiroshi Inoue**
**Yukio Shimosato · R. Yoshiyuki Osamura**

# Bronchial carcinoid tumor with gangliocytic- and paraganglionlike differentiation

Received: 13 March 2002 / Accepted: 24 June 2002 / Published online: 14 December 2002
© Springer-Verlag 2002

Sirs,

neuroendocrine tumors of the lung show a spectrum of histological variations ranging from classic carcinoid tumors to small-cell carcinoma [1]. We encountered a case of bronchial "carcinoid tumor with gangliocytic- and paraganglionlike differentiation." A 65-year-old man was admitted due to an abnormal shadow on his chest radiograph. He was asymptomatic, but a well-circumscribed coin lesion was seen in the right upper lung field. He underwent right upper lobectomy and dissection of mediastinal lymph nodes. Examination of the digestive tract, including abdominal computed tomography, duodenography, and barium enema, showed no apparent abnormalities. No hormonal signs or symptoms were recorded.

The 25×18 mm polypoid tumor involving the right upper lobe bronchus was well demarcated, and its cut surface was yellow or yellowish-white in color (Fig. 1). No necrotic foci were seen in the tumor. The tumor was composed of two different parts, containing three types of tumor cells. The major part of the tumor showed the trabecular, papillary and ribbonlike arrangement of medium-sized neoplastic cells, typical of carcinoid tumor (Fig. 2a). The polygonal to cuboidal cells contained round to ovoid nuclei. Nuclear atypia was minimal. The cells were focally arranged in rosettes. Mitotic figures were not seen. Some regions of the tumor showed proliferation of large round cells similar to ganglion cells surrounded by smaller spindle-shaped cells and fibrillary components (Fig. 2b). The ganglionlike cells possessed plump eosinophilic cytoplasm and vesicular nuclei with prominent nucleoli. The cells were embedded in fibrillar tissue somewhat resembling the nervous tissue. The neoplastic tissue showed transitional or mixed features. No regional lymph nodes were involved histologically. Histochemically, abundant argyrophilic granules were observed in the cytoplasm of both the carcinoidlike and smaller paraganglionlike tumor cells (Fig. 2c, d). Ganglionlike cells were only mildly argyrophilic. The immunohistochemical findings are summarized in Table 1. Some of the carcinoid cells and the smaller paraganglionlike cells were immunoreactive for chromogranin A, and these cells were mostly argyrophilic. The ganglionlike cells were negative for chromogranin A. While most carcinoid cells were weakly positive for synaptohysin in the cytoplasm (Fig. 2e), the ganglionlike cells were strongly

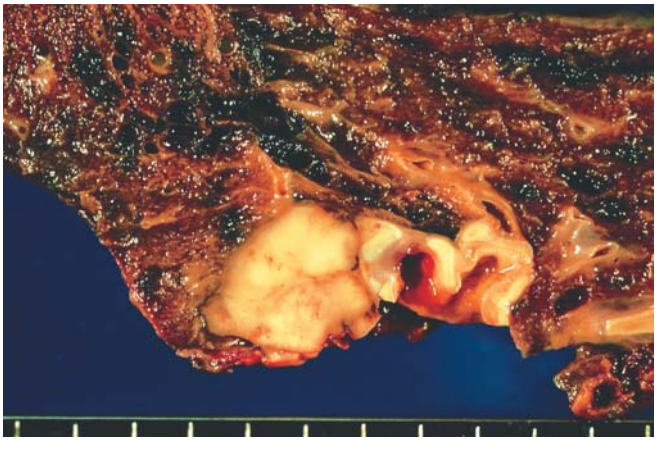


**Fig. 1** Gross findings. The 25×18 mm polypoid tumor involving the right upper lobe bronchus was well demarcated, and its cut surface was yellow or yellowish-white in color

M. Nakamura (✉) · H. Hatanaka · Y. Tsutsumi · H. Kijima
Y. Ueyama · R.Y. Osamura
Department of Pathology, Tokai University School of Medicine,
Isehara, Kanagawa 259-1193, Japan
e-mail: mnakamur@is.icc.u-tokai.ac.jp
Tel.: +81-463-931121, Fax: +81-463-911370

Y. Abe
National Kanagawa Hospital, Hadano, Kanagawa 257-8585, Japan

H. Inoue
Department of Surgery, Tokai University School of Medicine,
Isehara, Kanagawa 259-1193, Japan

Y. Shimosato
Department of Pathology, Keio University School of Medicine,
Shinjuku, Tokyo 160-8582, Japan

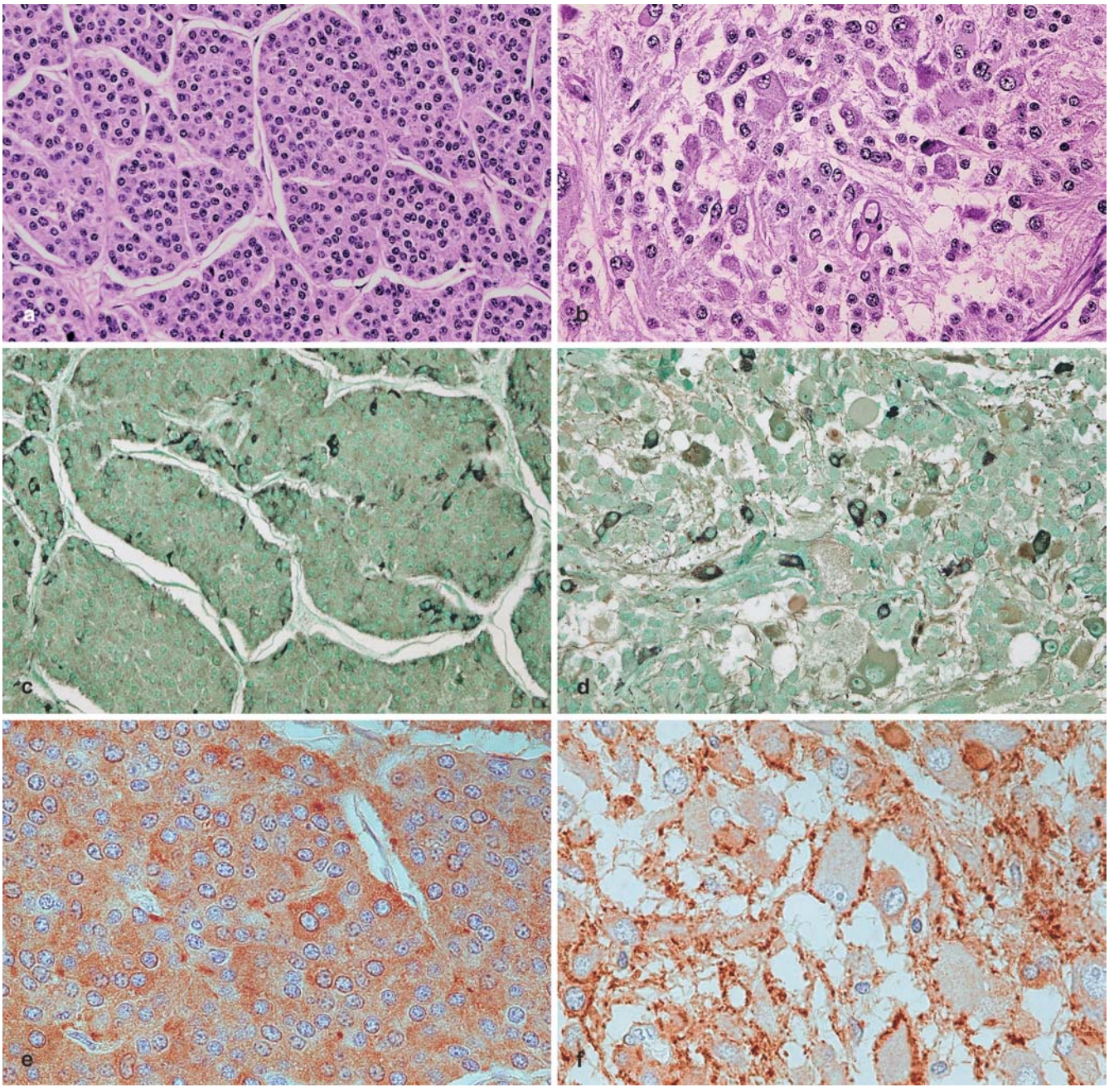



**Fig. 2a–f** Histological findings. **a** The carcinoid tumor cells possessed round to oval nuclei with no appreciable atypia, HE, ×75. **b** The ganglionlike cells had abundant cytoplasm, vesicular nuclei and prominent nucleoli; hematoxylin and eosin, ×75. **c**, **d** Abundant argyrophilic granules were present in the cytoplasm of both carcinoid cells (**c**) and paraganglion like cells (**d**) as determined by Grimelius' staining, ×75. **e** The carcinoid tumor cells were weakly positive for synaptophysin in the cytoplasm; ×150. **f** The ganglionlike cells were positive for synaptophysin at the cell surface; ×150

positive beneath the cell membrane in a synaptic vesicle-like fashion (Fig. 2f).

Gangliocytic paraganglioma is a rare benign tumor of the duodenum, which is composed of three types of cells, i.e., epithelioid cells with an endocrine pattern of growth, ganglion cells, and spindle cells [3, 4]. The morphological features in this case were consistent with so-called gangliocytic paraganglioma. A case of pulmonary gangliocytic paraganglioma has been reported [2]. While the immunohistochemical results presented here suggest that gangliocytic and paraganglionlike regions were considered to be abnormal morphological differentiation of the carcinoid tumor cells toward neuroectodermal appearance. The tumor cells resembling paraganglionlike cells expressing chromogranin A and the neuroendocrine markers were regarded as a variation of carcinoid tumor cells. In our opinion, “carcinoid tumor with gangliocytic- and paraganglionlike differentiation” is an adequate diagnostic term in this case.

**Table 1** Histochemical and immunohistochemical analyses (*NCAM* neural cell adhesion molecule, *NSE* neuron-specific enolase, *EMA* epithelial membrane antigen, *GFAP* glial fibrillary acidic protein; *GRP* gastrin-releasing peptide, *HCG* human chorionic gonadotropin, *PP* pancreatic polypeptide, *ACTH* adrenocorticotropic hormone, ++ more than one-half of tumor cells positive, + a modest number of tumor cells positive, – negative)

| Staining/ maker | Antibody source (dilution) | Cell type | | |
|---|---|---|---|---|
| | | Carcinoid tumor | Ganglionlike | Paraganglionlike |
| Argyrophilia (Grimelius) | | + | – | + |
| Chromogranin A | Immunotech | ++[a] | – | ++ |
| Synaptophysin | Dako (50) | + | ++[b] | – |
| NCAM (CD56) | Novocastra (30) | + | + | + |
| NSE | Dako (30) | – | ++ | + |
| S-100 protein | Dako (200) | +[a] | ++ | ++ |
| EMA | Dako (100) | – | – | – |
| Neurofilament | Dako (200) | – | + | – |
| GFAP | Dako (50) | – | – | – |
| Keratin | Dako (100) | + | ++ | ++ |
| Vimentin | Dako (100) | – | ++ | ++ |
| Calcitonin | Dako (200) | – | + | – |
| Serotonin | Dako (10) | – | – | – |
| GRP | Dako (200) | – | + | – |
| HCG | Dako (100) | – | – | – |
| PP | Dako (10,000) | – | – | – |
| Gastrin | Dako (400) | – | – | – |
| Somatostatin | Dako (300) | – | – | – |
| ACTH | Dako (200) | – | – | – |

[a] Positive on sustentacular cells of carcinoid tumor
[b] Positive on the cell surface

## References


1. Gould VE, Linnoila RI, Memoli VA, Warren WH (1983) Neuroendocrine cells and neuroendocrine neoplasms of the lung. Pathol Annu 18:287–330
2. Hironaka M Fukayama M, Takayashiki N, Saito K, Sohara Y, Funata N (2001) Pulmonary gangliocytic paraganglioma. Case report and comparative immunohistochemical study of related neuroendocrine neoplasms. Am J Surg Pathol 25:688–693
3. Perrone T, Sibley RK, Rosai J (1985) Duodenal gangliocytic paraganglioma. Am J Surg Pathol 9:31–41
4. Scheithauer BW, Nora FE, Lechargo J, Wick MR, Crawford BG, Weiland LH, Carney JA (1986) Duodenal gangliocytic paraganglioma. Clinicopathological and immunocytochemical study of 11 cases. Am J Clin Pathol 86:559–565

Virchows Arch (2003) 442:186–187
DOI 10.1007/s00428-002-0736-4

LETTER TO THE EDITOR

**Michal Zamecnik · Michal Michal**

# Ovarian carcinoma of hypercalcemic type: myoid features and lack of estrogen and progesterone receptors

Received: 17 September 2002 / Accepted: 9 October 2002 / Published online: 30 November 2002
© Springer-Verlag 2002

**Keywords** Ovarian carcinoma · Hypercalcemia · Estrogen receptor · Progesterone receptor

Sir, Ovarian carcinoma of hypercalcemic type (OCHT) is a distinctive tumor of young women. Histogenesis of OCHT is still unresolved [3, 4, 10]. The following three origins are discussed: (1) surface-epithelial cells, (2) germ cells, and (3) sex cord cells. As both surface-epithelial and sex cord-stromal tumors arise from hormone-dependent tissue, which is reflected by frequent expression of estrogen receptors (ERs) and progesterone receptors (PRs) in these tumors [7, 9, personal observation], we have tried to examine the ER and PR (1D5, 1A6, Immunotech) in our cases of OCHT. We think that a presence of ER and PR could support one of the above-mentioned histogenetic hypotheses, because undifferentiated tumors of both surface-epithelial and sex cord-stromal cell origins should express these receptors (even if only in a small percentage of neoplastic cells) at least in some cases. On the contrary, invariable hormone receptor negativity would rather suggest a germ cell origin of OCHT, because germ cell tumors are ER and PR negative [9]. To confirm recent observation of myoid features in OCHT [4], we examined our cases for alpha-smooth muscle actin (1A4), desmin (D33), and calponin (CALP) (all from Dako). In addition, the following antibodies were used to further characterize the phenotype of OCHT: Melan A (A103), CD99 (12E7), CD34 (Qbend 10), glial fibrillary acidic protein (GFAP; polyclonal), neuron-specific enolase (NSE; polyclonal), chromogranin A (DAK-A3), synaptophysin (SY38), neurofilament protein (2F11) (all from Dako), alpha-inhibin (R1, Serotec), and CD10 (56C6, Novocastra).

Only unquestionable OCHTs showing typical histological features with follicle-like structures (Fig. 1) and with expression of cytokeratin were included in our study. We examined altogether seven cases of OCHT. The age of the patients ranged from 18 years to 51 years (average 31.9 years). Antibodies to both ER and PR gave entirely negative results in all OCHTs. Actin was strongly positive in scattered neoplastic cells in 4 of 7 (57%) tumors. Actin-positive cells were also observed in an additional three tumors, but in these cases it was not possible to recognize with certainty whether the actin-positive cells were neoplastic or represented only non-neoplastic scattered myoid stromal cells. Calponin was expressed in scattered neoplastic cells in all tested lesions (Fig. 2). In comparison with actin, it labeled a higher number of cells. Scattered CD10-positive cells (Fig. 3) were present in 5 of 7 (71%) tumors. CD99 showed focal expression in four (57%) tumors. The rest of the tested antibodies were negative in all tumors.

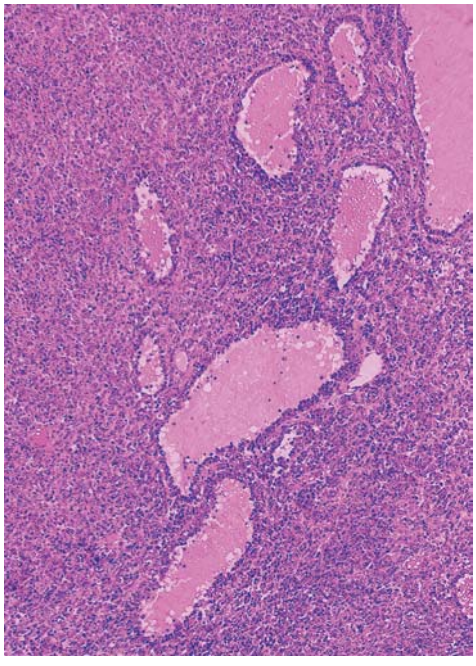


**Fig. 1** A typical picture of ovarian carcinoma of hypercalcemic type showing sheets of undifferentiated cells punctured with follicle-like spaces. Original magnification, ×40

M. Zamecnik (✉) · M. Michal
Sikl's Department of Pathology, Faculty Hospital,
Alej Svobody 80, 32318 Pilsen, Czech Republic
e-mail: zamecnik@medima.cz
Fax: +420-37-7440539

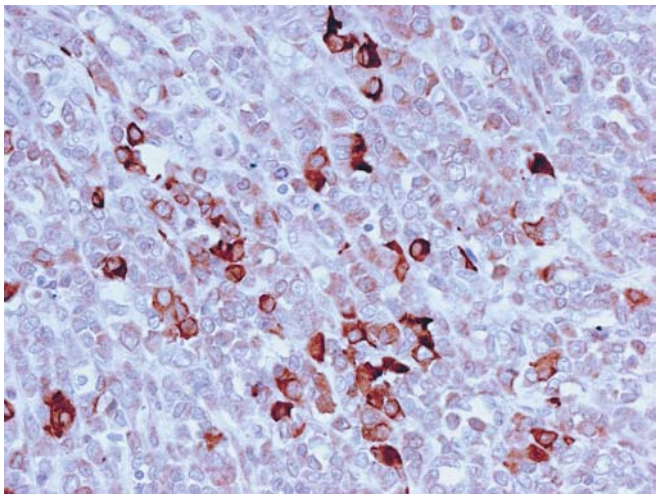


**Fig. 2** Immunoreactivity of neoplastic cells for calponin. Streptavidin-biotin complex technique; original magnification, ×200

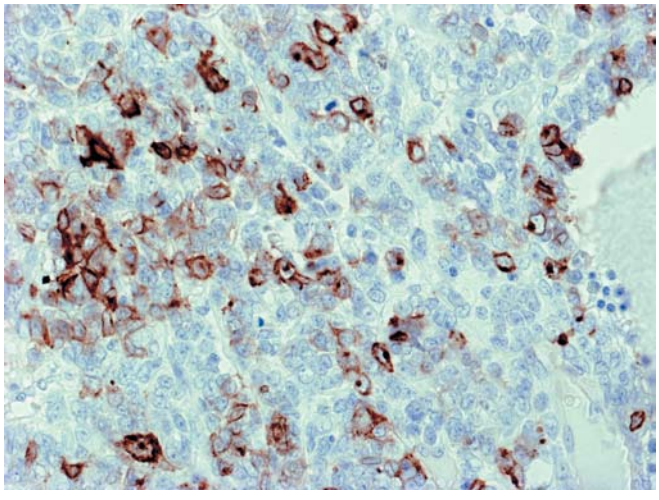


**Fig. 3** A tumor area with CD10 positive cells. Similar result was given with anti-CD99. SABC technique; original magnification, ×200

Our results show that OCHT is an ER- and PR-negative neoplasm. This does not support a surface-epithelial or sex cord-stromal cell origin and it favors a remaining germ cell derivation. We can also confirm an observation of actin positivity in scattered cells of OCHT, which was described by Lamovec et al. [4]. The myoid phenotype is further supported by immunohistochemical positivity with calponin antibody [6]. The immunohistochemical myoid marker expression is at variance with ultrastructural findings. Ultrastructurally, OCHTs showed epithelial features without any myoid differentiation [3, 10]. However, myoid differentiation in OCHT, as shown by our immunohistochemical staining, appears to be only focal and incomplete, such that it could be easily missed at the ultrastructural level. Therefore, meticulous ultrastructural study of OCHT is needed to resolve this question in the future. Expression of CD99 and CD10 has not yet been described in OCHT. CD99 is a marker for sex cord differentiation [1], and CD10 occurs in mesonephric [8] and endometrial stromal lesions [5]. However, both CD99 and CD10 have a low specificity, being observed in many other neoplasms [1, 2] and, therefore, they are of little value for diagnosis as well as for histogenetic consideration of OCHT. Occasionally reported neuroendocrine differentiation [10] revealed by chromogranin A, NSE or synaptophysin positivity was not found in our series.

From a practical viewpoint, an expression of myoid markers and negativity for ERs and PRs can be helpful in the differential diagnosis of OCHT. Unlike OCHT, undifferentiated ovarian carcinomas (that can mimic OCHT) have not been described to express myoid markers. With respect to hormone receptors, some undifferentiated surface-epithelial carcinomas contain ERs and/or PRs [9]. Expression of receptors was described also in the sex cord-stromal cell tumors [7]. Thus positivity for ERs and/or PRs would point against the diagnosis of OCHT.

In conclusion, OCHT often expresses myoid markers such as calponin and actin, and it appears to be consistently negative with antibodies to the ER and PR. These features can be helpful in the diagnosis of OCHT. In our view, the immunohistochemical phenotype favors more a germ cell origin rather than a surface-epithelial or sex cord-stromal cell origin.

## References


1. Choi YL, Kim HS, Ahn G (2000) Immunoexpression of inhibin alpha subunit, inhibin/activin betaA subunit and CD99 in ovarian tumors. Arch Pathol Lab Med 124:563–569
2. Chu P, Arber DA (2000) Paraffin-section detection of CD10 in 505 nonhematopoietic neoplasms. Frequent expression in renal cell carcinoma and endometrial stromal sarcoma. Am J Clin Pathol 113:374–382
3. Dickersin GR, Kline IW, Scully RE (1982) Small cell carcinoma of the ovary with hypercalcemia: a report of eleven cases. Cancer 49:188–197
4. Lamovec J, Bracko M, Cerar O (1995) Familial occurrence of small-cell carcinoma of the ovary. Arch Pathol Lab Med 119:523–527
5. McCluggage WG, Sumathi VP, Maxwell P (2001) CD10 is a sensitive and diagnostically useful immunohistochemical marker of normal endometrial stroma and of endometrial stromal neoplasms. Histopathology 39:273–278
6. Miettinen MM, Sarlomo-Rikala M, Kovatich AJ, Lasota J (1999) Calponin and h-caldesmon in soft tissue tumors: consistent h-caldesmon immunoreactivity in gastrointestinal stromal tumors indicates traits of smooth muscle differentiation. Mod Pathol 12:756–762
7. Mulvany NJ, Riley CB (1997) Granulosa cell tumors of unilocular cystic type. Pathology 29:348–353
8. Ordi J, Nogales FF, Palacin A, Marquez M, Pahisa J, Vanrell JA, Cardesa A (2001) Mesonephric adenocarcinoma of the uterine corpus: CD10 expression as evidence of mesonephric differentiation. Am J Surg Pathol 25:1540–1545
9. Teufel G, Geyer H, de Gregorio G, Fuchs A, Kleine W, Pfleiderer A (1983) Estrogen and progesterone receptors in malignant ovarian neoplazma. Geburtshilfe Frauenheilkd 43:732–740 (in German)
10. Young RH, Oliva E, Scully RE (1994) Small cell carcinoma of the ovary, hypercalcemic type. A clinicopathological analysis of 150 cases. Am J Surg Pathol 18:1102–1116

 © Springer-Verlag 2003

# ANNOUNCEMENTS

8–9 April 2003
**National Breast Pathology Course**

This two day course for Pathologists will cover all aspects of Breast Pathology

Course Tutor: Dr. S.E. Pinder

Residential and non residential options available

*For further information please contact:*
Education Administrators
Nottingham International Breast Education Centre
City Hospital, Hucknall Road, Nottingham NG5 1PB
Tel.: 0115 969 1689; Fax: 0115 962 7707
E-mail: enquiries@nibec.co.uk; www.nibec.co.uk

9–11 May 2003
**6th International Course on Bone Marrow Biopsy Pathology**
Hanover, Germany

Under the auspices of the European Association for Hematopathology

Bone marrow histology has evolved into an integral part of modern haematological diagnostics. Moreover, it affords unique access to a biological understanding of important diseases affecting the haematopoietic system. The courses offered by the European Bone Marrow Working Group under the auspices of the European Association for Hematopathology are intended to provide high quality educational sessions in bone marrow histopathology and to bring together people who have a particular interest in this field. In addition to state-of-the-art lectures focusing on selected topics, there will be workshops where participants are invited to contribute their own interesting and instructive cases. Topics will be chronic myeloproliferative disorders, lymphoma, hypoplastic states and MDS, reactive and therapy-related changes.

Course fee: 300 €

*For further information* see
http://www.mh-hannover.de/institute/pathologie/kongress or
contact Institute of Pathology, Medizinische Hochschule Hannover
Carl-Neubergstr. 1, 30625 Hannover, Germany
E-Mail: Laenger.Florian@MH-Hannover.de
Tel.: 0049 511 532-4501; Fax: -5799

12–16 May 2003
**Diagnostic Histopathology of Breast Disease**
London, UK

May 12–16, 2003, at Hammersmith Hospital (Imperial College Faculty of Medicine), London, UK. A week-long course designed for pathologists at Consultant and Senior Trainee level. The course provides a comprehensive coverage of the Histopathology of Breast Disease, with special emphasis on areas that pose diagnostic difficulties. The participants will be given ample time to study histological preparations, followed by illustrated discussion of the cases. There will be special sessions dealing with the interpretation of core biopsies and fine needle aspirations. There will also be two daily talks dealing with specific topics, given by eminent breast pathologists and followed by discussion. The topics will include reporting breast biopsies, immunohistochemistry, receptor assessment, c-erbB-2, prognostic factors, proliferative lesions/ carcinoma in situ, problems in breast pathology, a practical approach to the diagnosis of breast lymphomas and molecular pathology. The faculty will include Ian Ellis, Christopher Elston, Andrew Hanby, Kristin Henry, Stephen Humphreys, Sunil Lakhani, Andrew Lee, Sarah Pinder, Sami Shousha, and Clive Wells.

*Further details from:*
Wolfson Conference Centre, Hammersmith Hospital
Du Cane Road, London W12 ONN, UK
(Tel (44) 20 8383 3117/3227/3245; Fax (44) 20 8383 2428
e-mail wcc@ic.ac.uk)

12–23 May 2003
**International Course on Laboratory Animal Science**
Utrecht, The Netherlands

A two-week intensive course on laboratory animal science will be organized at the Department of Laboratory Animal Science – Utrecht, The Netherlands in May 2003. This course has been offered once a year since 1993.

The objective of this course is to present basic facts and principles that are essential for the humane use and care of animals and for the quality of research.

The contents of the course are in line with recommendations of the Federation of European Laboratory Animal Science Associations (FELASA) regarding the training of the young scientist whose research involves the use of vertebrate animals.

The course may also be of interest for those who intend to set up a similar course at their own institution. For this purpose, during the course the acquisition of teaching materials can be discussed with the course committee.

*For information and application forms please contact*:
Prof. Dr. L.F.M. van Zutphen or Mr. Stephan van Meulebrouck
Department of Laboratory Animal Science
Faculty of Veterinary Medicine, P.O. Box 80.166
3508 TD Utrecht, The Netherlands
Phone: *31-30-2532033; Fax: *31-30-2537997
E-mail: pdk@las.vet.uu.nl
Internet: http://las.vet.uu.nl (click 'Education').

9–11 June 2003
**Multi-Disciplinary Courses on Breast Disease**

Three day course. The first part is multi-disciplinary. Thereafter the different specialties meet to accommodate their own special requirements.

Course Tutors: Dr. I.O. Ellis, Dr. S.E. Pinder, Dr. A.H.S. Lee

| | | |
|---|---|---|
| Course fees: | NHS | £370.00 |
| | Non-NHS | £415.00 |
| | Overseas | £550.00 |

includes refreshments but not accommodation

*For further information please contact:*
Education Administrators
Nottingham International Breast Education Centre,
City Hospital, Hucknall Road, Nottingham NG5 1PB
Tel.: 0115 969 1689; Fax: 0115 962 7707
E-mail: enquiries@nibec.co.uk; www.nibec.co.uk

6 September 2003
**EUROPEAN BOARD OF PATHOLOGY**
**7th EXAMINATION 2003**
Ljubljana, Slovenia

The Seventh Examination of the European Board of Pathology will be held in Ljubljana, Slovenia, Saturday September 6, 2003. This Examination precedes the 19th Congress of the ESP.

*For information about the examination and application forms can be obtained from:*
Prod. Dr. J.G. van den Tweel
(chairman of The Examination Board)
Utrecht University Medical Center
Department of Pathology, H 04.312
P.O. Box 85500
3508 GA Utrecht
Fax: ++31-30-2544990
Tel.: ++31-30-2506565
e-mail: j.vandentweel@lab.azu.nl *or*
W.vanBragt@lab.azu.nl (secretary)
The same information is also available from Internet:
http:www.uems.be/pathol.htm, see index 2 and 3

13 October 2003
**Continuing Medical Education**

One day Multi-Disciplinary Update courses

Course fee: £95.00

*For further information please contact:*
Education Administrators
Nottingham International Breast Education Centre
City Hospital, Hucknall Road, Nottingham NG5 1PB
Tel.: 0115 969 1689; Fax: 0115 962 7707
E-mail: enquiries@nibec.co.uk; www.nibec.co.uk

17–19 November 2003
**Multi-Disciplinary Courses on Breast Disease**

Three day course. The first part is multi-disciplinary. Thereafter the different specialties meet to accommodate their own special requirements.

Course Tutors: Dr. I.O. Ellis, Dr. S.E. Pinder, Dr. A.H.S. Lee

| | | |
|---|---|---|
| Course fees: | NHS | £370.00 |
| | Non-NHS | £415.00 |
| | Overseas | £550.00 |

includes refreshments but not accommodation

*For further information please contact:*
Education Administrators
Nottingham International Breast Education Centre,
City Hospital, Hucknall Road, Nottingham NG5 1PB
Tel.: 0115 969 1689; Fax: 0115 962 7707
Email: enquiries@nibec.co.uk; www.nibec.co.uk

# EUROPATH NEWS 1/2003

European Society
of
Pathology

**Editors**
Prof. Niki J. Agnantis
University Department of Pathology
Medical School of Ioannina
GR-45110 Ioannina, Greece
Tel.: +302-651-097795
Fax: +302-651-097858
e-mail: nagnanti@cc.uio.gr

Dr. Bjørn Risberg
Department of Pathology
The Norwegian Radium Hospital
0310 Oslo, Norway
Tel.: +47-22934174
Fax: +47-22508554
e-mail: brisberg@labmed.uio.no

**The newsletter of the European Society of Pathology, EUROPATH NEWS, is sponsored by Leica Microsystems Nussloch GmbH**

## *Newsletter of the European Society of Pathology*

Dear Colleagues,

Happy New Year to you and your families. We are very pleased to convey to you the first 2003 issue of our ESP Newsletter. You will quickly notice that there has been a change in editors. Prof. Sir Colin Berry, after his recent retirement, has decided to end his collaboration as Co-Editor of the Europath News. On behalf of the Executive Committee of ESP, I would like to express my sincere thanks for his priceless contribution to the evolution of the Europath News, since its reappearance in 1996. Thus, I now have the pleasure of presenting to you the new assistant editor, Dr. Bjorn Risberg, a very active pathologist from the team of Prof. J.M. Nesland, who is already hard at work at the Society's website.

This issue begins with the Address by the President of the European Society of Pathology, Prof. Gianni Bussolati. It continues with Prof. Jahn Nesland's account of news from the Executive Committee meeting in Amsterdam and a report by Prof. M. Sobrinho-Simões, Past-President of ESP, on the role of EScoP and EUROCELLPATH in international training

The current Newsletter also includes announcements of forthcoming conferences, seminars and tutorial courses, as well as a report on the BIOPATH III. Furthermore, information is provided about the constituted Working Groups. Do not hesitate to furnish us with material on the activities of your department and even, through Europath News, share your problems with us. Last but not least, remember that we must increase the number of ESP members. This is a vital matter for the continuity of our Society. You can easily sign up by using the application form for membership (which is included in each issue of the Europath News) or going to our new **website** (whose address is also included). At the same time, you could exert influence on the younger staff in your department to join us.

With warmest thanks and regards,



Prof. Niki J. Agnantis
Chief Editor



Dr. Bjørn Risberg
Assistant Editor

## Address by the President of the European Society of Pathology, Gianni Bussolati

Dear Member,

I do hope you have already planned to come to Ljubljana for our Congress in September 2003 (http://www.cd-cc.si/ecp).

Prof. Dusan Ferluga and other Slovenian colleagues of the Organizing Committee have done their best to produce a very attractive program, providing a good balance of the different areas of interest of our discipline and including a long list of experts and of the best of possible speakers, who will present Keynote Lectures, Symposia, Special Presentations, Round Table Discussions, Short Courses and Slide Seminars. In addition to an update on current diagnostic standards, space will be given to modern techniques and breakthroughs, such as those made real by molecular genetics.

All practising pathologists and scientists are kindly invited to present their scientific achievements

and exchange their professional experiences through Free Paper and Poster Sessions. The best Free Papers will be acknowledged by giving the authors the opportunity to present their achievements at the plenary session, at which the authors of the three best Poster Presentations will additionally receive special Awards.

Pre-congress meetings on pulmonary pathology and on non-neoplasic nephropathology have been arranged, and a three-day Joint Meeting of the European and North American Society of Head and Neck Pathology has also been organized.

In the run-up to its bi-annual meeting, the Society is also heavily involved in a number of other activities.

On 10–13 May, Gavino Faa is organizing the XIIIth EurocellPath Course in Cagliari, Sardinia. The present course is devoted to molecular pathology.

EurocellPath courses are traditionally dedicated to young pathologists wishing to meet experts and to discuss scientific topics. Scientists interested in the molecular mechanisms of carcinogenesis, in genetic disregulations as diagnostic tools in Pathology, and in the molecular pathology of metabolic diseases will find in Sardinia splendid occasions for being mentally stimulated. I would also note that the location is „notorious“ for its very enjoyable character.

EScoP branch courses will be held on 25–28 May in Moscow, on 7–9 June in Ankara and on 14–18 June in Krakow, reproducing courses already successfully completed in Turin on Head and Neck Pathology (course leader: A. Cardesa), Thyroid Pathology (course leader: M. Sobrinho-Simões), and Pulmonary Pathology (course leader: H. Popper).

On 21–24 June, Jahn Nesland will also organize a conference on Tumor Cell Invasion, to be held in Lillehammer, Norway.

As you can see, in our Society you can find many opportunities to open your mind to new areas and to go deeper into topics of your present interest.

Many good reasons to be proud to be a member of the European Society of Pathology.

Yours sincerely,

Gianni Bussolati



Gianni Bussolati
President of the European Society of Pathology

## News from the Executive Committee meeting in Amsterdam, 6 October 2002

The President, Prof. Gianni Bussolati, reported on a high level of activity, including several trips around Europe. A visit to Istanbul for further planning of a ESP congress in year 2007, included discussions with representatives of the four Turkish societies and a visit to potential congress centres. The very successful Intercongress meeting in Baveno was also mentioned.

The European School of Pathology has given or arranged for courses in Turin, Moscow and Krakow. A search for new places in Eastern Europe to enable further expansion of the school is underway. The courses in Turin 2003 will be on pancreatic and liver pathology.

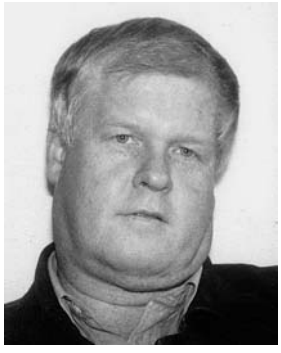
The Treasurer, Prof. Urbain van Haelst, reported that ESP now has 1164 members. Of these members, 34% subscribe to an electronic version of Virchows Archiv only. A closer link to national societies was discussed.

The upcoming congress in Ljubljana was discussed. Prof. D. Ferluga reported on the development of the scientific programme, with the second announcement having been scheduled to be distributed before Christmas 2002. Deadline for submission of abstracts will be 1 March 2003. The importance of poster sessions was discussed.

Prof. Torres and Prof. Soares reported on the development of the 2nd Intercontinental Congress of Pathology in Iguassu, Brazil, in 2004. At the IAP Congress in Amsterdam, 2000 CD-ROMs about it were distributed. Both the scientific and social programme are exciting and should appeal to us all. A satellite meeting will take place in Rio immediately prior to the congress in Iguassu. A deal with Brazilian airlines grants us a special offer, allowing for a stop-over in Rio.

Candidates for President-elect and four members of the Executive Committee must be proposed prior to the General Assembly, to take place in Ljubljana later this year. Several candidates have already been proposed, and all members are invited to come up with proposals. Proposals can be submitted to the Secretary.

Oslo, 5 January 2003



Jahn M. Nesland
Secretary ESP



# The role of the European School of Pathology (EScoP) and the European Course on Cellular Pathology (EUROCELLPATH) in international training

Manuel Sobrinho-Simões, MD, PhD
Medical Faculty of Porto, University Hospital of S. João and IPATIMUP –
Institute of Molecular Pathology and Immunology of the University of Porto, Portugal
Past-President of the European Society of Pathology

The quality of post-graduate training in Pathology in Europe has always been a major concern for the European Society of Pathology (ESP).

For many years the greatest problem stemmed from the huge differences among European countries regarding the models of medical education and specialty training.

In the eighties the situation started to change. The political evolution of Europe and the need for „harmonization" and „increased mobility of professionals" created the conditions to address the problem of pathology training in a more coherent manner. Curiously, another problem appeared at that time: the creation and progressive importance of molecular pathology. This new development added an extra difficulty to the aim of achieving balanced pathology training throughout the world.

Since the ESP has no official role in the European Board exams nor in the accreditation of any national training programme, it was decided that it should concentrate its efforts on the creation of good and reproducible international training conditions. In order to attain this objective, the Executive Committee of ESP launched, in 1990, two tutorial training „programmes" for residents and young pathologists: the European Course on Cellular Pathology (EUROCELLPATH) and the European School of Pathology (EScoP). These two "programmes" were created together with Pathology Update, an educational series of ESP, within the framework of the European Institute for Continuing Medical Education in Pathology (EICME-Path), a sort of umbrella organization of the ESP for its scientific educational activities.

Mention should be given to the crucial role played by Jean Alexis Grimaud and Gianni Bussolati in the creation of EUROCELLPATH and EscoP, respectively. The present chairmen of the two „programmes" are Fred Bosman (Institut Universitaire de Pathologie, Rue du Bugnon, 25, CH-1011 Lausanne, Switzerland; e-mail: Fred.Bosman@chuv.hospvd.ch) and Mauro Papotti (Dept. of Pathology, University of Turin, Via Santena, 7, 10126 Torino, Italy; e-mail: mauro.papotti@unito.it). Jahn Nesland was the driving force behind the creation and maintenance of Pathology Update until 1997. (The ESP is now discussing the best way to reactivate the publication of the papers and other materials that are presented in EUROCELLPATH and EScoP courses).

From the beginning it was decided that EUROCELLPATH and EScoP should play complementary roles, allowing for combined training in classic histopathology and molecular pathology. It was also decided that the courses of both „programmes" should be organized in a residential format, enabling the faculty to be together with the participants for the whole of the learning period.

The courses organized to date within the framework of EScoP and EUROCELLPATH are summarized below in Tables 1 and 2, respectively.

The courses of the EScoP are oriented around organ pathology and use the discussion of histological slides as their main educational tool. (Each participant has his own microscope and set of slides). The slide-seminar type of sessions is complemented by lectures on the new developments in immunohistochemistry and molecular biology as applied to surgical pathology.

The EScoP courses were first organized in Turin in 1991 and within seven years covered almost all fields of surgical pathology (Table 1). In the late nineties, the decision was made to start repeating (and updating) some of the courses (e.g. breast and pulmonary pathology) and to organize replicas of the courses in Poland and Russia in order to facilitate the attendance of Eastern European pathologists (Table 1). The format and all the characteristics of the courses in Warsaw, Moscow and Krakow, namely, their residential and tutorial nature, mimick those organized in Turin.

In contrast to EScoP, the courses of EUROCELLPATH, which are also organized in a tutorial format, rotate throughout Europe (Table 2). Instead of being organ-oriented, the EUROCELLPATH courses are disease-oriented and emphasise so-called molecular biopathology. Eight of the 12 courses organized to date have dealt with basic mechanisms of cancer initiation and cancer development and the remaining four with the etiopathogenesis of inflammatory processes (Table 2). As one would expect from the present trend towards molecular medicine, the vast majority of the titles of the courses stress a molecular/genetic approach (Table 2).

The faculties of EUROCELLPATH courses have been composed – and will continue being composed in the future – of a mixture of basic scientists and surgical pathologists interested in translational research. The programme of each course is designed to fill the gap between basic biomedical sciences and applied diagnostics from a surgical pathology standpoint.

Both EScoP and EUROCELLPATH courses are mainly attended by residents and young pathologists

from throughout Europe (30 to 40 participants per course). There are, however, in most courses, mainly as a result of the existing protocols between Europe and Latin America and Africa, a number of participants from outside Europe.

Summing up, the ESP has been trying hard, since 1990, to expose both experienced surgical pathologists and young pathologists/residents to two types of graduate courses that cover the spectrum from classic morphology to molecular pathology and integrate, in the frame of anatomic pathology, the brave new world of genes and molecules. The challenge is not only to be able to improve substantially the training of residents but also to increase the molecular biology knowledge of experienced pathologists.

**Table 1** EScoP courses

| Year | Site | Title | Organizers |
|---|---|---|---|
| 1991 | Turin | Non-neoplastic liver and GI pathology | W. Bogomoletz and D.J. Pollock |
| | | Ovarian pathology | F. Nogales |
| | | Breast pathology | V. Eusebi and R. Millis |
| 1992 | Turin | Pulmonary pathology | B. Corrin |
| | | Thyroid pathology | M. Sobrinho-Simões, G. Bussolati, E. Fonseca and L. David |
| | | GI and pancreatic endocrine pathology | E. Solcia, C. Bordi and C. Capella |
| | | Pituitary, adrenal and parathyroid pathology | C. Capella, S. Schroder and L. Grimelius |
| 1993 | Turin | Hematopathology (I) | A. Georgii |
| 1994 | Turin | Uterine pathology | J. Prat |
| | | Hematopathology (II) | A. Georgii |
| | | Breast pathology | V. Eusebi and H. Peterse |
| 1995 | Turin | Quantitative pathology | Y. Collan |
| | | Neuropathology | D. Schiffer |
| | | Head and neck pathology | A. Cardesa, P.J. Slootweg and R. Simpson |
| 1996 | Turin | Uropathology | F. Algaba |
| | | Dermatopathology (neoplasms) | D. Meister |
| 1997 | Turin | Tumors of liver and pancreas | G. Kloppel and H. Denk |
| | | Tumors of GI tract | K. Geboes |
| 1998 | Turin | Soft tissue tumors | T. Krausz, T. Mentsel and A.P. Dei Tos |
| | | Breast pathology | V. Eusebi and H. Peterse |
| 1999 | Turin | Pulmonary pathology | H. Popper |
| | | Cytopathology | W.Olszewski |
| | Warsaw | Breast pathology | H. Peterse |
| 2000 | Turin | Ovarian pathology | J. Prat and X. Matias-Guiu |
| | | GI pathology | K. Geboes and J.F. Flejou |
| 2001 | Turin | Pathology of lymph nodes and spleen | C. De Wolf Peters |
| | | Pathology of bone marrow and thymus | A. Marx, A. Tierens and R. Achten |
| | Warsaw | Ovarian pathology | J. Prat and X. Matias-Guiu |
| | Moscow | GI pathology | K. Geboes and J.F. Flejou |
| 2002 | Turin | Head and neck pathology | A. Cardesa, R. Simpson and P.J. Slootweg |
| | | Thyroid and parathyroid pathology | M. Sobrinho-Simões, G. Bussolati, E. Fonseca and M.Papotti |
| | Krakow | GI pathology | K. Geboes |
| | Moscow | Pulmonary pathology | H. Popper |

**Table 2** EUROCELLPATH courses

| Year | Site | Title | Organizers |
|---|---|---|---|
| I. 1990 | Lyon, France | Cell pathology | J.A. Grimaud and P. Stoebner |
| II. 1991 | Nyon, Switzerland | Cellular and molecular basis of the stromal reaction to epithelial tumours | J.A. Grimaud and G. Gabbiani |
| III. 1992 | Lyon, France | Extracellular matrix in pathology | J.A. Grimaud and G. Gabbiani |
| IV. 1994 | Dalfsen, The Netherlands | Molecular pathobiology of cancer | F. Bosman |
| V. 1995 | Oslo, Norway | The metastatic process | J.M. Nesland |
| VI. 1996 | Caminha, Portugal | Molecular pathology in oncology: Is there a meeting point for surgical pathologists and cancer researchers? | M.J. Bento, R. Seruca, F. Sansonetty, M. Seixas and M. Sobrinho-Simões |
| VII. 1997 | Metsovo, Greece | Stromal reaction in preneoplastic and early cancerous lesions | N. Agnantis |
| VIII. 1998 | Belfast, Ireland | Molecular and quantitative analysis of early neoplasia | P. Toner |
| IX. 1999 | Paris, France | Cellular and molecular changes in inflammation | P. Bedossa, J.A. Grimaud, A. Janin, P. Bertheau and J.F. Flejou |
| X. 2000 | Lillehammer, Norway | Molecular mechanisms in development and treatment of cancer | J.M. Nesland, W. Danielsen, E. Emilsen and R. Gurvitsj |
| XI. 2001 | Ghent, Belgium | Molecular mechanisms in chronic inflammatory diseases | C. Cuvelier |
| XII. 2002 | Berlin, Germany | Cancer as a disease of genes and gene regulation | S. Hauptmann |

## INTERNATIONAL ACADEMY OF PATHOLOGY

INTRAEUROPEAN-MEDITERRANEAN CONFERENCE

**Dates: 8–10 May, 2003**

Meeting Venue: Astir Palace Resort,
Vouliagmeni, Athens, Greece

Topics

**Breast Cancer:** Sunhil Lakhani, London, UK

**Endometrial Cancer:** Jaime Prat, Barcelona, Spain

**Pigmented Lesions of the Skin:** Martin C. Mihm, Jr, Boston, MA, USA

**Prostate Neoplasia:** Rodolfo Montironi, Ancona, Italy

***Organized by the Hellenic Division***

*Please visit our home page to see the content of the programme and other useful information*
*www.mednet.gr/hsap/intraeuropean.htm*

***Conference Secretariat***

*Alex. Soutsou 8, 106 71 Athens, Greece*
*Phone: +301-363-4944, Fax: +301-363-1690, e-mail: infor@era.gr*

## 13th EuroCellPath Course, 10–13 May 2003, Cagliari, Italy

Dear Colleagues, Members of ESP

The 13th EuroCellPath Course will be held in Cagliari on 10–13 May 2003. Under the title "Molecular mechanisms and molecular diagnostic tools in pathology", it will explore the following topics:

1. Molecular mechanisms in carcinogenesis
2. Genetic disregulations as diagnostic tools in surgical pathology
3. Molecular pathology of metabolic diseases
4. Subjects of proffered papers

For a detailed schedule of the entire conference, please see below. All of you are cordially and strongly invited to participate, especially young pathologists and 4th- to 5th-year residents.

Best regards to all of you,

Carlo D. Baroni

P.S. For more information please contact me (e-mail: carlo.baroni@uniroma1.it) or visit the ESP Website

## 13th EuroCellPath Course: Detailed Schedule of Events

### Saturday, 10 May 2003

| | |
|---|---|
| 17.00 –18.00 | Registration |
| 18.00 –19.00 | Welcome and presentation of the programme |
| 19.00 – 19.45 | Opening lecture<br>Mitochondrial DNA in human diseases: from neurodegenerative disorders to cancer<br>*M. Sobrinho-Simões, Portugal* |
| 20.00 | Welcoming cocktail |

### Sunday, 11 May 2003

Molecular mechanisms in carcinogenesis

Chairperson: C. Baroni

| | |
|---|---|
| 08.45 – 09.00 | Introduction, *C. Baroni, Italy* |
| 09.00 – 09.30 | Circulating tumor cells in the metastatic process<br>*J. M. Nesland, Norway* |
| 09.30 – 10.00 | Molecular progression of breast cancer<br>*G. Stanta, Italy* |
| 10.00 – 10.30 | Molecular mechanisms in normal and neoplastic liver cell growth<br>*A. Columbano, Italy* |
| 10.30 – 11.00 | Coffee break |
| 11.00 – 11.30 | Dysplasia in inflammatory chronic bowel disease: molecular mechanisms<br>*K. Geboes, Belgium* |
| 11.30 – 12.00 | Molecular progression in pancreas carcinoma<br>*A. Scarpa, Italy* |
| 12.00 – 12.30 | Molecular progression in gastric cancer<br>*R. Riddell, U.K.* |
| 12.30 – 13.00 | Discussion |
| 13.00 – 15.00 | Lunch break |
| 15.00 – 15.30 | Molecular progression in colon cancer<br>*R. Fodde, The Netherlands* |
| 15.30 – 16.00 | Different types of epithelial cadherin alterations play different roles in human carcinogenesis<br>*M. Sobrinho-Simões, Portugal* |
| 16.00 – 16.30 | Molecular pathology in gastro-pancreatic endocrine tumours<br>*C. Bordi, Italy* |
| 16.30 – 17.30 | Discussion |
| 17.30 – 18.00 | Free papers „Molecular mechanisms in carcinogenesis“ |
| 20.00 | Dinner with Sardinian folk groups |

### Monday, 12 May 2003

Genetic disregulations as diagnostic tools in pathology

Chairperson: J. Nesland

| | |
|---|---|
| 08.45 – 09.00 | Introduction, *G. Bevilacqua, Italy* |
| 09.00 – 09.30 | Cytokeratins in the diagnosis and differential diagnosis of tumors<br>*P. Van Eyken, Belgium* |
| 09.30 – 10.00 | Molecular pathology in the differential diagnosis of thyroid tumors<br>*L. Ruco, Italy* |

| | |
|---|---|
| 10.00 – 10.30 | Molecular profiles of lymphomas<br>*M. Chilosi, Italy* |
| 10.30 – 11.00 | Coffee break |
| 11.00 – 11.30 | Progress in diagnostic hematopathology relies on the interaction of pathologists and molecular geneticians<br>*C. Peeters, Belgium* |
| 11.30 – 12.00 | Alterations of p53 and Rb growth pathways in breast cancer: correlations with proliferation, apoptosis and clinical outcome<br>*N. Agnantis, Greece* |
| 12.00 – 12.30 | Discussion |
| 12.30 – 15.00 | Lunch break |
| 15.00 – 15.30 | Molecular pathology in the progression from Barrett's oesophagus to adenocarcinoma<br>*F. Bosman, Switzerland* |
| 15.30 – 16.00 | Molecular biology in neuroendocrine tumors<br>*G. Bussolati, Italy* |
| 16.00 – 16.30 | The pathologist facing the sentinel lymph node<br>*G. Viale, Italy* |
| 16.30 – 17.30 | Discussion |
| 17.30 – 18.00 | Free papers „Molecular diagnostic tools in pathology" |

**Tuesday, 13 May 2003**

Molecular pathology in metabolic disease

Chairperson: G. Monga

| | |
|---|---|
| 08.45 – 09.00 | Introduction, *G. Faa, Italy* |
| 09.00 – 09.30 | Metals and neurodegenerative disease<br>*H. Koslowski, Poland* |
| 09.30 – 10.00 | Phosphoturic tumors and oncogenic osteomalacia<br>*P. Bianco, Italy* |
| 10.00 – 10.30 | Molecular regulation of fibrosis in kidney disease<br>*T. Faraggiana, Italy* |
| 10.30 – 11.00 | Coffee break |
| 11.00 – 11.30 | Molecular mechanisms in iron storage diseases<br>*P. Brissot, France* |
| 11.30 – 12.00 | Hemochromatosis: from molecular mechanisms to clinical consequences<br>*R. Crichton, Belgium* |
| 12.00 – 12.30 | Alpha-1-antitrypsina deficiency: molecular pathology<br>*P.P. Coni, Italy* |
| 12.30 – 13.00 | Molecular mechanisms of tumor invasion and metastasis<br>*V. Castronovo, Belgium* |
| 13.00 – 14.00 | Discussion |
| 14.00 | End of the course |

## International Workshop on Intestinal Permeability in Health and Disease, 23–24 May 2003, Patras, Greece

### Conference & Cultural Center of the University of Patras

Invitation

The organizing committee of the International Workshop on Intestinal Permeability in Health and Disease has the great pleasure of inviting you to Patras, Greece, on 23–24 May 2003. Patras, a city with history that can be traced back to prehistoric times, is located on the northern coast of the Peloponnese and has functioned in the last two centuries as Greece's main link to Central Europe. The metropolitan area has a population of over 250,000 people. The city is famous for its Annual Carnival, Venetial Castle and the internationally known wine company of Achaia Claus. The University of Patras was founded in 1964 and is now located on a 600-acre campus just outside the city at the foot of mountain Panachaikos. Its 18 academic departments offer a wide range of undergraduate and graduate courses and degrees. We are looking forward to your participation in what we believe will be an exciting meeting on Intestinal Permeability in Health and Disease, designed to bring together basic and clinical scientists of diverse specialties in an effort to elucidate an emerging and novel field in medicine. See you in Patras in May 2003.

*General Fees:* 75 Euros, Students free

*Congress venue*

The congress will be held at the University of Patras Convention Center, located on the University Campus. Transportation to and from the hotels will be provided.

*Official language*

English

*Social and cultural events*

Reception at the Achaia Claus winery
Visit to Olympia
Visit to Delphi

*The Organizing Committee*

Scopa Chrisoula
Vagianos Constantin
Charonis Aristidis
Skoutelis Athanassios
Kouraklis Gregory

*Important dates*

*Workshop:* 23–24 May 2003

*Deadline for the receipt of abstracts*

15 February 2003

*Scientific program*

The program will consist of half-hour presentations by the invited speakers, a poster session and ample time for discussion of the topics presented.

*Topics include*

- Molecular basis of intestinal permeability
- Interaction between bacterial and intestinal epithelium
- Endocrine and immunological functions of the intestine
- Effect of inflammation on gut barrier function
- Clinical conditions affecting intestinal permeability (jaundice, sepsis, etc. )
- The impact of luminal content on barrier function

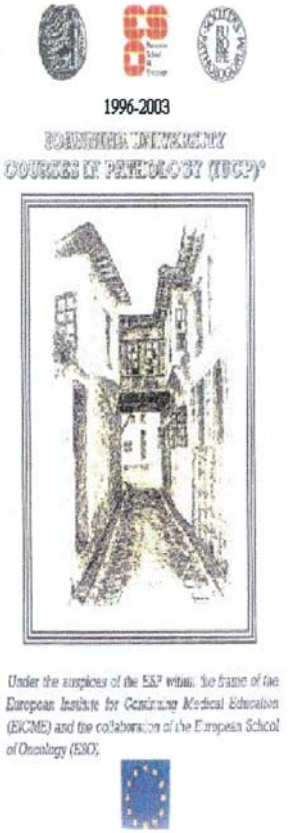
*Invited speakers include*

Alexandridis, T. (Greece)
Anderson, R. (Sweden)
Charonis, A. (Greece)
Deitch, E. (USA)
Filos, K. (Greece)
Jeppson, B. (Sweden)
Kotzabassi, C. (Greece)
Menger, M. (Germany)
Rowlands, B. (England)
Scopa, C. (Greece)
Vagianos, C. (Greece)
Viswanathan, V. (USA)

*Secretariat*

Synedra
Agiou Nikolaou 57
GR-262 21 Patras, Greece
Tel.: +30-610-242999
Fax: +30-610-242997
e-mail: synedra@pat.forthnet.gr




**Ioannina University Courses in Pathology (IUCP)**

**Part one:** Kidneys Pathology-Oncology
27–28 May, 2003
**Part two:** Bladder Pathology-Oncology
29–31 May, 2003

**Faculty**
Alamanos I (Gr)
Briasoulis E (Gr)
Eleftheriades E (Gr)
Kanavaros P (Gr)
Liapis H (USA)
Leontsini M (Gr)
Mairinger T (A)
Mikuz G (A)
Nakopoulou L (Gr)
Pantzaki A (Gr)
Papakostas V (Gr)
Pavlaki K (Gr)
Pentheroudakis G (Gr)
Petraki C (Gr)
Sofikitis N (Gr)
Sotsiou F (Gr)
Tsili A (Gr)

*Registration fees for each part:*
EUROS 400 (200 for residents)
Accommodation (double room, shared)
and full board are included
Account number in EUROS: 359/616930-96
National Bank of Greece, Ioannina, Greece

*Correspondence:*
Prof. Niki J. Agnantis, M.D.,
Institute of Pathology,
University of Ioannina,
Medical School,
University Campus,
45110 Ioannina, Greece
Tel.: +302-651-097795, Fax: +302-651-097858
e-mail: nagnanti@cc.uoi.gr.

For further information please contact
our home page at
http://medlab.cs.uoi.gr/iucp

***(Third announcement)***

**Director-Coordinator: Prof. Niki J. Agnantis**

# The Montebello Conference 2003

## Tumour Cell Invasion



The Montebello Centre,
Mesnali, Lillehammer, Norway

June 21-24, 2003

http://www.Montebelloconf.org

# Welcome to the Montebello Conference 2003

This years conference is dedicated Tumour Cell Invasion and we invite pathologists, cell biologists and clinicians to attend. Guest speakers will provide "state of the art" lectures and you are invited to present your own work as a free paper or a poster. The conference will take place in The Montebello Centre, Mesnali, Lillehammer during the period June 21.–24. 2003. The centre has a modern auditorium and many recreation facilities. Lillehammer, known for hosting the Winter Olympic Games, offers a peaceful and beautiful natural setting, being situated on the shore of Norway's largest lake, Mjøsa. Combining this with a friendly and open atmosphere, as well as challenging discussions, we believe this will be a rewarding experience

The number of participants is limited to 80. Please register at your first convenience. Registration fee is 330 Euro for non-ESP members and 280 Euro for members of ESP. Accommodation with full boarding (breakfast, lunch, dinner) is 460 Euro in single room and 410 Euro per person in double room for the whole conference.

We invite you to submit an abstract for free presentation and look forward seeing you in Lillehammer.

## The Montebello Conference organizing committee

Raisa Gurvitsj
Wencke Danielsen
Ben Davidson
Elisabeth Emilsen
Jahn M. Nesland

**Correspondence** Jahn M. Nesland
Dept. of Pathology
The Norwegian Radium Hospital
Montebello
NO-0310 Oslo, Norway

**Telephone** 47-22935620 • **Telefax** 47-22730164 • **e-mail**: j.m.nesland@labmed.uio.no

**Registration at the web site**: http://www.Montebelloconf.org

# Preliminary programme

**June 21, Saturday**

| | |
|---|---|
| 16.00 | Transport from Oslo airport, Gardermoen 2 hrs. Arrival in the afternoon. Tea/Coffee – sandwiches |
| 18.00–19.00 | Check in / Registration |
| 19.00–19.15 | Welcome in the Auditorium. *Jahn M. Nesland* |
| 19.15–20.00 | Epithelial – Mesenchymal Transitions in Tumour Progression. *Jean Paul Thiery, Paris* |
| 20.00–20.30 | Sight-seeing The Montebello Centre |
| 20.30 | Dinner |

**June 22, Sunday** 07.30–08.30 Breakfast
**Basement membrane / Stromal modulation**

| | |
|---|---|
| 08.30–09.15 | Basement membrane / Stromal composition. *Giulio Gabbiani, Geneva* |
| 09.15–10.00 | Regulation BM / Stromal degradation. *Fred Bosman, Lausanne* |
| 10.00–10.30 | Break |
| 10.30–11.15 | Dental matrix. A model for stromal modulation. *Ole Petter Lyngstadaas, Oslo* |
| 11.15–11.45 | Cancer initiation and cancer invasion in gastric carcinoma. *Manuel Sobrinho-Simões, Porto* |
| 11.45–12.00 | Break |
| 12.00–12.30 | Squamous cell carcinoma of the upper respiratory tract – development and progression. *Antonio Cardesa, Barcelona* |
| 12.30–13.00 | The role of adhesion molecules and extracellular matrix proteins in the progression of carcinomas of the upper respiratory tract. *Carlo Baroni, Rome* |
| 13.00–13.30 | Regulation of proteolysis in breast carcinomas. *Ben Davidson, Oslo* |
| 13.30–15.30 | Lunch |
| 15.30–17.00 | Free presentations |
| 17.00–17.15 | Break |
| 17.15–18.00 | Tumour lymphangiogenesis. *Kari Alitalo, Helsinki* |
| 20.00 | Dinner |

**June 23, Monday** 07.30–08.30 Breakfast
**Intracellular regulatory mechanisms in tumour cell invasion**

| | |
|---|---|
| 08.30–09.15 | The cadherin / catenin system. *Marc Mareel, Gent* |
| 09.15–10.00 | Intracellular signalling in malignant melanomas. *Vivi Ann Flørenes, Oslo* |
| 10.00–10.30 | Break |
| 10.30–15.30 | Sightseeing |
| 16.00–16.45 | Stromal interactions in malignant lymphomas. *Jan Delabie, Oslo* |
| 16.45–17.30 | Ovarial carcinoma – Regulation of tumour cell invasion. *Reuven Reich, Jerusalem* |
| 17.30–18.15 | Interaction glioblastoma cells and stromal elements. |
| 19.00 | Conference Dinner and Party |

**June 24, Tuesday** 07.30–08.30 Breakfast
**Cell cycle regulation and models for analysing tumour cell invasion**

| | |
|---|---|
| 08.30–09.15 | Cell cycle regulation. *Jiri Bartek, Copenhagen* |
| 09.15–10.00 | Autocrine / paracrine regulation and interaction with growth factor receptor signalling. *Jahn M. Nesland* |
| 10.00–10.45 | Special lecture: Three dimentional models for analysing cancer cell / stromal interaction. *José Costa, Yale* |
| 10.45–11.00 | *Concluding remarks. Jahn M. Nesland* |
| 11.00–12.00 | Lunch |
| 12.00 | Bus leaves for Oslo airport, Gardermoen |


ESCoP
European School of Pathology
Pathology of the Pancreas
Prof. G. Kloppel, Kiel
Pathology of the Liver & Biliary Tract
Prof. P. Bedossa, Paris
INSTITUTE FOR SCIENTIFIC INTERCHANGE FOUNDATION
2003 courses
September 19 - 25 Turin, Italy
AIM
Post-graduate residential course for young European pathologists based on workshops, slide seminars and few lectures to update and standardise participants' diagnostic ability.
FEE
• Registration is 300 Euro.
• Full board accomodation (to be paid upon departure) is 75 Euro/day/person.
• A limited number of EScoP scholarships (for ESP Members) is also available upon request
DATES
Pancreas Pathology
Sept. 19-20, 2003
Liver & Biliary Tract Pathology
Sept 21-25, 2002
PLACE & ORGANIZATION
Institute for Scientific Interchange (ISI)
Villa Gualino,
Viale S. Severo 65,
10133 Torino, Italy.
Phone Office
+39 011 6603090
Phone Residence
+39 011 6603555
E-mail: isi@isi36a.isi.it
PAST COURSES
1991 Liver & GI path (non neopl)
Ovarian pathology
Breast pathology
1992 Pulmonary pathology
Endocrine pathology
1993 Haematopathology
1994 Haematopathology
Uterine pathology
Breast pathology
1995 Quantitative pathology
Neuropathology
Head & Neck pathology
1996 Uropathology
Dermatopathology (neopl)
1997 Tumors of liver & pancreas
Tumors of GI tract
1998 Soft tissue tumors
Breast pathology
1999 Lung pathology
Cytopathology
2000 Ovarian pathology
GI pathology
2001 Hematopathology
2002 Head & Neck Pathology
Thyroid & parathyroid Path.
FUTURE COURSES
2004 Pathology of the Uterus
Pathology of the Bladder
Pathology of the Prostate
APPLY before April 30 to
European School of Pathology
c/o Dept Pathology, Univ Turin, Via Santena 7,
I-10126 Torino Italy Fax +39 011 6635267
E-mail mauro.papotti@unito.it
Note: By end June, a letter will confirm or reject the application. Do not send money now, please.
To EScoP
RE: Preliminary application
Surname: ..... Name: ..... Sex: .....
Date & place of birth: ..... Citizenship: .....
Full address.....
.....
Phone: ..... Fax: ..... E-mail: .....
application for 2 courses
application for 1 course
Sept. 19-21
Sept. 21-25
I apply for: EScoP scholarship
EU grant, if available
Member of ESP
non member (I apply for 2003 ESP membership)
I enclose a brief curriculum vitae stating my experience in pathology
Date.....
Signature: .....

## Euroworkshop BIOPATH III on Interdisciplinary Perspectives of Diagnostic Pathology, Cell Biology, and Morphometry, Madrid, Spain, 6 – 8 December, 2002

The Euroworkshop BIOPATH III on Interdisciplinary Perspectives of Diagnostic Pathology, Cell Biology, and Morphometry, supported by the European Commission (HPCF-2000–0001), was held at the Instituto de Investigaciones Biomedicas, CSIC & UAM, 28029 Madrid, Spain, from 6–8 December 2002. This third and last event of a threefold series focussing on interdisciplinary research in biochemistry, cell biology, and diagnostic surgical pathology offered young colleagues working in any one of these fields a broad and detailed insight into recent developments and potential interactions among the fields. The workshop was divided into three parts, namely, separate sessions dealing with (I) cell biology and glycosciences, (II) molecular pathology and digital imaging in pathology (including electronic information transfer), and (III) joint sessions presenting potential tools and applications of cell biology and pathology.

In detail: The joint sessions discussed the synthesis, structure, biological activities, and visualization of specific mammalian lectins. The biological importance of carbohydrate-interacting-proteins such as galectins has been recognized by several researchers, and is at present beyond all doubt. The biological functions include both activation and depression of cell proliferation and apoptosis, cellular differentiation, and invasion. This broad functional spectrum is in accordance with the structural flexibility of carbohydrates and their environment-dependent conformational changes. The carbohydrate structural determination of lectins is, therefore, of great scientific interest, and offers, in addition to structural modelling, a modern and suitable approach to the design of neo-molecules for diagnostic and therapeutic applications. In addition, these techniques permit the identification of new diseases, such as congenital disorders of glycosylation, as exemplarily and thoroughly discussed by E. Berger (Zurich). This broad spectrum of galectin functions is of specific interest in malignant diseases and raises the question of potential prognostic markers. In accordance with published data on lung cancer, Iacobelli (Chieti) indicated the prognostic value of expression of galectin-3 and its ligand MAC-2 BP in human breast cancer. S. Andre (Munich) demonstrated biochemical strategies to design adhesion-blocking therapeutics based upon galectins. This lecture was completed by J. Kopitz (Heidelberg), who indicated that the ganglioside sialidase, GM1 and galectins are essentially involved in control of neuroblastoma cells.

The pathology sessions focussed on sampling strategies with limited data sets to be applied in histology, cytology, or molecular pathology including gene arrays (K. Kayser, Heidelberg), geographic pathology (Y. Collan, Turku), and machine vision in diagnostic and investigative pathology (P. Hamilton, Belfast), whereas J. Salibury (London) presented recent developments in 3D reconstruction, and J. Szymas (Poznan) explained the use of telepathology for quality control in diagnostic pathology. These lectures provided our young colleagues with a survey of appropriate and effective implementation of electronic tools and artificial intelligence in diagnostic pathology. The section on supplementary molecular pathology was opened by E. Vollmer (Borstel), who described a new fixative HOPE for protein analysis in paraffin-embedded tissue, and followed E. Santinelli (Ancona), who analysed the prognostic significance of molecular pathology tools in breast carcinoma patients. These data were completed by additional studies guided by N. Agnantis (Ioannina). The use of molecular pathology in chronic non-malignant diseases was worked out by L. Carvalho (Coimbra) and T. Goldmann (Borstel) on interstitial lung diseases and tuberculosis, respectively.

The joint sessions included basic data on measurement techniques for molecular biochemistry and determination of molecular structure (J.F.G. Vliegenthart [Utrecht], K. Bock [Valby]) and interactions (M. Martin-Lomas [Sevilla], I. Wilson [Vienna]), which were expanded upon by lectures dealing with general structures of animal lectins (A. Romero [Madrid]), and domain/confirmation analysis of specific lectins (H.C. Siebert [Munich], C-lactose (J. Jimenez-Barbero [Madrid]), the hevein domain (J.L. Asenio [Madrid]), or lectin activities of human interleukins (J.O. Zanetta [Lille]).



A detailed poster discussion, a round table forum on integration of glycosciences, cell biology, and pathology, and training courses for sampling techniques, telepathology, molecular modelling, and gene arrays finally completed this interesting and strenuous workshop. The program and abstracts have been published in the *Electronic Journal of Pathology and Histology*, vol. 8.3 (September 2002), and can be viewed at the website http://ampat.amu.edu.pl/biopath/biopath2002.htm.

Speaking on behalf of at least the majority – if not all participants – I wish to express my gratitude to the local organizers Dr. A. Villalobo and Dr. J. Jimenez-Barbero (Madrid) and their collaborators as well as to Dr. H.-J. Gabius (Munich) and Dr. K. Kayser (Heidelberg), who implemented this scientifically outstanding workshop organized by tireless, warm-hearted hosts.

J. Szymas, Poznan

**Working Group of Pulmonary Pathology**
by Helmut Popper

*Address for information:*
Helmut H. Popper, M.D.,
e-mail: ppopper@kfunigraz.ac.at
Fax: +43–316–380–9636
Laboratories for Molecular Cytogenetics, Environmental and Respiratory Tract Pathology,
Institute of Pathology,
University of Graz

**Working Group on Head and Neck Pathology**
by Antonio Cardesa

*Information address:*
Prof. Antonio Cardesa,
Dept. Anatomic Pathology,
Hospital Clinic, Villarroel 170,
08036 Barcelona, Spain
(Tel: +34 93 227 5450,
Fax: +34 93 227 5717,
e-mail: acardesa@clinic.ub.es)

*New address:*
Prof. Henrik B. Hellquist, Chairman,
Department of Laboratory Medicine and Pathology,
Hamad Hospital, P.O. Box 3050,
Doha, Qatar

**Working Group on Endocrine Pathology**
by Gianni Bussolati

***E.C.E.P***
The European Club of Endocrine Pathology



***The European Club of Endocrine Patholgoy***
***Via Santena 7, Torino 10126, Italy***
***Tel.: +39-11-6706505, Fax: +39-11-6635267***
***e-mail: fassina@uxl.unipd.it***

All infomation, graphics and materials contained in this site are © 1997 by European Club of Endocrine Pathology
Prof. Ambrogio Fassina
© All right reserved

**Important message to all ESP members who want to send material for publication in the *Europath News*, which will appear four times a year (February, May, August, November) incorporated in *Virchows Archiv*: the material should be sent to one of the editors 2 months ahead of time by e-mail:**

**nagnanti@cc.uoi.gr** **brisberg@labmed.vio.no**

**Slide seminar in the Internet**

**Diagnostic histopathology cases presented at the European School of Pathology courses in Turin are going to be shown via Internet.**

**You are kindly invited to visit the site at http://www.isi.it/pathology/index.htm.**

**Working Group of Uropathology**
by Gregor Mikuz

*Addresses for information:*
Gregor Mikuz M.D., FRCPath (Chairman), Institute of Pathology University Innsbruck, Muellerstrasse 44, 6020 Innsbruck, Austria (gregor.mikuz@uibk.ac.at)

Ferran Algaba M.D.(Vice-chairman), Fundacion Puigvert, C/Cartagena 340 –350, 08025 Barcelona, Spain (19612itp@comb.es)

Antonio Lopez-Beltran M.D. (Secretary), Unit of Anatomical Pathology, Faculty of Medicine, 14004 Cordoba, Spain (Em1lobea@uco.es)

Margaret Constance Parkinson BSc, M.D. (Secretary), (HP) Fourth Floor Rockefeller Building, University Street, London WC1E6JJ, UK (Rmkdhmp@ucl.ac.uk)

Rodolfo Montironi M.D., FRCPath (Treasurer), Institute of Pathology, University of Ancona, 60020 Torrette / Ancona, Italy (r.montironi@popcsi.unian.it)

Michael J Mihatsch MD (Nephropathology), Institute of Pathology, University Basel, 4003 Basel, Switzerland (Mihatschmj@uhbs.ch)

**Working Group of Cytopathology**
by Fernando Schmitt

*Address for information:*
Prof Fernando Schmitt, IPATIMUP, Rua Roberto Frias S/N, 4200 Porto, Portugal (e-mail: fernando.schmitt@ipatimup.pt, Fax: +351–225570799)

**A message from the Editors to the Chairpersons of the formulated ESP Working Groups**

**Dear Colleagues,**
**If you are interested in presenting your activities to the EUROPATH NEWS, please send your material by e-mail 2 months ahead of publication.**

**PLEASE NOTE:**
**Due to the restricted number of pages in each issue, texts will appear on a "first come, first served" basis.**

**For information concerning ESP activities, please contact**

**ESP web-site: http://www.Europathology.org**

**Working Group of Gynaecology**
by Manfred Dietel

*Addresses for information:*
e-mail: manfred.dietel@charite.de

**Working Group on Molecular Pathology**

Foundation meeting:
Baveno Monday, 20 May 2002
For further information use the following e-mail addresses:

For Prof. Dr. Heinz Hofler:
renate.hartmann@lrz.tu-muenchen.de
(his secretary's e-mail address)

For Prof. Generoso Bevilacqua:
g.bevilacqua@med.unipi.it

**Electron Microscopy Working Group:**

*Address for information:*
Dr. Brian Eyden (PhD), Head of Diagnostic Electron Microscopy, Christie Hospital NHS Trust, Manchester M20 4BX, United Kingdom
Tel.: +44 161 446 3292
Fax: +44 161 446 3300
e-mail:
Brian.Eyden@christie-tr.nwest.nhs.uk

## The European Society of Pathology

Dear Colleague,

It will surely not have escaped your attention that *Virchows Archiv* is now the Official Journal of the European Society of Pathology.

But did you realise what benefits membership in the society offer you?

- A subscription to the journal *Virchows Archiv* at no extra charge – this is automatically sent to every member every month.
- Access to the journal online (take a look at http://link.springer.de). If you are already a member of ESP but have not yet registered for your free electronic access, you will find the necessary form to complete online here too.
- A discount of 20% on most titles published by Springer. To take advantage of this, simply send your order directly to the publisher, with details of your membership.
- Attendance at the Society's conferences at a reduced fee.

If you have not yet joined the European Society of Pathology, why not do so now? Simply complete and return the form enclosed. If you are already a member, please wait for our renewal letter for 2003.

We look forward to welcoming you as a member in 2003

Yours sincerely

M. Sobrinho-Simões
President
European Society of Pathology

U. van Haelst
Treasurer
European Society of Pathology

G. Klöppel
Managing Editor
Virchows Archiv




# Application for Membership of the
## EUROPEAN SOCIETY OF PATHOLOGY (E.S.P.)

***Please, type or use block letters to fill in this form!***



FAMILY NAME: .....

First Name(s): .....

Male ❑ Female ❑

Place and date of birth: .....

Title/Present Position: Prof. ❑ Dr. ❑ Resident ❑

Other : .....

*Please, clearly indicate which one of rhe following addresses should be used for subsequent correspondence, mailings, and listing in Membership Directory:*

❑ PRIVATE ADDRESS:

Name: .....

Street: .....

City: .....

Postcode/zip: .....

State/Country: .....

❑ INSTITUTE / OFFICE ADDRESS:

(This address will be used for subsequent correspondence and listing in Membership Directory)

Name Institute: .....

Department: .....

Street: .....

City: .....

Postcode/zip: .....

State/Country: .....

Tel. (+ ext): .....

Telefax: .....

E-mail: .....

FIELDS OF INTEREST: .....

.....

Date: .....

Signature of Applicant: .....

---

Please mail or fax the completed application form to:

E.S.P. - OFFICE OF THE TREASURER,
Prof. Dr. U. VAN HAELST,
van Cranenborchstraat 6,
NL – 6525 BN Nijmegen
The Netherlands.

Tel: xx 31. 24. 323 19 50
Fax: xx 31. 24. 322 23 04
E-mail: <Treasurer.ESP@vanHaelst.100.nl>

Your acceptance as a member of E.S.P. will be confirmed in due time.

Membership fee for 2003:

including subscription to the combined printed and electronic version of the Society's journal "Virchows Archiv": 89.00 EUR

including subscription to the electronic version only of "Virchows Archiv": 69.00 EUR





# Different to the rest!

## The NEW Leica ASP 300 Tissue Processor



ASP300/HBU/E

On the surface, all tissue processors may seem the same. But now Leica Microsystems offers you something different: a uniquely simplified instrument using the latest user-friendly, colour touch screen system. Smart design and proven technology are combined to create a new standard in automated tissue processing. Allow us to show you in your laboratory why the Leica ASP300 is different.


Leica Microsystems Nussloch GmbH
Heidelberger Strasse 17-19
D-69226 Nussloch

Phone +49 6224 143 0
Fax +49 6224 143 200
www.leica-microsystems.com


Leica
MICROSYSTEMS

Virchows Arch (2003) 442:209–210 © Springer-Verlag 2003

SOCIETY NEWS

# Invitation to the 19th European Congress of Pathology

On behalf of the European Society of Pathology (ESP) and the Organising Committee, we take great pleasure in inviting you to the 19th European Congress of Pathology, which will be held in Ljubljana, Slovenia, 6–11 September 2003.

Slovenia is not a large country, but at the hub of routes of trade and movement from east to west and north to south, it has always played a larger part in European events than its size would suggest. Slovenia is now an independent Central European state, on the sunny side of the Alps, bordering Italy, Austria, Hungary and Croatia. The landscape embraces rolling countryside leading to the Pannonian plain to the east, rugged Karst bordering the Adriatic Sea to the southwest, and the Alps to the north and west. The Slovenian nation of only two million today has survived mainly due to its culture, language and vitality. A bone flute, 30,000 years older than any other known in the world, and Europe's oldest bone needle, testify to the roots of culture here.

Its capital, Ljubljana, has a picturesque unity, composed of an architectural heritage spanning Roman Emona, through Renaissance and Baroque Ljubljana, to Secession Art Nouveau and Modern Ljubljana, so strongly marked by the influence of the world famous Slovenian architect, Jo e Plečnik. Ljubljana is an university city. The roots of the University go back to the seventeenth century with Academia Operosorum, the fourth Academy of Sciences in Europe. A Philharmonic Society dates back three centuries.

Ljubljana's congress tradition began in 1821, when the three emperors of the Holy Alliance met here to discuss the post-Napoleonic fate of Europe. These traditions have been brought together in the new Cultural and Congress Centre Cankarjev dom, with a capacity of 3,600, located in the heart of Ljubljana. Cankarjev dom is well equipped with all modern technical facilities and has an experienced in-house team to ensure the necessary high standards for scientific sessions and exhibitions. All Congress venues, and most hotels, are within walking distance of the centre of the city. Particular attention will be paid to stimulating the participation of trainees and young pathologists by securing as low a registration fee as possible, and inexpensive accommodations.

The European Society of Pathology has been succeeding in establishing its ever more continuous activity and influence. The old idea of a common programme of continuous education of pathologists has been realised through a number of courses organised each year by the European School of Pathology, at its headquarters in Turin and other centres throughout Europe. An increasing number of Working Groups within the European Society of Pathology, devoted to various fields, promote a continuous exchange of professional experiences and other information, the establishment of common diagnostic standards and collaboration on common research projects.

The biannual ESP Congresses retain a major role in fulfilling the main aims of the ESP in pathology education, exchange of the most recent research achievements and, particularly, in keeping together all branches of pathology, that otherwise tend to split according to organ systems, disease processes and the increasing number of techniques. The Congresses also keep together pathologists from the whole of Europe, irrespective of geographical and political borders.

We believe that the 19th European Congress of Pathology will continue the traditional approaches of previous Congresses and will serve to increase both links with European national and international pathology societies and intercontinental links, particularly with the International Academy of Pathology. The framework of the Congress Scientific Programme has been created with the strong impact and assistance of the ESP Working Groups, the ESP Executive/Scientific Committee and the Advisory Council as well as companion Societies. The programme covers all areas of pathology, provides information ranging from current diagnostic standards to recent advances in science and modern techniques, particularly those of molecular genetics, and includes a number of "hot" topics of today and tomorrow, which will be

presented by the best, internationally recognised experts at Keynote Lectures, Symposia, Special Presentations, Round Table Discussions, Short Courses and Slide Seminars. One evening is devoted to ESP Working Group Meetings, both business and scientific. Interesting Satellite Symposia will be organised by supporting companies, two by the main sponsor of the Congress Main Sponsor, Ventana Medical Systems S.A.

Furthermore, all practising pathologists and scientists are kindly invited to present their scientific achievements and exchange their professional experiences through Free Paper and Poster Sessions. The best Free Papers will be acknowledged by giving the authors the opportunity to present their achievements at the plenary session, at which the authors of the three best Poster Presentations will additionally receive special Awards.

All who are coming to Ljubljana are kindly invited to join us at two one-day Pre-Congress Meetings, prior to the Congress Opening Ceremony on Saturday: one on Pulmonary Pathology and the other devoted to non-neoplastic Nephropathology. There will also be a three-day Joint Meeting of the European and North American Society of Head and Neck Pathology. All Pre-Congress Meetings and a whole day Examination by the European Board of Pathology will be organised by using the facilities of the new building of the Faculty of Medicine, University of Ljubljana.

Culture kept the Slovenian national identity alive over the centuries and it still plays an important role in people's lives. The Congress will also highlight the traditional close connection between medicine and art. Some novel events are planned: an exhibition of the work of pathologists/painters and, especially, a Gala Concert on Monday evening in the main Gallus Concert Hall of the Congress Centre in Ljubljana, by pathologists/musicians from all over the world. A social programme is offered which reflects the warmth and hospitality of the Slovenian people.

The Second Millennium we have entered provides major challenges for all biomedical sciences, and the 19th European Congress of Pathology is a challenge for the Organisers. We sincerely hope that attendance at the Ljubljana Congress in 2003 will be a fruitful, enjoyable and memorable experience in every respect for all participants, and will give new impetus to our medical speciality in Slovenia.

We look forward to seeing you in September 2003 in Ljubljana.



Gianni Bussolati
President
European Society
of Pathology



Du an Ferluga
President
19th European Congress
of Pathology

Virchows Arch (2003) 442:211–217
DOI 10.1007/s00428-002-0741-7

REVIEW ARTICLE

**Rodolfo Montironi · Roberta Mazzucchelli**
**Theodorus Kwast**

# Morphological assessment of radical prostatectomy specimens. A protocol with clinical relevance

Received: 11 September 2002 / Accepted: 22 October 2002 / Published online: 16 January 2003
© Springer-Verlag 2003

**Abstract** The increase in prostate cancer detection has induced a sharp increase in the number of radical prostatectomies Proper examination of radical prostatectomy (RP) specimens by pathologists is critical in determining the need for adjuvant treatment and prediction of patient outcome. The pathology report should include relevant clinical information as well as provide prognostically useful information derived from the macroscopic examination and microscopic evaluation of the RP specimen.

**Keywords** Prostate cancer · Radical prostatectomy

## Introduction

The incidence of prostate cancer (PCa) has risen dramatically in the past decade, probably owing to early detection programs that employ digital rectal examination, serum prostate-specific antigen, and transrectal ultrasonography [16]. The increase in PCa detection has induced a sharp increase in the number of radical prostatectomies (RPs) [2, 5]. The popularity of surgical treatment is due in part to improvements in technique that decrease the risk of impotence, including nerve-sparing prostatectomy. One of the main issues for pathologists and urologists is the identification in RP specimens of those prognostic factors that could accurately predict patient outcome.

The contemporary status of the prognostic factors was addressed at two international consensus conferences: 1999 College of American Pathologists (CAP) Conference [5] and 1999 World Health Organization (WHO) Second International Consultation on Prostate Cancer [4]. A group of clinicians, pathologists and statisticians analysed the existing predictive factors and stratified them into categories reflecting the strength of published evidence and taking into account the opinions of the Prostate Working Group members of the CAP [5]. In particular, factors were ranked according to the CAP categorical ranking (Table 1):

- Category I: factors proven to be of prognostic importance and useful in clinical patient management
- Category II: factors that have been extensively studied biologically and clinically but whose importance remains to be validated in statistically robust studies
- Category III: all other factors not sufficiently studied to demonstrate their prognostic value.

The CAP categorical ranking was fully endorsed by the WHO conference [4]. In particular, the adoption of all the pathology factors grouped in category I was recommended; the factors grouped in category II may be included based on local discretion; and adoption of any of the factors in category III was not recommended [4].

The aim of this paper is to give an overview of:

- Handling and sectioning of RP specimens
- Pathology reporting of RP specimens

## Handling of RP specimens

Routine protocol-based tissue sampling ensures consistent and thorough examination by trainees and consultants. The issue has been addressed in the last few years by different groups and societies, among which are the Association of Directors of Anatomic Pathology [2] and the Col-

This paper is based on the morphological analyses of 393 radical prostatectomy specimens of the Italian PROSIT Study (a prospective, randomized trial). (Study coordinators: Prof. F. Pagano, Padua; Prof. A. Bono, Varese. Reviewing pathologist: Rodolfo Montironi, Ancona. See Appendix for the full list of participating centres).

R. Montironi (✉) · R. Mazzucchelli
Institute of Pathological Anatomy,
University of Ancona School of Medicine,
Umberto 1° Hospital60020 Torrette, Ancona, Italy
e-mail: r.montironi@unian.it
Tel.: +39-071-5964830, Fax: +39-071-889985

T. Kwast
Department of Pathology,
Josephine Nefkens Institute,
Erasmus MC, Rotterdam, The Netherlands

**Table 1** Categorical ranking of prognostic factors according the 1999 CAP Conference. Adapted from reference [5]

| |
|---|
| Category 1. Factors proven to be of prognostic importance and useful in clinical patient management: |
| Perioperative serum prostate specific antigen (PSA) |
| Histological grade (Gleason) |
| TNM stage |
| Surgical margin status |
| Category 2. Factors that have been extensively studied biologically and clinically but whose importance remains to be validated in statistically robust studies: |
| Tumour volume in needle biopsy specimens (recommended) |
| Tumour volume in radical prostatectomy specimens (recommended) |
| Histological type |
| DNA ploidy |
| Category 3. All other factors not sufficiently studied to demonstrate their prognostic value: |
| Perineural invasion |
| Microvessel density (angiogenesis) |
| Nuclear roundness, chromatin texture, other karyometric factors |
| Proliferation markers |
| Neuroendocrine differentiation |
| Prostate-specific antigen derivatives |
| All other factors (oncogenes, tumour suppressor genes, apoptosis genes, etc.) |

lege of American Pathologists [5, 12, 22, 25]. Bostwick and Montironi [6] and Mazzucchelli et al. [16] incorporated the conclusions of each of these contemporary statements to create a standardised approach to examination of RP specimens. The recommendations are as follows.

## Size and weight

The fresh (unfixed) RP specimen is weighed and may be measured in three dimensions, e.g. width, height and length. The volume of the specimen is calculated as the volume of an ellipse [15]:

$$(\text{Width} \times \text{Height} \times \text{Length}) \times 0.532$$

Although recording the weight of RP specimens is important for documentation, especially when supplemented by comments related to the completeness of resection, the value of recording dimensions in addition to weight is of less obvious value. Because the resected prostate is an irregular structure, symmetrical in only one axis about the sagittal plane, linear measurements are less accurate and reproducible than specimen weight.

To enhance a quick and uniform penetration of the fixative, the prostate specimen is injected with 10% neutral-buffered formalin solution using a fine hypodermic needle (0.6×25 mm, for instance). After plunging the needle deep into the prostatic tissue, formalin solution is slowly injected while the needle is slowly retracted. Formalin injection is performed in a systematic way, at multiple 0.5-cm-spaced sites at all sides of the RP specimen. In total, approximately 100 ml formalin solution is injected. (For details see ref. [13]). This procedure does not lead to damage to the morphology of the prostatic tissue. The rationale behind the injection procedure is that, during immersion in a formalin solution, the fixative only slowly diffuses toward the centre of the specimens. When the periphery of the prostate is fixed, the presence of cross-linked proteins is thought to hinder further diffusion of the fixative toward the centre of the specimen (so-called crust effect).

The entire surface of the RP specimen is inked using two different colours for each side in order to recognise the left and right. Green and red (or blue) are usually used. By immersing the inked gland into a mordant, such as Bouin's solution or acetic acid, the ink is fixed to the surface. The India ink could be preferred to the two-colour procedure because the black-coloured margins are more easily identified when the sections are examined under the microscope. Inking is important because the surface of the prostate is a fibromuscular tissue that does not form a discrete histological boundary with extraprostatic, pelvic soft tissue. Because proximity of tumour to margin cannot be predicted based on the gross appearance of the cut surface of the prostate, the entire surface should be inked. Inking each side with different colour helps retain orientation as sections are obtained and provides a cross-check for section location. The RP specimen is then immersed in 300 ml to 400 ml formalin solution and allowed to fix for 24 h.

### *Sectioning procedure*

For sectioning, the seminal vesicles (SVs) are removed from the RP specimen (Fig. 1). Each SV is cut into two halves using a ''sandwich'' technique. The apical and basal parts of the prostate are removed by a transversal cut at 4 mm from the distal and proximal margins, respectively. Optionally, the distal urethral margin may be removed from the apical part and examined separately. The apical and proximal parts are then sectioned as follows: slices are cut parasagittally at 4-mm intervals and perpendicularly to the inked surface.

The prostate specimen is step-sectioned at 4-mm intervals perpendicular to the long axis (apical-basal) of

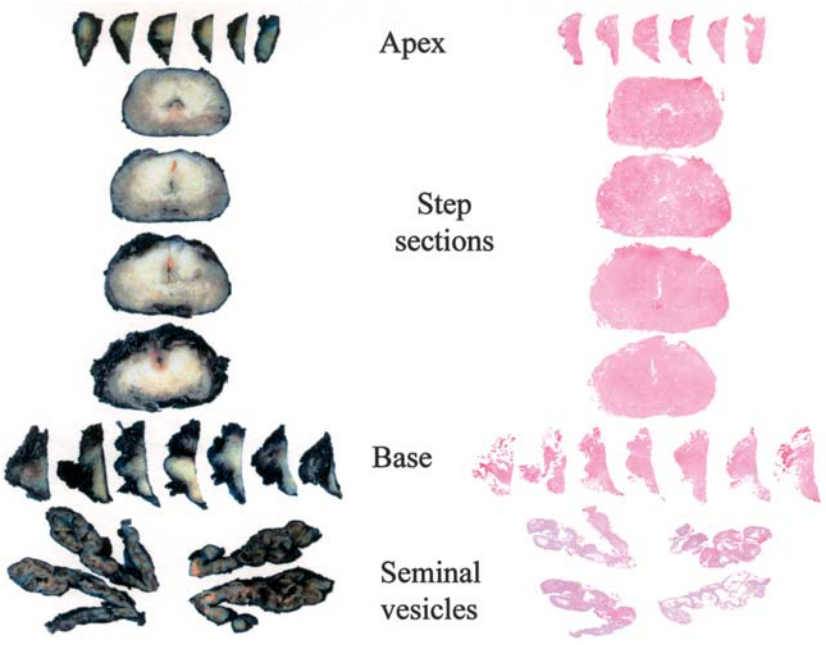



**Fig. 1** Serial coronal sections, parallel to an initial en-face section of the apex, the apical and proximal parts and the seminal vesicles (*left*). The corresponding histological sections are also shown (*right*) (*source* [16])

the gland. A slicing machine should be used. Serial coronal sections, parallel to an initial en-face section of the apex, are taken until the junction of the SVs is approached. The whole-mount sections are identified in a consecutive manner with capital letters, always starting from the most apical section. In this way, the whole RP specimen is available for histological examination as originally described by Stamey et al. [23]. When the India ink is used, a cut is made with a scalpel in the right antero-lateral aspect of each slice to mark the right side.

There is not yet a consensus among pathologists as to whether the whole gland should be embedded for sectioning. The rationale for total embedment of the prostate is based on the fact that the gross appearance of the sectioned prostate is an unreliable guide for tumour distribution. In addition, during the PSA era, tumours have become smaller in size and multifocality of cancer is a frequent finding [27]. Whether the greater time and materials involved in prosecting and examining sections of totally embedded prostate is worthwhile is unclear. Even totally embedding a prostate does not mean that the margins will be completely sampled, unless serial sections are made of each block.

The dilemma of choosing between whole mount sections and quadrant sections is one of balancing aesthetics and greater ease in examining sections against the cost of time and materials and the logistical problem of storing glass slides and paraffin blocks of unconventional size. The only significant difference in the histopathology of these two different processing methods is that whole mounts are often thicker sections.

The cut specimen may be post-fixed for 24 h. The en-face section is then processed as a single section; alternatively, the en-face sections are submitted as quadrants following a systematic numbering scheme. In particular, the cut specimen is dehydrated in graded alcohols, cleared in xylene, embedded in paraffin and examined histologically as 5-μm-thick, whole-mount, haematoxylin and eosin-stained sections (Fig. 1). Special moulding and inclusion cassettes should be used. The slides should be at least 76 mm long and 50 mm wide. Cover-slips of a similar size have to be used.

When cancer is not readily identified in the histological slides, the pathologist should proceed as follows: (1) If the prostate is totally embedded, then the diagnostic needle biopsies should be reviewed to assess the approximate location of the tumour. Sections of the prostatectomy of this area should be re-cut after block-flipping. (2) If the prostate was not totally embedded then this should be done. Immunostaining with antibody against CAM 5.2 should be applied to identify the so-called ‘‘minimal residual cancer’’ [18].

## Pathology reporting of RP specimens

The pathology report should include clinical relevant information (Table 2) as well as provide clinically useful information derived from the macroscopic examination (Table 3) and microscopic evaluation (Table 4) of the RP specimen [26]. The reporting pathologist should pay particular attention to the evaluation of the prognostic factors included in the College of American Pathologists categories 1 and 2, e.g. factors proven to be of prognostic importance and useful in clinical patient management and factors extensively studied biologically and clinically but whose importance remains to be validated in statistically robust studies: histological type, grade and volume of cancer, the extent of local invasion and stage of cancer as well as the surgical margins status. The explanatory notes of these factors are given hereafter.

**Table 2** Clinical information. Adapted from reference [26]

1. Patient identification
   a. Identification number
   b. Name
   c. Age (birth date)
2. Clinical information
   a. Relevant history and preoperative findings (previous diagnosis, treatment, includes PSA, imaging)
   b. Operative findings
   c. Anatomic site(s) of specimen(s)
   d. Procedure
      – Retropubic procedure

Nerve sparing

Standard radical
– Perineal procedure

3. Responsible physician(s)

**Table 3** Macroscopic examination. Adapted from reference [26]

1. Specimen
   a. Organ(s)/tissues included
   b. Unfixed/fixed (specify fixative)
   c. Opened/unopened
   d. Orientation (if indicated by surgeon)
   e. Structures included in specimen
      – Prostate
      – Seminal vesicles
      – Segments of vasa deferentia
      – Bladder neck
      – Urethra
      – Other(s) (specify)
   f. Size (three dimensions)
   g. Weight (prostate separately)
   h. Obstruction of urethra (partial/complete)
   i. Descriptive features (e.g., nodular hyperplasia)
   j. Results of intraoperative consultation
2. Tumour (if identified)
   a. Location(s)
   b. Size(s)
   c. Descriptive features
   d. Extent of local invasion
3. Regional lymph nodes
   a. Location
   b. Number (each location, if possible)
4. Blocks submitted for microscopic evaluation
   a. Tumour(s) (each grossly recognisable tumour)
   b. Blocks from other anatomic locations within the prostate (to evaluate for multicentricity)
   c. Blocks to determine extent of invasion
      – Prostatic capsule and periprostatic tissue adjacent to each tumour including inked margins
      – Seminal vesicles
      – Periprostatic tissue at bases of seminal vesicles
   d. Apex
   e. Prostate base margin
   f. All lymph nodes
   g. Frozen section tissue fragment(s)(unless saved for special studies)
   h. Other tissues (specify)

Special studies (specify) (e.g. immunohistochemistry, ploidy analysis, S phase fraction)

**Table 4** Microscopic evaluation. Adapted from reference [26]

1. Tumour
   a. Location(s)
   b. Histological type
   c. Gleason score with primary and secondary grades
   d. Extent of local invasion
      – 1 Extraprostatic extension
      – 2 Seminal vesicle involvement
2. Margins (location and extent of margins involved with tumour)
3. Regional lymph nodes
   a. Number (specify location)
   b. Number involved by tumour
      – 1 specify location, if possible
      – 2 size of metastatic deposit (i.e. if <2 mm = micrometastasis)
      – 3 extracapsular extension, if present
4. Additional pathologic findings, if present
   a. High-grade intraepithelial neoplasia (PIN)
   b. Therapy-related changes
   c. Other(s)
5. Metastasis to other organ(s) or structure(s) (specific sites)
6. Other tissue(s)/organ(s)
7. Results/status of special studies
8. Comments
   a. Correlation with intraoperative consultation
   b. Correlation with other specimens, as appropriate
   c. Correlation with clinical information, as appropriate

**Table 5** Histological classification of carcinoma of the prostate. Adapted from reference [26]

1. Adenocarcinoma (conventional, not otherwise specified)
2. Special variants of adenocarcinoma and other carcinomas
   – Prostatic duct adenocarcinoma
   – Mucinous (colloid) adenocarcinoma
   – Signet ring cell carcinoma
   – Adenosquamous carcinoma
   – Squamous cell carcinoma
   – Basaloid and adenoid cystic carcinoma
   – Transitional cell carcinoma
   – Small cell carcinoma
   – Sarcomatoid carcinoma
   – Lymphoepithelioma-like carcinoma
   – Undifferentiated carcinoma, not otherwise specified

## Histological type of cancer

The histological classification of prostate carcinoma is shown in Table 5. In general, more than 95% of cases of prostatic carcinoma are acinar adenocarcinoma. In recent years, a number of new and unusual histological variants or subtypes have been identified. These variants represent the spectrum of changes that can occur in adenocarcinoma. The biological behaviour of many of these variants may differ from typical adenocarcinoma, and proper clinical management depends on accurate diagnosis and separation from tumours arising in other sites. It is recommended that subtypes, such as small cell, ductal and mucinous, should be reported if they are noted histologically. Mixtures of different histological types should be indicated.

**Table 6** Gleason grades (pattern). Adapted from reference [26]

| |
|---|
| – Grade 1 – Single, separate, closely packed acini |
| – Grade 2 – Single acini, more loosely arranged, less uniform |
| – Grade 3 – Single acini of variable size, and separation, cribriform and papillary patterns |
| – Grade 4 – Irregular masses of acini and fused epithelium, can show clear cells |
| – Grade 5 – Anaplastic carcinoma |

**Table 7** Gleason scores (grouping). Scores may be grouped into differentiation or prognostic categories. Adapted from reference [5]

| |
|---|
| 2–4: Well differentiated |
| 5–6: Moderately well differentiated |
| 7: Moderately poorly differentiated |
| 8–10: Poorly differentiated |
| or |
| 2–6: Well differentiated |
| 7: Moderately differentiated |
| 8–10: Poorly differentiated |

## Histological grade of cancer

Differentiation grade is one of the strongest and more useful predictors, according to numerous univariate and multivariate studies. The Gleason grading system is recommended for use in all prostatic cancer specimens (Table 6) [3, 9, 10, 19, 24]. The Gleason score is the sum of the primary (most predominant) Gleason grade and the secondary (second most predominant) Gleason grade. Where no secondary Gleason grade exists, the primary Gleason grade is doubled to arrive at a Gleason score. The primary and secondary grades should be reported in parenthesis after the Gleason score, i.e. Gleason score 7 (3, 4) or 7 (3+4). If Gleason must be compressed for evaluation or reporting purposes, the groups should be 2–5, 6, 7, and 8–10, or 2–6, 7, and 8–10. In RP specimens, where more than one separate tumour is identified, the Gleason scores of the individual tumours may be reported separately or at the very least the Gleason score of the most significant lesion should be recorded. For instance, if there is a large Gleason score 5 transition zone cancer and a separate smaller Gleason score 7 peripheral zone cancer, both scores or at least the latter score should be reported rather than the scores being averaged. Gleason scores may be grouped into differentiation or prognostic categories (Table 7).

Another grading system may be used according to institutional preference (e.g. WHO, MD Anderson) but the Gleason score must be included to facilitate comparison of data. It is not possible to apply the Gleason and the WHO schemes when the patient was under androgen blockade before surgery. In such situations, the pathologist should indicate the degree of regression [17].

## Volume of cancer

A consensus for a standard method of volume determination has not yet evolved. Volume is most precisely determined by stereological methods, using either planimetry or point counting based on overlaid grids. However, the time and labour involved in these approaches will probably not lead to their wide acceptance. It is recommended that, at the very least, the proportion (percentage) of prostatic tissue involved by tumour be included for all specimens.

## Extent of local invasion

Extent of local invasion includes extraprostatic extension (EPE) and SV involvement. EPE is the preferred term for the presence of tumour beyond the confines of the prostate gland [1, 11]. Tumour abutting on or admixed with fat constitutes EPE. EPE may also be reported when tumour involves perineural spaces in the neurovascular bundles, even in the absence of periprostatic fat involvement. In certain locations, such as the anterior prostate and bladder neck regions, there is paucity of fat. In these locations EPE is determined when the tumour extends beyond the confines of the normal glandular prostate. At the apex, tumour admixed with skeletal muscle elements does not constitute EPE. The amount of EPE carries prognostic importance. Different ways have been used to define the amount of EPE. If it is equal to or less than two high-power (40×) microscopic fields, then EPE is focal according to some authors [16]. Any amount in excess of two high-power fields is considered to be either non-focal or extensive.

## Staging

The protocol recommends the use of the TNM Staging System for carcinoma of the prostate of the American Joint Committee on Cancer (AJCC) and the International Union Against Cancer (UICC) as shown below [8, 21]. The most recent revision was published in 2002. Clinical classification (cTNM) is usually carried out by the referring physician before treatment during initial evaluation of the patient or when pathologic classification is not possible (Table 8). The prefix symbol ‘‘p’’ refers to the pathologic classification of the TNM (pTNM), as opposed to the clinical classification. Pathologic classification is based on gross and microscopic examination (Table 9). By AJCC/UICC convention, the designation ‘‘T’’ of the TNM classification refers exclusively to the first resection of a primary tumour. Therefore, pT entails a resection of the primary tumour or biopsy adequate to evaluate the highest pT category; pN entails removal of nodes adequate to validate lymph-node metastasis (Table 10); and pM implies microscopic examination of distant lesions (Table 11).

Tumour remaining in a resection specimen following previous (neoadjuvant) treatment of any type (radiation therapy alone, chemotherapy therapy alone, or any combined modality treatment) is codified by the TNM using a prescript ‘‘y’’ to indicate the post-treatment status of the tumour (e.g., ypT1). The classification of residual

**Table 8** Primary tumour, clinical (cT) (2002 revision). Adapted from reference [26]

| | |
|---|---|
| TX | Primary tumour cannot be assessed |
| T0 | No evidence of primary tumour |
| T1 | Clinically inapparent tumour not palpable or visible by imaging |
| T1a | Tumour incidental histological finding in 5% or less of tissue resected |
| T1b | Tumour incidental histological finding in more than 5% of tissue resected |
| T1c | Tumour found in one or both lobes by needle biopsy, but not palpable or visible by imaging (elevated PSA) |
| T2 | Tumour confined within the prostate |
| T2a | Tumour involves one-half of one lobe or less |
| T2b | Tumour involves more than half of one lobe, but not both lobes |
| T2c | Tumour involves both lobes |
| T3 | Tumour extends through the prostatic capsule* |
| T3a | Extracapsular extension (unilateral or bilateral) |
| T3b | Tumour invades the seminal vesicle(s) |
| T4 | Tumour is fixed or invades adjacent structures other than the seminal vesicles, bladder neck, external sphincter, rectum, levator muscles and/or pelvic wall |

**Table 9** Primary tumour, pathologic (pT) (2002 revision). There is no pathologic T1 category

| | |
|---|---|
| pT2 | Organ confined |
| T2a | Tumour involves one-half of one lobe or less |
| T2b | Tumour involves more than half of one lobe, but not both lobes |
| T2c | Tumour involves both lobes |
| pT3 | Extraprostatic extension |
| pT3a | Extraprostatic extension |
| pT3b | Seminal vesicle extension |
| pT4 | Invasion of bladder*, rectum |

**Table 10** Regional lymph nodes (N)

| | |
|---|---|
| NX | Regional lymph nodes cannot be assessed |
| N0 | No regional lymph-node metastasis |
| N1 | Metastasis in regional lymph node or nodes |

**Table 11** Distant metastasis (M). When more than one site of metastasis is present, the most advanced category (pM1c) is used

| | |
|---|---|
| MX | Distant metastasis cannot be assessed |
| M0 | No distant metastasis |
| M1 | Distant metastasis |
| M1a | Non-regional lymph node(s) |
| M1b | Bone(s) |
| M1c | Other site(s) |

disease may be a predictor of postoperative outcome. In addition, the ypTNM classification provides a standardised framework for the collection of data needed to accurately evaluate new neoadjuvant therapies.

### Positive surgical margins

Surgical margins should be designated as ''negative'' if tumour is not present at the inked margin and as ''positive'' if tumour cells touch the ink at the margin. Positive surgical margins should not be interpreted as EPE. If the surgical margin is positive, the pathologist should state this explicitly, although this finding is not relied on for pathologic staging. The examining pathologist should be aware of false-positive margins due to the penetration of ink into cracks present on the external surface. The main cause for discrepancy in the definition of a positive margin is seen in situations in which cancer was very close but not clearly touching the inked margin or when the colour used to identify the margin appeared very pale.

The specific locations of the positive margins should be documented and there should be some indication (e.g. number of positive blocks, linear extent in millimetres) of the extent of margin positivity. The apex should be closely examined because of its unusual susceptibility to positive margins [6, 7, 20].

There is no full consensus on the definition of the T category in the situation in which the prostate base/bladder beck is involved and the margin is positive. This problem is likened to the fact that the basal prostatic stroma blends imperceptively into the bladder neck musculature and, therefore, to the difficulty in defining the exact transition point from prostate base to bladder neck, even though the latter is composed of distinct bundles of smooth muscle fibres. Microscopic involvement of bladder neck muscle fibres in RP specimens should be defined as pT4 [14]. Others [25] think that the microscopic involvement of bladder neck muscle fibres in RP specimens should not be equated with a pT4 designation, the latter generally requiring gross involvement of the bladder neck.

Tumour remaining in a patient after therapy with curative intent (e.g. surgical resection) is categorised by a system known as R classification. This classification may be used by the surgeon to indicate the known or assumed status of the completeness of the surgical resection. For the pathologist, the R classification is relevant only to the margins of surgical resection specimens; patients with tumour involving the resection margins on pathologic examination may be assumed to have residual tumour. Such patients may be classified as to whether the involvement is macroscopic or microscopic (Table 12).

**Table 12** Residual tumour in the patient

| | |
|---|---|
| RX | Presence of residual tumour cannot be assessed |
| R0 | No residual tumour |
| R1 | Microscopic residual tumour |
| R2 | Macroscopic residual tumour |

Tumour that is locally recurrent after a documented disease-free interval following surgical resection is classified according to the TNM categories but modified with the prefix ''r'' (e.g. rpT1).

## Conclusions

Substantial effort has been expended in the recent years in describing the available factors and determining their

predictive value for staging, cancer recurrence and patient survival. The pathologists derive many clinically important predictive factors in PCa from light microscopic examination of RP specimens. The goal is to tailor the therapeutic approach to the clinical, morphological and molecular features of each patient.

## Appendix

(For full details of the study see: J Clin Pathol 2002; 55:508–513)

The following urologists and pathologists participated in the Italian PROSIT study: M. Polito, G. Muzzonigro, D. Minardi, R. Montironi (Ancona); F.P. Selvaggi, S. Palazzo, P. Bufo (Bari); S. Guazzieri, R. Bertoldin, C. Doglioni, E. Macrì (Belluno); A. Lembo, L. Canclini, D. Chinaglia (Bergamo); S. Cosciani-Cunico, T. Zambolin, M. Tanello, R. Tardanico (Brescia); E. Usai, R. Migliari, G. Muscas, E. Valdes, C. Varsi (Cagliari); S. Ferretti, P. Palladini, C. DiGregorio (Carpi); G.C. Comeri, G. Conti, Q. Lunetta, G. Scola (Como); G. Signorelli, E. Andretta, R. Giordano, E. Nisi (Dolo); M. Rizzo, R: Bartoletti, A. Amorosi (Firenze); E: Martini, P. Andreassi, T. Ventura (L'Aquila); W. Artibani, R. Piazza, C. De Gaetani (Modena); D. Fontana, R. Tarabuzzi, L. Gulbetta, E. Bollito (Orbassano); F. Pagano, T. Prayer-Galetti, M. Gardiman (Padova); G. Fiaccavento, P. Belmonte, G. Sacchi (Portogruaro); S. Rocca Rossetti, C. Terrone, G. Palestro, D. Galliano (Torino); G. Muto, F. Bardari, O. Campobasso, .M. Pisacane (Torino); A. Manganelli, G. De Rubertis, M.T. Del Vecchio (Siena); D. Potenzoni, A. Gregori, L. Serra (San Secondo Parmense), G. Anselmo, A. Checchin, G.A. Arrigoni (Treviso); C. Selli, C. Scott, C.A.Beltrami (Udine); F. Zattoni, P. Galassi (Udine); A.V. Bono, C. Fava, M. Salvadore (Varese); A. Tasca, A. Meneghini, S. Meli, A. Armani (Vicenza).

## References


1. Amin MB, Grignon D, Bostwick D, Epstein JI, Reuter V, Troncoso P, Ro JY, Ayala AA (1998) Recommendations for reporting resected prostatic carcinomas with commentary. Pathol Case Rev 3:223–232
2. Association of Directors of Anatomic and Surgical Pathology (1996) Recommendations for the reporting of resected prostate carcinomas. Hum Pathol 27:321–323
3. Bostwick DG (1994) Gleason grading of prostatic needle biopsies: correlation with grade in 316 matched prostatectomies. Am J Surg Pathol 18:796–803
4. Bostwick DG, Foster CS, Algaba F, Hutter RVP, Montironi R, Mostofi FK et al (2000) Prostate tissue factors. In: Murphy G, Denis L, Khoury S, Partin A, Denis L (eds) Prostate cancer. Second International Consultation on Prostate Cancer, Co-Sponsored by WHO and UICC, 27–29 June 1999, Plymbridge Distributors Ltd, Paris
5. Bostwick DG, Grignon DJ, Hammond EH, Amin MB, Cohen M, Crawford D et al (2000) Prognostic factors in prostate cancer. Collage of American Pathologists consensus statement 1999. Arch Pathol Lab Med 124:995–1000
6. Bostwick DG, Montironi R (1997) Evaluating radical prostatectomy specimens: therapeutic and prognostic importance. Virchows Arch 430:1–16
7. Epstein JI (1991) The evaluation of radical prostatectomy specimens: therapeutic and prognostic implications. Pathol Annu 26:159–210
8. Fleming ID, Cooper JS, Henson DE, et al (eds) (1997) AJCC manual for staging of cancer, 5th edn. Lippincott Raven, Philadelphia
9. Gleason DF (1992) Histologic grading of prostate cancer: a perspective. Hum Pathol 23:273–279
10. Gleason DR, Mellinger GT, the Veterans Administration Cooperative Urological Research Group (1974) Prediction of prognosis for prostate adenocarcinoma by combined histological grading and clinical staging. J Urol 111:58–64
11. Grignon DJ, Sakr WA (1996) Pathologic staging of prostate carcinoma. What are the issues. Cancer 78:337–340
12. Henson DE, Hutter RVP, Farrow G (1994) Practice protocol for the examination of specimens removed from patients with carcinoma of the prostate gland. A publication of the Cancer Committee, College of American Pathologists. Arch Pathol Lab Med 118:779–783
13. Hoedemaeker RF, Ruijter ETG, Ruizeveld-de Winter JA, van der Kaa CA, The BIOMED II MPC study group, van der Kwast TH (1998) Processing radical prostatectomy specimens. A comprehensive and standardized protocol. J Urol Pathol 9:211–222
14. Hoedemaeker RF, Vis AN, Van der Kwast TH (2000) Staging prostate cancer. Microsc Res Technique 51:423–429
15. Littrup PJ, William CR, Egglin TK, Kane RA (1991) Determination of prostate volume with transrectal US for cancer screening. II. Accuracy of in vitro and in vivo techniques. Radiology 179:49–53
16. Mazzucchelli R, Santinelli A, Lopez-Beltran A, Scarpelli M, Montironi R (2002) Evaluation of prognostic factors in radical prostatectomy specimens with cancer. Urol Int 68:209–215
17. Montironi R, Bartels PH, Thompson D, et al (1996) Androgen-deprived prostate adenocarcinoma: evaluation of treatment-related changes versus no distinctive treatment effect with a Bayesian belief network. Eur Urol 30:307–315
18. Montironi R, Schulman CC (1998) Pathological changes in prostate lesions after androgen manipulation. J Clin Pathol 51:5–12
19. Partin AW, Kattan MW, Subong ENP, et al (1997) Combination of prostate-specific antigen, clinical stage, and Gleason score to predict pathological stage of localized prostate cancer: a multi-institutional update. JAMA 277:1445–1451
20. Sakr WA, Wheeler TM, Blute M, et al (1996) Staging and reporting of prostate cancer; sampling of the radical prostatectomy specimen. Cancer 78:366–369
21. Sobin LH, Wittekind C (eds) (2002) TNM classification of malignant tumours: International Union Against Cancer, 6th edn. Wiley-Liss, New York
22. Srigley JR, Amin MB, Bostwick DG, Grignon DJ, Hammond EH for the members of the Cancer Committee, College of American Pathologists (2000) Updated protocol for of the examination of specimens from patients with carcinomas of the prostate gland. A basis for checklists. Arch Pathol Lab Med 124:1034–1039
23. Stamey TA, McNeal JE, Freiha FS, Redwine E (1988) Morphometric and clinical studies on 68 consecutive radical prostatectomies. J Urol 139:1235–1241
24. Steinberg DM, Sauvageot J, Piantadosi S, Epstein JI (1997) Correlation of prostate needle biopsy and radical prostatectomy Gleason grade in academic and community settings. Am J Surg Pathol 21:566–576
25. True LD (1994) Surgical pathology examination of the prostate gland. Practice survey by American Society of Clinical Pathologists. Am J Clin Pathol 102:572–579
26. www.cap.org/html/ftpdirectory/html/prostate.html
27. Yang XJ, Lecksell K, Potter SR, Epstein JI (1999) Significance of small foci of Gleason score 7 or greater prostate cancer on needle biopsy. Urol 54:528–532

Virchows Arch (2003) 442:218–225
DOI 10.1007/s00428-003-0760-z

REVIEW ARTICLE

J. Sträter · P. Möller

# CD95 (Fas/APO-1)/CD95L in the gastrointestinal tract: fictions and facts

Received: 1 November 2002 / Accepted: 7 January 2003 / Published online: 11 February 2003
© Springer-Verlag 2003

**Abstract** CD95 is a member of the tumor necrosis factor receptor family. It is constitutively expressed on the basolateral membrane of intestinal epithelial cells (IEC) and induces apoptosis when cross-linked by its natural ligand, CD95L. The significance of providing such a death-inducing mechanism in IEC is not yet clear. In recent years a multitude of studies have been published addressing the question of where and under which conditions CD95L is produced in the gut in the normal and neoplastic situation. Although some of these studies have considerably influenced our view on the role of the CD95/CD95L system, it appears necessary to critically review published data which are in part confusing and contradictory. To date compelling evidence of CD95L expression in untransformed IEC is lacking, and involvement of the CD95/CD95L system in the physiological epithelial cell turnover appears unlikely. Whereas CD95L is overexpressed in T-cells under inflammatory conditions, its significance for mucosal damage in inflammatory bowel diseases is obscured by possible redundancies in cell death mechanisms. Finally, recent data indicate that the intriguing CD95L counterattack concept in gastrointestinal tract cancer needs to be revised.

**Keywords** Ligand · Colorectal cancer · Inflammatory bowel disease · Regeneration · CD95

## Introduction

Apoptosis, programmed cell death, is a fundamental biological process with tremendous implications for the maintenance of tissue homeostasis. In the small and large bowel, intestinal epithelial cells (IEC) divide at the base of the crypts, migrate up along the crypt or crypt-villus axis and are eliminated at the villus tips (small intestine) or luminal surface epithelium (colorectum) [16]. The number of eliminated cells must be in balance with the number of cells generated by mitosis at the crypt base and thus must be tightly regulated to prevent hyperplasia or tumor formation. Initial evidence that apoptosis is involved in epithelial cell loss in the gut was provided by data from Gavrieli and colleagues [22] who demonstrated DNA fragmentation, a hallmark of apoptosis, mostly in cells at the intestinal villus tips using the newly established terminal deoxyribonucleotidyl transferase mediated biotin-dUTP nick end labeling (TUNEL) technique. The specificity of the TUNEL technique was initially called into question when Ansari and coworkers [5] detected DNA fragmentation in epithelial cells in the very same villus compartment using the related in situ nick end labeling technique which lacked morphological features of apoptotic cell death. The number of stained cells and the intensity of nick-end labeling in the villus tips proved to increase with delayed fixation of the tissue [28]. Finally, however, the occurrence of apoptosis in the cell loss compartment was confirmed under more stringent conditions both in the small [28] and large intestine [57]. Quantitative analysis of the frequency of apoptosis in the villus tips of the murine small intestine suggest that programmed cell death is in fact a main regulator of the epithelial cell number in the gut [28]. The molecular mechanisms leading to the induction of apoptosis at the end of an IEC's life, however, remain to be determined.

Apoptosis may not only be important for cell loss in the physiological process of IEC turnover. It also plays a pivotal role in inflammatory conditions in which programmed cell death of immune cells and possibly epithelial cells is an important way to cut down the immune response and avoid autoimmunity but, on the other hand, may also contribute to tissue damage. Finally, although apoptosis had long been neglected in cancer research, it is obvious that tumor formation is not only a problem of dysregulated proliferation but also of prolonged survival of tumor cells, mostly due to (relative) resistance to apoptotic stimuli.

J. Sträter (✉) · P. Möller
Department of Pathology, University of Ulm,
Albert-Einstein-Allee 11, 89081 Ulm, Germany
e-mail: joern.straeter@medizin.uni-ulm.de
Tel.: +49-731-50023320
Fax: +49-731-50023884

A subset of members of the tumor necrosis factor (TNF) receptor superfamily, a group of type I transmembrane proteins containing one to five cystein-rich repeats in their extracellular domain, have become central points of interest in apoptosis research, as they are able directly to induce programmed cell death and are therefore referred to as the "death receptors." CD95 (APO-1/Fas) is probably the best studied of these death receptors [32, 49]. CD95-mediated apoptosis is triggered by its natural ligand, CD95L, which is a member of the TNF superfamily of cytokines [62, 64]. Engagement of CD95 by CD95L or cross-linking CD95 antibodies leads to recruitment of intracellular proteins that form a complex known as the death-inducing signaling complex (DISC) [36]. DISC formation finally results in activation of the effector caspase-3, either by extensive direct activation of the initiator caspase-8 (type I signaling pathway) or via an enhancing mitochondrial loop and formation of the apoptosome containing active caspase-9 (type II signaling pathway). The intracellular mechanisms leading to death receptor mediated apoptosis have been described in detail in several comprehensive reviews [38, 67] and are not further considered here.

CD95 is found in a variety of normal organs and tissues and is also constitutively expressed on the basolateral surface of IEC all along the crypt(villus) axis [40, 44]. In recent years a plethora of articles have been published dealing with the possible role of the CD95/CD95L apoptosis-inducing system in the gut under normal, inflammatory, and neoplastic conditions. The present review tries to shed some light on the maze of pertinent literature and critically discuss what seems to be fact and what may rather be fiction.

## CD95L immunohistochemistry: much darkness and little light

Given the broad tissue distribution of CD95 [40], expression of CD95L must be much more restricted and tightly regulated to prevent inadequate tissue damage. In addition to experimental in vitro studies, one of the central points in our understanding of the role the CD95/CD95L system may play is the question of where and under which circumstances CD95L is expressed. Some papers which have addressed this question have considerably influenced our view on this apoptosis-inducing system. Given the abundance of publications, in part contradictory, in this highly competitive field of research, it may help towards a correct interpretation of published data if we consider some methodological aspects.

Molecular techniques using tissue homogenates such as reverse transcriptase polymerase chain reaction (RT-PCR) and Western blotting are sensitive tools for the detection of CD95L but are not able to give any hint as to its cellular producers. Most studies therefore rely on immunohistochemistry to locate CD95L in tissue sections in situ. A report in *Science* by Giordano et al. [23], however, provoked the first doubts about the specificity of two different CD95L antibodies used in this study [20, 56]. Although the debate on poor reagent specificity was taken up later in *Cell Death and Differentiation* [7, 19, 29] and is still continuing, some of the CD95L antibodies with questionable sensitivity and/or specificity are still widely used for the detection of CD95L and may contribute to some of the confusion in this field.

Giordano et al. [23] reported constitutive CD95L expression in thyrocytes, which was detected by immunohistochemistry and flow cytometric analysis using two commercially available antibodies: the rabbit polyclonal IgG antibody C-20 (Santa Cruz Biotechnology, Santa Cruz, Calif., USA) and the monoclonal mouse IgG1 antibody 33 (Transductions Laboratories, Lexington, Ky., USA). In a reply to this paper Fiedler et al. [20] confirmed that antibody C-20 recognized CD95L in CD95L-transfected 293T cells in immunoblots and stained these cells in immunofluorescence. However, they complained about a background staining in untransfected control cells which was especially high in immunofluorescence studies. Moreover, antibody C-20 failed to label CD95L-transfected cells in fluorescent-activated cell scan (FACS) analyses. Smith et al. [55] in a similar FACS experiment found C-20 not to bind to CD95L-transfected KFL cells in which surface CD95L expression was verified using the monoclonal antibodies NOK-1 (Pharmingen) and Alf-1.2, while, conversely, C-20 gave (falsely) positive results when unstimulated ($CD95L^-$) Jurkat cells were analyzed. By immunocytochemistry we observed staining of CD95L-transfected CV1/EBNA cells and untransfected control cells to comparable extents with this antibody. Moreover, when results from immunohistochemistry on tissue sections were compared to those from in situ-hybridization C-20 proved to yield an unacceptably high background or unspecific staining [60]. Very similar results were obtained with the polyclonal anti-CD95L antibody N-20 (Santa Cruz Biotechnology) [60]. Thus, although these antibodies may be suitable for the analysis of CD95L by protein immunoblotting, they lack sufficient specificity when used in immunohistochemistry and, in the case of C-20, FACS analysis.

The specificity of the second CD95L reagent used by Giordano et al. [23], the monoclonal antibody (mAb) 33, was first called into question when Stokes et al. [56] found CD95L in normal thyrocytes by Western blot analysis with this antibody (thus so far confirming the Giordano et al. data) but failed to detect CD95L mRNA by either RT-PCR or ribonuclease protection assay. This antibody was further reported not to bind to CD95L immunoprecipitated from CD95L-transfected 293T cells but to a (different) 37-kDa protein in the supernatant which was also detected in untransfected cells [20]. Later it was shown that mAb 33 detects a protein with different mobility in two-dimensional electrophoresis than CD95L detected by other CD95L-specific antibodies such as G247-4 (Pharmingen, San Diego, Calif., USA) [19]. In line with these data, mAb 33 not only stained CD95L-transfected CV1/EBNA cells and untransfected controls to a comparable extent in immunocytochemistry but also

immunohistochemically labeled tonsillar squamous epithelium, which was negative for CD95L with the mAb G247-4 and in in situ-hybridization [60]. Taken together, available data strongly suggest that mAb 33 (additionally to CD95L?) binds to a cross-reactive protein and cannot be recommended for the detection of CD95L. Although it was suggested in a recent editorial that mAb 33 should be removed from the market [7], mAb 33 has been one of the most widely used antibodies for the immunohistochemical detection of CD95L.

## CD95/CD95L in the normal intestinal epithelium

Soon after the description of CD95 we demonstrated that the normal epithelium of the small and large intestines constitutively express CD95 at the basolateral cell surface, and that this expression is uniform all along the crypt(villus) axis [40, 44]. Moreover, normal, freshly isolated colonic crypt cells rapidly entered apoptosis when incubated in vitro with an agonistic CD95 antibody [58], although relatively high antibody concentrations were needed. The significance of this functional expression of CD95 on intestinal epithelial cells remained unclear, although the observation that epithelial cells in vitro were equally sensitive to CD95 ligation, regardless of their position along the crypt axis, seemed to argue against an involvement of this apoptosis-inducing system in the physiological regeneration of the gut epithelium.

A first hint of the possible function of CD95 in the gut was expected from addressing the question of which cells in the gut mucosa expressed CD95L. A recently published study proposed that intestinal epithelial cells themselves express CD95L at the luminal surface where CD95/CD95L coexpression coincides with a high frequency of TUNEL-positive (apoptotic) epithelial cells. The authors suggested that physiological (homeostatic) cell loss in the colon is due to CD95L-induced autocrine epithelial cell apoptosis [11]. CD95L expression in this study was examined by immunohistochemistry using two different antibodies: the polyclonal antibody C-20 (Santa Cruz Biotechnology), which is of doubtful specificity in immunohistochemistry (see above), and the monoclonal antibody G247-4 (Pharmingen). Unfortunately, the stainings obtained with the latter antibody were not shown in the paper, but results were reported to be "similar to those obtained with the polyclonal antibody." A study of our own with the same monoclonal antibody detected no CD95L in the normal epithelium of the colon (manuscript in preparation) or appendix [59]. By in situ-hybridization we found CD95L mRNA expression in a few scattered lamina propria cells but not in the normal epithelium of the stomach or small and large intestines. The only exception to this rule were Paneth cells which strongly expressed CD95L [45], although the significance of this observation is not yet clear. Absence of CD95L mRNA in colonocytes was later confirmed with this technique by Ueyama et al. [66] while another group [42] reported CD95L mRNA expression in 1 of 12 cases at the tip of the crypt in radioactive in situ-hybridization after 100 days of exposure. Unfortunately, this finding was not very well documented in their publication. Finally, we did not detect CD95L in normal colon epithelial cells on the transcriptional level when its expression in a pure fraction of isolated colonic crypt cells was examined by RT-PCR [61]. Taken together, published data are contradictory, but evidence of a lack of CD95L expression in normal IEC is accumulating.

Independently of the question of whether normal gut epithelium expresses CD95L the development of hyperplastic or neoplastic lesions in the gut mucosa has not been reported in CD95 knock-out mice [2]. An unpublished study of our own detected no differences in morphology or apoptotic cell counts in the gut mucosa of *lpr* and *gld* mice bearing defects in (functional) expression of CD95 and CD95L, respectively, and wild-type animals. Thus an involvement of the CD95/CD95L system in the physiological turnover of the gut epithelium appears unlikely.

## Activation-induced cell death

Probably the best studied function of the CD95/CD95L system is its central role in the regulation of immune processes and in what has been called activation-induced cell death. In vitro, prolonged activation of T-lymphocytes by ligation of the T-cell receptor/CD3-complex results in an induction of CD95L expression, enabling them to kill neighboring $CD95^+$ cells in a juxtacrine or paracrine way or, in the case of CD95L secretion, even to commit autocrine suicide [3, 14, 37]. Although all cytotoxic T-cells can use the CD95/CD95L pathway to induce death, it is most important for $CD4^+$ cells, especially those of the Th1 phenotype [34] and probably essential for the down-modulation of immune processes and the prevention of autoimmunity [38]. Mutations leading to a loss of functional CD95 (*lpr*) and CD95L expression (*gld*) in mice result in a phenotype which is characterized by lymphadenopathia and splenomegalia due to an abnormal accumulation of T-lymphocytes and development of an autoimmune disorder resembling systemic lupus erythematosus [46].

Circumstantial evidence strongly suggests an involvement of the CD95/CD95L system in inflammatory conditions including in the gut: the CD95 receptor is up-regulated together with HLA-DR antigens on the surface of colon epithelial cells by interferon-$\gamma$ [44]. This increase in CD95 expression is accompanied by but is not a prerequisite for interferon-$\gamma$ induced further sensitization of cells towards CD95-mediated cell death [51] which may at least in part be caused by up-regulating caspase-8 expression via the Stat1 pathway [21]. HLA-DR-expressing IEC are able to process and present antigen to and activate $CD4^+$ T-lymphocytes, especially under the influence of interferon-$\gamma$ [30]. Activated T-lymphocytes may then in turn produce CD95L and induce activation-induced cell death. Although experimental data

are still lacking, it is tempting to speculate that $CD95^+$ IEC acting as nonprofessional antigen-presenting cells under the influence of interferon-$\gamma$ are victims of activation-induced CD95L expression in T-cells and are driven into apoptosis possibly to down-modulate antigenic stimulation.

## CD95/CD95L in ulcerative colitis

Although death of immune and epithelial cells may be important in the regulation of immune responses, it becomes deleterious when apoptosis runs out of control. Reports on CD95 expression in IEC opened the possibility that mucosal damage in certain inflammatory bowel diseases is due to inappropriate CD95-mediated IEC death. Ulcerative colitis (UC) was one of the first diseases of the gut in which the CD95/CD95L system was reported to be involved. In contrast to Crohn's disease, which seems to be characterized by resistance of T-cells to multiple apoptotic signals [31], CD95L expression is significantly increased in lamina propria T-cells of UC lesions, and this is accompanied by higher numbers of apoptotic cell counts [33, 58, 63, 66]. Both lamina propria inflammatory cells and IEC apparently undergo apoptosis and death of the latter gives rise to small defects of the epithelial layer [58]. Thus CD95-induced mucosal defects may contribute to a decrease in the epithelial barrier function, a well-known phenomenon in UC [1, 24].

In addition to in situ observations in humans, some mouse models also suggest a role of the CD95 system in UC. For example, lamina propria $CD4^+$ T-cells from mice, in which a colitis resembling UC was induced by transfer of $CD4^+$ T-cell receptor (TCR) $\alpha\beta$ T-cells from athymic mice into histocompatible severe combined immunodeficiency mice, exhibited CD95-dependent cytotoxic activity in vitro [12]. Treatment of diseased severe combined immunodeficiency mice with antagonistic CD95 antibodies significantly blocked apoptosis of lamina propria T-cells [13]. A similar CD95-dependent cytotoxic activity in vitro was shown using lamina propria cells from mice in which colitis was induced by transfer of wild-type bone marrow cells into animals deficient in both T-cells and natural killer cells [54]. In this model, however, colitis also developed when bone marrow cells from *gld* (i.e., CD95L-deficient) instead of wild-type mice were transferred, whereas colitis was less severe after transferring cells with defects in another cytotoxic molecule, perforin.

These results point to the fact that expression of CD95L is not the only way by which cytotoxic T-lymphocytes kill target cells, a problem which is further highlighted by recent studies by Merger et al. [43]. When these authors induced enteritis in mice by injecting T-cell-activating anti-CD3 antibodies and compared tissue damage in wild-type mice to animals with defects in TNF-$\alpha$ receptors, CD95, and perforin expression, they observed significantly diminished mucosal injury only in perforin knockout mice. Nevertheless, damage was further reduced in mice bearing combined defects of perforin and CD95L, suggesting that several cytotoxic molecules synergistically contributed to mucosal injury in this model.

Although there is good evidence that CD95L is significantly overexpressed by lamina propria cells in UC, it is probably not the only death inducer. Future studies must address further the possible redundancies in cell death mechanisms leading to tissue damage in inflammatory bowel disease.

## Cell death in viral infections

The same redundancies exist in the repertoire possessed by cytotoxic T-cells and natural killer (NK) cells to kill viral-infected cells. Although early studies suggested that apoptosis-induction in virus infections is confined to two pathways, the perforin/granzyme and the CD95 pathways [41], it has become clear that death receptors other than CD95 are also involved, namely TNFR-1 [17] and two receptors of the TNF-related apoptosis-inducing ligand (TRAIL), TRAIL-R1 and TRAIL-R2 [52]. We recently observed that TRAIL-R1 and TRAIL-R2 which, as with CD95, are members of the TNFR family containing a death domain, are constitutively expressed on colonic epithelial cells. Interestingly, the homogeneous distribution of TRAIL-R1 along the crypt axis was strikingly similar to that of CD95. Moreover, in the colon carcinoma cell line, CaCo2, surface expression of TRAIL-R1 and TRAIL-R2 was increased upon infection with cytomegalovirus, and this up-regulation was accompanied by a sensitization of cells towards TRAIL-induced apoptosis [61]. Comparable data on the role of CD95 in viral infection of colonic epithelial cells are lacking, but constitutive coexpression of CD95 and apoptosis-mediating TRAIL-receptors may provide a mechanism to allow rapid elimination of virally infected intestinal epithelial cells and thus local containment of the infection. The importance of death receptors for the elimination of virus-bearing cells is highlighted by the fact that some viruses produce factors, such as the viral FLICE-inhibitory protein (vFlip), which specifically inhibit death receptor-mediated apoptosis of host cells [65].

## CD95/CD95L in neoplastic lesions: immunoprivilege and the counterattack hypothesis

The observation that some extralymphatic tissues with limited potential to regenerate, for example, the testis [8] or eye [26], constitutionally expressed CD95L led to an intriguing concept that placed the CD95/CD95L system in the center of the molecular mechanisms maintaining immune privilege [25]. According to this hypothesis, an inflammation which would cause fatal damage in these tissues is prevented by presentation of CD95L to infiltrating immune cells which in turn express and are sensitive to CD95. It rapidly became clear that this

concept had considerable impact on transplantation immunology since it presented a promising chance to circumvent graft rejection. Initial findings in transplantation experiments using $CD95L^+$ grafts were most encouraging. When tissue from murine testis was grafted under the kidney capsule of allogeneic animals, (constitutionally $CD95L^+$) testis grafts from wild-type mice survived while grafts from (functionally $CD95L^-$) *gld* mice were rejected [8]. Similarly, graft rejection of murine allogeneic pancreatic islet cells was prevented when cotransplanted with syngeneic myoblasts genetically engineered to express CD95L, whereas graft survival was not enhanced with cotransplantation of unmodified myoblasts [39].

The concept of immune privilege also opened discussion of a new immune escape mechanism by tumor cells when CD95L was found to be expressed in some melanoma or colon carcinoma cell lines [27, 47]. While these tumor cells were themselves resistant to CD95 ligation, they were able to drive cocultured (CD95-expressing and CD95-sensitive) Jurkat cells, a T-cell leukemia line, into CD95-dependent apoptosis in vitro. These observations precipitated into the so-called tumor counterattack hypothesis [47], proposing that tumors also represented immunoprivileged tissues, in that they escape the immune system by actively killing tumor-infiltrating lymphocytes via CD95/CD95L interactions.

## In vivo expression of CD95L in carcinomas of the gastrointestinal tract

As this hypothesis is based upon in vitro studies of tumor cell lines, it was important to demonstrate that the CD95L counterattack also takes place in tumors in vivo. Shortly after the publication of the concept in 1996, a series of papers was released reporting on CD95L expression in carcinomas of the gastrointestinal tract and their metastases. Bennett et al. [9] reported CD95L expression in all esophageal carcinomas studied (two adenocarcinomas and four squamous carcinomas). This finding was later confirmed by Younes et al. [70] who detected CD95L in at least a few tumor cells in all of 15 squamous carcinomas and 13 adenocarcinomas. Moreover, expression of CD95L in more than 25% of tumor cells was correlated with a higher incidence of lymph node metastasis in this study. The same group also studied CD95L expression in Barrett's metaplasia and found 11 of 20 samples of Barrett's mucosa without dysplasia and all cases with (low- or high-grade) dysplasia to be $CD95L^+$ in immunohistochemistry [69]. Bennett et al. [10] reported CD95L expression in 100% of gastric adenocarcinomas studied and recognized an increase in lymphocyte apoptosis in tumor areas with high CD95L expression. Similarly, O'Connell et al. [48] found CD95L expression in all of 31 colonic adenocarcinomas studied. Younes et al. [69] confirmed CD95L expression in adenocarcinomas of the colon and, additionally, reported (mostly focal) positivity for CD95L in the majority of colorectal adenomas.

CD95L expression in liver metastases of colorectal adenocarcinomas, which was first reported by Shiraki et al. [53] and later confirmed by Mann et al. [42] and by Yoong et al. [68], is of particular interest because hepatocytes express and are highly sensitive to CD95 [40, 50]. CD95 sensitivity of hepatocytes was impressively demonstrated by intraperitoneal injection of agonistic CD95 antibodies into mice, which rapidly died due to acute liver failure [50]. In vitro, CD95L-expressing colon cancer cells kill hepatocytes in coculture cytotoxic assays [68]. Taken together, these findings suggest that hepatocytes at the margin of colorectal liver metastases are driven into apoptosis by CD95L expression in tumor cells, thus facilitating the invasion of the tumor into surrounding liver tissue.

Despite this overwhelming body of data the CD95L counterattack is still far from being established as a relevant feature in carcinomas of the gastrointestinal tract. All the studies mentioned above rely on immunohistochemistry with CD95L antibodies of questionable specificity (see above). In an immunohistochemical study of our own using the monoclonal anti-CD95L antibody G247-4 we detected focal weak or moderate CD95L expression in tumor cells in a mere 11% of 129 colonic adenocarcinomas, while it was found in a significant proportion of tumor-infiltrating immune cells in the majority of cases (manuscript in preparation). These data are at variance with the much higher rate of CD95L expression in colonic carcinoma cells reported by others [48].

In addition to immunohistochemistry, some groups [42, 53] have used RT-PCR to detect CD95L in primary colonic carcinomas and liver metastases. Although convincing CD95L mRNA expression is shown in these studies in liver metastases and at least some of the primaries, RT-PCR on tissue homogenates is not a suitable means of clarifying whether detected transcripts derived from tumor-infiltrating immune or tumor cells.

Two studies [10, 48] confirmed CD95L expression in tumors by nonradioactive in situ-hybridization. Controls in these experiments were carried out by adding an excess of unlabeled to the labeled CD95L-specific probe. These controls, however, only confirm specificity of the detection system, they do not exclude unspecific binding of the probe. Moreover, given the relatively low sensitivity of nonradioactive in situ-hybridization, the high percentage of positive tumors in these studies is somewhat surprising in the light of data presented by Mann et al. [42]. This group performed radioactive in situ-hybridization and detected CD95L mRNA in 30% of primary colorectal to carcinomas and in 50% of liver metastases, but only after 100 or more days of exposure, indicating very weak expression. Thus the expression of CD95L in cancer cells of the gastrointestinal tract may occur but definitely at a much lower incidence than some early studies suggested.

## The counterattack hypothesis on retreat

Furthermore, there are also some recent experimental data, some of which again originate from transplantation immunologists, which call into question the concept of immune privilege and counterattack. For instance, when pancreatic islets or islet cells engineered to express CD95L on their surface were transplanted into allogeneic mice, islet cells were rejected even more rapidly than untransfected controls due to an unexpected invasion of granulocytes [4, 35]. Similarly, CD95-resistant CT26 colon carcinoma cells, which were subcutaneously injected into mice, rapidly regressed when infected with an adenoviral vector encoding CD95L. This regression was also accompanied by a dense infiltrate of the tumor by neutrophil granulocytes [6]. Thus the in vivo consequences of CD95L expression in tumor cells are far from clear. Moreover, a recent study even denies the ability of CD95L-expressing colon cancer cell lines to induce apoptosis in CD95-sensitive target cells in vitro [18].

On the other hand, there is now growing evidence that instead of being killed by tumor cells tumor-infiltrating cytotoxic cells express CD95L themselves and undergo CD95-dependent death in an auto- or paracrine way following MHC-restricted recognition of tumor antigens [71]. B7-H1, a new member of the B7 family of costimulatory molecules, was recently shown to be abnormally expressed on tumor cells and to drive activated tumor-reactive T-cells into apoptosis [15]. Activation of T-cells by CD3/TCR ligation in the presence of a B7-H1/immunoglobulin fusion product was accompanied by an up-regulation of CD95L, and T-cell apoptosis could be significantly inhibited by neutralizing antibodies to CD95L [15].

Even though the counterattack hypothesis has considerably stimulated research in tumor (and transplantation) immunology, in the light of the current literature it is evident that its role in the immune escape of tumor cells has been overestimated. Instead of killing directly, tumor cells may have evolved more subtle ways to force immune cells into death, i.e., via CD95-dependent suicide or fratricide.

## Summary and conclusions

Although constitutive expression of CD95 in the normal intestinal epithelium was recognized soon after its description in 1989, its functional role in the gastrointestinal tract remains unresolved. Research on CD95/CD95L has been severely compromised, particularly by uncritical use of reagents with questionable specificity. To date, compelling evidence of CD95L-expression in the normal intestinal epithelium is lacking, and an involvement of the CD95/CD95L system in the physiological turnover of epithelial cells in the gut is unlikely. The fact that many cells, IEC included, show increased CD95 expression and become sensitized towards CD95-mediated apoptosis upon treatment with interferon-$\gamma$ while activated ($CD4^+$ Th1-cells and $CD8^+$) T-cells express CD95L, is consistent with the idea that it is involved in inflammatory processes. Although CD95L expression in lamina propria cells has repeatedly been shown in ulcerative colitis, experimental data in animal models do not unequivocally support a dominant role of CD95L as a mediator of mucosal damage in this inflammatory bowel disease. Difficulty in determining the significance of a certain death-inducing molecule may be explained by possible redundancy in the capacity of immune cells to confer cytotoxicity. Finally, while the fascinating tumor counterattack concept suggested that CD95L expression by tumor cells may be the main mechanism of immune evasion of malignant tumors, there is now growing evidence that instead of being killed directly, tumor-infiltrating immune cells are eventually forced to commit CD95L-mediated suicide or induce fratricide upon activation by tumor antigens.

**Acknowledgements** This work was supported by grants from the Deutsche Krebshilfe to J.S. (10-1644-Str 1) and from the Deutsche Forschungsgemeinschaft (SFB518 TPA13) and the IZKF Ulm to P.M.

## References

1. Abreu MT, Palladino AA, Arnold ET, Kwon RS, McRoberts JA (2000) Modulation of barrier function during Fas-mediated apoptosis in human intestinal epithelial cells. Gastroenterology 119:1524–1536
2. Adachi M, Suematsu S, Kondo T, Ogasawara J, Tanaka T, Yoshida N, Nagata S (1995) Targeted mutation in the Fas gene causes hyperplasia in peripheral lymphoid organs and liver. Nat Genet 11:294–300
3. Alderson MR, Tough TW, Davis-Smith T, Braddy S, Falk B, Schooley KA, Goodwin RG, Smith CA, Ramsdell F, Lynch DH (1995) Fas ligand mediates activation-induced cell death in human T lymphocytes. J Exp Med 181:71–77
4. Allison J, Georgiou HM, Strasser A, Vaux DL (1997) Transgenic expression of CD95 ligand on islet beta cells induces a granulocytic infiltration but does not confer immune privilege upon islet allografts. Proc Natl Acad Sci USA 94:3943–3947
5. Ansari B, Coates PJ, Greenstein B, Hall PA (1993) In situ end labelling (ISEL) detects DNA strand breaks in apoptosis and in other physiological and pathological states. J Pathol 170:1–8
6. Arai H, Gordon D, Nabel EG, Nabel GJ (1997) Gene transfer of Fas ligand induces tumor regression in vivo. Proc Natl Acad Sci USA 94:13862–13867
7. Baker JR Jr, Bretz JD (2000) Specificity questions concerning the clone 33 anti-fas ligand antibody. Cell Death Differ 7:8–9
8. Bellgrau D, Gold D, Selawry H, Moore H, Franzusoff A, Duke RC (1995) A role for CD95 ligand in preventing graft rejection. Nature 377:630–632
9. Bennett MW, O'Connell J, O'Sullivan GC, Brady C, Roche D, Collins JK, Shanahan F (1998) The Fas counterattack in vivo: apoptotic depletion of tumor-infiltrating lymphocytes associated with Fas ligand expression by human esophageal carcinoma. J Immunol 160:5669–5675
10. Bennett MW, O'Connell J, O'Sullivan GC, Roche D, Brady C, Kelly J, Collins JK, Shanahan F (1999) Expression of Fas ligand by human gastric adenocarcinomas: a potential mechanism of immune escape in stomach cancer. Gut 44:156–162

11. Bennett MW, O'Connell J, Houston A, Kelly J, O'Sullivan GC, Collins JK, Shanahan F (2001) Fas ligand upregulation is an early event in colonic carcinogenesis. J Clin Pathol 54:598–604
12. Bonhagen K, Thoma S, Bland P, Bregenholt S, Rudolphi A, Claesson MH, Reimann J (1996) Cytotoxic reactivity of gut lamina propria CD4+ alpha beta T cells in SCID mice with colitis. Eur J Immunol 26:3074–3083
13. Bregenholt S, Petersen TR, Claesson MH (2001) The majority of lamina propria CD4 (+) T-cells from scid mice with colitis undergo Fas-mediated apoptosis in vivo. Immunol Lett 78:7–12
14. Dhein J, Walczak H, Bäumler C, Debatin K-M, Krammer PH (1995) Autocrine T-cell suicide mediated by APO-1/(Fas/CD95). Nature 373:438–441
15. Dong H, Strome SE, Salomao DR, Tamura H, Hirano F, Flies DB, Roche PC, Lu J, Zhu G, Tamada K, Lennon VA, Celis E, Chen L (2002) Tumor-associated B7-H1 promotes T-cell apoptosis: a potential mechanism of immune evasion. Nat Med 8:793–800
16. Eastwood GL (1977) Progress in gastroenterology: gastrointestinal epithelial renewal. Gastroenterology 72:962–975
17. Elkon KB, Liu CC, Gall JG, Trevejo J, Marino MW, Abrahamsen KA, Song X, Zhou JL, Old LJ, Crystal RG, Falck-Pedersen E (1997) Tumor necrosis factor alpha plays a central role in immune-mediated clearance of adenoviral vectors. Proc Natl Acad Sci USA 94:9814–9819
18. Favre-Felix N, Fromentin A, Hammann A, Solary E, Martin F, Bonnotte B (2000) The tumor counterattack hypothesis revisited: colon cancer cells do not induce T cell apoptosis via the Fas (CD95, APO-1) pathway. J Immunol 164:5023–5027
19. Fiedler P, Eibel H (2000) Antibody mAb33 from Transduction Laboratories detects human CD95L in ELISA but not in immunoblots. Cell Death Differ 7:126–128
20. Fiedler P, Schaetzlien CE, Eibel H (1998) Constitutive expression of FasL in thyrocytes. Science 279:2015
21. Fulda S, Debatin KM (2002) IFNgamma sensitizes for apoptosis by upregulating caspase-8 expression through the Stat1 pathway. Oncogene 21:2295–2308
22. Gavrieli Y, Sherman Y, Ben-Sasson SA (1992) Identification of programmed cell death in situ via specific labeling of nuclear DNA fragmentation. J Cell Biol 119:493–501
23. Giordano C, Stassi G, DeMaria R, Toldaro M, Richiusa P, Papoff G, Ruberti G, Bagnasco M, Testi R, Galluzo A (1997) Potential involvement of Fas and its ligand in the pathogenesis of Hashimoto's thyroiditis. Science 275:960–963
24. Gitter AH, Wullstein F, Fromm M, Schulzke JD (2001) Epithelial barrier defects in ulcerative colitis: characterization and quantification by electrophysiological imaging. Gastroenterology 121:1320–1328
25. Griffith TS, Ferguson TA (1997) The role of FasL-induced apoptosis in immune privilege. Immunol Today 18:240–244
26. Griffith TS, Brunner T, Fletcher SM, Green DR, Ferguson TA (1995) Fas ligand induced apoptosis as a mechanism of immune privilege. Science 270:1189–1192
27. Hahne M, Rimoldi D, Schröter M, Romero P, Schreier M, French LE, Schreier P, Bornand T, Fontana A, Lienard D, Cerottini J, Tschopp J (1996) Melanoma cell expression of Fas (APO-1/CD95) ligand: implications for tumor immune escape. Science 274:1363–1366
28. Hall PA, Coates PJ, Ansari B, Hopwood D (1994) Regulation of cell number in the mammalian gastrointestinal tract: the importance of apoptosis. J Cell Sci 107:3569–3577
29. Herr I, Posovsky C, Bohler T, Debatin K-M (2000) mAb 33 from Transduction Laboratories specifically binds to human CD95-L. Cell Death Differ 7:129–130
30. Hershberg RM, Framson PE, Cho DH, Lee LY, Kovats S, Beitz J, Blum JS, Nepom GT (1997) Intestinal epithelial cells use two distinct pathways for HLA class II antigen processing. J Clin Invest 100:204–215
31. Ina K, Itoh J, Fukushima K, Kusugami K, Yamaguchi T, Kyokane K, Imada A, Binion DG, Musso A, West GA, Dobrea GM, McCormick TS, Lapetina EG, Levine AD, Ottaway CA, Fiocchi C (1999) Resistance of Crohn's disease T cells to multiple apoptotic signals is associated with a Bcl-2/Bax mucosal imbalance. J Immunol 163:1081–1090
32. Itoh N, Yonehara S, Ishii A, Yonehara M, Mizushima S-I, Sameshima M, Hase A, Seto Y, Nagata S (1991) The polypeptide encoded by the cDNA for human cell surface Fas can mediate apoptosis. Cell 66:233–243
33. Iwamoto M, Koji T, Makiyama K, Kobayashi N, Nakane PK (1996) Apoptosis of crypt epithelial cells in ulcerative colitis. J Pathol 180:152–159
34. Ju ST, Cui H, Panka DJ, Ettinger R, Marshak-Rothstein A (1994) Participation of target Fas protein in apoptosis pathway induced by CD4+ Th1 and CD8+ cytotoxic T cells. Proc Natl Acad Sci USA 91:4185–4189
35. Kang SM, Schneider DB, Lin Z, Hanahan D, Dichek D, Stock PG, Baekkeshov S (1997) Fas ligand expression in islets of Langerhans does not confer immune privilege and instead targets them for rapid destruction. Nat Med 3:738–743
36. Kischkel FC, Hellbardt S, Behrmann I, Germer M, Pawlita M, Krammer PH, Peter ME (1995) Cytotoxicity-dependent APO-1 (Fas/CD95)-associated proteins form a death-inducing signaling complex (DISC) with the receptor. EMBO J 14:5579–5588
37. Klas C, Debatin K-M, Jonker RR, Krammer PH (1993) Activation interferes with the APO-1 pathway in mature human T cells. Int Immunol 5:625–630
38. Krammer PH (2000) CD95's deadly mission in the immune system. Nature 407:789–795
39. Lau HT, Yu M, Fontana A, Stoeckert CJJ (1996) Prevention of islet allograft rejection with engineered myoblasts expressing FasL in mice. Science 273:109–112
40. Leithäuser F, Dhein J, Mechtersheimer G, Koretz K, Brüderlein S, Henne C, Schmidt A, Debatin K-M, Krammer PH, Möller P (1993) Constitutive and induced expression of APO-1, a new member of the nerve growth factor/tumor necrosis factor receptor superfamily. Lab Invest 69:415–429
41. Lowin B, Hahne M, Mattmann C, Tschopp J (1994) Cytolytic T-cell cytotoxicity is mediated through perforin and Fas lytic pathways. Nature 370:650–652
42. Mann B, Gratchev A, Böhm C, Hanski ML, Foss HD, Demel G, Trojanek B, Schmidt-Wolf I, Stein H, Riecken EO, Buhr HJ, Hanski C (1999) FasL is more frequently expressed in liver metastases of colorectal cancer than in matched primary carcinomas. Br J Cancer 79:1262–1269
43. Merger M, Viney JL, Borojevic R, Steele-Norwood D, Zhou P, Clark DA, Riddell R, Maric D, Podack ER, Croitoru K (2002) Defining the roles of perforin, Fas/FasL, and tumor necrosis factor $\alpha$ in T cell induced mucosal damage in the mouse intestine. Gut 51:155–163
44. Möller P, Koretz K, Leithäuser F, Brüderlein S, Henne C, Quentmeier A, Krammer PH (1994) Expression of APO-1 (CD95), a member of the NGF/TNF receptor superfamily, in normal and neoplastic colon epithelium. Int J Cancer 57:371–377
45. Möller P, Walczak H, Riedl S, Sträter J, Krammer PH (1996) Paneth cells express high levels of CD95 ligand transcripts. A unique property among gastrointestinal epithelia. Am J Pathol 149:9–13
46. Nagata S, Suda T (1995) Fas and Fas ligand: lpr and gld mutations. Immunol Today 16:39–43
47. O'Connell J, O'Sullivan GC, Collins JK, Shanahan F (1996) The Fas counterattack: Fas-mediated T cell killing by colon cancer cells expressing Fas ligand. J Exp Med 184:1075–1082
48. O'Connell, Bennett MW, O'Sullivan GC, Roche D, Kelly J, Collins JK, Shanahan F (1998) Fas ligand expression in primary colon adenocarcinomas: evidence that the Fas counterattack is a prevalent mechanism of immune evasion in human colon cancer. J Pathol 186:240–246
49. Oehm A, Behrmann I, Falk W, Pawlita M, Maier G, Klas C, Li-Weber M, Richard S, Dhein J, Trauth BC, Ponsting W, Krammer PH (1992) Purification and molecular cloning of the APO-1 cell surface antigen, a member of the tumor necrosis/nerve growth factor receptor superfamily. J Biol Chem 267:10709–10715

50. Ogasawara J, Watanabe-Fukunaga R, Adachi M, Matsuzawa A, Kasugai T, Kitamura Y, Itoh N, Suda T, Nagata S (1993) Lethal effect of the anti-Fas antibody in mice. Nature 364:806–809
51. Reyher U von, Sträter J, Kittstein W, Gschwendt M, Krammer PH, Möller P (1998) Colon carcinoma cells use different mechanisms to escape CD95-mediated apoptosis. Cancer Res 58:526–534
52. Sedger LM, Shows DM, Blanton RA, Peschon JJ, Goodwin RG, Cosman D, Wiley SR (1999) IFN-gamma mediates a novel antiviral activity through dynamic modulation of TRAIL and TRAIL receptor expression. J Immunol 163:920–926
53. Shiraki K, Tsuji N, Shioda T, Isselbacher KJ, Takahashi H (1997) Expression of Fas ligand in liver metastases of human colonic adenocarcinomas. Proc Natl Acad Sci USA 94:6420–6425
54. Simpson SJ, De Jong YP, Shah SA, Comiskey M, Wang B, Spielman JA, Podack ER, Mizoguchi E, Bhan AK, Terhorst C (1998) Consequences of Fas-ligand and perforin expression by colon T cells in a mouse model of inflammatory bowel disease. Gastroenterology 115:849–855
55. Smith D, Sieg S, Kaplan D (1998) Aberrant detection of cell surface Fas ligand with anti-peptide antibodies. J Immunol 160:4159–4160
56. Stokes TA, Rymaszewski M, Arscott PL, Wang SH, Bretz JD, Bartron J, Baker JrJR (1998) Constitutive expression of FasL in thyrocytes. Science 279:2015
57. Sträter J, Koretz K, Günthert AR, Möller P (1995) In situ detection of enterocytic apoptosis in normal colonic mucosa and in familial adenomatous polyposis. Gut 37:819–825
58. Sträter J, Wellisch I, Riedl S, Walczak H, Koretz K, Tandara A, Krammer PH, Möller P (1997) CD95 (APO-1/Fas)-mediated apoptosis in colon epithelial cells: a possible role in ulcerative colitis. Gastroenterology 113:160–167
59. Sträter J, Mariani SM, Walczak H, Rücker FG, Leithäuser F, Krammer PH, Möller P (1999) CD95 ligand (CD95L) in normal human lymphoid tissues: a subset of plasma cells are prominent producers of CD95L. Am J Pathol 154:193–201
60. Sträter J, Walczak H, Hasel C, Melzner I, Leithäuser F, Möller P (2001) CD95 ligand (CD95L) immunohistochemistry: a critical study on 12 antibodies. Cell Death Differ 8:273–278
61. Sträter J, Walczak H, Pukrop T, von Müller L, Hasel C, Kornmann M, Mertens T, Möller P (2002) TRAIL and its receptors in the colonic epithelium: a putative role in the defence of viral infections. Gastroenterology 122:659–666
62. Suda T, Takahashi T, Golstein P, Nagata S. Molecular cloning and expression of the Fas ligand, a novel member of the Tumor Necrosis Factor family (1993) Cell 75:1169–1178
63. Suzuki A, Sugimura K, Ohtsuka K, Hasegawa K, Suzuki K, Ishizuka K, Mochizuki T, Honma T, Narisawa R, Asakura H (2000) Fas/Fas ligand expression and characteristics of primed CD45RO+ T cells in the inflamed mucosa of ulcerative colitis. Scand J Gastroenterol 35:1278–1283
64. Takahashi T, Tanaka M, Inazawa J, Abe T, Suda T, Nagata S (1994) Human Fas ligand: gene structure, chromosomal location and species specificity. Int Immunol 10:1567–1574
65. Thome M, Schneider P, Hofmann K, Fickenscher H, Meinl E, Neipel F, Mattmann C, Burns K, Bodmer JL, Schroter M, Scaffidi C, Krammer PH, Peter ME, Tschopp J (1997) Viral FLICE-inhibitory proteins (FLIPs) prevent apoptosis induced by death receptors. Nature 386:517–521
66. Ueyama H, Kiyohara T, Sawara N, Isozaki K, Kitamura S, Kondo S, Miyagawa J, Kanayama S, Shinomura Y, Ishikawa H, Ohtani T, Nezu R, Nagata S, Matsuzawa Y (1998) High Fas ligand expression on lymphocytes in lesions of ulcerative colitis. Gut 43:48–55
67. Walczak H, Krammer PH (2000) The CD95 (APO-1/Fas) and the TRAIL (APO-2L) apoptosis systems. Exp Cell Res 256:58–66
68. Yoong KF, Afford SC, Randhawa S, Hubscher SG, Adams DH (1999) Fas/Fas ligand interaction in human colorectal hepatic metastases. Am J Pathol 154:693–703
69. Younes M, Schwartz MR, Finnie D, Younes A (1999) Overexpression of Fas ligand (FasL) during malignant transformation in the large bowel and in Barrett's metaplasia of the esophagus. Hum Pathol 30:1309–1313
70. Younes M, Schwartz MR, Ertan A, Finnie D, Younes A (2000) Fas ligand expression in esophageal carcinomas and their lymph node metastases. Cancer 88:524–528
71. Zaks TZ, Chappell DB, Rosenberg SA, Restifo NP (1999) Fas-mediated suicide of tumor-reactive T cells following activation by specific tumor: selective rescue by caspase inhibition. J Immunol 162:3273–3279

Virchows Arch (2003) 442:226–230
DOI 10.1007/s00428-003-0762-x

ORIGINAL ARTICLE

**Sébastien Lepreux · Christophe Laurent · Brigitte Le Bail · Jean Saric · Charles Balabaud · Paulette Bioulac-Sage**

# Multiple telangiectatic focal nodular hyperplasia: vascular abnormalities

Received: 5 September 2002 / Accepted: 10 December 2002 / Published online: 20 February 2003
© Springer-Verlag 2003

**Abstract** The aim of this study was to look for vascular abnormalities in the liver of patients with multiple telangiectatic focal nodular hyperplasia. Four patients, all women on oral contraceptives, were included in this study. In none of the cases was the diagnosis of multiple telangiectatic focal nodular hyperplasia made preoperatively. In the nodules, the pathological aspect was quite characteristic with dilated sinusoidal areas surrounding compact areas. Compact areas comprised portal tract-like structures with vessels, mainly thickened arteries, usually amidst an inflammatory reaction. A ductular reaction of varied intensity was present in three cases. The non-nodular liver was grossly normal. However, in rare areas, there were obvious or minor vascular abnormalities looking like minimal abnormalities seen inside telangiectatic nodules. These results seem to support the concept that multiple telangiectatic focal nodular hyperplasia is a non-specific reaction to focal ischemia induced by various mechanisms such as hepatic vein thrombosis induced, perhaps, by oral contraceptives.

**Keywords** Focal · Nodular · Hyperplasia

## Introduction

Telangiectatic focal nodular hyperplasia (TFNH) differs strikingly from solid FNH because there is no central scar and few fibrous bands [1, 2, 6]. There is subtle architectural distortion, little or even no reactive ductules and marked sinusoidal dilatation and occasional hemorrhagic and necrotic centers. These telangiectatic nodules are often multiple and described under the term multiple FNH syndrome [6].

We took advantage of the multiplicity of the nodules and their vascular aspect to look more specifically for vascular abnormalities in the liver of patients with multiple TFNH (MTFNH). We wish to report, here, our findings.

## Clinical history

Cases with multiple benign nodules were retrieved from our files. Among the five cases with the diagnosis of multiple telangiectatic FNH, four were included in this study, and one case was rejected because the quality of the sampled material was not guaranteed. The main clinical, radiological and surgical findings are presented in Table 1.

## Materials and methods

All resected specimens had been previously adequately sampled (all abnormal nodules as well as numerous areas of the non-nodular liver at distance from nodules). In addition to the routine stains (H&E, trichrome, Perls, reticulin), additional sections were prepared for immunostaining with antibodies anti-cytokeratin (CK)7, $\alpha$-smooth muscle actin ($\alpha$SMA), and CD34.

## Results

In none of the cases was the diagnosis of MTFNH made preoperatively by imaging techniques or by the surgeon.

S. Lepreux · B. Le Bail · P. Bioulac-Sage
Service d'Anatomie Pathologique,
Hôpital Pellegrin, CHU Bordeaux, France

C. Laurent · J. Saric
Service de chirurgie digestive et de transplantation hépatique,
Hôpital St André, CHU Bordeaux, France

S. Lepreux · B. Le Bail · C. Balabaud · P. Bioulac-Sage (✉)
GREF INSERM EMI 9917,
Université Bordeaux 2 146,
rue léo Saignat, 33076 Bordeaux Cedex, France
e-mail: paulette.bioulac-sage@gref.u-bordeaux2.fr
Tel.: +33-5- 57571771
Fax: +33-5-56514077

**Table 1** Clinical, radiological, surgical and pathological data. *RH* right hepatectomy, *OC* oral contraceptives, *TFNH* telangiectatic focal nodular hyperplasia

| Case | Age (years)/ sex | OC | Main clinical signs/disease | Imaging techniques/number of nodules (size largest one) | Clinical, radiological diagnosis | Surgery (year) | Pathology |
|---|---|---|---|---|---|---|---|
| 1 | 45/female | 20 years | Abdominal bleeding | 1 large subcapsular and central hematoma | Ruptured adenoma | RH (1992) | Hemorrhagic nodule (+ or − necrotic) plus numerous small TFNH (from 1 cm to 1 mm) |
| 2 | 44/female | 22 years | Abdominal pain | 8 (6 cm) | Adenomatosis | Segments VI, VII (1998) | TFNH (1:6 cm, plus several <1 cm) |
| 3 | 36/female | 12 years | Resection of colon cancer | 3* (6 cm) | ? | RH (1998) | TFNH (1:6 cm, and 3:1 cm) |
| 4 | 50/female | 27 years | Abdominal pain | 9 (6 cm) | Adenomatosis | RH (2002) | TFNH (3:8, 5, 4 cm and 2<2 cm) |

* No liver tumor (US) was found prior to resection of the cancer. Prior to chemotherapy, magnetic resonance imaging of the liver was performed which revealed nodules

### Telangiectatic nodules

Their size varied from 6 cm to a few millimeters. Their color was slightly different from the non-nodular tissue (more pink with or without hemorrhagic areas); they were not encapsulated and poorly delineated. Under low-power microscopic examination, the aspect was very characteristic with dilated sinusoidal areas surrounding compact areas. The global liver architecture seemed preserved; however, there was approximation of portal tract-like structures. Compact areas comprised portal tract-like structures with vessels, mainly arteries with many sections, usually amidst an inflammatory reaction (Fig. 1). Arteries had a thickened wall, they were sometimes surrounded by some connective tissue forming short fibrous septa. Bile ducts were rare as well as portal veins (Fig. 1). A ductular reaction of varied intensity was present in three cases (not shown). Few rows of hepatocytes separated this compact zone from the dilated sinusoidal area. Sinusoidal dilatation could be minor, moderate, or major with the complete disappearance of hepatocytic plates, or extensive with necrosis and hemorrhage (not shown). In the more dilated areas, many cells were $\alpha$SMA positive (not shown), and there was no expression of CD34. Conversely, in sinusoids from the compact zone, endothelial cells expressed more or less CD34, but hepatic stellate cells did not express $\alpha$SMA. In addition, many arterioles were clearly seen particularly in the compact hepatocytic zone on $\alpha$SMA immunostaining (not shown). Hepatic veins were rarely observed. Some large veins were abnormal with a thickened wall and thrombosed small branches.

In case 1, the main nodule was hemorrhagic and partly necrotic. The other nodules were typical MTFNH.

### Non-nodular liver

The non-nodular liver was grossly normal. In rare areas, there were obvious or minor vascular abnormalities such as thickened hepatic veins with partially occluded small branches amidst inflammatory cells, sclerosed portal veins, remnants of portal tracts composed mainly of arteries without portal vein and bile ducts amidst an inflammatory reaction, portal tract approximation, and sinusoidal dilatation looking like minimal abnormalities seen inside telangiectatic nodules in three cases (Fig. 2) (Table 1).

## Discussion

Multiple telangiectatic FNH are rare but not exceptional. They occur in women taking oral contraceptives. Their mode of discovery is similar to that observed for adenomas (by chance, with abdominal pain). The nature of the bleeding nodule in case 1 remains unknown because not enough viable tissue remains. The presence of hemorrhagic areas in some TFNH supports, however, the idea that TFNH can bleed.

The diagnosis of MTFNH was missed both by radiologists and surgeons because the nodules did not have the characteristics of FNH (imaging techniques, macroscopy). The pathological diagnosis of MTFNH is easy if ductular proliferation is present [1, 2]. In the absence of ductular reaction, the diagnosis should be evoked once the diagnosis of adenoma has been ruled out when one of the following signs is present: a rim of sinusoidal dilatation, circling a few rows of hepatocytes with, in their middle, abnormal arteries (in size or number) mixed with some inflammatory cells and extracellular matrix components.

It is interesting to note that the same type of vascular lesions were present both in the nodules and in the non-

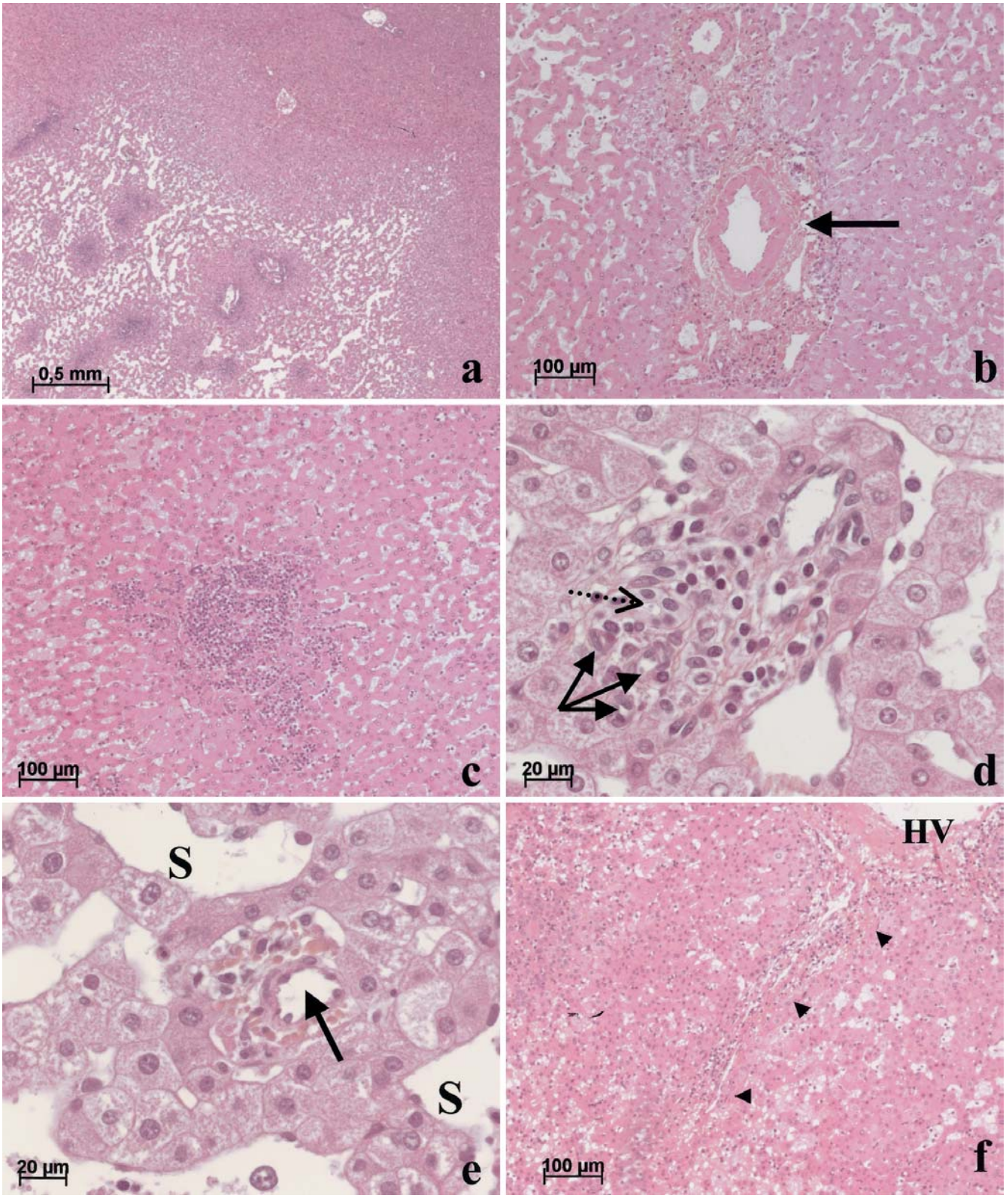



**Fig. 1** Telangiectatic nodule. **a** Typical aspect of a telangiectatic nodule with compact areas surrounded by sinusoidal dilatation. Portal tract-like structures are numerous. *Top* Normal liver. H&E. **b** A portal tract-like structure with many arterial sections, ductular proliferation, mild inflammatory reaction. Sinusoidal dilatation is not observed in the first rows of hepatocytes. **c** A portal tract-like structure with an intense inflammatory reaction. **d** In this portal tract there are several arterial sections (*thick arrows*). The portal vein and the bile duct (*dotted arrow*) are still identifiable. There is a mild inflammatory reaction. **e** In this portal tract-like structure, an isolated artery (*arrow*) surrounded by some connective tissue and inflammatory cells probably corresponds to a remnant of a small portal tract. At a short distance, sinusoids (*S*) are dilated. **f** This large hepatic vein (*HV*) has a thick wall, the abutting branch (*arrowhead*) is partly occluded and amidst inflammatory cells

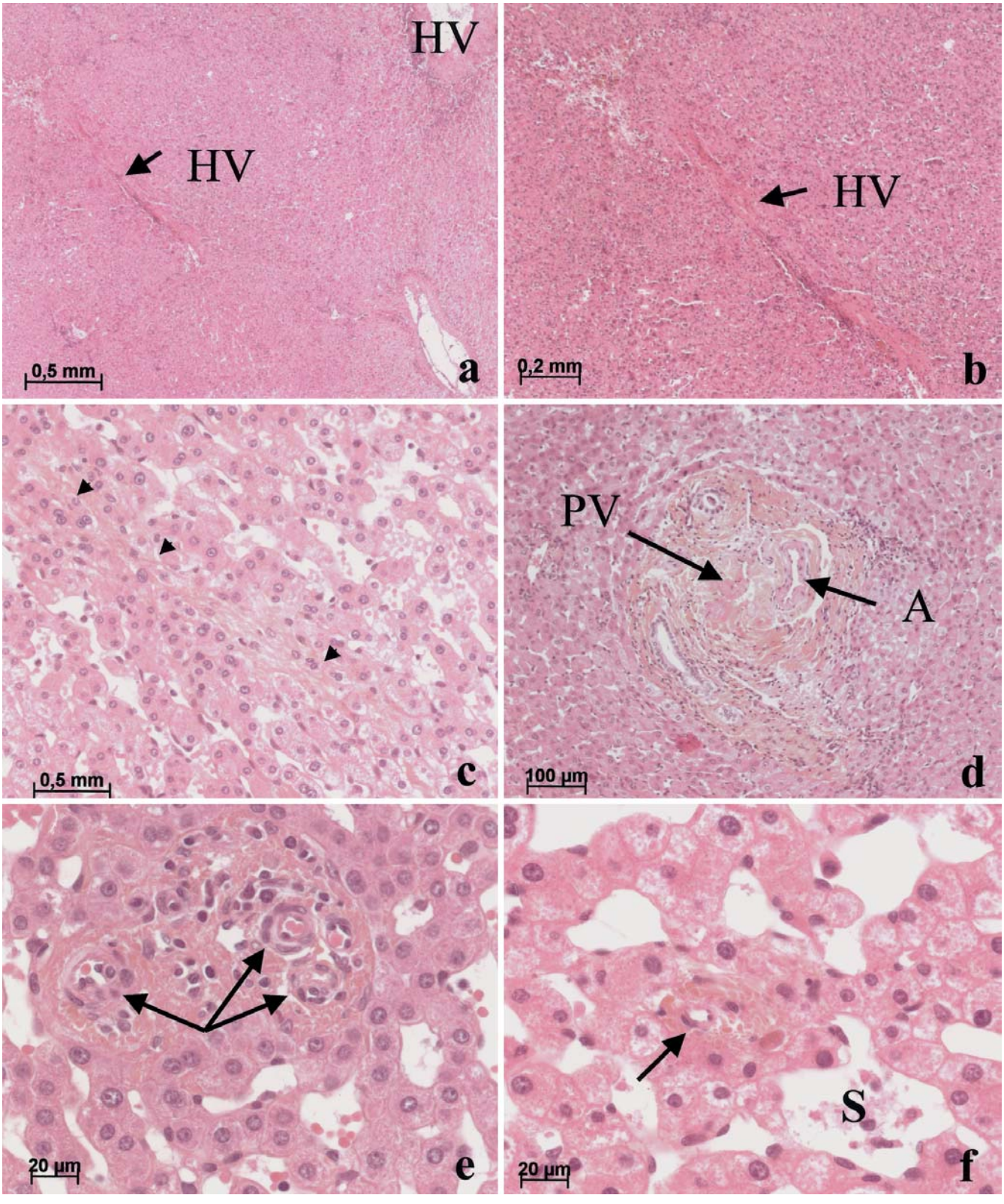



**Fig. 2** Non-nodular liver. **a, b, c** A damaged area with a large hepatic vein (*HV*) with a thickened wall, a partly occluded branch (*arrowhead*) with slight sinusoidal dilatation. **d** A phlebosclerosed portal vein (*PV*) nearby an artery (*A*) inside a fibrotic portal tract. **e** A portal tract-like structure with many arterial sections (*arrows*), a mild inflammatory reaction. This zone is to be compared with Fig. 1b. **f** An isolated artery (*arrow*) amidst mild fibrosis. This zone is to be compared with Fig. 1e. *S* dilated sinusoids

nodular liver in at least three cases, suggesting a link between the two.

It is thought that in FNH increased arterial flow hyperperfuses the local parenchyma leading to secondary hepatocellular hyperplasia [5]. In the last years, the idea has emerged that FNH could be a non-specific reaction to focal ischemia induced by various mechanisms such as hepatic vein thrombosis induced for example by oral contraceptives [4, 7]. This focal lesion induced the formation of arterio-venous shunts (between the hepatic artery and the hepatic veins) leading to an angiogenic process (hypertrophy of arteries). The presence of multiple nodules of various size from several centimeters to a few millimeters and of minor abnormalities in the non-nodular liver looking like MTFNH suggests that MTFNH is a diffuse process of vascular origin. It is not yet possible to say whether the *primum movens* is of arterial or venous origin. Because MTFNH affects women taking oral contraceptives, it seems appropriate to make a hypothetical link between oral contraceptives, vascular disease and MTFNH formation. It is of interest to note that the new generation of oral contraceptives could be more deleterious to the veins (in relation to their progesterone content) than the old ones [3].

## References


1. Fabre A, Audet P, Vilgrain V, Nguyen BN, Valla D, Belghiti J, Degott C (2002) Histologic scoring of liver biopsy in focal nodular hyperplasia with atypical presentation. Hepatology 35:414–420
2. Nguyen BN, Flejou JF, Terris B, Belghiti J, Degott C (1999) Focal nodular hyperplasia of the liver: a comprehensive pathologic study of 305 lesions and recognition of new histologic forms. Am J Surg Pathol 23:1441–1454
3. Vandenbroucke JP, Rosing J, Bloemenkamp KWM, Middeldorp S, Helmerhorst FM, Bouma BN, Rosendaal FR (2001) Oral contraceptives and the risk of venous thrombosis. N Engl J Med 344:1527–1535
4. Wanless IR (2000) Epithelioid hemangioendothelioma, multiple focal nodular hyperplasias, and cavernous hemangiomas of the liver. Arch Pathol Lab Med 124:1105–1107
5. Wanless IR, Mawdsley C, Adams R (1985) On the pathogenesis of focal nodular hyperplasia of the liver. Hepatology 5:1194–1200
6. Wanless IR, Albrecht S, Bilbao J, Frei JV, Heathcote EJ, Roberts EA, Chiasson D (1989) Multiple focal nodular hyperplasia of the liver associated with vascular malformations of various organs and neoplasia of the brain: a new syndrome. Mod Pathol 2:456–462
7. Wanless IR, Terris B, Bioulac-Sage P, et al (2000) Focal Hyperplasia (FH) of liver associated with localized hepatic vein thrombosis: a lesion with some features of “focal nodular hyperplasia”. Mod Pathol 13:191A

Virchows Arch (2003) 442:231–237
DOI 10.1007/s00428-002-0744-4

ORIGINAL ARTICLE

**Silvana Geleff · Sebastian F. Schoppmann**
**Georg Oberhuber**

# Increase in podoplanin-expressing intestinal lymphatic vessels in inflammatory bowel disease

Received: 13 August 2002 / Accepted: 30 October 2002 / Published online: 16 January 2003
© Springer-Verlag 2003

**Abstract** Ulcerative colitis (UC) and Crohn's disease (CD) are two presentations of inflammatory bowel diseases (IBDs). Whereas the inflammation in UC is confined to the mucosa/submucosa, CD is considered a transmural disease with characteristic lymphoid aggregates with or without epithelioid granulomas in the subserosa. Here we examined and quantified the distribution of lymphatic capillaries in small- and large-bowel resection specimens (non-IBD $n$=8; CD $n$=20 and UC $n$=13) using immunohistochemical staining with anti-human podoplanin antibody, an established marker for lymphatic endothelium. In normal small intestine, the lymphatic network originated in the capillaries beneath the surface epithelial cells, whereas it started in the lower third of the mucosa of the large intestine. Lymphatic microvessel counts revealed a statistically highly significant increase ($P$<0.005 in the muscularis mucosae, $P$=0.012 in the tunica submucosa and $P$=0.012 in the tunica subserosa) in IBDs when compared with normal intestine. Numerical differences between CD and UC samples were not significant. Prominence of lymphatic capillaries could also be observed in areas where fibrosis replaced chronic inflammation. These findings suggested that lymph-vessel proliferation in IBDs may be triggered by chronic inflammation irrespective of its organization and is maintained in fibrotic end-stage disease.

**Keywords** Crohn's disease · Immunohistochemistry · Inflammatory bowel disease · Lymphatic vessels · Podoplanin · Ulcerative colitis

S. Geleff · G. Oberhuber (✉)
Institute of Clinical Pathology, University of Vienna,
Waehringer Guertel 18–20, A-1090 Vienna, Austria
e-mail: pathologie@t-online.de
Tel.: +43–1-404003650, Fax: +43–1-4053402

S. F. Schoppmann
Department of Surgery, Vienna General Hospital,
University of Vienna, Austria

## Introduction

Crohn's disease (CD) and ulcerative colitis (UC) are inflammatory disorders of the gut of unknown etiology. One major differential diagnostic criterion between both diseases is that CD may involve all areas of the gastrointestinal (GI) tract with approximately one-third of the patients showing inflammation of the colon only. UC is essentially confined to the colon and is usually uniform and continuous in mucosal and occasionally submucosal inflammation. CD represents an inflammatory condition with skip lesions, granulomas, transmural inflammation and fissures as pathological features [21, 22]. Characteristically the inflammatory infiltrate is organized into so-called lymphoid aggregates in particular in the subserosal fatty tissue. These are follicle-like structures composed mainly of mononuclear cells and in many cases also of epithelioid cell granulomas. Although in the majority of cases these criteria permit histological discrimination, progression of disease and longstanding therapy may render the distinction between the two entities impossible.

It is thought that the pathologic mechanisms of inflammatory bowel disease (IBD) are primarily based on impaired immune responses including a dysregulation of local immune defense in which the constant influx of leukocytes provides a basis for the development of chronic inflammation [24]. However, it is unclear how and why chronic inflammation presents with formation of lymphoid aggregates and granulomas in CD but not in UC. One possible explanation was that UC is considered to represent a Th2 immunological response whereas CD is thought to be Th1 based [10]. Alternatively, the organization of the inflammatory infiltrate may be an expression of the immunological state of the individual patient. The intestinal microcirculation has also been implicated in the pathogenesis of IBD, in particular the observation of the proximity of infiltrates and blood/lymphatic vessels in CD which has led in the past to a classification of CD as a variant of granulomatous vasculitis [31]. Presently, vasculitis is not considered a constant feature of

CD, although rare cases with distinct granulomatous involvement of arteries have been described [14]. Lymphoid aggregates may also develop near or within lymphatic vessels, thus suggesting them to be the morphological substrate of an ongoing immunological response, e.g., to microorganisms. A previous report showed that there was an association between lymphoid aggregates, granulomas and capillary vessels consistent with lymphatic vessels [18]. Unfortunately, at that time no specific immunohistological makers for labeling of lymphatic vessels in formalin-fixed specimens were available.

It is now possible to selectively stain lymphatic vessels using a polyclonal antibody recognizing human podoplanin [3, 4, 28], an approximate38-kDa membrane protein which was originally detected on the surface of rat glomerular epithelial cells (podocytes) and was found to be linked to flattening of foot processes in experimental nephrosis [2, 15]. Human podoplanin shows features of a type-I membrane protein with several conserved O-glycosylation sites [3]. As heavily O-glycosylated mucoproteins were recently identified as counter receptors for selectins that mediate adhesion of inflammatory cells [25], it is possible that podoplanin may be involved in adhesion of inflammatory cells to lymphatic endothelia.

In the present study, we present data on podoplanin-expressing lymphatic vessels in resection specimens of patients with CD, UC (*n*=47) and of controls without evidence of IBD (*n*=8). The aim of the study was to determine the distribution and the quantity of lymphatic vessels in CD and in UC in order to reveal potential differences between both diseases. Furthermore, the association of lymphoid aggregates/granulomas and lymphatic vessels as well as the presence of lymphatic capillaries in fibrosis were examined.

## Materials and methods

### Human tissues

Specimens were obtained through surgical resection of small and large bowel from 20 patients diagnosed with CD (10 males and 10 females; median age 35 years, range 22–68 years). All patients underwent surgery due to the development of complications (fistulae and stenoses). When possible, up to three blocks with active lesions were chosen for each case. A total of 27 blocks with the disease originated from the small bowel and 7 blocks were taken from the large intestine.

As a second group, colonic resection specimens from 13 patients with UC undergoing surgery for intractable disease were analyzed (median age 52 years, range 34–78 years, all of them male patients). Blocks were taken from areas of active disease.

The diagnosis of CD and UC was based on the histology of resection specimens, clinical symptoms, blood tests, gastrointestinal endoscopy with biopsy and/or radiologic findings. Negative controls included resection margins from colon cancer specimens (*n*=8).

All tissues were fixed in neutral buffered 4% formalin and were paraffin embedded; 4-µm-thick sections were stained with hematoxylin and eosin for orientation, and immunohistochemistry was performed on consecutive sections.

### Monoclonal and rabbit antibodies

Rabbit anti-human podoplanin IgG was prepared as described [3]. Mouse monoclonal antibodies to CD31 (clone JC 70A) and to CD68 (clone PGM1), alkaline phosphatase-conjugated goat anti-mouse IgG, alkaline phosphatase-anti-alkaline phosphatase complex, peroxidase-conjugated swine anti-rabbit IgG and peroxidase-conjugated rabbit anti-swine IgG were from Dako (Glostrup, Denmark). Mouse monoclonal antibody to CD2 (clone AB 75) was from Novocastra Laboratories (Newcastle upon Tyne, UK). Biotinylated horse anti-mouse IgG, goat anti-rabbit IgG and streptavidin-peroxidase complex were purchased from Vector Laboratories (Burlingame, CA).

### Immunohistochemistry

For immunostaining of 3-µm-thick deparaffinized serial sections of small and large intestine, the following pretreatment was required: protease digestion (protease XXIV; Sigma, Deisenhofen, Germany) was used for CD68 (clone PGM1) and microwave treatment (600 W for 10 min) was performed for CD31, CD2 and anti-human podoplanin IgG. Sections were incubated with primary antibodies for 1 h at 20°C, followed by biotinylated horse anti-mouse IgG or goat anti-rabbit IgG for 30 min and detection by a streptavidin-peroxidase complex, according to the manufacturer's instructions. Peroxidase reaction product was visualized using diaminobenzidine (Serva, Heidelberg, Germany). A summary of primary antibodies and immunohistochemical procedures is given in Table 1.

For double immunostaining, deparaffined and rehydrated sections were subjected to microwave pretreatment and incubated with several combinations of primary antibodies: (1) monoclonal antibodies to CD31, followed by anti-human podoplanin IgG; (2) monoclonal antibodies to CD2, followed by anti-human podoplanin IgG; and (3) monoclonal antibodies to CD68, followed by anti-human podoplanin IgG. Secondary antibodies were in each case alkaline phosphatase-conjugated goat anti-mouse IgG followed by alkaline phosphatase-anti-alkaline phosphatase complex and peroxidase-conjugated swine anti-rabbit IgG followed by peroxidase-conjugated rabbit anti-swine IgG. Detection was performed for the monoclonal antibodies with blue alkaline phosphatase substrate kit (Vector, Burlingame, CA) according to the instructions of the manufacturer; peroxidase product was visualized using 3-amine-9-ethylcarbazole (AEC, Sigma, Deisenhofen, Germany) and $H_2O2$.

### Quantification of lymphatic capillaries and granulomas/lymphoid aggregates

In the 20 cases of active CD, the number of granulomas and of lymphoid aggregates was counted in each region of the bowel wall. Lesions with aggregates of CD2-positive lymphoid cells and

**Table 1** Monoclonal antibodies and antisera used in this study

| Molecule/ antibody | Clone | Pretreatment, antibody dilution | Source |
|---|---|---|---|
| CD31 | JC70A | MW, 1:40 | Dako |
| CD68 | PGM1 | Protease, 1: | Dako |
| CD2 | AB75 | Autoclave 1:40 | Novocastra |
| Podoplanin | Polyclonal | MW. 1:800 | Breiteneder-Geleff et al. [3] |

small clusters of CD68-positive epithelioid cells with or without giant cells were defined as a granulomas.

The number of podoplanin-positive lymphatic capillaries was assessed in CD, UC and normal bowel (non-IBD). Because of their richness in lymphatic capillaries in all cases, the focus was on the submucosal and subserosal layers. Accumulation of small lymphatic vessels expressing podoplanin (called 'hot spots' in analogy to previous investigations on microvessel density in tumors [20, 23, 29]) were selected at a low magnification (×40 magnification). Four hot spots were used per section for a modified microvessel density count [32] using a final magnification of ×200, corresponding to a field size of 0.739 $mm^2$. Only microvessels stained with podoplanin and visible lumina were considered countable, because small nerve fibers also expressed podoplanin and potentially could be confused with collapsed lymphatic capillaries. Using CD31 it turned out that all small vessels had lumina. Median vessel density and the highest vessel count ('top count') of four fields were assessed separately and values were evaluated for statistical significance using paired groups in Mann-Whitney test and Wilcoxon test.

### Quantification of lymphatic capillaries spanning the lamina muscularis mucosae

Lymphatic vessels spanning the muscularis mucosae were counted in sections from IBD as well as in controls samples. The number of lymphatics per millimeter of muscularis mucosae was determined in each section (at magnification 100× the number of crossing lymphatics was counted in four fields with a total length of 3.68 mm) using a measuring ocular for calibration.

## Results

### Lymphatic vessels in normal small and large intestine

In the wall of normal small and large intestine, lymphatic capillaries were identified as small, weakly stained, inconspicuous vessels when stained with anti-panendothelial antibody CD31 (Fig. 1). Immunohistochemistry with anti-human podoplanin IgG in consecutive sections revealed their geographic distribution. In the small intestine, the central lacteal was prominent in all villi of the mucosa, opposed to the few lymphatic capillaries located at the base of the crypts near the smooth muscle layer in colonic mucosa, confirming previous reports [5]. Lymphatic vessels that cross the muscular layer of the mucosa are comma-shaped small structures with a tiny lumen. Their number per millimeter of smooth muscle layer was 2.17 as a minimum and 4.07 as a maximum, corresponding to a median of 2.97 crossing vessels. Lymphatics were more prominent in loose connective tissue of the submucosal layer both in the large and the small intestine. Evaluation of the lymphatic microvessel density of the submucosa in eight samples (small and large intestine) gave a median number (median of four counts) of 4.75 (range 3–6.25) and a highest number (highest number of four counts) of 6.75 (range 6–8) capillaries in the submucosa. Lymphatic vessels (with small or barely visible lumina) were seen to span the muscularis propria and to be easily recognized in the subserosa where they characteristically 'accompany' middle-sized arteries and veins. Their density amounted to a median of 4.875 lymphatics per middle power field (range 3.5–5.75) and a top count of 7 (range 5–8).

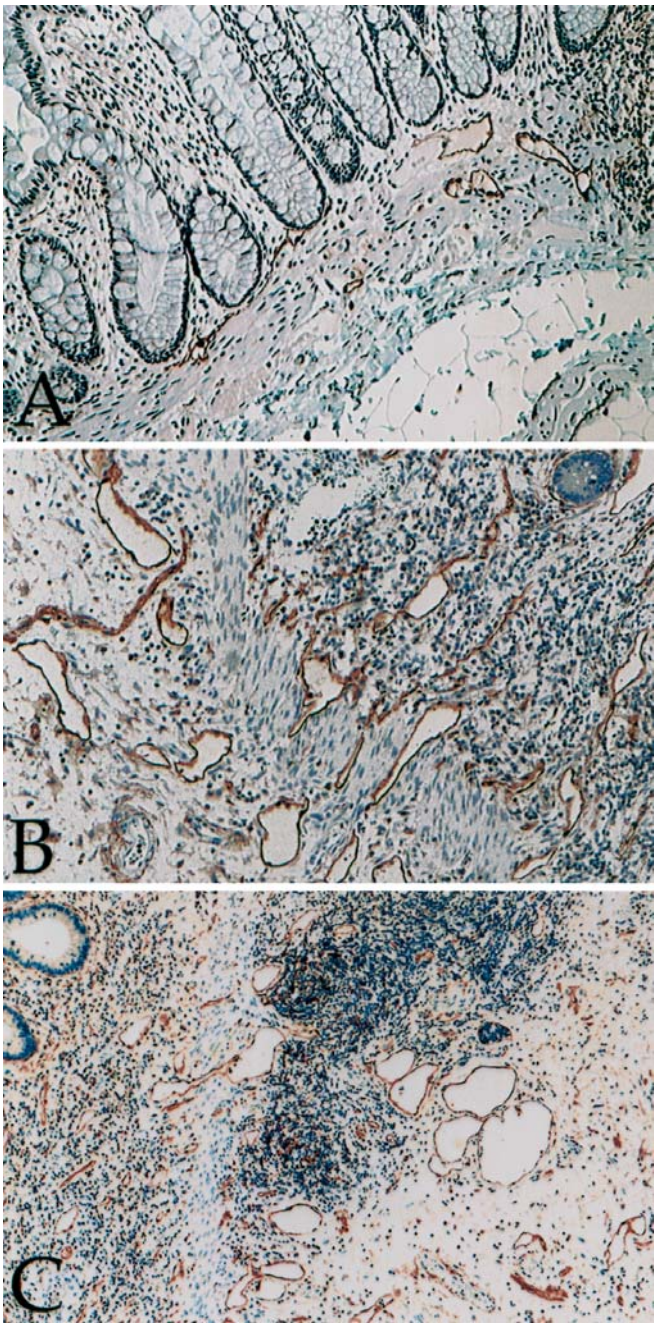



**Fig. 1** Distribution of lymphatics in the lamina muscularis mucosae and the submucosa in normal intestinal sections and in those from patients with inflammatory bowel disease, demonstrated by immunohistochemical staining with anti-human podoplanin IgG. In the control sample few podoplanin-expressing capillaries can be seen (**A**). By contrast in sections from the small intestine of patients with Crohn's disease (**B**) and ulcerative colitis (**C**) many tortuous vessels can be seen crossing the smooth muscle bundles of the muscularis mucosae. In addition, numerous lymphatic capillaries are located in areas of the submucosa rich in mononuclear cells (**B**, **C**)

**Table 2** Statistical evaluation of the distribution of the lymphatic capillaries in the submucosa using paired groups in the Wilcoxon test

| | Median Value | Top count of 4 |
|---|---|---|
| Crohn's disease/normal intestine | $P$=0.012 | $P$=0.012 |
| Ulcerative colitis/normal intestine | $P$=0.012 | $P$=0.012 |
| Ulcerative colitis/Crohn's disease | $P$=0.126 | $P$=0.213 |

**Table 3** Statistical evaluation of the distribution of the lymphatic capillaries in the subserosa using paired groups in the Wilcoxon test

| | Median Value | Top count of 4 |
|---|---|---|
| Crohn's disease/normal intestine | $P$=0.025 | $P$=0.033 |
| Ulcerative colitis/normal intestine | $P$=0.017 | $P$=0.017 |
| Ulcerative colitis/Crohn's disease | $P$=0.060 | $P$=0.529 |

## Lymphatic vessels in the large intestine in UC

The highest density of lymphatic capillaries was observed in the submucosa and subserosa in IBD. As the mucosa was often missing in the active lesions due to ulceration, the first layer in which lymphatics were quantified was the muscularis mucosae. In UC the median count of lymphatic capillaries per millimeter of smooth muscle layer was increased to 4.67 (range 3.43–6.52) compared with normal large intestine. Paired groups in the Mann-Whitney and the Wilcoxon tests gave a high significance to the difference between normal and UC colonic samples ($P$<0.005).

The density of lymphatic capillaries in the submucosa in UC amounted to a median count of 11.46 (range 3.5–20.5) and a top count of 15.3 lymphatic capillaries (range 4–26). These differences correspond to $P$=0.012 and $P$=0.012. The results of the statistical evaluation using the Wilcoxon test reflect a similar trend, as can be seen in Table 2 emphasizing the significant increase in lymphatic microvessel density relative to normal intestinal submucosa. Lymphatic microvessel density in the subserosa of UC samples was 8.19 (median count; range 4–15.25) and 12 (top count; range 6–22). This corresponds to statistically highly significant differences ($P$=0.017 and $P$=0.017, respectively) when compared with normal large intestine. The values obtained with the Wilcoxon test were similar and are depicted in Table 3.

## Lymphatic vessels in CD

### *Small intestine*

The majority (27 of 34) of our samples was derived from CD of the terminal ileum where active lesions were usually severe. Areas rich in lymphoid aggregates (with or without granulomas) contained podoplanin-positive capillaries with small- to medium-sized lumina, which were often filled with CD2-positive lymphocytes. Lymphatic capillaries were either located in or around each lymphoid aggregate. Depending on the plane of sectioning, these capillaries could be seen either at the center or the periphery of any lymphoid aggregate or granuloma. In our collective, each lymphoid aggregate with or without granuloma displayed a minimum of one associated lymphatic capillary. These results confirmed in part previous observations that a significant percentage of granulomas in CD was associated with lymphatic vessels [17] (Fig. 2).

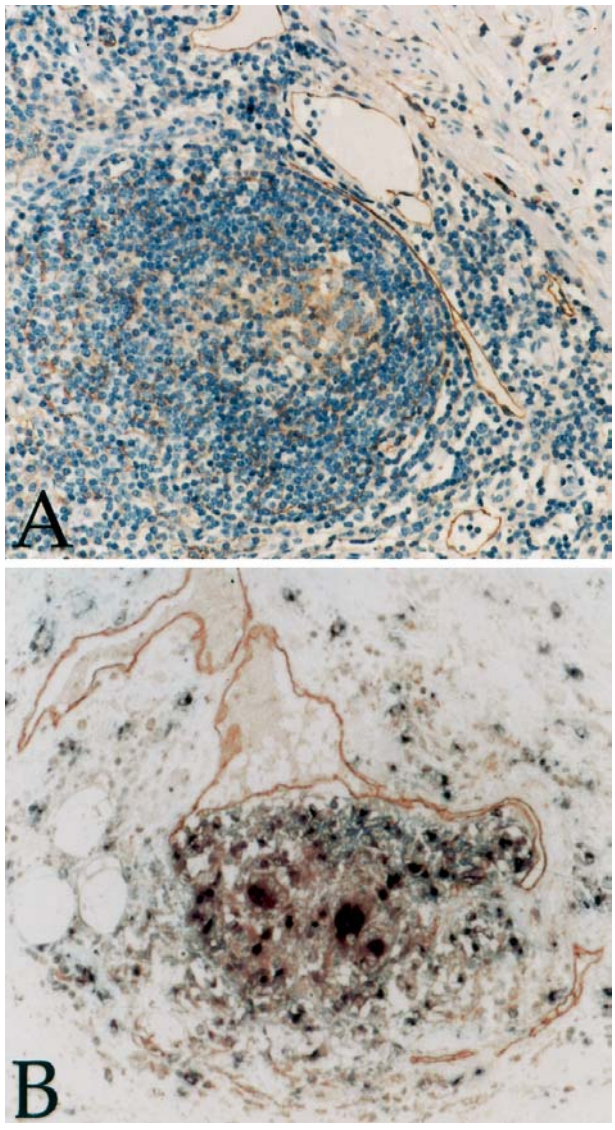



**Fig. 2** Lymphoid aggregates/granulomas contain numerous lymphatic capillaries in Crohn's disease. Lymphoid aggregates are prominent in the submucosa of small intestine. Here, thin and often dilated podoplanin-positive lymphatic capillaries can be seen in the periphery (**A**). These distended vessels can also be co-localized in epithelioid cell granulomas that contain CD68-positive giant cells (double staining with anti-human podoplanin and anti-human CD68 IgGs, **B**)

The median count of lymphatics in the submucosa of the small intestine was 12.925 (range 5.375–21.875) per middle power field and the top count was 21.11 (range 9–40).

There were fewer lymphoid aggregates in the subserosa than in the submucosa in our collective of CD specimens (median counts 21.12 in the submucosa versus 12.11 in the subserosa). Lymphatic capillaries tended to gather at certain points at the border between the outer layer of the muscularis propria and the subserosa. This was the area where large blood vessels cross the smooth muscle layer. When additional fistulae (3 of 20 cases) were present, the clustering of lymphatics around larger blood vessels in the subserosa was very prominent. Lymphatic vessel counts in the subserosa of the small intestine in CD mounted to 8.39 (median value; range 4.25–22.375) and 13.62 (top counts; range 6–33).

*Large intestine*

The samples of the large intestine ($n$=7) from patients with CD reflected a similar trend. Here the median submucosal lymphatic microvessel count was 15.82 (range 13.875–22.5) per middle power field and the top count was 24.42 (range 16–35).

The overall distribution of lymphatic vascular clusters in the subserosa was similar to that in the small intestine. Lymphatic vessel counts in Crohn samples of the large intestine were 8.96 (median count; range 6.125–12.125) and 13.85 (top count; range 8–20) in the subserosa.

Statistical evaluation of the microvessel density in the submucosa of all Crohn samples relative to the submucosa of normal intestine pointed to highly significant differences both with the Mann-Whitney ($P$=0.012 for median value and $P$=0.012 for top counts) and the Wilcoxon test (Table 2). A similar situation was found when matching lymphatic microvessel density in the subserosa in normal and CD subserosa ($P$=0.017 and $P$=0.017, respectively). The values obtained with the Wilcoxon test were similar (Table 3).

The number of lymphatic vessels associated with lymphoid aggregates combined with granulomas was 17.41 in the submucosa and 12.43 in the subserosa (median counts) and was comparable with the number of lymphatic vessels not associated with lymphoid aggregates combined with granulomas which was 16.53 and 12.28, respectively. In all our CD samples, the muscularis mucosae presented as a thick and irregular bundle of smooth muscle cells. The number of the lymphatic capillaries crossing the muscularis mucosae was significantly increased in CD: the median count was 5.27 per millimeter of muscularis mucosae compared with 2.97 in normal intestine. Paired groups in Mann-Whitney test and the Wilcoxon test gave a statistically significant difference ($P$<0.005).

There was no statistically significant difference between the lymphatic microvessel density in both the submucosa and the subserosa between CD and UC: $P$=0.402 versus $P$=0.06 for the submucosa and $P$=0.695 versus $P$=0.197 for the subserosa.

*Persistence of increased number of lymph vessels in intestinal fibrosis*

All of our specimens originated from end-stage intestines in which inflammation and edema did not respond to steroid therapy and had inexorably progressed to stenosis and/or fistulation. The submucosa and subserosa of specimens derived from fistulating CD had areas with focal chronic inflammation and areas with fewer mononuclear cells set against a background of fibrosis; whereas, in terminal UC fibrosis was mainly concentrated in the submucosa. Both patterns contributed to increased microvessel density as prominent, often ectatic lymph vessels were also observed in areas with fibrosis. The numeric difference between lesions associated and not-associated with lymphatics was not significant (ratio=1.3). We concluded that these patterns represented overlapping aspects of a chronic inflammatory disease.

## Discussion

Observations on the organization of the lymphatic network in the human intestine have so far been limited. Little is known about lymphatics in chronic IBD except the fact that dilated lymphatic vessels are one of the characteristic features of CD [13] and that capillaries resembling lymphatic vessels are associated with subserosal lymphoid aggregates and granulomas which constitute a histological hallmark of the disease. Here, we present data on the distribution of lymphatic vessels in small and large intestine in normal tissues and in IBD using immunohistochemistry with antibodies to human podoplanin, a specific marker of lymphatic endothelium.

In this study, we demonstrated for the first time a significant increase in the number of lymphatic capillaries in the muscularis mucosae, submucosa and subserosa of the small and large intestine in CD relative to normal intestine. Also we were able to demonstrate a close association between lymphoid aggregates and podoplanin-positive lymphatic capillaries in CD. To our surprise a similar statistically significant increase in lymphatic vessels was observed in our collective of UC samples. It is still unclear why lymphoid aggregates are common in the subserosal tissue in CD but not in UC. One explanation is that these follicle-like structures are histological signs of an attempt to clear yet unknown infectious agents.

Our data suggest that the development of lymphatic vessels may be caused by similar mechanisms in both IBDs and that the trigger for the development of lymphoid aggregates is independent of lymphatic vessel formation. Also in our specimens derived from end-stage disease which presented with a mixture of chronic inflammation and resulting fibrosis, the increase in the number of lymphatic capillaries was a persistent feature and did not disappear once leukocytes became scarce.

Information about microvascular function in IBD is limited and restricted to the endothelium of blood vessels. Cell culture experiments using human intestinal

microvascular cells derived from end-stage intestines of CD and UC patients showed that increased leukocyte adhesiveness occurred in both diseases [6]. This provided further evidence that chronic inflammation depended on secondary non-immune cell dysfunction. There are no functional data in IBD concerning the traffic of leukocytes through lymphatic capillaries to the regional lymph nodes.

The increase in number of lymphatic vessels may be the result of an increased demand on their physiological functions rather than being a major pathophysiological factor. In the gut, the physiological role of lymphatic capillaries is defined by two main 'clearance' functions: (1) removal of excessive interstitial fluids and (2) transport of lymphocytes to regional lymph nodes. It is clear that in IBD interstitial fluids accumulate as a result of inflammation that has to be removed. Several mechanisms for fluid accumulation have been proposed. Besides inflammation-associated phenomena, leakage of albumin and water was proposed to be linked to loss of interstitial and vascular sulfated glycosaminoglycans [19]. Also, modifications at the level of the cellular junctions of lymphatic capillaries, with a prevalence of the patent type of junction in CD [12], were observed.

It is also obvious that lymphatic traffic involving the mucosa, but also the remainder of the bowel wall and regional lymph nodes, does increase in IBD. Lymphatic capillaries are considered to be involved in this process, in particular in the removal of lymphocytes from the target organ to mesenterial lymph nodes. Chemokines such as "secondary lymphoid-tissue chemokine" (SLC), which are expressed not only on high endothelial venules (HEVs) but also on the lymphatic endothelium may play a role in mediating the migration of lymphocytes into efferent lymphatics [1, 7]. Other chemokines potentially involved in lymphatic traffic are the beta-chemokines RANTES, MCP-1 and MCP-3, which bind to dermal lymphatic endothelium supporting the notion that they may play a role in directing the migration of T cells to regional lymph nodes [8]. Most likely, this increased cell traffic will also stimulate lymphangiogenesis by yet unknown mechanisms or factors. Considerable evidence has emerged from studies of expression patterns of mucosal and microvascular cytokines and adhesion molecules [16, 27, 33, 34] in IBDs.

Up to now, it has, to our best knowledge, not been elucidated whether the cytokines and chemokines involved support or block lymphatic traffic through lymphatic vessels and whether they stimulated formation of lymphatic vessels in IBD. Recent studies found an association of lymphangiogenesis and expression of vascular endothelial growth factor (VEGF)-C in inflammatory cells in a model of cornea neovascularization and in tumor-associated lymphangiogenesis [17, 26]. When using in situ hybridization for VEGF-C mRNA in our IBD sections, we found a varying number of VEGF-C-expressing mononuclear cells throughout the intestinal wall, in particular in or near lymphoid aggregates (results not shown). Another possible mechanism that could lead to lymphangiogenesis and the accumulation of immunocompetent cells could be related to obstruction of efferent lymphatic routes. Previous studies in experimental enteritis in pigs have shown that chronic obstruction of mesenterial lymphatics using a formalin injection into the regional lymph nodes provoked hyperplasia of lymphatic tissue, granuloma-like lesions, edema and mucosal ulcerations that progressed to transmural inflammation, fibrosis and fistulating disease [11]. Most of the described features are also found in CD.

The finding that NOD2 frame-shift mutations are associated with susceptibility to CD has supported the view that a reduced ability to neutralize bacteria may be responsible for the disease at least in a subgroup of patients [9, 30]. It is possible that in all chronic/granulomatous inflammations the increased density of lymphatic microvessel is an expression of an elimination mechanism to ensure a quick delivery of leukocytes/infectious agents to the regional lymph node.

## References


1. Brandtzaeg P, Farstad IN, Haraldsen G (1999) Regional specialization in the mucosal immune system: primed cells do not always home along the same track. Immunol Today 20:267–277
2. Breiteneder-Geleff S, Matsui K, Soleiman A, Meraner P, Poczewski H, Kalt R, Schaffner G, Kerjaschki D (1997) Podoplanin, novel 43-kd membrane protein of glomerular epithelial cells, is down-regulated in puromycin nephrosis. Am J Pathol 151:1141–1151
3. Breiteneder-Geleff S, Soleiman A, Horvat R, Amann G, Kowalski H, Kerjaschki D (1999) Verh Dtsch Ges Pathol 83:270–275
4. Breiteneder-Geleff S, Soleiman A, Kowalski H, Horvat R, Amann G, Kriehuber E, Diem K, Weninger W, Tschachler E, Alitalo K, Kerjaschki D (1999) Angiosarcomas express mixed endothelial phenotypes of blood and lymphatic capillaries. Am J Pathol 154:385–394
5. Fenoglio CM, Kaye GI, Lane N (1973) Distribution of human colonic lymphatics in normal, hyperplastic, and adenomatous tissue. Gastroenterology 64:51–66
6. Freemont AJ (1988) Functional and biosynthetic changes in endothelial cells of vessels in chronically inflamed tissues: evidence for endothelial control of lymphocyte entry into diseased tissues. J Pathol 155:225–230
7. Gunn MD, Tangemann K, Tam C, Cyster JG, Rosen SD, Williams LT (1998) A chemokine expressed in lymphoid high endothelial venules promotes the adhesion and chemotaxis of naive T lymphocytes. Proc Natl Acad Sci U S A 95:258–263
8. Hub E, Rot A (1998) Binding of RANTES, MCP-1, MCP-3, and MIP-1alpha to cells in human skin. Am J Pathol 152:749–757
9. Hugot JP, Chamaillard M, Zouali H, Lesage S, Cezard JP, Belaiche J, Almer S, Tysk C, O'Morain CA, Gassull M, Binder V, Finkel Y, Cortot A, Modigliani R, Laurent-Puig P, Gower-Rousseau C, Macry J, Colombel JF, Sahbatou M, Thomas G (2001) Association of NOD2 leucine-rich repeat variants with susceptibility to Crohn's disease. Nature 411:599–603
10. Kakazu T, Hara J, Matsumoto T, Nakamura S, Oshitani N, Arakawa T, Kitano A, Nakatani K, Kinjo F, Kuroki T (1999) Type 1 T-helper cell predominance in granulomas of Crohn's disease. Am J Gastroenterol 94:2149–2155
11. Kalima TV, Saloniemi H, Rahko T (1976) Experimental regional enteritis in pigs. Scand J Gastroenterol 11:353–362

12. Kovi J, Duong HD, Hoang CT (1981) Ultrastructure of intestinal lymphatics in Crohn's disease. Am J Clin Pathol 76:385–394
13. Levine S, Haggit RC (1992) Colon. In: Sternberg SS (ed) Histology for Pathologists, Raven Press, New York, pp 573–590
14. Matson AP, Van Kruiningen HJ, West AB, Cartun RW, Colombel JF, Cortot A (1995) The relationship of granulomas to blood vessels in intestinal Crohn's disease. Modern Pathol 8:680–685
15. Matsui K, Breiteneder-Geleff S, Kerjaschki D (1998) Epitope-specific antibodies to the 43-kD glomerular membrane protein podoplanin cause proteinuria and rapid flattening of podocytes. J Am Soc Nephrol 9:2013–2026
16. Meenan J, Spaans J, Grool TA, Pals ST, Tytgat GNJ, van Deventer SJH (1997) Altered expression of alpha4beta7, a gut homing integrin, by circulating and mucosal T cells in colonic mucosal inflammation. Gut 40:241–246
17. Mimura T, Amano S, Usui T, Kaji Y, Oshika T, Ishii Y (2001) Expression of vascular endothelial growth factor C and vascular endothelial growth factor receptor 3 in corneal lymphangiogenesis. Exp Eye Res 72:71–78
18. Mooney EE, Walker J, Hourihane DOB (1995) Relation of granulomas to lymphatic vessels in Crohn's disease. J Clin Pathol 48:335–338
19. Murch SH, MacDonald TT, Walker-Smith JA, Levin M, Lionetti P, Klein NJ (1993) Disruption of sulphated glycosaminoglycans in intestinal inflammation. Lancet 341:711–714
20. Obermair A, Bancher-Todesca D, Bilgi S, Kaider A, Kohlberger P, Müllauer-Ertl S, Leodolter S, Gitsch G (1997) Correlation of vascular endothelial growth factor expression and microvessel density in cervical intrapithelial neoplasia. J Natl Cancer Inst 89:1212–1217
21. Petras RE (1989) Non-neoplastic intestinal disease. In: Sternberg SS (ed) Diagnostic surgical pathology, vol.2. Raven Press, New York, pp 967–1014
22. Price AB, Morson BC (1975) Inflammatory bowel disease. The surgical pathology of Crohn's disease and ulcerative colitis. Human Pathol 6:7–29
23. Rubin MA, Buyyounouski M, Bagiella E, Sharir S, Neugut A, Benson M, de la Taille A, Katz AE, Olsson CA, Ennis RD (1999) Microvessel density in prostate cancer: lack of correlation with tumor grade, pathologic stage and clinical outcome. Urology 53:542–547
24. Sartor RB (1997) Pathogenesis and immune mechanisms of chronic inflammatory bowel diseases. Am J Gastroenterol 92:5S–11S
25. Sassetti C, Tangemann K, Singer MS, Kershaw DB, Rosen SD (1998) Identification of podocalyxin-like protein as a high endothelial venule ligand forl-selectin: parallels to CD34. J Exp Med 187:1965–1975
26. Schoppmann SF, Birner P, Stöckl J, Kalt R, Ullrich R, Caucig C, Kriehuber E, Nagy K, Alitalo K, Kerjaschki D (2002) Tumor-associated macrophages express lymphatic endothelial growth factors and are related to peritumoral lymphangiogenesis. Am J Pathol 161:947–956
27. Schuermann GM, Aber-Bishop AE, Facer P, Lee JC, Rampton DS, Dore CJ, Polak JM (1993) Altered expression of cell adhesion molecules in uninvolved gut in inflammatory bowel disease. Clin Exp Immunol 94:341–347
28. Sleeman JP, Krishnan J, Kirkin V, Baumann P (2001) Markers for the lymphatic endothelium: in search of the holy grail? Microsc Res Tech 55:61–69
29. Tomisaki S, Ohno S, Ichiyoshi Y, Kuwano H, Maehara Y, Sugimachi K (1996) Microvessel quantification and its possible relation with liver metastasis in colorectal cancer. Cancer 77:1722–1728
30. Van Heel DA, McGovern DP, Jewell DP (2001) Crohn's disease: genetic susceptibility, bacteria, and innate immunity. Lancet 357:1902–1904
31. Wakefield AJ, Dhillon AP, Sawyer AM, Pounder RE, Lewis AAM, Rowles PM, Pittilo RM (1989) Pathogenesis of Crohn's disease: multifocal gastrointestinal infarction. Lancet 2:1057–1062
32. Weidner N, Semple JP, Welch WR, Folkman J (1991) Tumor angiogenesis and metastasis- correlation in invasive breast cancer. N Engl J Med 324:1–8
33. Woywodt A, Ludwig D, Neustock P, Kruse A, Schwarting K, Jantschek G, Kirchner H, Stange EF (1999) Mucosal cytokine expression, cellular markers and adhesion molecules in inflammatory bowel disease. Eur J Gastroenterol Hepatol 11:267–276
34. Yacyshyn BR, Lazarovits A, Tsai V, Matejko K (1994) Crohn's disease, ulcerative colitis, and normal intestinal lymphocytes express integrins in dissimilar patterns. Gastroenterology 107:1364–1371

Virchows Arch (2003) 442:238–244
DOI 10.1007/s00428-002-0749-z

ORIGINAL ARTICLE

**Daniela Petz · Sabine Klauck**
**Friedrich-Wilhelm Röhl · Peter Malfertheiner**
**Albert Roessner · Christoph Röcken**

# Feasibility of histological grading and staging of chronic viral hepatitis using specimens obtained by thin-needle biopsy

Received: 12 March 2002 / Accepted: 20 November 2002 / Published online: 28 January 2003
© Springer-Verlag 2003

**Abstract** We performed a retrospective study to investigate the feasibility of grading and staging of chronic viral hepatitis on specimens obtained by means of thin-needle biopsy (TNB; 20G) using the modified Ishak-system (J Hepatol 1995; 22:696–699). Specimens obtained using large-needle biopsy (LNB; 17G) served as a control. A total of 100 biopsy specimens from 88 patients were included in the study. Of the patients, 30 suffered from chronic hepatitis B, 54 from chronic hepatitis C, and 4 from both; 59 specimens were obtained by TNB and 41 by LNB. All four categories of the Ishak-system, i.e., interface hepatitis, confluent necrosis, lobular inflammation and portal inflammation, could be applied to TNB specimens and provided similar total scores to those observed in LNB specimens. Specimens obtained by TNB facilitated the diagnosis of liver cirrhosis. However, they bore the risk of underestimating the presence of cirrhosis in favor of advanced bridging fibrosis, whereas no differences were found in the overall recognition of liver fibrosis. Intra- and interobserver variabilities were not affected by the needle size. For the interobserver agreement, the kappa values for the category of inflammation ranged from 0.003 to 0.419 (TNB) and 0.096 to 0.470 (LNB) and for staging we noted kappa values of 0.351 (TNB) and 0.456 (LNB). Reproducibility increased when a tolerance of ±1 was accepted for grading (total score) and staging; in this case, observer variability was less than 20%. This study showed that grading and staging of chronic viral hepatitis is feasible in TNB specimens and that intra- and interobserver variability poses a greater problem than needle size.

**Keywords** Menghini · Histopathology · Liver biopsy

D. Petz · A. Roessner · C. Röcken (✉)
Department of Pathology, Otto-von-Guericke-University,
Leipziger Strasse 44, 39120 Magdeburg, Germany
e-mail: christoph.roecken@medizin.uni-magdeburg.de
Tel.: +49-391-6713179, Fax: +49-391-67190188

S. Klauck · P. Malfertheiner
Department of Gastroenterology,
Hepatology and Infectious Diseases,
Otto-von-Guericke-University, Magdeburg, Germany

F.-W. Röhl
Department of Biometrics, Otto-von-Guericke-University,
Magdeburg, Germany

## Introduction

Liver biopsies are obtained from patients with chronic viral hepatitis to confirm the diagnosis, to estimate the severity of inflammation (grading), to determine the stage of fibrosis (staging), to correlate the histological findings with the clinical presentation, to detect dysplasia and neoplasia, and to help disclose the possible presence of other liver diseases. In addition, histological examination of the liver is extremely valuable in assessing the prognosis and monitoring the effects of therapy on the liver in long-term follow-up [17, 21].

Adequate sampling is essential for the histological interpretation of the biopsy specimen, and different needle sizes are available for taking a liver biopsy: a large-needle biopsy (LNB) with a minimum core diameter of 1.0 mm, e.g., the Menghini type, is recommended for the investigation of diffuse liver diseases [10, 28], and thin-needle biopsy (TNB) with an internal diameter of less than 1.0 mm is used for the investigation of focal lesions [7, 9, 13, 26, 28]. The risk of complications following liver biopsy depends on the needle size used and it increases in quadratic proportion to the caliber of the cannula [20]. There are clinical situations in which a LNB carries a high risk of complications or is even contraindicated (e.g., thrombocytopenia <50 gpt/l, prothrombin time <50%, ascites, or Child-Pugh stages B and C), and only a TNB can be obtained. In a recent study [23], it was shown that LNB (17 G) and TNB (20 G) yielded similar histopathological diagnoses with regard to diversity, frequency, and reliability. However, the size of the specimen obtained with TNB may influence the quality of grading and staging of chronic viral hepatitis. In the present study, we aimed to determine whether grading and staging of chronic viral hepatitis is feasible in speci-

mens obtained by TNB, which putative limitations it may provide, and which influence it has on intra- and interobserver variability.

## Materials and methods

### Patient and case selection

The period of this retrospective study was July 1997 to April 2000. One-hundred biopsy specimens from 88 patients were retrieved from the archive of the Department of Pathology. Selection was based on the needle size used (TNB and LNB) as well as clinical and serological evidence of chronic infection with hepatitis B or C. Criteria for exclusion were clinical and histopathological alterations not related to viral hepatitis, such as autoimmune hepatitis, alcohol- and drug-abuse, hemochromatosis, Wilson's disease, or $\alpha$1-antitrypsin deficiency. Specimens containing mass lesions, such as hepatocellular carcinoma or cholangiocarcinoma were excluded.

### Liver biopsy procedure

Once written informed consent had been given, liver samples were obtained by percutaneous needle biopsy. The Menghini needle biopsy using a 1.4-mm needle (LNB; 17 G; Sonocan wing, B. Braun Melsungen AG, Melsungen, Germany) was performed using an intercostal approach under local anesthesia with approximately 5 ml 1% lidocaine hydrochloride, incision of the skin with a stylet, and assistance by ultrasonography. TNB was performed to obtain specimens for histology and not cytology with a 0.9-mm modified Menghini cutting needle (20 G; Sonocan wing, B. Braun Melsungen AG, Melsungen, Germany), also under the guidance of ultrasonography, but using a subcostal approach. The real-time ultrasound equipment was furnished with 3.5 MHz convex array transducers with a needle guide lateral attachment (Siemens Elegra, Germany). The procedures were performed in a hospital setting and patients were kept under observation at least for a period of 24 h. The selection of the biopsy procedure (LNB vs TNB) was performed arbitrarily (not randomized and not standardized) immediately prior to the procedure. The selection was influenced by the patient's request (whether local anesthesia and incision of the skin was approved or not), size of the intercostal space, and whether the biopsy site was demonstrable by ultrasound.

### Specimen processing

All specimens were fixed immediately in 10% neutralized formalin and subsequently embedded in paraffin. Deparaffinized serial sections were stained using a hematoxylin and eosin stain (H&E), periodic-acid Schiff reagent with (PAS-D) and without (PAS) diastase pretreatment, Masson's trichrome stain, reticulin stain, and iron stain. At least eight sections (three sections stained with H&E and one section for each special stain) were evaluated per biopsy specimen. The amount of tissue obtained was estimated by measuring the length of the formalin-fixed core cylinder prior to embedding. A core cylinder consisting of more than four pieces was regarded as fragmented.

### Evaluation

Grading and staging of chronic viral hepatitis was performed according to the modified Histological Activity Index (Ishak-system) [14]. All specimens were evaluated twice (intraobserver variability) by each of two independent observers (interobserver variability). At the time of the study, observer A was a medical student with special training in histopathology and observer B a qualified histopathologist with 10 years of experience. To ensure blinding, the repeat interval between the first and second examination round was 6–12 months. Afterward, both observers performed a third examination together using a discussion microscope. Each specimen was discussed and a uniform consensus was agreed. The observers were blinded against needle size during each examination round.

### Statistical analysis

Statistical analyses (correlation coefficient and ANOVA) were performed using SPSS 6.11 program (SPSS Inc., Chicago, IL, USA). Mean values, standard deviation, minimum and maximum were calculated to describe the database. The differences between the two groups in Table 1 were tested using the $\chi^2$-test for qualita-

**Table 1** Characteristics of patients

| Characteristic | Total $n$=100 | TNB $n$=59 | LNB $n$=41 | $P$ value |
|---|---|---|---|---|
| Age (years ±SD) | 50.28±12.97 | 49.81±13.13 | 50.95 ±12.86 | 0.692 |
| Gender (female/male) | 42/58 | 23/36 | 19/22 | 0.463 |
| Hepatitis B [no. (%)] | 33 (33) | 19 (32) | 14 (34) | 0.885 |
| Hepatitis C [no. (%)] | 63 (63) | 38 (64) | 25 (61) | 0.867 |
| Hepatitis B and C [no. (%)] | 4 (4) | 2 (3) | 2 (5) | 1.000 |
| Time interval after diagnosis (months ±SD) | 71.90±88.80 | 80.10±96.60 | 60.00±75.90 | 0.553 |
| Prothrombin time (quick one-stage) (% ±SD) | 90.88±16.93 | 88.26±17.83 | 94.58±15.01 | 0.120 |
| Partial thromboplastin time (s ±SD) | 33.67±4.40 | 34.07±4.83 | 33.09±3.67 | 0.489 |
| Platelet count ($\times 10^9$/l ±SD) | 182.52±78.56 | 165.54±52.00 | 206.95±78.65 | 0.026 |
| Albumin (g/l ±SD) | 43.17±7.11 | 42.78±7.27 | 43.74±6.92 | 0.599 |
| Alanine aminotransferase (µmol/s×l ±SD) | 1.71±1.35 | 1.92±1.40 | 1.40±1.22 | 0.020 |
| Aspartate aminotransferase (µmol/s×l ±SD) | 1.58±1.37 | 1.90±1.53 | 1.14±0.94 | 0.009 |
| Bilirubin (µmol/l ±SD) | 17.35±14.68 | 18.93±15.68 | 15.06±12.95 | 0.385 |
| γ-glutamyl transpeptidase (µmol/s×l ±SD) | 1.47±1.57 | 1.65±1.68 | 1.22±1.37 | 0.110 |
| Clinically no liver cirrhosis [no. (%)] | 60 (60) | 35 (59) | 25 (61) | 0.933 |
| Liver cirrhosis* [no. (%)] | 40 (40) | 24 (41) | 16 (39) | 0.868 |
| Interferon therapy [no. (%)] | 26 (26) | 18 (31) | 8 (20) | 0.340 |
| Length of biopsy (mm ±SD) | 27.07±14.28 | 28.15±15.03 | 25.51±13.16 | 0.236 |
| Fragmentation [no. (%)] | 24 (24) | 16 (27) | 8 (20) | 0.381 |

*Liver cirrhosis as shown by ultrasound or clinical data

tive variables, and the two tailed *t*-test for continuous variables. A *p* value of <0.05 was considered to be significant. The level of intra- and interobserver disagreement was assessed by means of the kappa value (Cohen's kappa) [2]. The kappa value is a measure of agreement adjusted for the chance expected agreement. The kappa value is 0 if agreement is no better than chance. If agreement is perfect, the coefficient is 1. According to Landis and Koch [16], the strength of agreement was considered slight for values between 0 and 0.190, fair for values between 0.200 and 0.390, moderate for values between 0.400 and 0.590, substantial for values between 0.600 and 0.790, and almost perfect for values greater than 0.800.

## Results

### Patient characteristics

Table 1 summarizes the clinical characteristics of the patients. Patient characteristics did not differ significantly between the two groups (LNB vs TNB) except for three parameters (Table 1); in patients who underwent TNB, the platelet count was significantly lower ($p$=0.026) and serum levels of alanine aminotransferase (ALT; $p$=0.020) and aspartate aminotransferase (AST; $p$=0.009) were significantly higher than those who underwent LNB.

### Comparison of grading and staging

Table 2 summarizes the results of the uniform consensus reached by both observers. In four biopsy specimens (all TNB), no grading and staging was performed, because only fibrous tissue (with and without bile ducts) and no liver parenchyma was enclosed. Chronic viral hepatitis was assessed with regard to periportal or periseptal interface hepatitis (A), confluent necrosis (B), focal lytic necrosis, apoptosis, focal inflammation (lobular inflammation; C), and portal inflammation (D). A maximum score for any of the four categories was not observed in any of the remaining 96 biopsy specimens. Grading of interface hepatitis (A; maximum possible score 4) ranged between 0 and 3, and of lobular inflammation (C; maximum possible score is 4) it ranged between 0 and 2 and was identical between specimens obtained by TNB or LNB. In the whole series, just one specimen, which had been obtained by LNB, enclosed zone 3 necrosis in some areas (B; maximum possible score 6). The grading of portal inflammation (D; maximum possible score 4) ranged between 0 and 3 (LNB). Every specimen obtained by TNB enclosed some portal inflammation that ranged between 1 and 2 (TNB). Again, a maximum score was not observed.

Staging of chronic hepatitis (S; maximum possible score 6 – cirrhosis, probable or definite) ranged between 0 and 6. The absence of portal fibrosis (stage 0) was found in specimens obtained by LNB only. The lowest stage in specimens obtained by TNB was 1 (fibrous expansion of some portal areas, with or without short fibrous septa; Table 3). Specimens obtained by TNB facilitated the diagnosis of liver cirrhosis (stage 6) in 18% of the cases investigated, compared with 22% of the specimens obtained by LNB. No differences were found in the overall recognition of liver fibrosis (Table 2).

Finally, the mean values for the individual categories for grading and staging showed no significant differences between specimens obtained by TNB or LNB (Table 2) and was not influenced by the underlying disease, i.e., chronic hepatitis B or C.

**Table 3** Kappa values for grading and staging. $O_A$ and $O_B$ denote two independent observers; *1* and *2* denote first and second examination round

| Observer | TNB | LNB |
|---|---|---|
| Grading | | |
| $O_{A1}$ vs $O_{A2}$ | 0.084 | 0.272 |
| $O_{B1}$ vs $O_{B2}$ | 0.206 | 0.306 |
| $O_{A2}$ vs $O_{B2}$ | 0.275 | 0.261 |
| Staging | | |
| $O_{A1}$ vs $O_{A2}$ | 0.370 | 0.394 |
| $O_{B1}$ vs $O_{B2}$ | 0.389 | 0.482 |
| $O_{A2}$ vs $O_{B2}$ | 0.351 | 0.456 |

**Table 2** Comparison of the frequency of score values for each category of the Ishak-system [14] after consensus was reached. *A* periportal or periseptal interface hepatitis (maximum possible score *4*), *B* confluent necrosis (*6*), *C* focal lytic necrosis, apoptosis, focal inflammation (*4*), *D* portal inflammation (*4*), and *S* stage of liver fibrosis (*6*)

| Score | Grading | | | | | | | | | | Staging | |
|---|---|---|---|---|---|---|---|---|---|---|---|---|
| | A | | B | | C | | D | | Total score | | S | |
| | TNB (*n*) | LNB (*n*) | TNB (*n*) | LNB (*n*) | TNB (*n*) | LNB (*n*) | TNB (*n*) | LNB (*n*) | TNB (*n*) | LNB (*n*) | TNB (*n*) | LNB (*n*) |
| 0 | 7 | 5 | 55 | 40 | 17 | 6 | 0 | 1 | 0 | 1 | 0 | 6 |
| 1 | 28 | 24 | 0 | 1 | 37 | 35 | 39 | 24 | 5 | 2 | 14 | 8 |
| 2 | 18 | 9 | 0 | 0 | 1 | 0 | 16 | 14 | 8 | 4 | 5 | 4 |
| 3 | 2 | 3 | 0 | 0 | 0 | 0 | 0 | 2 | 17 | 16 | 7 | 5 |
| 4 | 0 | 0 | 0 | 0 | 0 | 0 | 0 | 0 | 17 | 8 | 10 | 6 |
| 5 | | | 0 | 0 | | | | 8 | 6 | 9 | 3 | |
| 6 | | | 0 | 0 | | | | 0 | 3 | 10 | 9 | |
| 7 | | | | | | | | 0 | 1 | | | |
| Total no. of biopsies | 55 | 41 | 55 | 41 | 55 | 41 | 55 | 41 | 55 | 41 | 55 | 41 |
| *p* value | 0.597 | | 0.427 | | 0.091 | | 0.141 | | 0.232 | | 0.108 | |

**Table 4** Intra- ($O_{A1}$ vs $O_{A2}$; $O_{B1}$ vs $O_{B2}$) and interobserver ($O_{A2}$ vs $O_{B2}$) variabilities in grading and staging of chronic viral hepatitis. $O_A$ and $O_B$ denote two independent observers; *1* and *2* denote first and second examination rounds

| Observer | Differences in maximum score of grading | | | | Differences in staging | | | |
|---|---|---|---|---|---|---|---|---|
| | ±0 *n* (%) | ±1 *n* (%) | ≥±2 *n* (%) | Total *n* (%) | ±0 *n* (%) | ±1 *n* (%) | ≥±2 *n* (%) | Total *n* (%) |
| TNB | | | | | | | | |
| $O_{A1}$ vs $O_{A2}$ | 26 (47) | 27 (49) | 2 (4) | 55 (100) | 26 (47) | 24 (44) | 5 (9) | 55 (100) |
| $O_{B1}$ vs $O_{B2}$ | 20 (36) | 25 (45) | 10 (19) | 55 (100) | 27 (49) | 18 (33) | 10 (18) | 55 (100) |
| $O_{A2}$ vs $O_{B2}$ | 24 (44) | 22 (40) | 9 (17) | 55 (100) | 25 (45) | 23 (42) | 7 (12) | 55 (100) |
| LNB | | | | | | | | |
| $O_{A1}$ vs $O_{A2}$ | 18 (44) | 16 (39) | 7 (17) | 41 (100) | 20 (49) | 16 (39) | 5 (12) | 41 (100) |
| $O_{B1}$ vs $O_{B2}$ | 18 (44) | 18 (44) | 5 (12) | 41 (100) | 23 (56) | 18 (44) | 0 | 41 (100) |
| $O_{A2}$ vs $O_{B2}$ | 17 (41) | 19 (46) | 5 (12) | 41 (100) | 22 (54) | 11 (27) | 8 (19) | 41 (100) |

**Table 5** Strength of agreement (kappa values) of all pathological features using Ishak-system ($O_{A2}$ vs $O_{B2}$). $O_A$ and $O_B$ denote two independent observers, *1* and *2* first and second examination rounds, and *N.D.* coefficient not determined

| Category | | TNB | LNB |
|---|---|---|---|
| A | Periportal or periseptal interface hepatitis (piecemeal necrosis) | 0.390 | 0.338 |
| B | Confluent necrosis | N.D. | N.D. |
| C | Focal (spotty) lytic necrosis, apoptosis and focal inflammation | 0.003 | 0.096 |
| D | Portal inflammation | 0.419 | 0.470 |
| S | Fibrosis | 0.351 | 0.456 |

Fragmentation of the specimens was found in a total of 24 biopsies, of which 16 (27%) were obtained by TNB, and eight (20%) by LNB ($p$=0.381). Ten (41%) fragmented specimens showed evidence of advanced fibrosis or cirrhosis (stages 5 or 6).

### Comparison of clinical diagnosis of liver cirrhosis with histological staging

In 38 patients, cirrhosis of the liver was diagnosed clinically; a TNB was obtained from 23 and a LNB from 15 patients. Stage 6 was diagnosed histologically in ten (44%) specimens obtained by TNB and in nine (60%) obtained by LNB. Stage 5 was diagnosed histologically in six (26%) specimens obtained by TNB and in three (20%) obtained by LNB. If stages 5 and 6 are combined, then the difference between specimens obtained by TNB (70%) and LNB (80%) is less apparent. In the remaining patients, the biopsy specimens showed either stage 3 (TNB two patients; LNB two patients) or stage 4 (TNB three patients; LNB one patient).

In two patients only, liver biopsy (TNB in both cases) showed advanced fibrosis (stage 5) with no clinical signs of liver cirrhosis. Finally, in two cases with a clinical diagnosis of liver cirrhosis, the specimens obtained with TNB provided insufficient amounts of tissue to facilitate disease staging (see above).

### Intra- and interobserver variabilities

Table 4 shows the intra- and interobserver variabilities for grading and staging of chronic hepatitis during the first (1) and second (2) examination rounds by observers A and B.

The intraobserver variability was not significantly influenced by the needle size. Observer A ($O_{A1}$ vs $O_{A2}$) and observer B ($O_{B1}$ vs $O_{B2}$) reached similar total scores for grading (ranging from 36% to 47%) and staging (ranging from 47% to 56%) in specimens obtained by TNB and LNB (Table 4). The intraobserver variability improved to at least 81% for both observers when a tolerance of ±1 was accepted for grading (total score) and staging (Table 4).

The interobserver variabilities ($O_{A2}$ vs $O_{B2}$) showed similar results. The same total score for grading was reached in 44% of the specimens obtained with TNB and in 41% of the specimens obtained with LNB, whilst staging was identical in 45% of the specimens obtained with TNB and 54% obtained with LNB. Again, interobserver variability improved to at least 81% when a tolerance of ±1 was accepted for grading (total score) and staging (Table 4).

Table 3 shows the corresponding kappa value and Table 5 shows the Ishak-system [14] summarizing the strength of agreement between TNB and LNB for all pathological features. The intra- and interobserver variabilities showed no significant differences regarding grading and staging between specimens obtained with TNB and those obtained with LNB (Table 3, Table 4, and Table 5).

## Discussion

The aim of the present study was to determine whether grading and staging of chronic viral hepatitis can be ap-

plied to specimens obtained by TNB, which putative limitations it may provide, and which influence it has on intra- and interobserver variability. Disease activity and progression was assessed according to the modified Ishak-system [14].

TNB provided an inadequate amount of tissue in four patients, and only fibrous tissue and no liver parenchyma was obtained. This is related to the needle size. Previously we have shown that TNB bears a greater risk of supplying an inadequate amount of tissue than LNB [23], which repeat sampling may help to overcome.

A comparison of the mean values of the grading categories A, B, C, and D showed no significant differences between TNB and LNB. However, minor differences were apparent by direct comparison. Bridging necrosis (B) was found in a single specimen obtained by LNB; this is probably not related to the needle size, since bridging necrosis is generally a rare observation in chronic hepatitis and is more commonly found in acute hepatitis [3, 5, 18, 27]. The extent of portal inflammation (D) showed a broader range in specimens obtained by LNB (range 0–3) compared with specimens obtained by TNB (range 1–2). Previously we have shown that core biopsies obtained by TNB are significantly longer than those obtained by LNB and that the length of the core biopsy, within a given biopsy group, correlates with the number of portal tracts [23]. Despite being longer, specimens obtained by TNB enclose a significantly smaller number of portal tracts (approximately 6.7) than LNB (approximately 9.7) [23]; this smaller number of portal tracts may influence grading of portal inflammation. In contrast, Westin et al. [27] proposed that less than three portal tracts limits the ability to evaluate chronic hepatitis. Thus the number of portal tracts enclosed may influence grading of portal inflammation; however, this putative difference had no effect on the mean value in our series. Apart from the number of portal tracts, other factors may influence grading and staging. The quality of individual paraffin sections (i.e., staining intensity and thickness of the section) may vary, but this is a non-systematic error affecting both biopsy groups. Finally, we noticed that both observers were more cautious when grading slim or fragmented specimens. The most obvious difference between TNB and LNB is the thickness of the core cylinder, and even blinding against the needle size – as carried out during the whole study – does not exclude a systematic error related to the needle size. Even an inexperienced pathologist learns quickly to differentiate between TNB and LNB specimens.

A comparison of the mean values of staging also showed that both needle sizes facilitated the diagnosis of liver cirrhosis as either probable or definite (stage 6). Further histological patterns commonly observed in advanced liver fibrosis and cirrhosis such as fragmentation, lack of central veins, and presence of a thin rim of collagen, which aid in the evaluation of the stage of the disease, were identified in specimens obtained by both TNB and LNB [4]. The clinical diagnosis of liver cirrhosis is often based on different variables including clinical signs, endoscopic, and ultrasound findings. Most clinical signs are neither specific nor very sensitive [15]. Thus histological evidence of cirrhosis is still the gold standard. We compared the clinical diagnoses of liver cirrhosis with the histological diagnoses in our series. Specimens obtained by TNB and LNB confirmed the clinical diagnosis of liver cirrhosis in 43% and 60% of cases, respectively. Thus, clinical suspicion of cirrhosis was confirmed less commonly in specimens obtained by TNB than by LNB. However this difference was not significant. When clinical diagnoses are compared with histological diagnoses it may be necessary to include stage 5 (incomplete cirrhosis) since this category defines a transition between advanced bridging fibrosis and cirrhosis and hence does not exclude the presence of cirrhosis in a biopsy specimen. Combining categories 5 and 6, the difference between TNB (70%) and LNB (80%) was less apparent, which suggests that at least in some cases TNB bears the risk of underestimating stage 6 as stage 5, while the overall recognition of liver fibrosis was not influenced by the needle size (Table 2). In two cases where cirrhosis was suspected clinically, the amount of tissue obtained by TNB was unsatisfactory. The cylinder enclosed only fibrous tissue and no liver parenchyma. Therefore, although liver cirrhosis was likely to be present, it escaped definitive histological diagnosis in the biopsy specimen. One of these two patients subsequently underwent liver resection and cirrhosis was confirmed in the resection specimens.

The observer variability is a measure of the reliability and reproducibility of a diagnostic procedure. In 1994, the ‘‘French METAVIR Cooperative Study Group’’ [1] showed that one observer is sufficient to assess general pathological features of chronic hepatitis, such as fibrosis, piecemeal necrosis, and overall disease activity. However, dual observation is needed for more in-depth studies, such as characterization of specific features of chronic hepatitis or numerical scoring. Agreement exists when two observers give the same score for a given case. In this respect, the agreement in grading and staging of chronic hepatitis showed no significant differences between TNB and LNB and was found to be approximately 45%. On first sight, this appears to be a low figure for both techniques. Comparing both needle sizes, we obtained similar, but relatively lower values of kappa for TNB and LNB specimens. A possible reason for these low kappa values is that the level of experience of the pathologists may have influenced observer variations. The highest kappa values were obtained for portal inflammation and interface hepatitis where the category definitions are relatively clear. Low kappa values were obtained for focal necrosis, which in the Ishak-system [14] is defined as the number of necroinflammatory foci. When judging focal necrosis, inflammation, and apoptosis, a point of potential disagreement is the absence of a practical definition for the term ‘‘focus’’ in the Ishak-system [14]. However, this raises the question of what difference in the total score is clinically significant. Scheuer et al. [24] considered semi-quantitative scoring systems to be of limited use, and the addition of individ-

ual categories to a total score may be misleading. However, like ourselves, Westin et al. [27] used the Ishak-system [14] and tolerated a difference in the interobserver variability of ±1 for each category (A, B, C, or D). In our series, if an observer variability of ±1 is tolerated for the total score, then agreement is reached in 80% of patients for both TNB and LNB. Thus, specimens obtained by TNB and LNB show no significant differences in reliability and reproducibility in grading and staging of chronic hepatitis.

Our results do not support the notion that TNB, in general, is unsuitable for grading and staging of chronic viral hepatitis. Both, TNB and LNB are similarly sensitive to intra- and interobserver variability, which is influenced by the scoring system applied and, as shown here, not by the needle size. Each biopsy procedure is biased by the putative risk of a sampling error. The sample obtained may not be representative for the organ and disease under investigation. For this reason it has become common practice in diagnostic surgical pathology of the stomach and colon to obtain multiple biopsies. As yet, no specific sampling procedure has been developed for the liver covering the putative heterogeneous distribution of a diffuse liver disease. In this respect, TNB of the liver applied by an experienced clinician may be an advantage over LNB. The small needle size of TNB is associated with a decreased risk of complications and may thus be superior in obtaining biopsy specimens from different organ sites, providing a more representative sampling. TNB appears to bear the risk of underestimating liver cirrhosis (stage 6), but the question is whether this difference is clinically relevant as long as stage 5 (incomplete cirrhosis) is noted, and the histopathological report points out that this does not exclude complete cirrhosis.

Some potential limitations may have influenced our results. TNB and LNB were not obtained from the same patients and selection was not randomized. The clinical data from our two patient groups (TNB vs LNB) differed in platelet count and serum transferase levels. In the TNB group, the platelet count was significantly lower than in the LNB group. However, there is not enough evidence to suggest that the platelet count in chronic liver disease is correlated with histological signs of disease activity or progression. The serum levels of both transferases (ALT and AST) are significantly higher in the TNB group than in the LNB group. In patients with chronic hepatitis, the serum transferases show characteristic episodic fluctuations, and serum levels are usually lower in patients with longstanding disease. The correlation between serum transferases and extent of disease is still a matter of debate. Some authors have found correlations [8, 22, 25], while others have not [11, 12, 19]. Even in advanced and aggressive liver disease, serum ALT can be within normal limits [6]. Thus, the significant differences in platelet count and serum transferases may indicate a case selection bias, but had no influence on inter- and intraobserver variablity.

In conclusion, we demonstrate here that specimens obtained by TNB (20G) can be used for grading and staging of chronic viral hepatitis. However, they bear a risk in providing an inadequate amount of tissue and of underestimating the presence of liver cirrhosis in favor of advanced bridging fibrosis. Further studies will have to investigate the representativeness of TNB specimens for disease activity and stage by comparing paired biopsies (TNB and LNB) obtained from the same patients and whether multiple sampling with TNB is advantageous over single biopsies using LNB.

## References


1. Bedossa P (1994) Intraobserver and interobserver variations in liver biopsy interpretation in patients with chronic hepatitis C. The French METAVIR Cooperative Study Group. Hepatology 20:15–20
2. Bortz J, Lienert GA, Boehnke K (ed) (1990) Verteilungsfreie Methoden in der Biostatistik. Springer Berlin Heidelberg New York.
3. Boyer JL, Klatskin G (1970) Pattern of necrosis in acute viral hepatitis. Prognostic value of bridging (subacute hepatic necrosis). N Engl J Med 283:1063–1071
4. Chevallier M, Guerret S, Chossegros P, Gerard F, Grimaud JA (1994) A histological semiquantitative scoring system for evaluation of hepatic fibrosis in needle liver biopsy specimens: comparison with morphometric studies. Hepatology 20:349–355
5. Cooksley WG, Bradbear RA, Robinson W, Harrison M, Halliday JW, Powell LW, Ng HS, Seah CS, Okuda K, Scheuer PJ (1986) The prognosis of chronic active hepatitis without cirrhosis in relation to bridging necrosis. Hepatology 6:345–348
6. Di Bisceglie AM (1999) Chronic hepatitis C viral infection in patients with normal serum alanine aminotransferases. Am J Med 107:53S–55S
7. Edoute Y, Tibon-Fisher O, Ben Haim S, Malberger E (1992) Ultrasonically guided fine-needle aspiration of liver lesions. Am J Gastroenterol 87:1138–1141
8. Fanning L, Kenny E, Sheehan M, Cannon B, Whelton M, O'Connell J, Collins JK, Shanahan F (1999) Viral load and clinicopathological features of chronic hepatitis C (1b) in a homogeneous patient population. Hepatology 29:904–907
9. Gebel M, Horstkotte H, Koster C, Brunkhorst R, Brandt M, Atay Z (1986) Ultrasound-guided fine needle puncture of the abdominal organs: indications, results, risks. Ultraschall Med 7:198–202
10. Glaser J, Pausch J (1995) The risk of liver biopsy. Z Gastroenterol 33:673–676
11. Haber MM, West AB, Haber AD, Reuben A (1995) Relationship of aminotransferases to liver histological status in chronic hepatitis C. Am J Gastroenterol 90:1250–1257
12. Healey CJ, Chapman RW, Fleming KA (1995) Liver histology in hepatitis C infection: a comparison between patients with persistently normal or abnormal transaminases. Gut 37:274–278
13. Holtkamp W, Theilmeier A, Droese M, Ebert R, Reis HE (1990) Ultrasonically guided fine-needle puncture. The limits of the method in the abdomen and retroperitoneal space. Dtsch Med Wochenschr 115:809–812
14. Ishak K, Baptista A, Bianchi L, Callea F, De Groote J, Gudat F, Denk H, Desmet V, Korb G, MacSween RN, Phillips MJ, Portman BG, Poulsen H, Scheuer PJ, Schmid M, Thaler H (1995) Histological grading and staging of chronic hepatitis. J Hepatol 22:696–699
15. Kutcher R, Smith GS, Sen F, Gelman SF, Mitsudo S, Thung SN, Reinus JF (1998) Comparison of sonograms and liver histologic findings in patients with chronic hepatitis C virus infection. J Ultrasound Med 17:321–325

16. Landis JR, Koch GG (1977) The measurement of observer agreement for categorical data. Biometrics 33:159–174
17. Lindor KD, Bru C, Jorgensen RA, Rakela J, Bordas JM, Gross JB, Rodes J, McGill DB, Reading CC, James EM, Charboneau JW, Ludwig J, Batts KP, Zinsmeister AR (1996) The role of ultrasonography and automatic-needle biopsy in outpatient percutaneous liver biopsy. Hepatology 23:1079–1083
18. MacSween RN (1980) Pathology of viral hepatitis and its sequelae. Clin Gastroenterol 9:23–45
19. McCormick SE, Goodman ZD, Maydonovitch CL, Sjogren MH (1996) Evaluation of liver histology, ALT elevation, and HCV RNA titer in patients with chronic hepatitis C. Am J Gastroenterol 91:1516–1522
20. Menghini G (1970) One-second biopsy of the liver--problems of its clinical application. N Engl J Med 283:582–585
21. Pasha T, Gabriel S, Therneau T, Dickson ER, Lindor KD (1998) Cost-effectiveness of ultrasound-guided liver biopsy. Hepatology 27:1220–1226
22. Reedy DW, Loo AT, Levine RA (1998) AST/ALT ≥1 is not diagnostic of cirrhosis in patients with chronic hepatitis C. Dig Dis Sci 43:2156–2159
23. Röcken C, Meier H, Klauck S, Wolff S, Malfertheiner P, Roessner A (2001) Large needle biopsy versus thin needle biopsy in diagnostic pathology of liver diseases. Liver 21:391–397
24. Scheuer PJ (1997) Chronic hepatitis: what is activity and how should it be assessed? Histopathology 30:103–105
25. Sheth SG, Flamm SL, Gordon FD, Chopra S (1998) AST/ALT ratio predicts cirrhosis in patients with chronic hepatitis C virus infection. Am J Gastroenterol 93:44–48
26. Weiss H, Weiss A, Scholl A (1988) Fatal complication of fine-needle biopsy of the liver. Dtsch Med Wochenschr 113:139–142
27. Westin J, Lagging LM, Wejstal R, Norkrans G, Dhillon AP (1999) Interobserver study of liver histopathology using the Ishak score in patients with chronic hepatitis C virus infection. Liver 19:183–187
28. Wrba F, Renner F (1998) Recommendations for clinicopathologic quality standards in gastroenterology and hepatology. Consensus report of the Austrian Society of Gastroenterology ahd Hepatology and the Austrian Society of Pathology. Z Gastroenterol 36:917–923

Virchows Arch (2003) 442:245–251
DOI 10.1007/s00428-002-0743-5

ORIGINAL ARTICLE

**Paweł Surowiak · Piotr Dzięgiel · Rafał Matkowski
Mirosław Sopel · Andrzej Wojnar · Jan Kornafel
Maciej Zabel**

# Prognostic value of immunocytochemical determination of parathyroid hormone-related peptide expression in cells of mammary ductal carcinoma. Analysis of 7 years of the disease course

Received: 15 August 2002 / Accepted: 1 November 2002 / Published online: 25 January 2003
© Springer-Verlag 2003

**Abstract** Parathyroid hormone-related peptide (PTHrP) participates in the development of humoral hypercalcaemia of malignancy. The peptide is thought to affect growth and differentiation of normal and neoplastic cells. The present study aimed at evaluation of the relationship between survival time and development of distant metastases in patients with ductal mammary carcinoma on the one hand and PTHrP expression on the other. Immunocytochemical reactions using mouse monoclonal (clone 212–10.7) anti-PTHrP (38–64) antibodies were performed in paraffin sections originating from 47 patients with ductal mammary carcinoma. Expression of the protein was quantified employing a scale, considering the number of positive cells and intensity of the reaction (immunoreactive score, IRS). Survival time of the patients, determined during the course of a 7-year observation was also analysed. The obtained results demonstrated a relationship between intensity of PTHrP expression and the survival time. Patients with high expression of PTHrP (IRS>6) manifested longer survival than patients with lower PTHrP expression (IRS≤6; Cox'es *F* test, $P<0.05$). Moreover, in the group with the lower PTHrP expression, a negative relationship was detected between expression of the protein and the survival time (Cox'es model, $P<0.05$). No relationship was detected between PTHrP expression and the development of distant metastases.

**Keywords** Mammary carcinoma · Parathyroid hormone-related peptide · Immunocytochemistry

P. Surowiak (✉) · P. Dzięgiel · M. Sopel · M. Zabel
Department of Histology and Embryology,
University School of Medicine,
ul.Cha ubińskiego 6a, 50–356 Wroc aw, Poland
e-mail: pawel.surowiak@interia.pl
Tel.: +4871-784-0081, Fax: +4871-784-0082

R. Matkowski · J. Kornafel
Department of Gynaecological Oncology,
University School of Medicine, Wroc aw, Poland

A. Wojnar
Institute of Pathomorphology,
Lower Silesian Oncology Centre, Wroc aw, Poland

M. Zabel
Department of Histology and Embryology,
University of Medical Sciences,
Poznań, Poland

## Introduction

Parathyroid hormone-related peptide (PTHrP) was identified in 1987 in the course of studies on humoral hypercalcaemia of malignancy. It was isolated from tumour cells and, originally, it was suggested to play role in the control of calcium turnover [4]. The *PTHrP* gene consists of nine exons [10]. The process of alternate splicing of mRNA for PTHrP yields three different mRNAs that code three distinct proteins (1–139, 1–141, 1–173) of a common N-terminal sequence consisting of 139 amino acids, but of different C-terminal fragments [19, 20]. Numerous studies have demonstrated that a recombined PTHrP (1–34) induces hypercalcaemia and bone resorption, stimulates phosphate transport and augments cAMP synthesis in kidneys and in bone cells [32]. The fragment also is responsible for physiological function of PTHrP [25]. The fragment 67–86 stimulates transport of calcium ions across the placenta from the mother to her foetus [1]. The so-called osteostatin (107–111) acts antagonistically to the fragment 1–34, i.e. it inhibits activity of osteoclasts [7, 8].

Many studies demonstrated expression of the protein in several normal tissues, including mammary gland, skin, myocardium, kidneys, testes, pancreas, brain, uterus, etc. [12, 21, 27, 33, 35, 40]. The hormone was found to be present already at the morula stage of embryos [34]. Deletion of the *PTHrP* gene has lethal consequences [16]. The protein is also produced by endothelial cells and participates in the control of smooth muscle tonus in

**Table 1** Evaluation of the reaction results using the immunoreactive score scale. Final result represents the product of scores in the two columns

| Percentage of cells with positive reaction | | Intensity of the colour reaction | |
|---|---|---|---|
| No cells with positive reaction | 0 | No colour reaction | 0 |
| <10% cells with positive reaction | 1 | Low intensity colour reaction | 1 |
| 10–50% cells with positive reaction | 2 | Moderate intensity of colour reaction | 2 |
| 51–80% cells with positive reaction | 3 | High intensity of colour reaction | 3 |
| >81% cells with positive reaction | 4 | | |

vascular walls, uterus, stomach, intestines and urinary bladder [22, 23, 24]. In the course of lactation, it participates in milk ejection [30]. Human and cow milk contain significant amounts of PTHrP [3]. Liapis et al. reported that PTHrP expression in the milk gland increased during the course of lactation and was augmented in adenosis and simple or atypical hyperplasia relative to healthy epithelium [18]. The presence of PTHrP was noted in 60% normocalcaemic cases of breast carcinoma [31] but a significantly higher expression of the hormone can be detected in cases with metastases to bones [11]. Divergent opinions prevail as to the prognostic significance of PTHrP expression in cells of breast carcinoma. Yoshida et al. reported that the intensity of the hormone manifestation was closely related to advancement of the tumour and reflected a less favourable prognosis [38]. However, Kissin et al. observed no correlation between PTHrP expression and survival of the patients [17].

Also in cases of colonic and prostate carcinomas, PTHrP expression was reported to exhibit correlation with development of bone metastases [2, 29].

PTHrP is suggested to play role in the control of cell growth and differentiation. In cultures of human keratinocytes, the protein was found to exert anti-proliferative and pro-differentiation function [14, 15]. In studies on cell lines, mitogens such as epidermal growth factor or insulin-like growth factor augment expression of PTHrP [36]. The phenomenon resembles expression control in cell cycle engaged genes, such as, e.g. *c-myc*. Studies on transgenic mice showed that PTHrP overexpression in epithelial cells of mammary gland ducts induced hypoplasia of the organ [30]. Experiments performed on cultures of colon carcinoma cells demonstrated that PTHrP overexpression augmented adhesion of the cells to type-I collagen, which might indicate a certain role of the protein in development of metastases [37].

The present study aimed at evaluation of the relationship between survival time and development of distant metastases in patients with ductal mammary carcinoma at the G2 grade of tumour cell differentiation and the second stage of clinical advancement on the one hand and PTHrP expression on the other.

## Materials and methods

The studies were performed on samples of ductal mammary carcinoma of the histological grade – G2, originating from 47 patients, who underwent surgery in 1993–1994 at the Lower-Silesian Centre of Oncology in Wroclaw. All the patients manifested the second stage of clinical advancement of the tumour. At the first stage of the therapy, all the patients underwent mastectomy using Patey's procedure. Subsequently, they were treated with tamoxifen. The patients were periodically subjected to clinical, radiological and ultrasonographic control.

Samples of the studied cancers were fixed in 10% buffered formalin and then, embedded in paraffin. The preparations were stained with haematoxylin and eosin and evaluated histopathologically. In all the studied cases, sections were incubated with mouse monoclonal (clone 212–10.7) antibodies against epitope 38–64 of human parathyroid hormone-related peptide (Calbiochem, CA), biotinylated antibodies, streptavidin-biotinylated peroxidase (ABC) (LSAB2, Dako, Denmark), and activity of the latter was estimated using DAB (Dako, Denmark). Deparaffinised sections were digested with neuraminidase (Calbiochem, CA) to unblock antigenic determinants. In each case, the negative control was included with Primary Negative Control (Dako, Denmark) and then LSAB2 and DAB. Intensity of the immunocytochemical procedure was evaluated using the immunoreactive score (IRS) according to Remmele [26]. The applied scale took into account both intensity of the colour reaction and percentage of cells that exhibited the positive reaction. Final result represented the product of the two parameters and its values ranged between 0 and 12 (Table 1).

Survival of the patients, determined during 7-year observations, was also analysed. The relationship was analysed between survival time (expressed in quarter units) and expression of the protein. In order to define correlation between studied variables, Cox'ex model was employed. The relationship between intensity of PTHrP expression and a number of relapses was examined using the Kruskall-Wallis test since the number of relapses in our studies involved one of four values only (0–3). The relationship between PTHrP expression and survival time was tested also using Kaplan-Meier analysis. In the statistical analysis of the results, the Statistica software was used.

## Results

The mean age of the studied patients was 60.39± 10.18 years. Clinical analysis of the studied patients documented the death of 12 patients. Distant metastases developed in 9 patients, and 6 of the patients died. In 5 patients, the metastases were localised in bones and 4 of the patients carried also metastases in other organs/tissues. Following surgery, all the patients were treated with tamoxifen. In 13 cases, radiotherapy was also employed. As already mentioned in the Introduction, all the studied tumours demonstrated differentiation of G2 grade and the second stage of clinical advancement (TNM) (Table 2 and Table 3).

The immunocytochemical tests demonstrated variable intensity of reactions in individual tumours (Fig. 1a, b). Mean expression of PTHrP was 6.36±3.26. The studies demonstrated absence of direct correlations between pa-

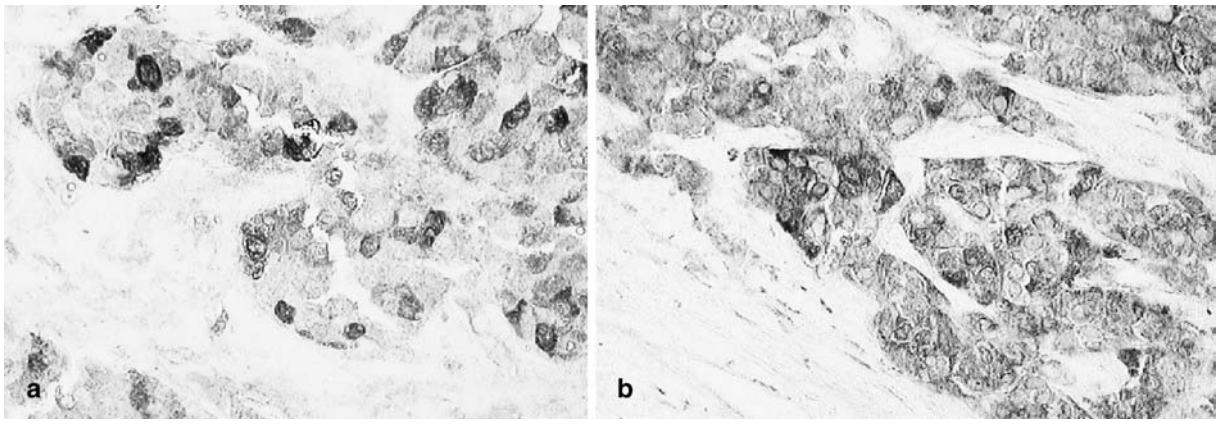
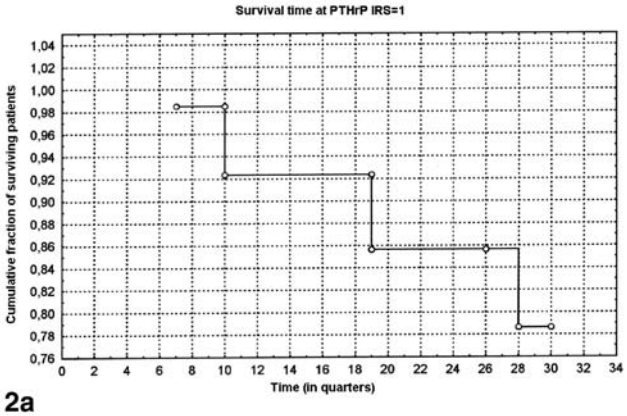


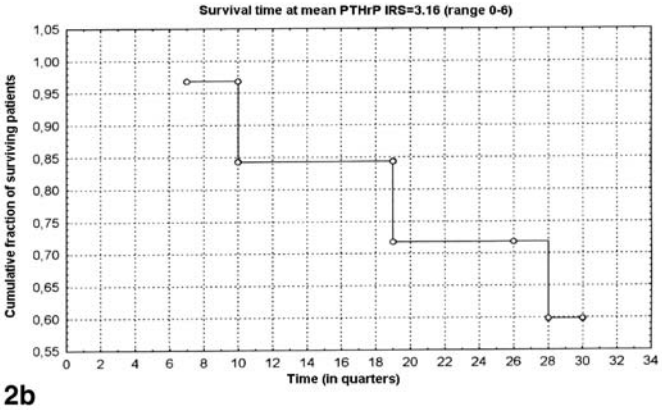

**Fig. 1a, b** Examples of variable intensity of parathyroid hormone-related peptide expression in mammary carcinoma cells (**a**, **b**: ×200)

**Table 2** Clinical data on the studied group of patients. + alive, – deceased, *0–3* number of metastases

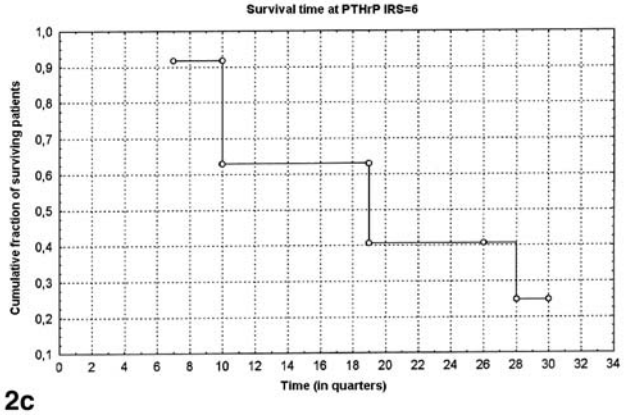
| Patient no. | PTHrP (IRS) | Age (years) | Alive/deceased | Metastases | I – metastasis | II – metastasis | III – metastasis |
|---|---|---|---|---|---|---|---|
| 1 | 2 | 69 | + | 0 | – | – | – |
| 2 | 12 | 72 | + | 0 | – | – | – |
| 3 | 9 | 52 | + | 0 | – | – | – |
| 4 | 12 | 69 | + | 0 | – | – | – |
| 5 | 9 | 78 | – | 2 | Liver | Bones | – |
| 6 | 4 | 82 | – | 3 | Liver | 2nd breast | Left groin |
| 7 | 6 | 59 | – | 2 | Bones | Lungs | – |
| 8 | 4 | 58 | + | 0 | – | – | – |
| 9 | 9 | 82 | + | 0 | – | – | – |
| 10 | 9 | 72 | + | 0 | – | – | – |
| 11 | 8 | 43 | + | 0 | – | – | – |
| 12 | 12 | 48 | + | 0 | – | – | – |
| 13 | 6 | 54 | + | 0 | – | – | – |
| 14 | 8 | 55 | + | 1 | Scar | – | – |
| 15 | 3 | 67 | – | 3 | Bones | Skin | Lungs |
| 16 | 12 | 60 | + | 0 | – | – | – |
| 17 | 12 | 63 | + | 0 | – | – | – |
| 18 | 0 | 63 | + | 0 | – | – | – |
| 19 | 4 | 74 | – | 0 | – | – | – |
| 20 | 0 | 50 | + | 0 | – | – | – |
| 21 | 8 | 72 | + | 0 | – | – | – |
| 22 | 6 | 80 | – | 0 | – | – | – |
| 23 | 9 | 65 | + | 0 | – | – | – |
| 24 | 9 | 53 | – | 1 | Liver | – | – |
| 25 | 6 | 54 | + | 0 | – | – | – |
| 26 | 2 | 48 | + | 0 | – | – | – |
| 27 | 2 | 67 | + | 0 | – | – | – |
| 28 | 0 | 44 | + | 0 | – | – | – |
| 29 | 2 | 49 | + | 0 | – | – | – |
| 30 | 0 | 53 | + | 0 | – | – | – |
| 31 | 8 | 49 | + | 0 | – | – | – |
| 32 | 6 | 62 | + | 0 | – | – | – |
| 33 | 9 | 70 | – | 2 | Liver | Bones | – |
| 34 | 9 | 49 | + | 1 | – | – | – |
| 35 | 9 | 68 | + | 0 | – | – | – |
| 36 | 9 | 76 | + | 0 | – | – | – |
| 37 | 6 | 64 | + | 0 | – | – | – |
| 38 | 2 | 48 | + | 0 | – | – | – |
| 39 | 2 | 79 | – | 0 | – | – | – |
| 40 | 2 | 48 | + | 0 | – | – | – |
| 41 | 9 | 69 | + | 2 | 2nd breast | Lungs | – |
| 42 | 8 | 48 | + | 1 | Bones | – | – |
| 43 | 12 | 44 | + | 0 | – | – | – |
| 44 | 6 | 48 | – | 0 | – | – | – |
| 45 | 2 | 49 | – | 0 | – | – | – |
| 46 | 12 | 65 | + | 0 | – | – | – |
| 47 | 2 | 47 | – | 0 | – | – | – |
| Medium | 6.36±3.26 | 60.39±10.18 | | | | | |



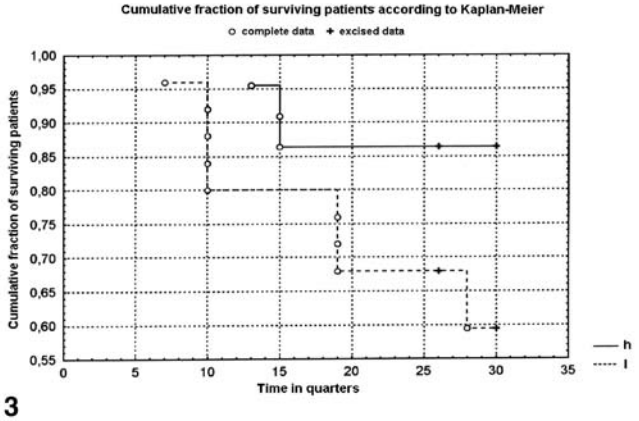

2a




2b




2c




3

**Fig. 2a–c** Examples of Kaplan–Meier's patient survival curves in group l, demonstrating the following parathyroid hormone-related peptide (PTHrP) expression intensity: **a** IRS=1, **b** IRS=3–16 (mean expression in group l), **c** IRS=6. In the subgroup A 78% patients, in subgroup B 60% patients and in subgroup C only 25% patients survived till the 28th quarter

**Fig. 3** Kaplan–Meier's analysis of relationship between intensity of parathyroid hormone-related peptide (PTHrP) expression (IRS) and survival of patients (in quarters of a year) in patients of l group, with low expression of the protein (IRS 0–6) and in patients of h group, with high PTHrP expression (IRS>6)

tient survival time and intensity of PTHrP expression (Cox'es model: $Chi^2$=0.72, *P*=0.39). In order to examine the relationship between PTHrP expression, expressed in the scale of 0–12, and patient survival time, subgroups of the studied cases were formed, one including patients with low PTHrP expression (IRS≤6, 22 patients), designated "l" and the other including patients with high PTHrP expression (IRS>6, 25 patients), designated "h".

The so-distinguished groups were subjected to statistical analysis. Computations employing the Cox'es model of proportional hazard demonstrated that low expression of PTHrP in the former group was related to patients' survival ($Chi^2$=4.01, *P*=0.045), and the beta exponent for the group amounted to 0.35. No such relationship could be detected in the group of patients with high PTHrP expression (Cox'es model: 2=0.61, *P*=0.43, beta exponent: –0.31).

In order to illustrate better the relationship between intensity of PTHrP expression and survival time in group I, calculations were performed using the Kaplan-Meier's analysis. Mean survival was examined for PTHrP of IRS=1, IRS=6 and for IRS=3.16, the mean value for group I. At IRS=1, 78% of patients survived 30 quarters, at IRS=3.16 only 60% patients survived such a period, while at IRS=6 only 25% patients survived the period (Fig. 2a, b, c).

Subsequently, mean survival of patients was compared in the groups l and h. Cox'es *F* test as well as Kaplan-Meier analysis demonstrated that mean survival time in the group of patients with high PTHrP expression exceeded that in the group with low expression of the protein (*P*=0.03, Fig. 3).

At the subsequent stage of statistical analysis, the relationship was examined between intensity of PTHrP expression and development of distant metastases. In the calculations, metastases to bones were not taken into account. The Kruskall-Wallis test demonstrated no relationship between PTHrP expression and the number of relapses (*n*=47, H=3.34, *P*=0.34). Regression of the Cox'es proportional hazard documented no relationship between PTHrP expression and the relapse-free survival time of the patients, measured in quarters ($Chi^2$=0.11, df=1, *P*=0.74).

The model of logistic regression demonstrated no relationship between intensity of PTHrP expression and development of metastases to bones ($Chi^2$=0.87, df=1, *P*=0.35).

**Table 3** Clinical data on the studied group of patients. *ca. ductale* ductal carcinoma, *G* grade of differentiation, *P* mastectomy according to Patey, *T* tamoxifen, *rtg* radiotherapy

| Patient no. | Diagnosis | G | T | T (cm) | N | N (cm) | M | I therapy | II therapy | III therapy |
|---|---|---|---|---|---|---|---|---|---|---|
| 1 | ca. ductale | 2 | 2 | 4 | 1 | 1 | 0 | P | T | rtg |
| 2 | ca. ductale | 2 | 1 | 1.5 | 1 | 1 | 0 | P | T | – |
| 3 | ca. ductale | 2 | 2 | 3 | 1 | 1 | 0 | P | T | – |
| 4 | ca. ductale | 2 | 2 | 3 | 0 | – | 0 | P | T | – |
| 5 | ca. ductale | 2 | 2 | 3.5 | 1 | 1.5 | 0 | P | T | rtg |
| 6 | ca. ductale | 2 | 1 | 2 | 1 | 1 | 0 | P | T | – |
| 7 | ca. ductale | 2 | 2 | 3 | 0 | – | 0 | P | T | rtg |
| 8 | ca. ductale | 2 | 2 | 3 | 1 | 1 | 0 | P | rtg | T |
| 9 | ca. ductale | 2 | 2 | 3 | 1 | 1 | 0 | P | T | – |
| 10 | ca. ductale | 2 | 2 | 2.5 | 0 | – | 0 | P | T | – |
| 11 | ca. ductale | 2 | 2 | 3 | 1 | 1 | 0 | P | T | rtg |
| 12 | ca. ductale | 2 | 2 | 3 | 1 | 1 | 0 | P | T | – |
| 13 | ca. ductale | 2 | 2 | 4 | 1 | 1 | 0 | P | T | – |
| 14 | ca. ductale | 2 | 2 | 4 | 1 | 1 | 0 | P | rtg | T |
| 15 | ca. ductale | 2 | 2 | 4 | 1 | 2 | 0 | P | T | rtg |
| 16 | ca. ductale | 2 | 2 | 3 | 1 | 1 | 0 | P | T | rtg |
| 17 | ca. ductale | 2 | 2 | 3.5 | 1 | 1 | 0 | P | T | rtg |
| 18 | ca. ductale | 2 | 2 | 5 | 1 | 1 | 0 | P | T | – |
| 19 | ca. ductale | 2 | 2 | 3.5 | 1 | 1 | 0 | P | T | rtg |
| 20 | ca. ductale | 2 | 2 | 4.5 | 0 | – | 0 | P | T | – |
| 21 | ca. ductale | 2 | 2 | 2.3 | 0 | – | 0 | P | T | – |
| 22 | ca. ductale | 2 | 2 | 4 | 0 | – | 0 | P | rtg | T |
| 23 | ca. ductale | 2 | 2 | 5 | 1 | 1 | 0 | P | rtg | T |
| 24 | ca. ductale | 2 | 2 | 2.5 | 1 | 2 | 0 | P | T | rtg |
| 25 | ca. ductale | 2 | 2 | 4 | 1 | 2 | 0 | P | T | – |
| 26 | ca. ductale | 2 | 2 | 4 | 1 | 1 | 0 | P | T | – |
| 27 | ca. ductale | 2 | 2 | 4 | 1 | 1 | 0 | P | T | – |
| 28 | ca. ductale | 2 | 2 | 4.5 | 0 | – | 0 | P | T | – |
| 29 | ca. ductale | 2 | 2 | 5 | 1 | 1 | 0 | P | T | – |
| 30 | ca. ductale | 2 | 2 | 4.5 | 0 | – | 0 | P | T | – |
| 31 | ca. ductale | 2 | 2 | 3 | 1 | 1 | 0 | P | T | – |
| 32 | ca. ductale | 2 | 2 | 4 | 1 | 1 | 0 | P | T | – |
| 33 | ca. ductale | 2 | 2 | 2.5 | 1 | 2 | 0 | P | T | – |
| 34 | ca. ductale | 2 | 2 | 4 | 1 | 1 | 0 | P | T | – |
| 35 | ca. ductale | 2 | 2 | 3 | 1 | 1 | 0 | P | T | rtg |
| 36 | ca. ductale | 2 | 2 | 2.5 | 0 | – | 0 | P | T | rtg |
| 37 | ca. ductale | 2 | 2 | 4 | 1 | 1 | 0 | P | T | rtg |
| 38 | ca. ductale | 2 | 2 | 4 | 1 | 1 | 0 | P | T | – |
| 39 | ca. ductale | 2 | 2 | 3.5 | 1 | 1 | 0 | P | T | – |
| 40 | ca. ductale | 2 | 2 | 5 | 1 | 1 | 0 | P | T | – |
| 41 | ca. ductale | 2 | 2 | 2.5 | 1 | 1 | 0 | P | T | – |
| 42 | ca. ductale | 2 | 2 | 3 | 1 | 1 | 0 | P | T | – |
| 43 | ca. ductale | 2 | 2 | 3 | 0 | – | 0 | P | T | – |
| 44 | ca. ductale | 2 | 2 | 4 | 0 | – | 0 | P | rtg | T |
| 45 | ca. ductale | 2 | 2 | 3.5 | 1 | 1 | 0 | P | T | rtg |
| 46 | ca. ductale | 2 | 1 | 1.5 | 1 | 1 | 0 | P | T | – |
| 47 | ca. ductale | 2 | 2 | 3.5 | 1 | 1 | 0 | P | T | rtg |

## Discussion

Statistical analysis has failed to detect any relationship between PTHrP expression and development of metastases to bones. This observation contradicts several publications [5, 6], the authors of which have demonstrated a clear-cut positive correlation between PTHrP manifestation and tumour's capacity to form metastases to bones. Most probably, this reflects the fact that in the group we have studied bone metastases that have developed in five cases only.

The performed studies also have failed to document a relationship between intensity of PTHrP expression and development of distant metastases, either when the number of metastases or when the time of their development was analysed. The result contradicts the hypothesis advanced following studies on cultured cells of colon carcinoma. In the studies, overexpression of PTHrP promoted adhesion of the cells to type-I collagen and the phenomenon has been linked to effects of PTHrP expression on metastatic spread [37]. In our studies, in which a 7-year clinical course of patients with mammary carcinoma was analysed, no relationship has been disclosed between manifestation of the protein on the one hand and the number or timing of metastases on the other. Such results might have reflected the highly uniform character of the studied group with respect to histological differentiation and clinical advancement, which still remain the principal denominators of prognosis [9].

The obtained results have shown that the relationship between PTHrP expression intensity and survival time of the patients has varied depending on the level of expression. Cases that exhibited higher expression (IRS>6) of the protein survived longer that those that expressed less PTHrP (IRS≤6). Surprisingly, the two groups examined independently of each other showed distinct types of relationship with survival time. In the l group, higher expression of the studied hormone has proven to be associated with worse prognosis. However, in the h group, no relationship could have been detected between PTHrP expression intensity and the survival time. The probable explanation of the phenomenon may involve distinct effects exerted on cell biology by the protein expressed in the cell in physiological quantities relative to effects of the overexpressed protein. This may be exemplified by overexpression of HER-2 protein or P-glycoprotein, which represent prognostically unfavourable factors only when overexpressed in the cell [28, 39]. In the case of PTHrP, a reciprocal effect can be noted: overexpression of the protein (group h, IRS>6) is a prognostically favourable factor. This is probably linked to anti-proliferative and pro-differentiative effects of the hormone, more intense than that observed in physiological circumstances [14, 15]. The observed phenomenon may be related to observations of transgenic mice in which overexpression of PTHrP was found to induce aplasia of the mammary gland [30]. This confirms also the anti-proliferative effect of PTHrP overexpression on mammary gland epithelial cells. It has been shown that mammary carcinomas may be accompanied by augmented expression of receptor of the tyrosine kinase group, mainly HER-2 and EGFR. The augmented expression is thought to be associated with unequivocally unfavourable prognosis [13, 28]. For our considerations, this seems significant since expression of PTHrP in cells has been found to become more intense under effects of ligands of the receptors (EGF, IGF-1). Possibly, the longer survival in cases associated with more intense PTHrP expression may result from inhibition by the hormone of tyrosine kinase function due to negative-feedback effects.

The negative correlation between survival time and PTHrP expression in the I group remains difficult to explain. Yoshida et al. documented the reciprocal correlation between intensity of the hormone manifestation and survival time but this pertained to the entire group of patients and not only among patients with lower PTHrP expression [38]. One of the possible causes of the divergent results of ours might involve the fact that the quoted author examined cases of various grades of differentiation while our material comprised only G2 cases. Moreover, Yoshida et al. detected a positive correlation between PTHrP expression extent and grade of differentiation. Their results might have reflected uniform character of the studied group. They have noted higher concentrations of the studied protein in less differentiated cases and, according to the College of American Pathologists [9], grade of differentiation represents one of the most significant and best recognised prognostic indices. Thus, the variable might have affected the final result of statistical calculations. Studies performed on a more uniform group of patients allow detection of more subtle relationships.

The negative correlation between intensity of PTHrP expression and survival time in group l may be explained by co-expression of PTHrP and of the receptor for the hormone on prostate carcinoma cells, described by Bryden et al. [2]. This suggests a potential for autocrine stimulation which may disturb function of other systems of growth regulation.

## References


1. Abbas SK, Ratclife WA, Moniz C, Dixit M, Caple IW, Silver M, Fowden A, Care AD (1994) The role of parathyroid hormone-related protein in calcium homeostasis in the fetal pig. Exp Physiol 79:527–536
2. Bryden AA, Hoyland JA, Freemont AJ, Clarke NW, George NJ (2002) Parathyroid hormone related peptide and receptor expression in paired primary prostate cancer and bone metastases. Br J Cancer 86:322–325
3. Budayr AA, Halloran BP, King JC, Diep D, Nissenson RA, Strewler GJ (1988) High levels of parathyroid hormone-like protein in milk. Proc Natl Acad Sci U S A 86:7183–7185
4. Burtis WJ, Wu T, Bunch C, Wysolmerski JJ, Insogna KL, Weir EC (1987) Identification of a novel 17,000-dalton parathyroid hormone like adenylate cyclase-stimulating protein from a tumor associated with humoral hypercalcemia of malignancy. J Biol Chem 262:7151–7156
5. Chirgwin JM, Guise TA (2000) Molecular mechanisms of tumor-bone interactions in osteolytic metastases. Crit Rev Eukaryot Gene Exp 10:159–178
6. Diel IJ (2001) Prognostic factors for skeletal relapse in breast cancer. Cancer Treat Rev 27:153–157
7. Fenton AJ, Kemp BE, Kent GM, Mosseley JM (1991) A carboxyl-terminal peptide from the parathyroid hormone-related protein inhibits bone resorption by osteoclasts. Endocrinology 129:1762–1768
8. Fenton AJ, Martin TJ, Nicholson GC (1994) Carboxyl-terminal parathyroid hormone-related protein inhibits bone resorption by isolated chicken osteoclasts. J Bone Miner Res 9:515–519
9. Fitzgibbons PL, Page DL, Weaver D, Thor AD, Allred DC, Clark GM, Ruby SG, O`Malley F, Simpson JF, Connoly JL, Hayes DF, Edge SB, Lichter A, Schnitt SJ (2000) Prognostic factors in breast cancer. College of American Pathologist Consensus Statement 1999. Arch Pathol Lab Med 124:966–978
10. Gillespie MT, Martin TJ (1994) The parathyroid hormone-related protein gene and its expression. Mol Cell Endocrinol 100:143–147
11. Grill V, Ho P, Body JJ, Johanson N, Lee SC, Kukreja SC, Moseley JM, Martin TJ (1991) Parathyroid hormone-related protein: elevated levels in both humoral hypercalcemia of malignancy and hypercalcemia complicating metastatic breast cancer. J Clin Endocrinol Metab 73:1309–1315
12. Ikeda K, Weir EC, Mangin M, Dannies PS, Kinder B, Deftos LJ, Brown M, Broadus AE (1988) Expression of messenger RNAs encoding a parathyroid hormone-like peptide in normal human parathyroid adenomas. Mol Endocrinol 2: 1230–1236
13. Jardines L, Weiss M, Fowble B, Greene M (1993) neu (c-erbB-2/HER-2) and the epidermal growth factor receptor (EGFR) in breast cancer. Pathology 61:268–282
14. Kaiser SM, Laneuville P, Rhim JS, Kremer R, Goltzman D (1992) Enhanced growth of a human keratinocyte cell line induced by antisense RNA for parathyroid hormone related peptide. J Biol Chem 261:13623–13628

15. Kaiser SM, Laneuville P, Rhim JS, Kremer R, Goltzman D (1994) Antisense mediated inhibition of parathyroid hormone-related peptide (PTHrP) production in a keratinocyte cell line impedes differentiation. Mol Endocrinol 8:277–289
16. Karaplis AC, Luz A, Glowacki J Bronson RT, Tybulewicz VL, Kronenberg HM, Mulligan RC (1994) Lethal skeletal dysplasia from targetet disruption of the parathyroid hormone-related peptide gene. Genes Dev 8:277–289
17. Kissin MW, Henderson MA, Danks JA, Hayman JA, Bennett RC, Martin TJ (1993) Parathyroid hormone related protein in breast cancer of widely varying prognosis. Eur J Surg Oncol 19:134–142
18. Liapis H, Crouch EC, Grosso LE, Kitzawa S, Wick MR (1993) Expression of parathyroidlike protein in normal, proliferative, and neoplastic human breast tissues. Am J Pathol 143:1169–1178
19. Mangin M, Jkeda K, Dreyer BE, Broadus AE (1998) Isolation and characterisation of the human parathyroid hormone-like peptide gene. Proc Natl Acad Sci U S A 86:2408–2412
20. Martin TJ, Moseley JM (1992) Biochemistry and pathology of PTH-related gene products. J Endocrinol Invest 15[Suppl 6]:171–177
21. Merendino JJ JR, Insogna KL, Milstone LM, Broadus AE, Stewart AF (1986) A parathyroid hormone-like protein from cultured human keratinocytes. Science 231:388–390
22. Molk LS, Ajiwa E, Martin TJ, Thompson JC, Cooper CW (1989) Parathyroid related protein relaxes gastric smooth muscle and shows cross desensitization with parathyroid hormone. J Bone Mineral Res 4:433–439
23. Mok LS, Nickols GA, Thompson JC, Cooper CW (1989) Parathyroid hormone as a smooth muscle relaxant. Endocr Rev 10:420–436
24. Nickols GA, Nana AD, Nickols MA, Dipette DJ, Asimakis GK (1989) Hypotension and cardiac stimulation due to the parathyroid hormone related protein, humoral hipercalcemia of malignancy factor. Endocrinology 125:834–841
25. Orloff JJ, Wu TL, Stewart AF (1989) Parathyroid hormone-like proteins: biochemical responses and receptor interaction. Endocr Rev 10:476–495
26. Remmele W, Stenger HE (1987) Vorschlag zur einheitlichen Definition eines Immunreaktiven Score (IRS) fuer den immunohistochemischen Oestrogenrezeptor- Nachweis (ER-ICA) im Mammakarzinomgewebe. Pathologe 8:138–140
27. Rodda CP, Kubota M, Heath JA (1988) Evidence for novel parathyroid hormone-related protein in fetal lamb parathyroid gland and sheep placenta: comparison with a similar protein implicated in humoral hipercalcemia of malignancy. J Endocrinol 117:261–271
28. Ross JS, Flechter JA (1999) HER-2/neu (c-erb-B2) gene and protein in breast cancer. Am J Clin Pathol 112[Suppl 1]:53–67
29. Sidler B, Alpert L, Henderson JE, Deckelbaum R, Amizuka N, Silva JE, Goltzman D, Karaplis AC (1996) Amplification of the parathyroid hormone-related peptide gene in a colonic carcinoma. J Clin Endocrinol Metab 81:2841–2847
30. Sopel M, Murawski M, Zabel M (1996) PTHrP (parthyroid hormone-related peptide)—a new multifunctional peptide hormone (in Polish). Post Biol Kom 23:127–142
31. Southby J, Kissin MW, Danks JA, Hayman JA, Moseley JM, Henderson MA, Bennett RC, Martin TJ (1990) Immunohistochemical localisation of parathyroid hormone-related protein in human breast cancer. Cancer Res 50:7710–7716
32. Steward AF, Broadus AE (1990) Clinical review 16: parathyroid hormone-related proteins: coming of age in the 1990s. J Clin Endocrinol Metab 71:1410–1414
33. Thiede MA, Rodan GA (1988) Expression of calcium-mobilizing parathyroid hormone-like peptide in lactating mammary tissue. Science 242:278–280
34. Van De Stolpe A, Karperien M, Lowik CWGM, Juppner H (1993) Parathyroid related peptide as an endogenous inducer of parietal endoderm differentiation. J Cell Biol 120:235–243
35. Weir EC, Brines ML, Ikeda K, Burtis WJ, Broadus AE, Robbins RJ (1990) Parathyroid hormone-related peptide gene is expressed in the mammalian central nervous system. Proc Natl Acad Sci U S A 87:108–112
36. Woodget JR (1989) Early gene induction by growth factors. Br Med Bull 45:529–540
37. Ye Y, Seitz PK, Cooper CW (2001) Parathyroid hormone-related protein overexpression in the human colon cancer cell line HT-29 enhances adhesion of the cells to collagen type I. Regul Pept 101:19–23
38. Yoshida A, Nakamura Y, Shimizu A, Harada M, Kameda Y, Nagano A, Inaba M, Asaga T (2000) Significance of parathyroid hormone-related protein expression in breast carcinoma. Breast Cancer 7:215–220
39. Zabel M, Dietel M (1993) Endocrine markers in malignant tumor cells producing parathyroid hormone-related peptide. Exp Clin Endocrinol 101:297–302
40. Zabel M, Kaczmarek A, Ramlau R, Matecka-Nowak M (1991) Significance of P-glycoprotein in the multidrug resistance of neoplasms to cytostatics (in Polish). Nowotwory XLI:37–45

Virchows Arch (2003) 442:252–257
DOI 10.1007/s00428-003-0759-5

ORIGINAL ARTICLE

**Motoji Sawabe · Akihiko Hamamatsu · Tateki Ito · Tomio Arai · Kumiko Ishikawa · Kouji Chida · Naotaka Izumiyama · Naoko Honma · Kaiyo Takubo · Masamitsu Nakazato**

# Early pathogenesis of cardiac amyloid deposition in senile systemic amyloidosis: close relationship between amyloid deposits and the basement membranes of myocardial cells

Received: 21 October 2002 / Accepted: 7 January 2003 / Published online: 26 February 2003
© Springer-Verlag 2003

**Abstract** Despite a number of in vitro studies of transthyretin (TTR) amyloidogenesis the early stage of in vivo amyloidogenesis in the human heart is largely unknown. A heart with a mild degree of cardiac amyloidosis removed from a 90-year old woman at autopsy was selected for analysis. The genotype of the TTR was the wild type. An immunohistochemical study with anti-TTR antibody was performed on serial paraffin sections, and 17 TTR-positive lesions less than 50 μm in diameter consisting of 13 interstitial and 4 vascular lesions were identified. The early interstitial lesions start as thick membranous deposits between interfacing myocardial cells. They are Congophilic with green birefringence and positive for apolipoprotein E but negative for amyloid P component. The TTR-positive amyloid extends along intercellular spaces and becomes larger, involving several myocardial fibers. The media is the initial site of arteriolar involvement. According to the in vitro studies of amyloid fibrillogenesis, the most critical step is formation of the nucleus under supersaturated conditions. The supersaturated conditions are speculated to be achieved by binding to proteoglycans or lipid membranes. Our results indicate that the basement membrane of myocardial cells is the initial site of amyloid deposition, providing a suitable place for concentration of TTR.

**Keywords** Amyloidosis · Prealbumin · Immunohistochemistry · Heart · Aged, 80 years and over

M. Sawabe (✉) · A. Hamamatsu · T. Ito · T. Arai · K. Ishikawa · K. Chida
Departments of Pathology and Cardiology,
Tokyo Metropolitan Geriatric Hospital,
35-2 Sakae-cho, Itabashi, 173-0015 Tokyo, Japan
e-mail: sawabe@tmig.or.jp
Tel.: +81-3-39641141
Fax: +81-3-39641982

N. Izumiyama · N. Honma · K. Takubo
Department of Clinical Pathology,
Tokyo Metropolitan Institute of Gerontology,
35-2 Sakae-cho, Itabashi, 173-0015 Tokyo, Japan

M. Nakazato
Third Department of Internal Medicine,
Miyazaki Medical College,
5200 Kihara, Kiyotake, 889-1692 Miyazaki, Japan

## Introduction

Transthyretin (TTR) is a serum protein that transports approximately one-quarter of thyroxine and all retinol binding protein in the blood. TTR usually forms a tetramer that is capable of binding thyroxine, whereas the monomeric form, which is rich in $\beta$-sheets, readily forms amyloid fibrils. Interstitial deposition of either the wild or mutant type of TTR causes systemic amyloidosis. The amyloidosis caused by wild type TTR is senile systemic amyloidosis (SSA; ATTR amyloidosis), and the amyloid deposition occurs mainly in the heart. Familial amyloidotic polyneuropathy and familial amyloidotic cardiomyopathy are caused by deposition of mutant type TTR. Although SSA is a relatively rare disease, TTR amyloid deposition itself is a common aging phenomenon in the extremely elderly population. Among the elderly autopsy cases who have died at 85 years of age or over, 25% show various degree of TTR-amyloid deposition in the heart [3]. Recent in vitro studies indicate that the rate-limiting step of amyloidogenesis is nucleus formation from early amyloid intermediates under supersaturated conditions [18]. After nucleation the amyloid fibrils grow rapidly in a cascading manner, but it is still uncertain where the amyloid fibrillogenesis takes place in vivo, and which microstructures or biomolecules create the supersaturated conditions. Although the histological features of SSA have been described in a few reports [17, 21], its early pathogenesis has never been studied to our knowledge. To elucidate the early pathogenesis of amyloid deposition of TTR we have performed immunohistochemical and electron microscopic studies on serial sections of myo-

cardium obtained from a patient with mild cardiac amyloidosis.

## Materials and methods

Information on 20 autopsy cases (10 men, 10 women) who died in the 10th decade of life and had unremarkable hearts were retrieved from the autopsy database of the Department of Pathology of Tokyo Metropolitan Geriatric Hospital, Tokyo, Japan. Mild cardiac amyloid deposition of TTR had been found in one of the men and four of the women, and a 90 year-old woman was selected for study on the basis of the degree of amyloid deposition. The patient had died of advanced pancreatic head cancer, and her cardiac function was normal. Gross examination of the heart showed mild senile atrophy with 220 g heart weight, mild aortic valvular calcification, and mild coronary arteriosclerosis. The heart was histologically normal except for mild deposition of TTR amyloid in the myocardium. From one largest transverse section of ventricles, four paraffin blocks were made, among which two sets of more than 60 serial sections 4 μm thick were obtained from the anteroseptal and posterolateral portions of the left ventricle. Every other section was used for immunohistochemistry with anti-TTR antibody, and the remaining sections used for Congo red staining, immunostaining with anti-apolipoprotein E (apoE) and anti-amyloid P, or electron microscopic study. The dye used for Congo red staining was Congo red 1B 227 (Chroma, Denmark). The slides were stained with 0.5% Congo red in 50% ethanol solution for 30 min and differentiated in 95% and 100% ethanol for a few seconds.

The immunohistochemical study was performed by the streptavidin-biotin method using a LSAB kit (Dako, Kyoto, Japan). The paraffin sections were deparaffinized, hydrated, and pretreated by 5-min incubation with 100% formic acid for anti-TTR and anti-amyloid P, or by 10-min heating in a pressure cooker for anti-apoE. The slides were then treated with avidin and biotin solutions (X0590, Dako) at 37°C for 10 min to block endogenous biotin. The primary antibodies were a rabbit polyclonal anti-transthyretin (A0002, Dakol) used in a 1:100 dilution; a rabbit polyclonal anti-human apoE (A299, IBL, Gunma, Japan) used in a 1:100 dilution; and a rabbit polyclonal anti-amyloid P protein (NCL-PCOMp, Novocastra Laboratories, Newcastle, UK) used in a 1:300 dilution. If the entire TTR-positive lesion was contained in the serial sections, it was included in our study.

Molecular analysis was performed by one of us (M.N.) according to the previously reported method [19]. In brief, DNA was purified from frozen kidney by proteinase K digestion and phenol-chloroform extraction. The polymerase chain reaction was performed with three sets of primers that cover exons 2, 3, and 4 of the TTR gene including the intron-exon boundaries. The amplicons were then directly sequenced by the dye-terminator method using DNA sequencer Model 373A (Applied Biosystems, Japan).

Written informed consent was obtained from the family of the patient at the time of autopsy. The use of autopsy materials for medical education and research is generally permitted in accordance with the Preservation of Autopsy Law of Japan.

## Results

Histological examination revealed numerous TTR-positive microscopic nodules up to 500 μm in diameter scattered throughout the interstitium of the myocardium. Examination of serial sections results in identification of 17 small lesions less than 50 μm in diameter, consisting of 13 interstitial and 4 vascular lesions. As shown in Figs. 1 and 2, the early interstitial lesions are thick membranous deposits located at the interfaces between two myocardial

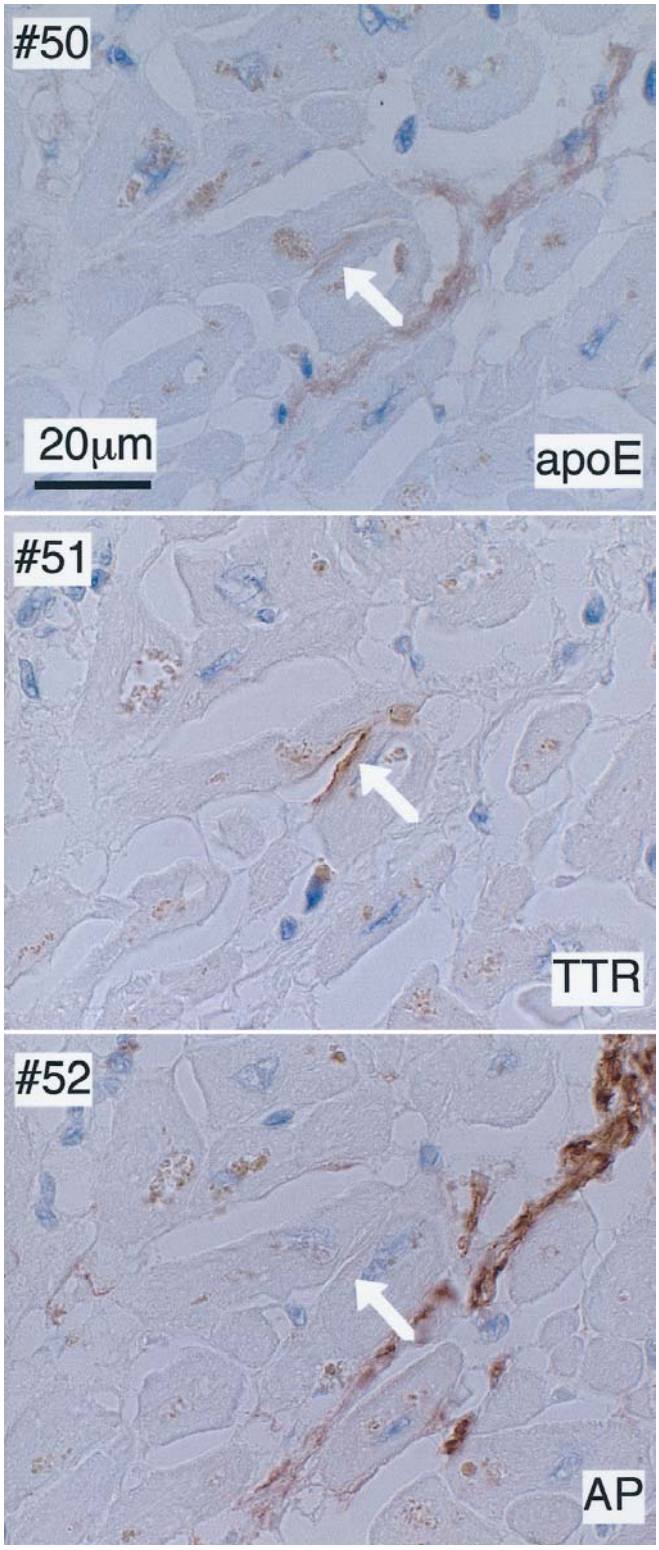



**Fig. 1** The smallest transthyretin (*TTR*) positive interstitial lesion, measuring 19×7 μm, observed in serial sections of a heart with mild senile cardiac amyloidosis. The interface of two adjacent myocardiocytes (*white arrows*) are positive for TTR and apolipoprotein E (*apoE*), as shown in #51 and #50, respectively, and negative for amyloid P (*AP*) in #52. Note the apoE and AP immunoreactivity of the elastic fibers. Original magnification, ×750

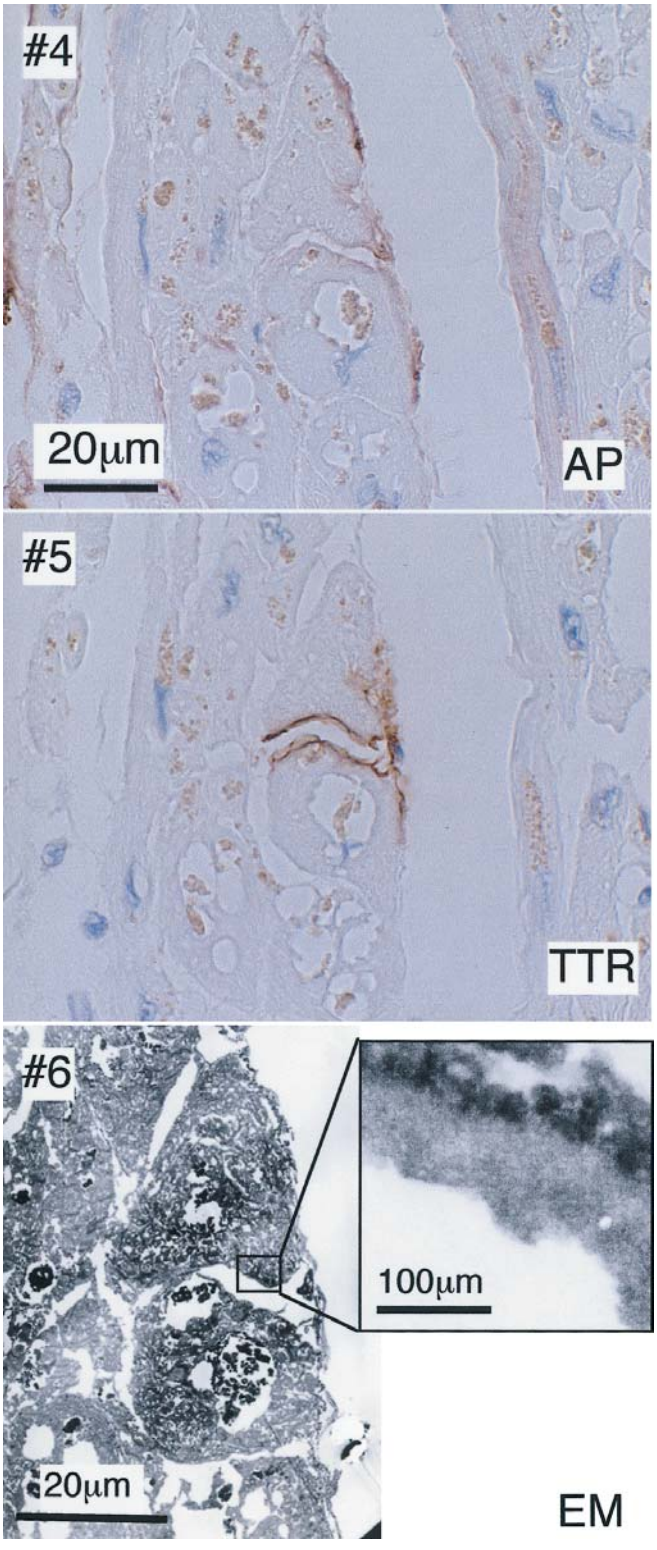



**Fig. 2** The early transthyretin (*TTR*) positive interstitial lesion, measuring 27×36 μm. The interface of two myocardiocytes and adjacent interstitium are positive for TTR, as shown in #5, and negative for amyloid P (*AP*) in #4. The electron micrographs in #6 show thickening of the basal lamina. No nonbranching amyloid fibrils are observed, probably because of autolysis and long-term formalin fixation. Original magnification, ×750, ×1,200 (*EM*), and ×40,000 (*EM*, *inset*)

cells. The smallest lesion measures 19×7 μm (Fig. 1). The other part of the cell surfaces than the interfaces is not affected initially and the cytoplasm of the myocardial cells is negative for TTR. These early lesions are Congophilic with green birefringence and positive for apoE but negative for amyloid P. The electron microscopic study reveals four- to fivefold thickening of the basal lamina (usually 20- to 30 nm-thick cell coat), but fails to identify nonbranching amyloid fibrils due to poor preservation of electron microscopic structures caused by autolysis and long-term formalin fixation (Fig. 2). These early lesions never involve nerve fascicles.

The TTR-positive amyloid extends along the intercellular spaces and becomes larger, involving several myocardial cells (Fig. 3). The TTR-positive deposits become less homogeneous in density and more fibrillar as the deposits increase in size. In the large nodules more than 50 μm in diameter the amyloid encircles the myocardial cells and makes them atrophic. These large nodules are positive for amyloid P.

Four TTR-positive vascular lesions are identified, including three arteriolar lesions and one capillary lesion. The smallest nodular deposition is found in the media and measures 20 μm in diameter (Fig. 4). The larger lesions involve the intima, adventitia, and surrounding interstitium as well. One capillary lesion shows amyloid deposition between a dilated capillary and adjacent myocardial cells.

Since the results of the molecular analysis revealed no mutations in the sequence of the TTR genome in the objective case, the genotype was the wild type.

## Discussion

Three major factors have been proposed to explain the development of amyloidogenesis: (a) the chemical properties of the amyloid precursor proteins (APPs), (b) the microenvironment at the site of deposition, and (c) proteolysis of amyloid fibrils [15, 16, 25, 30, 31]. APPs must be rich in $\beta$-sheets to be folded into the amyloid fibrils. While TTR itself is rich in $\beta$-sheets, some proteins, such as amyloid $\beta$ precursor protein, must be cleaved by specific proteases before polymerization. Genomic mutations associated with amino acid changes occasionally render APPs more likely to form amyloid fibrils, and mutant type TTR is mostly amyloidogenic and more prone to form amyloid fibrils than wild-type TTR by way of production of amyloidogenic intermediates [13].

The local microenvironment seems to play a significant role in amyloid deposition in systemic amyloidosis, and in vitro studies have suggested that nucleus formation under supersaturated conditions is the critical rate-limiting step of amyloidogenesis [18]. It is conceivable that the mechanism of concentration of APPs exists in vivo as well, and the interaction with proteoglycans or lipid membranes is thought to be important in this concentrating process [22, 23, 29]. Our data indicate a close relationship between TTR deposits and the basement

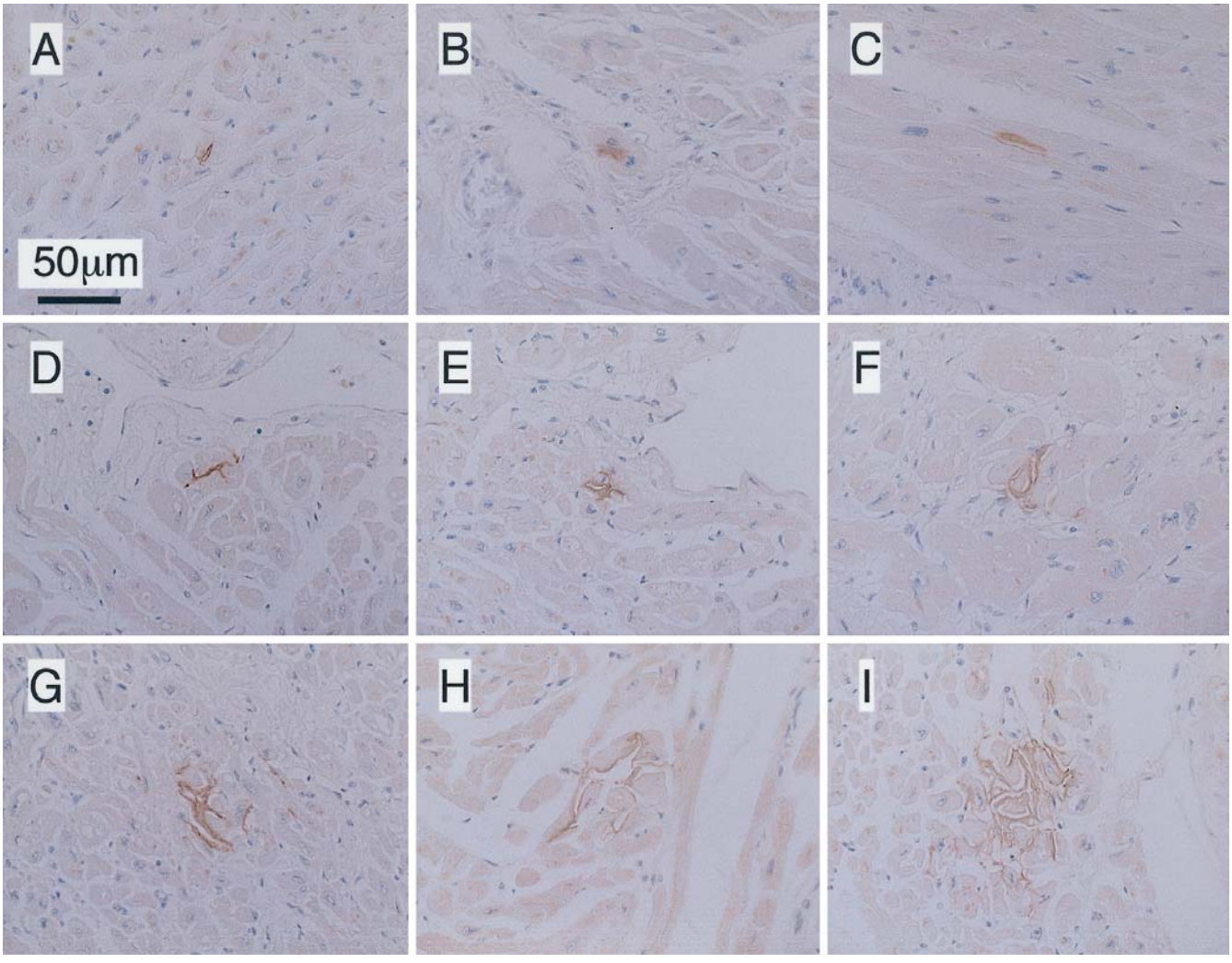



**Fig. 3** Development of transthyretin (TTR) positive interstitial lesions in a heart with mild senile cardiac amyloidosis. All photographs were taken at the center of the lesions at the same magnification, ×300. **A**–**C** Tiny TTR-positive early lesions are found in the center of the photographs *in the upper row*. They are located at the interfaces of two myocardial cells, which are seen on the transverse sections (**A**, **B**) and on the longitituidinal section (**C**). **D**–**F** The medium-sized lesions which involve several myocardial cells are shown in the figures *in the middle row*. **G**–**I** The figures *in the lower row* show typical amyloid nodules more than 50 μm in diameter

membranes of myocardial cells, and this suggests that certain unidentified biomolecules in the basement membrane facilitate concentration of TTR and formation of amyloid fibrils. Heparan sulfate, the predominant type of proteoglycan in the basement membrane, is the most likely candidate for the molecule responsible for concentration of TTR. It remains unknown why the TTR amyloid is located at the interfaces of myocardial cells rather than at the other part of the cell surfaces which is facing the interstitium.

Amyloid P and apoE coexist with APPs in all types of amyloid deposits and are regarded as important modifying factors of amyloidogenesis. Amyloid P prevents in vitro proteolysis of amyloid fibrils in cases of Alzheimer's disease and AA amyloidosis [28]. It is definitely related to in vivo amyloidogenesis, since it is present in immunoglobulin light chain amyloidosis (primary or AL amyloidosis), but absent in the preamyloidotic condition known as light chain deposition disease [5]. In the experimental model of amyloid P knock-out mice the induction of reactive amyloidosis (AA amyloidosis) was retarded, which clearly demonstrated the participation of amyloid P in the process of amyloidogenesis in vivo [1]. The significant role of amyloid P in amyloidogenesis in vivo was also proved by the high-resolution ultrastructural studies. Inoue et al. [11] reported that TTR amyloid fibrils are composed of amyloid P containing cores and TTR-rich superficial layers. Similar configurations of amyloid fibrils were reported from the same author in other forms of amyloidosis including AA and $\beta_2$-microglobulin amyloidoses and Alzheimer's disease [8, 9, 10]. The central location of amyloid P within the amyloid fibrils indicates that amyloid P is assembled from the earliest stage of amyloidogenesis. In our study the earliest amyloid

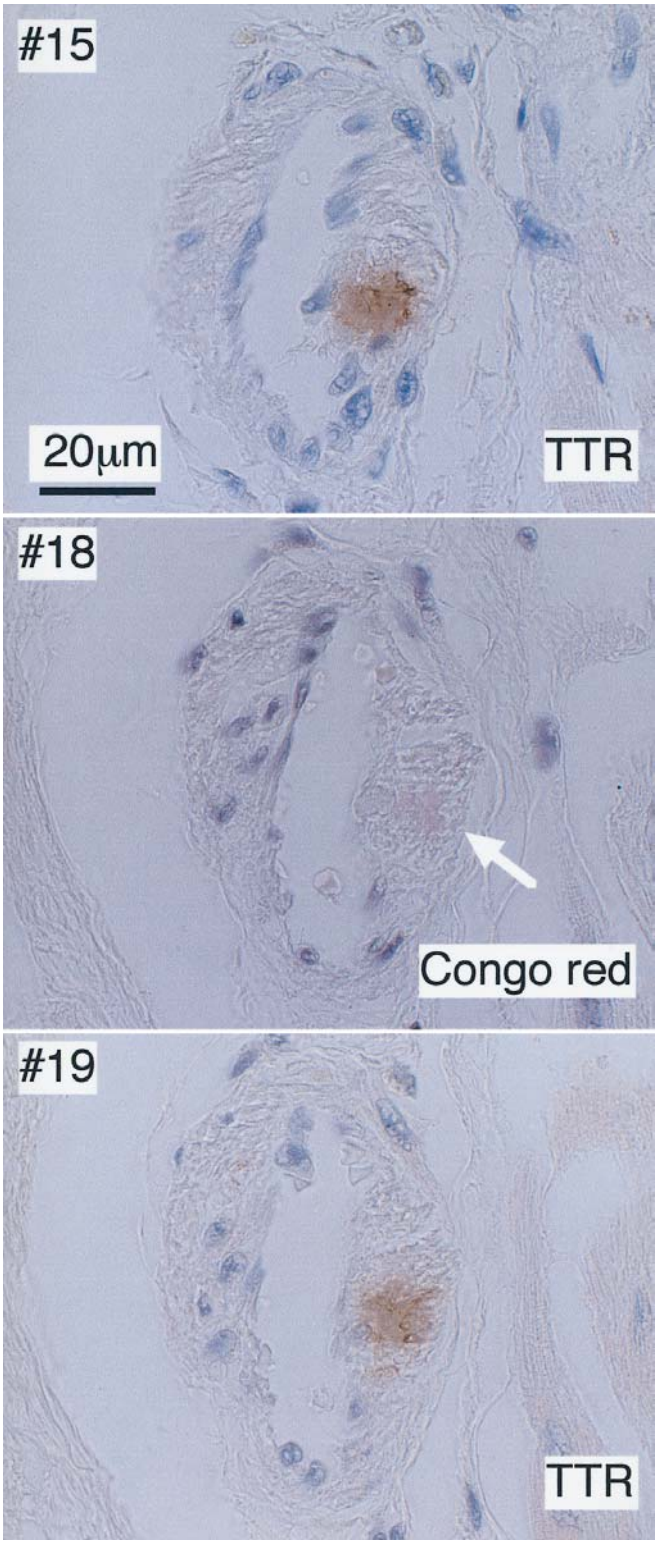



**Fig. 4** The smallest transthyretin-positive arteriolar lesion, measuring 20 μm in diameter. The media of the arteriole contains a nodular Congophilic amyloid deposit, as shown in #18 (*white arrow*), which is positive for transthyretin in #15 and #19. Note the inhomogeneous density of the deposits. Original magnification, ×750

deposits lack immunoreactivity for amyloid P. The precise reasons for disagreement between their model and our results are currently unclear. This inconsistency may be related to the fact that the pentosomes of amyloid P, subunits of amyloid P, lose immunoreactivity once assembled into 8.5-nm-wide pentagonal units [7]. Another possible explanation is that the low sensitivity of anti-amyloid P antibody might have resulted in false negative immunoreactivity in our study, although the elastic fibers were at least intensely positive as shown in Figs. 1 and 2.

There was a strong correlation between apoE genotype and sporadic and late-onset Alzheimer's disease. ApoE coexists with $\beta$-amyloid fibrils in senile plaques of Alzheimer's disease, and apoE, especially $apoE_4$, interacts with $\beta$-APPs and facilitates amyloid fibrillogenesis in vitro [2]. The importance of apoE in other types of amyloidogenesis than Alzheimer's disease is, however, controversial. In the same way as amyloid P component, ApoE is present in AL amyloidosis, but absent in light chain deposition disease [6]. On the other hand, no differences in the degrees of reactive amyloidosis were observed between apoE knock-out mice and wild mice [4], and no association was found between apoE genotypes and AA, AL, and ATTR amyloidoses [14, 20]. The apoE immunoreactivity in the earliest lesions in our study suggests that apoE is involved in the early stage of TTR amyloidogenesis.

An experimental model of SSA was recently developed by producing transgenic mice bearing the wild-type human TTR gene [27]. Interestingly, nonfibrillar, non-Congophilic TTR-positive deposits have been found in the heart and kidneys of these mice. Despite failure to demonstrate amyloid fibrils on electron microscopy in our study the Congophilic property of the TTR deposits strongly suggests complete formation of amyloid fibrils even in the earliest stage. There were no such nonfibrillar, non-Congophilic TTR-positive deposits in the 20 senile hearts examined in our study. It seems that TTR deposits are incapable of remaining in their nonfibrillar, non-Congophilic form in the human heart under physiological conditions and easily convert into amyloid fibrils. By contrast, nonfibrillar, non-Congophilic TTR deposition has been recently reported in the early stages of familial amyloidotic polyneuropathy [24].

The cardiac amyloidosis is caused by several types of amyloidosis and each type has different clinicopathological features. Our unpublished data from elderly autopsy cases show that the cases of cardiac amyloidosis of ventricular form are composed of equal numbers of senile systemic amyloidosis and AL amyloidosis. In cardiac amyloidosis of atrial form senile systemic amyloidosis is also a predominant type, comprising two-thirds of the cases, followed by AL amyloidosis and isolated atrial amyloid. AA amyloidosis is a rare cause of cardiac amyloidosis [21]. In senile systemic amyloidosis, the cardiac amyloid deposits are mainly nodular in the advanced stages and infrequently involve blood vessels, as shown in our study. In contrast, the amyloid deposits are located around the cardiac fibers and show frequent

vascular involvement in AL amyloidosis [21]. In isolated atrial amyloid, the cardiac atrium is one and only site of amyloid involvement (local amyloidosis) and atrial natriuretic peptide positive amyloid deposits are mainly located around the cardiac fibers [12]. The ultrastructural study of isolated atrial amyloid shows formation of atrial natriuretic peptide positive amyloid fibrils within atrial myocardial cells [26]. This intracellular localization of amyloid fibrils within myocardial cells are not seen in any type of systemic amyloidosis, such as AL, ATTR, or AA amyloidosis.

In conclusion, the basement membranes of the myocardial cells seem to contribute to the concentration of TTR and formation of amyloid fibrils in the early stage of TTR amyloidogenesis.

**Acknowledgements** We are grateful to all of the clinical technologists of the Department of Pathology of Tokyo Metropolitan Geriatric Hospital for preparing the serial sections and immunohistochemical slides.

## References

1. Botto M, Hawkins PN, Bickerstaff MC, Herbert J, Bygrave AE, McBride A, Hutchinson WL, Tennent GA, Walport MJ, Pepys MB (1997) Amyloid deposition is delayed in mice with targeted deletion of the serum amyloid P component gene. Nat Med 3:855–859
2. Castaño EM, Prelli F, Wisniewski T, Golabek A, Kumar RA, Soto C, Frangione B (1995) Fibrillogenesis in Alzheimer's disease of amyloid $\beta$ peptides and apolipoprotein E. Biochem J 306:599–604
3. Cornwell GG III, Murdoch WL, Kyle RA, Westermark P, Pitkänen P (1983) Frequency and distribution of senile cardiovascular amyloid. A clinicopathologic correlation. Am J Med 75:618–623
4. Elliott-Bryant R, Cathcart ES (1997) Apolipoprotein E and apolipoprotein A-1 knock-out mice readily develop amyloid A protein amyloidosis. Clin Immunol Immunopathol 85:104–108
5. Gallo G, Picken M, Frangione B, Buxbaum J (1988) Nonamyloidotic monoclonal immunoglobulin deposits lack amyloid P component. Mod Pathol 1:453–456
6. Gallo G, Wisniewski T, Choi-Miura NH, Ghiso J, Frangione B (1994) Potential role of apolipoprotein-E in fibrillogenesis. Am J Pathol 145:526–530
7. Inoue S (1995) Ultrastructural organization of connective tissue microfibrils in the posterior chamber of the eye in vivo and in vitro. Cell Tissue Res 279:291–302
8. Inoue S (2001) Basement membrane and $\beta$ amyloid fibrillogenesis in Alzheimer's disease. Int Rev Cytol 210:121–161
9. Inoue S, Kisilevsky R (1996) A high resolution ultrastructural study of experimental murine AA amyloid. Lab Invest 74:670–683
10. Inoue S, Kuroiwa M, Ohashi K, Hara M, Kisilevsky R (1997) Ultrastructural organization of hemodialysis-associated $\beta$2-microglobulin amyloid fibrils. Kidney Int 52:1543–1549
11. Inoue S, Kuroiwa M, Saraiva MJ, Guimarães A, Kisilevsky R (1998) Ultrastructure of familial amyloid polyneuropathy amyloid fibrils: examination with high-resolution electron microscopy. J Struct Biol 124:1–12
12. Kawamura S, Takahashi M, Ishihara T, Uchino F (1995) Incidence and distribution of isolated atrial amyloid: histologic and immunohistochemical studies of 100 aging hearts. Pathol Int 45:335–342
13. Kelly JW (1998) The alternative conformations of amyloidogenic proteins and their multi-step assembly pathways. Curr Opin Struct Biol 8:101–106
14. Kindy MS, de Beer FC, Markesbery WR, Pras M, Aksentijevich I, Kastner D, Kyle R, Solomon A, Woo P (1995) Apolipoprotein E genotypes in AA and AL amyloidoses. Amyloid 2:159–162
15. Müller D, Roessner A, Röcken C (2000) Distribution pattern of matrix metalloproteinases 1,2,3, and 9, tissue inhibitors of matrix metalloproteinases 1 and 2, and $\alpha$2-macroglobulin in cases of generalized AA- and AL amyloidosis. Virchows Arch 437:521–527
16. Picken MM (2001) The changing concepts of amyloid. Arch Pathol Lab Med 125:38–43
17. Pitkänen P, Westermark P, Cornwell GG III (1984) Senile systemic amyloidosis. Am J Pathol 117:391–399
18. Rochet JC, Lansbury PT Jr (2000) Amyloid fibrillogenesis: themes and variations. Curr Opin Struct Biol 10:60–68
19. Saito F, Nakazato M, Akiyama H, Kitahara Y, Date Y, Iwasaki Y, Harasawa S, Hisaki R, Horie T, Kinukawa N, Watanabe T, Sakamaki T, Yagi H, Hoshii Y, Yutani C, Kanmatsuse K (2001) A case of late onset cardiac amyloidosis with a new transthyretin variant (lysine 92). Hum Pathol 32:237–239
20. Satoh S, Tokuda T, Ikeda S, Sekijima Y, Yanagisawa N, Hidaka H, Kametani F (1996) No association between apolipoprotein E $\varepsilon$4 allele and the age of onset in type I familial amyloid polyneuropathy. Neurosci Lett 204:209–211
21. Smith TJ, Kyle RA, Lie JT (1984) Clinical significance of histopathologic patterns of cardiac amyloidosis. Mayo Clin Proc 59:547–555
22. Snow AD, Wight TN (1989) Proteoglycans in the pathogenesis of Alzheimer's disease and other amyloidoses. Neurobiol Aging 10:481–497
23. Snow AD, Bramson R, Mar H, Wight TN, Kisilevsky R (1991) A temporal and ultrastructural relationship between heparan sulfate proteoglycans and AA amyloid in experimental amyloidosis. J Histochem Cytochem 39:1321–1330
24. Sousa MM, Cardoso I, Fernandes R, Guimarães A, Saraiva MJ (2001) Deposition of transthyretin in early stages of familial amyloidotic polyneuropathy: evidence for toxicity of nonfibrillar aggregates. Am J Pathol 159:1993–2000
25. Stix B, Kähne T, Sletten K, Raynes J, Roessner A, Röcken C (2001) Proteolysis of AA amyloid fibril proteins by matrix metalloproteinases-1, -2, and -3. Am J Pathol 159:561–570
26. Takahashi M, Hoshii Y, Kawano H, Gondo T, Yokota T, Okabayashi H, Shimada I, Ishihara T (1998) Ultrastructural evidence for the formation of amyloid fibrils within cardiomyocytes in isolated atrial amyloid. Amyloid 5:35–42
27. Teng MH, Yin JY, Vidal R, Ghiso J, Kumar A, Rabenou R, Shah A, Jacobson DR, Tagoe C, Gallo G, Buxbaum J (2001) Amyloid and nonfibrillar deposits in mice transgenic for wild-type human transthyretin: a possible model for senile systemic amyloidosis. Lab Invest 81:385–396
28. Tennent GA, Lovat LB, Pepys MB (1995) Serum amyloid P component prevents proteolysis of the amyloid fibrils of Alzheimer disease and systemic amyloidosis. Proc Natl Acad Sci USA 92:4299–4303
29. Terzi E, Hölzemann G, Seelig J (1995) Self-association of $\beta$-amyloid peptide (1–40) in solution and binding to lipid membranes. J Mol Biol 252:633–642
30. Westermark P (1998) The pathogenesis of amyloidosis: understanding general principles. Am J Pathol 152:1125–1127
31. Westermark P, Sletten K, Johnson KH (1996) Ageing and amyloid fibrillogenesis: lessons from apolipoprotein AI, transthyretin and islet amyloid polypeptide. Ciba Found Symp 199:205–222

Virchows Arch (2003) 442:258–265
DOI 10.1007/s00428-002-0751-5

ORIGINAL ARTICLE

**N. Ohike · A. Jürgensen · M. Pipeleers-Marichal · G. Klöppel**

# Mixed ductal-endocrine carcinomas of the pancreas and ductal adenocarcinomas with scattered endocrine cells: characterization of the endocrine cells

Received: 1 October 2002 / Accepted: 28 November 2002 / Published online: 6 February 2003
© Springer-Verlag 2003

**Abstract** We compared the histological and immunohistochemical features of mixed ductal-endocrine carcinomas of the pancreas with those of ductal adenocarcinomas (DACs) containing scattered tumor-associated endocrine cells (SECs). Three pancreatic neoplasms fulfilled the WHO criteria for mixed ductal-endocrine carcinomas. Two of them showed moderately to poorly differentiated glandular structures composed of both mucin producing and neuroendocrine cells. The third mixed ductal-endocrine carcinoma was of the composite type showing DAC structures and a solid component with small epithelial cells, most of them of neuroendocrine nature. In 32 of 34 cases of DAC located in the head (30 cases) and body to tail (4 cases) of the pancreas and showing lymph-node metastases, SECs were found, but they were few in number and irregularly distributed in the tumors. In three DACs a few SECs were also detected in lymph-node metastases. Double staining for chromogranin A and the proliferation marker Ki-S5 revealed that all SECs that were not intimately integrated into the neoplastic glandular epithelium failed to show proliferative activity and changes of the expression of tumor suppressor genes (p53 and DPC 4). These findings suggest that only those SECs that belong to the proliferative cell fraction may be of neoplastic origin, while the majority of SECs probably constitute a tumor-associated but non-neoplastic cell population. These features contrast with those of mixed ductal-endocrine carcinomas, in which all endocrine cells are a component of the neoplasm.

N. Ohike (✉)
First Department of Pathology,
Showa University School of Medicine,
1-5-8 Hatanodai, Shinagawa-ku, 142-8555 Tokyo, Japan
e-mail: ohike@med.showa-u.ac.jp
Tel.: +813-3784-8119
Fax: +813-3784-8249

A. Jürgensen · G. Klöppel
Department of Pathology, University of Kiel, Germany

M. Pipeleers-Marichal
Department of Pathology, Academic Hospital,
Free University of Brussels, Belgium

**Keywords** Pancreatic ductal adenocarcinoma · Mixed ductal-endocrine · Scattered endocrine cells · Immunohistochemistry

## Introduction

Pancreatic ductal adenocarcinomas (DACs) with an endocrine component may be separated into mixed ductal-endocrine carcinomas or DACs with scattered tumor-associated endocrine cells (SECs). Mixed ductal-endocrine carcinomas are defined histologically according to the World Health Organization (WHO) criteria [17] as follows: a malignant epithelial neoplasm in which the ductal and endocrine cells are intimately admixed in the primary tumor and in its metastases and in which the endocrine cells comprise at least one-third to one-half of the tumor tissue. Only few cases of mixed ductal-endocrine carcinoma of the pancreas adhering to these criteria have been documented so far [4, 20, 34, 37]. Because they are so rare, even pathologists tend to be ignorant of the pathological and biological features of this tumor and are uncertain of the differential diagnosis versus DACs with SECs.

The occurrence of SECs in DACs has been considered to be a general phenomenon [3, 4, 10, 14, 18, 27, 30, 32, 36], but it remains unclear whether SECs are neoplastic or not. Recent reports have suggested that most SECs are non-neoplastic, because they usually lack cellular atypia and comprise only a small population. In addition, SECs are scarcely observed in invasive and metastatic sites [14, 32].

We have collected three cases of mixed ductal-endocrine carcinoma of the pancreas. In this study, we compared the histological and immunohistochemical features of mixed ductal-endocrine carcinomas with those in DACs with SECs, in order to find out whether the two tumor groups share some features or whether they can be clearly distinguished from each other. In addition, we addressed the question whether the SECs show the same

proliferative activity and expression of tumor suppressor gene products as DAC cells.

## Materials and methods

From our consultation files at the Department of Pathology of the University of Kiel, we selected three cases (accounting for approximately 0.5% of all DACs) that fulfilled the criteria for mixed ductal-endocrine carcinoma. In addition, we investigated 34 cases of DAC that showed regional lymph-node metastases. The pancreatic tumors from two patients with mixed ductal-endocrine carcinoma (cases 1 and 3) and from all patients with DACs were removed surgically. In one case of mixed ductal-endocrine carcinoma (case 2; also previously published [29]) the specimen was obtained at autopsy within 2 h of death. All three patients had a metastasizing carcinoma in the head of the pancreas, and each primary tumor was more than 3 cm in diameter. The first patient (case 1) was a 60-year-old man who died 9 months after surgery. The second patient (case 2), an 84-year-old woman, died 4 months after hospital admission. The third patient (case 3) was a 65-year-old man whose outcome is unknown. Among the patients with DACs were 16 men and 18 women. Their age ranged from 47 years to 80 years, with a mean of 63.7 years. The site of the primary tumor was the head of the pancreas in 30 cases and the body to tail in 4 cases. The tumor tissue from both primary and metastatic sites was fixed in 10% formalin and routinely processed for paraffin embedding. The sections were stained with hematoxylin and eosin (H&E) and periodic acid-Schiff (PAS).

### Immunohistochemistry

From the paraffin-embedded tissue blocks, 3-μm sections were cut for immunohistochemical staining. A total of 15 antibodies were used: two chromogranin A (CGA) monoclonal antibodies (Ventana Medical Systems, Tucson, AZ, USA, for single staining; Linaris, Wertheim-Bettingen, Germany, for double staining, at a dilution of 1:2); synaptophysin polycloncal antibody (Dako, Glostrup, Denmark, 1:50); cytokeratin (CK) 7 monoclonal antibody (Dako, 1:25); carcinoembryonic antigen (CEA) monoclonal antibody (Dako, 1:100); carbohydrate antigen (CA) 19–9 monoclonal antibody (gift of Dr. Kalthoff, Kiel, 1:200); MUC1 monocloncal antibody (Novocastra, Newcastle, UK, 1:100); trypsin monoclonal antibody (Ventrex Laboratories, Portland, OR, USA, 1:5000); insulin monoclonal antibody (BioGenex, San Ramon, CA, USA, 1:40); glucagon polyclonal antibody (BioGenex, 1:60); somatostatin polyclonal antibody (Dako, 1:200); pancreatic polypeptide (PP) polyclonal antibody (Dako, 1:10000); Ki-S5 (which recognizes a formalin-resistant epitope of the Ki-67 proliferation antigen [19]) monoclonal antibody (Department of Pathology, University of Kiel, Germany); p53 monoclonal antibody (Oncogene Research Products, Boston, MA, USA, 1:20); and deleted in pancreatic cancer-4 (DPC4) monoclonal antibody (Santa Cruz Biotechnology, Santa Cruz, CA, USA, 1:30). The immunostaining for CGA and hormone markers was carried out using the alkaline phosphatase–anti-alkaline phosphatase (APAAP) technique and for remaining antibodies the avidin-biotin-peroxidase complex method was used. The synaptophysin, CK7 and MUC1 immunostaining was performed on an automated stainer (Ventana). The immunoreaction was detected with new fuchsin or 3,3'-diaminobenzidine (DAB). For double staining with Ki-S5 and CGA, Ki-S5 immunostaining was first applied using the EnVision-horseradish peroxidase (HRP) method and DAB was used as a brown chromogen. Subsequently, CGA staining was performed using the APAAP technique and new fuchsin was used as a red chromogen. The tissue samples were subjected to pressure cooker treatment for 3.5 min prior to CEA, Ki-S5, p53, and DPC4 immunostaining. Ductal differentiation was defined as the presence of ductal or glandular structures, mucin production and CA19–9 or CEA expression, while endocrine cells were characterized by the presence of CGA and/or hormone expression [17]. The Ki-S5 labeling index (LI) was calculated as percentage of positive cells in at least 1000 tumor cells.

### Reactivity scores of SECs in DACs compared with endocrine cells in the surrounding tissues

The number of SECs in DACs, of SECs in non-neoplastic ducts and of islet cells in the surrounding tissues that were positive for each hormone was graded (score 0–2) on an arbitrary scale, as follows: 0, no positive cells present; 1, one or a few positive cells present in one or a few areas; 2, positive cells present in several or many areas or several or many positive cells present in or associated with a duct.

## Results

### Histopathological findings in mixed ductal-endocrine carcinomas

In case 1, the tumor was a moderately to poorly differentiated adenocarcinoma showing a cribriform growth pattern with a solid component. The cribriform glandular structures contained PAS-positive material (Fig. 1). Goblet-like cells with intracellular mucin were interspersed. The tumor cells had enlarged nuclei and faintly eosinophilic, granular cytoplasm. Mitotic cells were frequent. Immunohistochemically, approximately 50% of the tumor cells stained for CGA and synaptophysin. Simultaneously, the gland-forming tumor cells were CK 7 positive and showed apical positivity for CEA and CA 19–9 but not MUC1 and trypsin. Hormonal reactivity was not detected. The Ki-S5 LI was 48.2%.

In case 2, most of the tumor was a moderately to poorly differentiated adenocarcinoma with small glandular structures, a mucinous (colloid) component and also small solid cell clusters and cords supported by a dense stroma (Fig. 2). Immunohistochemically, the findings for CGA, synaptophysin, CEA and CA 19–9 were similar to those in case 1. In addition, there was an intense staining for CK 7 diffusely and for MUC1 in about 50% of the tumor cells, while somatostatin expression was detected in approximately 30% of the cells. No trypsin positive cells were found. Ki-S5-positive cells were hardly observed, probably due to technical reasons.

In case 3, the tumor was composed of well to moderately differentiated DAC structures and a solid component of rather small cells (Fig. 3). Occasionally, small gland-like lumina were found within the solid component. The DAC and the solid component were well separated from each other. Immunohistochemically, the DAC component showed CK 7, CEA and CA 19–9 positivity, while the solid carcinoma component displayed large clusters of cells positive for CGA and synaptophysin, that accounted for about 30–50% of the tumor cells. Hormonal reactivity was not detected. The Ki-S5 LI of areas of small cell carcinoma (67.1%) was higher than that of areas of DAC.

The three tumors were classified into two types: combined tumors consisting of glandular and solid

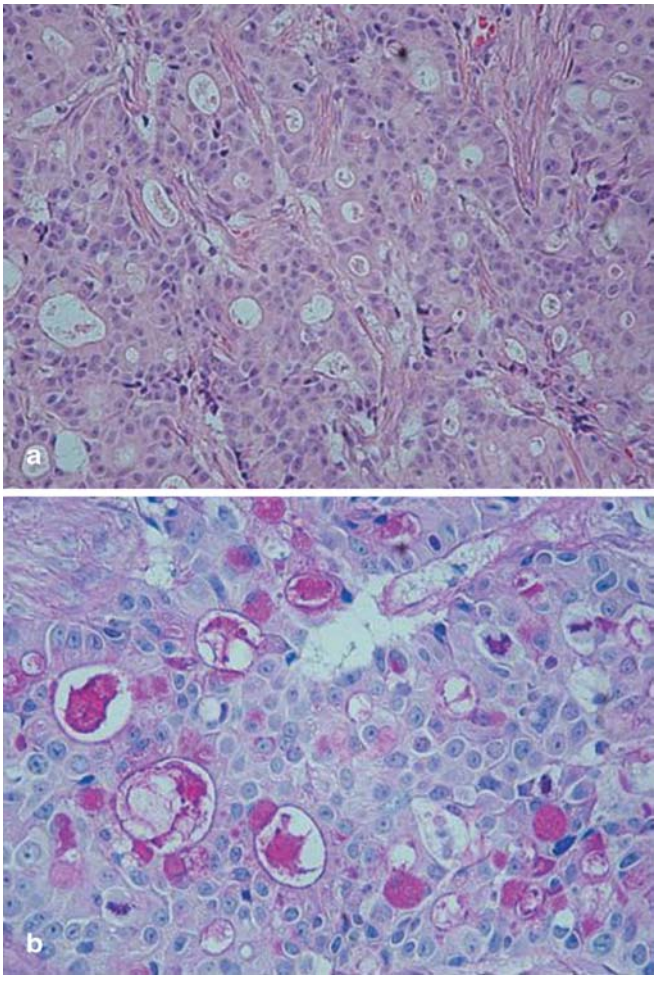



**Fig. 1** Histological features of mixed ductal-endocrine carcinoma (case 1). The tumor reveals a moderately differentiated adenocarcinoma showing cribriform glandular structures and goblet-like cells. H&E, ×120 (**a**) and PAS, ×250 (**b**)

structures with immunopositivity for CGA, synaptophysin, CEA and CA 19–9 (cases 1 and 2), and a composite tumor composed of areas of DAC and areas of endocrine neoplasm (case 3).

## Histopathological findings in DACs with SECs

Three types of SEC in DACs were distinguished and designated as types A to C. Type-A cells were more or less oval in shape and lined up along the base of the neoplastic glands, sometimes showing a periglandular arrangement (Fig. 4, Fig. 5). Some cells appeared to bud off from the neoplastic ducts. Type-A cells were all lacking in cellular atypia. Type-B cells were situated at the base of the neoplastic glands, forming clusters similar to Langerhans' islets and were usually associated with type-A cells (Fig. 4a, Fig. 5). Type-B cells also did not show any cellular atypia. Type-C cells consisted mainly of triangular or rectangular-shaped cells situated between

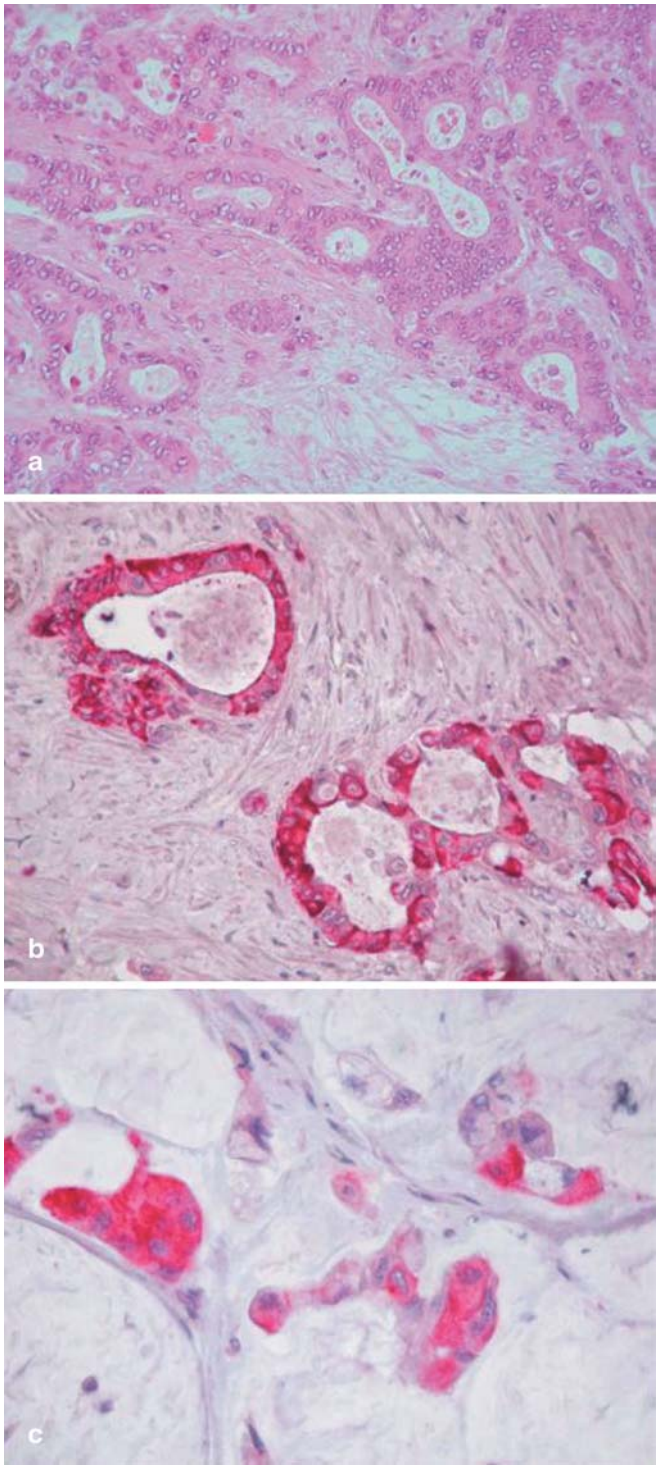



**Fig. 2** Histological features of mixed ductal-endocrine carcinoma (case 2). The tumor shows a moderately differentiated adenocarcinoma (**a**), including ductal structures (**b**), and mucinous carcinomatous structures (**c**). Tumor cells show a diffuse expression of chromogranin A (CGA) (**b**, **c**). H&E, ×120 (**a**) and CGA, ×250 (**b**, **c**)

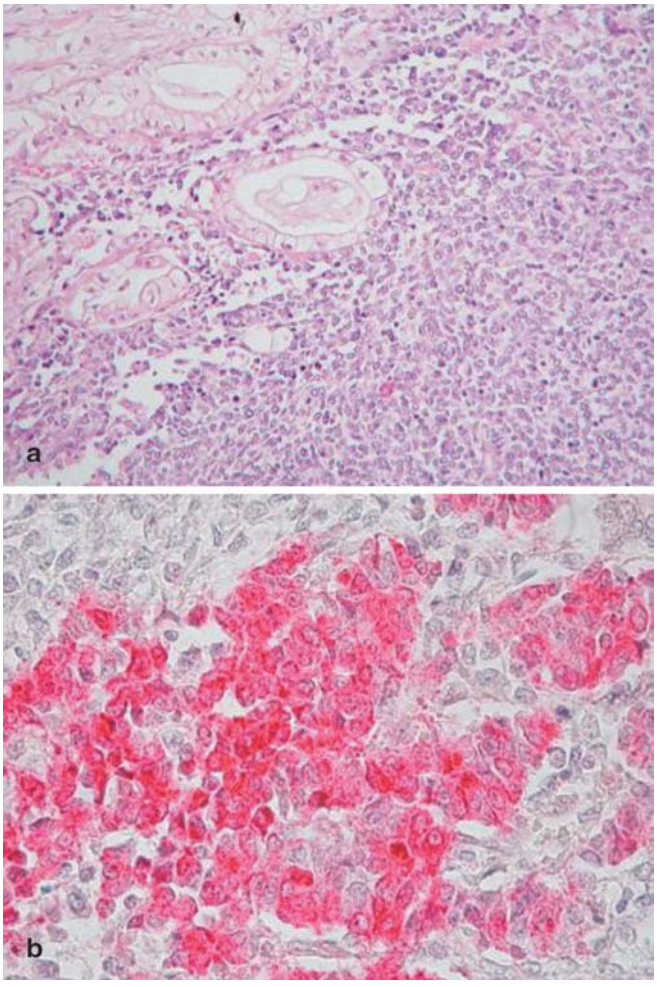



**Fig. 3** Histological features of mixed ductal-endocrine carcinoma (case 3). **a** Small cell carcinoma component adjacent to ductal adenocarcinomas. The small cell carcinoma component displayed chromogranin A (CGA)-positive cell clusters (**b**). H&E, ×120 (**a**) and CGA, ×250 (**b**)

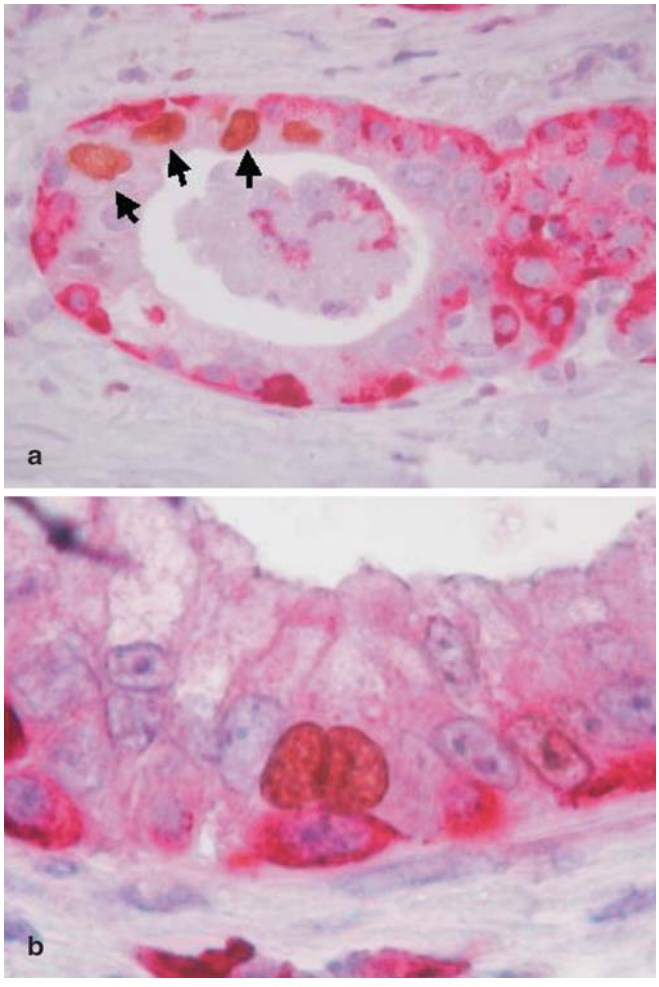



**Fig. 4** Ductal adenocarcinoma structures with attached chromogranin A (CGA)-positive scattered tumor-associated endocrine cells (SECs) of A and B type. Only the neoplastic columnar cells are Ki-S5 positive (*arrows*). Double immunostaining for CGA and Ki-S5, ×250 (**a**), ×1000 (**b**)

neoplastic duct cells with their apexes stretching far toward the neoplastic lumen (Fig. 6a). Moreover, polygonal-shaped cells within the multilayered malignant glands were also included in this type (Fig. 6b). Type-C cells usually showed cellular atypia. A and B type cells were more common in the vicinity of non-cancerous pancreatic tissue than in the central regions of the tumors and tended to also be associated with well-differentiated neoplastic ducts. In some cases, there were ductuloinsular complex-like structures consisting of neoplastic glands and A and B type cells. A and B type cells were occasionally connected with islets. On the other hand, type-C cells appeared to be randomly distributed and were also observed in the perineural space in three cases (Fig. 6b). Type-C cells were often present in neoplastic glands with mucinous or intestinal (goblet cell) metaplasia and in mucinous carcinomatous areas.

Most DACs were G1 (12 of 32) or G2 (15 of 32) tumors. SECs were found in 32 of 34 DACs (Table 1). Type-A cells were identified in 31 cases (91%), type-B cells in 24 (71%) and type-C cells in 13 (38%). There were significantly fewer type-C cells than type A and B cells in about four-fifths of the cases. In lymph nodes with DAC metastases, SECs were found in only three cases, and they consisted only of type-C cells. In two cases, they were observed not only in peripancreatic lymph nodes but also in distant lymph nodes.

## Double staining for CGA and Ki-S5 in DACs with SECs

In primary sites, the double-stained cells were type-C cells in six cases (Fig. 6), three of which were the cases that also had SECs (type-C cells) in metastatic lymph nodes (Table 1). The rate of Ki-S5-positivity of type C cells was more than 10% in two of the three cases. A- and B-type cells were not Ki-S5 positive (Fig. 4).

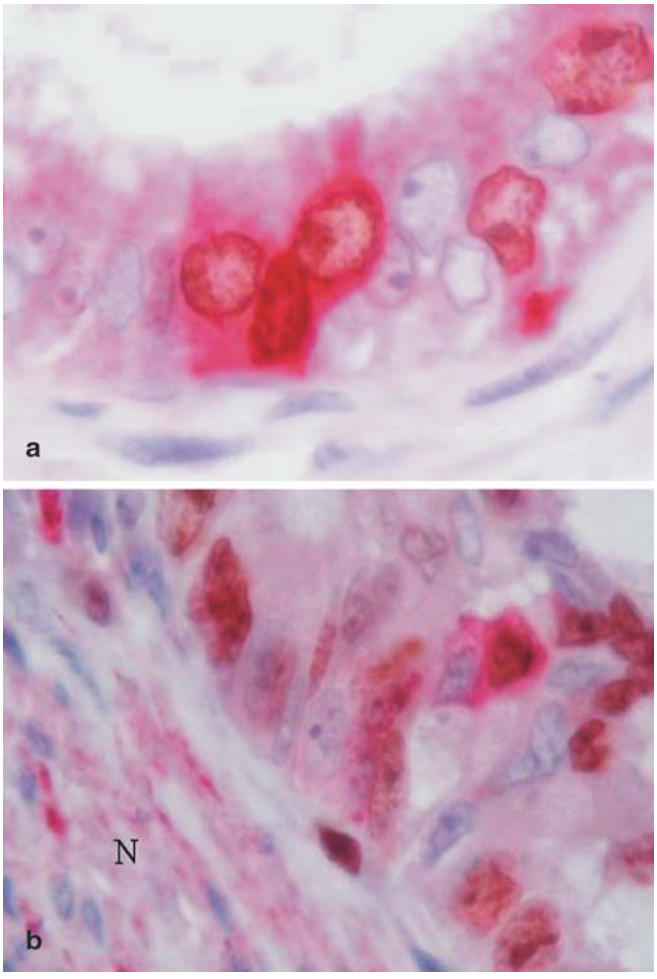



**Fig. 5** p53 nuclear accumulation and deletion of DPC4 are detected in ductal carcinoma cells, but not in A- and B-type cells. Immunostaining for p53, ×250 (**a**) and for DPC4, ×250 (**b**)

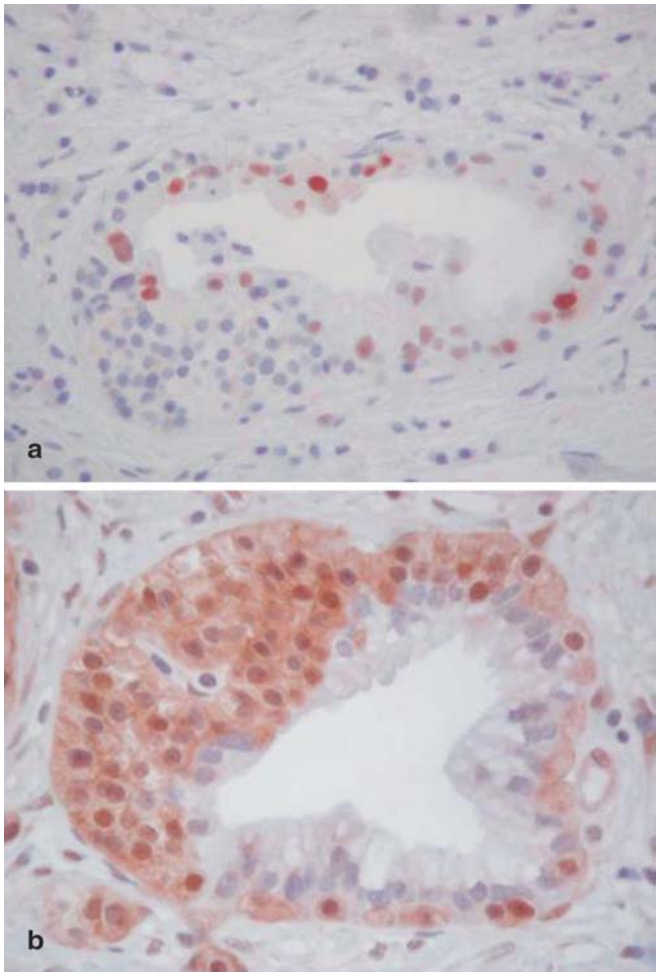



**Fig. 6** Chromogranin A (CGA) and Ki-S5 positive cells intermingled with neoplastic columnar cells. *N* nerve. Double immunostaining for CGA and Ki-S5, ×1000 (**a**, **b**)

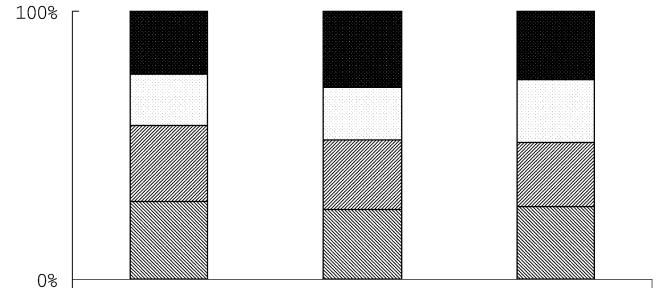
**Table 1** Results of the immunohistochemical analysis of scattered tumor-associated endocrine cells (SECs) in ductal adenocarcinomas (DACs), *A,B* non-neoplastic SECs, *C* neoplastic SECs

| | Incidence | Cell type | Incidence | Double-stained cells (Ki-S5+CGA) | Islet hormone expression |
|---|---|---|---|---|---|
| Primary tumor | 32/34 | A,B | 31/34, 24/34 | 0 | 17/18 |
| C | 13/34 | 6/34 | 0 | | |
| Lymph-node metastases | 3/34 | A,B | 0 | 0 | 0 |
| C | 3/34 | 3/34 | 0 | | |

## Hormonal reactivity of SECs in DACs compared with endocrine cells in the surrounding tissues

SECs were found in the surrounding non-neoplastic ducts or ductules, especially in those with hyperplastic or metaplastic changes. Ductuloinsular complex-like structures were also observed in some cases. However, islet cells in the surrounding area or intermingled within tumors seemed to be increased in most of the cases. In one case, the islets were densely aggregated and enlarged, suggesting a focal increase in PP cells, as can be seen in the PP lobe.

Among 18 randomly studied cases, 17 DACs had islet hormone-immunoreactive cells. Only A- and B-type cells contained hormones (Table 1). Thirteen cases showed reactivity for two or more hormones. SECs with hormonal reactivity were not observed in metastatic lymph nodes. Figure 7 shows the proportional positivity for each hormone of SECs in DACs, in non-neoplastic ducts, and islets. It demonstrates that the proportional distribution of the different islet cell types is approximately the same at all three sites.




| | SECs in DACs | SECs in non-neoplastic ducts | Islet cells |
|---|---|---|---|
| ■ *PP* | 19 | 23 | 34 |
| □ *som.* | 15 | 16 | 31 |
| ▨ *glu.* | 23 | 21 | 32 |
| ▧ *ins.* | 23 | 21 | 36 |

**Fig. 7** Proportional hormone expression in scattered tumor-associated endocrine cells (SECs) associated with ductal adenocarcinomas (DACs) compared with that of SECs in non-neoplastic pancreatic ducts and with islet cells. The bar graph shows the proportional distribution of hormones at different sites in 18 randomly studied cases. In the table at the bottom the scores of these 18 cases for each hormone were totaled. *PP* pancreatic polypeptide, *som.* somatostatin, *glu.* glucagon, *ins.* insulin

Comparison of genetic changes (p53 and DPC4) in mixed ductal-endocrine carcinomas and in DACs with SECs

Of the cases of mixed ductal-endocrine carcinoma, cases 1 and 2 lacked p53 nuclear expression and deletion of DPC4, while case 3 showed p53 nuclear expression. Case 3 was not examined for DPC4 expression because there was not enough tissue available. Of the DACs, eight cases that had a relatively large number of SECs (including type A cells in 7 cases, type B cells in 6, and type C cells in 6) were studied. p53 nuclear expression was detected in five cases, diffuse deletion of DPC4 was detected in four cases and focal deletion in three cases. Four of these cases showed both p53 expression and DPC4 deletions. SECs of the A and B type did not show p53 and DPC4 abnormalities (Fig. 5).

## Discussion

Two types of mixed ductal-endocrine carcinoma were distinguished in our series, a combined tumor consisting of intermingeled ductal and neuroendocrine cells forming glandular and solid structures (cases 1 and 2), and a composite tumor consisting of DAC structures embedded in or next to a solid cell compartment. The ductal phenotype of the tumor cells was characterized by CEA and CA 19–9 positivity, trypsin negativity and in one case (case 2) also by MUC1 expression, while the neuroendocrine phenotype was identified by CGA and synaptophysin expression. In case 3, the ductal structures and the solid endocrine cell component were clearly separated from each other, comparable to one of Klimstra's cases of mixed acinar-endocrine carcinomas with segregated areas of acinar and endocrine cells [13, 35]. In cases 1 and 2, the ductal and endocrine cells were intimately intermingled and occasionally seemed to form amphicrine cells, i.e., cells coexpressing exocrine (ductal) and endocrine markers. This notion was further substantiated by double staining the tumor cells of case 2 with PAS and synaptophysin, which revealed single cells that contained both reaction products (data not shown). Amphicrine cells with coexpression of trypsin and synaptophysin were also observed in an acinar cell carcinoma [13, 35].

We found three cases in the English-language literature that appeared to represent mixed ductal-endocrine carcinomas of the composite type. Leteurtre et al. [20] reported a 74-year-old man who had a metastasizing carcinoma in the head of the pancreas, histologically showing distinct features of a differentiated DAC component and a trabecular or acinar endocrine carcinoma with somatostatin immunopositivity. Terada et al. [37] reported a 62-year-old man who had a metastasizing carcinoma in the body to tail of the pancreas, possibly evolved from an endocrine tumor that had already been present as gastrinoma in Zollinger-Ellison syndrome 24 years earlier. Histologically, the tumor consisted of a poorly differentiated DAC component and a trabecular or ribbon-like endocrine carcinoma. Schron and Mendelsohn [37] reported a 62-year-old woman who had a metastasizing carcinoma in the head of the pancreas, histologically showing features of a poorly differentiated adenocarcinoma and a solid endocrine tumor. The remaining two cases (a case in a 65-year-old man described by Eusebi et al. [4] and a case in a 62-year-old patient published by Sessa et al. [34]) cannot be clearly classified from the illustrations and descriptions, but their histological features seem to resemble those of case 2 (combined tumor) of our series. Apart from these cases, there are a number of other reports in the literature that describe "mixed pancreatic tumors" [1, 5, 23, 24, 25, 31, 33, 35, 40]. Judging from the illustrations and descriptions (see below), they do not fulfill the strict criteria of truly mixed tumors, as defined in the WHO classification [16].

As for hormone production, expression of somatostatin has often been detected immunohistochemically in non-functional cases of mixed ductal-endocrine carcinoma [4, 20, 33], including one of our cases (case 2). Gastrin, however, was detected in cases that presented with a hormonal syndrome [23, 37]. On the basis of the clinical data available, including our cases, the prognosis of the mixed ductal-endocrine carcinoma was as poor as that of ordinary DACs [22]. Also, high proliferative activity was detected in two of our cases. The reason why the tumor in case 2 had no Ki-S5 positive cells is unclear, but it must have been a false-negative reaction, because the tumor had the features of a high-grade DAC. Variants of non-ductal tumors such as endocrine tumors with entrapped ducts and acini [9, 24, 25, 31, 39, 41], mucin-producing endocrine tumors [26], acinar cell carcinomas with endocrine component [6, 7, 12, 40], or mixed acinar-

endocrine carcinomas [13, 35] may be mistaken for mixed ductal-endocrine carcinomas. However, they should be strictly distinguished, because their behavior is dictated by their acinar or endocrine elements [14, 17]. For the differential diagnosis versus so-called collision tumors composed of two topographically separate components, the presence of mixed-type metastases may be needed.

Recently Kim et al. [11] proposed two models of multi-step progression for mixed glandular-neuroendocrine gastric carcinomas; model 1 is a common genetic pathway with p53 mutation through three sequential tumors: at the beginning there is a homogeneous adenocarcinoma. This gradually transforms into a genetically heterogeneous adenocarcinoma and finally displays an adenocarcinoma with neuroendocrine component. Model 2 is an uncommon genetic pathway resulting from a non-dysjunctional mitosis in which dual differentiation initially and concurrently arises from a single precursor cell.

Capella et al. [2] have reported that p53 nuclear accumulation is frequently present in the composite type of mixed endocrine-exocrine tumors [described as mixed adenocarcinoma-carcinoid or mixed poorly differentiated endocrine (small cell) carcinoma] of the gastrointestinal tract, while no genetic changes were noticed in the combined type (described as mixed diffuse carcinoma-carcinoid). Accordingly, we could speculate that there is a genetically different carcinogenesis between the combined tumors of our cases 1 and 2 having no p53 mutation and the composite tumor of our case 3 having a p53 mutation.

In our series, SECs were usually not very numerous in the single DAC, but they occurred in almost all of the tumors (94%), as described in previous reports [3, 10, 14, 18, 27, 30, 32]. However, it remains unclear whether SECs are neoplastic or not. We separated SECs into three types (A, B, and C) in the expectation that SECs are heterogeneous and may include both non-neoplastic and neoplastic cells. Our findings showed that most SECs consisted of A and B type cells, i.e., cells lined up along the base of neoplastic glands (A type), sometimes forming clusters (B type) that had no proliferative activity and no genetic changes (i.e., expression of p53 and deletion of DPC4). In addition, A- and B-type cells showed a hormonal profile similar to that of the SECs that were associated with non-neoplastic ducts and islets, which were involved in the carcinoma-associated pancreatitis that surrounds the tumor. Only a few SECs belonged to type-C cells, i.e., cells situated between neoplastic duct cells or within multilayered malignant glands, which apart from their localization in the primary tumor were also occasionally observed in metastatic sites beyond the pancreas. Since the type-C cells were intimately integrated into the epithelial lining of the neoplastic ductular structures and showed proliferative activity, we regarded them as neoplastic, deriving from neoplastic columnar cells. Interestingly, approximately the same percentage of neoplastic endocrine cells has been observed in adenocarcinomas of other non-endocrine organs [2].

As to the cause and effect of the close association between the non-neoplastic SECs (A- and B-type cells) and the neoplastic glands, it is interesting to note that this phenomenon is found especially in well-differentiated DACs and is only rarely seen in poorly differentiated carcinomas. It therefore appears that when neoplastic glands spread into preexisting pancreatic parenchyma, they entrap, and attach to, islet cells, if these neoplastic glands are well differentiated and thus closely resemble non-neoplastic ducts. This is the most likely explanation, since islet cells may attach to non-neoplastic ducts in the same way as they do to neoplastic ducts, particularly in chronic pancreatitis [15]. The reason for the association between the endocrine cells and the neoplastic columnar cells is not known, but it is tempting to speculate that it is mediated by certain adhesion molecules that are only produced by well-differentiated DACs. Whether the function of the attached endocrine cells and entrapped islets is also influenced by factors released by the cancer cells is another interesting question that has been discussed in detail in connection with the frequent development of diabetes in DAC [28, 30].

The observation that SECs occur particularly in well-differentiated DACs may also explain why Tezel et al. [38] found that DACs showing neuroendocrine differentiation had a better prognosis than DACs without such differentiation. Kamisawa et al. [8] also reported that DACs with SECs had a slightly better prognosis than DACs without SECs. In addition, they observed three adenocarcinomas with diffuse immunoreactivity for neuron-specific enolase and synaptophysin. However, from the illustration, it appears that these three cases did not represent ordinary DACs, but intraductal papillary-mucinous neoplasms, which differ in their endocrine cell distribution from DACs [21]. From studies on the prognostic value of grading of DACs, it is well known that patients with G1 and G2 DACs have a significantly longer survival than patients with G3 DACs [22].

In summary, mixed ductal-endocrine carcinomas, irrespective of whether they are of the combined or composite type, can be distinguished from DACs with SECs. While most of these SECs appear to be non-neoplastic, a minor fraction seems to belong to the neoplastic cell population of the DACs.

**Acknowledgements** We are grateful to Dr. G. Fischer, Wilhelmshaven, Germany, and Dr.Voudouris, Ludwigsburg, Germany, for providing case material and follow-up information.

## References

1. Arihiro K, Inai K (1991) Malignant islet cell tumor of the pancreas with multiple hormone production and expression of CEA and CA19–9. Report of an autopsy case. Acta Pathol Jpn 41:150–157
2. Capella C, La Rosa S, Uccella S, Billo P, Cornaggia M (2000) Mixed endocrine-exocrine tumors of the gastrointestinal tract. Semin Diagn Pathol 17:91–103
3. Chen J, Baithun SI, Pollock DJ, Berry CL (1988) Argyrophilic and hormone immunoreactive cells in normal and hyperplastic pancreatic ducts and exocrine pancreatic carcinoma. Virchows Arch 413:399–405

4. Eusebi V, Capella C, Bondi A, Sessa F, Vezzadini P, Mancini AM (1981) Endocrine-paracrine cells in pancreatic exocrine carcinomas. Histopathology 5:599–613
5. Gullo L, De Giorgio R, D'Errico A, Grigioni W, Parenti M, Corinaldesi R (1992) Pancreatic exocrine carcinoma producing adrenocorticotropic hormone. Pancreas 7:172–176
6. Hassan MO, Gogate PA (1993) Malignant mixed exocrine-endocrine tumor of the pancreas with unusual intracytoplasmic inclusions. Ultrastruct Pathol 17:483–493
7. Hoorens A, Lemoine NR, McLellan E, Morohoshi T, Kamisawa T, Heitz PU, Stamm B, Rüschoff J, Wiedenmann B, Klöppel G (1993) Pancreatic acinar cell carcinoma. An analysis of cell lineage markers, p53 expression, and Ki-ras mutation. Am J Pathol 143:685–698
8. Kamisawa T, Fukuyama M, Tabata I, Isawa T, Tsuruta K, Okamoto A, Koike M (1996) Neuroendocrine differentiation in pancreatic duct carcinoma special emphasis on duct-endocrine cell carcinoma of the pancreas. Pathol Res Pract 192:901–908
9. Kashiwabara K, Nakajima T, Shinkai H, Fukuda T, Oono Y, Kurabayashi Y, Kojima T, Nagamachi Y (1991) A case of malignant duct-islet cell tumor of the pancreas immunohistochemical and cytofluorometric study. Acta Pathol Jpn 41:636–641
10. Kay D, DeLellis RA, Dayal Y, Lloyd RV, Duggan MA, Tallberg K, et al. (1985) Ductal adenocarcinomas of the pancreas with neuroendocrine cells: An immunohistochemical study. Lab Invest 52:33A–34A
11. Kim KM, Kim MJ, Cho BK, Choi SW, Rhyu MG (2002) Genetic evidence for the multi-step progression of mixed glandular-neuroendocrine gastric carcinomas. Virchows Arch 440:85–93
12. Klimstra DS, Heffess CS, Oertel JE, Rosai J (1992) Acinar cell carcinoma of the pancreas: a clinicopathologic study of 28 cases. Am J Surg Pathol 16:815–837
13. Klimstra DS, Rosai J, Heffess CS (1994) Mixed acinar-endocrine carcinomas of the pancreas. Am J Surg Pathol 18:765–778
14. Klöppel G (2000) Mixed exocrine-endocrine tumors of the pancreas. Semin Diagn Pathol 17:104–108
15. Klöppel G, Bommer G, Commandeur G, Heitz P (1978) The endocrine pancreas in chronic pancreatitis. Immunocytochemical and ultrastructural studies. Virchows Arch 377:157–174
16. Klöppel G, Solcia E, Longnecker DS, Capella C, Sobin LH (1996) Histological typing of tumours of the exocrine pancreas. Second edition. WHO International histological classification of tumours. Springer, Berlin Heidelberg New York
17. Klöppel G, Hruban RH, Longnecker DS, Adler G, Kern SE, Partanen TJ (2000) Ductal adenocarcinoma of the pancreas. In: Hamilton SR, Aaltonen LA (eds) Pathology and genetics of tumours of the digestive system. WHO Classification of Tumours. IARC Press, Lyon, pp 221–230
18. Kodama T, Mori W (1983) Morphological behavior of carcinoma of the pancreas. 2. Argyrophil cells and Langerhans' islets in the carcinomatous tissues. Acta Pathol Jpn 33:483–493
19. Kreipe H, Wacker HH, Heidebrecht HJ, Haas K, Hauberg M, Tiemann M, Parwaresch R (1993) Determination of the growth fraction in non-Hodgkin's lymphoma by monoclonal antibody Ki-S5 directed against a formalin-resistant epitope of the Ki-67 antigen. Am J Pathol 142:1689–1694
20. Leteurtre E, Brami F, Kerr-Conte J, Quandalle P, Lecomte-Houcke M (2000) Mixed ductal-endocrine carcinoma of the pancreas: a case study with mixed ductal-endocrine metastasis double labeled for cytokeratin 19 and synaptophysin. Arch Pathol Lab Med 124:284–286
21. Longnecker DS, Adler G, Hruban RH, Klöppel G (2000) Intraductal papillary-mucinous neoplasms of the pancreas. In: Hamilton SR, Aaltonen LA (eds) Pathology and genetics of tumours of the digestive system. WHO Classification of Tumours. IARC Press, Lyon, pp 237–240
22. Lüttges J, Schemm S, Vogel I, Hedderich J, Kremer B, Klöppel G (2000) The grade of pancreatic ductal carcinoma is an independent prognostic factor and is superior to the immunohistochemical assessment of proliferation. J Pathol 191:154–161
23. Mihas AA, Ceballos R, Mihas A, Gibson RG (1978) Zollinger-Ellison syndrome associated with ductal adenocarcinoma of the pancreas. N Engl J Med 298:144–146
24. Nonomura A, Kono N, Mizukami Y, Nakanuma Y, Matsubara F (1992) Duct-acinar-islet cell tumor of the pancreas. Ultrastruct Pathol 16:317–329
25. Okada Y, Mori H, Tsutsumi A (1995) Duct-acinar-islet cell tumor of the pancreas. Pathol Int 45:669–676
26. Ordonez NG, Balsaver AM, Mackay B (1988) Mucinous islet cell (amphicrine) carcinoma of the pancreas associated with watery diarrhea and hypokalemia syndrome. Hum Pathol 19:1458–1461
27. Permert J, Mogaki M, Andrén-Sandberg A, Kazakoff K, Pour PM (1992) Pancreatic mixed ductal-islet tumors. Is this an entity? Int J Pancreatol 11:23–29
28. Permert J, Larsson J, Westermark GT, Herrington MK, Christmanson L, Pour PM, Westermark P, Adrian TE (1994) Islet amyloid polypeptide in patients with pancreatic cancer and diabetes. N Engl J Med 330:313–318
29. Pipeleers D, Couturier E, Gepts W, Reynders J, Somers G (1983) Five cases of somatostatinoma: clinical heterogeneity and diagnostic usefulness of basal and tolbutamide-induced hypersomatostatinemia. J Clin Endocrinol Metab 56:1236–1242
30. Pour PM, Permert J, Mogaki M, Fujii H, Kazakoff K (1993) Endocrine aspects of exocrine cancer of the pancreas. Their patterns and suggested biologic significance. Am J Clin Pathol 100:223–230
31. Reid JD, Yuh SL, Petrelli M, Jaffe R (1982) Ductuloinsular tumors of the pancreas: a light, electron microscopic and immunohistochemical study. Cancer 49:908–915
32. Sakaki M, Sano T, Hirokawa M, Takahashi M, Kiyoku H (2002): Immunohistochemical study of endocrine cells in ductal adenocarcinomas of the pancreas. Virchows Arch 441:249–255
33. Schron DS, Mendelsohn G (1984) Pancreatic carcinoma with duct, endocrine, and acinar differentiation. A histologic, immunocytochemical, and ultrastructural study. Cancer 54:1766–1770
34. Sessa F, Bonato M, Frigerio B, Capella C, Solcia E, Prat M, Bara J, Samloff IM (1990) Ductal cancers of the pancreas frequently express markers of gastrointestinal epithelial cells. Gastroenterology 98:1655–1665
35. Shimoike T, Goto M, Nakano I, Sato T, Migita Y, Ito T, Yanase T, Sezai S, Suzuki T, Nawata H (1997) Acinar-islet cell carcinoma presenting as insulinoma. J Gastroenterol 32:839–835
36. Suda K, Hashimoto K (1979) Argyrophil cells in the exocrine pancreas. Acta Pathol Jpn 29:413–419
37. Terada T, Matsunaga Y, Maeta H, Endo K, Horie S, Ohta T (1999) Mixed ductal-endocrine carcinoma of the pancreas presenting as gastrinoma with Zollinger-Ellison syndrome: an autopsy case with a 24-year survival period. Virchows Arch 435:606–611
38. Tezel E, Nagasaka T, Nomoto S, Sugimoto H, Nakao A (2000) Neuroendocrine-like differentiation in patients with pancreatic carcinoma. Cancer 89:2230–2236
39. Tomita T, Bhatia P, Gourley W (1981) Mucin producing islet cell adenoma. Hum Pathol 12:850–853
40. Ulich T, Cheng L, Lewin KJ (1982) Acinar-endocrine cell tumor of the pancreas. Report of a pancreatic tumor containing both zymogen and neuroendocrine granules. Cancer 50:2099–2105
41. Vantyghem MC, Kerr-Conte J, Evrard A, Farah R, Racadot A, Proye C, Lefebvre J, Lecomte-Houcke M (1999) Endo-exocrine tumor of the pancreas masquerading as an insulinoma. Pancreas 19:314–318

Virchows Arch (2003) 442:266–270
DOI 10.1007/s00428-002-0757-z

ORIGINAL ARTICLE

**Koh Furuta · Shingo Yoshioka · Satoko Okabe · Masato Ikeda · Mihoko Oginosawa · Seiyo Ikeda · Yoshifuku Nakayama · Masahiro Kikuchi · Stanley R. Hamilton**

# Expressions of two adenomatous polyposis coli and E-cadherin proteins on human colorectal cancers

Received: 1 October 2002 / Accepted: 10 December 2002 / Published online: 11 February 2003
© Springer-Verlag 2003

**Abstract** Mutations in the adenomatous polyposis coli (APC) gene contribute to the progression of colorectal tumorigenesis. Despite the importance, few studies regarding the localization of this protein on surgically resected human colorectal cancer specimens using immunohistochemistry have been reported so far because of the unavailability of the antibodies for this use. The goal of this study has been to provide the APC protein expression and to validate the APC molecular studies. We took advantage of an immunohistochemistry procedure of applying the unique detergent-mediated antigen retrieval technique to frozen sections and examined the expressions of one amino (N)-terminal (AC4) and one carboxy (C)-terminal APC antibody (HG2). Further, we compared the stainings of APC antibodies with those of the E-cadherin antibody using a quantitative image analysis. E-cadherin is a critical morphogenetic regulator during embryogenesis and recent evidence strongly suggests that downregulation of E-cadherin expression in cancers is associated with a high rate of invasion and metastasis. The analysis indicated statistically that normal epithelia showed stronger staining than cancer cells ($P<0.05$). Further, in normal epithelia, the amino (N)-terminal APC antibody (AC4) showed a positive correlation with another carboxy (C)-terminal APC antibody (HG2). E-cadherin showed no positive correlation with other APCs in either the normal epithelia or cancer cells. This study verified reduced expressions of APCs and E-cadherin proteins in colorectal cancer cells. This suggests that the normal APC and E-cadherin protein expressions in benign epithelium are progressively and independently lost in the sporadic colorectal cancers.

**Keywords** APC · E-cadherin · Immunohistochemistry · Colon cancer · Antigen retrieval

K. Furuta (✉)
Department of Clinical Chemistry and Laboratory Medicine,
National Cancer Center Hospital,
5-1-1 Tsukiji, Chuo-ku, 104-0045 Tokyo, Japan
e-mail: kfuruta@ncc.go.jp
Fax: +81-3-35423815

S. Yoshioka · S. Ikeda · Y. Nakayama
Department of Surgery, School of Medicine, Fukuoka University,
Fukuoka, Japan

S. Yoshioka · S. Okabe · Y. Nakayama · M. Kikuchi
Department of Pathology, School of Medicine, Fukuoka University,
Fukuoka, Japan

M. Ikeda
Department of Occupational Health Economics,
School of Health Sciences, University of Occupational and
Environmental Health, Kitakyushu, Japan

M. Oginosawa
Department of Medical Technology 1,
School of Health Sciences, University of Occupational and
Environmental Health, Kitakyushu, Japan

S. R. Hamilton
Division of Pathology and Laboratory Medicine,
University of Texas, MD Anderson Cancer Center,
Houston, Texas, USA

## Introduction

Mutations in the adenomatous polyposis coli (APC) gene contribute to the progression of colorectal tumorigenesis. Germline mutations in APC result in an autosomal dominantly inherited disease called familial adenomatous polyposis (FAP), which is characterized by the development of multiple colorectal adenomatous polyps that are prone to develop carcinomas later. Somatic mutations are linked to the development of sporadic colorectal tumors including small benign adenomas [6, 14, 16, 17, 24]. The APC gene is localized to the human chromosome 5q21 and is expressed in all tissues that have been tested [3, 9, 11]. The product of the APC gene is a 300-kDa protein composed of 2843 amino acids [6, 10, 19]. Both germline and somatic mutations are almost all either nonsense or frame-shift mutations that result in a carboxy-terminal truncation of the APC gene product [6, 13, 14, 16, 17, 21].

E-cadherin is a member of the cadherin family of cell adhesion molecules [23]. This molecule is a critical morphogenetic regulator during embryogenesis, and

recent evidence strongly suggests that downregulation of E-cadherin expression in cancers is associated with a high rate of invasion and metastasis [5, 23].

Despite the importance, few studies [19] regarding the localization of this APC protein on surgically resected human colorectal cancer specimens using immunohistochemistry have been reported so far. This is because there are no available antibodies for this purpose. We took advantage of an immunohistochemistry procedure by applying the unique detergent-mediated antigen retrieval technique to frozen sections. We examined the APC protein expressions and validated the APC molecular studies. Further we compared the expressions of APC protein with those of E-cadherin protein by analyzing the paired sets of slides, and the relationship between two proteins was indicated.

## Materials and methods

### Colorectal mucosae and neoplasms

Tissue from surgical specimens resected from patients with primary sporadic colorectal cancer between 1997 and 1998 was provided by the Frozen Tissue Bank in the Department of Pathology of Fukuoka University School of Medicine. Seventeen cancers together with normal epithelia close to the cancerous areas were selected for this study. The mean age of these 17 patients was 66 years, with a range from 34 years to 87 years. The sex ratio (male:female) was 2:1. Tumor locations were as follows: cecum, three cases; transverse colon, four cases; descending colon, one case; sigmoid colon, two cases; rectum, seven cases. Histological type and its differentiation was as follows: well-differentiated adenocarcinoma, 10 cases; moderately differentiated adenocarcinoma, 5 cases; mucinous adenocarcinoma, 1 case; signet-ring-cell carcinoma, 1 case. Staging information based on the Dukes classification was as follows: Dukes A, 6 cases; Dukes B, 1 case; Dukes C, 10 cases.

### Antibodies

The anti-human APC N-terminal mouse monoclonal antibody AC4 (a gift from Oncogene Science, Uniondale, NY) was used at 6.9 μg/ml; anti-human APC C-terminal mouse monoclonal antibody HG2 (Oncogene Science, Uniondale, NY) at 9.8 μg/ml; anti-human E-cadherin mouse monoclonal antibody (Takara Shuzo Co., Shiga, Japan) at 2 μg/ml: anti-human Ki-67 (MIB-1) mouse monoclonal antibody (Immunotech, Marseille, France) at 1: 200 dilution. Ki-67 staining served as a positive control of immunohistochemistry procedures. As a negative control, the primary antibody was omitted.

### Immunohistochemistry

Three-micron-thick cryostat tissue sections on silane-coated slides were stained using an alkaline phosphatase immunohistochemistry technique with the mouse monoclonal APC (AC4, HG2), E-cadherin, and Ki-67 antibodies. The sections were air dried at room temperature for 1 h, treated with −20°C acetone for 20 min and air dried at room temperature for another hour. The sections were permeabilized with detergent (NP40) for 5 min at room temperature for antigen retrieval [4] and were incubated with skim milk for 30 min to eliminate non-specific background immunostaining. Staining of AC4 and HG2 without antigen retrieval was far from satisfactory. Therefore, various antigen retrieval methods, such as using microwave, autoclave, or detergent, were tested. Among them the present detergent method produced the best result both in quality of staining and in reproducibility. Following the detergent antigen retrieval, sections were incubated for 30 min at room temperature with APC (AC4, HG2) and Ki-67 antibodies diluted with 0.05 M Tris buffer, pH 7.4 or with E-cadherin antibody diluted with 1× TNC (Tris Base, NaCl, and $CaCl_2$) buffer, pH 7.4.

The sections were next treated for 30 min at room temperature with affinity-purified horse biotinylated anti-mouse IgG (BA-2000, Vector Laboratories, Burlingame, CA) diluted 1:200 for anti-APC (AC4, HG2), E-cadherin, and Ki-67 antibodies, followed by incubation in alkaline phosphatase-conjugated streptavidin (D-396, Dako, Kyoto, Japan) diluted 1:100 for 30 min at room temperature. The alkaline phosphatase activity was visualized using naphthol-AS-BI-phosphate as substrate (Sigma, St.Louis, MO) and new fuchsin as a coupler (Merek, Darmstadt, Germany). A red reaction product appeared within 10–15 min, at which time the reaction was terminated by transferring the sections to the fixing buffer. After 30–60 s of counterstaining with hematoxylin, sections were dehydrated in graded ethanol, isopropanol, and xylene and cover-slipped with mounting medium.

### Evaluation of expression by image analysis

Areas of tissue represented in slides from each of the 17 cases of human primary colorectal cancer were categorized as “normal” or “cancer” depending on their histopathologic features. The side opposite the sample on each slide was underlined by a marker indicating the histopathologic features such as “normal” or “cancer”. This underlining was performed to avoid the effects of non-specific staining in necrosis, and stroma on the image analysis described below. In each underlined category, three high-power view fields (×200 magnification) were randomly selected and captured by a charge-coupled device (CCD) camera (Spot, Diagnostic Instruments, Sterling Heights, MI) on the light microscope for computerized image analysis. Even in a single high-power view field, heterogeneity in staining was observed. To minimize this staining heterogeneity, each high-power view field was divided into ten regions of interest (ROIs). Each ROI was not necessarily the same size. Consequently the ROI selection was performed throughout the selected “normal” or “cancer” areas randomly. No special attention was paid to the leading edge of the invasive colorectal cancers. This was done to maintain the randomness in ROI selection. Although the number of high-power view fields seemed quite limited, the preliminary study indicated that three randomly selected high-power view fields was, statistically, necessary and sufficient. In each ROI, area (A) and mean intensity (I) of positive staining were measured. In the preliminary study, APC staining was done on three cases. After staining procedures, ten high-power view fields per case were randomly selected, and similar image analysis procedures were performed. After these, statistical analysis between cancerous and normal mucosa was done. This analysis revealed that the necessary and sufficient number of fields was three not ten. Therefore, we decided to use three fields for this study. The value of A×I in each ROI was

**Table 1** Comparison of immunohistochemistry staining positivity. Areas of tissue represented in slides from each of the 17 cases of human primary colorectal cancer were categorized as “normal” or “cancer” depending on their histopathological features. Each high-power view field was divided into ten regions of interest (ROIs). In each ROI, area (A) and mean intensity (I) of positive staining were measured. The value of A×I in each ROI was summed up and used for comparison of immunohistochemistry staining positivity. *APC* adenomatous polyposis coli

| | Normal | Cancer | *P* value* |
|---|---|---|---|
| APC (AC4) | 3.857 | 3.222 | 0.0012 |
| APC (HG2) | 3.461 | 2.702 | 0.0086 |
| E-cadherin | 6.152 | 4.715 | 0.0002 |

* Testing of the effects of cancer was executed using ANOVA

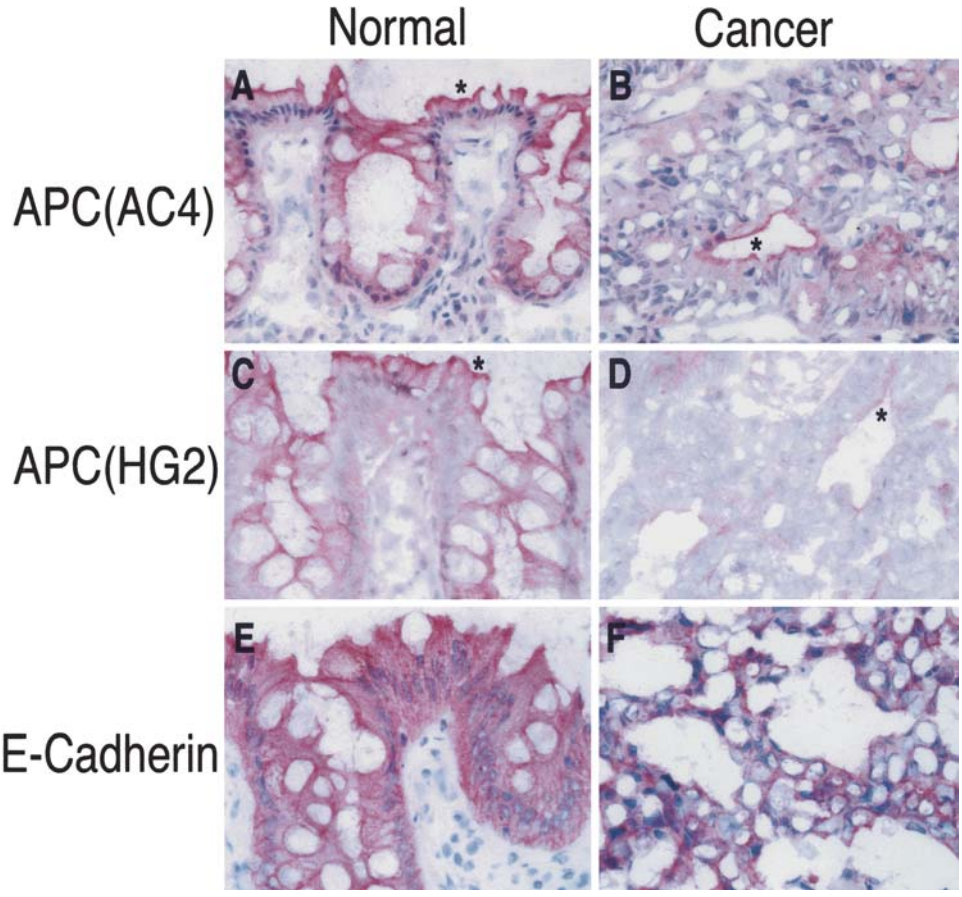



**Fig. 1** Immunohistochemical expression of adenomatous polyposis coli (APC), and E-cadherin in human colorectal cancers. Staining of APC and E-cadherin is shown. The *left column* (**A**, **C**, and **E**) shows staining of the normal epithelia. The *right column* (**B**, **D**, and **F**) shows staining of cancer (magnification, ×200; counterstained with methyl green). **A**, **C** (normal) and **B**, **D** (cancer): In normal colorectal epithelia, the APC antibody, of which the epitope is in either N-terminal (AC4) or C-terminal (HG2), showed membranous to cytoplasmic staining. Positive staining accumulated at the apical portion of the epithelia (*). In the cancer region, cytoplasmic staining was seen. Weakly enhanced apical staining was also seen in cancer glands (*). The staining patterns of these two APC antibodies were generally similar; however, HG2 showed a higher background than AC4. In the staining of each antibody, a quantitative statistical image analysis indicated that the normal epithelia showed stronger staining than that in the cancer region ($P<0.05$). **E** (normal) and **F** (cancer): In both the normal epithelia and the cancer regions, E-cadherin revealed the highest immunoreactivities among the three noted antibodies. Cytoplasmic to membranous staining was seen in the normal epithelia. In the cancer regions, membranous to cytoplasmic staining was observed. In the staining, a quantitative statistical image analysis indicated that the normal epithelia showed stronger staining than that in the cancer regions ($P<0.05$)

summed up and used for comparison of immunohistochemistry staining positivity (Table 1). Thus, a total of 3060 ROIs were analyzed. Image analysis was performed on a Macintosh computer using the public domain NIH Image program (developed at the U.S. National Institutes of Health and available from the Internet by anonymous FTP from zippy.nimh.nih.gov or on floppy disk from the National Technical Information Service, Springfield, Virginia, part number PB95–500195GEI).

### Statistics

The differences between expressions of APC (AC4, HG2) and E-cadherin in normal epithelia and in cancer were evaluated using analysis of variance (ANOVA). The dependent variable was each protein such as APC (AC4, HG2) and E-cadherin, and independent variables were the histopathologic diagnoses of the specimens: normal epithelia or cancer, the individual cases, and the interaction of the two variables. The analysis of difference was done using the *F* test.

The intra-class correlation coefficients [20] between a selection of two of three proteins were calculated in order to evaluate the relationship between them.

## Results

In the normal colorectal epithelia, the APC antibody, of which the epitope is either N-terminal (AC4) or C-terminal (HG2), showed membranous to cytoplasmic staining. Positive staining accumulated at the apical portion of the epithelia. In cancer regions, cytoplasmic staining was seen. Not strong but weakly enhanced apical staining was also seen in cancer glands. No remarkable nuclear localization of APC proteins was visible. The staining patterns of these two APC antibodies were generally similar; however, HG2 showed a higher back-

**Table 2** Correlations among three antibodies assessed using intraclass correlation (IC). The underlined number indicates the existence of a statistically significant correlation between two proteins. *APC* adenomatous polyposis coli

| | APC (AC4) | | APC (HG2) | | E-cadherin | |
|---|---|---|---|---|---|---|
| | IC | *P* value | IC | *P* value | IC | *P* value |
| Normal | | | | | | |
| APC(AC4) | | | 0.423 | 0.0367 | –0.250 | 0.8432 |
| APC(HG2) | | | | | –0.389 | 0.9464 |
| Cancer | | | | | | |
| APC(AC4) | | | –0.007 | 0.5090 | 0.028 | 0.4534 |
| APC(HG2) | | | | | –0.536 | 0.9896 |

ground than AC4 (Fig. 1A, B, C, D). In both normal epithelia and cancer regions, E-cadherin revealed the highest immunoreactivities among these three antibodies. Cytoplasmic to membranous staining was seen in normal epithelia. No remarkable apical staining was seen. In cancer regions, membranous to cytoplasmic staining was observed (Fig. 1E, F).

In the staining of each antibody, a quantitative statistical image analysis indicated that normal epithelia showed stronger staining than that of a cancer region ($P<0.05$) (Table 1). Further, in normal epithelia, amino (N)-terminal APC antibody (AC4) showed positive correlation with another carboxy (C)-terminal APC antibody (HG2). In cancer regions, no positive correlations between these two antibodies were seen ($P<0.05$). In both normal epithelia and in cancer regions, E-cadherin showed no positive correlation with other APCs (Table 2).

## Discussion

To our knowledge, our current study is among the first to describe the localization of the N-terminal (AC4) and the C-terminal APC (HG2) antibodies on surgically resected human colorectal cancer specimens. It has been reported that APC is involved in cell adhesion [22]. The APC antibodies are specific for epitopes close to the N- and C-termini of APC [1]. Moreover, as most naturally occurring APC mutations delete the N- but not the C-terminal regions of the protein [12, 15], these antibodies have the potential to discriminate expression of truncated mutant and wild-type APC in cytological preparations. This study indicated that an APC antibody, of which the epitope is in either N-terminal or C-terminal, became highly expressed in normal epithelia relative to a cancer region (AC4: $P=0.0012$; HG2: $P=0.0086$; Table 1). Further, the fact that a statistically significant correlation was observed only in normal epithelia ($P=0.0367$), not in a cancer region ($P=0.509$), suggested that the normal APC protein expression in benign epithelium is progressively lost in the sporadic colorectal cancers (Table 2) [7]. Recently, Bienz and Clevers [2] reviewed the current status of the APC molecules from the viewpoint of a wingless signal transduction pathway. In their article, they introduced the concept that APC contains nuclear export signals (NES) [8, 18] and, further, some of the mutant and truncated APC retained only the N-terminal NES. This indicates that AC4 could detect various truncated APC proteins including nuclear APC. Although our current staining data could not show any nuclear localization of mutant APC, this N-terminal antibody (AC4) may have an important potential in future studies of colorectal tumorigenesis.

Further, a statistical relationship between APC (N-terminal and C-terminal) and E-cadherin protein expressions in surgically resected human colorectal cancers was analyzed. The current image analysis data indicated that the E-cadherin protein did not significantly correlate with the two APCs either in the normal epithelia or in cancer (Table 2). This indicated that E-cadherin acts rather independently compared with the two APCs, although it has a negative role in tumor progression.

In conclusion, we took advantage of an immunohistochemistry procedure with the unique detergent-mediated antigen retrieval technique to frozen sections by which we could examine the expressions of two APC and E-cadherin proteins in human surgically resected sporadic colorectal cancers and verify reduced expressions of APCs and E-cadherin in colorectal cancer cells statistically using quantitative image analysis. This study suggests that the normal APC and E-cadherin protein expressions in benign epithelium is progressively and independently lost in the sporadic colorectal cancers.

**Acknowledgements** We thank Mr. Robert Debold for his English correction of this article. This work was supported in part by Bristol Myers Squibb Unrestricted Grant.

## References

1. Alman BA, Li C, Pajerski ME, Diaz-Cano S, Wolfe HJ (1997) Increased beta-Catenin protein and somatic APC mutations in sporadic aggressive fibromatoses (desmoid tumors). Am J Pathol 151:329–334
2. Bienz M, Clevers H (2000) Linking colorectal cancer to Wnt signaling. Cell 103:311–320
3. Bodmer WF, Bailey CJ, Bodmer J, Bussey HJ, Ellis A, Gorman P, Lucibello FC, Murday VA, Rider SH, Scambler P, et al (1987) Localization of the gene for familial adenomatous polyposis on chromosome 5. Nature 328:614–616
4. Brown D, Lydon J, Mclaughin M, Stuarttilley A, Tyszkowski R, Alper S (1996) Antigen retrieval in cryostat tissue sections and cultured cells by treatment with sodium dodecyl sulfate (SDS). Histochem Cell Biol 105:261–267
5. Dogan A, Wang ZD, Spencer J (1995) E-Cadherin expression in intestinal epithelium. J Clin Pathol 48:143–146

6. Groden J, Thliveris A, Samowitz W, Carlson M, Gelbert L, Albertsen H, Joslyn G, Stevens J, Spirio L, Robertson M, et al (1991) Identification and characterization of the familial adenomatous polyposis coli gene. Cell 66:589–600
7. Hao X, Frayling IM, Willcocks TC, Han W, Tomlinson IP, Pignatelli MN, Pretlow TP, Talbot IC (2002) Beta-catenin expression and allelic loss at APC in sporadic colorectal carcinogenesis. Virchows Arch 440:362–366
8. Henderson BR (2000) Nuclear-cytoplasmic shuttling of APC regulates beta-Catenin subcellular localization and turnover. Nat Cell Biol 2:653–660
9. Herrera L, Kakati S, Gibas L, Pietrzak E, Sandberg AA (1986) Gardner syndrome in a man with an interstitial deletion of 5q. Am J Med Genet 25:473–476
10. Kinzler KW, Nilbert MC, Su LK, Vogelstein B, Bryan TM, Levy DB, Smith KJ, Preisinger AC, Hedge P, McKechnie D, et al (1991) Identification of FAP locus genes from chromosome 5q21. Science 253:661–665
11. Leppert M, Dobbs M, Scambler P, O'Connell P, Nakamura Y, Stauffer D, Woodward S, Burt R, Hughes J, Gardner E, et al (1987) The gene for familial polyposis coli maps to the long arm of chromosome 5. Science 238:1411–1413
12. Miyaki M, Konishi M, Kikuchi-Yanoshita R, Enomoto M, Igari T, Tanaka K, Muraoka M, Takahashi H, Amada Y, Fukayama M, et al (1994) Characteristics of somatic mutation of the adenomatous polyposis coli gene in colorectal tumors. Cancer Res 54:3011–3020
13. Miyoshi Y, Ando H, Nagase H, Nishisho I, Horii A, Miki Y, Mori T, Utsunomiya J, Baba S, Petersen G, et al (1992) Germline mutations of the APC gene in 53 familial adenomatous polyposis patients. Proc Natl Acad Sci U S A 89:4452–4456
14. Miyoshi Y, Nagase H, Ando H, Horii A, Ichii S, Nakatsuru S, Aoki T, Miki Y, Mori T, Nakamura Y (1992) Somatic mutations of the APC gene in colorectal tumors: mutation cluster region in the APC gene. Hum Mol Genet 1:229–233
15. Nagase H, Nakamura Y (1993) Mutations of the APC (adenomatous polyposis coli) gene. Hum Mutat 2:425–434
16. Nishisho I, Nakamura Y, Miyoshi Y, Miki Y, Ando H, Horii A, Koyama K, Utsunomiya J, Baba S, Hedge P (1991) Mutations of chromosome 5q21 genes in FAP and colorectal cancer patients. Science 253:665–669
17. Powell SM, Zilz N, Beazer-Barclay Y, Bryan TM, Hamilton SR, Thibodeau SN, Vogelstein B, Kinzler KW (1992) APC mutations occur early during colorectal tumorigenesis. Nature 359:235–237
18. Rosin-Arbesfeld R, Townsley F, Bienz M (2000) The APC tumour suppressor has a nuclear export function. Nature 406:1009–1012
19. Smith KJ, Johnson KA, Bryan TM, Hill DE, Markowitz S, Willson JK, Paraskeva C, Petersen GM, Hamilton SR, Vogelstein B, et al (1993) The APC gene product in normal and tumor cells. Proc Natl Acad Sci U S A 90:2846–2850
20. Snedecor GW, Cochran WG (1989) Statistical Methods, 8th edn. Iowa State University Press, Iowa, USA
21. Su LK, Johnson KA, Smith KJ, Hill DE, Vogelstein B, Kinzler KW (1993) Association between wild type and mutant APC gene products. Cancer Res 53:2728–2731
22. Su LK, Vogelstein B, Kinzler KW (1993) Association of the APC tumor suppressor protein with catenins. Science 262:1734–1737
23. Takeichi M (1991) Cadherin cell adhesion receptors as a morphogenetic regulator. Science 251:1451–1455
24. Vogelstein B, Kinzler KW (1993) The multistep nature of cancer. Trends Genet 9:138–141

Virchows Arch (2003) 442:271–277
DOI 10.1007/s00428-002-0752-4

ORIGINAL ARTICLE

**A. Alkushi · J. Irving · F. Hsu · B. Dupuis · C. L. Liu · M. Rijn · C. B. Gilks**

# Immunoprofile of cervical and endometrial adenocarcinomas using a tissue microarray

Received: 23 May 2002 / Accepted: 29 October 2002 / Published online: 12 February 2003
© Springer-Verlag 2003

**Abstract** Adenocarcinomas of the uterine cervix show a wide range of morphological features, and can be confused with endometrial adenocarcinoma in biopsy or curetting specimens. The objective of this study was to use tissue microarray technology to evaluate the immunoprofile of a large set of uterine adenocarcinomas with an extended panel of antibodies, comparing the profile of primary cervical and endometrial adenocarcinomas. A tissue microarray was constructed using paraffin-embedded, formalin-fixed tissues from 141 hysterectomy specimens. Duplicate 0.6-mm cores were obtained from 57 cervical adenocarcinomas (16 in situ and 41 invasive) and 84 endometrial adenocarcinomas. Tissue array sections were immunostained with 21 commercially available antibodies [B72.3, CD 99, carcinoembryonic antigen (CEA), c-kit, pancytokeratin, CK 5/6, CK 7, CK8/18, CK19, CK 20, CK 22, EMA, estrogen receptor (ER), KP-1, melan-A, p53, PLAP, S-100, synaptophysin, TTF-1, and vimentin] utilizing the avidin-biotin (ABC) technique. Hierarchical clustering analysis of the tumors was done based on the immunostaining results. Only ER ($P$<0.001), CEA ($P$=0.04), vimentin ($P$<0.001), and CK 8/18 ($P$=0.002) showed a significantly different frequency of positivity in endometrial relative to cervical adenocarcinomas. ER, vimentin, and CK 8/18 were more likely to be expressed in endometrial adenocarcinomas, while cervical adenocarcinomas more frequently expressed CEA. We were able to identify immunoprofiles that were highly specific for endocervical adenocarcinoma ($ER^-$, $vimentin^-$, $CK\ 8/18^-$, $CEA^+$) or endometrial adenocarcinoma ($ER^+$, $vimentin^+$, $CK\ 8/18^+$, $CEA^-$), but most tumors showed an intermediate, nonspecific immunophenotype. Hierarchical clustering analysis was useful in the interpretation of these intermediate immunophenotypes. Papillary serous adenocarcinoma of the endometrium was less likely to express vimentin ($P$=0.002) than endometrioid carcinoma of the endometrium.

**Keywords** Endometrial carcinoma · Cervical adenocarcinoma · Immunohistochemistry · Tissue microarray

A. Alkushi · J. Irving · F. Hsu · B. Dupuis · C. B. Gilks (✉)
Department of Pathology and Genetic Pathology Evaluation Center,
Department of Pathology,
1st floor JPPN, Vancouver General Hospital,
855 W. 12th Avenue, Vancouver, BC V5Z 1M9, Canada
e-mail: bgilks@vanhosp.bc.ca
Tel.: +604-875-5555 ext. 63305
Fax: +604-875-5707

C. L. Liu
Department of Biochemistry, Stanford University,
Stanford, CA

M. Rijn
Department of Pathology,
Stanford University, Stanford, CA

## Introduction

Adenocarcinoma of the uterine cervix and endometrium have long been recognized as distinct entities, with different etiologies, behavior and treatments. There is, however, considerable overlap in the morphological features of adenocarcinoma arising at these two sites. This morphological overlap can make their histological differentiation a diagnostic problem in biopsy or curetting specimens, especially with a small biopsy, or when adenocarcinoma is present in both components of a fractional dilation and curettage specimen [4, 17, 23]. This distinction has preoperative clinical significance as the choice of definitive therapy may rest on the site of origin of the tumor, and it is not uncommon for the preoperative clinical, hysteroscopic, radiologic and pathologic examination to fail in identifying the primary site with certainty.

Tissue microarrays allow the assessment of hundreds of tissue cores on a single slide [13]. In this technique, small tissue cores are retrieved from selected regions of archival tissue blocks, and hundreds of such samples are precisely arrayed in a new paraffin block. These tissue samples can then be analyzed using immunohistochem-

istry, fluorescence in situ hybridization (FISH) or RNA in situ hybridization. We utilized a tissue microarray with samples from 141 cases to evaluate the immuoprofile of uterine adenocarcinomas of cervical and endometrial origin with a panel of 21 different antibodies. The data generated was submitted to hierarchical clustering analysis [8], to identify groups of tumors with related immunoprofiles.

## Materials and methods

### Study material

The study material consisted of slides and selected tissue blocks from 141 hysterectomy specimens retrieved from the archives of the Department of Pathology and Laboratory Medicine, Vancouver General Hospital (Table 1). These specimens were accessioned between 1984 and 2000. Fifty-seven were cases of cervical adenocarcinoma (16 in situ and 41 invasive tumors), and 84 were endometrial carcinomas. Cervical carcinoma cases were centered in the endocervical canal, while the endometrial carcinoma cases were in the uterine fundus. No cases with tumor centered in the lower uterine segment, or tumor extensively involving both the fundus and endocervical canal, such that determination of the primary site of the tumor was problematic, were included in this study. A wide range of morphological types of cervical adenocarcinoma were included (endocervical, villoglandular, endometrioid, clear cell, papillary serous, adenosquamous, glassy cell, adenoid cystic, and poorly differentiated type). Fifty-four endometrial carcinomas were of endometrioid type, five with focal mucinous differentiation. Of these, twenty-five were low-grade (FIGO grade 1) endometrial carcinomas of endometrioid type, and twenty-nine were high-grade (FIGO grade 3) endometrial adenocarcinomas of endometrioid type. The rest of the endometrial carcinomas were papillary serous carcinoma ($n$=30). Institutional ethics approval was obtained for this retrospective immunohistochemical study.

### Construction of tissue microarray

All hematoxylin and eosin (H&E) stained slides for these cases were reviewed, a slide with representative tumor was selected from each case, and an area of tumor was circled on the slide. The corresponding formalin-fixed, paraffin-embedded blocks were retrieved from the hospital archives and the area corresponding to the selected area on the slide was circled on the block with a felt marker for tissue microarray construction. All tissues were fixed in 10% neutral buffered formalin. Using a tissue microarrayer (Beecher Instruments, Silver Spring, MD), the area of interest in the donor block was cored twice with a 0.6-mm diameter needle and transferred to a recipient paraffin block.

### Immunohistochemistry

The avidin-biotin (ABC) method was used for immunostaining. The recipient block was sectioned at 4 $\mu$m, and transferred to silanized glass slides. Each of these unstained sections was deparaffinized with xylene, and rehydrated through a series of graded alcohols. A section from the array was then stained with haematoxylin and eosin, to assess adequacy. Further sections were stained with the panel of antibodies listed in Table 2 using a Ventana (Tuscon AZ) automated immunohistochemical stainer according to the manufacturer's guidelines. $CEA_{(p)}$ refers to the polyclonal anti-carcinoembryonic antigen (CEA) antibody, while $CEA_{(m)}$ refers to the monoclonal anti-CEA antibody. Antigen retrieval was done as indicated in Table 2. Microwave antigen retrieval consisted of placing the slides in 10 mM citrate buffer (pH 6.0) in a pressure cooker (Nordic Ware), and microwaving on high power until the buffer had boiled under pressure for 4 min. At this point, microwaving was stopped and the slides were incubated in the pressure cooker for a further 20 min, removed and rinsed. Proteinase antigen retrieval consisted of a 4-min incubation in protease-1 solution (Ventanna) according the supplier's recommended protocol. We did not use biotin blocking for this study as we have determined that with the antigen retrieval protocols used, in our experience, we do not see endogenous biotin reactivity (seen as granular cytoplasmic staining) in uterine tumors, in contrast to our experience with thyroid, renal and hepatocellular neoplasms.

Two pathologists (AA, CBG) scored the immunostaining using a two-headed microscope. Tumor cell cytoplasmic or nuclear staining (as appropriate, according to the antigen being detected) was scored as technically unsatisfactory/uninterpretable, negative (<5% cells positive), weak positive (5–50% of cells showing weak or moderately intense positivity), or strong positive (>50% of cells positive or 5–50% of cells showing intense immunoreactivity). Scoring results then were simplified into either negative or positive (combining weak and strong positive results) and unsatisfactory/uninterpretable results were eliminated from further consideration. Score results for the duplicate cores were consolidated into one score/case where positive staining would always supercede either a negative or uninterpretable result, and a negative result would supercede an uninterpretable result.

### Statistical and clustering analysis

Fisher's exact and Chi-Square tests were used to analyze 2×2 tables generated to compare the immunohistochemical scoring results of cervical and endometrial adenocarcinomas. Calculations were done using SPSS, version 9.0 software. Correction for making multiple comparisons was made, and significance was called at $P$<0.05, after correction.

**Table 1** Cases used in the tissue microarray

| Cervical adenocarcinoma | | Endometrial carcinoma | |
|---|---|---|---|
| Type | No. of cases | Type/grade | No. of cases |
| In situ | 16 | Grade-I endometrioid | 25 |
| Endocervical type | 11 | Grade-III endometrioid | 29 |
| Villoglandular | 2 | Papillary serous carcinoma | 30 |
| Endometrioid | 4 | | |
| Clear cell carcinoma | 4 | | |
| Papillary serous | 5 | | |
| Intestinal type (mucinous) | 1 | | |
| Adenosqumous carcinoma | 3 | | |
| Adenosqumous – glassy cell | 4 | | |
| Adenoid cystic | 1 | | |
| Poorly differentiated | 6 | | |
| Total | 57 | Total | 84 |

**Table 2** Antibodies used in this study. *N* no antigen retrieval, *M* microwave, *E* trypsin digestion

| Antigen | Clone | Supplier | Dilution | Antigen retrieval |
|---|---|---|---|---|
| B72.3 | BRST-3 | Signet | 1:10,000 | N |
| CD-68 | KP-1 | Dako | 1:400 | N |
| CD 99 | O13 | ID Labs | 1:20 | M |
| $CEA_{(m)}$ | TF 3H8–1 | Ventana | 1:5 | N |
| $CEA_{(p)}$ | Polyclonal | Dako | 1:10,000 | N |
| c-kit | Polyclonal | Santa Cruz | 1:100 | N |
| Pankeratin | Polyclonal | Dako | 1:4000 | E |
| CK 5/6 | D5/16B4 | Zymed | 1:100 | M |
| CK 7 | OV-TL 12/30 | Dako | 1:200 | E |
| CK 8/18 | CAM 5.2 | Becton/Dickinson | 1:50 | E |
| CK19 | RCK108 | Dako | 1:500 | E |
| CK 20 | Ks20.8 | Dako | 1:500 | E |
| CK 22 | cocktail | Biomeda | 1:10 | E |
| EMA | E29 | Dako | 1:200 | N |
| ER | 6F11 | Novocastra | 1:50 | M |
| Melan-A | Dako | A103 | 1:50 | M |
| p53 | DO-7 | Dako | 1:400 | M |
| S-100 | Polyclonal | Dr. A Marks[a] | 1:1000 | N |
| Synaptophysin | Polyclonal | Dako | 1:200 | M |
| TTF-1 | 8G7G3/1 | Dako | 1:100 | M |
| Vimentin | V9 | Biogenix | 1:20,000 | M |

[a] Dr. A. Marks, Banting and Best Dept. of Medical Research, University of Toronto

**Table 3** Immunohistochemical findings

| | Cervical adenocarcinoma | | Endometrial carcinoma | | *P* value* |
|---|---|---|---|---|---|
| | In situ | Invasive | Endometrioid | PSCE | |
| Pankeratin | 92% (11/12) | 100% (37/37) | 94% (47/50) | 100% (23/23) | |
| CK 8/18 | 66% (8/12) | 63% (24/38) | 94% (48/51) | 91% (20/22) | 0.002 |
| CK7 | 92% (12/13) | 94% (34/36) | 96% (51/53) | 100% (24/24) | |
| CK20 | 0% (0/15) | 2% (1/39) | 0% (0/52) | 0% (0/23) | |
| CK19 | 88% (7/8) | 83% (29/35) | 88% (42/48) | 94% (17/18) | |
| CK22 | 100% (7/7) | 97% (34/35) | 100% (49/49) | 100% (20/20) | |
| CK5/6 | 25% (3/12) | 33% (13/39) | 34% (18/53) | 8% (2/24) | |
| EMA | 69% (9/13) | 95% (35/37) | 98% (52/53) | 100% (25/25) | |
| $CEA_{(m)}$ | 33% (5/15) | 30% (11/37) | 17% (9/52) | 5% (1/22) | |
| $CEA_{(p)}$ | 78% (7/9) | 80% (28/35) | 61% (30/49) | 25% (5/20) | 0.04 |
| ER | 33% (4/12) | 11% (4/37) | 73% (37/51) | 36% (8/22) | <0.001 |
| Vimentin | 0% (0/13) | 10% (4/39) | 92% (48/53) | 52% (12/23) | <0.001 |
| Synaptophysin | 0% (0/11) | 0% (0/39) | 21% (11/52) | 13% (3/23) | |
| c-kit | 0% (0/12) | 13% (5/38) | 19% (10/53) | 12% (3/25) | |
| Melan-A | 0% (0/16) | 0% (0/38) | 0% (0/52) | 0% (0/22) | |
| CD 99 | 50% (4/8) | 47% (16/34) | 62% (31/50) | 41% (9/22) | |
| S-100 | 0% (0/7) | 6% (2/36) | 0% (0/49) | 0% (0/17) | |
| B72.3 | 17% (2/12) | 43% (16/37) | 60% (32/53) | 61% (14/23) | |
| TTF-1 | 0% (0/8) | 0% (0/36) | 0% (0/49) | 6% (1/18) | |
| CD 68 | 0% (0/8) | 3% (1/35) | 0% (0/50) | 0% (0/20) | |

**P* value comparing the immunostaian result in cervical and endometrial adenocarcinomas, $P<0.05$ is considered significant. Differences are not statistically significant unless indicated

Hierarchal clustering analysis of our tissue microarray data was performed using software tools that were originally designed for analyzing cDNA microarray data [8]. An Excel macro, TMA-Deconvoluter [14], was designed and written specifically for processing of raw tissue microarray staining data into a format compatible for use with the previously developed Cluster software [8]. The clustered data was then graphically viewed using TreeView (Cluster and Treeview software are freely available programs that can be accessed at http://rana.lbl.gov/EisenSoftware.htm).

## Results

Table 3 summarizes the immunohistochemical findings. For most antibodies tested there was no significant difference in immunostaining between cervical and endometrial carcinomas; however, for four antigens [estrogen receptor (ER) ($P<0.001$), vimentin ($P<0.001$), CK 8/18 ($P=0.002$), CEA ($P=0.04$ for the polyclonal antibody, and $P$ not significant for the monoclonal antibody)], there was a significant difference in the frequency of immunostaining. The first three antigens were more frequently expressed in endometrial adeno-

**Table 4** Cervical adenocarcinoma subtypes

| | Cervical adenocarcinoma | | Endometrial adenocarcinoma, endometrioid type |
|---|---|---|---|
| | Endocervical type | Other type | |
| $CEA_{(p)}$ | 100% (12/12) | 70% (16/23) | 61% (30/49) |
| ER | 10% (1/10) | 11% (3/27) | 73% (37/51) |
| Vimentin | 8% (1/12) | 11% (3/27) | 92% (48/52) |
| CK 8/18 | 63% (7/11) | 60% (16/27) | 94% (48/51) |

**Table 5** Cervical versus endometrial adenocarcinoma immunoprofiles

| | Cervical adenocarcinoma | Endometrioid endometrial carcinoma | *P* value |
|---|---|---|---|
| Cervical carcinoma pattern ($ER^-$, $Vimentin^-$, $CEA_{(p)}^+$) | 64% (21/33) | 4% (2/47) | <0.001 |
| Endometrial carcinoma pattern ($ER^+$, $Vimentin^+$, $CEA_{(p)}^-$) | 0% (0/33) | 23% (11/47) | 0.002 |
| Extended cervical carcinoma pattern ($ER^-$, $vimentin^-$, CK $8/18^-$, $CEA_{(p)}^+$) | 21% (7/33) | 2% (1/47) | 0.005 |
| Extended endometrial carcinoma pattern ($ER^+$, $vimentin^+$, CK $8/18^+$, $CEA_{(p)}^-$) | 0% (0/33) | 21% (10/47) | 0.005 |

**Table 6** Endometrioid versus papillary serous endometrial adenocarcinoma

| | Endometrial carcinoma | | | *P* value* |
|---|---|---|---|---|
| | Grade-I endometrioid | Grade-III endometrioid | Papillary serous carcinoma | |
| Estrogen receptor | 76% (19/25) | 69% (18/26) | 36% (8/22) | 0.08 |
| Vimentin | 88% (22/25) | 92% (26/27) | 52% (12/23) | 0.002 |

**P* value comparing the immunostaining results for endometrioid endometrial carcinoma and papillary serous carcinoma of endometrium

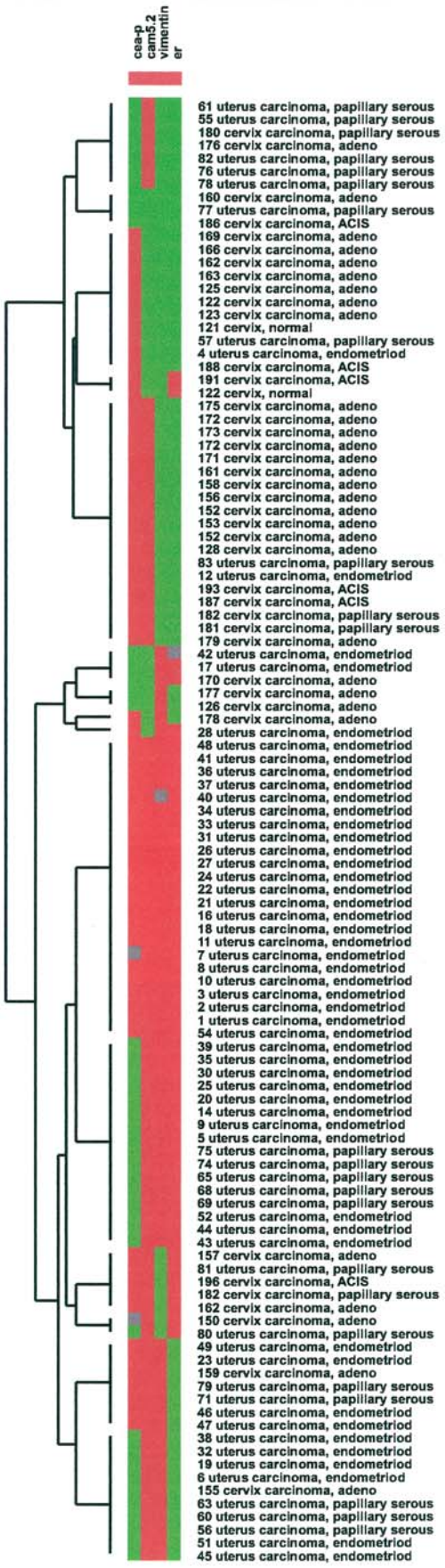
carcinomas than in cervical adenocarcinomas, whereas CEA showed the opposite pattern.

Table 4 shows the frequency of CK 8/18, ER, vimentin, and $CEA_{(p)}$ expression in different subtypes of invasive cervical adenocarcinoma. All endocervical (mucinous) type cervical adenocarcinomas expressed CEA as detected with the polyclonal antibody ($CEA_{(p)}$) and 70% of the other cervical adenocarcinoma subtypes expressed this protein. CEA was also present in more than half of the endometrial adenocarcinomas. The staining of endocervical type cervical adenocarcinomas was indistinguishable from other subtypes of cervical adenocarcinoma with respect to ER, vimentin, and CK 8/18 immunostaining.

As the combination of ER, CEA and vimentin staining has previously been shown to aid in differentiation between cervical and endometrial adenocarcinoma [2], we determined how many tumors showed a typical cervical adenocarcinoma staining profile ($ER^-$, $vimentin^-$, and $CEA_{(p)}^+$) or a typical endometrial adenocarcinoma staining profile ($ER^+$, $vimentin^+$, and $CEA_{(p)}^-$) (Table 5). For the purposes of this analysis, we excluded cervical papillary serous carcinomas, which are rare in the cervix. While most cervical adenocarcinomas were $ER^-$, $vimentin^-$, and $CEA_{(p)}^+$ (21 of 33, 64%), occasional endometrial adenocarcinomas also showed this staining pattern (2 of 47, 4%), so that this immunoprofile has a sensitivity and specificity of 64% and 91%, respectively, for the diagnosis of cervical adenocarcinoma. No cervical adenocarcinomas showed a staining pattern for these three antigens typical of endometrial adenocarcinoma, relative to 11 of 47 (23%) endometrial adenocarcinomas. Thus, this immunoprofile ($ER^+$, $vimentin^+$, and $CEA_{(p)}^-$) has a sensitivity of 23% and specificity of 100% for the diagnosis of endometrial adenocarcinoma.

Our analysis identified one novel discriminating marker in the differential diagnosis between endometrial and cervical adenocaricnomas, CK 8/18, and this antigen was then added to the immunoprofile for distinguishing between endometrial and cervical adenocarcinomas. The extended cervical-type pattern ($ER^-$, $vimentin^-$, CK $8/18^-$, $CEA_{(p)}$) has a sensitivity of 21% and specificity of 87.5% for the diagnosis of cervical adenocarcinoma. The endometrial-type pattern ($ER^+$, $vimentin^+$, CK $8/18^+$, $CEA_{(p)}$) has a sensitivity of 21% and specificity 100% for the diagnosis of endometrial adenocarcinoma. With either the limited (three antibodies) or extended (four antibodies) immunoprofiles, a majority of tumors do not show either a cervical-type or endometrial-type pattern, but instead have an intermediate immunophenotype, not characteristic of either primary site.

The result of hierarchical clustering analysis with the four antibodies showing a difference in staining between endometrial and endocervical adenocarcinoma is shown in Fig. 1. This shows that although cases of cervical and endometrial adenocarcinoma tend to cluster on separate branches of the dendrogram, there is considerable overlap, with some cases of cervical adenocarcinoma sharing the same immunophenotype as endometrial adenocarcinomas.




One antibody (vimentin) showed a significant difference in frequency of positivity when endometrioid and papillary serous carcinomas of the endometrium were compared (Table 6). ER was also expressed less frequently in papillary serous carcinomas than endometrioid carcinomas, but this difference was not statistically significant.

## Discussion

The preoperative distinction of cervical and endometrial adenocarcinomas is clinically important as stage-1 "low risk" endometrial adenocarcinoma can be treated by simple hysterectomy alone, while the treatment of cervical adenocarcinoma is generally by radiotherapy with or without subsequent hysterectomy [23]. We took advantage of recently described tissue microarray technology [13] to study a large number of cases of cervical and endometrial adenocarcinoma with multiple antibodies. Although only small amounts of the tumor are sampled in tissue microarrays, there is now convincing evidence that immunohistochemical staining of two or more cores/case gives results that are highly representative of whole sections of tumor [3, 18, 19, 22].

The earliest identified immunophenotypic difference between cervical and endometrial adenocarcinoma was the increased frequency and intensity of CEA immunoreactivity in cervical adenocarcinomas [5], an observation since confirmed in multiple studies [4, 7, 15, 17]. These studies have given a wide range of results, with 50–100% of cervical adenocarcinomas reported to be CEA positive, compared with 0–50% of endometrial adenocarcinoma studies [4, 5, 7, 15, 17]. Differences in staining techniques, antibodies (in particular monoclonal versus polyclonal anti-CEA antibodies), and case selection presumably account for the wide range of reported results. We found that the polyclonal anti-CEA antiserum was more discriminatory than the monoclonal antibody, with 35 of 44 (80%) cervical adenocarcinomas versus 35 of 69 (51%) endometrial adenocarcinomas staining positively with $CEA_{(p)}$. Of note, CEA was expressed by all endocervical (mucinous) type cervical adenocarcinomas relative to 70% of other types of cervical adenocarcinomas. This reduces the value of CEA immunostaining as a marker of cervical adenocarcinoma since these other histological subtypes of cervical adenocarcinoma are more difficult to differentiate from endometrial carcinoma, and would be the cases where one would be most likely to resort to immunostaining as a diagnostic aid.

Vimentin has also been consistently demonstrated to be differentially expressed in endometrial and cervical adenocarcinomas, being present in most endometrial

**Fig. 1** Graphical representation of the hierarchical clustering analysis. Positive staining is indicated by a *red cube*, absence of staining as *green*, and no available data as *gray* for each of the antibodies indicated at the top of the figure. Each case is listed at the right of the figure

adenocarcinomas and in a much smaller percentage of cervical adenocarcinomas [2, 4, 6, 7, 17]. Our findings are in agreement with these previous studies, with vimentin immunoreactivity in only 4 of 52 (8%) cervical adenocarcinomas, including only one tumor of endocervical type, relative to 60 of 76 (79%) endometrial adenocarcinomas, including 92% of endometrioid endometrial carcinomas. Thus, vimentin expression is most consistently negative in typical endocervical-type cervical adenocarcinomas and positive in endometrioid-type endometrial adenocarcinomas, with unusual subtypes more likely to give an "aberrant" staining pattern. Staining for ER protein has also been found to be of help in distinguishing between cervical and endometrial adenocarcinomas, with 70–90% of endometrial adenocarcinomas being $ER^+$, compared with 10–40% of cervical adenocarcinomas [9, 10, 16, 17]. We found 8 of 49 (16%) cervical adenocarcinomas to be $ER^+$, compared with 45 of 73 (62%) endometrial carcinomas. Our relatively low figure for the endometrial adenocarcinomas most probably reflects the inclusion of a relatively high proportion of papillary serous and high-grade endometrioid carcinomas in this study, as they are $ER^+$ in only 36% and 69% of cases, respectively. We identified one additional antibody that may help in differentiation between cervical and endometrial adenocarcinoma; cytokeratin 8/18 is more frequently expressed in endometrial than cervical adenocarcinomas.

McCluggage et al. suggested that a panel of ER, CEA and vimentin will allow distinction between cervical and endometrial adenocarcinoma, based on their study of 56 cases [17]. We found that this panel of three antibodies had a sensitivity and specificity of 64% and 96%, respectively, for the diagnosis of cervical adenocarcinoma, and a sensitivity of 23% and specificity of 100% for the diagnosis of endometrial adenocarcinomas. Thus, most tumors do not conform exactly to a "typical" immunophenotypic profile of either cervical or endometrial adenocarcinoma, with rare endometrial adenocarcinomas having an immunophenotype characteristic of cervical adenocarcinoma, i.e., $ER^-$, $vimentin^-$ and $CEA^+$. When we added CK 8/18 to the profile, the specificities of endometrial adenocarcinoma staining pattern ($CEA_{(p)}^-$ / $ER^+$/$vimentin^+$/CK $8/18^+$) or cervical adenocarcinoma staining pattern ($CEA_{(p)}^+$/$ER^-$/$vimentin^-$/CK $8/18^-$) were not significantly improved, while there was a drop in sensitivity. Thus, although CK 8/18 was differentially expressed in cervical and endometrial adenocarcinomas, it did not help to define immunoprofiles characteristic of cervical and endometrial adenocarcinomas. Even with the more limited panel of CEA, ER and vimentin, most tumors have an immunophenotype that is intermediate between the typical patterns of cervical and endometrial adenocarcinomas.

Although our primary objective was to compare cervical and endometrial adenocarcinomas, other novel observations emerged as a result of the broad screening approach using many antibodies and a large number of cases. Comparing papillary serous carcinoma to endometrioid carcinoma revealed that vimentin is less frequently expressed in papillary serous adenocarcinoma than in endometrioid type endometrial adenocarcinoma. These two types of endometrial carcinoma represent the prototype of types 2 and 1 of endometrial carcinoma, respectively, and these differences presumably reflect differences in molecular events during oncogenesis for these tumors. Halperin et al. found that ER is less frequently expressed in papillary serous carcinoma than endometrial adenocarcinoma of endometrioid type [12]. Although we observed a difference in the frequency of ER immunoreactivity between these two types of tumors, the difference was not statistically significant ($P$=0.08). This result does highlight one aspect of studies such as this one, using multiple immunohistochemical markers. If we had studied only ER, the difference we observed with 37 of 51 (73%) endometrioid adenocarcinomas and 8 of 22 (36%) papillary serous carcinomas staining positively for ER would have been highly significant ($P$=0.004), but this effect is lost in the present study when correction is made for multiple comparisons.

Application of hierarchical clustering analysis allowed us to graphically demonstrate the relatedness of cervical and endometrial adenocarcinoma immunoprofiles. Hierarchical clustering analysis is a method of dealing with complex sets of data and offers a possible systematic approach to complex immunophenotypes. Clustering analysis has been successfully applied to gene-expression data, based on the expression of thousands of genes, and has been remarkably successful in its ability to group tumors according to their primary site based on gene expression profiles [1, 11, 20, 21]. The dynamic range of immunostaining scores is significantly narrower than that obtained for mRNA levels in gene microarray experiments, however, and, as a result, the clustering of tumors based on immunoreactivity can be expected to be less well defined than is seen in gene expression array studies. When individual tumors are stained with multiple antibodies, a complex immunophenotype is generated that in typical cases is readily interpretable but, as shown previously, is more often than not atypical for at least some of the markers used. For example, what is the significance of a tumor in a D&C specimen with the immunoprofile of $CEA_{(p)}^-$/$ER^-$/$vimentin^+$/CK $8/18^+$? By reviewing the graphical display of the clustering analysis (Fig. 1) we can see that this immunophenotype was seen in ten tumors, including six endometrioid-type endometrial adenocarcinomas, three papillary serous adenocarcinomas of endometrium and one cervical adenocarcinoma. It thus is not a specific immunoprofile but is more suggestive of an endometrial rather than endocervical primary site. This application of clustering analysis allows a more objective interpretation of immunoprofiles based on staining with multiple antibodies and holds great promise for the immunohistochemical subclassification of tumors according to primary site; however, there is clearly a need for better, more tissue-specific, antigen targets.

## References


1. Alizadeh AA, Eisen MB, Davis RE, Ma C, Lossos IS, Rosenwald A, Boldrick JC, Sabet H, Tran T, Yu X, Powell JI, Yang L, Marti GE, Moore T, Hudson J, Lu L, Lewis DB, Tibshirani R, Sherlock G, Chan WC, Greiner TC, Weisenburger DD, Armitage JO, Warnke R, Staudt LM, et al (2000) Distinct types of diffuse large B-cell lymphoma identified by gene expression profiling. Nature 403:503–511
2. Azumi N, Battifora H (1987) The distribution of vimentin and keratin in epithelial and non-epithelial neoplasms. A comprehensive immunohistochemical study on formalin- and alcohol-fixed tumors. Am J Clin Pathol 88:286–296
3. Camp RL, Charette LA, Rimm DL (2000) Validation of tissue microarray technology in breast carcinoma. Lab Invest 80:1943–1949
4. Castrillon DH, Lee KR, Nucci MR (2002) Distinction between endometrial and endocervical adenocarcinoma: an immunohistochemical study. Int J Gynecol Pathol 21:4–10
5. Cohen C, Shulman G, Budgeon LR (1982) Endocervical and endometrial adenocarcinoma: an immunoperoxidase and histochemical study. Am J Surg Pathol 6:151–157
6. Dabbs DJ, Geisinger KR, Norris HT (1986) Intermediate filaments in endometrial and endocervical carcinomas. The diagnostic utility of vimentin patterns. Am J Surg Pathol 10:568–576
7. Dabbs DJ, Sturtz K, Zaino RJ (1996) The immunohistochemical discrimination of endometrioid adenocarcinomas. Hum Pathol 27:172–177
8. Eisen MB, Spellman PT, Brown PO, Botstein D (1998) Cluster analysis and display of genome-wide expression patterns. Proc Natl Acad Sci U S A 95:14863–14868
9. Fujiwara H, Tortolero-Luna G, Mitchell MF, Koulos JP, Wright TC Jr. (1997) Adenocarcinoma of the cervix. Expression and clinical significance of estrogen and progesterone receptors. Cancer 79:505–512
10. Ghandour FA, Attanoos R, Nahar K, Gee JW, Bigrigg A, Ismail SM (1994) Immunocytochemical localization of oestrogen and progesterone receptors in primary adenocarcinoma of the cervix. Histopathology 24:49–55
11. Golub T R, Slonim D K, Tamayo P, Huard C, Gaasenbeek M, Mesirov JP, Coller H, Loh ML, Downing JR, Caligiuri MA, Bloomfield CD, Lander ES (1999) Molecular classification of cancer: class discovery and class prediction by gene expression monitoring. Science 286:531–537
12. Halperin R, Zehavi S, Habler L, Hadas E, Bukowsky I, Schneider D (2001) Comparative immunohistochemical study of endometrioid and serous papillary carcinoma of the endometrium. Eur J Gynaecol Oncol 22:122–126
13. Kononen J, Bubendorf L, Kallioniemi A, Barlund M, Schraml P, Leighton S, Torhorst J, Mihatsch MJ, Sauter G, Kallioniemi OP (1998) Tissue microarrays for high-throughput molecular profiling of tumor specimens. Nat Med 4:844–847
14. Liu CL, Prapong W, Natkuman Y, Alizadeh A, Montgomery K, Gilks CB, van de Rijn M (2002) Software tools for high-throughput analysis and archiving of immunohistochemistry staining data obtained with tissue microarrays. Am J Pathol 161:1557–1565
15. Maes G, Fleuren G, Bara J, Nap M (1988) The distribution of mucins, carcinoembryonic antigen, and mucus-associated antigens in endocervical and endometrial adenocarcinomas. Int J Gynecol Pathol 7:112–122
16. Masood S, Rhatigan RM, Wilkinson EW, Barwick KW, Wilson WJ (1993) Expression and prognostic significance of estrogen and progesterone receptors in adenocarcinoma of the uterine cervix. An immunocytochemical study. Cancer 72:511–518
17. McCluggage WG, Sumathi VP, McBride HA, Patterson A (2002) A panel of immunohistochemical stains, including carcinoembryonic antigen, vimentin, and estrogen receptor, aids the distinction between primary endometrial and endocervical adenocarcinomas. Int J Gynecol Pathol 21:11–15
18. Nocito A, Bubendorf NA, Maria Tinner E, Suess K, Wagner U, Forster T, Kononen J, Fijan A, Bruderer J, Schmid U, Ackermann D, Maurer R, Alund G, Knonagel H, Rist M, Anabitarte M, Hering F, Hardmeier T, Schoenberger AJ, Flury R, Jager P, Luc Fehr J, Schraml P, Moch H, Mihatsch MJ, Gasser T, Sauter G (2001) Microarrays of bladder cancer tissue are highly representative of proliferative index and histological grade. J Pathol 194:349–357
19. Parker R, Cupples J, Lesack D, Grant D, Huntsman D, Gilks CB (2002) Assessment of inter observer variation in the immunohistochemical determination of estrogen receptor status using a breast cancer tissue microarray. Am J Clin Pathol 117:723–728
20. Perou CM, Sorlie T, Eisen MB, van de Rijn M, Jeffrey SS, Rees CA, Pollack JR, Ross DT, Johnsen H, Akslen LA, Fluge O, Pergamenschikov A, Williams C, Zhu SX, Lonning PE, Borresen-Dale AL, Brown PO, Botstein D (2000) Molecular portraits of human breast tumours. Nature 406:747–752
21. Sorlie T, Perou CM, Tibshirani R, Aas T, Geisler S, Johnsen H, Hastie T, Eisen MB, van De Rijn M, Jeffrey SS, Thorsen T, Quist H, Matese JC, Brown PO, Botstein D, Eystein Lonning P, Borreson-Dale AL (2001) Gene expression patterns of breast carcinomas distinguish tumor subclasses with clinical implications. Proc Natl Acad Sci U S A 98:10869–10874
22. Torhorst J, Bucher C, Kononen J, Haas P, Zuber M, Kochli OR, Mross F, Dietrich H, Moch H, Mihatsch M, Kallioniemi OP, Sauter G (2001) Tissue microarrays for rapid linking of molecular changes to clinical endpoints. Am J Pathol 159:2249–2256
23. Zaino RJ (2002) The fruits of our labors: Distinguishing endometrial from endocervical adenocarcinoma. Int J Gynecol Pathol 21:1–3

Virchows Arch (2003) 442:278–283
DOI 10.1007/s00428-002-0756-0

ORIGINAL ARTICLE

**Eunsil Yu · Eun Kyung Choi · Chong Jai Kim**

# Expression of promyelocytic leukemia protein increases during the differentiation of human neuroblastoma cells

Received: 20 August 2002 / Accepted: 6 October 2002 / Published online: 11 February 2003
© Springer-Verlag 2003

**Abstract** The promyelocytic leukemia (PML) protein, whose fusion with retinoic acid receptor $\alpha$ is responsible for the tumorigenesis of acute promyelocytic leukemia, acts as a tumor suppressor in various types of human cancers. We analyzed the expression patterns of PML, in both primary neuroblastic tumors ($n$=20) and two human neuroblastoma (NB) cell lines, SMS-KCNR (KCNR) and SH-SY5Y (SY5Y). The expression of PML, revealed as speckled or microgranular staining in the nuclei, was positively correlated with the differentiation status of NB cells in vivo, and was upregulated during the differentiation of KCNR and SY5Y cells following retinoic acid treatment. Screening of PML expression in human brain and sympathetic ganglia showed restricted expression of PML in mature neurons and glial cells, a result that was consistent with that in differentiated NB tumors. All these findings strongly suggest that increased PML expression is associated with growth inhibition and differentiation of human NB cells, and that it is of critical significance in the biology of NBs and in human nervous system development.

**Keywords** PML · Neuroblastoma · Retinoic acid · Differentiation

E. Yu
Department of Diagnostic Pathology,
University of Ulsan College of Medicine, Asan Medical Center,
138-736 Seoul, Korea

E. K. Choi
Department and Radiation Oncology,
University of Ulsan College of Medicine, Asan Medical Center,
138-736 Seoul, Korea

C. J. Kim (✉)
Department of Pathology,
Seoul National University College of Medicine,
28 Yongon-dong, Chongno-gu, 110-799 Seoul, Korea
e-mail: cjkim@plaza.snu.ac.kr
Tel.: +82-2-7603549
Fax: +82-2-7457966

## Introduction

The promyelocytic leukemia (PML) protein, encoded by the PML gene, is a nuclear phosphoprotein which is fused with the retinoic acid receptor $\alpha$ (RAR$\alpha$) gene in acute promyelocytic leukemia (APL) by the t(15;17) translocation [4, 13]. These two fusion products – PML/RAR$\alpha$ and RAR$\alpha$/PML – retain the DNA and hormone-binding domains of RAR$\alpha$ and most of the functional domains of PML, and interfere with PML and RAR/RA receptor X (RXR). This type of alteration in RAR, which is found in the majority of APL cases, seems to play a significant role in the development of APL by blocking promyelocytic differentiation [8, 11, 32].

Although detailed functional aspects of PML should be further clarified, recent investigations have revealed many important biological functions of PML. PML acts as a tumor suppressor, plays a role in the development of apoptosis, and mediates interferon function and immune surveillance [3, 18, 22, 24, 27, 31, 34]. In a PML knockout mice model, PML is critical for retinoic acid (RA)-dependent transactivation of the $p21^{WAF1/CIP1}$ gene, which regulates terminal myeloid differentiation, and dimethylbenzanthracene-treated $PML^{-/-}$ mice developed more tumors, such as B and T cell lymphomas, than their controls, indicating that PML functions as a tumor suppressor [30]. PML is also known to interact with other proteins, including p53, Rb, and Daxx which are of critical importance in growth control and apoptosis of the cells [2, 25, 35]. It has recently been shown that PML/RAR$\alpha$ blocks the interaction between Rb and histone deacetylase, thereby inhibiting repression of the expression of E2F target genes by the tumor suppressor Rb. This finding suggests that the derangement of Rb-mediated transcriptional suppression by PML is a contributory factor in APL tumorigenesis [15].

Neuroblastoma (NB) is one of the most common solid tumors of childhood and represents another type of human cancer, one that is responsive to RA treatment. RA treatment induces neuronal differentiation and growth arrest in RA-sensitive NB cell lines [1, 14]. Treatment

with RA activates signaling pathways that lead to growth inhibition and differentiation of the cells. RA treatment can modulate neurotrophin responsiveness of NB cells by regulation of trkA and trkB neurotrophin receptors [20]. RA treatment also induces secretion of biologically active transforming growth factor-$\beta$1 and increases the expression of its receptors in SMS-KCNR cells, which is accompanied by neuronal differentiation of the cells [7]. The overexpression of Ras-GRF, a neuron-specific Ras exchange factor of the central nervous system, in the SK-N-BE NB cells by transfection accelerated neuronal differentiation, indicating that the Ras-GRF and/or Ras-pathway is an important component of RA-induced differentiation of these cells [29]. It has also been shown that RA-mediated activation of the phosphatidylinositol 3-kinase/Akt signaling pathway is necessary for the neuronal differentiation of SH-SY5Y cells [19]. Despite the fact that NB and APL exhibit similar degrees of RA sensitivity, the significance of PML in NB has not been investigated. In the present study therefore, we analyzed the expression patterns of PML in NB. Both the size and number of PML dots dramatically increased in NB cell lines following RA treatment, and also in neuronal and Schwannian cells in primary neuroblastic tumors. Our findings strongly suggest that PML expression is related to growth inhibition and differentiation of NBs and is potentially of critical importance in the biology of the human nervous system.

## Materials and methods

### Cell culture and viable cell counting

KCNR and SY5Y human NB cell lines were cultured in RPMI 1640 containing 10% fetal bovine serum, 2 mM glutamine, and antibiotics (penicillin 100 IU/ml + streptomycin 50 mg/ml) in a 24-well plate. The cells were treated with control solvent and all-trans retinoic acid (Sigma, St. Louis, MI, USA) at the concentration of 5 $\mu$M. For viable cell counting after RA treatment, $2\times10^5$ cells were split in a six-well plate, and RA was applied the next day (day 0) at a concentration of 5 $\mu$M. Viable cell numbers were counted on day 5 after trypan blue staining.

### 3H-deoxythymidine uptake analysis

Five thousand cells were split in a 96-well plate in quadruplicate and kept overnight. On the next day (day 0), RA was added to individual wells and the cells were cultured for four additional days. On day 4, 1 $\mu$Ci of $^3$H-deoxythymidine was applied to each well and the cells were harvested after 24 h (day 5). The radioactivity was measured using a liquid scintillation counter.

### Immunofluorescence staining of PML

KCNR and SY5Y cells were split by placement overnight in a 24-well plate containing round cover slips at the density of $2\times10^4$ cells/well. Commencing the next day, the cells began 5-day treatment with control solvent and RA at a concentration of 5 $\mu$M. The cells were fixed for 10 min with cold methanol on ice and washed with PBS. For PML detection, the cells were incubated for an hour at room temperature in a murine monoclonal antibody against PML (PG-M3; Santa Cruz Biotechnology, Santa Cruz, CA, USA), diluted at 1:100 in PBS. Fluorescein isothiocyanate (FITC)-conjugated secondary antibody was complexed with the primary antibody. After staining, the slides were mounted with Fluoromount G (Fischer Scientific, Pittsburgh, PA, USA). The cells were analyzed using a Leiz confocal scanning microscope.

### Immunohistochemistry

For the analysis of PML expression in primary NBs, twenty NB tumor cases were collected from the files of the Departments of Pathology at Seoul National University Children's Hospital and Asan Medical Center, Seoul, Korea. The tumors were obtained from 9 boys and 11 girls, and their clinicopathologic characteristics are summarized in Table 1. For the comparison of PML expression pattern in the human nervous system, a fetal brain from a fetal autopsy case (gestational age: 21 weeks, pre-term premature rupture of membrane), a brain from an autopsy (a 15-year-old

**Table 1** Clinicopathologic profile of patients and promyelocytic leukemia (PML) immunoreactivity. *NB* neuroblastoma, *GNB* ganglioneuroblastoma, *GN* ganglioneuroma

| Case | Sex/age | Site | Stage | Histology | PML expression[a] |
|---|---|---|---|---|---|
| 1 | Male/3 years | Adrenal | IV | NB | – |
| 2 | Female/2 years | Adrenal | IV | NB | – |
| 3 | Male/9 months | Mediastinum | I | NB | – |
| 4 | Male/3 years | Lymph node | IV | NB | – |
| 5 | Male/4 months | Adrenal | II | NB | – |
| 6 | Male/1 years | Mediastinum | II | NB | – |
| 7 | Female/9 years | Retroperitoneum | IV | GNB | + |
| 8 | Female/2 years | Mediastinum | IV | GNB | + |
| 9 | Female/11 years | Adrenal | IV | GNB | + |
| 10 | Male/2 years | Retroperitoneum | IV | GNB | + |
| 11 | Female/6 years | Retroperitoneum | IV | GNB | + |
| 12 | Male/3 years | Adrenal | IV | GNB | + |
| 13 | Female/7 years | Lymph node | III | GNB | + |
| 14 | Female/3 years | Adrenal | III | GN | + |
| 15 | Male/10 years | Adrenal | I | GN | + |
| 16 | Female/4 years | Mediastinum | I | GN | + |
| 17 | Female/3 years | Mediastinum | I | GN | + |
| 18 | Female/7 years | Adrenal | IV | GN | + |
| 19 | Female/13 years | Mediastinum | I | GN | + |
| 20 | Male/5 years | Mediastinum | I | GN | + |

[a] PML immunoreactivity in poorly differentiated neuroblastic cells (NB) and neuronally differentiating/differentiated cells (GNB or GN)

male who died of Askin tumor of the chest wall), and sympathetic ganglia were also retrieved from the files of the Department of Pathology, Seoul National University Hospital, and were included in the analysis.

Representative 5-$\mu$m-thick paraffin sections were taken from each case, and immunohistochemical staining for PML was performed using a monoclonal anti-PML antibody (PG-M3). Briefly, the sections were deparaffinized and rehydrated through xylene and graded ethanol, and endogenous peroxidase was quenched with 3% hydrogen peroxide in methanol. After rehydration, the slides in jars underwent antigen retrieval, consisting of two courses of 5-min incubation in a microwave oven, in 0.01 mol/l sodium citrate buffer (pH 6.0). After microwave treatment, the sections were allowed 20 min to cool down to room temperature, then kept in PBS buffer and incubated overnight with 1:20 diluted murine monoclonal anti-PML antibody (PG-M3). Biotinylated secondary antibody was applied for 30 min. After PBS washing, the slides were incubated in streptavidin conjugated to horseradish peroxidase in Tris-HCl buffer for 30 min. Diaminobenzidine was used as a chromogen, and the slides were counterstained with Meyer's hematoxylin.

## Results

### PML expression in neuroblastoma cell lines

To evaluate whether PML expression is regulated by RA treatment, KCNR and SY5Y cells were treated with RA for 5 days at a concentration of 5 $\mu$M. All of the cells showed barely detectable PML dots before RA treatment on immunofluorescence staining, but the intensity of labeling and the number and size of the PML dots markedly increased after RA treatment in both cell lines (Fig. 1). Treatment with RA resulted in 49% and 55% reduction in growth of KCNR and SY5Y cells, respectively, as assessed by viable cell counting. These findings were consistent with the changes in $^3$H-deoxythymidine uptake (Fig. 2).

### PML expression in neuroblastic tumors and nervous system

To compare the PML expression pattern with that of the in vitro cell line model, immunohistochemical staining for PML expression was performed in 20 cases of neuroblastic tumors with varying degrees of differentiation; 6 cases of neuroblastoma, 7 of ganglioneuroblastoma, and 7 of ganglioneuroma. Clinicopathologic profiles of individual cases are summarized in Table 1. PML expression was not found in undifferentiated or poorly differentiated neuroblastic cells, while distinct PML dots were easily found in both neuronally differentiating cells and terminally differentiated ganglion cells found in ganglioneuroblastoma and ganglioneuroma cases (Fig. 3). PML expression, revealed as microgranular or finely speckled nuclear staining, was also detected as diffuse nuclear staining in endothelial cells of vessels in individual tumors and Schwannian cells of ganglioneuroblastoma and ganglioneuroma.

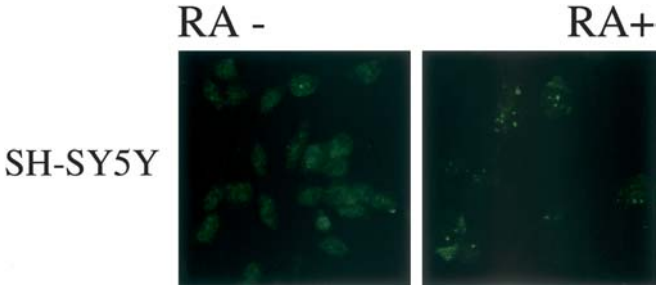



**Fig. 1** Retinoic acid-induced, increased expression of promyelocytic leukemia (PML) in the SH-SY5Y neuroblastoma cells. PML immunoreactivity is barely detectable in control cells (RA–) while there is a prominent increase of PML expression in retinoic acid (RA)-treated cells (RA+). The cells were treated with RA for 5 days at the concentration of 5 $\mu$M, and immunofluorescence stained with anti-PML antibody (PG-M3) (×800)

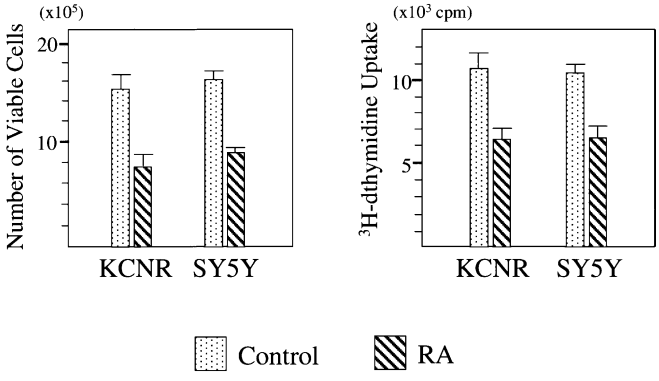



**Fig. 2** Growth inhibition of SMS-KCNR and SH-SY5Y cells following retinoic acid (RA) treatment for 5 days at the concentration of 5 $\mu$M. **A** Number of viable cells counted after trypan-blue staining. **B** $^3$H-deoxythymidine uptake analysis

In normal nervous system tissues, PML immunoreactivity was also restricted to mature cortical neurons, oligodendroglia, and astrocytes of the adult brain, while the neuronal precursor cells of the developing fetal brain did not express PML. The findings in sympathetic ganglia were basically identical to those of ganglioneuroma. Mature ganglion cells showed granular immunoreactivity for PML, and Schwann cells were also frequently labeled (Fig. 4).

## Discussion

The PML protein belongs to a family of proteins that is characterized by the presence of a $C_3HC_4$ ring finger, one or two additional Cys/His-rich motifs and an $\alpha$-helical coiled-coil domain [10, 26]. The wild-type PML protein concentrates within subnuclear domains which are defined as nuclear bodies at the ultrastructural level, and thereby exhibits a speckled pattern by immunostaining [12]. Immunohistochemical screening of PML expression has been performed in various types of human cancers. PML overexpression has been documented in Kaposi's

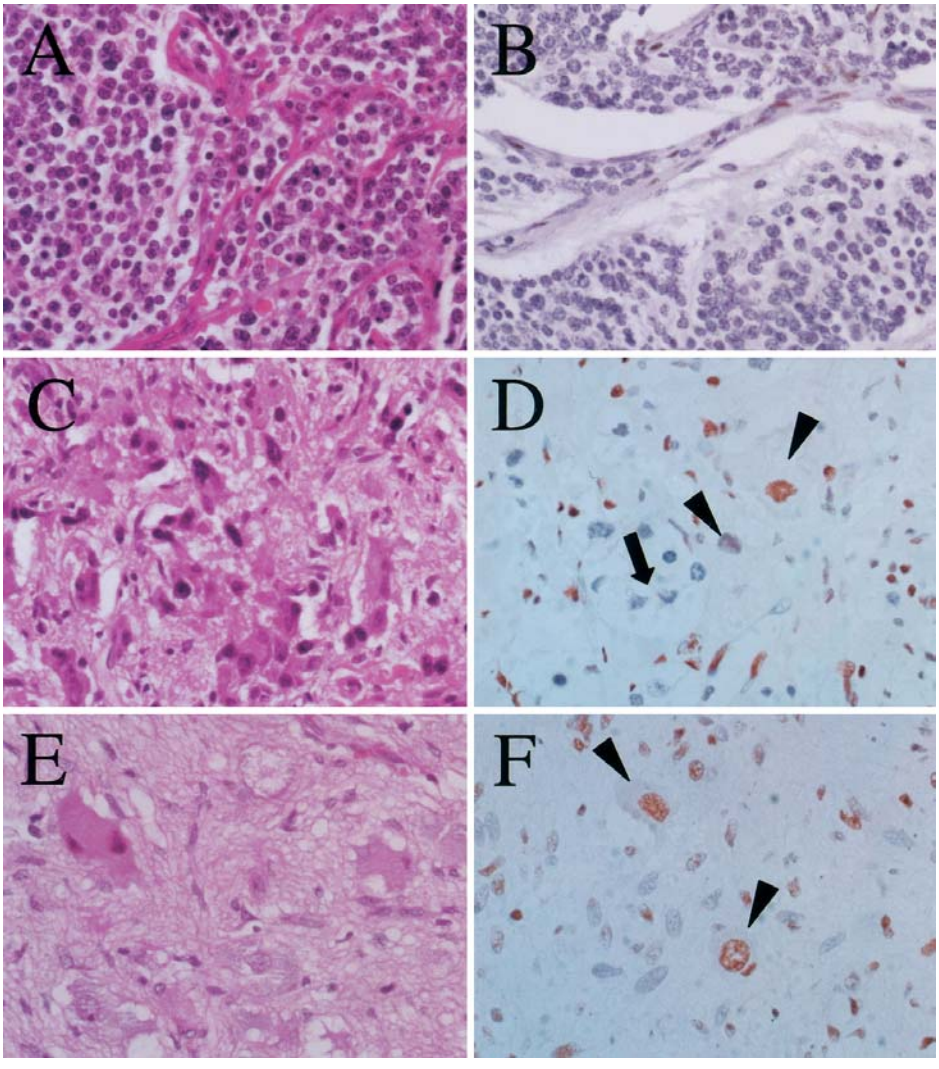



**Fig. 3** Promyelocytic leukemia (PML) expression in neuroblastic tumors. **A**, **B** PML is not expressed in poorly differentiated neuroblastic cells of neuroblastoma. Only intervening fibroblastic cells are stained positive on immunostaining (**A** H&E, ×400, **B** PML immunostaining, ×400). **C**, **D** PML expression in cells undergoing neuronal differentiation (*arrowheads*) in ganglioneuroblastoma. Schwann cells and endothelial cells are also immunoreactive for PML. Poorly differentiated neuroblastic cells do not show immunoreactivity (*arrow*) (**C** H&E, ×400, **D** PML immunostaining, ×400). **E**, **F** PML expression in both terminally differentiated ganglion cells (*arrowheads*) and Schwann cells of ganglioneuroma (**E** H&E, ×400, **F** PML immunostaining, ×400)

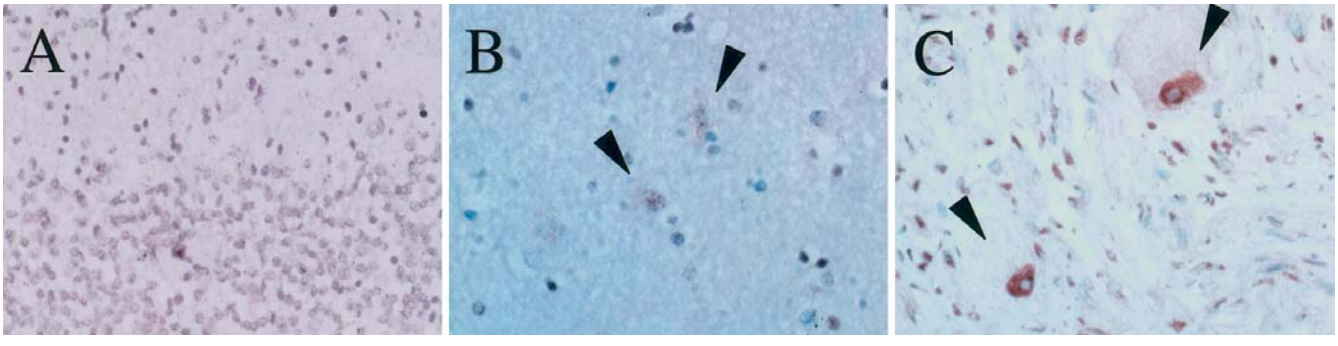



**Fig. 4** Expression of promyelocytic leukemia (PML) in the human nervous system. **A** Developing fetal cortical plate at the gestational age of 21 weeks revealing no immunoreactivity for PML in neuronal precursor cells (×400). **B** Mature cortical neurons (*arrowheads*) and glial cells of the cerebral cortex showing PML immunoreactivity in contrast to fetal cortical cells. The brain was obtained from a 15-year-old male. **C** PML immunoreactivity in sympathetic ganglia demonstrating a staining pattern basically identical with that of ganglioneuroma. Both mature ganglion cells (*arrowheads*) and Schwann cells have nuclear PML staining (×400)

sarcoma, Hodgkin's disease, squamous cell carcinomas of the larynx and esophagus, hepatocellular carcinomas and uterine cervical carcinomas, while its expression is downregulated in carcinomas of the prostate and breast, as well as in small cell carcinomas of the lung [5, 6, 9, 33].

Although the basic mechanisms underlying this differential regulation of PML expression in various types of

cancers largely remain unknown, it is thought that both the specific cell type and the proliferative state of individual tumors are closely related to the expression level of PML [9]. The majority of the epithelial tissues express low levels of PML. While normal liver cells do not express PML, PML expression is increased in cirrhotic liver and hepatocellular carcinomas, these being conditions of increased proliferation. Furthermore, PML is more strongly expressed at the periphery than at the center of single nodular hepatocellular carcinomas, and the peripheral portion is the place where the tumor is growing and expanding [5]. Zhang and colleagues found more interesting results in lung tumors. They compared PML expression level in normal lung with that in different types of lung cancers; adenocarcinoma, squamous cell carcinoma and small cell carcinoma [33]. PML expression was readily observed in normal lung, adenocarcinomas and squamous cell carcinomas, while it was not expressed in small cell carcinomas. Double immunohistochemical staining of PML and proliferation marker Ki-67 revealed an inverse correlation between the expressions of the two. Normal lung, adenocarcinomas, and squamous cell carcinomas were characterized by much lower Ki-67 labeling than that of small cell carcinoma. While the findings in these tumors clearly indicate that PML expression is related to the proliferative state of human cancers, PML expression is paradoxically lost when carcinomas of the breast turn to become invasive and in highly infiltrating, poorly differentiated, breast cancer cells [16]. Therefore, the functional aspects of PML in individual human cancers with different histogenetic bases should be open for further investigation.

The increased nuclear expression of PML detected in the present study during the differentiation of primary NB cells and RA-treated cell lines strongly suggests the functional importance of PML in the regulation of growth and differentiation of NB cells, as well as in human nervous system development. Furthermore, the screening of PML expression in developing and mature human brain and sympathetic ganglia demonstrated that the regulation of PML in NB mimics that of normal human nervous system development. This result is consistent with the prior observation that PML is strongly expressed in mature neurons and glial cells [28]. In the context of PML expression showing positive correlation with the differentiation status of NB cells, further clarification is required regarding the ability of PML to directly activate the cellular machineries involved in the neuronal differentiation of NB cells on a transcriptional level by different experimental systems, and the cell cycle machinery is one of the potential candidates that is regulated by PML. PML expression has been linked to changes in key regulators of cell cycle such as cyclin-dependent kinase (CDK), cyclin, and CDK inhibitors [18]. It has been reported that human breast cancer cells were G1 arrested, and the expression of CDK2 and cyclin D1 reduced, while that of $p21^{WAF1}$ and p53 significantly increased, when PML was overexpressed [17]. HeLa cells stably transfected with PML also showed an increased cell number in G1 phase with significant reduction in phosphorylated Rb [23]. RA treatment of NB cells is also associated with dramatic changes in cell cycle regulators. G1 cyclin/CDKs are completely downregulated in RA-treated SMS-KCNR cells along with an increase in the expression $p27^{Kip1}$ and G1 cyclin-bound $p27^{Kip1}$ [21].

In summary, the present study is the first to show that PML expression increases during neuronal differentiation of NB cells in vivo and in vitro. In the context that a similar pattern is seen in the human nervous system, it is highly likely that PML is of critical functional importance in the nervous system development and also in the biology of neuroectodermal tumors.

**Acknowledgements** This work was supported in part by a Korea Research Foundation Grant (KRF-1998–021-F000139) to E. Yu, E.K. Choi, and C.J. Kim, in part by 2002 BK21 Project for Medicine, Dentistry and Pharmacy and in part by a grant of the 1999 Korean National Cancer Control Program, Ministry of Health and Welfare, Republic of Korea.

## References

1. Abemayor E, Sidell N (1989) Human neuroblastoma cell lines as models for the in vitro study of neoplastic and neuronal cell differentiation. Environ Health Perspect 80:3–15
2. Alcalay M, Tomassoni L, Colombo E, Stoldt S, Grignani F, Fagioli M, Szekely L, Helin K, Pelicci PG (1998) The promyelocytic leukemia gene product (PML) forms stable complexes with the retinoblastoma protein. Mol Cell Biol 18:1084–1093
3. Borden KL, Campbell Dwyer EJ, Salvato MS (1997) The promyelocytic leukemia protein PML has a pro-apoptotic activity mediated through its RING domain. FEBS Lett 418:30–34
4. Borrow J, Goddard AD, Sheer D, Solomon E (1990) Molecular analysis of acute promyelocytic leukemia breakpoint cluster region on chromosome 17. Science 249:1577–1580
5. Chan JY, Chin W, Liew CT, Chang KS, Johnson PJ (1998) Altered expression of the growth and transformation suppressor PML gene in human hepatocellular carcinomas and in hepatitis tissues. Eur J Cancer 34:1015–1022
6. Cho Y, Lee I, Maul GG, Yu E (1998) A novel nuclear substructure, ND10: distribution in normal and neoplastic human tissues. Int J Mol Med 1:717–724
7. Cohen PS, Letterio JJ, Gaetano C, Chan J, Matsumoto K, Sporn MB, Thiele CJ (1995) Induction of transforming growth factor beta 1 and its receptors during all-trans-retinoic acid (RA) treatment of RA-responsive human neuroblastoma cell lines. Cancer Res 55:2380–2386
8. Dyck JA, Maul GG, Miller WH Jr, Chen JD, Kakizuka A, Evans RM (1994) A novel macromolecular structure is a target of the promyelocyte-retinoic acid receptor oncoprotein. Cell 76:333–343
9. Gambacorta M, Flenghi L, Fagioli M, Pileri S, Leoncini L, Bigerna B, Pacini R, Tanci LN, Pasqualucci L, Ascani S, Mencarelli A, Liso A, Pelicci PG, Falini B (1996) Heterogeneous nuclear expression of the promyelocytic leukemia (PML) protein in normal and neoplastic human tissues. Am J Pathol 149:2023–2035
10. Goddard AD, Borrow J, Freemont PS, Solomon E (1991) Characterization of a zinc finger gene disrupted by the t(15;17) in acute promyelocytic leukemia. Science 254:1371–1374
11. Grignani F, Ferrucci PF, Testa U, Talamo G, Fagioli M, Alcalay M, Mencarelli A, Grignani F, Peschle C, Nicoletti I,

Pelicci PG (1993) The acute promyelocytic leukemia-specific PML-RARα fusion protein inhibits differentiation and promotes survival of myeloid precursor cells. Cell 74:423–431
12. Hodges M, Tissot C, Howe K, Grimwade D, Freemont PS (1998) Structure, organization, and dynamics of promyelocytic leukemia protein nuclear bodies. Am J Hum Genet 63:297–304
13. Kakizuka A, Miller WH, Umesono K, Warrell RP Jr, Frankel SR, Murty VV, Dmitrovsky E, Evans RM (1991) Chromosomal translocation t(15;17) in human acute promyelocytic leukemia fuses RARα with a novel putative transcription factor, PML. Cell 66:663–674
14. Kaplan DR, Matsumoto K, Lucarelli E, Thiele CJ (1993) Induction of TrkB by retinoic acid mediates biologic responsiveness to BDNF and differentiation of neuroblastoma cell lines. Neuron 11:321–331
15. Khan MM, Nomura T, Kim H, Kaul SC, Wadhwa R, Zhong S, Pandolfi PP, Ishii S (2001) PML-RARα alleviates the transcriptional repression mediated by tumor suppressor Rb. J Biol Chem 276:43491–43494
16. Koken MH, Linares-Cruz G, Quignon F, Viron A, Chelbi-Alix MK, Sobczak-Thepot J, Juhlin L, Degos L, Calvo F, de The H (1995) The PML growth-suppressor has an altered expression in human oncogenesis. Oncogene 10:1315–1324
17. Le XF, Vallian S, Mu ZM, Hung MC, Chang KS (1998) Recombinant PML adenovirus suppresses growth and tumorigenicity of human breast cancer cells by inducing G1 cell cycle arrest and apoptosis. Oncogene 16:1839–1849
18. Liu JH, Mu ZM, Chang KS (1995) PML suppresses oncogenic transformation of NIH/3T3 cells by activated neu. J Exp Med 181:1965–1973
19. Lopez-Carballo G, Moreno L, Masia S, Perez P, Barettino D (2002) Activation of the phosphatidylinositol 3-kinase/Akt signaling pathway by retinoic acid is required for neural differentiation of SH-SY5Y human neuroblastoma cells. J Biol Chem 277:25297–25304
20. Lucarelli E, Kaplan DR, Thiele CJ (1995) Selective regulation of TrkA and TrkB receptors by retinoic acid and interferon-gamma in human neuroblastoma cell lines. J Biol Chem 270:24725–24731
21. Matsuo T, Thiele CJ (1998) p27Kip1: a key mediator of retinoic acid induced growth arrest in the SMS-KCNR human neuroblastoma cell line. Oncogene 16:3337–3343
22. Mu ZM, Chin KV, Liu JH, Lozano G, Chang KS (1994) PML, a growth suppressor disrupted in acute promyelocytic leukemia. Mol Cell Biol 14:6858–6867
23. Mu ZM, Le XF, Vallian S, Glassman AB, Chang KS (1997) Stable overexpression of PML alters regulation of cell cycle progression in HeLa cells. Carcinogenesis 18:2063–2069
24. Nason-Burchenal K, Gandini D, Botto M, Allopenna J, Seale JR, Cross NC, Goldman JM, Dmitrovsky E, Pandolfi PP (1996) Interferon augments PML and PML/RARα expression in normal myeloid and acute promyelocytic cells and cooperates with all-trans retinoic acid to induce maturation of a retinoic acid resistant promyelocytic leukemia cell line. Blood 88:3926–3936
25. Pearson M, Pelicci PG (2001) PML interaction with p53 and its role in apoptosis and replicative senescence. Oncogene 20:7250–7256
26. Reddy BA, Etkin LD, Freemont PS (1992) A novel zinc finger coiled-coil domain in a family of nuclear proteins. Trends Biochem Sci 17:344–345
27. Ruggero D, Wang ZG, Pandolfi PP (2000) The puzzling multiple lives of PML and its role in the genesis of cancer. Bioessays 22:827–835
28. Terris B, Baldin V, Dubois S, Degott C, Flejou JF, Henin D, Dejean A (1995) PML nuclear bodies are general targets for inflammation and cell proliferation. Cancer Res 55:1590–1597
29. Tonini R, Mancinelli E, Balestrini M, Mazzanti M, Marteganni E, Ferroni A, Sturani E, Zippel R (1999) Expression of Ras-GRF in the SK-N-BE neuroblastoma accelerates retinoic-acid-induced neuronal differentiation and increases the functional expression of the IRK1 potassium channel. Eur J Neurosci 11:959–966
30. Wang ZG, Delva L, Gaboli M, Rivi R, Giorgio M, Cordon-Cardo C, Grosveld F, Pandolfi PP (1998) Role of PML in cell growth and the retinoic acid pathway. Science 279:1547–1551
31. Wang ZG, Ruggero D, Ronchetti S, Zhong S, Gaboli M, Rivi R, Pandolfi PP (1998) Pml is essential for multiple apoptotic pathways. Nat Genet 20:266–272
32. Weis K, Rambaud S, Lavau C, Jansen J, Carvalho T, Carmo-Fonseca M, Lamond A, Dejean A (1994) Retinoic acid regulates aberrant nuclear localization of PML-RAR in acute promyelocytic leukemia cells. Cell 76:345–356
33. Zhang P, Chin W, Chow LT, Chan AS, Yim AP, Leung SF, Mok TS, Chang KS, Johnson PJ, Chan JY (2000) Lack of expression for the suppressor PML in human small cell lung carcinoma. Int J Cancer 85:599–605
34. Zhong S, Salomoni P, Pandolfi PP (2000) The transcriptional role of PML and the nuclear body. Nat Cell Biol 2:E85–E90
35. Zhong S, Salomoni P, Ronchetti S, Guo A, Ruggero D, Pandolfi PP (2000) Promyelocytic leukemia protein (PML) and Daxx participate in a novel nuclear pathway for apoptosis. J Exp Med 191:631–640

Virchows Arch (2003) 442:284–293
DOI 10.1007/s00428-002-0735-5

ORIGINAL ARTICLE

**Susanne Annette Steimle-Grauer · Marianne Tinguely · Laila Seada · Christian Fellbaum · Martin-Leo Hansmann**

# Expression patterns of transcription factors in progressively transformed germinal centers and Hodgkin lymphoma

Received: 5 July 2002 / Accepted: 18 September 2002 / Published online: 5 February 2003
© Springer-Verlag 2003

**Abstract** The World Health Organization (WHO) classification of Hodgkin lymphoma (HL) distinguishes two types: Classical Hodgkin lymphoma (CHL) and nodular lymphocyte predominant Hodgkin lymphoma (NLPHL). Both groups have in common that they mostly derive from B cells with rare classical cases originating from T cells. They differ in their histomorphology, immunophenotype, and clinical behavior. One of the subtypes of CHL, designated as lymphocyte-rich classical Hodgkin lymphoma (LRCHL), shares some morphological features with NLPHL. The transcription factors BSAP, BOB.1, Oct2 and MUM1 are sequentially expressed in normal B-cell development. In order to investigate the relationship between the CHL subgroups and NLPHL, we examined the protein expression of these transcription factors using immunohistochemistry in 15 reactive processes and 4 different subtypes of 58 HL cases. Our findings underline the B-cell origin of HL, without evidence, that reactive processes like progressively transformed germinal centers (PTGCs) are precursor lesions of HL. Furthermore, they demonstrate that LRCHL is distinct from NLPHL and that it is closely related to the mixed cellularity CHL (MCHL) in respect of BSAP, BOB.1, and Oct2 expression. It therefore occupies an intermediate position between MCHL and NLPHL. Based on MUM1 staining, LRCHL exhibits a more mature phenotype than NLPHL.

**Keywords** Hodgkin lymphoma · Transcription factors · BSAP/Pax5 · Oct2 · BOB.1/OBF1 · MUM1/IRF4

Both authors, S.A. Steimle-Grauer and M. Tinguely, contributed equally to this work.

S.A. Steimle-Grauer (✉) · M. Tinguely · L. Seada · C. Fellbaum · M.-L. Hansmann
Senckenbergisches Institute of Pathology,
Johann Wolfgang Goethe-University of Frankfurt,
Theodor-Stern-Kai 7, 60596 Frankfurt am Main, Germany
e-mail: Steimle-Grauer@em.uni-frankfurt.de
Tel.: +49-69-63015761
Fax: +49-69-63015241

## Introduction

Hodgkin lymphoma (HL) is one of the most common lymphomas in the Western world. Its cellular origin has been a controversial issue for years. Single-cell analyses of Hodgkin and Reed Sternberg (HRS) cells revealed a majority of about 98% of classical Hodgkin lymphoma (CHL) as being derived from B cells and only about 2% from T cells [6, 12, 29, 43]. In recent years, intensive research has confirmed the division into two main groups, the CHL and the rare nodular lymphocyte predominant Hodgkin lymphoma (NLPHL). They are distinguished by their different morphology as well as by their immunophenotype. The malignant lymphocytic and histiocytic (L&H) cells in NLPHL express B-cell associated molecules as CD20, CD79a, J-chain and immunoglobulins, but lack CD30 and CD15. In contrast, the HRS cells in CHL typically express CD30 and often CD15 but, in most instances, are devoid of CD20, CD79a, J-chain and immunoglobulins [41, 52]. Genotypically, all HLs contain rearranged immunoglobulin genes; however, both types have different patterns [5, 19, 22, 23, 26, 27].

In 1995, four cases of a variant of classical Hodgkin's disease were described as follicular Hodgkin's disease [2]. Recently, this variant of CHL, which morphologically resembled NLPHL in terms of nodular growth and lymphocyte richness, and CHL in terms of the immunophenotype, was designated as the common nodular variant of lymphocyte-rich classical Hodgkin lymphoma (LRCHL). The nodules in LRCHL, predominantly consisting of B cells, differ from those in NLPHL in that they represent expanded mantle zones with atrophic germinal centers (GCs) [1, 13]. Single-cell analyses for immunoglobulin gene rearrangements of LRCHL revealed that its tumor cells are derived from antigen experienced B cells with a mutation pattern similar to that of CHL (Bräuninger et al. unpublished observations).

To gain new insights into the cellular origin and the maturation stage of HL, we first examined the localization of the tumor cells in HL, focusing on LRCHL and NLPHL. Thereafter, B-cell specific activator protein

(BSAP/Pax5) [32, 35, 36], B-cell Oct binding factor1 (OBF-1/BOB.1) [11, 16, 20, 25, 42], octamer binding protein2 (Oct2) [15, 44, 45] and multiple myeloma-1 protein (MUM1/IRF4) [9, 49, 50] were selected for immunohistochemistry, because of their sequential expression at different stages of B-cell development and their importance for the regulation of gene expression during B-cell development. Their expression pattern in HL was evaluated by considering staining intensity and localization of the tumor cells with respect to the lymph-node architecture. Reactive lymphoid tissue and progressively transformed germinal centers (PTGCs) were taken for comparison.

## Materials and methods

Seventy-three paraffin-embedded tissue samples were retrieved from the files of the Senckenbergisches Institute of Pathology, reference center for lymph-node pathology, Johann Wolfgang Goethe-University, Frankfurt am Main, and reviewed according to the World Health Organization (WHO) classification. For immunohistochemistry of transcription factors, 11 cases of NLPHL and 47 cases of CHL were investigated. The latter group included 12 cases of the common nodular variant of LRCHL, 12 cases of mixed cellularity CHL (MCHL) and 23 cases of nodular sclerosis CHL (NSHL). In addition, reactive lesions were included, comprising five lymph nodes with signs of a lymphadenitis (LA) and ten lymph nodes with PTGCs.

### Immunohistochemistry

Immunohistochemistry was performed on paraffin-embedded, formalin-fixed lymph-node tissue. Nonmalignant lymph nodes with LA and no signs of progressive GC transformation were used as positive controls. Sections 4–5 µm thin were cut, dried, deparaffinized in xylene and rehydrated in graded alcohol. Before the staining procedure, antigen retrieval was carried out by heating in citrate buffer (pH 6.0, 10 mmol) for BSAP and BOB.1 and EDTA buffer (pH 8.0, 1 mmol) for Oct2 and MUM1. The primary antibodies (all from Santa Cruz Biotechnology, CA) for staining were as follows: BSAP staining – Pax-5 antibody (C-20, polyclonal goat), Oct2 staining – Oct2 antibody (C-20, polyclonal rabbit), BOB.1 staining – BOB.1 antibody (C-20, polyclonal rabbit) and for MUM1 staining – IRF-4/ICSAT antibody (M-17, polyclonal goat). Staining procedure was carried out with a GENESIS RSP 200 (Fa. Tecan, Deutschland GmbH, Germany) according to standard protocols. Streptavidin-biotin-coupled alkaline phosphatase (StrAviGen Multi Link Kits, Biogenex) and Fast Red as chromogen (Biogenex) were used to detect the bound antibodies. Counterstaining was performed with hemalaun (Sigma).

## Results

### Transcription factors in LA

*Immunohistochemical findings of transcription factors in GCs of LA*

- BSAP. In the GCs of reactive LA, an intense nuclear staining of small lymphocytes in the follicular mantle and a weak to moderate positivity of GC cells (some dark-zone centroblasts and some light-zone centrocytes) was seen. A moderate staining of some interfollicular blasts was also detectable (Fig. 1A).
- Oct2. A strong nuclear positivity of GC cells was found. The small lymphocytes in the follicular mantle zone were characterized by a less intense nuclear staining. A few lymphoid cells in the marginal zone and in the interfollicular areas showed an intense nuclear staining as well (Fig. 1B).
- GC cells, a few dispersed mantle zone cells, and a few interfollicular lymphocytes exhibited a strong nuclear positivity. The small mantle zone lymphocytes showed a weak nuclear staining (Fig. 1C).
- MUM1. A strong MUM1 expression was preferentially localized in GC cells of the light zone and in plasma cells. Centrocytes showed a strong nuclear and less intense cytoplasmic staining whereas plasma cells often presented with an intense nuclear and cytoplasmic immunostaining. Lymphocytes of the mantle zone were usually negative for MUM1. Furthermore, a positive reaction of some lymphocytes in the T-cell area was detected (Fig. 1D).

### Transcription factors in PTGCs

*Morphological findings in PTGCs*

Ten lymph nodes showing between one to six PTGCs were investigated. In contrast to the alterations in LA, GCs seem to be broken up and consist of sheets of blasts as well as centrocyte clusters. The mantle zones seem to invade and dissect the GC structures, leading to an irregular border between mantle zone and GC.

*Immunohistochemical findings of transcription factors in PTGCs*

- BSAP. Small lymphocytes with an intense nuclear staining were concentrated in the enlarged and irregularly shaped mantle zone. A few strongly positive cells were interspersed in the interfollicular area. Centroblast-like cells showed weak to moderate immunostaining in their nuclei (Fig. 1a).
- Oct2 and BOB.1. Cells showing an intense nuclear positivity for Oct2 and BOB.1 were not clearly defined to GC structures anymore, rather scattered throughout the follicular mantle and along the outer border of the mantle zone. Less intensely stained small lymphocytes of the mantle zone were also detected (Fig. 1b, c).
- MUM1. Intense nuclear and less intense cytoplasmic stained medium sized cells were irregularly dispersed over the PTGC. The mantle zones often remained free from strongly positive cells whereas the interfollicular areas were full of them (Fig. 1d).

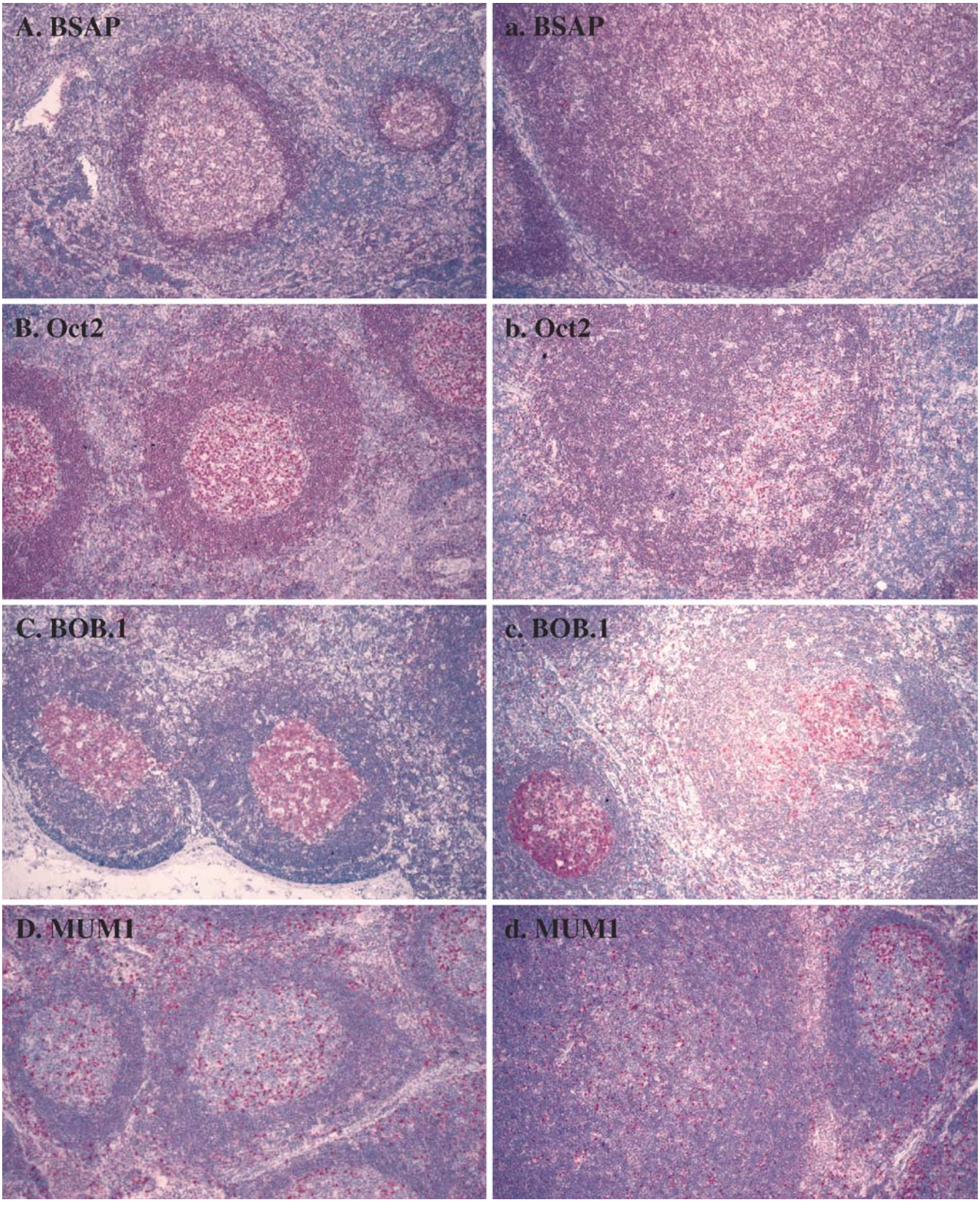



**Fig. 1A–D** Transcription factors in normal germinal centers (GCs) (**A**–**D**) and progressively transformed germinal centers (PTGCs) (*a*–*d*) of lymphadenitis, ×100. **A***a* Intense nuclear BSAP staining in mantle zone cells, weak to moderate positivity in GC cells. **B***b* Strong nuclear Oct2 positivity in GC cells, less intense staining in mantle zone cells. **C***c* Strong nuclear BOB.l positivity in GC cells, weaker staining in some mantle zone cells. **D***d* Strong nuclear MUM1 expression, preferentially localized in GC cells of the light zone and in plasma cells. Negative mantle zone cells

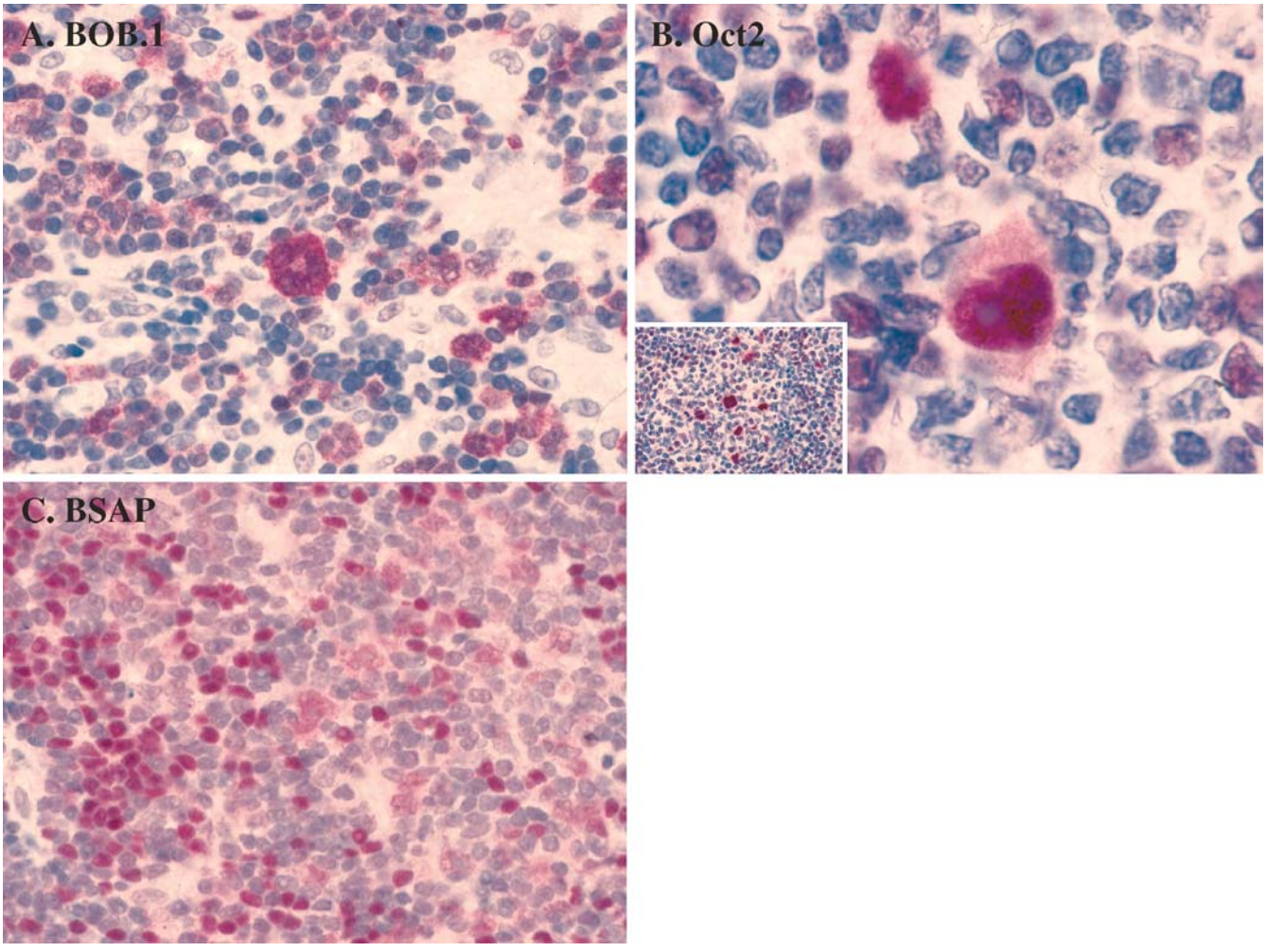



**Fig. 2** Transcription factors in nodular lymphocyte predominant Hodgkin lymphoma (NLPHL). **A** Strong nuclear BOB.1 staining of lymphocytic and histiocytic (L&H) cells, ×400. **B** Strong nuclear Oct2 staining of L&H cells; in addition, a faint spill over to the cytoplasm, ×1000. Strong nuclear staining of L&H cells (*inset*, ×400). **C** L&H cells, weaker BSAP stained than mantle zone cells, ×400

**Table 1** Staining pattern of transcription factors in tumor cells of Hodgkin lymphoma subgroups. +++ strong, ++ moderate, + weak, – no staining; *n* analyzed cases per subgroup: for each HL subgroup 0–4 cases could not be evaluated for technical reasons for some stains (BSAP, Oct2, BOB.1). Therefore, the number of actually evaluated cases can be different from n in the text. *Bold print* prevailing staining pattern in the majority of analyzed cases, referring to more than 75% of the tumor cells. *Brackets with numbers* staining pattern in the remaining cases

| | BSAP | Oct2 | BOB.1 | MUM1 |
|---|---|---|---|---|
| NLPHL (*n*=11) | **++** | **+++** | **+++** (-)[1] | **++** (–)[1] |
| LRCHL (*n*=12) | **–** (++)[2] | **+++** (-)[3] | **–** (++)[4] | **++** |
| MCHL (*n*=12) | **–** (++)[2] | **–** (++)[4] | **–** (++)[5] | **+++** |
| NSHL (*n*=23) | **–** (++)[4] | **–** (++)[6] | **–** (++)[7] | **+++** |

[1] One case with no stained tumor cells
[2] Three cases with more than 75% of tumor cells positive
[3] Five cases with only a minority of or no tumor cells positive
[4] Four cases with more than 75% of tumor cells positive
[5] Two cases with more than 75% of tumor cells positive
[6] Seven cases with more than 75% of tumor cells positive
[7] One case with more than 75% of tumor cells positive

## Transcription factors in HL subtypes

Table 1 shows the staining pattern of transcription factors in tumor cells of HL subgroups.

### *Morphological findings in NLPHL*

The lymph-node architecture was partially or totally replaced by a nodular or combined nodular and diffuse infiltrate. In particular, the nodular infiltrate consisted predominantly of small lymphocytes, histiocytes, epithelioid cells and intermingled L&H cells. Immunophenotypically, L&H cells were positive for B-cell markers, but negative for CD30 and CD15. The background was mixed up with numerous CD57 positive T cells.

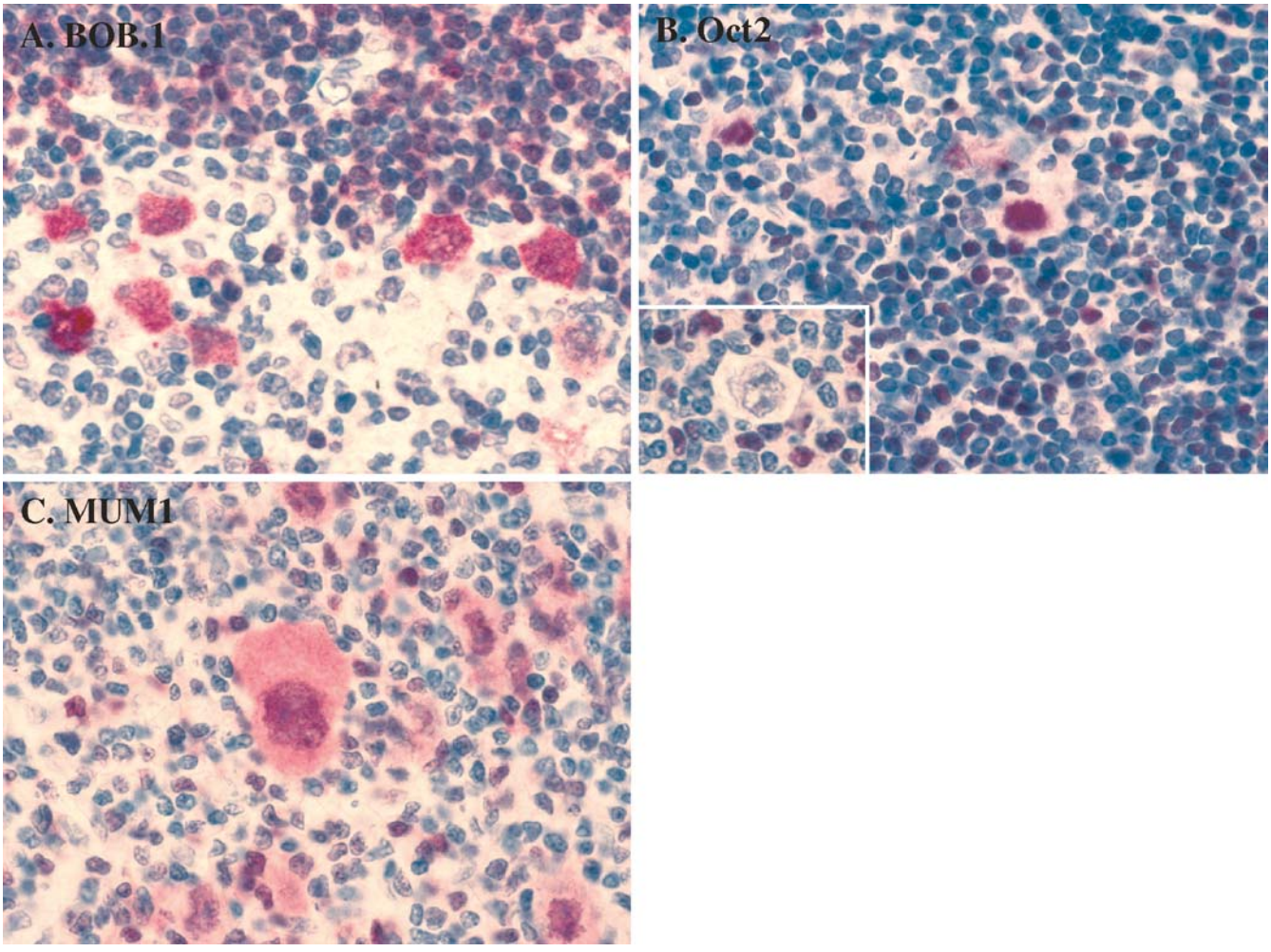



**Fig. 3** Transcription factors in lymphocyte-rich classical Hodgkin lymphoma (LRCHL). **A** Strong nuclear BOB.1 stained Hodgkin and Reed Sternberg (HRS) cells laying next to weaker stained mantle zone cells, ×400. **B** Intense nuclear Oct2 staining and negativity (*inset*) in HRS cells, two different cases, ×400. **C** Nuclear MUM1 positivity in HRS cells with a spill over to the cytoplasm, ×400

*Immunohistochemical findings of transcription factors in NLPHL*

- BSAP. The malignant L&H cells showed a moderate nuclear positivity, clearly weaker than the staining of normal mantle zone cells. There was no difference in the staining intensity according to the localization of the L&H cells. In addition, a weak cytoplasmic staining was observed in some cells of a few cases. BSAP was expressed in more than 75% of the malignant cells in all cases examined (Fig. 2C).
- Oct2 and BOB.1. The prevailing staining pattern was a strong nuclear one with occasional cells showing a faint cytoplasmic expression of Oct2 or BOB.1. Oct2 was highly expressed in all cases, BOB.1 in 10 of the 11 cases in the majority of tumor cells. For BOB.1 one case showed no tumor cell staining (Fig. 2A, B).
- MUM1. MUM1 was expressed inconsistently in NLPHL. The L&H cells showed a moderate nuclear staining in addition to a weaker cytoplasmic one. In eight cases, more than 75% of the malignant cells were positive. In the remaining three cases, two had less than 50% of the malignant cells positive and one case was negative. In addition to the malignant cells, plasma cells and mature lymphocytes in the nodules as well as in T zones were strongly positive.

*Morphological findings in LRCHL*

LRCHL presents with a nodular background mixed with histiocytes and few neutrophils and eosinophils. Besides the presence of a varying proportion of neoplastic cells, exhibiting morphologic features of L&H cells, many tumor cells have the cytomorphological appearance of classical HRS cells. The neoplastic cells are often scattered within the expanded mantle zones, thereby rarely forming aggregates. These cells express CD30 and/or CD15. A few cells are positive for CD20, but negative for the J-chain. Furthermore, small GCs can be identified

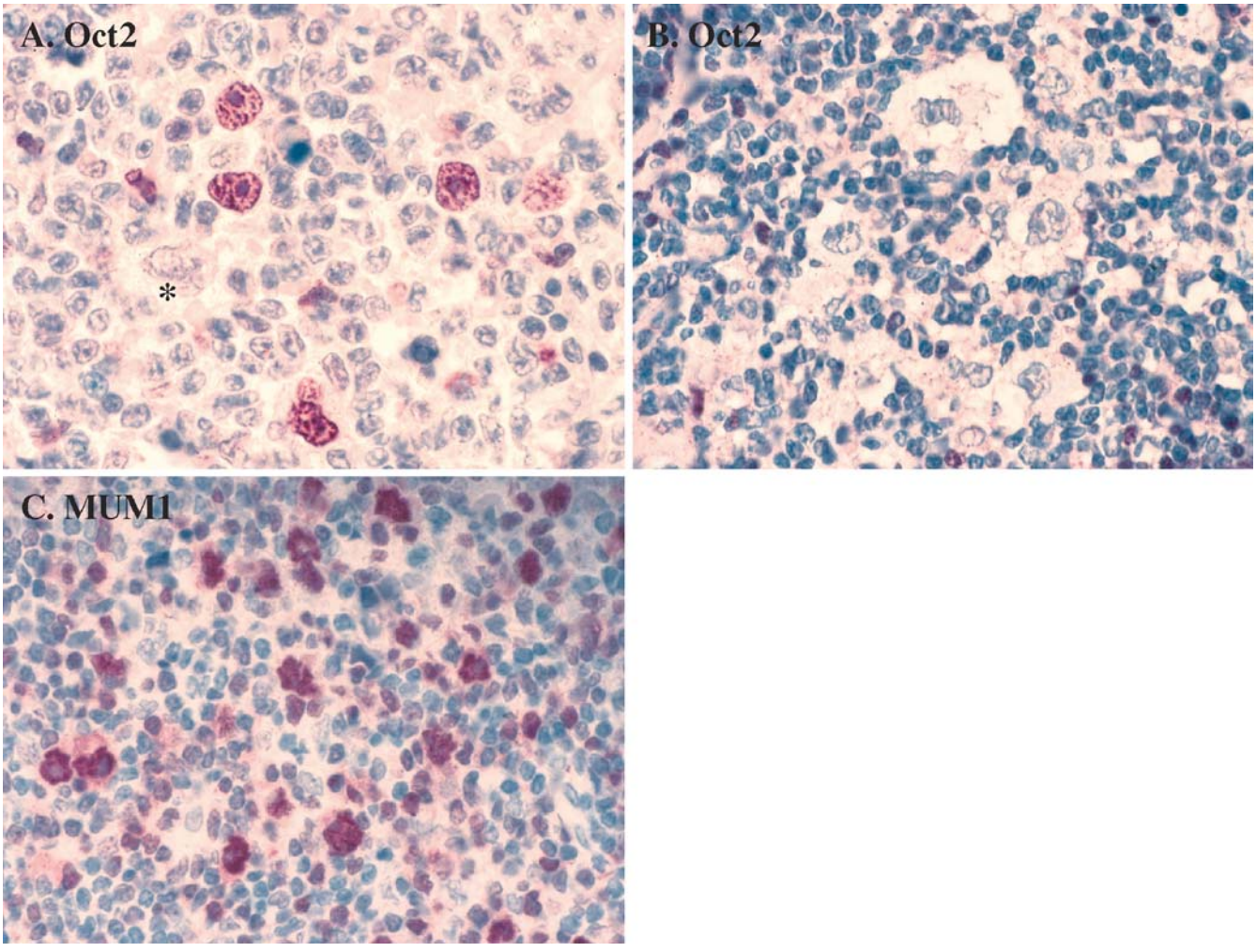



**Fig. 4** Transcription factors in mixed cellularity classical Hodgkin lymphoma (MCHL) and nodular sclerosis classical Hodgkin lymphoma (NSHL). **A** Nuclear Oct2 expression in a majority of Hodgkin and Reed Sternberg (HRS) cells of MCHL, laying next to a negative HRS cell in the same case (*), ×400. **B** No Oct2 expression in lacunar cells of NSHL, ×400. **C** Consistent nuclear MUM1 expression in HRS cells of NSHL and by-stander cells, ×400

in the periphery of the nodular structures, distinguishing these nodules from those of NLPHL, which do not contain GCs. Immunostaining with CD21 confirms the presence of eccentrically placed small GCs with a sharply depicted meshwork of follicular dendritic cells (FDCs). The mantle zone is expanded and contains an ill-defined loose meshwork of FDCs. The neoplastic cells are trapped in this meshwork and often surrounded by T-cell rosettes (CD3+).

*Immunohistochemical findings of transcription factors in LRCHL*

- BSAP. In eight cases, the majority of neoplastic cells were completely negative or expressed BSAP only in less than 50% of their malignant cells. Only three cases expressed BSAP in more than 75% of their tumor cells. The staining intensity was comparable to that of NLPHL.
- Oct2 and BOB.1. The staining intensity was similar to that in NLPHL. In contrast to NLPHL, in LRCHL more cases were negative for Oct2 and BOB.1. For Oct2, seven cases expressed Oct2 either in all neoplastic cells or in at least the majority (75%). Three cases remained completely negative, whereas in two cases only a minority of malignant cells was positive. For BOB.1, six cases remained negative, two presented with less than 50% of their tumor cells positive and four with at least the majority positive. Only three cases were positive for Oct2 and BOB.1 (Fig. 3A, B).
- MUM1. The neoplastic cells showed a strong nuclear staining pattern in addition to a less intense cytoplasmic expression of MUM1. In all cases, at least 75% of the cells were positive. Furthermore, a prominent moderate to strong nuclear positivity of rosetting cells

was observed, corresponding presumably to activated T cells (Fig. 3C).

*Morphological findings in NSHL and MCHL*

The morphology and immunophenotype of both subtypes presented with the known, classical features.

*Immunohistochemical findings of transcription factors in NSHL and MCHL*

- BSAP. As expected from the classical immunophenotype, the majority of NSHL and MCHL cases were negative for BSAP. In detail, 18 of the NSHL and seven of the MCHL cases remained negative in the overwhelming majority of tumor cells. In four cases of NSHL nearly all of the tumor cells expressed BSAP. In MCHL, three cases presented with their majority of tumor cells positive. The nuclear staining intensity was moderately strong.
- Oct2 and BOB.1. The staining intensity for both markers was moderate in most cases. In both subtypes, Oct2 was more frequently expressed than BOB.1, which was negative in most cases. Four cases of MCHL and only seven cases of NSHL showed a moderate to strong nuclear positivity for Oct2 in more than 75% of their tumor cells. In the majority of tumor cells, six cases of MCHL and 14 of NSHL remained negative; 18 cases of NSHL and seven cases of MCHL were negative for BOB.1. Only in one case of NSHL and in two cases of MCHL was BOB.1 expressed in more than 75% of the malignant cells (Fig. 4A, B).
- MUM1. In contrast to NLPHL and LRCHL, in all cases 100% of the malignant HRS cells showed a strong nuclear positivity with a weak to moderately strong spill over to the cytoplasm. In addition, some of the HRS cells were surrounded by positive small lymphocytes (Fig. 4C).

## Discussion

NLPHL was first described by Jackson in 1937 as an "early HD" [18]. In the past decade, evidence has accumulated that NLPHL exhibits features of a B-cell lymphoma with its own characteristics. Differences between the CHLs have been shown regarding the antigen profile, the immunoglobulin gene rearrangement pattern as well as the clinical behavior and prognosis [1, 5, 8, 26].

The common nodular variant of LRCHL, on the one hand, shares morphological, genotypical and clinical features with NLPHL; on the other hand, it presents with the same immunophenotype as CHL [8]. PTGCs were reported in association with 15% of patients with NLPHL and about 2% of cases with CHL [12]. Therefore, the

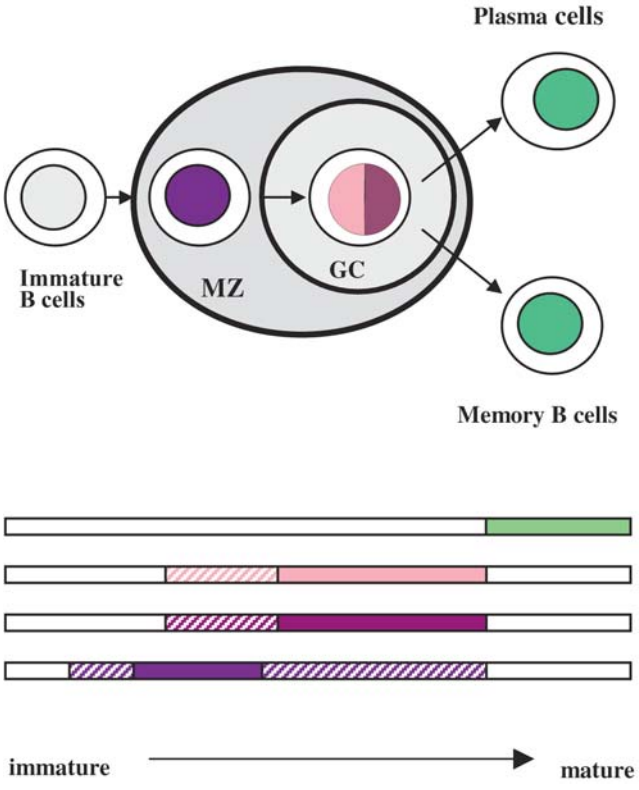



**Fig. 5** Predominant, nuclear expression of transcription factors in B cells during the germinal center pathway. *Blue* BSAP, *purple* Oct2, *pink* BOB.l, *green* MUM1. *Intense/hatched colors* represent the strong/weaker expression of transcription factors; *bars* represent correlation between intensity of expression and maturation stage of B cells. *MZ* mantle zone, *GC* germinal center

issue was raised whether these disorders play a role as precursor lesions of HL.

B lymphopoiesis, like other developmental processes, entails the ordered, sequential expression of structural and regulatory genes. Different transcription factors are differentially expressed during B-cell maturation and are important for the regulation of gene expression during B-cell development. Whereas BSAP, regulated by the Pax5 gene, usually starts occurring in early developmental stages, Oct2 and its cofactor BOB.1 were not seen later until MUM1 was expressed in mature B cells. This expression pattern can be correlated with the GC pathway of B cells (Fig. 5).

Expression of transcription factors in LA and PTGCs

The expression of transcription factors in LA in our series reflects the maturation stage of the B cells in the different GC areas (Fig. 1). It is in agreement with numerous reports in the literature, based on murine models and on human tissue [21]. According to the observation of Saez et al., we found mature lymphocytes positive for Oct2 and BOB.1 in the T-cell area [39]. Previous investigations addressed the question whether PTGCs are precursor

lesions of HL. However, immunohistochemical studies using an extended panel of antibodies against CD20, CD45RA, CD45RO, CD3, CD43, CD57, EMA, CD30 and CD21 could not show any relationship between the expression pattern of PTGCs and NLPHL [31]. Just as single-cell analyses did not reveal any evidence that PTGCs are clonally related to NLPHL [7]. Congruent with these data from the literature, we did not find evidence that could predict the evolution from PTGCs toward a HL in our study.

## Expression of BSAP in HL

The Pax5 gene is expressed exclusively in the B-lymphoid lineage within the hematopoetic system. BSAP functions both as a transcriptional activator and repressor of the Pax5 gene. It also seems to play a role in Ig class switching [32, 33, 34, 35, 36, 38]. Pax5 gene transcription is initiated in pro B-cells and is abundant at the pre-B and mature B-cell differentiation stages, but absent in terminally differentiated plasma cells [3]. This finding might be explained by the fact that BSAP has an important repressor function for Ig heavy chain expression by suppressing the activity of the 3' alpha heavy chain enhancer.

In NLPHL, all cases showed BSAP expression. In contrast, the LRCHL cases exhibited a mirror image with only few HRS cells in some cases presenting a moderately intense nuclear positivity for BSAP. In the other CHL, the number of positive cases was variable, ranging from 4 of 23 cases in NSHL to 3 of 12 in MCHL. Our findings in NSHL were similar to the study of Krenacs et al., but only in partial agreement with his results in NLPHL, where only 50% of cases were positive [21]. We found similar results in NLPHL to Foss et al. [10]. However, by using monoclonal antibodies, his group detected BSAP in a variable number of HRS cells in around 80% of CHL (NSHL, MCHL) [10]. To our knowledge, this is the first investigation of BSAP expression in LRCHL in a representative number of cases. On the genomic level, the mutation pattern of rearranged Ig genes of HRS cells in LRCHL is similar to that observed in other CHL, namely heavily mutated IgV genes and a fraction of cases with obviously crippling V gene mutations (Bräuninger et al., unpublished observations). Our immunohistochemical investigations on the protein level underline the B-cell nature of both the classical and the lymphocyte predominant HLs. Based on the expression pattern of BSAP, LRCHL behaves more like CHL with similarities to MCHL. In addition, BSAP protein expression may facilitate the delineation between NLPHL and LRCHL.

## Expression of Oct2 and BOB.1 in HL

BOB.1 protein is a B-cell specific co-activator of the Oct1 and Oct2 transcription factors [11, 42, 47]. In combination, the transcription factors Oct1 and Oct2 and their co-activator BOB.1 regulate immunoglobulin gene transcription [16, 20, 24]. Whereas Oct1 is a ubiquitous transcription factor implicated in the control of genes expressed by all cells, Oct2 is largely B-lineage specific and has been implicated in the control of B-lymphocyte-specific gene expression [15, 40, 44, 45, 48]. Oct1 and Oct2 can replace each other, whereas BOB.1 as a specific cofactor is required to activate the immunoglobulin gene promoter [11, 25, 47].

For Oct2 and BOB.1, we observed three major groups of expression patterns: In the first group, a simultaneous expression of Oct2 and BOB.1 was seen. The percentage of positive tumor cells was high, ranging from 75% to 100%, accompanied by an intense staining confined to the nuclei, with some cases showing a faint cytoplasmic positivity. This first group was represented by NLPHL. These results are in agreement with recently published data for NLPHL by Stein et al. [46] and are in line with CD20 expression commonly observed in this entity. The findings are in accordance with Re et al. who detected Oct2 and BOB.1 transcripts in the lymphocyte-predominant-derived cell line DEV [37].

The second group was characterized by an exclusive expression of Oct2 or BOB.1, which means that we found either an expression of Oct2 or BOB.1 in the same case. The percentage of cases with positive signals for these factors was lower than in the first group. The staining intensity was as strong as in group one. This pattern was found in most LRCHL. As an exception to the above-mentioned observations, we found three cases simultaneously positive for Oct2 and BOB.1 in LRCHL. These particular cases were negative for CD20. In the literature, there are only four cases of LRCHL investigated for the expression of Oct2 and BOB.1 by immunohistochemistry. In two cases, no positivity – neither for Oct2 nor BOB.1 – could be detected [37]. In the two other cases, only a faint staining for Oct2 and no or only moderate staining for BOB.1 was reported [39].

The third group showed no expression of Oct2 and BOB.1 in the majority of the cases. This is especially true for BOB.1. Nevertheless, about a quarter of these cases showed positivity for Oct2 in the majority of tumor cells. This group was represented by NSHL and MCHL.

Our observations on the expression patterns of Oct2 and BOB.1 in HL are identical to the findings of Saez et al. [39]. Lack of immunoglobulin gene expression has been shown by in situ hybridization in cases of CHL, despite the detection of potentially functional IgVDJ gene rearrangements in most of these cases [27]. The unexpected finding on the lack of Oct2 and BOB.1 expression in primary HRS cells of CHL (2 of 20 cases of LRCHL) was previously discussed by Re et al., where a novel mechanism involved in transcriptional deregulation of immunoglobulin genes in CHL was suggested [37]. Likewise, downregulation of BOB.1 and Oct2 was described in CHL, but not in NLPHL and correlated with immunoglobulin transcription in these cases [37, 46].

Expression of MUM1 in HL

MUM1 is a myeloma-associated oncogene transcriptionally activated as a result of t(6;14)(p25,q32) chromosomal translocation and by virtue of its juxtaposition to the immunoglobulin heavy chain gene locus [17]. It belongs to the interferon regulatory factor family which is generally induced by interferon and therefore plays an important role in antiviral defense and in cellular proliferation [14, 30, 49]. The physiological function has not yet been elucidated, except that it cooperates with PU.1 as a transcriptional regulator in lymphoid cells [4, 51]. Findings in mice suggest a prerequisite role for MUM1 in lymphocyte activation and in terminal B-cell differentiation [28]. In normal reactive lymph nodes, the spectrum of MUM1 expression ranged from that of a centrocyte to a plasmablast/plasma cell [9]. The factor is reported to be strongly expressed in lymphoplasmacytoid lymphoma, multiple myeloma, diffuse large B-cell lymphoma as well as in a few cases of Hodgkin's disease, but also in T-cell lymphomas including adult T-cell leukemia/lymphoma and anaplastic large cell lymphoma [9].

In the present study, MUM1 was constitutively expressed in all of the CHL and exhibited a strong nuclear and a weaker cytoplasmic labeling. In LRCHL, the majority of HRS cells were positive, but not always in 100% of the malignant cells, as seen in MCHL and NSHL. In NLPHL, MUM1 expression was more inconsistent, with around 25% of cases lacking positivity or presenting only occasional cells as positive. Our results, although a little more heterogeneous, are in accordance with those of Falini et al. [9], who reported positivity in only two cases of his study. Furthermore, to our knowledge, only Tsuboi et al. have reported MUM1 expression in one case of LRCHL [50].

In conclusion, the immunohistochemical detection of the transcription factors BSAP, BOB.1 and Oct2 confirms the B-cell origin of HL. We show, that LRCHL is a distinct entity that shares some similarities with MCHL and NSHL and takes an intermediate position between NLPHL and MCHL. Though our data do not allow to clearly assign a HL type to a precise stage of B-cell maturation, LRCHL seems to exhibit a more mature phenotype than NLPHL, taking into consideration the MUM1 expression. Although, the expression of transcription factors in HL is very heterogeneous, their simultaneous implementation for differential diagnosis may be useful.

**Acknowledgements** M.T. is supported by the Swiss National Science Foundation and the Janggen-Pöhn-Stiftung, Switzerland. We thank Ralf Lieberz and Anja Mottok for excellent technical assistance.

## References

1. Anagnostopoulos I, Hansmann ML, Franssila K, Harris M, Harris NL, Jaffe ES, Han J, van Krieken JM, Poppema S, Marafioti T, Franklin J, Sextro M, Diehl V, Stein H (2000) European Task Force on Lymphoma project on lymphocyte predominance Hodgkin disease: histologic and immunohistologic analysis of submitted cases reveals 2 types of Hodgkin disease with a nodular growth pattern and abundant lymphocytes. Blood 96:1889–1899
2. Ashton-Key M, Thorpe PA, Allen JP, Isaacson PG (1995) Follicular Hodgkin's disease. Am J Surg Pathol 19:1294–1299
3. Barberis A, Widenhorn K, Vitelli L, Busslinger M (1990) A novel B-cell lineage-specific transcription factor present at early but not late stages of differentiation. Genes Dev 4:849–859
4. Brass AL, Zhu AQ, Singh H (1999) Assembly requirements of PU.1-Pip (IRF-4) activator complexes: inhibiting function in vivo using fused dimers. EMBO J 18:977–991
5. Bräuninger A, Küppers R, Strickler JG, Wacker HH, Rajewsky K, Hansmann ML (1997) Hodgkin and Reed-Sternberg cells in lymphocyte predominant Hodgkin disease represent clonal populations of germinal center-derived tumor B cells. Proc Natl Acad Sci U S A 94:9337–9342
6. Bräuninger A, Hansmann ML, Strickler JG, Dummer R, Burg G, Rajewsky K, Küppers R (1999) Identification of common germinal-center B-cell precursors in two patients with both Hodgkin's disease and non-Hodgkin's lymphoma. N Engl J Med 340:1239–1247
7. Bräuninger A, Yang W, Wacker HH, Rajewsky K, Küppers R, Hansmann ML (2001) B-cell development in progressively transformed germinal centers: similarities and differences compared with classical germinal centers and lymphocyte-predominant Hodgkin disease. Blood 97:714–719
8. Diehl V, Sextro M, Franklin J, Hansmann ML, Harris N, Jaffe E, Poppema S, Harris M, Franssila K, van Krieken J, Marafioti T, Anagnostopoulos I, Stein H (1999) Clinical presentation, course, and prognostic factors in lymphocyte-predominant Hodgkin's disease and lymphocyte-rich classical Hodgkin's disease: report from the European Task Force on Lymphoma Project on Lymphocyte-Predominant Hodgkin's Disease. J Clin Oncol 17:776–783
9. Falini B, Fizzotti M, Pucciarini A, Bigerna B, Marafioti T, Gambacorta M, Pacini R, Alunni C, Natali-Tanci L, Ugolini B, Sebastiani C, Cattoretti G, Pileri S, Dalla-Favera R, Stein H (2000) A monoclonal antibody (MUM1p) detects expression of the MUM1/IRF4 protein in a subset of germinal center B cells, plasma cells, and activated T cells. Blood 95:2084–2092
10. Foss HD, Reusch R, Demel G, Lenz G, Anagnostopoulos I, Hummel M, Stein H (1999) Frequent expression of the B-cell-specific activator protein in Reed-Sternberg cells of classical Hodgkin's disease provides further evidence for its B-cell origin. Blood 94:3108–3113
11. Gstaiger M, Knoepfel L, Georgiev O, Schaffner W, Hovens CM (1995) A B-cell coactivator of octamer-binding transcription factors. Nature 373:360–362
12. Hansmann ML, Fellbaum C, Hui PK, Moubayed P (1990) Progressive transformation of germinal centers with and without association to Hodgkin's disease. Am J Clin Pathol 93:219–226
13. Hansmann ML, Weiss LM. Stein H, Harris NL, Jaffe ES (1999) Pathology of lymphocyte predominance Hodgkin's disease. In: Mauch PM, Armitage JO, Diehl V, Hoppe RT, Weiss LM (eds) Hodgkin's disease. Lippincott Williams & Wilkins, Philadelphia, pp 169–180
14. Harada H, Taniguchi T, Tanaka N (1998) The role of interferon regulatory factors in the interferon system and cell growth control. Biochimie 80:641–650
15. He X, Treacy MN, Simmons DM, Ingraham HA, Swanson LW, Rosenfeld MG (1989) Expression of a large family of POU-domain regulatory genes in mammalian brain development. Nature 340:35–41
16. Hess J, Nielsen PJ, Fischer KD, Bujard H, Wirth T (2001) The B lymphocyte-specific coactivator BOB.1/OBF.1 is required at multiple stages of B-cell development. Mol Cell Biol 21:1531–1539
17. Iida S, Rao PH, Butler M, Corradini P, Boccadoro M, Klein B, Chaganti RS, Dalla-Favera R (1997) Deregulation of MUM1/IRF4 by chromosomal translocation in multiple myeloma. Nat Genet 17:226–230

18. Jackson (1937) Classification and prognosis of Hodgkin's disease and allied disorders. Surg Gynecol Obstet 64:465
19. Kanzler H, Küppers R, Hansmann ML, Rajewsky K (1996) Hodgkin and Reed-Sternberg cells in Hodgkin's disease represent the outgrowth of a dominant tumor clone derived from (crippled) germinal center B cells. J Exp Med 184:1495–1505
20. Kim U, Qin XF, Gong S, Stevens S, Luo Y, Nussenzweig M, Roeder RG (1996) The B-cell-specific transcription coactivator OCA-B/OBF-1/Bob-1 is essential for normal production of immunoglobulin isotypes. Nature 383:542–547
21. Krenacs L, Himmelmann AW, Quintanilla-Martinez L, Fest T, Riva A, Wellmann A, Bagdi E, Kehrl JH, Jaffe ES, Raffeld M (1998) Transcription factor B-cell-specific activator protein (BSAP) is differentially expressed in B cells and in subsets of B-cell lymphomas. Blood 92:1308–1316
22. Küppers R, Rajewsky K, Zhao M, Simons G, Laumann R, Fischer R, Hansmann ML (1994) Hodgkin disease: Hodgkin and Reed-Sternberg cells picked from histological sections show clonal immunoglobulin gene rearrangements and appear to be derived from B cells at various stages of development. Proc Natl Acad Sci U S A 91:10962–10966
23. Küppers R, Rajewsky K, Bräuninger A, Hansmann ML (1998) L&H cells in lymphocyte-predominant Hodgkin's disease. N Engl J Med 338:763–765
24. Laumen H, Nielsen PJ, Wirth T (2000) The BOB.1 / OBF.1 co-activator is essential for octamer-dependent transcription in B cells. Eur J Immunol 30:458–469
25. Luo Y, Roeder RG (1995) Cloning, functional characterization, and mechanism of action of the B-cell-specific transcriptional coactivator OCA-B. Mol Cell Biol 15:4115–4124
26. Marafioti T, Hummel M, Anagnostopoulos I, Foss HD, Falini B, Delsol G, Isaacson PG, Pileri S, Stein H (1997) Origin of nodular lymphocyte-predominant Hodgkin's disease from a clonal expansion of highly mutated germinal-center B cells. N Engl J Med 337:453–458
27. Marafioti T, Hummel M, Foss HD, Laumen H, Korbjuhn P, Anagnostopoulos I, Lammert H, Demel G, Theil J, Wirth T, Stein H (2000) Hodgkin and Reed-Sternberg cells represent an expansion of a single clone originating from a germinal center B-cell with functional immunoglobulin gene rearrangements but defective immunoglobulin transcription. Blood 95:1443–1450
28. Mittrucker HW, Matsuyama T, Grossman A, Kundig TM, Potter J, Shahinian A, Wakeham A, Patterson B, Ohashi PS, Mak TW (1997) Requirement for the transcription factor LSIRF/IRF4 for mature B and T lymphocyte function. Science 275:540–543
29. Müschen M, Rajewsky K, Bräuninger A, Baur AS, Oudejans JJ, Roers A, Hansmann ML, Küppers R (2000) Rare occurrence of classical Hodgkin's disease as a T cell lymphoma. J Exp Med 191:387–394
30. Nelson N, Kanno Y, Hong C, Contursi C, Fujita T, Fowlkes BJ, O'Connell E, Hu-Li J, Paul WE, Jankovic D, Sher AF, Coligan JE, Thornton A, Appella E, Yang Y, Ozato K (1996) Expression of IFN regulatory factor family proteins in lymphocytes. Induction of Stat-1 and IFN consensus sequence binding protein expression by T cell activation. J Immunol 156:3711–3720
31. Nguyen PL, Ferry JA, Harris NL (1999) Progressive transformation of germinal centers and nodular lymphocyte predominance Hodgkin's disease: a comparative immunohistochemical study. Am J Surg Pathol 23:27–33
32. Nutt SL, Thevenin C, Busslinger M (1997) Essential functions of Pax-5 (BSAP) in pro-B cell development. Immunobiology 198:227–235
33. Nutt SL, Urbanek P, Rolink A, Busslinger M (1997) Essential functions of Pax5 (BSAP) in pro-B cell development: difference between fetal and adult B lymphopoiesis and reduced V-to-DJ recombination at the IgH locus. Genes Dev 11:476–491
34. Nutt SL, Morrison AM, Dorfler P, Rolink A, Busslinger M (1998) Identification of BSAP (Pax-5) target genes in early B-cell development by loss- and gain-of-function experiments. EMBO J 17:2319–2333
35. Nutt SL, Heavey B, Rolink AG, Busslinger M (1999) Commitment to the B-lymphoid lineage depends on the transcription factor Pax5. Nature 401:556–562
36. Nutt SL, Eberhard D, Horcher M, Rolink AG, Busslinger M (2001) Pax5 determines the identity of B cells from the beginning to the end of B-lymphopoiesis. Int Rev Immunol 20:65–82
37. Re D, Müschen M, Ahmadi T, Wickenhauser C, Staratschek-Jox A, Holtick U, Diehl V, Wolf J (2001) Oct-2 and Bob-1 deficiency in Hodgkin and Reed Sternberg cells. Cancer Res 61:2080–2084
38. Rolink AG, Nutt SL, Melchers F, Busslinger M (1999) Long-term in vivo reconstitution of T-cell development by Pax5-deficient B-cell progenitors. Nature 401:603–606
39. Saez AI, Artiga MJ, Sanchez-Beato M, Sanchez-Verde L, Garcia JF, Camacho FI, Franco R, Piris MA (2002) Analysis of Octamer-Binding Transcription Factors Oct2 and Oct1 and their coactivator BOB.1/OBF.1 in Lymphomas. Mod Pathol 15:211–220
40. Scheidereit C, Heguy A, Roeder RG (1987) Identification and purification of a human lymphoid-specific octamer-binding protein (OTF-2) that activates transcription of an immunoglobulin promoter in vitro. Cell 51:783–793
41. Schmid C, Pan L, Diss T, Isaacson PG (1991) Expression of B-cell antigens by Hodgkin's and Reed-Sternberg cells. Am J Pathol 139:701–707
42. Schubart DB, Rolink A, Kosco-Vilbois MH, Botteri F, Matthias P (1996) B-cell-specific coactivator OBF-1/OCA-B/Bob1 required for immune response and germinal centre formation. Nature 383:538–542
43. Seitz V, Hummel M, Marafioti T, Anagnostopoulos I, Assaf C, Stein H (2000) Detection of clonal T-cell receptor gamma-chain gene rearrangements in Reed-Sternberg cells of classic Hodgkin disease. Blood 95:3020–3024
44. Singh H, Sen R, Baltimore D, Sharp PA (1986) A nuclear factor that binds to a conserved sequence motif in transcriptional control elements of immunoglobulin genes. Nature 319:154–158
45. Staudt LM, Singh H, Sen R, Wirth T, Sharp PA, Baltimore D (1986) A lymphoid-specific protein binding to the octamer motif of immunoglobulin genes. Nature 323:640–643
46. Stein H, Marafioti T, Foss HD, Laumen H, Hummel M, Anagnostopoulos I, Wirth T, Demel G, Falini B (2001) Down-regulation of BOB.1/OBF.1 and Oct2 in classical Hodgkin disease but not in lymphocyte predominant Hodgkin disease correlates with immunoglobulin transcription. Blood 97:496–501
47. Strubin M, Newell JW, Matthias P (1995) OBF-1, a novel B cell-specific coactivator that stimulates immunoglobulin promoter activity through association with octamer-binding proteins. Cell 80:497–506
48. Sturm RA, Das G, Herr W (1988) The ubiquitous octamer-binding protein Oct-1 contains a POU domain with a homeo box subdomain. Genes Dev 2:1582–1599
49. Taniguchi T, Harada H, Lamphier M (1995) Regulation of the interferon system and cell growth by the IRF transcription factors. J Cancer Res Clin Oncol 121:516–520
50. Tsuboi K, Iida S, Inagaki H, Kato M, Hayami Y, Hanamura I, Miura K, Harada S, Kikuchi M, Komatsu H, Banno S, Wakita A, Nakamura S, Eimoto T, Ueda R (2000) MUM1/IRF4 expression as a frequent event in mature lymphoid malignancies. Leukemia 14:449–456
51. Yee AA, Yin P, Siderovski DP, Mak TW, Litchfield DW, Arrowsmith CH (1998) Cooperative interaction between the DNA-binding domains of PU.1 and IRF4. J Mol Biol 279:1075–1083
52. Zukerberg LR, Collins AB, Ferry JA, Harris NL (1991) Coexpression of CD15 and CD20 by Reed-Sternberg cells in Hodgkin's disease. Am J Pathol 139:475–483

Virchows Arch (2003) 442:294–297
DOI 10.1007/s00428-002-0717-7

CASE REPORT

**H. J. M. Mertens · M. Nap · M. P. G. Leers · T. H. B. Salemans**

# Multiparameter flow cytometry in the diagnosis of a gynaecologic double tumor: a case report

Received: 8 April 2002 / Accepted: 3 September 2002 / Published online: 26 February 2003
© Springer-Verlag 2003

**Abstract** *Purpose:* An uncommon clinical presentation of metastatic tumor will often lead to additional diagnostic examinations. The patient of the present study was known to have endometrial cancer which was thought to be limited to the endometrium. Three months postoperatively, she developed ascites due to spread of the tumor, which is rarely seen in low-stage endometrial cancer. *Method:* Multiparameter flow cytometry using both cell phenotype information and DNA ploidy was performed. *Results:* Retrospectively, the patient was diagnosed as having a DNA-diploid epithelial tumor of the endometrium as well as a DNA-aneuploid epithelial tumor in the left fallopian tube. It was shown that 3 months after primary surgery she developed ascites caused by metastatic tumor from the primary fallopian tube cancer. *Conclusion:* The complete diagnosis was made using multiparameter flow cytometry which, at present, is not routinely applied in gynecologic pathology.

**Keywords** Endometrial cancer/fallopian tube cancer · Tumor diagnosis · DNA flow cytometry

## Introduction: clinical history

In a nearby hospital a 76-year-old women was seen because of postmenopausal blood loss. She was in good health and did not smoke or use any medication. Physical examination showed no abnormalities. Using ultrasound, the endometrium was thickened and the ovaries were normal. Cytologic examination of a cervical smear was normal (Pap I) and histopathologic examination of a pipelle aspiration of the endometrium showed adenocarcinoma.

An abdominal hysterectomy with bilateral salpingo-oophorectomy was performed. There was no ascites and no signs of macroscopic tumor spread. No peritoneal washing was done. The operation was uneventful.

Histopathologic examination showed a well-differentiated adenosquamous carcinoma of the endometrium. Both myometrium and cervix were not involved. The ovaries were histologically normal. In the left fallopian tube a small tumor focus was described, classified as adenocarcinoma in situ. The tumor was diagnosed as endometrial cancer FIGO grade IA; adjuvant therapy was not indicated [3].

Three months after surgery the patient was referred to our department because of dyspnea caused by ascites. Cytologic examination of cells in the peritoneal fluid showed adenocarcinoma cells. Because of the rarity of positive ascites cytology in a patient with endometrial cancer FIGO grade IA, it was decided to revise the original histopathologic examination.

H.J.M.M. Mertens (✉)
Maaslandziekenhuis Sittard,
Department of Obstetrics and Gynaecology,
Research Institute Growth and Development GROW,
Walramstraat 23, 6131 BK Sittard, Maastricht, The Netherlands
e-mail: h.mertens@orbisconcern.nl
Tel.: +31-464-597787
Fax: +31-464-597463

M. Nap · M.P.G. Leers
Department of Pathology, Atrium Medical Center Heerlen,
The Netherlands

T.H.B. Salemans
Department of Obstetrics and Gynaecology,
Atrium Medical Center Heerlen, The Netherlands

## Methods

### Histopathologic examination

Histopathologic examination revealed an endometrial adenosquamous carcinoma. Moreover, the single tumor mass in the left fallopian tube was found to be locally invasive. Differentiation between primary endometrial cancer spread to the tube (usually per continuitatem), primary tube cancer spread to the endometrium or the presence of two primary tumors simultaneously was not possible using routinely histopathologic examination. For further examinations, a new technique was applied.

Multiparameter flow cytometry

Cytokeratins are specific markers for epithelial cells. Adenocarcinoma that consists of malignant glandular cells are well marked by those cytokeratins [15]. After preparing a single-cell suspension, cells retained enough cytoskeletal remnants to allow immunocytochemical detection of these cytokeratins. Labeling of the cytokeratins allows a restriction of the flow-cytometric analysis to the epithelial compartment of the tumor without admixture of normal cells (inflammatory and endothelial cells, stromal compartment) [10]. DNA was stained using the intercalation dye propidium iodide. The fluorescence intensity of individual cells stained with DNA specific dyes is proportional to DNA content of the cells.

*Preparation of cell suspension*

Two 50-µm-thick sections were cut from each paraffin block. Subsequently, these tissue sections were deparaffinized twice in xylene, 30 min each, and then rehydrated in a descending ethanol series. Sections were then rinsed in phosphate buffered saline (PBS; pH 7.2–7.4). The sections were placed in a glass tube with cold citrate solution (2 mg citric acid/ml aqua dest; pH 6.0), and then subjected to a 120-min heating step in an 80°C water bath. After a short cooling-down period, a 10-min mild pepsin digestion step followed, at 37°C in a freshly prepared solution containing 1 mg/ml pepsin (Sigma, St. Louis, MO, USA) in 0.1 N HCl. A single-cell suspension was obtained by vortexing and filtering of the sample through a 50-µm mesh nylon filter. The cell suspension was then centrifuged at 400×*g*, and the cell pellet was re-suspended in PBS, supplemented with 1% bovine serum albumin (BSA/PBS buffer; Sigma).

*Multiparameter flow cytometry*

The single-cell suspension was aliquoted into 100-µl samples. The samples were incubated with a single monoclonal antibody directed to CK 7 (OV/TL 12–30; Dako A/S, Glostrup, Denmark; 1:50), CK 20 (Ks20.8; Dako; 1:50) or pan-CK (MNF116; Dako; 1:50). After an overnight incubation at room temperature, antibody binding was made visible by incubating the single cells with fluorescein isothiocyanate (FITC) labeled goat-anti-mouse Ig (Dako A/S; 1:10) for 1.5 h at room temperature. The samples were rinsed twice in PBS and finally DNA was stained using propidium iodide (PI, 1.0 µM, Sigma) in PBS containing 0.1 mg/ml RNAse (Serva, Heidelberg, Germany). The samples were allowed to stand for a minimum of 1 h in the dark at 4°C before flow cytometric analysis. As a negative control for background staining by the primary antibody, a proportion of the cell suspension was incubated with a non-relevant mouse Ig (Dako; 1:50).

Samples were analyzed using a PARTEC PAS III flow cytometer (Partec GmbH, Münster, Germany). Cells were excited with a single 488-nm argon laser. FITC fluorescence was detected through a 515–545 nm BP filter and PI fluorescence through a 600-nm LP filter. At least 10,000 relevant events were collected for each sample. FITC signals were recorded as logarithmic amplified data, while the PI signals were recorded as linear amplified data. The following settings were used: 512 V and 438 V on photomultiplier tubes for FL1 (FITC) and FL3 (PI), respectively. Compensation was performed afterwards during analysis using the N-color compensation module of the PAS software program (Partec GmbH, Münster, Germany).

The lack of a known DNA-diploid reference population in nuclei from paraffin-embedded tissues makes the identification of this population difficult. Because the incidence of tumors with a DNA index smaller than 1.0 is rare, it has been established in a DNA cytometry consensus conference that it is recommended that the first peak in the DNA histogram may be assumed to represent the DNA-diploid population [16]. DNA histograms with a coefficient of variation of the G0/G1 peak less than 5% were considered as good quality measurements.

## Pathologic findings

A (normal) diploid DNA pattern was seen in the cells of the endometrial carcinoma: a single large peak that represented 2 N DNA content of cells in the G0/G1 phase of the cell cycle and a smaller peak that represented the double DNA content (4 N) of cells in the G2/M phase. In Fig. 1, both the DNA histograms of the tumor mass in the left fallopian tube and the cells in the ascites are shown. Both are different from the DNA histogram of the endometrial carcinoma. These latter DNA patterns are aneuploid in both cases: they show an extra peak that represents cells with DNA content of 1.4×2N.

The DNA histogram of the endometrial cancer shows two different stem lines: one at the distance of 1 and one at an additional distance at 1.4. The DNA index in the endometrial carcinoma is 1. The tumor mass of the left fallopian tube and the cells in the ascites show an abnormal DNA index. In both tumors the DNA index is 1.4.

We concluded that our patient initially had two primary tumors simultaneously: both endometrial cancer and fallopian tubal cancer. The DNA index of the malignant cells in the ascites and the fallopian tubal cancer were the same; the DNA index of the endometrial cancer mass was different. For that reason, cells in the ascites most likely originated from the primary fallopian tube carcinoma.

## Discussion

The woman of the present study originally complained of postmenopausal blood loss. In about 10–20% of women with postmenopausal blood loss, the bleeding is caused by malignancies of the reproductive tract. Endometrial cancer is involved in 12–15% of these situations [3]. It is the most common gynecologic malignancy in developed countries in women between 50 years and 70 years of age. With increasing age, it is more likely that postmenopausal bleeding is caused by endometrial cancer [15].

Endometrial cancer can be histologically classified as either low, intermediate or high grade with different histological subtypes. In this specific case, the endometrial tumor was classified as an adenosquamous carcinoma, which is a combination of high-grade adenocarcinoma components mixed with areas of squamous differentiation.

Staging of the disease is done according to the FIGO system. Endometrial cancer usually spreads along the surface of the endometrium, infiltrates myometrium to the peritoneum and parametria, and eventually spreads through the lymphatic veins or blood vessels. It may also spread via the fallopian tubes to the ovaries or peritoneal cavity [3].

Because spread of endometrial cancer is known to be a growth process *per continuitatem*, the initial remark in the pathology report of a tumor focus in the left fallopian tube

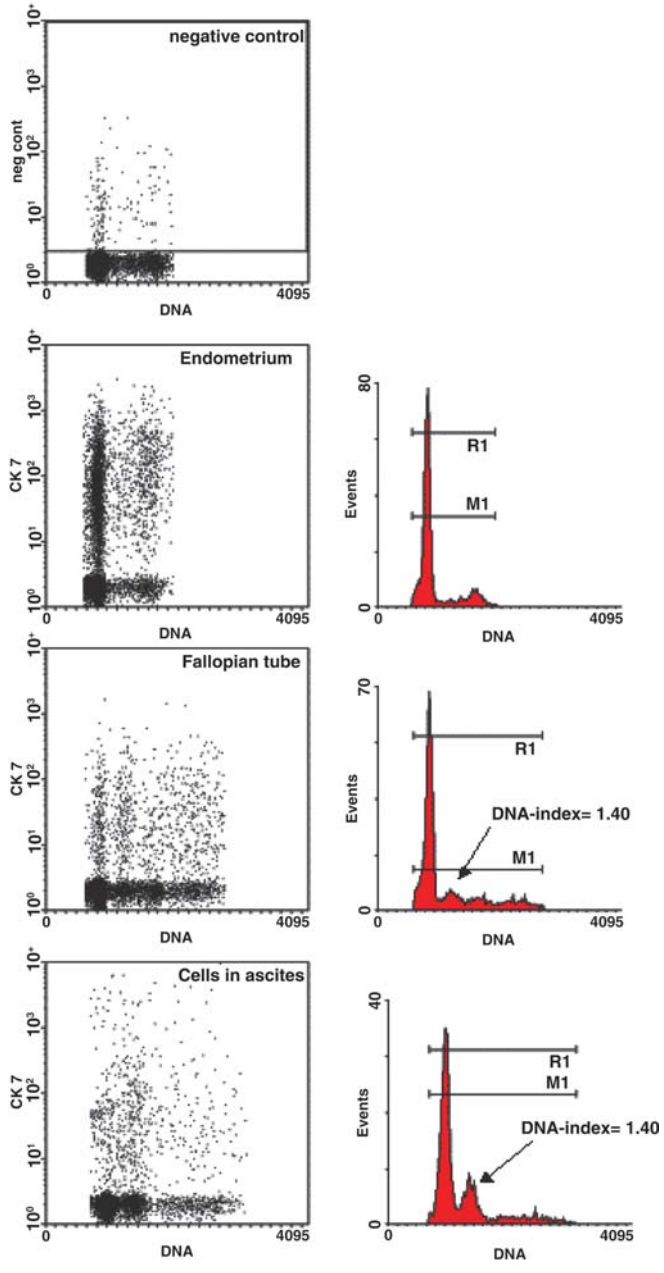



**Fig. 1** Shown in this figure are the dotplots (*left panel*) and the DNA histograms (*right panel*) of the multiparameter cytokeratin/DNA flow cytometry analyses of the endometrium, fallopian tube and cells in the ascites of the patient. In the *upper row*, the negative control corresponding to these analyses is shown. The measurements were performed exclusively in the gate of the cytokeratin-positive cells. Analysis of the endometrium showed a normal diploid DNA content. An additional high G0/G1 peak with the accompanying lower G2/M peak in the tumor cells of the fallopian tube and cells in the ascites reflect abnormal DNA content in both types of tumor cells. The DNA content from the (normal) diploid G0/G1 peak in both types of tumor cells is the same (DNA index = 1.40)

should have been reason for further investigations. The unexpected early presentation of peritoneal tumor metastasis in this patient led to further investigations of the original specimen, in comparison with the present tumor-born ascites. Histological review showed that the tumor focus in the fallopian tube was part of the surface lining and not a luminal tumor fragment. Besides, there was infiltration present of the supporting stroma. Rules for classification of fallopian tube cancer have recently been rewritten, according the FIGO Committee of Gynaecologic Oncology [6].

This observation and the way of tumor spread made a stage-I adenosqamous carcinoma of the endometrium unlikely. However, merely histologic examination did not prove the foci of tumors in the fallopian tube and the endometrium to be two different processes.

Other techniques, such as immunohistochemistry of steroid receptor in the endometrial and tubal carcinoma, were also incapable of further discrimination, which showed the same receptor expression pattern for both tumors. Both tumor locations originate from the same Mullerian epithelium, giving rise to similar phenotypic tumor cell characteristics [2, 11].

Flow cytometry can be used to analyze the DNA content of individual cells. In the past, this technique could be applied with confidence to either cells from cultures or single cells prepared from fresh tissue or frozen tissue [10]. The use of formalin-fixed material suffered from loss of cell surface antigens and unstable DNA analysis.

Recently, a technical modification was described in which the preparation of single-cell suspensions from formalin-fixed, paraffin-embedded material could be made successfully without loss of antigenicity, with high cell recovery and with DNA histograms of perfect quality [10]. Using this approach, it is also possible to selectively label epithelial cells in a subpopulation of interest [8, 10]. By this method it was possible to compare cells from both histological sections with cells from the ascites.

In the present study, the diploid DNA index of the endometrial tumor location was in sharp contrast with the aneuploid DNA index of 1.4, both in the tubal focus and in the malignant cells in the ascites. The absence of even a small aneuploid peak in the endometrial tumor is in favor of two different tumor processes. Since we could demonstrate a similar DNA content in the fallopian tubal cancer and in the malignant cells in the ascites, the latter cells are suggested to be metastases originating from the primary fallopian tube carcinoma.

Metastatic cells do not always retain the DNA profile of their primary tumor, but the majority of all metastases show the same profile as the primary tumor [17, 19]. Studies that describe a different DNA content in metastases and in the primary tumor are predominantly based on uniparameter flow cytometry. Contamination of these samples with normal cells (inflammatory cells, stromal components, etc.) may mask small DNA index abnormalities as a not observable aneuploid DNA peak. Using multiparameter flowcytometry with cytokeratin cell labeling, we specifically select tumor cells. Measurements in selected populations represent better tumor cell DNA content.

Primary fallopian tube carcinoma comprises only 0.3–1.1% of all gynecologic malignancies [1, 2, 7, 9, 18]. The differentiation between primary malignant tumors of the fallopian tube and metastatic tumor masses is often difficult because of widespread disease [5, 9, 18]. Tumor masses in the fallopian tube are generally metastatic from the ipsilateral ovary, which has been spread by direct invasion or from a contralateral ovary by transcoelomic spread [1, 7, 12, 13]. Primary adenocarcinoma of the fallopian tube with papillary features, as seen in this patient, is the most common histological type of primary tube cancer (>90%) [7, 8, 9, 11, 12, 13].

Primary tube cancer is treated like ovarian cancer: one should try to debulke completely. Adjuvant multi-chemotherapy with a cisplatinum-combined treatment should be given after surgery [2, 4, 5, 7, 9, 12, 14, 18]. The patient of the present study received 175 mg/m$^2$ taxol and 75 mg/m$^2$ cisplatinum 4 months after primary surgery. After four doses, chemotherapy was stopped because of progressive disease and 9 months after primary surgery she died; autopsy was not allowed.

Correct pre- or peri-operative diagnosis of primary tube cancer is uncommon [1, 5, 13]. Difficulties in diagnosing primary tube cancer exist due to its rarity, the complaints and clinical features are not specific [1, 12]. Because of these difficulties in diagnosing primary fallopian tubal cancer, a delay in treatment is not uncommon [12]. This new histopathologic technique, which has recently become more feasible in normal practice, enables early correct diagnoses in uncommon clinical or histopathologic manifestations of well-known primary tumors.

## References


1. Borghi L, Ballotta MR, Bianchini E et al (1994) Primary carcinoma of fallopian tube: experience of six cases. Eur J Obstet Gynecol Reprod Biol 57:161–166
2. Cabrero I, Young RH, Vamvakas EC et al (1999) Carcinoma of the fallopian tube: a clinical pathological study of 105 cases with observations on staging and prognostic factors. Gynecol Oncol 72:367–379
3. Copeland LJ (1996) Update on endometrial cancer. Clin Obstet Gynecol 39:627–728
4. Cormio G, Gabriele A, Maneo A et al (1997) Second-look laparotomy in the management of fallopian tube carcinoma. Acta Obstet Gynecol Scand 76:369–372
5. Daskalakis G, Kiosses E, Katsetos C et al (1998) Primary carcinoma of the fallopian tube. Eur J Gynaecol Oncol 19:384–385
6. FIGO Committee on Gynecologic Oncology (2000) Cancer of the Fallopian Tube. I J Gynecol Obstet 70:209–262
7. Friedrich M, Heinsen C, Schweizer J et al (1998) Primary tubal carcinoma: a retrospective analysis of four cases with a literature review. Eur J Gynaecol Oncol 19:138–143
8. Hellstrom A (1998) Primary fallopian tube cancer: a review of the literature. Med Oncol 15:6–14
9. Jeregzek B, Jessem J, Kobierska A (1996) Primary cancer of the fallopian tube, report of 26 patients. Acta Obstet Gynecol Scand 75:281–286
10. Leers MPG, Schutte B, Theunissen PHMH et al (1999) Heat pretreatment enables high resolution DNA flow cytometry of paraffin embedded tumor tissue. Cytometry 35:260–266
11. Navani SS, Cabrero I, Young RH et al (1996) Endometrioid carcinoma of the Fallopian tube: a clinicopathologic analysis of 26 cases. Gynecol Oncol 63:371–378
12. Ng P, Lawton F (1998) Fallopian tube carcinoma – a review. Ann Acad Med 27:693–697
13. Pai RR, Sahu KK, Raghuveer CV (1996) Primary carcinoma of the fallopian tube. A clinicopathologic study. Indian J Cancer 33:92–96
14. Rauthe G, Vahrson HW, Burkhardt E (1998) Primary cancer of the fallopian tube. Treatment and results of 37 cases. Eur J Gynaecol Oncol 19:356–362
15. Schaafsma HE, Ramaekers FCS (1994) Cytokeratin subtyping in normal and neoplastic epithelium: basic principles and diagnostic applications. Pathol Annu 29:21–62
16. Shankey TV, Rabinovitch PS, Bagwell B et al (1993) Guidelines for implementation of clinical DNA cytometry. Cytometry 14:472–477
17. Smit VT, Fleuren GJ, Houwelingen van JC et al (1990) Flow cytometric DNA ploidy analysis of synchronously occurring multiple malignant tumors of the female genital tract. Cancer 66:1843–1849
18. Wang PH, Yuan CC, Chao HT et al (1998) Prognosis of primary fallopian tube adenocarcinoma: report of 25 patients. Eur J Gynaecol Oncol 6:571–574
19. Zangwill BC, Balsara G, Dunton C et al (1993) Ovarian carcinoma heterogeneity as demonstrated by DNA ploidy. Cancer 71:2261–2267

Virchows Arch (2003) 442:298–301
DOI 10.1007/s00428-002-0755-1

CASE REPORT

**Daniel Azorín · José L. Rodríguez-Peralto · Elena García-García · Javier Salamanca**

# Cutaneous papillary squamous cell carcinoma. Report of three new cases and review of the literature

Received: 10 July 2002 / Accepted: 3 December 2002 / Published online: 19 February 2003
© Springer-Verlag 2003

**Abstract** Squamous cell carcinoma is one of the most common malignant cutaneous tumors. Several histological variants have been described; the papillary subtype is one of the most infrequent, with only four cases having being reported previously. We report three new cases of this unusual variant of cutaneous squamous cell carcinoma, review the literature and consider the main differential diagnoses. Polymerase chain reaction performed in our three cases did not demonstrate human papilloma virus infection.

**Keywords** Squamous cell carcinoma · Papillary · Cutaneous

## Introduction

Squamous cell carcinoma (SCC) is one of the most common malignant cutaneous tumors, frequently arising on the sun-exposed skin of elderly patients [1]. Several histological subtypes have been described, including classical, verrucous, acantholitic, spindle cell, clear cell, signet ring cell, pigmented, desmoplastic, and papillary [5]. Papillary squamous cell carcinoma (PSCC) is one of the rarest variants of cutaneous SCC. Microscopically, PSCC consists of exophytic, pedunculated masses with large papillary fronds permeated by fibrovascular cores.

Only four cases of cutaneous PSCC have previously been reported in the literature [2, 3, 4]. We report three new cases (two of them in the same patient) of this unusual variant of cutaneous SCC and review the four cases previously described.

D. Azorín · J. L. Rodríguez-Peralto (✉) · E. García-García · J. Salamanca
Department of Pathology,
Hospital Universitario 12 de Octubre,
Ctra. de Andalucía Km. 5 400, 28041 Madrid, Spain
e-mail: jrodriguezp.hdoc@salud.madrid.org
Tel.: +34-91-3908710

## Clinical history

Patient 1

A 66-year-old man, 14-year status post-kidney transplant, diagnosed of leishmaniasis in 1992, presented with a fast-growing, painful, bleeding mass on the left arm. The tumor, a 5×4-cm pedunculated lesion, was surgically removed (Fig. 1). Seven months after the first surgical excision, the patient presented with a new painful, pedunculated, 4×4-cm mass on the right leg of 4-month duration, which was surgically removed. Three months after the second surgical excision and 10 months after the first, the patient is alive and without evidence of recurrence or metastases.

Patient 2

A 78-year-old woman, with multiple classic cutaneous SCCs (Fig. 2) and actinic keratosis surgically removed 1 year before, presented with a slowly growing, 3×1.5-cm, pedunculated tumor on the right leg. The lesion was surgically removed and the patient is alive without evidence of recurrence or metastases 2 months after excision.

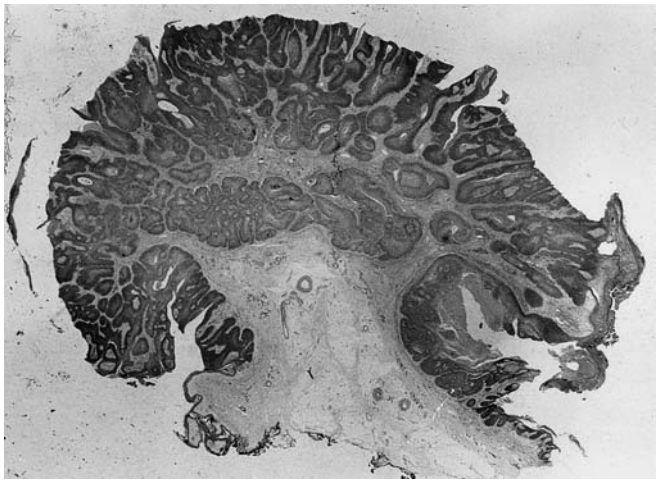


**Fig. 1** Case 1. Scanning magnification of the lesion located in the arm, which shows a pedunculated tumor with a papillary growth pattern

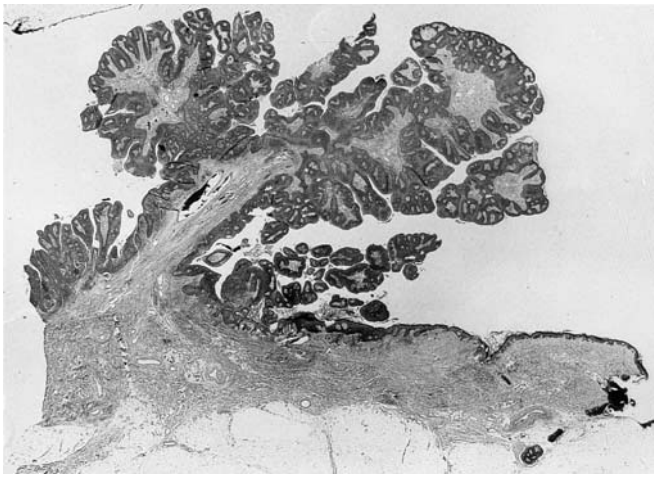


**Fig. 2** Case 2. Panoramic view showing a prominent papillary growth pattern



**Fig. 3** Detail of papillary structures formed by a squamous cell proliferation lying over a fibrovascular core

## Materials and methods

The tumors were surgically excised and routinely fixed in neutral buffered formalin prior to normal protocolized processing with hematoxylin and eosin staining. Polymerase chain reaction amplification of human papilloma virus (HPV) was done using a commercially available kit (Master Diagnostica, Granada, Spain). Appropriate controls were included.

## Results

The three tumors showed similar microscopic features. They consisted of squamous cell proliferations with an exophytic, pedunculated, papillary growth pattern. The papillary structures were formed by a keratinocytic epidermal growth lying over fibrovascular cores forming a central stalk (Fig. 3).

The tumor cells were basically of transitional type, small sized, with dark, basophilic cytoplasm, indistinct

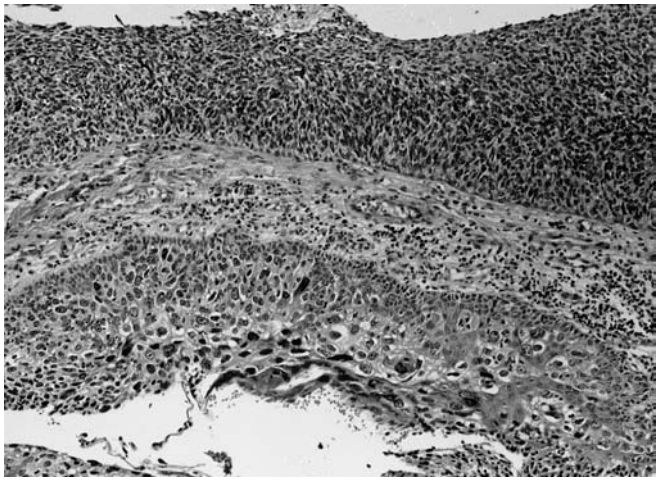


**Fig. 4** High power shows a transitional-like cell proliferation on one side of the papillary structure (*top*) and a squamous cell proliferation with abundant clear cytoplasm on the other (*bottom*). Both types of cells display nuclear atypia and mitoses

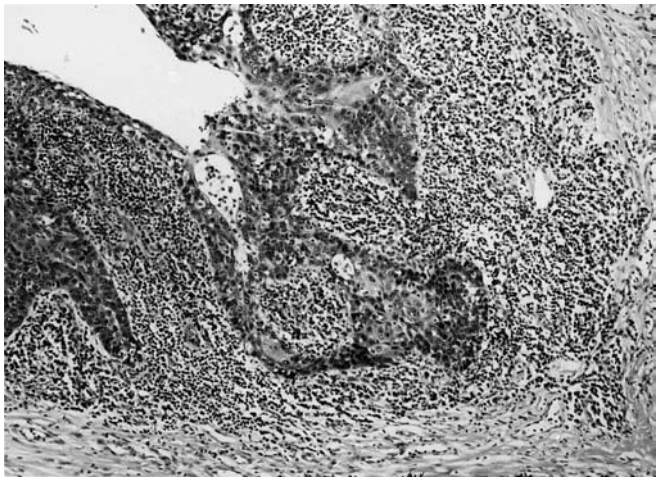


**Fig. 5** Small focus showing irregularity of the basal layer with increased inflammatory response. This is an apparent microinvasion of the fibrovascular core

membranes and scattered intercellular bridges. In some areas, usually at the periphery of the tumor, the cells had abundant clear cytoplasm with well-defined cytoplasmic membranes. Both types of cells showed marked nuclear atypia, pleomorphism with bizarre forms and high typical and atypical mitotic indices (Fig. 4). Keratin pearls, eddy bodies and tricholemmal keratinization were not found.

The dermo-epidermal interface was obscured by a moderate infiltrate of lymphocytes and plasma cells. Deep invasion was not seen, but focal involvement of the fibrovascular cores was present in one tumor (Fig. 5).

The three tumors were negative on polymerase chain reaction screening for HPV, HPV 6/11, HPV 16, HPV 18 and HPV 31/33.

**Table 1** Review of the published cases. *ANED* alive with no evidence of disease, *DNED* died with no evidence of disease

| | Sex | Age (years) | Size (cm) | Inmuno-suppression | Location | Follow-up (months) | Evolution | Dermal invasion | Clear cells | HPV |
|---|---|---|---|---|---|---|---|---|---|---|
| Landman [2] (1990) | | | | | | | | | | |
| Case 1 | Female | 105 | 2 | No | Cheek | 18 | ANED | Yes | Yes | No |
| Case 2 | Female | 87 | 2 | No | Forehead | 18 | ANED | Yes | No | No |
| Masouye [4] (1991) | Female | 85 | 7 | No | Flank | 12 | DNED | No | Yes | No |
| Martin III [3] (1994) | Male | 37 | 1.7 | Yes | Scalp | ? | ? | No | No | No |
| Present cases (2002) | | | | | | | | | | |
| Case 1 | Male | 66 | 5 | Yes | Arm | 10 | ANED | No | Yes | No |
| Case 2 | Male | 66 | 4 | Yes | Leg | 3 | ANED | Yes | Yes | No |
| Case 3 | Female | 78 | 3 | No | Leg | 2 | ANED | No | Yes | No |

## Discussion

SCC is the second most common type of skin cancer after basal cell carcinoma. This tumor typically arises on the sun-exposed skin of elderly patients, but has also been linked to immunosuppression, arsenic exposure, radiation, chronic ulceration and HPV infection [1].

Although cutaneous SCC is usually easily treated, its prognosis depends on tumor size, location, histologic differentiation, depth or perineural invasion and histologic subtype [1]. Among the several histologic subtypes of cutaneous SCC reported in the literature, the papillary variant is one of the most infrequent [5].

The papillary growth pattern is a common finding in urinary or respiratory tract transitional cell carcinomas and has also been described in adenocarcinomas of the digestive or female genital tracts. However, in the skin, pure PSCC has only been reported on four prior occasions (Table 1). Since the first two cases described by Landman et al. in 1990 [2], only two more have been published [3, 4]. Three cases occurred in women and one in a man. The women were immunocompetent while the man had had a cardiac transplant and was consequently immunosuppressed. The average age of all patients was 78.5 years, with a range of 37–105 years, and the immunosuppressed man was the youngest. Two of the reported tumors were located in sun-exposed areas. The duration of growth was less than 1 year in all cases. The sizes ranged from 1.7 cm to 7 cm, with an average of 3.2 cm. The present three tumors were masses of 5×4 cm and 4×4 cm, located in non-sun-exposed areas of a 66-year-old post-renal transplanted immunosuppressed man, and a 3×1.5-cm lesion on a sun-exposed area of a 78-year-old woman.

Microscopically, the four previously reported cases showed papillary growth composed of atypical squamous cell proliferation with abundant mitotic figures overlying fibrovascular cores. Two of these cases had a superficial clear cell component [2, 4]. Focal dermal invasion was present in the first two cases [2]. Immunohistochemical staining with anti-HPV was negative in three cases [2, 4] and there was no amplification of HPV-DNA in the fourth [3]. Our cases had a transitional-like deep component with superficial clear cell differentiation, and only one case showed focal stalk invasion. The three lesions were negative for HPV on polymerase chain reaction.

The four earlier cases were tumor free after a follow-up ranging from 12 months to 18 months. The absence of recurrence or metastases during that period suggests a non-aggressive course by cutaneous PSCC. Our two patients are alive without recurrence or metastases at 10, 3 and 2 months after surgical resection.

Differential diagnosis must be performed with cutaneous SCCs of an exophytic growth pattern, like verrucous carcinoma or verrucous Bowen disease [5, 6]. Typical PSCC presents a prominent exophytic papillary growth pattern with fibrovascular cores and many layers of markedly atypical transitional-like squamous cells with numerous mitotic figures. Verrucous carcinoma is predominantly located in mucosas and composed of downward-growing irregular strands of large squamous cells with no or very mild nuclear atypia and a strikingly bland cytology. It never presents the markedly exophytic papillary pattern characteristic of PSCC. Bowen disease is a highly atypical squamous carcinoma in situ that shows full-thickness involvement of the epidermis with preservation of the basal layer. The verrucous variant of this entity presents papillomatous projections but lacks true fibrovascular cores characteristic of PSCC. Moreover, PSCC is composed of atypical cells that may not fulfil the epidermal thickness and, as in our case, may be of transitional type.

In summary, we presented three cutaneous PSCCs, two in an immunosuppressed 66-year-old man and one in a sun-exposed area of a 78-year-old woman. We emphasized the well-defined clinico-pathological features and non-aggressive course of this neoplasm, as well as its relationship with actinic radiation or immunosuppression.

## References

1. Alam M, Ratner D (2001) Cutaneous squamous-cell carcinoma. N Engl J Med 344:975–983
2. Landman G, Taylor RM, Friedman KJ (1990) Cutaneous papillary squamous cell carcinoma. A report of two cases. J Cutan Pathol 17:105–110

3. Martin RW 3rd, Farmer ER, Rady PL, Tyring SK (1994) Cutaneous papillary squamous cell carcinoma in a inmunosuppressed host. J Cutan Pathol 21:476–477
4. Masouye I, Kapanci Y (1991) A third case of cutaneous papillary squamous cell carcinoma. J Cutan Pathol 18:142–143
5. Rinker MH, Fenske NA, Scalf LA, Glass LF (2001) Histologic variants of squamous cell carcinoma of the skin. Cancer Control 8:354–363
6. Strayer DS, Santa Cruz DJ (1980) Carcinoma in situ of the skin: a review of histopathology. J Cutan Pathol 7:244–259

Virchows Arch (2003) 442:302–303
DOI 10.1007/s00428-003-0781-7

LETTER TO THE EDITOR

**Fumio Ide · Kenji Mishima · Ichiro Saito**

# Ectomesenchymal chondromyxoid tumor of the anterior tongue with myxoglobulosislike change

Received: 25 November 2002 / Accepted: 24 January 2003 / Published online: 27 February 2003
© Springer-Verlag 2003

Sir,

Ectomesenchymal chondromyxoid tumor (ECT) of the anterior tongue is rare [5]. Since for the original largest series from the Armed Forces Institute of Pathology [7] only seven additional cases have been reported in the English-language literature [1, 4, 8, 9]. We report a unique example of ECT with focal microscopic globoid body formation, reminiscent of myxoglobulosis.

A 52-year-old woman presented with a painless reddish-brown mass of the tongue which was unchanged for over 15 years. Clinical examination showed a soft cystic polypoid submucosal tumor on the tip of the tongue. Clinical diagnosis of hemangioma was rendered. Twenty years after simple excision she is well with no evidence of tumor. The resected mass measured 3×2×1.5 cm and the cut surface was gelatinous with cystic areas of hemorrhage. Histological examination revealed a well circumscribed multilobular myxohyaline tumor within the submucosa (Fig. 1a). It was composed of netlike sheets of small round- to spindle-shaped tumor cells with scattered chondroid foci (Fig. 1b). Mucin-filled cleftlike spaces and congested vascular channels were conspicuous (Fig. 1c). Plasmacytoid tumor cells and ductal differentiation were not observed anywhere in lesion. There were no salivary gland tissues in multiple sections. Tumor cells showed intense immunoreactivity with vimentin and glial fibrillary acidic protein and were focally positive for S-100 protein and CD57. They were negative for AE1/AE3 and $\alpha$-smooth muscle actin. Interestingly, multiple mucin-pooled pseudocysts were filled with round hyalinized globules (Fig. 1d). Many of the intraluminal globules had centers which contained of viable tumor cells, but some were composed entirely of acellular amorphous mass. The cellular globules stained with mucicarmine and alcian blue and showed metachromasia by toluidine blue.

Our case was originally filed as myoepithelioma of the tongue but the diagnosis was revised to that of ECT after the publication of the report by Smith et al. [7]. In this context, we reviewed comprehensively the English literature and found two other examples [2, 6]. An unusual feature of the present ECT is the microscopic presentation of focal globoid body formation. The only similar description is the swirling formation by Smith et al. [7], suggestive of neural differentiation. The globoid bodies in our case were reminiscent in some respects of myxoglobulosis in salivary mucoceles [3]. The well known myxoglobulosis of the appendix may occur as a consequence of a unique reparative reaction of the capsule granulation tissue in response to the extravasated mucin. However, the globoid body formation is apparently unrelated to the organizing process. We prefer the idea that unlike granulation tissue-based globular organization in mucoceles, myxoglobulosislike change in ECT is a peculiar form of hyaline degeneration occurring in ischemic tumor islands.

F. Ide (✉) · K. Mishima · I. Saito
Department of Pathology,
Tsurumi University School of Dental Medicine,
2-1-3 Tsurumi, Tsurumi-ku, Yokohama 230-8501, Japan
e-mail: ide-f@tsurumi-u.ac.jp
Tel.: +81-45-5808360
Fax: +81-45-5722888

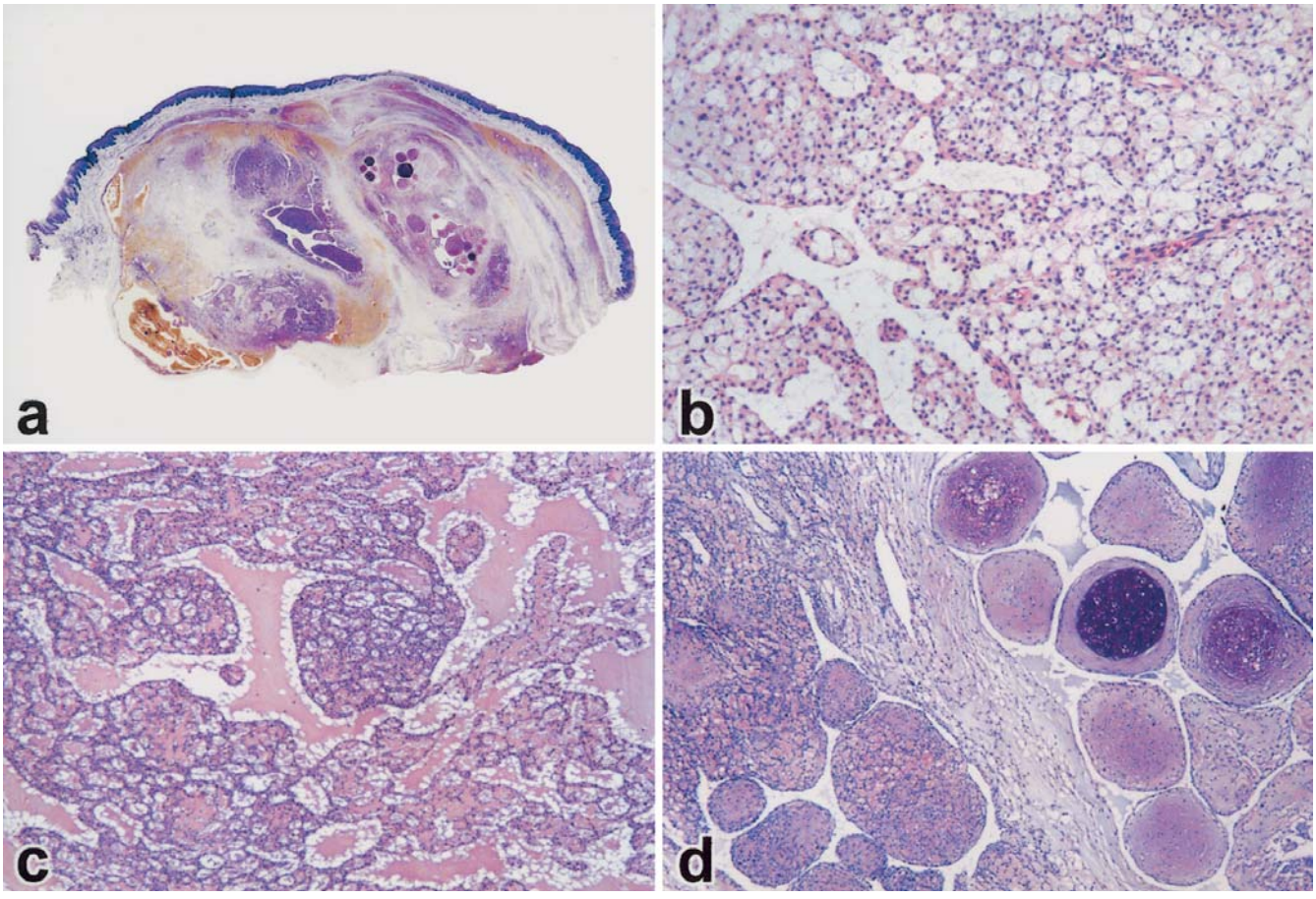



**Fig. 1** **a** Scanning magnification of a well-demarcated multilobular submucosal tumor. Focal globoid body formation is highlighted. Toluidine blue staining. **b** Characteristic netlike growth pattern. Hematoxylin and eosin. **c** Cleftlike spaces filled with mucin. Mucicarmine staining. **d** Cellular and paucicelluar globules in pseudocyst. Toluidine blue staining

## References


1. Carlos R, Aguirre JM, Pineda V (1999) Ectomesenchymal chondromyxoid tumor of the tongue. Med Oral 4:361–365
2. Casas LE de las, Hoerl HD, Oberley TD, Hafez GR, Sempf JM, Shalkham JE, Kurtycz DFI (2001) Myoepithelioma presenting as a midline cystic tongue lesion: cytology, histology, ancillary studies, and differential diagnosis. Diagn Cytopathol 24:403–407
3. Ide F, Kusama K (2002) Myxoglobulosis-like change in a lower lip mucocele. Histopathology 40:575–576
4. Kannan R, Damm DD, White DK, Marsh W, Allen CM (1996) Ectomesenchymal chondromyxoid tumor of the anterior tongue. A report of three cases. Oral Surg Oral Med Oral Pathol 82:417–422
5. Mills SE, Gaffey MJ, Frierson HF (2000) Tumors of the upper aerodigestive tract and ear, 3rd series. In: Atlas of tumor pathology, fascicle 26. Armed Forces Institute of Pathology, Washington, pp 330–332
6. Rogers TR, Johnson JV, Newland JR (1989) Pleomorphic adenoma of the anterior tongue in a 12-year-old girl. J Oral Maxillofac Surg 47:89–90
7. Smith BC, Ellis GL, Meis-Kindblom JM, Williams SB (1995) Ectomesenchymal chondromyxoid tumor of the anterior tongue. Nineteen cases of a new clinicopathologic entity. Am J Surg Pathol 19:519–530
8. Visscher JGAM de, Kibbelaar RE, van der Waal I (2003) Ectomesenchymal chondromyxoid tumor of the anterior tongue. Report of two cases. Oral Oncol 39:83–86
9. Wal JE van der, van der Waal I (1996) Ectomesenchymal chondromyxoid tumor of the anterior tongue. Report of a case. J Oral Pathol Med 25:456–458

 © Springer-Verlag 2003

# ANNOUNCEMENTS

8–9 April 2003
**National Breast Pathology Course**

This two day course for Pathologists will cover all aspects of Breast Pathology

Course Tutor: Dr. S.E. Pinder

Residential and non residential options available

*For further information please contact:*
Education Administrators
Nottingham International Breast Education Centre
City Hospital, Hucknall Road, Nottingham NG5 1PB
Tel.: 0115 969 1689; Fax: 0115 962 7707
E-mail: enquiries@nibec.co.uk; www.nibec.co.uk

9–11 May 2003
**6th International Course on Bone Marrow Biopsy Pathology**
Hanover, Germany

Under the auspices of the European Association for Hematopathology

Bone marrow histology has evolved into an integral part of modern haematological diagnostics. Moreover, it affords unique access to a biological understanding of important diseases affecting the haematopoietic system. The courses offered by the European Bone Marrow Working Group under the auspices of the European Association for Hematopathology are intended to provide high quality educational sessions in bone marrow histopathology and to bring together people who have a particular interest in this field. In addition to state-of-the-art lectures focusing on selected topics, there will be workshops where participants are invited to contribute their own interesting and instructive cases. Topics will be chronic myeloproliferative disorders, lymphoma, hypoplastic states and MDS, reactive and therapy-related changes.

Course fee: 300 €

*For further information* see
http://www.mh-hannover.de/institute/pathologie/kongress or
contact Institute of Pathology, Medizinische Hochschule Hannover
Carl-Neubergstr. 1, 30625 Hannover, Germany
E-Mail: Laenger.Florian@MH-Hannover.de
Tel.: 0049 511 532-4501; Fax: -5799

12–16 May 2003
**Diagnostic Histopathology of Breast Disease**
London, UK

May 12–16, 2003, at Hammersmith Hospital (Imperial College Faculty of Medicine), London, UK. A week-long course designed for pathologists at Consultant and Senior Trainee level. The course provides a comprehensive coverage of the Histopathology of Breast Disease, with special emphasis on areas that pose diagnostic difficulties. The participants will be given ample time to study histological preparations, followed by illustrated discussion of the cases. There will be special sessions dealing with the interpretation of core biopsies and fine needle aspirations. There will also be two daily talks dealing with specific topics, given by eminent breast pathologists and followed by discussion. The topics will include reporting breast biopsies, immunohistochemistry, receptor assessment, c-erbB-2, prognostic factors, proliferative lesions/ carcinoma in situ, problems in breast pathology, a practical approach to the diagnosis of breast lymphomas and molecular pathology. The faculty will include Ian Ellis, Christopher Elston, Andrew Hanby, Kristin Henry, Stephen Humphreys, Sunil Lakhani, Andrew Lee, Sarah Pinder, Sami Shousha, and Clive Wells.

*Further details from:*
Wolfson Conference Centre, Hammersmith Hospital
Du Cane Road, London W12 ONN, UK
(Tel (44) 20 8383 3117/3227/3245; Fax (44) 20 8383 2428
e-mail wcc@ic.ac.uk)

12–23 May 2003
**International Course on Laboratory Animal Science**
Utrecht, The Netherlands

A two-week intensive course on laboratory animal science will be organized at the Department of Laboratory Animal Science – Utrecht, The Netherlands in May 2003. This course has been offered once a year since 1993.

The objective of this course is to present basic facts and principles that are essential for the humane use and care of animals and for the quality of research.

The contents of the course are in line with recommendations of the Federation of European Laboratory Animal Science Associations (FELASA) regarding the training of the young scientist whose research involves the use of vertebrate animals.

The course may also be of interest for those who intend to set up a similar course at their own institution. For this purpose, during the course the acquisition of teaching materials can be discussed with the course committee.

*For information and application forms please contact*:
Prof. Dr. L.F.M. van Zutphen or Mr. Stephan van Meulebrouck
Department of Laboratory Animal Science
Faculty of Veterinary Medicine, P.O. Box 80.166
3508 TD Utrecht, The Netherlands
Phone: *31-30-2532033; Fax: *31-30-2537997
E-mail: pdk@las.vet.uu.nl
Internet: http://las.vet.uu.nl (click 'Education').

9–11 June 2003
**Multi-Disciplinary Courses on Breast Disease**

Three day course. The first part is multi-disciplinary. Thereafter the different specialties meet to accommodate their own special requirements.

Course Tutors: Dr. I.O. Ellis, Dr. S.E. Pinder, Dr. A.H.S. Lee

| | | |
|---|---|---|
| Course fees: | NHS | £370.00 |
| | Non-NHS | £415.00 |
| | Overseas | £550.00 |

includes refreshments but not accommodation

*For further information please contact:*
Education Administrators
Nottingham International Breast Education Centre,
City Hospital, Hucknall Road, Nottingham NG5 1PB
Tel.: 0115 969 1689; Fax: 0115 962 7707
E-mail: enquiries@nibec.co.uk; www.nibec.co.uk

6 September 2003
**EUROPEAN BOARD OF PATHOLOGY**
**7th EXAMINATION 2003**
Ljubljana, Slovenia

The Seventh Examination of the European Board of Pathology will be held in Ljubljana, Slovenia, Saturday September 6, 2003. This Examination precedes the 19th Congress of the ESP.

*For information about the examination and application forms can be obtained from:*
Prod. Dr. J.G. van den Tweel
(chairman of The Examination Board)
Utrecht University Medical Center
Department of Pathology, H 04.312
P.O. Box 85500
3508 GA Utrecht
Fax: ++31-30-2544990
Tel.: ++31-30-2506565
e-mail: j.vandentweel@lab.azu.nl *or*
W.vanBragt@lab.azu.nl (secretary)
The same information is also available from Internet:
http:www.uems.be/pathol.htm, see index 2 and 3

6–11 September 2003
**19th European Congress of Pathology**

Ljubljana, Slovenia

The largest congress of pathologists in Europe in 2003, covering basic diagnostic standards, update scientific achievements and recent technical advances in all areas of pathology at 4 keynote lectures, 30 symposia, 21 short courses, 21 slide seminars, 14 special presentations, 2 round table discussions and free paper and poster sessions. Internationally recognized invited speakers are from throughout Europe and the USA.

**March 31, 2003 is the deadline for abstracts.**

*Updated information on the congress website:* http://www.cd-cc.si

13 October 2003
**Continuing Medical Education**

One day Multi-Disciplinary Update courses

Course fee: £95.00

*For further information please contact:*
Education Administrators
Nottingham International Breast Education Centre
City Hospital, Hucknall Road, Nottingham NG5 1PB
Tel.: 0115 969 1689; Fax: 0115 962 7707
E-mail: enquiries@nibec.co.uk; www.nibec.co.uk

17–19 November 2003
**Multi-Disciplinary Courses on Breast Disease**

Three day course. The first part is multi-disciplinary. Thereafter the different specialties meet to accommodate their own special requirements.

Course Tutors: Dr. I.O. Ellis, Dr. S.E. Pinder, Dr. A.H.S. Lee

| | | |
|---|---|---|
| Course fees: | NHS | £370.00 |
| | Non-NHS | £415.00 |
| | Overseas | £550.00 |

includes refreshments but not accommodation

*For further information please contact:*
Education Administrators
Nottingham International Breast Education Centre,
City Hospital, Hucknall Road, Nottingham NG5 1PB
Tel.: 0115 969 1689; Fax: 0115 962 7707
Email: enquiries@nibec.co.uk; www.nibec.co.uk

Virchows Arch (2003) 442:307–308 © Springer-Verlag 2003

SOCIETY NEWS

# Invitation to the 19th European Congress of Pathology

On behalf of the European Society of Pathology (ESP) and the Organising Committee, we take great pleasure in inviting you to the 19th European Congress of Pathology, which will be held in Ljubljana, Slovenia, 6–11 September 2003.

Slovenia is not a large country, but at the hub of routes of trade and movement from east to west and north to south, it has always played a larger part in European events than its size would suggest. Slovenia is now an independent Central European state, on the sunny side of the Alps, bordering Italy, Austria, Hungary and Croatia. The landscape embraces rolling countryside leading to the Pannonian plain to the east, rugged Karst bordering the Adriatic Sea to the southwest, and the Alps to the north and west. The Slovenian nation of only two million today has survived mainly due to its culture, language and vitality. A bone flute, 30,000 years older than any other known in the world, and Europe's oldest bone needle, testify to the roots of culture here.

Its capital, Ljubljana, has a picturesque unity, composed of an architectural heritage spanning Roman Emona, through Renaissance and Baroque Ljubljana, to Secession Art Nouveau and Modern Ljubljana, so strongly marked by the influence of the world famous Slovenian architect, Jo e Plečnik. Ljubljana is an university city. The roots of the University go back to the seventeenth century with Academia Operosorum, the fourth Academy of Sciences in Europe. A Philharmonic Society dates back three centuries.

Ljubljana's congress tradition began in 1821, when the three emperors of the Holy Alliance met here to discuss the post-Napoleonic fate of Europe. These traditions have been brought together in the new Cultural and Congress Centre Cankarjev dom, with a capacity of 3,600, located in the heart of Ljubljana. Cankarjev dom is well equipped with all modern technical facilities and has an experienced in-house team to ensure the necessary high standards for scientific sessions and exhibitions. All Congress venues, and most hotels, are within walking distance of the centre of the city. Particular attention will be paid to stimulating the participation of trainees and young pathologists by securing as low a registration fee as possible, and inexpensive accommodations.

The European Society of Pathology has been succeeding in establishing its ever more continuous activity and influence. The old idea of a common programme of continuous education of pathologists has been realised through a number of courses organised each year by the European School of Pathology, at its headquarters in Turin and other centres throughout Europe. An increasing number of Working Groups within the European Society of Pathology, devoted to various fields, promote a continuous exchange of professional experiences and other information, the establishment of common diagnostic standards and collaboration on common research projects.

The biannual ESP Congresses retain a major role in fulfilling the main aims of the ESP in pathology education, exchange of the most recent research achievements and, particularly, in keeping together all branches of pathology, that otherwise tend to split according to organ systems, disease processes and the increasing number of techniques. The Congresses also keep together pathologists from the whole of Europe, irrespective of geographical and political borders.

We believe that the 19th European Congress of Pathology will continue the traditional approaches of previous Congresses and will serve to increase both links with European national and international pathology societies and intercontinental links, particularly with the International Academy of Pathology. The framework of the Congress Scientific Programme has been created with the strong impact and assistance of the ESP Working Groups, the ESP Executive/Scientific Committee and the Advisory Council as well as companion Societies. The programme covers all areas of pathology, provides information ranging from current diagnostic standards to recent advances in science and modern techniques, particularly those of molecular genetics, and includes a number of "hot" topics of today and tomorrow, which will be

presented by the best, internationally recognised experts at Keynote Lectures, Symposia, Special Presentations, Round Table Discussions, Short Courses and Slide Seminars. One evening is devoted to ESP Working Group Meetings, both business and scientific. Interesting Satellite Symposia will be organised by supporting companies, two by the main sponsor of the Congress Main Sponsor, Ventana Medical Systems S.A.

Furthermore, all practising pathologists and scientists are kindly invited to present their scientific achievements and exchange their professional experiences through Free Paper and Poster Sessions. The best Free Papers will be acknowledged by giving the authors the opportunity to present their achievements at the plenary session, at which the authors of the three best Poster Presentations will additionally receive special Awards.

All who are coming to Ljubljana are kindly invited to join us at two one-day Pre-Congress Meetings, prior to the Congress Opening Ceremony on Saturday: one on Pulmonary Pathology and the other devoted to non-neoplastic Nephropathology. There will also be a three-day Joint Meeting of the European and North American Society of Head and Neck Pathology. All Pre-Congress Meetings and a whole day Examination by the European Board of Pathology will be organised by using the facilities of the new building of the Faculty of Medicine, University of Ljubljana.

Culture kept the Slovenian national identity alive over the centuries and it still plays an important role in people's lives. The Congress will also highlight the traditional close connection between medicine and art. Some novel events are planned: an exhibition of the work of pathologists/painters and, especially, a Gala Concert on Monday evening in the main Gallus Concert Hall of the Congress Centre in Ljubljana, by pathologists/musicians from all over the world. A social programme is offered which reflects the warmth and hospitality of the Slovenian people.

The Second Millennium we have entered provides major challenges for all biomedical sciences, and the 19th European Congress of Pathology is a challenge for the Organisers. We sincerely hope that attendance at the Ljubljana Congress in 2003 will be a fruitful, enjoyable and memorable experience in every respect for all participants, and will give new impetus to our medical speciality in Slovenia.

We look forward to seeing you in September 2003 in Ljubljana.



Gianni Bussolati
President
European Society
of Pathology



Du an Ferluga
President
19th European Congress
of Pathology

Virchows Arch (2003) 442:309–316
DOI 10.1007/s00428-002-0748-0

REVIEW ARTICLE

**Burkhard Helpap · Bernd J. Schmitz-Dräger · Peter W. Hamilton · Giovanni Muzzonigro · Andrea B. Galosi · Karl H. Kurth · David Lubaroff · David J. Waters · Michael J. Droller**

# Molecular pathology of non-invasive urothelial carcinomas (part I)

Received: 2 November 2002 / Accepted: 26 November 2002 / Published online: 11 February 2003
© Springer-Verlag 2003

**Abstract** An international consultation on the diagnosis of non-invasive urothelial neoplasms was held in Ancona, Italy in May 2001. Besides histology and problems of classification, one group of experts (Committee no. 3) discussed the molecular pathology and cytometry of non-invasive urothelial carcinomas. In the following first part, special immunohistochemical and molecular markers for stratifications in bladder cancer were discussed including different cytokeratins (clone 34$\beta$E12, CK 20), cell proliferation markers (Ki67/MIB-1, PCNA, AgNOR, DNA-cytometry), tumor suppressor genes and oncogenes (p53, p21, erb-B2, bcl-2), different receptor expressions of epidermal growth factor and vascular endothelial growth factor and others. These molecular markers were analyzed in diagnosis of urothelial carcinomas, recurrences, progression and response to treatment.

**Keywords** Papillary bladder cancer · Non-invasive · Cell proliferation · Cytokeratins · Tumor suppressor genes

Authors were part of Committee no. 3, International Consultation on the Diagnosis of Non-Invasive Urothelial Neoplasms, Ancona, Italy, 11-12 May 2001

B. Helpap (✉)
Institute of Pathology, Hegau-Klinikum, 78207 Singen, Germany
e-mail: pathologie@hegau-klinikum.de
Tel.: +49-773-1892100
Fax: +49-773-1892105

B. J. Schmitz-Dräger
Department of Urology, Euromed Clinic, 90763 Fürth, Germany

P. W. Hamilton
Department of Pathology, Centre for Health Care Informatics, Belfast, N. Ireland

G. Muzzonigro · A. B. Galosi
Institute of Urology,
Azienda Ospedaliera Umberto 1 - University of Ancona, Ancona, Italy

K. H. Kurth
Department of Urology, University of Amsterdam, Amsterdam, The Netherlands

D. Lubaroff
Department of Urology, University of Iowa, Iowa City, Iowa, USA

D. J. Waters
Gerald P Murphy Cancer Foundation, Seattle, WA, USA

M. J. Droller
Department of Urology, Mount Sinai Medical Center,
1 Gustave L. Levy Place, Box 1272, New York, NY, 10029, USA

## Introduction

The traditional designation of bladder cancer as either "non-invasive" or "invasive" was based on whether or not the lamina propria was involved. The lack of involvement was taken to imply a relatively benign situation, while muscle invasion was considered a potentially life-threatening situation. Several clinical observations called this somewhat simplistic separation of tumor types into question and suggested that "papillary" bladder cancer actually comprised a variety of different types of bladder cancer whose intrinsic biological potential represented fundamentally distinct pathways of development. (The same was suggested to characterize muscle-invasive cancer, but validation of this concept remains preliminary.)

Approximately 70-75% of bladder cancers are "papillary" at their initial clinical presentation. Of these, 70-75% are mucosally confined (stage Ta) and 30% are invasive of the lamina propria (stage T1). Only 2-4% of the mucosally confined tumors (which are generally of high grade) are likely to progress. In contrast, 30-50% of stage T1 tumors have this potential. However, aggressive behavior is generally restricted to those tumors that are high grade, that have penetrated the lamina propria extensively, and that are accompanied by flat carcinoma in situ either adjacent to the tumor or at distant sites. The majority of bladder cancers (nearly all of those that are mucosally confined and 50-70% of those that have infiltrated the lamina propria) will not progress [16]. On the other hand, 70-75% of all "papillary" tumors are likely to recur.

Tumor recurrence is one of the most frequent events encountered in the treatment of non-invasive bladder cancer. This is either because of a "field effect" that characterizes carcinogenesis of the general urothelium, or as a result of implantation of tumor cells that may occur either naturally during tumor growth or because of the shedding of cells during transurethral resection.

Specific risk factors associated with tumor recurrence include tumor grade (which likely reflects the more extensive involvement of the urothelium in higher grade disease), multifocality (which may reflect either inadequate resection or field effect and a greater risk as well for tumor cell implantation following resection), and the status of the urothelium surrounding the tumor which is a component of the field-effect phenomenon with endoscopically invisible cancer remaining in the bladder following initial therapy.

Over the past decade, studies on molecular and genetic aspects of urothelial cancer described chromosomal defects that coincided with the pathways of tumor development suggested by these disparate lesions. However, the nature of these correlations was only broadly defined and their precision and detail was felt to require additional study and validation. This has prompted ongoing investigations designed to examine variables that might be used to predict the potential behavior of a given diathesis and to explore histologically and cytologically based modalities of identifying and characterizing the various types of urothelial cancers and their distinct biological potentials.

In May 2001, an international meeting in Ancona/Italy was held about international consultation on the diagnosis of noninvasive urothelial neoplasms. In four committees the following topics were discussed: histological morphology of urothelial papillary neoplasms and preneoplastic nonpapillary lesions in committee 1 and 2, and in committee 4 detection methods other than morphology, molecular pathology and cytometry.

The objectives of the committee no3 are to review the histology, morphometry, and molecular alterations in Ta relative to T1 bladder cancer and to assess the value of various tissue and cellular markers in stratifying patients for likely recurrence, progression, and response to treatment. Large conclusive studies on the utility of tissue or cellular markers in distinguishing between Ta and T1 cancers over and above that information offered by conventional histology in staging and grading these tumors are presently lacking. Efforts have been made to distinguish tumors of low malignant potential from those of high malignant potential [18]. However, within each broad category, a heterogeneity in intrinsic biological potential persists. This report therefore focuses on tissue factors that may provide predictive information that is additive to conventional pathology and discusses cellular factors that may aid in identifying patients at high risk for cancer progression. Specific adjuncts to standard histological and cytological techniques together with specific procedures in identifying and characterizing various markers in tissue and cytological preparations that will be reviewed include quantitative histology and quantitative cytology, flow cytometry, and immunocytology.

## Immunohistochemical and molecular markers for stratifications in papillary bladder cancer

Immunohistochemical and molecular markers might be used as an adjunct to histology to predict: (1) tumor recurrence, (2) biological behavior of Ta and T1 bladder cancers, and (3) tumor progression; and to monitor treatment response during follow-up. Application of tissue and cellular markers in approaching these is outlined in Table 1 and Table 2.

Several markers that characterize the histology and cellular appearance of a tumor have been considered to provide important information that may be predictive of disease recurrence. These include Ki67 or in its tissue form as MIB-1, cytokeratins, CK20, 34 beta E12, mutations in chromosome 9p21, and mutations of FGF3. In addition, epidermal growth factor (EGF) receptor and vascular endothelial growth factor (VEGF) receptor expression in the surrounding tissue have been suggested to predict the likelihood of tumor recurrence [15, 16, 17, 18, 22, 24, 32, 33, 52] (Table 2).

Similarly, a number of substances have been proposed as markers to provide information that may be predictive of disease progression. Some of these have been proposed as independent markers, while others have been suggested

**Table 1** Immunohistochemical and cell kinetic analyses of flat and papillary urothelial lesions of the urinary bladder [16]

| Diagnosis | Palisading (yes/no) | Cytokeratin 34$\beta$E12 expression pattern basal/diffuse | Mib 1 labeling index, low/high, expression basal/diffuse |
|---|---|---|---|
| Normal | Yes | Basal | Low, basal |
| Hyperplastic lesions | Yes | Basal | Low, basal |
| Reactive atypia | Yes | Basal | Low, basal |
| Dysplasia mild | Yes | Basal | Low/ moderate, basal |
| Papilloma | Yes | Basal | Low, basal |
| Low malignant potential | Yes | Basal | Low, basal |
| Papillary carcinoma noninvasive | Yes | Basal | Low, basal |
| Minimal invasive (pT1a) | Yes | Basal | Low, basal |
| Invasive (pT1b, c) | No | Diffuse | Moderate, diffuse |
| >pT2 | No | Diffuse | Moderate/high |
| Diffuse carcinoma in situ | No | Diffuse | High diffuse |

**Table 2** Prognostic factors of urothelial carcinomas of the urinary bladder [16]

| Grading<br>Staging | Low-grade | | | High-grade | | |
|---|---|---|---|---|---|---|
| | GIa. b<br>pTa | →<br>→ | GIIa<br>pT1 | GIIb<br>pT1 | GIII<br>pT1 | Cais<br>pTis |
| Nucleoli location | Singular/central | | | Singular→multiple<br>Prominent eccentric | | |
| Frequency of nuclei with nucleoli | 1 | – | 3 | 40 | – | 70 |
| AgNOR frequency/nucleus | 5 | – | 7 | 10 | – | 15 |
| PCNA | 5 | – | 20% | 30 | – | 60% |
| Ki67/Mib1 (basal) | 4 | – | 6% | – | | |
| Ki67/Mib1 (diffus) | 10 | – | 12% | 20 | 40% | 78% |
| DNA cytometry | Euploid–tetraploid | | | Aneuploid | | |
| p53 | 10 | – | 30% | 50–70% | | 80% |
| p21 | | | ≤40% | | ≤90% | |
| erb B2 | 45 | – | 55% | 55 | – | 80% |
| bcl2 | 15 | – | 25% | 25 | 60% | 90% |
| EGF receptor | + | | + | + | + | + |
| CEA | + membrane bound | | | + | + | + diffuse |
| Blood group | ± | | + | – | – | – |
| Antigen ABH cytokeratin 34ßE12 | Basal | | | Diffuse | | |
| Cytokeratin 20 | Superficial | | | Diffuse | | |
| Recurrences | | | + | + | + | + |

**Table 3** Candidate tissue markers for stratification of the prognosis of papillary bladder cancer

| | |
|---|---|
| Disease recurrence | |
| – | Tissue markers in tumor<br>(e.g. p53, Ki67/MIB-1, CK20, 34ßE12, Chr. 9p21,FGF3 mutation) |
| – | Tissue markers in surrounding tissue<br>(e.g. EGF-R, VEGF) |
| Disease progression | |
| – | Tissue markers in tumor<br>(e.g. p53, Rb, p21, cadherins, MMPs, TIMPs, Cathepsins, bcl-2, bax, CK 22, 34ßE12, FGF3 mutation) |
| – | Tissue markers in surrounding tissue<br>(e.g. EGF-R, VEGF) |
| Response to treatment | |
| – | Tissue markers in tumor<br>(e.g. p53, Rb, p21, MDR) |
| – | Tissue markers in surrounding tissue |

to add to information provided by the histology of the presenting lesion. These include p53, RB, p21, cadherins, MMPs, TIMPs, cathepsins, bcl-2, bax, cytokeratin 22, 34 beta E12, and FGF3 mutation (Table 2, Table 3).

Of possible equal importance are those markers that have been proposed to provide information that may be predictive of response to treatment. These have included p53, RB, p21, and MDR. The ability of a marker to predict tumor response accurately may be dependent in part on the treatment itself. For this reason, it may be important to evaluate tumor marker data from patients that have been treated with a number of different agents (Table 2).

In considering the vast literature in this area, it is important to realize that the results of tissue marker studies may be highly dependent on the manner in which tissue is collected and processed. Given the variability in results and the often varying conditions by which tissue is collected, processed, and the various assays performed, it seems clear that strict standardization of methodology will be needed to improve our ability to make meaningful comparisons between different studies and to conduct multi-institutional studies that ultimately provide interpretable data and that can validate the usefulness of a particular marker.

As an adjunct to this, the technique of laser capture microdissection may provide a method to collect a tissue sample that is of precise interest for purposes of characterizing the role of a particular marker in prognosis. The expression of a marker at both the message and the protein level may be advisable in many of these studies. In addition, in situ techniques such as immunohistochemistry and in situ hybridization may have the distinct advantage of affording precise localization of markers to particular cell types and/or to extracellular regions.

Analytic and quantitative methods, including flow cytometry and image analysis, may provide objective assessments of bladder cancer using both histological sections and specimens used for cytological analysis. Through the quantitative assessment of nuclear size,

**Table 4** The value of proliferation marker Ki-67/MIB-1 in predicting tumor recurrence in papillary bladder cancer

| Author (year), reference | No. of patients | Results | | Remarks |
|---|---|---|---|---|
| | | Univariate | Multivariate | |
| Pfister (1999) [36] | 244 | | n.s. | Versus "clinico-pathological index"* |
| Liukkonen (1999) [29] | 207 | n.s. | n.s. | |
| Wu (2000) [53] | 93 | 0.05 | 0.016 | |
| Gontero (2000) [11] | 214 | 0.048 | 0.029 | |
| Rodriguez-Alonso (2002) [37] | 210 | | 0.05 | Including 35 T2a tumors |

n.s., not significant
* Included: grades G2–3, T1, multifocality, >3 cm

nuclear shape, nuclear roundness, nucleolar number, nucleolar size, and nucleolar shape, AgNOR staining, quantification of nuclear DNA content, and assessment of nuclear chromatin texture, predictive information may conceivably be obtained [19] (Table 2).

Large conclusive studies on the association between putative tissue and cellular markers and outcomes both in terms of the intrinsic biology and natural history of the various forms of papillary bladder cancer and the efficacy of various treatments are lacking. Although much information is available and much work has been done, the validation of the usefulness of a particular substance proposed as a marker requires further study for clinical validation.

Current evidence suggests that Ki67 or tissue MIB-1 may be the strongest candidate for a marker to predict recurrence, while p53 expression may be the strongest candidate to predict cancer progression [16]. It will be imperative to standardize tissue handling and laboratory assays with further studies and to determine whether the use of markers is likely to be effective not only in a predictive but also in a cost-effective sense. The practical utility of markers will therefore rest upon whether they provide information that is additive to conventional pathology and clinical staging.

The following are descriptions of the current status of immunohistochemical, molecular, and genetic markers, cytometry and morphometry, and the use of analytical and quantitative techniques in dealing with the objectives of predicting recurrence, prognosis, and response to treatment. Although highly technical in nature, they provide a basis for further study and for the placement of other clinical and laboratory observations in the context of what may be needed to further refine our ability to characterize and understand the intrinsic biological potential of the various forms of bladder cancer.

## Disease recurrence

A variety of different markers have been correlated with tumor recurrence in papillary bladder cancer (Table 2, Table 3). Most detailed data are available for the p53 tumor suppressor gene and the proliferation marker Ki-67/ MIB-1.

Several trials have addressed the impact of immunohistochemical p53 accumulation in predicting tumor recurrence in patients with papillary bladder cancer. While in some of the mostly smaller trials, univariate analysis showed a correlation between p53 accumulation and tumor recurrence; none of the studies reported p53 accumulation to provide additive information if compared with clinical parameters [9, 11, 29, 36, 37, 46, 48, 53].

Proliferation marker Ki-67/MIB-1 has also been studied in a number of trials (Table 4). In 3 of 5 major investigations, an independent prognostic value was reported for Ki-67/MIB-1. In the negative findings by Pfister et al. [36], Ki-67/MIB-1 staining was compared with a clinico-pathological score combining a variety of parameters known to be correlated with tumor recurrence (grade G2-3 tumors, stage T1, multifocality, tumor size >3 cm). Even when this procedure is adequate, the investigation of any marker is only reasonable after exploiting all other available information. Nevertheless, there is substantial evidence that a large number of Ki-67/MIB-1-positive tumor cells can be correlated with tumor recurrence [13].

Implication of the loss of expression of cytokeratin (CK) 20 are highly controversial. While Alsheikh et al. [1] did not see a significant correlation with tumor recurrence, Harnden et al. [14] found a decreased CK20 expression to be an independent ($p<0.0001$) predictor of tumor recurrence in papillary disease. In this connection it is very important if the study with CK20 is based on low- or high-grade tumors. The expression pattern of CK20 in low-grade urothelial carcinoma is low in contrast to high values in high-grade tumors [16] (Table 2, Table 3).

Shariat et al. [44] studied the role of E-cadherin on the clinical outcome in 53 patients with carcinoma in situ. Decreased E-cadherin expression was independently associated with disease recurrence ($p=0.019$). Recent investigations suggested a potential role for cyclin D1 expression [30]and low p27Kip1 protein expression [43], with both factors providing independent prognostic information concerning tumor recurrence in papillary bladder tumors [23]. Lipponen and Eskelinen [27, 26] observed a short recurrence-free interval in Ta/T1 bladder cancer patients with decreased E-cadherin expression even in multivariate analysis. More recently, a mutation in the FGF3 gene has been demonstrated to be signifi-

**Table 5** The value of immunohistochemical p53 accumulation in predicting tumor progression in papillary bladder cancer. *n.r.* not reported

| Author (year), reference | No. of patients | mAb | Results | | Remarks |
|---|---|---|---|---|---|
| | | | Univariate | Multivariate | |
| Sarkis (1993) [38] | 43 | 1801 | 0.003 | 0.002 | T1 |
| Thomas (1994) [47] | 25 | CM1-Serum | 0.007 | n.s. | T1 |
| Gardiner (1994) [10] | 28 | CM1, 1801, DO-7 | n.s. | n.s. | T1 |
| Sarkis (1994) [39] | 33 | 1801 | 0.002 | 0.004 | TIS |
| Vatne (1995) [51] | 73 | 1801 | n.s. | n.s. | T1 |
| Serth (1995) [42] | 69 | 1801 | 0.001 | 0.0029 | T1 |
| Tetu (1996) [46] | 265 | Anti-serum | n.s. | n.s. | |
| Burkhard (1997) [2] | 46 | DO-7 | n.r. | n.s. | |
| Casetta (1997) [4] | 59 | DO-7 | 0.02 | 0.009 | TaG1 |
| Schmitz-Dräger (1997) [40] | 61 | DO-1 | 0.0022 | 0.0135 | |
| Grossman (1998) [12] | 45 | DO-1 | 0.04–0.005**/§ | n.r. | T1 |
| Hermann (1998) [20] | 143 | 1801 | 0.05 | 0.05 | T1 |
| Malmström (1999) [31] | 261 | DO-7 | n.r. | 0.0005 | Prospective randomized trial, BCG, MMC |
| Liukkonen (1999) [29] | 207 | CM-1 | 0.002 | n.s. | |
| Leissner (2001) [25] | 70 | 1801 | n.s. | n.s. | Ta G2 only |
| Rodriguez-Alonso (2002) [37] | 210 | DO-7 | n.r. | 0.05 | T1, T2a |

n.s., not significant
** Different statistical tests
§ Combination with RB

cantly correlated with tumor recurrence but not with disease progression in papillary bladder cancer (Table 3).

For loss of heterozygosity (LOH) specifically on chromosomes 9, 11 and 17, some groups have reported a significant correlation with tumor recurrence [7, 34, 49]. For most trials, however, patient numbers are small, and multivariate analysis is lacking. Orlow et al. [34] showed that homozygous deletion of that INK4A gene (chr. 9p) correlated with a lower recurrence-free survival ($p$=0.040). Furthermore, those deletions affecting both proteins encoded by the INK4A gene, p16 and p19(ARF), and thus deregulating both the pRb and p53 pathways, were clearly correlated with clinicopathological parameters of an unfavorable prognosis.

The impact of several other factors, e.g., epithelial growth factor receptor (EGFr) expression [29], apoptotic marker Bcl-2 [53], HER/2neu [47] and MDM 2 or p21 expression [36, 40], has been addressed in larger trials but has not displayed a significant correlation with tumor recurrence.

## Disease progression

The predictive value of alterations of the p53 tumor suppressor gene in bladder cancer [38] as a marker of disease progression in papillary bladder cancer has been the subject of many studies (Table 5). Information from multivariate analysis is available in 16 such studies. In 8 of them an additive prognostic value compared with clinical markers of tumor progression was observed, in the other 8 studies no significant difference was reported. Although the sample size in the positive trials tended to be slightly larger than in the negative studies, the actual question remains open. Technical differences might underlie these discrepancies. While four of seven trials using monoclonal antibody (mAb) 1801 and three of five studies using mAb DO-7 had a positive result, no trial using the CM-1 antiserum showed a positive finding [41].

In contrast to multiple trials addressing the question of tumor recurrence, proliferation marker Ki-67/MIB-1 has not been extensively studied with regard to tumor progression in papillary tumors. Two larger trials report different results on the additive prognostic relevance of this marker [29, 37]. The situation is similar for the loss of E-cadherin expression with one trial on 53 patients with Tis reporting a significant correlation with tumor progression [44], while in another study this difference was not confirmed [26].

p21(waf1/cip1) protein is a cyclin-dependent kinase inhibitor able to arrest the cell at the G1 phase by inhibiting DNA replication through interaction with the proliferating cell nuclear antigen (PCNA). Decreased expression has been correlated with unfavorable prognosis specifically in invasive tumors [5]. For papillary bladder cancer none of the four larger trials identified the p21WAF1/CIP1 protein expression as an independent prognostic parameter of tumor progression [5, 25, 28, 30, 45].

In contrast to numerous reports on invasive bladder cancer [6], the role of Rb tumor suppressor protein inactivation in papillary tumors has rarely been addressed. Grossman et al. [12] studied p53 accumulation along with Rb expression in 45 patients with T1 bladder cancer. Patients with abnormal expression of either or both proteins had a significant increase in tumor progression ($p \leq 0.04$ and $p$=0.005, respectively).

Matrix metalloproteinases (MMPs) and the tissue inhibitors of metalloproteinases (TIMPs) have been associated with high-grade lesions, tumor invasion and metastasis in many human cancers. Several studies on the impact of different MMPs and TIMPs in invasive bladder tumors and on the diagnostic use of these markers in bladder cancer have been reported, but there are no conclusive trials (Table 3).

## Response to treatment

The issue of the use of molecular markers to predict response to treatment in superficial bladder cancer has not yet been systematically addressed. Although P53 protein accumulation might be considered, reports from six trials have been negative concerning an independent prognostic value for tumor recurrence [3, 21, 31, 35, 50, 54]. Study size has been small in most trials and different therapeutic regimens have been employed in the larger ones.

Flam et al. [8] investigated the relevance of an immunohistochemical loss of CK 18 expression on tumor recurrence and tumor progression in superficial tumors but failed to show any significance. Zlotta et al. [54] found alterations of Ki-67 and p21WAF1/CIP1 expression to be correlated with tumor recurrence after BCG therapy. However, none of these markers provided additive prognostic information as compared with established clinical markers.

## Conclusion

Although several of the new molecular markers appear highly promising, divergent results of different trials suggest that none of them is yet ready to be included in the clinical management of patients with papillary bladder cancer.

The problems remain study size, endpoints, populations, retrospective designs, antigen retrieval (microwave), antibodies used, statistical problems (multifactorial analysis), means of assessment (reproducibility, scoring system), and differences between genetic alteration and immunohistochemical findings (proteomics).

What seems needed is standardization of marker research (e.g., variability index), arrays, metaanalysis/combined analysis, network trials, as well as evaluation of other factors beyond the biology of the tumor that may play a role, such as treatment, surgeon, the surrounding phenotypically normal tissue, and host factors (e.g., acetylation, GST, Cyt p450, smoking, Th1 cytokine secretion). Perhaps some of these issues will be discussed in the next WHO classification of tumors of the urothelial system.

## References


1. Alsheikh A, Mohamedali Z, Jones E, Masterson J, Gilks CB (2001) Comparison of the WHO/ISUP classification and cytokeratin 20 expression in predicting the behavior of low-grade papillary urothelial tumors. World Health Organization/International Society of Urologic Pathology. Mod Pathol 14:267-272
2. Burkhard FC, Markwalder R, Thalmann GN, Studer UE (1997) Immunohistochemical determination of p53 overexpression-an easy and readily available method to identify progression in superficial bladder cancer? Urol Res 25[Suppl]:31-35
3. Caliskan M, Türkeri LN, Mansuroglu B, Toktas G, Aksoy B, Ünlüer E, Akdas A (1997) Nuclear accumulation of mutant p53 protein: a possible predictor of failure of intravesical therapy in bladder cancer. Br J Urol 79:373-377
4. Casetta G, Gontero P, Russo R, Pacchioni D, Tizzani A (1997) P53 expression compared with other prognostic factors in OMS grade-I stage-Ta transitional cell carcinoma of the bladder. Eur Urol 32:229-236
5. Chow NH, Tzai TS, Cheng HL, Liu HS, Chan SH, Tong YC (2000) The clinical value of p21WAF1/CIP1 expression in superficial bladder cancer. Anticancer Res 20:1173-1176
6. Cote RJ, Dunn MD, Chatterjee SJ, Stein JP, Shi SR, Tran QC, Hu SX, Xu HJ, Groshen S, Taylor CR, Skinner DG, Benedict WF (1998) Elevated and absent pRb expression is associated with bladder cancer progression and has cooperative effects with p53. Cancer Res 58:1090-1094
7. Edwards J, Duncan P, Going JJ, Grigor KM, Watters AD, Bartlett JM (2001) Loss of heterozygosity on chromosomes 11 and 17 are markers of recurrence in TCC of the bladder. Br J Cancer 85:1894-1899
8. Flam TA, Chopin DK, Leleu C, Abbou CC, Steg A, Desligneres S, Boccon-Gibod L (1990) Immunohistochemical markers defined by monoclonal antibodies and response to bacillus Calmette-Guerin endovesical immunotherapy for superficial bladder tumors. Eur Urol 17:338-342
9. Friedrich MG, Riethdorf S, Erbersdobler A, Tiemer C, Schwaibold H, Solter JK, Huland E, Riethdorf L, Conrad S, Hammerer PG, Huland H (2001) Relevance of p53 gene alterations for tumor recurrence in patients with superficial transitional cell carcinoma of the bladder. Eur Urol 39:159-166
10. Gardiner RA, Walsh MD, Allen V, Rahman S, Samaratunga ML, Seymour GJ, Lavin MF (1994) Immunohistological expression of p53 in primary pT1 transitional cell bladder cancer in relation to tumour progression. Br J Urol 73:526-532
11. Gontero P, Casetta G, Zitella A, Ballario R, Pacchioni D, Magnani C, Muir GH, Tizzani A (2000) Evaluation of P53 protein overexpression, Ki67 proliferative activity and mitotic index as markers of tumour recurrence in superficial transitional cell carcinoma of the bladder. Eur Urol 38:287-296
12. Grossman HB, Liebert M, Antelo M, Dinney CP, Hu SX, Palmer JL, Benedict WF. (1998) p53 and RB expression predict progression in T1 bladder cancer. Clin Cancer Res 4:829-834
13. Hake R, Vorreuther R, Borchmann P, Lukowsky S, Thiele J, Fischer R (1993) Monoclonal antibodies (Mib1, pC10, 486p and p53) as prognostic factors to detect recurrent transitional cell carcinoma of the bladder. Verh Dtsch Ges Pathol 77:236-240
14. Harnden P, Mahmood N, Southgate J (1999) Expression of cytokeratin 20 redefines urothelial papillomas of the bladder. Lancet 353: 974-977
15. Helpap B (1992) Grading and prognostic significance of urologic carcinomas. Urol Int 48:245-257
16. Helpap B (2002) The new WHO-classification of urothelial carcinomas of the urinary bladder. Verh Dtsch Ges Pathol 86:57–66

17. Helpap B, Köllermann J (1999) Proliferative pattern of exophytic and superficially invasive and noninvasive low-grade urothelial carcinoms. Hum Pathol 30:145-150
18. Helpap B, Köllermann J (2000) Assessment of basal cell status and proliferative patterns in flat and papillary urothelial lesions. A contribution to the new WHO classification of urothelial tumors of the urinary bladder. Hum Pathol 31:745-759
19. Helpap B, Loesevitz L, Bulatko A (1994) Nucleolar and argyrophilic nucleolar organizer region counts in urothelial carcinomas with special emphasis on grade II tumors. Virchows Arch 425:265-226
20. Hermann GG, Horn T, Steven K (1998) The influence of the level of lamina propria invasion and the prevalence of p53 nuclear accumulation on survival in stage T1 transitional cell bladder cancer. J Urol 159:91-94
21. Hudson MA, Nadler RB, Swanson PE, Humphrey PA (1995) P53 protein accumulation in superficial bladder cancer: a predictor of tumor progression which is not affected by intravesical BCG therapy. J Urol 153:531
22. Köllermann J, Helpap B (2001) High risk superficial bladder carcinoma-pT1G3: the significance of its diagnosis on trans-urethral resection specimens. Urol Integr Invest 6:24-30
23. Krokolopoulou P, Christodoulou P, Konstatinidou AE, Thomas-Tsagli E, Kapralos P, Davaris P (2000) Cell cycle regulators in bladder cancer: A multivariate survival study with emphasis on p27Kip1. Hum Pathol 31:751-760
24. Krüger S, Kahl M, Fabian T, Hörlin A, Herrmann G, Müller H, Schneider M (1993) Morphometrical, cytochemical and immunohistochemical studies on the proliverative activity of urinary bladder carcinoms. Verh Dtsch Ges Pathol 77:231-235
25. Leissner J, Hohenfellner R, Thuroff JW, Koppen C, Wolf HK (2001) Prognostic significance of histopathological grading and immunoreactivity for p53 and p21/WAF1 in grade 2 pTa transitional cell carcinoma of the urinary bladder. Eur Urol 39:438-445
26. Lipponen PK, Eskelinen MJ (1995) Reduced expression of E-cadherin is related to invasive disease and frequent recurrence in bladder cancer. J Cancer Res Clin Oncol 121:303-308
27. Lipponen P, Aaltomaa S, Eskelinen M (1996) Expression of the apoptosis supressing bcl-2 protein in transitional cell bladder tumours. Histopathol 28:135-140
28. Lipponen P, Aaltomaa S, Eskelinen M, Ala-Opas M, Kosma VM (1998) Expression of p21(waf1/cip1) protein in transitional cell bladder tumours and its prognostic value. Eur Urol 34:237-234
29. Liukkonen T, Rajala P, Raitanen M, Rintala E, Kaasinen E, Lipponen P (1999) Prognostic value of MIB-1 score, p53, EGFr, mitotic index and papillary status in primary superficial (Stage pTa/T1) bladder cancer: a prospective comparative study. The Finnbladder Group. Eur Urol 36:393-400
30. Liukkonen T, Lipponen P, Raitanen M, Kaasinen E, Ala-Opas M, Rajala P, Kosma VM (2000) Evaluation of p21WAF1/CIP1 and cyclin D1 expression in the progression of superficial bladder cancer. Finbladder Group. Urol Res 28:285-292
31. Malmstrom PU, Wijkstrom H, Lundholm C, Wester K, Busch C, Norlen BJ (1999) 5-year followup of a randomized prospective study comparing mitomycin C and bacillus Calmette-Guerin in patients with superficial bladder carcinoma. Swedish-Norwegian Bladder Cancer Study Group. J Urol 161:1124-1127
32. Moch H, Sauter G, Gudat F, Waldman F, Mihatsch MJ (1993) Ki-67-fraction, p53-alteration and numerical chromosomal aberrations (chromosomes 7 and 17) in formalin fixed bladder carcinomas. Verh Dtsch Ges Pathol 77:226-230
33. Offner FA, Schöfer G, Hittmair A, Öfner D, Grünewald K, Weyrer K, Mattern D, Eberle J, Mikuz G, Feichtinger H (1993) Proliferative activity and p53 expression in transitional cell carcinomas of the urinary bladder. Verh Dtsch Ges Pathol 77:241-246
34. Orlow I, LaRue H, Osman I, Lacombe L, Moore L, Rabbani F, Meyer F, Fradet Y, Cordon-Cardo C (1999) Deletions of the INK4A gene in superficial bladder tumors. Association with recurrence. Am J Pathol 155:105-113
35. Peyromaure M, Weibing S, Sebe P, Verpillat P, Toublanc M, Dauge MC, Boccon-Gibod L, Ravery V (2002) Prognostic value of p53 overexpression in T1G3 bladder tumors treated with bacillus Calmette-Guerin therapy. Urology 59:409-413
36. Pfister C, Moore L, Allard P, Larue H, Lacombe L, Tetu B, Meyer F, Fradet Y (1999) Predictive value of cell cycle markers p53, MDM 2, p21, and Ki-67 in superficial bladder tumor recurrence. Clin Cancer Res 5:4079-4084
37. Rodriguez-Alonso A, Pita-Fernandez S, Gonzalez-Carrero J, Nogueira-March JL (2002) Multivariate analysis of survival, recurrence, progression and development of mestastasis in T1 and T2a transitional cell bladder carcinoma. Cancer 94:1677-1684
38. Sarkis AS, Dalbagni G, Cordon-Cardo C, Zhang ZF, Sheinfeld J, Fair WR, Herr HW, Reuter VE (1993) Nuclear overexpression of p53 protein in transitional cell bladder carcinoma: a marker for disease progression. J Natl Cancer Inst 85:53-59
39. Sarkis AS, Dalbagni G, Cordon-Cardo C, Zhang Z-F, Sheinfeld J, Fair WR, Herr HW, Reuter VE (1994) Association of p53 nuclear overexpression and tumor progression in carcinoma in situ of the bladder. J Urol 152:388-392
40. Schmitz-Dräger BJ, Kushima M, Goebell P, Jax TW, Gerharz C-D, Bültel H, Schulz WA, Ebert T, Ackermann R (1997) P53 and mdm2 in the development and progression of bladder cancer. Eur Urol 32:487-493
41. Schmitz-Dräger BJ, Goebell P, Ebert T, Fradet Y (2000) P53 immunohistochemistry as a prognostic marker in bladder cancer: playground for urologic scientists? Eur Urol 38:691-700
42. Serth J, Kuczyk MA, Bokemeyer C, Hervatin C, Nafe R, Tan HK, Jonas U (1995) p53 immunohistochemistry as an independent prognostic factor for superficial transitional cell carcinoma of the bladder. Br J Cancer 71:201-205
43. Sgambato A, Migaldi M, Faraglia B, Garagnani L, Romano G, De Gaetani C, Ferrari P, Capelli G, Trentini GP, Cittadini A (1999) Loss of P27Kip1 expression correlates with tumor grade and with reduced disease-free survival in primary superficial bladder cancers. Cancer Res 59:3245-3250
44. Shariat SF, Pahlavan S, Baseman AG, Brown RM, Green AE, Wheeler TM, Lerner SP (2001) E-cadherin expression predicts clinical outcome in carcinoma in situ of the urinary bladder. Urology 57:60-65
45. Stein JP, Ginsberg DA, Grossfeld GD, Chatterjee SJ, Esrig D, Dickinson MG, Groshen S, Taylor CR, Jones PA, Skinner DG, Cote RJ (1998) Effect of p21WAF1/CIP1 expression on tumor progression in bladder cancer. J Natl Cancer Inst 90:1072-1079
46. Tetu B, Fradet Y, Allard P, Veilleux C, Roberge N, Bernard P (1996) Prevalence and clinical significance of HER/2neu, p53 and Rb expression in primary superficial bladder cancer. J Urol 155:1784-1788
47. Thomas DJ, Robinson MC, Charlton R, Wilkinson S, Shenton BK, Neal DE (1994) P53 expression, ploidy and progression in pT1 transitional cell carcinoma of the bladder. Br J Urol 73:533-537
48. Toktas G, Turkeri LN, Unluer E, Atug F, Murat C, Ozveren B, Caliskan M, Akdas A (1999) Prognostic significance of p53 protein accumulation in stage pT1 transitional cell carcinoma of the bladder. Int Urol Nephrol 31:437-441
49. Tsukamoto M, Matsuyama H, Oba K, Yoshihiro S, Takahashi M, Naito K (2002) Numerical aberrations of chromosome 9 in bladder cancer. A possible prognostic marker for early tumor recurrence. Cancer Genet Cytogenet 134:41-45
50. Tzai TS, Chow NH, Lin JS, Yang WH, Tong YC (1998) The expression of p53 and bcl-2 in superficial bladder transitional cell carcinoma and its role in the outcome of postoperative intravesical chemotherapy. Anticancer Res 18:4717-4721
51. Vatne V, Maartmann Moe H, Hoestmark J (1995) The prognostic value of p53 in superficially infiltrating transitional cell carcinoma. Scand J Urol Nephrol 29:491-495

52. Wagner U, Sauter G, Moch H, Novotna H, Epper R, Mihatsch MH, Waldman FM (1995) Patterns of p53, erbB-2, and EGF-r Expression in premalignant lesions of the urinary bladder. Hum Pathol 26:970-978
53. Wu TT, Chen JH, Lee YH, Huang JK (2000) The role of bcl-2, p53, and ki-67 index in predicting tumor recurrence for low grade superficial transitional cell bladder carcinoma. J Urol 163:758-760
54. Zlotta AR, Noel JC, Fayt I, Drowart A, Van Vooren JP, Huygen K, Simon J, Schulman CC (1999) Correlation and prognostic significance of p53, p21WAF1/CIP1 and Ki-67 expression in patients with superficial bladder tumors treated with bacillus Calmette-Guerin intravesical therapy. J Urol 161:792-798

Virchows Arch (2003) 442:317–321
DOI 10.1007/s00428-002-0750-6

ORIGINAL ARTICLE

**M. Vieth · R. Kushima · F. Borchard · M. Stolte**

# Pyloric gland adenoma: a clinico-pathological analysis of 90 cases

Received: 1 October 2002 / Accepted: 28 November 2002 / Published online: 26 March 2003
© Springer-Verlag 2003

**Abstract** *Background:* Pyloric gland adenoma is a rarely described neoplasia of the gastric mucosa. Recent publications have shown that similar lesions are also found in the gallbladder, the main pancreatic duct, the duodenum and the cervix of the uterus. Apart from case reports, few clinical data are available on these patients. We therefore conducted a search of the archived material collected between 1990 and 2000 for more clinical data on patients with this rare lesion. *Patients and methods:* Between 1990 and 2000, 90 patients were diagnosed as having a pyloric gland adenoma in the stomach (77 patients), duodenal bulb (7 patients), duodenum (1 patient), bile duct (3 patients) or gallbladder (2 patients). *Results:* Pyloric gland adenomas account for 2.7% of all gastric polyps and occur predominantly in old age (73±12.8 years), more frequently in women (75%) than in men. The predilection site in the stomach is the corpus mucosa (64%) and they are often found in patients suffering from autoimmune gastritis (36%). At the time of diagnosis, pyloric gland adenomas measure 16.1±9.1 mm in size. In 30% of gastric pyloric adenomas, transition to well-differentiated adenocarcinoma has been noted. *Discussion:* In our material, pyloric gland adenoma is the third most common neoplastic polypoid lesion in the stomach. Since a search through the literature revealed only a few case reports on this lesion, it is possible that for some reason this lesion might be diagnosed more often than reported. *Conclusion:* Our study revealed that 30% of the gastric pyloric gland adenomas showed continuous transition to well-differentiated adenocarcinoma at the time of the initial diagnosis. This underscores the malignant potential of the lesion, and the need for polypectomy.

**Keywords** Pyloric gland adenoma · Stomach · Duodenum · Bile duct · Clinical data · Adenocarcinoma

This work is dedicated to Professor Dr. med. Kurt Elster who passed away 26 October 2001.

M. Vieth
Institute of Pathology,
University of Magdeburg, 39120 Magdeburg, Germany

R. Kushima
Department of Pathology, Shiga University of Medical Science,
Seta Ohtsu, 520-2192 Shiga, Japan

F. Borchard
Institute of Pathology, Klinikum Aschaffenburg,
63739 Aschaffenburg, Germany

M. Stolte (✉)
Institute of Pathology, Klinikum Bayreuth,
Preuschwitzerstrasse 101, 95445 Bayreuth, Germany
e-mail: Michael.Vieth@Medizin.Uni-Magdeburg.de
Tel.: +49-921-4005600
Fax: +49-921-4005609

## Introduction

Pyloric gland adenoma of the gastric mucosa was first described by Elster in 1976 [7] but misinterpreted as adenoma-like hyperplasia of mucoid glands. Borchard et al. described a pyloric gland adenoma showing transition to moderately differentiated adenocarcinoma on the occasion of two tutorials of the International Academy of Pathology (IAP) in Germany held in 1986 and 1987 (F. Borchard, personal communication). The first characterization of two cases by mucin analysis was published by Borchard et al. [3] in 1990. A similar lesion was described by Watanabe [19] in the World Health Organization (WHO) classification of gastric tumors in 1990. Similar adenomas of the gastric type were subsequently described in gastric mucosa heterotopia in the duodenum [12], in the pancreatic duct [1] and, in particular, in the gallbladder [9, 11, 17] and the cervix of the uterus [8, 13].

In a previous publication reporting on 18 patients with a pyloric gland adenoma, we found an elevated frequency of p53 expression in these adenomas relative to gastric adenomans of the intestinal type [10]. Apart from the six initial descriptions of pyloric gland adenomas in the stomach published between 1976 and 1990, our search of the literature revealed no further publications. Despite the description by Watanabe [19], our search through the literature revealed the absence of the entity of pyloric

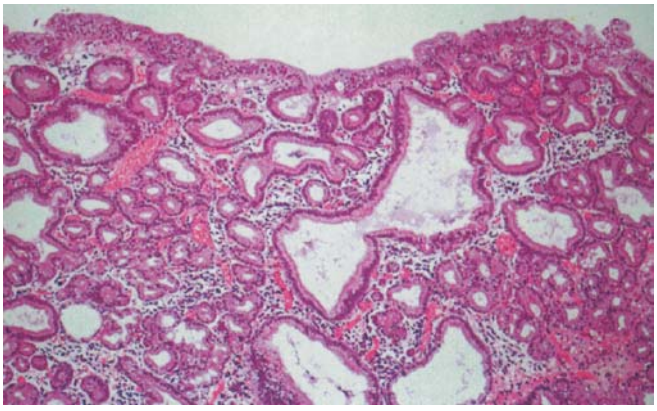


**Fig. 1** Low power view of a pyloric gland adenoma composed of prismatic columnar epithelium showing basal nuclei and pale eosinophilic cytoplasm and forming some ectatic foveolae (H&E ×20)

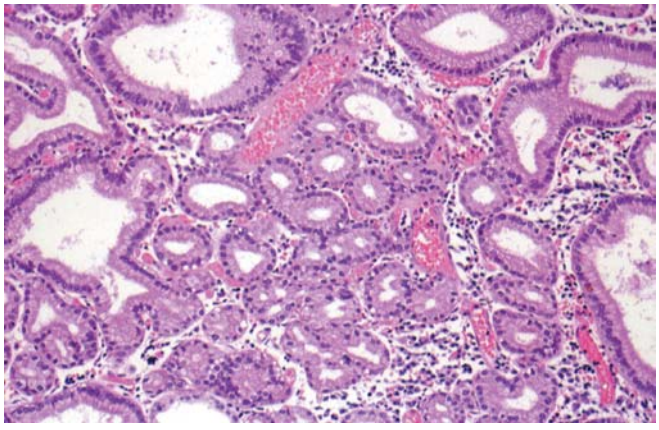


**Fig. 2** Larger view of Fig. 1. Pyloric gland adenoma with round basal nuclei (H&E ×200)

gland adenoma in all classifications of gastric tumors. Presumably, most of these adenomas are diagnosed routinely but are not reported.

For this reason, we carried out a clinico-pathological analysis of all pyloric gland adenomas of the upper gastrointestinal tract diagnosed in 90 patients during the period between 1990 and 2000.

## Patients and methods

In order to determine the incidence of pyloric gland adenoma, we evaluated the records of all gastric polyps diagnosed at the Institute of Pathology in Bayreuth during the period between 1990 and 2000. For the specific clinico-pathological analysis of the patients with pyloric gland adenoma, the following criteria were applied:

- Age and sex distribution
- Distribution of the location of the adenoma
- Status of the gastric mucosa
- Incidence of carcinoma in pyloric gland adenoma

Pyloric gland adenomas from 90 patients were investigated. In 68 (75%) of these patients, the diagnosis was established primarily in forceps biopsy material. Of these patients, 65 (96%) were then submitted to endoscopic polypectomy. In 21 (23%) of the patients, the primary diagnosis was established in the polypectomy specimen, in a single case in the gastrectomy specimen.

The diagnosis of pyloric gland adenoma was made on the basis of the criteria proposed by Watanabe [19]: this type of adenoma is mainly composed of closely packed pyloric type glands. The glands are lined by cuboidal or columnar mucus-secreting cells immunohistochemically positive for mucin 6, with paradoxical concavalin A staining being specific for the mucin of pyloric gland cells, mucus neck cells and Brunner's gland cells. Immunohistochemistry with antibodies against mucin 2 (intestinal goblet cells), mucin 5-AC (gastric surface epithelium) and mucin 6 (deep foveolar gastric epithelium) antigen helps to differentiate pyloric gland adenomas and other polypoid lesions of the stomach such as hyperplastic polyps, foveolar hyperplasia and tubular adenoma, which show mainly positivity for the surface mucin 5-AC [4, 10]. All cases were confirmed independently by the four authors. A typical pyloric gland adenoma is shown in Fig. 1, Fig. 2, Fig. 3, and Fig. 4.

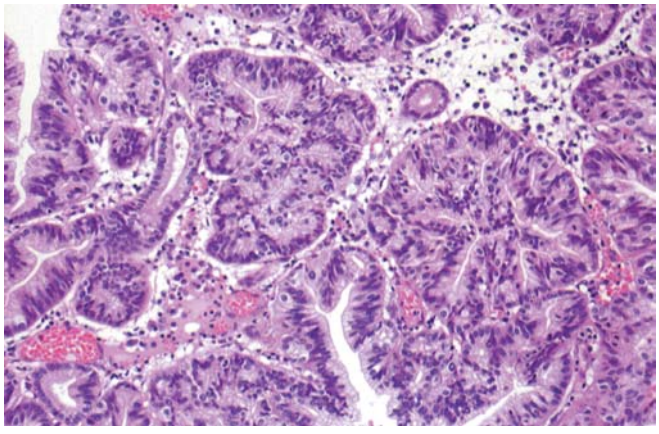


**Fig. 3** Pyloric gland adenoma with continuous transition to well-differentiated adenocarcinoma with hyperchromatic bizarre nulcei and bizarre structure of foveolae. The stellar pattern of the glands represents invasive tubules within the lamina propria with back to back formation. Characteristically, the cytology is not suspicious on low-power view (H&E ×40)

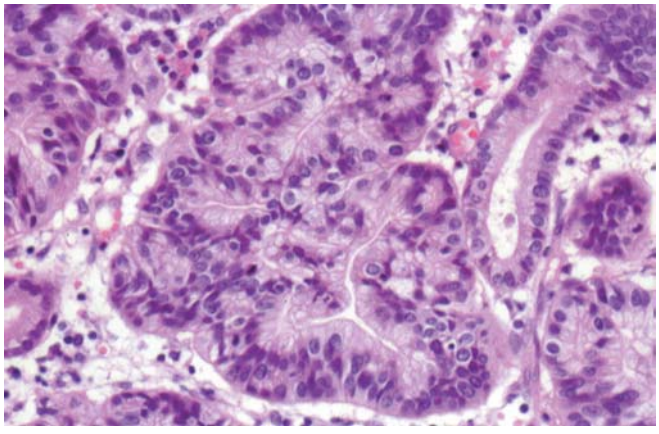


**Fig. 4** Larger view of Fig. 3. Focus of well-differentiated adenocarcinoma with invasive tubules in the tunica propria with hyperchromatic bizarre nuclei, prominent nucleoli and typically pale eosinophilic cytoplasm (H&E ×200)

In case of adenocarcinoma, the diagnosis was based on the definition of gastric neoplasia by the WHO [19] and analysis of the mucin distribution and proliferative markers [18].

The classification and grading of gastritis in patients with pyloric gland adenoma was done in accordance with the updated Sydney System [5]. An ex-Hp gastritis was always diagnosed when only a low-grade, non-active superficial gastritis was found, with no evidence of *Helicobacter pylori* in slides stained with the Warthin-Starry silver stain [15].

## Results

### Incidence of pyloric gland adenoma among our gastric polyps

The incidence of gastric polyps diagnosed at the Institute of Pathology in Bayreuth between 1900 and 2000 is shown in Table 1. The harmless fundic gland polyps (Elster's polyps), which are readily diagnosed via the endoscope and in our material are the most common of the gastric polyps [6], have not been considered in the present study. In our statistics, pyloric gland adenoma is very rare, accounting for only 2.7% of all gastric polyps. Among the polypous neoplasias of the gastric mucosa, however, pyloric gland adenomas occupy third place after tubular adenomas of the intestinal type and adenocarcinomas, just edging out the tubulopapillary and the extremely rare papillary adenomas.

### Age and sex distribution

Pyloric gland adenomas occur predominately in old age, more frequently in women than in men. In our material, the sex distribution was 55 (61%) women to 35 (39%) men, the average age of the women being 75±12.8 years, that of the men 70±13.3 years (Table 2).

### Distribution of the location of the adenoma

The predilection site for pyloric gland adenoma in the upper digestive tract is the stomach. Of all pyloric gland adenomas, 85% are found in the stomach, whereas 15% are found extra-gastric. Corpus/fundic mucosa is the most frequent location where 64% of all pyloric gland adenomas are found, followed by the duodenal bulb (7.9%), the cardia (7.9%), the antrum (6.7%) and the intermediate zone of the gastric mucosa (5.6%). Individual pyloric gland adenomas are also found in the region of the angulus, in the descending part of the duodenum, the bile duct and the gallbladder (Table 3). At the time of the diagnosis, pyloric gland adenomas were already relatively large, the mean diameter of our polyps being 16.1±9.1 mm (Table 4).

**Table 1** Gastric polyp registry including all gastric polyps diagnosed between 1990 and 2000 at the Institute of Pathology in Bayreuth excluding fundic gland cysts

| | *n*=2778 |
|---|---|
| Tumor-like lesions | |
| Total: | 1890 |
| Hyperplastic polyps | 60.1% |
| Inflammatory fibroid polyps | 3.5% |
| Pancreatic heterotopia | 1.2% |
| Brunner's heterotopia | 0.3% |
| Peutz-Jeghers polyps | 0.3% |
| Juvenile polyps | 0.2% |
| Cronkhite-Canada polyps | 0.1% |
| Neoplasias | |
| Total: | 888 |
| Adenomas: | |
| Tubular: | 20.3% |
| Tubulopapillary | 1.2% |
| Papillary | 0.1% |
| Pyloric gland | 2.7% |
| Adenocarcinomas | 6.1% |
| Carcinoids | 2.7% |
| Metastases | 1.2% |

**Table 2** Age and sex distribution of patients with pyloric gland adenomas

| | Pyloric gland adenomas | |
|---|---|---|
| | All patients | Patients with transition to carcinoma |
| Sex | 55 females: 35 males (2.5:1) | 15 females: 10 males (1.5:1) |
| Age (years) | 73±12.8 | 74±9.2 |
| Females | 75±12.8 | 78±9.2 |
| Males | 70±13.3 | 69±6.2 |

**Table 3** Location of pyloric gland adenomas

| | *n* |
|---|---|
| Stomach | 77 (85%) |
| Extra-gastric | 13 (15%) |
| Gall bladder | 2 (2%) |
| Bile duct | 3 (3%) |
| Bulb | 7 (8%) |
| Duodenum | 1 (1%) |
| Antrum | 6 (7%) |
| Intermediate zone | 4 (5%) |
| Corpus | 58 (64%) |
| Cardia | 7 (8%) |
| Residual stomach (BII) | 2 (2%) |
| Total | 90 (100%) |

**Table 4** Size distribution of pyloric gland adenomas (stomach only)

| | Transition to carcinoma | Without carcinoma |
|---|---|---|
| Size in millimeters | 16±9 | 17±7 |

**Table 5** Status of gastric mucosa

| Gastritis-status | *n* (%) |
|---|---|
| Normal | 2 (3.8%) |
| *H. pylori* | 22 (41.5%) |
| -active | 16 (30.2%) |
| -ex-*H. pylori* | 6 (11.3%) |
| Chemical | 11 (20.8%) |
| Autoimmune | 18 (33.9%) |

**Table 6** Frequency of gastric pyloric gland adenomas with transition to well-differentiated adenocarcinoma (mucosal type)

| | *n* |
|---|---|
| Gastric pyloric gland adenomas without adenocarcinoma | 54 (100%) |
| Gastric pyloric gland adenomas with transition to adenocarcinoma | 23 (30%) |
| Location of gastric carcinoma in pyloric gland adenoma | |
| Antrum | 2 (9%) |
| Intermediate zone | 2 (9%) |
| Corpus | 18 (78%) |
| Cardia | 1 (4%) |
| Location other than the stomach | |
| Duodenum | 1 |
| Bile duct | 1 |

### Status of the unaffected gastric mucosa

In 53 of 90 patients with gastric pyloric gland adenoma, we were able to examine biopsies from the antrum and corpus obtained simultaneously or later. It was found that pyloric gland adenomas in our material developed mainly in atrophic autoimmune gastritis of the corpus and fundus mucosa (34%), while Hp gastritis was seen in 30%, an ex-Hp gastritis in 11% and chemical reactive gastritis (C-gastritis) in 20%. The diagnosis of autoimmune gastritis was made whenever marked atrophy of parietal cells and diffuse lymphocytic infiltration was present in the tunica propria. Further criteria were proliferation of neuroendocrine cell complexes, foveolar hyperplasia and, in the majority of the cases, the finding of intestinal metaplasia. Only in 3.8% of the patients was a normal gastric mucosa observed. In a single male patient, a concomitant tubular adenoma of the intestinal type was found elsewhere, in a further male patient a carcinoid tumor, and in one patient an additional gastric carcinoma (Table 5). No difference in the distribution of gastritis was detected between cases with and without transition to adenocarcinoma. None of the cases showed so-called corpus dominant active *Helicobacter* gastritis.

### Incidence of carcinoma in the pyloric gland adenomas

In the polypectomy ($n$=76) or surgical specimen ($n$=1) obtained from patients with gastric pyloric gland adenoma, we diagnosed transition to a well-differentiated tubular adenocarcinoma of the gastric type in 26% ($n$=20) of the cases. Three further tubular adenocarcinomas were moderately differentiated but, despite one T2 carcinoma, still limited to the mucosa. Most cases showed only small foci of adenocarcinoma. In total, 30% of all pyloric gland adenomas showed transition to carcinoma. All carcinomas were of the gastric type; no diffuse type of carcinoma was present. The detection rate of carcinoma in a pyloric gland adenoma correlates with the diameter of the adenoma (Table 6).

## Discussion

The first clinico-pathological analysis of a large number of patients with pyloric gland adenoma diagnosed over a period of 10 years at our institute shows, in the first instance, that, at 2.7% of all gastric polyps, this lesion is not that rare as indicated by only few reported cases in the literature. After all, following adenomas of the intestinal type and polypous adenocarcinoma of the stomach, it is the third most common epithelial neoplastic polyp of the gastric mucosa.

The fact that, following the first case reports of pyloric gland adenoma in 1976, 1986, 1987 and 1990 [3, 4, 7, 18], to date, only our own work on the p53 expression in pyloric gland adenomas in comparison with intestinal type adenomas has been published [10] suggests that most cases of pyloric gland adenomas diagnosed are either not published or underdiagnosed.

Our work also confirms that these adenomas are also found in gastric heterotopic mucosa and gastric metaplasia in the duodenum [12], in the pancreatic duct [1] and in the gall bladder [11, 17]. In addition, we have also found three pyloric gland adenomas in the common bile duct. Most commonly, this adenoma arises in the gastric mucosa. Here, the predilection site (64%) is the corpus mucosa. In our work, this correlates well with the status of the gastric mucosa in the antrum and corpus, since, in common with the adenomas of the intestinal type [12], pyloric gland adenomas apparently are preferentially found (34%) in an atrophic autoimmune gastritis of the corpus mucosa. Since atrophic autoimmune gastritis is found predominantly in advanced age, and then mostly in women, this is presumably also the explanation for the observation that pyloric gland adenomas in our material are more commonly seen in women (ratio female:male = 55:35) of advanced age (women: 75±12.8 years; men: 70±13.3 years). Concerning the association with autoimmune gastritis, it could only be speculated on whether the neoplastic change of the deep gastric epithelium might be caused by neuroendocrine stimulation by proliferated neuroendocrine cell complexes. Further studies are necessary to investigate this issue. To date, no data have been published on the incidence of gastric carcinomas arising in pyloric gland adenomas. Our analysis shows that, as in the case of adenomas of the intestinal type [4, 14], pyloric gland adenomas are precancerous lesions [16], since 30%

reveal transition to a gastric-type gastric carcinoma. Since it appears to be more or less certain that a relatively large percentage of early gastric carcinomas initially arise as gastric carcinomas of the gastric type that can convert secondarily into a gastric carcinoma of the intestinal type [2], it is possible that gastric carcinomas of the gastric type have arisen in previously non-diagnosed pyloric gland adenomas.

## Conclusion

In conclusion, our analysis shows that, although pyloric gland adenomas are rare gastric polyps, they nevertheless occupy third place in the list of neoplastic polyps, arise mainly in atrophic autoimmune gastritis and, therefore, present mainly in the corpus of elderly patients. The finding of transition to gastric type adenocarcinoma in 30% of our cases indicates that this adenoma is a precancerous lesion and that endoscopic polypectomy is indicated.

## References


1. Bakotic BW, Robinson MJ, Sturm PD, Hruban RH, Offerhaus GJ, Albores-Saavedra J (1999) Pyloric gland adenoma of the main pancreatic duct. Am J Surg Pathol 23:227–231
2. Bamba M, Sugihara H, Kushima R, Okada K, Tsukashita S, Hattori T (2001) Time dependent expression of intestinal phenotype in signet ring cell carcinomas of the human stomach. Virchows Arch 438:49–56
3. Borchard F, Ghanei A, Koldovsky U, Hengels KJ, Bückmann FW (1990) Gastrale Differenzierung in Adenomen der Magenschleimhaut. Immunhistochemische und elektronenmikroskopische Untersuchungen. Verh Dtsch Ges Pathol 74:528
4. Cornaggia M, Capella C, Riva C, Finzi G, Solcia E (1986) Electron immunocytochemical localization of pepsinogen I (PgI) in chief cells, mucous-neck cells and transitional mucous-neck/chief cells of the human fundic mucosa. Histochemistry 85:5–11
5. Dixon MF, Genta RM, Yardley JH, Correa P (1996) Classification and grading of gastritis. The updated Sydney System. International workshop on the histopathology of gastritis, Houston 1994. Am J Surg Pathol 20:1161–1181
6. Eidt S, Stolte M (1989) Gastric glandular cysts – investigations into their genesis and relationship to colorectal epithelial tumors. Z Gastroenterol 27:212–217
7. Elster K (1976) Histologic classification of gastric polyps. In: Morson BC (ed) Pathology of the gastro-intestinal tract. Springer, Berlin Heidelberg New York, pp 78–92
8. Ishii K, Hidaka E, Katsuyama T, Ota H, Shiozawa T, Tsuchiya S (1999) Ultrastructural features of adenoma malignum of the uterine cervix: demonstration of gastric phenotypes. Ultrastruct Pathol 23:375–381
9. Itoi T, Watanabe H, Ajioka Y, Ooohashi Y, Takei K, Nishikura K, Nakamura Y, Horic A, Saito T (1996) APC, K-ras codon 12 mutations and p53 gene expression in carcinoma and adenoma of the gall-bladder suggest two genetic pathways in gall-bladder carcinogenesis. Pathol Int 46:333–340
10. Kushima R, Müller W, Stolte M, Borchard F (1996) Differential p53 protein expression in gastric adenomas of gastric and intestinal types: possible sequence of p53 alteration in the stomach carcinogenesis according to histological and mucin histochemical phenotypes. Virchows Arch 428:223–227
11. Kushima R, Remmele W, Stolte M, Borchard F (1996) Pyloric gland type adenoma of the gallbladder with squamoid spindle cell metaplasia. Pathol Res Pract 192:963–969
12. Kushima R, Rüthlein HJ, Stolte M, Hattori T, Borchard F (1999) Pyloric gland-type adenoma arising in heterotopic gastric mucosa of the duodenum with dysplastic progression of the gastric type. Virchows Arch 435:452–457
13. Mikami Y, Hata S, Fujiwara K, Imajo Y, Kohno I, Manabe T (1999) Florid endocervical glandular hyperplasia with intestinal and pyloric gland metaplasia: worrisome benign mimic of "adenoma malignum". Gynecol Oncol 74:504–511
14. Oberhuber G, Stolte M (2000) Gastric polyps: an update of their pathology and biological significance. Virchows Arch 437:581–590
15. Oberhuber G, Puspök A, Dejaco C, Hammer J, Zauner C, Pfeffel F, Fiedler R, Pötzi R, Allerberger F, Wrba F (1996) Minimal chronic inactive gastritis: indicator of pre-existing *Helicobacter pylori* gastritis? Pathol Res Pract 192:1016–1021
16. Schmitz JM, Stolte M (1997) Gastric polyps as precancerous lesions. Gastroenterol Clin North Am 1:29–46
17. Takei K, Watanabe H, Itoi T, Saito T (1996) p53 and Ki-67 immunoreactivity and nuclear morphometry of "carcinoma-in-adenoma" and adenoma of the gall bladder. Pathol Int 46:908–917
18. Tsukashita S, Kushima R, Bamba M, Sugihara H, Hattori T (2001) MUC gene expression and histogenesis of adenocarcinoma of the stomach. Int J Cancer 94:166–170
19. Watanabe H, Jass JR, Sobin LH (1990) Histological typing of oesophageal and gastric tumours. Springer, Berlin Heidelberg New York

Virchows Arch (2003) 442:322–328
DOI 10.1007/s00428-003-0769-3

ORIGINAL ARTICLE

**R. Kremser · P. Obrist · G. Spizzo · H. Erler · D. Kendler · G. Kemmler · G. Mikuz · C. Ensinger**

# Her2/neu overexpression in differentiated thyroid carcinomas predicts metastatic disease

Received: 25 September 2002 / Accepted: 27 December 2002 / Published online: 8 March 2003
© Springer-Verlag 2003

**Abstract** To investigate the prognostic value of Her2/neu expression in differentiated thyroid carcinomas 103 patients were retrospectively investigated. All of them received surgical and an identical follow-up treatment. The patients with papillary and follicular thyroid cancer were further separated into two groups concerning their clinical development, including one group without distant metastasis (follow-up of minimum 8 years). The second group presented with distant metastases as a sign of an aggressive behaviour. Her2/neu was immunohistochemically detected on sections from formalin-fixed, paraffin-embedded tissues using c-erbB-2/Her-2/neu oncoprotein Ab-17 monoclonal antibody (mAb). In statistical analysis using the Mann-Whitney U-test and $\chi^2$ test, Her2/neu protein overexpression was significantly correlated with prognosis. Both tumour entities without distant metastases showed significantly less cytoplasmic immunostaining than patients with development of metastases. Concerning the clinical outcome, Her2/neu overexpression may be regarded as a prognostic factor in differentiated thyroid carcinomas. Moreover, in addition to standard radioiodine elimination therapy, application of Herceptin could lead to new successful therapeutic concepts for a number of patients with progressive thyroid cancer.

R. Kremser · P. Obrist · G. Mikuz · C. Ensinger (✉)
Institute of Pathology, University of Innsbruck,
Muellerstr. 44, 6020 Innsbruck, Austria
e-mail: christian.ensinger@uibk.ac.at
Tel.: +43-512-5073668
Fax: +43-512-582088

G. Spizzo
Division Hematology & Oncology,
University of Innsbruck, 6020 Innsbruck, Austria

H. Erler · D. Kendler
Institute of Nuclear Medicine,
University of Innsbruck, 6020 Innsbruck, Austria

G. Kemmler
Institute of Psychiatrics (Division Biostatistics),
University of Innsbruck, 6020 Innsbruck, Austria

**Keywords** Her2neu · Thyroid cancer · Metastasis · Prognosis

## Introduction

Cancer results from alterations in critical regulatory genes controlling cell proliferation, differentiation and single cell survival. Specific genes, the proto-oncogenes, are able to induce cell transformation when they are abnormally expressed after amplifications or mutations. As a consequence of such alterations, the oncogenes induce abnormal cell proliferations and tumour development [8].

The c-erbB-2 gene (also known as Her2/neu), located on human chromosome 17 at q21, encodes a transmembrane glycoprotein of MW 185 kDa (p185) [3], which is a homologue to the epidermal growth factor (EGF) receptor and has tyrosine kinase activity [27]. The natural ligands of p185 are not yet completely identified, but an interaction with important cellular signal transduction proteins is known [14].

A redundant amplification of c-erbB-2 genes and overexpression of Her2/neu protein was first detected in human breast cancer and ovarian cancer [4, 25, 38]. Furthermore, it was found in lung and gastric cancers [24], recognising Her2/neu overexpression as an important factor concerning growth and progression of malignant cells, even if some of the mechanisms are still to be clarified.

Many authors [13, 24, 30, 33, 34, 35, 38] found Her2/neu overexpression not only resulting from tumour development, but also as an initial factor of neoplastic proliferation. Yu and Hung (1991) showed in their experiments that the activated Her2/neu oncogene is able to increase metastatic potential in 3T3 cells [37]. An overexpression of Her2/neu in human lung and breast cancer seems to also lead to an increased metastatic potential of the cells [6, 28, 36].

Patients with differentiated thyroid cancer receiving an identical treatment are presenting with a very different clinical course and are, therefore, interesting for evalu-

ating oncogenic influences responsible for these variations. In our study, we used the clinical outcome with or without metastases to define two groups of patients. The prognostic value of immunohistochemically detectable Her2/neu levels in their tumour tissues were investigated to facilitate clinical decisions regarding therapy and perhaps apply modern strategies of antigene-directed treatment procedures.

## Materials and methods

Patients and tumours

This retrospective study included 103 patients with differentiated thyroid cancer diagnosed at the Institute of Pathology between 1983 and 1999, according to the World Health Organization (WHO) classification [12] and reclassified according to a modified classification described by Rosai et al. [22]. Patients were treated at the Institute of Nuclear Medicine of the University Innsbruck (Austria), and all of them underwent total thyroidectomy and an identical therapeutic follow-up: patients with tumours of stages 2–4 (larger than 1 cm) were treated with radio-iodine therapy, and the serum thyroglobulin levels were measured periodically in order to detect tumour recurrences as soon as possible. Paraffin blocks and clinical history were available for all cases. Concerning the clinical course, the patients were separated into two groups, without (group 1) and with (group 2) distant metastases. The presence of cervical lymph-node metastases was not criterion for group 2, due to the fact that cervical lymph-node metastases are not a statistically significant prognostic indicator [5].

In the first group, 36 patients (23 female/13 male) were included, their tumours were diagnosed in the years between 1988 and 1993, with a minimum follow-up of 8 years. During this time, after surgery and radio-iodine elimination therapy, they did not develop tumour recurrences or metastatic disease. This group is described in detail in Table 1.

The second group with 61 patients (43 female/18 male) was diagnosed in the years 1983–1999 with development of distant metastases. In eight cases, we additionally investigated metastatic tissues. This group is further described in Table 2 and Table 3. Six cases of the series were excluded from the study due to loss of immunoreactivity.

**Table 1** Non-metastasising group demonstrating number of patients in several subgroups. *PTC* papillary thyroid cancer, *FTC* follicular thyroid cancer

| | No. | Sex | | Stage | | | | Intensity | | | Score | | | | | | |
|---|---|---|---|---|---|---|---|---|---|---|---|---|---|---|---|---|---|
| | | Female | Male | T2 | T3 | T4 | N1 | 1 | 2 | 3 | 0 | 2 | 4 | 6 | 8 | 9 | 12 |
| PTC | 22 | 15 | 7 | 19 | 2 | 1 | 2 | 5 | 7 | 10 | 0 | 5 | 5 | 8 | 1 | 3 | 0 |
| Classical type | 8 | 4 | 4 | 6 | 1 | 1 | 2 | 3 | 4 | 1 | 0 | 3 | 3 | 1 | 1 | 0 | 0 |
| Follicular variant | 11 | 9 | 2 | 11 | 0 | 0 | 0 | 2 | 3 | 6 | 0 | 2 | 2 | 6 | 0 | 1 | 0 |
| Large cell variant | 2 | 1 | 1 | 2 | 0 | 0 | 0 | 0 | 0 | 2 | 0 | 0 | 0 | 1 | 0 | 1 | 0 |
| Oxyphilic variant | 1 | 1 | 0 | 0 | 1 | 0 | 0 | 0 | 0 | 1 | 0 | 0 | 0 | 0 | 0 | 1 | 0 |
| FTC | 14 | 8 | 6 | 9 | 2 | 3 | 0 | 2 | 11 | 1 | 0 | 2 | 8 | 4 | 0 | 1 | 0 |
| Minimal invasive | 9 | 4 | 5 | 7 | 2 | 0 | 0 | 2 | 6 | 1 | 0 | 2 | 5 | 1 | 0 | 1 | 0 |
| Broad invasive | 5 | 4 | 1 | 2 | 1 | 2 | 0 | 0 | 5 | 0 | 0 | 3 | 2 | 0 | 0 | 0 | 0 |

**Table 2** Metastasising group demonstrating number of patients in several subgroups

| | No. | Sex | | Stage | | | | Intensity | | | Score | | | | | | |
|---|---|---|---|---|---|---|---|---|---|---|---|---|---|---|---|---|---|
| | | Female | Male | T2 | T3 | T4 | N1 | 1 | 2 | 3 | 0 | 2 | 4 | 6 | 8 | 9 | 12 |
| PTC | 21 | 10 | 11 | 6 | 6 | 9 | 13 | 0 | 3 | 18 | 0 | 0 | 1 | 4 | 1 | 9 | 6 |
| Classical type | 9 | 1 | 8 | 1 | 3 | 5 | 6 | 0 | 1 | 8 | 0 | 0 | 0 | 3 | 1 | 4 | 1 |
| Follicular variant | 11 | 8 | 3 | 5 | 3 | 3 | 6 | 0 | 2 | 9 | 0 | 0 | 1 | 1 | 0 | 5 | 4 |
| Large cell variant | 1 | 1 | 0 | 0 | 0 | 1 | 1 | 0 | 0 | 1 | 0 | 0 | 0 | 0 | 0 | 0 | 1 |
| FTC | 40 | 33 | 7 | 6 | 15 | 19 | 18 | 2 | 13 | 25 | 0 | 2 | 9 | 8 | 0 | 14 | 7 |
| Minimal invasive | 0 | 0 | 0 | 0 | 0 | 0 | 0 | 0 | 0 | 0 | 0 | 0 | 0 | 0 | 0 | 0 | 0 |
| Broad invasive | 40 | 33 | 7 | 6 | 15 | 19 | 18 | 2 | 13 | 25 | 0 | 2 | 9 | 8 | 0 | 14 | 7 |

**Table 3** Sites of metastases. *Adr.Gl.* adrenal gland, *Ln Abd.* abdominal lymph nodes

| | No. | Sites of metastases | | | | | | | |
|---|---|---|---|---|---|---|---|---|---|
| | | Bone | Lung | Hilus | Mediastinum | Liver | Brain | Adr.Gl. | Ln Abd. |
| PTC | 21 | 5 | 13 | 3 | 2 | 1 | 2 | 1 | 2 |
| Classical type | 9 | 3 | 5 | 2 | 0 | 0 | 1 | 1 | 2 |
| Follicular variant | 11 | 2 | 7 | 0 | 2 | 1 | 1 | 0 | 1 |
| Large cell variant | 1 | 0 | 1 | 1 | 0 | 0 | 0 | 0 | 0 |
| FTC | 40 | 23 | 21 | 6 | 4 | 2 | 0 | 0 | 3 |
| Minimal invasive | 0 | 0 | 0 | 0 | 0 | 0 | 0 | 0 | 0 |
| Broad invasive | 40 | 23 | 21 | 6 | 4 | 2 | 0 | 0 | 3 |

### Her2/neu-antibody

For immunohistochemistry, a mouse monoclonal antibody (mAb) against c-erbB2/Her-2/neu of the c-erbB family was used. It was designed as a cocktail of two mAbs directed against different epitopes in the cytoplasmic domain of the c-erbB-2 protein: the cytoplasmic domain of recombinant human c-erbB-2/Her-2 oncoprotein (e2–4001) and keyhole limpet haemocyanin (KLH) conjugate of a synthetic peptide, aa 1242–1255,(TAENPEYLGLDVPV) from the C-terminus of the human c-erbB-2 protein (3B5) [15] (c-erbB-2/Her-2/neu oncoprotein Ab-17 clone e2–4001+3B5; Neomarkers, Vienna, Austria).

### c-erbB2 staining and scoring

The routinely processed tumour samples were formalin fixed (4%) and paraffin embedded. Sections (5 μm) on poly-L-lysine-coated slides were used after drying in an oven for 10 h at 56°C. After dewaxing and peroxidase blocking, the pretreatment procedure for antigen retrieval was done in citrate buffer (pH 6.5) for 15 min at 86°C. Then the slides were allowed to cool down for 30 min and washed with Tris buffer (pH 6.5) for 10 min (20°C). The immunoreactions were performed for 30 min with the 1:50 diluted Ab-17 primary antibody at 20°C. After washing in Tris buffer, slides were incubated for 60 min with antimouse antibodies of the EnVision kit (20°C) (Dako, Vienna, Austria). Finally, the preparations were developed in diaminobenzidine (DAB) and counterstained with haemalum.

### Controls

For every case, the evaluation of the immunoreactions was done on slides with tumour parts as well as adjacent normal thyroid tissue as internal control. In addition, negative controls (without primary antibody) were performed. Moreover, in this series, Her2/neu positive (Dako score +++) and negative (Dako score −) breast cancer slides were stained. The Dako cytospin slides (Hercep test) were used as a supplementary control. The complete set of slides was incubated within one process.

### Evaluation

Scoring of the c-erbB2/ Her2/neu immunostaining was independently performed by two pathologists (P.O. and C.E.). Both assessors were unaware of clinical outcome. The presence of clearly visible dark brown precipitation was considered as immunoreaction. Only cytoplasmic staining was considered for evaluation, independently of pronounced membranous or perinuclear reaction.

Evaluation included the proportion of reactive cells within the tumours as well as the staining intensity. The proportion score described the estimated fraction of positively stained tumour cells (0: no visible reaction; 1: less than 10%; 2: 10–50%; 3: 50–80%; 4: more than 80% of tumour cells stained). The intensity score represented the estimated staining intensity (0: no staining; 1: weak; 2: moderate; 3: strong reaction intensity). As total score, the product of proportion score and intensity score, ranging from 0 to 12, was calculated.

### Fluorescence in-situ hybridisation

Fluorescence in-situ hybridisation (FISH) was performed on ten cases (five papillary and five follicular thyroid carcinomas, with each one total score of 2 and two with total score of 6 and 12) of our series on formalin-fixed, paraffin-embedded tissues using the PathVysion Her-2 DNA probe kit (VYSIS, product no. 30–161060). Samples were pretreated and hybridised according to the manufacturers instructions.

### Statistical analysis

The intensity score and total score were analysed using the non-parametric Mann-Whitney U-test. Data of the two groups were analysed in association with histological tumour type and clinicopathological parameters. As a level of significance, $P<0.05$ was used. For evaluating clinicopathological parameters and the association with Her2neu levels, the $\chi^2$ test was used. All data were processed with the SPSS for Windows statistical software.

## Results

### Immunohistochemistry

The tumours presented with a heterogeneous distribution of Her2/neu positive cells partly as single cells in negative surrounding or sometimes arranged in variably sized cell clusters. In some tumours, large stained areas were also observed.

In papillary thyroid cancer (Fig. 1) specimens, the invasive borders and lymphatic invasions showed a stronger immunostaining than central tumour parts; while, in follicular tumours (Fig. 2), no regularity concerning the distribution of the immunoreaction could be observed. In papillary thyroid cancers, most of the stained tumour cells showed mainly cytoplasmic positivity with partly membraneous and perinuclear accumulation of the oncoprotein; while, in follicular thyroid carcinomas, no membraneous reactivity could be detected. The metastases presented an identical staining pattern to the primary tumours.

In normal adjacent thyroid tissue only in single thyreocytes a very weak reaction was observed. The control slides with breast cancer tissues stained correctly positive and negative but revealed also partly cytoplasmic reactivity in the positive controls.

In the evaluated series of differentiated thyroid carcinomas, we found six cases without adequate immunohistochemical reaction, not only with the Her2/neu antibody, but also with thyroglobulin antibodies used as process control in normal thyroid tissue parts. This phenomenon could be due to excessive formalin fixation of the samples. All six cases were excluded from the study.

### Fluorescence in-situ hybridisation

In addition, the FISH analysis revealed a two-fold amplification (copy number of 4 in two chromosomes 17) of the Her2neu gene in two of ten cases (20%). Both tumours belonged to the group with total score 12, including one papillary and one follicular thyroid cancer, and were among the metastasising group. No highly amplified genes were found in this series.

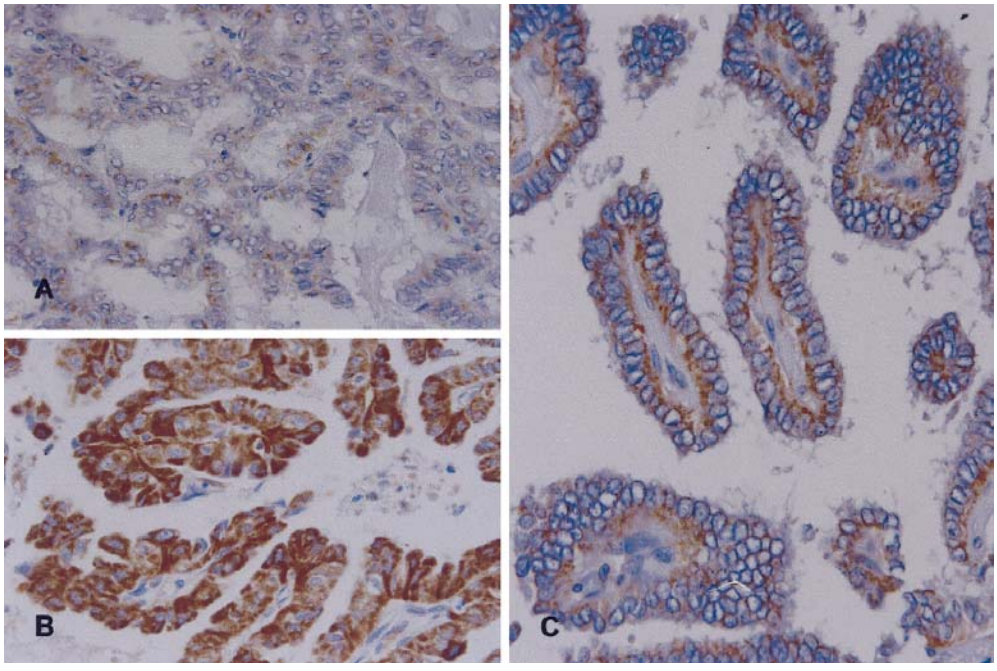



**Fig. 1** Papillary thyroid carcinomas with different reactivity of tumour cells with Her2neu antibody in follicular variant with low-staining intensity counted as score 1 (**A**), and in classical type of papillary thyroid cancer with high intensity (**B**: score 3) and medium intensity (**C**: score 2)

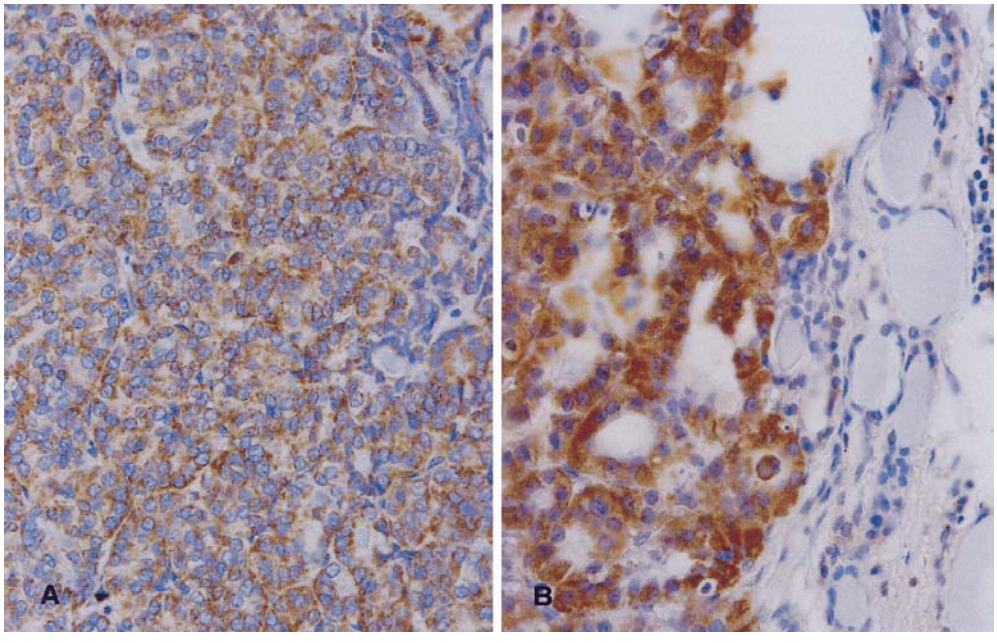



**Fig. 2** Follicular thyroid cancer examples with medium staining intensity scored as 2 (**A**) and high reactivity counted as 3 (**B**) and only minimal reactivity in adjacent regular thyroid tissue

Statistical analysis

All tumours in the groups without (Table 1) and with (Table 2 and Table 3) distant metastasis showed expression of Her2/neu. Patients' sex showed no association with Her2/neu expression, but their ages correlated significantly (Table 4). Increased tumour stage presented with a tendency towards higher Her2/neu expression. Cervical lymph-node metastases did not correlate with Her2/neu levels.

Follicular thyroid cancer samples associated with the clinical outcome brought a significant difference concerning intensity ($P$=0.001) and total score ($P$=0.02). The same analysis of the papillary tumours was significantly different too, concerning intensity ($P$=0.01) and total score ($P$=0.003). Comparing the two groups independently of the histological type, also highly significant differences concerning the intensity of the staining ($P$=0.001) and the total score ($P$<0.001) were found. No correlation of Her2/neu expression with any site of metastases, histological subtypes or variants could be demonstrated (Table 4).

Comparing clinicopathological parameters with development of metastases, a highly significant correlation

**Table 4** Statistical analysis correlating Her2neu expression with clinicopathological parameters. *PTC* papillary thyroid cancer, *FTC* follicular thyroid cancer, *ns* not significant

| Variables | *P* value | |
|---|---|---|
| | Intensity | Total score |
| Sex | n.s. | n.s. |
| Age | 0.003 | 0.009 |
| Stage T | n.s. | 0.01 |
| Cervical lymph-node metastases | n.s. | n.s. |
| Distant metastases | <0.001 | <0.001 |
| Metastases in PTC | 0.01 | 0.003 |
| Metastases in FTC | 0.001 | 0.02 |
| Any site of metastasis | n.s. | n.s. |
| Histology | | |
| PTC | n.s. | n.s. |
| FTC | n.s. | n.s. |
| Other subtypes and variants | n.s. | n.s. |

($P$<0.001) with patients' ages was found with increased metastasis in older patients (over 50 years). No relationship to patients' sex was found. Only two sites of distant metastases correlated with histological tumour types: lung metastases were mainly found in follicular thyroid cancers ($P$=0.004), and liver metastases occurred in papillary thyroid cancers ($P$=0.047).

## Discussion

The role of the erbB2 proto-oncogene in thyroid carcinomas is controversially discussed, especially the prognostic significance of amplification and overexpression. Lemoine et al. [18] analysed a large series of benign and malignant thyroid tumours by means of Southern-blot analysis, polymerase chain reaction (PCR) and immunohistochemistry, without detection of abnormalities in structure or expression of c-erbB-2. So they concluded that activation of this oncogene is not necessarily involved in neoplastic transformation. Haugen et al. [11] investigated the c-erbB-2 protein expression in frozen thyroid cancer specimens and found, in papillary thyroid carcinomas, immunoreactivity at the cell membrane but also cytoplasmic reactivity, similar to our observations. Additionally, in these specimens, the Her2/neu mRNA levels were analysed and found to be significantly elevated. Utrilla et al. (1999) [29] showed only papillary and medullary thyroid (c-cell derived) tumours with a cytoplasmic reaction against Her2/neu, and no immunoreactivity with c-erbB-2 could be detected in follicular thyroid carcinomas using the same antibodies. It was concluded that an elevated c-erbB-2 expression was a typical feature of papillary thyroid tumours. In contrast, in our series, no significant difference within the group of differentiated thyroid carcinomas could be found, probably due to the application of different antibodies and additionally used antigen retrieval techniques.

Our cases presented with a highly significant correlation between Her2/neu expression within papillary as well as follicular thyroid carcinomas and the clinical course concerning metastatic disease. Also, Akslen et al. (1993) [2] examined the prognostic value of c-erbB-2 expression in papillary thyroid carcinomas and found significant correlations between the intensity of the cytoplasmic reaction and extrathyroidal tumour invasion as well as tumour recurrences. Evaluating separately the membraneous reaction brought no correlation with these parameters, but membraneous reactivity was correlated with lack of lymph-node metastases. In our series, predominantly occurring cytoplasmic staining was not associated with cervical lymph-node metastases (Table 4). Also other authors described in different tumour entities such as invasive bladder cancer [17] or breast carcinomas [10, 23] no significant relationship between Her2/neu expression and lymphatic spread.

Similar to the results of Akslen concerning cytoplasmic reactivity [1], we did not find an association between patients' sex and Her2/neu expression in tumours. However, in our cases, highly significant correlations between patients' ages and development of distant metastases as well as between cytoplasmic Her2/neu overexpression and age were found. In their series of papillary thyroid carcinomas, they described an association of lacking c-erbB-2 staining with reduced survival, especially in females, but they did not mention the histological grade of these cases, although they described high-grade histological features to be associated with decreased survival [1]. Similar to these observations, single tumour samples in our series showed in small regions of poorly differentiated tumour parts a distinct reduced reactivity.

The occurrence of cytoplasmic immunoreactions of Her2/neu is not completely understood. Potter et al. [20] discovered a 155-kDa (p155) protein reacting with the antibody. P155 could be localised in the mitochondrial cristae, explaining the partly granular aspect of the staining. In bladder cancer c-erbB-2 amplifications, high mRNA levels and a strong cytoplasmic immunoreaction were observed, correlating with high levels of p155 [7]. It seems to represent reactions with a homologue of the c-erbB2 protein, which might be due to an alteration or an instability of the oncoprotein itself or the mRNA. Soares et al. [26] discussed the occurrence of an unglycosylated form of the c-erbB-2 protein, fitting with the cytoplasmic staining in their series of papillary thyroid cancer, indicating that these proteins tend to stay in the cytoplasmic compartments instead of proceeding to their cell sites [9]. It could also reflect a rapid turnover of c-erbB-2 in the thyroid, leading to its internalisation and degradation as described for the mammary gland [16]. It is difficult to estimate the biological role of cytoplasmic Her2/neu parts, because not much is known about the interaction of Her2/neu with cellular regulations. However, it seems to be an important factor in thyroid tumour development [2], especially concerning extra-thyroidal growth as well as survival [1].

In human breast cancer, membraneous reaction is specific for the c-erbB-2 protein expression and significantly associated with the amplification of the gene. In our FISH analysis, we found only a twofold Her2/neu gene amplification in 20% of the investigated specimens, indicating a minor role in thyroid tumour development. The constellation of mainly cytoplasmic Her2/neu reactivity and lack of highly amplified Her2/neu genes in thyroid carcinomas seem to restrict Herceptin utilisation to a few patients with clearly membraneous staining only.

Her2/neu is known to be overexpressed in several human neoplasms, but the prognostic or therapeutic significance varies within different tumour types. Revillion et al. [21] compared in their review several tumour series concerning the importance of Her2/neu in relation to clinical parameters. Due to the impact of therapeutic use of Herceptin, breast cancer is the best investigated neoplasm concerning Her2/neu at the moment. C-erbB-2 positive tumours had a significantly lower oestrogen and progesterone receptor status, which is important for a possible hormone therapy [19]. Younger patients presented with significantly higher Her2/neu levels than postmenopausal women.

Several studies indicate that a higher Her2/neu level is an independent prognostic parameter for an aggressive behaviour of tumours [9, 19, 20]. Berchuck et al. [4] examined the prognostic value of Her2/neu in ovarian carcinomas and observed a worse response on therapy and a worse clinical outcome. Experimentally in Her2/neu-rich ovarian carcinoma cell lines, a significantly higher motility could be observed [32]. These cells dissociated faster than the cells of a normal population, indicating Her2/neu influence on cellular motility and association with worse clinical outcome. Westermark et al. [31] already found in 1982 that cells of malignant glioma cell lines presented with higher motility and faster dissociated cell colonies after adding EGF.

For the first time, we are able to present Her-2/neu protein overexpression as a predictive factor in differentiated thyroid carcinomas, in both papillary and follicular thyroid carcinomas, concerning the development of distant metastases. Our results of Her2/neu overexpression are correlating with a tendency to more aggressive behaviour and a worse clinical outcome of human carcinomas. It seems that a fewer number of patients suffering from papillary thyroid cancer presenting with membrane-pronounced staining pattern, in addition to standard iodine elimination therapy with the danger of bone-marrow depression, could benefit from further antitumoral strategies with modern antibody therapies.

**Acknowledgements** We thank Ines Tschörner (Institute of Pathology) for her excellent technical assistance.

## References

1. Akslen LA, Varhaug JE (1995) Oncoproteins and tumor progression in papillary thyroid carcinoma: presence of epidermal growth factor receptor, c-erbB-2 protein, estrogen receptor related protein, p21-ras protein, and proliferation indicators in relation to tumor recurrences and patient survival. Cancer 76:1643–1654
2. Akslen LA, Myking AO, Salvesen H, Varhaug JE (1993) Prognostic impact of EGF-receptor in papillary thyroid carcinoma. Br J Cancer 68:808–812
3. Allgayer H, Babic R, Gruetzner KU, Tarabichi A, Schildberg FW, Heiss MM (2000) C-erbB-2 is of independent prognostic relevance in gastric cancer and is associated with the expression of tumor-associated protease systems. J Clin Oncol 18:2201–2209
4. Berchuck A, Kamel A, Whitaker R, Kerns B, Olt G, Kinney R, Soper JT, Dodge R, Clarke-Pearson DL, Marks P (1990) Overexpression of HER-2/neu is associated with poor survival in advanced epithelial ovarian cancer. Cancer Res 50:4087–4091
5. Carcangiu ML, Zampi G, Pupi A, Castagnoli A, Rosai J (1985) Papillary carcinoma of the thyroid. A clinicopathologic study of 241 cases treated at the University of Florence, Italy. Cancer 55:805–828
6. Chazin VR, Kaleko M, Miller AD, Slamon DJ (1992) Transformation mediated by the human HER-2 gene independent of the epidermal growth factor receptor. Oncogene 7:1859–1866
7. Coombs LM, Pigott DA, Sweeney E, Proctor AJ, Eydmann ME, Parkinson C, Knowles MA (1991) Amplification and overexpression of c-erbB-2 in transitional cell carcinoma of the urinary bladder. Br J Cancer 63:601–608
8. Cooper GM (ed) (1997) The cell, a molecular approach. ASM Press, Washington DC
9. Daneker G, Mercurio A, Guerra L, Wolf B, Salem R, Bagli D, Steele G (1987) Laminin expression in colorectal carcinomas varying in degree of differentiation. Arch Surg 122:1470–1474
10. Gullick WJ, Love SB, Wright C, Barnes DM, Gusterson B, Harris AL, Altman DG (1991) C-erbB-2 protein overexpression in breast cancer is a risk factor in patients with involved and uninvolved lymph nodes. Br J Cancer 63:434–438
11. Haugen DR, Akslen LA, Varhaug JE, Lillehaug JR (1992) Expression of c-erbB-2 protein in papillary thyroid carcinomas. Br J Cancer 65:832–837
12. Hedinger C, Williams ED, Sobin LH (1989) The WHO histological classification of thyroid tumors: a commentary on the second edition. Cancer 63:908–911
13. Hou L, Shi D, Tu SM, Zhang HZ, Hung MC, Ling D (1992) Oral cancer progression and c-erbB-2/neu proto-oncogene expression. Cancer Lett 65:215–220
14. Hung MC, Lau YK (1999) Basic science of HER-2/neu: a review. Semin Oncol 26:51–59
15. Hynes NE, Stern DF (1994) The biology of erbB-2/neu/HER-2 and its role in cancer. Biochim Biophys Acta 1198:165–184
16. Kornilova T, Taverna D, Hoeck W, Hynes NE (1992) Surface expression of erb B2 protein is post-transcriptionally regulated in mammary epithelial cells by epidermal growth factor and by the culture density. Oncogene 7:511–519
17. Kruger S, Weitsch G, Buttner H, Matthiensen A, Bohmer T, Marques F, Feller AC, Bohle A (2002) Her2 overexpression in muscle-invasive urothelial carcinomas of bladder. Int J Cancer 102:514–518
18. Lemoine NR, Wyllie FS, Lillehaug JR, Staddon SL, Hughes CM, Aasland R, Shaw J, Varhaug JE, Brown CL, Gullick WJ (1990) Absence of abnormalities of the c-erbB-1 and c-erbB-2 proto-oncogenes in human thyroid neoplasia. Eur J Cancer 26:777–779
19. Lovekin C, Ellis IO, Locker A, Robertson JF, Bell J, Nicholson R, Gullick WJ, Elston CW, Blamey RW (1991) C-erbB-2 oncoprotein expression in primary and advanced breast cancer. Br J Cancer 63:439–443 (erratum 64:202)
20. de Potter CR, Van Daele S, Van de Vijver MJ, Pauwels C, Maertens G, De Boever J, Vandekerckhove D, Roels H (1989) The expression of the neu oncogene product in breast lesions

and in normal fetal and adult human tissues. Histopathology 15:351–362
21. Revillion F, Bonneterre J, Peyrat JP (1998) ERBB2 oncogene in human breast cancer and its clinical significance. Eur J Cancer 34:791–808
22. Rosai J, Carcangiu ML, DeLellis RA (1992) Tumors of the thyroid gland. In: Rosai J (ed) Atlas of tumor pathology, third series, fascicle 5. Armed Forces Institute of Pathology, Washington D.C., pp 96–116
23. Schneider J, Pollan M, Ruibal A, Jimenez E, Lucas AR, Nunez NI, Tejerina A (1999) Histologic high grade and CD44 are independent predictors of a node invasion in early (T1) breast cancer. Tumour Biol 20:319–330
24. Schneider PM, Hung MC, Chiocca SM, Manning J, Zhao XY, Fang K, Roth JA (1989) Differential expression of the c-erbB-2 gene in human small cell and non-small cell lung cancer. Cancer Res 49:4968–4971
25. Slamon DJ, Clark GM, Wong SG, Levin WJ, Ullrich A, McGuire WL (1987) Human breast cancer: correlation of relapse and survival with amplification of the HER-2/neu oncogene. Science 235:177–182
26. Soares P, Sambade C, Sobrinho-Simoes M (1994) Expression of C-erb B2 in tumours and tumour-like lesions of the thyroid. Int J Cancer 56:459–461
27. Stern DF, Heffernan PA, Weinberg RA (1986) P185, a product of the neu proto-oncogene, is a receptorlike protein associated with tyrosine kinase activity. Mol Cell Biol 6:1729–1740
28. Tan M, Yao J, Yu D (1997) Overexpression of the c-erb-2 gene enhanced intrinsic metastasis potential in human breast cancer cells without increasing their transformation abilities. Cancer Res 57:1199–1205
29. Utrilla JC, Martin-Lacave I, San Martin MV, Fernandez-Santos JM, Galera-Davidson H (1999) Expression of c-erbB-2 oncoprotein in human thyroid tumours. Histopathology 34:60–65
30. Weiner DB, Nordberg J, Robinson R, Nowell PC, Gazdar A, Greene MI, Williams WV, Cohen JA, Kern JA (1990) Expression of the neu gene-encoded protein (P185neu) in human non-small cell carcinomas of the lung. Cancer Res 50:421–425
31. Westermark B, Magnusson A, Heldin CH (1982) Effect of epidermal growth factor on membrane motility and cell locomotion in cultures of human clonal glioma cells. J Neurosci Res 8:491–507
32. Wiechen K, Karaaslan S, Dietel M (1999) Involvement of the c-erbB-2 oncogene product in the EGF-induced cell motility of SK-OV-3 ovarian cancer cells. Int J Cancer 83:409–414
33. Xia W, Lau YK, Zhang HZ, Liu AR, Li L, Kiyokawa N, Clayman GL, Katz RL, Hung MC (1997) Strong correlation between c-erbB-2 overexpression and overall survival of patients with oral squamous cell carcinoma. Clin Cancer Res 3:3–9
34. Yokota J, Yamamoto T, Miyajima N, Toyoshima K, Nomura N, Sakamoto H, Yoshida T, Terada M, Sugimura T (1988) Genetic alterations of the c-erbB-2 oncogene occur frequently in tubular adenocarcinoma of the stomach and are often accompanied by amplification of the v-erbA homologue. Oncogene 2:283–287
35. Yoshida K, Tsuda T, Matsumura T, Tsujino T, Hattori T, Ito H, Tahara E (1989) Amplification of epidermal growth factor receptor (EGFR) gene and oncogenes in human gastric carcinomas. Virchows Arch 57:285–290
36. Yu D, Wang SS, Dulski KM, Tsai CM, Nicolson GL, Hung MC (1994) C-erbB-2/neu overexpression enhances metastatic potential of human lung cancer cells by induction of metastasis-associated properties. Cancer Res 54:3260–3266
37. Yu DH, Hung MC (1991) Expression of activated rat neu oncogene is sufficient to induce experimental metastasis in 3T3 cells. Oncogene 6:1991–1996
38. Zhang X, Silva E, Gershenson D, Hung MC (1989) Amplification and rearrangement of c-erb B proto-oncogenes in cancer of human female genital tract. Oncogene 4:985–989

Virchows Arch (2003) 442:329–335
DOI 10.1007/s00428-003-0786-2

ORIGINAL ARTICLE

**Elin Richardsen · Tanja Ukkonen · Tone Bjørnsen · Elin Mortensen · Lars Egevad · Christer Busch**

# Overexpression of IGBFB2 is a marker for malignant transformation in prostate epithelium

Received: 20 September 2002 / Accepted: 30 January 2003 / Published online: 1 April 2003
© Springer-Verlag 2003

**Abstract** Insulin-like growth factor binding protein 2 (IGFBP2) has been shown to be overexpressed in prostatic intraepithelial neoplasia (PIN) and invasive cancer and the serum level to parallel that of prostate-specific antigen (PSA) in prostate cancer. A combination of cDNA and tissue microarray results recently demonstrated overexpression of IGFBP2 in hormone refractory prostate cancer, indicating that the IGF system may be part of a key growth regulatory pathway in prostate cancer. The present study reexamines the immunohistochemical expression of IGFBP2 and its relationship to grade in tissue from 193 radical prostatectomy specimens from patients with localized prostate adenocarcinoma. We found a significant overexpression of IGFBP2 in all instances of PIN and in more than 90% of cancers regardless of the grade. An intense overexpression was noted in the neuroendocrine cells in normal glands as well as in cancer. The IGFBP2 expression was also analyzed in 18 cases of biopsy diagnosed prostate cancer. In all these cases, the glands interpreted as invasive cancer in hematoxylin-eosin stained sections overexpressed IGFBP2, without a significant correlation to grade. We conclude that overexpression of IGFBP2 is a powerful marker for malignant transformation in the prostate epithelium and suggest that optimized immunohistochemical detection of IGFBP2 expression may be an adjunct tool in the diagnosis of prostate cancer.

E. Richardsen (✉) · T. Ukkonen · T. Bjørnsen · E. Mortensen · C. Busch
Department of Pathology,
University Hospital of Northern Norway,
9038 Tromsø, Norway
e-mail: elin.richardsen@unn.no
Tel.: +47-7-7627208
Fax: +47-7-7627204

L. Egevad
Department of Pathology and Cytology,
Karolinska Hospital,
171 76 Stockholm, Sweden

**Keywords** Prostate · Benign hyperplasia (BPH) · Prostatic intraepithelial neoplasia (PIN) · Invasive carcinoma · Insulin-like growth factors · IGFBP2

## Introduction

The insulin-like growth factors (IGFs) I and II are produced by a variety of tissues and are potent mitogens in normal and malignant cells [2, 27]. They play an important role in cell proliferation and metabolism [9]. In biological fluids [26], they are non-covalently bound to IGF-binding proteins (IGFBPs), which are a family of six proteins binding IGFs with high specificity. IGFBP2 is a major prostatic IGFBP. IGFBP2 has previously been indicated to be immunohistochemically overexpressed in prostate cancer and prostatic intraepithelial neoplasia (PIN) [12, 32, 34, 35] A combination of cDNA and tissue microarray results validated overexpression of IGFBP2 in malignant gliomas [28] and hormone refractory prostate cancer [4], indicating that the IGF system may be a key growth regulatory pathway in prostate cancer. This study and the differences in correlation to grade reported in previous studies provoked our interest to test IGFBP2 immunoexpression in two independent materials of prostate cancer without regard to possible hormone sensitivity.

The aim was to assess the extent and pattern of expression in high-grade PIN, and in the different grades of prostate cancer, to determine whether immunohistochemical demonstration of IGFBP2 overexpression is a consistent marker of malignant transformation of prostate epithelium and whether its assessment could have a value as an adjunct tool in the often-difficult diagnosis of prostate cancer.

## Materials and methods

### Patients

Paraffin blocks from total prostatectomy specimens were obtained from the archives of the Departments of Pathology, University

Hospitals in Tromsø, Norway and Uppsala, Sweden. The former group consisted of 119 and the latter of 74 patients with prostate cancer. Using total prostatectomy specimens, 16 patients were diagnosed with PIN along with cancer; using transurethral resection material (TUR) 14 patients were shown to have benign hyperplasia (BPH) without cancer; and 15 specimens from patients were diagnosed as normal. These specimens were all extracted from the archives of Department of Pathology, Tromsø. Initially 18 specimens with BPH were retrieved. After review by a uro-pathologist of these specimens initially judged as normal, four cases were diagnosed as PIN because of cellular atypia and were hence excluded.

Blocks with core biopsies from 16 patients who were examined because of suspicious digital rectal examination findings or elevated serum prostate-specific antigen (PSA) levels. Biopsies in which a diagnosis of carcinoma was made based on judgement of hematoxylin-eosin stained slides were used to assess whether IGFBP2 immunostaining detected these lesions.

### Tissue preparation

The total prostatectomy specimens were processed as described [10], i.e., whole-mount sections were prepared at 3–4 mm, stained with hematoxylin-eosin and examined for the distribution of cancer. From the slide with the largest tumor area, representative tumor areas were serially sectioned at 4 $\mu$m for immunohistochemistry. The malignancy of the tumor occupying these areas was graded 1–5 and scored 2–10 according to Gleason [14]. One to five areas with cancer were marked in each case and punched out using a cylindrical metal punch device with 10-mm diameter. Tissue arrays of each 5–6 punched cylinders were made by melting them into one block. These tissue-array blocks were then sectioned at 4-$\mu$m for hematoxylin-eosin staining and for immunohistochemistry.

PIN is either low grade or high grade [3, 13], reflecting the degree of cellular atypia as well as architectural abnormality. Blocks from 16 cases in which areas with high-grade PIN had been identified were punched, all specimens being from patients operated with total prostatectomy. A set of multiblocks for PIN were sectioned and stained as above.

### Immunohistochemistry

Sections from the multiblocks were stained with hematoxylin-eosin. Areas with normal tissue, BPH, PIN and carcinoma of all grades were encircled.

- 4-$\mu$m-thick paraffin sections were heated at 60°C for at least 15 min
- Sections were deparaffinized for 3×5 min in xylene, 2×2 min in 100% EtOH, 2×2 min in 90% EtOH, in $dH_2O$, rinsed in PBS pH 7.4
- Retrieval with cooking in citrate buffer pH 7.3 in microwave oven (Whirlpool) at 450 W, 2 h and 10 min
- Staining performed with Dako EnVision+ system, peroxidase (DAB), rabbit kit (Dako, Copenhagen, Denmark), as described according to manufacturer:
  - Peroxidase blocking (step 1) was for 5 min
  - Primary antibody polyclonal goat anti-IGFBP2 (Santa Cruz Biotechnology, Inc., CA., USA) was incubated for 30 min (concentration 1:800), (step 2)
  - Secondary antibody biotinylated rabbit anti-goat immunoglobulins (Dako) was incubated for 30 min (concentration 1:600)
  - Peroxidase-labeled polymer was incubated for 30 min (step 3)
  - Liquid DAB+ substrate chromogen was incubated for 4 min (step 4)
- Tissue sections were counterstained with hematoxylin and dipped in the bluing reagent (Scott's liquid: 41.7 mM $NaHCO_3$, 81.1 mM $MgSO_4 \times 7H_2O$ in $dH_2O$), mounted and cover-slipped.

All steps—except step 4—were performed on a Kinetic Slide Stainer (Biocare Medical, Walnut Creek, CA, USA) at +24°C on an Orbital shaker (Biocare Medical). Step 4 was done at room temperature on a shaker. All of the specimens in both materials as well the controls and the core biopsies were stained with monoclonal antibody identifying high-molecular-weight cytokeratins (34$\beta$E12, Dako recognizing cytokeratins 1, 5, 10 and 14) to mark basal cells. In areas diagnosed as carcinoma, all glands were lacking basal cells.

### Assessment of type, extent and intensity of the immunohistochemical staining

The immunostaining results were assessed semi-quantitatively using a modified McCarthy's H scoring system [23]. The whole section was scanned at low power and the percentage of tumor cells that were negative, weakly, moderately or strongly stained was estimated. Each percentage figure was multiplied by 0, 1, 2 or 3, respectively, reflecting the intensity of their staining: none, weak, moderate or strong.

#### *Immunoexpression score*

Immunoexpression score (IEXP-SC)=AOX × ISI, where AOX = percentage cellular area of the tumor with overexpression and ISI = immunostaining intensity. The product gives a score from 0 to 300, which was expressed as:

| | |
|---|---|
| *negative* | $-\text{IEXP} - \text{SC} = 0 - 50$ |
| *weakly positive* | $-\text{IEXP} - \text{SC} = 51 - 100$ |
| mod*erately positive* | $-\text{IEXP} - \text{SC} = 101 - 200$ |
| *stongly positive* | $-\text{IEXP} - \text{SC} = 201 - 300$ |

## Results

### Gleason score distribution

As displayed in Fig. 1, regarding the distribution of Gleason scores, the Tromsø material showed a tendency toward higher scores. The majority represented Gleason

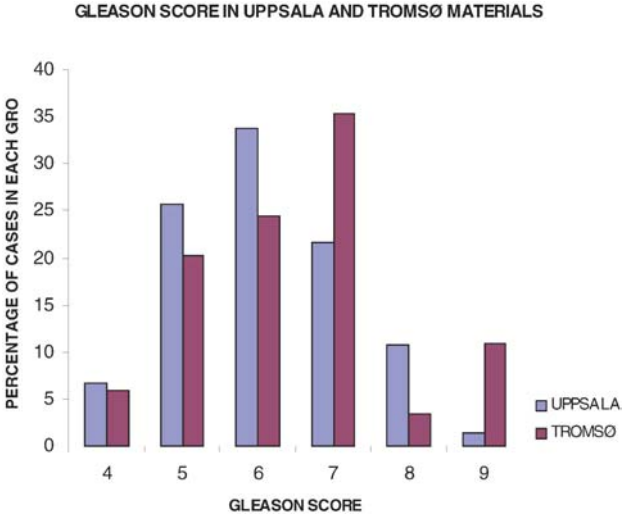



**Fig. 1** Distribution of Gleason scores in the Tromsø and Uppsala materials

**Table 1** Overexpression of insulin-like growth factor binding protein 2 (IGFBP2) in normal prostate epithelium, prostatic intraepithelial neoplasia (PIN) and cancer

| | Tromsø material | | Uppsala material | |
|---|---|---|---|---|
| | Overexpressed Area (%) | No. cases/total (%) With overexpression | Overexpressed Area (%) | No. of cases/total (%) With overexpression |
| Normal epithelium | 0 | 0/96 (0%) | 0 | 0/61 (0%) |
| PIN* | 100 | 26/26 (100%) | 100 | 31/31 (100%) |
| Cancer** | >90 | 103/119 (87%) | >90 | 56/74 (76%) |
| <90 $E_{max}$ | 16/119 (13%) $E_{max}$ | <90 $E_{max}$ | 18/74 (24%) $E_{max}$ | |

* Areas with PIN were from the same sections as areas with carcinoma. Only the IGFBP2 overexpression in PIN lesions was noted. The intensity was not graded. In BPH (from the archives) there was an expression of IGFBP-2, but the intensity of the staining was very weak in all specimens and was indistinguishable from that in normal epithelium

** The total number of cancers in both material was 193. In all cancers IGFBP2 was overexpressed. The extent of the staining was assessed as > or <90%. There was a significant difference between the two materials (87% of the cases with carcinoma in Tromsø material overexpressed IGFBP2 in >90%, 76% of the tumor area compared with in the Uppsala material overexpressed IGFBP2 in >90; uncorrelated Chi-square *P* value=0.03)

scores 5–7 and fewer cases with scores 4, 8 and 9. The slides from both materials were analyzed by two pathologist (E.R. and C.B.). In Uppsala, the urologists are somewhat more reluctant to perform radical prostatectomy in patients with higher grade carcinoma than the Tromsoe tradition. This could possibly explain the difference in grade distribution between the two materials.

## Immunohistochemical expression of IGFBP2

The overall distribution of the extent of IGFBP2 expression in the two materials is given in Table 1 and Fig. 2.

### *Normal epithelium*

Prostate tissue contains both stromal and epithelial cells. The stroma surrounds the acinar structures, which consist of two types of epithelial cells: luminal epithelial cells and the basal cells. The normal luminal epithelial cells showed a very weak expression of IGFBP2 with a granular of positive staining in the supranuclear region of the cells, probably corresponding to the Golgi apparatus, but mostly they were negative (Fig. 3 A, B). Basal cells were negative.

Normal glands seen in the core biopsies showed a slightly stronger staining pattern than in similar glands in total prostatectomy specimens.

### *Benign prostatic hyperplasia*

All cases of BPH were almost negative or very weakly stained. The intensity of the staining was judged as either 0 or 1. The staining was granular, again mostly localized to Golgi-area of the cytoplasm (Fig. 3C) and was essentially identical to the normal glands, with slight variability, mainly with variable degree of distension of the acini.

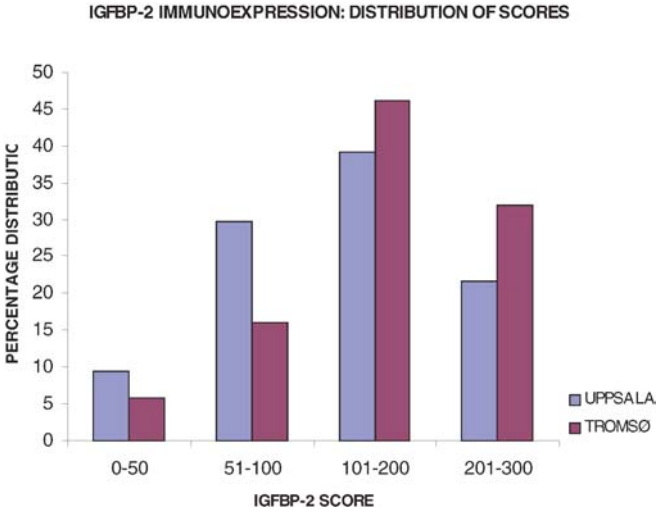



**Fig. 2** Distribution of insulin-like growth factor binding protein 2 (IGFBP2) scores in the Uppsala and Tromsø materials

### *Prostatic intraepithelial neoplasia*

Sections from 16 patients with areas of high-grade PIN were analyzed. There was an overexpression of IGFBP2 in all PIN lesions. The staining was variable; some showed a pancytoplasmatic staining, some a more diffuse granular staining in the cytoplasm of the epithelial cells, and in others the staining was more localized to the Golgi area in the cytoplasma (Fig. 3D, E). The intensity of the staining varied but was significantly stronger than in normal epithelium or hyperplasia.

### *Invasive carcinoma*

The pattern of positive staining for IGFBP2 in carcinoma was the same as that described for PIN above (Fig. 3F, G). The staining was mostly granular and most concentrated in the Golgi area of the cytoplasm, but there was also pancytoplasmatic and diffuse granular staining. The

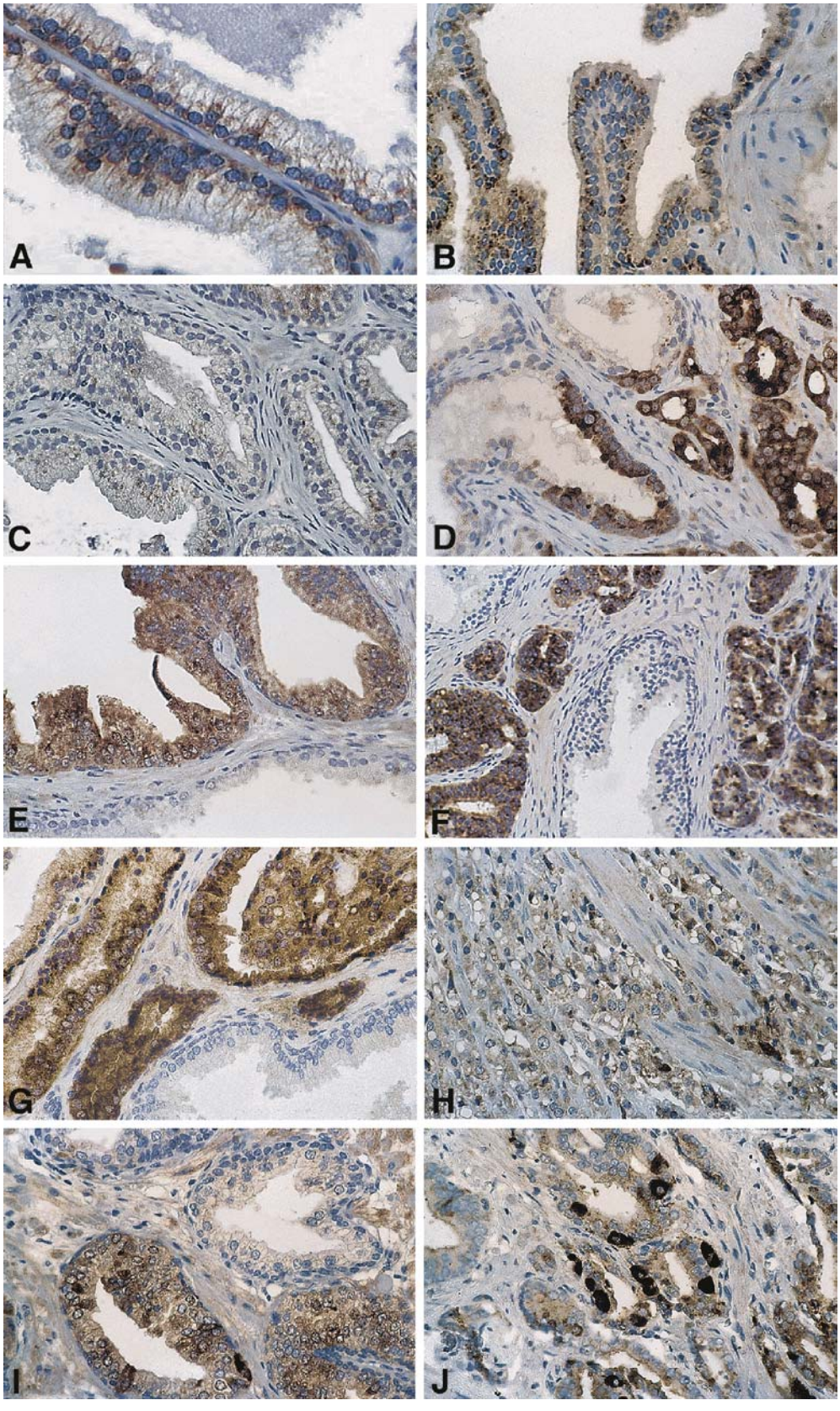



**Fig. 3 A–I** Immunoexpression of insulin-like growth factor binding protein 2 (IGFBP2) in: normal glandular epithelium (**A**), hyperplastic epithelium (**B** and **C**), normal glandular epithelium with adjacent emerging prostatic intraepithelial neoplasia (PIN) and to the right invasive carcinoma (**D**), PIN (**E**), normal glands intermingled with invasive cancer Gleason grade 3 (**F**), normal glands and Gleason grade-3 and grade-4 glands of invasive cancer (**G**), poorly differentiated cancer Gleason grade 5 (**H**), and glandular structures with intensely IGFBP2-positive cells resembling neuroendocrine cells (**I**). **J** Chromogranin immunostaining of cells of the type seen in **I** (**J**)

staining intensity of tumor cells was assessed by comparing them to the staining of adjacent normal epithelial cells. Thus, there was a very distinct difference in the staining pattern between normal epithelium and specimens with high-grade PIN or cancer. As seen in Table 1, the majority of cases with invasive carcinoma (87% and 76% in the Tromsø and Uppsala material, respectively) showed an overexpression in more than 90% of the cancer cells. In the remaining cases, all showed overexpression, most of them in more than 50% of the tumor cells.

The distribution of IGFBP2 immunoexpression scores showed show a significant difference between the Uppsala and the Tromsø materials: 87% of the cases with carcinoma from Tromsø material overexpressed IGFBP2 in more than 90%, while 76% of the tumor area relative to that in the Uppsala material overexpressed IGFBP2 in more than 90% (uncorrelated Chi-square $P$ value=0.03). This difference could possibly be due to the fact that the Uppsala material is about 5 years older than the Tromsø material. This could influence antigen retrieval.

In some of the cases with carcinoma, there were a few cells with very strong positive IGFBP2 staining (Fig. 3I). These cells were also positive for chromogranin A (Fig. 3J), i.e., they were of the neuroendocrine type [1].

The stromal cells, i.e., smooth muscle cells and fibroblasts were occasionally weakly stained and were independent of whether it was in normal prostate tissue, BPH, PIN or carcinoma.

In Tromsø material, the stromal cells adjacent to carcinoma were stained in 37 of 119 cases, and in 24 of 119 cases with normal prostate tissue. In the Uppsala material, the stromal cells were stained in 18 of 74 areas with carcinoma, and 9 of 74 areas with normal prostate tissue (in the same cases). Thus, in many cases, there was no expression in stromal cells at all.

### Statistical analysis

Fisher's exact probability test was used to evaluate whether there was a difference in IGFBP2 expression in Tromsø material relative to the Uppsala material, and whether there was a change in IGFBP2 expression with a change of Gleason grade [29]. We did find a significant difference in Tromsø material relative to the Uppsala material, in that the proportion of cases where more than 90% of tumor cells were stained was higher in the Tromsø material, but the extent and pattern of IGFBP2 expression was the same in low-grade carcinoma as in high-grade carcinoma in both materials.

## Discussion

We chose to investigate whether overexpression of IGFBP2 was consistent enough to have a potential in distinguishing PIN or invasive cancer from the normal in operative specimens or core biopsies. Some reports indicated that it may be so, because of elevated IGFBP2 in serum in patients with prostate cancer [6], and a recent study validated overexpression of IGFBP2 with tissue microarray technique, in patients with hormone refractory prostate cancer [4]. We compared two different materials from two centers to determine possible differences in the immuno-reactivity of IGFBP2, which might be due to different routines in sample handling.

Our data indicate that there is a rather dramatic and distinct overexpression associated with malignant transformation, i.e., in PIN and invasive carcinoma, seen as increased extent and intensity of IGFBP2 immunoreactivity.

Normal prostate epithelium tissue and that of BPH were negative or very weakly positive and localized to the Golgi area in the cytoplasm. We were unable to demonstrate any differences between PIN and carcinoma regarding extent and/or intensity of the staining. The over-expression in both PIN and carcinoma varied from weak, moderately to strong, and the expression from diffuse granular staining, to strong pancytoplasmatic staining. Others have reported that IGFBP2 expression was stronger with increased malignancy grade [35]. We did not find a significant correlation between the grade of prostate cancer and the expression of IGFBP2, however (not illustrated). Regarding the Gleason grade distribution, there was a slight but significant difference between the Tromsø and the Uppsala materials, however.

A possible explanation could be that a difference in a combination of immunohistochemistry and mRNA hybridization has indicated a significantly higher expression of IGFBP2 and IGFBP3 in PIN and cancer relative to normal prostatic epithelium [34], but with no correlation between IGFBP2 expression and stage or grade. In another study [12], a correlation between increasing malignancy grade and increased IGFBP2 expression was noted. However, here determination of the mRNA content in tissue samples was performed, not in situ hybridization, nor immunohistochemistry. Thus, this technique does not take the composition of the tissue compartment into account. For example, the lower grades may have a larger relative stromal component than the higher grades. This could distort the results and give higher values in high-grade cancer due to less "dilution" by stroma.

A recent case-control study from Northern Sweden measured levels of IGF-I, IGFBP1, IGFBP2, IGFBP3 and insulin in plasma samples from 149 men who had a diagnosis of prostate cancer between 1 month and 10 years after blood collection and were compared with 298 control men. The authors found an increased risk of prostate cancer in men with elevated plasma IGF-I, particularly in younger men. Prostate cancer risk was not associated with levels of IGFBP1, IGFBP2 or insulin. However, patients with established prostatic carcinoma have been shown to have elevated serum IGFBP2 levels, which parallel the PSA levels [6].

The IGFs I and II are produced by a variety of tissues and are potent mitogens in normal and in malignant cells. They play an important role in cell proliferation and

metabolism [9, 11, 24]. In biological fluids, they are non-covalently bound to IGFBPs, which are a family of six proteins binding IGFs with high specificity. One of these is IGFBP2, localized to chromosome 2, region q33-q34. In the male reproductive tract, IGFBP2 plays an important role, both as a regulator of normal and abnormal function. IGFBP2 is in high concentration in seminal plasma [20, 25] as well as in prostate epithelial and stromal cells.

In normal glandular epithelium and in BPH, the IGFBP2 expression has been previously shown to be weaker than in carcinoma. [15, 16, 17, 21, 31, 32, 33, 34, 35]. BPH involves varying amount of stroma, epithelium and smooth muscle. Normal prostate epithelial cells secrete IGFBP2 and IGFBP4. IGFBP2 expression in prostatic stromal cells from patients with BPH is dramatically reduced and that may be because growth of stromal cells may be promoted both by a relief from inhibition, due to reduced IGFBP2, as well as via potentiation of IGF-II action by IGFBP5 [7, 33]. In malignant prostate epithelium, IGFBP4-mRNA and IGFBP5 immunoreactivity are elevated relative to normal epithelium. IGFBP6 is present in both benign and malignant epithelium [33]. IGFBP5 is made by fibroblasts and is supposed to be sequestered in epithelium. Apparently, the IGF system plays a key role in the cross talk between stroma and epithelium normally, as well as in BPH and cancer. The regulation is complex and much is yet to be learned about the details.

In recent years the new and powerful techniques using cDNA microarrays and tissue microarrays have helped to identify some very interesting molecules, which are supposed to be of particular interest for prostate cancer. Above all, P503S, P504S, P510S and hepsin as well as members of the protein kinase C family have been indicated to be powerful markers for malignant transformation using immunohistochemistry [5, 8, 18, 19, 22, 36, 37]. The relative sensitivity and specificity of the new potential malignancy markers including IGFBP2 need to be carefully studied in large clinical materials. Possible functional relationships between them also need to be clarified.

This study has extended previous observations regarding overexpression of IGFBP2 in PIN and prostate cancer and has tested its validity in two independent materials using the same immunohistochemical technique. Furthermore, the overexpression has been quantified and we have shown that it might become an important adjuvant diagnostic tool in PIN and prostate cancer in routine diagnostic work. As mentioned, we are presently comparing IGFBP2 overexpression with that of p504s and other indicated malignancy markers for prostate cancer.

We conclude that IGFBP2 immunostaining of prostate tissue may well help in the diagnosis of cancer. This possibility will be tested in a large material of primarily negative core biopsies in a forthcoming study and compared with other markers for malignant transformation.

The IGFBP2 overexpression already at the preinvasive stage is extremely interesting and should provoke further studies into the mechanisms responsible. So far, very little is known or understood regarding the complex regulation of IGFs, IGF receptors and IGFBPs in cancer.

## References


1. Abrahamsson PA, di Sant'Agnese PA (1993) Neuroendocrine cells in the human prostate gland. J Androl 14:307–309
2. Bondy CA, Werner H, Roberts CT, LeRoith D (1990) Cellular pattern of insuline-like growth factor-I (IGF.I) and type I IGF receptor gene expression in early organogenesis: comparison with IGF-II gene expression. J Mol Endocrinol 4:1386–1398
3. Bostwick DG, Brawer MK (1987) Prostatic intraepithelial neoplasia and early invasion in prostate cancer. Cancer 59:788–794
4. Bubendorf L, Kolmer M, Kononen J, Koivisto P, Mousses S, Chen Y, Mahlamaki E, Schraml P, Moch H, Willi N, Elkahloun AG, Pretlow TG, Gasser TC, Mihatsch MJ, Sauter G, Kallioniemi OP (1999) Hormone therapy failure in human prostate cancer: analysis by complementary DNA and tissue microarrays. J Natl Cancer Inst 91:1758–1764
5. Chaib H, Cockrell EK, Rubin MA, Macoska JA (2001) Profiling and verification of gene expression patterns in normal and malignant human prostate tissues by cDNA microarray analysis. Neoplasia 3:43–52
6. Cohen P, Peehl DM, Stamey TA, Wilson KF, Clemmons DR, Rosenfeld RG (1992) Elevated levels of insulin-like growth factor-binding protein-2 in the serum of prostate cancer patients. J Clin Endocrinol Metab 79:1031–1035
7. Cohen P, Nunn SE, Peehl DM (2000) Transforming growth factor-$\beta$ induces growth inhibition and IGF-binding protein-3 production in prostatic stromal cells: abnormalities in cells cultured from benign prostatic hyperplasia tissue. J Endocrinol 164:215–223
8. Cornford P, Evans J, Dodson A, Parsons K, Woolfenden A, Neoptolemos J, Foster CS (1999) Protein kinase C isoenzyme patterns characteristically modulated in early prostate cancer. Am J Pathol 154:137–44
9. Dhanasekaran SM, Barrette TR, Ghosh D, Shah R, Varambally S, Kurachi K, Pienta KJ, Rubin MA, Chinnaiyan AM (2001) Delineation of prognostic biomarkers in prostate cancer. Nature 412:822–826
10. Egevad L, Engström K, Busch C (1998) A new method for handling radical prostatectomies enabling fresh tissue harvesting, whole mount sections and landmarks for alignment of sections. J Urol Pathol 9:17–28
11. Ferry JR, Katz LEL, Grimberg A, Cohen P, Weinzimer SA (1999) Cellular actions of insulin-like growth factor binding proteins. Horm Metab Res 31:192–202
12. Figueroa JA, De Raad S, Tadlock L, Speights VO, Rinehart JJ (1998) Differential expression of insuline-like growth factor binding proteins in high versus low Gleason score prostate cancer. J Urol 159:1379–1383
13. Foster CS (2000) Cellular features distinguishing benign and malignant phenotypes in prostatic biopsies. Hum Pathol 31:1445–1447
14. Gleason DF (1977) Histologic grading and clinical staging of prostatic carcinoma. In: Tannenbaum M (ed) Urologic pathology. Lea and Fiebiger, Philadelphia, pp 171–198
15. Grimberg A, Cohen P (1999) Growth hormone and prostate cancer: guilty by association? J Endocrinol Invest 22:64–73
16. Grimberg A, Cohen P (2000) Role of insuline-like growth factors and their binding proteins in growth control and carcinogenesis. J Cell Physiol 183:1–9
17. Ho JP, Baxter RC (1997) Insulin-like growth factor-binding protein-2 patients with prostate carcinoma and benign prostatic hyperplasia. Clin Endocrinol 46:145–154
18. Jiang Z, Woda BA, Rock KL, Xu Y, Savas L, Khan A, Pihan G, Cai F, Babcook JS, Rathanaswami P, Reed SG, Xu J, Fanger

GR (2001) P504S: a new molecular marker for the detection of prostate carcinoma. Am J Surg Pathol 25:1397–1404
19. Jiang Z, Wu CL, Woda BA, Dresser K, Xu J, Fanger GR, Yang XJ (2002) P504S/alpha- Methyl-CoA Racemase: a useful marker for diagnosis of small foci of prostatic carcinoma on needle biopsy. Am J Surg Pathol 26:1169–1174
20. Kelley KM, Youngman OH Gargosky SE, Gucev Z, Matsumoto T, Hwa V, Lilly NG, Simpson DM, Rosenfeldt RG (1996) Insulin-like growth factor-binding proteins (IGFBPS) and their regulatory dynamics. Int J Biochem Cell Biol 28:619–637
21. Luo J, Duggan DJ, Chen Y, Sauvageot J, Ewing CM, Bittner ML, Trent JM, Isaacs WB (2001) Human prostate cancer and benign prostatic hyperplasia: molecular dissection by gene expression profiling. Cancer Res 61:4683–4688
22. Magee JA, Araki T, Patil S, Ehrig T, True L, Humphrey PA, Catalona WJ, Watson MA, Milbrandt J (2001) Expression profiling reveals hepsin overexpression in prostate cancer. Cancer Res 61:5692–5696
23. McCarthy KS Jr, Miller LS, Cox EB, Konrath J, McCarthy Sr (1985) Estrogen receptor analyses: correlation of biochemical and immunohistochemical methods using monoclonal antireceptor antibodies. Arch Pathol Lab Med:716–721
24. Menouny M, Binoux M, Babajko S (1998) IGFBP-2 expression in a human cell line is associated with increased IGFBP-3 proteolysis, decreased IGFBP-1 expression and increased tumorgenicity. Int J Cancer 77:874–879
25. Monti S, Di Silverio F, Lanzara S, Varasano P, Martini C, Tosti-Croce C, Sciarra F (1998) Insuline-like growth factor-I and –II in human benign prostatic hyperplasia: relationship with binding proteins 2 and 3 and androgens. Steroids 63:362–366
26. Rajaram S, Baylink DJ, Mohan S (1997) Insuline-like growth factor-binding proteins in serum and other biological fluids: regulation and functions. Endocr Rev 18:801–831
27. Roopmathy R, Valentinis B, Cohen P (1997) Insuline-like growth factor (IGF)-binding Protein-3 induces apoptosis and mediates the effects of transforming growth factor-$\beta$1 on programmed cell death through a p53 and IGF-independent mechanism. J Biol Chem 272:12181–12188
28. Sallinen SL, Kononen J, Sallinen PK, Haapasalo HK, Helin HJ, Pauli TH, Schraml P, Kallioniemi OP, Kononen J (2000) Identification of differentially expressed genes in human gliomas by DNA microarray and tissue chip techniques. Cancer Res 60:6617–6622
29. Shousha S, Peston D (1997) Immunohistochemical demonstration of oestrogen and progesterone receptors in paraffin sections of breast carcinoma. Curr Diagn Pathol 4:176–180
30. Stamey T, McNeal JE, Yemoto CM, Sigal BM, Johnstone JM (1999) Biological determinants of cancer progression in men with prostate cancer. JAMA 281:1395–1400
31. Stattin P, Bylund A, Rinaldi S, Biessy C, D\echaud H, Stenman U-H, Egevad L, Riboli E, Hallmans G, Kaaks R (2000) Plasma insulin like growth factor-I, inslunin-like growth factor binding proteins, and prostate cancer risk: a prospective study. J Natl Cancer Inst 92:1910–1917
32. Tennant MK, Thrasher JB, Twomey PA, Birnbaum RS, Plymate SR (1996) Insulin-like growth factor-binding protein-2 and -3 expression in benign human prostate epithelium, prostate intraepithelial neoplasia, and adenocarcinoma of the prostate. J Clin Endocrinol Metab 81:411–420
33. Tennant MK, Thrasher JB, Twomey PA, Birnbaum RS, Plymate SR (1996) Insulin-like growth factor-binding proteins (IGFBP)-4, -5, and -6 in the benign and malignant human prostate: IGFBP-5 messenger ribonucleic acid localization differs from IGFBP-5 protein localization. J Clin Endocrinol Metab 81:3783–3792
34. Tennant MK, Thrasher JB, Twomey PA, Drivdahl RH, Birnbaum RS, Plymate SR (1996) Protein and messenger ribonucleic acid (mRNA) for the type 1 insulin-like growth factor IGF) receptor is decreased and IGF-II mRNA is increased in human prostate carcinoma compared to benign prostate epithelium. J Clin Endocrinol Metab 81:3774–3782
35. Thrasher JB, Tennant MK, Twomey PA, Hansberry KL, Wettlaufer JN, Plymate SR (1996) Immunohistochemical localization of insulin-like growth factor binding proteins 2 and 3 in prostate tissue: clinical correlations. J Urol155:999–1003
36. Xu J, Stolk JA, Zhang X, Silva SJ, Houghton RL, Matsumura M, Vedvick TS, Leslie KB, Badaro R, Reed SG (2000) Identification of differentially expressed genes in human prostate cancer using subtraction and microarray. Cancer Res 60:1677–1682
37. Yang XJ, Wu CL, Woda BA, Dresser K, Tretiakova M, Fanger GR, Jiang Z (2000) Expression of alpha-Methylacyl-CoA racemase (P504S) in atypical adenomatous hyperplasia of the prostate. Am J Surg Pathol 26:921–925
38. Zhang W, Wang H, Song SW, Fuller GN (2002) Insulin-like growth factor binding protein 2: gene expression microarrays and the hypothesis-generation paradigm. Brain Pathol12:87–94

Virchows Arch (2003) 442:336–342
DOI 10.1007/s00428-003-0787-1

ORIGINAL ARTICLE

**Yves Allory · Delphine Ouazana · Eric Boucher · Nicolas Thiounn · Annick Vieillefond**

# Papillary renal cell carcinoma

## Prognostic value of morphological subtypes in a clinicopathologic study of 43 cases

Received: 18 October 2002 / Accepted: 3 February 2003 / Published online: 4 April 2003
© Springer-Verlag 2003

**Abstract** A series of 43 papillary renal cell carcinomas (PRCCs) were analyzed to investigate the prognostic value of the morphological subtyping (type 1/type 2) proposed by Delahunt and Eble [6]. Twenty-six cases were type 1 (small cuboid cells arranged in single or double layers), 13 cases were type 2 (voluminous eosinophilic cells with irregular pseudostratification pattern), and four cases with oncocytic cells (large eosinophilic cells with round regular nuclei) were distinct from type 2 and grouped apart. All type-1 and oncocytoid-type PRCCs were staged pT1 or pT2, whereas 8/13 type-2 PRCCs were staged pT3 or pT4. Follow-up information (range, 3–113 months; median, 43 months) showed 12 deaths from disease: 2 in the type-1 group,10 in the type-2 group, 0 in the oncocytoid-type group. The Kaplan-Meier analysis showed that pejorative outcome was associated ($P<0.001$) with high stage (pT3/pT4), high nuclear grade (3/4), morphological type 2, absence of foam cells, and abundant fibrous stroma. The multivariate analysis showed that stage and morphological type were independently associated with survival ($P<0.05$). These results support the clinical interest of morphological subtyping of PRCCs in the prognosis evaluation of the patients. The four oncocytoid-type PRCCs had a favorable outcome, but additional data are required to evaluate this type of neoplasm.

A. Vieillefond
Service d'Anatomie Pathologique, Hôpital Cochin, Paris, France

D. Ouazana · N. Thiounn
Service d'Urologie, Hôpital Cochin, Paris, France

Y. Allory (✉)
Service d'Anatomie Pathologique,
Hôpital Tenon, 4 rue de la Chine, 75020 Paris, France
e-mail: yves.allory@tnn.ap-hop-paris.fr
Tel.: +33-1-56016677
Fax: +33-1-56017876

E. Boucher
Laboratoire d'Anatomie Pathologique,
Hôpital militaire de Percy, Clamart, France

**Keywords** Kidney · Neoplasm · Prognosis · Renal cell carcinoma · Papillary renal cell carcinoma

## Introduction

In the revised classification of renal cell neoplasia [15, 30], papillary renal cell carcinoma (PRCC) is recognized as a distinct tumor type, supported by multiple morphological [1, 4, 8, 18, 20, 22, 24], immunohistochemical [10, 24], and genetic [5, 12, 13, 14, 16] studies. PRCCs represent approximately 15–20% of renal epithelial tumors [3, 18, 20] and are typically characterized by a predominant papillary pattern (more than 50% at least of the tumor) [1, 18, 24], a cytokeratin 7-positive immunophenotype [10], and recurrent cytogenetic alterations consistently showing trisomy or tetrasomy of chromosomes 7 and 17, and with a high-frequency loss of chromosome Y, trisomies 12, 16, and 20 [5, 12, 13, 14, 16]. Most studies suggested that PRCC had a more favorable prognosis than conventional (clear cell) renal cell carcinomas (CRCC) [3, 18, 20, 22]. However, large and recent studies, taking into account the stage and the nuclear grade, have revealed a similar prognosis for PRCC in comparison with CRCC [19, 21]. These discrepancies might be related to the broad range of morphological and cytogenetic variants described in PRCC. Indeed, various architectural variants—including trabecular, tubular, solid, and collecting duct-like patterns—and cytological subtypes—basophilic, eosinophilic, or clear cell—have been described [1, 8, 18, 22, 23, 24, 25, 26, 27, 31], and 20% of PRCCs at least have been reported lacking the typical trisomy 17 [5, 11, 13, 14]. Recently, Delahunt and Eble [6] have proposed the existence of two PRCC subtypes, type 1 with papillae covered by a single or double layer of small cells with scanty cytoplasm, and type 2 with papillae covered by cells with abundant eosinophilic cytoplasm, arranged in a pseudostratified or irregularly stratified manner [6]. Interestingly, the tumor stage at diagnosis was significantly higher in type-2 than in type-1 PRCCs, suggesting

these subtypes could be clinicopathologic entities with a different prognosis [6].

In this study, we report a series of 43 consecutively diagnosed cases of PRCC, aiming to: (1) investigate the possibility to classify all the PRCC cases as type 1 or 2, (2) confirm the clinicopathologic features of types 1 and 2, and (3) evaluate the prognostic impact of these morphological subtypes in patients' survival.

## Material and methods

### Case selection

Cases of PRCC diagnosed between January 1992 and July 1998 were retrieved from the files of the Department of Pathology, Cochin Hospital, Paris, France. We included 43 cases according to the following criteria: (1) the carcinoma had a main diameter of more than 1 cm and showed papillary architecture in at least 50% of the tumor (solid variant with packed papillae were included [25]) according to the revised classification of renal tumor [15, 30]; (2) the differential diagnosis (i.e., metanephric adenoma, oncocytoma, CRCC with papillary pattern, eosinophilic chromophobe cell carcinoma, and collecting duct carcinoma) were excluded; (3) the PRCC was not associated with another renal malignant tumor; (4) the demographic data (age, sex) and follow-up information (disease-free and overall survival) obtained from clinical charts were available. Forty cases were treated by radical nephrectomy; three cases were treated by partial nephrectomy with safe margins (one patient with a 2-cm-diameter tumor, two patients with a congenital single kidney).

### Morphological study

Gross examination data (tumor size, extent) were obtained from pathology reports. Hematoxylin–eosin–saffron-stained sections from all cases were reviewed concomitantly by two pathologists (E.B., A.V.), and the following features were evaluated:

1. Type of architecture, classified as papillary, solid-variant, or mixed
2. Cytoplasm characteristics, including size (small or tall) and staining (basophilic or eosinophilic, respectively, if the tumor was predominantly of one cell type, or mixed if both components were conspicuous within the tumor
3. Nuclear size and pleomorphism
4. Tumor necrosis
5. Psammoma bodies
6. Macrophages appearing as foam cells within fibrovascular cores and/or within necrotic area
7. Stroma, described as "scanty" or "abundant and fibrous"
8. Tumor extension through the capsule and/or within (small and large) vessels

The tumors were classified as type-1 PRCC (papillae covered with a single or double layer of small cuboid cells with scanty cytoplasm) or type-2 PRCC (papillae covered by large eosinophilic

**Table 1** Main clinicopathologic features of papillary renal cell carcinoma (*SD* standard deviation, *DOD* dead of disease)

| | | Type 1 ($n$=26) | Type 2 ($n$=13) | Oncocytoid type ($n$=4) |
|---|---|---|---|---|
| Age of patient (years) | Mean ± SD | 61±15 | 59±18 | 56±20 |
| | Range | 29–84 | 18–78 | 38–76 |
| Sex of patient | Male | 24 | 12 | 4 |
| | Female | 2 | 1 | 0 |
| Follow-up (months) | Median ± SD | 47±24 | 22±29 | 44±7 |
| | Range | 9–113 | 3–108 | 41–57 |
| DOD[d] ($n$) | | 2 | 10 | 0 |
| Tumor size (cm) | Mean ± SD | 5.5±3.9 | 6.7±4.4 | 4.5±1.7 |
| | Range | 2–20 | 2.5–15 | 2–6 |
| Stage[a,c] | pT1 | 20 | 4 | 4 |
| | pT2 | 6 | 0 | 0 |
| | pT3 | 0 | 8 | 0 |
| | pT4 | 0 | 1 | 0 |
| Architecture | Tubulopapillary | 22 | 11 | 2 |
| | Solid variant | 0 | 1 | 0 |
| | Mixed | 4 | 1 | 2 |
| Grade[b,c] | 1 | 0 | 0 | 0 |
| | 2 | 26 | 1 | 3 |
| | 3 | 0 | 10 | 1 |
| | 4 | 0 | 2 | 0 |
| Cytoplasm[c] | Basophilic[c] | 4 | 0 | 0 |
| | Eosinophilic[c] | 0 | 9 | 4 |
| | Mixed[c] | 22 | 4 | 0 |
| Necrosis | | 22 | 11 | 4 |
| Psammoma bodies | | 9 | 3 | 1 |
| Foam cells[c] | | 17 | 3 | 3 |
| Conspicuous stroma[d] | | 3 | 10 | 1 |

[a] Sobin et al. [30]
[b] Fuhrman et al. [9]
[c] Statistically different between type 1 and type 2, using Kruskal-Wallis test ($P$<0.01)
[d] Statistically different between type 1 and type 2, using Fisher's exact test ($P$<0.01). Other features are not significantly different between type 1 and 2

cells arranged in a pseudostratified or irregularly stratified manner), defined by Delahunt and Eble [6]. Tumor stage was assigned according to the TNM staging system of the International Union Against Cancer (UICC) [29, 30]. Tumor grade was evaluated on the basis of nuclear size and pleomorphism as described by Fuhrman et al. [9].

### Statistical analysis

The clinicopathologic features of papillary renal cell carcinoma were tested for their association with the histological types 1 and 2, using for continuous variables the student *t*-test (age, tumor size, follow-up time), and for qualitative variables Fisher's exact test (ratio of male to female, necrosis, psammoma bodies, foam cells, stroma, deaths), or the Kruskal-Wallis test (stage, grade, cytoplasm). Survival was defined as the time between surgery and patient death. For the analysis, only deaths with PRCC listed as the underlying cause were considered as events. The Kaplan-Meier method was used to analyze the cumulative survival of patients and the effect of the following parameters on survival: age, tumor size, stage, grade, type 1 or type 2, cytoplasm staining, psammoma bodies, foam cells, stroma, and necrosis. Statistical differences between the groups were determined with the log rank test. A multivariate analysis using the Cox proportional hazards regression model was used to test for independent prognostic value. The statistical analysis was performed with Statistica software (version 5.1; Statsoft France, Paris, France).

## Results

The results are summarized in Table 1. There were 40 men and 3 women in the series, and the mean age at surgery was 60 years.

### Type-1 and type-2 classification

According to the criteria defined by Eble and Delahunt, 28 cases were easily classified as type-1 or -2 PRCCs, but histological subtyping was problematic in 15 cases. Seven of fifteen cases were made of medium-sized cells; we agreed to classify them on the basis of pseudostratification only. Four of fifteen cases displayed significant foci of overlapping features, with papillae covered by small cuboidal cells in the vicinity of large eosinophilic cells; we decided arbitrarily to class them as type-2 PRCCs. Four of fifteen other cases were made of large cells with a striking oncocytic appearance; because of this distinct feature, we decided to consider them separately from the type-2 PRCCs. Eventually, 26 cases were classified as type-1 PRCCs, 13 cases were classified as type-2 PRCCs, and four cases with an oncocytoid pattern were grouped apart.

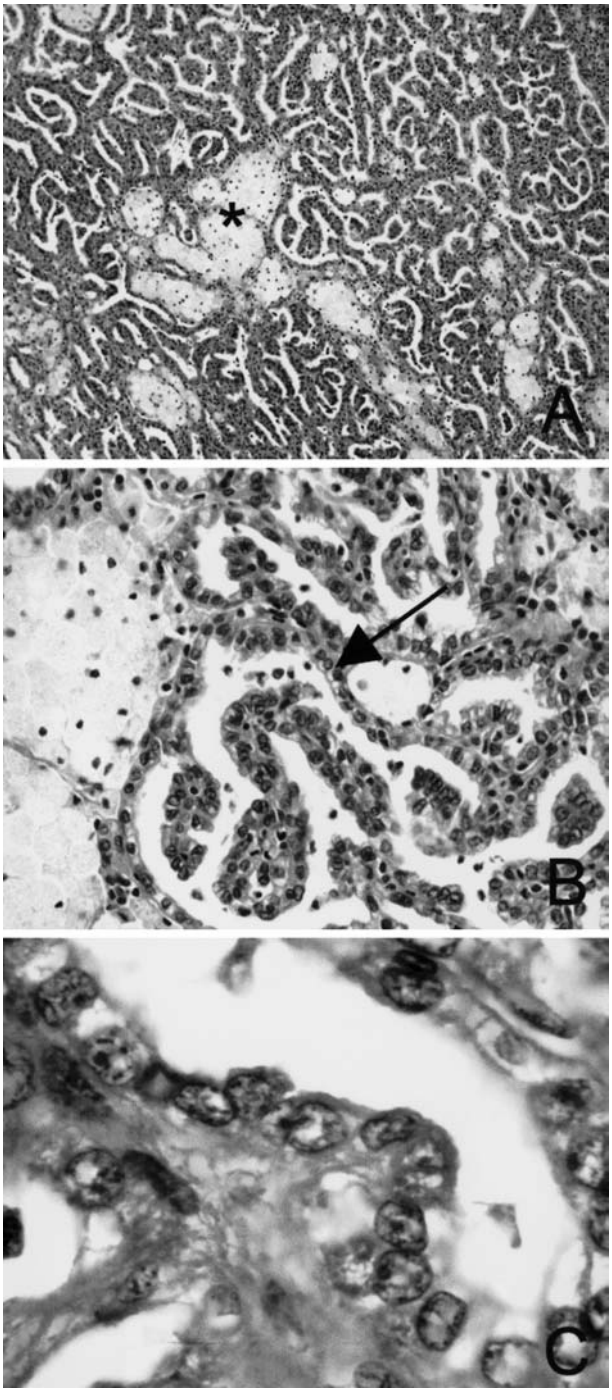



**Fig 1A–C** Type-1 papillary renal cell carcinoma with: (**A**) foam cells within the papillae (*asterisk*); (**B**) small, cuboid monostratified cells (*arrow*); and (**C**) small, regular nuclei

### Comparisons between type-1 and type-2 PRCCs

The mean age of the patients and the male to female ratio was not significantly different between the two groups. The main tumor was associated with distant papillary adenomas (size less than 0.5 cm) in 6 of 26 cases in type-1 PRCCs, and 1 of 13 cases in type-2 PRCCs. The mean size of the main tumor was 5.5 cm in type-1 and 6.7 cm in type-2 PRCCs, without statistical difference. The architecture was predominantly papillary, without difference between the two groups. In type-1 PRCCs, the stalk of papillae was covered by small and cuboid cells with small ovoid nuclei, arranged in a regular and monostratified pattern (Fig. 1). In type-2 PRCCs, the cells lining papillae were large and columnar, predominantly eosinophilic,

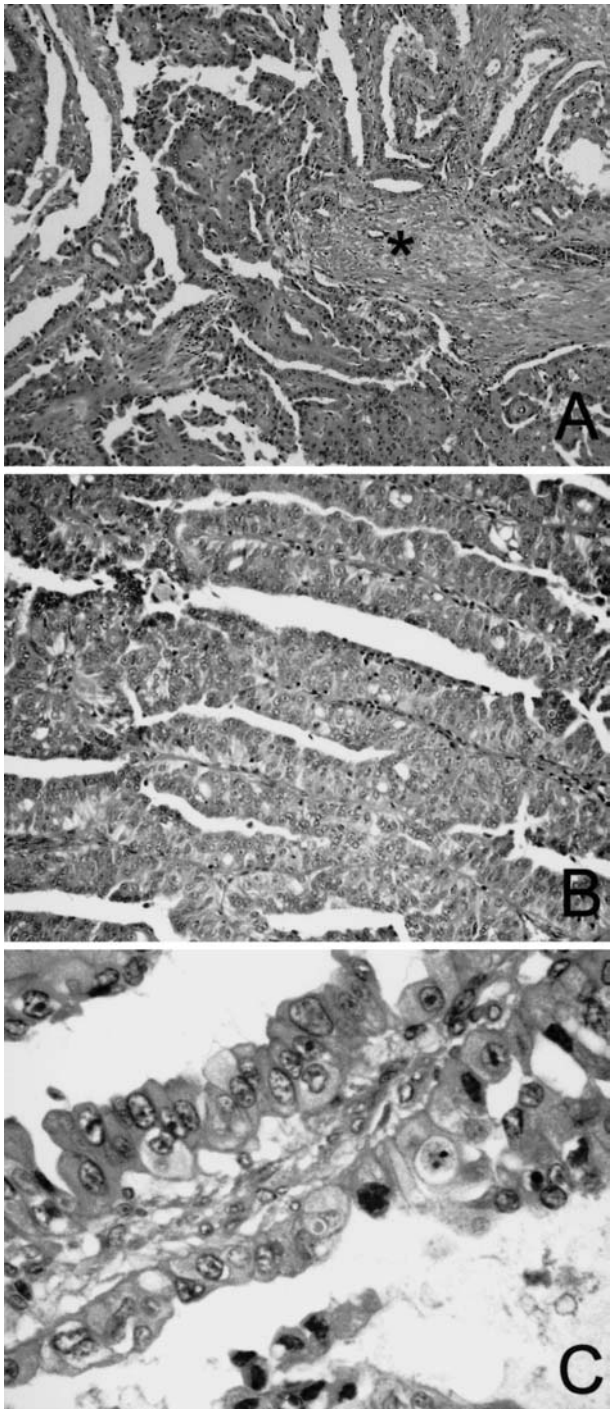



**Fig. 2A–C** Type-2 papillary renal cell carcinoma with: (**A**) abundant fibrous stroma (*asterisk*); (**B**) broad pseudostratified papillae; and (**C**) large and irregular nuclei

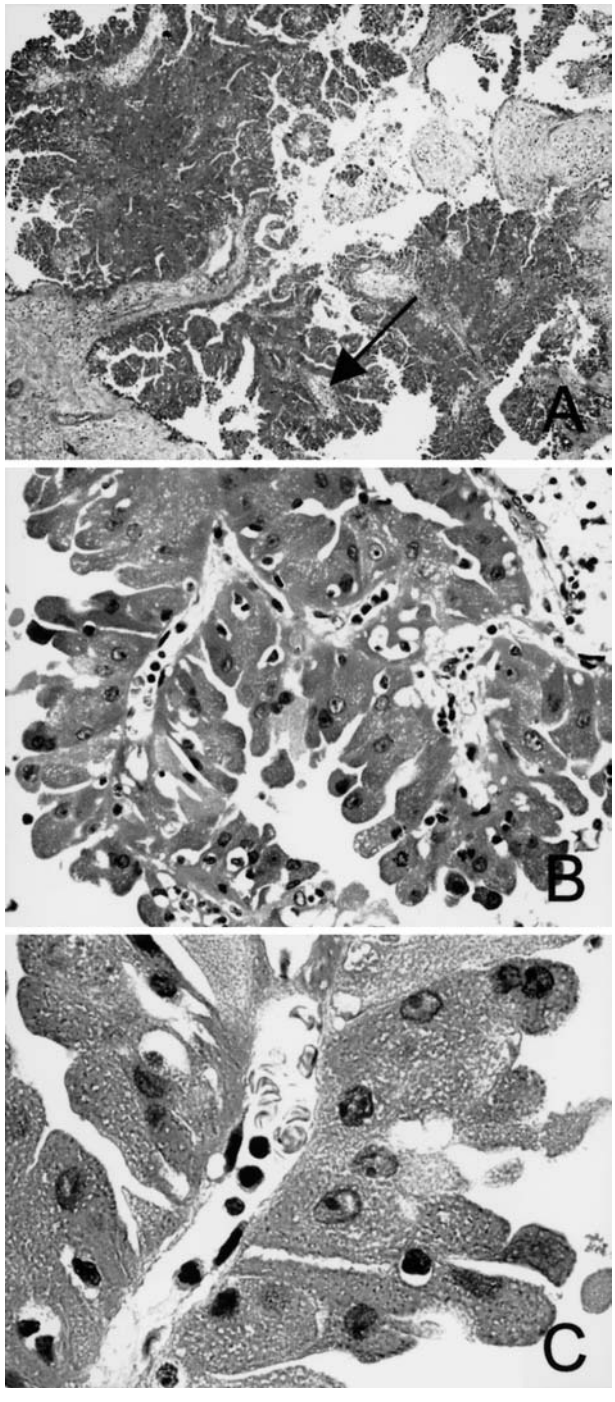



**Fig. 3A–C** Oncocytoid-type papillary renal cell carcinoma with: (**A**) predominant papillary architecture and foam cells within the stalks (*arrow*); (**B**) mono- or pseudostratified pattern; and (**C**) oncocytic feature due to voluminous eosinophilic cytoplasms, regular nuclei, and low nucleus to cytoplasm ratio

with large irregular nuclei and an irregular pseudo- or multistratification pattern (Fig. 2). The nuclear grade was significantly higher in type-2 than in type-1 PRCCs ($P<0.01$). Four type-2 cases had areas with collecting duct-like pattern, with distorted tubules in a desmoplastic stroma. Sarcomatoid cells were noted within two of these latter cases. The diagnosis of collecting-duct carcinoma was excluded by *Ulex europaeus* lectin negative staining. Foci of necrosis with cholesterol clefts were frequently observed in both type-1 and type-2 PRCCs, without statistical difference. A significant fibrovascular stroma, enlarging papillae or surrounding tumoral tubules, was more often noticed in type-2 (10/13) than in type-1

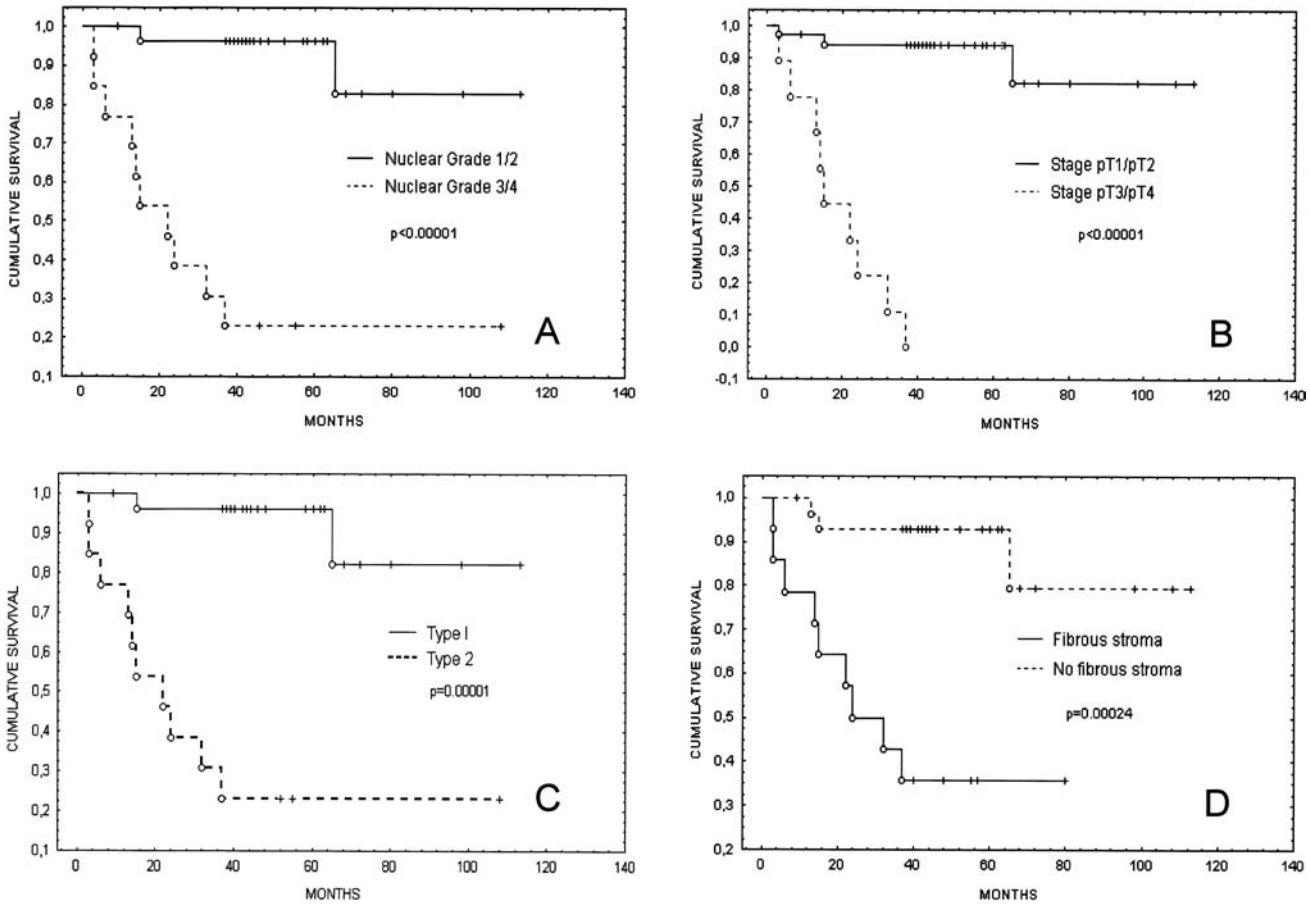



**Fig. 4A–D** Cumulative survival of patients, stratified by: (**A**) the nuclear grade; (**B**) the tumor stage; (**C**) the morphological type 1 or 2; and (**D**) the fibrous stroma

PRCCs (3/26; $P<0.01$). Carcinomatous islets filling the lumen of small blood and/or lymphatic vessels surrounding the tumor were frequently noticed in type-2 (8/13), but never in type-1 PRCCs (0/26). The stage was significantly higher in type-2 than in type-1 PRCCs. No type-1 case extended through the renal capsule or into the renal vein. All type-1 cases were staged pT1 or pT2, whereas eight type-2 cases were staged pT3 or pT4 (two cases with extension into the renal vein, and eight cases with extension in the perirenal adipose tissue). Lymph node metastases were noticed at initial surgery in seven cases of type-2, but in none of type-1 PRCCs.

## Characteristics of oncocytoid-type PRCCs

The mean age and sex ratio of the oncocytoid-type PRCC patients were not significantly different from the patients of type-1 and -2 PRCCs. There was no multifocality, and the mean tumor size was 4.5 cm. Tumoral cells were medium- to large-sized and eosinophilic, with a round regular nucleus, and a low nucleus to cytoplasm ratio. Nuclei had often a conspicuous nucleolus. The nuclear grade was 2 in three cases and 3 in one case. These cytological features gave the cells a distinct oncocytic pattern (Fig. 3), which was lacking in the type-2 PRCCs that were characterized by large, irregular nuclei and abundant eosinophilic cytoplasm. The tumors were made of papillary structures with mono- or pseudostratified pattern. In two of four cases, solid areas were present with packed papillae. Foam cells were focally noticed within the stalks of papillae. The stroma was inconspicuous. All four cases showed extensive necrosis as observed in type-1 and -2 PRCCs. These four cases were staged pT1. We propose to designate them as oncocytoid-type PRCCs.

## Prognosis analysis

The median follow-up time was 43 months (range 3–113 months). Two of twenty-six patients with type-1 PRCC, and 10 of 13 patients with type-2 PRCC died of disease. No deaths occurred in patients with oncocytoid-type PRCC. The Kaplan-Meier analysis (Fig. 4) showed a worse prognosis for patients with: (1) high stage (pT3 or pT4), (2) tumor size $\geq$7 cm, (3) high grade (grade 3 or 4), (4) type-2 PRCC, (5) absent or rare foam cells, and (6) abundant fibrous stroma. The prognosis was not related

**Table 2** Multivariate analysis of prognostic parameters survival

| | Estimate | SD | *P* |
|---|---|---|---|
| Stage | 4.75 | 0.63 | 0.029 |
| Grade | 1.59 | 0.95 | 0.207 |
| Type I or 2 | 4.31 | 0.65 | 0.038 |
| Stroma | 0.05 | 1.07 | 0.818 |

to: (1) age (using median age as cut-off value), (2) psammoma bodies, or (3) necrosis. A multivariate survival analysis using the Cox proportional hazards model showed that only stage and histological type (1 or 2) were independently associated with survival ($P<0.05$; Table 2).

## Discussion

Papillary renal cell carcinoma is a well-recognized distinct tumor type among renal tumors, even though this group exhibits a large range of morphological variants [1, 4, 6, 8, 18, 20, 22, 24, 25, 26, 27]. Delahunt and Eble [6] have recently proposed a subtyping of PRCC into two morphological subtypes: type 1 (small cells with scanty cytoplasm arranged in a single or double layer), and type 2 (cells with voluminous and usually eosinophilic cytoplasm, arranged in a pseudo- or irregularly stratified manner), which could be associated with a favorable or a pejorative prognosis, respectively [6]. In the present series, 65% of the cases were easily classified as type 1 or type 2. The other cases were somehow equivocal because of overlapping features, but we proposed to classify them using the following additional criteria: (1) cases with medium-sized cells were classified on the basis of pseudostratification only, (2) cases with papillae covered both by small basophilic cells and large eosinophilic cells were classified as type 2. Despite these difficulties, 39 of 43 cases could be grouped in type 1 or 2, with morphological features mostly similar to those initially described by Delahunt and Eble [6].

In our series, four cases were classified as a distinct group with a oncocytoid pattern due to large eosinophilic cells with round regular nuclei. These tumors were made of a mixture of solid areas with tightly packed papillae and true papillary structures, with scattered foci of foam cells, and cytokeratin 7-positive tumoral cells. Regarding to the oncocytoma's features reviewed by Amin [2], the papillary architecture (either typical or solid variant) and necrosis seemed too extensive to be compatible with the diagnosis of oncocytoma. Such oncocytoid PRCCs have already been reported in adults [22, 31]. Unfortunately, cytogenetic data were lacking, as in the present series, so we cannot demonstrate further whether theses cases belong to the PRCC group. The four patients with oncocytoid PRCC remained free of disease after radical nephrectomy, suggesting a favorable outcome. However, a larger series of similar cases will be necessary to evaluate reliably the prognosis of the oncocytoid PRCC phenotype.

Previous studies on prognosis factors in PRCC have demonstrated that stage, nuclear grade, and DNA aneuploidy are correlated with a poor outcome [1, 3, 8, 19, 21, 22]. The impact of morphological features of PRCC in patients' survival remains controversial [1, 22]. The morphological subtyping proposed by Delahunt and Eble includes cell volume and pseudostratification [6]. Both these authors and Jiang et al. have observed that tumor size and stage are significantly higher in type-2 than in type-1 PRCCs [6, 11]. In our series, eight type-2 cases showed extrarenal extension (seven of which with lymph node metastasis), whereas all type-1 cases were confined to the kidney, confirming that type-1 and type-2 PRCCs might be related to different clinical behavior. Moch et al., reporting a series of 588 renal tumors, including 64 PRCC, found that type 1 behaved less aggressively than type 2 [19]. Recently, Delahunt et al. have studied a series of 66 PRCCs for which morphological type 1 and 2, AgNOR score, and Ki-67 index were independently associated with survival, providing evidence of the clinical relevance of the type-1 and -2 classification [7]. In this study, the univariate analysis showed that stage, tumor size, nuclear grade, morphological subtyping, and fibrous stroma were associated with survival. Furthermore, stage and morphological subtyping were found in multivariate analysis to be independent predicting factors of survival, whereas nuclear grade was not significantly associated with survival. Even though the tumor stage at diagnosis remains the main prognostic factor, our results confirm the prognosis impact of the classification proposed by Delahunt and Eble. Of note, when we compared outcome between type-1 and type-2 PRCCs grouped together with oncocytoid type, the difference was less marked (due to the favorable outcome of the four oncocytoid cases) but remained significant (due to the very poor outcome of the 13 type-2 cases; data not shown).

Given the distinct outcome related to types 1 and 2, future studies will aim to find out the molecular basis. Delahunt et al. have demonstrated that tumor growth kinetics is significantly lower in type-1 than in type-2 PRCCs [7]. The genetic alterations in type-1 and -2 PRCCs were reported to be different, with more frequent chromosome gains of 7p and 17p and allelic imbalance in type 1 than in type 2, and a sporadic c-*met* mutation restricted to type-1 PRCCs [11, 17, 28]. Delahunt et al. have suggested that these results supported the hypothesis of two different entities, and in particular that type-2 do not evolve from type-1 PRCCs [7]. On the contrary, in our series we observed some cases with mixed features of type 1 and type 2, rather suggestive, at least for these cases, of a type-1 to type-2 tumoral progression. We propose that type 2 might be a heterogeneous group including both cases arising from type 1 and cases arising de novo. Further molecular studies will test this hypothesis.

## References


1. Amin MB, Corless CL, Renshaw AA, Tickoo SK, Kubus J, Schultz DS (1997) Papillary (chromophil) renal cell carcinoma: histomorphological characteristics and evaluation of conventional pathologic prognostic parameters in 62 cases. Am J Surg Pathol 21:621–635
2. Amin MB, Crotty TB, Tickoo SK, Farrow GM (1997) Renal oncocytoma: a reappraisal of morphological features with clinicopathologic findings in 80 cases. Am J Surg Pathol 21:1–12
3. Amin MB, Amin MB, Tamboli P, Javidan D, Stricker H, De-Peralta Venturina M, Deshpande A, Menon M (2002) Prognostic impact of histologic subtyping of adult renal epithelial neoplasms. An experience of 405 cases. Am J Surg Pathol 26:281–291
4. Boczko S, Fromowitz FB, Bard RH (1979) Papillary adenocarcinoma of kidney: a new perspective. Urology 14:491–495
5. Corless CL, Aburatani H, Fletcher JA, Housman DE, Amin MB Weinberg DS (1996) Papillary renal cell carcinoma: quantitation of chromosomes 7 and 17 by FISH, analysis of chromosome 3p for LOH, and DNA ploidy. Diagn Mol Pathol 5:53–64
6. Delahunt B, Eble JN (1997) Papillary renal cell carcinoma: a clinicopathologic and immunohistochemical study of 105 tumors. Mod Pathol 10:537–544
7. Delahunt B, Eble JN, McCredie MR, Bethwaite PB, Stewart JH, Bilous AM (2001) Morphologic typing of papillary renal cell carcinoma: comparison of growth kinetics and patient survival in 66 cases. Hum Pathol 32:590–595
8. el-Naggar AK, Ro JY, Ensign LG (1993) Papillary renal cell carcinoma: clinical implication of DNA content analysis. Hum Pathol 24:316–321
9. Fuhrman SA, Lasky LC, Limas C (1982) Prognostic significance of morphological parameters in renal cell carcinoma. Am J Surg Pathol 6:655–663
10. Gatalica Z, Kovatich A, Miettinen M (1995) Consistent expression of cytokeratin 7 in papillary renal-cell carcinoma. An immunohistochemical study in formalin-fixed, paraffin-embedded tissues. J Urol Pathol 3:205–211
11. Jiang F, Richter J, Schraml P, Bubendorf L, Gasser T, Sauter G, Mihatsch MJ, Moch H (1998) Imbalances in papillary renal cell carcinoma: genetic differences between histological subtypes. Am J Pathol 153:1467–1473
12. Kattar MM, Grignon DJ, Wallis T, Haas GP, Sakr WA, Pontes JE, Visscher DW (1997) Clinicopathologic and interphase cytogenetic analysis of papillary (chromophilic) renal cell carcinoma. Mod Pathol 10:1143–1150
13. Kovacs G (1989) Papillary renal cell carcinoma. A morphological and cytogenetic study of 11 cases. Am J Pathol 134:27–34
14. Kovacs G, Fuzesi L, Emanual A, Kung HF (1991). Cytogenetics of papillary renal cell tumors. Genes Chromosom Cancer 3:249–255
15. Kovacs G, Akhtar M, Beckwith BJ, Bugert P, Cooper CS, Delahunt B, Eble JN, Fleming S, Ljungberg B, Medeiros LJ, Moch H, Reuter VE, Ritz E, Roos G, Schmidt D, Srigley JR, Storkel S, van den Berg E, Zbar B (1997) The Heidelberg classification of renal cell tumours. J Pathol 183:131–133
16. Lager DJ, Huston BJ, Timmerman TG, Bonsib SM (1995) Papillary renal tumors. Morphologic, cytochemical, and genotypic features. Cancer 76:669–673
17. Lubensky IA, Schmidt L, Zhuang Z, Weirich G, Pack S, Zambrano N, Walther MM, Choyke P, Linehan WM, Zbar B (1999) Hereditary and sporadic papillary renal carcinomas with c-met mutations share a distinct morphological phenotype. Am J Pathol 155:517–526
18. Mancilla-Jimenez R, Stanley RJ, Blath RA (1976) Papillary renal cell carcinoma: a clinical, radiologic, and pathologic study of 34 cases. Cancer 38:2469–2480
19. Moch H, Gasser T, Amin MB, Torhorst J, Sauter G, Mihatsch MJ (2000) Prognostic utility of the recently recommended histologic classification and revised TNM staging system of renal cell carcinoma: a Swiss experience with 588 tumors. Cancer 89:604–614
20. Mydlo JH, Bard RH (1987) Analysis of papillary renal adenocarcinoma. Urology 30:529–534
21. Onishi T, Ohishi Y, Goto H, Suzuki M, Miyazawa Y (1999) Papillary renal cell carcinoma: clinicopathological characteristics and evaluation of prognosis in 42 patients. BJU Int 83:937–943
22. Orain I, Buzelin F, Ferry N (1987) Tubulopapillary tumors of the kidney. A proposal of 20 new cases and a review of the literature. J Urol 93:1–9
23. Perot C, Bougaran J, Boccon-Gibod L, Storkel S, Leverger G, Akker J van den, Taillemite JL, Couturier J (1999) Two new cases of papillary renal cell carcinoma with t(X;1)(p11;q21) in females. Cancer Genet Cytogenet 110:54–56
24. Renshaw AA, Corless CL (1995) Papillary renal cell carcinoma. Histology and immunohistochemistry. Am J Surg Pathol 19:842–849
25. Renshaw AA, Zhang H, Corless CL, Fletcher JA, Pins MR (1997) Solid variants of papillary (chromophil) renal cell carcinoma: clinicopathologic and genetic features. Am J Surg Pathol 21:1203–1209
26. Renshaw AA, Morgan TW, Fletcher JA (1998) A sarcomatoid renal cell carcinoma with a "hobnail pattern" and immunohistochemical and cytogenetic features of papillary carcinoma. J Urol Pathol 9:93–102
27. Renshaw AA, Granter SR, Fletcher JA, Kozakewich HP, Corless CL, Perez-Atayde AR (1999) Renal cell carcinomas in children and young adults: increased incidence of papillary architecture and unique subtypes. Am J Surg Pathol 23:795–802
28. Sanders ME, Mick R, Tomaszewski JE, Barr FG (2002) Unique patterns of allelic imbalance distinguish type-1 from type-2 sporadic papillary renal cell carcinoma. Am J Pathol 161:997–1005
29. Sobin LH, Witteking CH (eds) (1997) International Union Against Cancer. TNM classification of malignant tumors (5th edn). Wiley-Liss, New York
30. Storkel S, Eble JN, Adlakha K, Amin M, Blute ML, Bostwick DG, Darson M, Delahunt B, Iczkowski K (1997) Classification of renal cell carcinoma: workgroup no. 1. Union Internationale Contre le Cancer (UICC) and the American Joint Committee on Cancer (AJCC). Cancer 80:987–989
31. Thoenes W, Storkel S, Rumpelt HJ (1986) Histopathology and classification of renal cell tumors (adenomas, oncocytomas and carcinomas). The basic cytological and histopathological elements and their use for diagnostics. Pathol Res Pract 181:125–143

Virchows Arch (2003) 442:343–348
DOI 10.1007/s00428-003-0758-6

ORIGINAL ARTICLE

**Harald Seeberger · Constanze Knörr · Christian Mainhardt · Hans Konrad Müller-Hermelink · Axel Greiner**

# Tumor-infiltrating T cells with similar antigen binding sites in different mucosa-associated lymphoid tissue type B cell lymphomas

Received: 24 June 2002 / Accepted: 6 December 2002 / Published online: 19 February 2003
© Springer-Verlag 2003

**Abstract** B cell lymphomas of mucosa-associated lymphoid tissue (MALT)-type arise on the background of chronic inflammation due to either autoimmunity or infection at various sites of the organism. Characteristically the tumor-infiltrating T cells found in large numbers in MALT-type lymphomas are predominantly of $CD4^+$ phenotype and may have impact on tumor pathogenesis. To assess whether the chromosomal translocation t(11;18)(q21; q21) that is specific for at least a subset of MALT-type lymphomas may have an impact on tumor environment, we investigated the antigen binding sites of tumor-infiltrating T cells from one t(11;18)-positive tumor of the thyroid and one t(11;18)-negative tumor of the stomach. MHC Allelotyping was performed and revealed common alleles in HLA-DR and HLA-DQ loci. Cloning and sequencing of the complementary determining region 3 in $V_{\beta 2}$ chains of T cell receptors demonstrated the use of identical $J_{\beta}$segments in both patients, suggestive for recognition of the same antigen. We therefore suggest that tumor-infiltrating $CD4^+$ T cells are tightly integrated in MALT-type lymphoma immunoarchitecture irrespective of genetic background and localization of the tumors.

**Keywords** Mucosa-associated lymphoid tissue type lymphoma · Tumor-infiltrating T cells · T-cell receptor · Complementary determining region 3

H. Seeberger · C. Knörr · H. K. Müller-Hermelink · A. Greiner (✉)
Institute of Pathology, University of Würzburg,
Josef-Schneider-Strasse 2, 97080 Würzburg, Germany
e-mail: path040@mail.uni-wuerzburg.de
Tel.: +49-931-20147785
Fax: +49-931- 20147440

C. Mainhardt
Department of Transfusion Medicine,
University of Würzburg, Josef-Schneider-Strasse 2,
97080 Würzburg, Germany

## Introduction

B cell lymphomas of mucosa-associated lymphoid tissue (MALT) type are extranodal low-grade malignancies of memory B cells [12] that develop at various, almost exclusively mucosal sites of the organism. The tumors are preceded by chronic inflammation due to either infection or autoimmunity [15]. Contrary to the general view that B cell lymphoma is an entirely autonomous growth from the beginning, findings in MALT-type lymphomas suggest that tumor-infiltrating T cells are important in lymphoma containment and progression [14, 17]. It has been shown that T helper lymphocytes ($CD4^+$) preserve the tumor-host immunoarchitectural relationship [19], which is in contrast to solid tumors, in which cytotoxic T cells ($CD8^+$) have been associated with immunosurveillance [29]. It was suggested that environmental antigens such as *Helicobacter pylori* lead to T cell activation and thus promote MALT-type lymphoma survival [14]. However, as a unique feature of MALT-type lymphoma B cells, the tumor-produced immunoglobulin recognizes autoantigens rather than *H. pylori* antigens [8].

Recently the chromosomal translocation t(11;18)(q21; q21) was found to be specific for 30–50% of all MALT-type lymphomas [3, 24, 27]. The presence of this chromosomal aberration has an impact on clinical outcome since it renders gastric MALT-type lymphomas resistant to *H. pylori* eradication therapy [2, 20], and may might also affect the immunological background and Tcell environment of the tumors. We therefore investigated tumor-infiltrating T cells of two diverse MALT-type lymphoma cases that differed in respect to the presence of the t(11;18)(q21; q21), preceding lesion (autoimmunity vs. *H. pylori* infection) and the site of tumor development (thyroid vs. stomach). By characterizing the antigen-binding sites (complementary determining region 3, CDR3) of the T cell receptor (TCR) in combination with MHC allelotyping, we characterized the immunological background that affects MALT-type lymphoma development.

## Materials and methods

### Sample preparation

Tumor specimens were obtained immediately after surgical removal for preparation of cell suspensions, snap-freezing in liquid nitrogen and routine fixation for histological examination. The diagnosis was confirmed by routine histology and immunohistochemistry according to the Revised European-American Lymphoma (REAL) classification [12] and WHO classification, respectively [13]. Both tumors were extranodal marginal zone B cell lymphoma of MALT-type originating in the stomach (patient no. 1) and the thyroid (patient no. 2). In patient no. 2 peripheral blood lymphocytes were isolated by density-gradient centrifugation [17].

### Flow cytometry

Flow cytometry was performed to determine the percentage of $CD4^+$, $CD8^+$, and $V_{\beta 2}$ T cells in tumor and peripheral blood. The analysis was carried out on a FACScan (Beckton Dickinson, Heidelberg, Germany) using the program Lysis II (Beckton Dickinson) for data acquisition and analysis as described elsewhere [17]. The following antibodies were used: anti-CD4 (R-8886, Sigma, Deisenhofen Germany), anti-CD8 (R-806, Dako, Hamburg, Germany), and anti-$TCR_{V\beta 2}$ (MPB2D5, Beckman-Coulter, Krefeld, Germany).

### Immunostaining

Immunohistochemical staining was performed on 4 μm cryostat sections of fresh frozen surgical specimens. The immunoperoxidase method was applied by a three-step incubation procedure with diluted affinity-purified anti-mouse antibody (Dako) and serum from mouse as control, as described in detail elsewhere [7].

### Isolation of genomic DNA and HLA genotyping

For each patient genomic DNA was isolated from malignant B cells using TRIzol reagent (Life Technology, Paisley, UK) according to the manufacturer's instructions. The precipitated DNA was dissolved in 8 mM NaOH and adjusted to a concentration of 50 ng/μl. For the subsequent HLA genotyping 240 μg genomic DNA was used.

For HLA class I and class II analysis we used the Dynal AllSet SSP HLA-A (or HLA-B, DR, DQ) low-resolution assays (Dynal, Oslo, Norway) containing 24 (48, 24, 8, respectively) different sequence-specific primer (SSP) mixes for the HLA-A (HLA-B, DR, DQ loci, respectively). Sample DNA, AmpliTaq DNA-polymerase (Perkin Elmer, Weiterstadt, Germany) and the PCR solution (Dynal) were added, and PCR was performed according to the manufacturer's instructions. Finally, the amplified alleles were detected by agarose gel electrophoresis.

### RNA extraction and cDNA synthesis

Total RNA was extracted from 20–25 approximately 10no. no. μm thick cryostat-sections of nitrogen-frozen tumor tissue or from $2\times10^5$ peripheral blood lymphocytes using TRIzol reagent according to the manufacturer's instructions. First-strand cDNA synthesis was carried out with 1 μg total RNA in a volume of 5 μl plus 2 μl dT-15 primer (220 μM) and 1 μl a hexamer random primer (50 nM) by incubating at 65°C for 10 min. After chilling on ice deoxyribonucleoside triphosphates and dithiothreitol at final concentrations of 1 mM and 10 mM respectively, 25 U recombinant RNAsin (Promega, Heidelberg, Germany), reverse transcriptase buffer, and 0.2 U Moloney murine leukemia virus reverse transcriptase (Gibco BRL, Gaithersburg, Md. USA) were added to a final volume of 25 μl. After incubation at 37°C for 70 min the samples were boiled for 4 min.

Quality and amount of cDNA was estimated by glyceraldehyde-3-phosphate dehydrogenase (GAPDH)-specific PCR.

### T cell receptor V$\beta$ family specific polymerase chain reaction

Aliquots of cDNA were amplified in parallel in reactions containing one of 23 TCR $V_\beta$ family specific primers ($V_{\beta 1–10}$ and $V_{\beta 12–24}$) and the TCR $C_\beta$ consensus primer [6]. The primer $V_{\beta 11}$ was excluded since it did not give any result in testing experiments [10]. The amplifications were performed in the GeneAmp PCR system 2400 (Perkin-Elmer Cetus, Emeryville, Calif., USA) in a final volume of 25 μl containing 1 μl of cDNA, 2.5 μl of 10× PCR buffer (USB, Braunschweig, Germany), 1.5 μl 25 mM $MgCl_2$, 0.5 μl 10 mM deoxyribonucleoside triphosphates, 0.5 μl 2 pmol/μl of each primer and 0.5 U of cloned Taq DNA polymerase (USB). Amplifications consisted of 35 cycles of denaturation at 94°C for 60 s, annealing of primers at 60°C for 45 s and extension of primers at 72°C for 90 s and a final extension step of 10 min at 72°C.

### Evaluation of TCR V$\beta$ length polymorphism

PCR products were subjected to electrophoresis using the ABI 373A sequencer (Applied Biosystems, Weiterstadt, Germany). The evaluation of TCR $V_\beta$ length polymorphism was performed using the Genescan software version 1.2.2. (Applied Biosystems). The evaluation of oligoclonality in the different $V_\beta$ families was performed as described in detail elsewhere [25].

### Cloning and sequencing of TCR V$\beta$2 transcripts

PCR products obtained with the primers $V_{\beta 2}$ and $C_\beta$ were cloned into PCRscript (Stratagene, Heidelberg, Germany), which was used to transform ultracompetent *Escherichia coli* (Stratagene). White colonies were picked and grown overnight in 3 ml Luria-Bertani medium. The double-stranded DNA template from the colonies was sequenced by the chain-termination method [28] using the Taq dye deoxy termination cycle sequencing kit (Applied Biosystems, Weiterstadt, Germany). Analysis was performed on the automatic sequencer ABI 373A (Applied Biosystems).

## Results

### B cell lymphomas of MALT-type contain a high proportion of tumor-infiltrating T cells with clonal expansions

The tumors were typical marginal zone B cell lymphomas with respect to their morphology and immunophenotype (Table 1). The proportion of tumor-infiltrating T cells was high and showed a prevalence of $CD4^+$ helper cells. The cases differed in respect to localization of the tumor and its initial lesion which was associated with chronic *Helicobacter pylori* infection in patient no. 1 and long-lasting Hashimoto's disease in patient no. 2. Moreover, the cytogenetic background of the tumors differed since the t(11;18)(q21; q21) was present in patient no. 2 and absent in patient no. 1 as determined by fluorescence in situ hybridization [27].

Using a TCR $V_\beta$ family-specific PCR assay we characterized the tumor-infiltrating T cells of the tumor tissues. Transcripts for all 23 $V_\beta$ families investigated

**Table 1** Characteristics of the MALT-type lymphomas investigated

| | Localization of tumor | Immunophenotype | t (11;18) (q21; q21) | $CD3^+4^+$ (%) | $CD3^+8^+$ (%) | Clinical background |
|---|---|---|---|---|---|---|
| Patient no. 1 | Stomach | $CD19^+$<br>$CD23^-$<br>$CD5^-$<br>$IgD^-$<br>$IgM^+$, $\kappa$ | Negative | 13 | 7 | *H. pylori* associated chronic gastritis |
| Patient no. 2 | Thyroid | $CD19^+$<br>$CD23^-$<br>$CD5^-$<br>$IgD^-$<br>$IgM^+$, $\lambda$ | Positive | 39 | 3 | 8 years duration Hashimotothyroiditis |

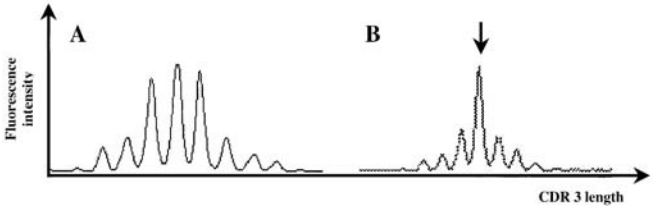



**Fig. 1** Electropherograms of TCR $V_{\beta 2}$ transcripts from tumor-infiltrating T cells of two different MALT-type lymphomas. Patient no. 1 (stomach) shows a normal length distribution (*A*), whereas patient no. 2 (thyroid) exhibits a clonal expansion (*B*, *arrow*).

were found in both patients, indicating a nonrestricted T cell repertoire. Clonal expansions of tumor-infiltrating T cells resulted in a dominant band in Genescan analysis and were found in patient no. 2 in 11 (48%) and in patient no. 1 in 17 (74%) of the 23 TCR $V_\beta$ families. The $V_\beta$ families 1, 5, 10, 19, and 23 showed clonal expansions in both tumors, whereas the $V_\beta$ families 6, 12, and 13 lacked clonal expansions in either tumor (data not shown). The remaining $V_\beta$ families showed clonal expansions in only one of the patients each (e.g., $V_{\beta 2,}$ Fig. 1a, b).

Immunostaining of tumor sections with a TCR $V_{\beta 2}$-specific antibody confirmed the data obtained by RT-PCR: a large numer of clustering T cells expressing the $V_{\beta 2}$ chain is found in patient no. 2 (Fig. 2A), indicating clonal expansion, whereas patient no. 1 showed scattered $V_{\beta 2}$ T cells within the tumor tissue (Fig. 2A). For further investigation we focused on this specific T cell subset.

## Similar antigen-binding regions in the T cell receptor from tumor-infiltrating T cells of the gastric and the thyroid MALT-type lymphoma

First we cloned and sequenced TCR $V_{\beta 2}$ transcripts of tumor-infiltrating T cells from the two patients, and then we deduced the amino acid sequence of CDR3. Patient no. 1 who showed no clonal T cell expansion displayed TCR $V_{\beta 2}$ transcripts with a CDR3 of 16 amino acids (aa) in length (43% of all transcripts), 20 aa (14%) and 21 aa (43%). However, in patient no. 2 there was a preference of $V_{\beta 2}$ transcripts with a CDR3 length of 20 aa (62.5%) as expected from Genescan analysis, reflecting the clonally expanded T cells. The remaining $V_{\beta 2}$ transcripts were 19 aa (12.5%) and 21 aa (25%) in length. We found identical $J_\beta$segments in tumor-infiltrating T cells from both patients (Fig. 2B). Transcripts with CDR3 length of 20 aa displayed $J_\beta$ 1.5-segments. Here 15 aa out of 20 aa are shared, resulting in a sequence homology of the whole CDR3 in 75%. Transcripts with CDR3 length of 21 aa displayed $J_\beta$ 2.1 segments. Here 14 aa of 21 aa are shared, resulting in a sequence homology of still 66.66%.

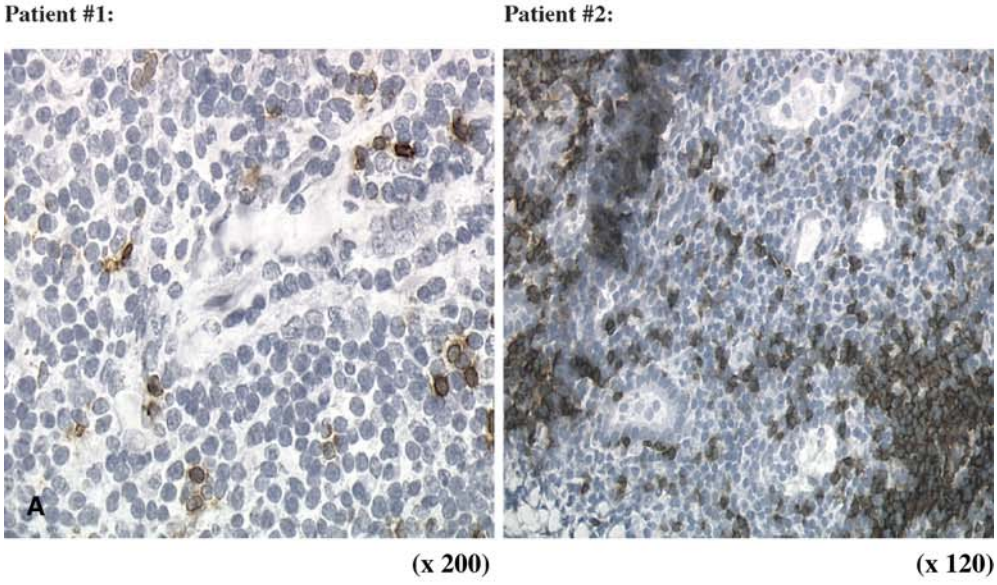
However, when comparing CDR3 of tumor-infiltrating T cells with peripheral T cells in patient no. 2 we did not find transcripts with identical length using the same $J_\beta$ segments (Fig. 2B). Moreover, the peripheral blood showed no clonal expansion of T cells with TCR $V_{\beta 2}$.

We determined the percentage of $CD4^+$ and $CD8^+$ T cells by FACS analysis and compared tumor-infiltrating T cells with peripheral T cells. The ratio of $CD4^+$ to $CD8^+$ T cells was drastically enhanced in the tumor (Table 2). However, the percentage of T cells expressing TCR $V_{\beta 2}$ was identical in the two compartments. This special T cell subset consists in the peripheral blood predominantly and in the tumor almost exclusively of $CD4^+$ T cells (Table 2).

## Patients share common alleles in their HLA loci

The HLA genotyping was done at low resolution level and characterized patient no. 1 as follows: HLA-A: 02xx, 03xx; HLA-B: 08xx, 18xx, HLA-DRB1: 03xx; HLA-DQB1: 02xx, resulting in the phenotypic specificities HLA-A 02, 03; HLA-B 08, 18; HLA-DR 17 (3); HLA-DQ 02. The genotype of patient- no. 2 was: HLA-A: 01xx, 02xx; HLA-B: 08xx, 50xx; HLA-DRB1: 03xx, 08xx; HLA-DQB1: 02xx, 04xx, resulting in the phenotypic profiles HLA-A 01, 02; HLA-B 08, 50 (21); HLA-DR 17 (3), 08; HLA-DQ 02, 04. In conclusion, the patients shared in the HLA class I locus the alleles HLA-A 02 and HLA-B 08, and in the class II locus, which is most important for the interaction of antigen-presenting cells with $CD4^+$ helper T cells, the alleles HLA-DR 03 and HLA-DQ 02.

**Fig. 2. A** Immunohistochemistry with anti-TCR $V_{\beta 2}$ showing scattered lymphocytes within the tumor that infiltrates glandular structures in patient 1, and numerous T cell expansions within the tumor of patient 2. **B** Comparison of the amino acid sequence of antigen-binding CDR3 in tumor-infiltrating T cells of the two patients and in tumor-infiltrating and peripheral T cells of patient 2. *Underlined* $J_\beta$ segments; *arrows* $J_\beta$ segments found in both patients in transcripts of identical CDR3 length




**Patient #1: tumor-infiltrating T cells**

| Vβ 2 | CDR 3 | | Jβ |
|---|---|---|---|
| CSA | L D L E Q Y F G P G T R L T V T | | 2.7 |
| CSA | R S G E L F F G E G S S L T V L | | 2.2 |
| CSA | R S G E L F F G E G S S L T V L | | 2.2 |
| CSA | K P G Y S N Q P Q H F G D G T R L S I L | ← | 1.5 |
| CSA | R D G R G S Y N E Q F F G P G T R L T V L | ⇠ | 2.1 |
| CSA | R D G R G S Y N E Q F F G P G T R L T V L | ⇠ | 2.1 |
| CSA | R D P S D L N Y G Y T F G S G T R L T V V | | 1.2 |

**Patient #2: tumor-infiltrating T cells**

| Vβ 2 | CDR 3 | | Jβ |
|---|---|---|---|
| CSA | R N P S D E T Q Y F G P G T R L L V L | | 2.5 |
| CSA | E L A R G N Q P Q H F G D G T R L S I L | ← | 1.5 |
| CSA | S M Q G S N E K L F F G S G T Q L S V L | | 1.4 |
| CSA | S M Q G S N E K L F F G S G T Q L S V L | | 1.4 |
| CSA | G M G G S N E K L F F G S G T Q L S V L | | 1.4 |
| CSA | S M Q G S N E K L F F G S G T Q L S V L | | 1.4 |
| CSA | R A G T G A G E T Q Y F G P G T R L L V L | | 2.5 |
| CSA | C P D D K A G N E Q F F G P G T R L T V L | ⇠ | 2.1 |

**Patient #2: peripheral T cells**

| Vβ 2 | CDR 3 | Jβ |
|---|---|---|
| CSA | D P A G D G E L F F G E G S R L T V L | 2.2 |
| CSA | R K P Q G Y N E Q F F G P G T R L T A L | 2.1 |
| CSA | R V M G V V D G Y T F G S G T R L T V V | 1.2 |
| CSA | R A S S G G Y E Q Y F G P G T R L T V T | 2.7 |
| CSA | G D R H S G A S V L T F G A G S R L T V L | 2.6 |
| CSA | R E L G G S T Y E Q Y F G P G T R L T V T | 2.7 |
| CSA | R E R L S S G A N V L T F G A G S R L T V L | 2.6 |
| CSA | R E R L S S G A N V L T F G A G S R L T V L | 2.6 |
| CSA | G G W Q D R P R E T Q Y F G P G T R L L V L | 2.5 |
| CSA | S G G L A G A S Y N E Q F F G P G T R L T V L | 2.1 |
| CSA | R V G V A G G S G Y N E Q F F G P G T R L T V L | 2.1 |

**B**

**Table 2** Peripheral blood T cells and tumor-infiltrating T cells of patient no. 2

| | All T cells | | TCR $V_{\beta 2}$ T cells | |
|---|---|---|---|---|
| | CD4/CD8 | TCR $V_{\beta 2}$ (%) | $CD4^+$ (%) | $CD8^+$ (%) |
| Peripheral blood | 0.33 | 2.95 | 70 | 30 |
| Tumor | 13.0 | 2.94 | 91 | 9 |

## Discussion

Tumor-infiltrating T cells in MALT-type lymphoma play an important role for tumor development, maintenance, and progression [14, 19]. However, it is unclear whether the T cells interact with the tumor in a paracrine way as proposed by in vitro data using CD40 ligand and cytokine stimulation [17] or more specifically by antigen and cognate interaction mediated by HLA class II molecules. To address this question we chose two patients with comparable HLA background but divergent MALT-type lymphomas in respect to localization, preceding lesion and cytogenetic aberrations. Between these two patients we found similarities in the antigen-binding regions of the T cell receptor, which is expressed mainly by the identical $J_\beta$ segments in $V_{\beta 2}$ transcripts with identical CDR3 length. Although the hypervariable nucleotide region of CDR3 was diverse, the finding of identical $J_\beta$ segments alone might indicate the recognition of a similar antigen in both tumors [4, 22, 23]. This notion is further strengthened by a comparison of tumor-infiltrating and peripheral T cells within one patient, as demonstrated in patient no. 2. We therefore suggest the action of a similar antigen in both MALT-type lymphoma patients that could be, for example, an autoantigen or bacterial antigen. *H. pylori* antigens could serve as ideal candidates because some of them (e.g., heat shock proteins) are widespread and share autoantigen features [16, 18]. This would explain findings of regression of salivary gland MALT-type lymphoma after *H. pylori* eradication [1]. However, a specific antigen in MALT-type lymphoma should also result in biased or restricted antigen receptor use of the tumor cells, but this has not been found so far [11, 26]. Furthermore, no unique autoantigen or *H. pylori* antigen binding by the tumor immunoglobulin has been found among all MALT-type lymphomas investigated [8, 9]. Another explanation for similar antigen receptors in tumor-infiltrating T cells may be reactivity towards a tumor-associated antigen that is specifically expressed on malignant B cells and would argue for an tumor directed activity of the $CD4^+$ T cells.

Recently the chromosomal translocation t(11;18)(q21; q21) specific for MALT-type lymphoma was demonstrated to involve the genes API2 and MALT1 [5] that could support autonomous growth [21]. However, our findings demonstrated similarity in the antigen receptor of tumor-infiltrating T cells irrespective of the t(11;18)(q21; q21), indicating that a common immunoarchitecture of early MALT-type lymphomagenesis might persist independently of the acquired cytogenetic alteration.

Although only two cases were investigated and further work is required to verify our findings for MALT-type lymphoma in general, this study underlines the importance of tumor-infiltrating T cells of MALT-type lymphomas in establishing an immunological background that tends to be surprisingly similar, even in MALT-type lymphomas that differ in localization, preceding lesions and cytogenetic background.

**Acknowledgements** This work was supported by the Interdisziplinäres Zentrum für klinische Forschung (IZKF) Würzburg, grant B3, and the Wilhelm-Sander-Stiftung, grant 94.025.2. We thank P. Starostik for critically reading the manuscript.

## References

1. Alkan S, Karcher DS, Newman MA, Cohen P (1996) Regression of salivary gland MALT lymphoma after treatment for Helicobacter pylori. Lancet 348:268–269
2. Alpen B, Neubauer A, Dierlamm J, Marynen P, Thiede C, Bayerdorfer E, Stolte M (2000) Translocation t(11;18) absent in early gastric marginal zone B-cell lymphoma of MALT type responding to eradication of Helicobacter pylori infection. Blood 95:4014–4015
3. Auer IA, Gascoyne RD, Connors JM, Cotter FE, Greiner TC, Sanger WG, Horsman DE (1997) t(11;18)(q21;q21) is the most common translocation in MALT lymphomas. Ann Oncol 8:979–985
4. Chott A, Probert CS, Gross GG, Blumberg RS, Balk SP (1996) A common TCR beta-chain expressed by CD8+ intestinal mucosa T cells in ulcerative colitis. J Immunol 156:3024–3035
5. Dierlamm J, Baens M, Wlodarska I, Stefanova-Ouzounova M, Hernandez JM, Hossfeld DK, De Wolf-Peeters C, Hagemeijer A, Van den Berghe H, Marynen P (1999) The apoptosis inhibitor gene API2 and a novel 18q gene, MLT, are recurrently rearranged in the t(11;18)(q21;q21) associated with mucosa-associated lymphoid tissue lymphomas. Blood 93:3601–3609
6. Genevee C, Diu A, Nierat J, Caignard A, Dietrich PY, Ferradini L, Roman-Roman S, Triebel F, Hercend T (1992) An experimentally validated panel of subfamily-specific oligonucleotide primers (V alpha 1-w29/V beta 1-w24) for the study of human T cell receptor variable V gene segment usage by polymerase chain reaction. Eur J Immunol 22:1261–1269
7. Greiner A, Marx A, Müller-Hermelink HK, Schmausser B, Petzold K, Kruger H (1992) Vascular autoantibodies in amyotrophic lateral sclerosis. Lancet 340:378–379
8. Greiner A, Marx A, Heesemann J, Leebmann J, Schmausser B, Müller-Hermelink HK (1994) Idiotype identity in a MALT-type lymphoma and B cells in Helicobacter pylori associated chronic gastritis. Lab Invest 70:572–578
9. Greiner A, Knörr C, Qin Y, Schultz A, Marx A, Kroczek RA, Müller-Hermelink HK (1998) CD40 ligand and autoantigen are involved in the pathogenesis of low-grade B-cell lymphomas of mucosa-associated lymphoid tissue. Dev Immunol 6:187–195
10. Haedicke W, Greiner A, Seeberger H, Müller-Hermelink HK (1999) Oligoclonal expansions of T-cell repertoire in gastric mucosa associated lymphoid tissue type B-cell lymphoma and adjacent gastritis. Diagn Mol Pathol 8:138–144
11. Hallas C, Greiner A, Peters K, Müller-Hermelink HK (1998) Immunoglobulin VH genes of high-grade mucosa-associated lymphoid tissue lymphomas show a high load of somatic

mutations and evidence of antigen-dependent affinity maturation. Lab Invest 78:277–287
12. Harris NL, Jaffe ES, Stein H, Banks PM, Chan JK, Cleary ML, Delsol G, De Wolf Peeters C, Falini B, Gatter KC, Müller-Hermelink HK, et al (1994) A revised European-American classification of lymphoid neoplasms: a proposal from the International Lymphoma Study Group. Blood 84:1361–1392
13. Harris NL, Jaffe ES, Diebold J, Flandrin G, Muller-Hermelink HK, Vardiman J, Lister TA, Bloomfield CD (2000) The World Health Organization classification of neoplastic diseases of the haematopoietic and lymphoid tissues: report of the Clinical Advisory Committee Meeting, Airlie House, Virginia, November 1997. Histopathology 36:69–86
14. Hussell T, Isaacson PG, Crabtree JE, Spencer J (1996) Helicobacter pylori-specific tumour-infiltrating T cells provide contact dependent help for the growth of malignant B cells in low-grade gastric lymphoma of mucosa-associated lymphoid tissue. J Pathol 178:122–127
15. Isaacson PG (1993) Pathogenesis and early lesions in extranodal lymphoma. Toxicol Lett 67:237–247
16. Kawahara Y, Yokota K, Mizuno M, Yunoki N, Uesu T, Okada H, Kobayashi K, Hirai Y, Oguma K, Tsuji T (1999) Antibodies to human gastric epithelial cells and heat shock protein 60 in Helicobacter pylori positive mucosa associated lymphoid tissue lymphoma. Gut 45:20–23
17. Knörr C, Amrehn C, Seeberger H, Rosenwald A, Stilgenbauer S, Ott G, Müller-Hermelink HK, Greiner A (1999) Expression of costimulatory molecules in low-grade mucosa-associated lymphoid tissue-type lymphomas in vivo. Am J Pathol 155:2019–2027
18. Kobayashi K, Yokota K, Yoshino T, Kawahara Y, Dey A, Hirai Y, Oguma K, Akagi T (1998) Detection of Helicobacter pylori associated antigen and heat shock protein 60 on follicular dendritic cells in the germinal centres of low grade B cell lymphoma of gastric mucosa associated lymphoid tissue (MALT). J Clin Pathol 51:396–398
19. Koulis A, Diss T, Isaacson PG, Dogan A (1997) Characterization of tumor-infiltrating T lymphocytes in B-cell lymphomas of mucosa-associated lymphoid tissue. Am J Pathol 151:1353–1360
20. Liu H, Ruskon-Fourmestraux A, Lavergne-Slove A, Ye H, Molina T, Bouhnik Y, Hamoudi RA, Diss TC, Dogan A, Megraud F, Rambaud JC, Du MQ, Isaacson PG (2001) Resistance of t(11;18) positive gastric mucosa-associated lymphoid tissue lymphoma to Helicobacter pylori eradication therapy. Lancet 357:39–40
21. Lucas PC, Yonezumi M, Inohara N, McAllister-Lucas LM, Abazeed ME, Chen FF, Yamaoka S, Seto M, Nunez G (2001) Bcl10 and MALT1, independent targets of chromosomal translocation in malt lymphoma, cooperate in a novel NF-kappa B signaling pathway. J Biol Chem 276:19012–19019
22. McHeyzer-Williams MG, Davis MM (1995) Antigen-specific development of primary and memory T cells in vivo. Science 268:106–111
23. Oksenberg JR, Panzara MA, Begovich AB, Mitchell D, Erlich HA, Murray RS, Shimonkevitz R, Sherritt M, Rothbard J, Bernard CC, et al (1993) Selection for T-cell receptor V beta-D beta-J beta gene rearrangements with specificity for a myelin basic protein peptide in brain lesions of multiple sclerosis. Nature 362:68–70
24. Ott G, Katzenberger T, Greiner A, Kalla J, Rosenwald A, Heinrich U, Ott MM, Muller-Hermelink HK (1997) The t(11;18)(q21;q21) chromosome translocation is a frequent and specific aberration in low-grade but not high-grade malignant non-Hodgkin's lymphomas of the mucosa-associated lymphoid tissue (MALT-) type. Cancer Res 57:3944–3948
25. Puisieux I, Even J, Pannetier C, Jotereau F, Favrot M, Kourilsky P (1994) Oligoclonality of tumor-infiltrating lymphocytes from human melanomas. J Immunol 153:2807–2818
26. Qin Y, Greiner A, Hallas C, Haedicke W, Müller-Hermelink HK (1997) Intraclonal offspring expansion of gastric low-grade MALT-type lymphoma: evidence for the role of antigen-driven high-affinity mutation in lymphomagenesis. Lab Invest 76:477–485
27. Rosenwald A, Ott G, Stilgenbauer S, Kalla J, Bredt M, Katzenberger T, Greiner A, Ott MM, Gawin B, Dohner H, Müller-Hermelink HK (1999) Exclusive detection of the t(11;18)(q21;q21) in extranodal marginal zone B cell lymphomas (MZBL) of MALT type in contrast to other MZBL and extranodal large B cell lymphomas. Am J Pathol 155:1817–1821
28. Sanger F, Nicklen S, Coulson AR (1977) DNA sequencing with chain-terminating inhibitors. Proc Natl Acad Sci U S A 74:5463–5467
29. Wang RF, Rosenberg SA (1999) Human tumor antigens for cancer vaccine development. Immunol Rev 170:85–100

Virchows Arch (2003) 442:349–355
DOI 10.1007/s00428-003-0763-9

ORIGINAL ARTICLE

**E. Fokkema · E. G. E. de Vries · H. J. M. Groen · C. Meijer · W. Timens**

# Expression of apoptosis-related proteins and morphological changes in a rat tumor model of human small cell lung cancer prior to and after treatment with radiotherapy, carboplatin, or combined treatment

Received: 11 October 2002 / Accepted: 20 December 2002 / Published online: 21 February 2003
© Springer-Verlag 2003

**Abstract** *Purpose*: In order to understand the apoptosis pathway in tumor cells, differences in cell morphology and expression of apoptosis-related proteins induced by radiation and/or chemotherapy, were investigated in a rat double tumor model comparing cisplatin-sensitive and -resistant human small cell lung cancer tumors. *Methods*: The cisplatin-sensitive human small cell lung cancer cell line (GLC4) and its cisplatin-resistant subline (GLC4–CDDP) were each injected subcutaneously in a different hind limb of the rat. After 15–17 days, radiation (10 Gy), carboplatin (25 mg/kg, intraperitoneal), combined treatment, or no treatment was administered. In combined treatment, carboplatin was administered 24 h before radiation. Tumors were removed and fixed 72 h after carboplatin or 48 h after radiation. Paraffin-embedded slides were stained with hematoxylin/eosin for morphology. Expression of the apoptosis-related proteins p53, p21, Rb, bcl–2, bax, c–myc, Fas and Fas–L was assessed immunohistochemically. *Results*: In the GLC4 tumor, carboplatin treatment increased tumor cell size, tumor cell size heterogeneity, and number of apoptotic tumor cells. After radiation and combined treatment, these changes were more pronounced and multinuclear giant cells were observed. In GLC4–CDDP tumors, minimal changes were detected after carboplatin. Following radiation slight increases in tumor cell size, tumor cell size heterogeneity and number of apoptotic tumor cells were observed. No multinuclear giant cells were seen. After combined treatment, GLC4–CDDP showed cellular changes comparable to those in GLC4 cells after radiation or combined treatment, but no giant cells were observed. Untreated, both tumors were equally positive for p53, bax, Fas, Fas–L, c–myc and negative for Rb. Contrary to GLC4, untreated GLC4–CDDP tumors showed no p21 and bcl–2 expression. After combined treatment, an increase in number of bcl–2 positive cells was found in GLC4–CDDP tumors. No p21 was induced in GLC4–CDDP by any treatment modality. In GLC4 tumors, p21 was induced by radiation alone. No further changes in protein expression were induced by any treatment in GLC4 tumors. *Conclusion:* Following therapy, morphological changes in cell size and cell size heterogeneity were more pronounced in GLC4 than in GLC4–CDDP tumors. However, morphological changes in GLC4–CCDP tumors after treatment indicate that carboplatin plus radiotherapy may be effective also in cisplatin resistant tumor cells. An increase in p21 in GLC4 after radiation might facilitate apoptosis. The increase in number of Bcl–2 positive cells after combined treatment and the consistently negative p21 status after any treatment in GLC4–CDDP may protect these tumor cells from apoptosis as a part of their resistance mechanism to cisplatin.

**Keywords** Apoptosis · Small cell lung cancer · Rat · Platinum resistance

E. Fokkema · H. J. M. Groen
Department of Pulmonary Diseases,
University Hospital Groningen,
The Netherlands

E. G. E. de Vries · C. Meijer
Department of Medical Oncology,
University Hospital Groningen, The Netherlands

W. Timens (✉)
Department of Pathology,
University Hospital Groningen,
P.O. Box 30.001, 9700 RB Groningen, The Netherlands
e-mail: w.timens@path.azg.nl
Tel.: +31-50-3614684
Fax: +31-50-3632510

## Introduction

In the recent past, several studies have shown advantage of combined treatment of tumors with radiation and chemotherapy above single modality treatment with radiation alone. For instance, combining a standard radiation regimen with cisplatin showed a better response

and survival rate in cervical cancer [12, 21] and non-small cell lung cancer [22]. In head and neck cancer, a benefit of combining radiotherapy with cisplatin or carboplatin and 5-fluorouracil [1, 3, 4, 19, 24] was observed. However, not all tumor types may respond to such an extent to combined treatment. Biological parameters that determine radiation-sensitive or -resistant tumors, and sensitivity toward additional chemotherapy are important for optimizing therapy. Efficacy of radiation and/or chemotherapy depends on two modes of tumor cell death: programmed cell death (apoptosis) or necrosis. Presently, apoptosis is thought to be of major importance. Activation of the apoptosis pathway by radiation or chemotherapy may be reflected by changes in expression of apoptosis-related proteins, such as p53, p21, Rb, bcl–2, bax, c–myc, Fas and Fas–ligand (Fas–L) [5, 9]. These proteins are key proteins in the apoptosis pathway, which may be up- or downregulated, mutated, or absent in tumor cells, affecting the functionality of the apoptosis route and thereby providing a possible mechanism for therapy resistance [20]. Although changes in expression of these apoptosis-related proteins induced by radiation and chemotherapy have been reported [5, 9, 25], the exact contribution of these treatment modalities to the modulation of apoptosis in human tumors has not yet been fully revealed. Since drug resistance is a considerable problem in treatment of lung cancer, we established a double tumor model in the rat, with one tumor derived from a cisplatin-sensitive human small cell lung cancer (SCLC) cell line [11] and the other from its cisplatin-resistant subline, which shows cross-resistance to carboplatin [10, 17]. Both tumors were implanted in the same animal, each in a different hind limb. In this study, carboplatin was used as cytotoxic agent because recent human studies have been performed with carboplatin instead of cisplatin [3, 7] partially because of its milder toxicity profile than cisplatin. We investigated morphological changes and differences in expression of apoptosis-related proteins in the cisplatin-sensitive and the cisplatin-resistant tumors, shortly after radiation, carboplatin, or combined treatment. Differences in protein expression were evaluated between both tumors. In this study we investigated whether these proteins are up– or downregulated by radiation, chemotherapy, or combined treatment, and whether these changes are different between therapy-sensitive and -resistant human tumors. This may provide more insight in mechanisms of induction of apoptosis and mechanisms of drug resistance. This information may help optimize clinical treatment of patients.

## Materials and methods

### Chemicals

RPMI 1640 medium and fetal calf serum (FCS) were both purchased from Life Technologies (Paisley, Scotland). Bovine serum albumin (BSA) was obtained from Serva (Heidelberg, Germany), human AB serum from Sigma–Aldrich (Zwijndrecht, the Netherlands) and Matrigel from Becton Dickinson (Bedford, MA). Ketamine (Ketalar) was obtained from Parke–Davis (Munich, Germany), xylazine (Rompun) from Bayer (Leverkusen, Germany), and carboplatin from Bristol–Myers Squibb (Woerden, the Netherlands). Diaminobenzidine tetrahydrochloride (DAB) was purchased from ICN Biomedicals (Zoetermeer, the Netherlands), imidazol from Merck (Darmstadt, Germany), and mounting medium from International Medical (Zutphen, the Netherlands). Phosphate buffered saline (PBS, 150 mM NaCl, 7.6 mM $Na_2HPO4$, 1.6 mM $KH_2PO4$, pH 7.35) and Tris–buffer (0.1 M Tris–HCl at pH 9.0) were freshly made in our laboratory. Antigen retrieval (AR) solution consisted of 2% blocking reagent from Boehringer Mannheim (Mannheim, Germany) with 0.2% sodium dodecyl sulfate (SDS) in maleic acid buffer (pH 6.0).

### Animals and tumor induction

HSDHam/RNUrnu rats (Harlan, Horst, the Netherlands, 180–200 g) were used as hosts for both tumors. Experiments were approved by the local animal ethics committee of the Groningen University. Prior to tumor cell injection, rats were anaesthetized with $N_2O$ and halothane.

The SCLC cell line GLC4 and its subline with in-vitro acquired, stable cisplatin resistance GLC4–CDDP [10, 17] were used in our model. The GLC4–CDDP subline is characterized by an increased glutathione level, decreased DNA–platination, increased DNA repair capacity, but unchanged cellular platinum level, relative to GLC4 [10, 11, 16, 17]. Both cell lines express a p53 mutation. According to the method described by Hendrikse et al. [8], tumors were induced subcutaneously in the rat. In short, both cell lines were cultured in RPMI medium with 10% FCS, and harvested in exponentional growth phase. After washing cells twice with cold (4°C) PBS, cells were resuspended in ice-cold (0°C) PBS. For injection, $7.5\times10^6$ GLC4 cells and $20\times10^6$ GLC4–CDDP cells in 0.1 ml PBS added to 0.1 ml Matrigel were aspirated into separate syringes and kept on ice. Different cell numbers for each cell line were used to compensate for differences in growth rate in order to allow an equal tumor size after the growth period. Matrigel was used to facilitate cell growth after injection. The mixtures of cell suspension and Matrigel were injected subcutaneously in the hind limbs of the rat immediately after aspiration. GLC4 tumor cells were injected in the left limb and GLC4–CDDP cells in the right limb of the same animal. After reaching a size of 1.5–2 cm in diameter, tumors were treated as described below.

### Treatment design

Tumors were either irradiated with 10 Gy (1 Gy/min), treated with bolus carboplatin intraperitoneally (25 mg/kg body weight), or with a combined treatment of intraperitoneal carboplatin (25 mg/kg) and radiation (10 Gy). Untreated tumors served as controls. Carboplatin dosing was based on previous studies by Los et al. [14, 15] and was administered 24 h prior to radiation. Rats were sacrificed 48 h after radiotherapy, and tumors were excised. Each treatment modality was administered to at least three animals. All animals in each group were sacrificed at approximately 2.5 weeks after tumor cell injection, providing sufficient and equal tumor growth. Tumor size measurements were performed in the living animal by measuring the subcutaneously located tumor mass in three dimensions immediately prior to treatment and immediately prior to excision.

### Tissue preparation and evaluation of morphology

Immediately after excision, tumors were fixed in formalin (10%) for at least 24 h. Thereafter tumor tissue was embedded in paraffin. From all tumors, 3-μm sections were cut and placed on APES-coated slides. Prior to further processing, slides were deparaffinized. One slide per tumor was stained with standard hematoxylin/eosin and evaluated by a pathologist. These slides were evaluated for global morphological changes, regarding tumor cell size and

tumor cell size heterogeneity, relative number of tumor cells in apoptosis, and multinucleated "giant tumor cells".

### Immunohistochemistry

For all immunohistochemistry purposes except for c–myc staining, epitope demasking was performed by preheating. Slides were covered with AR solution and incubated in a pressure cooker three times for 10 min at 115°C with 5 min cooling at room temperature in between. For c–myc, AR was performed by incubating slides overnight at 80°C in Tris–buffer. After AR, slides were washed with PBS and incubated for 30 min with 0.3% $H_2O_2$ in PBS to block endogenous peroxidase activity and washed again with PBS. Subsequently, slides were incubated with the primary antibody diluted in PBS/1% BSA for 1 h. Primary antibodies used were: mouse monoclonal anti-p53, clone BP53–12–1 from Biogenex (San Ramona, CA; 1:800); mouse monoclonal anti-p21 (WAF 1), clone EA10 from Calbiochem (Cambridge, MA; 1:50); mouse monoclonal anti-Rb (NCL–Rb) from Novocastra Laboratories (Newcastle upon Tyne, UK; 1:50); mouse monoclonal anti-c–myc, clone 9E10.3 from Neomarkers (Hoersholm, Denmark; 1:150); mouse monoclonal anti-bcl–2, clone 124 from Dako (Glostrup, Denmark; 1:50); rabbit anti-bax N–20 from SantaCruz (Heidelberg, Germany; 1:600); mouse monoclonal anti-Fas, clone CH–11 from Upstate Biotechnology (Lake Placid, NY; 1:100); mouse monoclonal anti-Fas–L from Transduction Laboratories (Lexington, KY; 1:160).

Depending on the primary antibody, a rabbit anti-mouse immunoglobulin conjugated to peroxidase (Dako, Glostrup, Denmark; 1:50), a goat anti-rabbit conjugated to peroxidase (Dako, Glostrup, Denmark; 1:50), or a biotinylated rabbit anti-mouse antibody (Dako, Glostrup, Denmark; 1:300) were used for the second step (diluted in PBS/1% BSA/1% AB serum). Depending on the secondary antibody, goat anti-rabbit conjugated to peroxidase, rabbit anti-goat antibody conjugated to peroxidase (1:50), or streptavidin conjugated to peroxidase (1:300) (all from Dako, Glostrup, Denmark) were used for the third step (diluted in PBS/1% BSA/1% AB serum). After each step, the slides were washed with PBS. To visualize the bound antibodies, slides were incubated in DAB medium (25 mg DAB in 50 ml PBS with 50 mg imidazole and 50 µl 30% $H_2O2$) for 7 min. Slides were counterstained with hematoxylin for 2 min and rinsed with $H_2O$. After dehydration, slides were covered using mounting medium. Tissue of different human tumors staining positive for p53, Rb, p21, or c–myc were used as positive controls for these stainings. For Fas staining human liver tissue, for Fas–L human testis and for bcl–2 and bax human tonsil tissue were used as positive control. As negative control for the staining procedure, the primary antibody was omitted.

### Staining analysis

All stained tumors were evaluated for percentage of positive cells, for intensity of staining in a semi-quantitative way by grading from negative (0) to strongly positive (4) and for localization of staining (nucleus, cytoplasmatic or membrane located), all without knowledge of prior treatment. At least 20 microscopic fields were counted at a magnification of ×100.

### Statistics

Morphological variables and expression of apoptotic proteins were compared prior to and after treatment between treatment arms and tumor types. Immunohistochemistry staining results were analyzed with a non–parametric Mann–Whitney U test to establish differences between tumors and treatment arms. $P$ values <0.05 were considered as statistically significant.

## Results

### Tumor growth

A growth period of at least 2 weeks was required to reach sufficient tumor size of about 2 cm diameter for both tumor types, in the hind limb of the animals. Tumors were slightly larger after treatment (Table 1). Microscopy of the tumors showed clearly viable tumor cells. Especially after treatment, but also in controls, central areas with non–vital cells were observed, possibly due to ischemia in these fast-growing tumors or partially due to a treatment effect.

### Morphological changes

Untreated GLC4 tumors showed a more disorganized and heterogeneous aspect at histological examination, relative to GLC4–CDDP tumors. In contrast to GLC4 tumor cells, GLC4–CDDP tumor cells showed a more organized aspect in which cells show a more cohesive growth pattern. GLC4 tumors showed more heterogeneity in cell size and cell density in hematoxylin/eosin staining. These tumors consisted partly of large cells (diameter about 23.2 µm) and partly of small cells (diameter about 12 µm). GLC4–CDDP tumors mainly consisted of small cells (diameter about 14 µm). Figure 1 shows typical examples of morphological changes due to the various treatments in GLC4 and GLC4–CDDP tumors. Treatment with carboplatin alone induced increase of cell size, up to 26 µm, increased cell size heterogeneity and increased number of cells undergoing apoptosis in GLC4 tumors. Only minimal morphological changes were observed in GLC4–CDDP tumors. In GLC4 tumors, radiation alone induced a more pronounced increase in cell size and cell size heterogeneity. Furthermore it induced "multinucleated giant cells" with diameters of about 35 µm, and increased the number of cells undergoing apoptosis. In GLC4–

**Table 1** Mean tumor size (standard deviation) prior to and after treatment, immediately before resection. $P$ value indicates result of paired samples $t$-test, comparing sizes before and after treatment

| Tumor type | Treatment | $n$ | Mean tumor diameter (mm) before treatment (SD) | Mean tumor diameter (mm) after treatment (SD) | $P$ value |
|---|---|---|---|---|---|
| GLC4 | Control | 3 | 15.7 (4.6) | NA | |
| | Carbo | 2 | 15.3 (2.9) | 19.7 (7.9) | 0.02 |
| | rt | 2 | 14.2 (4.0) | 16.3 (4.1) | 0.03 |
| | Carbo/rt | 4 | 16.5 (6.6) | 18.9 (7.0) | 0.01 |
| GLC4–CDDP | Control | 3 | 13.6 (4.2) | NA | |
| | Carbo | 2 | 16.5 (9.0) | 20.7 (10.9) | <0.01 |
| | rt | 2 | 14.5 (5.3) | 17.2 (5.1) | 0.01 |
| | Carbo/rt | 4 | 15.4 (6.1) | 17.8 (7.7) | 0.01 |

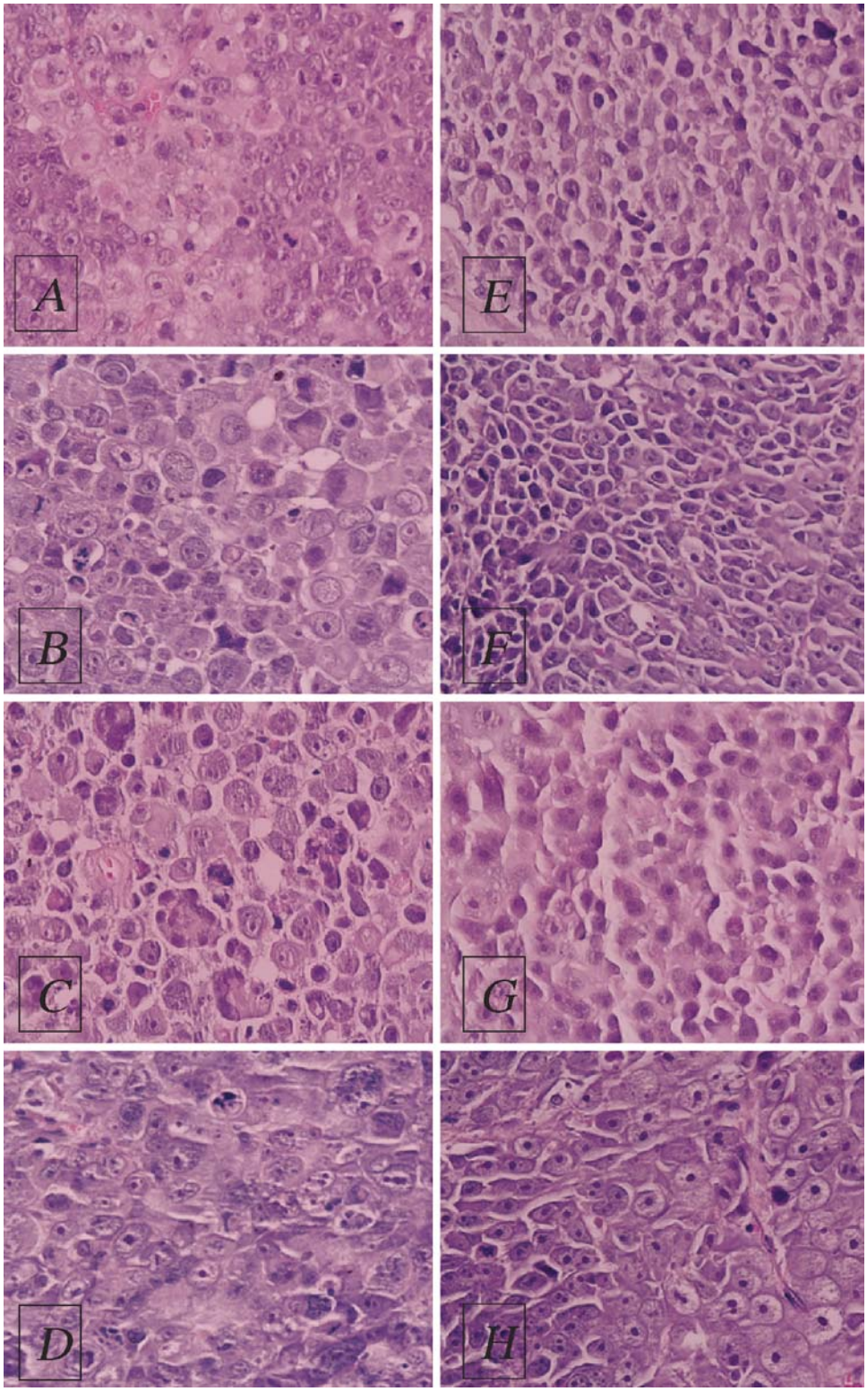



**Fig. 1** Examples of tumor tissue at magnification of ×100 from GLC4 and GLC4–CDDP prior to and after treatment. The *left panel* shows GLC4 tumors without treatment (**A**), treated with carboplatin (**B**), treated with radiation (**C**), and treated with combined treatment (**D**). The *right panel* shows GLC4–CDDP tumors without treatment (**E**), treated with carboplatin (**F**), treated with radiation (**G**), and treated with combined treatment (**H**)

CDDP tumors, radiation alone induced a slight increase in cell size and cell size heterogeneity and in number of cells undergoing apoptosis, but less pronounced than in GLC4 tumors. In GLC4–CDDP tumors treated with radiation alone, no "multinucleated giant cells" were observed. In GLC4 tumors, combined treatment induced an increase in cell size, as well as in cell size heterogeneity and in "multinucleated giant cells" comparable to changes after radiation. In GLC4–CDDP tumors, combined treatment induced cellular changes comparable to those in GLC4 tumors after radiation or combined treatment, although no giant cells were observed. This indicates that combined

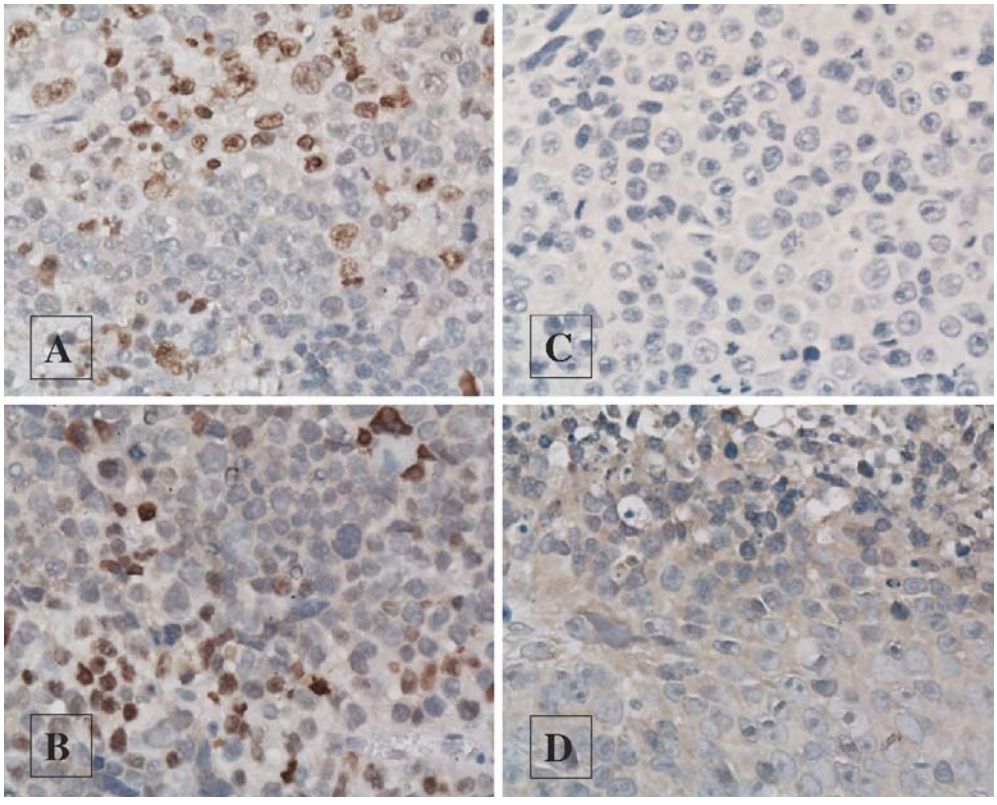



**Fig. 2** Examples of antigen staining at magnification of ×100. **A** p21 staining in untreated GLC4 tumor. **B** p21 staining in GLC4 tumor after radiation. **C** Bcl–2 staining in untreated GLC4–CDDP tumor. **D** bcl–2 staining in GLC4–CDDP after radiation

**Table 2** Changes in GLC4 and GLC4–CDDP cell morphology after treatment relative to untreated tumors. – unchanged, not present, + slight increase, ++ marked increase

| Morphology | Treatment | | |
|---|---|---|---|
| | Carboplatin | Radiation | Radiation and carboplatin |
| GLC4 | | | |
| Cell size | + | ++ | ++ |
| Cell size heterogeneity | + | ++ | ++ |
| Giant cells | – | + | + |
| Apoptosis | + | ++ | ++ |
| GLC4–CDDP | | | |
| Cell size | – | + | ++ |
| Cell size heterogeneity | – | + | ++ |
| Giant cells | – | – | – |
| Apoptosis | – | + | ++ |

treatment also affects cisplatin–resistant cells. An overview of morphological changes is given in Table 2.

## Immunohistochemistry

### *Untreated tumors*

Untreated, both tumor types highly expressed p53, bax, c–myc, Fas and Fas–L. Mean staining percentages (standard deviation) for untreated GLC4 tumor cells were 92±8% for p53, 32±18% for p21, 75±7% for bcl–2, 100±0% for bax, and 60±35% for Fas–L. Mean staining percentages (standard deviation) for untreated GLC4–CDDP tumor cells were 97±6% for p53, 0±0% for p21, 0±0% for bcl–2, 93±12% for bax, and 92±10% for Fas–L. All tumors were negative for Rb and showed 100% of cells positive for Fas and c–myc.

Untreated GLC4–CDDP tumors lacked p21 protein expression, contrary to GLC4 tumors.

### *After treatment*

In GLC4, p21 expression was mainly observed in the most vital tumor regions, and this expression increased after radiation alone to 80±14% and, to a lesser extent, 60±14% after combined treatment, although the latter was statistically not significant. GLC4–CDDP tumors still lacked p21 after any treatment modality.

In untreated GLC4 tumors, 75% of the cells stained positive for bcl–2, while untreated GLC4–CDDP tumors showed no bcl–2 expression at all. Impressive increase in number of bcl–2 positive cells was observed after treatment in GLC4–CDDP tumors. (Fig. 2). In GLC4–CDDP tumors, after treatment, the number of cells expressing bcl–2 increased from no expression to 85–100% expression, depending on treatment type. Treatment with carboplatin resulted in a slightly less but still impressive increase in bcl–2 expression (85±7%), compared to radiation (100±0%) and combined treatment (93±12%). Bcl–2 expression was highest around zones

with non–vital cells, in contrast to p21 expression, as observed in GLC4.

No clear alteration of expression of p53, Rb, c–myc, Fas, bax and Fas–L expression was observed after any treatment. Intensity of Fas staining was slightly higher around zones of non-vital cells.

## Discussion

Scarce data are available concerning changes in expression of apoptosis related proteins in human tumors before and after treatment by chemotherapy and/or radiation. The human tumor model used in this study with a therapy-sensitive and a therapy-resistant counterpart provides a unique way to investigate these possible changes and to investigate differences shortly after treatment by carboplatin, radiation or a combined treatment. The model may prove to be useful to evaluate the clinically relevant potentiation of combined treatment.

To validate our model, we first evaluated morphological changes following treatment. GLC4 showed more sensitivity to treatment than GLC4–CDDP, resulting in more pronounced morphological changes and the appearance of multinucleated giant cells after radiation and combined treatment. However, it should be taken into account that our experiments were conducted at equimolar carboplatin dose for the cisplatin-sensitive and -resistant tumors. In a previous in vitro study, GLC4–CDDP also showed cross–resistance against radiation. This study further showed that incubation with carboplatin before radiation could enhance the effect of radiation on cell survival [6]. In our study, we observed an increase in morphological changes in GLC4–CDDP after combined treatment, indicating a radio-sensitizing effect of carboplatin. No multinucleated giant was observed in GLC4–CDDP tumors in contrast to GLC4. This type of tumor cell seems to continue dividing its nucleus without dividing its cytoplasm. This phenomenon has been previously observed after radiation in several cell lines with mutant p53 or without p53 [2, 13, 18]. Mutated p53 may result in disruption of cell cycle checkpoints and genomic instability leading to generation of more multinuclear giant cells. Furthermore, human bladder carcinoma cell lines irradiated with 6 Gy in G1 phase showed more giant cells and multinucleated cells than cells irradiated in S phase [13]. This could explain why not all cells in the tumors obtained from our tumor model were affected, since the tumor cells may be in different cell cycle phases at the time of treatment. Although both GLC4 and GLC4–CDDP in our study showed p53 mutation, GLC4 cells were the most sensitive to generate multinucleated and giant cells at equimolar carboplatin dose. Nevertheless, both tumor types showed evidence of changes in cell morphology, especially after combined treatment. The main interest in the present study was to establish the effect of the combined treatment with carboplatin and radiation on apoptosis-related proteins. Several clinical studies in patients with solid tumors have shown the benefit of the addition of chemotherapy to radiation in the treatment of non–small cell lung cancer, cervical carcinoma [12, 22, 23], and head and neck cancer [1, 3, 4, 24]. The cytotoxic agent potentially acts as a radiosensitizer in the tumor cells, possibly by priming the apoptotic route which makes the cells more susceptible to radiation. In this study, we investigated the effect of treatment on the expression of apoptosis-related proteins, such as p53, p21, Rb, bcl–2, bax, c–myc, Fas and Fas–L. Except for an increase in p21 expression after radiation, no major changes in the expression of these proteins in GLC4 tumors were observed after any therapy. However, untreated GLC4 tumors already showed a strong positivity for p53, c–myc, bax, Fas and Fas–L. Therefore, a further increase of these proteins may be undetectable by immunohistochemistry. In contrast to GLC4, we observed a clear increased presence of bcl–2 protein after treatment with radiotherapy, chemotherapy or combination, in GLC4–CDDP tumors. Bcl–2 was mainly located in the zones around areas with apoptotic cells. Bcl–2 is known as a protein that protects against apoptosis. Induced expression of bcl–2 might be a response to cell damage-induced onset of apoptosis and a last effort of these cells to try to avoid apoptosis under these conditions. However, what seems to be induction could also be a selection of tumor cells able to upregulate bcl–2, which protects them from apoptosis. This would then suggest, at least partial, therapy resistance.

Furthermore, we observed a clear difference in p21 expression between GLC4 and GLC4–CDDP tumors, as GLC4–CDDP tumors showed no p21 prior to and after treatment. P21 is a protein that acts downstream of p53 in cell cycle regulation. The lack of p21 expression in GLC4–CDDP can potentially also prevent apoptosis. Therefore, induction of bcl–2 and lack of p21 might both protect these tumor cells from apoptosis and play a role in their resistance to cisplatin. Another possibility is that the increased bcl–2 expression is caused by selection of bcl–2-positive cells which survive apoptosis. Despite the possible protection by bcl–2 against apoptosis, the morphological changes in GLC4–CDDP tumors after treatment indicate that carboplatin plus radiotherapy may be effective also in cisplatin-resistant tumor cells.

In conclusion, following therapy, morphological changes in cell size and cell size heterogeneity were more pronounced in GLC4 than in GLC4–CDDP tumors. No major changes in the expression of apoptosis–related proteins in GLC4 tumors were observed after any treatment. In GLC4–CDDP, all treatment modalities induced bcl–2 in combination with a consistently negative p21 status in these tumor cells, providing a possible protection from apoptosis. However, morphological changes in GLC4–CDDP tumors after especially combined treatment, indicate that degenerative processes are going on, including apoptosis or at least initiation of apoptosis, as observed in previous studies [2, 13, 18]. This indicates that carboplatin plus radiotherapy may be effective in treatment of cisplatin-resistant tumor cells.

## References


1. Adelstein DJ, Lavertu P, Saxton JP, Secic M, Wood BG, Wanamaker JR, Eliachar I, Strome M, Larto MA (2000) Mature results of a phase III randomized trial comparing concurrent chemoradiotherapy with radiation therapy alone in patients with stage III and IV squamous cell carcinoma of the head and neck. Cancer 88:876–883
2. Bracey TS, Williams AC, Paraskeva C (1997) Inhibition of radiation-induced G2 delay potentiates cell death by apoptosis and/or the induction of giant cells in colorectal tumor cells with disrupted p53 function. Clin Cancer Res 3:1371–1381
3. Calais G, Alfonsi M, Bardet E, Sire C, Germain T, Bergerot P, Rhein B, Tortochaux J, Oudinot P, Bertrand P (1999) Randomized trial of radiation therapy versus concomitant chemotherapy and radiation therapy for advanced-stage oropharynx carcinoma. J Natl Cancer Inst 91:2081–2086
4. Cheng SH, Tsai SY, Yen KL, Jian JJ, Chu NM, Chan KY, Tan TD, Cheng JC, Hsieh CY, Huang AT (2000) Concomitant radiotherapy and chemotherapy for early-stage nasopharyngeal carcinoma. J Clin Oncol 18:2040–2045
5. Dewey WC, Ling CC, Meyn RE (1995) Radiation-induced apoptosis: relevance to radiotherapy. Int J Radiat Oncol Biol Phys 33:781–796
6. Groen HJM, Sleijfer S, Meijer C, Kampinga HH, Konings AW, de Vries EGE, Mulder NH (1995) Carboplatin- and cisplatin-induced potentiation of moderate–dose radiation cytotoxicity in human lung cancer cell lines. Br J Cancer 72:1406–1411
7. Groen HJM, van der Leest AHD, Snoek WJ, Nossent B, Oosterhuis B, Nabers H, Smit WJGM, Timmer PR, Otter R, van Putten JWG, Fokkema E, Hoekstra HJ, Hermans J, Szabo BG, de Vries EGE, Mulder NH (1999) Phase III study of continuous carboplatin over 6 weeks with radiation versus radiation alone in stage III non-small cell lung cancer (NSCLC). Proc Am Soc Clin Oncol 17:466a
8. Hendrikse NH, de Vries EGE, Eriks-Fluks L, van der Graaf WTA, Hospers GAP, Willemsen AT, Vaalburg W, Franssen EJ (1999) A new in vivo method to study P-glycoprotein transport in tumors and the blood–brain barrier. Cancer Res 59:2411–2416
9. Hickman, JA (1992) Apoptosis induced by anticancer drugs. Cancer Metastasis Rev 11:121–139
10. Hospers GAP, Mulder NH, de Jong B, de Ley L, Uges DRA, Fichtinger-Schepman AMJ, Scheper RJ, de Vries EGE (1988) Characterization of a human small cell lung carcinoma cell line with acquired resistance to cis-diamminedichloroplatinum(II) in vitro. Cancer Res 48:6803–6807
11. Hospers GAP, Meijer C, de Leij L, Uges DRA, Mulder NH, de Vries EGE (1990) A study of human small-cell lung carcinoma (hSCLC) cell lines with different sensitivities to detect relevant mechanisms of cisplatin (CDDP) resistance. Int J Cancer 46:138–144
12. Keys HM, Bundy BN, Stehman FB, Muderspach LI, Chafe WE, Suggs CL, Walker JL, Gersell D (1999) Cisplatin, radiation, and adjuvant hysterectomy compared with radiation and adjuvant hysterectomy for bulky stage IB cervical carcinoma. N Engl J Med 340:1154–1161
13. Leonhardt EA, Trinh M, Forrester HB, Dewey WC (1998) Persistent decrease in viability as a function of X irradiation of human bladder carcinoma cells in G1 or S phase. Radiat Res 149:343–349
14. Los G, Verdegaal EM, Mutsaers PH, McVie JG (1991) Penetration of carboplatin and cisplatin into rat peritoneal tumor nodules after intraperitoneal chemotherapy. Cancer Chemother Pharmacol 28:159–165
15. Los G, Smals OAG, van Vugt MJH, van der Vlist M, den Engelse L, McVie JG, Pinedo HM (1992) A rationale for carboplatin treatment and abdominal hyperthermia in cancers restricted to the peritoneal cavity. Cancer Res 52:1252–1258
16. Meijer C, Mulder NH, Hospers GAP, Uges DRA, de Vries EGE (1990) The role of glutathione in resistance to cisplatin in a human small cell lung cancer cell line. Br J Cancer 62:72–77
17. Meijer C, Mulder NH, Timmer–Bosscha H, Sluiter WJ, Meersma GJ, de Vries EGE (1992) Relationship of cellular glutathione to the cytotoxicity and resistance of seven platinum compounds. Cancer Res 52:6885–6889
18. Peled A, Schwartz D, Elkind NB, Wolkowicz R, Li R, Rotter V (1996) The role of p53 in the induction of polyploidity of myelomonocytic leukemic M1/2 cells. Oncogene 13:1677–1685
19. Pignon JP, Bourhis J, Domenge C, Designe L (2000) Chemotherapy added to locoregional treatment for head and neck squamous-cell carcinoma: three meta-analyses of updated individual data. MACH-NC Collaborative Group. Meta-analysis of chemotherapy on head and neck cancer. Lancet 355:949–955
20. Reed JC (1999) Dysregulation of apoptosis in cancer. J Clin Oncol 17:2941–2953
21. Rose PG, Bundy BN, Watkins EB, Thigpen JT, Deppe G, Maiman MA, Clarke-Pearson DL, Insalaco S (1999) Concurrent cisplatin-based radiotherapy and chemotherapy for locally advanced cervical cancer. N Engl J Med 340:1144–1153
22. Schaake-Koning C, van den Bogaert W, Dalesio O, Festen J, Hoogenhout J, van Houtte P, Kirkpatrick A, Koolen M, Maat B, Nijs A (1992) Effects of concomitant cisplatin and radiotherapy on inoperable non-small-cell lung cancer. N Engl J Med 326:524–530
23. Trovo MG, Minatel E, Franchin G, Gobitti C, Roncadin M, De Paoli A, Arcicasa M, Boz G, Bortolus R (1992) Radiotherapy enhanced by cis-platinum in stage III non-small cell lung cancer: a phase II study. Radiother Oncol 23:241–244
24. Vokes EE, Kies MS, Haraf DJ, Stenson K, List M, Humerickhouse R, Dolan ME, Pelzer H, Sulzen L, Witt ME, Hsieh YC, Mittal BB, Weichselbaum RR (2000) Concomitant chemoradiotherapy as primary therapy for locoregionally advanced head and neck cancer. J Clin Oncol 18:1652–1661
25. Wouters BG, Giaccia AJ, Denko NC, Brown JM (1997) Loss of p21Waf1/Cip1 sensitizes tumors to radiation by an apoptosis-independent mechanism. Cancer Res 57:4703–4706

Virchows Arch (2003) 442:356–363
DOI 10.1007/s00428-003-0768-4

ORIGINAL ARTICLE

**Keiko Mashimo · Shigeru Sato · Youkichi Ohno**

# Chronic effects of ethanol on cultured myocardial cells: ultrastructural and morphometric studies

Received: 17 October 2002 / Accepted: 17 December 2002 / Published online: 19 February 2003
© Springer-Verlag 2003

**Abstract** Ultrastructural alterations of the myocardium due to chronic ethanol exposure were investigated using an in vitro system – mouse ventricular myocardial cells in a monolayer culture, which were spontaneously and synchronously contracting – by chronic exposure to 12.5, 50, and 200 mM ethanol for up to 21 days. Morphometric analyses revealed that exposure to 12.5 mM ethanol for 14 days induced an increase in the number of residual bodies, which are lysosomes containing electron-dense, amorphous materials. Some cells exposed to 50 mM ethanol for 14 days contained an accumulation of glycogen granules, increasing in inverse proportion to the mitochondrial volume. The volumetric proportion of myofibrils on day 14 decreased as the ethanol dose became lower, and was in proportion to large and giant mitochondria within the limits of three ethanol groups. Dose-dependent increases in the size and volumetric proportion of mitochondria were observed after the 14-day exposure; at a low dose (12.5 mM) mitochondria of usual size tended to increase, whereas at a high dose (200 mM) giant mitochondria increased. Coincidentally with this mitochondrial increase or gigantism, all ethanol groups showed higher beat rates than the control. Consequently, it is most likely that chronic 14-day exposures to these three ethanol doses remodel the cellular function of the in vitro myocardium in different ways; the 200-mM dose induced mitochondrial hypertrophy, an adaptive response to switch myocardial energy metabolism over to some special one; the 50-mM dose was a boundary dose; and the 12.5-mM dose mostly mimicked the chronic in vivo administration of ethanol and induced slightly degenerative alterations – increased residual bodies and lysosomes, decreased myofibrils and lowered mitochondrial respiratory function.

**Keywords** Ethanol · Myocardial cells · Culture · Ultrastructure · Mouse

K. Mashimo (✉) · Y. Ohno
Department of Legal Medicine,
Nippon Medical School, 1-1-5 Sendagi, Bunkyo-ku,
113-8602 Tokyo, Japan
e-mail: kei-mam@nms.ac.jp
Tel.: +81-3-38222131
Fax: +81-3-58145680

S. Sato
Central Institute for Electron Microscopic Researches,
Nippon Medical School,
Bunkyo-ku, 113-8602 Tokyo, Japan

## Introduction

Some chronic alcoholics suffer from a variety of cardiac disorders, such as tachycardia, cardiac hypertrophy and alcoholic cardiomyopathy. An examination of the ultrastructure of alcoholics' hearts revealed dilatation of the sarcoplasmic reticulum (SR) and transverse (T)-tubules, an increased number or swelling of mitochondria, increased lysosomes, myofibrillar lysis and increased lipid droplets and lipofuscin [1, 5, 15, 39]. Using the in vivo hearts of animals chronically fed ethanol, however, no consistent view of ultrastructural alterations has yet been achieved, despite the efforts of many investigators [3, 6, 8, 10, 11, 12, 14, 17, 21, 25, 33, 34].

Using an in vitro system with spontaneously and synchronously contracting myocardial cells in a monolayer culture, we previously succeeded in finding ethanol-induced acute ultrastructural changes in the myocardium over a 24-h period, such as a rapid increase and subsequent dose-dependent return to normalcy of glycogen granules, a dose-dependent occurrence of mitochondrial fusion, and an appearance of giant mitochondria at large doses (200 mM and 500 mM), suggesting a dysfunction in the energy-generating systems [27, 28]. In addition, ethanol concentrations up to 200 mM did not induce any degenerative or lethal changes in cultured myocardial cells during a 24-h exposure, though 500 mM did [23]. The present study employed the same in vitro ventricular myocardium isolated from humoral and other indirect effects so as to elucidate the direct effects of chronic ethanol exposure for up to 21 days at a wide range of concentrations (12.5, 50 and 200 mM) on the

ultrastructure of the ventricular myocardium, which is a continuation of our previous study on acute effects [27].

## Materials and methods

### Culture and ethanol exposure

Ventricular myocardial cells in monolayer sheets were prepared according to previously reported procedures [27]. Briefly, ventricles were excised from neonatal mice (ddy, 0-day old), and were minced into 1- to 2-$mm^3$ pieces. Tissue fragments were gently agitated at 37°C in a Hank's salt solution containing 0.05% Bactotrypsin (Difco) and 0.01% DNase (Boehringer Mannheim). This trypsinization was repeated several times. The supernatant cell suspension after each trypsinization was transferred into cold Eagle's minimum essential medium (Eagle MEM) with 10% fetal bovine serum (FBS; HyClone), which was centrifuged. Cells were suspended in Eagle MEM with 20% FBS and filtered through a nylon mesh (200 mesh/inch). After a pre-incubation for 4 h to exclude non-muscle cells, unattaching cells were inoculated in gelatin-coated MicroWell Modules (Nunc) at a concentration of $1.8\times10^4$ cells/well. The mice were cared for in accordance with "The Regulations of Animal Experimentation of Nippon Medical School", which are based on "The Guidelines of the International Committee on Laboratory Animals, 1974".

After cultivation for 5 days, myocardial cells grew to contact mutually so that they formed a monolayer sheet and contract synchronously. And then, the culture medium was replaced with Eagle MEM containing 10% FBS buffered with 10 mM HEPES (*N*-(2-hydroxyethyl)piperazine-*N'*-(2-ethanesulfonic acid)) or 20 mM BES (*N,N-bis*-(hydroxyethyl)-2-aminoethanesulfonic acid) (pH 7.4), and the cultured cells were then placed in a $CO_2$-free environment at 37°C. From 1 h to 2 h later, the chronic exposure to ethanol (0, 12.5, 50 and 200 mM) was started by replacing the normal medium with one containing ethanol. Culture modules were placed in a culture dish which was either wrapped in Parafilm to prevent the ethanol from evaporating or put into a sealed glass container with an ethanol solution having the same concentration as that of the culture medium so that the ethanol vapor would maintain the given ethanol concentration of the culture medium. Over a period of 2 days, the ethanol concentration of the medium decreased by about 10% when wrapped in Parafilm and by about 5% in the glass container. The medium was renewed every 1–2 days.

### Beat rate and ultrastructure

Spontaneous contractions of ventricular myocardial cells in a monolayer were counted through a phase-contrast inverted microscope (TMD, Nikon, Tokyo) at 3 h after the change of the ethanol medium, since the beat rate of the cells accelerated dose dependently just after the change [22, 23].

The cells were fixed and prepared for an electron microscope examination on the 7th, 14th and 21st days of exposure to ethanol, according to a method previously reported [27]. The chronic-exposure experiments were performed in triplicate.

### Morphometric analysis

The ratios of the area of intracellular organelles – glycogen granules, myofibrils, lysosomes, residual bodies (a kind of lysosome containing electron-dense, amorphous materials) and mitochondria – to cytoplasm were obtained using the following procedure. Each type of intracellular organelle in an electron microscope photograph was painted with a different color. An image of the colored photograph was taken with an image scanner (Hewlett Packard, ScanJet CX/T) using the Adobe Photoshop program (Adobe Systems Inc, San Jose, CA, USA). The color for a particular type of organelle was selected with Photoshop and its area was measured using the Image 1.62 program (NIH, MD, USA).

### Statistics

An analysis of the variance of the beat rate was performed using a two-factor analysis of variance (ANOVA) for time and ethanol concentration. Following one-factor ANOVA for ethanol concentration, a multiple comparison was performed on each day using two-tailed Dunnett's test. Morphometric data were analyzed using a non-parametric Kruskal-Wallis rank test for ethanol concentration; then, a multiple comparison was performed using the Tukey test as a post-hoc test. Correlation analysis was performed using Pearson's correlation. Results are considered statistically significant when $P<0.05$.

## Results

### Spontaneous contractions

The control monolayer sheets of ventricular myocardial cells continued contracting spontaneously and synchronously as a whole even on day 14 of ethanol experiment, and most of them also did on day 21; but the contractions gradually slowed throughout the experimental period (Fig. 1). Most of the ethanol-exposed sheets continued contracting on day 14 of exposure, while some of them ceased contracting. On day 21, parts of the sheets of the ethanol groups contracted weakly and other

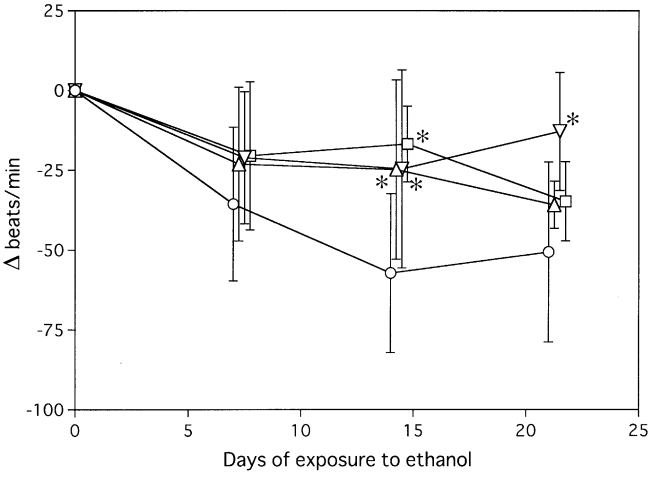



**Fig. 1** Time course of changes in the beat rates of mouse ventricular myocardial cells in monolayer cultures. The beat rate was counted 3 h after the ethanol medium was replaced with a fresh one. The values represent changes in beats per minute from those on the day when ethanol exposure started, and are the average of three independent series of ethanol exposures. *Symbols* for the same exposure time are shifted little by little to the right in order of ethanol concentration so as to show deviations. The number of samples decreased gradually as cell sheets were fixed in sequence for microscopic observation from 11 to 14 on day 7, and 5 to 9 on day 14 to 3 to 5 on day 21. Statistical multiple comparisons were performed using two-tailed Dunnett's test. *Circle* 0 mM; *triangle* 12.5 mM; *inverted triangle* 50 mM; *square* 200 mM. *$P<0.05$ versus corresponding time control

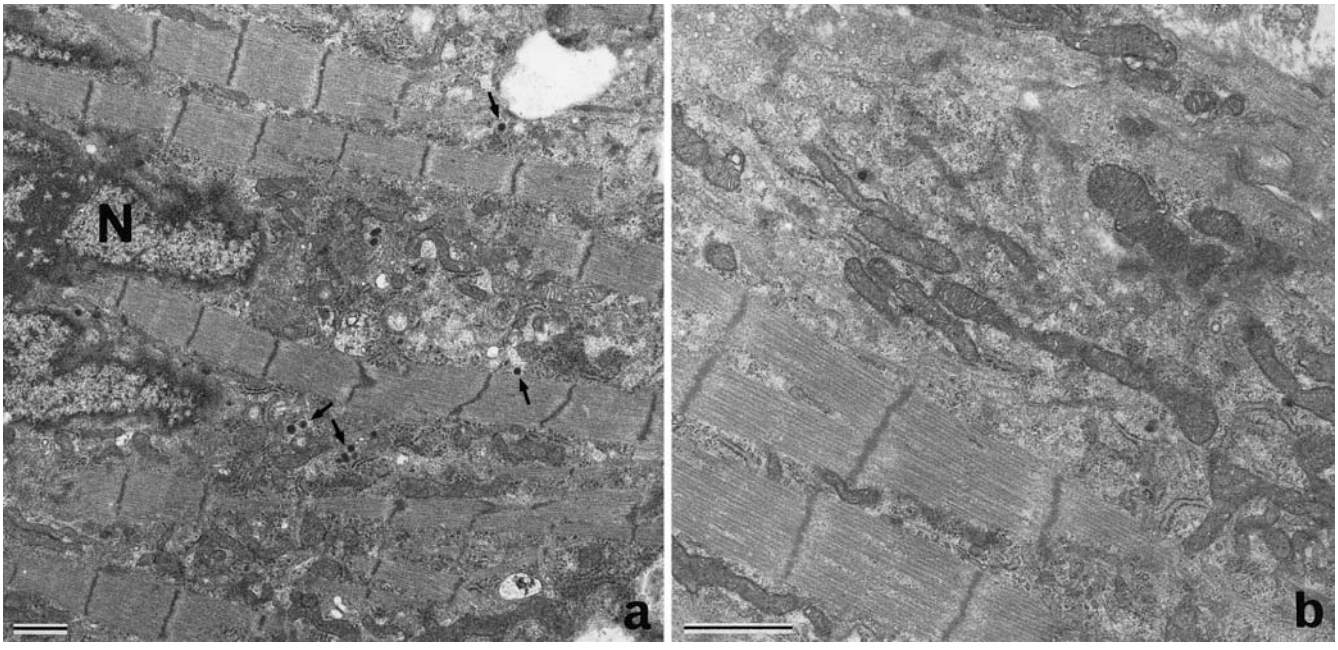



**Fig. 2** Electron microscope photographs of mouse ventricular myocardial cells in a monolayer after cultivation for 6 days (**a**) and 26 days (**b**) in the normal medium. *N* nucleus. *Bars* 1 μm. **a**, **b** The control ultrastructure was almost the same as that of the normal myocardium in vivo even on day 26. Specific granules like atrial specific granules observed in the atrial myocardium in vivo were seen in the early period of cultivation (*arrows*). **a** ×7000. **b** ×14,000

parts did not, while all of the control myocardial sheets but one contracted.

Parts of the monolayer sheets detached from the substratum but still contracted on day 7 of ethanol experiment and, thereafter, regardless of ethanol exposure. Some of the ethanol-exposed sheets detached as a whole from the substratum. After cultivation for 33 days, spontaneous contraction was observed in some cases, but not in others, regardless of ethanol exposure.

The absolute beat rates on the day of the start of ethanol exposure ranged approximately from 100 beats/min to 180 beats/min. Then, for statistical analysis, the beat rate of each sheet of myocardial cells was normalized with that on the start day (day 0) (Fig. 1).

The beat rates of all the ethanol groups changed in a similar way regardless of the concentration of ethanol. However, the beat rate of the control group was always slower than those of the ethanol groups ($P<0.01$ for ethanol concentration by two-factor ANOVA). In particular, there was a statistically significant difference between each of the ethanol groups exposed for 14 days and the corresponding time control group according to Dunnett's test (Fig. 1). In addition, there was a statistically significant difference between the 50-mM group on day 21 and the corresponding control group.

## Ultrastructure

Figure 2a shows the typical ultrastructure of control ventricular myocardial cells in a monolayer culture. This ultrastructure was almost the same as that of the normal myocardium in vivo, except that the cultured cells contained elongated mitochondria and increased numbers of glycogen granules and rough endoplasmic reticulum (rER) [27]. Even on day 21 of ethanol exposure, the corresponding control ultrastructure exhibited only slight changes, apart from a reduced amount of glycogen granules (Fig. 2b). Finally, on day 28, some of the control myocardial cells ceased contracting, as mentioned above, and exhibited a degenerative or necrotic ultrastructural appearance (data not shown).

**Table 1** Changes in amount of glycogen granules in cultured ventricular myocardial cells after chronic exposure to ethanol. The amount of glycogen granules in normal myocardial cells after culture for 5 days is regarded as +1

| Concentrationof ethanol (mM) | Days of ethanol exposure | | |
|---|---|---|---|
| | 7 | 14 | 21 |
| 0 | +~+++ | ±~+ | ± |
| 12.5 | ± | ± | ± |
| 50 | +~+++ | +~+++ | ± |
| 200 | + | ± | ± |

The amount of glycogen granules gradually decreased over 21 days in all experimental groups except the 50-mM ethanol one (Table 1). In some series of cells exposed to 50 mM ethanol, the amount of glycogen granules, which was in accumulated form, remained at an elevated level until day 14 (Fig. 3a; asterisks).

The amounts of myofibrils in the control and ethanol-exposed cultures were almost the same throughout a 21-

day period, except for a reduced amount after 14-day exposure to 12.5 mM ethanol and 21-day exposure to 200 mM ethanol (Fig. 3). The lengths of sarcomeres were measured with a vernier caliper and did not change due to ethanol exposure (data not shown). The amount of SR also remained nearly unaffected by ethanol, though it tended to decrease in the early stages for 12.5 mM ethanol and to increase after a 14-day exposure to 200 mM ethanol. SR and T-tubules had a tendency to dilate slightly if at all in ethanol groups, but within the normal range.

The amount of rER tended to decrease gradually in the control cells over 21 days, and also in all ethanol groups, though the 12.5-mM group exhibited a smaller decrease. The number of lysosomes (Fig. 3b, c, f; small arrows) and residual bodies (Fig. 3c, f; large arrowheads) increased in the ethanol groups, especially after a 14-day exposure to 12.5 mM ethanol.

Specific granules, which seem to correspond to atrial specific granules containing atrial natriuretic peptide (ANP), were occasionally seen in the perinuclear region of the control and 50-mM and 200-mM groups till day 7 but not thereafter (Fig. 2a, small arrows). Hardly any were observed for 12.5-mM exposure even on day 3 and thereafter.

Mitochondrial fusion was occasionally observed following ethanol exposure in a dose-dependent manner (Fig. 3b, e; small arrowheads): on no or rare occasions for 12.5 mM on days 7–21, on a few occasions for 50 mM on days 7–21, and on more occasions for 200 mM on days 7–14. Giant mitochondria were observed following ethanol exposure in a dose-dependent manner (Table 2) and their appearance almost paralleled the occurrence of mitochondrial fusion: on very few occasions for 12.5 mM ethanol, almost the same as for the control; on more occasions for 50 mM, especially on day 14 and day 21; and on a much larger number of occasions for 200 mM (Fig. 3b, d, e), especially on day 14. In addition, for 200 mM ethanol strange-shaped giant mitochondria, which seemed to be formed by the fusion of a thick, elongated mitochondrion and a round, giant one, were often observed (Fig. 3d, e; large arrows).

**Table 2** Incidence of giant mitochondria and changes in area occupied by mitochondria in cultured ventricular myocardial cells after chronic exposure to ethanol. Giant mitochondria have a cross-sectional area five times larger than that of usual-sized mitochondria. The area occupied by mitochondria in normal myocardial cells after culture for 5 days is regarded as ++. *g* hardly any giant mitochondria were detected, *G* giant mitochondria were occasionally detected, *GG* giant mitochondria were frequently detected, *GGG* giant mitochondria were very frequently detected

| Concentrationof ethanol (mM) | Days of ethanol exposure | | |
|---|---|---|---|
| | 7 | 14 | 21 |
| 0 | g<br>++ | G<br>++ | g<br>+~++ |
| 12.5 | g<br>+~++ | G<br>++~++++ | G<br>++ |
| 50 | G<br>++ | G~GG<br>++~++++ | G~GG<br>++~+++ |
| 200 | G~GG<br>++~+++ | GG~GGG<br>++~++++ | g~GG<br>+~++ |

The cytoplasmic area occupied by mitochondria increased after a 14-day exposure to all concentrations of ethanol (Table 2; Fig. 3c, d) and returned to the previous level on day 21 in the 12.5-mM and 200-mM ethanol groups, but not in the 50-mM group (Table 2). However, there was a difference in mitochondrial size on day 14 between the 12.5-mM ethanol group and the groups exposed to 50 mM or more: mitochondria were the usual size but rather elongated in shape in 12.5 mM ethanol (Fig. 3c) compared with the control ones (Fig. 2a, b), while they were larger in diameter or more gigantic in 50 mM and 200 mM ethanol (Fig. 3d, e).

## Morphometric analysis

Ultrastructural changes due to ethanol exposure seemed to be the most marked on day 14. Then, in order to confirm this impression, the cross-sectional areas of organelles occupying the cytoplasm after 14-day exposure to 0–200 mM ethanol were digitized and statistically analyzed.

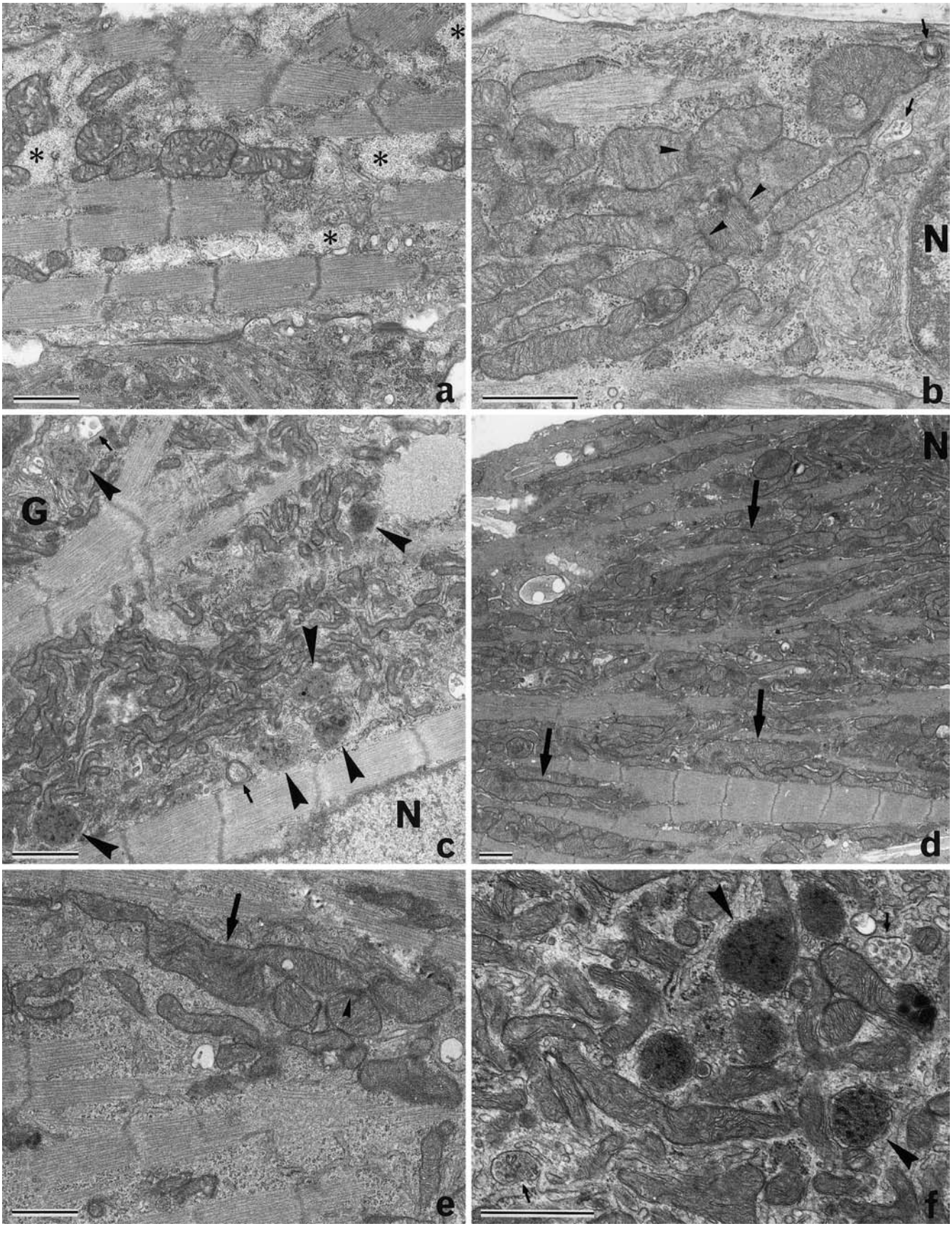
Glycogen granules took two forms: focally accumulated and monoparticulate scattered among myofibrils and cytoplasm. We counted here only glycogen granules in accumulated form, and they increased only for 50 mM ethanol in some chronic series but not in other series (Fig. 4) without any statistical significance between the control and the 50-mM group.

The amount of myofibrils decreased as the ethanol dose became lower among all ethanol groups (Fig. 4; $P$=0.03 by Kruskal-Wallis test). There was a significant difference between the control and the 12.5-mM group using the Tukey test.

The number of lysosomes and residual bodies increased for the 12.5-mM ethanol group compared with the control and other higher concentration groups (Fig. 4; $P$<0.03 by Kruskal-Wallis test), though there were statistical differences among the groups only for residual bodies (12.5 mM vs control or 200 mM).

The cross-sectional area of a usual mitochondrion was here estimated to be about 0.55 $\mu m^2$, which was obtained by averaging the areas of control mitochondria. The term "giant mitochondria" is used here to mean those with a cross-sectional area more than five times as large as that of usual ones, as mentioned in a previous study [27]. In addition, for convenience we refer to mitochondria with a cross-sectional area more than three times but less than five times as large as that of usual ones as "large mitochondria", and to mitochondria with a cross-sectional area up to three times as large as that of usual ones as "usual-sized mitochondria".

The ratio of cross-sectional area of mitochondria to the area of the cytoplasm dose dependently increased (Fig. 5; $P$=0.037 by Kruskal-Wallis test), with a significant difference for 200 mM ethanol compared with the control. The ratio of large or giant mitochondria either


a
b
N
c
G
N
d
N
e
f

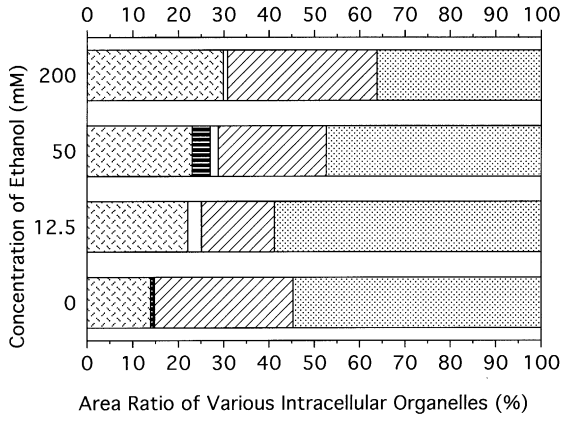



**Fig. 4** Ratios of the cross-sectional area of mitochondria (*hatched lines*), accumulated glycogen granules (*horizontal stripes*), lysosomes + residual bodies (*open bar*), myofibrils (*diagonal stripes*), and unspecified cytoplasm excluding these organelles (*dots*) to that of total cytoplasm of ventricular myocardial cells after 14-day exposure to ethanol (mean of four values for all groups)

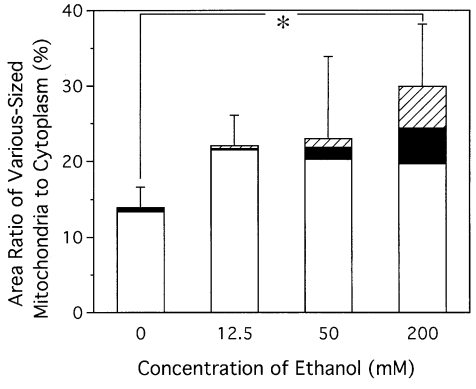



**Fig. 5** Ratios of the cross-sectional area of usual-sized (*open*), large (*shaded*) and giant (*diagonal lines*) mitochondria to that of cytoplasm of ventricular myocardial cells after 14-day exposure to ethanol (mean of four values for all groups). The terms, usual-sized, large and giant mitochondria, are used to mean those less than 3 times, 3–5 times and 5 times or more as large, respectively, as usual ones in cross-sectional area. The *bars* represent SD for total mitochondria. Multiple comparisons were performed using Tukey test. **P*<0.05 for total mitochondria

**Fig. 3** Electron microscope photographs of mouse ventricular myocardial cells in a monolayer exposed to a medium containing 12.5 mM ethanol for 14 days (**c**, **f**), those exposed to 50 mM for 14 days (**a**) and those exposed to 200 mM for 14 days (**d**, **e**) and 21 days (**b**). *N* nucleus, *small arrows* lysosomes, *small arrowheads* mitochondrial fusion, *large arrowheads* residual bodies. *Bars* 1 μm. **a** Glycogen granules in lumps (*asterisks*) were abundant. **b** Mitochondria became gigantic, while myofibrils became fewer. Cell size was diminished. **c** Mitochondria were more abundant and rather elongated in form compared with the control cells. Lysosomes and residual bodies were seen. Golgi apparatus (*G*) was swollen. **d**, **e** The area occupied by mitochondria increased greatly. Mitochondria were larger in diameter, more gigantic or branched (*large arrows*) in form. **f** Residual bodies were seen in the perinuclear region. **a** ×12,000, **b** ×17,500, **c** ×12,000, **d** ×6000, **e** ×12,000, **f** ×21,000

to cytoplasm or to total mitochondria (Fig. 5) also increased dose dependently ($P<0.03$ for all these four ratios by Kruskal-Wallis test), and there were statistical significances in all these ratios for 200 mM ethanol compared with the control. There were additional statistical significances between the 200-mM ethanol group and either of other ethanol groups (data not shown).

The ratios of the cross-sectional area of myofibrils to that of total mitochondria were 228, 76, 122 and 122 for the control, 12.5-mM, 50-mM and 200-mM groups, respectively; the ratios for all ethanol groups were half or less that of the control ($P=0.049$ by Kruskal-Wallis test), and there was a statistically significant difference between the 12.5-mM and the control group.

As far as three ethanol groups were concerned, there was a significant correlation between the ratio of myofibrils to cytoplasm and that of large and giant mitochondria to cytoplasm (correlation coefficient = 0.678; $P=0.013$ by Pearson's correlation).

The remaining unspecified area of the cytoplasm excluding glycogen granules, lysosomes, residual bodies, myofibrils and mitochondria dose dependently decreased (Fig. 4; $P=0.009$ by Kruskal-Wallis test) with a statistical significance for 200 mM compared with the control.

## Discussion

There are a few reports describing the ultrastructure of cardiomyocytes in long-term culture (15 days to 1.5 months) derived from neonatal rats [19, 35] and adult mammals [9, 16, 29, 30]. These studies pointed out that the continuance of contractile activity was a key factor in the long-term maintenance of the contractile apparatus. However, hardly any ultrastructural photographs have been demonstrated. In this study, neonatal mouse ventricular myocardial cells in a monolayer culture were found to maintain their initial ultrastructure (Fig. 2) and spontaneous contractions (Fig. 1) for up to approximately 1 month, making them suitable for the observation of the effects of ethanol on the myocardium for a chronically long time, though the amounts of glycogen granules and rER and beat rate gradually decreased.

Like in the alcoholic hearts in vivo, in cultured mouse myocardial cells chronically exposed to ethanol (Fig. 3, Fig. 4, Fig. 5), mitochondriosis (a large accumulation of small mitochondria) and increased numbers of lysosomes (human alcoholics [1, 5, 15, 39]) and the mitochondrial enlargement and proliferation (animal alcoholics [3, 6, 8, 17, 34]) were also observed, but not mitochondrial swelling, myofibrillar lysis, contraction bands, dilatation of the SR and T-tubules or lipid deposition. The swelling of mitochondria and dilatation of the SR are considered to be probably related to malnutrition [15, 33] or anoxia [13, 15]. Thus, the ethanol-induced ultrastructural changes observed only in vivo might possibly be attributed to anoxic circumstances induced by ethanol-caused hemostasis, or artifacts due to immersion fixation during sampling.

Biochemical studies on mouse hearts in vivo [2] indicated that mitochondria may be the primary organelles affected by chronic ethanol feeding. Following chronic 14-day exposure to ethanol, in addition to a dose-dependent mitochondrial increase in volumetric proportion, a dose-dependent increase in mitochondrial size was recognized (Table 2; Fig. 3, Fig. 4, Fig. 5). The augmentation of mitochondrial size with normal internal structure was also reported in the myocardium in vivo after experimental chronic ethanol intake [3, 11, 17, 21, 25], though the size was at most double and the volumetric proportion of mitochondria scarcely changed. The mechanism of mitochondrial enlargement has been so far attributed to either a deceleration of division and degradation [21, 25] or mitochondrial fusion [3, 7, 24, 27, 31, 37]. The mitochondria of the cultured mouse myocardial cells in the present study might become enlarged by fusion, since mitochondrial fusion (Table 2; Fig. 3b, e) and strange-shaped giant mitochondria (Fig. 3d, e) were simultaneously observed.

The formation of giant mitochondria was observed in aged and diseased organs [38]. Is the formation of giant mitochondria a degenerative process? Wakabayashi and his co-workers [18], however, suggested that the formation of giant mitochondria may be an adaptive process to unfavorable environments at a subcellular level. In addition, some studies have claimed that enlarged mitochondria acquire the capacity to produce ATP. Chronic ethanol feeding concurrently induced the formation of giant mitochondria and increased succinate dehydrogenase activity in baboon liver [20]. Skulachev [36] speculated that giant mitochondria may serve as intracellular structures to transmit $\Delta\bar{\mu}H$ (electrochemical $H^+$ potential difference), which is a transient intermediate of oxidative phosphorylation. Such is possibly also the case with the cultured myocardial cells in this study; higher ethanol doses are likely to switch mitochondrial metabolism and morphogenesis over to some special one through ethanol-induced disturbances in the energy producing system.

There was an interesting coincidence between mitochondrial gigantism (Table 2; Fig. 3, Fig. 5) and the higher contraction rate (positive chronotropism) (Fig. 1) of cultured mouse ventricular myocardial cells after chronic 14-day exposure to 200 mM ethanol, since such a synchrony was also observed in these cells after acute 1-h exposure to 200 mM ethanol [22, 23]. In cultured rat cardiomyocytes exposed to fentanyl (a synthetic opioid), a similar coincidence has been also reported and was found to be accompanied by the increased secretion of ANP [26]. Since the in vitro mouse myocardium in this study lacks neural and humoral effects, it is likely that ethanol-induced positive chronotropism (Fig. 1) is an intrinsic characteristic of the ventricular myocardium itself, and it seems to be partly associated with tachycardia, which is often observed in human chronic alcoholics [4]. However, the exact reason and mechanism of the coincidence between the mitochondrial and chronotropic increment remains unclear.

Changes in the myocardial glycogen content due to chronic ethanol feeding is a controversial issue. In this study, the amount of glycogen granules markedly increased in inverse proportion to the mitochondrial volume in some series of 14-day exposures to 50 mM ethanol (Table 1; Fig. 3a and Fig. 4), though hardly any were detected after exposure to other doses of ethanol. An ethanol concentration of 50 mM might be on a boundary line of energy metabolism between dysfunction of glycogen metabolism and mitochondrial hypertrophy.

Surprisingly, the amount of myofibrils after 14-day exposure to ethanol decreased as the ethanol dose became lower; the amount of myofibrils was half in the 12.5-mM ethanol group, but equal in the 200-mM group compared with the control group (Fig. 4). Moreover, in the 12.5-mM group, SR, which might be an index of contraction ability, also decreased compared with any other groups including the control one. Preedy and Peters [32] suggested chronic ethanol feeding enhanced degradation of rat cardiac contractile proteins.

However, the ratios of the cross-sectional area of myofibrils to that of total mitochondria, which might be an index of mitochondrial respiratory function, for all ethanol groups were half or less than that for the control one. In particular, the ratio for the 12.5-mM group was only about one-third of that for the control one, though the mitochondria of the 12.5-mM groups seemed ultrastructurally the same as those of the control group, being elongated in form and usual in size but not enlarged (Fig. 2, Fig. 3 and Fig. 5). Meanwhile, within the limits of three ethanol groups, the area of the myofibrils increased in proportion to that of large and giant mitochondria. Therefore, it is likely that respiratory function of usual-sized mitochondria observed in myocardial cells exposed to 12.5–200 mM ethanol for 14 days is lower than that in the control cells. As a result, myocardial cells exposed to 12.5 mM ethanol are not able to maintain the amount of contraction apparatus probably due to shortage of ATP, whereas cells exposed to 200 mM ethanol are able to maintain their contraction apparatus by being supplied with ATP from enlarged, hypertrophied mitochondria.

Throughout the wide range of doses of ethanol used in this study, the lowest dose, 12.5 mM, highly mimicked the chronic in vivo administration of ethanol; after chronic 14-day exposure, the number of lysosomes and residual bodies increased compared with the control and higher ethanol doses (Fig. 4). Moreover, usual-sized mitochondria tended to increase in number (Fig. 3c and Fig. 5), while myofibrils decreased (Fig. 4), which was identical with mitochondriosis observed in various pathological conditions. These ultrastructural changes seem very similar to those seen in the in vivo hearts of rodent [3] and human [39] alcoholics. Taken together, chronic doses ranging from 12.5 mM to 50 mM, concentrations of ethanol which were usually observed in humans after drinking, might be very suitable doses in this in vitro system for investigating the chronic effects of ethanol.

**Acknowledgements** The authors would like to thank Dr. Takeshi Haseba for his critical reading of the manuscript.

## References


1. Alexander CS (1967) Electron microscopic observations in alcoholic heart disease. Br Heart J 29:200–206
2. Alexander CS, Forsyth GW, Nagasawa HT, Kohlhoff JG (1977) Alcoholic cardiomyopathy in mice: myocardial glycogen, lipids and certain enzymes. J Mol Cell Cardiol 9:235–245
3. Alexander CS, Sekhri KK, Nagasawa HT (1977) Alcoholic cardiomyopathy in mice: electron microscopic observations. J Mol Cell Cardiol 9:247–254
4. Brigden W, Robinson J (1964) Alcoholic Heart Disease. Br Med J 2:1283–1289
5. Bulloch RT, Pearce MB, Murphy ML, Jenkins BJ, Davis JL (1972) Myocardial lesions in idiopathic and alcoholic cardiomyopathy: study by ventricular septal biopsy. Am J Cardiol 29:15–25
6. Burch GE, Colcolough HL, Harb JM, Tsui CY (1971) The effect of ingestion of ethyl alcohol, wine and beer on the myocardium of mice. Am J Cardiol 27:522–528
7. Coleman R, Silbermann M, Gershon D, Reznick AZ (1987) Giant mitochondria in the myocardium of aging and endurance-trained mice. Gerontology 33:34–39
8. Czarnecki CM, Schaffer SW, Evanson OA (1985) Ultrastructural features of ethanol-induced cardiomyopathy in turkey poults. Comp Biochem Physiol A Physiol 82:939–943
9. Decker ML, Behnke-Barclay M, Cook MG, Lesch M, Decker RS (1991) Morphometric evaluation of the contractile apparatus in primary cultures of rabbit cardiac myocytes. Circ Res 69:86–94
10. Édes I, Tószegi A, Csanády M, Bozóky B (1986) Myocardial lipid peroxidation in rats after chronic alcohol ingestion and the effects of different antioxidants. Cardiovasc Res 20:542–548
11. Ettinger PO, Lyons M, Oldewurtel HA, Regan TJ (1976) Cardiac conduction abnormalities produced by chronic alcoholism. Am Heart J 91:66–78
12. Fahimi HD, Kino M, Hicks L, Thorp KA, Abelman WH (1979) Increased myocardial catalase in rats fed ethanol. Am J Pathol 96:373–390
13. Ganote CE, Seabra-Gomes R, Nayler WG, Jennings R (1975) Irreversible myocardial injury in anoxic perfused rat hearts. Am J Pathol 80:419–50
14. Hall JL, Rowlands Jr DT (1970) Cardiotoxicity of alcohol: an electron microscopic study in the rat. Am J Pathol 60:153–164
15. Hibbs RG, Ferrans VJ, Black WC, Weilbaecher DG, Walsh JJ, Burch GE (1965) Alcoholic cardiomyopathy: an electron microscopic study. Am Heart J 69:766–779
16. Horackova M, Mapplebeck C (1989) Electrical, contractile, and ultrastructural properties of adult rat and guinea-pig ventricular myocytes in long-term primary cultures. Can J Physiol Pharmacol 67:740–750
17. Jaatinen P, Saukko P, Sarviharju M, Kiianmaa K, Hervonen A (1994) Effects of lifelong ethanol consumption on the ultrastructure and lipopigmentation of rat heart. Alcohol Alcohol 29:269–282
18. Karbowski M, Kurono C, Wozniak M, Ostrowski M, Teranishi M, Nishizawa Y, Usukura J, Soji T, Wakabayashi T (1999) Free radical-induced megamitochondria formation and apoptosis. Free Radic Biol Med 26:396–409
19. Kira Y, Nakaoka T, Hashimoto E, Okabe F, Asano S, Sekine I (1994) Effect of long-term cyclic mechanical load on protein synthesis and morphological changes in cultured myocardial cells from neonatal rat. Cardiovasc Drugs Ther 8:251–262
20. Lieber CS, Casini A, DeCarli LM, Kim C, Lowe N, Sasaki R, Leo MA (1990) S-adenosyl-L-methionine attenuates alcohol-induced liver injury in the baboon. Hepatology 11:165–172
21. Mall G, Mattfeldt T, Volk B (1980) Ultrastructural morphometric study on the rat heart after chronic ethanol feeding. Virchows Arch 389:59–77
22. Mashimo K (1985) Chronotropic responses to ethanol of mouse atrial and ventricular myocardial cells in culture. Jpn J Physiol 35:659–671
23. Mashimo K, Sato S, Ohno Y (2001) Acute cytotoxic effects of ethanol on cultured mouse myocardial cells in a monolayer: enzymatic, chronotropic and ultrastructural studies. Jpn J Alcohol Drug Depend 36:142–153
24. Matsuhashi T, Karbowski M, Liu XR, Usukura J, Wozniak M, Wakabayashi T (1998) Complete suppression of ethanol-induced formation of megamitochondria by 4-hydroxy-2,2,6,6-tetramethyl-piperidine-l-oxyl (4-OH-TEMPO). Free Radic Biol Med 24:139–147
25. Mattfeldt T, Mall G, Volk B (1980) Morphometric analysis of rat heart mitochondria after chronic ethanol treatment. J Mol Cell Cardiol 12:1311–1319
26. Mekhail NA, Doss DN, Bravo EL, Estafanous FG (1994) Fentanyl stimulates atrial natriuretic peptide secretion. J Mol Cell Cardiol 26:425–434
27. Mikami K, Sato S, Watanabe T (1990) Acute effects of ethanol on cultured myocardial cells: an ultrastructural study. Alcohol Alcohol 25:651–660
28. Mikami K, Sato S, Nakazawa N, Asano G, Watanabe T (1993) Ethanol-elicited structural and biochemical alterations in mitochondrial ATPase in cultured myocardial cells. Virchows Arch 63:365–371
29. Moses RL, Claycomb WC (1982) Ultrastructure of terminally differentiated adult rat cardiac muscle cells in culture. Am J Anat 164:113–131
30. Nag AC, Cheng M, Fischman DA, Zak R (1983) Long-term cell culture of adult mammalian cardiac myocytes: electron microscopic and immunofluorescent analyses of myofibrillar structure. J Mol Cell Cardiol 15:301–317
31. Porta EA, Hartroft WS, de la Iglesia FA (1967) Structural and ultrastructural hepatic lesions associated with acute and chronic alcoholism in man and experimental animals. In: Maickel RP (ed) Biochemical factors in alcoholism. Pergamon, Oxford, pp 201–238
32. Preedy VR, Peters TJ (1989) Synthesis of subcellular protein fractions in the rat heart in vivo in response to chronic ethanol feeding. Cardiovasc Res 23:730–736
33. Rossi MA (1980) Alcohol and malnutrition in the pathogenesis of experimental alcoholic cardiomyopathy. J Pathol 130:105–116
34. Segel LD, Rendig SV, Choquet Y, Chacko K, Amsterdam EA, Mason DT (1975) Effects of chronic graded ethanol consumption on the metabolism, ultrastructure, and mechanical function of the rat heart. Cardiovasc Res 9:649–663
35. Simpson DG, Terracio L, Terracio M, Price RL, Turner DC, Borg TK (1994) Modulation of cardiac myocyte phenotype in vitro by the composition and orientation of the extracellular matrix. J Cell Physiol 161:89–105
36. Skulachev VP (1980) Membrane electricity as a convertible energy currency for the cell. Can J Biochem 58:161–175
37. Sun CN, Dhalla NS, Olson RE (1969) Formation of gigantic mitochondria in hypoxic isolated perfused rat hearts. Experientia 25:763–764
38. Tandler B, Hoppel CL (1986) Studies on giant mitochondria. Ann N Y Acad Sci 488:65–81
39. Tsiplenkova VG, Vikhert AM, Cherpachenko NM (1986) Ultrastructural and histochemical observations in human and experimental alcoholic cardiomyopathy. J Am Coll Cardiol 8:22A–32A

Virchows Arch (2003) 442:364–371
DOI 10.1007/s00428-003-0775-5

ORIGINAL ARTICLE

**Moriz Buzello · Christoph Boehm · Stephan Orth · Bernhard Fischer · Heimo Ehmke · Eberhard Ritz · Gerhard Mall · Kerstin Amann**

# Myocyte loss in early left ventricular hypertrophy of experimental renovascular hypertension

Received: 27 September 2002 / Accepted: 16 January 2003 / Published online: 2 April 2003
© Springer-Verlag 2003

**Abstract** Left ventricular hypertrophy (LVH) develops very early in experimental renovascular hypertension after clipping of one renal artery and is accompanied by a remodeling of cardiac structure which has not yet been investigated in detail. It was the aim of the present study to analyze changes in cardiomyocyte number and volume in LVH after 2 weeks of renovascular hypertension. Sprague-Dawley rats were subjected to clipping of the left renal artery (2K1C) or sham operation (sham). One group of 2K1C rats received antihypertensive treatment with dihydralazine. The experiment was terminated after 2 weeks. Hearts were investigated using stereological methods, electron microscopy, immunohistology for the proliferation marker proliferating cell nuclear antigen, the pro- and anti-apoptotic proteins Bax and Bcl-2 as well as the TUNEL technique. After 2 weeks, systolic blood pressure and relative left ventricular weight were significantly higher in untreated 2K1C animals than in sham and dihydralazine-treated 2K1C rats. Volume fraction of interstitial tissue and capillary length density were not different, whereas wall thickness of intramyocardial arteries was significantly higher in untreated 2K1C (5.12±0.7 μm) than in sham (3.92±0.6 μm) and in dihydralazine-treated 2K1C (3.91±0.7 μm) rats. Cardiomyocyte diameter and volume were significantly higher in untreated 2K1C than in sham animals. The number of cardiomyocytes per left ventricle was significantly lower in untreated 2K1C rats (5.5±1.6 vs 3.9±6.9 $\times 10^7$). Using immunohistochemistry, no direct evidence of apoptosis was found, but a relative higher expression of the anti-apoptotic protein bcl-2 expression was seen in untreated 2K1C than in sham animals. This may reflect a protective mechanism as a consequence of earlier occurring apoptosis. These observations document that experimental renovascular hypertension induces a rapidly developing LVH characterized by marked cardiac remodeling and substantial loss of cadiomyocytes.

**Keywords** Hypertension · Renal · Left ventricular hypertrophy · Remodeling · Apoptosis

M. Buzello · C. Boehm · B. Fischer
Department of Pathology,
University of Heidelberg, Germany

K. Amann (✉)
Department of Pathology,
University of Erlangen-Nürnberg,
Krankenhausstrasse 8-10, 91054 Erlangen, Germany
e-mail: kerstin.amann@patho.imed.uni-erlangen.de
Tel.: +49-9131-8522291
Fax: +49-9131-8522601

G. Mall
Department of Pathology,
University of Darmstadt, Germany

E. Ritz
Department of Internal Medicine,
University of Heidelberg, Germany

H. Ehmke
Department of Physiology,
University of Hamburg, Germany

S. Orth
Department of Nephrology and Hypertension,
Inselspital Bern, Switzerland

## Introduction

Experimental renovascular hypertension is characteristically associated with a pronounced left ventricular hypertrophy (LVH). Histopathological studies in rats with 2 kidney/1 clip (2K1C) Goldblatt hypertension of more than 6–8 weeks duration demonstrated an increase in cardiomyocyte volume, interstitial cardiac fibrosis, and thickening of myocardial vascular walls [1, 2, 3, 4], consistent with the view that renovascular hypertension induces a slowly progressive cardiac remodeling.

This view was challenged by several recent observations of rapid and substantial increases in left ventricular weight to body weight ratio and by re-expression of the atrial natriuretic peptide gene, a molecular marker of LVH, within the first 1–2 weeks after induction of 1K1C or 2K1C hypertension [5, 6, 7, 8]. Thus, renovascular

hypertension appears to induce a very rapid cardiac remodeling, which may be explained by a concurrent activation of several signaling cascades leading to hypertrophic growth, such as an increase in systemic blood pressure, stimulation of the systemic renin–angiotensin system, activation of the sympathetic nervous system as well as an enhanced release of local growth factors such as angiotensin II (Ang II) and endothelin-1 (ET-1) [1, 5, 7, 8, 9, 10].

The histopathology of these early cardiac changes, however, has not yet been investigated. This is of particular importance, as non-specific factors such as tissue swelling could contribute to the early increase in left ventricular mass. In addition, it is not known whether the increase in left ventricular mass is simply accomplished by generalized hypertrophy of all cardiomyocytes or whether it involves a structural reorganization that would require a coordinated growth and loss of cells.

Therefore, it was the aim of the present study to investigate the early changes in cardiomyocyte geometry, i.e., cardiomyocyte number and mean cardiomyocyte volume, after 2 weeks of experimental renovascular hypertension. To assess the importance of changes in systemic blood pressure in the genesis of these changes, one experimental group was treated with the non-specific antihypertensive drug dihydralazine to control for blood pressure.

## Methods

### Animal model

The study was performed in 44 male Sprague-Dawley rats (Ivanovas Co., Kissleg, Germany, mean initial body weight: 163 g) which were housed in single cages at constant temperature (20°C) and humidity (25%). The animals received standard rat diet (Altromin, Lage, Germany).

After an adaptation period of 3 days, the left renal artery was clipped (2K1C) in 27 animals, as described in detail previously [11]. Seventeen animals served as controls: they were sham operated (sham), i.e., the animals were anesthetized and the operation was performed without clipping of the left renal artery. Three days after the operation, treatment with dihydralazine (4.5 mg/day in the drinking fluid) was started in ten animals of the 2K1C group (2K1C + dihydralazine).

### Experimental design

1. Sham operated controls (sham; *n*=17)
2. Untreated 2K1C (2K1C; *n*=17)
3. Dihydralazine-treated 2K1C (2K1C + dihydralazine; *n*=10)

Systolic blood pressure was measured regularly by means of tail plethysmography in conscious animals, taking great care that the dose of dihydralazine provided a good 24-h blood-pressure control.

### *Perfusion fixation and tissue sampling*

Two weeks after clipping of the left renal artery, the experiment was terminated by retrograde perfusion fixation. The abdominal aorta was catheterized under ketamine/diazepam anesthesia (100 mg/kg or 2.5 µg/kg, respectively) and blood samples were taken. The viscera were rinsed with 10% dextran solution (to avoid tissue edema) containing 0.5 g/l procaine hydrochloride (2 min) to guarantee complete relaxation of the vasculature. Ten seconds after starting the aortic perfusion, the vena cava was incised to drain the blood. After dextran infusion, the vascular system was perfused with 0.2 M phosphate buffer containing 3% glutaraldehyde for 12 min [12].

After perfusion, the heart and aorta of each animal were excised. Weight and volume of the heart as well as of the left ventricle were determined, and tissue sampling and section staining were performed according to the orientator method [13]. Uniformly random tissue sampling was achieved by preparing a set of equidistant slices of the left ventricle and the interventricular septum with a random start. Two slices of the left ventricle were selected by area weighted sampling and processed accordingly [13]. Eight pieces of the left ventricular muscle including the septum were prepared and embedded in Epon-Araldite. Semithin sections (1 µm) were stained with methylene blue and basic fuchsin and examined under the light microscope with oil immersion and phase contrast at a magnification of 1000:1 [14].

In several animals per group, ultrathin sections (0.08 µm) were prepared and stained with uranyl acetate and lead citrate. Ultrathin sections were qualitatively examined using a Zeiss EM 10 electron microscope (Zeiss Co., Oberkochen, Germany).

For immunohistochemical analysis, five untreated 2K1C and five sham-operated animals were perfused with ice-cold NaCl (0.9%). Their hearts were cut into two transverse parts; one half was snap frozen, the other was fixed in paraformaldehyde. Afterward, frozen sections (8 µm) and paraffin sections (4 µm) were prepared for immunohistochemistry [15], hematoxylin and eosin, and sirius red staining (for detection of collagen).

### *Immunohistochemistry and immunofluorescence using confocal laser microscopy*

*TUNEL assay.* Cardiomyocytic DNA degradation was assessed in situ on transmural paraffin sections of the heart using terminal deoxynucleotidyl transferase-mediated dUTP nick-end-labeling (TUNEL) with direct fluorescence. As a pretreatment, the serial sections were exposed to 0.1% Triton X100 (0.1% Triton X100 in SSC buffer, 10 min). The apoptosis detection kit was applied following manufacturers' instructions (In Situ Cell Death Detection; AP, Boehringer, Mannheim, Germany). As a positive control, tissue supplied by the manufacturers was used (glandula tonsillaris). Additionally, one transmural serial paraffin section was exposed to Tris buffer solution with 0.1 mg/ml DNase I + bovine serum albumin (BSA; Serva, Heidelberg, Germany; 10 min). A transmural TUNEL assay without TdT (terminal deoxynucleotidyl transferase) was used as negative control. The TUNEL staining was performed with fluorescein-dUTP omitting the alkaline phosphatase (AP)-converting step. Propidium iodide (50 µg/ml) was used for counterstaining of nuclei.

*Bax and Bcl-2 immunohistochemistry.* The expression of the pro-apoptotic Bax gene and the anti-apoptotic Bcl-2 gene was determined using primary unconjugated antibodies (anti-Bax, polyclonal, 1:100; anti-Bcl-2, polyclonal, 1:250, Pharmingen, Boston, USA). After blocking of non-specific binding (casein block + 1 mg/ml human IgG, Gamma-Venin, Aventis-Behring, Marburg, Germany, and bovine serum albumin, Serva, Heidelberg, Germany; 15 min), the transmural paraffin sections were incubated with the primary antibodies at previously determined dilutions (20 h, 4°C). Afterward, slices were rinsed with buffer and incubated with 20% goat serum (Dianova, Hamburg, Germany; 20 min). Then slices were rinsed and incubated with a goat anti-rabbit IgG biotin (polyclonal antibody, 1:20, Biogenex, San Ramon, USA; room temperature, 30 min), the super-sensitive label AP-conjugated streptavidin (Biogenix, San Ramon, USA; 30 min) and Fast Red substrate (Dako, Hamburg, Germany). After washing, the sections were briefly counterstained with hematoxylin and coverslipped. Specificity of immunofluorescence reaction was tested with streptavidin-fluorescein isothiocyanate.

*Immunohistochemistry for proliferating cell nuclear antigen.* The nuclear expression of the cell-cycle associated protein proliferating cell nuclear antigen (PCNA) was assessed as a marker of cell activation and proliferation on paraffin transmural sections of the heart using a primary unconjugated antibody (anti-PCNA, monoclonal, 1:150; Immunotech, Marseille, France) as described in detail elsewhere [15]. All antibodies had been tested for specificity in the rat previously. Negative controls were performed by omitting the primary antibody. To reduce run-to-run variations in the staining intensity, all stainings of the same antibody were performed in the same run for 2K1C and sham sections.

*Morphometrical and stereological analysis*

All investigations were performed in a blinded manner, i.e., the observer was unaware of the study group to which the animal belonged. According to the orientator method, stereological analysis was performed on eight random samples of differently orientated sections of the left ventricular myocardium per animal [12, 13, 14]. Length density ($L_V$) of capillaries, i.e., the length of capillaries per unit tissue volume, and the volume density ($V_V$) of cardiac capillaries, i.e., the volume of capillaries per unit myocardial tissue volume, were measured in eight systematically subsampled areas per section using a Zeiss eyepiece (Zeiss Co. Oberkochen, Germany) with 100 points for point counting. The length density of myocardial capillaries ($L_V$) was determined using the equation $L_V=2Q_A$ (where $Q_A$ is area density, e.g., the number of capillary transects per area of myocardial reference tissue) [12, 13, 14]. Total capillary length per heart was calculated using the volume of the left ventricle according to the formula $L=L_V\times V$ [12, 13, 14] where $V=m/\delta$, and $\delta$ being 1.04 g/mm$^3$ for rat cardiac tissue [16]. Intercapillary distance, i.e., the distance between the centers of two adjacent intramyocardial capillaries, was calculated according to a modification of the formula of Henquell and Honig [14]. $V_V$ of capillaries, interstitial tissue and cardiomyocytes was obtained using the point counting method according to the equation $P_P=V_V$ (where $P_P$ is point density). Reference volume was the total myocardial tissue (exclusive of non-capillary vessels, i.e., arterioles and veins). Intramyocardial arteries with a minimal lumen diameter between 20 $\mu$m and 100 μm were investigated using a semiautomatic image analyzing system (Videoplan, Contron Co. Eching, Germany) as described in detail previously [14]. Cardiomyocyte geometry was determined using a model-based approach. Cardiomyocyte diameter (md) and cardiomyocyte length (l) were analyzed on longitudinal sections using a semiautomatic image analyzing system (Videoplan, Contron Co. Eching, Germany; magnification 1:1000, oil immersion, phase contrast) and corrected for contraction by standardizing on sarcomere length. Mean cardiomyocyte volume ($v_{myo}$) was derived from $v_{myo}=\pi$ (md/2)$^2\times$l, and the number of cardiomyocytes per volume of myocardium was calculated according to $n=V_{Vmyo}\times$ left ventricular volume/$v_{myo}$ (with $V_{Vmyo}$= volume density of cardiomyocytes).

*Quantitative immunohistochemical analysis*

*TUNEL assay.* Apoptosis of cardiac cells was evaluated using a confocal microscope (TCS NT, Leica, Bensheim, Germany). Chromatin alterations and the histochemical detection of double DNA cord breaks were analyzed. The investigations were performed on a minimum area of 0.58 cm$^2$ per heart. This was done in a blinded manner, i.e., the observer was unaware of the study-group to which the animal belonged. The number of cardiomyocytes per area labeled using the TUNEL technique was counted. The area was measured using a semi-quantitative image analyzing system (Videoplan, Contron Co. Eching, Germany) as described in detail previously [14]. Cardiomyocyte density was visible by counterstaining (nuclei and $\alpha$-sarcomeric actin) with propidium iodide.

*Bax and Bcl-2 immunohistochemistry.* The intensity of the protein expression was quantified by two independent investigators using light microscopy and a semi-quantitative scoring system (0, no expression; 1, weak expression; 2, moderate expression; 3, strong expression) at a magnification of ×400 in a blinded manner [15]. Staining intensity was calculated as the mean score of the two observers. Using this scoring system, the protein expression was analyzed in 100 fields per heart (total myocardial area: 6.25 mm$^2$). In addition, the area of Bax- and Bcl-2 expression was analyzed using the point-counting method and a Zeiss eyepiece (Zeiss Co. Oberkochen, Germany) [14]. Interobserver error did not exceed 5%.

*PCNA assay.* The number of PCNA-positive cells (cardiomyocytes) per area myocardium was counted using a light microscope at a magnification of ×400 [15]. The investigations were performed on a minimum area of 0.58 cm$^2$ in each heart. The reference area was measured using a semi-quantitative image analyzing system (Videoplan, Contron Co. Eching, Germany) as described in detail [14]. Again the analysis was done in a blinded manner by two independent observers; the mean of the two observers was calculated for each animal.

Statistics

All data are expressed as mean±standard deviation. After testing for normality distribution (Lilliefors-test) one-way analysis of variance (ANOVA; using SPSS) was performed, followed by the least-significant difference test to assess the differences between the groups. The zero hypothesis was rejected at probability of error $P<0.05$. Differences in immunohistochemical investigations were investigated using the Wilcoxon and the Fisher's exact tests.

## Results

### Description of the model

Table 1 describes the model used in this experiment. At the beginning, body weight and blood pressure were

**Table 1** Description of the animal model (mean±standard deviation)

| | Body weight (g) | Left ventricular weight[#]/body weight ratio (mg/g) | Systolic blood pressure (mmHg) |
|---|---|---|---|
| Sham-operated controls ($n$=12) | 289±15 | 2.53±0.24 | 116±7 |
| Untreated 2K1C ($n$=12) | 236±46[*] | 3.41±0.56[*+] | 137±9[*+] |
| 2K1C + dihydralazine ($n$=10) | 249±11[*] | 2.83±0.32 | 109±13 |
| ANOVA | $P<0.05$ | $P<0.05$ | $P<0.05$ |

[*]$P<0.05$ vs sham-operated controls
[+]$P<0.05$ vs 2K1C + dihydralazine
[#]After perfusion fixation

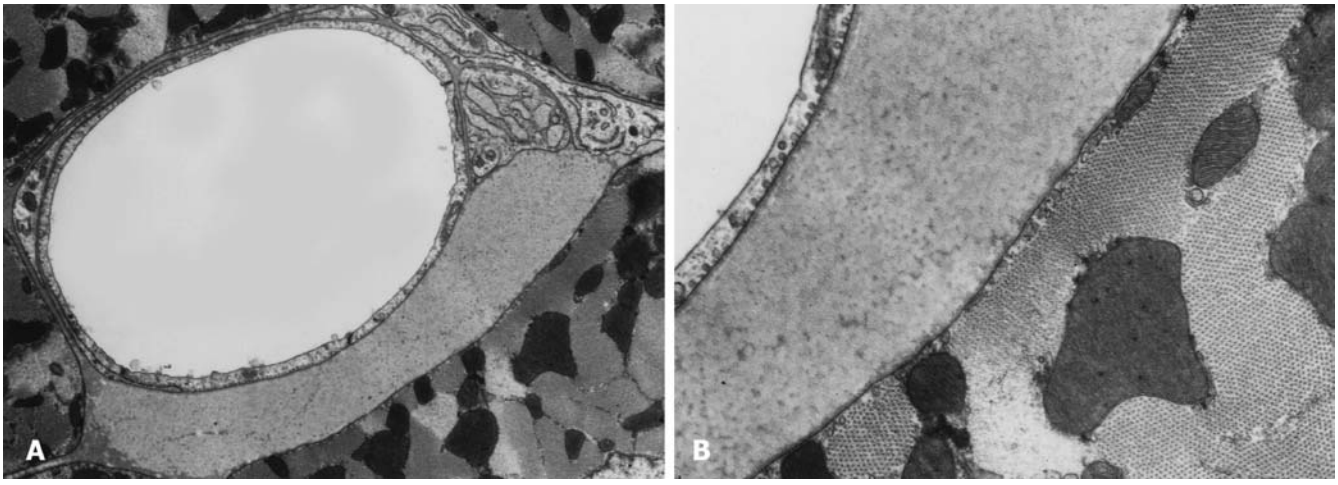



**Fig. 1** Early ultrastructural changes in left ventricular hypertrophy of untreated 2 kidney/1 clip (2K1C) rats. Please note pericytic activation and focal perivascular accumulation of fibrillar material (**A**) which, at higher magnifications (**B**), was identified as type-IV collagen. The ultrastructure of the cardiomyocyte and the endothelium is not altered. Ultrathin sections, magnifications: 1:7000 (**A**) and 1:18000 (**B**)

**Table 2** Changes of cardiac interstitial tissue, arteries and capillaries (mean±standard deviation)

| | Interstitial volume density (%) | Capillary length density (mm/mm$^3$) | Intercapillary distance (μm) | Wall thickness of intramyocardial arteries (μm) |
|---|---|---|---|---|
| Sham-operated controls ($n$=12) | 2.49±0.4 | 3976±849 | 17.1±2.9 | 3.92±0.6 |
| Untreated 2K1C ($n$=12) | 2.8±0.5 | 3498±710 | 18.6±2 | 5.12±0.7$^{*+}$ |
| 2K1C + dihydralazine ($n$=10) | 2.54±0.3 | 3539±657 | 18.3±1.7 | 3.91±0.7 |
| ANOVA | n.s. | n.s. | n.s. | $P$<0.05 |

*$P$<0.05 vs sham-operated controls
$^+P$<0.05 vs 2K1C + dihydralazine

**Table 3** Cardiomyocyte geometry (mean±standard deviation)

| | Mean cardiomyocyte diameter (μm) | Mean cardiomyocyte volume (μm$^3$) | Mean number of cardiomyocytes per left ventricle (×10$^7$) | Volume density of cardiomyocytes (%) |
|---|---|---|---|---|
| Sham-operated controls ($n$=12) | 12.6±1.4 | 12,395±3601 | 5.5±1.6 | 86.2±1.12 |
| Untreated 2K1C ($n$=12) | 15±1.6* | 17,145±3204* | 3.9±0.7* | 86.5±2.16 |
| 2K1C + dihydralazine ($n$=10) | 13.6±1 | 13,337±2220 | 4.5±1.0 | 85.9±2.25 |
| ANOVA | $P$<0.05 | $P$<0.05 | $P$<0.05 | n.s. |

*$P$<0.05 vs sham-operated controls

comparable in all groups (data not shown). In another study using intraarterial blood pressure measurements in the same experimental model of 2K1C, we found that blood pressure significantly increased on day 4 after the operation, reaching a steady-state level on days 10–14. At the end of the study, body weight was significantly ($P$<0.05) lower in both 2K1C groups than in sham. Systolic blood pressure and relative left ventricular weight, i.e., left ventricular weight/body weight ratio, were significantly ($P$<0.05) higher in untreated 2K1C (+35%) than in sham and 2K1C+dihydralazine groups (Table 1). Left ventricular volume was not significantly different among the three groups (0.75±0.07 mm$^3$ in sham, 0.70±0.09 mm$^3$ in 2K1C+D and 0.79±0.08 mm$^3$ in 2K1C). The hemoglobin and hematocrit levels were comparable in all three groups (data not shown). Serum creatinine was comparable in sham (0.54±0.04 mg/dl) and untreated 2K1C (0.55±0.05 mg/dl) groups; it was slightly increased in the dihydralazine-treated 2K1C group (0.60±0.05 mg/dl, $P$<0.05 vs sham).

## Structural changes of the heart

Structural changes of the heart are shown in Table 2 and Table 3, and in Fig. 1, Fig. 2 and Fig. 3). Volume density of interstitial tissue, length density of cardiac capillaries and mean intercapillary distance were not significantly

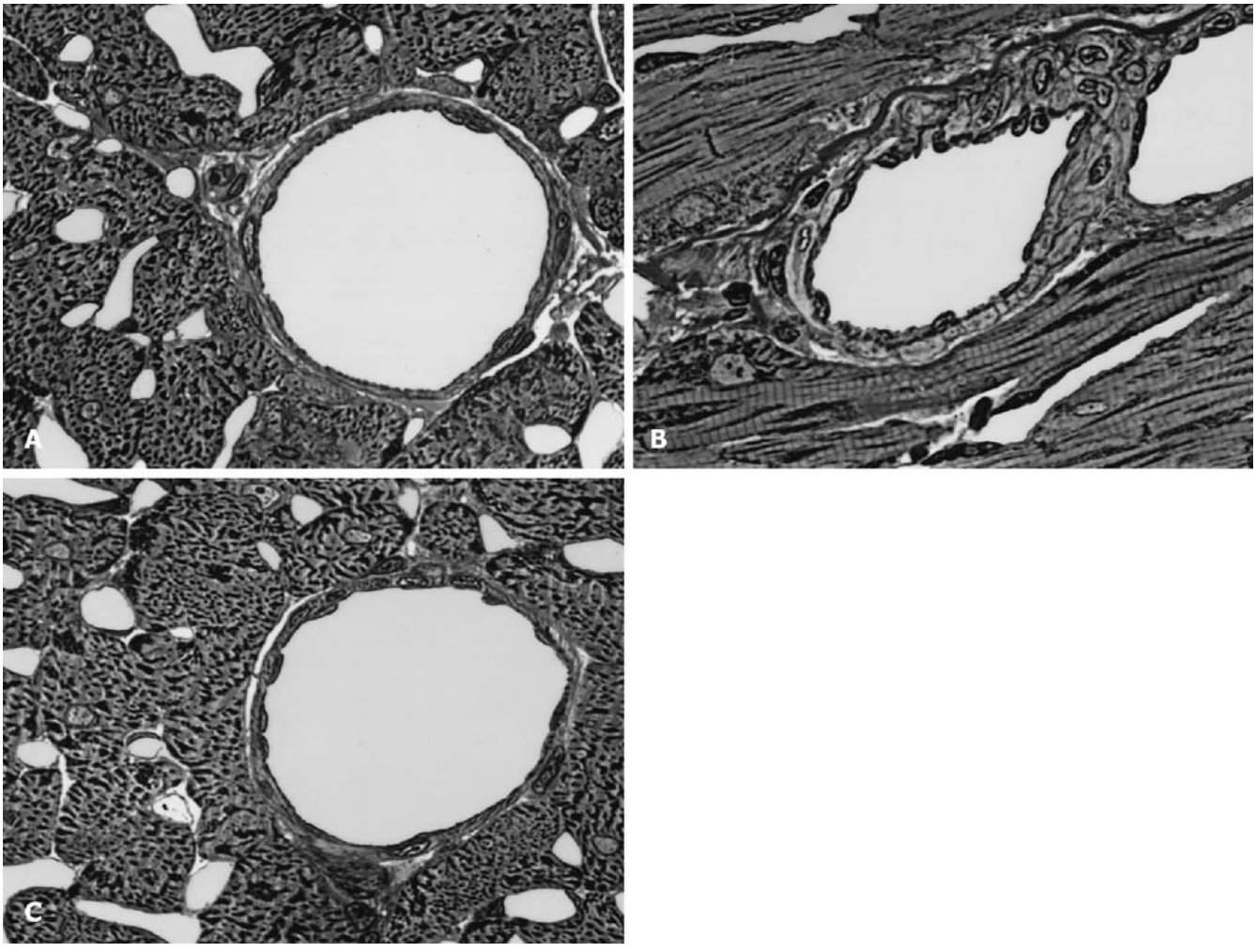



**Fig. 2** Structural changes of intramyocardial arteries in left ventricular hypertrophy of untreated 2 kidney/1 clip (2K1C) rats. Please note a marked increase in wall thickness due to hypertrophy of vascular smooth muscle cells in untreated 2K1C rats (**B**) relative to sham-operated controls (**A**) and dihydralazine-treated 2K1C rats (**C**). Semithin sections, magnification: 1:630

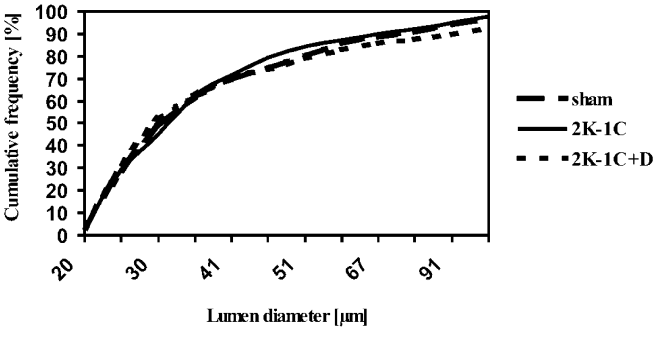



**Fig. 3** Cumulative frequency of lumen diameters. There is no significant difference in the cumulative frequencies of lumen diameters between the groups indicating the absence of a systematic sampling artifact

different among the three experimental groups (Table 2). Also the volume density of the interstitial tissue was not significantly different between both 2K1C groups and sham by light microscopy (Table 2). This was confirmed by Sirius red stains of the heart. Using electron microscopy, only a focal increase in perivascular collagen type IV was seen in the untreated and dihydralazine-treated 2K1C animals (Fig. 1).

Wall thickness of intramyocardial arterioles was significantly ($P<0.05$) higher in untreated 2K1C than in sham and 2K1C+dihydralazine groups (Table 2, Fig. 2). Lumen diameters were not significantly different among the three groups (32.6±6.5 µm in sham, 36.2±8.6 µm in untreated 2K1C and 28.4±7.7 µm in 2K1C+dihydralazine). The mean number of intramyocardial arteries that were used for the measurements was not significantly different among the groups (38±15.5 in sham, 56±13.9 in 2K1C+D and 40±17 in 2K1C). To exclude sampling artifacts, the cumulative frequency of sections as a function of vessel diameter was plotted (Fig. 3). Since

no significant differences in vessel diameter were seen among the three groups, systematic sampling artifacts can be excluded. In contrast, analysis of the cumulative frequencies of different classes of wall thickness showed a systematic shift to the right for the untreated 2K1C group compared with dihydralazine-treated 2K1C group and sham operated controls, indicating a higher prevalence of intramyocardial arteries with greater wall thickness (data not shown). Mean diameter of cardiomyocytes as well as mean cardiomyocyte volume were significantly ($P<0.05$) higher in untreated 2K1C rats than in sham-operated controls (Table 3), while sarcomere length was not significantly different (data not shown). In dihydralazine-treated 2K1C rats, mean cardiomyocyte diameter and volume were comparable to those of sham-operated animals. In parallel, the number of cardiomyocytes per left ventricle was significantly ($P<0.05$) lower in untreated 2K1C than in sham-operated rats. In dihydralazine-treated 2K1C rats, cardiomyocyte number per left ventricle was slightly higher than in untreated 2K1C rats; it was no longer significantly different from sham-operated animals (Table 3).

### Immunohistochemical investigations of the heart

Immunohistochemistry was performed on transmural sections of the hearts of untreated 2K1C and sham-operated control animals. The total number of TUNEL-positive cardiomyocyte nuclei per area of myocardium was numerically higher in the untreated 2K1C group (3.55±2.35) than in sham-operated controls (2.53±1.68), but the difference was not statistically significant. The total number of PCNA-positive cardiomyocyte nuclei per area of myocardium was comparable in untreated 2K1C (252±59) and sham (270±41) animals. The relative area of Bcl-2-positive cardiomyocytic cytoplasm ($A_{ABcl\text{-}2}$) was significantly ($P<0.05$) higher in the hearts of untreated 2K1C rats (3.75±0.89) than in sham-operated controls (1.20±0.27). The intensity of cytoplasmic Bcl-2 staining was also significantly ($P<0.05$) higher in untreated 2K1C rats (2.03±0.62) than in sham-operated controls (1.51±0.20). In contrast, the relative area of cytoplasmic Bax positivity ($A_{ABax}$) was comparable between the two groups, as was the intensity of cytoplasmic Bax staining. Consequently, the ratio of cardiac cytoplasmic Bcl-2/Bax-expression area, as an index of the apoptotic state, increased from 0.57 in sham to 1.60 (+282%) in untreated 2K1C rats compared with sham-operated controls ($P<0.05$).

## Discussion

The present study documents that LVH develops very early (<2 weeks) in the course of renovascular hypertension in 2K1C rats. It is accompanied by a marked structural remodeling of the myocardium with a significant increase in wall thickness of intramyocardial arterioles, a tendency toward an increase in non-vascular interstitial tissue and lower capillary length densities. In addition, stereological analysis of cardiomyocyte geometry using a model-based approach, documented cardiomyocyte hypertrophy and a significantly lower number of cardiomyocytes per left ventricle in untreated 2K1C rats compared with sham-operated controls. These structural changes of the heart were partly, but not completely, prevented by non-specific antihypertensive treatment with dihydralazine. Since systolic blood pressure was completely normalized in dihydralazine-treated 2K1C rats, we could dissociate blood pressure-dependent from blood pressure-independent mechanisms.

In the present study, the increase (+37.5%) in the left ventricular weight to body weight ratio as an index of LVH was similar to that observed in previous studies with longer duration of renovascular hypertension [2, 3, 4, 5]. Using light microscopy, only a minor increase in interstitial tissue was found in untreated 2K1C rats compared with sham-operated controls. Using electron microscopy, however, marked focal perivascular deposits of collagen type IV were seen in the hearts of untreated 2K1C rats, indicating the beginning of myocardial fibrosis due to hypertensive tissue damage. This finding is consistent with the study of Mall et al. [3] who found that it takes 12 weeks before a significant difference in interstitial tissue is found. After 8 weeks, a significantly lower capillary length density in 2K1C relative to sham animals was demonstrated in the study of Mall et al. [3]. In the present short-term study, a tendency toward reduced capillary supply was seen, but this difference was not statistically significant. This finding may suggest that the changes in capillary length density develop later in the course of LVH, whereas wall thickening of intramyocardial arteries is already present in the early phase of renovascular hypertension. Early thickening of intrarenal arteries in experimental hypertension was also found in studies by Helmchen et al. [17, 18].

So far changes in cardiomyocyte geometry in LVH have only been investigated in a limited number of studies. Using a morphometric approach—the left ventricles were divided into endocardial and epicardial zones (which we did not do, using the orientator technique)—Anversa and coworkers [19, 20] found an increase in epicardial volume of about 37% with proportional increase of myocytes. Dämmrich and Pfeifer [21] analyzed cardiomyocyte number and volume in Sprague-Dawley rats after the induction of LVH by aortic banding. Their results were comparable to ours [20]. In addition, Gerdes et al. [22] measured the cell volume of isolated cardiomyocytes and found similar results to our in vivo study.

An important and unexpected finding of the study was that the number of cardiomyocytes per left ventricle was significantly lower in untreated 2K1C animals than in sham-operated controls. This loss of cardiomyocytes was partly, but not entirely, prevented by normalization of systolic blood pressure with dihydralazine. In hearts with marked ventricular hypertrophy and no signs of cardiac

failure, a decrease in cardiomyocyte number was first described in 1994 by Olivetti et al. [23] in subjects with hypertensive cardiac hypertrophy. The authors reasoned that the loss of cardiomyocytes was due to necrosis. In a subsequent study, they discovered that their findings could be explained by apoptosis, since DNA breakpoints, DNA condensation, and fragmentation were present in cardiomyocytes from hypertrophic hearts [24].

In order to obtain further insights into the regulation of cardiomyocyte hypertrophy and loss of cells in early LVH, we analyzed the hearts of untreated 2K1C and sham-operated control rat hearts using the TUNEL technique and immunohistochemistry with antibodies against pro- and anti-apoptotic proteins [25]. Although we found no differences between untreated 2K1C and sham-operated control rats with respect to the number of apoptotic or proliferating cardiomyocytes, we demonstrated a threefold increase of the anti-apoptotic protein Bcl-2, whereas cardiac expression of the pro-apoptotic protein bax was comparable in both groups, thus yielding an increased Bcl-2/Bax ratio. These results point to activation of anti-apoptotic mechanisms by day 14 of hypertensive LVH [25]. It is well known that the TUNEL assay does present methodological problems and the fractions of cells reported in the literature undergoing apoptosis using this assay have frequently been exaggerated. Using electron microscopy, we did not detect apoptotic cardiomyocytes, but this is not astonishing at all as the putative apoptotic process induced by the clipping of the renal artery may have been completed 2 weeks after clipping. This interpretation is supported by the observation of Teiger et al. [26] who detected apoptotic cardiomyocytes only during the first 7 days of LVH, with a peak at day 4 when cardiac hypertrophy had been induced by aortic banding. Rodriguez-Feo and coworkers [27] recently found a significant increase in the Bax/Bcl-2 ratio and in the percentage of apoptotic cardiomyocytes in the hearts of 19-week-old spontaneously hypertensive rats (SHRs) relative to age-matched normotensive Wistar Kyoto controls. This increase in the rate of apoptosis was found very early in the SHR, even before LVH had developed [27]. This finding provides further support to the notion that apoptosis may occur early in the course of hypertension, i.e., long before any structural evidence of cardiac damage is detectable. It is well known that levels of the potentially pro-apoptotic factor Ang II vary greatly in the first 2 weeks of 2K1C hypertension [28]. Thus, the direct pro-apoptotic effect of Ang II may be at least one potential explanation for the decrease in myocyte number in 2K1C rats, but this remains speculative since we did not measure Ang II levels in our experiment. Treatment with the non-specific antihypertensive agent dihydralazine resulted in complete normalization of systolic blood pressure (as assessed by tail plethysmography), but this intervention prevented only partly the various cardiac structural alterations. The fact that arterial wall thickness was completely normalized in dihydralazine-treated 2K1C rats argues for a central role of blood pressure in the development of this alteration. Since cardiomyocyte hypertrophy and the loss of cardiomyocytes were only partly prevented by dihydralazine, a potential role of blood pressure-independent factors, such as endocrine and paracrine growth factors, has to be considered. A likely candidate involved is Ang II, as the experimental model of 2K1C hypertension is characterized by particularly strong stimulation of the systemic renin–angiotensin system. Previous studies have demonstrated potent, blood pressure-independent effects of Ang II on cardiomyocyte growth in vitro [29, 30] and in vivo [31, 32].

In conclusion our data document that LVH in renovascular hypertension develops as early as several days after clipping of the renal artery and is characterized by complex myocardial remodeling. The most important features of this early cardiac remodeling process are hypertrophy and a specific loss of cardiomyocytes, possibly due to an earlier increase in apoptotic activity that was no longer present in the present study 2 weeks after induction of hypertension. Alternatively, myocyte loss due to necrosis has to be considered. The cardiac remodeling processes are partly independent of the increase in blood pressure and provide the setting for the well-known clinical consequences of LVH such as arrhythmias and heart failure.

**Acknowledgements** Dres. M. Buzello, C. Boehm, B. Fischer were recipients of grants from the Graduiertenkolleg "Nieren- und Kreislaufregulation" of Deutsche Forschungsgemeinschaft (DFG). The work was further supported by the Deutsche Forschungsgemeinschaft (SFB 423, project B8). The authors thank Z. Antoni, H. Derks, G. Gorsberg, P. Rieger and H. Ziebart for excellent technical support. We further acknowledge the help of Dr. rer. nat. J. Sikora and PD Dr. Ph. A. Schnabel, Department of Pathology, University of Heidelberg, in performing the TUNEL technique and Dr. med. F. Zimmermann, Department of Immunology, University of Heidelberg, for the introduction into confocal laserscanning microscopy.

## References

1. Hocher B, George I, Rebstock J, Bauch A, Schwarz A, Neumayer HH, Bauer C (1999) Endothelin system-dependent cardiac remodeling in renovascular hypertension. Hypertension 33:816–822
2. Smith SH, McCaslin M, Sreenan C, Bishop SP (1988) Regional myocyte size in two-kidney, one clip renal hypertension. J Mol Cell Cardiol 20:1035–1042
3. Mall G, Mattfeldt T, Rambausek M, Hasslacher C, Mann J, Ritz E (1989) Reaction patterns of the myocardial interstitium in different models of cardiac hypertrophy-sterological investigations. Gegenbaurs Morphol Jahrb 135:151–158
4. Fischer M, Wiest G, Tekesin I, Amann K, Mann J, Hasslacher, Derks H, Mall G (1992) Effects of combined renovascular hypertension and diabetes mellitus on myocardial cells, non-vascular interstitium and capillaries: a stereological study on rat hearts. Virchows Arch 420:499–506
5. Ehmke H, Faulhaber J, Münter K, Kirchengast M, Wiesner RJ (1999) Chronic $ET_A$ receptor blockade attenuates cardiac hypertrophy independently of blood pressure effects in renovascular hypertensive rats. Hypertension 33:954–960
6. Ito H, Hiroe M, Hirata Y, Fujisaki H, Adachi S, Akimoto H, Ohta Y, Marumo F (1994) Endothelin $ET_A$ receptor antagonist blocks cardiac hypertrophy provoked by hemodynamic overload. Circulation 89:2198–2203

7. Wiesner RJ, Ehmke H, Faulhaber J, Zak R, Rüegg JC (1997) Dissociation of left ventricular hypertrophy, $\beta$-myosin heavy chain gene expression, and myosin isoform switch in rats after ascending aortic stenosis. Circulation 95:1253–1259
8. Massart PE, Donckier J, Kyselovic J, Godfraind T, Heyndrickx GR, Wibo M (1999) Carvedilol and lacidipine prevent cardiac hypertrophy and endothelin-1 gene overexpression after aortic banding. Hypertension 34:1197–1201
9. Katholi RE (1983) Renal nerves in the pathogenesis of hypertension in experimental animals and humans. Am J Physiol 245:F1–F14
10. Johansson M, Elam M, Rundquist B, Eisenhofer G, Herlitz H, Lambert G, Friberg P (1999) Increased sympathetic nerve activity in renovascular hypertension. Circulation 99:2537–2542
11. Della-Bruna R, Bernhard I, Gess B, Schricker K, Kurtz A (1995) Renin gene and angiotensin II $AT_1$ receptor gene expression in the kidneys of normal and of two-kidney/one clip rats. Pflugers Arch 430:265–272
12. Mattfeldt T, Mall G (1987) Growth of capillaries and myocardial cells in the normal rat heart. J Mol Cell Cardiol 19:1237–1246
13. Mattfeld T, Mall G, Gharehbaghi H, Möller P (1990) Estimation of surface area and length with the orientator. J Microsc 159:301–317
14. Törnig J, Amann K, Ritz E, Nichols C, Zeier M, Mall G (1996) Arteriolar wall thickening, capillary rarefaction and interstitial fibrosis in the heart of rats with renal failure. The effect of ramipril, nifedipine and moxonidine. J Am Soc Nephrol 7:669–677
15. Amann K, Kronenberg G, Gehlen F, Wessels S, Orth S, Münter K, Ehmke H, Mall G, Ritz E (1998) Cardiac remodelling in experimental renal failure—an immunohistochemical study. Nephrol Dial Transplant 13:1958–1966
16. Wiest G, Gharehbaghi H, Amann K, Simon T, Mattfeldt T, Mall G (1992) Physiological growth of arteries in the rat heart parallels the growth of capillaries, but not of myocytes. J Mol Cell Cardiol 24:1423–1431
17. Helmchen U, Kneissler U, Bohle RM, Reher A, Groene HJ (1984) Adaptation and decompensation of intrarenal small arteries in experimental hypertension. J Cardiovasc Pharmacol 6[Suppl 4]:696–705
18. Helmchen U, Bohle RM, Kneissler U, Groene HJ (1984) Intrarenal arteries in rats with early two-kidney, one clip hypertension. Hypertension 6:11187–11192
19. Loud AV, Anversa P, Giacomelli F, Wiener J (1978) Absolute morphometric study of myocardial hypertrophy in experimental hypertension. I. Determination of myocyte size. Lab Invest 38:586–596
20. Anversa P, Loud AV, Giacomelli F, Wiener J (1978) Absolute morphometric study of myocardial hypertrophy in experimental hypertension. II. Ultrastructure of myocytes and interstitium. Lab Invest 38:597–609
21. Dämmrich J, Pfeifer U (1983) Cardiac hypertrophy in rats after supravalvular aortic constriction. Virchows Arch 43:265–286
22. Gerdes AM, Moore JA, Hines JM, Kirkland PA, Bishop SP (1986) Regional differences in myocyte size in normal rat heart. Anat Rec 215:420–426
23. Olivetti G, Melissari M, Balbi T, Quaini F, Cigola E, Sonnenblick EH, Anversa P (1994) Myocyte cellular hypertrophy is responsible for ventricular remodelling in the hypertrophied heart of middle aged individuals in the absence of cardiac failure. Cardiovasc Res 28:1199–1208
24. Olivetti G, Abbi R, Quaini F, Kajstura J, Cheng W, Nitahara JA, Quaini E, Di Loreto C, Beltrami CA, Krajewski S, Reed JC, Anversa P (1997) Apoptosis in the failing human heart. N Engl J Med 336:1131–1141
25. Korsmeyer SJ, Shutter JR, Veis DJ, Merry DE, Oltvai ZN (1993) Bcl-2/Bax: a rheostat that regulates an antioxidant pathway and cell death. Semin Cancer Biol 4:327–332
26. Teiger E, Than VD, Richard L, Wisnewsky C, Tea BS, Gaboury L, Tremblay J, Schwartz K, Hamet P (1996) Apoptosis in pressure overload-induced heart hyper trophy in the rat. J Clin Invest 97:2891–2897
27. Rodriguez-Feo JA, Fortes J, Aceituno E, Farre J, Ayala R, Castilla C, Rico L, Gonzalez-Fernandez F, Garcia-Duran M, Casado S, Lopez-Farre A (2000) Doxazosin modifies Bcl-2 and Bax protein expression in the left ventricle of spontaneously hypertensive rats. J Hypertens 18:307–315
28. Guan S, Fox J, Mitchell KD, Navar LG (1992) Angiotensin and angiotensin converting enzyme tissue levels in two-kidney, one clip hypertensive rats. Hypertension 20:763–767
29. Ito H, Hirata Y, Adachi S, Tanaka M, Tsujino M, Koike A, Nogami A, Murumo F, Hiroe M (1993) Endothelin-1 is an autocrine/paracrine factor in the mechanism of angiotensin II-induced hypertrophy in cultured rat cardiomyocytes. J Clin Invest 92:398–403
30. Moreau P, dUscio LV, Shaw S, Takase H, Barton M, Lüscher TF (1997) Angiotensin II increases tissue endothelin and induces vascular hypertrophy; reversal by $ET_A$-receptor antagonist. Circulation 96:1593–1597
31. Kim S, Ohta K, Hamaguchi A, Yukimura T, Miura K, Iwao H (1995) Angiotensin II induces cardiac phenotypic modulation and remodeling in vivo in rats. Hypertension 25:1252–1259
32. Mervaala E, Muller DN, Schmidt F, Park JK, Gross V, Bader M, Breu V, Ganten D, Haller H, Luft FC (2000) Blood pressure-independent effects in rats with human renin and angiotensinogen genes. Hypertension 35:587–594

Virchows Arch (2003) 442:372–380
DOI 10.1007/s00428-003-0773-7

ORIGINAL ARTICLE

**Andréa M. A. Costa · Beatriz Tuchweber · Thierry Lamireau · Ibrahim M. Yousef · Charles Balabaud · Jean Rosenbaum · Alexis Desmoulière**

# Role of apoptosis in the remodeling of cholestatic liver injury following release of the mechanical stress

Received: 14 September 2002 / Accepted: 19 December 2002 / Published online: 26 March 2003
© Springer-Verlag 2003

**Abstract** It has been known for a long time that portal fibrosis consecutive to experimental common bile duct ligation is reversible following obstacle removal, but the mechanisms involved remain unknown. We have studied the effect of bilioduodenal anastomosis and of simple biliary decompression on the remodeling of the lesion in bile duct-ligated rats. Rats were subjected to common bile duct ligation for 7 days or 14 days. Bilioduodenal anastomosis was performed after 14 days of bile duct ligation and animals sacrificed at intervals. In other animals, after 7 days or 14 days of ligation, the common bile duct was merely decompressed by bile aspiration and animals sacrificed 24 h later. Collagen deposition, $\alpha$-smooth muscle actin expression and apoptosis were evaluated. Bile was collected and the bile acid profile assessed. After anastomosis, collagen deposition and $\alpha$-smooth muscle actin expression decreased and were back to control values after 7 days. These parameters remained practically unchanged 24 h after biliary decompression. Bile duct ligation by itself induced apoptosis of some fibroblastic and bile ductular cells after 7 days; this was back to normal after 14 days. After anastomosis or decompression, apoptosis of both fibroblastic and bile ductular cells increased greatly and was accompanied by ultrastructural features of extracellular matrix degradation. Total bile acid content decreased after common bile duct ligation, the proportion of dihydroxylated bile acids decreasing and that of trihydroxylated bile acids increasing. Biliary decompression and anastomosis did not modify total concentration and composition of the biliary bile acid pool. In summary, we show that mere biliary decompression, by relieving the mechanical stress, is as effective as bilioduodenal anastomosis to induce apoptosis of portal cells that likely triggers portal fibrosis regression.

**Keywords** Myofibroblast · Fibrosis · Liver · Extracellular matrix · Bile acids

A. M. A. Costa · T. Lamireau · C. Balabaud · J. Rosenbaum · A. Desmoulière (✉)
Groupe de Recherches pour l'Etude du Foie,
INSERM E0362, Université Victor Segalen Bordeaux 2,
146 rue Léo-Saignat, 33076 Bordeaux cedex, France
e-mail: Alexis.Desmouliere@gref.u-bordeaux2.fr
Tel.: +33-557-571771
Fax: +33-556-514077

A. M. A. Costa
Departamento de Histologia e Embriologia,
Universidade do Estado do Rio de Janeiro,
Rio de Janeiro, Brazil

B. Tuchweber
Département de Nutrition,
Université de Montréal,
Montréal, Canada

I. M. Yousef
Département de Physiologie,
Université de Montréal,
Montréal, Canada

## Introduction

Liver fibrosis is the main complication of many chronic liver diseases such as chronic viral hepatitis and alcoholic liver disease. It is also a major complication of biliary diseases whether intra- or extra-hepatic. The potential reversibility of liver fibrosis is a key issue. Reversibility of experimental cholestatic liver fibrosis following obstacle removal was observed a long time ago [3, 4]. More recently, Hammel et al. [14] studied a group of patients with cholestatic liver fibrosis who underwent surgical decompression of an obstructed biliary system. By comparing liver-biopsy specimens obtained before and after surgery, they observed in some patients a significant regression of the liver fibrosis after decompression. However, the mechanisms involved in fibrosis resolution remain essentially unknown.

The animal model of bile duct proliferation and fibrosis after ligation of the common bile duct has been widely used, because it simulates many histological features of human chronic biliary fibrosis. Bile duct ligation is quickly followed by extracellular matrix

deposition in the portal tracts and differentiation of portal fibroblasts into $\alpha$-smooth muscle actin-positive myofibroblasts. These cells proliferate and play a dominant role in the development of portal fibrosis [7]. At the same time, bile duct epithelial cells also proliferate resulting in the formation of neoductules. The fate of the proliferating bile duct epithelial cells during regression of the portal lesion induced by bilioduodenal anastomosis has been studied by Bhatal and Gall who showed that these cells underwent apoptosis. However, although Ramm et al. [27] observed the disappearance of portal myofibroblasts after the release of the extrahepatic obstruction, the mechanism and the kinetics of the disappearance of these cells have not been ascertained.

We were the first to show that apoptosis mediates the decrease in cellularity during the transition between skin granulation tissue and scar [6]. This observation has now been extended to other organs. Thus, in the liver, it has been shown that myofibroblasts derived from hepatic stellate cells disappear by apoptosis during the spontaneous resolution of rat liver fibrosis induced by carbon tetrachloride treatment [16]. Altogether, the regulation of apoptotic phenomena during tissue repair may be important in scar establishment and development of pathological scarring when apoptosis fails to occur.

The aim of this study was to evaluate, in portal fibrosis induced in rats by common bile duct ligation, the role of portal myofibroblasts apoptosis during the fibrotic tissue remodeling observed after bilioduodenal anastomosis. Furthermore, we examined whether biliary decompression alone was able to induce cell apoptosis in the lesions. Thus, after bile duct obstruction, animals were subjected to either bilioduodenal anastomosis or simple biliary decompression to characterize the very early stages of possible reversal of liver lesions induced by common bile duct ligation. Finally, an analysis of the bile was performed to study whether modifications in bile acid concentration could partly be involved in cell death and fibrosis resolution.

## Materials and methods

### Animals and surgery

Male Sprague-Dawley rats weighing 200–250 g were used. All animals were housed in a temperature- and humidity-controlled room under a constant light cycle where they had free access to food and drinking water. All protocols were in full compliance with the University of Montreal and of Bordeaux guidelines for animal care. Rats were subjected to common bile duct ligation as described before [36]. Experimental procedures were as follows.

Control animals underwent sham surgery as described previously [36]. Since there was no difference between results of the various sham-operated rats, data are presented together as controls. A first group of animals was subjected to bile duct ligation and sacrificed after 7 days ($n$=4) or 14 days ($n$=4). In another group ($n$=9), on the 14th day after bile duct ligation, bile flow was reconnected by a Roux-en-y choledochojejunostomy between the dilated stump of the common bile duct and the first jejunum loop under sodium pentobarbital anesthesia (45 mg/kg intraperitoneally) as previously described [38]. Animals were sacrificed 1 ($n$=3), 2 ($n$=3), and 7 ($n$=3) days later. Finally, other animals ($n$=10) subjected to bile duct ligation for 7 days ($n$=5) or 14 days ($n$=5) were submitted to a simple biliary decompression. To this end, rats were anesthetized with sodium pentobarbital and the liver exposed by a longitudinal midline incision. To carry out decompression of the common bile duct, the contents of the dilated duct were drained by needle puncture, and animals sacrificed 24 h later. In all animals, blood samples were taken at the time of sacrifice and routine liver function blood tests (bilirubin, alkaline phosphatase, GGT, and transaminases) were performed on an automated analyzer in the Biochemistry Department of Montreal University or of Pellegrin Hospital in Bordeaux. Data were calculated as mean values ±SD. A student's $t$-test for unpaired samples, with Welch correction was used for statistical analysis. A $P<0.05$ was considered significant.

Other groups of animals were subjected to bile analysis. In animals with bile duct ligation for a duration of 7 days ($n$=3) or 14 days ($n$=3), bile flow was reconnected by choledochojejunostomy. Twenty four hours after the operation, the common bile duct was cannulated with a PE 20 cannula and bile collected every 15 min for 30 min. Sham-operated animals ($n$=6) served as controls. These sham-operated animals underwent the same manipulation as the choledochojejunostomy group, except the actual reconnection between bile duct and intestine. Other experimental groups with bile duct ligation for 7 days ($n$=3) or 14 days ($n$=3) were subjected to a simple decompression. Animals were then kept for 5 h under sedation. After the 5-h period, the bile was collected as described above. Groups of sham-operated animals ($n$=6) served as controls; they were anesthetized and operated on as before except that the decompression was not applied. Basal values for biliary bile acid content and composition were obtained from additional groups of rats that underwent laparotomy without bile duct ligation. In all animals, during bile collection, body temperature was monitored using a rectal thermistor and kept at 36°C with a heating lamp.

### Histochemistry, immunohistochemistry and apoptosis detection

Fresh tissue samples were routinely formalin fixed and paraffin embedded. Tissue sections (5 $\mu$m) were stained with hematoxilin-eosin for routine histology or Sirius red [saturated picric acid in distilled water containing 0.1% (w/v) Sirius red F3B (BDH Chemicals Ltd., Poole, UK)] to allow visualization of fibrosis [20]. $\alpha$-Smooth muscle actin expression was evaluated using immunohistochemistry with a specific monoclonal antibody [33] as previously described [36]. Apoptosis was detected using the TdT-mediated dUTP-X nick end labeling (TUNEL) method [12]. Briefly, formalin-fixed, paraffin-embedded sections were pretreated with proteinase K (10 $\mu$g/ml; Roche Diagnostics, Meylan, France) for 20 min. Then, the ApopTag Plus in situ apoptosis detection kit (Oncor, Gaithersburg, MD) was used following manufacturer instructions.

Sirius red staining was scored semi-quantitatively, in 20 random, low-power (×5 objective) fields per animal using the following score: − staining present only in portal tract; + staining present in portal tract and around proliferating bile ducts; ++ staining present in incomplete septa penetrating into the parenchyma; +++ staining present in well-organized septa connecting portal tracts. The amount of cells expressing $\alpha$-smooth muscle actin was also scored in 20 random low-power fields per animal: − positive cells only in vessel walls; + scarce positive cells in portal tract connective tissue (<20% of the portal tract connective tissue surface); ++ numerous positive cells in portal tract connective tissue (20–60% of the portal tract connective tissue surface); +++ large amount of positive cells in portal tract connective tissue (>60% of the portal tract connective tissue surface). Semi-quantitative evaluation was estimated by two different researchers, and inter-observer reproducibility was greater than 95%. Moreover, minimal differences were observed among animals from the same group.

Apoptotic cells were counted in 30 portal zones per animals with a ×20 objective. The percentage of bile duct epithelial cells

and of non-bile duct epithelial cells (including portal fibroblasts and inflammatory cells) positive for TUNEL was also evaluated. All values are expressed as mean±SD. The student's *t*-test was used to evaluate significance of differences between two groups; a $P<0.05$ was considered significant.

### Transmission electron microscopy

Liver fragments were processed for transmission electron microscopy using established procedures. Briefly, small liver fragments (approximately 1 $mm^3$) were immersed in 1% osmium tetroxide in 0.1 M cacodylate buffer (pH 7.2) for 2 h, washed, dehydrated in graded ethanols, and Epon embedded. Semi-thin sections were stained with toluidine blue to orientate the tissue. Thin sections were contrasted with uranyl acetate and lead citrate and observed with a Philips CM-120 transmission electron microscope (Philips SA, Zurich, Switzerland).

### Bile acid analysis

The conjugated and total bile acids in bile were determined using liquid chromatrography-electrospray tandem mass spectrometry (LC-MS) in accordance with a technique that we have recently published [26]. Specific bile acid species were determined in selected samples using gas-chromatography-mass spectrometry (GC-MS) with a technique similar to that previously described [8]. All values are expressed as mean±SD. Comparison of multiple means was performed using analysis of variance (ANOVA) with the Statview 2.0 software (Abacus Concepts Inc., Berkeley, CA); a $P<0.05$ was considered significant.

## Results

### Biochemical analysis

Before anastomosis or decompression, serum bilirubin was elevated at 7 days after bile duct ligation (122.4±43.2 $\mu M\ l^{-1}$) and remained elevated at 14 days after bile duct ligation (94.0±64.5 $\mu M\ l^{-1}$) compared with control values obtained in sham-operated animals (4.2±0.9 $\mu M\ l^{-1}$; $P<0.005$ and $P<0.03$, respectively). Bilirubin levels decreased after bilioduodenal anastomosis and were almost normal after 7 days (7.8±1.1 $\mu M\ l^{-1}$). Twenty four hours after decompression, we observed in the group ligated for 7 days a significant decrease in bilirubin concentration (66.8±15.6 $\mu M\ l^{-1}$) compared with the values obtained in the absence of decompression ($P<0.02$); for animals ligated for 14 days, the decrease observed after decompression (76.2±37.0 $\mu M\ l^{-1}$) was not significantly different from those obtained without decompression.

Without anastomosis or decompression, the values for alkaline phosphatase, GGT, ASAT and ALAT were 348±69 IU $l^{-1}$, 19±4 IU $l^{-1}$, 480±125 IU $l^{-1}$, and 111±48 IU $l^{-1}$, respectively, in animals ligated for 7 days, and 264±13 IU $l^{-1}$, 405±241 IU $l^{-1}$, 376±76 IU $l^{-1}$, and 127±34 IU $l^{-1}$, respectively, for animals ligated for 14 days. These blood biochemical parameters were within control range 7 days after anastomosis, as previously described [2]. Twenty four hours after decompression of animals bile duct ligated for 7 days or 14 days, there was no significant modifications of these parameters (not shown).

### Hematoxylin-eosin, Sirius red and $\alpha$-smooth muscle actin staining

The results of semi-quantitative analysis of Sirius red and of $\alpha$-smooth muscle actin staining are shown in Table 1. In animals ligated for 7 days and 14 days, as already described [36], the development of the portal lesion was illustrated by bile duct proliferation and deposition of extracellular matrix. Seven days after bile duct ligation, incomplete septa penetrated into the parenchyma; at 14 days after bile duct ligation, the septa interconnected adjacent portal tracts (Fig. 1a). At 7 days after bile duct ligation, numerous $\alpha$-smooth muscle actin-expressing myofibroblasts were observed in portal tracts, mainly around proliferating bile ducts; at 14 days after bile duct ligation, the amount of portal myofibroblasts increased (Fig. 1b). Twenty four hours after bilioduodenal anastomosis, portal lesions remained unchanged. Forty-eight

**Table 1** Evaluation of Sirius red staining and of $\alpha$-smooth muscle actin- and TUNEL-positive cells in portal areas. In control animals, Sirius red staining was detected in portal areas and around centrolobular veins; $\alpha$-smooth muscle actin was present exclusively in vessel walls (portal vessels and centrolobular veins); no apoptotic cells were detected. Values are expressed as means±SD

| | Sirius red staining | $\alpha$-Smooth muscle actin-positive cells | TUNEL-positive cells (%) |
|---|---|---|---|
| Bile duct ligation for 7 days | | | |
| Without decompression | ++ | ++ | 5.2±0.4 |
| 24 h after decompression | ++ | ++ | 8.1±0.4[a] |
| Bile duct ligation for 14 days | | | |
| Without anastomosis or decompression | +++ | +++ | 1.6±0.3 |
| 24 h after anastomosis | +++ | +++ | 11.3±0.6[b] |
| 48 h after anastomosis | ++ | ++ | 8.7±0.5[b] |
| 7 days after anastomosis | + | – | 0.9±0.5 |
| 24 h after decompression | +++ | +++ | 11.8±0.7[c] |

[a] $P<0.05$ compared with bile duct-ligated animals for 7 days without decompression
[b] $P<0.05$ compared with bile duct-ligated animals for 14 days without anastomosis
[c] $P<0.05$ compared with bile duct-ligated animals for 14 days without decompression

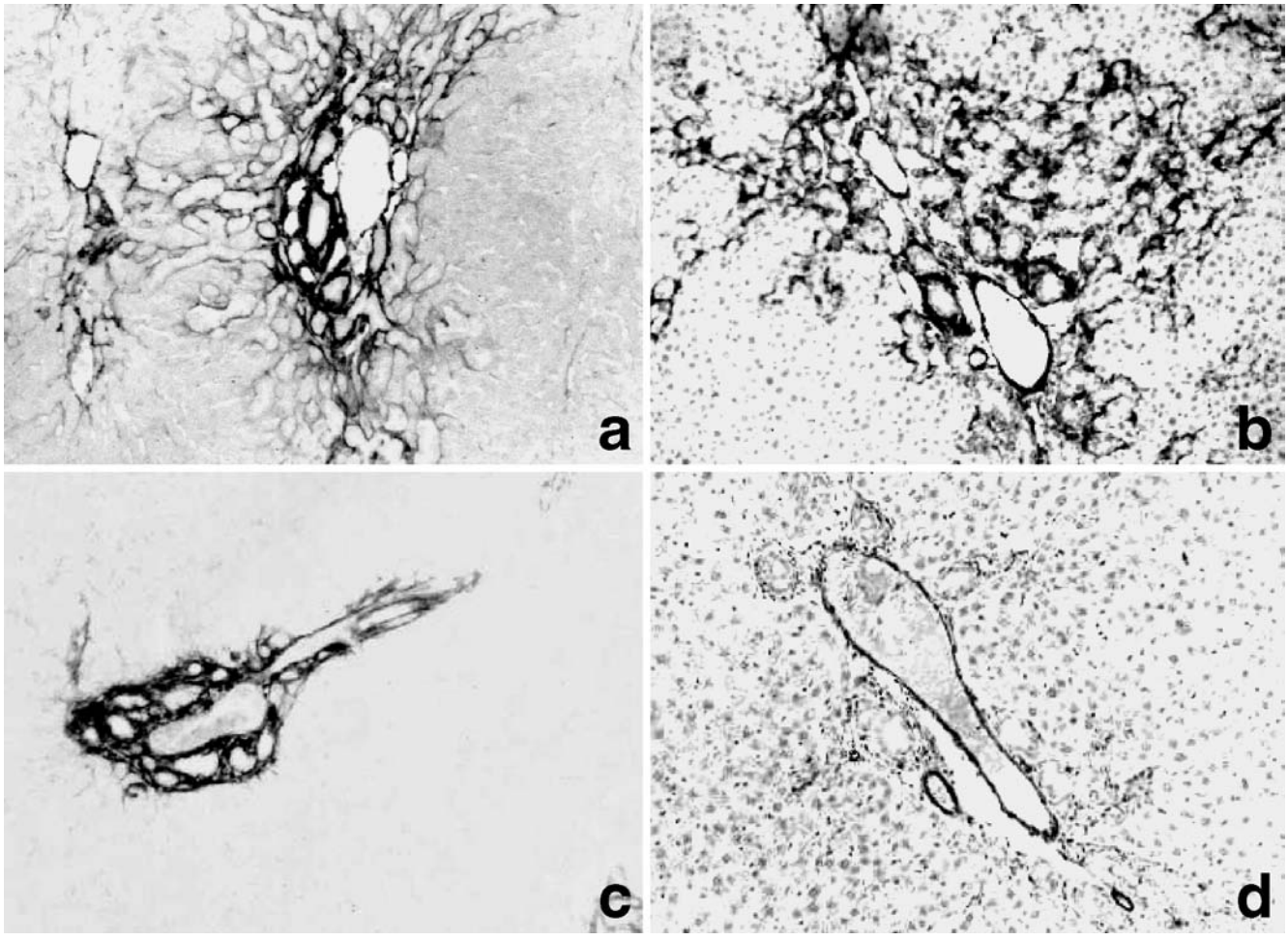



**Fig. 1** Sirius red staining (**a**, **c**) and immunohistochemistry for $\alpha$-smooth muscle actin (**b**, **d**) in bile duct-ligated animals for 14 days (**a**, **b**) and 7 days after bilioduodenal anastomosis (**c**, **d**). Fourteen days after common bile duct ligation, a large amount of collagenous deposition in enlarged portal areas (**a**) and numerous cells expressing $\alpha$-smooth muscle actin forming layers around proliferating bile ducts (**b**) are observed. At 7 days after bilioduodenal anastomosis, only a scarce deposition of collagen is observed in portal areas (**c**), while cells expressing $\alpha$-smooth muscle are observed only in vessel walls (**d**). ×100

hours after anastomosis, numerous bile ducts were still present but showed signs of disorganization; a slight decrease in the amount of collagen and of myofibroblastic cells expressing $\alpha$-smooth muscle actin was observed. At 7 days after bilioduodenal anastomosis, the collagen deposition was reduced with a scarce deposition of collagen still present in the portal areas (Fig. 1c); bile duct number was reduced, and cells expressing $\alpha$-smooth muscle actin were observed only in vessel walls (Fig. 1d). Twenty four hours after decompression, histological parameters such as collagen deposition, amount of myofibroblasts expressing $\alpha$-smooth muscle actin and bile duct proliferation were similar to that observed in animals bile duct-ligated for 7 days and 14 days, with no major features of reorganization.

## Apoptosis evaluation

Quantitative evaluation of apoptosis is summarized in Table 1. In animals ligated for 7 days and 14 days, apoptosis in portal zones was marked at 7 days (Table 1; Fig. 2a) but practically absent at 14 days (Table 1; Fig. 2b). Portal cells showing apoptosis included fibroblastic, inflammatory, and bile duct epithelial cells. Many hepatocytes in periportal location were also positive for TUNEL at both time points. After bilioduodenal anastomosis, apoptosis significantly increased with a peak at 24 h (Table 1; $P<0.01$ compared with the bile duct-ligated animals without anastomosis); there were scarce apoptotic cells in the parenchyma, the majority of apoptotic cells being present in portal regions where non-bile duct epithelial cells and bile duct epithelial cells positive for TUNEL staining represented 57.2±7.8% and 39.6±4.3%, respectively, of the total apoptotic cells in the portal area. At 2 days after bilioduodenal anastomosis, the number of apoptotic cells decreased relative to 24 h after bilioduo-

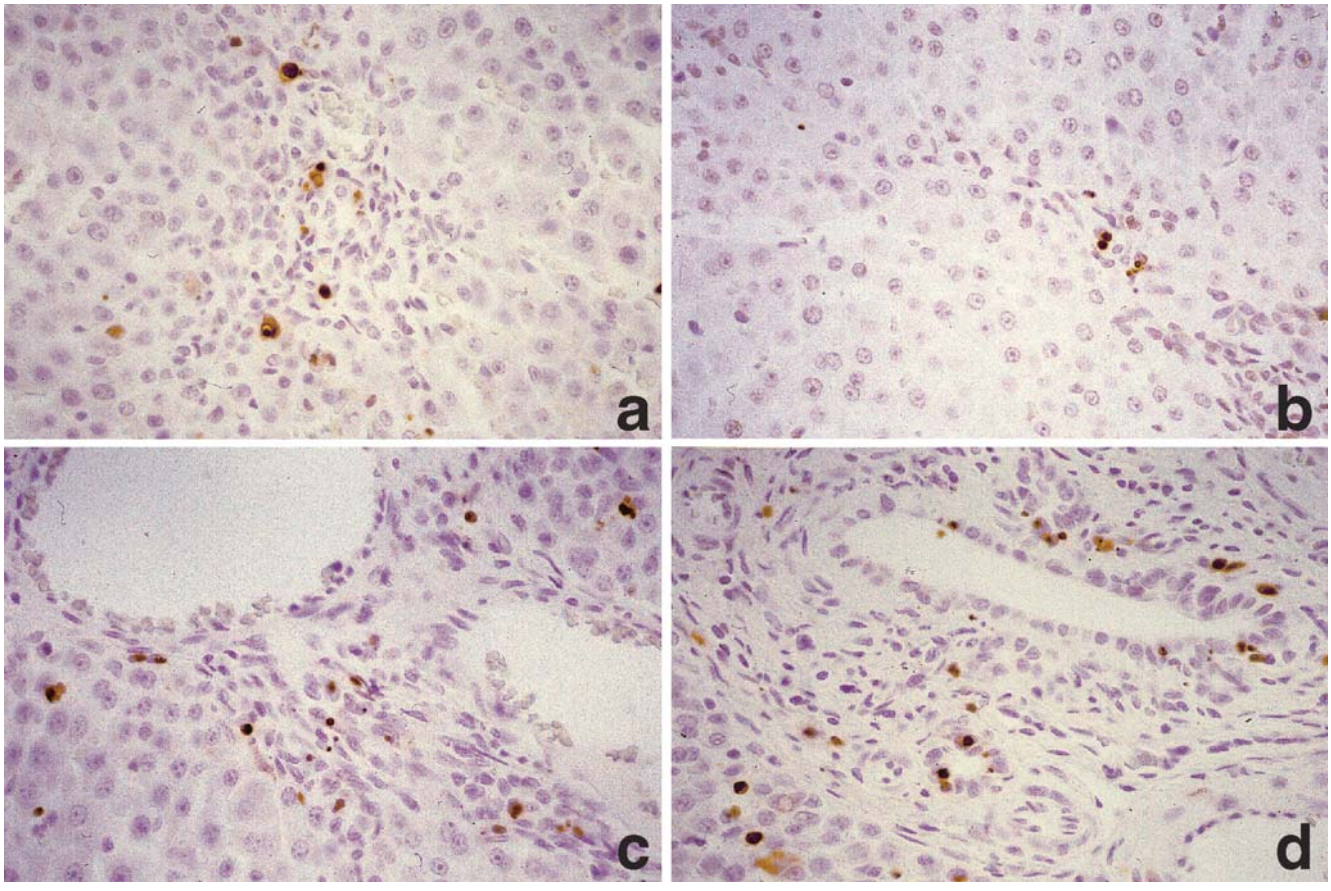



**Fig. 2** TUNEL staining for apoptotic cells. Seven days after common bile duct ligation (**a**), positive cells are observed, mainly at the border between the extending portal area and the parenchyma; 14 days after common bile duct ligation (**b**), a few positive cells are still present at the periphery of the portal area. Twenty-four hours after decompression in animals bile duct-ligated for 7 days (**c**), numerous positive cells are clearly identified in the portal areas; the number of positive cells was higher after decompression in animals bile duct-ligated for 14 days (**d**); ×200

denal anastomosis (Table 1), but remained significantly higher than the bile duct-ligated animals without anastomosis (Table 1; $P<0.05$). Seven days after anastomosis, there were few positive cells for TUNEL staining in portal tracts. Twenty-four hours after decompression, the amount of apoptotic cells in portal areas significantly increased in animals ligated for both times (7 days and 14 days) compared with bile duct-ligated animals without decompression (Table 1; $P<0.02$). The number of apoptotic cells was, however, significantly higher in the animals that had common bile duct ligation for 14 days (Table 1; Fig. 2d) than in those that had common bile duct ligation for 7 days (Table 1; Fig. 2c; $P<0.05$). Few hepatocytes were positive for TUNEL following decompression. The amount and the type of cells positive for TUNEL staining in portal areas 24 h after decompression were very similar to those observed 24 h after bilioduodenal anastomosis, i.e., about 60% of TUNEL-positive non-bile duct epithelial cells and 40% of TUNEL-positive bile duct epithelial cells.

## Electron microscopy examination

As already described [7], after bile duct ligation, thick collagen bundles in portal tract connective tissue and typical myofibroblasts with microfilament bundles were observed around bile ducts (Fig. 3a). Twenty-four hours after bilioduodenal anastomosis, extracellular matrix rearrangement and cellular apoptosis were observed. Collagen bundles with typical features of degradation such as fibrils with varying diameters and twisted fibrils were observed (Fig. 3b). Twenty four hours after anastomosis, many cells showing features of apoptosis (chromatin condensation, loss of contact with neighboring cells) were observed; these cells were fibroblastic or myofibroblastic cells and bile duct epithelial cells (Fig. 3, c–e). Twenty four hours after bile duct decompression, similar features of extracellular matrix remodeling and of apoptosis were observed in portal fibroblastic cells (Fig. 3f).

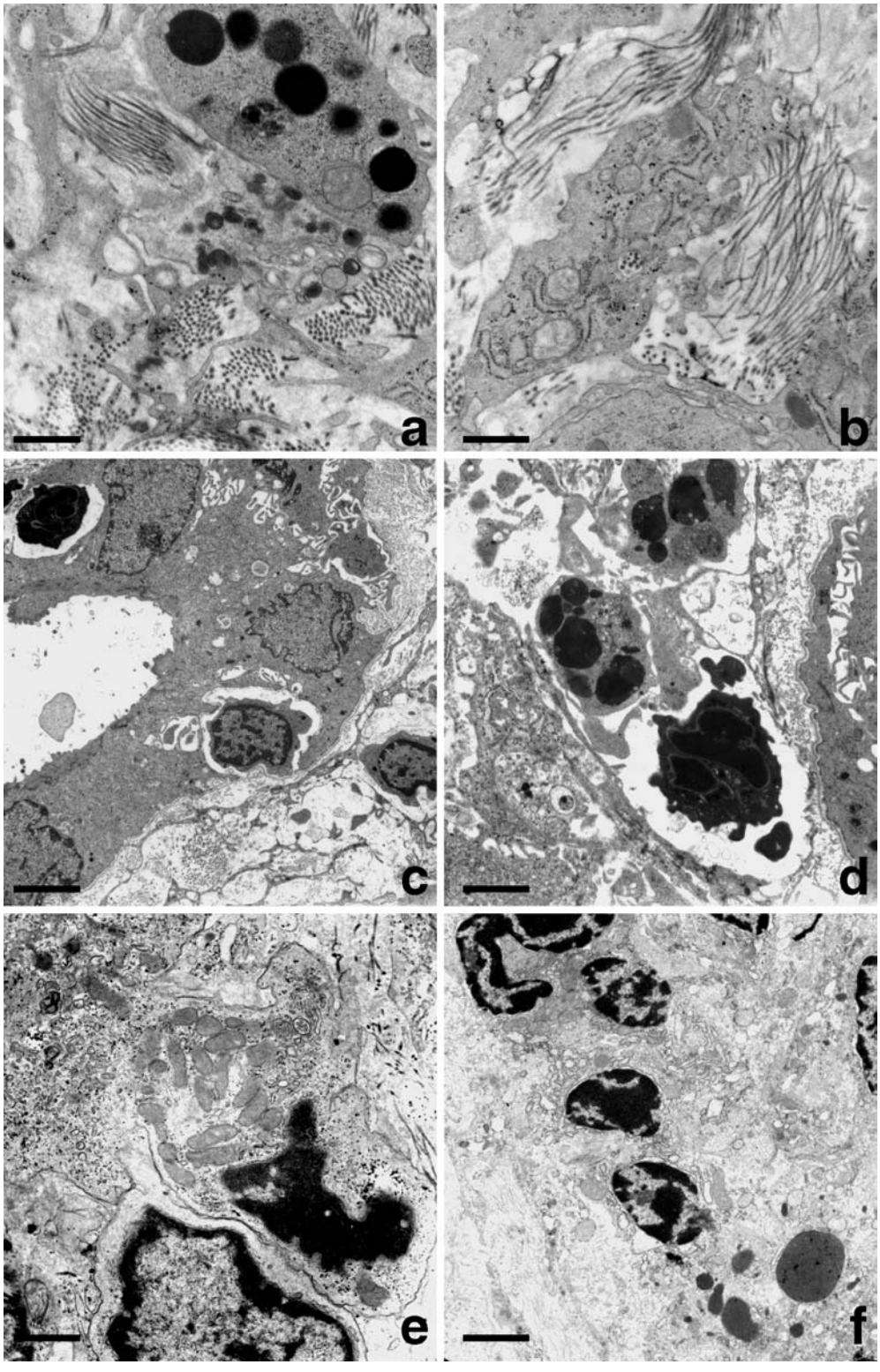



**Fig. 3** Ultrastructural observations in portal tracts of animals bile duct-ligated for 14 days (**a**), and 24 h after bilioduodenal anastomosis (**b**–**e**) or biliary decompression (**f**). In control animals (**a**), large bundles of collagen are observed in the portal connective tissue. Twenty-four hours after anastomosis, collagen fibrils showing features of degradation (bundle dissociation and variable fiber diameters) are present (**b**). Ultrastructural features of apoptosis, such as chromatin condensation, loss of contact with neighboring cells together with a preservation of organelles (mitochondria and endoplasmic reticulum) are observed after both anastomosis (**c**–**e**) or decompression (**f**). Those cells include bile duct epithelial cells (**c**) and portal fibroblastic cells (**d**, **e** and **f**). *Bars* 170 $\mu$m (**a** and **b**); 40 $\mu$m (**c** and **d**); 65 $\mu$m (**e** and **f**)

## Bile analysis

Changes in biliary bile acid concentration and bile acid composition are shown in Table 2. The concentration of total bile acids in bile duct-ligated rats without bilioduodenal anastomosis or decompression was significantly decreased relative to normal sham-operated animals ($P<0.05$). There were no significant differences between groups at 7 days and 14 days after bile duct ligation. After bile flow reconnection by anastomosis or decompression, the concentrations showed a tendency to increase in most groups, but differences were not statistically significant as

**Table 2** Total biliary bile acid concentration and bile acid profile after bilioduodenal anastomosis (BDL) or decompression following bile duct ligation. Bile acid analysis was carried out before and 24 h after anastomosis or 5 h after decompression. 99% of bile acids were in tauroconjugated form. Values are expressed as means±SD

| Groups | Total bile acid (mM) | % Distribution pattern | | | |
|---|---|---|---|---|---|
| | | Mono-hydroxylated | Di-hydroxylated | Tri-hydroxylated | Tetra-hydroxylated |
| Controls | 28.0±7.5 | 0.33±0.07 | 13.9±2.1 | 81.8±2.5 | 3.8±0.5 |
| Anastomosis at 7 days after BDL | | | | | |
| Without anastomosis | 14.19±2.61* | 0 | 2.12±0.33* | 96.4±1.2* | 1.52±0.71 |
| After anastomosis | 21.60±13.27 | 0.21±0.18 | 5.14±1.92* | 90.4±3.9* | 4.27±2.06 |
| Anastomosis at 14 days after BDL | | | | | |
| Without anastomosis | 17.7±8.3* | 0 | 1.65±0.06* | 97.52±0.57* | 0.83±0.73 |
| After anastomosis | 13.0±11.1 | 0.02±0.03 | 2.78±2.17* | 94.2±3.76* | 2.9±2.5 |
| Decompression at 7 days after BDL | | | | | |
| Without decompression | 12.9±6.5* | 0.07±0.03 | 1.9±0.3* | 96.7±0.2* | 1.2±0.03 |
| After decompression | 40.0±12.52 | 0.04±0 | 2.6±0.15* | 95.9±0.7* | 1.42±0.59 |
| Decompression at 14 days after BDL | | | | | |
| Without decompression | 14.3±7.85* | 0.01±0.01 | 1.79±0.53* | 96.6±0.9* | 1.59±0.52 |
| After decompression | 24.0±13.4 | 0.08±0.04 | 5.40±1.77* | 92.35±2.53* | 2.16±1.40 |

* $P<0.05$ compared with controls (sham-operated animals)

there were considerable variations between individual rats after surgery.

Analysis of biliary bile acid composition in control rats showed that the most abundant bile acids were trihydroxylated bile acids in taurine-conjugated form. GC-MS technique indicated that those were cholic acid and beta muricholic acid (70% and 8%, respectively); whereas, the dihydroxylated bile acids were mainly chenodeoxycholic and deoxycholic acid (5.6% and 4.0%, respectively). The remainder of the bile acids in the pool were contributed by ursodeoxycholic acid (a dihydroxylated bile acid), lithocholic acid (a monohydroxylated bile acid), and by tetrahydroxylated bile acids. After bile duct ligation, the proportion of dihydroxylated bile acids decreased while that of trihydroxylated bile acids increased significantly. GC-MS analysis showed, however, that the main change was in the contribution of beta muricholic acid, which increased to an average of 85% relative to 8% in sham-operated animals. The proportion of cholic acid decreased to about 3% relative to 70% in sham-operated animals. The pattern of change was similar at 7 days or 14 days after bile duct ligation. In animals with decompression or bilioduodenal anastomosis, there was a tendency toward the reversal of these abnormalities that was however not statistically significant.

## Discussion

In this study, we have demonstrated an important involvement of apoptosis in the tissue remodeling induced by bilioduodenal anastomosis or decompression in bile duct-ligated rats. Bilioduodenal anastomosis stimulated the regression of the cholestatic lesion with a decrease of the cellularity by apoptosis of the portal cells (mainly fibroblastic, inflammatory, and bile duct cells) and the remodeling of the extracellular matrix. Furthermore, the simple release of the pressure by decompression was sufficient to rapidly induce an important apoptotic process.

During the development of the lesion, apoptosis was much more marked in the sub-acute phase (at 7 days) when the proliferation of portal cells is important [36], than at 14 days. The presence of bile duct epithelial cell apoptosis in this setting has already been described by Gall and Bhathal [10]. However, we describe here for the first time the occurrence of portal fibroblast apoptosis during the development of the lesion. This is reminiscent of the apoptosis that was also observed in activated hepatic stellate cells during the course of carbon tetrachloride-induced liver fibrosis [16]. In agreement with the data of Miyoshi et al. [23], we have also observed a significant number of hepatocytes undergoing apoptosis. This finding may explain why, following bile duct ligation, the liver volume does not increase significantly [18] despite a large increase in the size of portal tracts.

Although apoptosis occurred in the course of bile duct ligation, its rate was significantly enhanced after either anastomosis or decompression. Apoptotic cells were mainly observed in portal areas, and were mostly bile duct epithelial and myofibroblastic cells. Indeed, compared with the toxin-induced chronic liver damage, there is, in this model, little liver necrosis and inflammation, and bile duct proliferation is essentially followed by a marked expansion of a fibroblast population in the periductular stroma that rapidly expresses $\alpha$-smooth muscle actin [36]. The factors controlling the rate of apoptosis in the course of bile duct ligation and following pressure release may be multiple. First, bile duct ligation results in an increase in bilirubin concentration in serum and in bile. High bilirubin levels may be protective against apoptosis triggered by oxidant-related stimuli

[35]. Thus, anastomosis or decompression that lower bilirubin concentration may induce the loss of this protective factor. However, bilirubin is also a pro-apoptotic factor by itself, notably on neural cells [29, 32] and it is thus difficult to assess its exact role. Second, it is known that bile acids can exert various toxic effects on cells, including apoptosis, depending on many factors, such as their degree of hydrophobicity. We have recently shown that hydrophobic bile acids were cytotoxic and induced apoptosis of cultured biliary epithelial cells [19]. We have also shown as others that bile duct ligation induced changes in total bile acid concentration and bile acid composition. The proportion of dihydroxylated bile acids decreased and that of trihydroxylated bile acids increased. As also shown by Naito et al. [24], beta muricholic acid became the predominant trihydroxylated form, while cholic acid contribution decreased markedly. Following anastomosis or decompression, there was a trend toward the normalization of these values. Similar to ursodeoxycholic acid, beta muricholic acid has been shown to be protective against taurolithocholate-induced cholestasis [22] and may also be protective against toxic effects of cholic or chenodeoxycholic acids [37]. Ursodeoxycholic acid specifically protects hepatocytes against apoptosis [28]. Thus, provided that beta muricholic acid behaves similarly, a decrease in its concentration, together with other modifications in the bile acid composition of bile, may shift the balance toward apoptosis.

While changes in bile composition are probably of importance, it is likely that the main factor in inducing a higher apoptosis rate following anastomosis or decompression is the decreased biliary pressure.

Mechanical forces can regulate gene expression in different cell types [5, 15, 30]. Mechanical stimulation in dermal fibroblasts cultured in a three dimensional collagen network leads to an increase of extracellular matrix synthesis and inhibition of its degradation [17]. Similar mechanisms may occur in portal fibroblasts in bile duct-ligated animals. However, it is well known that the release of the pressure by bilioduodenal anastomosis leads to extracellular matrix remodeling with regression of the fibrosis [1, 38]. We show here that the release of the pressure either by anastomosis or decompression can very early induce a remodeling of the lesion, characterized by the induction of apoptosis in bile duct epithelial cells and portal myofibroblasts, together with extracellular matrix modifications. After release of the pressure, cells may die by apoptosis because they lose their contacts with extracellular matrix, as shown by Meredith et al. [21], or cell apoptosis may be induced by changes in the mechanical properties of the extracellular matrix as recently demonstrated [9, 13, 25]. These two mechanisms are likely to occur during experimental liver fibrosis remodeling. In our experiments, we have indeed observed ultrastructural evidence of extracellular matrix degradation that may be explained by a decreased expression of matrix proteinase inhibitors as shown by Iredale et al. [16] during the recovery from carbon tetrachloride-induced liver fibrosis. It is noteworthy that portal fibroblasts are not directly exposed to a mechanical stress as they are embedded in the portal matrix, whereas bile duct epithelial cells are direct targets. It is thus likely that the fate of portal fibroblasts is dictated in part by signals originating from bile duct cells. This is supported by data from Swartz et al. [34] showing that mechanically stressed bronchial epithelial cells elaborate soluble factors that elicit matrix remodeling in unstressed lung fibroblasts. Following bile duct obstruction, bile duct epithelial cells are known to synthesize growth factors such as PDGF-BB [11] that can act as survival factors for many cell types [31]. Interruption of this signaling secondary to bile duct cell apoptosis could provide an explanation for portal fibroblast apoptosis.

In conclusion, we have shown, in the model of cholestatic fibrosis induced by common bile duct ligation, that the withdrawal of intraductal pressure (by bilioduodenal anastomosis or decompression) is a sufficient stimulus to induce apoptosis in bile duct epithelial and portal fibroblastic cells, and to elicit extracellular matrix remodeling. Those data are important in the understanding of mechanisms involved in regression of cholestatic diseases and highlight the role of mechanical stimuli on cell growth, phenotype and death.

**Acknowledgements** This work was supported in part by the Région Aquitaine in France, by the Medical Research Council of Canada and by Fundação de Amparo à Pesquisa do Estado do Rio de Janeiro (Brazil). We thank the staff of the Biochemistry Department of Pellegrin Hospital (Bordeaux) for performing liver function tests.

## References

1. Abdel-Aziz G, Lebeau G, Rescan PY, Clement B, Rissel M, Deugnier Y, Campion JP, Guillouzo A (1990) Reversibility of hepatic fibrosis in experimentally induced cholestasis in rat. Am J Pathol 137:1333–1342
2. Aronson DC, Chamuleau RA, Frederiks WM, Gooszen HG, Heijmans HS, James J (1993) Reversibility of cholestatic changes following experimental common bile duct obstruction: fact or fantasy? J Hepatol 18:85–95
3. Birns M, Masek B, Auerbach O (1962) The effects of experimental acute biliary obstruction and release on the rat liver. A histochemical study. Am J Pathol 40:95–112
4. Cameron GR, Prasad LBM (1960) Recovery from biliary obstruction after spontaneous restoration of the obstructed common bile-duct. J Pathol Bacteriol 80:127–136
5. Chiquet M (1999) Regulation of extracellular matrix gene expression by mechanical stress. Matrix Biol 18:417–426
6. Desmoulière A, Redard M, Darby I, Gabbiani G (1995) Apoptosis mediates the decrease in cellularity during the transition between granulation tissue and scar. Am J Pathol 146:56–66
7. Desmoulière A, Darby I, Costa AMA, Raccurt M, Tuchweber B, Sommer P, Gabbiani G (1997) Extracellular matrix deposition, lysyl oxidase expression, and myofibroblastic differentiation during the initial stages of cholestatic fibrosis in the rat. Lab Invest 76:765–778
8. Dionne S, Tuchweber B, Plaa GL, Yousef IM (1994) Phase I and Phase II metabolism of lithocholic acid in hepatic acinar zone 3 necrosis. Evaluation in rats by combined radiochromatography and gas liquid chromatrography-mass spectrometry. Biochem Pharmacol 48:1187–1197

9. Fluck J, Querfeld C, Cremer A, Niland S, Krieg T, Sollberg S (1998) Normal human primary fibroblasts undergo apoptosis in three-dimensional contractile collagen gels. J Invest Dermatol 110:153–157
10. Gall JA, Bhathal PS (1990) A quantitative analysis of the liver following ligation of the common bile duct. Liver 10:116–125
11. Grappone C, Pinzani M, Parola M, Pellegrini G, Caligiuri A, DeFranco R, Marra F, Herbst H, Alpini G, Milani S (1999) Expression of platelet-derived growth factor in newly formed cholangiocytes during experimental biliary fibrosis in rats. J Hepatol 31:100–109
12. Gravieli Y, Sherman Y, Ben-Sasson SA (1992) Identification of programmed cell death in situ via specific labeling of nuclear DNA fragmentation. J Cell Biol 119:493–501
13. Grinnell F, Zhu M, Carlson MA, Abrams JM (1999) Release of mechanical tension triggers apoptosis of human fibroblasts in a model of regressing granulation tissue. Exp Cell Res 248:608–619
14. Hammel P, Couvelard A, O'Toole D, Ratouis A, Sauvanet A, Flejou JF, Degott C, Belghiti J, Bernades P, Valla D, Ruszniewski P, Levy P (2001) Regression of liver fibrosis after biliary drainage in patients with chronic pancreatitis and stenosis of the common bile duct. N Engl J Med 344:418–423
15. Hsieh AH, Tsai CM, Ma QJ, Lin T, Banes AJ, Villarreal FJ, Akeson WH, Sung KL (2000) Time-dependent increases in type-III collagen gene expression in medical collateral ligament fibroblasts under cyclic strains. J Orthop Res 18:220–227
16. Iredale JP, Benyon RC, Pickering J, McCullen M, Northrop M, Pawley S, Hovell C, Arthur MJ (1998) Mechanisms of spontaneous resolution of rat liver fibrosis. Hepatic stellate cell apoptosis and reduced hepatic expression of metalloproteinase inhibitors. J Clin Invest 102:538–549
17. Kessler D, Dethlefsen S, Haase I, Plomann M, Hirche F, Krieg T, Eckes B (2001) Fibroblasts in mechanically stressed collagen lattices assume a "synthetic" phenotype. J Biol Chem 276:36575–36585
18. Krahenbuhl S, Talos C, Lauterburg BH, Reichen J (1995) Reduced antioxidative capacity in liver mitochondria from bile duct ligated rats. Hepatology 22:607–612
19. Lamireau T, Zoltowska M, Levy E, Yousef I, Rosenbaum J, Tuchweber B, Desmoulière A (2003) Effects of bile acids on biliary epithelial cells: proliferation, cytotoxicity, and cytokine secretion. Life Sci 72:1401–1411
20. Manabe N, Chevallier M, Chossegros P, Causse X, Guerret S, Trepo C, Grimaud JA (1993) Interferon-alpha 2b therapy reduces liver fibrosis in chronic non-A, non-B hepatitis: a quantitative histological evaluation. Hepatology 18:1344–1349
21. Meredith JE Jr, Fazeli B, Schwartz MA (1993) The extracellular matrix as a cell survival factor. Mol Biol Cell 4:953–961
22. Milkiewicz P, Roma MG, Elias E, Coleman R (2002) Hepatoprotection with tauroursodeoxycholate and beta muricholate against taurolithocholate induced cholestasis: involvement of signal transduction pathways. Gut 51:113–119
23. Miyoshi H, Rust C, Roberts PJ, Burgart LJ, Gores GJ (1999) Hepatocyte apoptosis after bile duct ligation in the mouse involves fas. Gastroenterology 117:669–677
24. Naito T, Kuroki S, Chijiiwa K, Tanaka M (1996) Bile acid synthesis and biliary hydrophobicity during obstructive jaundice in rats. J Surgical Res 65:70–76
25. Niland S, Cremer A, Fluck J, Eble JA, Krieg T, Sollberg S (2001) Contraction-dependent apoptosis of normal dermal fibroblasts. J Invest Dermatol 116:686–692
26. Perwaiz S, Tuchweber B, Mignault D, Gilat T, Yousef IM (2001) Determination of bile acids in biological fluids by liquid chromatrography-electrospray tandem mass spectrometry. J Lipid Res 12:114–119
27. Ramm GA, Carr SC, Bridle KR, Li L, Britton RS, Crawford DH, Vogler CA, Bacon BR, Tracy TF (2000) Morphology of liver repair following cholestatic liver injury: resolution of ductal hyperplasia, matrix deposition and regression of myofibroblasts. Liver 20:387–396
28. Rodrigues CM, Fan G, Ma X, Kren BT, Steer CJ (1998) A novel role for ursodeoxycholic acid in inhibiting apoptosis by modulating mitochondrial membrane perturbation. J Clin Invest 101:2790–2799
29. Rodrigues CM, Sola S, Castro RE, Laires PA, Brites D, Moura JJ (2002) Perturbation of membrane dynamics in nerve cells as an early event during bilirubin-induced apoptosis. J Lipid Res 43:885–894
30. Roelofsen J, Klein-Nulend J, Burger EH (1995) Mechanical stimulation by intermittent hydrostatic compression promotes bone-specific gene expression in vitro. J Biomech 28:1493–1503
31. Sano H, Ueda Y, Takakura N, Takemura G, Doi T, Kataoka H, Murayama T, Xu Y, Sudo T, Nishikawa S, Nishikawa SI, Fujiwara H, Kita T, Yokode M (2002) Blockade of platelet-derived growth factor receptor-$\beta$ pathway induces apoptosis of vascular endothelial cells and disrupts glomerular capillary formation in neonatal mice. Am J Pathol 161:135–143
32. Silva RF, Rodrigues CM, Brites D (2001) Bilirubin-induced apoptosis in cultured rat neural cells is aggravated by chenodeoxycholic acid but prevented by ursodeoxycholic acid. J Hepatol 34:402–408
33. Skalli O, Ropraz P, Trzeciak A, Benzonana G, Gillessen D, Gabbiani G (1986). A monoclonal antibody against alpha-smooth muscle actin: a new probe for smooth muscle differentiation. J Cell Biol 103:2787–2796
34. Swartz MA, Tschumperlin DJ, Kamm RD, Drazen JM (2001) Mechanical stress is communicated between different cell types to elicit matrix remodeling. Proc Natl Acad Sci U S A 98:6180–6185
35. Tomaro ML, Batlle AM (2002) Bilirubin: its role in cytoprotection against oxidative stress. Int J Biochem Cell Biol 34:216–220
36. Tuchweber B, Desmoulière A, Bochaton-Piallat ML, Rubbia-Brandt L, Gabbiani G (1996) Proliferation and phenotypic modulation of portal fibroblasts in the early stages of cholestatic fibrosis in the rat. Lab Invest 74:1–14
37. Yousef IM, Bouchard G, Tuchweber B, Plaa G (1997) Monohydroxy bile acid induced cholestasis: role of biotransformation. Drug Metab Rev 29:167–181
38. Zimmermann H, Reichen J, Zimmermann A, Sagesser H, Thenisch B, Hoflin F (1992) Reversibility of secondary biliary fibrosis by biliodigestive anastomosis in the rat. Gastroenterology 103:579–589

Virchows Arch (2003) 442:381–387
DOI 10.1007/s00428-003-0772-8

ORIGINAL ARTICLE

**A. Lopez-Beltran · R. J. Luque · A. Quintero · M. J. Requena · R. Montironi**

# Hepatoid adenocarcinoma of the urinary bladder

Received: 31 October 2002 / Accepted: 14 January 2003 / Published online: 25 March 2003
© Springer-Verlag 2003

**Abstract** Hepatoid adenocarcinoma is rare in the urinary bladder with only three well-illustrated previously reported cases. Pathological diagnosis is based on a combination of histological features resembling hepatocellular carcinoma and the positive immunostaining for alpha-fetoprotein. We present the clinicopathological features of four additional cases. The patients were males 66, 85, 61 and 68 years old. Hematuria was the initial symptom in all four patients. Two cases were treated by cystoprostatectomy and the remaining two by transurethral resection of the bladder. On histology, the cases showed a mixture of cells growing in a solid fashion and sheets or anastomosing trabeculae of hepatoid cells merging focally with a secondary glandular pattern of adenocarcinoma. Intracytoplasmic hyaline globules in all and bile production in three of the cases also supported the impression of hepatocytic differentiation. Immunoreactivity for alpha-fetoprotein, low molecular weight cytokeratin, alpha-1-antitrypsin, albumin, epithelial membrane antigen and a striking canalicular pattern when stained against polyclonal carcinoembryonic antigen (CEA), all indicate hepatocellular differentiation. The hepatic nature of the cells was further assessed by detecting the recently incorporated marker hepatocyte paraffin 1, by means of immunohistochemistry and albumin gene mRNA non-isotopic in situ hybridization, both of which had positive signals in all four cases. Three patients died 12, 14 and 19 months after diagnosis. The fourth patient was alive with disease at 26 months of follow-up. In conclusion, hepatoid adenocarcinoma seems to be an aggressive malignant neoplasm that is rare in the bladder whose correct diagnosis may need appropriate immunohistochemical and in situ hybridization means in addition to a complete patient clinical and pathological evaluation. The exact histogenesis and classification of these tumors remains to be established.

**Keywords** Hepatoid · Adenocarcinoma · Urinary bladder · Alpha-fetoprotein · Albumin · mRNA

A. Lopez-Beltran (✉)
Department of Pathology,
Cordoba University Medical School
and Reina Sofia University Hospital, Facultad de Medicina,
Avda. Menendez Pidal S/N, 14004 Cordoba, Spain
e-mail: em1lobea@uco.es
Tel.: +34-957-218993
Fax: +34-957-218229

R. J. Luque
Hospital Princesa Sofia, Jaen, Spain

A. Lopez-Beltran · A. Quintero
Biomedical Research Unit,
Reina Sofia University Hospital, Cordoba, Spain

M. J. Requena
Department of Urology,
Reina Sofia University Hospital, Cordoba, Spain

R. Montironi
Department of Pathology,
University of Ancona, Torrette, Italy

## Introduction

Hepatoid adenocarcinomas are extrahepatic tumors showing areas morphologically comparable to those of hepatocellular carcinomas [1, 2]. These areas are composed of cords of polygonal cells separated by sinusoids, occasionally featuring bile production and/or bile canaliculi formation [2]. In addition to this histological picture, hepatoid adenocarcinomas share with hepatocellular carcinoma immunohistochemical reactivity with anti-alpha-fetoprotein (AFP), anti-albumin, anti-alpha-1-antitrypsine (A1AT), anti-low molecular weight cytokeratin (LMWCK) and anti-epithelial membrane antigen (EMA) antibodies. Canalicular pattern of the immunoreaction against polyclonal anti-carcinoembryonic antigen (CEA; pCEA) antibody is also seen, together with elevated serum levels of AFP in most reported cases but not in all [1, 3]. Bile canaliculi formation can also be illustrated by electron microscopy. The recent introduction of the hepatocyte paraffin 1 (Hep Par 1), a monoclonal antibody which reacts with most hepatic cells in paraffin-embedded

tissues represents a useful tool to investigate hepatoid tissue origin [4, 17]. This can also be assessed detecting albumin gene mRNA by means of in situ hybridization (ISH), that to date remains the most specific single method for hepatic tissue origin [5, 6, 7, 16, 19, 22, 27].

Clinically, this variant of adenocarcinoma is characterized by its predilection for older patients, the aggressive course and poor prognosis. Early lymph node and visceral metastases are common [8, 10, 11, 12, 13, 14, 15].

Extra hepatic malignant neoplasms recapitulating the morphological features of hepatocellular carcinoma have been reported in a variety of organs, although it is more common in the stomach and the ovary [10, 12, 20]. This tumor does not occur in association with any germ-cell elements and seems to represent a somatic-derived variant of adenocarcinoma [18]. Hepatoid adenocarcinoma has subsequently been reported in the pancreas, lung, papilla of Vater, renal pelvis, ovary, and stomach [8, 10, 11, 12, 13, 14, 15, 21, 23, 24, 28]. In the urinary bladder, three cases have been reported so far [3, 25, 26] – in all instances identified by its distinctive histological appearance and production of AFP.

We report on the clinicopathological features, the immunohistochemical profile and the albumin gene mRNA expression in four additional cases of hepatoid adenocarcinoma of the urinary bladder. Current classification of AFP-producing bladder tumors is also reviewed.

## Materials and methods

Four cases of hepatoid adenocarcinoma of the urinary bladder were included in the study. Two of them were found in a retrospective study of bladder tumors from 927 patients seen at Reina Sofia University Hospital between 1980 and 1997. Two additional cases were seen in consultation. Clinical information was retrieved from patients' records in all cases.

Hematoxylin and eosin (H&E)-stained sections were available for review in all cases. Using standard published criteria [10], we independently confirmed the histological diagnosis in the study cases. Paraffin blocks showing the most representative areas of hepatoid differentiation were selected from all cases. Blocks were serially cut and stained with H&E, periodic acid/Schiff base (PAS) with diastase and Alcian blue (pH 2.5). Immunohistochemical staining was performed on unstained 5-$\mu$m-thick sections from formalin-fixed, paraffin-embedded tissues, using an automated immunostainer (Ventana Systems, Tucson, AZ) followed by a Streptavidin-biotin-labeled detection step [9]. All cases examined were subjected to heat-induced epitope retrieval. Positive and negative controls were used in each assay.

Non-isotopic mRNA ISH was performed using a probe and a method already published [5, 7, 22]. The albumin gene mRNA probe consisted of a 510-bp fragment that corresponded to the coding region of the albumin gene [6]. Oligo sequence of albumin mRNA (5'-ATA AGC CGA GCT AAA GAG AAA AAG AAG GGA AAT AAA GGT TAC CCA CCT CAT-3') labeled by digoxigenin was synthesized (MWG-Biotech AG, Germany). For the ISH technique, sections were cut from selected blocks and put on a polylysin-coated slide. Sections were then dewaxed in xylene and rehydrated through graded alcohol series. After digestion with proteinase K (250 $\mu$l; Dako) in 50 mmol/l Tris-HCl containing 1 mmol/l ethylene diamine tetraacetic acid (EDTA) for 15 min at 37°C, slides were post-fixed in paraformaldehyde 4% in phosphate-buffered saline (PBS), at 4°C for 5 min. Washing in PBS was

**Table 1** Clinicopathological features of four cases reporting of hepatoid adenocarcinoma of the bladder compared with previous reports. *AWD* alive with disease, *DOD* dead of disease, *HG* hyaline globules, *HPF* high power fields, *AFP* alpha fetoprotein, *TURB* transurethal resection of bladder

| Case no. (reference) | Age/sex | Gross | Grade/ stage | Symptoms /treatment | Follow-up (months) | HG | Spicular bodies | Bile pigment | Mitosis/ 10HPF | Preoperative serum AFP |
|---|---|---|---|---|---|---|---|---|---|---|
| Case 1 [25] | 68/Female | 2.5 cm | III $pT_{3a}$ | Hydronephosis/TURB | AWD | Yes | No | Yes | 10–15 | Not available |
| Case 2 [26] | 89/Female | 6.5x5.5 | III $pT_{2b}$ | Hematuria/cystectomy | Lost to follow-up | No | No | No | Not included | 12,700 $\mu$g/ml |
| Case 3 [3] | 71/Male | Not available | III $pT_2$ | Hematuria/TURB | AWD | Yes | No | No | <10 | Within normal limits |
| Present case 1 | 66/Male | 6x5 cm | III $pT_{3a}$ | Hematuria/cystectomy | Lung metastasis. DOD.14 months | Yes | Yes | Yes | 14 | 1065 $\mu$g/ml |
| Present case 2 | 85/Male | ** | III $pT_2$ | Hematuria/TURB | Lung metastasis. DOD.12 months | Yes | Yes | Yes | 15 | Not available |
| Present case 3 | 61/Male | 5x5 cm | III $pT_{3a}$ | Hematuria/cystectomy | Lung metastasis. DOD.19 months | Yes | Yes | Yes | 10 | 2025 $\mu$g/ml |
| Present case 4 | 68/Male | 1.5 cm | High $pT_1$ | Hematuria/TURB | AWD. Hepatoid change<5% | Yes | No | No | 8 | 1070 $\mu$g/ml |

** 80 g resected material, described at cystoscopy as large solid tumor

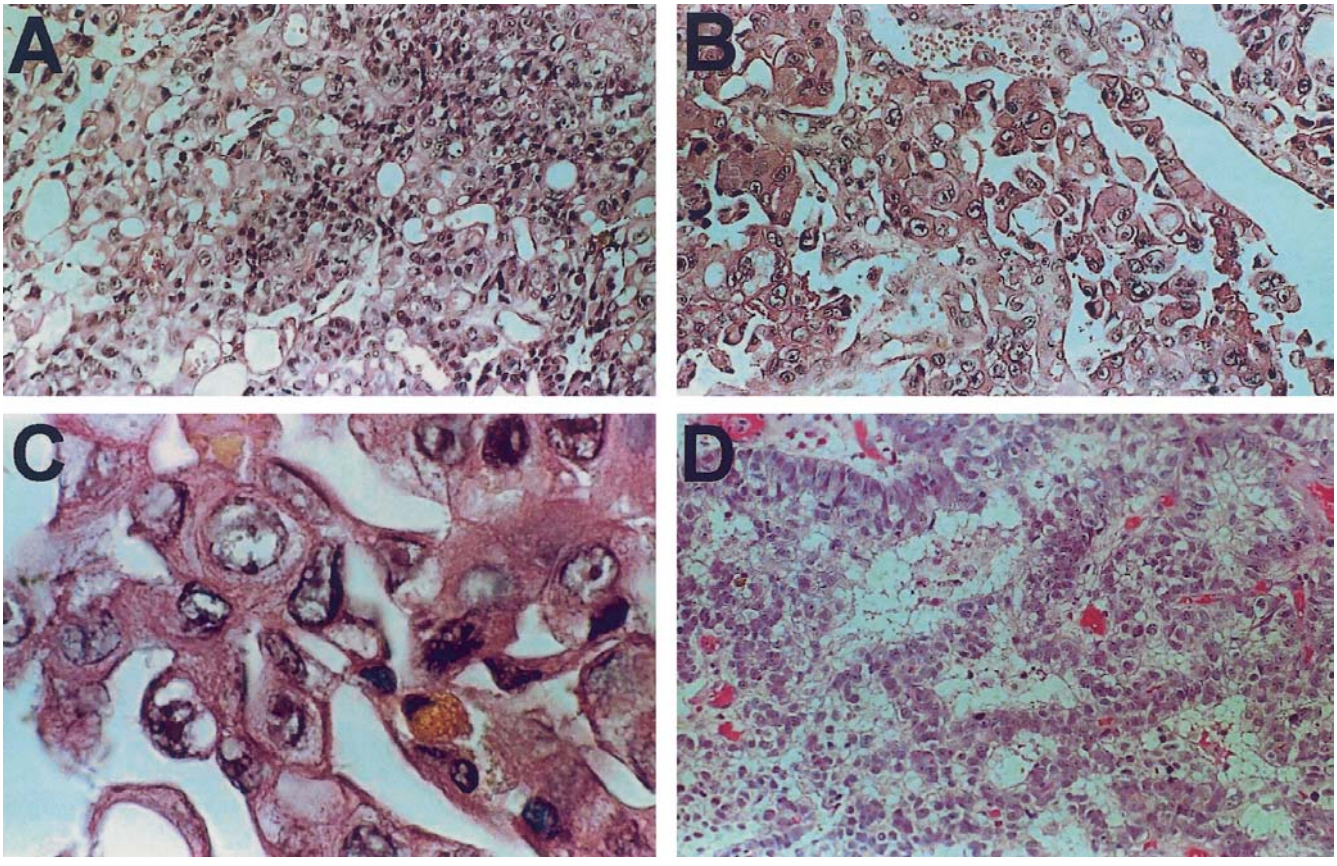



**Fig. 1** Hepatoid adenocarcinoma of the urinary bladder. Solid (**A**) and trabecular patterns (**B**) (**A** and **B**, H&E, ×100). Close-up view of hepatoid cells showing intracytoplasmic bile pigment (**C**) (H&E, ×250). Associated adenocarcinoma (**D**) (H&E, ×250)

performed for 3 min at 4°C and at room temperature. The hybridization mix contained 50% deionised formamide, 0.3 mol/l NaCl, 20 mmol/l Tris-HCl (pH 7.4), 5 mol/l EDTA, 10 mmol/l $NaH_2PO4$ (pH 8), 10% dextran sulfate, 1× Denhart's and 50 mg/ml yeast tRNA. Each section was covered with 25 $\mu$l of the hybridization solution. The sections were each covered with a siliconized coverslip. Hybridization was performed at 50°C for 16 h. Coverslips were removed and slides subjected to a stringent wash in 5× sodium chloride sodium citrate (SSC) for 10 min at 50°C and in 4× SSC for 20 min at 37°C. RNAse treatment was then performed at 37°C for 20 min (RNAse Boehringer, Mannheim, Germany), followed by a stringent wash in 2× SSC, 0.5× SSC and 0.1× SSC at 42°C for 20 min each. Slides were then rinsed in buffer 1 (100 mmol/l Tris-HCl, 150 mmol/l NaCl, pH 7.5) at room temperature before incubation with normal sheep serum diluted 1:50 for 30 min at room temperature and with polyclonal anti-digoxigenin antibody (Dako, Denmark) diluted 1:500 for 2 h at room temperature. After three washes in buffer1, sections were equilibrated in buffer 2 (100 mmol/l Tris-HCl, 100 mmol/l NaCl, 50 mmol/l $MgCl_2$, pH 9.5) for 2 min and incubated in buffer 2 with a freshly prepared color-substrate solution containing nitro blue tetrazolium salt (340 mg/ml), 5-bromo-4-chloro 3 indol phosphate toludium salt (170 mg/ml) and levamizole (1 mmol/l). Slides were washed in deionised water, counterstained with neutral green, quickly dehydrated, and mounted in Eukitt. Negative controls added to each case consisted of pretreated slides with ribonuclease A (250 mg/ml) before hybridization and omitting the probe cocktail during the ISH procedure. Sections of normal liver, added to each batch of slides, served as positive controls. Staining for albumin mRNA was regarded as positive if a distinct finely granular cytoplasmic staining was present, regardless of intensity [16].

## Results

### Clinicopathological features

Main clinical and pathological data on the reported cases is presented in Table 1. As seen, hematuria was the initial symptom in all the four patients. Two cases were treated by cystoprostatectomy and two by TURB. Mean age at diagnosis was 70 years (range 61–85 years of age). Mean follow-up was 15 months. On gross examination, tumors ranged 1.5–6 cm in width. All patients were male. All four patients had high-grade bladder tumors, and pathological stage (UICC, 2002) was T1 ($n$=1), T2 ($n$=1), and T3a ($n$=2). Two patients had associated urothelial carcinoma in situ. Three patients died of disease at 12–19 months. One patient was alive with disease at 26 months follow-up. All four patients had a previous history of recurrent bladder tumors.

On histology, a spectrum of histological patterns and cytological features was observed in the four bladder tumors. A variable proportion of tubular glands and papillary and trabecular structures was present in all tumors. Some of the glands were lined by columnar cells and by cells with abundant clear cytoplasm Fig. 1. The hepatoid foci were composed of cords or trabeculae of cells with abundant eosinophilic cytoplasm, large nuclei,

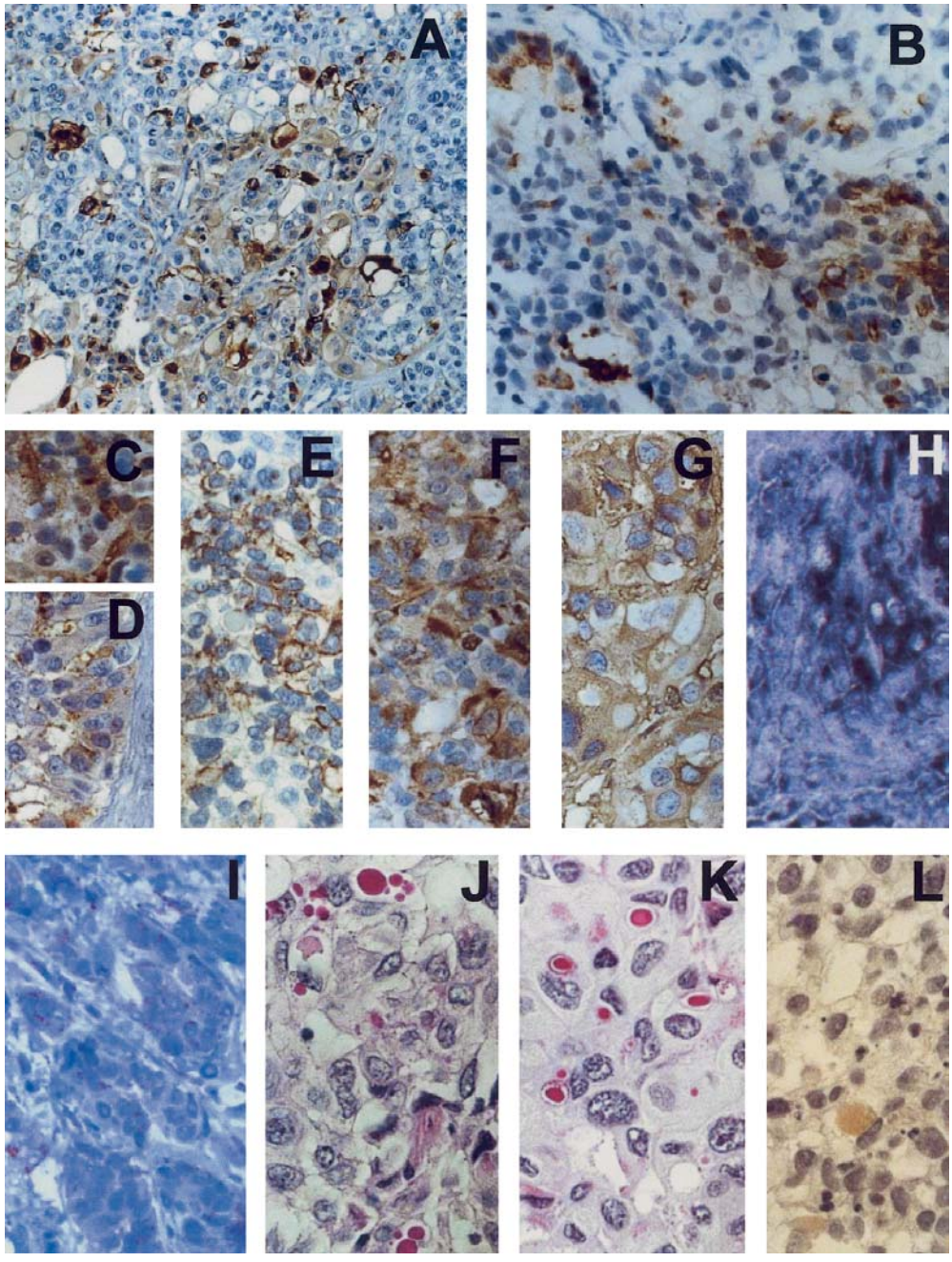



**Fig. 2** Hepatoid adenocarcinoma of the urinary bladder. Intracytoplasmic positive cells for alpha-fetoprotein (AFP) in hepatoid adenocarcinoma with solid (**A**) and conventional adenocarcinoma (**B**) patterns (×250). Canalicular (**C**) and intracytoplasmic (**D**) patterns of positive immunostain for pCEA (**C** ×400; **D** ×250). Positive immunostain for LMWCK (**E**), A1-AT (**F**), and albumin (**G**) (**E**, **F**, and **G**, ×250). (**H**) Intracytoplasmic positive signal for albumin gene mRNA (×250). (**I**) Positive focal granular immunostain for Hep Par 1(×250). Extracellular and intracellular hyaline globules in hepatoid adenocarcinoma after diastase PAS staining (**J**) occasionally featuring spicular bodies (**K**) and immunostain for AFP (**L**) (**J**, **K**, and **L**, ×250)

and prominent cherry red nucleoli Fig. 1. Occasionally, sinusoids were identified between the trabeculae, and these areas were indistinguishable from well-differentiated hepatocarcinoma. Bile pigment was seen within the cytoplasm of scattered neoplastic cells in three cases, reflecting an advanced degree of differentiation. Occasionally, the hepatoid cells were arranged as solid nests (so-called medullary pattern), as papillary structures, or in glandular configuration. Atypical mitoses were present focally. Intracellular and intercellular hyaline globules were found in all four cases (Fig. 2). Extensive lymphovascular permeation was seen in three cases.

Immunohistochemical studies
and albumin gene mRNA non-isotopic ISH

Immunohistochemical markers used in the study including the results for individual cases are given in Table 2. Focal AFP and pCEA expression was seen in all four cases examined. A focal canalicular pattern of pCEA expression, recapitulating bile canaliculi, was seen in three cases. A1AT, EMA, LMWCK and albumin gave a focal positive stain in hepatoid areas. The four cases focally expressed Hep Par 1. Hep Par 1 reactivity was characteristically granular and cytoplasmic and limited to foci of frank hepatoid differentiation (Fig. 2). Immunos-

**Table 2** Immunohistochemical results of four cases of hepatoid adenocarcinoma of the urinary bladder. *P* polyclonal antibody, *M* monoclonal antibody, *AFP* alpha-feto protein, HepPar1 (OCH1E5.2.10) hepatocyte paraffin 1 (clone OCH1E5.2.10), *LMW CK* low molecular weight cytokeratin, *A1AT* alpha 1 antitrypsin, *EMA* epithelial membrane antigen, *NSE* neurone-specific enolase, *βHCG* beta human chorionic gonadothropin

| Antiserum | Source | Type P/M | Dilution | Case no. 1 | Case no. 2 | Case no. 3 | Case no. 4 |
|---|---|---|---|---|---|---|---|
| AFP | Dako | P | 1:50 | + | + | + | + |
| HepPar1 (OCH1E5.2.10) | Dako | M | 1:80 | +* | +* | +* | +* |
| LMW CK | Biogenex | M | Prediluted | + | + | + | + |
| A1AT | Dako | P | 1:100 | + | + | + | + |
| EMA | Dako | M | 1:100 | + | + | + | + |
| pCEA | Dako | P | 1:300 | +** | +** | +** | +** |
| Chromogranin | Signet | M | Prediluted | – | – | – | – |
| NSE | Signet | M | Prediluted | – | – | – | – |
| βHCG | Dako | P | 1:200 | – | – | – | – |
| Albumin | Dako | P | 1:80 | + | + | + | + |

* Focal granular staining
** pCEA (polyclonal carcinoembryonic antigen) stained focally showing a striking canalicular pattern in three of four cases

tains for chromogranin, neurone specific enolase (NSE) and beta human chorionic gonadothropin (B-HCG) were negative in all four cases. Intracytoplasmic hyaline globules were immunoreactive for AFP (Fig. 2).

Albumin gene mRNA non-isotopic ISH showed positive signals in the cytoplasm of cells in hepatoid foci in all cases (Fig. 2).

## Discussion

The term hepatoid has been used in the literature to designate a heterogeneous variety of tumors from several organs [8, 10, 11, 12, 13, 14, 15, 21, 23, 24, 28] that can be grouped into three wide categories:

I. Germinal tumors with focal areas of hepatoid differentiation or somatic tumors that show germinal differentiation with some hepatoid areas. These lesions intensely stain for AFP (especially in the hepatoid areas), show scarce positivity for A1AT, and they are consistently negative for pCEA.
II. The second category that includes true hepatoid adenocarcinoma presents with strict morphological criteria of hepatoid differentiation, such as (i) formation of cords of polygonal cells separated by sinusoids or (ii) evidence of biliary pigment production or formation of biliary canaliculi. These tumors show a variable pattern of staining for AFP (frequently patchy), consistently stain for A1AT, albumin and half of the reported cases show few positive cells for pCEA sometimes with a sticking canalicular pattern. The four cases presented in this report belong to this category.
III. The third category (non-hepatoid AFP-producing carcinomas) includes tumors that produce AFP without any morphological feature of hepatocellular differentiation, aside from AFP production.

Using these criteria, hepatoid adenocarcinoma is rare in the urinary bladder with only three previously reported well-illustrated cases [3, 25, 26].

The four cases reported in this study had morphological and immunohistochemical criteria suggesting hepatocellular differentiation. These include a mixture of tubular or papillary adenocarcinoma with sheet-like or trabecular proliferation of neoplastic cells with abundant, eosinophilic cytoplasm and centrally located nuclei. Intracytoplasmic lumina and PAS-positive, diastase-resistant hyaline globules were occasionally present in neoplastic cells. Some of these intracytoplasmic globules that are called spicular bodies have a peripheral halo and spikes. In other instances, the hyaline globules are larger and may be seen both in the intracellular and extracellular compartments. These hyaline globules are not specific for hepatoid adenocarcinoma [25, 26]. Immunoreactive AFP is found in the cytoplasm of cells in the trabecular or sheet-like areas. It can also be found in the intracytoplasmic lumina and within the cytoplasm of the cells lining the glands or papillae in the adenocarcinoma component. AFP may be present in cancer tissues from patients in which AFP cannot be found in patient's preoperative serum. In most cases, a few cells are also stained by anti-polyclonal CEA antibody. pCEA stain is sometimes predominant along the surfaces of columnar epithelial cells exhibiting a canalicular pattern or in intracytoplasmic lumina. Also EMA, A1AT, and LMWCK were present in our cases, although they are not specific for hepatoid adenocarcinoma. Albumin that was also present in all the four reported cases is the most important protein produced by normal and neoplastic hepatocytes [7], and immunohistochemistry (IHC) with albumin antibodies has been used as a marker of hepatocellular differentiation [7]. Unfortunately, since albumin is ubiquitously present in plasma and extravascular spaces, immunohistochemical interpretation is hampered by strong background staining as happened in our cases [5, 6, 7]. In order to obviate the non-specific IHC staining with albumin, we have used albumin mRNA non-isotopic ISH. This, has proved a superior alternative to IHC in bladder

hepatoid adenocarcinoma [5, 6, 7, 16, 19, 22, 27] and, therefore, gave appropriate positive results in the four cases reported herein. Also the recently introduced marker of hepatocellular differentiation that reacts in paraffin material Hep Par 1 was tested in our cases by immunohistochemical means giving focal granular cytoplasmic staining in all four cases.

From a clinical point of view, it might be relevant for pathologists to arrive at the correct diagnosis of primary hepatoid adenocarcinoma, thus helping the clinicians in the appropriate management of these patients [3, 25, 26]. In addition, it has been shown that carcinomas with hepatoid features, irrespective of AFP production, have a poorer prognosis than AFP-producing carcinomas without hepatoid morphological features [14]. As seen in our cases, the final prognostic significance of hepatoid adenocarcinoma of the urinary bladder seems to be related to the advanced stage at diagnosis and the extensive vascular permeation seen in our cases. Conversely, the prolonged patient survival observed in case 4 in our series might be related to low pathological stage (pT1) of the tumor, a finding similar to the previously reported case of hepatoid adenocarcinoma of the renal pelvis (stage I) which appeared to have been cured by local excision [14].

Finally, the histogenesis of hepatoid adenocarcinoma remains a matter of debate [23]. For cases located in the digestive tract and for those associated with yolk sac or other germ-cell tumors, the presence of hepatoid areas has been explained on the bases of a common embryology [10, 11, 12, 13, 14, 15]. However, cases arising in such sites as lung, ovary or urinary bladder in the absence of any germ-cell component, are difficult to reconcile with such a hypothesis [10, 11, 12, 13, 14, 15]. A multi-potent cell origin or a differentiation of tumor cells in an endodermal direction may be responsible for the hepatoid characteristics of this rare tumor, a fact that needs to be demonstrated.

In conclusion, the term hepatoid adenocarcinoma should be strictly reserved for tumors with hepatoid morphological features and AFP secretion. Diagnostic criteria of these tumors would improve if at least one of the following criteria is additionally present: bile pigment, bile canaliculi by electron microscopy or by IHC against pCEA, positive immunoreaction against Hep Par 1, or albumin gene mRNA activity demonstrated by non-isotopic ISH.

**Acknowledgements** Supported by the grant FIS 00/0898 (Fondo de investigación sanitaria, Madrid, Spain).

## References

1. Arnould L, Drouer P, Fargeot P, Bernard A, Foucher P, Collin E, Petrella T (1997) Hepatoid adenocarcinoma of the lung. Report of a case of an unusual alpha-feto producing lung tumor. Am J Surg Pathol 21:1113–1118
2. Bostwick DG, Lopez-Beltran A (1999) Bladder biopsy interpretation. United Pathologists Press, New York, pp 173–196
3. Burgues O, Ferrer J, Navarro S, Ramos D, Botella E, Llombart-Bosch A (1999) Hepatoid adenocarcinoma of the urinary bladder. An unusual neoplasm. Virchows Arch 435:71–75
4. Chu PG, Ishizawa S, Wu E, Weiss LM (2002) Hepatocyte antigen as a marker of hepatocellular carcinoma. Am J Surg Pathol 26:978–988
5. D'Enico A, Baccarini P, Fiorentino M, Ceccarelli C, Bonazzi C, Ponzetto A, Scozaec JY, Mancini AM, Grigioni W (1996) Histogenesis of primary liver carcinomas: strengths and weakness of cytokeratin profile and Albumin mRNA detection. Hum Pathol 27:599–604
6. Dugalezyd A, Law SW, Demison OF (1982) Nucleotide sequence and the encoded amino acids of human serum Albumin mRNA. Proc Natl Acad Sci U S A 79:71–75
7. Foschini MP, Baccarini P, DalMonte PR, Sinard J, Eusebi V, Rosai J (1998) Albumin gene expression in adenocarcinomas with hepatoid differentiation. Virchows Arch 433:537–541
8. Gardiner GW, Lajoie G, Keith R (1992) Hepatoid adenocarcinoma of the papilla of Vater. Histopathology 20:541–544
9. Hsu SM, Raine L, Fanger H (1981) Use of avidin-biotin peroxidase complex (ABC) in immunoperoxidase techniques. A comparison between ABC and unlabelled antibody (PAP) procedures. J Histochem Cytochem 29:577–580
10. Ishikura H, Scully RF (1987) Hepatoid carcinoma of the ovary. A newly described tumor. Cancer 60:2775–2784
11. Ishikura H, Fukasawa Y, Ogasawara K, Natori T, Tsukuda Y, Aizawa M (1985) An AFP-producing gastric carcinoma with features of hepatic differentiation: a case report. Cancer 56:840–848
12. Ishikura H, Kirimoto K, Sakamoto M, Miyamoto Y, Yamagiwa H, Troh T, Aizawa M (1986) Hepatoid adenocarcinoma of the stomach: an analysis of seven cases. Cancer 58:119–126
13. Ishikura H, Kanda M, Ito M, Nosaka K, Mizuno K (1990) Hepatoid adenocarcinoma: a distinct subtype of alpha-fetoprotein producing lung carcinoma. Virchows Arch 417:73–80
14. Ishikura H, Ishiguro T, Eantus C, et al (1991) Hepatoid adenocarcinoma of the renal pelvis producing alpha-fetoprotein of hepatic type and bile pigment. Cancer 67:3051–3056
15. Ishikura H, Kishimoto T, Andachi H, Kakuta Y, Yoshiki T (1997) Gastrointestinal hepatoid adenocarcinoma: venous permeation and mimicry of hepatocellular carcinoma, a report of four cases. Histopathology 31:47–54
16. Krishna M, Lloyd RV, Batts KP (1997) Detection of albumin messenger RNA in hepatic and extrahepatic neoplasm. A marker of hepatocellular differentiation. Am J Surg Pathol 21:147–152
17. Maitra A, Murakata LA, Albores-Saavedra J (2001) Immunoreactivity for hepatocyte paraffin 1 antibody in hepatoid adenocarcinoma of the gastrointestinal tract. Am J Clin Pathol 115:689–694
18. Moran CA, Suster S (1997) Hepatoid yolk sac tumors of the mediastinum: a clinicopathologic and immunohistochemical study of four cases. Am J Surg Pathol 21:1210–1214
19. Murray GI, Paterson PJ, Ewen SWB, Melvin WT (1992) In situ hybridization of Albumin mRNA in normal liver and hepatocellular carcinoma with a digoxigenin labeled oligonucleotide probe. J Clin Pathol 45:21–24
20. Nagai E, Ueyama T, Takashi Y, Tsuneyoshi M (1993) Hepatoid adenocarcinoma of the stomach. Cancer 72:1827–1835
21. Nogales EF, Concha A, Plata C, Ruiz-Avila I (1993) Granulosa cell tumor of the ovary with diffuse true hepatic differentiation simulating stromal luteinization. Am J Surg Pathol 17:85–90
22. Papotti M, Pacchioni D, Negro F, Bonino F, Bussolati G (1994) Albumin gene expression in liver tumors: diagnostic interest in fine needle aspiration biopsies. Mod Pathol 7:271–275
23. Prat J, Bhan AK, Dickersin GR, Robboy SJ, Scully RE (1982) Hepatoid yolk sac tumor of the ovary (endodermal sinus tumor with hepatoid differentiation); a light microscopic, ultrastructural and immunohistochemical study of seven cases. Cancer 50:2355–2368

24. Roberts CC, Colby TV, Batts KP (1997) Carcinoma of the stomach with hepatocyte differentiation (hepatoid adenocarcinoma). Mayo Clin Proc 72:1154–1160
25. Sinard J, Macleary L Jr., Melamed J (1994) Hepatoid adenocarcinoma of the urinary bladder. Unusual localization or a newly recognized tumor type. Cancer 73:1919–1925
26. Yamada K, Fujioka Y, Ebihara Y, Kiriyama I, Suzuki H, Akimoto M (1994) Alpha-Fetoprotein producing undifferentiated carcinoma of the bladder. J Urol 152:958–960
27. Yamaguchi K, Nalesnik MA, Carr BI (1993) In situ hybridization of Albumin mRNA in normal liver and liver tumors: identification of hepatocellular origin. Virchows Arch 64:361–365
28. Yamamoto R, Ishikura H, Azuma M, Hareyama H, Makinoda S, Koyama Y, Nishi S, Fujimoto S (1996) Alpha-Fetoprotein production by a hepatoid adenocarcinoma of the uterus. J Clin Pathol 49:420–422

Virchows Arch (2003) 442:388–392
DOI 10.1007/s00428-002-0754-2

CASE REPORT

**Laurence de Leval · Jean-Olivier Defraigne · Gilberte Hermans · Florence Dôme · Jacques Boniver · Christian Herens**

# Malignant solitary fibrous tumor of the pleura: report of a case with cytogenetic analysis

Received: 5 September 2002 / Accepted: 10 December 2002 / Published online: 27 February 2003
© Springer-Verlag 2003

**Abstract** The majority of solitary fibrous tumors (SFTs) of the pleura are benign, but 10–30% locally recur or metastasize. Pathogenic factors relevant to the determinism of their biological properties are largely unknown. Cytogenetic data on SFTs of the pleura are sparse. We report herein a case of a malignant SFT of the pleura where successful karyotyping was obtained from the primary and recurrent tumors. The initial karyotype showed two abnormal clones: 48, XY; +8; +8; del(9)(q22; q32) [19] and 46, XY, t(1;16)(q25;p12) [7]. Culture of the recurrent tumor yielded one clone identical to the dominant clone of the initial karyotype. Demonstration of a recurrent abnormal karyotype largely supports its relevance to the malignant clone and suggests a role of supernumerary chromosome(s) 8 in the determinism of malignant behavior in SFT.

**Keywords** Solitary fibrous tumor · Pleura · Cytogenetics · Tetrasomy 8 · Malignant

## Introduction

Solitary fibrous tumor (SFT) of the pleura is a rare fibrous tumor thought to originate from submesothelial mesenchymal cells. Its overall incidence is low (2.8 cases per 100,000 tumor registrations at the Mayo Clinic) [12], but this tumor represents the second most common neoplasm of the pleura following diffuse malignant mesothelioma. The majority of SFT of the pleura are benign; however, a substantial number of cases (10–30% in large series) recur or metastasize [6, 11, 12].

There are no established criteria for assessing the biological behavior of SFTs. Microscopic features of malignancy include a high cellularity, cellular pleomorphism, a mitotic count higher than 4 per 10 high power fields (HPF), hemorrhage and necrosis [6]. Cytogenetic data on SFT of the pleura are sparse and restricted to few reports. The anomalies include trisomy 8 in two cases [1], translocation (2;3)(p21;p26) [10] in one patient, t (4;15)(q13;q26) in another [4] and a complex karyotype – 46, XY, t(6;17)(p11.2;q23), ins(9;12)(q22; q15q24.1), inv(16)(p13.1q24) – in one case [5]. The possible relationship of chromosomal changes to the biological properties of the tumors still needs to be proven.

We report a case of recurrent malignant SFT of the pleura harboring a 48, XY, +8, +8, del(9)(q22q32) karyotype.

L. de Leval (✉) · G. Hermans · F. Dôme · J. Boniver
Department of Pathology, C.H.U. Sart-Tilman,
Tour de Pathologie, B23, +1, 4000 Liège, Belgium
e-mail: L.deLeval@ulg.ac.be
Tel.: +32-4-3662405
Fax: +32-4-3662919

J.-O. Defraigne
Department of Thoracic and Cardiovascular Surgery,
C.H.U. Sart-Tilman, Liège, Belgium

C. Herens
Department of Genetics,
C.H.U. Sart-Tilman, Liège, Belgium

## Clinical history

A 54-year-old man presented with weight loss, bone pain, digital clubbing and mild superior vena cava syndrome. Skeletal symptoms were found to be related to hypertrophic osteoarthropathy. Chest imaging revealed a large right thoracic mass. From review of previous chest X-rays and medical history, it could be inferred that a right thoracic mass had been present for at least 12 years with progressive enlargement over the subsequent years. A percutaneous needle biopsy of the lesion was obtained and showed dense hyalinized collagenous tissue containing scarce cytologically bland fibroblast-like cells that were immunoreactive for CD34 and negative for cytokeratin, suggesting a SFT of the pleura. At thoracotomy, the tumor appeared to arise from the parietal pleura and had a smooth glistening surface with abundant vascularization. The tumor was cleaved from the lung despite massive bleeding. Postoperative period was unremarkable.

Control chest computed tomography (CT) scans performed at 6 months and 12 months after surgery showed a re-expansion of the previously collapsed right lung and no evidence of residual tumor. No additional therapy was administered. Bone pain disappeared but digital clubbing persisted. Eighteen months after surgery, thoracic

CT scan showed tumor recurrence in the right thorax. At rethoracotomy, massive tumoral extension in the right chest with infiltration of the visceral pleura and of the pericardium was found and "en-bloc" resection was not feasible. Tumor was resected together with the right lung and the right pericardial side.

The patient died 6 weeks after surgery of respiratory insufficiency due to extensive left bronchopneumonia. At autopsy, residual or recurrent tumor was found on the inner right thoracic wall and a 1-cm metastasis was found in the left lung. There was no evidence of tumor dissemination to other organs.

## Materials and methods

Tissues for light microscopy were fixed in 10% formalin or B5 and paraffin embedded in a standard manner. In addition to the routine hematoxylin and eosin stain, an indirect immunoperoxidase stain was performed with antibodies against CD34, CD99, desmin, actin, cytokeratin, Ki67 and epithelial membrane antigen.

Chromosome preparations of tumor cells were obtained after 5-day-old in situ cultures of an overnight collagenase disaggregated specimen of tumor biopsies [9]. Q-banded chromosomes were evaluated and classified according to ISCN nomenclature [7].

## Results

The primary tumor was a 25×14×13-cm sharply circumscribed mass with a smooth outer surface. Cut section showed a variegated appearance consisting of grayish-white firm tissue alternating with a partly necrotic and hemorrhagic fleshy tissue. Microscopic examination showed hypocellular collagenized areas demarcated from highly cellular areas with a solid "patternless", fascicular or focally hemangiopericytoma-like growth pattern, composed of spindly to plump cells with scant cytoplasm and mildly pleomorphic ovoid nuclei (Fig. 1A and B). In some areas, the tumor cells were loosely arranged in fascicular fashion and had slightly larger and more pleomorphic nuclei (Fig. 1C and D). Large zones of infarct-type necrosis were present. The mitotic rate was variable; cellular areas contained up to six mitoses per 10 HPF. The tumor cells were diffusely strongly positive for CD34 (Fig. 2), CD99 and vimentin but were negative for actin, desmin, EMA and cytokeratin. The Ki67 labeling index was estimated to be 10–15%. Based on histological and immunohistochemical findings, a diagnosis of SFT of the

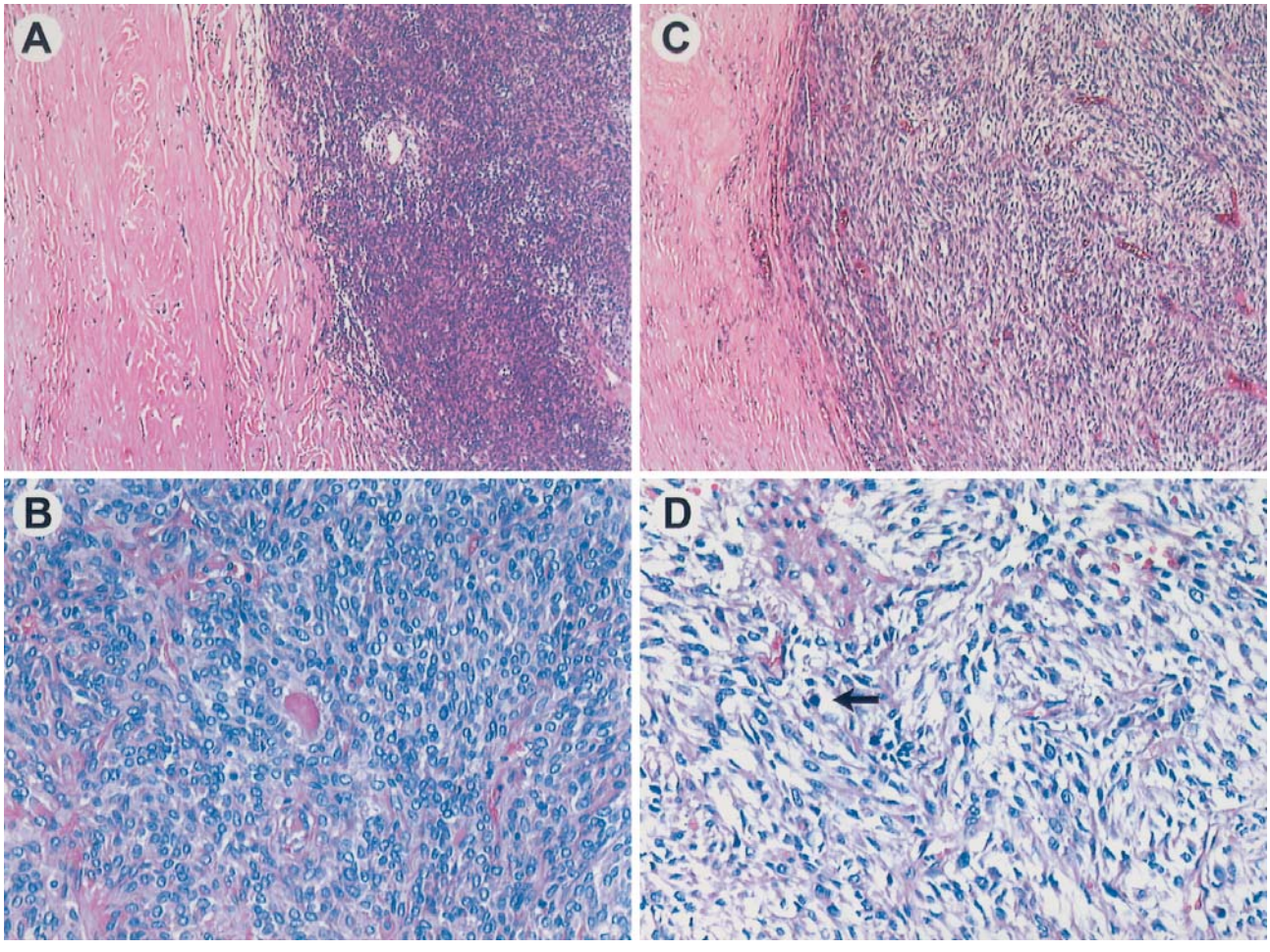



**Fig. 1** Microscopic features of the first resection specimen. The tumor consisted of hypocellular hyalinized tissue alternating with highly cellular areas (**A**, ×50) composed of short spindled cells with mildly pleomorphic nuclei (**B**, ×200). In some cellular areas, the cells were more loosely arranged in a fascicular fashion (**C**, ×50) and exhibited mitotic activity (*arrow*) (**D**, ×200)

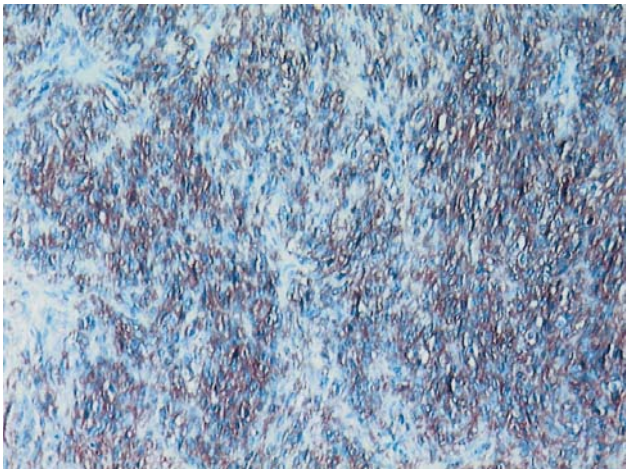


**Fig. 2** CD34 immunostaining of the tumor (immunoperoxidase technique, ×200)

pleura was made. Cytogenetic analysis was performed on 35 Q-banded metaphases. The karyotype was as follows: 48, XY; +8; +8; del(9)(q22; q32) [19] / 46, XY, t(1;16)(q25;p12) [7] / 46, XY [9] (Fig. 3, Fig. 4).

The re-excision specimen consisted of multiple fragments of soft fleshy partly necrotic tumor (in aggregate 40×20×7 cm) and a right pneumectomy. The lung was collapsed and showed multiple pleural-based tumor nodules. Microscopic examination disclosed a cellular tumor with focal hemangiopericytoma-like features composed of medium-sized spindle cells with mildly pleomorphic nuclei in a loose myxoid stroma, with a high mitotic rate (13 mitoses per 10 HPF; Fig. 5). The Ki67 labeling index was around 25%. The tumor was not infiltrating into the lung parenchyma and the hilar lymph nodes were free of tumor. Immunohistochemical findings were similar to those previously described for the primary tumor. Cytogenetic analysis was performed on 27 Q-banded metaphases: a 48, XY, +8, +8, del(9)(q22q32) karyotype was found in 26 cells.

## Discussion

We report here the cytogenetic findings in a malignant SFT of the pleura. Interestingly, successful karyotyping was obtained on two tumor samples taken from the first surgical specimen and from the recurrent tumor. An identical abnormal karyotype characterized by the presence of two additional chromosomes 8 and an interstitial deletion within the long arm of chromosome 9 (del(9)(q22q32)) was detected after culture of both samples. Recurrence of this abnormal karyotype largely supports its relevance to the malignant clone.

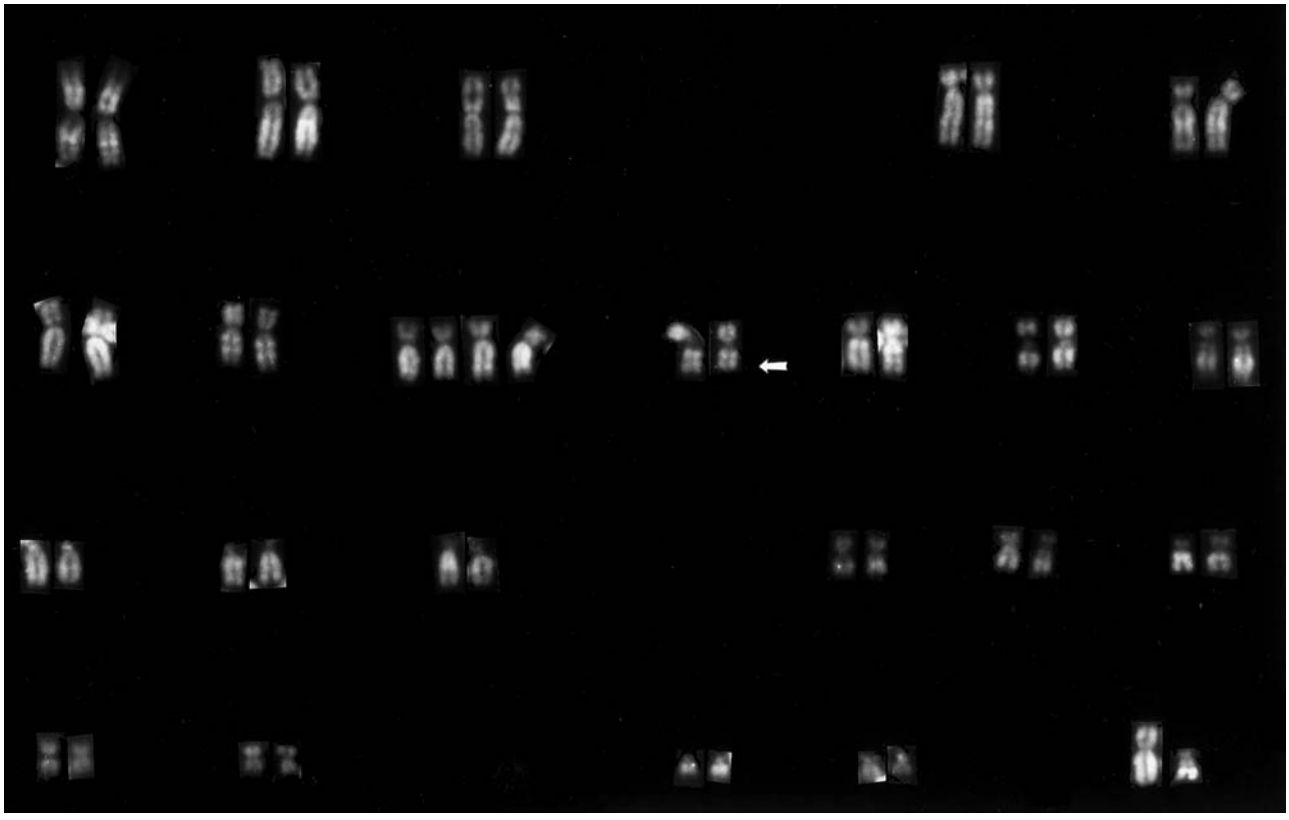


**Fig. 3** Q-banded preparation obtained after culture of the primary tumor. Tetrasomy 8, and interstitial deletion within the long arm of chromosome 9 [(q22q32)] (*arrow*) was observed on the first clone

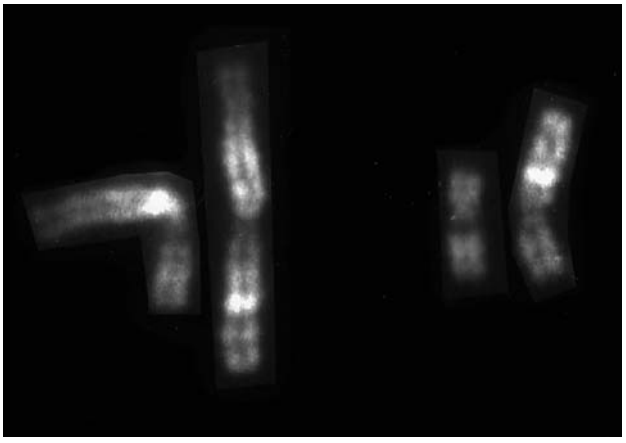


**Fig. 4** Q-banded preparation obtained after culture of the primary tumor. Partial karyotype of the second clone harboring a t(1;16)(q25;p12)

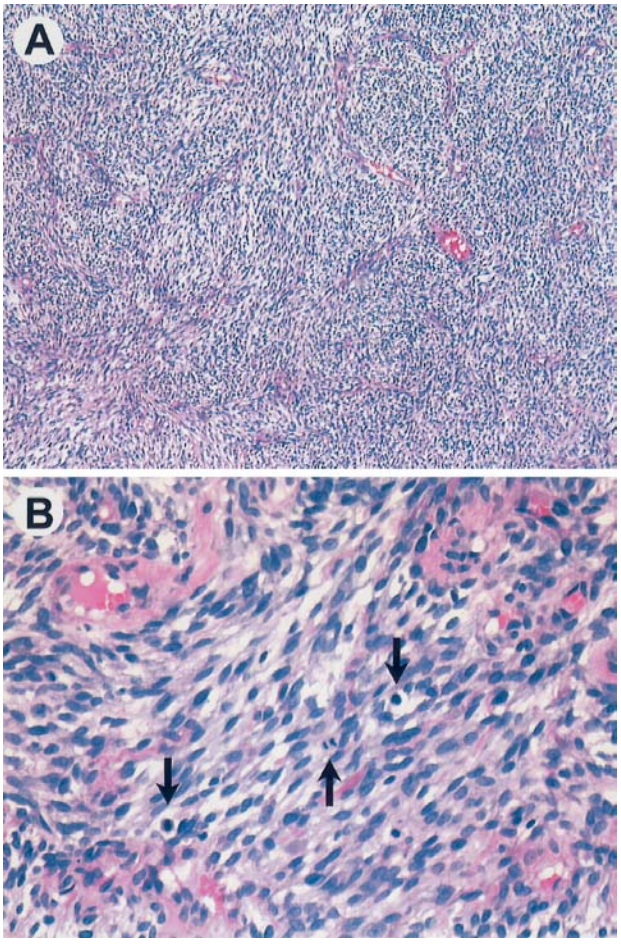



**Fig. 5** Microscopic features of the recurrent tumor. The recurrent tumor was homogeneously cellular, composed of spindle cells arranged in loose fascicles in a somewhat myxoid stroma with abundant vasculature (**A**, ×50) and showed brisk mitotic activity (*arrows*) (**B**, ×200)

Sparse data suggest that gain of chromosome 8 might be associated with tumorigenesis and/or tumor progression of pleural SFT. Trisomy 8 is indeed the only recurrent numerical anomaly reported so far by standard cytogenetics in SFT of the pleura, that has been described as the sole cytogenetic anomaly in two cases [1], but it is unclear from this preliminary report whether this anomaly was associated with benign or malignant variants of SFT. Based on a comparative genomic hybridization (CGH) study, Miettinen et al. found tumor size-related DNA copy number changes in SFT of the pleura. In this study, gain of the entire chromosome 8 was the most common change found alone or in association with other chromosomal gains and/or losses in four of eight tumors larger than 10 cm, suggesting that trisomy 8 might be related to tumor progression [11]. The finding of two additional chromosomes 8 in our tumor, which showed obvious malignant features, supports this hypothesis. However, the relationship between gain of chromosome 8 and tumor size or malignancy was not evident in the other CGH-based analysis of pleural SFT by Krismann et al., who found significant gains of chromosomes 8 and 15q in a subset of tumors but failed to identify any correlation with tumor size [8]. Of interest is that trisomy and/or tetrasomy 8 have also been described in other benign and malignant fibrous tumors (subsets of desmoid tumors and infantile fibrosarcomas) [2, 3, 13].

This is the first report of an interstitial deletion within the long arm of chromosome 9 in SFT of the pleura. In the two CGH-based analyses mentioned earlier, 9q has not been identified as a site of chromosomal loss in SFT of the pleura. Interestingly, in the case reported by Donner et al. [5], band 9q22 was also rearranged by an ins(9;12)(q22;q15;q24.1), raising the possibility that a gene on 9q22 might be relevant to the pathogenesis of SFT.

Mechanisms underlying tumor progression in SFT of the pleura are largely unknown. It has been suggested that malignant SFT may arise de novo or occur as transformation within a benign SFT [14]. In the case reported here, review of the clinical history and previous chest X-ray films clearly indicated accelerated growth in a previously benign slow-growing tumor, and indeed histopathological analysis of the first resection specimen confirmed an admixture of hypocellular benign areas and of highly cellular mitotically active zones. Cytogenetic findings failed to bring support to the “transformation” hypothesis. Instead, the peculiar finding of two distinct abnormal clonal karyotypes in addition to normal mitosis after culture of the first tumor specimen rather suggested two concurrent distinct clonal events. Whereas the clone harboring tetrasomy 8 was clearly associated with a malignant recurring component of the lesion, the significance of the clone harboring the (1;16) translocation remains speculative. It might be hypothesized that this anomaly was related to another malignant component of the tumor, possibly cured by the first surgical resection, or likely associated with the benign component of the tumor, and bearing no relationship to the malignant transforma-

tion. To our knowledge, none of SFT of the pleura, nor any other type of neoplasia was reported to have a similar translocation. Clearly, more cytogenetic data on SFT are needed before any conclusive interpretation of this translocation is possible.

**Acknowledgements** We thank Dr. G.P. Nielsen for critical reading of the manuscript and helpful comments. L.M. Dupuis and M.C. Petit are acknowledged for technical assistance. Laurence de Leval is a Research Associate of the Belgian National Fund for Scientific Research (F.N.R.S.).

## References

1. Berean K, Miller R, Horsman D (1994) Solitary fibrous tumor: cytogenetic analysis (abstract). Modern Pathol 7:149A
2. Dal Cin P, Brock P, Casteels-van Daele M, De Wever I, van Damme R, Van den Berghe H (1991) Cytogenetic characterization of congenital or infantile fibrosarcoma. Eur J Pediatr 150:579–581
3. Dal Cin P, Sciot R, Alys M, Delabie J, Stas M, De Wever I (1994) Some desmoid tumors are characterized by trisomy 8. Genes Chromosom Cancer 10:131–135
4. Dal Cin P, Pauwels P, Van den Berghe H (1999) Solitary fibrous tumor of the pleura with t(4;15)(q13;q26). Histopathology 35:86–95
5. Donner L, Silva M, Dobin S (1999) Solitary fibrous tumor of the pleura: a cytogenetic study. Cancer Genet Cytogenet 111:169–171
6. England D, Hochholzer L, McCarthy M (1989) Localized benign and malignant fibrous tumors of the pleura. Am J Surg Pathol 13:640–658
7. Mitelman S (ed) (1995) ISCN, An international system for human cytogenetic nomenclature. Karger, Basel
8. Krismann M, Adams H, Jaworska M, Müller K, Johnen G (2000) Patterns of chromosomal imbalances in benign solitary fibrous tumours of the pleura. Virchows Arch 437:248–255
9. Limon J, Dal Cin P, Sandberg A (1986) Application of long-term collagenase disaggregation for the cytogenetic analysis of human solid tumors. Cancer Genet Cytogenet 23:305–313
10. Mertens F, Willen R, Lillo-Gil R, Mitelman F, Mandahl N (1996) Translocation (2;3)(p21;p26) as the sole anomaly in a benign localized fibrous mesothelioma. Cancer Genet Cytogenet 92:90–91
11. Miettinen M, El-RIfae W, Sarlomo-Rikala M, Andersson L, Knuutila S (1997) Tumor size-related DNA copy number changes occur in solitary fibrous tumors but not in hemangiopericytomas. Mod Pathol 10:1194–1200
12. Okike N, Bernatz P,Woolner L (1978) Localized mesothelioma of the pleura. Benign and malignant variants. J Thorac Cardiovasc Surg 75:363–370
13. Sandberg A, Bridge J (2002) Updates on the cytogenetics and molecular genetics of bone and soft tissue tumors: congenital (infantile) fibrosarcoma and mesoblastic nephroma. Cancer Genet Cytogenet 132:1–13
14. Yokoi T, Tsuzuki T, Yatabe Y, Suzuki M, Kurumaya H, Koshikawa T, Kuhura H, et al (1998) Solitary fibrous tumour: significance of p53 and CD34 immunoreactivity in its malignant transformation. Histopathology 32:423–432

Virchows Arch (2003) 442:393–399
DOI 10.1007/s00428-003-0798-y

CASE REPORT

**Kazuto Yamazaki**

# Pulmonary well-differentiated fetal adenocarcinoma expressing lineage-specific transcription factors (TTF-1 and GATA-6) to respiratory epithelial differentiation: an immunohistochemical and ultrastructural study

Received: 13 August 2002 / Accepted: 6 March 2003 / Published online: 4 April 2003
© Springer-Verlag 2003

**Abstract** A case of pulmonary well-differentiated fetal adenocarcinoma was examined with conventional histological, immunohistochemical, and ultrastructural studies that revealed the distribution of lineage-specific transcription factors (TTF-1 and GATA-6). The patient was a 33-year-old Japanese woman, who underwent resection of the right lower lobe for the lung tumor. The tumor demonstrated an organized histology mimicking the epithelial differentiation of fetal lung with peculiar glands and moruloid cell nests, without mesenchymal proliferation. Adenocarcinoma cells forming the atypical glands were similar to the epithelial cells of the branching tubules in the pseudo glandular stage of the fetal lung. Distribution of TTF-1 was observed in many of the nuclei of the adenocarcinoma cells forming the glands. Tumor cells in the morula were primitive epithelial cells with some immunohistochemical neuroendocrine cell differentiation and some of them showed GATA-6-positive stains in the nuclei. In the ultrastructural study, adenocarcinoma cells showed little differentiation toward mucous cells and ciliated cells. Neuroendocrine granules were seen in a few tumor cells in the morula. In the present case, tumor cells forming the peculiar histological, molecular, and ultrastructural constructions showed partial and incomplete mimicry of the morphogenesis of respiratory epithelium.

**Keywords** Respiratory epithelial differentiation · Pulmonary blastoma · Morula · Neuroendocrine cell · Surfactant apoprotein A

K. Yamazaki (✉)
Department of Pathology,
Saiseikai Central Hospital,
1-4-17 Mita, Minatoku, 108-0073 Tokyo, Japan
e-mail: KazutoYamazaki@aol.com
Tel.: +81-3-34518211
Fax: +81-3-34516102

## Introduction

Pulmonary well-differentiated fetal adenocarcinoma is a rare malignant neoplasm that histologically resembles airway structures seen in the early phase of fetal lung development [2]. Some synonymous diagnostic names have been reported in the literature since the early introduction of Kradin et al. [6] and Kodama et al. [4], such as pulmonary endodermal tumor resembling fetal lung [9, 11, 12, 15], pulmonary adenocarcinoma of the fetal type [10, 13] and pulmonary blastoma lacking sarcomatous elements [2].

The lesion could be distinguished from pulmonary blastoma, which exhibits biphasic epithelial and stromal patterns [2, 3]. The tumor cells were reported to contain numerous complex, branching tubules resembling the developing fetal lung in its canalicular stage. Some of the epithelial cells were shown to have a neurosecretory-type differentiation [3, 4, 6, 9]. The particular histological feature of this adenocarcinoma is its presence in the morula area [12, 13]. Some reports have pointed out the existence of tumor cells similar to a common endodermal stem cell for the different types of epithelial cells within the lung [10].

Recently lineage-specific transcription factors to respiratory epithelial differentiation, such as thyroid transcription factor-1 (TTF-1) and GATA-6, have been attracting attention [1, 5, 14]. It is becoming clear that many of the key factors determining the process of branching morphogenesis, particularly of the respiratory organs, are highly conserved through evolution [14]. GATA-6 is one of the transcription factors conserving the zinc finger DNA-binding domain and found in the developing lung [1, 5, 14]. However, TTF-1 is a 38-kDa protein that is required for organogenesis and for maintaining the differentiated phenotypes of various tissue types including lung [17]. In the lung, TTF-1 expression is highest in bronchial and alveolar epithelial cells, where it mediates surfactant homeostasis by regu-

lating the expression of the lung epithelial markers, surfactant proteins A and B [2, 17]. In lung organogenesis, TTF-1 is a lineage or tissue-specific marker for peripheral airway epithelium or the terminal respiratory unit [7, 16]. Recently, GATA-6 and TTF-1 have been reported to directly interact or regulate surfactant protein-C gene expression [8].

We herein report on a rare case of typical pulmonary well-differentiated fetal adenocarcinoma with conventional histological, immunohistochemical, and ultrastructural studies that revealed the distribution of lineage-specific transcription factors (TTF-1 and GATA-6).

## Clinical history

The patient was a 33-year-old Japanese woman who complained of right back pain and hemosputum that had persisted for 3 months. She visited a hospital where an X-ray examination revealed an abnormal shadow in the right side of the chest. Transbronchial biopsy was carried out and a histopathological diagnosis of adenocarcinoma was made. When her right back pain gradually increased, she visited our hospital hoping for resection surgery. The patient was a non-smoker with no particular findings in her history. After the clinical evaluation of her tumor stage as c-T3N0M0, right lower lobe resection and the resection of associated lymph node were performed. On gross examination of the excised material from the patient's lung, no lymph-node metastasis was observed.

## Materials and methods

### Light microscopy and immunohistochemistry

The excised specimen was fixed in 15% formalin, embedded in paraffin wax, sectioned, and stained with hematoxylin and eosin (H&E). For immunohistochemistry, the antigens of pankeratin (AE1/AE3), epithelial membrane antigen (EMA), neuron-specific enolase (NSE), secretory component (SC), surfactant apoprotein A (SAP), CD56, somatostatin, synaptophysin (SP), chromogranin A (CG), carcinogenic embryonic antigen (CEA), alpha smooth muscle actin, muscle actin (HHF35), TTF-1 (mouse monoclonal antibody, ×200 for use, Dako, Denmark), and GATA-6 (goat polyclonal antibody, ×100 for use, Santa Cruz Biotechnology, Inc. CA, USA) were examined using an indirect streptavidin-biotin method (LSAB2 kit, Dako, Denmark). Immunostaining was done with or without antigen-retrieval techniques. Further immunonohistochemical investigations have similarly been done in order to find out whether surfactant protein B, (pro) surfactant protein C, as well as Clara cell protein CC10 were in the tumor tissue. Namely, using commercially available antibodies of CC10 (Santa Cruz Biotechnology), anti-surfactant protein B (SPB) (Chemicon International, CA, USA) and anti-human prosurfactant protein C (proSPC) (Research Diagnostics, Inc., NJ, USA), the tumor tissue and surrounding non-tumoral lung tissue were immunohistochemically examined.

### Electron microscopy

Small samples of tumor tissue were fixed in phosphate-buffered 2.5% glutaraldehyde, processed conventionally and embedded in epoxy resin. Ultrathin sections were stained with uranyl acetate and lead citrate, and examined under a JEOL-1200 EXII electron microscope.

## Results

### Macroscopic findings

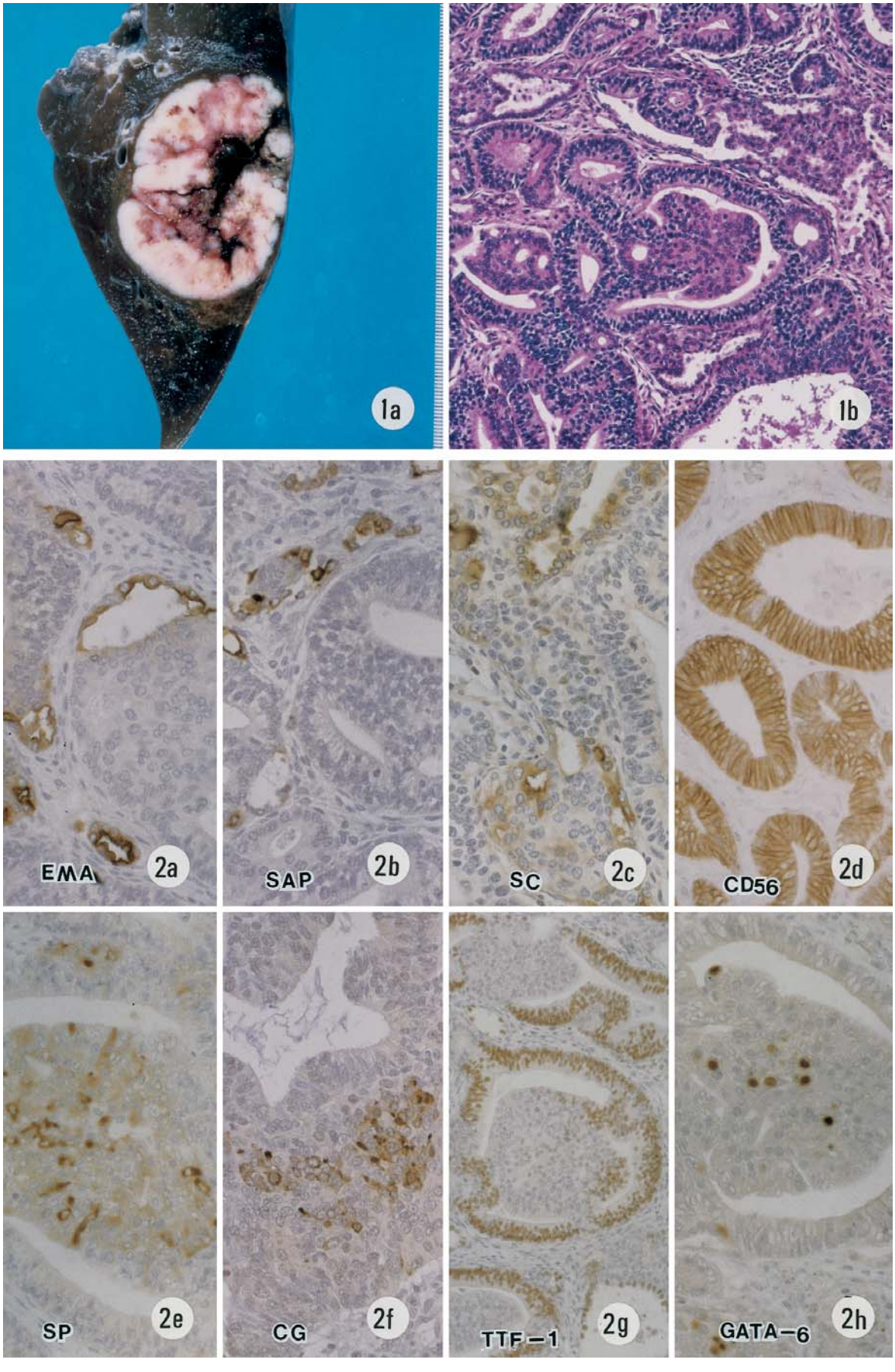
A peripherally located tumor measuring approximately 7×5×5 cm was observed in the excised lung tissue. The tumor was well demarcated and lacked evidence of either pleural indentation or pleural adhesion. The cut surface revealed a white yellow solid mass (Fig. 1a) with no cavity formation. At the center of the tumor some hemorrhage was observed.

### Conventional light microscopic findings

The tumor histology demonstrated irregular medium to large-sized glands, consisting of tall columnar epithelial tumor cells with oval and pseudostratified nuclei and chromatin condensation (Fig. 1b). The atypical glands looked like endometrial glands in the proliferative phase. The tumor cells sometimes showed the glycogen rich clear cytoplasm and perinuclear cytoplasmic vacuoles. Mitotic activity and necrosis were also occasionally seen. At the marginal area of the irregular glands, some morula of solid tumor cell nests were frequently formed (Fig. 1b). In these areas, the tumor cells consisted of medium-sized polyhedral or oval cells, with a slightly eosinophilic cytoplasm and rounded nuclei. Optically clear nuclei were occasionally seen. Between the endometrioid-like tumor glands, compressed irregular glands were sometimes seen. These glands were not lined with tall columnar endometrioid glandular epithelial cells but rather flattened epithelial cells (Fig. 1b). In the stroma of the tumor tissue, inconspicuous spindle-shaped cells with sparse myxomatous stroma were seen. Neither striated muscle nor cartilaginous components were observed. In the surrounding healthy lung tissue, slight obstructive pneumonia was seen. Slight vascular invasion by the cancer cells was noted. No metastatic tumor cells were seen in the 16 resected lymph nodes. A histopathological diagnosis of well-differentiated fetal adenocarcinoma of the lung was made (Fig. 1b).

**Fig. 1 a** Gross appearance of the excised tumor. **b** Tumor tissue at medium magnification. Well-differentiated adenocarcinoma, forming irregular glands. Photomicrograph, H&E stain. ×125

**Fig. 2** Light microscopic and immunohistochemical observations of the tumor tissue. **a** Tumor tissue at medium magnification. Well-differentiated adenocarcinoma, forming irregular glands. EMA immunostains, ×250. **b** Surfactant apoprotein A (SAP) immunostain, ×250. **c** Secretory component (SC) immunostain, ×250. **d** CD56 immunostain, ×250. **e** Synaptophysin (SP) immunostain, ×250. **f** Chromogranin A (CG) immunostain. ×250. **g** Fetal lung epithelial differentiation specific transcription factor, TTF-1 immunostain, ×125. **h** Fetal lung epithelial differentiation specific transcription factor, GATA-6 immunostain, ×250


1a
1b
EMA
2a
SAP
2b
SC
2c
CD56
2d
SP
2e
CG
2f
TTF−1
2g
GATA−6
2h

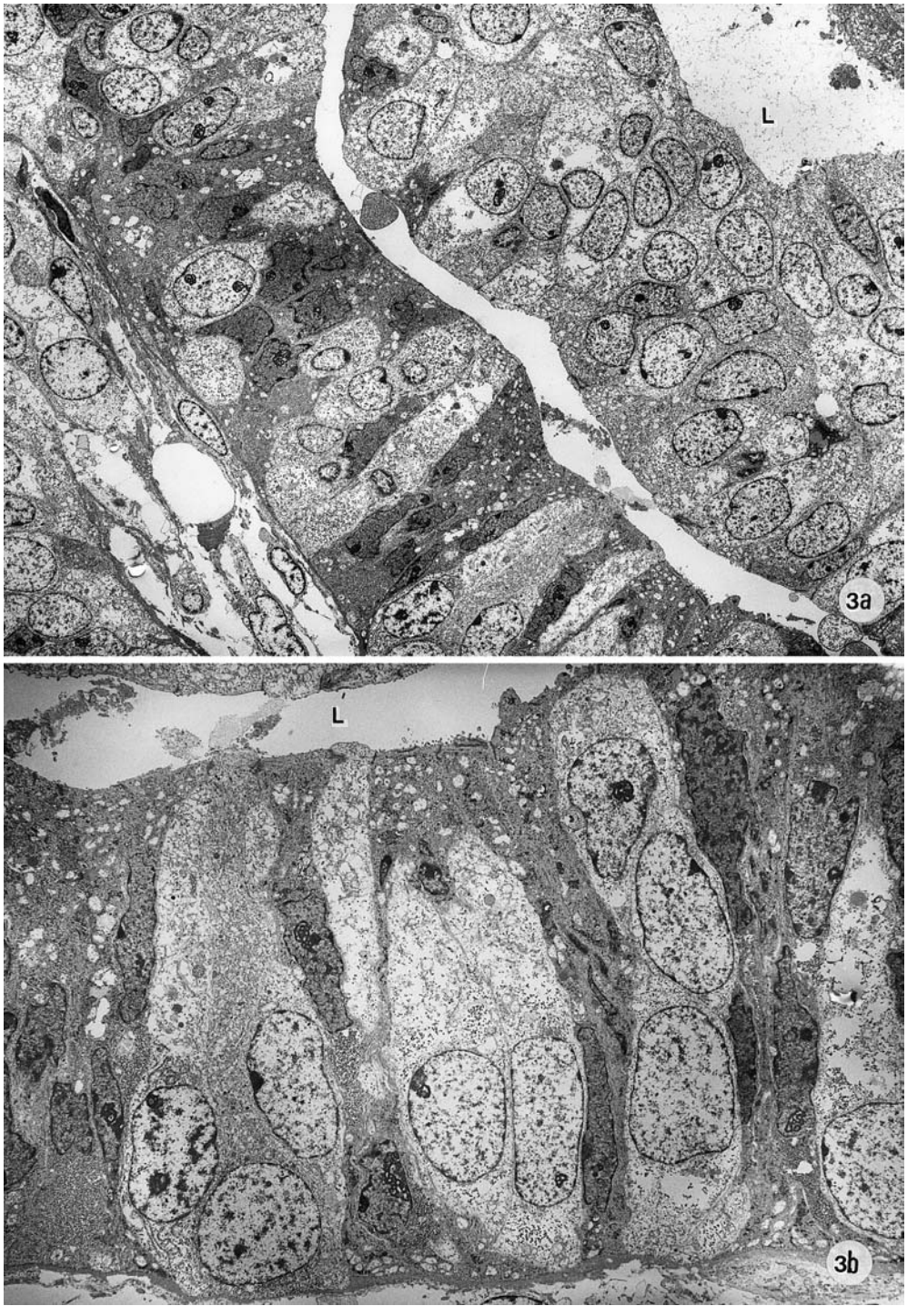
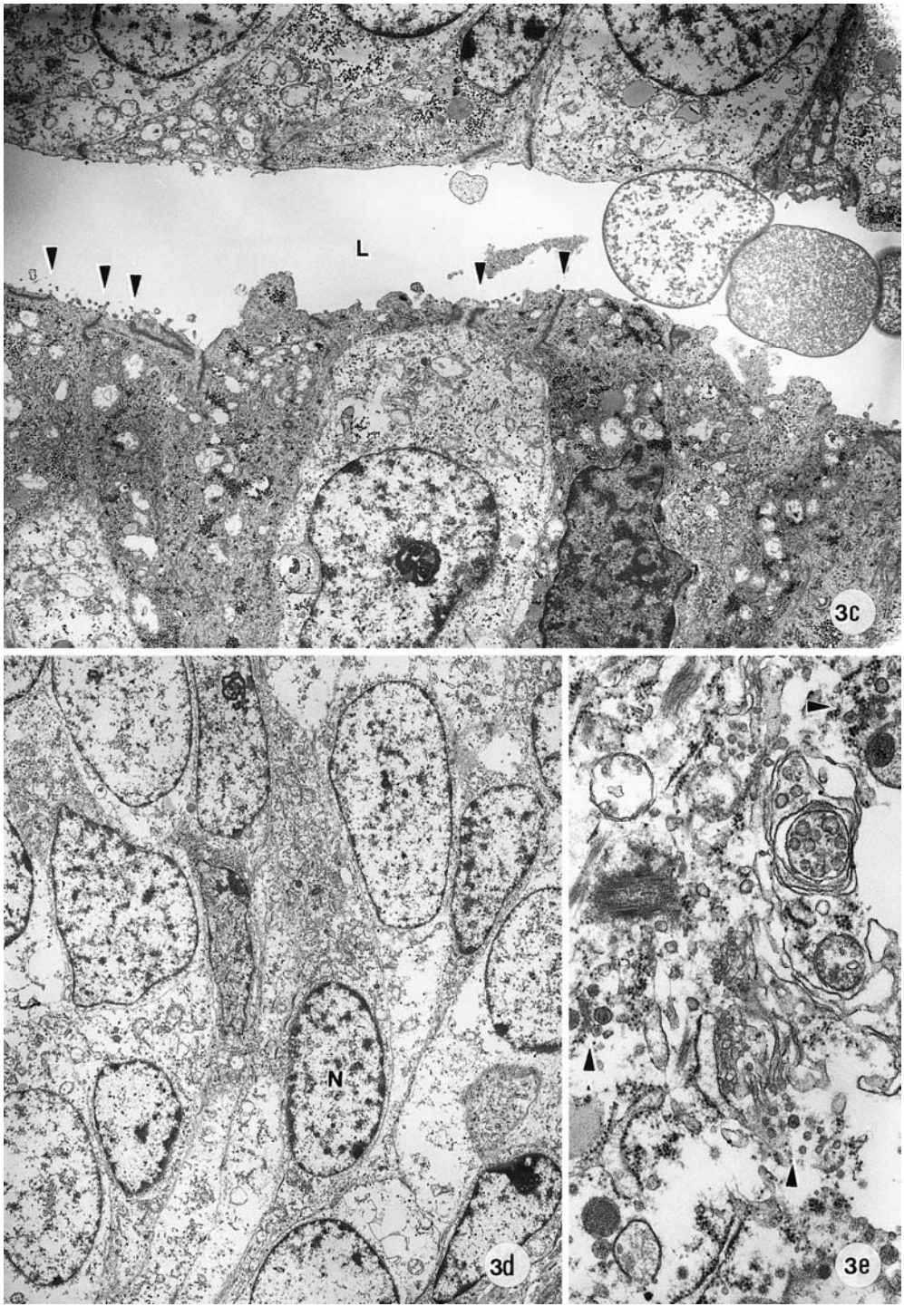



**Fig. 3** Transmission electron micrographs of adenocarcinoma cells and morula. **a** Low power view of the tumor tissue. Adenocarcinoma cells form a glandular structure (*lower left*). In the lumen (*L*), small aggregates of undifferentiated cells form the morula (upper right), ×1800. **b** Transmission electron micrographs of adenocarcinoma cells forming an atypical gland. Adenocarcinoma cells form the lumen (*L*) in the upper side of the figure; basal lamina at their base, ×3600. **c** High-power view of the apical portion of the adenocarcinoma cells. Junctional complex and apical microvilli are well developed (*arrowheads*). In the apical portion of the cytoplasm, mucin-secreting granules are inconspicuous but a few medium-sized granules are seen. Lumen (center: *L*), ×7200. **d** Nodular aggregates of morula cells having small solid pattern and rather opaque cytoplasmic density. A few tumor cells with neuroendocrine cell differentiation (*N*) ×4500. **e** Higher power view of the cytoplasm of the moruloid cell in **d** (*N*) with some small aggregates of neurosecretory-type granules (*arrowheads*), ×36,000

Light microscopic immunohistochemical findings

The immunohistochemical study revealed endometrioid-like tumor glands, irregular glands surfaced with compressed epithelial cells, and morula cell nests showing a slightly different staining pattern. The glands and morula cells nests both stained strongly positive for the antigen of pankeratin(AE1/AE3). EMA, SAP, and SC showed a similar staining pattern (Fig. 2a–c). The luminal surface of the compressed irregular glands between the endometrioid-like tumor glands also stained positive. The stained cells forming the compressed glands were not tall columnar cells but were rather flattened, somewhat similar to type-II pneumocytes or Clara cells. A small number of tumor cells forming the atypical glands stained positively for somatostatin. Some tall adenocarcinoma cells in the atypical glands stained positively for CD56 (Fig. 2d). The cytoplasm of some tumor cells in the

**Fig. 3 c–e**




morula stained positively for the antibodies against NSE, SP and CG (Fig. 2e, f). A small number of the epithelial tumor cells in the glands stained positively for CEA. Further immunonohistochemical investigations have been done in order to find out whether SPB, (pro) surfactant protein C (SPC), as well as Clara cell protein CC10 were in the tumor tissue. Few positive stains were seen by anti-human proSPC. A few positive immunostains of Clara cell protein CC10 were found in some cells in the morula cells nests and tumor glands. Many flattened cells forming the compressed irregular glands between endometrioid-like tumor glands were stained positively by anti-surfactant protein B antibody. Positive stains in tall adenocarcinoma cells were inconspicuous by these three antibodies. Some stromal cells in the tumor stroma stained positively for the anti-alpha smooth muscle actin and anti-muscle actin (HHF35) antibodies. A unique staining pattern was observed in the TTF-1 and GATA-6

staining (Fig. 2g, h). Distribution of TTF-1 was observed in many of the nuclei of the adenocarcinoma cells forming the glands (Fig. 2g). TTF-1 was also positive in cells forming the flattened glands (Fig. 2g). The nuclei of some tumor cells in the morula stained positively for the antibody against GATA-6 (Fig. 2h). Positive staining for both TTF-1 and GATA-6 was hardly seen in the mesenchymal cells.

### Electron microscopic findings

In the transmission electron microscopic study, adenocarcinoma cells and moruloid cells were discerned (Fig. 3a). When viewed under low magnification, adenocarcinoma cells in the tumor tissue formed dilated tubular atypical glands. Adenocarcinoma cells consisted of two cell types with either a dark or clear cytoplasm. The cytoplasm of the latter cell type was rich in glycogen, most of which was washed away during the tissue processing. Adenocarcinoma cells were similar to the epithelial cells of the branching tubules in the pseudo-glandular stage of the fetal lung (Fig. 3a, b). They showed little differentiation toward mucous or ciliated cells, but showed lamina at their base (Fig. 3b, c). Adenocarcinoma cells formed lumina with well-developed junctional complexes and apical microvilli (Fig. 3c). In the apical portion of the cytoplasm, mucin secreting granules were inconspicuous, although some medium-sized granules and dense core granules were seen (Fig. 3c). Formation of cilia was lacking. Poor microvillous specialization was observed.

Nodular aggregates of morula cells had small solid pattern and rather opaque cytoplasmic density. Small aggregates of undifferentiated cells with rather clear cytoplasm and scarce organella forming the morula-like structure (Fig. 3a, d). A few tumor cells in the morula cell masses possessed the characteristics of neuroendocrine cells (Fig. 3a, d, e). Figure 3e shows the cytoplasm of morula cells at a higher magnification with some small aggregates of neurosecretory-type granules. At the surface area of the morula, tumor cells could be seen with some differentiation similar to adenocarcinoma cells with apical and granular differentiation (Fig. 3a, c).

## Discussion

In the present case of pulmonary well-differentiated fetal adenocarcinoma, tumor cells were heterogeneous but organized mimicking, to some extent, the epithelial differentiation of the fetal lung [2, 3, 4, 6, 9, 10, 11, 12, 13, 15]. Adenocarcinoma cells forming the dilated atypical glands were similar to the epithelial cells of the branching tubules in the pseudo-glandular stage of the fetal lung. These adenocarcinoma cells were positive for CD 56 as described in some reports [3], but neuroendocrine differentiation was inconspicuous. Tumor cells in the morula were rather primitive epithelial cells, but some neuroendocrine cell differentiation was evident [3, 4, 6, 9]. In the tumor tissue, between the adenocarcinoma glands, some medium-sized compressed lumina could be observed, covered by a rather flattened type of epithelial cells expressing EMA, SAP, and SC. Those cells might be more differentiated cells similar to type-II pneumocytes lining the alveoli or Clara type cells [1, 17].

In the lung, specific transcription factors, such as TTF-1 and GATA-6, might be assumed to be putative "master genes" or important regulatory genes for respiratory epithelial differentiation, and have recently been attracting attention [2, 5, 14, 17]. GATA-6 is reported to have possibly important roles in vascular smooth muscle cell differentiation, terminal differentiation of the pulmonary epithelium, and their gene expression, at least in part interacting with the expression of TTF-1 and its potential target gene of surfactant protein [2, 5, 14]. In the most recent literature, GATA-6 and TTF-1 were reported to directly interact and regulate SPC gene expression [8]. Analysis of the transcriptional factors binding the promoters of lung-specific genes, such as SPA, SPB and SPC, is providing some important clues as to how expression of these lung-specific genes is regulated in time and space during physiological fetal development. Transcriptional factors of TTF-1 and GATA-6 play key roles at this level [2, 17]. In the present tumor tissue, TTF-1 and GATA-6 staining produced a unique pattern correlating to other immunohistochemical markers, such as EMA, SAP, SC, CD 56, CG, and SP. Distribution of TTF-1 was observed in many of the nuclei of the adenocarcinoma cells forming the glands, which were occasionally positive for CD56, but stained very sparsely for EMA, SAP, SC, CG, and SP. TTF-1 was additionally positive in the flattened gland-forming cells [5], which were also positive for EMA, SAP, and SC. Several times it has been mentioned that TTF-1 is involved in the regulation of the surfactant proteins, mainly in the regulation of SPC [2, 5, 8, 17]. Until now, it has not been completely clear whether in pulmonary adenocarcinomas the phenotypes of type-II and Clara cells can be found. Although only a case report is given in the present article, additional immunonohistochemical investigations have been done to find out whether SPB, proSPC, as well as Clara cell protein CC10 are in the tumor tissue. Few positive stains were seen by anti-human proSPC. A few positive immunostains of Clara cell protein CC10 were found in some cells in the morula cell nest tumor glands. Many flattened cells forming the compressed irregular glands between endometrioid-like tumor glands stained positively by anti-SPB antibody. Positive stains in tall adenocarcinoma cells were inconspicuous by these three antibodies. Tumor cells in the morula were primitive epithelial cells with some immunohistochemical neuroendocrine cell differentiation, the nuclei of some of which stained positive for GATA-6. Expression of each of the transcriptional regulatory molecules might be intimately relating to the morphological and immunohistochemical diverse differentiation of epithelial neoplastic cells in the present case.

The transmission electron microscopic study revealed both adenocarcinoma and moruloid cells. Adenocarcinoma cells were similar to the epithelial cells of the branching tubules in the pseudo-glandular stage of the fetal lung [4, 10]. They showed little differentiation toward mucous cells and ciliated cells [4]. A few tumor cells in the morula, which were mainly of undifferentiated type cells, possessed the characteristics of neuroendocrine cells, with neurosecretory-type granules [6, 12].

In the present case of pulmonary well-differentiated fetal adenocarcinoma, cancer cells formed histological and ultrastructural constructions while expressing various immunohistochemical markers, including lineage-specific transcription factors, such as TTF-1 and GATA-6, partially and incompletely simulating the morphogenesis of fetal lung epithelial morphogenesis. It might be useful to use these transcriptional factors as markers for cellular differentiation of these cancer cells [7, 16].

**Acknowledgements** Authors would like to acknowledge T. Nagai and K. Fujita for their electron microscopic technical assistance and Drs. K. Matsuoka, T. Aoki, H. Kodama, and H. Nomori for their valuable discussions.

## References

1. Bruno MD, Korfhagen TR, Liu C, et al (2000) GATA-6 activates transcription of surfactant protein A. J Biol Chem 275:1043–1049
2. Colby TV, Koss MN, Travis WD (1995) 21 mixed epithelial and mesenchymal tumors. Tumors of the lower respiratory tract. Armed Forces Institute of Pathology, Washington, DC, pp 395–417
3. Inoue H, Kasai K, Shinda J, et al (1992) Pulmonary blastoma. Comparison between its epithelial components and fetal bronchial epithelium. Acta Pathol Jpn 42:884–892
4. Kodama T, Shimosato Y, Watanabe S, et al (1984) Six cases of well-differentiated adenocarcinoma simulating fetal lung tubules in pseudoglandular stage. Comparison with pulmonary blastoma. Am J Surg Pathol 8:735–744
5. Koutsourakis M, Keijizer R, Visser P, et al (2001) Branching and differentiation defects in pulmonary epithelium with elevated Gata6 expression. Mech Dev 105:105–114
6. Kradin RL, Young RH, Dickersin GR, et al (1982) Pulmonary blastoma with argyrophil cells and lacking sarcomatous feature (pulmonary endodermal tumor resembling fetal lung). Am J Surg Pathol 6:165–172
7. Lau S, Luthringer DJ, Eisen RN (2002) Thyroid transcription factor-1: a review. Appl Immunohistochem Mol Morphol 10:97–102
8. Liu C, Glasser SW, Wan H, et al (2002) GATA-6 and thyroid transcription factor-1 directly interact and regulate surfactant protein-C gene expression. J Biol Chem 277:4519–4525
9. Manning JT Jr., Ordonez NG, Rosenberg HS, et al (1985) Pulmonary endodermal tumor resembling fetal lung. Report of a case with immunohistochemical studies. Arch Pathol Lab Med 109:48–50
10. Muller-Hermelink H, Kaiserling E (1986) Pulmonary adenocarcinoma of fetal type: alternating differentiation argues in favour of a common endodermal stem cell. Virchows Arch 409:195–210
11. Nakatani Y, Dickersin GR, Mark EJ (1990) Pulmonary endodermal tumor resembling fetal lung: a clinicopathologic study of five cases with immunohistochemical and ultrastructural characterization. Hum Pathol 21:1097–1107
12. Nakatani Y, Kitamura H, InayamaY, et al (1994) Pulmonary endodermal tumor resembling fetal lung. The optically clear nucleus is rich in biotin. Am J Surg Pathol 18:637–642
13. Nakatani Y, Kitamura H, Inayama Y, et al (1998) Pulmonary adenocarcinoma of fetal lung type: a clinicopathologic study indicating differences in histology, epidemiology, and natural history of low-grade and high-grade forms. Am J Surg Pathol 22:399–411
14. Shaw-White JR, Bruno MD, Whitsett JA (1999) GATA-6 activates transcription of thyroid transcription factor-1. J Biol Chem 274:2658–2664
15. Singh SP, Besner GE, Schauer GM (1997) Pulmonary endodermal tumor resembling fetal lung: report of a case in a 14-year-old girl. Pediatr Pathol Lab Med 17:951–958
16. Yatabe Y, Mitsudomi T, Takahashi T (2002). TTF-1 expression in pulmonary adenocarcinoma. Am J Surg Pathol 26:767–773
17. Warburton D, Schwarz M, Tefft D, et al (2000) The molecular basis of lung morphogenesis. Mech Dev 92:55–81

Virchows Arch (2003) 442:400–406
DOI 10.1007/s00428-003-0765-7

CASE REPORT

**Koichi Kawasaki · Takui Ito · Toshiaki Tsuchiya · Hitoshi Takahashi**

# Is angiomatosis an intrinsic pathohistological feature of massive osteolysis? Report of an autopsy case and a review of the literature

Received: 18 September 2002 / Accepted: 17 December 2002 / Published online: 26 March 2003
© Springer-Verlag 2003

**Abstract** We report here an autopsied patient who had died during the clinical course of massive osteolysis (MO), which is a rare chronic disease that begins insidiously and is characterized by progressive regional loss of bone. Since the original description by Gorham and Stout in 1955, vascular proliferation, e.g., hemangiomatosis, has been considered to be the characteristic feature related to the pathogenesis. However, no such vascular changes were observed in the present patient. It was also important to note that a significant number of cases of MO that showed no vascular proliferation have been described previously. Therefore, we consider that vascular proliferation is not always associated with the osteolysis in MO and that the increased vascularity, if any, may be one of the results of the disease rather than the cause.

**Keywords** Gorham's disease · Osteolysis · Skull · Autopsy · Angiomatosis · Pathogenesis

K. Kawasaki
Department of Neurosurgery and Pathology,
Brain Research Institute, Niigata University,
1 Asahimachi Niigata, 951-8585 Japan

T. Ito
Department of Orthopaedic Surgery,
Niigata University School of Medicine,
1 Asahimachi Niigata, 951-8585 Japan

T. Tsuchiya
Department of Internal Medicine,
National Nishi-Niigata Central Hospital,
1-14-1 Masago Niigata, 950-2085 Japan

H. Takahashi (✉)
Department of Pathology,
Brain Research Institute, Niigata University,
1 Asahimachi Niigata, 951-8585 Japan
e-mail: hitoshi@bri.niigata-u.ac.jp
Tel.: +81-25-2270633
Fax: +81-25-2270817

## Introduction

Massive osteolysis (MO) is a rare chronic disease that begins insidiously and is characterized by progressive regional loss of bone with resulting deformity [16]. The osteolysis is initially localized to one bone, and then frequently extends to multiple bones; joints and intervertebral disks pose no barriers to extension of the disease. Other bones in affected patients may appear perfectly normal [10, 11, 20, 23]. Spontaneous arrest of the osteolysis may sometimes occur [20]. Radiologically, the process is characterized by the disappearance of one or multiple adjacent bones, regardless of interposing joint spaces [20].

The microscopic features of MO were described originally by Gorham and Stout [10]. Subsequently, despite variations in histological appearance, vascular proliferation is now considered to be the most prominent and characteristic feature of the disease. We recently autopsied a patient who had died during the clinical course of MO and found no apparent proliferative vascular changes in any of the lesions. Here, we report the histopathological findings and discuss the significance of vascular proliferation in relation to the pathogenesis of MO.

## Clinical history

The patient, a woman, was 44 years old at the time of death. She had been healthy until the age of 29 years, when she first noticed increasing hollowness in the region of the occipital bone. As the affected area became painful and gradually increased in size, she visited a local hospital and subsequently underwent craniotomy and cranioplasty. However, the histological diagnosis of her illness was not established. At the age of 34 years, hoarseness and swallowing disturbance appeared, and radiation therapy (total, 31 Gy) was performed for an osteolytic lesion at the skull base. At the age of 35 years, further irradiation of the skull base (total, 28 Gy) was tried, but the osteolytic lesion expanded further. At the age of 36 years (Fig. 1A), posterior cranio-vertebral fixation, tracheotomy and gastrostomy were performed because of postural instability of the neck and associated dyspnea and dysphagia. At the age of 37 years, a biopsy specimen from the temporal bone showed edematous bone marrow tissue with osteolysis. Although no definite histopathological diagnosis was made, MO was suspected from the progressive clinical

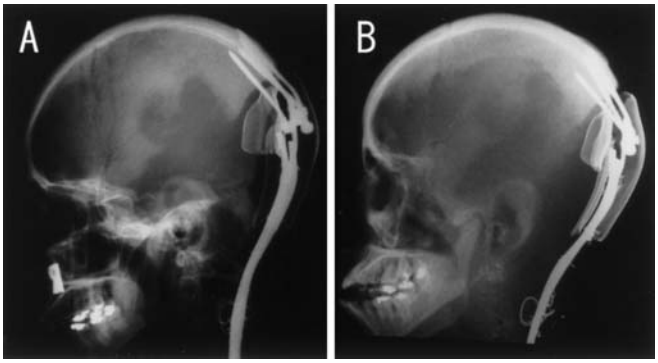



**Fig. 1** Lateral-view craniograms taken at 36 years (**A**) and 43 years (**B**), demonstrating progressive osteolysis

course and radiographic findings. The patient became deaf and dumb, and the osteolysis subsequently progressed to the left temporal bone. At the age of 42 years, left facial palsy appeared, and at the age of 43 years (Fig. 1B), she lost her left eyesight. At the age of 44 years, the osteolysis spread further over the facial, mandibular and vertebral bones. Because of increasing pain and neck instability, she became bedridden and eventually also lost her right eyesight. The patient died about 15 years after onset of the disease: a tracheal cannula was found to be out of place, and she was suspected to have committed suicide.

During the course of her illness, the results of laboratory tests – including blood, urine and cerebrospinal fluid examinations – were unremarkable. No history of trauma was recorded, and there was no family history of bone or kidney disorders.

## Materials and methods

Tissues removed at autopsy were fixed with 4% paraformaldehyde in 0.1 M phosphate buffer and embedded in paraffin. Sections, 4 μm thick, were stained with hematoxylin-eosin (H-E), azan-Mallory and silver impregnation for reticulin. For nervous tissue, Klüver-Barrera stain was also used.

The sections were also immunostained using the avidin-biotin-peroxidase complex method (ABC) with a Vectastain ABC kit (Vector, Burlingame, CA). The antibodies used were: mouse monoclonal antibodies against vimentin (Dakopatts, Denmark; diluted 1:100), CD-68 (Dakopatts; diluted 1:100), and rabbit polyclonal antibodies against factor VIII (Dakopatts; diluted 1:500). The primary incubations were carried out overnight at 4°C.

For electron microscopy, pieces of tissue from the osteolytic lesions were post-fixed in 1% osmium tetroxide, dehydrated through a graded ethanol series and embedded in Epon 812. Ultrathin sections were cut, stained with uranyl acetate and lead citrate, and examined with a Hitachi H-7100 electron microscope.

## Results

At autopsy, depressed deformities at the forehead, cheek and jaw were confirmed (Fig. 2A). The calvaria covering a large part of the left cerebral hemisphere (Fig. 2B, C), the bones forming the skull base except for the frontal and orbital bones, and the C1 and C2 vertebral bones showed a rubbery consistency and were easily deformed. Histologically, these affected bones had been completely replaced by fibrous tissues consisting of spindle-shaped fibroblastic cells of low cellularity in a loose collagenous background (Fig. 3A, B). These spindle-shaped cells were shown to be immunoreactive for vimentin. Other inter-

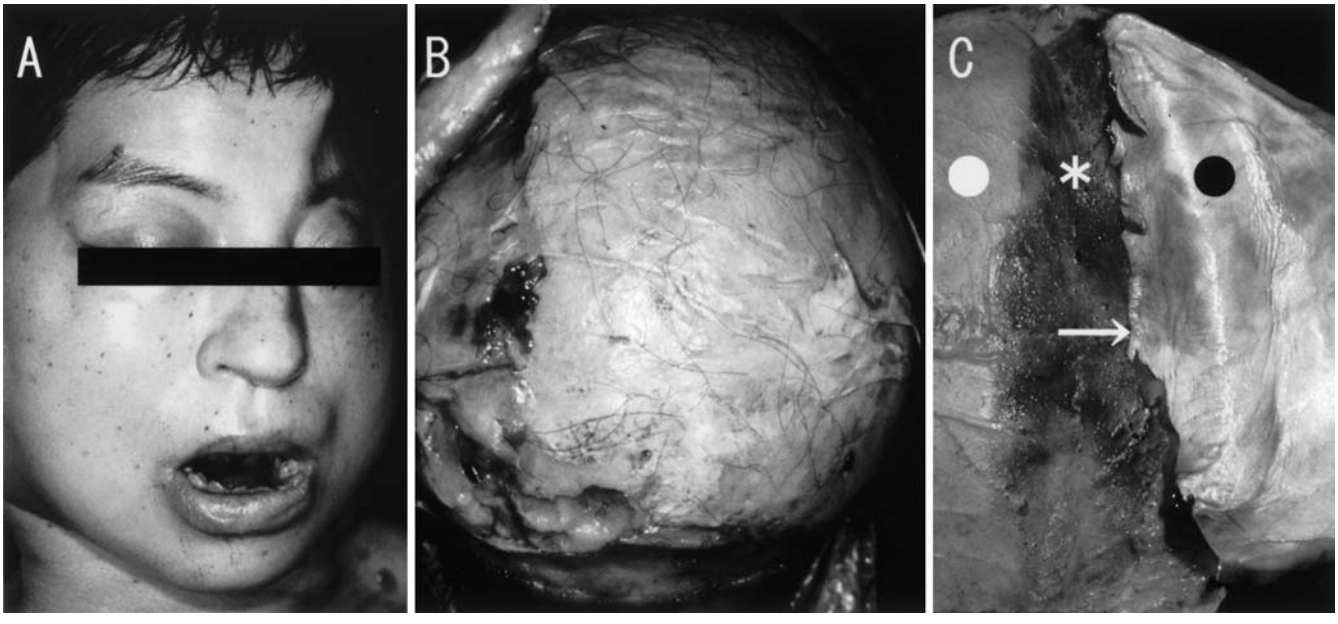



**Fig. 2** Photographs of the patient at autopsy. **A** Deformation of the face due to depressions of the forehead, cheek and jaw. **B** Convexity view of the calvaria. The *left side* is depressed, and replaced by fibrous tissue with a rubbery consistency. **C** Inside view of the calvaria. The dura mater tightly adhered to the inner surface of the calvaria that replaced by fibrous tissue with rubbery consistency (*black closed circle*) and was easily detached from the remainder (*white closed circle* and *asterisk*). *Arrow* indicates the cut edge of the dura mater. In the bone with normal appearance and consistency (*white closed circle*), sulci of the middle meningeal artery are clearly observed. The transitional area (*asterisk*) shows reddish discoloration

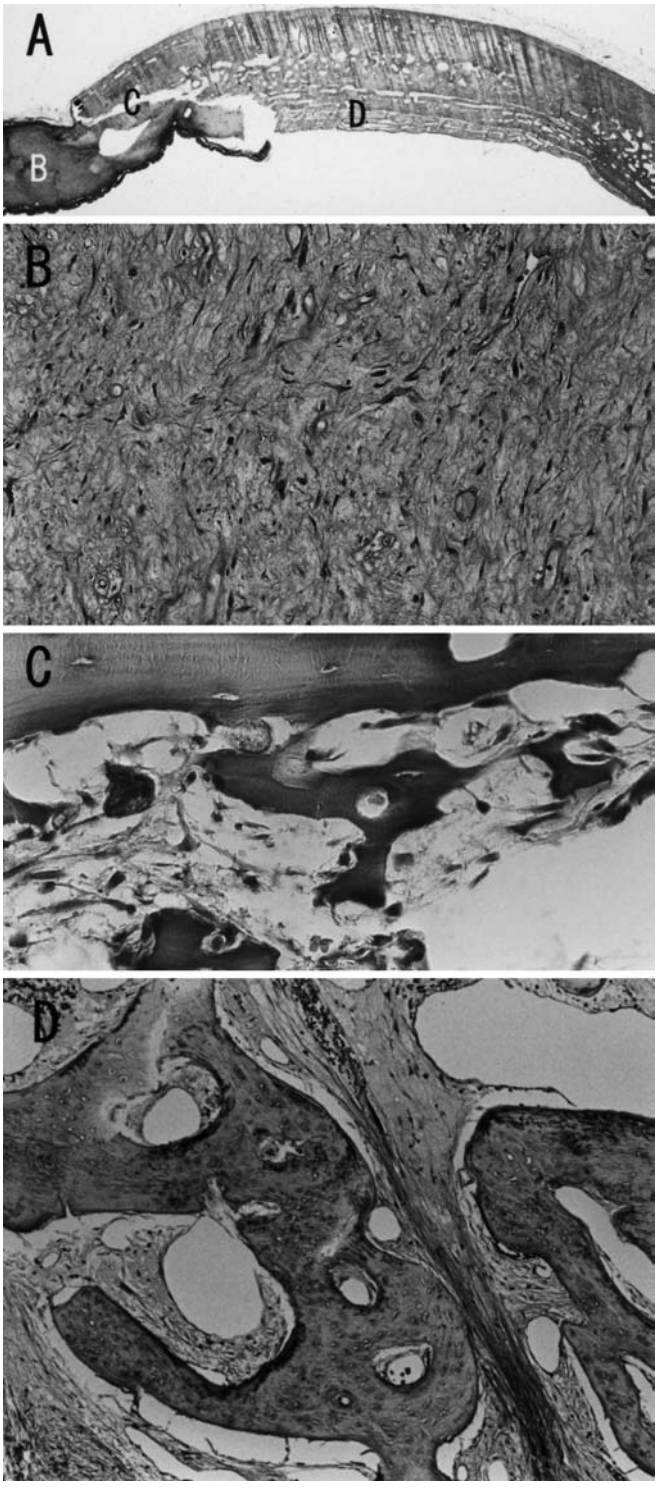



**Fig. 3** Transitional area between the lesion and the apparently normal bone (calvaria). **A** Coronal sections of the calvaria. **B**, **C** and **D** The areas described below (azan-Mallory stain, decalcified section, ×1.5). **B** Bone replaced by fibrous tissue containing spindle-shaped fibroblast-like cells. Some capillaries are present in this region (hematoxylin and eosin, decalcified section, ×120). **C** Histological architecture of the bone is well preserved with lamellar structures and haversian canals (hematoxylin and eosin, decalcified section, ×270). **D** Dilated vessels with thin walls are evident among irregularly shaped new bone trabeculae (hematoxylin and eosin, decalcified section, ×70)

mediate filament proteins, including desmin, keratin, neurofilament protein and glial fibrillary acidic protein, were completely immunonegative (data not shown). No vascular proliferation or angiomatosis was evident, even in the sections immunostained with anti-factor VIII antibody. In the transitional areas between the bones with a normal consistency and the fibrous tissues that had replaced them (Fig. 2C), the bone surfaces facing the fibrous tissues showed irregular moth-eaten outlines, but otherwise the bones were normal in appearance (Fig. 3C and Fig. 4A, B). Multinucleated eosinophilic osteoclasts, which were immunoreactive for CD-68, were frequently encountered in these areas (Fig. 4). New bone formation was observed beneath the inner surface of the calvaria around the lesion (Fig. 3A, D). Among the irregularly shaped new bone trabeculae, many dilated vessels with thin walls were evident.

Electron microscopy revealed that the spindle-shaped cells contained many intermediate filaments and short segments of rough endoplasmic reticulum in their cytoplasm, a characteristic feature of fibroblasts. There were no remarkable pathological findings in the nervous system, including the brain and spinal cord. The visceral organs were also unremarkable, including the lung.

## Discussion

In 1955, Gorham and Stout described the histological features of MO after reviewing eight cases [10], two of which were their own [11]. They found marked proliferation of thin-walled capillaries in the lesions and considered that this vascular proliferation, which they termed “hemangiomatosis”, was the most prominent histological feature [10]. Since then, the association of vascular proliferation with the bone lesions has been well documented in many cases of MO (Table 1) [1, 8, 11, 12, 13, 15, 16, 17, 18, 21, 22, 26, 27]. However, such a histological picture is not universal; it has also been described as fibrous connective tissue, numerous small-caliber blood vessels [1], vascular channels, mainly of the lymphatic type [11], cavernous lymphangioma [12], large thin-walled vessels [12], capillary hemangioma [13], dense fibrous tissue containing numerous vascular spaces [15], and fibrous tissue with numerous wide capillaries [18].

The cause of MO is unknown. Gorham et al. hypothesized that the active hyperemia caused by hemangiomatosis might disturb the normal balance between osteoclasts and osteoblasts, causing an excess of bone destruction over new bone formation [9]. Heyden et al. suggested that angiomatosis might induce local hypoxia and acidosis, and that this might favor the activity of local hydrolytic enzymes [15].

We diagnosed the present patient as having MO from the peculiar progressive clinical and radiographic findings: as this patient had no hereditary pattern, skin lesions or associated nephropathy, other syndromes of idiopathic osteolysis could be excluded [14]. Paget’s disease of bone

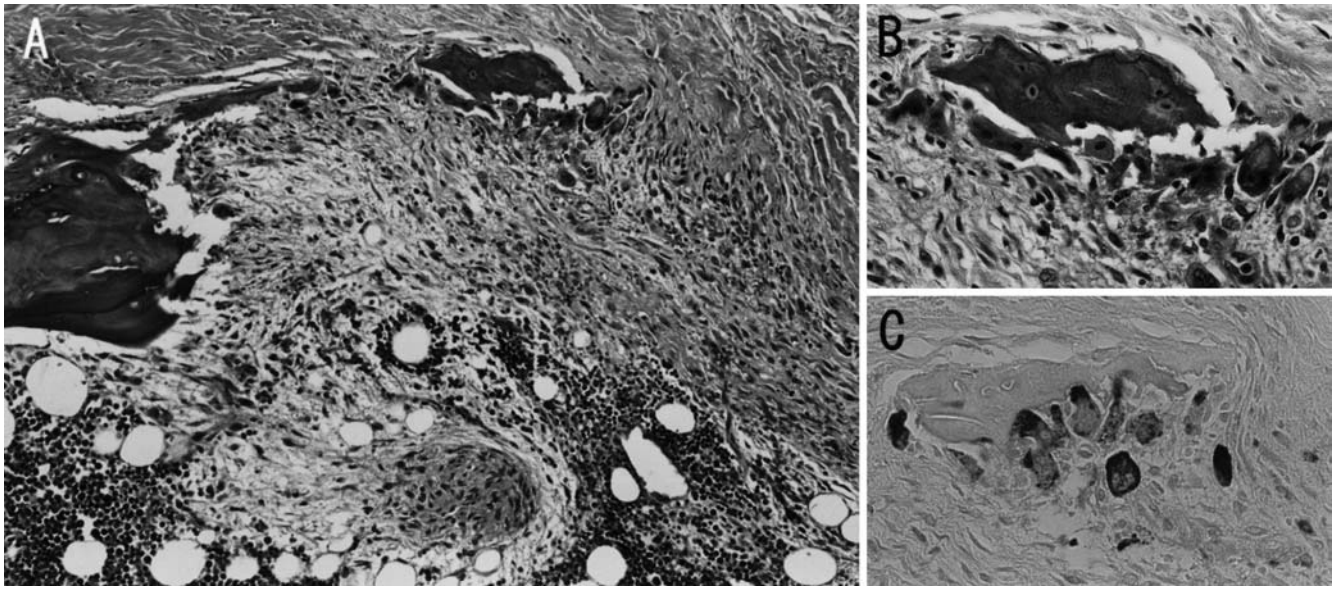



**Fig. 4** Transitional area between the lesion and the bone (cervical vertebra). Osteoclasts are closely associated with the bone fragments (hematoxylin and eosin, **A** ×130, **B** ×300). These osteoclasts are clearly positive for CD-68 (**C** ×300)

(osteitis deformans) should also be included in the differential diagnosis [6]: the disease is a common chronic osteolytic and osteosclerotic disease of uncertain cause that may involve one (monostotic) or more bones (polyostotic) and results in pain, skeletal deformities, and occasional sarcomatous transformation [7]. During the disease process, the clinical and radiological features can be easily detected [7]. Most importantly, in the present patient, the irregular, mosaic pattern of osteoid seen in Paget's disease [6, 7] was not found in any of the lesions.

During her illness, two biopsy examinations provided no specific findings that would have indicated the pathological diagnosis. Postmortem examination revealed no apparent proliferative vascular changes, including so-called angiomatosis, in any of the lesions. Therefore, the question arose as to whether this patient's bone disorder might have differed histologically from MO. However, cases of MO that showed no vascular proliferation have been reported previously (Table 1) [2, 3, 4, 5, 19, 20, 24, 25]. These cases, together with the present one, indicate that vascular proliferation is not always associated with the osteolysis in MO. Osteoclasts, considered to be the only cell type capable of absorbing bone [18], were found in the osteolytic lesions in the present case (Fig. 4). The presence of osteoclasts has also been confirmed in many previous cases (Table 1) [11, 15, 18, 19, 20, 21, 24, 25, 26, 27]. Recently, Spieth et al. [24] and Möller et al. [18] reported that, in MO, bone absorption was osteoclast specific. Thus it is possible that MO may be the consequence of local derangement of osteoclastic activity [18, 19].

In the present case, two types of vascular picture that were somewhat similar to the "hemangiomatosis" described by Gorham and Stout [10] were observed. One was found in the fibrovascular tissues among the new bone trabeculae, and not in the osteolytic lesions (Fig. 3D). It was considered that if a large part of the calvaria had been replaced by fibrous tissue, the altered part of the calvaria would not have been able to withstand gravity, and that periosteal reactive bone formation would have taken place in the dura mater beneath the healthy part of the calvaria around the lesion (Fig. 3A). Among the new bone trabeculae, fibrovascular tissue appeared (Fig. 3D), but no osteoclasts were found in these areas. New bone formation in MO has been confirmed histologically in previous reports (Table 1) [2, 15, 16, 21, 24]. Johnson and McClure [16] also described in detail the roentgenographic changes characteristic of new bone formation in MO.

The other type of vascular picture was evident in the region where fibrous tissue had replaced the bone, and a number of capillary-like vessels were observed there (Fig. 3B). However, the occurrence of such vessels (capillarization) appears to be related to the activation and proliferation of fibroblasts that participate in lesion repair. Diaz-Ramon et al. [4] described two stages in this process: the first stage, characterized by vascular proliferation in connective tissue (hemangiomatosis), is followed by a second stage where residual fibrous tissue replaces absorbed bone. In some previously reported cases of MO, vascular proliferation associated with new bone formation or fibrous tissue proliferation may have been described as "angiomatosis". However, it is unclear whether such vascular proliferation is truly a specific feature of MO.

In conclusion, progressive absorption of bone in MO is not always accompanied by pathologically significant vascular proliferation. We consider that the increased vascularity, if any, may be one of the results of the disease rather than the cause. Simultaneously, it seems question-

**Table 1** Review of cases of massive osteolysis. + present, – absent, *NM* not mentioned

| Study | Gender, age at 1st visit (years) | Duration of symptoms prior to pathological diagnosis (years) | Affected bones | Histology | Osteoclasts | Vascular proliferation | New bone formation | Autopsy/ biopsy |
|---|---|---|---|---|---|---|---|---|
| Anavi et al. [1] (1989) | Female, 24 | 12 | Mandible | Fibrous connective tissue, numerous small-caliber blood vessels | – | + | – | Biopsy |
| Chai et al. [2] (1984) | Male, 38 | NM | Skull | No increased vascularity | NM | – | + | Biopsy |
| | Male, 21 | NM | Skull | No vascular abnormality | NM | – | NM | Biopsy |
| Cherrick et al. [3] (1972) | Male, 27 | 7 | Mandible, maxilla | Fibrous connective tissue | – | – | NM | Biopsy |
| Diaz-Ramon et al. [4] (1996) | Male, 51 | NM | Craniofacial bone | Fibrous connective tissue | NM | – | – | Biopsy |
| El-Mofty [5] (1971) | Female, 55 | 15 | Mandible | Fibrous tissue | – | – | – | Biopsy |
| Frederiksen et al. [8] (1983) | Female, 66 | 3 | Maxillofacial bone | Highly vascularized collagenous tissue | – | + | NM | Biopsy |
| Gorham et al. [11] (1954) | Male, 16 | 2.5 | Clavicle, scapula, rib | Hemangiomatosis | + | + | NM | Autopsy |
| | Male, 44 | 0.5 | Clavicle, scapula, humerus | Vascular channels, mainly of lymphatic type | NM | + | NM | Biopsy |
| Halliday et al. [12] (1964) | Male, 23 | 2 | Ilium | Cavernous lymphangioma | NM | + | NM | Biopsy |
| | Male, 27 | 1 | Rib | Large, thin-walled vessels | NM | + | NM | Autopsy |
| | Male, 1.5 | 0.25 | Femur | Cavernous and capillary hemangioma | NM | + | NM | Biopsy |
| | Female, 15 | NM | Rib | Cavernous lymphangioma | NM | + | NM | Biopsy |
| Hambach et al. [13] (1958) | Male, 16 | 1.2 | Scapula, clavicula | Capillary hemangioma | NM | + | NM | Autopsy |
| Heyden et al. [15] (1977) | Male, 34 | 1 | Vertebrae, rib | Numerous thin-walled, capillary-like vessels | – | + | + | Biopsy |
| | Male, 3 | 0.5 | Iliac bone | Hemangioma-like structure | – | + | + | Biopsy |
| | Male, 15 | 1.25 | Scapula | Dense fibrous tissue contained numerous vascular space | + | + | + | Biopsy |
| Johnson et al. [16] (1958) | Female, 29 | 1 | Ischium | Highly vascular fibrous tissue | – | + | + | Biopsy |
| Kery et al. [17] (1970) | Female, 12 | 0.17 | Femur | Many thin-walled vessels | – | + | NM | Biopsy |
| | Male, 36 | 0.83 | Fibula | Thin-walled vessels were present | NM | + | NM | Biopsy |

able whether MO can be diagnosed with confidence only on the basis of morphology; fibrous tissue with increased vascularity may be a common feature, but does not appear to be a reliable diagnostic hallmark of MO. Only a few autopsy cases have so far been available for review [11, 12, 13]. Further studies are needed to establish the distinct pathology of MO, and to elucidate the mechanisms underlying the progressive osteolysis that characterizes the disease.

**Acknowledgements** We thank T. Hasegawa, S. Egawa, C. Tanda, J. Takasaki and Y. Ota for their technical help, and M. Machida and K. Abe for their help in preparing the manuscript.

**Table 1** (continued)

| Study | Gender, age at 1st visit (years) | Duration of symptoms prior to pathological diagnosis (years) | Affected bones | Histology | Osteoclasts | Vascular proliferation | New bone formation | Autopsy/ biopsy |
|---|---|---|---|---|---|---|---|---|
| Möller et al. [18] (1999) | Female, 77 | 0.25 | Femur | Fibrous tissue with numerous wide capillaries | + | + | NM | Biopsy |
| | Female, 70 | 0.5 | Femur | A stroma rich in fibers with numerous blood vessels | + | + | NM | Biopsy |
| | Female, 19 | NM | Rib | Fibrous tissue with dilated blood vessels | + | + | NM | Biopsy |
| | Female, 78 | 0.04 | Ischium, pubis | Markedly vascularized fibrous tissue | + | + | NM | Biopsy |
| | Female, 83 | NM | Humerus | Vascular fibrous tissue | + | + | NM | Biopsy |
| | Female, 56 | 0.17 | Humerus | Much vascular fibrous tissue | + | + | NM | Biopsy |
| Ohnishi et al. [19] (1993) | Male, 42 | 4 | Mandible | Fibrous connective tissue | + | − | NM | Biopsy |
| Ohya et al. [20] (1990) | Female, 46 | 0.17 | Mandible | Fibrous tissue | + | − | NM | Biopsy |
| | Male, 66 | 3 | Mandible | Dense collagenous fibrous tissue | + | − | NM | Biopsy |
| Poirier [21] (1968) | Male, 37 | 2 | Humerus | Some vascular fibrous tissue and numerous large vascular space | + | + | + | Biopsy |
| Sage et al. [22] (1974) | Female, 36 | 0.83 | Metatarsus | Fibrovascular tissue with two types of vessels | − | + | − | Biopsy |
| Shives et al. [23] (1993) | Male, 30 | NM | Radius, ulna | All cases but two showed increased vascularity in bone | NM | NM | NM | Biopsy |
| | Male, 27 | NM | Rib, vertebrae | | NM | NM | NM | Biopsy |
| | Female, 5 | NM | Sacrum, pelvis | | NM | NM | NM | Biopsy |
| | Male, 23 | NM | Sacrum, ilium | | NM | NM | NM | Biopsy |
| | Male, 14 | NM | Femur | | NM | NM | NM | Biopsy |
| | Male, 21 | NM | Metacarpals | | NM | + | NM | Biopsy |
| | Female, 32 | NM | Metacarpals | | NM | NM | NM | Biopsy |
| | Female, 37 | NM | Femur | | NM | − | NM | Biopsy |
| | Female, 7 | NM | Femur | | NM | NM | NM | Biopsy |
| | Male, 27 | NM | Rib, vertebrae | | NM | NM | NM | Biopsy |
| | Male, 15 | NM | Rib, vertebrae | | NM | NM | NM | Biopsy |
| Spieth et al. [24] (1977) | Female, 46 | 0.75 | Radius | Scar tissue with minimal remaining vasculature | + | − | + | Biopsy |
| Takeda et al. [25] (1987) | Female, 46 | 2 | Mandible | Replaced by fibrous tissue | + | − | NM | Biopsy |
| Tilling et al. [26] (1968) | Female, 5 | 10 | Metatarsus | Loose angioma-like tissue with thin-walled vessels | + | + | NM | Biopsy |
| Turra et al. [27] (1990) | Male, 19 | NM | Humerus | Numerous thin-walled vessels | + | + | NM | Biopsy |

## References


1. Anavi Y, Sabes WR, Mintz S (1989) Gorham's disease affecting the maxillofacial skeleton. Head Neck 11:550–557
2. Chai WX, Wu JP, Chen KF (1984) Massive osteolysis of the skull: long-term follow-up observations after cranioplasty. Report of two cases. Acta Neurochir 73:201–206
3. Cherrick HM, King OH, Dorsey JN (1972) Massive osteolysis (disappearing bone, phantom bone, acute absorption of bone) of the mandible and maxilla. J Oral Med 27:67–74
4. Diaz-Ramon C, Fernandez-Latorre F, Revert-Ventura A, Mas-Estelles F, Domenech-Iglesias A, Lazaro-Ventura A (1996) Idiopathic progressive osteolysis of craniofacial bones. Skeletal Radiol 25:294–297
5. EL-Mofty S (1971) Atrophy of the mandible (massive osteolysis). Oral Surg 31:690–700
6. Fechner RE, Mills SE (1993) Tumors of the bones and joints. Atlas of tumor pathology, 3rd Series, Fascicle 8. Armed Forces Institute of Pathology, Washington DC, pp 133–135
7. Fitzpatrick (1996) Metabolic and nontumorous bone disorders. In: Damjanov I, Linder J (eds) Anderson's pathology, 10th edn, vol 2. Mosby, St. Louis, pp 2606–2607
8. Frederiksen NL, Wesley RK, Sciubba JJ, Helfrick J (1983) Massive osteolysis of the maxillofacial skeleton: a clinical, radiographic, histologic, and ultrastructural study. Oral Surg Oral Med Oral Pathol Oral Radiol Endod 55:470–480
9. Gorham LW (1960) Circulatory changes associated with osteolytic and osteoblastic reactions in bone. Arch Intern Med 105:199–216
10. Gorham LW, Stout AP (1955) Massive osteolysis (acute spontaneous absorption of bone, phantom bone, disappearing bone). Its relation to hemangiomatosis. J Bone Joint Surg Am 37:985–1004
11. Gorham LW, Wright AW, Shultz HH, Maxon FC (1954) Disappearing bones: a rare form of massive osteolysis. Report of two cases, one with autopsy findings. Am J Med 17:674–682
12. Halliday DR, Dahlin DC, Pugh DG, Young HH (1964) Massive osteolysis and angiomatosis. Radiology 82:637–644
13. Hambach R, Pujman J, Maly V (1958) Massive osteolysis due to hemangiomatosis. Report of a case of Gorham's disease with autopsy. Radiology 71:43–47
14. Hardegger F, Simpson LA, Segmueller G (1985) The syndrome of idiopathic osteolysis. Classification, review, and case report. J Bone Joint Surg Br 67:89–93
15. Heyden G, Kindblom LG, Nielsen JM (1977) Disappearing bone disease. A clinical and histological study. J Bone Joint Surg Am 59:57–61
16. Johnson PM, McClure JG (1958) Observation on massive osteolysis, a review of the literature and report of a case. Radiology 71:28–41
17. Kery L, Wouters HW (1970) Massive osteolysis. Report of two cases. J Bone Joint Surg Br 52:452–459
18. Möller G, Priemel M, Amling M, Werner M, Kuhlmey AS, Delling G (1999) The Gorham-Stout syndrome (Gorham's massive osteolysis). A report of six cases with histopathological findings. J Bone Joint Surg Br 81:501–506
19. Ohnishi T, Kano Y, Nakazawa M, Sakuda M (1993) Massive osteolysis of the mandible: a case report. J Oral Maxillofac Surg 51:932–934
20. Ohya T, Shibata S, Takeda Y (1990) Massive osteolysis of the maxillofacial bones. Report of two cases. Oral Surg Oral Med Oral Pathol Oral Radiol Endod 70:698–703
21. Poirier H (1968) Massive osteolysis of the humerus treated by resection and prosthetic replacement. J Bone Joint Surg Br 50:158–160
22. Sage MR, Allen PW (1974) Massive osteolysis. Report of a case. J Bone Joint Surg Br 56:130–135
23. Shives TC, Beabout WB, Unni KK (1993) Massive osteolysis. Clin Orthop 294:267–276
24. Spieth ME, Greenspan A, Forrester DM, Ansari AN, Kimura RL, Gleason-Jordan I (1997) Gorham's disease of the radius: radiographic, scintigraphic, and MRI findings with pathologic correlation. A case report and review of the literature. Skeletal Radiol 26:659–663
25. Takeda Y, Kuroda M, Suzuki A, Fujioka Y, Takayama K (1987) Massive osteolysis of the mandible. Acta Pathol Jpn 37:677–684
26. Tilling G, Skobowytsh B (1968) Disappearing bone disease, morbus Gorham. Report of a case. Acta Orthop Scand 39:398–406
27. Turra S, Gigante C, Scapinelli R (1990) A 20-year follow-up study of a case of surgically treated osteolysis. Clin Orthop 250:297–302

Virchows Arch (2003) 442:407–408
DOI 10.1007/s00428-003-0767-5

LETTER TO THE EDITOR

**Adele Fornelli · Alberto Cavazza · Alessandra Cancellieri · Giulio Rossi · Loredana De Marco**

# Bronchioloalveolar carcinoma with nodular ("morule-like") features

Received: 29 July 2002 / Accepted: 29 October 2002 / Published online: 1 March 2003
© Springer-Verlag 2003

**Keywords** Bronchioloalveolar carcinoma · Lung · Nodular growth · Morule

Sir,

In the recent World Health Organization (WHO) classification of lung and pleural tumours [4], bronchioloalveolar carcinoma (BAC) was considered a variant of pulmonary adenocarcinoma characterised by an exclusive growth upon the wall of pre-existing alveoli ("lepidic growth"), without stromal infiltration. When these strict criteria are applied, BAC becomes a rare neoplasm. Traditionally, it is subdivided into two types: mucinous and non-mucinous, the latter being composed of type-II pneumocytes and/or Clara cells [1, 2]. We describe a non-mucinous BAC with peculiar foci of nodular growth, an apparently unreported finding in such a tumour.

The patient was a 51-year-old woman, non-smoker, presenting with dry cough and malaise. A chest X-ray revealed a diffuse opacity in the lower lobe of the left lung, which did not resolve with antibiotic therapy. A total body computed tomography (CT) scan was negative for extrapulmonary lesions. An explorative thoracotomy was performed, followed by a left pneumonectomy. Two years after surgery, the patient presented with multiple opacities in the controlateral lung, not biopsied and clinically interpreted as neoplastic recurrences. Chemotherapy was therefore administered, but the patient died of disease progression 6 years after surgery. No autopsy was performed.

Macroscopically, the lower lobe and the lingula showed an ill-defined area of parenchymal consolidation, 10 cm in diameter. Histologically, most of the lesion was composed of moderately atypical columnar cells, with overlapping nuclei, abundant eosinophilic cytoplasm and frequent apical snouting, growing along the alveolar wall (Fig. 1). In the material examined (ten blocks from the tumour), the underlying pulmonary architecture was always preserved, and no foci of stromal infiltration were present. Occasionally, multiple small intra-alveolar neoplastic nodules were observed, composed of cells morphologically identical to those lining the alveoli (Fig. 1). The nodules had a squamoid appearance, bearing some resemblance to the morules seen in endometrioid adenocarcinoma of the uterus or in well-differentiated foetal adenocarcinomas of the lung [3]: however, no obvious squamous differentiation was seen. The other lung parenchyma, the bronchial margin and the hilar lymph nodes were unremarkable.

Immunohistochemically, cytokeratin AE1/AE3, cytokeratin 7 and thyroid transcription factor (TTF)-1 were strongly expressed in the lepidic and in the nodular component of the tumour (Fig. 1), whereas chromogranin and synaptophysin were negative. Collagen IV and laminin confirmed the endo-alveolar location of the nodules (Fig. 1).

This lesion fulfils the morphologic criteria for non-mucinous BAC, being composed of neoplastic cells with an exclusive "lepidic" growth, in the absence of stromal invasion [4]. The peculiar feature of our case consists in the multiple foci of nodular growth, a finding which, to the best of our knowledge, has not been previously described in BAC. In our opinion, these foci should be considered non-invasive, based on the absence of both architectural complexity and stromal desmoplasia. It seems likely that this phenomenon represents just a

A. Fornelli · A. Cancellieri
Department of Pathology, Ospedale Maggiore, Bologna, Italy

A. Cavazza (✉)
Unità Operativa di Anatomia Patologica, Ospedale S. Maria Nuova, Viale Risorgimento 80, 42100 Reggio Emilia, Italy
e-mail: cavazza.alberto@asmn.re.it
Tel.: +39-0522-295917
Fax: +39-0522-296945

G. Rossi
Policlinico, Modena, Italy

L. De Marco
Ospedale Ramazzini, Carpi (Modena), Italy

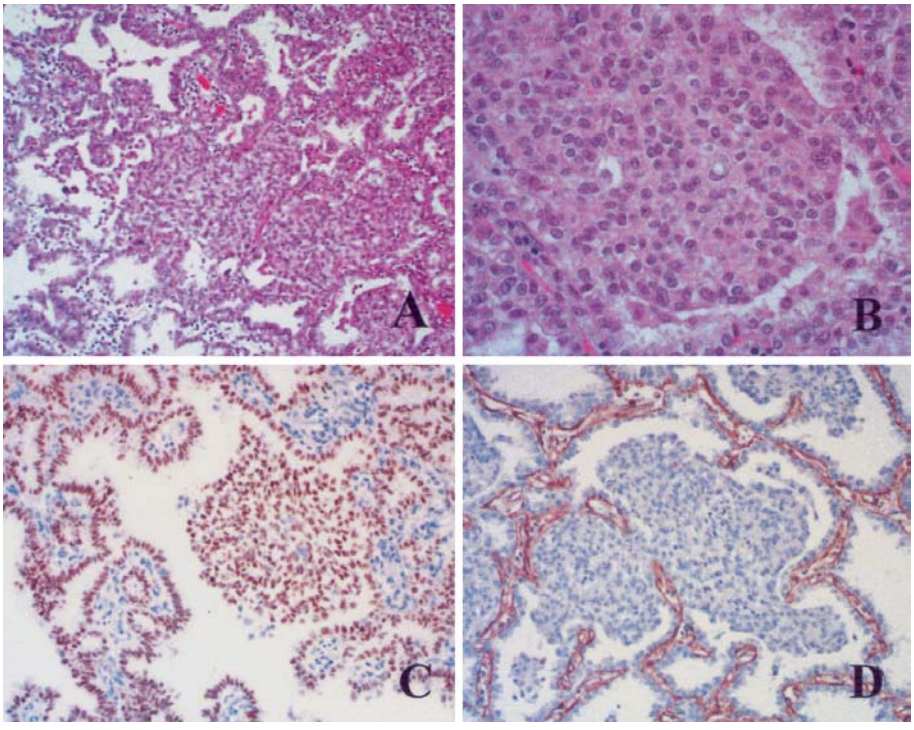



**Fig. 1** **A** The tumour has the classical features of non-mucinous bronchioloalveolar carcinoma. Focally, small nodules are present (haematoxylin and eosin, ×100), **B** at high magnification, the nodular areas have a squamoid, "morule-like" appearance. The cells forming the nodules are identical to those growing along the alveolar wall (haematoxylin and eosin, ×400), **C** the neoplastic cells are immunoreactive for TTF-1, both in the nodular and in the lepidic component (avidin biotin peroxidase complex, ×200) **D** collagen IV confirms the endoalveolar location of the nodules (avidin biotin peroxidase complex, ×400)

morphologic curiosity, to be differentiated from a real infiltration and still consistent with a diagnosis of BAC.

**Acknowledgements** The authors are grateful to Prof. Thomas V. Colby, Mayo Clinic, Scottsdale, for helpful suggestions.

## References

1. Clayton F (1988) The spectrum and significance of bronchioloalveolar carcinomas. Pathol Annu 23:361–394
2. Colby TV, Koss MN, Travis WD (1995) Atlas of tumor pathology. Tumors of the lower respiratory tract. AFIP, Washington
3. Koss MN, Hochholzer L, O'Leary T (1991) Pulmonary blastomas. Cancer 67:2368–2381
4. Travis WD, Colby TV, Corrin B, Shimosato Y, Brambilla E (1999) WHO international histological classification of tumours. Histological typing of lung and pleural tumours, 3rd edn. Springer, Berlin Heidelberg New York

Virchows Arch (2003) 442:409–411
DOI 10.1007/s00428-003-0777-3

LETTER TO THE EDITOR

**Rie Shibata · Makio Mukai · Yasunori Okada · Michiie Sakamoto · Tokuko Yamauchi · Koichi Kobayashi**

# A case of sclerosing hemangioma of the lung presenting as a gigantic tumor occupying the left thoracic cavity

Received: 16 August 2002 / Accepted: 14 January 2003 / Published online: 28 March 2003
© Springer-Verlag 2003

**Keywords** Hemangioma · Sclerosing · Lung · Thoracic · Tumor

Sir,

We report a case of sclerosing hemangioma of the lung that, over a period of 47 years, developed into a gigantic tumor that occupied the left thoracic cavity. This is the largest and most unusual case of sclerosing hemangioma of the lung. A 67-year-old woman was admitted to Keio University Hospital, Tokyo, Japan, in order to resect a gigantic tumor occupying the left thoracic cavity. She had a history of detection of an abnormal shadow on a chest X-ray 47 years previously when she was 20 years old, but she refused surgery at the time. Although there had been no symptoms for about 40 years, she developed exertional dyspnea by the age of 61 years, and 6 years later she could hardly walk. Physical examination showed a decrease in breath sounds in the left lung, but the laboratory data were within normal limits. Computed tomography (Fig. 1a) and magnetic resonance imaging (data not shown) revealed a giant mass occupying the entire left thoracic cavity. It was suspected to be a solitary fibrous tumor, and left pneumonectomy was performed. The patient's postoperative course was uneventful, and no recurrence has been noted throughout 2 years of follow-up.

The resected tumor measured 20×16×15 cm and weighed 2.3 kg. The cut surface of the tumor was dark red, and tan in some areas. Hemorrhagic areas were also seen (Fig. 1b). Although the tumor showed marked extrapulmonary growth, and the left lung had become extremely atrophic as a result of compression by the tumor (Fig. 1b, arrows), the tumor was in continuity with the left upper lobe. The tumor displayed four histological patterns: solid, papillary, hemorrhagic, and sclerotic (Fig. 2). The areas exhibiting the solid pattern contained characteristic round-polygonal cells with abundant clear to eosinophilic cytoplasm (pale cells). In the areas displaying the papillary pattern, papillary projections were lined by cuboidal cells. The areas showing the hemorrhagic pattern were composed of large blood-filled spaces lined by epithelial cells and were reminiscent of a cavernous hemangioma. The sclerotic area contained sparse tumor cells in dense fibrous tissue. Immunohistochemically, positive staining for epithelial membrane antigen and thyroid transcription factor-1 (TTF-1) was observed in both the pale cells and the lining cells. The lining cells were positive for cytokeratin (AE1/AE3, CAM5.2 and 34$\beta$E12), but only a small number of pale cells were positive for cytokeratin. Surfactant apoprotein A was observed in the lining cells but the pale cells were negative. The pale cells stained positively for neuron-specific enolase, but the lining cells were negative. Both the pale cells and the lining cells were negative for chromogranin and synaptophysin. Nuclear staining for estrogen receptors was detected in the pale cells, but both the pale cells and the lining cells were negative for progesterone receptors. All the cells were negative for carcinoembryonic antigen, HMB-45, CD34, CD31, factor VIII, smooth muscle actin, desmin, and S-100 protein.

In 1956, Liebow and Hubbell [5] described a pathological entity of the lung with distinctive variegated features that they called sclerosing hemangioma of the lung. They thought that it represented regressive changes in a hamartomatous angioma with prominent sclerosis.

R. Shibata (✉) · Y. Okada · M. Sakamoto
Department of Pathology,
Keio University School of Medicine,
35 Shinanomachi, Shinjuku-ku, 160-8582 Tokyo, Japan
e-mail: ries@sc.itc.keio.ac.jp
Tel.: +81-3-53633764
Fax: +81-3-33533290

M. Mukai
Division of Diagnostic Pathology,
Keio University School of Medicine,
35 Shinanomachi, Shinjuku-ku, 160-8582 Tokyo, Japan

T. Yamauchi · K. Kobayashi
Department of Surgery,
Keio University School of Medicine,
35 Shinanomachi, Shinjuku-ku, 160-8582 Tokyo, Japan

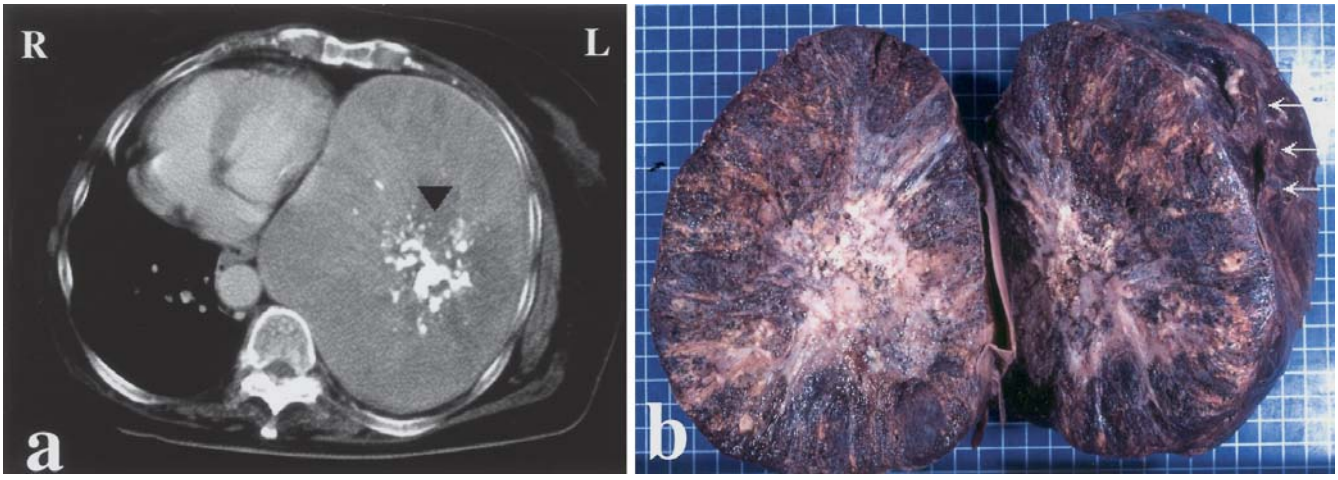



**Fig. 1** **a** Computed tomographic scan of the chest showing a gigantic mass in the left thoracic cavity. Calcification is seen in the center of the mass (*arrowhead*). **b** Cut surface of the resected tumor showing a mixture of hemorrhage and tan medullary areas and a well-defined border. A grayish-white lesion with calcification is seen in the center of the tumor. *Arrows* point to the atrophic lung tissue compressed by the tumor

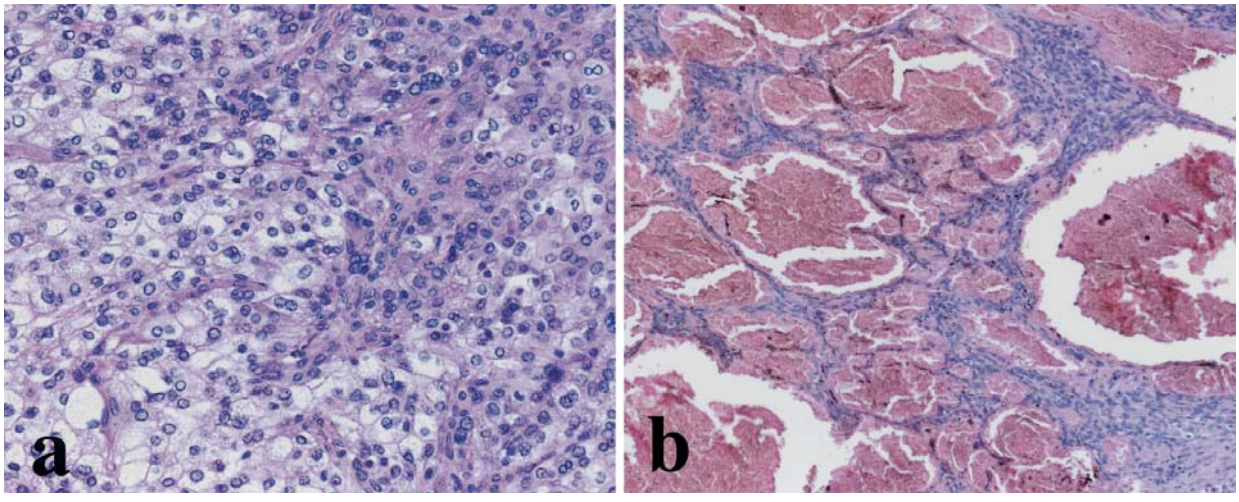



**Fig. 2** Microscopic features of the tumor. Hematoxylin and eosin stain. **a** Solid pattern (original magnification, ×200). **b** Hemorrhagic pattern (original magnification, ×100)

Although the nature of the pale cells has never been determined definitively, Niho et al. demonstrated the monoclonality of the pale cells and cuboidal lining cells [6]; thus, sclerosing hemangioma is considered to be a true neoplasm rather than a hamartoma.

Sclerosing hemangiomas of the lung have been reported to range in size from 0.4 cm to 8.0 cm [2]. To the best of our knowledge, our patient's tumor is the largest cited in the literature. Most patients with sclerosing hemangioma appear to have an asymptomatic course. Our patient had no definite symptoms for the first 40 years, but developed exertional dyspnea and difficulty walking because of obstruction of the large bronchi and compression of the left lung by the large tumor. Thus, the clinical course of our case suggests that sclerosing hemangioma of the lung is not self-limiting despite its benign nature.

Several cases of sclerosing hemangioma with regional lymph-node metastasis have been reported [1, 3, 8, 9]. Although the size of the tumors in these cases was generally larger (ranging from 5 cm to 8 cm), their histological features were no different from those of ordinary sclerosing hemangiomas without metastasis. Sclerosing hemangiomas of the lung are also known to occasionally cross over the fissures and bulge of the pleural surface and take on a polypoid appearance [2]. The tumor in the present case was special in that it occupied almost the entire left thoracic cavity as a result of extensive extrapulmonary growth over a long period—47 years. However, since the patient did not have any metastases, the ability for extrapulmonary growth is

insufficient to produce lymph-node metastases. All the tumor cells of our case were negative for Ki-67. The previous cases, which showed lymph-node metastasis might have higher proliferative activity. Further studies on many cases of sclerosing hemangioma will be necessary to elucidate the mechanism of metastasis.

The results of immunohistochemical staining in the present case are basically consistent with those in previous reports [1, 3, 4, 7]. Recently, Xu et al. demonstrated neurosecretory granules and neuroendocrine markers in the pale cells, and hypothesized that sclerosing hemangioma is a neuroendocrine neoplasm [10]. The pale cells in our case were also positive for neuron-specific enolase, but they were negative for chromogranin and synaptophysin. As in other reports [1, 3], the immunohistochemical findings in our case failed to support the hypothesis of a neuroendocrine neoplasm.

In conclusion, we have reported the largest and most unusual case of sclerosing hemangioma of the lung, with the tumor occupying the entire left thoracic cavity. Sclerosing hemangioma of the lung is a slow-growing benign tumor, but our case suggests that the tumor grows expansively and invasively in the lung without self-regression over a long clinical course. Thus, it is suggested that sclerosing hemangioma of the lung should be treated by resection of the tumor when it is first detected.

## References


1. Chan ACL, Chan JKC (2000) Pulmonary sclerosing hemangioma consistently expresses thyroid transcription factor-1 (TTF-1): a new clue to its histogenesis. Am J Surg Pathol 24:1531–1536
2. Dail DH (1994) Uncommon tumors. In: Dail DH (ed) Pulmonary pathology. Springer, Berlin Heidelberg New York, pp 1317–1329
3. Devouassoux-Shisheboran M, Hayashi T, Linnoila RI, Linnoila RI, Koss MN, Travis WD (2000) A clinicopathologic study of 100 cases of pulmonary sclerosing hemangioma with immunohistochemical studies: TTF-1 is expressed in both round and surface cells, suggesting an origin from primitive respiratory epithelium. Am J Surg Pathol 24:906–916
4. Leong AS, Chan KW, Seneviratne HS (1995) A morphological and immunohistochemical study of 25 cases of so-called sclerosing haemangioma of the lung. Histopathology 27:121–128
5. Liebow AA, Hubbell DS (1956) Sclerosing hemangioma (histiocytoma, xanthoma) of the lung. Cancer 9:53–75
6. Niho S, Suzuki K, Yokose T, Kodama T, Nishiwaki Y, Esumi H (1998) Monoclonality of both pale cells and cuboidal cells of sclerosing hemangioma of the lung. Am J Pathol 152:1065–1069
7. Rodriguez-Soto J, Colby TV, Rouse RV (2000) A critical examination of the immunophenotype of pulmonary sclerosing hemangioma. Am J Surg Pathol 24:442–450
8. Spencer H, Nambu S (1986) Sclerosing haemangiomas of the lung. Histopathology 10:477–487
9. Tanaka I, Inoue M, Matsui Y, Oritsu S, Akiyama O, Takemura T, Fujiwara M, Kodama T, Shimosato Y (1986) A case of pneumocytoma (so-called sclerosing hemangioma) with lymph node metastasis. Jpn J Clin Oncol 16:77–86
10. Xu HM, Li WH, Hou N, Zhang SG, Li HF, Wang SQ, Yu ZY, Li ZJ, Zeng MY, Zhu GM (1997) Neuroendocrine differentiation in 32 cases of so-called sclerosing hemangioma of the lung: identified by immunohistochemical and ultrastructural study. Am J Surg Pathol 21:1013–1022

Virchows Arch (2003) 442:412–414
DOI 10.1007/s00428-003-0779-1

LETTER TO THE EDITOR

**Ihab Abdulkader · José Cameselle-Teijeiro · Jerónimo Forteza**

# Signet-ring cells associated with pseudomembranous colitis

Received: 18 October 2002 / Accepted: 27 January 2003 / Published online: 3 April 2003
© Springer-Verlag 2003

Sir,

Signet-ring cells (SRCs) are most commonly associated with mucus-producing malignant epithelial tumors. They may also be found in thyroid lesions, nonepithelial neoplasm, and, in reactive conditions, in a variety of sites [2, 4]. Here we report the clinical, microscopic, and immunohistochemical features of two cases of pseudomembranous colitis showing benign SRCs.

Case 1 was a 49-year-old man was admitted to hospital due to bacterial meningitis treated with antibiotic therapy including cefotaxim and tobramycin. On the 5th day in hospital the patient developed severe abdominal pain and abdominal distension. At laparotomy features of toxic megacolon were found, and a partial left colon resection with colostomy was performed. Twelve months later he underwent another operation to reconstruct the intestinal transit, and in the postoperative period he had fecaloid peritonitis due to suture dehiscence as well as bleeding in the digestive tract due to subcardial ulcer, which were surgically treated. Currently, 3 years after he was first operated on, the patient is alive with a defect in the abdominal wall due to the repeated surgery.

Case 2 was a 69-year-old man with a history of partial right colon resection for well-differentiated adenocarcinoma without mucinous component. After surgery the patient developed abdominal pain, tenderness, distension, and fever and was treated with mefoxitin, amikacin, and clindamycin. Since the symptoms became more severe, on the 13th day after surgery he underwent resection of the remaining part of right colon and transverse colon. Another synchronous well differentiated adenocarcinoma without mucinous component was found in transverse colon. There is no follow-up.

I. Abdulkader · J. Cameselle-Teijeiro (✉) · J. Forteza
Department of Pathology,
Hospital Clínico Universitario,
Choupana s/n, 15706 Santiago de Compostela, Spain
e-mail: apjocame@usc.es
Tel.: +34-981-950858
Fax: +34-981-950889

Macroscopically, we found dilatation of the colon in both cases, the thickness of the wall was increased, and the mucosal surface displayed multiple yellow patches of exudate (Fig. 1). Furthermore, an anular (constrictive) mass of 3 cm diameter was found in case 2. Histologically the two specimens showed similar findings, with transmural acute inflammation and formation of pseudomembranes (Fig. 2a). Focally the crypt epithelia appeared distended and replaced by signet-ring shaped cells (Fig. 2), which were mucicarmine positive (Fig. 3a). Occasional SRCs were also seen in the pseudomembranes. The signet cells showed peripherally placed nuclei and intracytoplasmic vacuoles. The nuclei were not enlarged, displayed uniform chromatin distribution, and had either no nucleoli or mitotic figures. SRCs were not present in the lamina propria outside the crypts. Immunohistochemically the SRCs were positive for cytokeratins (20, clone CAM5.2, and clone AE1-AE3; Fig. 3b) and E-cadherin (Fig. 3c) while uniformly negative for CD68 (KP1), MIB-1, bcl-2, and p53.

The current SRC formation in pseudomembranous colitis has been reported only in four previous cases [1, 3, 4, 5]. As occurred in our patients, toxic megacolon developed after antibiotic therapy, showing a gross and microscopic picture of pseudomembranous colitis. The recognition of benign SRCs associated with pseudomembranous colitis has diagnostic implications. The occurrence of benign SRCs may present a diagnostic pitfall as they can simulate a carcinomatous infiltrate. Furthermore, the presence of SRCs in a patient with a history of colonic adenocarcinoma, as reported by Schiffman [4] and occurred in our second case strongly suggests recurrent carcinoma. However, primary and metastatic SRC carcinomas of the colon are uncommon and more related to ulcerative colitis. The E-cadherin–catenin complex is important for cell-cell adhesion of epithelial cells, and impairment of one or more components of this complex is associated with SRC carcinoma [6]. However, benign SRCs in our patients showed an immunohistochemical normal pattern of E-cadherin. We think that the associ-

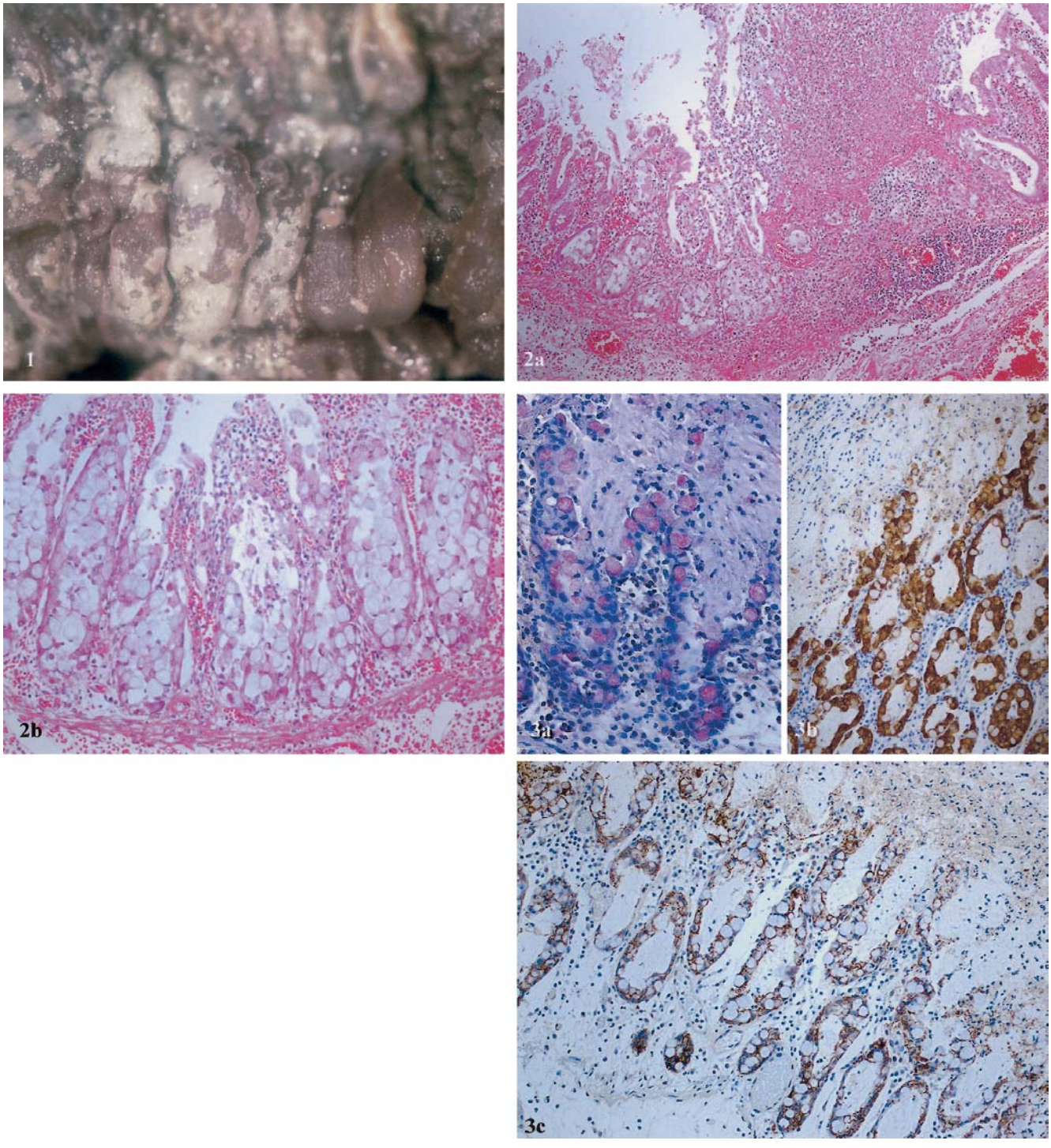



**Fig. 1** Pseudomembranous colitis. Gross appearance of lesion

**Fig. 2** **a** Area of colon involved by pseudomembranous colitis. The crypts are fillet with signet-ring cells. Hematoxylin and eosin, ×100. **b** Representative area showing numerous signet cell in colonic crypts. Hematoxylin and eosin, ×200

**Fig. 3** **a** Signet-ring cells showed cytoplasmic mucicarmine positivity. ×200. **b** The same cells were immunoreactive for cytokeratins (clone AE1-AE3). ×200. **c** Normal membrane staining for E-cadherin was observed in signet-ring cells. ×200

ation between benign SRCs and carcinoma is merely coincidental and not directly related.

Pathologists should be aware of the risk of misdiagnosing such lesions as SRC carcinoma. Attention to the history and to the microscopic features, which show the SRCs confined within the mucosa and completely surrounded by intact basal lamina, may avoid misdiagnosis. Immunohistochemical studies for collagen IV, laminin, and E-cadherin, as well as negativity for MIB-1 and p53 could also be helpful. Although some authors [1, 5] have claimed that the finding of SRCs in pseudomembranous colitis can be associated with a fulminant course, the follow-up in our case 1 does not support this hypothesis.

## References


1. Damiani S, Campidelli C (2002) Pseudomembranous colitis with signet-ring cells. Histopathology 41:176–177
2. Dehner LP (1987) Gastrointestinal tract. In: Grayson T (ed) Pediatric surgical pathology. Williams & Wilkins, Baltimore, pp 334–432
3. Michal M, Chlumska A, Mukensnabl P (1998) Signet-ring cell aggregates simulating carcinoma in colon and gallbladder mucosa. Pathol Res Pract 194:197–200
4. Schiffman R (1996) Signet-ring cells associated with pseudomembranous colitis. Am J Surg Pathol 20:599–602
5. Sidhu JS, Liu D (2001) Signet-ring cells associated with pseudomembranous colitis. Am J Surg Pathol 25:542–543
6. Zhou YN, Xu CP, Han B, Li M, Qiao L, Fan DC, Yang JM (2002) Expression of E-cadherin and beta-catenin in gastric carcinoma and its correlation with the clinicopathological features and patient survival. World J Gastroenterol 8:987–993

Virchows Arch (2003) 442:415
DOI 10.1007/s00428-003-0766-6

BOOK REVIEW

**Michael Sheaff**

# Sudha R. Kini: Color atlas of pulmonary cytopathology

Received: 29 November 2002 / Accepted: 29 November 2002 / Published online: 13 March 2003
© Springer-Verlag 2003

Dear Sirs,

Thank you for asking me to review this wonderful book. I would like to offer the following.

I have often thought that cytology has been undervalued as a means of diagnosis and morphological evaluation of disease processes. To some extent this is because cytology is considered by many outside the discipline to be a "dry" subject with black and white, benign or malignant conclusions. Practising pathologists will tell you that, in most organ systems, this is patently not the case and this is particularly so for pulmonary cytopathology.

This is amply illustrated by Dr. Kini's book on the subject. She uses a combination of high-quality photomicrographs and detailed text to demonstrate lesions with differential diagnosis. What I especially like about this book is its thoroughness to the point of being elementary (although always comprehensive). This is not to say that it is any way basic, since there is a wealth of information contained between its covers – some of which I have not found in other texts of lung pathology several times its size.

Another of its qualities is the approach from a practical diagnostic viewpoint, including technical considerations that do not seem to be part of recognised post-graduate training in the modern world. We are taken through the specimen handling from acquisition to slide preparation and then on to reading, discussing reasons for using a particular procedure and possible alternatives.

A couple of minor "niggles" are the splitting of text and illustrations, which I personally would prefer to see combined, and an occasional low-power photograph that does not seem to be very demonstrative. On the whole, however, the photographs are first class and illustrate the relevant findings admirably. The sections on the role of cytology in the diagnosis of idiopathic pulmonary fibrosis and bronchoalveolar lavage differential cell counts appear a little brief and could, I think, be more detailed. That said, there are several excellent points I would like to mention in addition to the overall high standard and these relate to the bibliography and the juxtaposition of adenocarcinomas with mesotheliomas – frequently such a difficult differential diagnosis.

In many ways Dr Hammar has provided the best review of the book in his Foreword and I would have to agree with almost everything that is contained therein. However, whether this is a book that "all diagnostic pathologists should own" is debatable and possibly overstating the mark. In any case, I found this book a pleasure to peruse and will refer to it regularly. It is so much more than just a pictorial atlas. It is a book that all diagnostic pathologists will want to have access to within their departments.

M. Sheaff (✉)
Department of Morbid Anatomy and Histopathology,
The Royal London Hospital,
Whitechapel, El 1BB London, England
e-mail: m.t.sheaff@qmul.ac.uk
Tel.: +020-7377-7347
Fax: +020-7377-7030

 © Springer-Verlag 2003

## ANNOUNCEMENTS

9–11 May 2003
**6th International Course on Bone Marrow Biopsy Pathology**
Hanover, Germany

Under the auspices of the European Association for Hematopathology

Bone marrow histology has evolved into an integral part of modern haematological diagnostics. Moreover, it affords unique access to a biological understanding of important diseases affecting the haematopoietic system. The courses offered by the European Bone Marrow Working Group under the auspices of the European Association for Hematopathology are intended to provide high quality educational sessions in bone marrow histopathology and to bring together people who have a particular interest in this field. In addition to state-of-the-art lectures focusing on selected topics, there will be workshops where participants are invited to contribute their own interesting and instructive cases. Topics will be chronic myeloproliferative disorders, lymphoma, hypoplastic states and MDS, reactive and therapy-related changes.

Course fee: 300 €

*For further information* see
http://www.mh-hannover.de/institute/pathologie/kongress or contact Institute of Pathology,
Medizinische Hochschule Hannover,
Carl-Neubergstr. 1, 30625 Hannover, Germany
E-Mail: Laenger.Florian@MH-Hannover.de
Tel.: 0049 511 532-4501; Fax: -5799

12–16 May 2003
**Diagnostic Histopathology of Breast Disease**
London, UK

May 12–16, 2003, at Hammersmith Hospital (Imperial College Faculty of Medicine), London, UK. A week-long course designed for pathologists at Consultant and Senior Trainee level. The course provides a comprehensive coverage of the Histopathology of Breast Disease, with special emphasis on areas that pose diagnostic difficulties. The participants will be given ample time to study histological preparations, followed by illustrated discussion of the cases. There will be special sessions dealing with the interpretation of core biopsies and fine needle aspirations. There will also be two daily talks dealing with specific topics, given by eminent breast pathologists and followed by discussion. The topics will include reporting breast biopsies, immunohistochemistry, receptor assessment, c-erbB-2, prognostic factors, proliferative lesions/ carcinoma in situ, problems in breast pathology, a practical approach to the diagnosis of breast lymphomas and molecular pathology. The faculty will include Ian Ellis, Christopher Elston, Andrew Hanby, Kristin Henry, Stephen Humphreys, Sunil Lakhani, Andrew Lee, Sarah Pinder, Sami Shousha, and Clive Wells.

*Further details from:*
Wolfson Conference Centre, Hammersmith Hospital
Du Cane Road, London W12 ONN, UK
(Tel (44) 20 8383 3117/3227/3245; Fax (44) 20 8383 2428
e-mail wcc@ic.ac.uk)

12–23 May 2003
**International Course on Laboratory Animal Science**
Utrecht, The Netherlands

A two-week intensive course on laboratory animal science will be organized at the Department of Laboratory Animal Science – Utrecht, The Netherlands in May 2003. This course has been offered once a year since 1993.

The objective of this course is to present basic facts and principles that are essential for the humane use and care of animals and for the quality of research.

The contents of the course are in line with recommendations of the Federation of European Laboratory Animal Science Associations (FELASA) regarding the training of the young scientist whose research involves the use of vertebrate animals.

The course may also be of interest for those who intend to set up a similar course at their own institution. For this purpose, during the course the acquisition of teaching materials can be discussed with the course committee.

*For information and application forms please contact*:
Prof. Dr. L.F.M. van Zutphen or Mr. Stephan van Meulebrouck
Department of Laboratory Animal Science
Faculty of Veterinary Medicine, P.O. Box 80.166
3508 TD Utrecht, The Netherlands
Phone: *31-30-2532033; Fax: *31-30-2537997
E-mail: pdk@las.vet.uu.nl
Internet: http://las.vet.uu.nl (click ‘Education’).

9–11 June 2003
**Multi-Disciplinary Courses on Breast Disease**

Three day course. The first part is multi-disciplinary. Thereafter the different specialties meet to accommodate their own special requirements.

Course Tutors: Dr. I.O. Ellis, Dr. S.E. Pinder, Dr. A.H.S. Lee

| | | |
|---|---|---|
| Course fees: | NHS | £370.00 |
| | Non-NHS | £415.00 |
| | Overseas | £550.00 |

includes refreshments but not accommodation

*For further information please contact:*
Education Administrators
Nottingham International Breast Education Centre,
City Hospital, Hucknall Road, Nottingham NG5 1PB
Tel.: 0115 969 1689; Fax: 0115 962 7707
E-mail: enquiries@nibec.co.uk; www.nibec.co.uk

6 September 2003
**EUROPEAN BOARD OF PATHOLOGY**
**7th EXAMINATION 2003**
Ljubljana, Slovenia

The Seventh Examination of the European Board of Pathology will be held in Ljubljana, Slovenia, Saturday September 6, 2003. This Examination precedes the 19th Congress of the ESP.

*For information about the examination and application forms can be obtained from:*
Prod. Dr. J.G. van den Tweel
(chairman of The Examination Board)
Utrecht University Medical Center
Department of Pathology, H 04.312
P.O. Box 85500
3508 GA Utrecht
Fax: ++31-30-2544990
Tel.: ++31-30-2506565
e-mail: j.vandentweel@lab.azu.nl *or*
W.vanBragt@lab.azu.nl (secretary)
The same information is also available from Internet:
http:www.uems.be/pathol.htm, see index 2 and 3

6–11 September 2003
**19th European Congress of Pathology**

Ljubljana, Slovenia

The largest congress of pathologists in Europe in 2003, covering basic diagnostic standards, update scientific achievements and recent technical advances in all areas of pathology at 4 keynote lectures, 30 symposia, 21 short courses, 21 slide seminars, 14 special presentations, 2 round table discussions and free paper and poster sessions. Internationally recognized invited speakers are from throughout Europe and the USA.

*Updated information on the congress website:*
http://www.cd-cc.si

13 October 2003
**Continuing Medical Education**

One day Multi-Disciplinary Update courses

Course fee: £95.00

*For further information please contact:*
Education Administrators
Nottingham International Breast Education Centre
City Hospital, Hucknall Road, Nottingham NG5 1PB
Tel.: 0115 969 1689; Fax: 0115 962 7707
E-mail: enquiries@nibec.co.uk; www.nibec.co.uk

17–19 November 2003
**Multi-Disciplinary Courses on Breast Disease**

Three day course. The first part is multi-disciplinary. Thereafter the different specialties meet to accommodate their own special requirements.

Course Tutors: Dr. I.O. Ellis, Dr. S.E. Pinder, Dr. A.H.S. Lee

| | | |
|---|---|---|
| Course fees: | NHS | £370.00 |
| | Non-NHS | £415.00 |
| | Overseas | £550.00 |

includes refreshments but not accommodation

*For further information please contact:*
Education Administrators
Nottingham International Breast Education Centre,
City Hospital, Hucknall Road, Nottingham NG5 1PB
Tel.: 0115 969 1689; Fax: 0115 962 7707
Email: enquiries@nibec.co.uk; www.nibec.co.uk

Virchows Arch (2003) 442:419–420 © Springer-Verlag 2003

SOCIETY NEWS

# Invitation to the 19th European Congress of Pathology

On behalf of the European Society of Pathology (ESP) and the Organising Committee, we take great pleasure in inviting you to the 19th European Congress of Pathology, which will be held in Ljubljana, Slovenia, 6–11 September 2003.

Slovenia is not a large country, but at the hub of routes of trade and movement from east to west and north to south, it has always played a larger part in European events than its size would suggest. Slovenia is now an independent Central European state, on the sunny side of the Alps, bordering Italy, Austria, Hungary and Croatia. The landscape embraces rolling countryside leading to the Pannonian plain to the east, rugged Karst bordering the Adriatic Sea to the southwest, and the Alps to the north and west. The Slovenian nation of only two million today has survived mainly due to its culture, language and vitality. A bone flute, 30,000 years older than any other known in the world, and Europe's oldest bone needle, testify to the roots of culture here.

Its capital, Ljubljana, has a picturesque unity, composed of an architectural heritage spanning Roman Emona, through Renaissance and Baroque Ljubljana, to Secession Art Nouveau and Modern Ljubljana, so strongly marked by the influence of the world famous Slovenian architect, Jo e Plečnik. Ljubljana is an university city. The roots of the University go back to the seventeenth century with Academia Operosorum, the fourth Academy of Sciences in Europe. A Philharmonic Society dates back three centuries.

Ljubljana's congress tradition began in 1821, when the three emperors of the Holy Alliance met here to discuss the post-Napoleonic fate of Europe. These traditions have been brought together in the new Cultural and Congress Centre Cankarjev dom, with a capacity of 3,600, located in the heart of Ljubljana. Cankarjev dom is well equipped with all modern technical facilities and has an experienced in-house team to ensure the necessary high standards for scientific sessions and exhibitions. All Congress venues, and most hotels, are within walking distance of the centre of the city. Particular attention will be paid to stimulating the participation of trainees and young pathologists by securing as low a registration fee as possible, and inexpensive accommodations.

The European Society of Pathology has been succeeding in establishing its ever more continuous activity and influence. The old idea of a common programme of continuous education of pathologists has been realised through a number of courses organised each year by the European School of Pathology, at its headquarters in Turin and other centres throughout Europe. An increasing number of Working Groups within the European Society of Pathology, devoted to various fields, promote a continuous exchange of professional experiences and other information, the establishment of common diagnostic standards and collaboration on common research projects.

The biannual ESP Congresses retain a major role in fulfilling the main aims of the ESP in pathology education, exchange of the most recent research achievements and, particularly, in keeping together all branches of pathology, that otherwise tend to split according to organ systems, disease processes and the increasing number of techniques. The Congresses also keep together pathologists from the whole of Europe, irrespective of geographical and political borders.

We believe that the 19th European Congress of Pathology will continue the traditional approaches of previous Congresses and will serve to increase both links with European national and international pathology societies and intercontinental links, particularly with the International Academy of Pathology. The framework of the Congress Scientific Programme has been created with the strong impact and assistance of the ESP Working Groups, the ESP Executive/Scientific Committee and the Advisory Council as well as companion Societies. The programme covers all areas of pathology, provides information ranging from current diagnostic standards to recent advances in science and modern techniques, particularly those of molecular genetics, and includes a number of "hot" topics of today and tomorrow, which will be

presented by the best, internationally recognised experts at Keynote Lectures, Symposia, Special Presentations, Round Table Discussions, Short Courses and Slide Seminars. One evening is devoted to ESP Working Group Meetings, both business and scientific. Interesting Satellite Symposia will be organised by supporting companies, two by the main sponsor of the Congress Main Sponsor, Ventana Medical Systems S.A.

Furthermore, all practising pathologists and scientists are kindly invited to present their scientific achievements and exchange their professional experiences through Free Paper and Poster Sessions. The best Free Papers will be acknowledged by giving the authors the opportunity to present their achievements at the plenary session, at which the authors of the three best Poster Presentations will additionally receive special Awards.

All who are coming to Ljubljana are kindly invited to join us at two one-day Pre-Congress Meetings, prior to the Congress Opening Ceremony on Saturday: one on Pulmonary Pathology and the other devoted to non-neoplastic Nephropathology. There will also be a three-day Joint Meeting of the European and North American Society of Head and Neck Pathology. All Pre-Congress Meetings and a whole day Examination by the European Board of Pathology will be organised by using the facilities of the new building of the Faculty of Medicine, University of Ljubljana.

Culture kept the Slovenian national identity alive over the centuries and it still plays an important role in people's lives. The Congress will also highlight the traditional close connection between medicine and art. Some novel events are planned: an exhibition of the work of pathologists/painters and, especially, a Gala Concert on Monday evening in the main Gallus Concert Hall of the Congress Centre in Ljubljana, by pathologists/musicians from all over the world. A social programme is offered which reflects the warmth and hospitality of the Slovenian people.

The Second Millennium we have entered provides major challenges for all biomedical sciences, and the 19th European Congress of Pathology is a challenge for the Organisers. We sincerely hope that attendance at the Ljubljana Congress in 2003 will be a fruitful, enjoyable and memorable experience in every respect for all participants, and will give new impetus to our medical speciality in Slovenia.

We look forward to seeing you in September 2003 in Ljubljana.



Gianni Bussolati
President
European Society
of Pathology



Du an Ferluga
President
19th European Congress
of Pathology

Virchows Arch (2003) 442:421–428
DOI 10.1007/s00428-003-0782-6

REVIEW ARTICLE

**Angelo P. Dei Tos**

# The reappraisal of gastrointestinal stromal tumors: from Stout to the KIT revolution

Received: 2 September 2002 / Accepted: 22 December 2003 / Published online: 26 February 2003
© Springer-Verlag 2003

**Abstract** For five decades gastrointestinal stromal tumors (GISTs) truly have represented one of the most confusing as well as neglected areas of both surgical pathology and clinical oncology. The recognition of the central role played by KIT expression in the development of the interstitial cell of Cajal and of the activating KIT mutations in the pathogenesis of GIST have been the keys for a more precise categorization of this long elusive clinicopathological entity. A Consensus Conference held at the National Institutes of Health in 2001 provided both an evidence-based definition and a practical scheme for the assessment of the risk of aggressive clinical behavior. This scheme is based on evaluation of the size and mitotic rate of the tumors, and its use is strongly advocated. On the basis of current data GISTs can be defined as a distinctive group of KIT-expressing mesenchymal neoplasms of the gastrointestinal tract, showing differentiation towards the interstitial cell of Cajal, also known as the gastrointestinal pacemaker cells. Metastatic GISTs have been a virtually incurable disease until the elucidation of the role of KIT mutations. STI-571 (imatinib mesylate) is a molecule that inhibits the function of various receptors with tyrosine kinase activity, such as abl, the bcr-abl chimeric product, platelet-derived growth factor receptor, and KIT. Following its successful use in the treatment of chronic myeloid leukemia, STI-571 has also proved extremely effective in targeting metastatic GIST. Data regarding the duration of the response to this therapy are not yet available, and therefore any overenthusiasm should be avoided. Nonetheless, the GIST story remains paradigmatic of a totally innovative approach to cancer therapy which until now is the most elegant translation of cancer biology experimental knowledge into clinical practice.

**Keywords** Gastrointestinal stromal tumor · Sarcoma · Tyrosine kinase receptors · KIT · Target therapy

A. P. Dei Tos (✉)
Departments of Pathology and Oncology,
Regional Hospital,Piazza Ospedale 1, 31100 Treviso, Italy
e-mail: apdeitos@ulss.tv.it

## Introduction

We live in an era in which the concept of "translational research" is having a profound impact upon medicine. During the past few years the opportunity to turn the observations provided by basic scientists into solutions immediately applicable to the treatment of patients has unequivocally evolved from the stage of hope to that of reality. In this context the story behind the redefinition of the clinicopathological entity known as gastrointestinal stromal tumor (GIST), is somewhat paradigmatic of the central role that pathology may play in this process.

The conceptual evolution of the classification of mesenchymal tumors of the gastrointestinal (GI) tract has been the subject of numerous previous articles [2, 33, 36, 49]. However, the recent introduction of STI-571 (imatinib mesylate, Glivec®), a receptor tyrosine kinase inhibitor that has proved extremely effective in the treatment of GISTs, has generated huge attention for this group of neoplasms [23, 42].

Ironically these lesions have truly have been one of the most confusing as well as neglected areas of both surgical pathology and clinical oncology. Neither reliable diagnostic nor prognostic criteria have been available until recently, when a Consensus Conference held at the National Institutes of Health (NIH) in April 2001 provided a solid, evidence-based rationale for GIST diagnosis and prognostication [13].

The recognition of the central role played by activating KIT mutations in the pathogenesis of GIST [20, 29, 46], which in most cases is associated with KIT protein (CD117) expression, has not only has been the key to such a major clinical advance but has provided pathologists with a reproducible genotypic as well as phenotypic marker [24, 50]. Effective palliation for a previously incurable disease has become available, and pathologists are responsible for the most accurate selection of patients.

## Diagnosing GISTs: from Stout to the KIT revolution

The first accurate description of mesenchymal neoplasms of the GI tract was one of the many invaluable contributions of Arthur Purdy Stout [17]. It is interesting to note that for more than two decades, until the advent of ultrastructural examination and subsequently of immunohistochemistry, these tumors were generally regarded as deriving from smooth muscle cells and were therefore variably classified as leiomyomas, bizarre leiomyomas [54], cellular leiomyomas [3], leiomyoblastomas, and leiomyosarcomas. Unfortunately, with the advent of electron microscopy and immunohistochemistry, unequivocal smooth muscle differentiation was hardly demonstrable in most cases examined [45, 61]. In consideration of such an "orphan" phenotype Mazur and Clark [32] in 1983 pragmatically pioneered the use of the more generic designation "stromal tumor." Both ultrastructural and immunohistochemical examination not only provided negative findings, as a minority of GI tract stromal tumors exhibited features of neuroectodermal differentiation. Herrera et al. [19] introduced the concept of "plexosarcoma" in 1984 to acknowledge the existence of autonomic neuronal differentiation in at least a small subset of cases. These entities were subsequently renamed as gastrointestinal autonomic nerve tumors (GANT) [27].

Fifty years following Stout's description the line differentiating this group of tumors remained to be elucidated. Pathologists were left with the impression of a heterogeneous group of lesions, exhibiting in some instances a myogenic phenotype and in others a neural or even a mixed one. Some cases did not exhibit any specific line of differentiation making the diagnostic approach even more frustrating [41]. Some enthusiasm was generated by the recognition that about two-thirds of GISTs express CD34 [34, 38]. However, the diagnostic utility of this observation was hampered by the poor specificity of this marker, which is now know to be expressed in a broad variety of spindle cell tumors, including those exhibiting smooth muscle or schwannian differentiation. As a consequence of the lack of reproducible diagnostic criteria GIST represented not more than a generic term to indicate any mesenchymal tumor arising in the GI tract. Importantly, some suggested distinguishing true smooth muscle and schwannian neoplasms (which may indeed arise in the GI tract and have to be properly recognized), but without being able to provide a meaningful definition for the nonneural, nonmyogenic ones.

The 1990s eventually brought the long awaited breakthrough. Researchers for many years had observed strong KIT expression in hematopoietic stem cells, mast cells, melanocytes, and interstitial cells of Cajal (ICC), which plays a major role in committing primitive cells towards a specific lineage [22, 25, 30]. KIT is a transmembrane tyrosine kinase receptor composed of an extracellular domain containing the ligand binding site and an intracellular domain containing the actual kinase enzymatic domain. Normal KIT receptors homodimerize following binding to a ligand know as "stem-cell" factor [4, 31] resulting in activation of the KIT kinase domain. The consequent phosphorylation of tyrosine residues is the prerequisite for activation of a variety of signal transduction pathways involved not only in differentiation but also proliferation, apoptosis, and tumorigenesis [18].

The ICC is a cell type sharing immunophenotypic and ultrastructural features of both smooth muscle and neuronal cells. The ICC acts as the interface between the autonomic neural network of the bowel wall and its muscle layers and has been therefore also popularized as the "gastrointestinal pacemaker" cell. KIT expression appears to play a key role in committing primitive mesenchymal cells towards interstitial ICC differentiation [26, 56], and in fact KIT deficient mice lack a functional ICC network and exhibit an aperistaltic gut [40].

In 1998 Hirota and coworkers [20] reported that some GISTs contained activating mutations in the *KIT* proto-oncogene which is associated with expression of KIT protein [20, 24, 29, 47, 50]. Although in some cases there exist activating mechanisms other than mutational events, as a direct result of mutations KIT proteins in GISTs are constitutionally activated in a ligand-independent manner [47]. It subsequently became evident that the prevalence of *KIT* mutations in GIST was much higher than initially believed [29]. It was also discovered that true neural as well as smooth muscle neoplasms of the GI tract entirely lack *KIT* mutations. As a consequence KIT expression was proposed as both the most sensitive and a specific phenotypic marker. On the basis of all these observations it was suggested to define GISTs as a distinctive group of KIT-expressing mesenchymal neoplasms of the GI tract showing differentiation towards ICC [24, 52]. It must also be emphasized that GANT exhibits identical KIT mutation and expression, therefore showing complete molecular genetic and morphological overlap with GISTs [28]. As a consequence GANT may no longer be regarded as a separate clinicopathological entity.

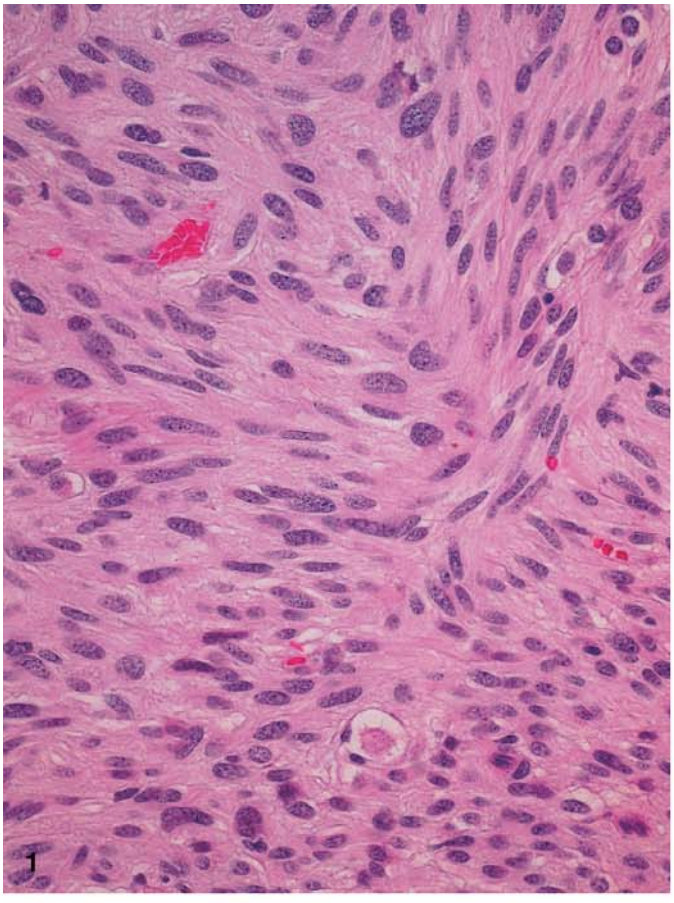
At the end of the 1990s pathologists were eventually able not only to accurately define this long elusive group of neoplasms but also to suggest a possible line of differentiation. However, the final and also the nicest part of the story was still to come: the discovery of KIT dysregulation provided the scientific rationale for a very innovative therapeutic approach.

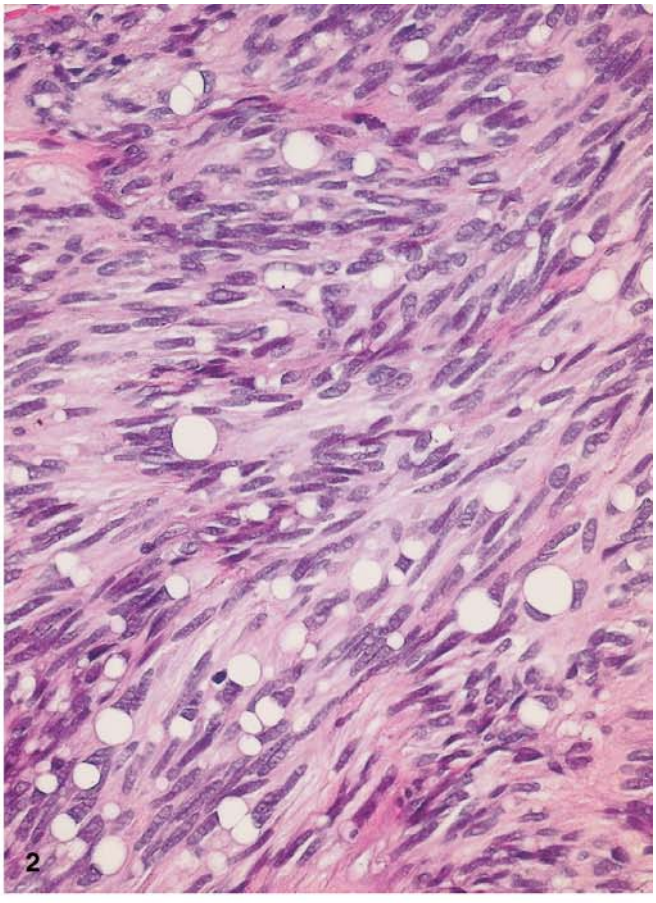
**Fig. 1** Gastrointestinal stromal tumor: spindle cell type. The neoplastic cells tend to have light eosinophilic cytoplasm, often with indistinct cell borders. Hematoxylin and eosin, ×40

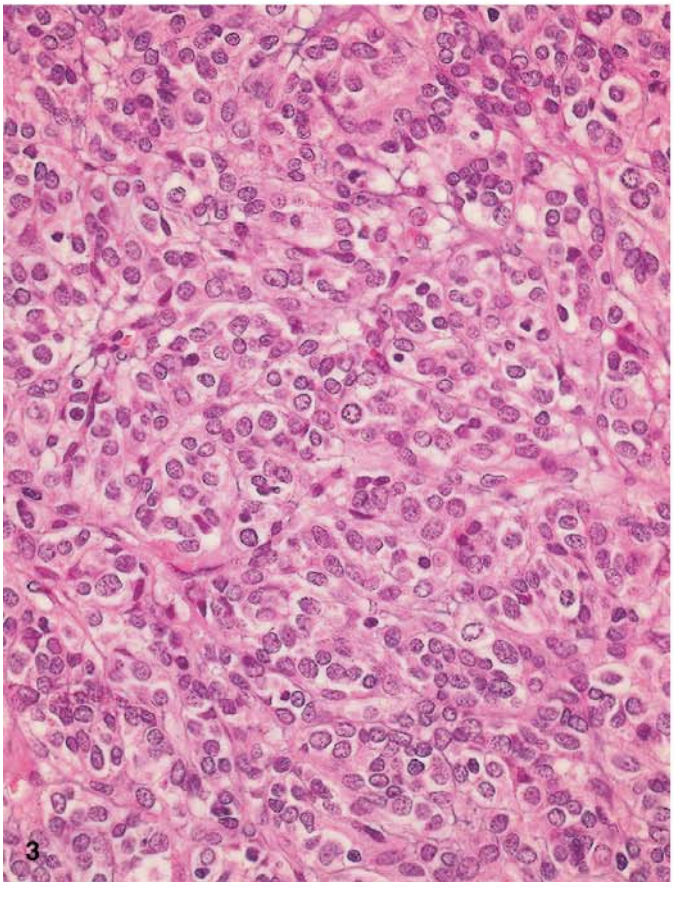
**Fig. 2** Gastrointestinal stromal tumor: spindle cell type. A peculiar feature, observed most often in gastric neoplasm, is the presence of striking juxtanuclear cytoplasmic vacuoles. Hematoxylin and eosin, ×40

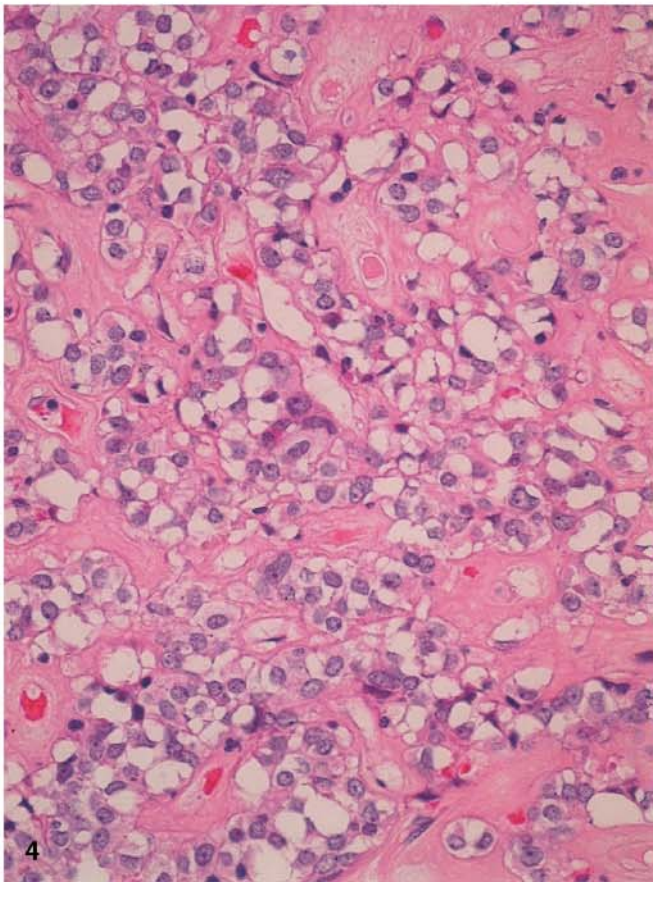
**Fig. 3** Gastrointestinal stromal tumor: epithelioid cell type. Hematoxylin and eosin, ×40

**Fig. 4** Gastrointestinal stromal tumor: epithelioid cell type. Clearing of cytoplasm is seen. Hematoxylin and eosin, ×40


1


2


3


4

## Targeted therapy in GIST

The first clinical use of STI-571 (imatinib mesylate) was to treat chronic myeloid leukemia, a hematological disorder whose cytogenetic hallmark is a balanced chromosome 9 and 22 translocation. This cytogenetic aberration leads to the formation of the BCR-ABL chimeric protein characterized by a constitutionally activated tyrosine kinase activity. STI-571 proved effective in blocking the ABL kinase activity both in vitro and in vivo [9, 10] and by early 2001 became available as an extremely effective treatment for patients with chronic myeloid leukemia. In the meantime STI-571 was seen not only to be effective in inhibiting the activity of ABL or of the BCR-ABL protein but could also block other transmembrane receptors with tyrosine kinase activity: namely KIT and platelet-derived growth factor receptor [5, 9, 57]. Growth arrest and apoptosis determined by STI-571 on human GIST cell lines was demonstrated [57], and soon thereafter the first patient affected by metastatic GIST was successfully treated [23].

The use of imatinib mesylate in cancer therapy is certainly one of the greatest success of translational research. In both chronic myeloid leukemia and GIST genetics and molecular pathology have provided fundamental insights regarding tumor biology and have also established a very basis for designing a new targeted therapy. At present hundreds of GIST patients are enrolled in clinical trials showing a disease response in about 50% of those with advanced unresectable or metastatic GIST and stable disease in another 28% [8]. Of course, an accurate assessment of the duration of the response is not yet available, and therefore more time need before definite conclusions can be drawn. However, if we consider that metastatic GIST has until now been a virtually incurable disease, these results undoubtedly present a major advance in cancer therapy. At the present time it is responsibility of the pathologists' community to provide clinicians with the highest diagnostic standards to ensure the most accurate selection of patients.

## The pathology of GIST

According to available data, GISTs account for about 2% of GI tract neoplasms [55]. However, this figure probably significantly underestimates the true incidence. GISTs tend to be distributed along the entire GI tract [11]. Some 50–60% of cases arise in the stomach, 20–30% in the small bowel [16, 58], 10% in the large bowel [59, 60], and 5% in the esophagus [37]. Lesions that are morphologically and immunophenotypically indistinguishable from conventional GISTs have also been seen to occur in extragastrointestinal locations such as mesentery, omentum, and retroperitoneum [35, 44].

The morphological diagnosis of GIST appears to be relatively simple. The majority of cases can be in fact be classified into three broad categories: spindle cell type (70%), epithelioid type (20%), and mixed spindle and epithelioid cell type (10%).

GISTs of spindle cell type are composed of uniform eosinophilic spindle cells organized in short fascicles or in a short storiform growth pattern (Fig. 1). The neoplastic cells tend to have light eosinophilic cytoplasm, often with indistinct cell borders. Nuclei tend to be oval shaped and uniform in appearance, often with vesicular chromatin. A peculiar albeit relatively infrequent feature, most often observed in gastric neoplasms, is by the presence of striking juxtanuclear cytoplasmic vacuoles (Fig. 2). This feature, in conjunction with the absence of ancillary diagnostic tools, led in the past to GISTs being misinterpreted as smooth muscle neoplasms. The presence of nuclear palisading is another potentially misleading histological feature, as is frequently observed in both smooth muscle and neural tumors. Cystic stromal degeneration and stromal hemorrhage may be a prominent feature.

GISTs of epithelioid type are composed of round-shaped cells exhibiting eosinophilic or clear cytoplasm (Figs. 3, 4). Nuclei tend to be round-to-ovoid and uniform with vesicular chromatin. In comparison with spindle-cell GISTs, tumor cells tend more frequently to exhibit a nested growth pattern.

GISTs of mixed cell type may feature abrupt transition between spindle cell and epithelioid areas or as an alternative the two cell types may be intermingled.

In approximately 10–20% of cases (of either spindle cell or epithelioid type) hyaline or fibrillary brightly eosinophilic structures known as skeinoid fibers are seen. These structures appear to be composed of nodular tangles of collagen fibers [39] and typically exhibit periodic acid–Schiff (PAS) positivity (Fig. 5). Skenoid fibers are more frequent in lesions arising in the small bowel, where the tumors also tend to show a nesting, paragangliomalike growth pattern [1, 39]. Nuclear pleomorphism is seen only exceptionally (Fig. 6).

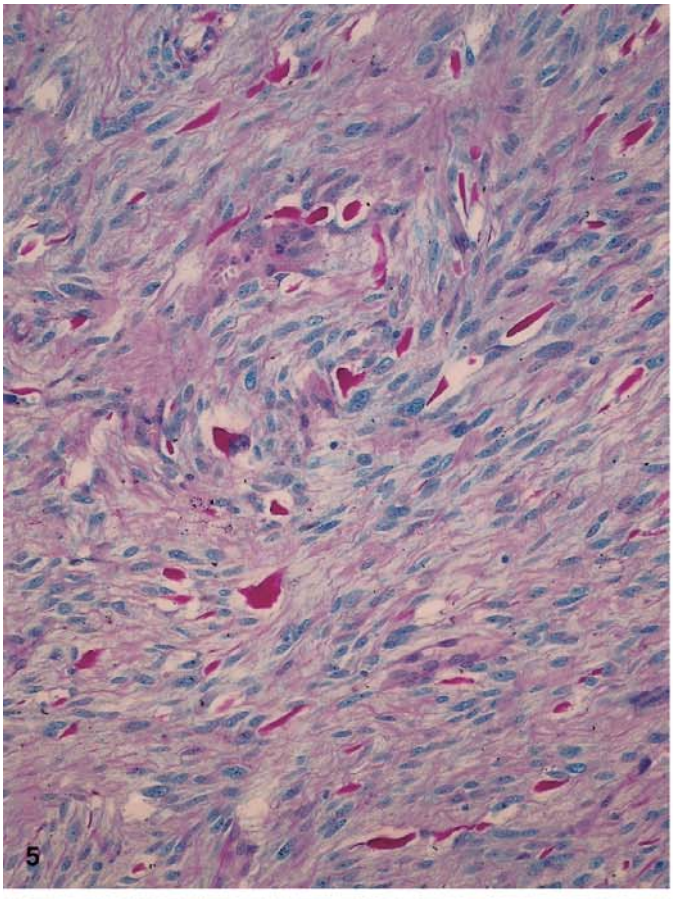
In view of the current clinical and therapeutic implications of KIT expression, immunophenotypic analysis has gained a major diagnostic role. As emphasized by the participants at the NIH Consensus Conference on GISTs, the term GIST should be limited to GI tract mesenchymal lesions displaying KIT (CD117) immunopositivity [13]. It should be noted that some exceptional lesions with typical cytoarchitectural features of GIST lack KIT expression. While this phenomenon is generally a technical artifact or sampling error, pathologists should be aware that a very small proportion of GISTs do lack *KIT* mutations and/or

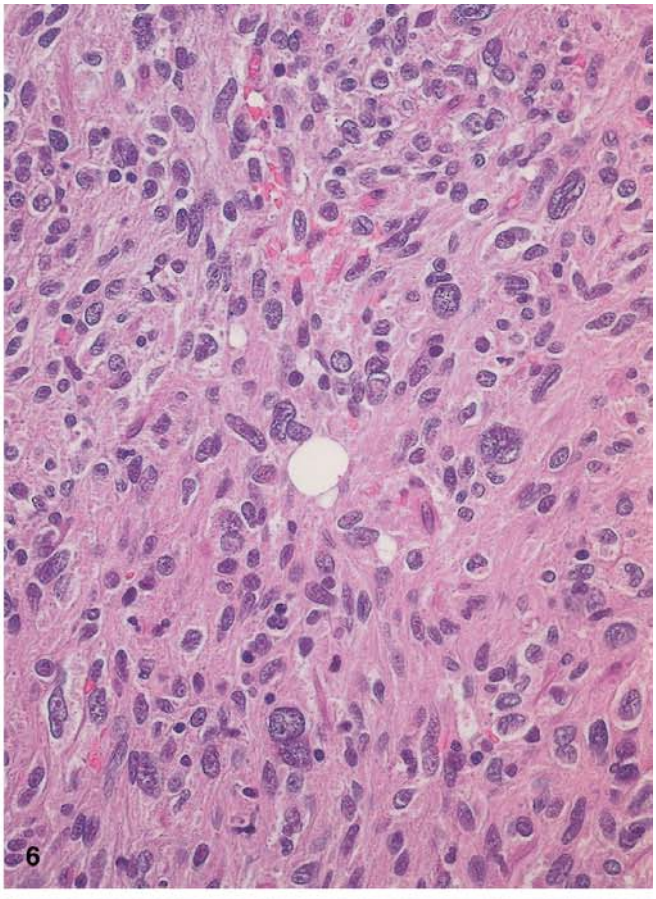
**Fig. 5** The presence of Periodic acid–Schif positive skeinoid fibers is most often observed in GIST arising in the small bowel. ×20

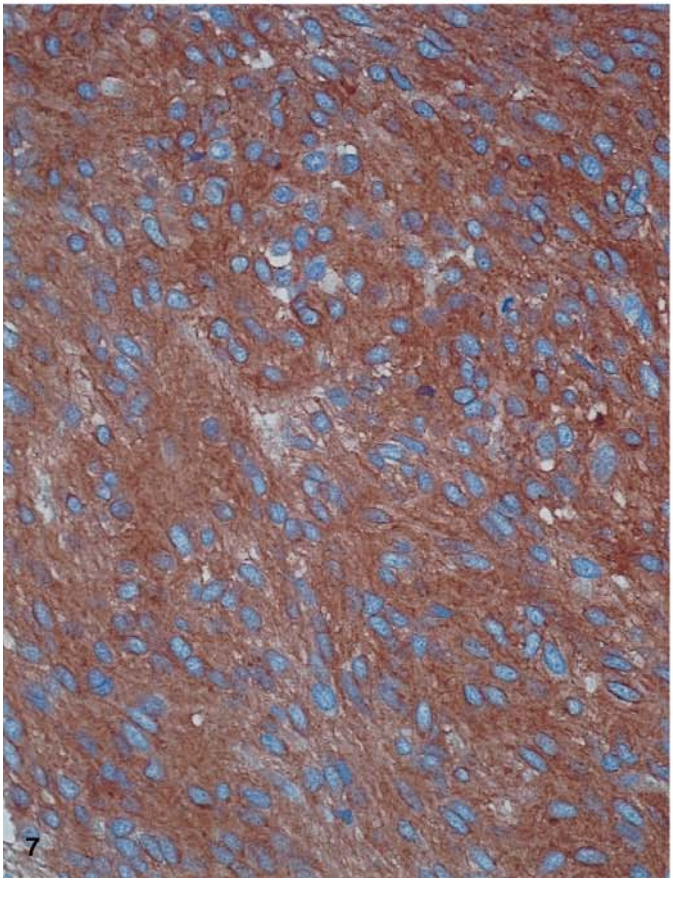
**Fig. 6** Nuclear pleomorphism is a rare finding in GISTs. Hematoxylin and eosin, ×40

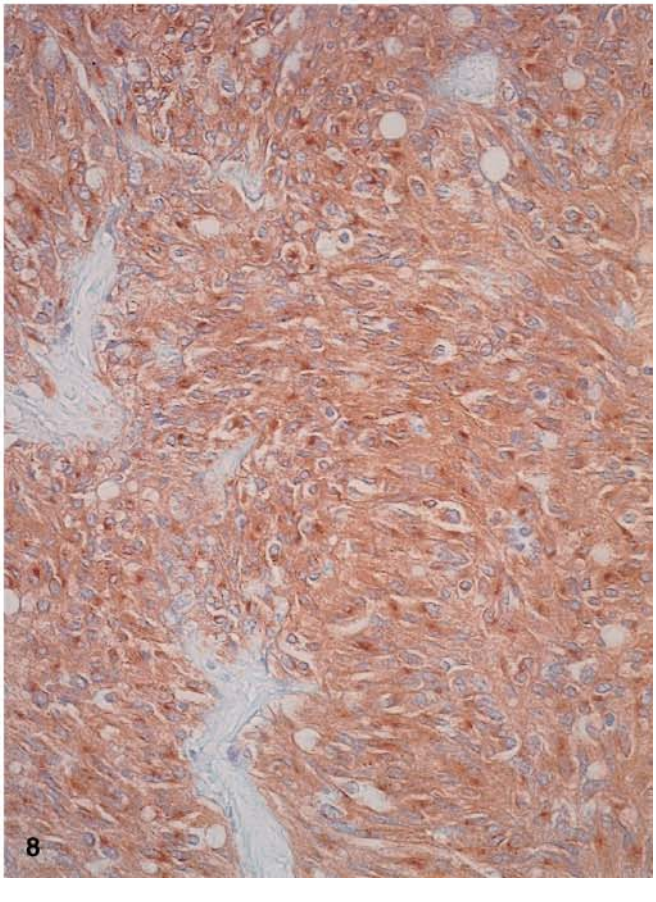
**Fig. 7** KIT immunoreactivity is typically cytoplasmic and diffuse. Immunoperoxidase, ×40

**Fig. 8** In some cases a paranuclear, dotlike accentuation of KIT immunopositivity is observed. Immunoperoxidase, ×20


5


6


7


8

KIT expression. The pattern of KIT expression is usually cytoplasmic and diffuse (Fig. 7). However, up to one-half of cases also show a dotlike accentuation of the staining (Fig. 8). More rarely a dotlike pattern is seen in the absence of diffuse cytoplasmic staining. The significance (if any) of these distinctive staining patterns has not yet been elucidated. KIT positivity is usually seen in the vast majority of neoplastic cells; however, expression can be rarely focal, therefore representing a potential diagnostic pitfall.

In view of the predictive value of KIT immunostaining strict application of quality controls protocols is mandatory to minimize false-positive and false-negative results. It is also important to optimize preclinical conditions (mainly the type of fixative and time of fixation) to ensure reproducibility [14].

The great interest generated by the successful administration of STI-571 therapy for GISTs has led to attempts to evaluate KIT expression in almost every tumor type. Many "out-of-context" positive results appear to elude any biological rationale, and at least some of them are probably technical artifacts [21].

With the advent of KIT immunostaining the other phenotypic markers have lost some of their diagnostic utility. Nonetheless it must be recalled that approximately two-thirds of GISTs show immunopositivity for CD34, one-third for smooth muscle actin, and about 5% for S-100 protein, indicating a certain degree of immunophenotypic heterogeneity [48]. Again, as all these markers are not specific for GIST, they must be used in a panel with CD117.

## GIST and prognosis

Ensuring proper classification is not the only task of diagnostic pathology. For decades pathologists have struggled in the attempt to identify both gross and microscopic parameters to predict the clinical behavior of GISTs. One of the main achievements of the NIH Consensus Conference is to have provided a simple scheme for assessing the risk for aggressive behavior (Table 1) [13]. Many studies have analyzed the prognostic relevance of a variety of parameters such as anatomical location [1, 2, 11], patient age [11], mucosal invasion, tumor necrosis, and high cellularity, rather often leading to conflicting conclusions [11, 37]. Nonetheless, two morphological features have emerged as fairly reliable predictors of outcome: mitotic rate and tumor size [2, 7, 12, 15, 33, 43, 44]

Of course, when focusing on the individual case, there remains the problem of lesions smaller than 2 cm that parenthetically feature KIT abnormalities totally identical to those present in larger ones [6] or with a very low mitotic rate that occasionally metastasize. As this certainly is a possibility experienced by numerous referral centers, the opportunity to continue to label small, mitotically inactive GISTs as benign has become the object of sharp debate. When appropriate follow-up is available, it seems as though any GIST presenting with clinical symptoms or signs may potentially behave aggressively. In view of current data, and despite the frustration that this approach may generate among clinicians, it is important that pathologists refrain from calling GISTs "benign" [13]. It might be that in the future pathologists will be able to devise better prognostic parameters; however, for the time being we must admit that that even the use of immunohistochemical proliferation markers, DNA ploidy, and computer-assisted image analysis have not proved useful in a clinical context. Most probably other approaches such as KIT molecular analysis or molecular profiling of GISTs will succeed in allowing more reliable prognostication. Importantly, recent data indicate better 5-year recurrence-free survival for GISTs carrying exon 11 missense mutations [51].

**Table 1** NIH Consensus Conference approach for defining risk of aggressive behavior in gastrointestinal stromal tumors (*HPF* high-power fields) [13]

| | Size[a] | Mitotic count[b] |
|---|---|---|
| Very low risk | <2 cm | <5 per 50 HPF |
| Low risk | 2–5 cm | <5 per 50 HPF |
| Intermediate risk | <5 cm | 6–10 per 50 HPF |
| | 5–10 cm | <5 per 50 HPF |
| High risk | >5 cm | >5 per 50 HPF |
| | >10 cm | Any mitotic rate |
| | Any size | >10 per 50 HPF |

[a] Size is the single largest dimension
[b] Ideally mitotic count should be standardized according to surface area examined (based on size of high-power fields), but there are no agreed definitions in this regard

The scheme developed by the panelists of the NIH Consensus Conference to assess the risk of aggressive behavior incorporates these uncertainties and therefore prudently avoids providing any criteria to distinguish benign from malignant GISTs. Pathologists are simply asked to evaluate the size and the mitotic rate, which are unarguably reasonably reproducible and easily determinable morphological parameters. In the era of molecular sophistication it may be argued that the use of unsophisticated tools such as "rulers" and "eyeballing" appears inappropriate. However, as this scheme is based on the only two existing reliable prognostic parameters, its use in routine pathology practice must nevertheless be strongly advocated.

## Conclusions

The effective palliation of patients with metastatic GIST is certainly one of the brightest successes in clinical oncology. This is the result of a combined effort of different subspecialties, and pathologists have certainly contributed significantly. While it appears possible that other tumor types may be effectively targeted with this approach [53], it is important that any future use of

STI571 continue to be based on a solid rationale, rather than on an emotional basis.

To avoid misinterpretation it must be emphasized that it is still unclear how durable the efficacy of this treatment is, as is the percentage of tumors that eventually become resistant to therapy. However, this story remains paradigmatic of a totally new approach to cancer therapy that until now has been the most elegant translation of cancer biology experimental knowledge into clinical practice.

KIT is certainly the ideal target for such an innovative therapeutic approach as it has proved to be biologically relevant and, in contrast with HER-2 which is involved in less than one-third of breast cancers, is present in the vast majority of GISTs. Hopefully other KIT will emergeome, and attempts to target other molecules such as EGFR, VGEFR and others are already under way. However, it must be emphasized that the GIST model is relatively simple compared with other cancer types. The complete elucidation of the many molecular mechanisms underlying the different carcinogenic pathways will remain the baseline for further developing effective targeted therapies.

## References


1. Appelman HD (1986) Smooth muscle tumors of the gastrointestinal tract. What we know now that Stout didn't know. Am J Surg Pathol 10 [Suppl 1]:83–99
2. Appelman HD (1990) Mesenchymal tumors of the gut: historical perspectives, new approaches, new results and does it make any difference? Monogr Pathol 31:220–246
3. Appelman HD, Hellwigh EB (1977) Cellular leiomyomas of the stomach in 49 patients. Arch Pathol Lab Med 101:373–377
4. Blume-Jensen P, Claesson-Welsh L, Siegbahn A, Zsebo KM, Westermark B, Heldin CH (1991) Activation of the human c-kit product by ligand-induced dimerization mediates circular actin reorganization and chemotaxis. EMBO J 10:4121–4128
5. Buchdunger E, Cioffi CL, Law N, Stover D, Ohno-Jones S, Druker BJ, Lydon NB (2000) Abl protein-tyrosine kinase inhibitor STI571 inhibits in vitro signal transduction mediated by c-kit and platelet-derived growth factor receptor. J Pharmacol Exp Ther 295:139–145
6. Corless CL. McGreevey L, Haley A, Town A, Heinrich MC (2002) KIT mutations are common in incidental gastrointestinal stromal tumours one centimeter or less in size. Am J Pathol 160:1567–1572
7. DeMatteo RP, Lewis JJ, Leung D, Mudan SS, Woodruff JM, Brennan MF (2000) Two hundred gastrointestinal stromal tumors. Recurrence patterns and prognostic factors for survival. Ann Surg 231:51–58
8. Demetri GD, von Mehren M, Blanke CD, Van den Abbeele AD, Eisenberg B, Roberts PJ, Heinrich MC, Tuveson DA, Singer S, Janicek M, Fletcher JA, Silverman SG, Silberman SL, Capdeville R, Kiese B, Peng B, Dimitrijevic S, Druker BJ, Corless C, Fletcher CD, Joensuu H (2002) Efficacy and safety of imatinib mesylate in advanced gastrointestinal stromal tumors. N Engl J Med 347:472–480
9. Druker BJ, Tamura S, Buchdunger E, Ohno S, Segal GM, Fanning S, Zimmermann J, Lydon NB l (1996) Effect of a selective inhibitor of the Abl tyrosine kinase on the growth of Bcr-Abl positive cells. Nat Med 2:561–566
10. Druker BJ, Talpaz M, Resta DJ, Peng B, Buchdunger E, Ford JM, Lydon NB, Kantarjian H, Capdeville R, Ohno-Jones S, Sawyers CL (2001) Efficacy and safety of a specific inhibitor of the BCR-ABL tyrosine kinase in chronic myeloid leukaemia. N Engl J Med 344:1031–1037
11. Emory TS, Sobin LH, Lukes L, Lee DH, O'Leary TJ (1999) Prognosis of gastrointestinal smooth muscle (stromal) tumors. Dependence on anatomic site. Am J Surg Pathol 23:82–87
12. Evans HL (1985) Smooth muscle tumors of the gastrointestinal tract. A study of 56 cases followed for a minimum of 10 years. Cancer 56:2242–2450
13. Fletcher CDM, Berman JJ, Corless C, Gorstein F, Lasota J, Longley BJ, Miettinen M, O'Leary TJ, Remotti H, Rubin BP, Shmookler B, Sobin LH, Weiss SW (2002) Diagnosis of gastrointestinal stromal tumours: a consensus approach. Hum Pathol 33:459–465
14. Fletcher CDM, Flecther JA (2002) Testing for Kit (CD117) in gastrointestinal stromal tumours: another HercepTest Appl Immunohistochem Mol Morphol 10:197–198
15. Franquemont DW (1995) Differentiation and risk assessment of gastrointestinal stromal tumors. Am J Clin Pathol 103:41–47
16. Goldblum JR, Appelman HD (1995) Stromal tumors of the duodenum. A histologic and immunohistochemical study of 20 cases. Am J Surg Pathol 19:71–80
17. Golden T, Stout AP (1941) Smooth muscle tumours of the gastrointestinal tract and retroperitoneal tissues. Surg Gynecol Obstet 73:784–710
18. Heinrich MC, Rubin BP, Longley JL, Fletcher JA (2002) Biology and genetic aspects of gastrointestinal stromal tumours: kit activation and cytogenetics alterations. Hum Pathol 3:484–495
19. Herrera GA, Pinto de Moraes H, Grizzle WE, Han SG (1984) Malignant small bowel neoplasm of enteric plexus derivation (plexosarcoma). Light and electron microscopic study confirming the origin of the neoplasm. Dig Dis Sci 29:275–284
20. Hirota S, Isozaki K, Moriyama Y, Hashimoto K, Nishida T, Ishiguro S, Kawano K, Hanada M, Kurata A, Takeda M, Muhammad Tunio G, Matsuzawa Y, Kanakura Y, Shinomura Y, Kitamura Y (1998) Gain-of-function mutations of c-kit in human gastrointestinal stromal tumors. Science 279:577–580
21. Hornick JL, Fletcher CDM (2002) Immunohistochemical staining for KIT in soft tissue sarcomas is very limited in distribution. Am J Clin Pathol 117:188–193
22. Isozaki K, Hirota S, Nakama A, Miyagawa J, Shinomura Y, Xu Z, Nomura S, Kitamura Y (1995) Disturbed intestinal movements, bile reflux to the stomach, and deficiency of c-kit expressing cells in Ws/Ws mutant rats. Gastroenterology 109:456–464
23. Joensuu H, Roberts PJ, Sarlomo-Rikala M, Andersson LC, Tervahartiala P, Tuveson D, Silberman SL, Capdeville R, Dimitrijevic S, Druker B, Demetri G (2001) Effect of the tyrosine kinase inhibitor STI571 in a patient with a metastatic gastrointestinal stromal tumour. N Engl J Med 344:1052–1056
24. Kindblom L-G, Remotti HE, Aldenborg F, Meis-Kindblom JM (1998) Gastrointestinal pacemaker cell tumor (GIPACT): gastrointestinal stromal tumors show phenotypic characteristics of the interstitial cells of Cajal. Am J Pathol 152:1259–1269
25. Kitamura Y, Go S (1979) Decreased production of mast cells in SI/Sid anemic mice. Blood 53:92–497
26. Kluppel M, Huizinga JD, Malysz J, Bernstein A (1998) Developmental origin and KIT-dependent development of the interstitial cell of Cajal in the mammalian small intestine. Dev Dyn 211:60–71
27. Lauwers GY, Erlandson RA, Casper ES, Brennan MF, Woodruff JM (1993) Gastrointestinal autonomic nerve tumors: a clinicopathologic, immunohistochemical and ultrastructural study of 12 cases. Am J Surg Pathol 17:887–897
28. Lee JR, Joshi V, Griffin JW, Lasota J, Miettinen M (2001) Gastrointestinal autonomic nerve tumor: immunohistochemical and molecular identity with gastrointestinal stromal tumor. Am J Surg Pathol 25:979–987
29. Lux ML, Rubin BP, Biase TL, Chen CJ, Maclure T, Demetri G, Xiao S, Singer S, Fletcher CD, Fletcher JA (2000) KIT extracellular and kinase domain mutations in gastrointestinal stromal tumors. Am J Pathol 156:791–795

30. Maeda H, Yamagata A, Nishikawa S, Yoshinaga K, Kobayashi S, Nishi K, Nishikawa S (1992) Requirement of c-kit for development of intestinal pacemaker system. Development 116:369–375
31. Majumder S, Brown K, Qiu FH, Besmer P (1988) c-Kit protein, a transmembrane kinase: identification in tissue and characterization. Mol Cell Biol 8:4896–4902
32. Mazur MT, Clark HB (1983) Gastric stromal tumors: reappraisal of histogenesis. Am J Surg Pathol 7:507–519
33. Miettinen M, Lasota J (2001) Gastrointestinal stromal tumors definition, clinical, histological, immunohistochemical and molecular genetic features and differential diagnosis. Virchows Arch 438:1–12
34. Miettinen M, Virolainen M, Sarlomo-Rikala M (1995) Gastrointestinal stromal tumors: value of CD34 antigen in their identification and separation from true leiomyomas and schwannomas. Am J Surg Pathol 19:207–216
35. Miettinen M, Monihan JM, Sarlomo-Rikala M, Kovatich AJ, Carr NJ, Emory TS, Sobin LH (1999) Gastrointestinal stromal tumors/smooth muscle tumors (GISTs) primary in the omentum and mesentery: clinicopathologic and immunohistochemical study of 26 cases. Am J Surg Pathol 23:1109–1118
36. Miettinen M, Sarlomo-Rikala M, Lasota J (1999) Gastrointestinal stromal tumors: recent advances in understanding of their biology. Hum Pathol 30:1213–1230
37. Miettinen M, Sarlomo-Rikala M, Sobin LH, Lasota J (2000) Esophageal stromal tumors. A clinicopathologic, immunohistochemical and molecular genetic study of 17 cases and comparison with esophageal leiomyomas and leiomyosarcomas. Am J Surg Pathol 24:211–222
38. Mikhael AI, Bacchi CE, Zarbo RJ, Ma CK, Gown AM (1994) CD34 expression in stromal tumors of the gastrointestinal tract. Appl Immunohistochem 2:89–93
39. Min K-W (1992) Small intestinal stromal tumors with skeinoid fibers. Clinicopathological, immunohistochemical and ultrastructural investigations. Am J Surg Pathol 16:145–155
40. Nakama A, Hirota S, Okazaki T, Nagano K, Kawano S, Hori M, Kitamura Y (1998) Disturbed pyloric motility in Ws/Ws mutant rats due to deficiency of c-kit-expressing interstitial cell of Cajal. Pathol Int 48:843–849
41. Newman PL, Wadden C, Fletcher CDM (1991) Gastrointestinal stromal tumours: correlation of immunophenotype with clinicopathologic features. J Pathol 164:107–117
42. Oosterom AT van, Judson I, Verweij J, Stroobants S, Donato di Paola E, Dimitrijevic S, Martens M, Webb A, Sciot R, Van Glabbeke M, Silberman S, Nielsen OS (2001) Safety and efficacy of imatinib (STI571) in metastatic gastrointestinal stromal tumours: a phase I study. Lancet 358:1421–1423
43. Ranchod M, Kempson RL (1977) Smooth muscle tumors of the gastrointestinal tract and retroperitoneum. A pathologic analysis of 100 cases. Cancer 39:255–262
44. Reith JD, Goldblum JR, Lytes RH, Weiss SW (2000) Extragastrointestinal (soft tissue) stromal tumors: an analysis of 48 cases with emphasis on histologic predictors of outcome. Mod Pathol 13:577–585
45. Ricci A, Ciccarelli O, Cartun RW, Newcombe P (1987) A clinicopathologic and immunohistochemical study of 16 patients with small intestinal leiomyosacomas. Limited utility of phenotyping. Cancer 60:1790–1799
46. Rubin BP, Fletcher JA, Fletcher CDM (2000) Molecular insights into the histogenesis and pathogenesis of gastrointestinal stromal tumors. Int J Surg Pathol 8:5–10
47. Rubin BP, Singer S, Tsao C, Duensing A, Lux ML, Ruiz R, Hibbard MK, Chen CJ, Xiao S, Tuveson DA, Demetri GD, Fletcher CD, Fletcher JA (2001) KIT activation is a ubiquitous feature of gastrointestinal stromal tumours. Cancer Res 61:8118–8121
48. Rudolph P, Chiaravalli AM, Pauser U, Oschlies I, Hillemanns M, Gobbo M, Marichal M, Eusebi V, Hofler H, Capella C, Kloppel G (2002) Gastrointestinal mesenchymal tumors immunophenotypic classification and survival analysis. Virchows Arch 441:238–248
49. Saint Aubain Somerhausen N de, Fletcher CDM (1998) Gastrointestinal stromal tumours: an update. Sarcoma 2:133–141
50. Sarlomo-Rikala M, Kovatich AJ, Barusevicius A, Miettinen M (1998) CD117: a sensitive marker for gastrointestinal stromal tumors that is more specific than CD34. Mod Pathol 11:728–734
51. Singer S, Rubin BP, Lux ML, Chen CJ, Demetri GD, Fletcher CD, Fletcher JA (2002) Prognostic value of KIT mutation type, mitotic activity, and histologic subtype in gastrointestinal stromal tumors. J Clin Oncol 20:3898–3905
52. Sircar K, Hewlett BR, Huizinga JD, Chorneyko K, Berezin I, Riddell RH (1999) Interstitial cells of Cajal as precursors of gastrointestinal stromal tumors. Am J Surg Pathol 23:377–389
53. Sjoblom T, Shimizu A, O'Brien KP, Pietras K, Dal Cin P, Buchdunger E, Dumanski JP, Ostman A, Heldin CH (2001) Growth inhibition of dermatofibrosarcoma protuberans tumors by the platelet-derived growth factor receptor antagonist STI571 through induction of apoptosis. Cancer Res 61:5778–5783
54. Stout AP (1967) Bizarre smooth muscle tumours of the stomach. Cancer 15:400–409
55. Thomas RM, Sobin LH (1995) Gastrointestinal cancer: incidence and prognosis by histologic type. SEER population-based data: 1973–1987. Cancer 75:154–170
56. Torihashi S, Nishi K, Tokutomi Y, Nishi T, Ward S, Sanders KM (1999) Blockade of KIT signalling induces transdifferentiation of interstitial cells of Cajal to a smooth muscle phenotype. Gastroenterology 117:140–148
57. Tuveson DA, Willis NA, Jack T, Griffin JD, Singer S, Fletcher CDM, Fletcher JA, Demetri GD (2001) STI571 inactivation of the gastrointestinal stromal tumor c-KIT oncoprotein: biological and clinical implications. Oncogene 20:5054–5058
58. Tworek JA, Appelman HD, Singleton TP, Greenson JK (1997) Stromal tumors of the jejunum and ileum. Mod Pathol 10:200–209
59. Tworek JA, Goldblum JR, Weiss SW, Greenson JK, Appelman HD (1999) Stromal tumors of the abdominal colon. A clinicopathologic study of 20 cases. Am J Surg Pathol 23:937–945
60. Tworek JA, Goldblum JR, Weiss SW, Greenson JK, Appelman HD (1999) Stromal tumors of the anorectum. A clinicopathologic study of 22 cases. Am J Surg Pathol 23:946–954
61. Welsh RA, Meyer T (1969) Ultrastructure of gastric leiomyomas. Arch Pathol 87:71–81

Virchows Arch (2003) 442:429–436
DOI 10.1007/s00428-003-0797-z

ORIGINAL ARTICLE

**Reinhard Ullmann · Massimo Bongiovanni · Iris Halbwedl · Susanna Petzmann · Margit Gogg-Kammerer · Anna Sapino · Mauro Papotti · Gianni Bussolati · Helmut H. Popper**

# Bronchiolar columnar cell dysplasia—genetic analysis of a novel preneoplastic lesion of peripheral lung

Received: 26 July 2002 / Accepted: 5 March 2003 / Published online: 9 April 2003
© Springer-Verlag 2003

**Abstract** Atypical adenomatous hyperplasia is the only known precursor lesion of lung adenocarcinomas (ACs) so far. Here, we describe a new dysplastic lesion in the bronchioles of peripheral lung for which we propose the name bronchiolar columnar cell dysplasia (BCCD). Eight of fourteen BCCDs were successfully analyzed by means of comparative genomic hybridization (CGH). The average number of chromosomal aberrations was 2.6 in BCCD and 14.7 in concomitant AC. Among the aberrations were losses of 3p, 9, 13, 14 and gains of 1q, 17, 19q and 20q. Summarizing our data from morphological and genetic analysis, we conclude that BCCD is a preneoplasia of the bronchiolar epithelium and most probably represents an additional precursor lesion of lung adenocarcinomas.

**Keywords** Bronchiolar dysplasia · Comparative genomic hybridization · Lung adenocarcinoma

## Introduction

While adenocarcinoma (AC) of the lung is the most common pulmonary carcinoma in industrialized countries, its proposed preneoplastic lesion, atypical adenomatous hyperplasia (AAH) is rare [10]. Although in the past few years pulmonary pathologists have put much effort on the detection of AAH, its occurrence is still unproportionally infrequent when compared with the dramatic increase of its carcinomatous counterpart. Improved diagnostic techniques that enable the diagnosis of early-stage carcinomas, e.g., high resolution and spiral computed tomography, have so far not contributed to an increase in the diagnosis of AAH.

In the pancreas and prostate, a precursor lesion of AC with columnar cell morphology is well established and has already been genetically connected to AC [1, 3, 8, 15]. Loss of heterozygosity (LOH) studies on normal epithelium adjacent to different lung carcinomas, including small cell carcinoma (SCLC), squamous cell carcinoma (SQCC) and AC indicate that the pathogenesis of these tumors differs significantly and suggest a special way of tumorigenesis in AC not comparable with that of SQCC and SCLC [17]. Here, we present the morphological and genetic analysis of a new potential preneoplastic lesion of lung AC arising in bronchioles, for which we propose the name bronchiolar columnar cell dysplasia (BCCD).

R. Ullmann · I. Halbwedl · S. Petzmann · M. Gogg-Kammerer · H. H. Popper (✉)
Laboratories of Molecular Cytogenetics,
Environmental and Respiratory Pathology, Institute of Pathology,
Auenbruggerplatz 25, 8036 Graz, Austria
e-mail: popper@uni-graz.at
Fax: +43-316-384329

M. Bongiovanni · A. Sapino · M. Papotti · G. Bussolati
Department of Biomedical Science and Oncology,
University of Torino,
Torino, Italy

## Materials and methods

Initiated by three consultation cases, which showed multiple bronchiolar dysplastic foci in bronchioles of fibrotic lung, we reviewed the most recent AC cases for a similar dysplasia. Of 25 consecutive cases of AC, 11 with dysplastic lesions were detected in formalin-fixed, paraffin-embedded tissues. The selection criteria were cytological and structural atypia confined to bronchiolar epithelium. The age of the patients ranged from 38 years to 78 years (Table 1). For histological evaluation, the first of a consecutive series of 5-μm sections was stained by hematoxylin and eosin (HE). For laser microdissection the sections were stained with diluted Harris hematoxylin solution (Merck, FRG). At least 500 cells per case were laser-microdissected (PALM, Bernried, FRG) by an experienced pathologist. Degenerate oligonucleotide primer polymerase chain reaction (DOP-PCR) consisted of six low-stringency and 34 high-stringency cycles using the Qiagen hot-start polymerase and the respective buffers provided by the manufacturer. In every round of PCR, a normal control was co-amplified and also analyzed using comparative genomic hybridization (CGH) against non-amplified DNA in a sex mismatched manner. Thresholds were determined that way that, with the exception of the telomeric regions and the X-chromosome, the complete 99% confidence interval was within this range in the male normal versus female normal hybridization. LOH analysis using two microsatellite markers located at 9p and one at 9q (D9S161, D9S970 and

**Table 1** Patient data: in the location column, far means at least 1 cm apart from the carcinoma, in most cases BCCD was found in normal control lung sections taken from another segment; close means adjacent to the carcinoma, usually the same segment, but always in an uninvolved bronchiole. *AC* adenocarcinoma, *BCCD* bronchiolar columnar cell dysplasia, *CGH* comparative genomic hybridization, *AAH* atypical adenomatous hyperplasia

| Case no. | Age (years) | Sex | Type of carcinoma | Precursor lesion | Proximity of BCCD | CGH successful in: |
|---|---|---|---|---|---|---|
| 1 | 60 | M | Anaplastic carcinoma, in situ AC | BCCD low grade | Far | BCCD, ** |
| 2 | 70 | M | No carcinoma, end stage lung fibrosis | BCCD high grade | | BCCD |
| 3 | 53 | F | No carcinoma, sclerodermia | BCCD high grade | | BCCD |
| 4 | 38 | M | No carcinoma, end stage lung fibrosis | BCCD high grade | | BCCD |
| 5 | 65 | M | Adenosquamous carcinoma | BCCD low and high grade | Far and close | BCCD |
| 6 | 70 | M | Mixed AC, papillary, tubular, bronchioloalveolar, solid, mucinous | BCCD low and high grade | Far | BCCD, AC |
| 7 | 72 | M | Mixed AC, tubular, acinar, solid | BCCD high grade | Far | BCCD, AC |
| 8 | 58 | M | Mixed AC, papillary, bronchioloalveolar, multicentric | BCCD high grade | Close | BCCD, AC |
| 9 | 54 | F | Mixed AC, tubular, papillary, multicentric | BCCD low grade, AAH | Far | * |
| 10 | 78 | M | Mixed AC, papillary, embryonal | BCCD high and low grade, AAH | Far | * |
| 11 | 58 | M | Mixed AC, papillary, bronchioloalveolar, multicentric | BCCD high grade | Close | * |
| 12 | 45 | M | Mixed AC, acinar, papillary, embryonal | BCCD low and high grade | Far | * |
| 13 | 60 | M | Mixed AC, papillary, bronchioloalveolar, multicentric | BCCD low and high grade, AAH | Close | * |
| 14 | 61 | M | Mixed AC, tubular, acinar | BCCD low grade | Far | * |

* In these cases the BCCD was too small or lost on subsequent sections, or the DNA was degraded
** In anaplastic carcinoma there were diffuse infiltrating single cells and small cell clusters of no more than four cells together—microdissection resulted in non-sufficient DNA

**Table 2** Features of bronchiolar columnar cell dysplasia (BCCD) grades in contrast to normal and regenerating bronchiolar epithelium. *Bas* basal cells, *Res* reserve cells, *Col* columnar cells, *Clara* Clara cells, *ACis* adenocarcinoma in situ

| | Normal | Regenerative | BCCD low grade | BCCD high grade | ACiS |
|---|---|---|---|---|---|
| Structural atypia | | | | | |
| Ordered layers from basal lamina | Bas-Res-Col/Clara | Present* | Present in part* | No* | no |
| Nuclear crowding | No | No | Yes, in middle layers* | Yes* | Yes |
| Cytologic atypia | | | | | |
| Nuclei: enlarged | No | No, slightly | Slightly | Moderate to severe (up to double size of normal) | Severe |
| Irregular contour | No | No | No | Yes | Yes |
| Condensed chromatin at nuclear membrane | No | No | Yes/No | Yes | Yes |
| Chromatin finely distributed | Yes | Yes | Yes | Yes/No | No |
| Chromatin condensed | No | No | Yes/No | Yes | Yes |
| Chromatin coarse | No | No | No | Yes | Yes |
| Multinucleation | No | No | No | Yes | Yes |
| Pseudoinclusions | No | No | No | Yes | Yes |
| Nucleoli: inconspicuous | Yes | Yes | Yes/No | No | No |
| Enlarged | No | Yes, slightly | Yes, slightly | Yes | Yes |
| Irregular contour | No | No | Yes, sometimes | Yes | Yes |

* Structural atypia and/or nuclear crowding is seen only in larger but not in terminal respiratory bronchioli or alveolar ducts

D9S1690) was performed in six cases, where enough material was available, as described previously [12].

## Results

BCCD could be characterized by structural as well as cytologic atypia. Structurally there was a loss of organization of the epithelial layers: basal and reserve cells were replaced by uniform atypical columnar cells, and with increase of dysplasia these uniform cells replaced also the various differentiated bronchiolar cells, cylindrical as well as cuboidal (Fig. 1, Fig. 2, Fig. 3a, b). Cytologically these dysplastic cells showed loss of polar orientation of the nuclei, enlargement of nuclei and nucleoli, irregular nuclear contours, a coarse and/or condensed chromatin, and sometimes multinucleation (Fig. 1, Fig. 2, Fig. 3a, b; Table 2). High-grade BCCD was clearly distinguishable from normal and regenerating epithelium, because the




**Fig. 1** **a** Focally mild bronchiolar columnar cell dysplasia (BCCD; case 9) in an area of branching small bronchioles. Each of these branches is surrounded by smooth muscle cells. There is a loss of basal and reserve but also columnar differentiated cells, and a disorganization of the nuclei; nuclei are enlarged, and chromatin in some nuclei is condensed. Nucleoli are enlarged in some cells and also show irregular contours; in some areas and in the larger bronchiolus normal epithelium is retained; HE ×300. *Arrows* highlight groups of dysplastic cells in the accompanying schema (**b**)

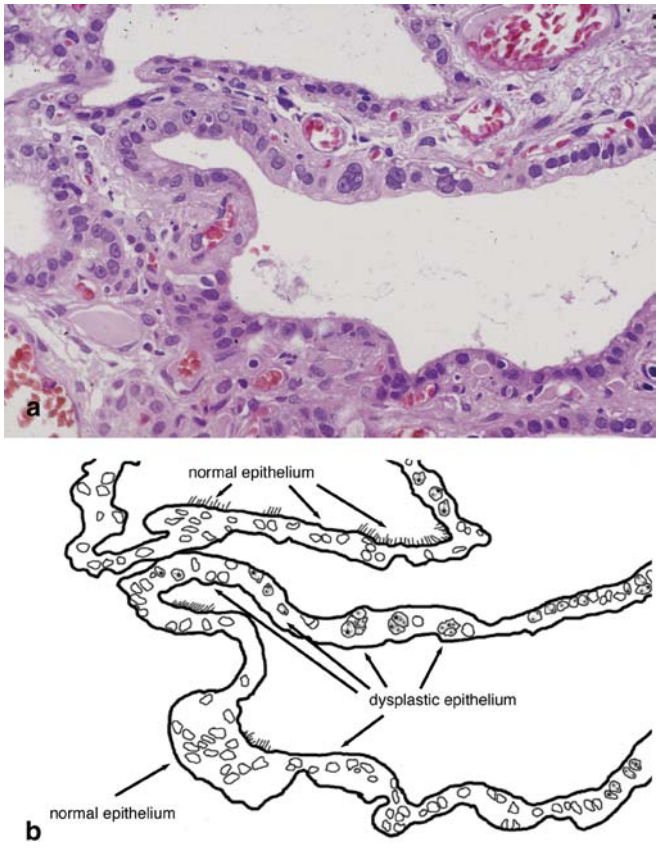



**Fig. 2** **a, b** Severe bronchiolar columnar cell dysplasia (BCCD) in a terminal respiratory bronchiole (case 4) and schema of the photograph; loss of polar orientation of the nuclei and multinucleation is seen, nuclei and nucleoli are enlarged, chromatin is condensed along the nuclear envelope; the dysplastic cells have completely replaced normal epithelium; reserve cells or Clara cells are no longer visible; there is also a sharp demarcation of BCCD from adjacent normal epithelium, where Clara and even a few ciliated cells are still visible; in this case, there is no structural atypia, because of just one epithelial layer; H&E ×380. *Arrows* highlight dysplastic epithelium in the accompanying schema (**b**)

cytologic atypia and structural derangement involved all epithelial layers. Low-grade BCCD was more difficult to assess, because cytologic atypia was confined to the basal layer. Therefore, it could only be separated from reactive or regenerative changes of the epithelium, when nuclear crowding and chromatin condensation were present. Also the evaluation of nuclear size and shape were helpful: In regeneration, there was a mixture of different cells present, for example basal cells with small round and dark stained nuclei, reserve cells with larger fine granular and lightly stained nuclei, and differentiated Clara cells with dome-shaped apical cytoplasm and round nuclei (Fig. 4a, b, c). In regenerating epithelium, differentiated epithelial cells could always be found. In addition, most often there was residual inflammation. In dysplasia there was a uniformity of cells and nuclei.

Grading of BCCD obviously was difficult, because the composition of the normal epithelium changes with bronchiolar generations: the percentage of ciliated columnar and triangular basal cells decrease toward the periphery while Clara cells and secretory columnar cells increase. In general, the number of the epithelial cell layers decreased toward the periphery from 3–5 layers in large bronchioles to a single cell layer in the third generation of terminal bronchioles. Therefore, structural disorganization as a criterion for dysplasia is limited to larger bronchioles. In terminal up to small bronchioli, the criteria for dysplasia has to rely on cytological atypia.

BCCD could be distinguished from retrograde infiltrating carcinoma, because in BCCD the epithelial proliferation is focal, embedded and surrounded by normal epithelium, whereas in retrograde infiltrating AC multi-layered epithelial papillae protruding out of normal epithelium were frequent. BCCD also had smaller nuclei and nucleoli than AC. Cribriform and papillary structures

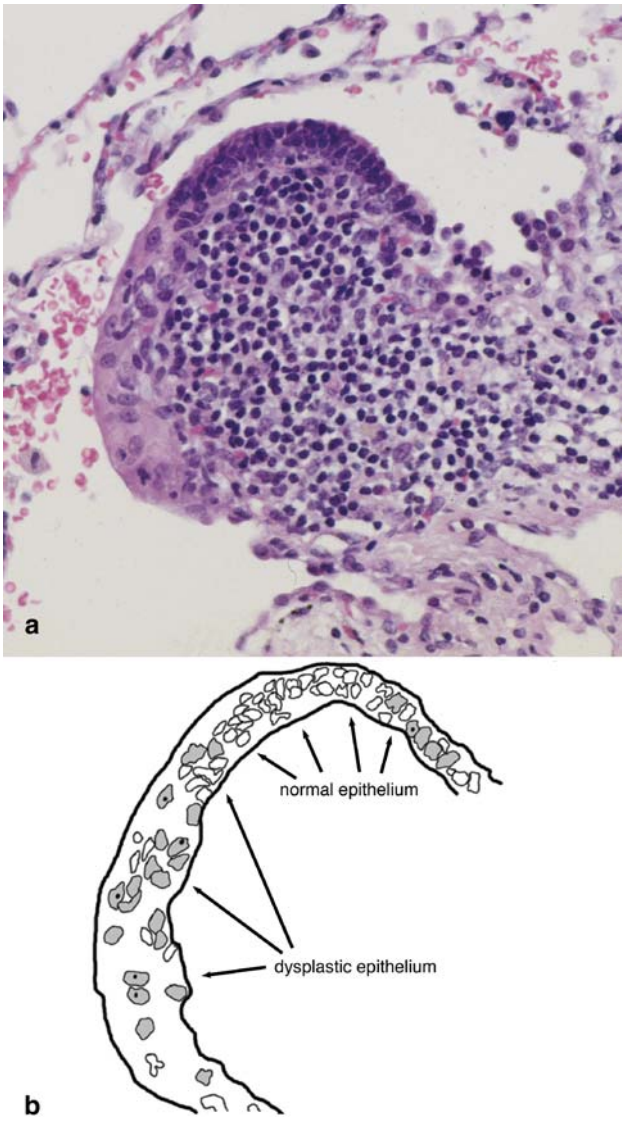



**Fig. 3** **a, b** Severe bronchiolar columnar cell dysplasia (BCCD; case 12) at the junction of a terminal bronchiole and a ductus alveolaris; the small size of BCCD is evident. At the top there are differentiated bronchiolar cells with small nuclei, whereas to the left side irregular shaped and enlarged atypical nuclei comprise this BCCD; at the bottom there is an alveolar duct again with normal epithelium; HE ×380. *Arrows* highlight dysplastic cells in the accompanying schema

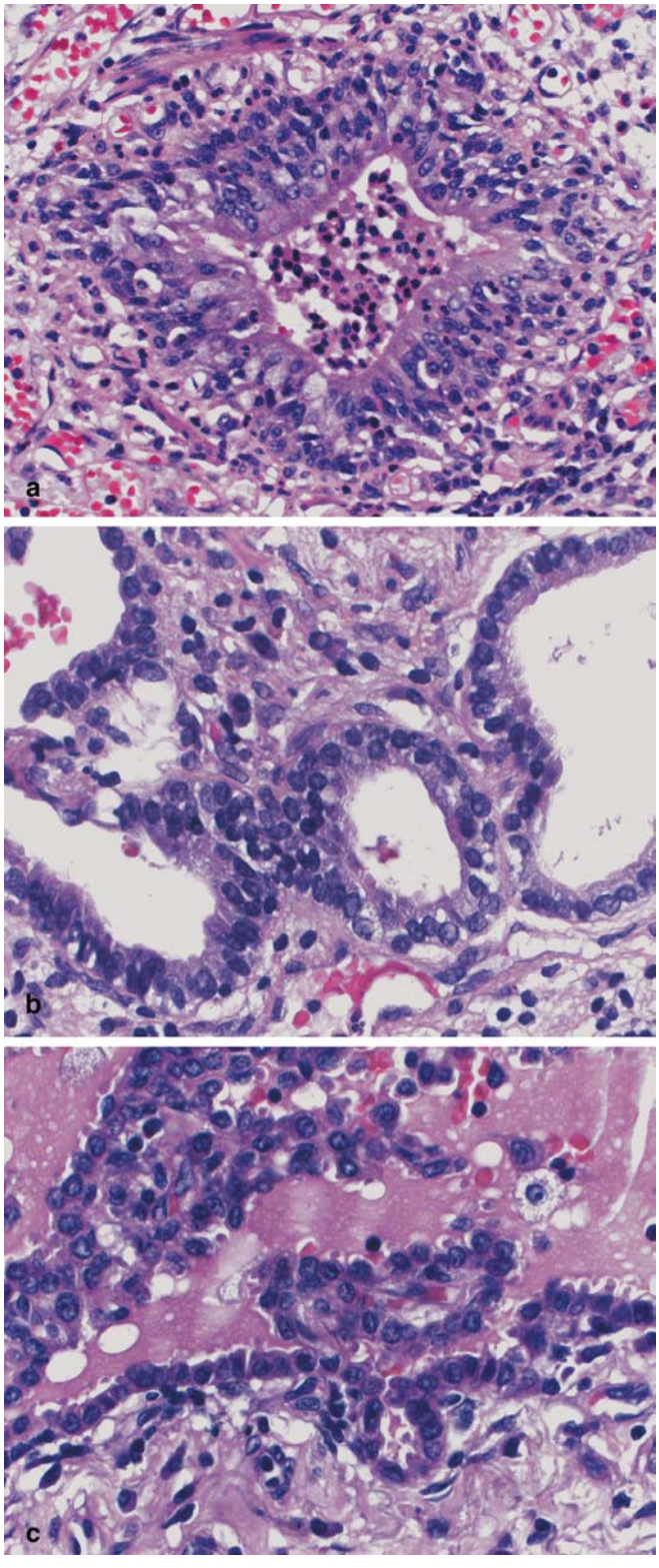



**Fig. 4** Regenerating epithelium in bronchioles. **a** A larger bronchiolus is shown. The epithelium is multi-layered; within the epithelium, enlarged lightly stained nuclei are seen, but without irregular nucleoli, and without chromatin condensation. The regenerating epithelium also shows different degrees of differentiation into the diverse cell types, such as tall columnar cells and some goblet cells. **b** A small bronchiolus is shown. The regenerating epithelium consists predominately of Clara cells mixed with reserve cells, the latter characterized by their lesser stained chromatin and cytoplasm. **c** Epithelial regeneration in a terminal bronchiolus is shown. The single layered epithelium is composed of Clara and reserve cells. The major difference to low-grade dysplasia is the non-uniformity of cells and nuclei due to ongoing cell differentiation, and the absence of chromatin condensation and irregular nucleoli. H&E ×320, ×480, ×480

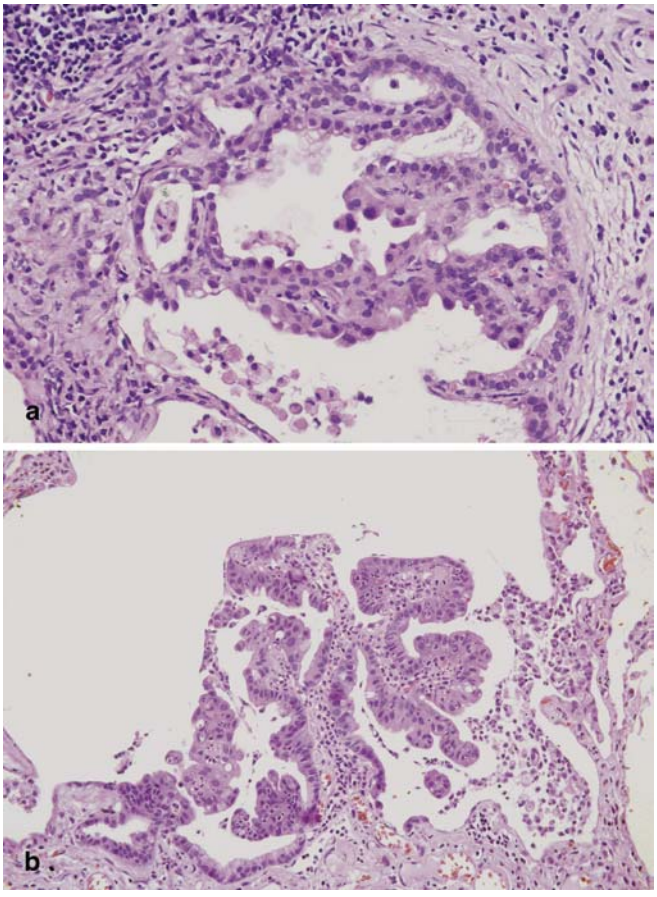



**Fig. 5** In-situ adenocarcinoma (case 1). **a** Tubular growth pattern with irregular formed cell bridges; some of these bridges also have a thin stroma stalk; at the edges remnants of normal bronchiolar epithelium is retained. **b** Papillary proliferation with multicellular papillae, some branches with a stroma stalk; in some areas there is nuclear crowding and nuclear polymorphism; in this case, there was an anaplastic carcinoma within the same lobe, but without a connection to these lesions; both lesions were close together, without invasion, and confined to the bronchiolar–alveolar junction; atypia is evident in both; H&E, ×200

were absent in BCCD, and there was no connection with the AC.

In one case also an in-situ AC with cribriform and papillary pattern (Fig. 5a, b) was seen in addition to BCCD and a diffuse infiltrating anaplastic carcinoma. Details of the other cases were given in Table 1.

### CGH and LOH studies

The average number of aberrations was 2.6 in BCCD and 14.7 in AC. The chromosomal aberrations found are summarized in Table 3. In three cases, we could compare the genetic aberrations of BCCD with that of the concomitant AC. Overlapping changes are highlighted in the table. The karyotypes of two isolated BCCDs and in addition a comparison of chromosomal aberrations in BCCD and coexisting carcinoma are shown (Fig. 6a, b, c). LOH was detected in two of six cases and confirmed the findings by CGH. Of 14 BCCD, 6 could not be evaluated by CGH, because of DNA degradation in combination with the small size of the lesions. The chromosomal regions of 1p36, 19p, 22, X and Y were not evaluated.

## Discussion

In this study, we describe a new dysplastic lesion of the lung, which we suppose to be another precursor of ACs. Unlike AAH, which can be detected macroscopically, BCCD detection requires high-magnification microscopy. This might be the reason why it has been overlooked so far, in addition to the fact that, on routine evaluation of ACs, not much attention is paid to adjacent or far away bronchioles. Atypical cell proliferations have already been recognized in the vicinity of different types of lung fibrosis, and it is known that ACs arise more frequently in the background of lung fibrosis [4, 13, 19]. In our series, we encountered three cases with lung fibrosis, all associated with high-grade BCCD. They all showed the same cytological atypia as those cases of BCCD associated with ACs in the same lobe or segment. Inflammation-associated atypia in regenerating epithelium might resemble BCCD, especially in the background of fibrosis. In these cases nuclear and nucleolar enlargement can prevail. The proliferation of Clara cells, which can extend into the alveolar region, as well as cuboidal transformed pneumocytes type II, which can dominate the bronchi-

**Table 3** Summary of chromosomal gains and losses in eight bronchiolar columnar cell dysplasia (BCCD) and three adenocarcinomas (ACs). BCCD and the coexisting AC are indicated by the same case number. Overlapping aberrations are highlighted in bold

| Tumor | Gains | Losses |
|---|---|---|
| BCCD 1 | 1q, 20q | 9p, 13q14–21 |
| BCCD 2 | 7q11.2, 17q, | 9 |
| BCCD 3 | 17, 19q, 20q13 | 3p12–23, 14q11.1–24 |
| BCCD 4 | – | – |
| BCCD 5 | – | 9q, 10q24-ter |
| BCCD 6 | – | – |
| AC 6 | 1q, 5p, 5q31-ter, 6p, 7, 14, 16, 17q | 3p, 4q28-ter, 6q, 8, 9q, 10q24-ter, 13, 15q14-ter, 17p, 18q, 20p |
| BCCD 7 | **7q11-q21** | 2p23-ter, **6q23-ter**, **12q23-ter**, 15q21-ter |
| AC 7 | 4q, 5p, **7q11–32**, 12p, 17 | 3p, 5q, **6q21-ter**, 8p, 9p, 11q24-ter, **12q22-ter**, 13q, 14q, 18, 20q |
| BCCD 8 | **13q32-ter**, **19q13.1** | **13q14–21** |
| AC 8 | 8q, 10q23-ter, **13q32-qter**, **19q13.1** | 3p12-p24, 4q24-ter, 9p23-q22, **13q13–21**, 14q |

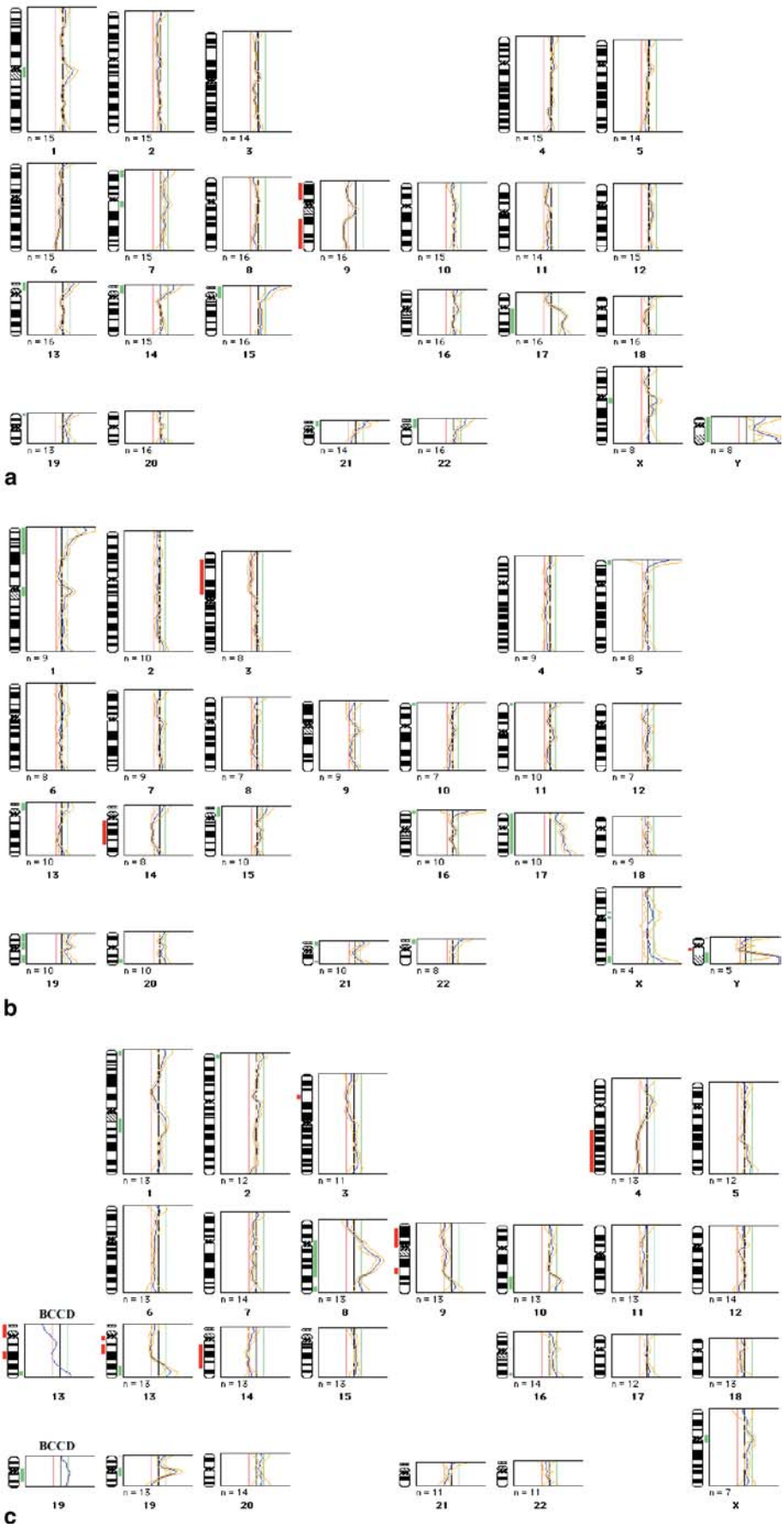



**Fig. 6 a**, **b** Chromosomal aberrations in two different bronchiolar columnar cell dysplasias (BCCDs) as detected by comparative genomic hybridization (CGH; cases 2 and 3). **c** Chromosomal changes in one BCCD and accompanying AC (case 8); changes in the BCCD are shown as *insets left* to the carcinoma chromosomes. Losses are shown on the *left side* of each idiogram in *red*, gains on the *right side* in *green*. The 99% confidence interval is shown in *brown*

oloalveolar junction, sometimes build up an epithelial multilayer. In the presence of inflammation-associated atypia, this may resemble dysplasia. One helpful criterion for the differential diagnosis is that in regenerative proliferation there is always a mixture of reserve and differentiated cells and never a sharp demarcation between restored and still regenerating epithelium. Therefore, specific cell types, such as columnar and Clara cells, can be recognized. The opposite is true for BCCD. In addition the other cytological features, such as irregular shaped nuclei and nucleoli, and coarse or condensed chromatin, are only seen in BCCD.

The resemblance of dysplastic and regenerating cells is not only of diagnostic impact, but also generates additional need to prove the neoplastic nature of these cells. Can the finding of chromosomal aberrations be taken as a proof for the neoplastic status of BCCD? The occurrence of chromosomal aberrations in normal and regenerative tissue has hardly been explored. In various organs, there is accumulating evidence that chromosomal aberrations can also be found in normal appearing cells in the epithelium as well as in stroma adjacent to carcinomas. Genetic changes in normal epithelium have also been found in the lung, but it seems, according to LOH studies, that the frequency and extent of chromosomal aberrations are highly dependent on the tumor type. In a LOH study done by Wistuba et al. in 90% of 22 SCLC and in 54% of 25 SQCC cases, the normal epithelium was affected by chromosomal changes; however, only 10% of 21 ACs showed LOH in the normal epithelium. The differences in the mean index of allelic loss, which also includes the extent of chromosomal aberrations, are even more significant: SCLC, 0.27; SQCC, 0.08; AC, 0.01 [17]. In a different study dealing with non-small cell lung cancer, and not distinguishing between SQCC and AC, the following frequencies of changes were found in the peritumoral normal bronchial cells: LOH at 5q21 in 37.5%, 3p21 in 22%, 9p21 in 27% and 17p in 13% [14]. Due to this rare occurrence of genetic changes in normal epithelium adjacent to AC, the finding of chromosomal aberrations seems to be a good indicator of neoplasia. The chromosomal aberrations found in BCCD, especially losses of 3p and chromosome 9 or parts of it, are very well known early aberrations in lung carcinomas and their preneoplastic lesions [5, 6, 7, 16, 18]. Also gains of 17q, which we have found in two of eight BCCDs, are frequent changes especially in non-small cell lung carcinomas [9, 11].

There are some clues indicating that BCCD precedes ACs. One is the topography, since AC like BCCD usually arises in the peripheral lung. The next one can be deduced by a comparison of BCCD with dysplasias from other organs. Despite some structural differences, the precursor lesions of ACs in prostate and pancreas share several morphological features with BCCD [1, 3]. In AAH, data derived from immunohistochemistry, flow cytometry and genetic analysis have revealed an overlap of abnormalities with AC [18]. Also a recent LOH study including AAH and the concomitant AC has genetically linked the preneoplasia to the carcinoma [18]. The chromosomal data acquired in our study also point to a connection between BCCD and AC. We succeeded to get CGH data on three BCCDs coexisting with AC. While one dysplasia showed no aberrations at all, in two cases BCCD and the carcinoma shared some chromosomal aberrations (Table 3). Also in AAH, overlapping abnormalities with AC have been described [2, 18].

According to our data derived from morphology, immunohistochemistry, and CGH, BCCD is a preneoplasia of the bronchiolar epithelium and most probably represents an additional precursor lesion of AC of the lung.

**Acknowledgements** We gratefully acknowledge the support by the Austrian Research Fund (FWF project P14759) and the Styrian Cancer Society Foundation (to HHP). RU and SP were supported by the Austrian National Bank Jubilee Fund (Projects OeNB 7645 and 8454), which is also gratefully acknowledged.

## References

1. Bostwick DG (2000) Prostatic intraepithelial neoplasia. Curr Urol Rep 1:65–70
2. Colby TV, Wistuba II, Gazdar A (1998) Precursors to pulmonary neoplasia. Adv Anat Pathol 5:205–215
3. Hruban RH, Adsay NV, Albores-Saavedra J, Compton C, Garrett ES, Goodman SN, Kern SE, Klimstra DS, Kloeppel G, Longnecker DS, Luttges J, Offerhaus GJ (2001) Pancreatic intraepithelial neoplasia: a new nomenclature and classification system for pancreatic duct lesions. Am J Surg Pathol 25:579–586
4. Hubbard R, Venn A, Lewis S, et al (2000) Lung cancer and cryptogenic fibrosing alveolitis. A population-based cohort study. Am J Respir Crit Care Med 161:5–8
5. Hung J, Kishimoto Y, Sugio K, et al (1995) Allele-specific chromosome 3p deletions occur at an early stage in the pathogenesis of lung carcinoma. JAMA 273:1908
6. Kishimoto Y, Sugio K, Hung JY, et al (1995) Allele-specific loss in chromosome 9p loci in preneoplastic lesions accompanying non-small-cell lung cancers. J Natl Cancer Inst 87:1224–1229
7. Kitamura H, Kameda Y, Ito T, et al (1999) Atypical adenomatous hyperplasia of the lung. Implications for the pathogenesis of peripheral lung adenocarcinoma. Am J Clin Pathol 111:610–622
8. Luttges J, Galehdari H, Brocker V, et al (2001) Allelic loss is often the first hit in the biallelic inactivation of the p53 and DPC4 genes during pancreatic carcinogenesis. Am J Pathol 158:1677–1683
9. Michelland S, Gazzeri S, Brambilla E, et al (1999) Comparison of chromosomal imbalances in neuroendocrine and non-small-cell lung carcinomas. Cancer Genet Cytogenet 114:22–30
10. Mori M, Rao SK, Popper HH, Cagle PT, Fraire AE (2001) Atypical adenomatous hyperplasia of the lung: a probable forerunner in the development of adenocarcinoma of the lung. Mod Pathol 14:72–84
11. Petersen I, Bujard M, Petersen S, et al (1997) Patterns of chromosomal imbalances in adenocarcinoma and squamous cell carcinoma of the lung. Cancer Res 57:2331–2335
12. Petzmann S, Ullmann R, Klemen H, et al (2001) Loss of heterozygosity on chromosome arm 11q in lung carcinoids. Hum Pathol 32:333–338
13. Samet JM (2000) Does idiopathic pulmonary fibrosis increase lung cancer risk? Am J Respir Crit Care Med 161:1–2
14. Sanz-Ortega J, Saez MC, Sierra E, et al (2001) 3p21, 5q21, and 9p21 allelic deletions are frequently found in normal bronchial

cells adjacent to non-small-cell lung cancer, while they are unusual in patients with no evidence of malignancy. J Pathol 195:429–434
15. Takayama H, Takakuwa T, Dong Z, et al (2001) Fas gene mutations in prostatic intraepithelial neoplasia and concurrent carcinoma: analysis of laser capture microdissected specimens. Lab Invest 81:283–288
16. Thiberville L, Payne P, Vielkinds J, et al (1995) Evidence of cumulative gene losses with progression of premalignant epithelial lesions to carcinoma of the bronchus. Cancer Res 55:5133–5139
17. Wistuba, II, Berry J, Behrens C, et al (2000) Molecular changes in the bronchial epithelium of patients with small cell lung cancer. Clin Cancer Res 6:2604–2610
18. Yamasaki M, Takeshima Y, Fujii S, et al (2000) Correlation between genetic alterations and histopathological subtypes in bronchiolo-alveolar carcinoma and atypical adenomatous hyperplasia of the lung. Pathol Int 50:778–785
19. Yasuhara K, Mitsumori K, Yoshimura H, et al (1995) Relationship between the development of pulmonary fibrosis and lung tumors in Syrian golden hamsters induced by N-methyl-N-nitrosourethane. Toxicol Pathol 23:551–559

Virchows Arch (2003) 442:437–443
DOI 10.1007/s00428-003-0803-5

ORIGINAL ARTICLE

**Jaw-Yuan Wang · Tsung-Jen Huang · Fang-Ming Chen · Ming-Chia Hsieh · Shiu-Ru Lin · Ming-Feng Hou · Jan-Sing Hsieh**

# Mutation analysis of the putative tumor suppressor gene *PTEN/MMAC1* in advanced gastric carcinomas

Received: 11 November 2002 / Accepted: 10 March 2003 / Published online: 15 April 2003
© Springer-Verlag 2003

**Abstract** A novel tumor suppressor gene, *PTEN/MMAC1*, located on chromosome band 10q23.3, encodes a 403-amino acid, dual-specificity protein phosphatase. The defects in this gene are responsible for the development of some advanced cancers. Inactivating alterations, including mutations and deletions, in the PTEN/MMAC1 gene have been identified in several types of human cancers and cancer cell lines. To clarify the participation of the *PTEN/MMAC1* gene in advanced gastric carcinogenesis, we screened their frequency of mutations in primary advanced gastric adenocarcinoma tissues. Cancer specimens and their corresponding normal tissues were obtained surgically from 60 patients with pathologically proven advanced gastric carcinoma at the Department of Surgery of Kaohsiung Medical University Hospital. All nine exons of the *PTEN/MMAC1* gene were amplified using polymerase chain reaction and screened for mutations by single-strand conformation polymorphism analysis and followed by direct sequencing. After neutral polyacrylamide gel electrophoresis, 17 patients (28.3%) showed an apparent electrophoretic mobility shift between the cancer and its paired normal tissue. These results from direct sequencing indicated that mutations consisted of eight cases (47.1%) of missense mutation, five silent mutations (29.4%), two nonsense mutations (11.8%), a 12-bp deletion (5.9%), and a mutation within the splice donor site of intron 6 (5.9%). The mutation hot spots at codons 45, 66, 82 and 204 in advanced gastric cancer have not been observed previously. Based on the present analysis, our study implicated that the mutations of the *PTEN/MMAC1* gene do not occur at a significant rate in human advanced gastric carcinoma, but the rare clustered mutation site (exons 2–6) perhaps suggested that *PTEN/MMAC1* might contribute to the gastric carcinogenesis and its progression.

**Keywords** *PTEN/MMAC1* · Tumor suppressor gene · Gene mutation · Gastric carcinoma

J.-Y. Wang · T.-J. Huang · F.-M. Chen · M.-F. Hou · J.-S. Hsieh (✉)
Department of Surgery,
Kaohsiung Medical University and Hospital,
Shih-Chuan 1st Road, No. 100, 807 Kaohsiung, Taiwan
e-mail: cy614112@ms14.hinet.net
Tel.: +886-7-3122805
Fax: +886-7-3114679

S.-R. Lin
MedicoGenomic Research Center,
Kaohsiung Medical University and Hospital,
Kaohsiung, Taiwan

M.-C. Hsieh
Department of Internal Medicine,
Kaohsiung Medical University,
Kaohsiung, Taiwan

## Introduction

A candidate tumor suppressor gene, *PTEN/MMAC1* (phosphatase and tensin homologue deleted on chromosome ten/mutated in multiple advanced cancers 1), also known as *TEP1* (transforming growth factor-$\beta$ regulated and epithelial cell enriched phosphatase 1), has recently been identified on human chromosome band 10q23.3 [19, 20, 35]. The *PTEN/MMAC1* gene contains nine exons and encodes a 403-amino acid, dual-specificity phosphatase with homology to the cytoskeleton proteins chicken tensin and bovine auxilin, cytoskeletal proteins that interact with adhesion molecules [5, 19, 20, 24, 35]. Mutations of the *PTEN/MMAC1* gene have been described in several types of tumors in different frequencies. Somatic mutations have been initially found in a variety of human cancer cell lines and primary tumors of the endometrium, brain, prostate, breast, and kidney [3, 11, 16, 20, 30, 32, 35, 40, 41]. Although subsequent studies revealed *PTEN/MMAC1* mutations in a wide variety of tumor types, some studies disclosed the low frequency of these gene mutations in other tumors [13, 16, 17, 23, 32] indicating that the *PTEN/MMAC1* gene might play a role in the tumorigenesis of some cancers but not others. Furthermore, it was reported that the *PTEN/MMAC1* gene might regulate tumor cell invasion and metastasis [35]. Thus,

this gene is probably correlated with some human cancer progression [1, 8, 12].

Despite the worldwide declining incidence of gastric cancer over the past decades, it remains a major medical problem and is the second most common fatal malignancy worldwide [37]. In Taiwan, gastric cancer is the third major cause of cancer-related death among males and the fifth major cause of cancer-related death among females. There are over 3000 new cases diagnosed every year, with over 2000 patients dying annually from this disease [6]. Despite advances in diagnostic and therapeutic techniques, only gastric cancer diagnosed at an early stage is likely to be cured by surgical procedure. The prognosis remains poor in the case of advanced disease due to the high incidence of metastasis and recurrence. The molecular pathogenesis of human cancer formation and progression is largely unknown. Recently, gastric carcinogenesis has been thought to be a multi-step process that is associated with a series of changes in the activation of oncogenes and inactivation of tumor suppressor genes [36]. However, the role of the *PTEN/MMAC1* gene leading to the development of human advanced gastric cancer remains poorly defined.

In the present study, we examined the mutation frequency and pattern of the *PTEN/MMAC1* gene in primary advanced gastric cancer specimens using polymerase chain reaction–single-strand conformation polymorphism (PCR-SSCP) analysis followed by direct sequencing. Our results observed mutations of *PTEN/MMAC1* in17 of 60 (28.3%) patients with advanced gastric cancer, showing a rare clustered mutation site, suggesting that the *PTEN/MMAC1* gene might have a critical role in the pathogenesis of human advanced gastric cancer.

## Materials and methods

### Tissue samples and DNA extraction

Between January 1999 and April 2001, 60 consecutive patients with advanced gastric carcinoma that underwent surgical resection at the Department of Surgery of Kaohsiung Medical University Hospital were enrolled in this study. All patients were proven to have a primary adenocarcinoma of the stomach with the depth of invasion into or beyond the muscularis propria with no evidence of any other malignancy. Clinicopathological descriptions were carried out according to the General Rules for the Gastric Cancer Study in Surgery and Pathology from the Japanese Research Society for Gastric Cancer (JRSGC) [14]. The cancer tissues with their matched normal tissues were collected immediately after surgical resection, frozen instantly in liquid nitrogen, and then stored at −80°C until analyzed. Genomic DNA was isolated from frozen primary gastric cancer and the paired normal tissues using the proteinase-K (Stratagene, La Jolla, CA) digestion and phenol/chloroform extraction procedures according to the method by Sambrook [33].

### PCR-SSCP analysis

Tumor DNAs were subjected to PCR-SSCP analysis to search for mutations. All nine exons of the *PTEN/MMAC1* gene were amplified using primers designed according to Chang et al. [4] with some modifications (Table 1). PCR amplification was performed within a reaction mixture containing 50 pmol forward and reverse primers, 100 ng genomic DNA, 2.5 U *Taq* DNA polymerase (Promega Corp., Madison, WI), 100 mmol/l each deoxynucleotide triphosphate (Promega), 3 $\mu$Ci [$\alpha$-$^{32}$P]-dCTP (New England Nuclear Research Products, Boston, MA), and 1× PCR buffer [10 mmol/l Tris-HCl (pH 8.3), 1.5 mmol/l $MgCl_2$, 50 mmol/l KCl, and 0.01% gelatin]. A programmable thermocycler (PTC-100, MJ Research, Watertown, MA) was used to perform amplifications. The PCR condition for each exon was as follows: 35 cycles of 1 min denaturation at 94°C, 1 min annealing at temperature shown in Table 1, 1 min extension at 72°C, and 5 min final extension at 72°C. The PCR products were heated at 94°C for 4 min and loaded onto polyacrylamide gels of GeneGel Excel 12.5/24 kit (Pharmacia Biotech Inc, San Francisco, CA) using the Genephore electrophoresis unit (Pharmacia Biotech). Gels were run for 6–7 h at 5–6 W,

**Table 1** Oligonucleotide primers for *PTEN/MMAC1* analysis

| Exon | Sequence | Annealing temperature (°C) | Product size (bp) |
|---|---|---|---|
| 1 | Forward: 5′-CTCCTCCTTTTTCTTCAGCC-3′<br>Reverse: 5′-TATGACCTAGCAACCTGACCA-3′ | 56 | 243 |
| 2 | Forward: 5′-TGACCACCTTTTATTACCA-3′<br>Reverse: 5′-AAGTATCTTTTTCTGTGGCTTA-3′ | 48 | 240 |
| 3 | Forward: 5′-ATAGAAGGGGTATTTGTTGGA-3′<br>Reverse: 5′-ACCTCACTCTAACAAGCAGATA-3′ | 56 | 293 |
| 4 | Forward: 5′-TTCAGGCAATGTTTGTTA-3′<br>Reverse: 5′-CTCGATAATCTGGATGACTCA-3′ | 48 | 225 |
| 5 | Forward: 5′-GCAACATTTCTAAAGTTACCTA-3′<br>Reverse: 5′-TCTGTTTTCCAATAAATTCTC-3′ | 48 | 386 |
| 6 | Forward: 5′-GAGTAACTATTCCCAGTCAGA-3′<br>Reverse: 5′-TAATTTGTTCAAATGCTTCAGA-3′ | 54 | 286 |
| 7 | Forward: 5′-ATCGTTTTTGACAGTTTG-3′<br>Reverse: 5′-CCAATGAAAGTAAAGTACA-3′ | 48 | 260 |
| 8 | Forward: 5′-AGGTGACAGATTTTCTTTTTTA-3′<br>Reverse: 5′-TAGCTGTACTCCTAGAATTA-3′ | 52 | 394 |
| 9 | Forward: 5′-GTTCATCTGCAAAATGGA-3′<br>Reverse: 5′-TGGTAATCTGACACAATGTCCTA-3′ | 50 | 397 |

and then they were stained using the Plusone DNA silver staining kit (Pharmacia Biotech).

### Direct sequencing

The PCR products were purified using the QIAEX II Gel Extraction Kit (Qiagen Inc., Valencia, CA) and then subjected to sequencing using a double-strand cycle sequencing system (Gibco BRL, Gaithersburg, MD). The purified products were then sequenced directly with T7 promoter/IRD800 (LI-COR, Lincoln, NE), which is a T7 promoter primer labeled with a heptamethine cyanine dye, or using DNA polymerase incorporating IRD-labeled dATP for sequencing reaction. Upon completion of the sequencing reaction, 4 μl formamide loading buffer was added to the reaction mixture, and the sample was heated to 95°C for 5 min, snap cooled and loaded onto the sequencing gel.

An automated DNA electrophoresis system (Model 4200; LI-COR) with a laser diode emitting at 785 nm and fluorescence detection between 815 nm and 835 nm was used to detect and analyze the sequencing ladder. Electrophoresis was performed on a 41-cm×25-cm×0.2-mm gel consisting of 6% Long Ranger gel matrix (AT Biochem; Malvern, PA) with 7 M urea and a running buffer consisting of 133 mM Tris base, 44 mM boric acid and 2.5 mM EDTA, pH 9 at 50°C. From each sequencing reaction, a 1.5-μl sample was loaded onto each lane. Following the loading of samples, electrophoresis was carried out at 2000-V constant voltage with the gel heated to 50°C. The PCR products were sequenced directly from both forward and reverse directions. Data collection and image analysis utilized an IBM486 (model 90) using the Base Image IR software supplied with the model 4200 DNA sequencer.

### Immunohistochemistry

To determine the impact of PTEN nonsense mutations on protein expression in advanced gastric carcinoma tissues, immunohistochemical staining was performed in cases with codon 66 nonsense mutations. Briefly, 4-$\mu$m paraffin sections were dewaxed in xylene and rehydrated with alcohol. The slides were then incubated in 3% hydrogen peroxide for 5 min to block endogenous peroxidase activity. After washing in Tris-buffered saline (TBS, pH 7.6), the slides were incubated with diluted primary mouse monoclonal antibodies against PTEN (#MS-1601-R7, 1:150; NeoMarkers, Fermont, CA, USA). The primary antibodies were detected using the avidin-biotin-complex-peroxidase technique (Vectastain Elite kit, Vector Laboratories, Inc., Burlingame, CA, USA) with biotinylated anti-mouse IgG as secondary antibody. The reaction was developed with diaminobenzidine-hydrogen peroxide (Sigma Chemical Company, St Louis, MO) as chromogen and the sections were subsequently counterstained with light hematoxylin.

## Results

Of all these patients, there were 39 males and 21 females (average age, 65 years; ranging from 31 years to 85 years). All gastric cancers and their adjacent normal gastric tissues were screened for the mutations of the *PTEN/MMAC1* gene in nine exons using the PCR-SSCP analysis. After neutral polyacrylamide gel electrophoresis, 17 patients (28.3%) showed an apparent electrophoretic mobility shift between the cancer and its paired normal tissue. Of 17 such differences, 4 were detected in exon 2 (cases 12, 17, 18, 19), 4 were detected in exon 3 (cases 21, 29, 38, 42), 4 were found in exon 4 (cases 9, 26, 31, 47), 1 was detected in exon 5 (case 7), and 4 were found in exon 6 (cases 6, 10, 11, 37) (Fig. 1). Moreover, the SSCP indicated that the mobility shift patterns of cases 17 and 18, cases 21 and 38, cases 26 and 31, and cases 11 and 37 were of similar type.

Direct sequencing analysis of the *PTEN/MMAC1* gene mutations revealed eight cases of missense mutation, five silent mutations, two nonsense mutations, a 12-bp deletion and one mutation within the splice donor site of intron 6 (Table 2). The results indicated that the mutation site in exon 2 was found to be at codon 31 (AAC→AAT) in one case, at codon 34 (GCT→GCG) in one case, and at codon 45 (GTA→GTG) in two cases (Fig. 2A), all resulting in silent mutations. The mutation sites in exon 3 were found to be at codon 62 (AAA→ATA) in one case,

**Table 2** Mutations of *PTEN/MMAC1* in advanced gastric cancer and clinicopathological features. *pT* pathological depth of tumor invasion, *pN* pathological status of lymph-node metastasis, *WD* well differentiated, *MD* moderately differentiated, *PD* poorly differentiated, *Signet* signet ring cell

| Case no. | Sex | Age (years) | pT | pN | Stage[a] | Histology | Exon | Mutated codon | Base substitution | Amino acid change |
|---|---|---|---|---|---|---|---|---|---|---|
| 6 | Male | 65 | t3 | n3 | III | PD | 6 | Codon 188 | TAT→TCT | Tyr→Ser |
| 7 | Female | 72 | t3 | n3 | III | PD | 5 | Codon 124 | TGT→TAT | Cys→Tyr |
| 9 | Male | 74 | t2 | n3 | III | Mucinous | 4 | Codon 76 | TAT→TAC | Silent mutation |
| 10 | Male | 69 | t3 | n3 | III | MD | Intron 6 | nt. 110262 | T→G | |
| 11 | Male | 60 | t3 | n2 | III | Signet | 6 | Codon 204 | CCA→ACA | Pro→Thr |
| 12 | Female | 58 | t2 | n2 | II | WD | 2 | Codon 31 | AAC→AAT | Silent mutation |
| 17 | Male | 63 | t2 | n1 | I | PD | 2 | Codon 45 | GTA→GTG | Silent mutation |
| 18 | Female | 64 | t2 | n2 | II | PD | 2 | Codon 45 | GTA→GTG | Silent mutation |
| 19 | Male | 70 | t3 | n3 | III | Signet | 2 | Codon 34 | GCT→GCG | Silent mutation |
| 21 | Male | 61 | t4 | n3 | IV | MD | 3 | Codon 66 | ACA→ACT | Nonsense mutation |
| 26 | Male | 67 | t3 | n1 | II | WD | 4 | Codon 82 | AAT→ACT | Asn→Thr |
| 29 | Female | 55 | t3 | n2 | III | PD | 3 | Codon 62 | AAA→ATA | Lys→Ile |
| 31 | Male | 59 | t3 | n3 | III | MD | 4 | Codon 82 | AAT→ACT | Asn→Thr |
| 37 | Female | 62 | t4 | n2 | III | PD | 6 | Codon 204 | CCA→ACA | Pro→Thr |
| 38 | Male | 66 | t2 | n3 | III | WD | 3 | Codon 66 | ACA→ACT | Nonsense mutation |
| 42 | Male | 68 | t2 | n2 | II | PD | 3 | Codon 67 | ATA→AAA | Ile→Lys |
| 47 | Female | 67 | t4 | n3 | IV | WD | 4 | Codon 75–78 | 12 bp deletion | |

[a] Staging according to Japanese Research Society for Gastric Cancer

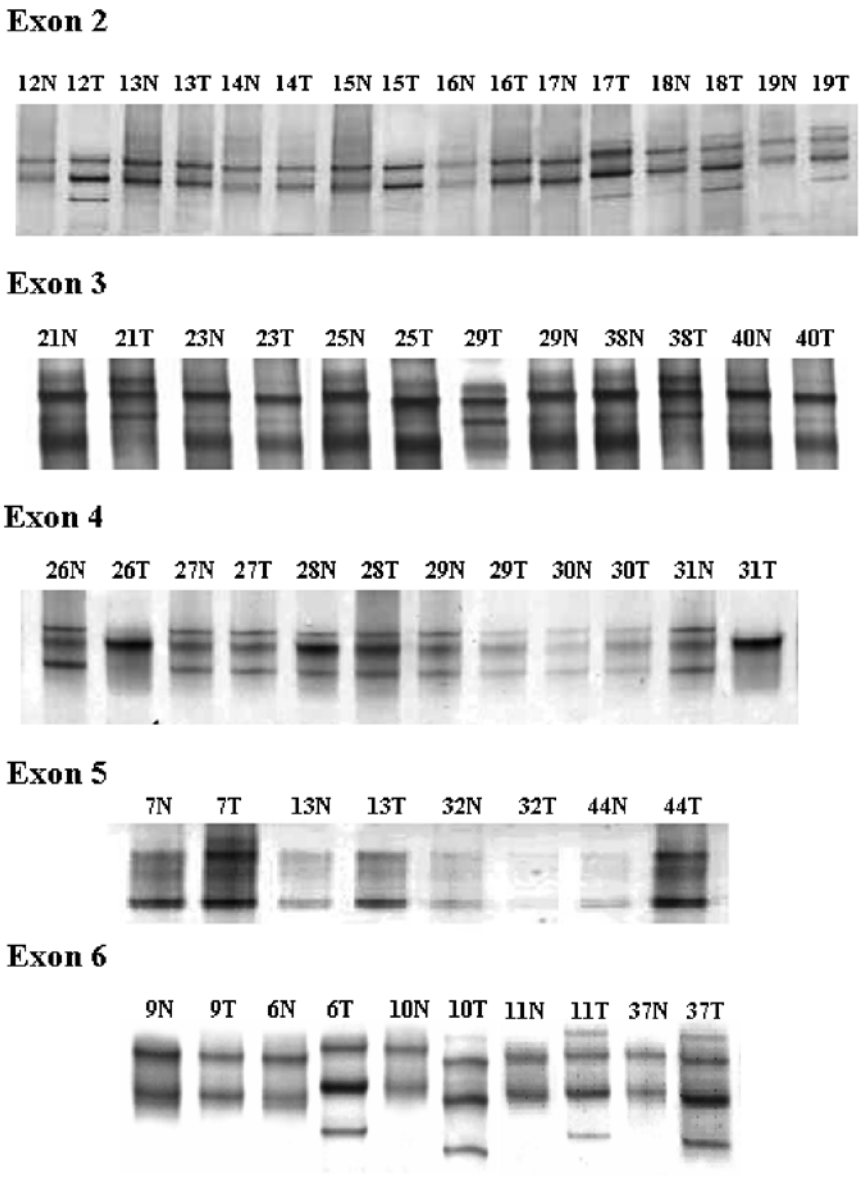



**Fig. 1** Polymerase chain reaction–single-strand conformation polymorphism analysis of *PTEN/MMAC1* mutations in human advanced gastric cancers. An electrophoretic mobility shift of the bands differs between the tumor (*T*) and its paired normal tissue (*N*), representing a different conformer of the fragment and suggesting the presence of mutations in exons 2–6

resulting in a change from lysine to isoleucine substitution, at codon 66 (ACA→ACT) in two cases, resulting in silent mutations, and at codon 67 (ATA→AAA) in one case, resulting in a change from isoleucine to lysine substitution. The mutation sites in exon 4 were found to be at codon 76 (TAT→TAC) in one case, resulting in a silent mutation, at codon 82 (AAT→ACT) in two cases (Fig. 2B), resulting in a change from asparagine to threonine substitution, a 12-bp deletion in codons 75–78. The mutation site in exon 5 was found to be at codon 124 (TGT→TAT) in one case, resulting in a change from cystine to tyrosine. The mutation sites in exon 6 were found to be at codon 188 (TAT→TCT) in one case (Fig. 2C), leading to a tyrosine to serine substitution; at codon 204 (CCA→ACA) in two cases (Fig. 2D), leading to proline to threonine substitution; and in intron 6 at nucleotide 110262 (T→G) in one case (Fig. 2E). Furthermore, a significantly reduced expression of PTEN protein was found in the nonsense-mutation PTEN patient (Fig. 3B) compared with the wild-type PTEN patient (Fig. 3A).

## Discussion

A series of genetic alterations, including activation of proto-oncogenes and inactivation of tumor suppressor genes, are an important process in human carcinogenesis. As tumors progress to more advanced stages, they require an increasing number of genetic alterations. Due to a variety of histological subtypes and exposure to a range of mutagenic substances, the molecular pathogenesis of gastric cancer is still largely unknown. Several candidate tumor suppressor genes have been found to be inactivated in gastric cancer, for example the *p53* and *APC* genes [25, 38]. However, other potential tumor suppressor genes that

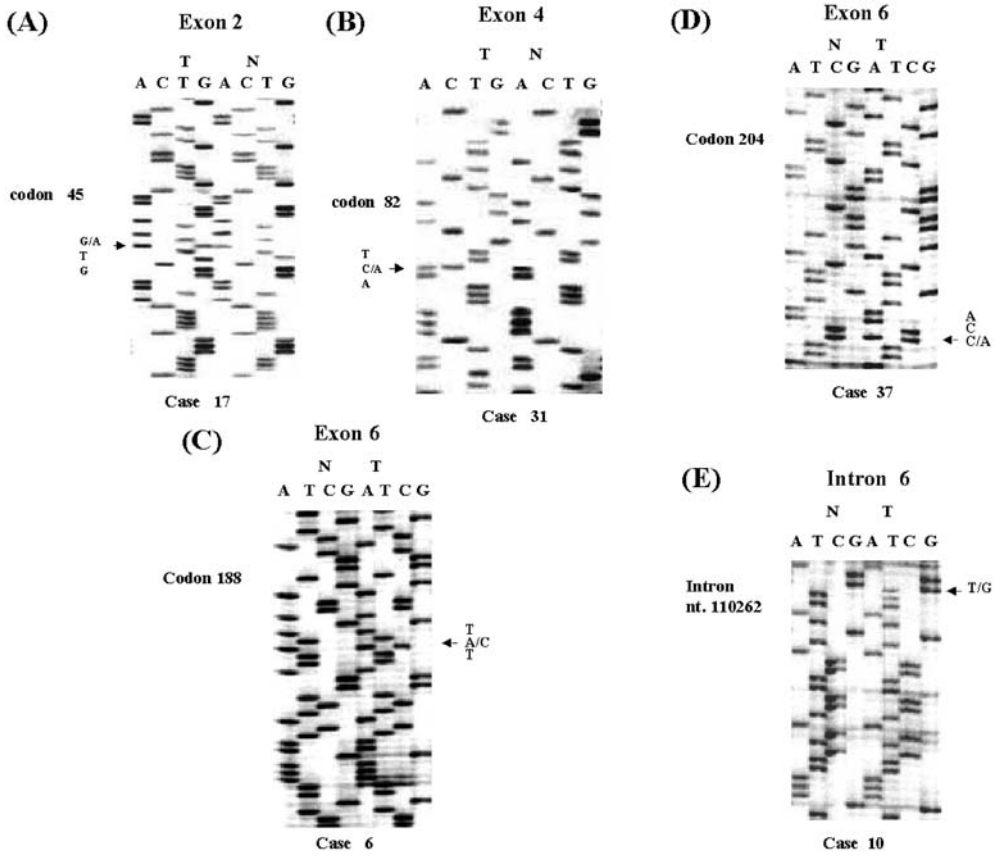



**Fig. 2** Nucleotide sequencing analysis of the *PTEN/MMAC1* gene mutations in human advanced gastric cancers. Each mutation in tumor cells (*T*) shown is matched to a normal adjacent gastric cancer (*N*). The codon at which the mutation occurs is indicated. Each sequence is shown 5′ (*bottom*) to 3′ (*top*). *Arrows* point to bands corresponding to mutated base pairs. **A** Sequencing gel shows GTA→GTG mutation in exon 2 at codon 45, resulting in a silent mutation. **B** Sequencing gel shows AAT→ACT mutation in exon 4 at codon 82, resulting in a change in the encoding amino acid from asparagine to threonine. **C** Sequencing gel shows TAT→TCT mutation in exon 6 at codon 188, resulting in a change in the encoding amino acid from tyrosine to serine. **D** Sequencing gel shows CCA→ACA mutation in exon 6 at codon 204, resulting in a change in the encoding amino acid from proline to threonine. **E** Sequencing gel shows T→G mutation in intron 6 at nucleotide 110,262

may play a role in gastric cancer have not been studied extensively.

The *PTEN/MMAC1* gene was recently identified as a tumor suppressor gene at 10q23.3, encoding a dual-specificity phosphatase that dephosphorylates both tyrosine phosphate and serine/threonine phosphate residues [19, 20, 35]. The in vivo role of *PTEN/MMAC1* appears to be dephosphorylation and inactivation of phosphotidylinositol 3,4,5-triphosphate through phosphoinositide-dependent kinase [26]. In fact, mutations and deletions of this gene have been described in a wide range of human cancers [20, 35], and germ-line mutations have also been identified in several rare autosomal dominant cancer-predisposing conditions such as Cowden's disease and Bannayan-Zonana syndrome [21, 22]. For instance, mutations of *PTEN/MMAC1* have been reported to occur in 33–50% of endometrial carcinomas [18, 31, 39], 25–44% of glioblastomas [2, 41], 0–21% of ovarian cancers [23, 26], 0–20% of prostate cancers [3, 4], and less than 5% in thyroid and breast cancers [21, 30]. Recent studies indicate that mutations of the *PTEN/MMAC1* gene seem to be infrequent in gastric cancer [4, 10, 27, 34], but the sample size analyzed is small and tumor specimens included both early and advanced gastric cancers in these investigations.

Previous researchers have described the *PTEN/MMAC1* gene as being associated with advanced stage and metastasis in endometrial and prostate carcinoma [29, 42], and that mutations of this gene are correlated with tumor progression and poor outcome in breast cancer and melanoma [7, 28]. Therefore, the analysis of the *PTEN/MMAC1* gene mutations in advanced gastric cancer might provide some information regarding the development and progression of gastric cancer. In the current study, we examined the mutation status of the *PTEN/MMAC1* gene in advanced gastric cancer and found somatic mutations in 17 of 60 (28.3%) primary tumor specimens, of which the mutation frequency is higher than published reports. The exact reason for our mutation rate being considerably higher than previous studies remains unclear. However, our tumor samples focusing on advanced gastric cancer, different histological subtypes, and an environmental

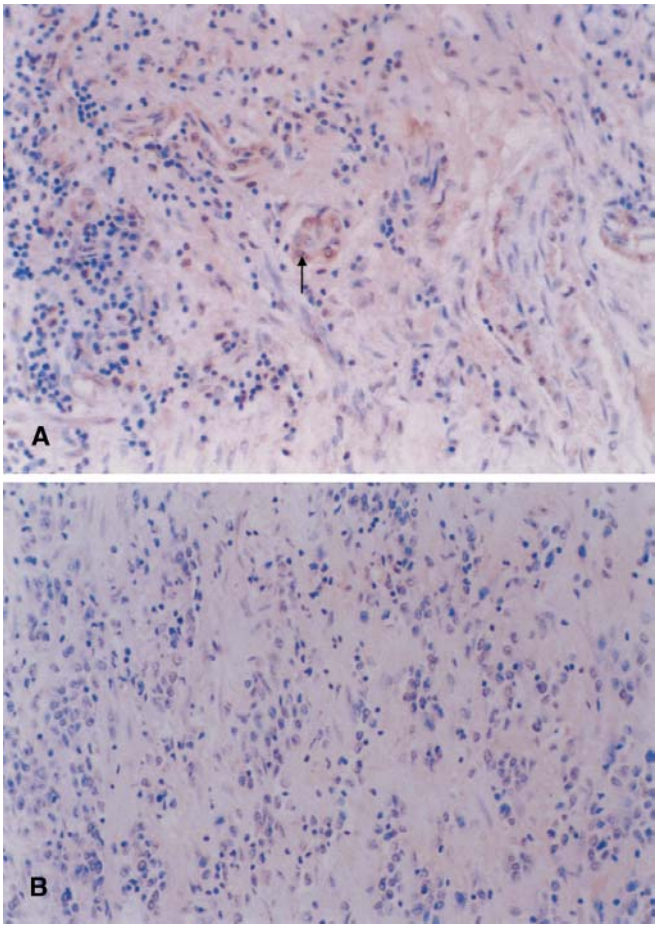



**Fig. 3** Immunohistochemical analysis of the effect of PTEN nonsense mutations on protein expression in advanced gastric carcinomas. **A** Normal expression of PTEN protein expression in the cytoplasm of cancer cells in the wild-type PTEN patient (*arrow*). **B** Absence of PTEN protein expression in the cytoplasm of cancer cells in the nonsense-mutation PTEN patient

carcinogen prevailing in a geographic region might be responsible for it. Kang et al. [15] pointed out that gastric carcinoma patients with silencing of the *PTEN/MMAC1* gene showed poor prognosis, and inactivation of the *PTEN/MMAC1* gene may play a vital role in the development and progression of gastric cancer. Also, the aberrant promoter methylation is suggested to be a major mechanism in the silencing of this gene [10, 15]. Moreover, we found that mutational patterns of the *PTEN/MMAC1* gene were clustered on exon 2 to exon 6, with the mutation hot spots at codons 45, 66, 82 and 204, leading to missense mutations on codons 82 and 204, and nonsense mutations on codon 66. Herein, mutations at codons 66, 82 and 204 might have a crucial role in the carcinogens or progression of gastric cancer. In addition, nonsense mutations of PTEN gene really reduced PTEN protein expression in advanced gastric cancer by immunohistochemistry. Fei et al. [10] observed that PTEN expression was significantly reduced or absent in gastric cancer tissues relative to matched non-tumorous gastric mucosa and healthy controls. We, therefore, suggest that in gastric cancers inactivation of the PTEN gene by mutation may contribute to its downregulation besides hypermethylation of the PTEN promoter [15]. Nevertheless, the actual role of PTEN expression in patients with advanced gastric cancer needs further investigation for confirmation. In contrast to most identified mutations of *PTEN/MMAC1* within exons 5–9, however, the specific mutation spectrum in advanced gastric cancer from our analysis is located within exons 2–6. Consequently, these controversial results concerning the mechanism of the *PTEN/MMAC1* gene alterations and these mutation clusters in hot spots in advanced gastric cancer need further investigation to elucidate the viewpoint. In addition, we found a mutation in intron 6 in one of 60 advanced gastric cancers, and whether this mutation in the intron affects transcriptional or post-transcriptional modulation has still to be investigated.

In conclusion, our study implicated that the mutations of the *PTEN/MMAC1* gene do not occur at a significant rate in human advanced gastric carcinoma, but the rare clustered mutation site perhaps suggested that the *PTEN/MMAC1* gene has an important role in the pathogenesis of these tumors. Thus, to clarify the role of the *PTEN/MMAC1* gene in the development and progression of gastric cancer, it will be necessary to investigate other mechanisms of inactivation of *PTEN/MMAC1*, including gene hypermethylation, since the present study could not exclude such mechanisms.

**Acknowledgement** This research was supported by a grant from the National Science Council of the Republic of China (NSC89–2314-B-037–120).

## References

1. Bose K, Crane A, Hibshoosh H, Manaukhani M, Sandweis L, Parsons R (2002) Reduced expression of PTEN correlates with breast cancer progression. Hum Pathol 33:405–409
2. Bostrom J, Cobbers JM, Wolter M, Tabatabai G, Weber RG, Lichter P, Collins VP, Reifenberger G (1998) Mutation of the PTEN (MMAC1) tumor suppressor gene in a subset of glioblastomas but not in meningiomas with loss of chromosome arm 10q. Cancer Res 58:29–33
3. Cairns P, Okami K, Halachmi S, Halachmi N, Esteller M, Herman JG, Jen J, Isaacs WB, Bova GS, Sidransky D (1997) Frequent inactivation of PTEN/MMAC1 in primary prostate cancer. Cancer Res 57:4997–5000
4. Chang JG, Chen YJ, Perng LI, Wang NM, Kao MC, Yang TY, Chang CP, Tsai CH (1999) Mutation analysis of the PTEN/MMAC1 gene in cancers of the digestive tract. Eur J Cancer 35:647-651
5. Dahia PL (2000) PTEN, a unique tumor suppressor gene. Endocr Relat Cancer 7:115–129
6. Anonymous (1997) Department of Health and Vital Statistics, vol. I. Department of Health, Taipei, pp 71–85
7. Depowski PL, Rosenthal SI, Ross JS (2001) Loss of expression of the PTEN gene protein product is associated with poor outcome in breast cancer. Mod Pathol 14:672–676
8. Dicuonzo G, Angeletti S, Garcia-Foncillas J, Brugarolas A, Okrouzhnov Y, Santini D, Tonini G, Lorino G, De Cesaris M, Baldi A (2001) Colorectal carcinomas and PTEN/MMAC1 gene mutations. Clin Cancer Res 7:4049–4053

9. Dong JT, Li CL, Sipe TW, Frierson HF Jr (2001) Mutations of PTEN/MMAC1 in primary prostate cancers from Chinese patients. Clin Cancer Res 7:304–308
10. Fei G, Ebert MP, Mawrin C, Leodolter A, Schmidt N, Dietzmann K, Malfertheiner P (2002) Reduced PTEN expression in gastric cancer and in the gastric mucosa of gastric cancer relatives. Eur J Gastroenterol Hepatol 14:297–303
11. Guldberg P, Thor Straten P, Birck A, Ahrenkiel V, Kirkin AF, Zeuthen J (1997) Disruption of the MMAC1/PTEN gene by deletion or mutation is a frequent event in malignant melanoma. Cancer Res 57:3660–3663
12. Harima Y, Sawada S, Nagata K, Sougawa M, Ostapenko V, Ohnishi T (2001) Mutation of the PTEN gene in advanced cervical cancer correlated with tumor progression and poor outcome after radiotherapy. Int J Oncol 18:493–497
13. Hu YC, Lam KY, Tang JC, Srivastava G (1999) Mutational analysis of the PTEN/MMAC1 gene in primary oesophageal squamous cell carcinomas. Mol Pathol 52:353–356
14. Japanese Research Society for Gastric Cancer (1995) The general rules for the gastric cancer study. Part I. Clinical, surgical, and conclusive findings. Part II. Histological findings. Kanehara and Co., Tokyo, pp 2–46
15. Kang YH, Lee HS, Kim WH (2002) Promoter methylation and silencing of PTEN in gastric carcinoma. Lab Invest 82:285–291
16. Kondo K, Yao M, Kobayashi K, Ota S, Yoshida M, Kaneko S, Baba M, Sakai N, Kishida T, Kawakami S, Uemura H, Nagashima Y, Nakatani Y, Hosaka M (2001) PTEN/MMAC1/TEP1 mutations in human primary renal-cell carcinomas and renal carcinoma cell lines. Int J Cancer 91:219–224
17. Kubo Y, Urano Y, Hida Y, Arase S (1999) Lack of somatic mutation in the PTEN gene in squamous cell carcinomas of human skin. J Dermatol Sci 19:199–201
18. Kurose K, Bando K, Fukino K, Sugisaki Y, Araki T, Emi M (1998) Somatic mutations of the PTEN/MMAC1 gene in fifteen Japanese endometrial cancers: evidence for inactivation of both alleles. Jpn J Cancer Res 89:842–848
19. Li DM, Sun H (1997) TEP1, encoded by a candidate tumor suppressor locus, is a novel protein tyrosine phosphatase regulated by transforming growth factor beta. Cancer Res 57:2124–2129
20. Li J, Yen C, Liaw D, Podsypanina K, Bose S, Wang SI, Puc J, Miliaresis C, Rodgers L, McCombie R, Bigner SH, Giovanella BC, Ittmann M, Tycko B, Hibshoosh H, Wigler MH, Parsons R (1997) PTEN, a putative protein tyrosine phosphatase gene mutated in human brain, breast, and prostate cancer. Science 275:1943–1947
21. Liaw D, Marsh DJ, Li J, Dahia PL, Wang SI, Zheng Z, Bose S, Call KM, Tsou HC, Peacocke M, Eng C, Parsons R (1997) Germline mutations of the PTEN gene in Cowden disease, an inherited breast and thyroid cancer syndrome. Nat Genet 16:64–67
22. Marsh DJ, Dahia PL, Zheng Z, Liaw D, Parsons R, Gorlin RJ, Eng C (1997) Germline mutations in PTEN are present in Bannayan-Zonana syndrome. Nat Genet 16:333–334
23. Maxwell GL, Risinger JI, Tong B, Shaw H, Barrett JC, Berchuck A, Futreal PA (1998) Mutation of the PTEN tumor suppressor gene is not a feature of ovarian cancers. Gynecol Oncol 70:13–16
24. Myers MP, Stolarov JP, Eng C, Li J, Wang SI, Wigler MH, Parsons R, Tonks NK (1997) P-TEN, the tumor suppressor from human chromosome 10q23, is a dual-specificity phosphatase. Proc Natl Acad Sci U S A 94:9052–9057
25. Nakatsuru S, Yanagisawa A, Ichii S, Tahara E, Kato Y, Nakamura Y, Horii A (1992) Somatic mutation of the APC gene in gastric cancer: frequent mutations in very well differentiated adenocarcinoma and signet-ring cell carcinoma. Hum Mol Genet 1:559–563
26. Obata K, Morland SJ, Watson RH, Hitchcock A, Chenevix-Trench G, Thomas EJ, Campbell IG (1998) Frequent PTEN/MMAC mutations in endometrioid but not serous or mucinous epithelial ovarian tumors. Cancer Res 58:2095–2097
27. Okami K, Wu L, Riggins G, Cairns P, Goggins M, Evron E, Halachmi N, Ahrendt SA, Reed AL, Hilgers W, Kern SE, Koch WM, Sidransky D, Jen J (1998) Analysis of PTEN/MMAC1 alterations in aerodigestive tract tumors. Cancer Res 58:509–511
28. Poetsch M, Dittberner T, Woenckhaus C (2001) PTEN/MMAC1 in malignant melanoma and its importance for tumor progression. Cancer Genet Cytogenet 125:21–26
29. Rasheed BK, Stenzel TT, McLendon RE (1997) PTEN gene mutations are seen in high-grade but not in low-grade gliomas. Cancer Res 57:4187–4190
30. Rhei E, Kang L, Bogomolniy F, Federici MG, Borgen PI, Boyd J (1997) Mutation analysis of the putative tumor suppressor gene PTEN/MMAC1 in primary breast carcinomas. Cancer Res 57:3657–3959
31. Risinger JI, Hayes AK, Berchuck A, Barrett JC (1997) PTEN/MMAC1 mutations in endometrial cancers. Cancer Res 57:4736–4738
32. Sakurada A, Suzuki A, Sato M, Yamakawa H, Orikasa K, Uyeno S, Ono T, Ohuchi N, Fujimura S, Horii A (1997) Infrequent genetic alterations of the PTEN/MMAC1 gene in Japanese patients with primary cancers of the breast, lung, pancreas, kidney, and ovary. Jpn J Cancer Res 88:1025–1028
33. Sambrook J, Fritsch EF, Maniatis T (1989) Molecular cloning: a laboratory manual. Cold Spring Harbor Laboratory, New York, pp 6.22–6.34
34. Sato K, Tamura G, Tsuchiya T, Endoh Y, Sakata K, Motoyama T, Usuba O, Kimura W, Terashima M, Nishizuka S, Zou T, Meltzer SJ (2002) Analysis of genetic and epigenetic alterations of the PTEN gene in gastric cancer. Virchows Arch 440:160–165
35. Steck PA, Pershouse MA, Jasser SA, Yung WK, Lin H, Ligon AH, Langford LA, Baumgard ML, Hattier T, Davis T, Frye C, Hu R, Swedlund B, Teng DH, Tavtigian SV (1997) Identification of a candidate tumour suppressor gene, MMAC1, at chromosome 10q23.3 that is mutated in multiple advanced cancers. Nat Genet 15:356–362
36. Tahara E (1995) Molecular biology of gastric cancer. World J Surg 19:484–490
37. Tahara E, Semba S, Tahara H (1996) Molecular biological observations in gastric cancer. Semin Oncol 23:307–315
38. Tamura G, Kihana T, Nomura K, Terada M, Sugimura T, Hirohashi S (1991) Detection of frequent p53 gene mutations in primary gastric cancer by cell sorting and polymerase chain reaction single-strand conformation polymorphism analysis. Cancer Res 51:3056–3058
39. Tashiro H, Blazes MS, Wu R, Cho KR, Bose S, Wang SI, Li J, Parsons R, Ellenson LH (1997) Mutations in PTEN are frequent in endometrial carcinoma but rare in other common gynecological malignancies. Cancer Res 57:3935–3940
40. Teng DH, Hu R, Lin H, Davis T, Iliev D, Frye C, Swedlund B, Hansen KL, Vinson VL, Gumpper KL, Ellis L, El-Naggar A, Frazier M, Jasser S, Langford LA, Lee J, Mills GB, Pershouse MA, Pollack RE, Tornos C, Troncoso P, Yung WK, Fujii G, Berson A, Steck PA (1997) MMAC1/PTEN mutations in primary tumor specimens and tumor cell lines. Cancer Res 57:5221–5225
41. Wang SI, Puc J, Li J, Bruce JN, Cairns P, Sidransky D, Parsons R (1997) Somatic mutations of PTEN in glioblastoma multiforme. Cancer Res 57:4183–4186
42. Whang YE, Wu X, Suzuki H, Reiter RE, Tran C, Vessella RL, Said JW, Isaacs WB, Sawyers CL (1998) Inactivation of the tumor suppressor PTEN/MMAC1 in advanced human prostate cancer through loss of expression. Proc Natl Acad Sci U S A 95:5246–5250

Virchows Arch (2003) 442:444–452
DOI 10.1007/s00428-003-0784-4

ORIGINAL ARTICLE

**Bence Sipos · Simone Möser · Holger Kalthoff · Virag Török · Matthias Löhr · Günter Klöppel**

# A comprehensive characterization of pancreatic ductal carcinoma cell lines: towards the establishment of an in vitro research platform

Received: 21 November 2002 / Accepted: 29 January 2003 / Published online: 12 April 2003
© Springer-Verlag 2003

**Abstract** There are a large number of stable pancreatic ductal carcinoma cell lines that are used by researchers worldwide. Detailed data about their differentiation status and growth features are, however, often lacking. We therefore attempted to classify commonly used pancreatic carcinoma cell lines according to defined cell biological criteria. Twelve pancreatic ductal adenocarcinoma cell lines were cultured as monolayers and spheroids and graded according to their ultrastructural features. The grading system was based on the integrity of membrane structures and on the presence of mucin granules, cell organelles, nuclear and cellular polymorphism, cell polarity, and lumen formation. On the basis of the resulting scores the cell lines were classified as well, moderately, or poorly differentiated. In addition, immunocytochemistry was performed for the markers cytokeratin 7, 8, 18, 19, carcinoembryonic antigen, MUC1 MUC2, MUC5, and MUC6. The population doubling time of monolayer cultures, determined by a tetrazolium salt based proliferation assay was correlated with the ultrastructural grade. The grading of the ultrastructural features of the monolayers, and particularly of the spheroids, revealed that Capan-1 and Capan-2 cells were well differentiated; Colo357, HPAF-2, Aspc-1, A818-4, BxPc3, and Panc89 cells were moderately differentiated and PancTu-I, Panc1, Pt45P1, and MiaPaCa-2 cells poorly differentiated. Membrane-bound MUC1 staining was a characteristic of well differentiated cell lines. The population doubling time of the monolayer cultures was related to the differentiation grade. No relationship was found between the p53, K-ras, DPC4/Smad4, or $p16^{INK4a}$ mutation status and the grade of differentiation. We conclude that the proposed ultrastructural grading system combined with the proliferative activity provides a basis for further comparative studies of pancreatic ductal adenocarcinoma cell lines.

**Keywords** Pancreatic ductal carcinoma · Cell lines · Differentiation · Ultrastructure · Proliferation

B. Sipos (✉) · S. Möser · G. Klöppel
Department of Pathology, University of Kiel,
Michaelisstrasse 11, 24105 Kiel, Germany
e-mail: s.bence@path.uni-kiel.de
Tel.: +49-431-5973400
Fax: +49-431-5973462

H. Kalthoff
Molecular Oncology Unit,
Department of Abdominal and Thoracic Surgery,
Michaelisstrasse 11, 24105 Kiel, Germany

V. Török
Second Department of Pathology,
Semmelweis University, Budapest, Hungary

M. Löhr
Second Department of Medicine,
University of Heidelberg-Mannheim, Mannheim, Germany

## Introduction

As is the case with other carcinomas, studies on the cell biology and genetics of ductal adenocarcinoma (DAC) of the pancreas are largely based on in vitro investigations employing various cell lines that are commonly available through cell culture collections. The data produced in these studies are often used to make general statements regarding the biological features of DACs and their response to certain stimuli, even if only a few cell lines were examined. However, DACs are quite heterogeneous. This is reflected in their grade of differentiation, which varies from tumor to tumor. It must therefore be anticipated that the various cell lines also reveal a great deal of diversity in structure and function, so that generalized interpretations of results need to be viewed cautiously. Interpretations of data would, however, be more meaningful if there were a cell line catalogue listing cell lines according to their morphological differentiation, functional properties, growth kinetics, and main genetic changes. In 1993 we made a first attempt to grade pancreatic carcinoma cell lines on the basis of their ultrastructural features [22]. Similar studies were also performed by Vila et al. [34], who detected ductal differentiation markers

such as MUC1, cytokeratin (CK) 7, and carbonic anhydrase II in four newly established pancreatic carcinoma cell lines and classified these cell lines on the basis of their phenotypical features into more and less differentiated groups. As helpful as these early studies were in providing a first phenotypic profile of pancreatic carcinoma cell lines, they were not yet systematic and failed to relate the structural, functional, and genetic features of a greater number of well established cell lines to their proliferation status. In an earlier study we analyzed the genetic alterations in 22 pancreatic carcinoma cell lines of known or potential ductal origin and found that more than 90% of the cell lines harbored alterations of the $p16^{INK4a}$, K-ras, and p53 genes, 36% of them DPC4/Smad4 genetic alterations [25].

In this study we systematically screened 12 DAC cell lines for their in vitro growth, fine structural differentiation, expression of functional markers, and cell population doubling time. To analyze in vitro growth we used not only the monolayer culture system but also the spheroid tumor model. Being a three-dimensional in vitro culture it facilitates direct cell-cell interactions and may therefore simulate in vivo growth more closely than the monolayer conditions. Our analysis revealed a conspicuous degree of heterogeneity among these 12 cell lines, which is best reflected by the ultrastructural grade of differentiation of spheroids and the population doubling time.

## Material and methods

Table 1 lists the pancreatic ductal carcinoma cell lines investigated in this study. The origin of each cell line was traced back to the respective sources and publications, to ascertain that they were truly generated from DACs. The histological typing of the tumors and their grade of differentiation according to the WHO classification [8] were deduced, if not explicitly mentioned in the original articles, from the descriptions and illustrations of the tumor's morphology. The histology and grade of the xenotransplants were studied in experiments by the authors [15] or have been described by other authors (se Table 1).

### Culture conditions

Cells were cultured as monolayers in RPMI 1640 with Glutamax (Gibco, Karlsruhe, Germany) containing 10% fetal calf serum (PAA Laboratories, Cölbe, Germany) under standard culture conditions (5% $CO_2$, 95% air in humidified chamber at 37°C).

### Generation of spheroids

Cells were trypsinized, counted in a hemocytometer and seeded onto nonadherent 96-well plates with U-form wells at a concentration of $10^4$/well in RPMI medium containing 10% fetal calf serum supplemented with 20% methyl cellulose (M-0512, Sigma-Aldrich, Sternheim, Germany). Spheroids were harvested after 96 h, pelleted, and washed in phosphate-buffered solution.

### Transmission electron microscopy

Monolayer cultures were grown to confluency on glass slides, washed twice in phosphate-buffered solution and fixed in 1–2.5% glutaraldehyde in 0.1 M cacodylate buffer. Some cell lines and the spheroids were fixed in a solution containing 0.05% picric acid, 2.5% glutaraldehyde, and 2% freshly prepared formaldehyde in 0.1 M cacodylate buffer. All samples were postfixed in 1% osmium tetroxide in cacodylate buffer. Following dehydration monolayer cultures were embedded in Epon in situ on the glass slides. Ultrathin sections, cut on a Leica Ultracut UCT ultramicrotome, were stained with uranyl acetate and lead citrate and examined under a Zeiss E902 electron microscope. At least 20 cells from each of two independent cultures of each cell line were photographed on Kodak electron microscope film.

### Ultrastructural grading

The ultrastructure of the monolayers and spheroids was evaluated on microphotographs according to the slightly modified criteria of Kern et al. [14]. The analysis included cellular polymorphism (variability of cell shape, amount of cytoplasm), nuclear polymorphism (nuclear membrane, chromatin, nucleoli), mucin granules (rare, abundant), cell organelles (Golgi apparatus, endoplasmic

**Table 1** Origin, histology and grade of differentiation of pancreatic ductal adenocarcinoma (PDAC) cell lines

| Cell line | Source of tumor cells | Histology and grade[a] of primary tumor | Histology and grade of transplanted tumor (in nude or SCID mice) | Principal investigator |
|---|---|---|---|---|
| A818-4 | Ascites | PDAC, G2 | G2[b] | H. Kalthoff (Germany) [25] |
| ASPC-1 | Ascites | PDAC, G2 | G2/G3 (focally G1) [5] | W.H. Chen and (USA) [5] |
| BxPc3 | Primary tumor | PDAC, G2 | G2/G3 [33] | M.H. Tan (USA) [33] |
| Capan-1 | Liver metastasis | PDAC, G1 | G1 [16] | J. Fogh (USA) [6] |
| Capan-2 | Primary tumor | PDAC, G1 | G1 [19] | J. Fogh (USA)[c] |
| Colo357 | Lymph node metastasis | PDAC, G1-G2 | G2/G3 (focally G1 and adenosquamous components) [23] | R. Morgan (USA) [26] |
| HPAF-2 | Ascites | PDAC, G2? | not known | R.S. Metzgar (Germany) [24] |
| MiaPaCa-2 | Primary tumor | PDAC, G3 | G3[b] | A. Yunis (USA) [35] |
| Panc1 | Primary tumor | PDAC, G3 | G3 [18] | M. Lieber (USA) [18] |
| Panc89 | Lymph node metastasis | PDAC, G2 | G2/G3 [28] | T. Okabe (Japan) [28] |
| PancTuI | Primary tumor | PDAC, G2-G3 | G3[b] | M. vov Bülow (Germany) [25] |
| Pt45P1 | Primary tumor | PDAC, G3 | G3[b] | H. Kalthoff (Germany) [25] |

[a] WHO grading system
[b] Unpublished data

**Table 2** Grading of ultrastructural features of monolayer cultures of PDAC cell lines (*grade 1* score 5–8, *grade 2* score 9–12, *grade 3* score 13–15)

| Cell line | Cellular polymorphism | Nuclear polymorphism | Cell membrane structures | Mucin granules | Cell organelles | Final score | Grade |
|---|---|---|---|---|---|---|---|
| Capan-1 | 1 | 2 | 1.5 | 1–2 (1.5) | 1 | 7 | 1 |
| Capan-2 | 1 | 2–3 (2.5) | 2 | 1–2 (1.5) | 1 | 8 | 1 |
| BxPc3 | 3 | 2 | 1–2 (1.5) | 1 | 1–2 (1.5) | 9 | 2 |
| HPAF-2 | 3 | 3 | 1 | 1 | 1 | 9 | 2 |
| Panc89 | 2 | 2 | 2 | 1 | 2 | 9 | 2 |
| A818-4 | 3 | 2 | 3 | 1 | 1 | 10 | 2 |
| Aspc-1 | 3 | 3 | 2 | 1 | 1 | 10 | 2 |
| Colo357 | 3 | 2 | 2 | 2 | 1 | 10 | 2 |
| PancTuI | 3 | 3 | 2–3 (2.5) | 1–2 (1.5) | 3 | 13 | 3 |
| MiaPaCa-2 | 3 | 2–3 (2.5) | 3 | 2 | 3 | 13.5 | 3 |
| Panc1 | 3 | 3 | 3 | 3 | 2–3 (2.5) | 14.5 | 3 |
| Pt45P1 | 3 | 3 | 3 | 2–3 (2.5) | 3 | 14.5 | 3 |

**Table 3** Grading of ultrastructural features of spheroids generated from cultured PDAC cells (*grade 1* score 7–11, *grade 2* score 12–16, *grade 3* score 17–21)

| Cell line | Cellular polymorphism | Nuclear polymorphism | Cell membrane structures | Mucin granules | Cell organelles | Lumen formation | Cell polarity | Final score | Grade |
|---|---|---|---|---|---|---|---|---|---|
| Capan-1 | 1 | 1 | 1–2 (1.5) | 1 | 1 | 1 | 1 | 7.5 | 1 |
| Capan-2 | 1–2 (1.5) | 2 | 1 | 1–2 (1.5) | 1 | 1 | 1–2 (1.5) | 9.5 | 1 |
| Colo357 | 2 | 1 | 2 | 1 | 1 | 2 | 3 | 12 | 2 |
| HPAF-2 | 3 | 3 | 1 | 1 | 1 | 1 | 3 | 13 | 2 |
| Aspc-1 | 2–3 (2.5) | 3 | 2 | 1 | 1 | 1 | 3 | 13.5 | 2 |
| A818-4 | 3 | 2 | 2 | 1 | 1 | 2 | 3 | 14 | 2 |
| BxPc3 | 3 | 2 | 1 | 1–2 (1.5) | 2 | 1–2 (1.5) | 3 | 14 | 2 |
| Panc89 | 3 | 3 | 1–2 (1.5) | 1 | 1–2 (1.5) | 1–2 (1.5) | 3 | 14.5 | 2 |
| PancTu-I | 3 | 3 | 2 | 2 | 2–3 (2.5) | 1 | 3 | 16.5 | 3 |
| Panc1 | 3 | 3 | 2 | 2 | 2 | 2 | 3 | 17 | 3 |
| Pt45P1 | 3 | 3 | 2 | 2 | 3 | 2 | 3 | 18 | 3 |
| MiaPaCa-2[a] | – | – | – | – | – | – | – | 20[b] | – |

[a] No spheroid formation
[b] Estimated score

**Table 4** Immunocytochemical features of monolayer cultures and spheroids generated from cultured PDAC cells (*m* membrane-bound staining pattern, *CK* cytokeratin, *CEA* carcinoembryonic antigen; – negative, + <10%, ++ 10–50%, +++ >50% of the cells stained)

| Cell line | Grade | CK7 | CK8, 18, 19[a] | Pan-CK[a] | Vimentin | MUC1 | MUC2 | MUC5 | MUC6 | CEA[a] |
|---|---|---|---|---|---|---|---|---|---|---|
| Capan-1 | 1 | +++ | + | +++ | ++ | +++ m | – | ++ | +++ | + |
| Capan-2 | 1 | +++ | +++ | +++ | – | +++ m | – | – | – | – |
| Colo357 | 2 | +++ | + | +++ | + | +++ | – | ++ | – | + |
| HPAF-2 | 2 | +++ | +++ | +++ | + | ++ | – | + | – | ++ |
| Aspc-1 | 2 | ++ | +++ | +++ | +++ | ++ | + | + | – | ++ |
| A818-4 | 2 | +++ | – | +++ | +++ | + | +++ | + | – | – |
| BxPc3 | 2 | +++ | + | +++ | + | ++ | + | + | – | ++ |
| Panc89 | 2 | +++ | + | ++ | – | + | + | + | – | ++ |
| PancTuI | 3 | +++ | ++ | +++ | +++ | + | – | – | +++ | + |
| Panc1 | 3 | – | +++ | +++ | +++ | + | – | – | – | – |
| Pt45P1 | 3 | +++ | ++ | +++ | +++ | ++ | + | +++ | – | – |
| MiaPaCa-2[a] | 3 | – | ++ | +++ | +++ | ++ | – | – | n.d. | – |

reticulum, mitochondria, microfilaments), cell membrane structures (cell junctions, interdigitations, microvilli), and in the case of spheroids additionally lumen formation and cell polarity (well to poorly developed). Each feature was evaluated in at least 20 intact cells from each series and given an individual score ranging from 1 to 3. The final score was calculated by adding the individual scores obtained for each cell line. To define the grade, the final scores were arbitrarily divided into three groups designated as grade 1 (final score, monolayer, 5–8; spheroid 7–11), grade 2 (final score, monolayer, 9–12; spheroid, 12–16), and grade 3 (final score, monolayer, 13–15; spheroid, 17–21; Tables 2, 3).

## Immunocytochemistry

Immunocytochemistry was performed on monolayer cultures and spheroids (Table 4). For monolayer cultures cells were grown on glass slides and fixed in 4% buffered paraformaldehyde for 1 h.

Then the cells were permeabilized by heating in a pressure cooker in Tris-EDTA-trisodium citrate buffer for 3 min. The spheroids were embedded in OCT medium, snap-frozen in isopentane-dry ice, and cut into 10-µm-thin cryostat sections. Primary antibodies were used to MUC1 (1:100, Novocastra, Newcastle, UK), MUC2 (1: 100, Novocastra), MUC5 (1:500, Mab2011, Chemicon, Temecula, Calif., USA), MUC6 (1: 100, Novocastra), cytokeratin 7 (1: 25, M 7018, Dako, Glostrup, Denmark), cytokeratin 8, 18, and 19 (1:10, CAM 5.2, 349205, Becton Dickinson, San Jose, Calif., USA), pan-cytokeratin (1:200, Kl-1, 1918, Immunotech, Marseille, France), vimentin (1:100, M 7020, Dako), carcinoembryonic antigen (1:100, M7072, Dako), synaptophysin (1:50, Dako), and chromogranin A (1:2, Linaris, Wertheim-Bettingen, Germany). Serum blocking and detection were performed with a peroxidase-based mouse and rabbit Vectastain Kit (Vector Laboratories, Burlingame, CA, USA) according to the manufacturer's instructions. The staining intensity was graded as mild, moderate or strong.

### Proliferation assay

Confluent cultures were trypsinized, counted in a hemocytometer, and seeded into 96-well plates in concentrations of $5\times10^3$, $10^4$, and $2\times10^4$ cells/well. The number of viable cells was detected with a colorimetric tetrazolium salt based assay (Cell Proliferation Assay, Roche Diagnostics, Mannheim, Germany) after 24, 48, 72, and 96 h. Each measurement was performed 12-fold in three independent series. Optical densities were plotted against incubation time. The highest proliferation rate was calculated from the curve.

### Genetic data

The data on the mutational status of the most frequent genetic changes (p53, K-ras, DPC4/smad4, p16) in the cell lines were obtained from earlier publications [3, 4, 13, 25, 27].

## Results

### Features of monolayer and spheroid cultures

The pancreatic ductal adenocarcinoma (PDAC) cell lines grew as adherent monolayer cultures. Capan-1 and Colo357 and to some extent Panc1 cells tended to form bi- or multilayers in postconfluent cultures. A subset of Capan-1 and MiaPaCa-2 cells detached after the cultures became confluent and grew as floating cell aggregates (Capan-1) or single cells (MiaPaCa-2). The cells varied highly in shape from cell line to cell line. Capan-1 and Capan-2 cultures were rather monomorphic and consisted of polygonal, cuboid, or round-oval cells. Panc89 cells were moderately polymorphic, polygonal, or oval. All other cultures exhibited marked polymorphism. Cell shapes ranged from polygonal, oval-round to spindle-shaped fibroblastoid. HPAF-2, Colo357, A818-4 cultures additionally contained bizarre giant cells.

All PDAC cell lines formed spheroids within 24 h except for MiaPaCa-2, the cells of which disaggregated during harvesting. Capan-1 and Capan-2 cells formed cohesive spheroids consisting of smaller cell aggregates with lumen formation. A818-4, BxPc3, Colo357, HPAF-2, Panc89, PancTu-I, and Pt45P1 cells developed well circumscribed spheroids. Aspc-1 and Panc-1 spheroids had an irregular outer surface.

### Ultrastructural features

Tables 2 and 3 show the results of the grading of the cell lines. The grade 1 cell lines, Capan-1 and Capan-2, differed little in their features. The nuclei of the monomorphous cells showed homogeneous chromatin and one to four round nucleoli. The abundant cytoplasm contained many electron dense or lamellar mucin granules, Golgi complexes, and elements of rough endoplasmic reticulum. The cells were connected by numerous cell junctions such as desmosomes and junctional complexes. Networks of intermediate filaments were anchored to the desmosomes. Capan-1 cells formed many interdigitations with neighboring cells. Capan-2 cells had well developed microvilli and glycocalyx on their surface. In spheroids both cell lines revealed marked lumen formation. Capan-1 cells and to some extent Capan-2 cells showed a polarization towards the outer surface of the spheroids, with mucin granules in apical position and nuclei at the opposite side. The lateral plasma membranes at the apical pole of the cells were connected by regular junctional complexes (Fig. 1a).

The grade 2 cell lines exhibited marked heterogeneity from cell line to cell line. The most striking difference between these lines and the grade 1 cell lines was the pronounced cellular and nuclear polymorphism. The nuclei of the polymorphic cells were irregular and sometimes highly segmented, occasionally with crude chromatin structure and with up to four nucleoli. In some cell lines a reduced number of interdigitations (A818-4, Aspc-1, Colo357) and desmosomes (Aspc-1, Colo357) was noted. In general the cells were well equipped with cell organelles, i.e., Golgi complexes, rough endoplasmic reticulum, and mucin granules. Lumen formation was seen in the spheroids, but the lumina were smaller and more irregular than in grade 1 spheroids. None of the grade 2 spheroids showed signs of polarization (Fig. 1b, c).

The grade 3 cell lines showed significantly fewer cell organelles, specialized membrane structures and mucin granules than the grade 2 cell lines. The cytoplasm contained elements of rough endoplasmic reticulum which were rarely organized in parallel structures. Golgi complexes were only seen in PancTu-I cells. Interdigitations were completely absent. Interestingly, PancTu-I spheroids formed well defined lumina. MiaPaCa-2 cells were not able to generate spheroids. We interpreted this phenomenon as loss of the capability to form cell-cell contacts and hence considered the MiaPaCa-2 cell line to be the most poorly differentiated line (Fig. 1d).

### Immunocytochemistry

Since there is no specific marker for PDACs or ductal differentiation, we used a panel of antibodies directed against various antigens (Table 4). CK7 was strongly expressed in 10 of the 12 cell lines. All but one cell line (A818-4) reacted with an antibody (CAM5.2) against

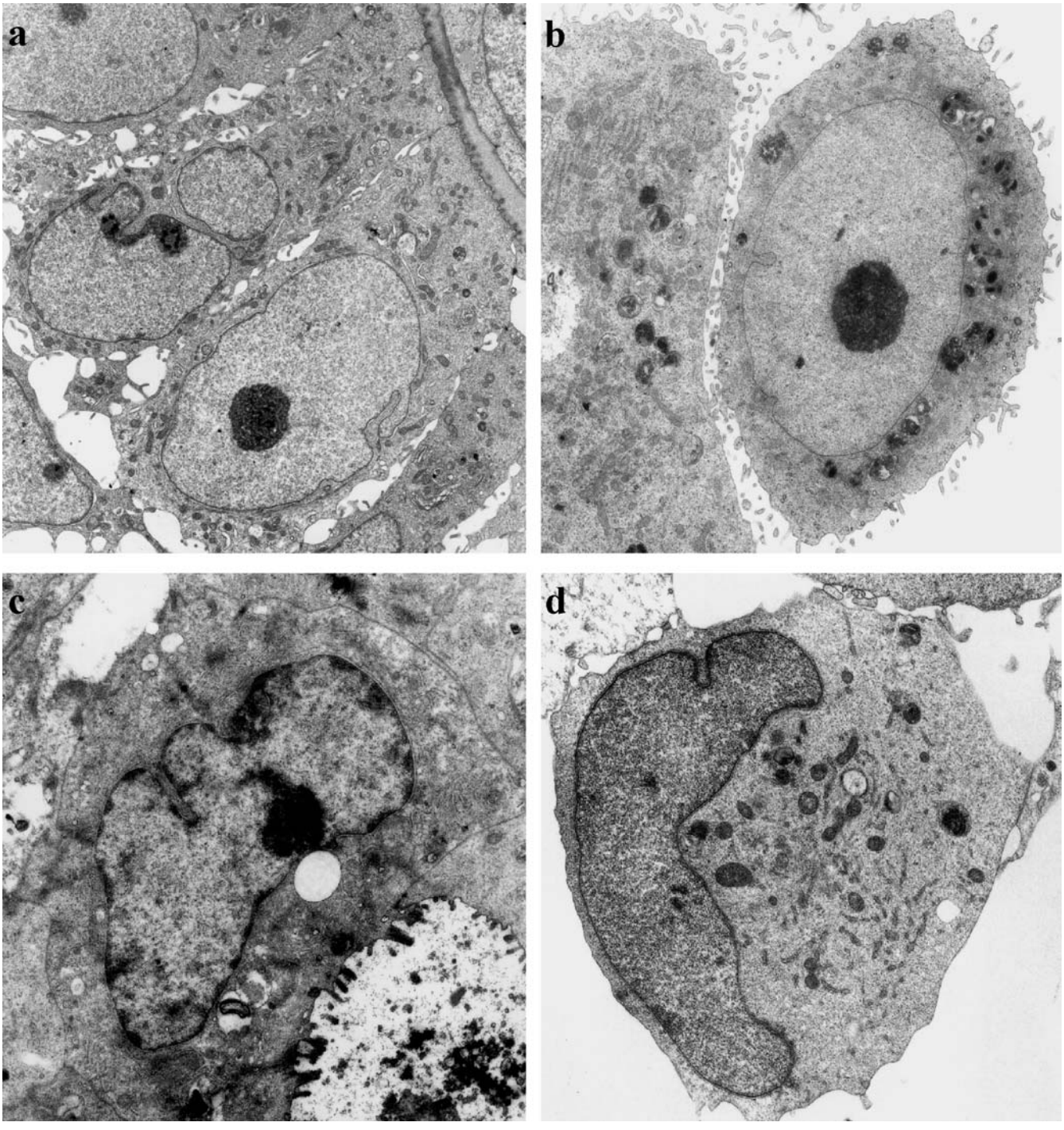



**Fig. 1** Ultrastructural features of PDAC cell lines. **a** Spheroid of Capan-2 cells showed polarity toward the surface, a number of microvilli and cell junctions, glycocalix on the surface. **b** Colo-357 cells in spheroid showed many microvilli, mucin granules, well developed Golgi apparatus and endoplasmic reticulum. **c** HPAF-2 cells in spheroid formed lumina with microvilli, numerous cell junctions. Note the markedly irregular nucleus with crude chromatin structure and membrane invagination. **d** MiaPaCa-2 cells in monolayer culture exhibited poorly developed membrane structures, cytoplasmic organelles and few mucin granules. Original magnification, ×3000

CK8, 18 and 19, and all cells were strongly positive for the broad spectrum CK marker Kl-1. Vimentin was variably expressed in grade 1 and grade 2 cell lines, and strongly expressed in all grade 3 cell lines. MUC1 was expressed in all cell lines. Grade 1 cell lines displayed a membrane-bound staining pattern and grade 2 and 3 cell lines faint to moderately strong cytoplasmic staining. The MUC2, MUC5, and MUC6 staining patterns appeared to

**Table 5** Genetic aberrations in PDAC cell lines [25]

| Cell line | Grade | K-ras | p53 | p16 | DPC4/smad4 |
|---|---|---|---|---|---|
| Capan-1 | 1 | Mut (p.m.) [4, 13] | Mut (p.m.) [4] | Mut[a] [27] | Mut (p.m.) [32] |
| Capan-2 | 1 | Mut (p.m.) [4, 13] | W.t. [4] | Mut (ins) [27] | N.d. (low protein expression)[b] |
| Colo357 | 2 | Mut (p.m.) [13] | W.t. [3, 13] | W.t. [27] | Mut (h.d.) [32][c] |
| HPAF-2 | 2 | Mut (p.m.) | Mut (p.m.) | Mut (del) | W.t. |
| Aspc-1 | 2 | Mut (p.m.) | Mut (frameshift) | Mut (frameshift) | W.t./Mut (p.m.) [32] |
| A818-4 | 2 | Mut (p.m.) | Mut | Mut (h.d.) | W.t |
| BxPc3 | 2 | W.t. [4, 13] | Mut (p.m.) [4, 13] | Mut[a] [27] | Mut (h.d.) [7] |
| Panc89 | 2 | W.t. [13]/Mut (p.m.) [36] | Mut (p.m.) | Mut (meth) | W.t. |
| PancTu-I | 3 | Mut (p.m.) | Mut (p.m.) | Mut (meth) | W.t. |
| Panc1 | 3 | Mut (p.m.) | Mut (p.m.) | Mut (h.d.) | W.t. |
| Pt45P1 | 3 | Mut (p.m.) | Mut (p.m.) | Mut (h.d.) | W.t. |
| MiaPaCa-2 | 3 | Mut (p.m.) | Mut (p.m.) | Mut (h.d.) | W.t. |

[a] No gene product detected
[b] Personal communication I. Schwarte-Waldhoff (Immunologisch-Molekularbiologisches Labor, Medizinische Universitatsklinik Bochum, Knappschaftskrankenhaus, Ruhr-Universität, Bochum, Germany)
[c] DPC4/Smad4 expressing Colo357 cell line exists also (personal communication, I. Schwarte-Waldhoff)

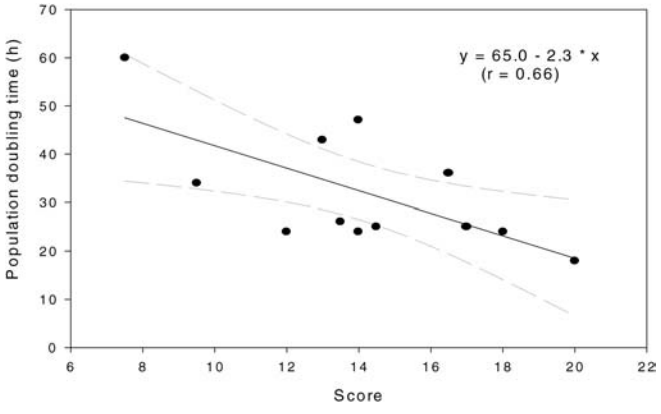



**Fig. 2** Correlation between ultrastructural grade (final score) of spheroids and population doubling time of monolayer cultures

be unrelated to the grade of differentiation. Carcinoembryonic antigen expression was quite evenly distributed among the cell lines. The neuroendocrine markers chromogranin and synaptophysin were negative in all cell lines (data not shown).

### Growth kinetics and correlation with ultrastructural grade

The population doubling time of the monolayer cultures ranged between 18 and 60 h. Grade I cell lines tended to have a higher population doubling time (47±13 h) than grade II (31.5±9.6 h) and grade III (25.7±6.5 h) cell lines. The limited number of cell lines did not allow a statistical analysis. The shortest doubling time was seen in MiaPaCa-2 cells and the longest in Capan-1 cells. These two cell lines represented the opposite ends of the ultrastructural grading spectrum (Fig. 2).

### Relationship between genetic alterations and ultrastructural grade

Table 5 shows the mutational status of the cell lines for K-ras (10/12), p53 (10/12), p16 (11/12), and DPC4/smad4 (1/8). There was no correlation between the K-ras, p53, p16, or DPC4/smad4 mutation rate and the ultrastructural grade of the cell lines.

## Discussion

Pancreatic carcinoma cell lines are so widely used for the study of tumorigenesis, tumor progression and tumor biology that it is definitely worth establishing a catalog of their principal features based on a comparative characterization of such cell lines. In a previous study we analyzed the K-ras, p53, p16, and DPC4/Smad4 status of 22 cell lines derived from pancreatic ductal carcinomas to determine their genetic profile [25]. In this study we analyzed the light microscopic, ultrastructural, and immunocytochemical features of 12 established pancreatic ductal carcinoma cell lines (including six of the previously tested series of 22 cell lines) when grown in monolayers and in three-dimensional cell cultures, i.e., spheroids. By establishing an ultrastructural grading system we were able to relate the fine structure of the individual cell lines to their population doubling time. This revealed a relationship between differentiation and growth.

We traced the source of the various cell lines tested to ensure that all derived from human pancreatic carcinomas showing ductal differentiation in the primary and, where available, in the xenograft. All cell lines were found to originate from PDACs, although of different degrees of differentiation.

The morphology of the monolayer cultures, as analyzed by phase contrast microscopy, differed from cell line to cell line. However, the differences allowed only a rough distinction between monomorphic and polymorphic

cell lines. Multicellular spheroids are thought to represent a model that is intermediate in complexity between monolayer cultures and solid in vivo tumors, in that they facilitate direct cell-cell interactions, which may influence metabolism, proliferation, and differentiation. Indeed, in the spheroids formed by several of our PDAC cell lines we saw cell polarization and lumen formation. On the basis of these criteria we found Capan-1 cells to be the most highly differentiated because their spheroids even resembled hollow spheres, a recently developed culture model of ductal differentiation characterized by cellular polarization towards the surface of the three dimensional cell aggregates [17]. On the other end of this spectrum were MiaPaCa-2 cells, which, in contrast to Capan-1 cells and all other PDAC cell lines analyzed, completely failed to grow as spheroids. These spheroids may therefore be regarded as a test system in which lumen formation and polarization, two of the most important in vivo criteria for PDAC differentiation, can be studied in vitro.

According to the WHO grading system [8], PDACs may be classified into three grades that can be used as prognostic markers [15, 20]. Originally this grading system also included an analysis of the ultrastructural features of the tumor cells [14, 15]. We applied similar criteria to the electron microscopic grading of our PDAC cell lines grown either as monolayers or spheroids. The main features that were scored, and that defined the grade were cellular and nuclear polymorphism and the presence of specialized membrane structures, cell organelles, polarity, and lumen formation, the latter two criteria applying only to spheroids. The features discriminating between grade 1 and grade 2 cell lines were cellular and nuclear polymorphism and loss of polarity of the outer cell layer of the spheroids. Grade 2 and grade 3 cell lines were distinguished mainly by the decreased number of mucin granules and cell organelles. Interestingly, all cell lines that were able to form spheroids also revealed lumen formation, even if the histology of the xenotransplants of the respective cell lines failed to show any clear glandular formations, as in the Panc1 cell line. This seems to indicate that the feature of glandular/ductal formation of a carcinoma may be retained longer in vitro under adequate growth conditions than in vivo.

The ultrastructural grading revealed that most (>80%) of the analyzed cell lines fall into either the grade 2 (50%) or grade 3 (33.3%) category, while the grade 1 PDAC cell lines formed the smallest group (16.7%). This does not reflect the distribution of grades among PDAC, which is 33% G1, 51% G2 and 16% G3 tumors [20], but is related to the general difficulty in culturing cell lines from well differentiated tumors. The grade assigned to the monolayer of a PDAC cell line did not differ from that of the accompanying spheroid. However, the two usually differed in their final scores. When we compared the final scores of the monolayer and spheroid of a cell line with the histological differentiation of its respective xenotransplant, it appeared that in the grade 2 group the final score for the spheroid reflected the capacity of the respective cell line for glandular differentiation in the xenotransplant better than the final score for the monolayer. For instance, the monolayer of BxPc3, a grade 2 cell line, had a lower final score than Aspc-1 or Colo357, although after xenotransplantation the latter two cell lines formed, at least focally, better differentiated tumors than BxPc-3 cells, which formed only moderately to poorly differentiated tumors. The spheroid scores for Aspc-1 and Colo 357 were, however, lower than that for BxPc3 and compared better with the cell lines' in vivo capacity for tumor differentiation. This suggests that their spheroids' ultrastructural score is the best determinant for the in vivo differentiation status of the tested PDAC cell lines. This is a notion, however, that needs to be confirmed in a larger study.

The expression patterns of cytokeratins are well defined characteristics of epithelial malignancies. CK7, 8, 18, and 19 are expressed in all human PDACs [9, 10, 29, 30], but decreasing expression of these cytokeratins is reported in the undifferentiated variant [12]. Vimentin, conversely, appears in undifferentiated carcinomas and is virtually absent from differentiated PDACs [12]. The disappearance of these cytokeratins and the appearance of vimentin may therefore be considered as a sign of dedifferentiation of PDAC in vivo. In vitro this observation is apparently of no relevance, since, irrespective of their ultrastructural differentiation, 10 of 12 PDAC cell lines expressed vimentin and to some extent also CK7, 8, 18, and 19, thereby confirming a number of other reports [12, 31]. None of the other immunocytochemical markers examined, i.e., MUC1, MUC2, MUC5, MUC6, CEA, synaptophysin, and chromogranin A, revealed any clear relationship with the ultrastructural differentiation of the cell lines. Hence they seem to be of no use in the characterization of PDAC cell lines. This applies particularly to MUC1 expression, which is a functional feature of PDACs [34]. MUC1 was expressed in all of our PDAC cell lines, confirming the data of other authors [2, 11]. Whether the membrane-bound MUC1 staining pattern seen in the spheroids of the Capan-1 and Capan-2 cell lines is a feature of highly differentiated PDAC cell lines needs to be confirmed by other studies. Interestingly, MUC2, which is virtually absent from PDACs in vivo but characterizes certain intraductal papillary mucinous neoplasms [1, 21], was expressed in 5 of 12 cell lines in this series, indicating that, as with vimentin, MUC2 is one of the markers whose reexpression is favored by in vitro conditions.

Because of the highly standardized culture conditions the population doubling time of monolayer cultures is a well reproducible feature of cell lines. We asked whether there is a relationship between the proliferation rate of the PDAC cell lines and their ultrastructural differentiation. As Fig. 2 shows, the population doubling time is related to the ultrastructural differentiation status of the cell lines. This is best exemplified by the cell lines with the highest degree of differentiation, Capan-1, and the lowest degree of differentiation, MiaPaCa-2, the two cell lines that also exhibited markedly differing proliferation rates. The fact that the correlation for the other cell lines is not better

may be explained in several ways. First, monolayer cultures are optimally supplied with nutrients and oxygen but have reduced cell-cell contacts and grow on an artificial surface. These conditions are highly artificial and may affect both the differentiation program and the proliferation rate. Second, the number of cell lines tested is too limited to reveal statistically significant differences. Third, in normal cells differentiation and proliferation are usually controlled by different signal transduction pathways, which may be affected differently by the genetic and epigenetic changes that lead to malignant transformation. Therefore differentiation and proliferation are not necessarily affected to the same extent in the PDAC cell lines.

In a previous publication on 22 PDAC cell lines we analyzed the most common genetic alterations in human PDAC, K-ras, p53, $p16^{Ink4}$, and DPC4/smad 4. The K-ras, p53, and $p16^{Ink4}$ genes were found to be mutated in over 90% of the cell lines, followed by mutations of DPC4/Smad4 in approximately 50% [25]. Eleven of the 12 cell lines in this series (which included six cell lines from the previous series [25]) also harbored $p16^{Ink4}$ mutations and 10/12 p53 and K-ras mutations, while DPC4/smad4 was mutated in only one of nine examined cell lines. From these results it was not possible to determine a correlation between differentiation and genetic alterations. It is possible that the genetic alterations that accompany the differentiation of tumor cells will not be detected until more is known about the genes that control the cellular differentiation process.

In conclusion, our study shows that the differentiation status of PDAC cell lines can be reliably determined by means of a detailed grading system based on the ultrastructural features. This system is best applied to spheroids, because this three dimensional culture model seems to offer a good correlate for the in vivo situation and is also related to the proliferation status of the monolayer cultures. The data from this study may be used to create a biological catalogue of PDAC cell lines listing their differentiation status and may be helpful in interpreting the relevance of many cell biological observations.

**Acknowledgements** The authors thank O. Bracker, R Köpke, B. Facompré, and A. Höltzl for their skillful technical assistance, Prof. Lüllmann-Rauch and Prof. A. Kadar for their helpful technical suggestions, and K. Dege for editing the manuscript. This work was supported by the Werner and Klara Kreitz Foundation, the IZKF, University of Kiel, and a Faculty Grant.

## References

1. Adsay NV, Pierson C, Sarkar F, Abrams J, Weaver D, Conlon KC, Brennan MF, Klimstra DS (2001) Colloid (mucinous noncystic) carcinoma of the pancreas. Am J Surg Pathol 25:26–42
2. Balagué C, Gambus G, Carrato C, Porchet N, Aubert JP, Kim YS, Real FX (1994) Altered expression of MUC2, MUC4, and MUC5 mucin genes in pancreas tissues and cancer cell lines. Gastroenterology 106:1054–1061
3. Barton CM, Staddon SL, Hughes CM, Hall PA, O'Sullivan C, Klöppel G, Theis B, Russell RC, Neoptolemos J, Williamson RC (1991) Abnormalities of the p53 tumour suppressor gene in human pancreatic cancer. Br J Cancer 64:1076–1082
4. Berrozpe G, Schaeffer J, Peinado MA, Real FX, Perucho M (1994) Comparative analysis of mutations in the p53 and K-ras genes in pancreatic cancer. Int J Cancer 58:185–191
5. Chen WH, Horoszewicz JS, Leong SS, Shimano T, Penetrante R, Sanders WH, Berjian R, Douglass HO, Martin EW, Chu TM (1982) Human pancreatic adenocarcinoma: in vitro and in vivo morphology of a new tumor line established from ascites. In Vitro 18:24–34
6. Fogh J, Wright WC, Loveless JD (1977) Absence of HeLa cell contamination in 169 cell lines derived from human tumors. J Natl Cancer Inst 58:209–214
7. Hahn SA, Schutte M, Hoque AT, Moskaluk CA, da Costa LT, Rozenblum E, Weinstein CL, Fischer A, Yeo CJ, Hruban RH, Kern SE (1996) DPC4, a candidate tumor suppressor gene at human chromosome 18q21.1. Science 271:350–353
8. Hamilton SR, Aaltonen LA (eds) World Health Organization classification of tumours. Pathology and genetics of tumours of the digestive system, 2000. IARC, Lyon
9. Herzig KH, Altmannsberger M, Fölsche UR (1994) Intermediate filaments in rat pancreatic acinar tumors, human ductal carcinomas, and other gastrointestinal malignancies. Gastroenterology 106:1326–1332
10. Heyderman E, Larkin SE, O'Donnell PJ, Haines AM, Warren PJ, Northeast A, Grant AG (1990) Epithelial markers in pancreatic carcinoma: immunoperoxidase localisation of DD9, CEA, EMA and CAM 5.2. J Clin Pathol 43:448–452
11. Hollingsworth MA, Strawhecker JM, Caffrey TC, Mack DR (1994) Expression of MUC1, MUC2, MUC3 and MUC4 mucin mRNAs in human pancreatic and intestinal tumor cell lines. Int J Cancer 57:198–203
12. Hoorens A, Prenzel K, Lemoine NR, Klöppel G (1998) Undifferentiated carcinoma of the pancreas: analysis of intermediate filament profile and Ki-ras mutations provides evidence of a ductal origin. J Pathol 185:53–60
13. Kalthoff H, Schmiegel W, Roeder C, Kasche D, Schmidt A, Lauer G, Thiele HG, Honold G, Pantel K, Riethmuller G (1993) p53 and K-RAS alterations in pancreatic epithelial cell lesions. Oncogene 8:289–298
14. Kern HF, Roher HD, von Bülow M, Klöppel G (1987) Fine structure of three major grades of malignancy of human pancreatic adenocarcinoma. Pancreas 2:2–13
15. Klöppel G, Lingenthal G, von Bülow M, Kern HF (1985) Histological and fine structural features of pancreatic ductal adenocarcinomas in relation to growth and prognosis: studies in xenografted tumours and clinico-histopathological correlation in a series of 75 cases. Histopathology 9:841–856
16. Kyriazis AP, Kyriazis AA, Scarpelli DG, Fogh J, Rao MS, Lepera R (1982) Human pancreatic adenocarcinoma line Capan-1 in tissue culture and the nude mouse: morphologic, biologic, and biochemical characteristics. Am J Pathol 106:250–260
17. Lehnert L, Lerch MM, Hirai Y, Kruse ML, Schmiegel W, Kalthoff H (2001) Autocrine stimulation of human pancreatic duct-like development by soluble isoforms of epimorphin in vitro. J Cell Biol 152:911–922
18. Lieber M, Mazzetta J, Nelson-Rees W, Kaplan M, Todaro G (1975) Establishment of a continuous tumor-cell line (panc-1) from a human carcinoma of the exocrine pancreas. Int J Cancer 15:741–747
19. Löhr M, Trautmann B, Göttler M, Peters S, Zauner I, Maillet B, Klöppel G (1994) Human ductal adenocarcinomas of the pancreas express extracellular matrix proteins. Br J Cancer 69:144–151
20. Lüttges J, Schemm S, Vogel I, Hedderich J, Kremer B, Klöppel G (2000) The grade of pancreatic ductal carcinoma is an independent prognostic factor and is superior to the immunohistochemical assessment of proliferation. J Pathol 191:154–161

21. Lüttges J, Zamboni G, Longnecker D, Klöppel G (2001) The immunohistochemical mucin expression pattern distinguishes different types of intraductal papillary mucinous neoplasms of the pancreas and determines their relationship to mucinous noncystic carcinoma and ductal adenocarcinoma. Am J Surg Pathol 25:942–948
22. Maillet B, De Grève J, Lemoine H, Kalthoff H, Schmiegel W, Klöppel G (1993) Phenotypical differentiation and genetic alterations in human pancreatic carcinoma cell lines. Int J Pancreatol 14:72–75
23. Meitner PA, Kajiji SM, LaPosta-Frazier N, Bogaars HA, Jolly GA, Dexter DL, Calabresi P, Turner MD (1983) "COLO 357," a human pancreatic adenosquamous carcinoma: growth in artificial capillary culture and in nude mice. Cancer Res 43:5978–5985
24. Metzgar RS, Gaillard MT, Levine SJ, Tuck FL, Bossen EH, Borowitz MJ (1982) Antigens of human pancreatic adenocarcinoma cells defined by murine monoclonal antibodies. Cancer Res 42:601–608
25. Moore PS, Sipos B, Orlandini S, Sorio C, Real FX, Lemoine NR, Gress T, Bassi C, Klöppel G, Kalthoff H, Ungefroren H, Löhr M, Scarpa A (2001) Genetic profile of 22 pancreatic carcinoma cell lines. Analysis of K-*ras*, *p53*, *p16* and *DPC4/Smad4*. Virchows Arch 439:798–802
26. Morgan RT, Woods LK, Moore GE, Quinn LA, McGavran L, Gordon SG (1980) Human cell line (COLO 357) of metastatic pancreatic adenocarcinoma. Int J Cancer 25:591–598
27. Naumann M, Savitskaia N, Eilert C, Schramm A, Kalthoff H, Schmiegel W (1996) Frequent codeletion of p16/MTS1 and p15/MTS2 and genetic alterations in p16/MTS1 in pancreatic tumors. Gastroenterology 110:1215–1224
28. Okabe T, Yamaguchi N, Ohsawa N (1983) Establishment and characterization of a carcinoembryonic antigen (CEA)- producing cell line from a human carcinoma of the exocrine pancreas. Cancer 51:662–668
29. Rafiee P, Ho SB, Bresalier RS, Bloom EJ, Kim JH, Kim YS (1992) Characterization of the cytokeratins of human colonic, pancreatic, and gastric adenocarcinoma cell lines. Pancreas 7:123–131
30. Santini D, Ceccarelli C, Martinelli GN, Pasquinelli G, Leone O, Marrano D, Mancini AM (1994) Expression of intermediate filaments in normal and neoplastic exocrine pancreas. Zentralbl Pathol 140:247–258
31. Schussler MH, Skoudy A, Ramaekers F, Real FX (1992) Intermediate filaments as differentiation markers of normal pancreas and pancreas cancer. Am J Pathol 140:559–568
32. Schutte M, Hruban RH, Hedrick L, Cho KR, Nadasdy GM, Weinstein CL, Bova GS, Isaacs WB, Cairns P, Nawroz H, Sidransky D, Casero RA Jr, Meltzer PS, Hahn SA, Kern SE (1996) DPC4 gene in various tumor types. Cancer Res 56:2527–2530
33. Tan MH, Nowak NJ, Loor R, Ochi H, Sandberg AA, Lopez C, Pickren JW, Berjian R, Douglass HO Jr, Chu TM (1986) Characterization of a new primary human pancreatic tumor line. Cancer Invest 4:15–23
34. Vila MR, Lloreta J, Schussler MH, Berrozpe G, Welt S, Real FX (1995) New pancreas cancers cell lines that represent distinct stages of ductal differentiation. Lab Invest 72:395–404
35. Yunis AA, Arimura GK, Russin DJ (1977) Human pancreatic carcinoma (MIA PaCa-2) in continuous culture: sensitivity to asparaginase. Int J Cancer 19:218–235
36. Hirai H, Okabe T, Ahraku Y, Fujisawa M, Unabe A, Takaku F (1985) Activation of the c-k-ras oncogene in a human pancreas carcinoma. Biochem Biophys Res Commun 127:168–174

Virchows Arch (2003) 442:453–461
DOI 10.1007/s00428-003-0794-2

ORIGINAL ARTICLE

**Jiří Ehrmann · Antonín Kolek · Rostislav Kod'ousek · Jana Zapletalová · Soňa Lísová · Paul Gerard Murray · Jiří Drábek · Zdeněk Kolář**

# Immunohistochemical study of the apoptotic mechanisms in the intestinal mucosa during children's coeliac disease

Received: 29 October 2002 / Accepted: 12 February 2003 / Published online: 16 April 2003
© Springer-Verlag 2003

**Abstract** Mechanisms leading to morphological changes of the small intestine during coeliac disease (CD) are not yet completely recognized; however, two main processes have been suggested recently: remodeling of mucosa by matrix metalloproteinases, and mucosal atrophy by apoptosis. The aim of this study was analysis of the expression of proteins regulating apoptosis in the small intestine of children with active CD (ACD) and potential CD (PCD). Jejunal biopsies of 43 children with PCD and untreated ACD and 21 control samples were analyzed by means of standard indirect immunohistochemical technique for Fas, Fas ligand (Fas-L), tissue transglutaminase (tTG), Bcl-2, and glutathione S-transferase (GST) expression. We found significantly lower numbers of Fas-expressing enterocytes in the ACD patients than in PCD patients and controls. Similarly, the number of Fas-positive mucosal lymphocytes was decreased in ACD when compared with PCD. The number of Fas-L- and tTG-expressing enterocytes and mucosal lymphocytes was higher in both PCD and ACD. On the other hand, the number of Bcl-2-positive mucosal lymphocytes in PCD as well as ACD was significantly lower. The expression of tTG in extracellular matrix was significantly higher in PCD and ACD when compared with controls. Our results showed that Fas and/or Fas-L, Bcl-2, and tTG may be involved in apoptotic pathways leading to mucosal atrophy in children with CD. tTG changes are in agreement with the presumed role of this protein in the pathogenesis of CD.

**Keywords** Coeliac disease · Apoptosis · Fas · Fas-L · Bcl-2 · tTG

J. Ehrmann Jr · R. Kod'ousek · S. Lísová · Z. Kolář (✉)
Laboratory of Molecular Pathology & Institute of Pathology,
Palacký University,
Hněvotínská 3, 77515 Olomouc, Czech Republic
e-mail: kolarz@tunw.upol.cz
Tel.: +42-585632465
Fax: +42-585632966

A. Kolek
Clinic of Pediatrics, Faculty of Medicine,
Palacký University,
I. P. Pavlova 6, 77520 Olomouc, Czech Republic

J. Zapletalová
Department of Biometry, Faculty of Medicine,
Palacký University,
Hněvotínská 3, 77515 Olomouc, Czech Republic

P. G. Murray
CRC Institute for Cancer Studies,
University of Birmingham,
B15 2TJ, UK

J. Drábek
Department of Immunology, HLA Laboratory,
Faculty of Medicine,
Palacký University,
I. P. Pavlova 6, 77520 Olomouc, Czech Republic

## Introduction

Coeliac disease (CD) is an inflammatory disease of the small intestine, characterized by abnormal reaction to gluten. Recent studies have shown an estimated prevalence of 1 in every 85–300 individuals in Europe [20]. Moreover, refractory or untreated CD is associated with some malignancies such as enteropathy-associated T-lymphoma, carcinoma of the esophagus, or carcinoma of the pharynx [11, 12]. Histologically, CD is characterized by inflammation and atrophy of mucosa of the small intestine. It has been suggested that mucosal atrophy is result of its remodeling by matrix metalloproteinases [41] and of excessive apoptotic enterocyte loss [6, 30]. Apoptosis of enterocytes is mediated by infiltrating both cytotoxic mucosal T lymphocytes and intraepithelial lymphocytes (IELs) via the perforin-granzyme mechanism [6, 22, 34, 43]. The effect of perforin can be modulated by some members of the Bcl-2 family and, in addition, other molecules are involved in the modulation of the enterocyte apoptosis, such as glutathione S-transferase (GST) and tissue transglutaminase (tTG) [15]. GST regulates programmed cell death by controlling

**Table 1** Primary antibodies used in the study (*Fas-L* Fas ligand, *GST* glutathione S-transferase, *tTG* tissue transglutaminase)

| Antibody | Clone | Dilution | Pretreatment | Secondary | Producer |
|---|---|---|---|---|---|
| Anti-Fas | N18 | 1:50 | Microwave 15 min | Polyclonal rabbit | Santa Cruz[a] |
| Anti-Fas-L | N20 | 1:50 | Microwave 15 min | Polyclonal rabbit | Santa Cruz[a] |
| Anti-Bcl-2 | 124 | Prediluted | Microwave 15 min | Monoclonal mouse | Dako[b] |
| Anti-GST | PI 353–10 | 1:50 | No | Monoclonal mouse | Dako[b] |
| Anti-tTG | CUB 7402 | 1:50 | Microwave 15 min | Monoclonal mouse | Dako[b] |

[a] Santa Cruz Biotechnology, Santa Cruz, Calif., USA
[b] Dako, Glostrup, Denmark

mitochondrial membrane permeability [16, 17]. Intestinal GST can also protect against cancer development [8]. Many authors have documented that tTG is involved in CD pathogenesis [25, 42]. It has been shown that tTG forms complexes with gliadin peptides. Deamidated gliadin is then recognized by specific intestinal T lymphocytes and it is also the main target of disease-specific autoantibodies. There is evidence that this complex formation develops in extracellular matrix and mucosal basement membranes [28, 29, 39, 48, 49]. Nevertheless, tTG is also considered as one of the important factors involved in programmed cell death [35, 36, 37, 45], and assessment of tTG expression within the cells could serve as an early indicator of apoptosis [1, 2, 18, 26]. Apoptosis of enterocytes mediated by cytotoxic T lymphocytes is activated mainly by a Fas–Fas ligand (Fas-L) interaction [3]. Therefore, the aim of our study was to analyze stage-dependent immunohistochemical expression of proteins Fas, Fas-L, tTG, Bcl-2, and GST, which could be involved in development of morphological changes during CD.

## Materials and methods

### Patients

All patients were treated in the Pediatric Clinic, Faculty of Medicine, Palacký University, Olomouc, during the period 1997–2000. The study was carried out on 25 children with active CD (ACD), mean age 7.6 years (median 7.0 years). This mean age is commonly observed at the time of diagnosis of CD in children in the Czech Republic. All subjects complained of symptoms of malabsorption (diarrhea, weight loss, growth disturbances). Histological examination of small intestine mucosa showed villous atrophy of type IIIc, according to the modified Marsh classification [23, 35], and the presence of antiendomysial antibody (anti-EMA) was confirmed in all cases. In 18 children with potential CD (PCD), mean age 10.9 years (median 11.0 years), the presence of anti-EMA, *HLA* alleles *DQA1*0501*, *DQB1*0201*, mucosal changes of modified Marsh type I (more than 40 intraepithelial lymphocytes per 100 enterocytes), and gluten challenge lasting more than 3 months were confirmed. In controls, 21 children without CD, mean age 7.6 years (median 5.0 years), jejunal biopsy was indicated for nonspecific gastrointestinal symptoms. Absence of anti-EMA and normal jejunal morphology (Marsh 0) were confirmed in all cases.

### Samples

Small intestine biopsy was performed either with capsule (pediatric small intestine capsule with two ports; T.C. Components/Engineers, England) or by endoscopy (Olympus GIF-E; Olympus XP-20). Histopathological mucosal changes were classified according to Marsh [23, 35]. Coeliac disease was diagnosed according to revised European Society for Paediatric Gastroenterology, Hepatology and Nutrition (ESPGHAN) criteria [51], and active and potential CD were classified according criteria proposed by Ferguson and Troncone [14, 47]. IgA class anti-endomysial antibodies (EMA) were analyzed by indirect immunofluorescence microscopy (The Binding Site, Birmingham, UK). Quantitative determination of serum IgA levels was performed by nephelometry (Behring). The *HLA-DQA1*0501* allele was tested using PCR by a pair of primers 5' CAG ACA ATT TAG ATT TGA CCC 3', 5' CAG TCA TAA CTC TCC TCA GC 3'. Investigation of the alleles in the *HLA-DQB1* locus was performed by PCR with published sequence-specific primers [31].

### Tissue processing and immunohistochemistry

Jejunal biopsy samples were fixed in formalin up to 24 h and embedded in paraffin. Specimens 5 $\mu$m thick were prepared on glass slides coated with Vectabond (Vector). A standard, indirect immunohistochemical technique, using biotinylated secondary anti-rabbit or anti-mouse antibody and streptavidin peroxidase after antigen retrieval, was used for detection of Fas, Fas-L, Bcl-2, tTG, and GST (Table 1). The primary antibody was omitted as a negative control. The grade of immunopositivity of Fas, Fas/L, Bcl-2, GST, and tTG was scored semiquantitatively at a magnification of ×400 in the following ranges: zero, up to 10% of positive cells; +, 11–29% of positive cells; ++, 30–59% of positive cells; +++, 60% or more positive cells. Moreover, the objectivity of this semiquantitative approach was validated by subsequent estimation of the percentage of Fas- and Fas-L-positive cells by a computer image-analysis system, Laboratory Universal Computer Image Analysis M (Laboratory Imaging, Prague, Czech Republic). Expression of all analyzed proteins was assessed separately in enterocytes, mucosal lymphocytes, and IELs. We also measured the ratio of Fas-positive glycocalyx of intestinal villi per total length of glycocalyx by LUCIA M. The positivity of cells was compared in both the cryptal regions and in the upper part of the villi. Moreover, the expression of tTG was also semiquantitatively estimated in the basement membrane of intestinal mucosa and in extracellular matrix.

### Statistics

The proportion of semiquantitative ranges (zero, +, ++, +++) in particular groups was expressed as a percentage. Then a two-way sample analysis with a confidence level of 0.95 and a significance level of $P \geq 0.05$, chi-square tests and Pearson correlation were used for comparison of these percentage values between controls, PCD patients, and ACD patients. The results are therefore expressed as percentage of proportion of semiquantitatively obtained ranges.

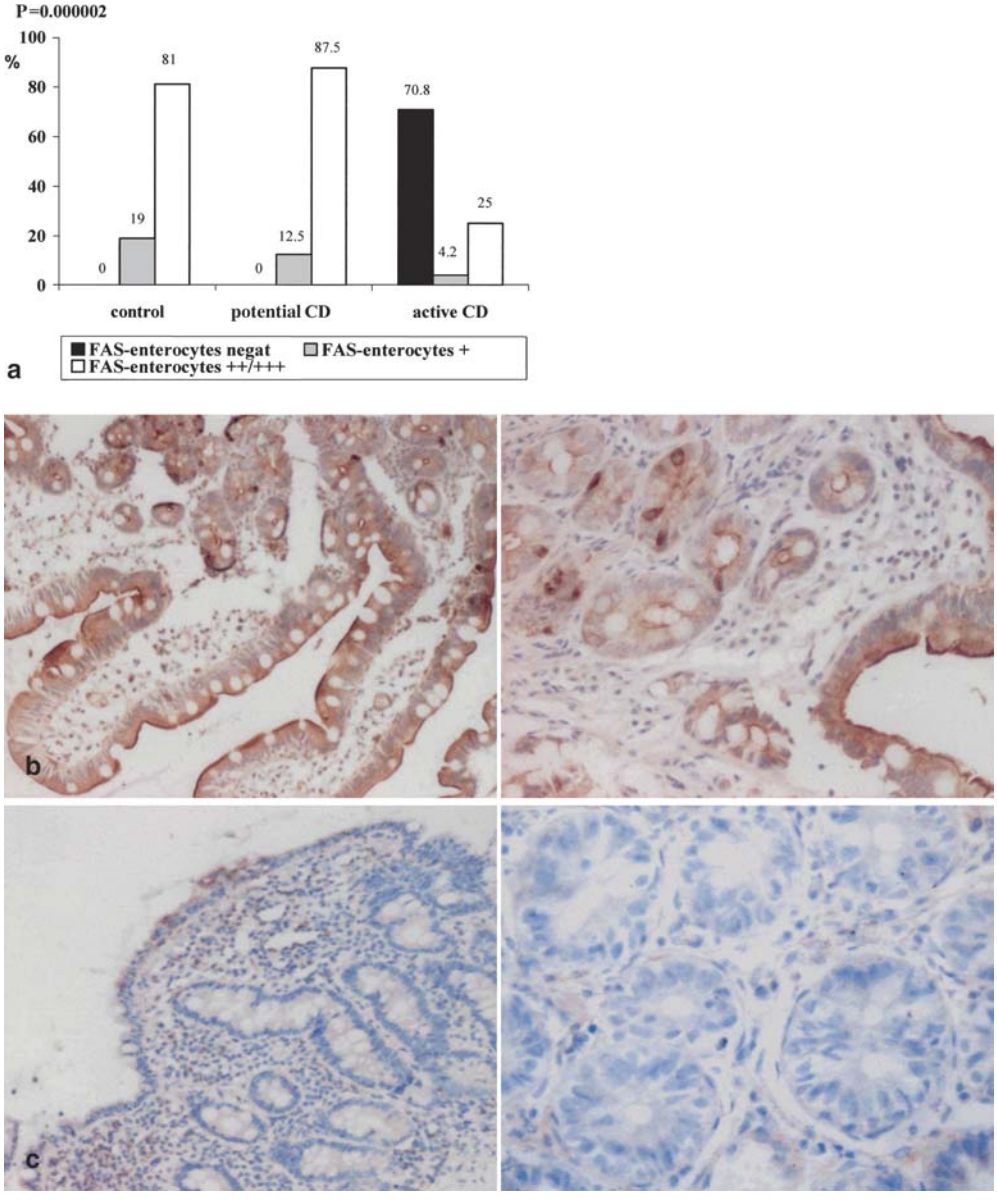



**Fig. 1** **a** The percentage of Fas-expressing enterocytes in all groups. **b** The Fas expression in enterocytes in potential coeliac disease (PCD). **c** The Fas-negative enterocytes within the intestinal crypt in active CD (ACD)

## Results

Fas expression

In all analyzed groups, there were more Fas-expressing enterocytes within the cryptal regions than Fas-expressing enterocytes in the upper part of the villi. However, the percentage of Fas-positive enterocytes was significantly lower ($P \leq 0.000002$) in the group of ACD patients (25%) when compared with the controls (81%) and the PCD (87%; Fig. 1). Similarly, the mean ratio of the Fas-positive glycocalyx length was 2.4% in the ACD patients, 32.3% in the PCD patients, and 53.3% in the controls ($P \leq 0.014$). Also, the percentage of Fas-positive mucosal lymphocytes of the ACD group was significantly lower (20.8%; $P \leq 0.003$) than the PCD group (75%; Fig. 2).

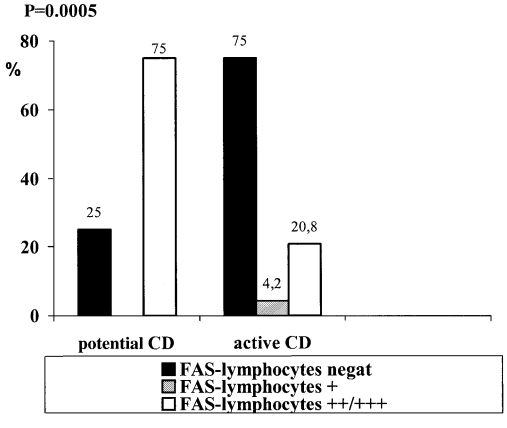



**Fig. 2** The percentage of Fas-expressing mucosal lymphocytes within the crypts

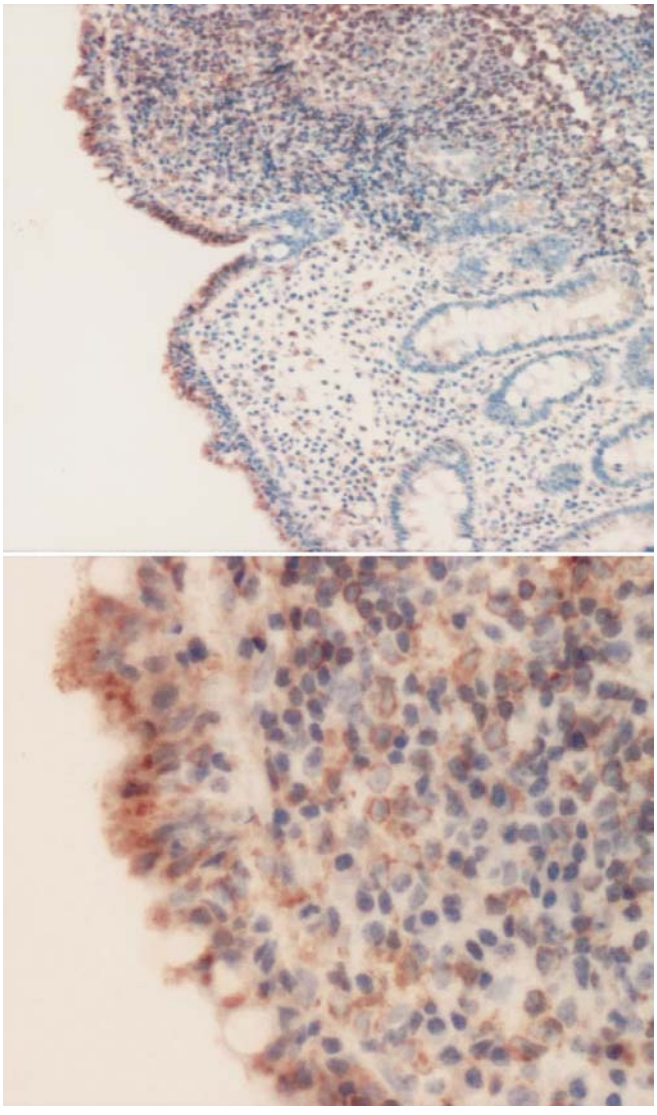


**Fig. 3** Fas ligand (Fas-L) expression within the cytoplasm of enterocytes in ACD with granular/microvesicular pattern

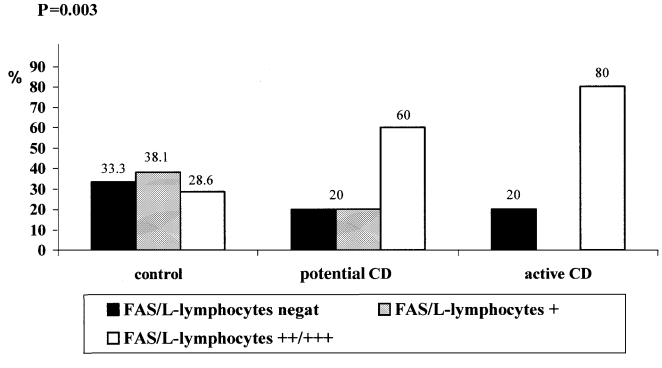
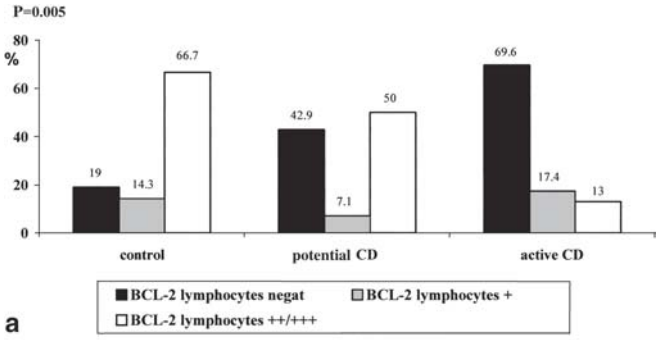



**Fig. 4** The percentage of Fas-L-expressing mucosal lymphocytes within the crypts



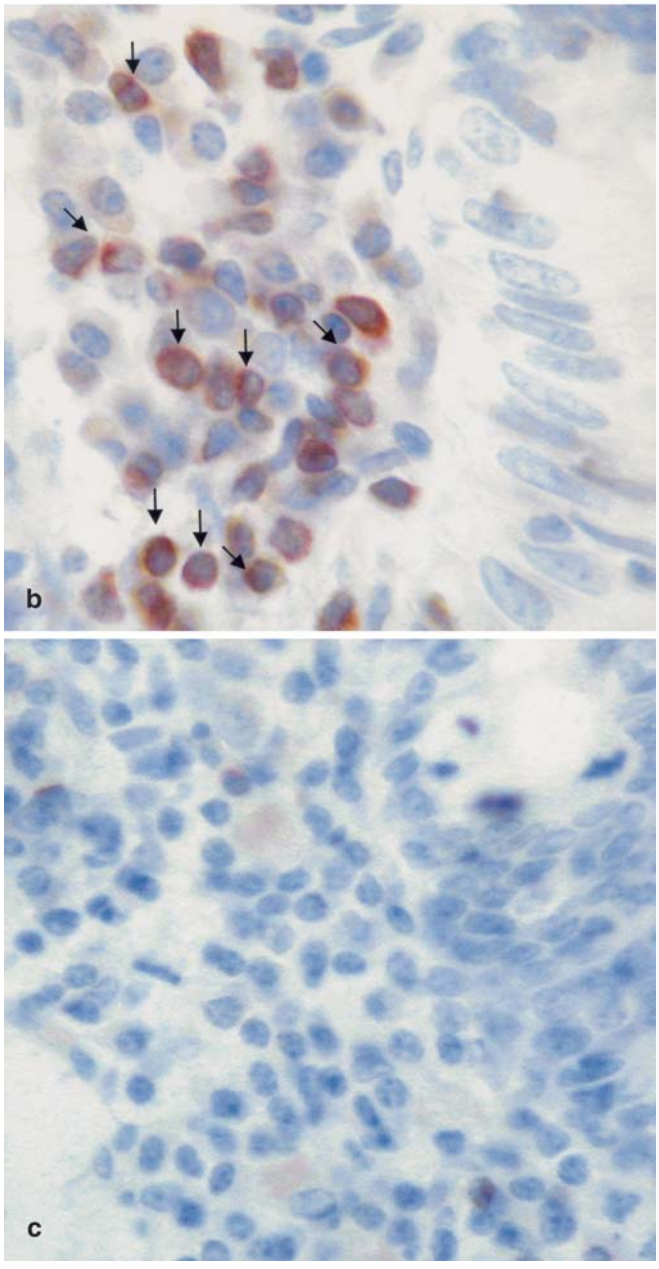




**Fig. 5** **a** The percentage of Bcl-2-expressing mucosal lymphocytes within the crypts. **b** The Bcl-2 expression in mucosal lymphocytes in PCD. **c** The Bcl-2-negative mucosal lymphocytes in ACD

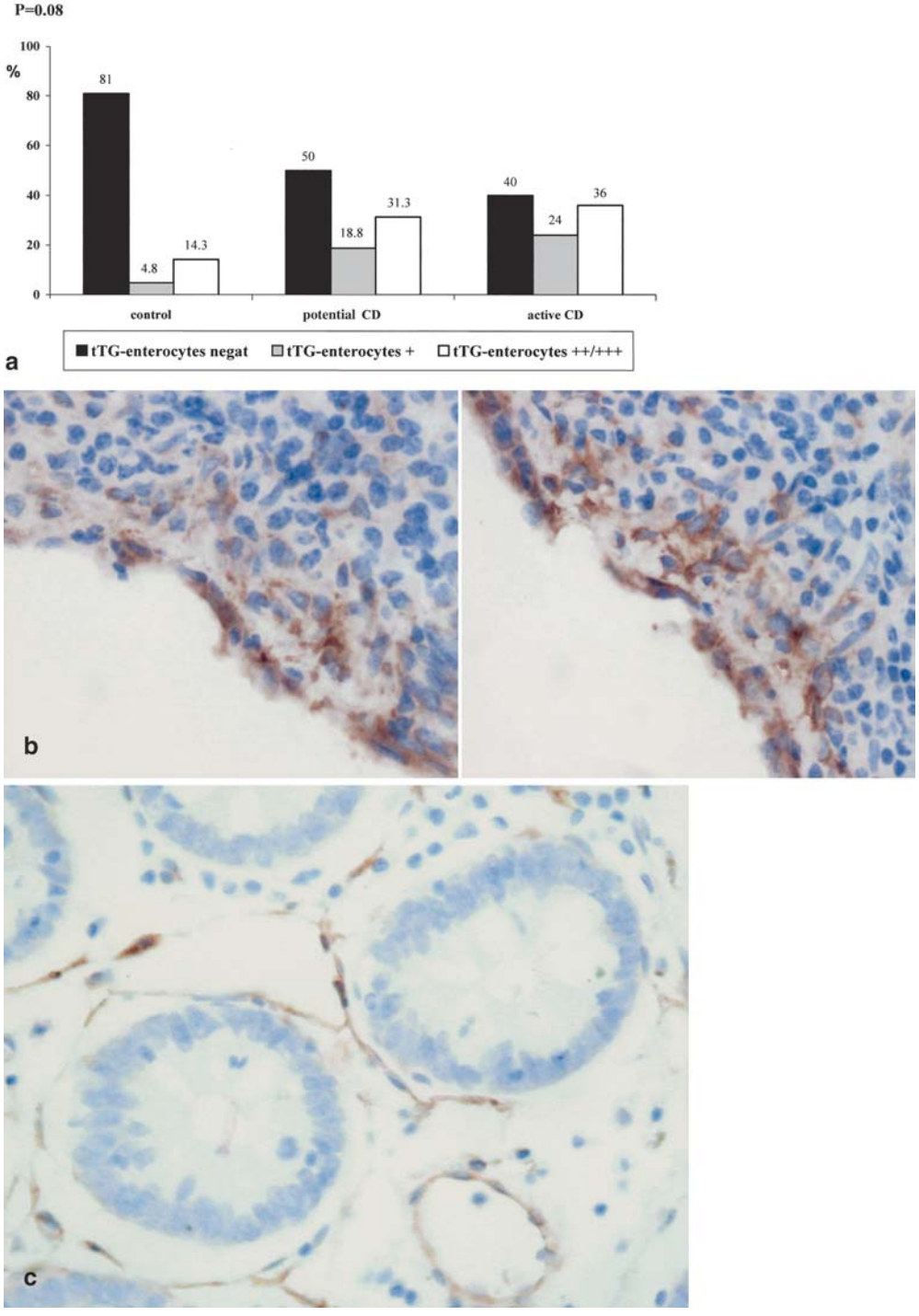



**Fig. 6** **a** The percentage of tissue transglutaminase (tTG) in the enterocytes **b** The tTG expression in the apical enterocytes in ACD **c** The tTG-negative enterocytes in the control

Fas-L expression

The percentage of Fas-L-positive enterocytes in the upper part of the villi was more than 80% in all groups; however, the proportion of Fas-L-positive enterocytes within the cryptal regions was significantly higher ($P \leq 0.006$) in the groups of ACD and PCD patients (84% and 86.7%, respectively) versus 76.2% in the controls. The expression of Fas-L antigen within the cytoplasm of enterocytes was typically granular/microvesicular in character (Fig. 3). The percentage of mucosal lymphocytes expressing Fas-L was significantly higher ($P \leq 0.003$) in the ACD and PCD groups (80% and 60%, respectively) compared with controls (28.6%; Fig. 4).

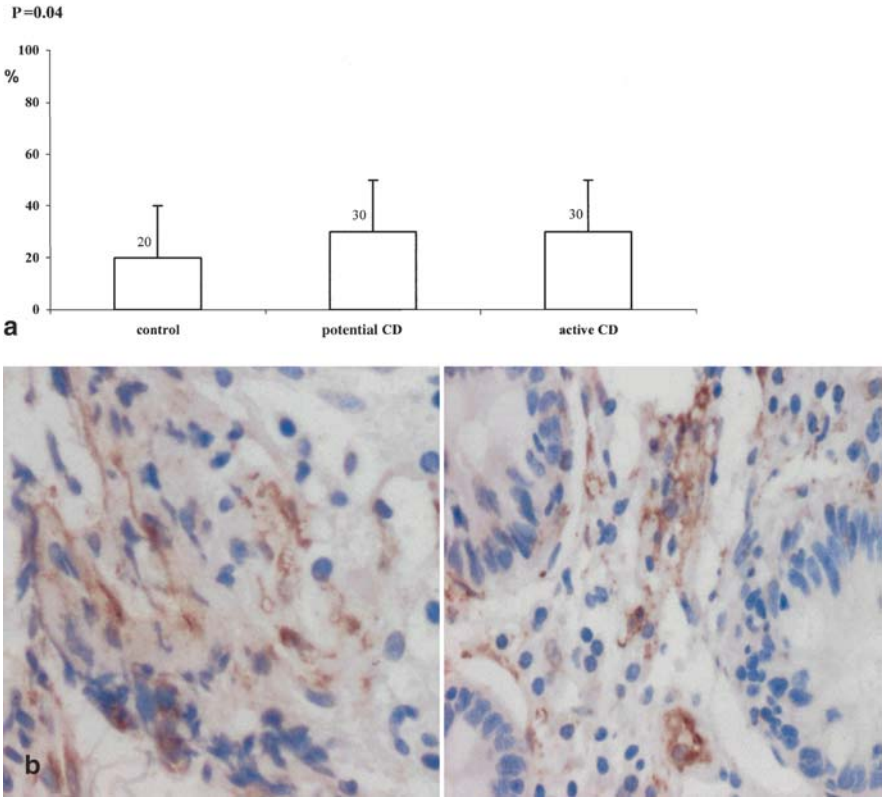



**Fig. 7** **a** The percentage of tTG in the basal membranes and extracellular matrix. **b** The tTG positivity in extracellular matrix in PCD

## Bcl-2 expression

We found significantly more ($P \leq 0.005$) Bcl-2-negative mucosal lymphocytes in the group with active CD (69.6% of Bcl-2 negative cells versus 42.9% in the potential CD and 19% in the controls; Fig. 5).

## tTG expression

The positivity of tTG in the enterocytes was not significantly higher in the group of ACD (60%) and PCD (50.1%) when compared with controls (19.1%), probably due to high heterogeneity (Fig. 6). Similarly, the positivity of tTG in the mucosal lymphocytes in the group of ACD was also not significantly higher (12% in ACD, 6.3% in PCD, and 0% in the controls; figures not shown). Surprisingly, on the other hand, the expression of tTG in the extracellular matrix and basement membranes was significantly higher ($P \leq 0.04$) in ACD (30%) and PCD (30%) patients when compared with controls (20%; Fig. 7).

## GST expression

We found more GST-positive enterocytes and mucosal lymphocytes in the PCD group (18.8% of positive enterocytes and 6.3% of positive mucosal lymphocytes)

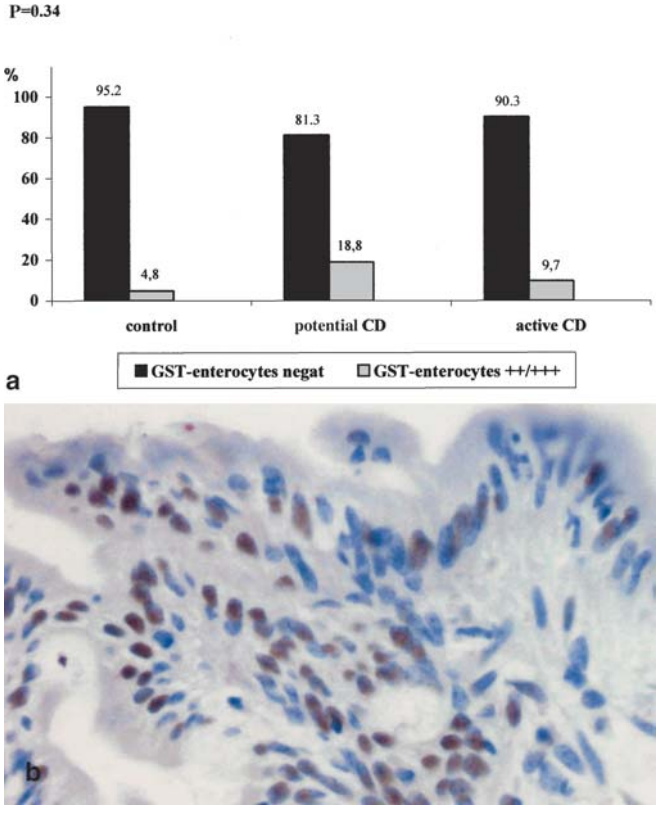



**Fig. 8** The percentage of glutathione S transferase (GST) expression in the enterocytes

when compared with other groups; however, these results did not reach statistical significance ($P \leq 0.34$; Fig. 8).

Intraepithelial lymphocytes (IELs)

The number of IELs expressing proteins Fas, Fas-L, Bcl-2, GST and tTG was very low and did not vary between ACD and PCD patients and controls.

## Discussion

Mechanisms leading to mucosal atrophy in CD are not yet completely understood; however, its remodeling by matrix metalloproteinases and excessive apoptotic enterocyte loss are probably the most important processes [5, 30, 41].

Among one of the early hallmarks of apoptosis is tTG expression [35, 36, 37, 45]. In our study we found increased numbers of tTG-expressing enterocytes in ACD and, to a lesser extent, in PCD. Therefore, even if these findings did not reach statistical significance (probably due to heterogeneity of cases), it may reflect expected increased loss of enterocytes in CD. Moreover, it is supported by our finding of increased caspase 8 expression, increased TUNEL index, and presence of PARP cleavage in these groups (preliminary data of our forthcoming study; data not shown). We also found non-significantly higher numbers of tTG-expressing mucosal lymphocytes in ACD, which also might be the result of increased apoptosis in these cells. Possible increased readiness of mucosal lymphocytes to undergo programmed cell death during active CD is also supported by the finding of decreased Bcl-2 positivity of these cells in this group. Di Sabatino et al. have also found increased apoptosis in mucosal lymphocytes in untreated active CD in their recent study [9]. On the contrary, in PCD, we revealed only low tTG expression within mucosal lymphocytes, which exhibited a high expression of Bcl-2. Therefore, we may hypothesize that mucosal lymphocytes in PCD are protected from apoptosis by the effect of Bcl-2 protein. However, it has to be noted that interpretation of results of tTG expression depends on analyzed cell type or tissue [46]. Expression of tTG in enterocytes and lymphocytes may be interpreted as an early marker of apoptosis. On the contrary, tTG expression in basement membranes (BM) and extracellular matrix (ECM) may be related to its role in CD pathogenesis [4, 10]. This is supported by our finding of significantly increased expression of tTG in BM and ECM both in the ACD and PCD groups. The significance of this finding, even if percentage difference is not striking (30% ACD, 30% PCD versus 20% control), is due to high homogeneity of these groups in extracellular tTG expression.

Possible explanation of the high number of Fas-negative enterocytes, almost completely Fas-negative glycocalyx, as well as high numbers of Fas-negative mucosal lymphocytes in ACD may offer Fas-L targeting and subsequent apoptotic loss of majority of FAS-bearing cells, leading to mucosal atrophy and perturbation of cell homeostasis within the mucosa of ACD patients [5]. We are not able to explain why the majority of the above-mentioned changes were found within the cryptal regions rather than in the upper part of the villi. Nevertheless, our hypothesis of Fas-L targeting is also supported by finding an increased number of Fas-L-bearing enterocytes and lymphocytes in both PCD and ACD patients. The active role of the Fas/Fas-L apoptotic pathway during PCD and ACD is also supported by the granular pattern of Fas-L expression in enterocytes. In agreement with previous works, it may suggest microvesicular localization of Fas-L, allowing prompt release of Fas-L-containing microvesicles to the surface of the cell, which is now considered as a new, effective mechanism for the rapid induction of autocrine/paracrine cell death [24, 50]. The presence of Fas-L on enterocytes is not contradictory; Fas-L expression was found not only in lymphocytes but also in other cell types [40, 52]. It is also know that some metalloproteinases (playing role in mucosal remodeling) react with Fas-L and influence apoptosis [27, 38]. Maiuri et al. [21] and Ciccocioppo et al. [7] have found increased Fas expression in enterocytes in areas of mucosal atrophy in untreated CD. However, the materials and methods used in this study were different. It is also known that various anti-Fas-L antibodies may be used and, even if the N20 antibody used in our study was not considered ideal for immunohistochemistry [44], we had not criticized background staining in our samples (see Fig. 3). Moreover, the studied patients were predominantly adults and, besides analysis of Fas/Fas-L expression, the authors did not estimate expression of other apoptosis-related proteins. The lower number of Fas-bearing cells in CD found in our study may reflect the fact that these cells were already destroyed by Fas-L-bearing elements.

It is well known that apoptosis is triggered by several mechanisms including receptor-mediated, mitochondria-mediated, and DNA damage-mediated pathways [13, 19, 32]. GST is considered, similarly to Bcl-2, as one of the important regulators of mitochondrial membrane permeability during apoptosis [16, 17]. Based on our finding of higher levels of GST expression in the enterocytes as well as in the lymphocytes in the PCD group, we can speculate that GST may play an antiapoptotic role.

We did not find any difference in expression of studied apoptosis-related proteins in IELs. It may be possible that not only IELs but also subepithelial lymphocytes play a more important role during apoptotic processes in the small intestine and that the role of IELs is related more to immunopathologic processes during the initial phases of CD.

We can conclude, together with others [7], that the Fas/Fas-L signaling pathway takes place during activation of apoptosis of enterocytes during potential and active coeliac disease. The results of our study also showed that infiltrating lymphocytes can be also eliminated during CD, probably by a receptor-mediated apoptotic pathway. Finally, our findings confirm that Fas/Fas-L, Bcl-2, and

tTG proteins are involved in apoptotic pathways leading to mucosal morphological changes in CD.

**Acknowledgements** We thank Mgr. Petra Řiháková for her technical assistance during preparation of the manuscript. This study was supported by grants IGA MZ CR NE 6197–3/2000 and MSM 151100001.

## References

1. Amendola A, Lombardi G, Oliverio S, et al. (1994) HIV-1 gp120-dependent induction of apoptosis in antigen-specific human T cell clones is characterized by "tissue" transglutaminase expression and prevented by cyclosporine A. FEBS Lett 339:258–264
2. Amendola A, Gougeon ML, Poccia F, et al. (1996) Induction of "tissue" transglutaminase in HIV pathogenesis: evidence for high rate of apoptosis of CD4+ T lymphocytes and accessory cells in lymphoid tissues. Proc Natl Acad Sci USA 93:11057–11062
3. Berke G (1995) The CTL's kiss of death. Cell 81:9-12
4. Brusco G, Muzi P, Ciccocioppo R, et al. (1999) Transglutaminase and coeliac disease: endomysial reactivity and small bowel expression. Clin Exp Immunol 118:371–375
5. Ciccocioppo R, Di Sabatino A, Gasbarrini G, et al. (1999) Apoptosis and gastrointestinal tract. Ital J Gastroenterol Hepatol 31:162–172
6. Ciccocioppo R, Di Sabatino A, Parroni R, et al. (2000) Cytolytic mechanisms of intraepithelial lymphocytes in coeliac disease (CoD). Clin Exp Immunol 120:235–240
7. Ciccocioppo R, Di Sabatino A, Parroni R, et al. (2000) Increased enterocyte apoptosis and Fas/Fas ligand system in celiac disease. Am J Clin Pathol 115:494–503
8. Clapper ML, Szarka CE (1998) Glutathione S-transferases: biomarkers of cancer risk and chemopreventive response. Chem Biol Interact 111:377–388
9. Di Sabatino A, Ciccocioppo R, D'Aló S, et al. (2001) Intraepithelial and lamina propria lymphocytes show distinct patterns of apoptosis whereas both populations are active in Fas based cytotoxicity in coeliac disease. Gut 49:380–386
10. Farrace MG, Picarelli A, Di Tola M, et al. (2001) Presence of anti-"tissue" transglutaminase antibodies in inflammatory intestinal diseases: an apoptosis-associated event? Cell Death Differ 8:767–770
11. Fassano A, Catassi C (2001) Current approaches to diagnosis and treatment of coeliac disease: an evolving spectrum. Gastroenterology 120:636–651
12. Feighery C (1999) Coeliac disease (clinical review). BMJ 319:236–239
13. Feldmann G, Haouzi D, Moreau A, et al. (2000) Opening of the mitochondrial permeability transition pore causes matrix expansion and outer membrane rupture in Fas-mediated hepatitis apoptosis in mice. Hepatology 31:674–683
14. Ferguson A, Arranz E, O'Mahony S (1993) Clinical and pathological spectrum of coeliac disease—active, silent, latent, potential. Gut 34:150–151
15. Fesus L, Thomazy V, Falus A (1987) Induction and activation of tissue transglutaminase during programmed cell death. FEBS Lett 224:104–108
16. Hall AG (1999) Glutathione and the regulation of cell death. Adv Exp Med Biol 457:199–203
17. Hall AG (1999) Review: The role of glutathione in the regulation of apoptosis. Eur J Clin Invest 29:238–245
18. Knight CR, Rees RC, Platts A, et al. (1993) Interleukin-2-activated human effector lymphocytes mediate cytotoxicity by inducing apoptosis in human leukaemia and solid tumour target cells. Immunology 79:535–541
19. Kroemer G, Petit P, Zamzami N, et al. (1995) The biochemistry of programmed cell death. FASEB J 9:1277–1287
20. Lebenthal E, Branski D (2002) Celiac disease: an emerging global problem. J Pediatr Gastroenterol Nutr 35:508–512
21. Maiuri L, Auricchio S, Coletta S, et al. (1998) Blockage of T-cell costimulation inhibits T-cell action in celiac disease. Gastroenterology 115:564–572
22. Maiuri L, Ciacci C, Raia V, et al. (2001) FAS engagement drives apoptosis of enterocytes of coeliac patients. Gut 48:418–424
23. Marsh MN, Growe PT (1995) Morphology of the mucosal lesion in gluten sensitivity. Baillieres Clin Gastroenterol 9:173–179
24. Martinez-Lorenzo MJ, Anel A, Gamen S, et al. (1999) Activated human T cells release bioactive Fas ligand and APO2 ligand in microvesicles. J Immunol 163:1274–1281
25. Marzari R, Sblattero D, Florian F, et al (2001) Molecular dissection of the tissue transglutaminase autoantibody response in celiac disease. J Immunol 166:4170–4176
26. Mastino A, Grelli S, Piacentini M, et al. (1993) Correlation between induction of lymphocyte apoptosis and prostaglandin E2 production by macrophages infected with HIV. Cell Immunol 152:120–130
27. Mitsiades N, Yu WH, Poulaki V, et al (2001) Matrix metalloproteinase-7-mediated cleavage of Fas ligand protects tumor cells from chemotherapeutic drug cytotoxicity. Cancer Res 61:577–581
28. Molberg O, McAdam SN, Korner R, et al. (1998) Tissue transglutaminase selectively modifies gliadin peptides that are recognized by gut-derived T cells in celiac disease. Nat Med 4:713–717
29. Molberg O, McAdam SN, Sollid LM (2000) Role of tissue transglutaminase in celiac disease. J Pediatr Gastroenterol Nutr 30:232–240
30. Moss SF, Attia L, Scholes JV, et al. (1996) Increased small intestinal apoptosis in coeliac disease. Gut 39:811–817
31. Mullighan CG, Bunce M, Welsh KI (1997) High resolution HLA-DQB1 typing using the polymerase chain reaction and sequence-specific primers. Tissue Antigens 50:688–692
32. Nagata S, Golstein P (1995) The Fas death factor. Science 267:1449–1456
33. Oberhuber G, Vogelsang H, Stolte M, et al (1996) Evidence that intestinal intraepithelial lymphocytes are activated cytotoxic T cells in celiac disease but not in giardiasis. Am J Pathol 148:1351–1357
34. Oberhuber G, Granditsch G, Vogelsang H (1999) The histopathology of coeliac disease: time for a standardized report scheme for pathologists. Eur J Gastroenterol Hepatol 11:1185–1194
35. Oliverio S, Amendola A, Rodolfo C, et al. (1999) Inhibition of "tissue" transglutaminase increases cell survival by preventing apoptosis. J Biol Chem 274:34123–34128
36. Piacentini M (1995) Tissue transglutaminase: a candidate effector element of physiological cell death. Curr Top Microbiol Immunol 200:163–175
37. Piredda L, Farrace MG, LoBello M, et al. (1999) Identification of "tissue" transglutaminase binding proteins in neural cells committed to apoptosis. FASEB J 13:355–364
38. Powell WC, Fingelton B, Wilson CL, et al. (1999) The metalloproteinase matrilysin proteolytically generates active soluble Fas ligand and potentiates epithelial cell apoptosis. Curr Biol 9:1441–1447
39. Quarsten H, Molberg O, Fugger L, et al. (1999) HLA binding and T cell recognition of a tissue transglutaminase-modified gliadin epitope. Eur J Immunol 29:2506–2514
40. Saas P, Walker PR, Hahne M, et al. (1997) Fas ligand expression by astrocytoma in vivo: maintaining immune privilege in the brain? J Clin Invest 99:1173–1178
41. Salmela MT, MacDonald TT, Black D, et al (2002) Upregulation of matrix metalloproteinases in a model of T cell-mediated tissue injury in the gut: analysis by gene array and in situ hybridization. Gut 51:540–547
42. Shan L, Molberg O, Parrot I, et al (2002) Structural basis for gluten intolerance in celiac sprue. Science 297:2275–2279

43. Shiner M, Eran M, Freier S, et al. (1998) Are intraepithelial lymphocytes in celiac mucosa responsible for inducing programmed cell death (apoptosis) in enterocytes? Histochemical demonstration of perforins in cytoplasmic granules of intraepithelial lymphocytes. J Pediatr Gastroenterol Nutr 27:393–396
44. Strater J, Walczak H, Hasel C, et al. (2001) CD95 ligand (CD95L) immunohistochemistry: a critical study on 12 antibodies. Cell Death Differ 8:273–278
45. Szondy Z, Molnar P, Nemes Z, et al. (1997) Differential expression of tissue transglutaminase during in vivo apoptosis of thymocytes induced via distinct signalling pathways. FEBS Lett 404:307–313
46. Thomazy V, Fesus L (1989) Differential expression of tissue transglutaminase in human cells. An immunohistochemical study. Cell Tissue Res 255:215–224
47. Troncone R, Greco L, Mayer M, et al. (1996) Latent and potential coeliac disease. Acta Paediatr (Suppl) 412:10–14
48. Uhlig H, Osman AA, Tanev ID, et al. (1998) Role of tissue transglutaminase in gliadin binding to reticular extracellular matrix and relation to coeliac disease autoantibodies. Autoimmunity 28:185–195
49. Van de Wal Y, Kooy Y, Van Veelen P, et al. (1998) Selective deamidation by tissue transglutaminase strongly enhances gliadin-specific T cell reactivity. J Immunol 161:1585–1588
50. Wagelie-Steffen AL, Hartmann K, Vliagoftis H, et al. (1998) Fas ligand (FasL, CD95L, APO-1L) expression in murine mast cells. Immunology 94:569–574
51. Walker Smith JA, Guandalini S, Schmitz J, et al. (1990) Revised criteria for diagnosis of coeliac disease. Arch Dis Child 65:909–911
52. Younes M, Schwartz MP, Finnie D, et al. (1999) Overexpression of Fas ligand (FasL) during malignant transformation in the large bowel and in Barrett's metaplasia of the esophagus. Hum Pathol 30:1309–1313

Virchows Arch (2003) 442:462–467
DOI 10.1007/s00428-003-0791-5

ORIGINAL ARTICLE

**Gian Kayser · Jan Dirk Baumhäkel · Tamas Szöke · Imre Trojan · Urs Riede · Martin Werner · Klaus Kayser**

# Vascular diffusion density and survival of patients with primary lung carcinomas

Received: 5 December 2002 / Accepted: 7 February 2003 / Published online: 5 April 2003
© Springer-Verlag 2003

**Abstract** *Aim:* To investigate the clinical significance of tumour vascularisation in operated lung cancer patients. *Materials and methods:* Histological slides obtained from 498 patients with potentially curative operated lung carcinomas in two different institutions of thoracic surgery were immunohistochemically stained with an anti-CD34 antibody and subjected to quantitative image analysis. Syntactic structure analysis measured the absolute and relative features of vessels, including the numerical tumour cells densities relative to their nearest neighbouring vessel. These data are associated with tumour volume, post-surgical TNM stage, and each patient's survival. *Results:* The clinical data, including sex distribution, age of patients, pTNM stages and survival, did not differ between the two institutions. The tumour vascularisation (volume fraction, Vv) amounted to 7% in lung carcinomas, was independent from cell type and increased in advanced tumour stages (pT4, pN3). Advanced tumour stages presented with a higher numerical vascular density and with maintained minimum diameter and circumference of vessels. Each patient's survival was closely associated with the pN stage, tumour volume, cell type and numerical density of tumour cells within a distance less than 20 μm from the nearest neighbouring vessel due to multivariate statistical analysis. *Conclusion:* Vascularisation of lung tumours becomes altered in advanced tumour stages. Of prognostic significance is the distribution of tumour cells in relation to the nearest neighbouring vessel only.

**Keywords** Lung cancer · Vascularisation · Survival · Syntactic structure analysis

G. Kayser (✉) · U. Riede · M. Werner
Institute of Pathology, University Freiburg,
Albertstrasse 19, 79104 Freiburg, Germany
e-mail: gkayser@ukl.uni–freiburg.de
Tel.: +49-761-2036820
Fax: +49-761-2036790

J. D. Baumhäkel · K. Kayser
Institute of Pathology, Charité, Humboldt University,
Berlin, Germany

T. Szöke · I. Trojan
Department of Thoracic Surgery,
University Szeged, Szeged, Hungary

## Introduction

Malignant and benign tumours commonly possess a specific texture and thus can be considered as "an organ embedded within a host organ" [5, 9]. Vascularisation (and tumour–induced neo-vascularisation) has been in focus for various tumour cell types, such as breast carcinomas, renal or colon carcinomas. The reported data of neo-vascularisation in these tumours are, however, contradictory. On the one hand, Teo et al. (2002) reported a higher vascular density in invasive ductal carcinomas of the breast in comparison with their non-invasive counterparts [23]. On the other hand, Kirkali et al. did not find an influence of vascularisation on clinical parameters of renal carcinoma patients, in contrast to the proliferation activity [12]. Only a weak angiogenic response of colorectal carcinomas has been observed by Pritchard et al. [13], whereas Vermeulen et al. [26] were able to demonstrate a high endothelial proliferation index and a high mircovessel density in so-called hotspots of colorectal carcinomas. In lung carcinomas, there is evidence that the density of intra-tumour vessels is of prognostic significance [11, 18, 20]. However, again the published results are contradictory: Slodkowska et al. reported a close relationship between the lymph-node status and the vascularisation of operated non-small cell lung cancer patients [18, 20], while other authors could not support these findings [14]. In addition to the "classical" prognostic factors that include the pTNM stage, clinical parameters—such as performance status, loss of weight, etc. and additional features such as proliferation index measured by immune histochemistry (Ki-67), expression of histo-blood group antigens A H, or binding capacities

to certain lectins—the prognostic significance of vascularisation remains, therefore, still undefined [1, 4, 7, 10].

We now report a study comprising 498 potentially curative operated lung carcinoma patients that analyses the tumour vascularisation in relation to several clinical parameters, including the pTNM stage and survival.

## Materials and methods

### Clinical data and immunohistochemistry

The study included 498 potentially curative operated lung carcinoma patients who underwent surgical treatment in the Department of Thoracic Surgery of the University of Szeged, Szeged, Hungary (246 patients) and in that of the Thoraxklinik, Heidelberg, Germany (252 patients) during the period 1 January 1990 until 30 December 1992. The fate of all included patients was obtained by intensive follow-up until 31 December 2000. Post-surgical tumour staging was performed and re-coded according to the rules of the Union Internationale Contra la Cancrum (UICC) [22, 25]. The tumour volume was calculated assuming a spherical formation with the radius being the mean of the three measured dimensions of the tumour. The tumours were classified according to the rules of the World Health Organization (WHO) [27] based on hematoxylin and eosin (HE)-stained slides, including additional staining such as periodic acid Schiff base (PAS), collagen, or immunohistochemistry (neuroendocrine, epithelial, or sarcomatous markers) if needed. Histological slides of 4- to 5-$\mu$m thickness were stained with a commercially available monoclonal antibody against CD34 (Dako, Hamburg, Germany) according to the prescriptions of the distributor by use of the Vectorstain ABC kit (Vector lab) and counterstained with hematoxylin. Positive and negative controls were performed as usual, i.e. in contemporary performance of slides known to contain vessels, and by omitting the first antibody. Tumour vessels were defined as all blood vessels lying within the tumour area.

### Morphometry and syntactic structure analysis

The immunohistochemically stained slides were thoroughly screened for hot spots and "less densely vascularised" areas at the tumour boundary. The areas of interest were taken from the tumour boundary at random, i.e. mixing spots with "normal" vascular density (four areas) and those of so-called hot-spots (two areas). The selected tumour areas were digitised into a RGB image using a colour CCD camera (JVC TK1070) at a magnification (×10) mounted to a Leica microscope into a 512×512 pixel matrix. Self-written programs based on the commercially available Digital Image Analysing System (DIAS, University Jena, Germany) allowed an automated detection of stained vessels by transferring the RGB colour space into a HSI (hue, saturation, intensity) space, with specific selection of the brown colour and appropriate threshold of the grey value intensity. The selected vessels then underwent morphometric computations based on stereological procedures, and their volume fractions, Vv, and surface fractions, Sv, were estimated. The measured absolute values included the minimum vascular diameter and vascular area. In addition, the minimum distance between nearest neighbouring vessels and the density of tumour cells in relation to their distance to the nearest located vessel were calculated using syntactic structure analysis. Details of performance and the theoretical background of the applied technique have been described elsewhere [6, 10, 11]. The obtained data were analysed statistically using descriptive and multivariate statistical procedures such as the Chi-square test, Kolmogoroff Smirnow test, multivariate discriminate analysis, and Kaplan Meier analysis including Cox regression. A commercially available statistical program package (NCSS 2000, Number Cruncher Statistical Systems, Kaysville, Utah, USA) serves for these purposes.

## Results

Synopsis of the material is presented in Table 1. The clinical figures obtained in the two different institutions were similar in terms of sex of the patients, the stated histological diagnoses, and tumour stages. The Hungarian patients were only slightly younger than the Germans. The same concordance held true for the survival of the patients and the expression of the analysed vascular features (not shown). Therefore, computations shown below do not differentiate between the materials of the two different institutions.

The density of vessels can be measured by calculating the Vv and the intensity of oxygen supply by calculating the Sv, which is the fraction of the vascular surface in relation to the volume embedding the vessels. The results in relation to cell type, pT and pN stage, and tumour localisation (central, peripheral) are given in Table 2. The vascular surface/tumour volume fraction Sv is in the same range, and amounts to 5.2 (%/μm) with a surprisingly low standard deviation (Table 2). It seems to be constant and independent of the cell types. A statistically significant increase ($P<0.05$) of Vv and Sv with increasing tumour stages can be noted, which is associated with increasing vascular density (or number of vessels/area unit) and not with an increased vascular volume.

The mean vascular diameter measured about 18 μm, which is in the range of about two cellular layers in living lung parenchyma. The theoretical circumference calculated on the basis of the minimum diameter amounts to 60–70 μm. Taking into account a randomly distributed arrangement of vessels, it computes to 100 μm, which is in the range of the measured mean circumference, i.e. the vessels are built in circular tubes and arranged in an anisotropic manner. The absolute values of the mean

**Table 1** Synopsis of material

| Parameter | Heidelberg | Szeged | Total |
|---|---|---|---|
| Men | 201 | 201 | 402 |
| Women | 45 | 51 | 96 |
| Age (years, mean±SD) | 60±8 | 57±9 | 59±7 |
| Cell type | | | |
| Squamous | 113 | 112 | 225 |
| Adeno | 94 | 96 | 190 |
| Large cell | 30 | 33 | 63 |
| Small cell | 9 | 11 | 20 |
| Tumour stages | | | |
| pT1 | 41 | 37 | 78 |
| pT2 | 152 | 150 | 302 |
| pT3 | 52 | 55 | 107 |
| pT4 | 1 | 10 | 11 |
| pN0 | 131 | 134 | 265 |
| pN1 | 61 | 59 | 120 |
| pN2 | 49 | 55 | 104 |
| pN3 | 5 | 4 | 9 |

**Table 2** Quantitative vascular features in lung carcinomas in relation to tumour cell type and pTN stage (mean and standard deviation)

| Feature | Numerical density of vessels | Vv (%) | Vv connective tissue (%) | Av (1/$\mu$m) | Smallest diameter ($\mu$m) | Mean circumference ($\mu$m) | Mean area ($\mu m^2$) |
|---|---|---|---|---|---|---|---|
| Squamous | 5.5±2.3 | 6.7±4.4 | 4.1±9.7 | 5.2±1.7 | 18.7±7.9 | 109±40 | 1765±1633 |
| Adeno | 5.4±2.5 | 6.5±5.1 | 4.7±12.5 | 5.2±2.2 | 18.3±8.1 | 108±47 | 1803±1341 |
| Large cell | 5.2±2.4 | 6.9±6.5 | 2.8±4.0 | 5.3±2.2 | 19.2±7.9 | 114±42 | 1901±1604 |
| Small cell | 5.2±2.1 | 7.5±5.0 | 2.9±2.1 | 5.3±2.1 | 18.9±5.6 | 119±47 | 2091±1541 |
| pT1 | 5.4±2.6 | 5.9±3.5 | 4.1±11.1 | 5.1±2.3 | 18.4±5.9 | 105±31 | 1472±935 |
| pT2 | 5.4±2.3 | 7.1±5.2 | 3.9±8.8 | 5.2±1.9 | 19.1±8.6 | 113±46 | 1984±2515 |
| pT3 | 5.2±2.1 | 6.1±3.9 | 4.9±13.1 | 4.7±1.7 | 17.4±7.1 | 104±40 | 1632±1484 |
| pT4 | 7.7±3.5 | 8.0±5.6 | 1.9±7.2 | 6.9±2.5 | 19.5±8.8 | 106±43 | 1409±1086 |
| pN0 | 5.2±2.2 | 6.7±5.1 | 3.9±9.1 | 5.1±2.1 | 19.2±8.6 | 112±45 | 1895±2518 |
| pN1 | 5.4±2.3 | 6.3±3.8 | 4.5±9.8 | 5.0±1.7 | 17.8±6.4 | 105±34 | 1633±1312 |
| pN2 | 5.6±2.6 | 7.0±4.9 | 4.6±13.2 | 5.2±2.1 | 18.0±7.4 | 109±45 | 1824±1791 |
| pN3 | 7.2±4.3 | 8.1±5.5 | 2.1±7.4 | 6.4±2.9 | 20.5±10.4 | 115±52 | 1714±1362 |
| Central | 5.4±2.4 | 5.5±3.3 | 6.4±16.3 | 4.7±1.7 | 15.5±6.3 | 98±36 | 1400±1077 |
| Peripheral | 5.2±2.4 | 6.0±4.3 | 4.9±11.8 | 4.7±1.9 | 17.3±6.9 | 106±41 | 1662±1624 |

**Table 3** Numerical densities of tumour cells in relation to the distance from the nearest neighbouring (supplying) vessel

| Feature | Numerical density <20 $\mu$m | Numerical density <40 $\mu$m | Numerical density <60 $\mu$m | Numerical density >60 $\mu$m |
|---|---|---|---|---|
| Squamous | 14.1±2.7 | 16.0±2.2 | 16.4±2.9 | 12.9±2.9 |
| Adeno | 15.6±2.8 | 19.4±4.9 | 20.9±2.3 | 16.3±3.3 |
| Large cell | 13.9±9.3 | 16.1±2.1 | 16.4±1.9 | 12.7±3.9 |
| Small cell | 12.5±2.7 | 13.7±3.6 | 13.5±4.3 | 10.4±4.3 |
| pT1 | 13.2±6.8 | 14.9±8.5 | 15.2±1.3 | 11.5±9.5 |
| pT2 | 17.3±2.1 | 20.9±4.8 | 22.3±5.7 | 17.8±5.1 |
| pT3 | 12.5±3.9 | 13.9±5.2 | 13.7±6.2 | 10.0±5.1 |
| pT4 | 15.0±4.9 | 18.5±7.5 | 19.7±9.5 | 15.6±9.0 |
| pN0 | 14.8±1.8 | 17.5±3.2 | 18.6±4.7 | 14.7±4.6 |
| pN1 | 15.9±2.5 | 18.3±3.1 | 18.8±3.5 | 15.4±3.9 |
| pN2 | 17.3±2.8 | 20.7±3.8 | 20.9±4.0 | 15.4±2.8 |
| pN3 | 14.3±3.4 | 17.6±6.1 | 19.1±8.8 | 15.1±8.0 |
| Central | 12.5±4.5 | 14.4±6.2 | 14.6±7.2 | 10.5±5.4 |
| Peripheral | 16.1±2.6 | 19.2±3.6 | 19.6±3.9 | 14.5±3.0 |

vascular area are characterised by a broad standard deviation, which reflects to the range of the vascular sizes.

The numerical density of tumour cells in relation to the distance of the nearest neighbouring vessel is shown in Table 3. The percentage of cells per unit area ($\mu m^2$) was highest at a distance 20 $\mu$m<d<60 $\mu$m, and decreased for tumour cells located at larger distances (Table 3, Fig. 1). The cellular density of small cell anaplastic and squamous cell carcinoma decreased remarkably after a 60-$\mu$m distance. Thus, they possess a different tumour cell arrangement related to the vessels than that of adenocarcinoma. These tumours still have a higher cellular density at distances greater than 60 $\mu$m than those less than 20 $\mu$m.

The survival analysis of the two cohorts revealed no differences between patients operated on at the two surgical institutions at a statistically significant level. As expected, a strong relationship between the pTN stage and the survival was observed, as exemplarily shown in Fig. 2. The same held true for other known parameters such as the pT stage or—at an even stronger statistical relationship—the tumour volume (not shown). Among vascular features, only the tumour cell density at a distance of less

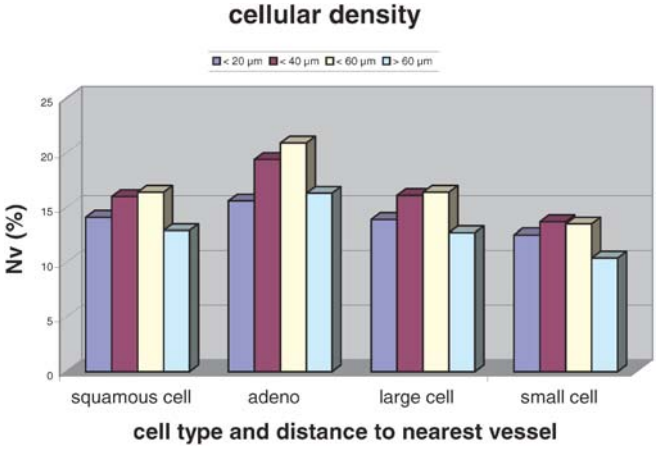



**Fig. 1** Cellular density in relation to distance to nearest neighbouring vessels (distances in microns)

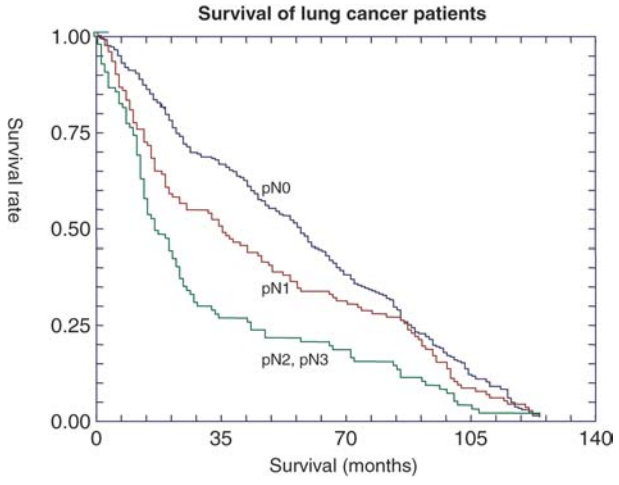



**Fig. 2** Survival rate of potentially curative operated lung carcinoma patients in relation to the pN stage ($n$=498)

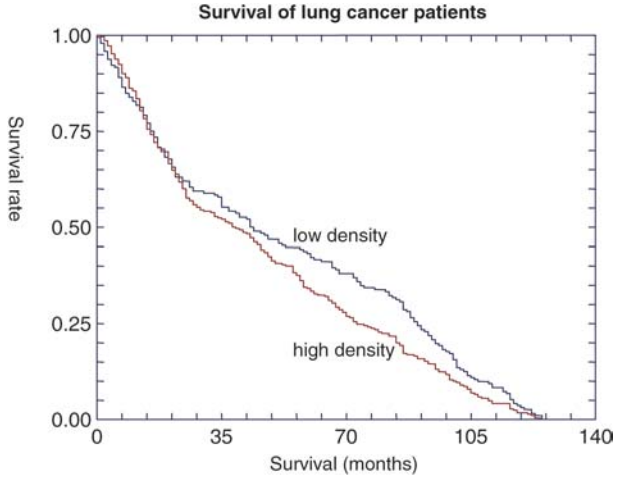



**Fig. 3** Survival rate of potentially curative operated lung carcinoma patients in relation to the tumour cell density at a distance <20 μm from the nearest neighbouring vessel ($n$=498, $P$<0.05)

than 20 μm reached a statistically significant level ($P$<0.05; Fig. 3). At larger distances, this feature was related to the patients' prognoses only at a statistical "trend" level ($P$<0.1). Multivariate analysis confirmed these findings (Table 4).

## Discussion

The nutrition of malignant tumours is provided by two kinds of vessels: those that are present in the host tissue and those that are created by the tumour itself. There is a controversial discussion about the range of newly formed vessels. Whereas several authors believe that angiogenesis plays an important role in malignancies of the breast or colon, others believe that there is evidence for only a weak angiogenic response, at least in colon/rectal cancer [2, 3, 5, 12, 13, 14, 15, 16, 17, 18, 24].

In this study, vessels were defined by structures that positively stained with the antibody CD34. This probe specifically recognises endothelial cells. The results obtained using this antibody are equivalent to those obtained by application of different endothelial-specific probes, such as Uleus europaeus agglutinin or CD31 [19, 26]. The benefits of the antibody CD34 are an easy to apply probe with excellent staining characteristics, the constraint, the theoretical chance that vascular endothelial cells might change their receptor and binding characteristics if exposed to or embedded in malignancies [19, 23, 24, 26] and, thus, escape the visualisation. Despite this theoretical chance, the applied antibody cannot be used to distinguish between "old or existent" and "tumour-induced" vessels [19]. With these prerequisites, the following vascular characteristics have been found in this study:

A. Stereological data. The volume (Vv) and the surface/volume (Sv) fraction of vessels in lung carcinomas are similar in the different cell types. The Vv accounts for 6–8% of the total tumour volume. These data are in general agreement with those reported by other authors [14, 18, 20]. Only tumours in advanced stages (pT4, pN4) possess a remarkably increased Sv (about 30% on average). These data indicate that advanced tumours, either in size or lymph-node invasion, are provided with an increased nutrition. An increased Sv is induced either by increased vascular density or decreased size of measured vessels. As shown in Table 2, the size-related features of the vessels, i.e. minimum diameter, mean circumference, or mean vascular area, remain nearly unchanged if computed in relation to the tumour stages. These findings contradict the hypothesis that the changes of Sv are induced by changes of the vascular size. The steep increase of Sv should, therefore, be associated with an increase of the numerical density of vessels, i.e. the number of vessels located in a "unit" volume. This theory is, indeed, supported by data shown in Table 3. The close

**Table 4** Multivariate analysis of survival of potentially curative operated lung carcinoma patients

| Feature | Rank | Z value | Probability level |
|---|---|---|---|
| pN | 1 | 5.21 | 0.000001 |
| Tumour volume | 2 | 2.26 | <0.02 |
| Cell type | 3 | 1.98 | <0.04 |
| Tumor cell density at a vascular distance <20 μm | 4 | 1.86 | <0.05 |

association between the vascular density in advanced lung carcinoma tumour stages and Sv fits into the theory that tumour-induced vascularisation is specifically occurring during these stages, i.e. after the lung carcinomas have reached "a certain age". Similar findings have been reported for the involvement of the immune system in lung carcinomas in terms of inflammation [8]. Again, only tumours at a "certain age" described by the tumour volume induce a notable reactive inflammation. A slight increase of the numerical density of the vessels with increasing tumour volume has been noted in our material, however, not at a statistically significant level. The Vv of connective tissue is similar in squamous cell and adenocarcinomas, and amounts to about a half of that in small cell lung cancer, which, in addition, possess a slightly increased Vv.

B. Absolute vascular features. In terms of a basis constraint, these features are subject to tissue shrinking effects induced by fixation and post-surgical diminishment of vascular lumen due to loss of the intravascular tension. Assuming that newly formed vessels are of approximately tubular formation, the minimum vascular diameter can be assumed to be an appropriate feature to be measured. It is independent of the cell type and the tumour stages; however, centrally located lung carcinomas possess on average smaller vessels when compared with peripherally located tumours.

C. Structural features. There exist only a few investigations that contribute to the relationship between tumour cells and their spatial relationship to the nearest vessels [9, 11, 12]. Kayser et al. [11] measured the percentage of S-phase tumour cells in relation to their distance from the nearest neighbouring vessel. The authors could demonstrate, that the numerical density of S-phase tumour cells is associated with the distance from the nearest vessel: the closer the vessel, the more likely a tumour cell can be found in a proliferation status. Kirkali et al. [12] reported an association of the proliferation activity in association with the angiogenesis in renal carcinomas, too. Vermeulen et al. [26] found an association of active endothelial cells analysed by the Ki-67 protein with so-called hot-spots. All these articles indicate that there is probably a close relationship between the functional activity of tumour cells and their distance to the tumour supply system, i.e. the vessels. We herein apply a new approach in so far as we perform a stereological analysis in relation to a vessel-associated reference space. All tumour cells located within a defined space having a vessel in its centre and being characterised by a maximum distance from the vascular surface are counted and the Nv fraction is calculated. In accordance with previous results, this technique is applied to steps of 20-μm distance from the vascular surface. The results indicate that the tumour cell density increased from a distance 0 μm to 60 μm, and decreased thereon. All lung tumour cell types behave similarly (Table 3, Fig. 1). In addition, this feature is independent of tumour stages (pT, pN) and location.

D. Vascularisation and prognosis. There is a discrepant debate about the role of vascular density with respect to the prognosis of patients suffering from malignant tumours. Some authors are convinced that the degree of tumour vascularisation is closely associated with the outcome of the patient, others are not [13, 15, 18, 20]. In lung carcinomas, Slodkowska et al. reported an association of vascular density with increased tumour involvement of lymph nodes [18, 20]. Other authors could not find a corresponding association [14]. Our results are of borderline significance. The analysis of the survival of our patients revealed no difference in the patients' survivals when treated in the two quite different surgical institutions. The survival analysis resulted in the expected data: the most important predictor for the survival of our patients was the lymph-node involvement. This was in agreement with data published by several authors [1, 4, 21]. The second prognostic indicator was the tumour volume, which ranged even before the pT stage, and was, of course, statistically not independent from the pT stage. The statistical significance of vascular features ranged behind these two parameters, and had—with the exception of tumour cell density close to a vessel—only the significance of a trend ($P<0.1$). Only the tumour cell density close to the surface of the vascular supply system indicated the outcome of the patient at a moderate to low significance. Our findings so far can explain both those findings indicating a prognostic significance and the controversial ones. Vascularisation is a necessity for a tumour to expand and survive. Its initialisation needs time, and its degree is associated with advanced tumour stages only. Therefore, only a weak association with the patient's survival can be expected. Similar to the association of tumour growth with the "immune response" of host tissue [11], the tumour needs time in order to activate the neovascularisation, i.e. it becomes more important in advanced tumour stages compared with early tumours. Whether there is interaction between activation of the immune system and of vascularisation cannot be answered by our study.

In aggregate, the degree of vascularisation in potentially curative operated lung carcinoma patients depends on the tumour stage and is characterised by an increased vascular density, especially an increase of the surface/volume fraction Sv. This feature is mainly induced by a higher vascular density and not by changes of vascular size. The outcome of the patients is only weakly correlated to vascular tumour parameters. The numerical density of tumour cells at a close to moderate distance from the vascular surface is the most significant feature.

**Acknowledgement** The authors gratefully acknowledge the financial support of the Verein zur Förderung des biologisch–technologischen Fortschritts in der Medizin e.V.

## References


1. Baumhäkel J, Kayser K, Kalman E, Kos J, Lah TT, Spiess E, Ebert W, Fiehn W, Werle B (2001) Histological and thermodynamic features of cathepsin B positive tumors of non small cell lung cancer obtained by syntactic structure analysis. Elec J Pathol Histol 7:06
2. Gelb AB, Sudilovski D, WU CD, Weis LM, Medeiros LI (1997) Appraisal of intratumoral microvessel density, Ki–67 score, DNA content and p53 protein expression as prognostic indicators in patient with locally confined renal cell carcinoma. Cancer 80:1768–1775
3. Gorelik E, Galili U, Raz A (2001) On the role of cell surface carbohydrates and their binding proteins (lectins) in tumor metastasis. Cancer Metastasis Rev 20:245–277
4. Kayser G, Gunzenhäuser I, Becker HD, Herth F, Kayser K (2001) Proliferationsrate beim kleinzelligen–anaplastischen Bronchialkarzinom—ein cytomorphologischer Parameter mit prognostischer Aussagekraft. Pathologe 23:326–332
5. Kayser K (1992) Analytical lung pathology. Springer, Berlin Heidelberg New York
6. Kayser K, Berthold S, Eichhorn S, Kayser C, Ziehms S, Gabius HJ (1997) Application of attributed graphs in diagnostic pathology. Anal Quant Cytol Histol 18:286–292
7. Kayser K, Bovin NV, Korchgina EY, Zeilinger C, Feng F–Y, Gabius H–J (1994) Correlation of expression of binding sites for synthetic blood group A–, B–, and H–trisaccharides and for sarcolectin with survival of patients with bronchial carcinoma. Eur J Cancer 30A:653–657
8. Kayser K, Bülzebruck H, Ebert W, Merkle NM, Vogt–Moykopf I (1986) Local tumor inflammation, lymph node metastasis, and survival of operated bronchus carcinoma patients. J Natl Cancer Inst 77:77–81
9. Kayser K, Gabius, HJ (1997) Graph theory and entropy concept. In: Graumann W (ed) Histochemistry. Progress in histochemistry and cytochemistry 32. Gustav Fischer, Stuttgart
10. Kayser K, Kayser G, Eichhorn S, Biechele U, Altiner M, Kaltner H, Zeng FY, Vlasova EV, Bovin NV, Gabius HJ (1998) Association of prognosis in surgically treated lung cancer patients with cytometric, histometric and ligand histochemical properties: with an emphasis on structural entropy. Anal Quant Cytol Histol 20:313–320
11. Kayser K, Richter B, Stryciak R, Gabius HJ (1997) Positive and negative correlations between vascularization and parameters derived from integrated nuclear fluorescence and syntactic structure analysis in human lung carcinomas. Anal Cell Pathol 15:73–83
12. Kirkali Z, Yorukoglu K, Ozkara E, Kazimoglu H, Mungan U (2001) Proliferative activity, angiogenesis and nuclear morphometry in renal carcinoma. Int J Urol 8:697–703
13. Leek RD, Lewis CE, Whitehouse R, Greenall M, Clarke J, Harris AL (1996) Association of macrophage infiltration with angiogenesis and prognosis in invasive breast carcinoma. Cancer Res 56:4625–4629
14. Lucchi M, Mussi A, Fontanini G, Faviana P, Ribechini A, Angeletti CA (2002) Small cell lung carcinoma (SCLC): the angiogenic phenomenon. Biotech Histochem 77:85–91
15. McLennan GT, Bostwick DG (1995) Microvessel density in renal cell carcinoma. Lack of prognostic significance. Urology 46:27–30
16. Pritchard AJ, Chatterjee T, Wilkinson M, Powe DG, Gray T, Hewitt RE (1995) Evidence for a weak angiogenic response to human colorectal cancers. Br J Cancer 71:1081–1086
17. Rintoul RC, Sethi T (2001) The role of extracellular matrix in small-cell lung cancer. Lancet Oncol 2:437–442
18. Sikora J, Slodkowska J, Kobos J, Radamyski A (1996) Tumor angiogenesis within lung adenocarcinomas and its correlation with metastasis. Elec J Pathol Histol 2.1:961–962
19. Sinowatz F, Plendl J (1996) Heterogeneity of endothelial cells. Elec J Pathol Histol 2.2:962–968
20. Slodkowska J, Sikora J, Kobos J, Radamyski A, Kuca P (1996) The clinicopathological assessment of proliferation, metastatic potential and angiogenesis of lung adenocarcinomas. Elec J Pathol Histol 2.2:962–963
21. Sloman A, D'Amico F, Yousem SA (1996) Immunohistochemical markers of prolonged survival in small cell carcinoma of the lung. An immunohistochemical study. Arch Pathol Lab Med 120:465–472
22. Sobin LH, Wittekind C (eds) (1998) UICC: TNM classification of malignant tumours, 5th edn. John Wiley and Sons Inc., New York
23. Teo NB, Shoker BS, Jarvis C, Martin L, Sloane JP, Holcombe C (2002) Vascular density and phenotype around ductal carcinoma in situ (DCIS) of the breast. Br J Cancer 86:905–911
24. Terayama N, Terada T, Nakanuma Y (1996) A morphometric and immunohistochemical study on angiogenesis of human metastatic carcinomas of the liver. Hepatology 24:816–819
25. Hermanek P, Hutter RVP, Sobin LH, Wagner G, Wittekind C (eds) (1998) UICC: TNM–Atlas. 4. Aufl. Springer, Berlin Heidelberg NewYork
26. Vermeulen P, Dirix LC, van Marck E, van Oosterom AT (1996) High endothelial proliferation index and high microvessel density in vascular hotspots suggest an active angiogenic process in human colorectal adenocarcinomas. Br J Cancer 74:1506–1510
27. World Health Organization (2000) International classification of malignant tumours. Geneva: World Health Organization, 3rd edn. Springer, Berlin Heidelberg New York

Virchows Arch (2003) 442:468–471
DOI 10.1007/s00428-003-0799-x

ORIGINAL ARTICLE

**Raf Sciot · Ivo De Wever · Maria Debiec-Rychter**

# Lipoblastoma in a 23-year-old male: distinction from atypical lipomatous tumor using cytogenetic and fluorescence in-situ hybridization analysis

Received: 14 January 2003 / Accepted: 4 March 2003 / Published online: 5 April 2003
© Springer-Verlag 2003

**Abstract** Lipoblastoma is a rare benign tumor that occurs primarily in infancy and early childhood. We present the rare presentation of a 12 cm sized intramuscular lipoblastoma of the thigh in a 23-year-old patient. On histology, the tumor strongly resembled an atypical lipomatous tumor due to the presence of lipoblasts and atypical stromal nuclei. The very focal lobulation and myxoid change presented the only histological hint towards a lipoblastoma. Cytogenetic and subsequent FISH evaluation of the tumor cells showed a 46,XY, t(8;15) (q12;q25) as chromosomal change with rearrangement of the PLAG1 gene. The present case indicates that lipoblastoma should enter the differential diagnosis of an 'atypical' deep seated fatty tumor in adults. The diagnostic value of cytogenetic/molecular analysis in the differential diagnosis of lipomatous tumors is underscored as well.

**Keywords** Lipoblastoma · Atypical lipomatous tumor · FISH · Cytogenetics · PLAG1 · gene 8q12

## Introduction

Adipose tissue tumors represent the most frequent soft-tissue neoplasms in adults, ordinary lipomas obviously being the most common type. Lipoblastomas are relatively rare benign fatty tumors that typically occur in young children, usually less than 8 years old. Lipoblastomas have been described to occur in older children and very rarely in elderly patients. Silverman et al. described a recurring lipoblastoma in a 48-year-old patient, although unequivocal proof for the diagnosis of lipoblastoma was lacking [10]. The term lipoblastomatosis refers to the lesions that infiltrate into the muscle. Because of the presence of lipoblasts, thin-walled plexiform capillary vessels and a myxoid stroma, lipoblastoma (tosis) may resemble malignant adipose tissue tumors such as myxoid liposarcoma and atypical lipomatous tumor [9].

Genetic alterations underlying the pathogenesis of lipomatous tumors are well known. The specific translocations, t(12;16) and t(12;22), generating TLS-CHOP and EWS–CHOP fusion transcripts, respectively, have been found in myxoid and round cell liposarcoma [6]. In atypical lipomatous tumors, characteristic supernumerary ring and/or giant marker chromosomes can be found with amplified sequences of chromosomal region 12q [1]. Lipoblastomas present with the rearrangements of chromosomal region 8q12 involving the *PLAG1* gene [3, 4].

We recently reported a histologically lipoblastoma-like atypical lipomatous tumor in a 14-year-old child [7]. We now present an opposite situation: an atypical lipomatous tumor-like lipoblastoma occurring in a 23-year-old patient, emphasizing the diagnostic relevance of cytogenetics and fluorescence in-situ hybridization (FISH).

R. Sciot (✉)
Department of Pathology; University Hospital,
Catholic University of Leuven, University Hospital St. Rafaël,
Minderbroedersstraat 12, 3000 Leuven, Belgium
e-mail: raf.sciot@uz.kuleuven.ac.be
Tel.: +32-16-336593
Fax: +32-16-336548

I. De Wever
Department of Surgery,
University Hospital, Catholic University of Leuven,
Leuven, Belgium

M. Debiec-Rychter
Center of Human Genetics,
University Hospital, Catholic University of Leuven,
Leuven, Belgium

## Materials and methods

The tumor was received fresh. Part of the specimen was fixed in 6% formalin. A minor part was snap-frozen in liquid nitrogen cooled isopentane. The fixed tissue was processed to paraffin and stained with hematoxylin & eosin.

Chromosome metaphases were obtained after short-term culture of a primary tumor sample, utilizing standard procedures. G-banded chromosomes were evaluated and classified according to the International System of Human cytogenetic nomenclature [8]. Metaphase dual-color FISH was performed using the combination of Spectrum Orange-labeled chromosome 8 centromeric (CEP8-

SO, Vysis Inc., Downers Grove, IL, USA) and biotin-labeled YAC164H8 DNA probes. The latter maps to exons 2–5 of the *PLAG1* gene at 8q12 [5]. Hybridization and detection was performed as previously described [2]. Hybridization signals were visualized using an epifluorescence microscope (Leica DMRB, Wetzlar, Germany) equipped with a cooled CCD camera and run by image analysis software (QUIPS, Vysis, IL, USA).

## Results

A 23-year-old male patient presented with a painless swelling in the right thigh. The tumor was noticed by the patient only 4 weeks before the surgical intervention. On imaging, an intramusular tumor was seen, showing the density of fat. The 12-cm-sized tumor was resected and showed the appearance of adipose tissue. The tumor was extensively sampled. On histology, the fatty nature of the tumor was confirmed. A striking variability in adipocyte

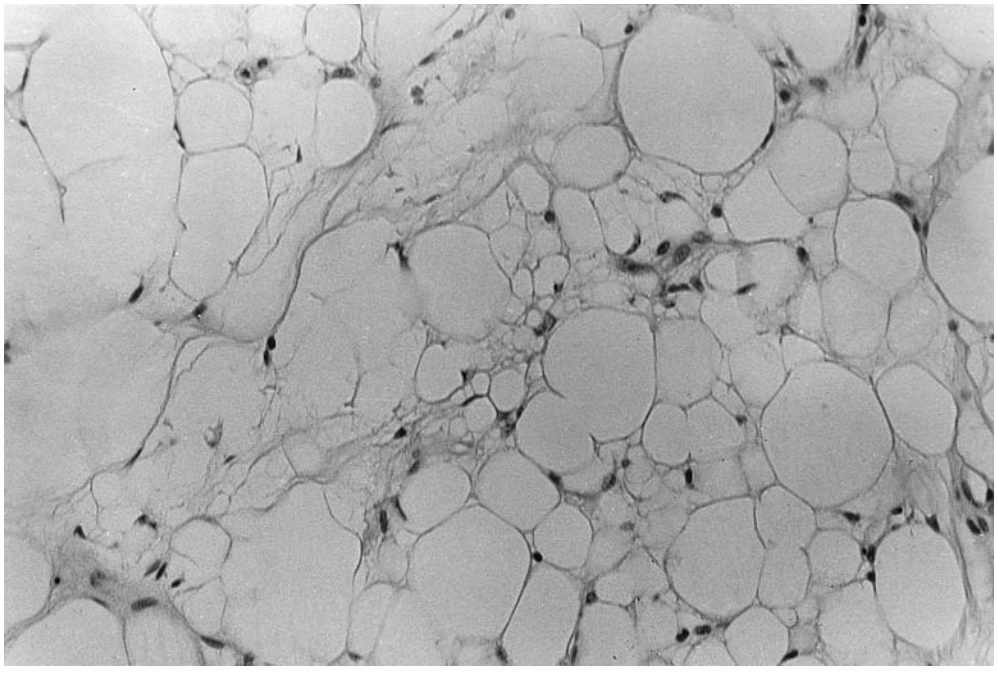


**Fig. 1** Hematoxylin and eosin stain, showing the variability in adipocyte size and lipoblasts

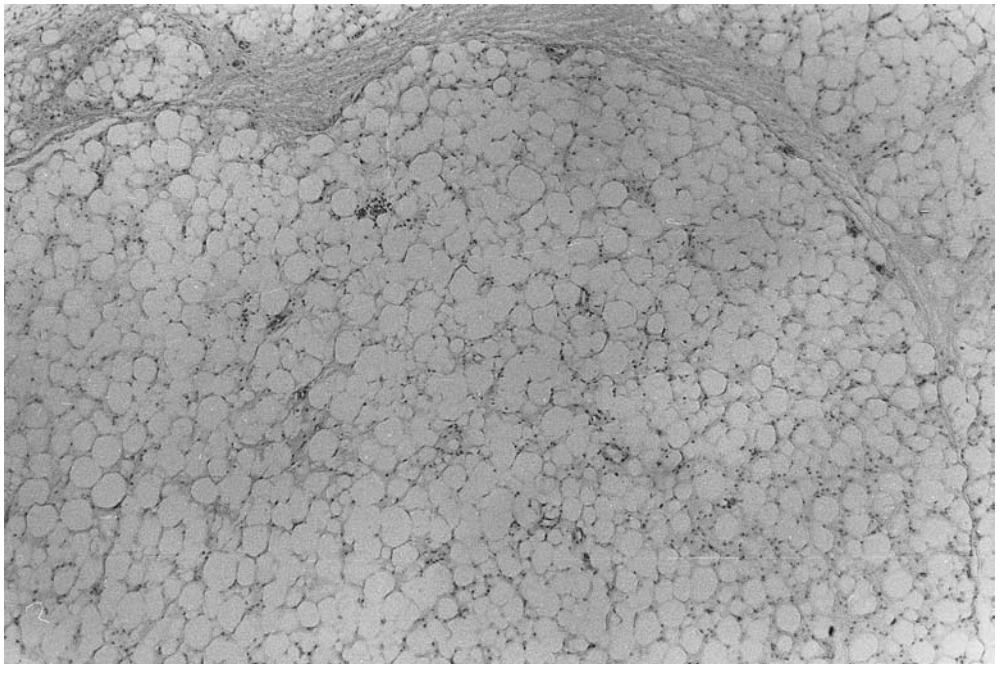


**Fig. 2** Hematoxylin and eosin stain, revealing the focal lobulation

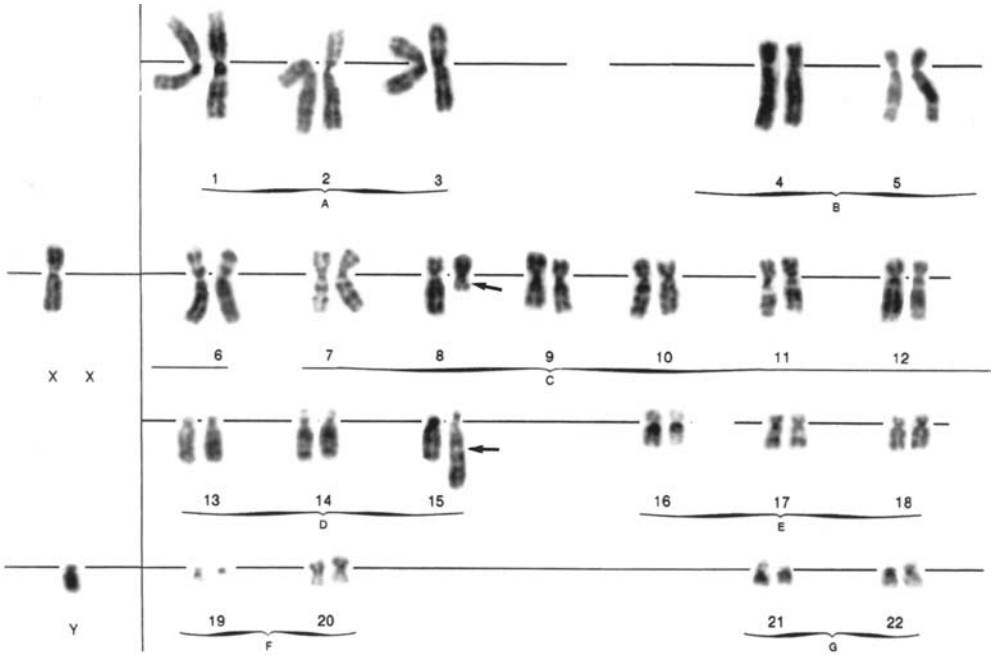



**Fig. 3** G-banded karyogram of the abnormal tumor metaphase showing 46,XY, t(8;15) (q12;q25) karyotype. *Arrows* point to the breakpoints

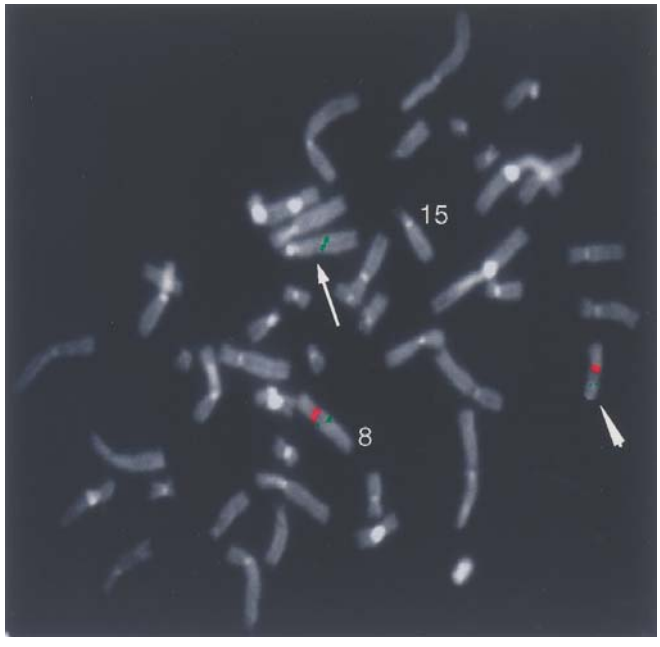



**Fig. 4** Dual-color fluorescence in-situ hybridization (FISH) analysis of neoplastic metaphase cell using SpectrumOrange-labeled chromosome 8 centromeric and biotin-labeled YAC164H5/*PLAG1* DNA probes. The split, green signal from the latter confirms *PLAG1* gene rearrangement. Derivative chromosomes 8 and 15 are indicated by the arrowhead and the arrow, respectively

size was seen as well as scattered hyperchromatic stromal nuclei. Multifocal lipoblasts were also present, mainly at the edge of the tumor (Fig. 1). Stromal myxoid changes as well as a vague lobulation were only very focally present (Fig. 2). There was no increased fibrosis.

Thirty-five G-banded metaphases were obtained from a 5-day-old culture of a tumor biopsy sample. A normal male karyotype, 46,XY, was found in 11 cells. The remaining metaphases displayed abnormal 46,XY,t(8;15) (q12;q25) karyotype (Fig. 3).

By metaphase FISH analysis, Spectrum Orange-labeled centromeric CEP8 and biotin-labeled YAC164H8/*PLAG1* specific probes revealed a green signal on the normal chromosome 8q12 as well as a split signal at the breakpoint sites of both derivative chromosomes, der (8) and der (15) (Fig. 4). This finding indicated the rearrangement of the *PLAG1* gene.

## Discussion

Lipoblastoma (tosis) is a fully benign tumor that shows characteristic histological features such as lobulation and an admixture of mature adipocytes and lipoblasts. Lipoblastoma (tosis) shows a typical 8q12 rearrangement, which brings about promoter swapping events in the *PLAG1* oncogene, resulting in activation of this gene [4]. Because of the presence of myxoid areas, lipoblasts and a plexiform chicken-wire capillary pattern, this lesion may be mistaken for a myxoid liposarcoma, certainly in the absence of clinical data. However, myxoid liposarcoma is not particularly characterized by a lobulation pattern, and this malignant tumor typically occurs in an older age group than does lipoblastoma. From a cytogenetic point of view, myxoid liposarcoma has a typical t(12;16) (q13;p11) translocation [6]. Because of the lipoblasts in lipoblastoma, atypical lipomatous tumor may also enter the differential diagnosis. The tumor about which we report in this paper was, on histology, first considered to be highly suggestive of an atypical lipomatous tumor,

because of the location, the size, the presence of lipoblasts and the age of the patient. A lipoblastoma was considered to be very unlikely, the only possible histological 'hint' being the very focal lobulation and myxoid change. For the patient, the differential diagnosis is of importance, since atypical lipomatous tumor is a low-grade sarcoma with no metastatic potential, but, when recurring, may dedifferentiate and thus gain a metastatic potential. To our surprise, the tumor did not reveal the typical ring chromosomes/giant markers of atypical lipomatous tumor, but showed involvement of 8q12 and rearrangement of the *PLAG1* gene, as seen in lipoblastoma.

This case, as well as our previous report, confirms that, on the one hand, lipoblastoma does rarely occur in elderly patients and that, on the other hand, atypical lipomatous tumor can present in children [7]. In addition, these findings show that cytogenetics and/or FISH are a very powerful diagnostic tool in a differential diagnostic setting and in tumors with an unusual clinical presentation.

**Acknowledgements** This text presents research results of the Belgian program on Interuniversity Poles of Attraction initiated by the Belgian Sate, Prime Minister's Office, Science Policy Programming. Its authors assume the scientific responsibility. The authors would like to thank Belinda Carleer and Lut Mekers for their excellent technical assistance. Michel Rooseleers is acknowledged for his photographic assistance.

## References

1. Dei Tos AP, Doglioni C, Piccinin S, Sciot R, Furlanetto A, Baiocchi M, Dal Cin P, Maestro R, Fletcher CDM, Tallini G (2000) Coordinated expression and amplification of the MDM 2, CDK4, and HMGI-C genes in atypical lipomatous tumours. J Pathol 190:531–536
2. Dierlamm J, Wlodarska I, Michaux L, La Starza R, Zeller W, Mecucci C, Van den Berghe H (1996) Successful use of the same slide for consecutive fluorescence in situ hybridization experiments. Genes Chromosomes Cancer 16:261–264
3. Gisselsson D, Hibbard MK, Dal Cin P, Sciot R, Hsi B-L, Kozakewich HP, Fletcher JA (2001) PLAG1 alterations in lipoblastoma: involvement in varied mesenchymal cell types and evidence for alternative oncogenic mechanisms. Am J Pathol 159:955–962
4. Hibbard MK, Kozakewich HP, Dal Cin P, Sciot R, Tan X, Xiao S, Fletcher JA (2000) PLAG1 fusion oncogenes in lipoblastoma. Cancer Res 60:4869–4872
5. Kas K, Voz ML, Roijer E, Astrom AK, Meyen E, Stenman G, Van de Ven WJ (1997) Promoter swapping between the genes for a novel zinc finger protein and beta-catenin in pleiomorphic adenomas with t(3;8) (p21;q12) translocations. Nat Genet 15:170–174
6. Knight JC, Renwick PJ, Dal Cin P, Van den Berghe H, Fletcher CD(1995) Translocation t(12;16) (q13;p11) in myxoid liposarcoma and round cell liposarcoma: molecular and cytogenetic analysis. Cancer Res 55:24–27
7. Kuhnen C, Mentzel T, Fisseler-Eckhoff A, Debiec-Rychter M, Sciot R(2002) Atypical lipomatous tumor in a 14-year-old patient distinction from lipoblastoma using FISH-analysis. Virchows Arch 441:299–302
8. Mitelman F (ed) (1995) ISCN, An international system for human genetic nomenclature. Karger, Basel
9. Sciot R, Mandahl N (2002) Lipoblastoma/lipoblastomatosis. In: Fletcher CDM, Unni KK, Mertens F (eds) Pathology and genetics. Tumours of soft tissue and bone. In: World Health Organization Classification of Tumours, IARC Press, pp 26–27
10. Silverman JS, Hamilton J, Tamsen A (1999) Benign recurring lipoblastoma in an adult versus well differentiated subcutaneous myxoid liposarcoma: clinicopathologic, immunohistochemical and molecular analysis of a unique case. Pathol Res Pract 195:787–792

Virchows Arch (2003) 442:472–481
DOI 10.1007/s00428-003-0785-3

ORIGINAL ARTICLE

**Jing An · De-Shan Zhou · Kazunori Kawasaki · Kotaro Yasui**

# The pathogenesis of spinal cord involvement in dengue virus infection

Received: 25 September 2002 / Accepted: 29 January 2003 / Published online: 15 April 2003
© Springer-Verlag 2003

**Abstract** To investigate the mechanisms of dengue (DEN) virus transmission within the spinal cord, severe combined immunodeficient mice were intracerebrally inoculated with DEN virus type 2. After inoculation, a high virus titer and antigens were detected in the brain and spinal cord. At early stages of the infection, ultrastructural examinations showed that a few virions were present in the cytoplasm of ependymal cells lining the central canal. As the infection progressed, virions were observed in the lumen of the rough endoplasmic reticulum (RER), RER-derived vesicles and the Golgi region of infected neurons. These data suggest that the inoculated DEN virus might spread to the neurons of the spinal cord via the cerebral spinal fluid and cause several neuronal pathological responses. Moreover, DEN virus was also observed in myelinated and unmyelinated nerve fibers and typical neuronal synapses. Some virion-containing vesicles appeared to be fused with the membrane of presynapses, indicating that neuron-to-neuron transport of DEN virus might occur in the spinal cord. Additionally, anterior, lateral and posterior horns of the spinal cord exhibited different numbers of the positive neurons and different staining intensities of the DEN antigen during the infection. This difference likely represents variation of susceptibility to the DEN virus among the neurons of the spinal cord.

**Keywords** Dengue virus · Neuron-to-neuron transportation · Viral spread · Electron microscopy · Spinal cord · Mouse

J. An
Department of Microbiology,
Third Military Medical University,
400038 Chongqing, China

D.-S. Zhou (✉)
Department of Histology and Embryology,
Third Military Medical University,
400038 Chongqing, China
e-mail: dszhou2000@yahoo.com
Tel.: +86-23-68752230
Fax: +86-23-65402973

K. Yasui
Department of Microbiology,
Tokyo Metropolitan Institute for Neuroscience,
2-6 Musaitai, Fuchu-City, 183-8526 Tokyo, Japan

K. Kawasaki
Institute for Biological Resources and Functions,
National Institute of Advanced Industrial Science and Technology,
1-1-1 Higaishi, Tsukuba, 305-8566 Ibaraki, Japan

## Introduction

Dengue (DEN) viruses are members of the flavivirus family. Four distinct serotypes of DEN viruses (DEN 1, 2, 3, 4) have been identified. These viruses are mosquito-borne human pathogens that can be spread rapidly in the tropics and subtropics. DEN viruses can cause either mild febrile illnesses (classical dengue fever) or life-threatening syndromes (dengue hemorrhagic fever/dengue shock syndrome, DHF/DSS) [23]. Typical signs of DHF/DSS are gastrointestinal bleeding and hypovolemic shock resulting from an increased vascular permeability. In recent years, unusual clinical manifestations, mostly cerebral and hepatic symptoms, have become more common in patients with DEN virus infection [20, 21, 26, 29]. Although the target cells for DEN virus infection remain unclear, nervous system involvement has been indicated by neurological manifestations including lethargy, confusion, and coma observed during the febrile phase of the infection as well as delayed cerebral symptoms such as paralysis of extremities, loss of sensation and manic psychosis [2, 5, 10, 17]. The pathophysiology of neuronal involvement in human cases of DEN virus infection was attributed to factors such as cerebral anoxia, cerebral edema, hepatic failure and metabolic acidosis. In previous studies, however, it has been reported that severe combined immunodeficient (SCID) mice xenografted with HepG2 or K562 cells showed neurological signs of kyphoscoliosis and flaccid paralysis after intraperitoneal inoculation of DEN virus type-2 (DEN-2). DEN viral antigens were detected in

neurons of the central nervous system (CNS) in these infected mice [1, 16]. Recent clinical studies also demonstrated that DEN virus antigens were found in the neurons of the CNS in fatal cases of DHF [18, 22]. These results supported the hypothesis that DEN virus may invade the CNS and directly induce pathological effects in neurons.

The aforementioned flaccid paralysis suggested that the neurons of the spinal cord are involved in the infection. However, mechanisms of viral transmission within the spinal cord and the nature of the neuronal injury have not been elucidated completely at the present time. Since SCID mice with an intracerebral (i.c.) inoculation of DEN-2 showed similar neuronal manifestations, such as flaccid paralysis and kyphoscoliosis, to those observed in HepG2-engrafted SCID mice inoculated intraperitoneally with DEN-2, we analyzed the mechanism of the virus spread within the spinal cord using i.c. inoculation in the animal model . Our results might be valuable for understanding pathogenesis of neuronal manifestations associated with DEN virus infection.

## Materials and methods

### Animals

Female SCID (C.B.-17/Icr Tac-scid) mice aged 14 weeks from Clea Co. (Tokyo, Japan) were maintained in specific pathogen-free facilities.

### Virus inoculum

DEN-2 (strain Tr1751) isolated from a patient with DEN fever was kindly provided by Dr. Oya A (National Institute of Infectious Diseases, Japan). The virus was propagated in *Aedes albopictus* mosquito cells (C6/36) and stored at −80°C until used [13]. The titer of virus stock was adjusted to $10^6$ pfu/ml.

### Virus infection

Each mouse was injected i.c. with $2.5\times10^4$ pfu (25 $\mu$l) DEN-2, and the infected animals were observed daily for signs of morbidity and especially for post-infection (p.i.) paralysis. Samples of the blood, brain and spinal cord were taken on days 1, 3, 5 and 7 p.i. and on the day of paralysis onset (DP). Ten mice were used for each time point (five for virus titration, two for histopathological and immunohistochemical examinations and three for ultrastructural observations). The serum and tissue samples obtained from each animal were immediately frozen at −80°C for titration of virus. Each control mouse was inoculated i.c. with 25 $\mu$l Eagle's minimum essential medium (MEM).

### Titration of virus

Tissue samples were homogenized with MEM containing 20% Haemaccel and 10 mM HEPES (pH 7.2–7.4). After centrifugation at 15,000 rev/min for 15 min at 4°C, the supernatant was collected and then analyzed for virus titer by the plaque method using a Vero cell monolayer culture under methycellulose overlay medium. Virus titer in the serum was also determined using the same plaque procedure.

### Histopathological and immunohistochemical examination

Specimens of the brains and spinal cords were taken out after perfusion with 4% paraformaldehyde in 0.1 M phosphate buffer (PB, pH 7.4) on days 1, 3, 5, 7 p.i. and DP (two mice for each time point, ten mice total), and then fixed with the same fixative solution for 2 h at 4°C. The specimens were further divided into two parts. One was processed for hematoxylin and eosin (HE) staining, and the other was used for immunohistochemical determination of DEN viral antigens. In brief, the specimens were rinsed in 0.01 M phosphate buffered saline and frozen immediately with liquid nitrogen in OTC compound. Cryo-sections (10 $\mu$m) were made using a cryostat. Two primary mouse monoclonal antibodies (mAbs), 504 and 301, were used for detecting DEN-2 viral antigens. Both mAbs react with DEN viruses [15]. Fluorescein isothiocyanate (FITC)-conjugated anti-mouse immunoglobulin G (Dako) was used as a secondary antibody. The sections were observed under a fluorescence microscope (Axioplan, Zeiss, Germany). Controls were stained with the secondary antibody only.

### Ultrastructural observation

The spinal cord of the infected mice was taken on days 1, 3, 5, 7 p.i and DP (three mice for each time point, fifteen mice total). Under ether anesthesia, the mice were perfused through the heart with Kreb's solution to remove blood and then with Karnovsky's fixative solution containing 4% paraformaldehyde and 2.5% glutaraldehyde in 0.1 M PB. The spinal cords were taken out and cut into small pieces (3–5 $mm^3$), then immersed in the same fixative solution for 2–3 h at 4°C. After washing with the same buffer, the specimens were post-fixed with 1% OsO4 in 0.1 M PB for 2 h at 4°C. Following osmication, the specimens were rinsed in distilled water and then block-stained with 1% aqueous uranyl acetate solution for 2–3 h at 25°C. After dehydration with a graded series of ethanol, the specimens were embedded in Epon Epoxy resin. Ultra-thin sections (60 nm) were prepared with a Reichert ultramicrotome. The sections were double-stained with lead citrate and uranyl acetate, then examined in an electron microscope (H-7000, Hitachi) [25].

## Results

### Clinical data

After i.c. inoculation with DEN-2 virus, the mice gradually showed bradykinesia, ruffle and kyphoscoliosis. On day 8 and day 9 p.i., the infected mice developed paralysis of hind and/or fore legs. All animals died around 24 h after showing paralysis.

### Growth of DEN-2 virus in the CNS

As shown in Fig. 1, the DEN-2 virus was not initially detectable in the spinal cord and brain of the infected mice. In the spinal cord, the virus was detected in 80% of mice with a titer of $10^{1.9}$ pfu/g on day 3 p.i. From day 5 to DP, the virus was detected in all animals with a titer of about $10^{5.1–5.7}$ pfu/g. There was no difference in the amount of DEN-2 virus in cervical, thoracic and lumber segments at the same time point p.i. (data not shown). In the brain, the virus was detected in 80% of mice with a titer of $10^{2.5}$ pfu/g on day 3. From day 5 to DP, the virus was detected in all mice with a titer of about $10^{5.1–6.3}$

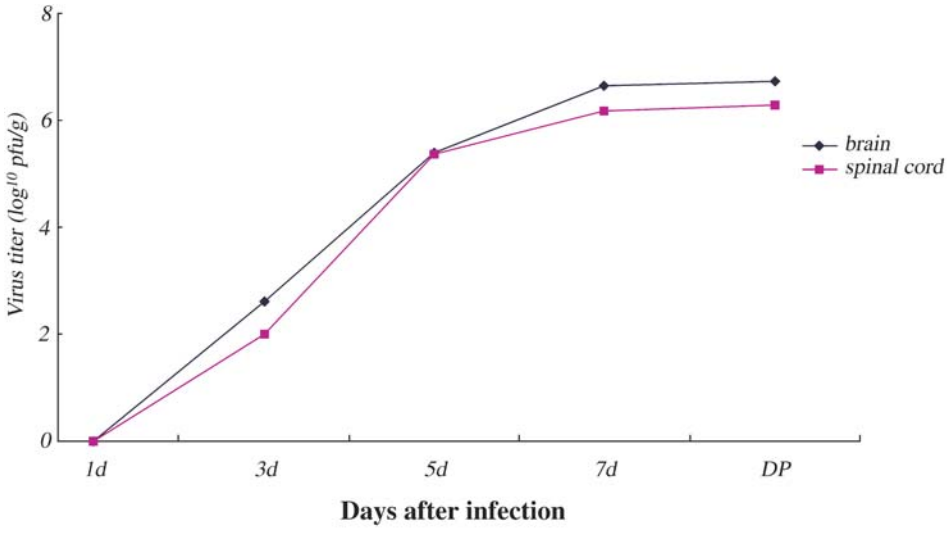



**Fig. 1** Growth curves of DEN-2 virus in the brain and spinal cord of infected mice after intracerebral (i.c.) inoculation. Virus titer is determined by plaque assay on a Vero cell monolayer culture. Value from the tissues of five mice is averaged for each time point. *DP* day of paralysis onset

pfu/g. In contrast, no virus was detected in the serum during infection.

## Distribution of DEN-2 virus in the CNS

By immunohistochemical staining, DEN viral antigen was observed in the spinal cord and brain (Fig. 2a, b, c). In the spinal cord, DEN viral antigens were weakly stained in a few neurons in the anterior horn on day 3 p.i. (Fig. 2a). After day 3, they were found with strong staining in many neurons in the same area. In contrast, DEN antigen-positive neurons were not observed in the lateral and posterior horn until day 5 p.i., by which time, the DEN antigen started to appear in the neurons in these areas. When a large number of DEN antigen-positive neurons with strong staining were observed in the lateral and posterior horn on day 7 p.i. and DP (Fig. 2b), some neurons were lost in the anterior horn. The cervical, thoracic and lumber segments showed a similar transmission pattern, as described above. It seems that the neurons in the anterior horn were more involved in the infection than those of the lateral horn and posterior horn of the spinal cord. In the brain, there were a few DEN-immunoreactive neurons showing a weakly positive response of DEN viral antigen in the hippocampus and basal ganglia from day 3 to day 5 p.i. With virus replication, many neurons were strongly stained on day 7 and DP (Fig. 2c). DEN viral antigen was not observed in the neurons on day 1 p.i. However, no DEN viral antigen was detected in neuroglia and ependymal cells of the CNS during any period of the infection. The control specimens were negative for DEN virus antigen.

## Histopathological observation

In HE staining, several pathological changes were found in the spinal cord sections of infected mice from day 5 after i.c. inoculation. Edema and congestion were seen from day 5 to DP. Neurons in the gray matter showed some denatured changes including hypochromatism, decreased Nissl substance, vacuolization and neuronophagia. Astrocyte swelling was occasionally seen. With the virus replication, loss of the neurons was observed in the anterior horn on DP.

Using transmission electron microscopy (TEM), typical spherical DEN virus particles were seen with diameters of about 45–55 nm and an electron-dense nucleocapsid was surrounded by an envelope lipid bilayer. At day 3 p.i., a number of virions were seen in the cytoplasm, but not in the rough endoplasmic reticulum (RER) and Golgi complex of the ependymal cells lining the central canal at multiple levels with some extension to the subependymal central gray matter (Fig. 3a, b, c). As the infection progressed, virions were found predominantly in the lumen of the RER, RER-derived vesicles and Golgi regions in the neurons (Fig. 4a, b, c, d, e, f, g). The RER showed irregular dilations and slight vesiculation in this phase of the infection. At later phases of the infection, many RER-derived vesicles containing virions were observed in the Golgi complexes of infected neurons (Fig. 4f, g). Membrane-bound vesicles containing virions were also found in myelinated and unmyelinated nerve fibers and on both sides of typical synapses (Fig. 5a, b, c). Some vesicles containing virion in the synapse were close to the presynaptic membrane and appeared to fuse with the membrane (Fig. 5d, e). During the infection, some neurons in the anterior horn gradually developed necrosis (Fig. 6) and were lost when the mice showed paralysis. Inflammatory cells were often seen in the spinal cord during the infection. However, morphological signs of apoptosis, e.g., pycnotic nucleus and margination of chromatin to the nuclear membrane, were not observed in the infected neurons. The ultrastructural features described above were not seen in specimens from uninfected mice.

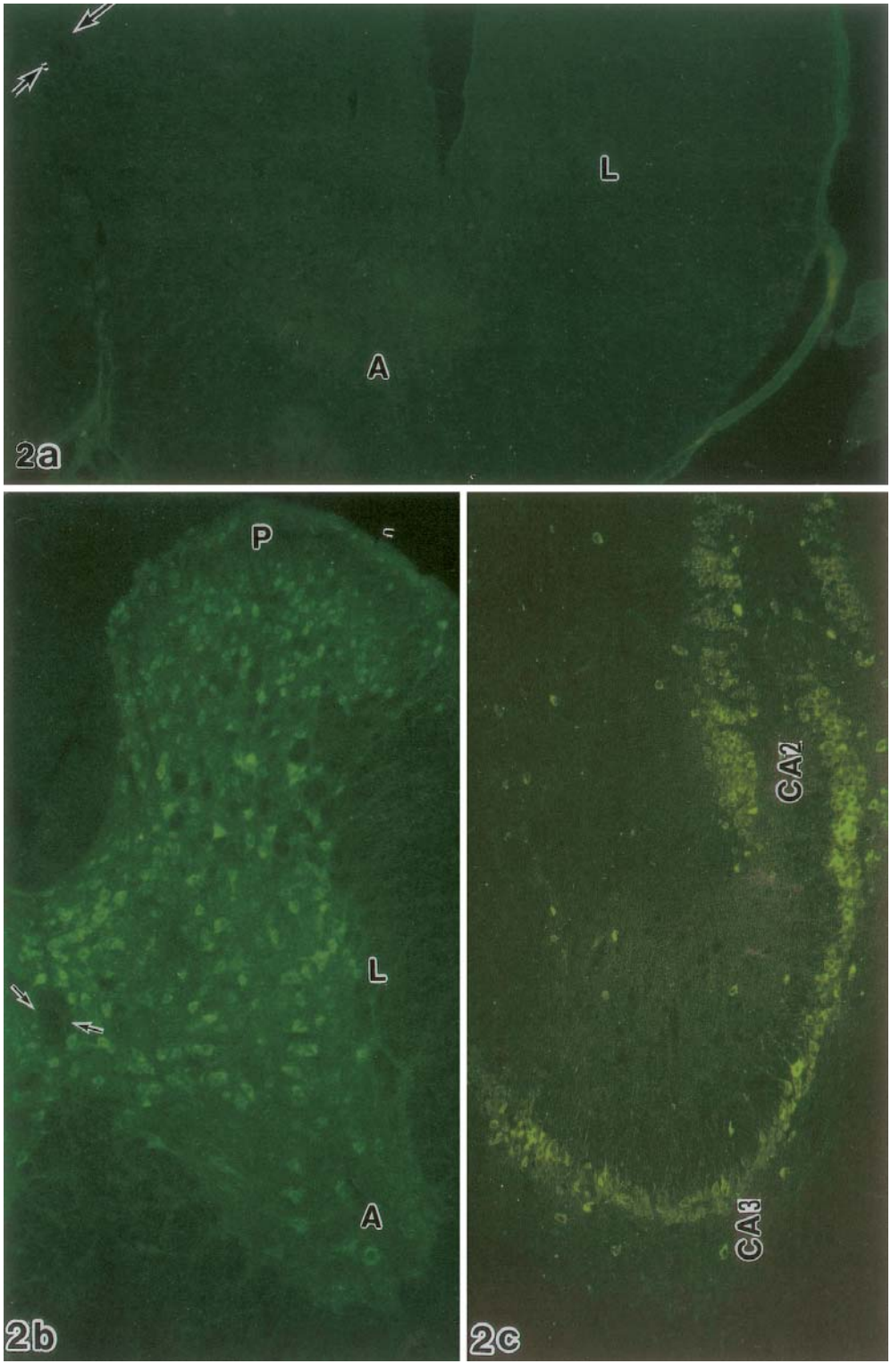



**Fig. 2** Immunostaining for DEN viral antigens on cryosections of the brain and spinal cord. **a** A few neurons weakly stained are observed in the anterior horn of the spinal cord at day 3 post-infection and no DEN viral antigen-positive neurons are found in lateral and posterior horns at this time (×150); **b** Many DEN viral antigen-positive neurons with strong staining are seen in whole gray matter of the spinal cord on the day of paralysis onset (×200); **c** A large number of DEN antigen-positive neurons with strong staining are seen in the CA3 and CA2 field of the hippocampus at day 7 post-infection (×170). *A* anterior horn, *L* lateral horn, *P* posterior horn, *Arrows* the central canal of the spinal cord

## Discussion

Infection of SCID mice or suckling mice by i.c. inoculation of viruses has been widely used as a convenient animal model for investigating viral infection in the CNS [8, 11, 24, 30]. For example, Pol et al. [30] inoculated cytomegalovirus (CMV) i.c. into newborn and SCID mice, and found that developing brain cells are inherently more susceptible to CMV infection, independent of the immune system. Charlier et al. [8] observed characteristics of flavivirus encephalitis and a protective effect of interferon on Montana Myotis leukoencephalitis virus

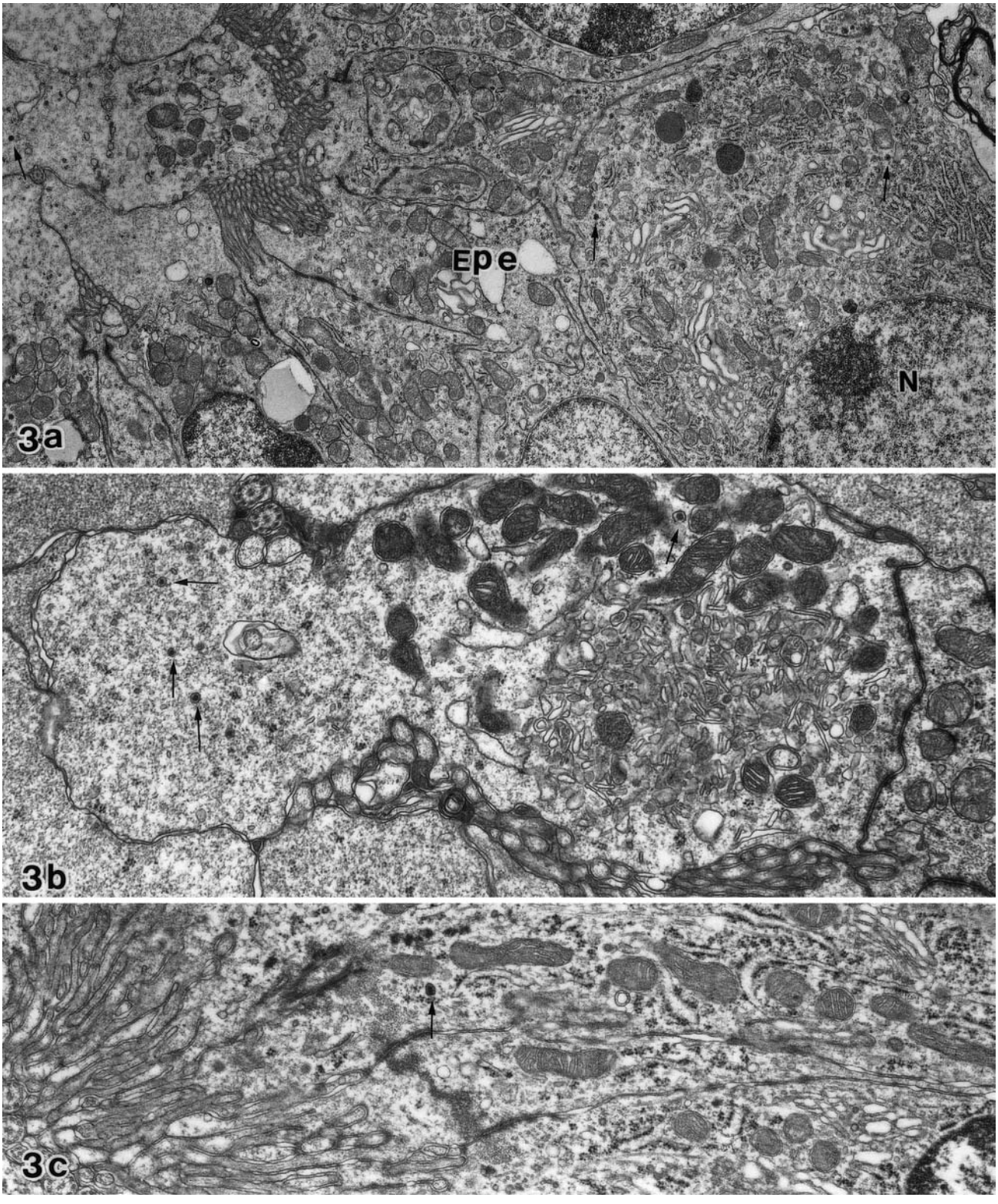



**Fig. 3** Electron micrographs showing the distribution of DEN viral particles in the ependymal cells of the central canal at day 3 post-infection. **a** Lower magnification showing the viral particles (*arrows*) in the cytoplasm of ependymal cells (*epe*) and subependymal cells. *N* nucleus (×8000). **b** Higher magnification of a part of an ependymal cell from a neighboring section of **a**, the viral particles (*arrows*) exist in the cytoplasm near the lumen of the central canal (×18,900). **c** Viral particle is seen in the cytoplasm of ependymal cells (*arrow*) (×20,200)

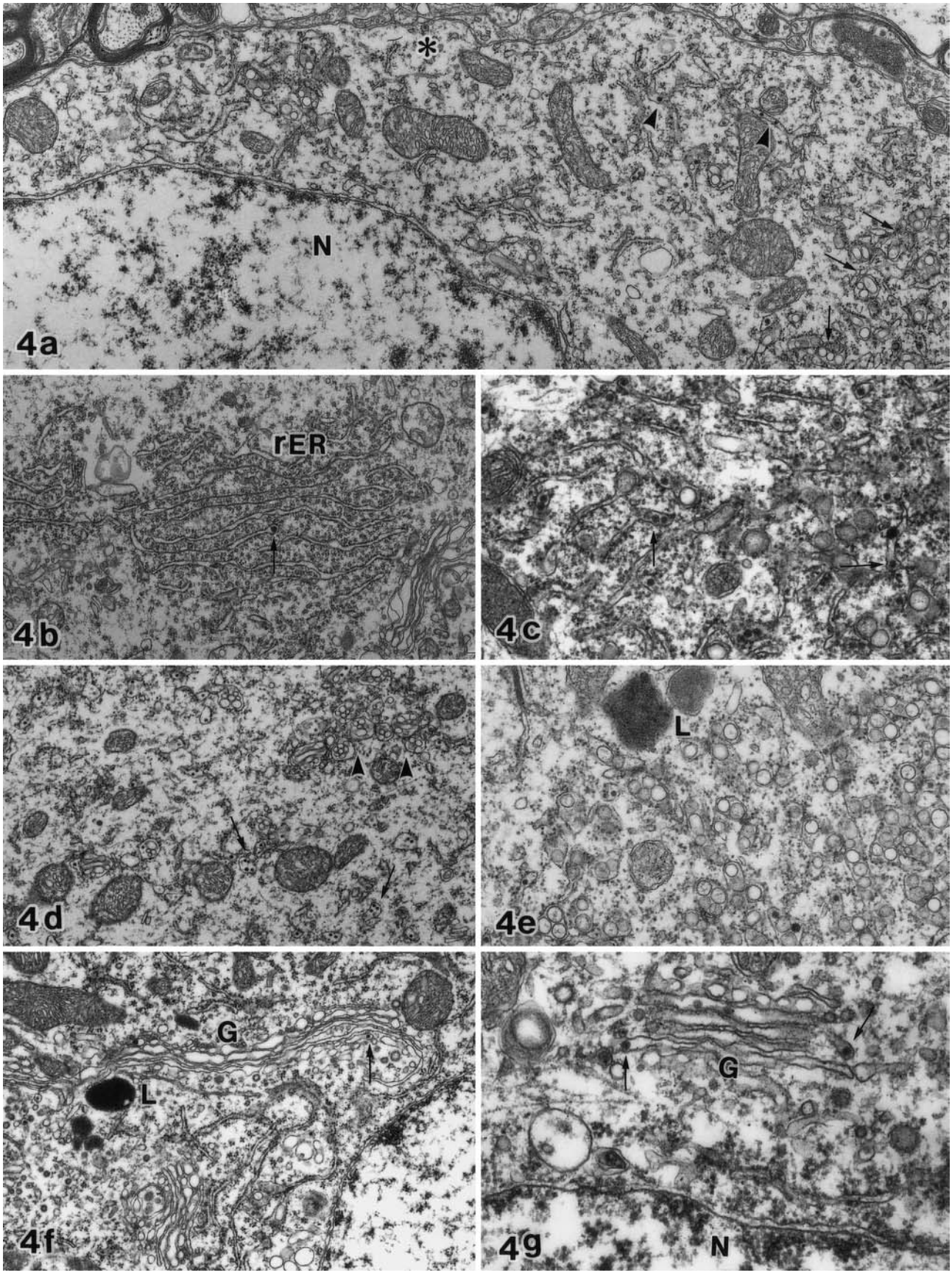



**Fig. 4** Legend see page 478

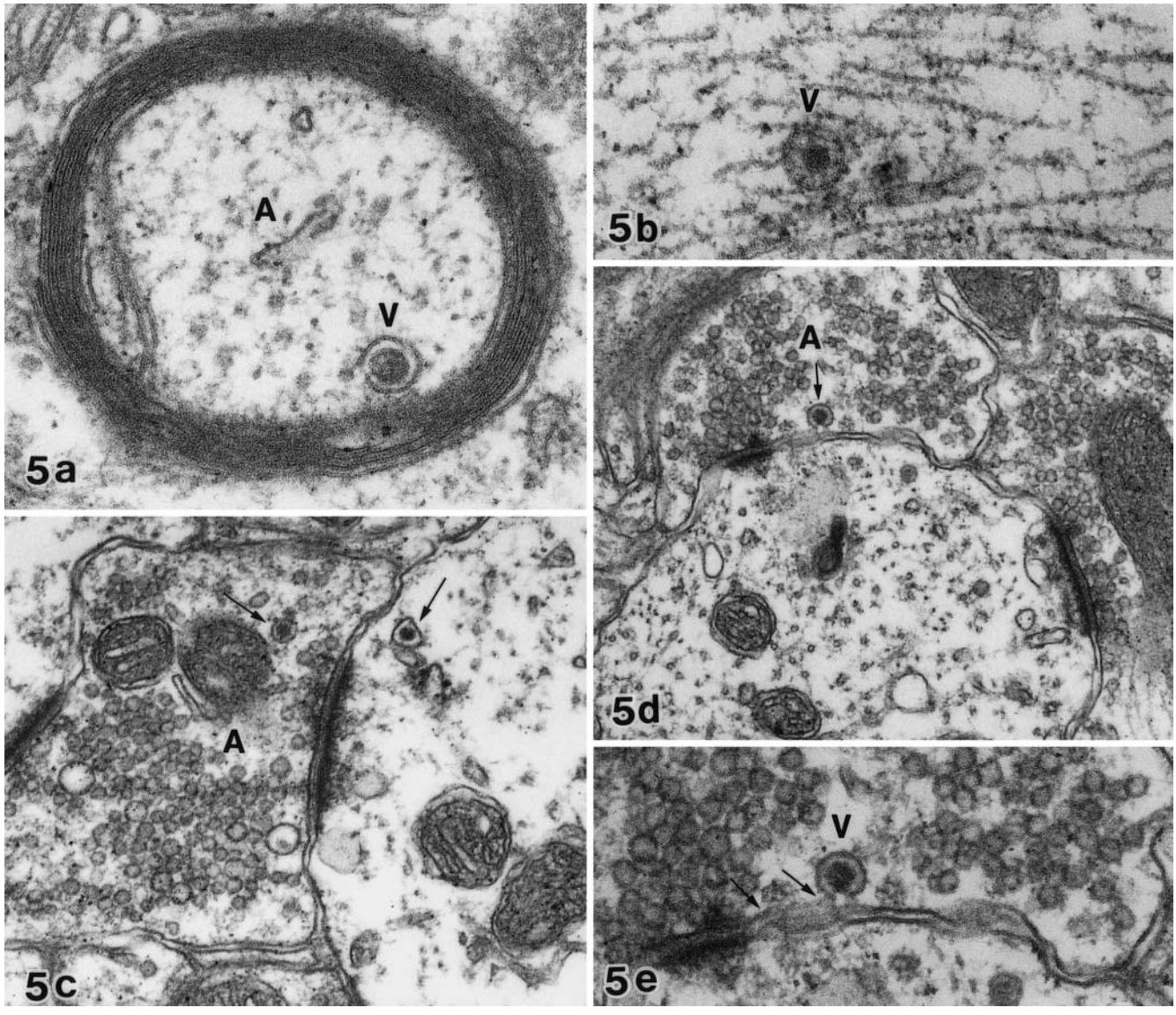



**Fig. 5** Electron micrographs representing a distribution of DEN-2 virions in the nerve fibers of infected neurons. **a** and **b** Membrane-bound vesicles carrying a virus particle are observed in the cross and longitudinal sections of myelinated (×103,000) and unmyelinated (×92,000) nerve fibers respectively at day 5 post-infection. *A* axon, *V* membrane-bound vesicles. **c** Showing typical synaptic features: mitochondria, clustered synaptic vesicles, the cleft and active zones of the pre- and post-synaptic membranes. Membrane-bound vesicles carrying a virus particle (*arrows*) are seen on both sides of the synapse at day 7 post-infection (×48,000); **d** Membrane-bound vesicle carrying a virus particle (*arrow*) near the end of an axon (*A*) appears to be fusing with the presynaptic membrane at day 7 post-infection (×35,000). **e** High magnification view of the membrane-bound vesicle indicated by the *arrows* in **d**. The vesicle membrane (*V*) seems to be fused with the presynaptic membrane (×80,000)

◀ **Fig. 4** One set of electron micrographs representing the replication of DEN virus in the neurons of the spinal cord during the infection. **a** A lower magnification micrograph views typical DEN virus particles (*arrowheads*) and membrane bounded vesicles (*arrows*) inside the rough endoplasmic reticulum (RER) of a neuron in the anterior horn at day 7 post-infection. A vesicle (*) containing virion adjacent to the membrane of the neuron is also observed. *N* nucleus (×12,500); **b** A virion (*arrow*) in the lumen of the RER is seen at day 3 post-infection. *rER* rough endoplasmic reticulum (×11,500). **c** Similar observations with b (*arrows*) are seen at day 5 post-infection (×30,000). **d** Many RER-derived vesicles (*arrowheads*), some of them containing virions (*arrows*), are observed in the infected neuron on the day of paralysis onset (×20,000). **e** Showing a large number of RER-derived vesicles in the infected cell on the day of paralysis onset. *L* lysosome (×28,000). **f** and **g** Electron micrographs showing the virions (*arrows*) within the Golgi complex (*G*) at day 3 (×12,700) and day 5 post-infection (×35,800), respectively. *L* lysosome, *N* nucleus

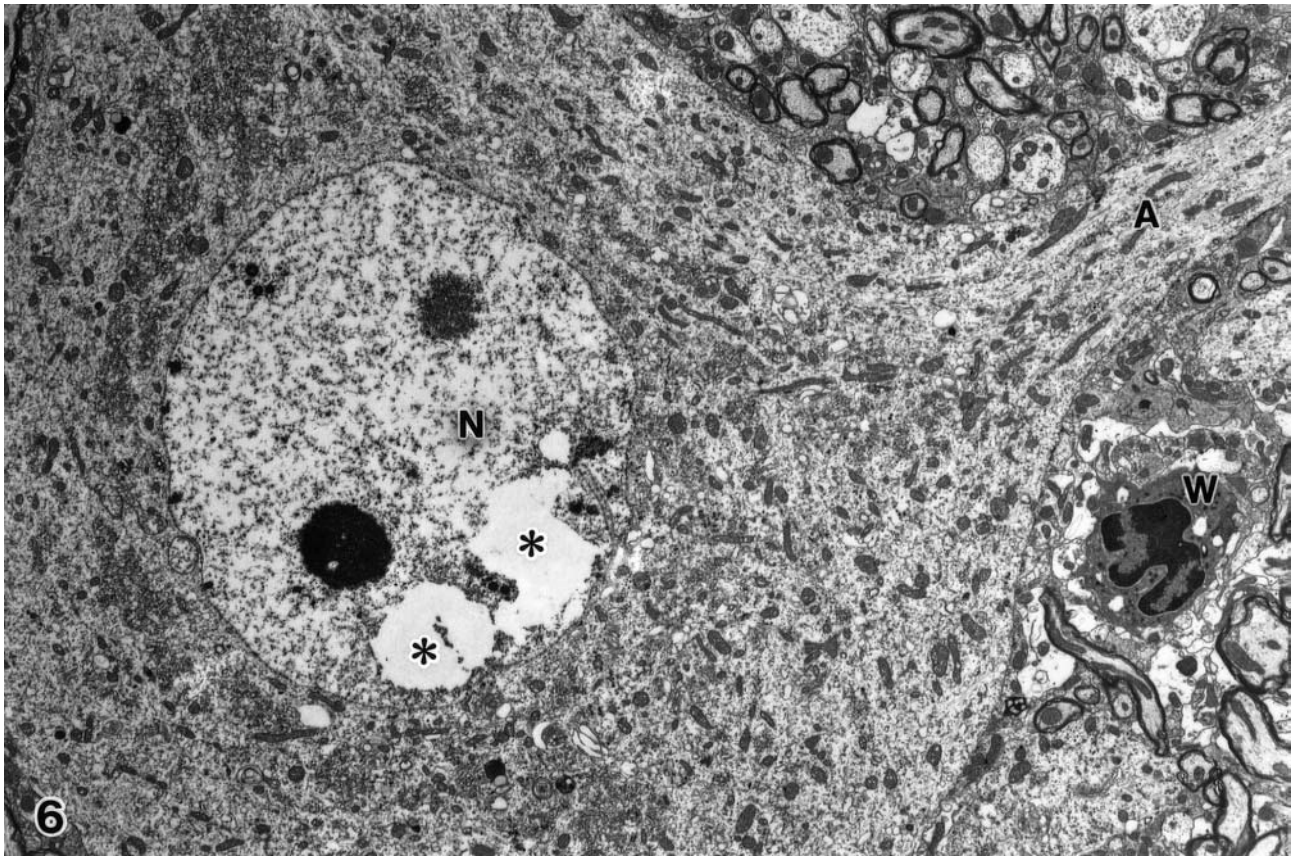



**Fig. 6** Electron micrograph of a neuron in the anterior horn of a paralyzed mouse showing that the nucleus (*N*) of a neuron gradually developed necrosis (*). Inflammatory cell, a white blood cell (*W*) near to the neuron is observed. *A* axon (×3500)

(MMLV) encephalitis using SCID mice infected by direct i.c. inoculation of MMLV. Shibuta et al. [24] also used the model of i.c. inoculation to observe the distribution of parainfluenza virus in the mouse brain. These studies indicated that the model of i.c. inoculation of viruses may be appropriate for studying the pathogenesis of CNS lesions caused by several viruses, including neurotropic and non-neurotropic viruses. Therefore, in the present study, we performed a histopathologic study to investigate the distribution of virus in the brain and spinal cord of SCID mice at various time points after i.c. inoculation of DEN-2 virus. Our results demonstrated that there was a possible route of virus spread within the spinal cord after viral invasion of the CNS, and the infection induced several pathological responses in neurons.

## Spread of the virus within the spinal cord

After i.c. inoculation, the DEN-2 virus entered the nervous system primarily via the central canal of the spinal cord in this study. This route was suggested by the fact that the virus was initially detected in the ependymal cells lining the central canal and viral replication progressed simultaneously in whole spinal cord and brain. The initial distribution of i.c. inoculated DEN-2 virus was similar to that described by Mims for India ink [19]. Mims found that the injected particles were not deposited at the point of the needle but tracked back along the needle and spread throughout the cerebrospinal fluid (CSF) space including the ventricular system, subarachnoid space, and the central canal of the spinal cord. It has been implicated [6] that the ependymal cells may constitute a resident fixed macrophage system, which may be the first line of defense against CNS invasion by various pathogens and may selectively absorb or phagocytize particular substances in the CSF. Several studies [6, 7] had demonstrated that a variety of viruses showed a selective affinity for ependymal cells in which viruses may replicate or transport through. In the present study, because there were only a few virions in the cytoplasm, not in RER or Golgi complexes, of the ependymal cells and the viral antigen was not observed in these cells immunochemically, it seems that the DEN-2 virus may have passed through the ependymal cells without replication and entered the subependymal central gray matter. Since the central canal is a patent CSF pathway in mice, we considered that i.c. inoculated DEN-2 virus particles might be delivered by the central canal CSF pathway for potential adsorption by ependymal cells in this study. It was partially consistent with results from Jackson et al. [14], who reported that i.c. inoculated sindbis virus spread

within the CNS via a CSF pathway and indicated that the route of spread by the central canal may be a common pathway in other viral infections.

Previously, Hase [12] reported that Japanese encephalitis virus moves via the interstitial space during the early phase of infection. Although no DEN virus was observed in the extracellular space in this study, we cannot exclude the existence of the same transport mechanism because it is difficult to observe the virus movement via interstitial space under EM. With progression of the infection, interestingly, DEN-2 virus was observed in the nerve fibers and the area of the pre- and post-synapse. Membrane-bound vesicles containing virion were very close to the presynaptic membrane, and some of them appeared to be fused with the membrane. These results suggested that, in addition to moving via interstitial space, the DEN virus might travel from neuron-to-neuron directly during the infection.

### Nature of neuronal injury

On day 3 p.i., only a few viral antigen-positive neurons were detected in the anterior horn. With progression of the infection, viral antigens were observed in the neurons with increased numbers and stronger staining in the anterior horn. They also appeared in the lateral and posterior horn. When infected mice showed paralysis, a large amount of viral antigen was observed in the lateral and posterior horns. The viral load in the anterior horn was decreasing due to the destruction of the neurons. These results suggested that the neurons in the anterior horn might be more sensitive to DEN virus infection than those in the lateral and posterior horns.

In the present study, mice infected with DEN-2 virus showed flaccid paralysis, and a high virus titer and viral antigens were detected in the spinal cord after infection. Meanwhile several histopathologic changes and neuronal denaturation changes were also observed in the spinal cord. Numerous RER-derived vesicles, which may correspond to DEN nucleocapsid, were seen in the neurons of infected mice in this system. They are similar to that of the previous studies with flavivirus [3, 4, 27, 28]. In the later phase of the infection, death of the infected neurons was observed in the anterior horn. This might be caused by the replication of the virus and account for the occurrence of flaccid paralysis in infected animals. These results indicated that neurons were target cells for DEN virus and the infection led to several pathological responses including neuronal necrosis. However, signs of apoptosis in infected neurons were not observed. This may be related to neuronal maturity since the mice used in our study were adults [9].

In conclusion, the results of the present study showed that the DEN virus might initially spread within the spinal cord by a central canal CSF pathway after i.c. inoculation and then be transmitted by traveling either through the interstitial space or transported directly from neuron to neuron. The replication of virus in the infected neurons results in several neuronal pathological responses, including neuronal necrosis. Certain clinical neuronal manifestations of the disease may be caused by these pathological alterations in the CNS.

**Acknowledgements** We thank Dr. Steve Coon, Laboratory of Development Neurobiology, NICHD, NIH, USA, for critically reading the manuscript. We are grateful to Dr. P. Zhang (Louisiana State University Health Science Center, USA) for helpful discussion while the manuscript was in preparation and Dr. Xiuwu Bian (Department of Pathology, Third Military Medical University, China) for pathological observations. This work was supported in parts by grants no. 30170848 from the National Science Foundation of China (NSFC) and 01J013 from Military Medicine Foundation.

## References

1. An J, Kimura-Kuroda J, Hirabayashi Y, Yasui K (1999) Development of a novel mouse model for dengue virus infection. Virology 263:70–77
2. Angibaud G, Luaute J, Laille M, Gaultier C (2001) Brain involvement in dengue fever. J Clin Neurosci 8:63–65
3. Barth OR (1992) Replication dengue viruses mosquito cell cultures: a model from ultrastructural observations. Mem Inst Oswaldo Cruz 87:565–574
4. Barth OR (1999) Ultrastructural aspects of the dengue virus (flavivirus) particle morphogenesis. J Submicrosc Cytol Pathol 31:407–412
5. Bhamarapravati N (1997) Pathology of dengue infection. In: Gubler DJ, Kuno G (eds) Dengue fever and dengue hemorrhagic fever. CAB International, New York, pp 115–133
6. Bleier R, Alberecht R, Cruce JAF (1975) Supraependymal cells of hypothalamic third ventricle: identification as resident phagocytes of the brain. Science 189:299–301
7. Bruni JE, Delbigio MR, Clattenburg RE (1985) Ependyma: normal and pathological. A review of the literature. Brain Res 356:1–19
8. Charlier N, Leyssen P, Paeshuyse J, Drosten C, Schmitz H, Van Lommel A, De Clercq E, Neyts J (2002) Infection of SCID mice with Montana Myotis leukoencephalitis virus as a model for flavivirus encephalitis. J Gen Virol 83:1887–1896
9. Despres P, Frenkiel MP, Ceccaldi PE, Duarte Dos Santos C, Deubel V (1998) Apoptosis in the mouse central nervous system in response to infection with mouse-neurovirulent dengue viruses. J Virol 72:823–829
10. George R, Lum CS (1997) Clinical spectrum of dengue infection. In: Gubler DJ, Kuno G (eds) Dengue fever and dengue hemorrhagic fever. CAB International, New York, pp 89–114
11. Griffin DE, Levine B, Tyor WR, Irani DN (1992) The immune response in viral encephalitis. Semin Immunol 4:111–119
12. Hase T (1993) Virus-neuron interactions in the mouse brain infected with Japanese encephalitis virus. Virchows Arch 64:161–170
13. Igarashi A (1978) Isolation of Singh's Aedes albopictus cell clone sensitive to Dengue and Chikungunya viruses. J Gen Virol 40:531–544
14. Jackson AC, Moench TR, Griffin DE, Johnson RT (1987) The pathogenesis of spinal cord involvement in the encephalomyelitis of mice caused by neuronadapted sindbis virus infection. Lab Invest 56:418–423
15. Kimura-Kuroda J, Yasui K (1986) Antigenic comparison of envelope protein E between Japanese encephalitis virus and some other flaviviruses using monoclonal antibodies. J Gen Virol 67:2663–2667
16. Lin YL, Liao C, Chen LK, Yeh CT, Liu CI, Ma SH, Huang YY, Huang YL, Kao CL, King CC (1998) Study of dengue virus infection in SCID mice engrafted with human K562 cells. J Virol 72:9729–9737

17. Lum LCS, Lam SK, Choy YS, George R, Harun F (1996) Dengue encephalitis: a true entity? Am J Trop Med Hyg 54:256–259
18. Miagostovich MP, Ramos RG, Nicol AF, Nogueira RM, Cuzzi-Maya T, Oliveria AV, Marchevsky RS, Mesquita RP, Schtzamyr HG (1997) Retrospective study on dengue fatal cases. Clin Neuropathol 16:204–208
19. Mims CA (1960) Intracerebral injections and the growth of viruses in the mouse brain. Br J Exp Pathol 41:52–60
20. Nimmannitya S, Thisyakorn U, Hemsrichart V (1987) Dengue haemorrhagic fever with unusual manifestations. Southeast Asian J Trop Med Public Health 18:398–406
21. Rajajee S, Mukundan D (1994) Neurological manifestations in dengue hemorrhagic fever. Indian Pediatr 31:688–690
22. Ramos C, Sanches G, Pabdi RH, Baquera J, Hernandez D, Ramos J, Flores A (1998) Dengue virus in the brain of a fatal case of hemorrhagic dengue fever. J Neurovirol 4:465–468
23. Rice CM (1996) Flaviviridae: the viruses and their replication. In: Fields BN, Knipe DM, Howley PM (eds) Fields Virology, 3rd edn. Lippincott-Raven, Philadelphia, pp 931–959
24. Shibuta H, Kanda T, Nozawa A, Sato S, Kumanishi T (1985) Experimental parainfluenza virus infection in mice: growth and spread of a highly pathogenic variant of parainfluenza 3 virus in the mouse brain. Arch Virol 83:43–52
25. Siritorn B, Kimura-Kuroda J, Zhou DS, Yasui K (1998) Neutralizing mechanism of a monoclonal antibody against Japanese encephalitis virus glycoprotein. Am J Trop Med Hyg 58:389–398
26. Solomon T, Dung NM, Vaughn DW, Kneen R, Thao LTT, Raengsakulrach B, Loan HT, Day NPJ, Farrar J, Myint KSA, Warrell MJ, James WS, Nisalak A, White NJ (2000) Neurological manifestations of dengue infection. Lancet 355:1053–1059
27. Steffan M, Marianneau P, Schwemling CC, Royer C, Schmitt C, Jaeck D, Wolf P, Gendrault JL, Keller FS (2001) Ultrastructural observation in hepatitis C virus-infected lymphoid cells. Microbes Infect 3:193–202
28. Takasaki T, Takada K, Kurane I (2001) Electron microscopy study of persistent dengue virus infection: analysis using a cell line persistently infected with dengue-2 virus. Intervirology 44:48–54
29. Thisyakorn U, Thisyakorn C (1994) Dengue infection with unusual manifestations. J Med Assoc Thai 77:410–413
30. van den Pol AN, Reuter JD, Santarelli JG (2002) Enhanced cytomegalovirus infection of developing brain independent of the adaptive immune system. J Virol 76:8842–8854

Virchows Arch (2003) 442:482–490
DOI 10.1007/s00428-003-0761-y

ORIGINAL ARTICLE

**Kimihide Kusafuka · Franck P. Luyten · Raymond De Bondt · Yuji Hiraki · Chisa Shukunami · Teruo Kayano · Tamiko Takemura**

# Immunohistochemical evaluation of cartilage-derived morphogenic protein-1 and -2 in normal human salivary glands and pleomorphic adenomas

Received: 24 September 2002 / Accepted: 20 December 2002 / Published online: 18 April 2003
© Springer-Verlag 2003

**Abstract** Cartilage-derived morphogenic protein (CDMP)-1 and -2 belong to the bone morphogenetic protein (BMP) family in the transforming growth factor (TGF)-$\beta$ superfamily. CDMP-1 and CDMP-2 were reported to play essential roles in limb cartilage and limb-joint formation in developing mice. Although pleomorphic adenoma of the salivary glands is an epithelial tumor, it frequently shows ectopic cartilaginous formation. These findings suggested that CDMP-1 and -2 may play essential roles in chondroid formation in salivary pleomorphic adenoma. To evaluate this hypothesis, we examined the expression and localization of CDMP-1 and -2 immunohistochemially in 20 normal human salivary glands and 35 pleomorphic adenomas. CDMP-1 was immunolocalized in the striated ducts and the intercalated ducts in the normal salivary glands. CDMP-1 was immunolocalized in the cuboidal neoplastic myoepithelial cells around the chondroid areas of the pleomorphic adenomas, whereas these molecules were not localized in the spindle-shaped neoplastic myoepithelial cells of the myxoid element or the lacuna cells of the chondroid element in these tumors. CDMP-2 was expressed neither in normal salivary glands nor any of the elements of the pleomorphic adenomas. Type-II collagen and aggrecan were immunolocalized throughout the matrix around the lacuna cells of the chondroid element, whereas type-X collagen was not immunlocalized in any epithelial or stromal elements, including the chondroid elements. Aggrecan was deposited not only on the chondroid matrix, but also on the myxoid stroma and intercellular spaces of the tubulo-glandular structures, whereas chondromodulin-I was deposited on the chondroid matrix. These results indicated that the cuboidal neoplastic myoepithelial cells around the chondroid areas expressed CDMP-1 and suggested that this molecule may play a role in the differentiation of neoplastic myoepithelial cells in pleomorphic adenoma. The phenotype of the lacuna cells was similar to that of mature to upper hypertrophic chondrocytes of the authentic cartilage. In conclusion, pleomorphic adenoma expressed CDMP-1 but not CDMP-2.

**Keywords** Cartilage-derived morphogenetic proteins · Cartilaginous matrix · Chondroid formation · Pleomorphic adenoma · Immunohistochemistry

K. Kusafuka (✉) · T. Takemura
Department of Pathology,
Japanese Red Cross Medical Center,
4-1-22 Hiroo, 150-8935 Tokyo, Japan
e-mail: kinkymus@ya2.so-net.ne.jp
Tel.: +81-3-34001311 ext 2866
Fax: +81-3-34091604

F. P. Luyten · R. De Bondt
Laboratory for Skeletal Development and Joint Disorders,
Katholieke Universiteit Leuven, Onderwijs & Navorsing,
Herestraat 49, 8th floor, 3000 Leuven, Belgium

Y. Hiraki · C. Shukunami
Department of Molecular Interaction and Tissue Engneering,
Institute for Frontier Sciences, Kyoto University,
53 Shogoinkawahara-cho, Sakyo-ku, 606-8507 Kyoto, Japan

T. Kayano
Forensic Dentistry,
Department of International Health Development,
Division of Public Health, Graduate School,
Tokyo Medical and Dental University,
Yushima 1-5-45, Bunkyo-ku, 113-8549 Tokyo, Japan

## Introduction

Pleomorphic adenoma of the salivary glands is characterized by the so-called "mixed" appearance of epithelial and mesenchymal-like elements. In previous studies, mesenchymal-like elements, including chondroid and myxoid elements, were shown to be related to neoplastic myoepithelial cells migrating into the stroma. Recently, we demonstrated that bone morphogenetic proteins (BMPs) were associated with chondroid formation in

pleomorphic adenoma [12, 14]. We also reported that co-expression of fibroblast growth factor (FGF)-2 and FGF receptor-1 in the lacuna cells in chondroid elements inhibited ossification of the chondroid elements [13]. Although FGF-2 is a strong angiogenic factor [5], pleomorphic adenoma is a hypovascular tumor due to the low density of CD34-positive endothelial cells, and there are no capillaries in the chondroid elements of such tumors [15]. Recently, we reported that the cartilage-specific matrix protein chondromodulin-I (ChM-I) was deposited on the inter-territorial matrix, especially around the lacunae, in the chondroid areas of pleomorphic adenomas [15]. As ChM-I was also shown to be a strong angio-inhibitor [8, 9], this matrix molecule plays an essential role in avascularity in chondroid elements of this type of tumor.

Cartilage-derived morphogenic protein (CDMP)-1 and -2 were extracted and cloned from fetal calf cartilage [1, 17]. CDMPs belong to the BMP family in the TGF-$\beta$ superfamily. Their carboxyterminal TGF-$\beta$ domains are 82% identical, thus defining a novel subfamily most closely related to BMP-5, BMP-6 and osteogenic protein-1 (BMP-7). Northern-blotting analysis showed that both genes were predominantly expressed in cartilaginous tissues [1]. On in situ hybridization and immunostaining of sections from human embryos, CDMP-1 was found predominantly at the stage of precartilaginous mesenchymal condensation and throughout the cartilaginous cores of the developing long bones, whereas CDMP-2 expression was restricted to the hypertrophic chondrocytes of ossifying long-bone centers [1]. CDMP-1 and its homologue growth/differentiation factor-5 (GDF-5) were discovered independently using degenerate polymerase chain reaction screening for BMP-like genes. Thus, CDMP-1 and -2 have been reported to be associated with cartilage formation in the limbs and limb-joint development [1, 17].

The findings presented here suggested that CDMPs may be associated with the chondroid formation of salivary pleomorphic adenoma. We examined the expression and localization of CDMP-1 and -2, in comparison with the localization of cartilaginous matrix proteins, in human normal salivary glands and pleomorphic adenoma using immunohistochemical methods.

## Materials and methods

### Antibodies (Table 1)

Anti-CDMP-1 and anti-CDMP-2 polyclonal affinity-purified antibodies were raised in chickens against the N-terminal sequence recombinant peptides QGKRPSKNLKARC and HGKRHGKKSRLRC, which are specific for CDMP-1 and -2, respectively. These antisera did not cross-react with each other or other BMP family members on Western blotting analysis [1, 4]. On Western-blotting analysis, the anti-CDMP-1 antibody revealed a single band of 34 kDa, and the anti-CDMP-2 antibody revealed a single band of 38 kDa [4]. Anti-type-II collagen monoclonal antibody (clone II-4C11; Fuji Yakuhin Kogyo, Toyama, Japan) and anti-type-X collagen monoclonal antibody (clone X53; Immunodiagnostika und Biotechnologie GmbH, Berlin, Germany) were purchased from the sources shown. The specificity of anti-type-II antibody was confirmed previously [12], and the specificity of anti-type-X collagen antibody raised against human recombinant type-X collagen was confirmed with endochondral ossification tissue in human neonatal vertebrae. Anti-aggrecan polyclonal antibody, a kind gift from Dr. T. Yada (Institute for Molecular Science of Medicine, Aichi Medical University, Nagoya, Japan), was raised against neonatal rat cartilage aggrecan as described previously [23, 24]. This antiserum against rat aggrecan recognized mouse and human aggrecan core protein on enzyme-linked immunosorbent assay (ELISA) and Western-blotting analysis, and cross-reacted with human aggrecan. Anti-ChM-I polyclonal antibody was raised in rabbits against mature recombinant human ChM-I protein [10]. On Western-blotting analysis, this antibody revealed a single diffuse band of 25 kDa. For identification of neoplastic myoepithelial cells, anti-S-100 protein polyclonal antiserum (Z311) and anti-$\alpha$ smooth muscle actin monoclonal antibody (M0851: clone 1A4) were purchased from Dako (Japan).

### Tissues

Thirty-five pleomorphic adenoma cases were chosen from the pathology files of the Japanese Red Cross Medical Center, Tokyo, Japan, from the period 1986 to 2000. Twenty specimens included normal salivary gland tissue. Two neonatal vertebral tissue specimens were used as controls. These specimens were fixed in 10% buffered formalin, routinely processed, and embedded in paraffin wax. Sections 3 $\mu$m thick were then prepared.

### Immunohistochemistry

Paraffin-embedded sections were deparaffinized in xylene and rehydrated. For CDMP-1 and -2 staining, deparaffinized sections were heated in citrate buffer, pH 5.0, for 15 min in a microwave oven (500 W), for antigen retrieval. For ChM-I staining, deparaffinized sections were first pre-treated with 0.1% hyaluronidase (H6254; Sigma Chemical Co., St. Louis MO, USA) in acetate buffer, pH 5.0, for 45 min at 37°C, followed by two washes with phosphate buffered-saline (PBS), and were then treated with 0.4% pepsin (P-6887; Sigma) in 1.0 N HCl solution for 45 min at 37°C. For type-X collagen staining, deparaffinized sections were first pre-

**Table 1** Antibodies used in the present study. *CDMP* cartilage-derived morphogenetic protein, *ChM-I* chondromodulin-I, *poly* polyclonal antibody, *mono* monoclonal antibody, *(C)* chicken, *(M)* mouse, *(R)* rabbit

| Antigen | Clone (animal) | Dilution | Sources |
|---|---|---|---|
| CDMP-1 | poly (C) | 1:100 | Dr. F.P. Luyten [1, 4] |
| CDMP-2 | poly (C) | 1:100 | Dr. F.P. Luyten [1, 4] |
| Type-II collagen | Mono (M) | 1:500 | Fuji Yakuhin Kogyo |
| Type-X collagen | Mono (M) | 1:20 | Immunodiagnostika und Biotechnologie |
| Aggrecan | Poly (R) | 1:1000 | Drs. T. Yada and K. Kimata [23, 24] |
| ChM-I | Poly (R) | 1:400 | Dr. Hiraki [10] |
| S-100 Protein | Poly (R) | 1:400 | Dako, Japan |
| $\alpha$-Smooth muscle actin | Mono (M) | 1:50 | Dako, Japan |

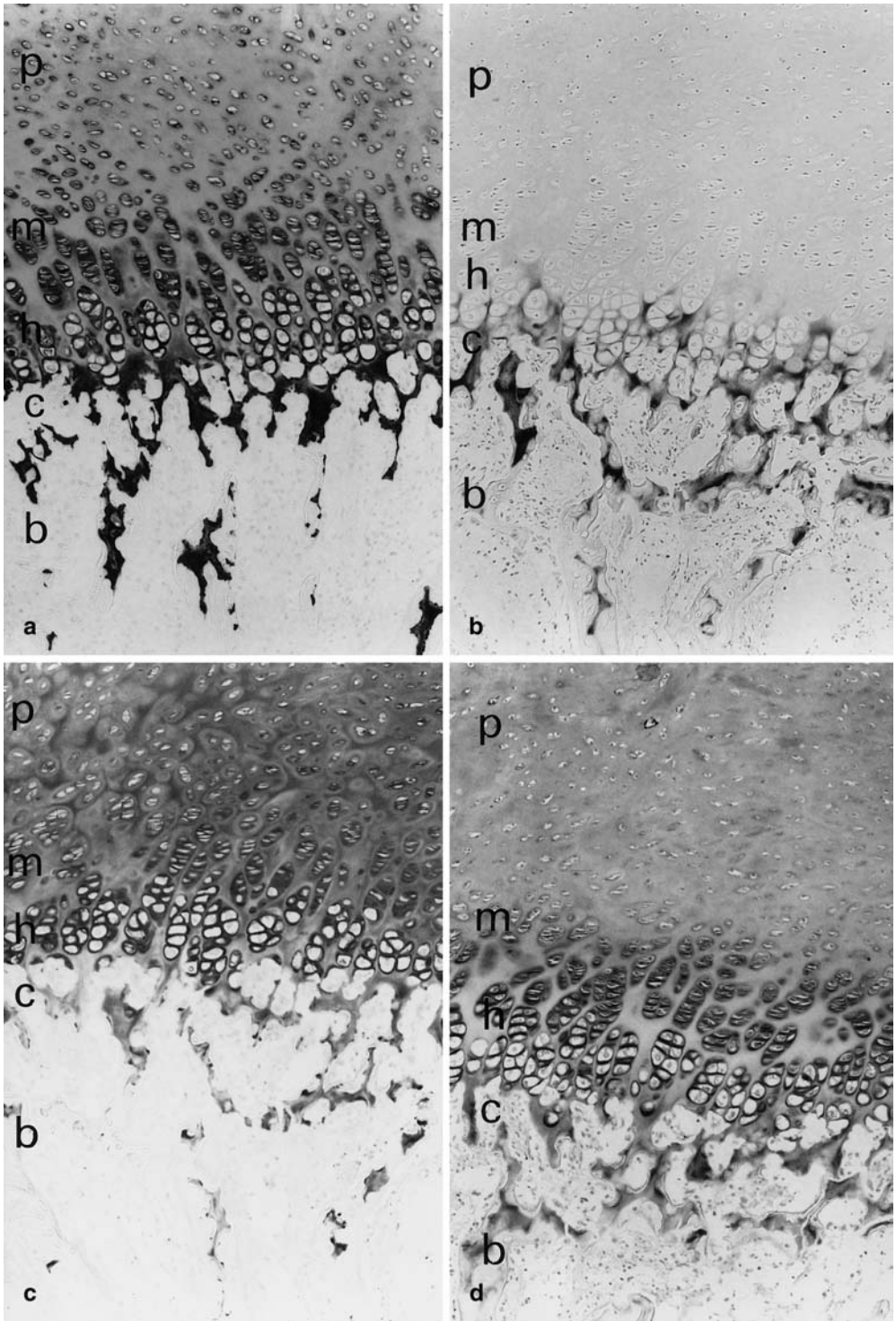



**Fig. 1** Results of the control studies for each antibody using endochondral ossification tissues of the neonatal vertebrae. *p* proliferating cartilage, *m* mature cartilage, *h* hypertrophic cartilage, *c* calcifying cartilage, *b* bone. **a** Moderate to strong reaction for type-II collagen was observed in the matrix of the mature to hypertrophic cartilage. Weak reaction for type-II collagen was seen in the proliferating cartilage (immunostaining ×100). **b** Strong reaction for type-X collagen was seen only in the matrix of the lower hypertrophic to calcifying cartilage (immunostaining ×100). **c** Strong reaction for aggrecan was observed in the inter-territorial matrix of the mature to hypertrophic cartilage (immunostaining ×100). **d** Moderate to strong reaction for chondromodulin-I was seen in the inter-territorial matrix of the hypertrophic cartilage, especially around the lacunae (immunostaining ×100)

treated with 0.1% pepsin in 0.5 M acetic acid solution for 2 h at 37°C, followed by two washes with PBS, and then treated with 2 mg/ml hyaluronidase for 30 min at 37°C. For aggrecan and type-II collagen stainings, deparaffinized sections were treated as described previously [15]. All sections were washed in PBS, and incubated for 30 min in 0.3% $H_2O_2$ in methanol to inactivate endogenous peroxidases. After incubation for 1 h at room temperature, sections were washed twice in PBS and incubated with biotinylated anti-chicken, rabbit or -mouse immunoglobulin antibody (61–3140; Zymed Laboratories Inc., San Fancisco, CA, USA, and Dako Japan Co., Kyoto, Japan). After two additional washes, they were incubated in peroxidase-conjugated streptavidin (P397; Dako Japan Co.) followed by two washes in PBS. Bound peroxidase was developed with 0.02% 3,3'-diaminobenzidine in 0.1 mol/Tris buffer, pH 7.6, in 0.005% $H_2O_2$ for 5 min, and counterstaining was performed with 5% methyl green. As negative controls, the primary antibodies were replaced with normal chicken, mouse or rabbit serum or PBS, or preabsorbed with recombinant peptides.

## Results

### Specificity of each antibody in human neonatal tissue

No immunoreactivities for CDMP-1 or CDMP-2 were observed in any layers of the vertebral cartilage tissue, whereas immunoreactivity for CDMP-1 was observed in the human osteoarthrotic articular cartilage, and CDMP-2 was detected in the human osteoarthrotic articular cartilage (data not shown) [4]. Immunoreactivity for type-II collagen was seen throughout the matrix of the tracheal cartilage and cartilaginous matrix of the vertebral tissue (Fig. 1a). Immunoreactivity for type-X collagen was observed in the lower hypertrophic to calcifying cartilaginous matrices of the endochondral bone formation tissues, but no immunoreactivity for type-X collagen was seen in the matrix of the tracheal cartilage (Fig. 1b). Immunoreactivity for aggrecan was observed in the matrix of the tracheal cartilage and especially in the matrix of the mature to hypertrophic cartilage of the vertebral tissue (Fig. 1c), whereas weak immunoreactivity was seen throughout the cartilaginous matrix. Strong immunoreactivity for ChM-I was observed in the interterritorial regions around the lacunae of the cartilaginous tissues, especially in the areas around the upper hypertrophic chondrocytes (Fig. 1d).

### Histology of pleomorphic adenoma cases examined

In the present study, the epithelial component consisted of tubulo-glandular structures, in which the inner cells and outer cells were 35 (100%) and 35 (100%) cases, respectively, whereas the stromal types of mesenchymal-like component composed of fibrous (19 cases: 54.3%), hyaline (14 cases: 40.0%), myxoid (32 cases: 91.4%) and chondorid elements (24 cases: 68.6%).

### CDMP expression in human normal salivary glands and pleomorphic adneomas

Table 2 and Table 3 summarize the results of the immunohistochemical analyses. Immunoreaction for CDMP-1 was seen in the striated ducts and intercalated ducts of the normal salivary glands, whereas no immunoreaction for CDMP-2 was seen in the normal salivary glands (Fig. 2a, b) Immunoreaction for CDMP-1 was seen in the cytoplasm of the cuboidal neoplastic myoepithelial cells around the chondroid elements (28.6%), whereas no immunoreaction for CDMP-1 was seen in the lacuna cells in the chondroid elements, or in the spindle-shaped neoplastic myoepithelial cells in the myxoid elements (0%; Fig. 2c, d, e). The neoplastic myoepithelial cells expressing CDMP-1 had a cuboidal shape in the hypocellular regions. Even these cells were positive for S-100 protein but negative for $\alpha$ smooth muscle actin. No immunoreaction for CDMP-2 was observed in any of the elements of the pleomorphic adenomas, including the neoplastic myoepithelial cells or the lacuna cells (0%) (Fig. 2f). No CDMP-1 or -2 immunoreactivity was seen in the negative controls in which the primary antibody was replaced with PBS or normal chicken serum, or preabsorbed with recombinant peptides of CDMP-1 or -2 (data not shown).

**Table 2** Percentage of positivity of cartilage-derived morphogenetic proteins (CDMPs) and matrix proteins in pleomorphic adenomas. Outer cells include the nests or cords of neoplastic myoepithelial cells. Stromal types indicate each ground substance in the case of matrix protein examination, or each stromal cell in the case of CDMP examination. *ChM-I* chondromodulin-I

| | Tubulo-glandular structures | | Stromal types | | | |
|---|---|---|---|---|---|---|
| | Inner cells | Outer cells | Fibrous | Hyaline | Myxoid | Chondroid |
| CDMP-1 | 0 | 0 | 0 | 0 | 10 (28.6%) | 0 |
| CDMP-2 | 0 | 0 | 0 | 0 | 0 | 0 |
| Type-II collagen | 0 | 0 | 0 | 0 | 0 | 24 (100%) |
| Type-X collagen | 0 | 0 | 0 | 0 | 0 | 0 |
| Aggrecan | 12 (34.3%) | 20 (57.1%) | 6 (31.6%) | 6 (42.9%) | 31 (96.9%) | 22 (91.7%) |
| ChM-I | 0 | 0 | 0 | 0 | 12 (37.5%) | 24 (100%) |
| | 35/35 | 35/35 | 19/35 | 14/35 | 32/35 | 24/35 |

**Table 3** Intensity of immunohistochemistry for cartilage-derived morphogenetic proteins (CDMPs) and matrix proteins in pleomorphic adenomas. *ChM-I* chondromodulin-I, *MEC* myoepithelial cells, – no staining, + weak staining, ++ moderate staining, +++ strong staining

| | Tubulo-glandular structures | | Stromal types | | | |
|---|---|---|---|---|---|---|
| | Inner cells | Outer cells | Fibrous | Hyaline | Myxoid | Chondroid |
| CDMP-1 | – | – | – | – | +++MEC | – |
| CDMP-2 | – | – | – | – | – | – |
| Type-II collagen | – | – | – | – | – | +++ |
| Type-X collagen | – | – | – | – | – | – |
| Aggrecan | + | ++ | + | + | +++ | +++ |
| ChM-I | – | – | – | – | ++ | +++ |

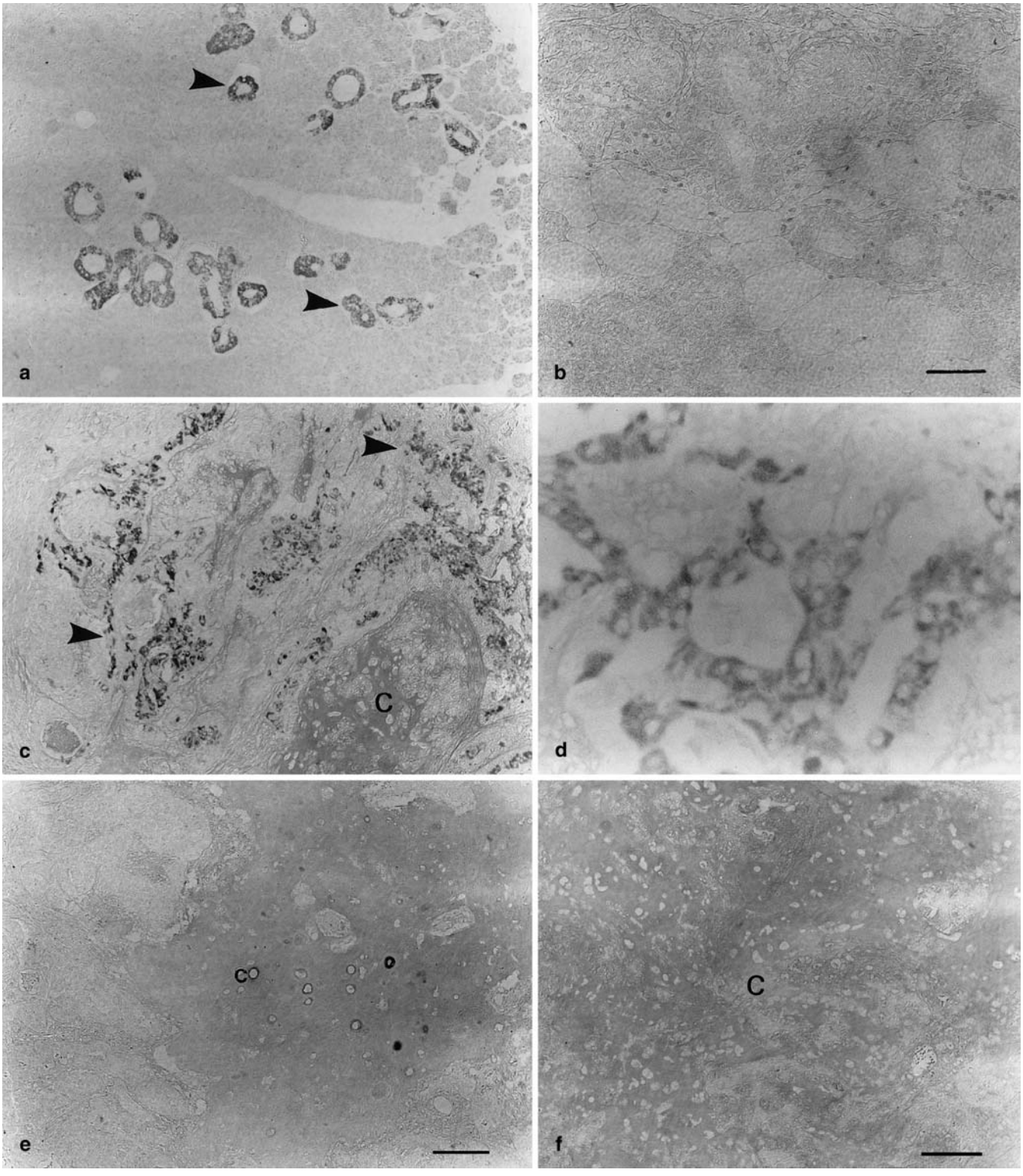



**Fig. 2 a** Moderate reaction for cartilage-derived morphogenic protein (CDMP)-1 was observed in the cytoplasm of the striated ducts and intercalated ducts (*arrows*) of the normal salivary glands (immunostaining ×100). **b** No reaction for CDMP-2 was seen in the normal salivary glands. *Scale bar* 100 μm (immunostaining ×100). **c** Moderate reaction for CDMP-1 was observed in the cytoplasm of the cuboidal neoplastic myoepithelial cells (*arrowheads*) in the hypocellular areas around the chondroid element (*C*) of the pleomorphic adenomas. There was no deposition of CDMP-1 on the stroma (immunostaining ×100). **d** Moderate reaction for CDMP-1 was seen in the cytoplasm of the cuboidal neoplastic myoepithelial cells in the myxoid areas. (immunostaining ×200). **e** No reaction for CDMP-1 was seen in the chondroid element (*C*) of the pleomorphic adenoma. *Scale bar* 100 μm (immunostaining ×100). **f** No reaction for CDMP-2 was seen in the chondroid element (*C*) of the pleomorphic adenoma. *Scale bar* 100 μm

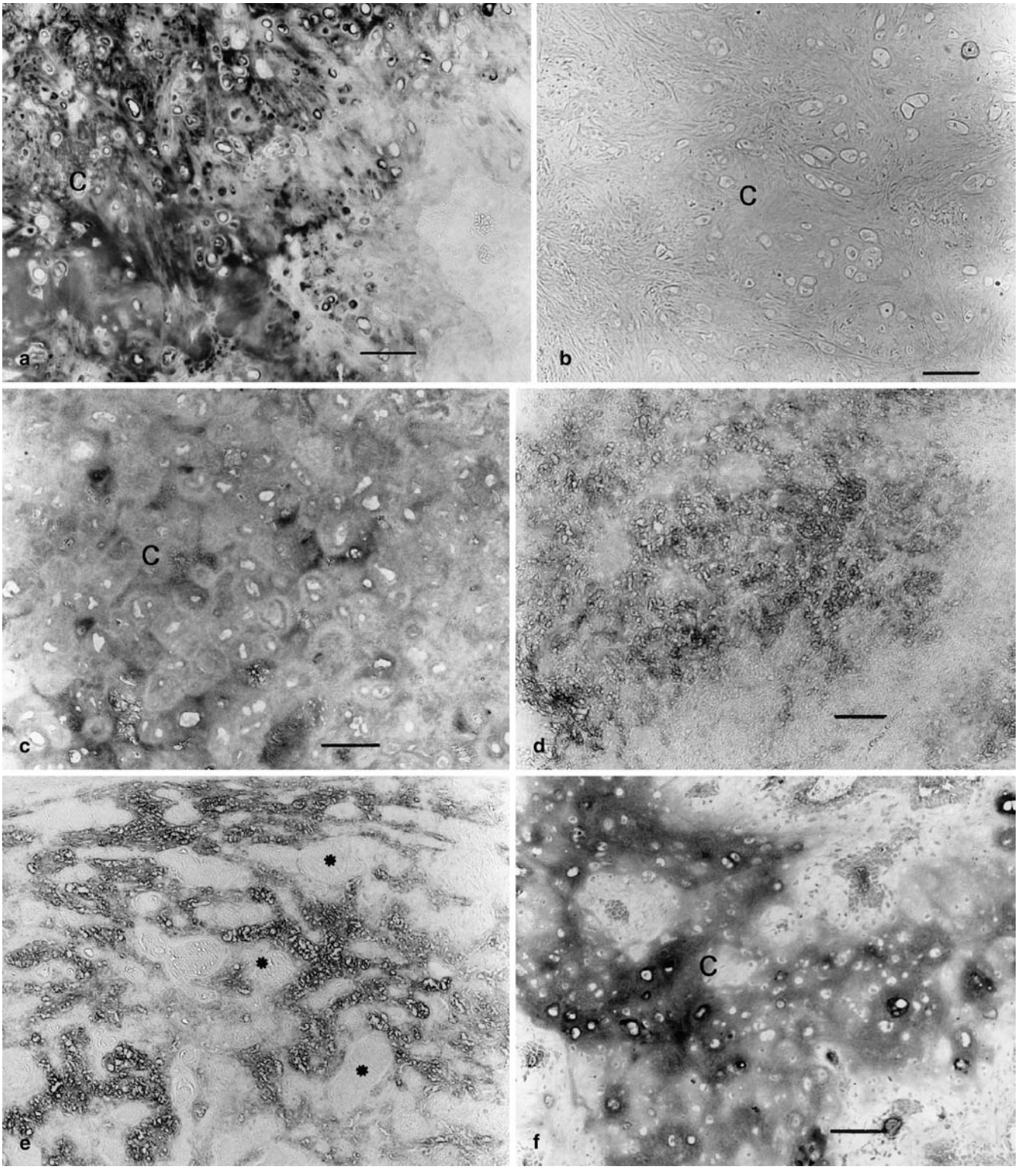



**Fig. 3** **a** Strong reaction for type-II collagen was seen only in chondroid matrix (*C*) of pleomorphic adenoma. *Scale bar* 100 $\mu$m (immunostaining ×100). **b** No reaction for type-X collagen was seen in the chondroid matrix (*C*) of the pleomorphic adenoma. *Scale bar* 100 $\mu$m (immunostaining ×100). **c** Moderate to strong reaction for aggrecan was observed in the chondroid matrix (*C*) of the pleomorphic adneoma. *Scale bar* 100 $\mu$m (immunostaining ×100). **d** Moderate reaction for aggrecan was seen in the myxoid stroma of the pleomorphic adenoma. *Scale bar* 100 $\mu$m (immunostaining ×100). **e** Moderate reaction for aggrecan was seen in the intercellular spaces of the epithelial element (*) of the pleomorphic adenoma (immunostaining ×100). **f** Moderate to strong reaction for chondromodulin-I (ChM-I) was observed in the chondroid matrix (*C*) of the pleomorphic adneoma. Especially, strong deposition of ChM-I was seen around the lacunae. *Scale bar* 100 $\mu$m (immunostaining ×100)

Characterization of chondroid elements in pleomorphic adenoma

No immunoreactions for type-II collagen, type-X collagen, aggrecan or ChM-I were seen in the normal salivary gland tissue (data not shown). Strong immunoreaction for type-II collagen was observed throughout the chondroid matrix (100%), but none was seen in other mesenchymal-like elements or epithelial elements (Fig. 3a). However, no immunoreaction for type-X collagen was seen in any elements in the salivary pleomorphic adenomas (0%) (Fig. 3b). Strong immunoreaction for aggrecan was consistently observed in the matrix of the chondroid elements (91.7%) (Fig. 3c). Such immunoreaction was also seen in small myxoid areas within or near the epithelial sheets, and occasionally in the inter-cellular spaces of the solid nests of the neoplastic myoepithelial cells or tubulo-glandular structures (Fig. 3d, e). Strong immunoreaction for ChM-I was observed on the inter-territorial spaces around the lacunae, while moderate immunoreaction was seen in the chondroid matrix (100%; Fig. 3f). Immunoreaction for ChM-I was observed in the neoplastic myoepithelial cells of the myxoid elements (37.5%). No immunoreaction was seen in the negative controls.

## Discussion

Pleomorphic adenoma is the most frequent type of benign tumor of the salivary glands. It is composed of epithelial and neoplastic myoepithelial cells, and the latter are believed to responsible for formation of myxoid and chondroid elements [2].

Recently, CDMP-1 and -2 were extracted and cloned from newborn calf cartilage. CDMPs are members of the BMP family in the TGF-$\beta$ superfamily [1, 17]. Known BMPs, which by definition are intimately involved in cartilage and bone formation in experimental model systems, are not expressed at significant levels in the chondroblasts or chondrocytes of the cartilage core of developing long bones, except in the hypertrophic chondrocytes, where both *Vgr*-1 (BMP-6) and osteogeneic protein-1 (BMP-7) are expressed [6, 18]. In developing human embryos, CDMP-1 was found predominantly at the stage of precartilaginous mesenchymal condensation and throughout the cartilaginous cores of the developing long bones, whereas CDMP-2 expression was restricted to the hypertrophic chondrocytes of ossifying long-bone centers [1]. On Northern-blotting analysis of neonatal tissue, CDMP-1 mRNA was only detected in newborn articular and cricoid cartilage as a band of 3 kb, whereas CDMP-2 mRNA was present in neonatal bovine articular and cricoid cartilage as a 4.6 kb band [1]. The expression pattern of CDMP-2, probably the bovine homologue of mouse GDF-6, suggested that it is involved in the terminal differentiation of chondrocytes (hypertrophy and calcification) and at the earliest stages of endochondral ossification, including angiogenesis and osteoblast differentiation [1, 17]. In addition, the relatively high levels of expression in neonatal cartilage suggested possible roles in the maintenance and stabilization of the cartilage phenotype after birth. Interestingly, neither CDMP-1 nor -2 were expressed in the axial skeleton. Recombinantly expressed CDMP-1 protein initiated and promoted chondrogenesis and to a limited extent osteogenesis both in vitro and in vivo [11, 17]. CDMP-1, therefore, increases the number of chondroprogenitor cells and accelerates chondrocyte differentiation to hypertrophy. In the present study, although myoepithelial cells are very scanty in the striated ducts, we demonstrated that CDMP-1 was expressed in the striated duct in the normal salivary glands. Therefore, this molecule may play a role in branching morphogenesis of this duct system rather than in maintenance of myoepithelial cells in the normal salivary glands. No expression of CDMP-2 was observed in the normal salivary glands or pleomorphic adenoma. In salivary pleomorphic adenoma, CDMP-1 was expressed in the cuboidal neoplastic myoepithelial cells in the hypocellular areas, which were considered to have a pre-chondroprogenitor phenotype, morphologically. This molecule may play a role in the acceleration of the transdifferentiation from cuboidal neoplastic myoepithelial cells to lacuna cells in an autocrine manner. No CDMP-1 or -2 expression was observed in the lacuna cells of the chondroid elements and, thus, CDMP-1 and -2 were not related to maintenance of the chondroid phenotype of the lacuna cells. Although CDMP-2 was expressed in the hypertrophic chondrocytes of the articular cartilage, this molecule was not expressed in the lacuna cells of the chondroid areas in the pleomorphic adenomas. CDMP-2 was expressed in lower hypertrophic to calcifying chondrocytes [1]. As the phenotype of the lacuna cells of the chondroid elements may be similar to that of mature to upper hypertrophic chondrocytes of authentic cartilage rather than that of lower hypertrophic to calcifying chondrocytes, these cells did not express CDMP-2. It was demonstrated recently that CDMP-1/GDF-5 signals preferentially through a heteromeric complex of BMP receptor-IB (Alk-6, type-I receptor) with BMP receptor II or activin receptor II (type-II receptor) [3, 19].

We reported previously that the chondroid areas of pleomorphic adenoma expressed type-II collagen protein and mRNA, and the lacuna cells were similar to the authentic chondrocytes in phenotype [12]. Type-X collagen is a marker of terminal differentiation of endochondral bone formation [20, 21], and this matrix molecule was deposited on the matrix of lower hypertrophic to calcifying cartilage of vertebral tissues. Analysis of pleomorphic adenoma revealed that ossification of the chondroid elements was extremely rare [2], and the expression of type-X collagen was not detected in any areas of the pleomorphic adenoma in the present study. The present study also demonstrated the deposition of type-II collagen and aggrecan in the stroma of the chondroid areas. Aggrecan is a cartilage-specific large aggregating chondroitin sulfate proteoglycan, which is a

marker of hypertrophic cartilage [16]; in other words, aggrecan was deposited in the chondroid matrix of pleomorphic adenoma. The BMP-2 produced by the spindle-shaped neoplastic myoepithelial cells may induce chondroid tissue using a paracrine mechanism [12], and the BMP-6 produced by the lacuna cells may maintain chondroid tissue using an autocrine mechanism in pleomorphic adenoma [14]. BMP-2 and FGF-2 were expressed in the spindle-shaped neoplastic myoepithelial cells of the myxoid areas of the pleomorphic adenomas, which may be related to the differentiation of neoplastic myoepithelial cells and mesenchymal-like tissue [12, 13, 14]. Recently, we reported that a cartilaginous matrix protein, ChM-I was deposited in the inter-territorial matrix of the chondroid areas, especially around the lacunae [15]. This matrix molecule was recently identified as a novel endothelial cell growth inhibitor [8]. ChM-I was reported to inhibit DNA synthesis and tube morphogenesis of cultured vascular endothelial cells [9], but this molecule stimulated DNA synthesis and proteoglycan synthesis in cultured growth plate chondrocytes [7]. In situ hybridization analysis indicated that ChM-I mRNA was expressed in the proliferating to upper hypertrophic chondrocytes in the growth plates of the long bones, but the expression of the gene was reduced and then abolished in the lower hypertrophic and calcified zone, allowing vascular invasion [22]. From the results of the immunohistochemical examination, ChM-I is considered to be a marker of upper hypertrophic cartilage.

In conclusion, pleomorphic adenoma of the salivary glands expressed CDMP-1 around the chondroid elements. As the phenotype of the lacuna cells of the chondroid element was more immature than that of the lower hypertrophic to calcifying chondrocytes, the pleomorphic adenoma did not express CDMP-2 in any of the elements in this type of tumor. Normal salivary glands expressed CDMP-1 in the striated ducts and intercalated ducts, whereas these tissues did not express CDMP-2. Thus, CDMP-1 may play important roles in the differentiation of neoplastic myoepithelial cells in this type of tumor and in branching morphogenesis of normal salivary glands. Taken together, we speculated that CDMP-1 may promote the transdifferentiation from cuboidal neoplastic myoepithelial cells to lacuna cells, which were phenotypically similar to mature to upper hypertrophic chondrocytes, in pleomorphic adenoma. However, CDMP-2 appears to be related to neither the chondroid formation of pleomorphic adenoma nor the branching morphogenesis of normal salivary glands.

**Acknowledgements** We are grateful to Susumu Sekiguchi, Kikuo Wakamatsu, Shoichi Hashimoto, Akira Niizeki, Hiroko Komatsuzaki and Eiji Shimada on the staff of the Department of Pathology, Japanese Red Cross Medical Center, Tokyo, Japan, for technical assistance. We wish to thank Mr. Takashi Yoshizawa at the Photo Studio, Tokyo Medical and Dental University, Tokyo, Japan, for microphotography. We also wish to thank Drs. Toshikazu Yada and Koji Kimata (Institute for Molecular Science of Medicine, Aichi Medical University, Nagoya, Japan) for generously providing specific antibody against aggrecan.

## References

1. Chang CS, Hoang B, Thomas JT, Vukicevic S, Luyten PF, Ryba JPN, Kozak AC, Reddi AH, Moos M Jr (1994) Cartilage-derived morphogenetic proteins: new members of the transforming growth factor-$\beta$ superfamily predominantly expressed in long bone during human embryonic development. J Biol Chem 269:28227–28234
2. Dardick I (1996) Pleomorphic adenoma (benign mixed tumor) (chapter 9). In: Color atlas/text of the salivary gland tumor pathology. Igaku-Shoin Inc, New York, pp 75–92
3. Erlacher L, McCartney J, Piek E, ten-Dijke P, Yanagishita M, Oppermann H, Luyten FP (1998) Cartilage-derived morphogenetic proteins and osteogenic protein-1 differentially regulate osteogenesis. J Bone Miner Res 13:383–392
4. Erlacher L, Ng C-K, Ullrich R, Krieger S, Luyten FP (1998) Presence of cartilage-derived morphogenetic proteins in articular cartilage and enhancement of matrix replacement in vitro. Arthritis-Rheum 41:263–273
5. Folkman J, Klangsburn M (1967) Angiogenic factors. Science 235:442–447
6. Helder MN, Ozkaynak E, Sampath TK, Luyten FP, Latin V, Oppermann H, Vukicevic S (1995) Expression pattern of osteogenic protein-1 (bone morphogenetic protein-7) in human and mouse development. J Histochem Cytochem 43:1035–1044
7. Hiraki Y, Tanaka H, Inoue H, Kondo J, Kmizono A, Suzuki F (1991) Molecular cloning of a new class of cartilage-specific matrix, chondromodulin-I, which stimulates growth of cultured chondrocytes. Biochem Biophys Res Commun 175:971–977
8. Hiraki Y, Inoue H, Iyama K, Kamizono A, Ochiai M, Shukunami C, Iijima S, Suzuki F, Kondo J (1997) Identification of chondromodulin-I as a novel endothelial growth inhibitor: purification and its localization in the avascular zone of epiphyseal cartilage. J Biol Chem 272:32419–32426
9. Hiraki Y, Kono T, Sato M, Shukunami C, Kondo J (1997) Inhibition of DNA synthesis and tube morphogenesis of cultured vascular endothelial cells by chondromodulin-I. FEBS Lett 425:321–324
10. Hiraki Y, Mitsui K, Endo N, Takahashi K, Hayami T, Inoue H, Shukunami C, Tokunaga K, Kono T, Yamada M, Takahashi HE, Kondo J (1999) Molecular cloning of human chondromodulin-I, a cartilage-derived growth modulating factor, and its expression in Chinese hamster ovary cells. Eur J Biochem 260:869–878
11. Hotten GC, Matsumoto T, Kimura M, Bechtold RF, Kron R, Ohara T, Tanaka H, Satoh Y, Okazaki M, Shirai T, Pan H, Kawai S, Pohl JS, Kudo A (1996) Recombinant human growth/differentiation factor 5 stimulates mesenchyme aggregation and chondrogenesis responsible for the skeletal development. Growth Factors 13:65–74
12. Kusafuka K, Yamaguchi A, Kayano T, Fujuwara M, Takemura T (1998) Expression of bone morphogenetic proteins in salivary pleomorphic adenomas. Virchows Arch 432:247–253
13. Kusafuka K, Yamaguchi A, Kayano T, Takemura T (1998) Immunohistochemical localization of fibroblast growth factors (FGFs) and FGF receptor-1 in human normal salivary glands and pleomorphic adenomas. J Oral Pathol Med 27:287–292
14. Kusafuka K, Yamaguchi A, Kayano T, Takemura T (1999) Immunohistochemical localization of bone morphogenetic protein-6 in salivary pleomorphic adenomas. Pathol Int 49:1023–1027
15. Kusafuka K, Hiraki Y, Shukunami C, Yamaguchi A, Kayano T, Takemura T (2001) Cartilage-specific matrix protein chondormodulin-I is associated with chondroid formation in salivary pleomorphic adenomas: immunohistochemical analysis. Am J Pathol 158:1465–1472
16. Luo W, Guo C, Zhang J, Chen TL, Wang PY, Vertel BM, Tanzer ML (2000) Aggrecan from start to finish. J Bone Miner Metab 18:51–56
17. Luyten FP (1997) Cartilage-derived morphogenetic protein-1. Int J Biochem Cell Biol 29:1241–1244

18. Lyons KM, Pelton RW, Hogan BLM (1989) Patterns of expression of murine Vgr-1 and BMP-2a RNA suggest that transforming growth factor-$\beta$-like genes coordinately regulate aspects of embryonic development. Genes Dev 3:1657–1668
19. Nishitoh H, Ichijo H, Kimura M, Matsumoto T, Makishima F, Yamaguchi A, Yamashita H, Enomoto S, Miyazono K (1996) Identification of type I and type II serine/threonine kinase receptors for growth/differentiation factor-5. J Biol Chem 271:21345–21352
20. Schmid TM, Popp RG, Linsenmayer TF (1990) Hypertrophic cartilage matrix: type X collagen, supramolecular assembly and calcification. Ann N Y Acad Sci 580:64–73
21. Schmid TM, Bonen DK, Luchene L, Linsenmayer TF (1991) Late events in chondrocyte differentiation: hypertrophy, type X collagen synthesis and matrix calcification. In Vivo 5:533–540
22. Shukunami C, Iyama K, Inoue H, Hiraki Y (1999) Spatiotemporal pattern of the mouse *chondromodulin-I* gene expression and its regulatory role in vascular invasion into cartilage during endochondral bone formation. Int J Dev Biol 43:39–49
23. Takeda M, Iwata H, Suzuki S, Brown KS, Kimata K (1986) Correction of abnormal matrix formed by cmd/cmd chondrocytes in culture by exogenously added cartilage proteoglycan. J Cell Biol 103:1605–1614
24. Zhao M, Takata T, Ogawa I, Yada T, Kimata K, Nikai H (1999) Immunohistochemical evaluation of the small and large proteoglycans in pleomorphic adenoma of the salivary glands. J Oral Pathol Med 28:37–42

Virchows Arch (2003) 442:491–495
DOI 10.1007/s00428-003-0802-6

ORIGINAL ARTICLE

**Baljit Singh · Thomas Tschernig · Martijn van Griensven · Armin Fieguth · Reinhard Pabst**

# Expression of vascular adhesion protein-1 in normal and inflamed mice lungs and normal human lungs

Received: 28 October 2002 / Accepted: 11 March 2003 / Published online: 17 April 2003
© Springer-Verlag 2003

**Abstract** Recently, vascular adhesion protein-1 (VAP-1) was implicated in adhesion and transmigration of lymphocytes across endothelial cells in liver and other organs. There is very little information on VAP-1 expression in normal and inflamed lungs. Therefore, we conducted a study to localize VAP-1 in normal mice and human lungs and in two distinct murine models of lung inflammation. Normal mice and human lungs revealed VAP-1 expression in the endothelium of large and mid-sized pulmonary vessels but not in alveolar septae, airway epithelium or blood cells. Mice that lack the $lpr^{-/-}$ gene and develop extensive lymphocytic infiltration in their lungs showed VAP-1 expression similar to the normal mice lungs. Mice subjected to cecal ligation and puncture developed acute lung inflammation and showed VAP-1 not only in endothelial cells but also in inflammatory cells in perivascular areas at 72 h after the procedure. We concluded that VAP-1 expression may contribute to the functional heterogeneity of endothelial cells within the lung to create distinct sites for the recruitment of inflammatory cells. Furthermore, since VAP-1 is expressed over a longer period of time in inflamed lungs, it may even be a suitable target for drug delivery and therapeutic manipulations.

**Keywords** VAP-1 expression · Pulmonary inflammation

B. Singh (✉)
Department of Veterinary Biomedical Sciences,
University of Saskatchewan,
52 Campus Drive, Saskatoon, SK S7N 5B4, Canada
e-mail: baljit.singh@usask.ca
Tel.: +1-306-9667408
Fax: +1-306-9667405

T. Tschernig · R. Pabst
Department of Anatomy,
Hannover Medical School,
Hannover, Germany

M. van Griensven
Department of Trauma Surgery,
Hannover Medical School,
Hannover, Germany

A. Fieguth
Department of Legal Medicine,
Hannover Medical School,
Hannover, Germany

## Introduction

Only recently have the endothelial cells of the human lung vasculature been characterized in some detail and a great variability documented. The von Willebrand factor expression depended on the diameter of the vessels with only a weak, mosaic-like staining of capillaries [1]. The endothelial markers CD31 and CD34 also varied not only with age but with the type of vessels, with the strongest staining of capillary endothelial cells by anti-CD34 [22] and an upregulation of adhesion molecules in lungs of patients with acute respiratory distress syndrome (ARDS) [21]. Lung inflammation is a multi-step host response to a variety of viral, bacterial and chemical stimuli [29]. This multi-step paradigm includes expression of inflammatory mediators and adhesion molecules to recruit inflammatory cells to the injury site. Adhesion molecules such as selectins, integrins and members of immunoglobulin superfamily play a critical role in inflammatory cell recruitment [10, 16]. Although significant progress has been made in the identification of various adhesion molecules involved in these processes, our understanding is still incomplete. For example, although $\beta 2$ integrins facilitate neutrophil recruitment into the lung, there are instances of $\beta 2$ integrin-independent recruitment [15, 20]. Furthermore, the mechanisms of inflammatory cell accumulation in perivascular sites in the lung are largely unknown [24].

Recently, vascular adhesion protein-1 (VAP-1), an amine oxidase, was identified as an adhesion receptor that promotes homing of lymphocytes to endothelial cells in peripheral lymph nodes and at sites of inflammation [27]. VAP-1, a 170-kDa sialoglycoprotein, is constitutively expressed on endothelial cells in the human liver but is largely absent from non-inflamed vessels in extra-lym-

phoid organs [17]. The expression of VAP-1 is upregulated in high endothelial venules in peripheral lymph nodes at the sites of inflammation [26]. The increased expression of VAP-1 in vessels of endocrine pancreas correlates with the degree of lymphocyte infiltration [4]. VAP-1 cooperates with selectins to promote binding of lymphocytes to the endothelial cells and their transmigration across the vascular barrier in the liver [18]. Furthermore, inhibition of VAP-1-associated monoamine oxidase activity reduces lymphocyte adhesion and their migration across endothelial cells [17]. The expression of VAP-1 is also increased in experimental arthritis and dermatitis in pig and dog [12]. In a rabbit model of acute peritoneal inflammation, anti-VAP-1 monoclonal antibody reduced granulocyte accumulation by 70% [30]. Therefore, VAP-1 has significant functional consequences for inflammatory cell recruitment.

There is very little information on the expression of VAP-1 in normal and inflamed lung [12]. Therefore, we investigated VAP-1 expression in normal mice and human lungs and two distinct mouse models of lung inflammation. Mice that are deficient in one of the death receptors (CD95), *lpr*$^{-/-}$, show extensive recruitment of lymphocyes into their lungs [1]. A cecal ligation and puncture (CLP) model of acute lung inflammation is characterized by infiltration of neutrophils into the lungs [7]. A different family of adhesion molecules (a novel subset of the Ig superfamily) are the junctional adhesion molecules (JAMs), which seem to play an important role in the transmigration of leukocytes through endothelia [11]. The lung vascular system has not been studied with respect to the expression of the JAM. We report that VAP-1 expression is restricted to the endothelium of pulmonary arteries and veins as well as to a subset of macrophages or histiocytes, while alveolar septae, airway epithelium and blood cells are mostly negative. The expression of VAP-1 remained unaltered in both the models of lung inflammation with additional localization in perivascular areas. In addition, an immunohistochemical expression of JAM-2 was not found.

## Materials and methods

### Mice and human lung samples

Lung tissues were obtained from normal mice (C57Bl/6) and from so called *lpr*$^{-/-}$ mice on a Black/6 background ($n$=5 each). Those mice have a mutation in the *lpr* gene, a deficient CD95 receptor. The reduced apoptosis led to lupus-like autoimmune reactions with accumulation of lymphocytes in the kidneys and lungs. Animals were euthanized at 10 weeks of age [1]. Lungs were also collected from mice ($n$=3) that underwent the CLP procedure; CLP is an established model to simulate sepsis-induced multi-organ pathology [3, 5, 25]. Briefly, the mice (C57Bl/6) were anesthetized (100 mg/kg body weight ketamine and 16 mg/kg body weight xylazine subcutaneous), and a mid-line laparotomy was performed. Cecum was exteriorized and a through-and-through hole was made with a 21-gauge needle. After making sure that the hole was patent, cecum was ligated at the ilio–cecal junction. The animals were euthanized at 72 h after the procedure and lungs were snap frozen in liquid nitrogen and stored at −70°C.

Human lung samples were obtained during autopsies from seven children who had died of sudden infant death (six male, one female; mean age: 5.4 months; mean post-mortem interval: 28 h, informed consent obtained) and two adults (male, 60/65 years old; traumatic death) in the Department of Legal Medicine of Hannover Medical School. The samples were stored at −70°C.

### Immunohistochemistry for VAP-1, JAM-2 and CD31

Seven-micron-thick sections were prepared from frozen lung tissues and placed on glass slides that were coated with polylysine. The immunocytochemistry was performed as described previously [18]. Briefly, the sections were fixed in acetone at −20°C for 10 min and incubated with rat anti-mouse VAP-1 (kind gift from Dr. M. Salmi and Dr. S. Jalkanen), JAM-2 (kind gift from Dr. B. Imhof) monoclonal antibody (1:50) or CD31 (Dako, Hamburg, Germany, 1:50) followed by rat immunogloublins (1:100 in 5% mouse serum in PBS) and rat alkaline phosphatase-anti-alkaline phosphatase (APAAP; 1:100 in PBS) for 30 min each. The secondary antibody steps were repeated with incubation times of 15 min each. A similar protocol was used for the human tissues except that rat immunoglobulins were prepared in 5% human serum in PBS. The color was developed with Fast blue (Sigma) as a substrate for the APAAP with subsequent counter-staining in hematoxylin for 25 s. Anti-human CD45 (1:75; Dako) and anti-mouse CD3 (1:500; Dako) were used as isotype controls for endothelial staining for human and mice lungs, respectively. To assess non-specific binding of secondary antibodies, primary antibody was omitted in some sections. The images were captured with a digital camera mounted on a Leitz light microscope.

## Results

### Normal mouse lung

The lung sections incubated without a primary antibody as well as isotype control antibodies remained unstained and indicated a lack of non-specific binding of the secondary antibodies to the tissues. Lung sections stained with VAP-1 antibody demonstrated distinct reaction in endothelial cells of pulmonary arteries (Fig. 1A, Table 1), veins and venules. VAP-1 did not stain bronchiolar epithelium and alveolar septae. JAM-2 did not stain any of the areas in the lung sections from normal mice, whereas labeling was found in spleen and lymph nodes (not shown).

### VAP-1 expression in inflamed mice lungs

The lungs from *lpr*$^{-/-}$ mice showed extensive periarterial infiltrates of lymphocytes as indicated by staining with an antibody against the T-cell receptor (TCR; Fig. 1D). VAP-1 staining in these inflamed lungs was restricted to pulmonary arteries, veins and venules as noticed in the lungs of the normal mice (Fig. 1E). In addition, VAP-1 reacted with perivascular vessels in the lungs from *lpr*$^{-/-}$ mice (Fig. 1F). Bronchiolar epithelium, alveolar septae and cells such as lymphocytes did not react with VAP-1. Mice subjected to CLP showed acute inflammation characterized by accumulation of neutrophils in the lungs. The pattern of VAP-1 staining was similar to the normal

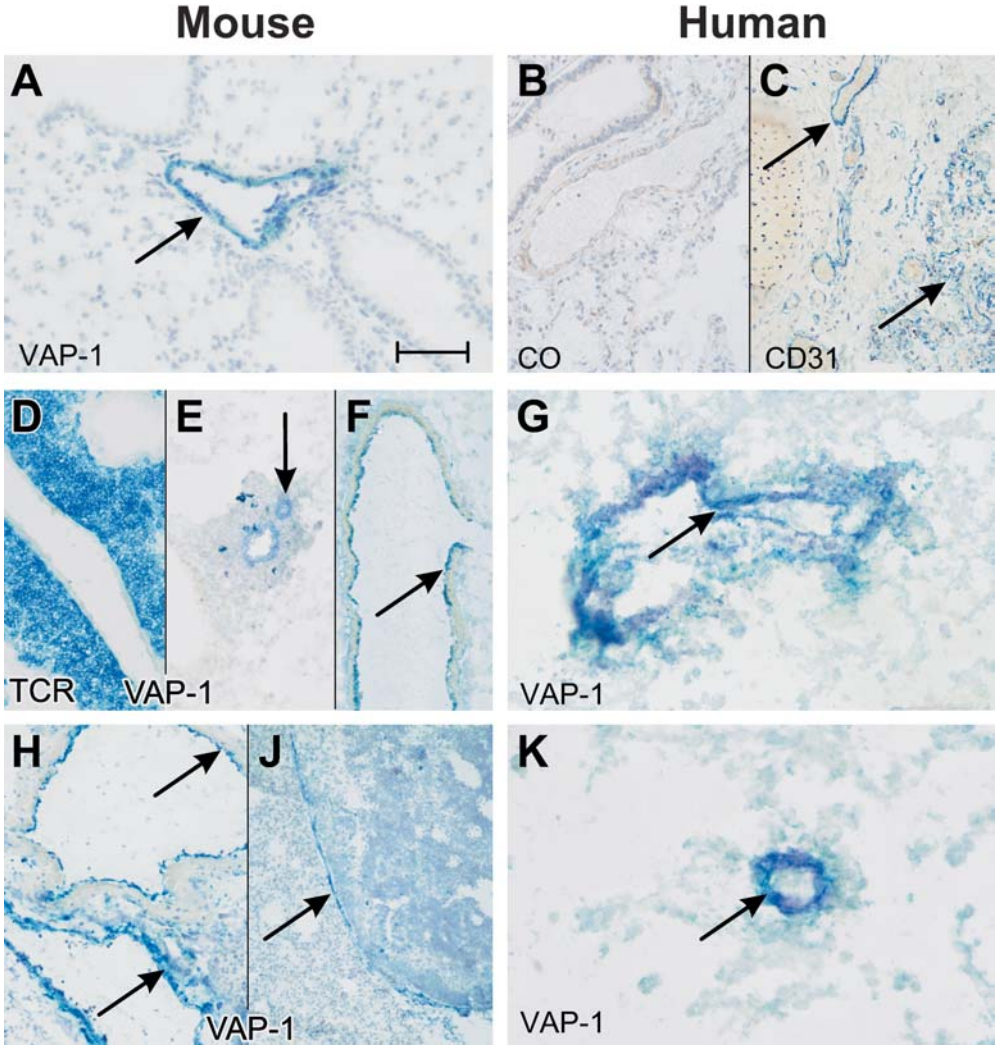



**Fig. 1** Immunohistologically stained representative cryostat sections of mice lung tissue (**A**, **D**, **E**, **F**, **H**, **J**) and human lung tissue (**B**, **C**, **G**, **K**) using the APAAP-technique with Fast Blue as the substrate (scale bar 100 µm, same magnification in all figure parts). In this representative lung section of a healthy mouse (**A**), a pulmonary artery was stained with the antibody against the vascular adhesion protein-1 (VAP-1) adhesion molecule (*arrow*), whereas the bronchial epithelium and alveolar capillaries were not labeled. In the lungs of mice with autoimmune inflammation ($lpr^{-/-}$ mice) perivascular cuffs consisting mainly of T lymphocytes were found (**D**, *TCR* T-cell receptor; notice the unstained endothelium serving as isotype negative control staining). In those infiltrates, VAP-1 positive vessels could be detected (**E**, *arrow*). VAP-1 expression was also found in those lung sections on pulmonary arteries and perivascular vessels (**F**, *arrow*; note the branching vessel not stained for VAP-1). A section of an inflamed lung of a cecal ligation and puncture model (CLP) mouse revealed a positive endothelium of arteries and veins (**H**, *arrows*). In addition, labeling of the endothelium of a sinus of a bronchial lymph node was found (**J**, *arrow*). Staining of human lung sections without a primary antibody showed no staining (**B**), whereas CD31 labeled all endothelial cells including the alveolar capillaries (**C**, *arrows*). VAP-1 staining was found in veins (**G**, *arrow*) but also in human pulmonary arteries (not shown) as well as in venules (**K**, *arrow*)

mice (Fig. 1H). The capsular sinuses of bronchial lymph nodes were also positive for VAP-1 staining (Fig. 1J).

## Normal human lung

Lung sections prepared from most of the human samples showed poorly preserved morphology especially of the bronchial epithelium. There was no non-specific binding of the secondary antibodies in the human lung sections (Fig. 1B). The panendothelial marker CD31 labeled all pulmonary arteries and veins as well as alveolar capillar-

**Table 1** Expression of VAP-1 in the lung vasculature. + complete staining except some small branching vessels in some sections, – complete absence of labeling; JAM-2 was not expressed at all

| | Mouse lung | | Human lung Sudden death |
|---|---|---|---|
| | Healthy | Inflamed | |
| Pulmonary artery | + | + | + |
| Pulmonary vein | + | + | + |
| Venule | + | + | + |
| Capillaries/septa | – | – | – |

ies (Fig. 1C). VAP-1 antibody stained the endothelium of pulmonary veins (Fig. 1G), arteries (not shown) and venules (Fig. 1K) but not alveolar septae and airway epithelium. There was no staining for JAM-2 in human lung tissues (Table 1).

## Discussion

A great variability in the expression of markers of endothelial cells of the human lung vasculature had been described before using antibodies against CD31, CD34 and von Willebrand factor [23]. The lack of staining of endothelial cells with the anti-JAM-2 antibody has so far to be taken with some reservation as modifications of the technique or other samples of lung tissue might show positive reactions. We report that VAP-1 expression is restricted to the endothelial and smooth muscle cells of pulmonary arteries and veins of normal and inflamed mice lungs, and normal human lungs. The expression was absent in the epithelial cells and alveolar septae of the lung. VAP-1 is a novel adhesion molecule that also has monoamine oxidase activity [13, 27]. Previously, constitutive expression of VAP-1 was reported in the endothelium of blood vessels in organs such as liver, kidney and peripheral lymph nodes, and also in smooth muscle cells of large vessels [27]. There is only one report that briefly mentions constitutive expression of VAP-1 in the endothelium of pulmonary venules [12]. In contrast, we report a lack of VAP-1 expression in alveolar septae of mice and human lungs that indicates its absence from lung capillaries. The CD31-expression was also found on capillaries in the investigated material documenting the preservation of endothelial markers in the investigated samples. This distinction in VAP-1 expression, vessels versus capillaries, shows phenotypic heterogeneity of endothelial cells within the same organ [32]. Although endothelial cells contain functional form of VAP-1, the functional implications of constitutively expressed VAP-1 remain unknown [2]. Since luminal expression of VAP-1 is a prerequisite for it to be functional, constitutive intracellular VAP-1 may have little, if any, influence on physiological trafficking of cells such as lymphocytes and neutrophils. However, VAP-1 that is constitutively expressed may act as a ready-to-use source of adhesive protein in early stages of inflammation.

We report the first data on VAP-1 expression in inflamed lungs. VAP-1 expression was found in both lymphocytic and neutrophilic inflammation in the lung, still localized in pulmonary arteries and veins but not in alveolar capillaries. It remains unclear whether this expression was unchanged or enhanced relative to normal tissue. Even in inflammation the alveolar capillaries remained negative for the staining against VAP-1. Mice with deletion of *lpr* gene used in our study showed extensive perivascular accumulation of lymphocytes in their lungs [9]. It is known that VAP-1 plays a role in lymphocyte circulation and homing in inflamed liver and kidney and anti-VAP-1 monoclonal antibody inhibits it [17, 19, 27]. VAP-1 also acts as a "molecular brake" during rolling of granulocytes and promotes their recruitment in acute peritoneal inflammation [30]. Although others have reported an increase in the expression of VAP-1 in the endothelium of blood vessels at sites of inflammation [26], we did not notice such an alteration in $lpr^{-/-}$ mice that have extensive lymphocytic recruitment and CLP mice that develop acute neutrophilic lung inflammation. VAP-1 is translocated to the luminal surface of endothelial cells in inflamed organs [12]. Therefore, VAP-1 in inflamed mice lungs may actually be present on the luminal surface of endothelium and we may have failed to detect it with immunohistology. Nevertheless, VAP-1 present in inflamed lungs may indicate its involvement in lymphocyte and neutrophil recruitment.

An interesting observation was the similarity of VAP-1 expression in CLP-induced acute lung inflammation to chronic lymphocytic inflammation in $lpr^{-/-}$ mice. These data, similar to observations by other investigators, indicate long-term stability of VAP-1 expression [13]. This sustained expression of VAP-1 may either be due to longevity of VAP-1 translocated to the luminal surface or its new production. The longevity of VAP-1 expression, irrespective of the mechanisms that cause it, is in contrast to other adhesion molecules such as selectins that are downregulated after their functional expression during the early phase of inflammation [6, 14]. The ability of endothelial cells in larger pulmonary vessels to retain VAP-1 for a longer period of time in inflammation makes it an attractive candidate to target therapeutic agents.

The most intriguing observation in our study was the expression of VAP-1 in perivascular areas of inflamed lungs relative to the normal. The functional implications of perivascular expression of VAP-1 remain unknown. It is generally accepted that inflammatory cell transmigration occurs in lung capillaries and not in blood vessels with smooth muscle cells [8, 24]. Although perivascular accumulation of inflammatory cells is a consistent feature in many lung diseases, the mechanisms of this phenomenon remain largely unknown [24, 28, 31]. Since VAP-1 promotes lymphocyte and neutrophil recruitment and it is expressed in pulmonary arteries and veins and in the perivascular areas in inflamed lungs, we speculate that it plays a role in perivascular recruitment of inflammatory cells. Therefore, it is critical to investigate the biology of VAP-1 in lung pathophysiology.

**Acknowledgements** The research was supported by a grant from Deutsche Forschungsgemeinschaft (SFB 587, B1). Dr. Baljit Singh was supported by a Study Visit Grant from the German Academic Exchange Program. The authors thank Dr. M. Salmi and Dr. S. Jalkanen for the VAP-1 antibody, and Dr. B. Imhof for the JAM-2 antibody.

## References


1. Adachi M, Suematsu S, Suda T, Watanabe D, Fukuyama H, Ogasawara J, Tanaka T, Yoshida N, Nagata S (1996) Enhanced and accelerated lymphoproliferation in Fas-null mice. Proc Natl Acad Sci U S A 93:2131–2136
2. Alexander JS, Granger DN (2000) Lymphocyte trafficking mediated by vascular adhesion protein-1: implications for immune targeting and cardiovascular disease. Circ Res 86:1190–1192
3. Bless NM, Tojo SJ, Kawarai H, Natsume Y, Lentsch AB, Padgaonkar VA, Czermak BJ, Schmal H, Friedl HP, Ward PA (1998) Differing patterns of P-selectin expression in lung injury. Am J Pathol 153:1113–1122
4. Bono P, Jalkanen S, Salmi M (1999) Mouse vascular adhesion protein 1 is a sialoglycoprotein with enzymatic activity and is induced in diabetic insulitis. Am J Pathol 155:1613–1624
5. Chinnaiyan AM, Huber-Lang M, Kumar-Sinha C, Barrette TR, Shankar-Sinha S, Sarma V, Padgaonkar VA, Ward PA (2001) Molecular signature of sepsis: multiorgan gene expression profiles of systemic inflammation. Am J Pathol 159:1199–1209
6. Crockett-Torabi E (1998) Selectins and mechanisms of signal transduction. J Leukoc Biol 63:1–14
7. Czermak BJ, Breckwoldt M, Ravage ZB, Huber-Lang M, Schmal H, Bless NM, Friedl HP, Ward PA (1999) Mechanisms of enhanced lung injury during sepsis. Am J Pathol 154:1057–1065
8. Doerschuk CM (2001) Mechanisms of leukocyte sequestration in inflamed lungs. Microcirculation 8:71–88
9. Fleck M, Kern ER, Zhou T, Podlech J, Wintersberger W, Edwards CK III, Mountz JD (1998) Apoptosis mediated by Fas but not tumor necrosis factor receptor 1 prevents chronic disease in mice infected with murine cytomegalovirus. J Clin Invest 102:1431–1443
10. Gahmberg CG, Valmu L, Kotovuori P, Ihanus E, Tian L, Pessa-Morikawa T (1998) Leukocyte integrins in inflammation. Cell Mol Life Sci 54:549–555
11. Imhof BA, Engelhardt B, Vadas MA (2001) Novel mechanisms of the transendothelial migration of lymphocytes. Trends Immunol 22:411–414
12. Jaakkola K, Nikula T, Holopainen R, Vahasilta T, Matikainen MT, Laukkanen ML, Huupponen R, Halkola L, Nieminen L, Hiltunen J, Parviainen S, Clark MR, Knuuti J, Savunen T, Kaapa P, Voipio-Pulkki LM, Jalkanen S (2000) In vivo detection of vascular adhesion protein-1 in experimental inflammation. Am J Pathol 157:463–471
13. Jalkanen S, Salmi M (2001) Cell surface monoamine oxidases: enzymes in search of a function. EMBO J 20:3893–3901
14. Kanwar S, Steeber DA, Tedder TF, Hickey MJ, Kubes P (1999) Overlapping roles for L-selectin and P-selectin in antigen-induced immune responses in the microvasculature. J Immunol 162:2709–2716
15. Klemm A, Tschernig T, Ermert L, Althoff A, Merkle M, Gebert A, Ermert M, Seeger W, Pabst R (2000) Blockade of leucocyte function-associated antigen-1 (LFA-1) decreases lymphocyte trapping in the normal pulmonary vasculature: studies in the isolated buffer-perfused rat lung. Clin Exp Immunol 121:375–383
16. Kuebler WM, Kuhnle GE, Groh J, Goetz AE (1994) Leukocyte kinetics in pulmonary microcirculation: intravital fluorescence microscopic study. J Appl Physiol 76:65–71
17. Lalor PF, Edwards S, McNab G, Salmi M, Jalkanen S, Adams DH (2002) Vascular adhesion protein-1 mediates adhesion and transmigration of lymphocytes on human hepatic endothelial cells. J Immunol 169:983–992
18. Lehmann C, Wilkening A, Leiber D, Markus A, Krug N, Pabst R, Tschering T (2001) Lymphocytes in the bronchoalveolar space reenter the lung tissue by means of the alveolar epithelium, migrate to regional lymph nodes, and subsequently rejoin the systemic immune system. Anat Rec 264:229–236
19. Martelius T, Salmi M, Wu H, Bruggeman C, Hockerstedt K, Jalkanen S, Lautenschlager I (2000) Induction of vascular adhesion protein-1 during liver allograft rejection and concomitant cytomegalovirus infection in rats. Am J Pathol 157:1229–1237
20. Mizgerd JP (2002) Molecular mechanisms of neutrophil recruitment elicited by bacteria in the lungs. Semin Immunol 14:123–132
21. Müller AM, Cronen C, Müller K-M, Kirkpatrick CJ (2002) Heterogeneous expression of cell adhesion molecules by endothelial cells in ARDS. J Pathol 198:270–275
22. Müller AM, Nesslinger M, Skipka G, Müller K-M (2002) Expression of CD34 in pulmonary endothelial cells in vivo. Pathobiology 70:11–17
23. Müller AM, Skrzynski C, Skipka G, Müller K-M (2002) Expression of von Willebrand factor by human pulmonary endothelial cells in vivo. Respiration 69:526–533
24. Pabst R, Tschernig T (2002) Perivascular capillaries in the lung: an important but neglected vascular bed in immune reactions? J Allergy Clin Immunol 110:209–214
25. Riedemann NC, Guo RF, Neff TA, Laudes IJ, Keller KA, Sarma VJ, Markiewski MM, Mastellos D, Strey CW, Pierson CL, Lambris JD, Zetoune FS, Ward PA (2002) Increased C5a receptor expression in sepsis. J Clin Invest 110:101–108
26. Salmi M, Kalimo K, Jalkanen S (1993) Induction and function of vascular adhesion protein-1 at sites of inflammation. J Exp Med 178:2255–2260
27. Salmi M, Yegutkin GG, Lehvonen R, Koskinen K, Salminen T, Jalkanen S (2001) A cell surface amine oxidase directly controls lymphocyte migration. Immunity 14:265–276
28. Schneider T, van Velzen D, Moqbel R, Issekutz AC (1997) Kinetics and quantitation of eosinophil and neutrophil recruitment to allergic lung inflammation in a brown Norway rat model. Am J Respir Cell Mol Biol 17:702–712
29. Springer TA (1990) Adhesion receptors of the immune system. Nature 346:425–434
30. Tohka S, Laukkanen M, Jalkanen S, Salmi M (2001) Vascular adhesion protein 1 (VAP-1) functions as a molecular brake during granulocyte rolling and mediates recruitment in vivo. FASEB J 15:373–382
31. Uhlig S, Brasch F, Wollin L, Fehrenbach H, Richter J, Wendel A (1995) Functional and fine structural changes in isolated rat lungs challenged with endotoxin ex vivo and in vitro. Am J Pathol 146:1235–1247
32. Wang Q, Pfeiffer GR, Stevens T, Doerschuk CM (2002) Lung microvascular and arterial endothelial cells differ in their responses to intercellular adhesion molecule-1 ligation. Am J Respir Crit Care Med 166:872–877

Virchows Arch (2003) 442:496–500
DOI 10.1007/s00428-003-0780-8

CASE REPORT

**J. Müller-Höcker · P. Rellecke**

# Chief cell proliferation of the gastric mucosa mimicking early gastric cancer: an unusual variant of fundic gland polyp

Received: 2 December 2002 / Accepted: 27 January 2003 / Published online: 16 April 2003
© Springer-Verlag 2003

**Abstract** We describe a hitherto unknown lesion of gastric chief cell proliferation mimicking structurally mucosal gastric cancer. The unremarkable cytology of the cells, their very low Ki-67 index, the inclusion of occasional parietal cells and especially ultrastructural evidence of chief cell differentiation proved helpful in the differentiation from early gastric cancer. The exact classification of the alteration remains unresolved. The presence of microcysts suggests that the lesion is a variant of fundic gland polyp formation.

**Keywords** Fundic gland polyp · Dysplasia · Gastric carcinoma

## Introduction

Gastric dysplasia is characterized by disorganization of mucosal architecture and nuclear abnormalities [9, 11, 12, 22] and by its tendency to progress to invasive cancer [17]. Especially low-grade dysplasia may be difficult to differentiate from epithelial atypia associated with inflammation and regeneration. This is especially true for damage due to nonsteroidal anti-inflammatory drugs/acetylsalicylic acid which may lead to considerable disturbance of mucosal architecture and nuclear atypia in the process of cell regeneration. Since gastric dysplasia is an important marker for carcinoma risk, and especially high-grade dysplasia is highly predictive for gastric carcinoma [3, 4, 6, 18], reactive nonneoplastic lesions must be clearly discriminated. Here we report an unusual lesion of oxyntic gastric chief cells mimicking early gastric cancer.

J. Müller-Höcker (✉)
Pathologisches Institut,
Ludwig-Maximilians-Universität,
Thalkirchner Strasse 36, 80337 Munich, Germany
e-mail: josef.mueller-hoecker@web.de
Tel.: +49-89-51604051

P. Rellecke
Medizinische Klinik II, Klinikum Großhadern,
Ludwig-Maximilians-Universität,
Munich, Germany

## Case report

A 75-year-old white man presented because of permanent epigastrical pain independent of food intake. There was no nausea or vomiting. The patient had a past medical history of hepatitis A and B, chronic obstructive lung disease because of chronic nicotine abuse (50 pack-years) and chronic alcohol consumption. Laboratory findings demonstrated elevated plasma levels of $\gamma$- glutamyltransferase (29 U/ml) and mean corpuscular hemoglobin (33.2 pg). There was a slight elevation in C-reactive protein and carcinoembryonic antigen. Other laboratory findings were unremarkable.

Gastroscopy showed a prominent lesion of the gastric mucosa at the major side in the cardia/corpus transition zone (10–12 mm in diameter). Endosonography revealed that the lesion was limited to the gastric mucosa without infiltrating deeper layers. The patient was treated with proton pump inhibitors for 3 months, relieving the episodes of epigastrical pain. Further technical examinations including abdominal ultrasonography, coloscopy, and magnetic resonance imaging revealed no further relevant findings except steatosis hepatis and osteochondrosis of the lumbar spine and arteriosclerotic plaques in the abdominal aorta.

Gastric biopsy specimens of the corpus and antrum were fixed in 4% buffered formalin, embedded in paraffin, and cut into 4-µm sections for light microscopic investigation. Staining for hematoxylin and eosin, Giemsa, and periodic acid–Schiff were performed. Immunohistochemical studies were performed for the detection of $\gamma$-enolase (1:30), chromogranin (1:150), Ki_67 (1:50) using the Ventana staining NexES (Ventana Medical Systems, Tucson, Ariz., USA; automated immunostainer), serotonin (1:200) with the alkaline phosphatase–antialkaline phosphatase system and gastrin (1:600) using the biotin-streptavidin-peroxidase system. For gastrin and synaptophysin a 15-min microwave pretreatment (citrate buffer) was administered. All the antisera were provided by Dako (Hamburg, Germany). For electron microscopy the biopsy material was deparaffinized in xylol, rehydrated, and treated with osmium (2% in a.dest.) for 1 h, dehydrated in acetone, and embedded in epon (polymerization at 78°C overnight) for preparation of semithin and ultrathin sections. Counterstaining was performed with uranyl acetate and led citrate following routine protocols.

## Results

Light microscopy of the corpus mucosa showed anastomosing cords of epithelial cells in the upper half of the mucosa. The cells had a monomorphous appearance with centrally placed round nuclei and an amphophilic cytoplasm (Fig. 1a, b). There was no mitosis, and MiB-1

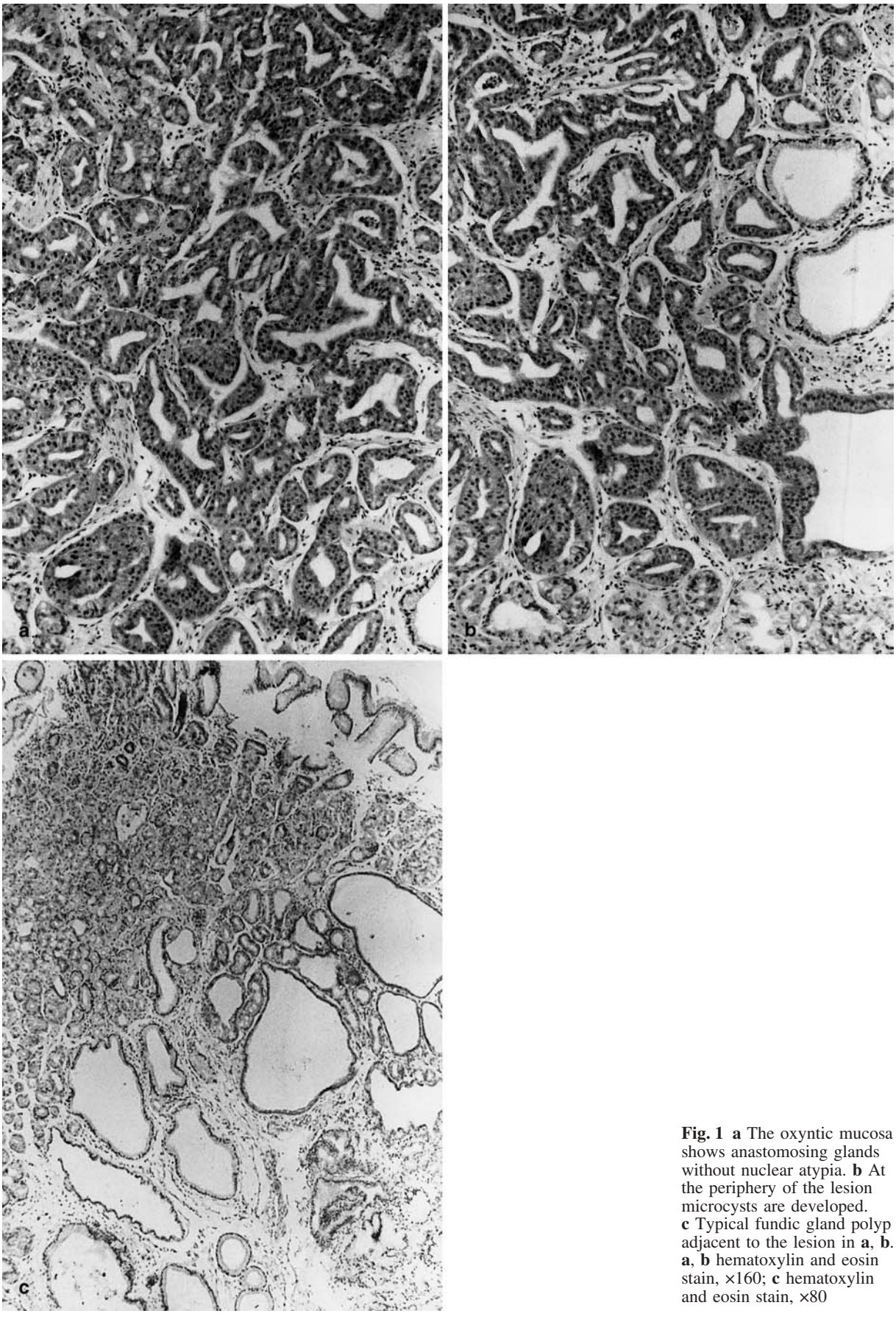



**Fig. 1** **a** The oxyntic mucosa shows anastomosing glands without nuclear atypia. **b** At the periphery of the lesion microcysts are developed. **c** Typical fundic gland polyp adjacent to the lesion in **a**, **b**. **a**, **b** hematoxylin and eosin stain, ×160; **c** hematoxylin and eosin stain, ×80

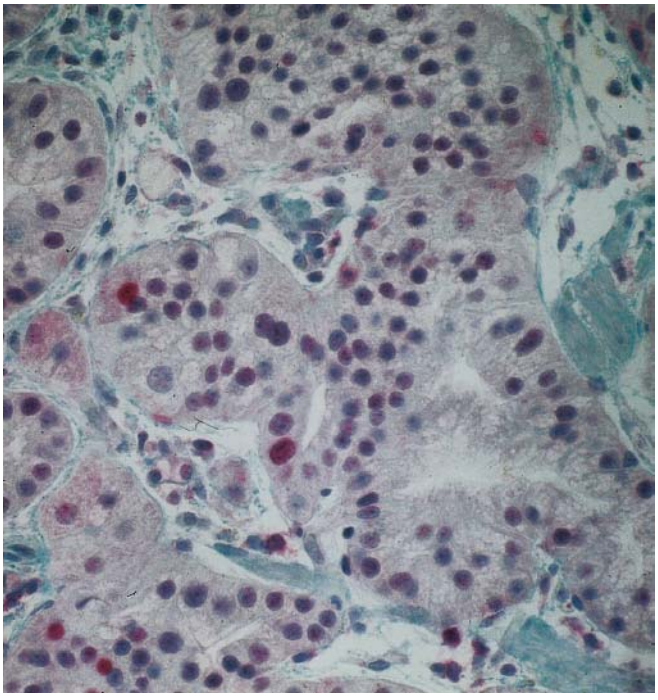


**Fig. 2** Staining for Ki-67 reveals only scattered red-colored nuclei; ×320

staining for Ki-67 (Fig. 2) revealed a low nuclear staining index (less than 5%). In the Giemsa stain single parietal cells were detected in close contact to the amphophilic cell cords. Adjacent to the lesion microcysts consisting of oxyntic gland and foveolar type cells were seen (Fig. 1b), merging into typical fundic gland polyp formation (Fig. 1c) in the neighborhood. The foveolar surface epithelium was intact. The mucosal stroma was moderately edematous with scarce lymphocytes and plasma cells. Immunohistochemistry gave no evidence of endocrine differentiation with various antibodies (chromogranin, $\gamma$-enolase, synaptophysin). The gastric mucosa of the antrum was regularly developed and showed only minor lymphocytic infiltrates. There were no erosive changes or signs of increased cellular proliferation in the proliferative compartment of the neck region. *Helicobacter pylori* was not detected.

Electron microscopy performed after reembedding the paraffin-embedded tissue revealed that the abnormal cells showed chief cell differentiation with large aggregates of rough endoplasmic reticulum throughout the cytoplasm being filled with proteinaceous material, while the amount of zymogen granula was reduced (Fig. 3a). In normal chief cells the rough endoplasmic reticulum is predominantly in a retronuclear position while zymogen granula accumulate in the apical cytoplasm (Fig. 3b). The typical internal vesicular structure was seen in parietal cells.

## Discussion

In this report we describe a hitherto unknown lesion of gastric mucosa which mimicked early gastric cancer both endoscopically and morphologically. Disturbance of mucosal architecture by anastomosing cords of monomorphous epithelial cells was the most alarming histological feature. In contrast to structural disturbance, cellular atypia was practically lacking. Immunohistochemistry ruled out a carcinoid lesion, and MiB-1 staining for Ki-67 revealed a very low proliferative compartment. The presence of occasional parietal cells was verified in the Giemsa stain. Only after reembedding for ultrastructural investigation was the true nature of the lesion identified. The chief cell differentiation found in the ultrastructural investigation was regarded as the strongest argument for the benign character of the lesion. This also ruled out especially adenoma of intestinal and pyloric gland type with certainty. Interestingly, the chief cells also showed evidence of disorganization at the subcellular level. While in regular chief cells the rough endoplasmatic reticulum is concentrated in a retronuclear basal position, and zymogen granules accumulate in the apical cytoplasma, most of the chief cells of the present lesion showed a loss of polarity and a random distribution of the rough endoplasmic reticulum.

The true nature of the alteration, however, remains to be clarified. Interestingly, microcysts of oxyntic glands existed and merged into a fundic gland polyp in the neighborhood. It is thought that fundic gland polyps (FGP) is a reactive alteration [5, 8, 19]. Its relationship to the structural disturbance of the mucosa in the present case remains unclear, however. Especially it cannot be determined whether they are reactive to the structural disorganization of the chief cells, or whether they are an active part of it. Assuming the latter, it may be hypothesized that the lesion described here is a variant of fundic gland polyp formation.

The pathogenesis of FGP is still unknown. FGPs occur almost exclusively in normal corpus or after *H. pylori* eradication [7, 16, 19]. FGPs have been reported to develop in the corpus mucosa during proton pump inhibitor therapy (for review see [21]). This issue is controversal, however [21]. Most plausible is that FGPs result from a functional-secretory impairment. This is underscored by their reversible occurrence after pentagastrine stimulation [15]. There is no evidence that cancerization in the stomach involves chief cells. In contrast, parietal cell carcinoma [1, 2, 14] and carcinoma with predominant Paneth cell differentiation have been reported [10, 13].

In summary, the tumorlike lesion of the gastric mucosa described here was made up of chief cells. Because of the striking architectural disturbance we had to exclude especially grade 1 adenocarcinoma, which may present as a tubular network without single cell infiltration [20]. Especially the presence of parietal cells within the lesion and the evidence of chief cell differentiation by ultra-

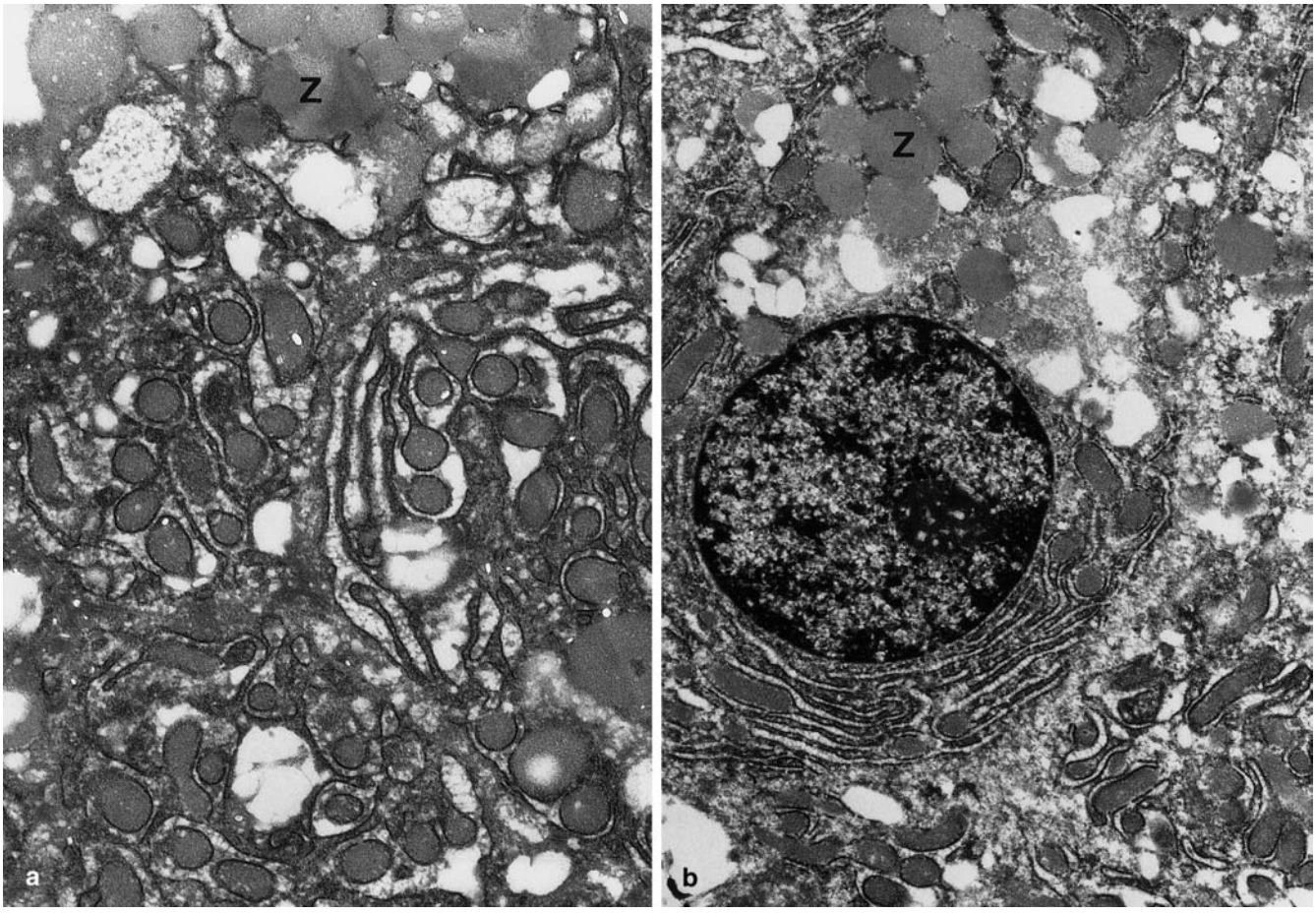



**Fig. 3** Ultrastructure after reembedding from primarily paraffin embedded tissue. **a** Atypical chief cell with a high amount of rough endoplasmatic reticulum (RER) throughout the cytoplasm. The RER is filled with proteinaceous material. Zymogen granula are also seen (*Z*). **b** Regular chief cell with concentration of the RER in a retronuclear position and accumulation of zymogen granula at the apical pole. **a** ×21,000; **b** ×16,500

structural investigation proved helpful for establishing the correct diagnosis.

**Acknowledgements** The authors thanks Prof. M. Stolte, Institute of Pathology, Klinikum Bayreuth, for valuable comments. The authors are indebted to Ms. Brigitte Schult and Ms. Maria Wittmeier for carefully preparing the manuscript and to Ms. Sabine Schäfer for valuable technical assistance.

## References

1. Byrne D, Holley MP, Cushieri A (1988) Parietal cell carcinoma of the stomach; association with long-term survival after curative resection. Br J Cancer 58:85–87
2. Capella C, Frigerio B, Cornaggia M, et al (1984) Gastric parietal cell carcinoma a newly recognized entity: light microscopic and ultrastructural features. Histopathology 8:813–824
3. Coma del Corral MJ, Pardo-Mindan FJ, Razquin S, Ojeda C (1990) Risk of cancer in patients with gastric dysplasia. Follow-up study of 67 patients. Cancer 65:2078–2085
4. Cusso X, Mones J, Ocana J, Medez C, Vilardell F (1993) Is endoscopic gastric cytology worthwhile? An evaluation of 903 cases of carcinoma. J Clin Gastroenterol 16:336–339
5. Elster K, Eidt H, Ottenjann R, et al (1977) Drüsenkörperzysten, eine polypoide Läsion der Magenschleimhaut. Dtsch Med Wochenschr 102:183–187
6. Fertitta AM, Comin U, Terruzzi V (1993) Clinical significance of gastric dysplasia: a multicenter follow-up study. Gastrointestinal Endoscopic Pathology Study Group. Endoscopy 25:265–268
7. Fiocca R (1995) The point of view of the gastroenterologist. G Ital End Dig 18:284–285
8. Hizawa K, Iida M, Matsumoto T, et al (1993) Natural history of fundic gland polyposis without familial adenomatosis coli: follow-up observations in 31 patients. Radiology 1989:429–432
9. Jarvis LR, Whitehead R (1985) Morphometric analysis of gastric dysplasia. J Pathol 147:133–138
10. Kazzaz BA, Eulderink F (1989) Paneth cell-rich carcinoma of the stomach. Histopathology 15:303–305
11. Ming S-C, Bajtai A, Correa P, et al (1984) Gastric dysplasia. Significance and pathologic criteria. Cancer 54:1794–1801
12. Nagayo T (1981) Dysplasia of the gastric mucosa and its relation to the precancerous state. Gann 72:813–823
13. Ooi A, Nakanishi I, Itoh T, Ueda H, Mai M (1991) Predominant Paneth cell differentiation in an intestinal type gastric cancer. Pathol Res Pract 187:220–225
14. Robey-Cafferty SS, Ro JY, McKee EG (1989) Gastric parietal cell carcinoma with an unusual, lymphoma-like histologic appearance: report of a case. Mod Pathol 2:536–540

15. Rohner HG (1977) Drüsenkörperzysten des Magens: Erscheinungsbild und mögliche Entstehungsmechanismen. Leber Magen Darm 7:62–64
16. Rösch W, Stolte M (1995) Helicobacter pylori is not found in patients with glandular cystic polyps of the stomach. Hepatogastroenterology 42:84–85
17. Rugge M, Farinati F, Baffa R, et al (1994) Gastric epithelial dysplasia in the natural history of gastric cancer: a multicenter follow-up study. Gastroenterology 107:1288–1296
18. Saraga EP, Gardiol D, Costa J (1987) Gastric dysplasia: a histologic follow-up study. Am J Surg Pathol 11:81–89
19. Stolte M, Bethke P, Seifert E, et al (1995) Observation of gastric glandular cysts in the corpus mucosa of the stomach under omeprazole treatment. Z Gastroenterol 33:146–149
20. Takahashi T, Iwama N (1985) Three-dimensional microstructure of gastrointestinal tumors. Gland pattern and its diagnostic significance. Pathol Annu 1:419–440
21. Vieth M, Stolte M (2001) Fundic gland polyps are not induced by proton pump inhibitor therapy. Am J Clin Pathol 116:716–720
22. Watanabe H, Jass JR, Sobin LH (1990) Histological typing of oesophageal and gastric tumours, 2nd edn. Springer, Berlin Heidelberg New York

Virchows Arch (2003) 442:501–503
DOI 10.1007/s00428-003-0764-8

LETTER TO THE EDITOR

**Fumio Ide · Kenji Mishima · Ichiro Saito**

# Solid-cystic tumor variant of odontogenic keratocyst: an aggressive but benign lesion simulating keratoameloblastoma

Received: 11 July 2002 / Accepted: 19 December 2002 / Published online: 10 April 2003
© Springer-Verlag 2003

Sir,

Keratoameloblastoma (KA), which was first described by Siar and Ng [9] under the descriptive term "combined ameloblastoma and odontogenic keratocyst," is a unique tumor within the spectrum of ameloblastoma. To our knowledge, only nine well-documented examples including a rarer papilliferous form have appeared in the English-language literature [1, 2, 5, 7, 9, 10]. We present an 18-year follow-up case of a solid-cystic tumor variant of odontogenic keratocyst (OKC) in the mandible that may be confused with KA. This case defies easy diagnostic and nosologic classification because it demonstrated combined features of KA and OKC, each belonging to a different pathologic entity.

A 49-year-old woman first presented in 1984 with a multilocular radiolucent lesion, measuring 4.5 cm in diameter, in the left mandible. A jaw cyst had been removed from the same site at another institution in 1973, but no further information of the initial biopsy was available. After cystectomy, conservative enucleation or curettage was performed three times (in 1985, 1986, and 1990) because of recurrence. However, in 1998, a honeycombed radiolucency appeared again. Through en-block resection, the lesion was under control for 4 years. During the clinical course, there was no evidence of involvement of the adjacent soft tissues or lymph nodes.

Surgical materials from 1984 to 1990 had essentially similar histological patterns. They showed a benign combined proliferation of solid epithelial follicles with marked central keratinization and multiple keratinizing cysts of varying size (Fig. 1A). Solid nests were in direct continuity with cysts and invaded the cancellous bone. The features diagnostic for ameloblastoma (e.g., peripheral palisading, reversed polarization of nuclei and subnuclear vacuolization) were exceptional (Fig. 1B). Thin squamous epithelial lining of keratinizing cysts had the characteristics of OKC and exhibited extensive proliferation in some areas (Fig. 1C). Notably, the finally resected specimen (in 1998) contained multiple separate OKCs within the marrow spaces (Fig. 2A, B). Some of them showed finger-like proliferations (Fig. 2C). Even on step sections, none involved the solid components.

The present solid-cystic epithelial lesion was originally regarded as KA but proved to be a solid form of OKC with the retrospective review. The patient's significantly excellent prognosis over a period of 18 years ruled out the possibility of highly differentiated squamous cell carcinoma arising in an OKC. There are review articles of clinical and histological observations that indicated that some OKCs behave as aggressive as a true neoplasm [3, 8]. Presumably, the neoplastic OKC family span a broad clinicopathologic spectrum from benign pure cystic form with infiltrative properties on one end [6] to cytologically malignant form with capability of metastasis [4] on the other, with the present solid-cystic form occupying an intermediate position, probably nearer to the benign end, in both morphology and behavior. Very recently, Vered et al. [11] reported a similar solid OKC in the maxilla with the infiltration into the surrounding soft tissues, but it is difficult to compare their lesion to ours because their case was published in the abstract form.

KA is a rare variant of ameloblastoma characterized histologically by an admixture of solid tumor islands resembling follicular ameloblastoma with extensive keratinization, and multiple keratinizing cysts bear characteristics of OKC [5, 7, 9, 10]. Overall, the present case showed architectural characteristics of KA; therefore, the question arises whether this lesion fits the criteria for KA. However, the lack of obvious palisading and reversed nuclear polarity of the peripheral tumor cells could not confirm the diagnosis of ameloblastoma. Interestingly, our case did not change its KA-like appearance for over 6 years, but recurred as an ordinary OKC 8 years after the surgery. Consequently, the present lesion belongs to a rare

F. Ide (✉) · K. Mishima · I. Saito
Department of Pathology,
Tsurumi University School of Dental Medicine,
2-1-3 Tsurumi, Tsurumi-ku, 230-8501 Yokohama, Japan
e-mail: ide-f@tsurumi-u.ac.jp
Tel.: +81-45-5808360
Fax: +81-45-5722888

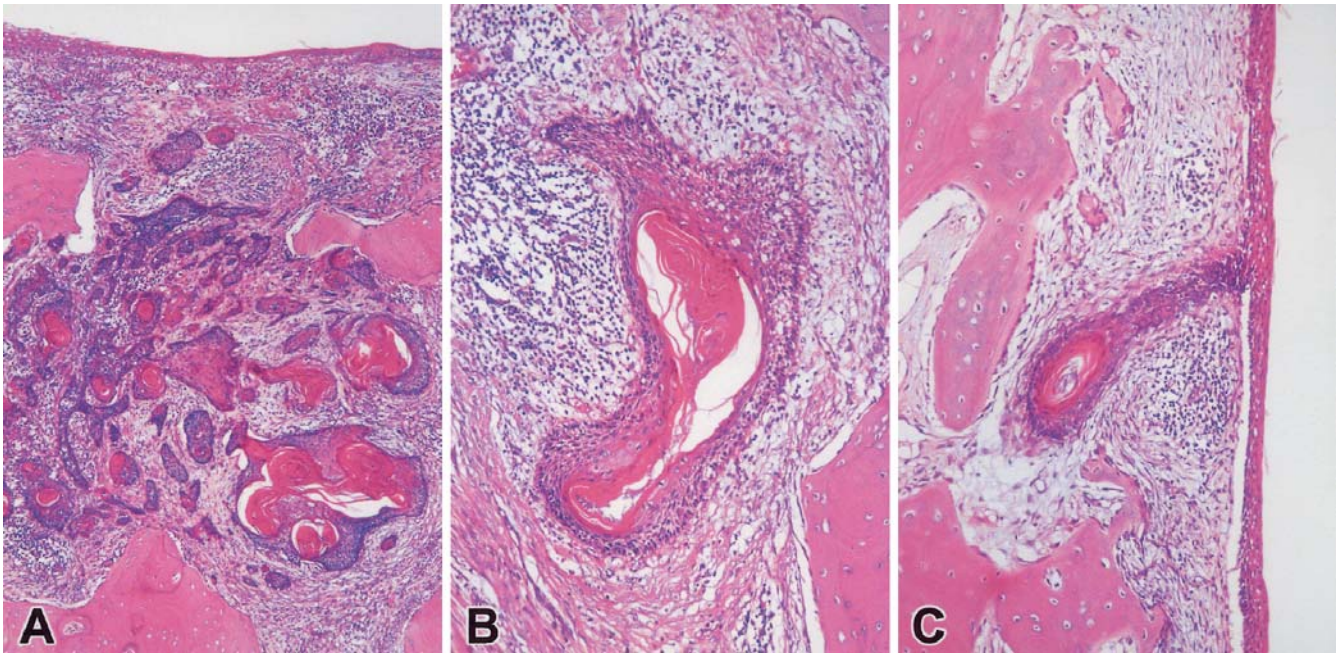



**Fig. 1** Solid-cystic epithelial lesion excised in 1984. **A** Solid component invading cancellous bone. **B** Representative solid follicle showing central keratinization. **C** Cystic component lined by thin squamous epithelium of uniform thickness. Note detachment and down-growth of cyst epithelium

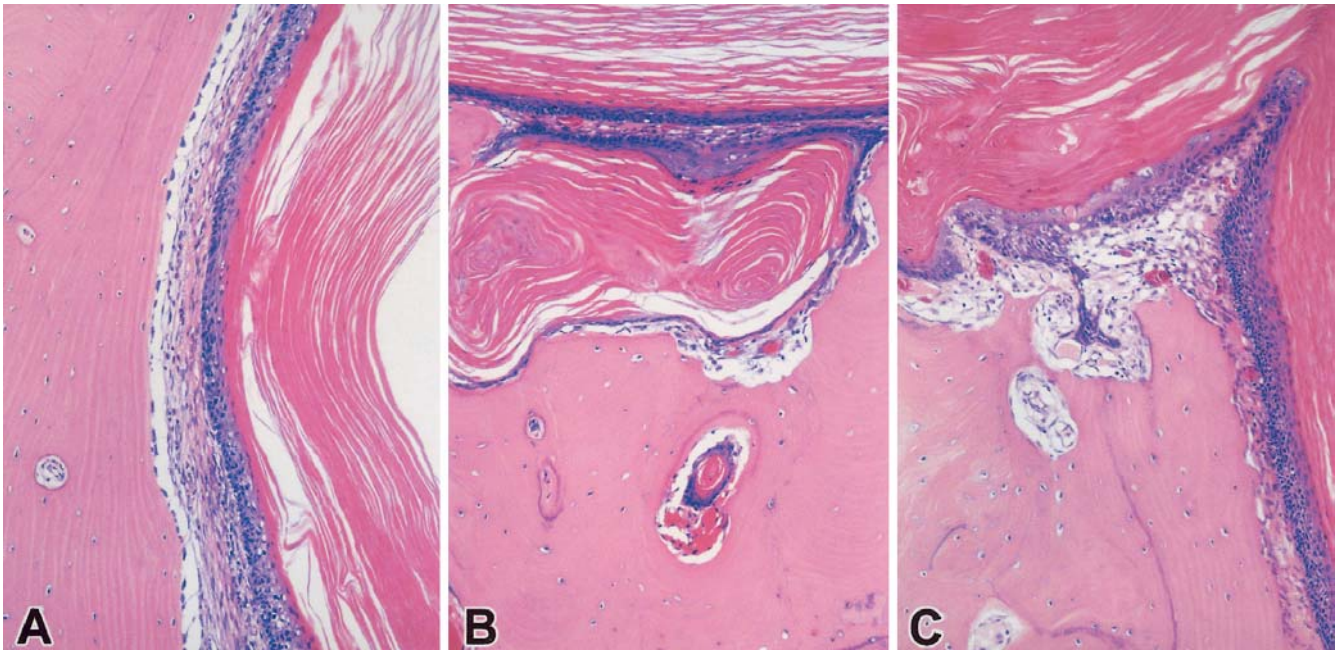



**Fig. 2** Multiple keratinizing cysts resected in 1998. **A** Lining epithelium showing pathognomonic features of odontogenic keratocyst. **B** Microcysts within marrow spaces. **C** Finger-like proliferation of cyst epithelium

neoplastic variant of OKC separable from KA. Based on our experience and that in the literature [3, 8], the solid form of OKC behaves as a benign, locally invasive tumor with a propensity for recurrence. It is important to realize that a solid-cystic tumor variant of OKC could be confused with KA.

## References

1. Altini M, Slabbert H de V, Johnston T (1991) Papilliferous keratoameloblastoma. J Oral Pathol Med 20:46–48
2. Collini P, Zucchini N, Vessecchia G, Guzzo M (2002) Papilliferous keratoameloblastoma of mandible: a papillary

ameloblastic carcinoma. Report of a case with a 6-year follow-up and review of the literature. Int J Surg Pathol 10:149–155
3. Ide F, Saito I (2003) Many faces of odontogenic keratocyst. Oral Oncol 39:204–205
4. Minic AJ (1992) Primay intraosseous squamous cell carcinoma arising in a mandibular keratocyst. Int J Oral Maxillofac Surg 21:163–165
5. Norval EJG, Thompson IOC, van Wyk CW (1994) An unusual variant of keratoameloblastoma. J Oral Pathol Med 23:465–467
6. Omura S, Kawabe R, Kobayashi S, Mizuki N (1997) Odontogenic keratocyst appearing as a soap-bubble or honeycomb radiolucency: report of a case. J Oral Maxillofac Surg 55:185–189
7. Said-Al-Naief NAH, Lumerman H, Ramer M, Kopp W, Kringstein GJ, Persenchino F, Torno R (1997) Keratoameloblastoma of the maxilla. A case report and review of the literature. Oral Surg Oral Med Oral Pathol Oral Radiol Endod 84:535–539
8. Shear M (2002) The aggressive nature of the odontogenic keratocyst: is it a benign cystic neoplasm? Part 1. Clinical and early experimental evidence of aggressive behavior. Oral Oncol 38:219–226
9. Siar CH, Ng KH (1993) 'Combined ameloblastoma and odontogenic keratocyst 'or' keratinizing amelobastoma'. Br J Oral Maxillofac Surg 31:183–186
10. Takeda Y, Satoh M, Nakamura S, Ohya T (2001) Keratoameloblastoma with unique histological architecture: an undescribed variation of ameloblastoma. Virchows Arch 439:593–596
11. Vered M, Dayan D, Buchner A (2002) Multicystic (solid) variant of keratocyst (abstract). J Oral Pathol Med 31:312–313

Virchows Arch (2003) 442:504–506
DOI 10.1007/s00428-003-0806-2

LETTER TO THE EDITOR

**Chris Jones · Reuben Tooze · Sunil R. Lakhani**

# Malignant adenomyoepithelioma of the breast metastasizing to the liver

Received: 18 September 2002 / Accepted: 15 January 2003 / Published online: 12 April 2003
© Springer-Verlag 2003

Sir,

Tumors with myoepithelial cell component have been recognized for some time within the salivary gland and, although rare, have also been described in the breast [2, 3, 5]. Examples include adenoid cystic carcinoma, adenomyoepithelioma, low-grade adenosquamous (syringomatous) carcinoma, pure malignant myoepithelioma (myoepithelial carcinoma) and poorly differentiated myoepithelial-rich breast carcinoma.

The morphology of tumors showing myoepithelial differentiation is generally different to that of tumors derived from luminal cells. Pure myoepithelial carcinomas tend to resemble sarcomas by having a predominantly spindle cell pattern of growth. Although there are only a few reports in the literature, it seems that no fewer than 50% of the published cases had an aggressive behavior [2]. Metastases have been described in five reports, with sites including ribs, lumbar spine, bones, lung and brain, lung, regional lymph nodes and jaw.

We have previously reported molecular cytogenetic data on pure myoepithelial carcinomas using comparative genomic hybridization (CGH) analysis [4]. While myoepithelial carcinomas showed overlap in the regions of DNA copy number change relative to ductal carcinomas of no special type (IDC-NST), they exhibited far fewer genetic alterations. The most common changes were losses at 11q, 16p, 16q, 17p and 17q, aberrations frequently seen in invasive ductal carcinomas. Given the rarity of myoepithelial cell transformation, and their aggressive behavior, these regions may harbor critical genes in breast tumorigenesis.

Unlike pure myoepithelial carcinomas, adenomyoepitheliomas of the breast contain a proliferation of both the luminal glandular component as well as myoepithelial cells. Reports in the literature are primarily as single case reports or small series [1]. Although generally considered to be benign, malignant and metastatic adenomyoepitheliomas have been reported. The epithelial component may form solid nests or groups, ducts, cystic trabecular, pseudo-papillary or papillary structures. The myoepithelial component is arranged around the epithelial component and can form solid strands, trabeculae or even larger sheets, and are usually polygonal or spindle shaped.

We report a case of adenomyoepithelioma in the breast with a pure spindle cell tumor metastases to the liver. CGH analysis was used to investigate the clonal relationship between the glandular and myoepithelial components of the primary lesion and the spindle cell metastasis.

## Case report

A 71-year-old woman presented with a 2-month history of a right breast mass which may have been present longer, as she had not undertaken breast self-examination for 3 years. A 2×3-cm mass in the lower outer quadrant of the right breast was reported as suspicious of carcinoma by mammography and fine-needle aspiration (FNA) cytology. Right segmental mastectomy with axillary node clearance was performed. The patient was treated with tamoxifen which was continued for 2 years until her death. At postmortem, multiple tumor deposits were found in the right lobe of the liver. No other evidence of metastatic disease was present. Detailed examination of the breast did not reveal any residual or recurrent tumor.

C. Jones · S. R. Lakhani (✉)
The Breakthrough Toby Robins Breast Cancer Research Centre,
Chester Beatty Laboratories, Institute of Cancer Research,
Fulham Rd, Mary-Jean Mitchell Green Building, London,
SW3 6JB, UK
e-mail: lakhani@icr.ac.uk
Tel.: +44-207-9706085
Fax: +44-207-9706084

R. Tooze
Department of Histopathology,
Addenbrookes' Hospital,
Cambridge, UK

S. R. Lakhani
The Royal Marsden Hospital,
London, UK

*Present address:*
R. Tooze, Department of Histopathology,
St James's University Hospital,
Leeds, UK

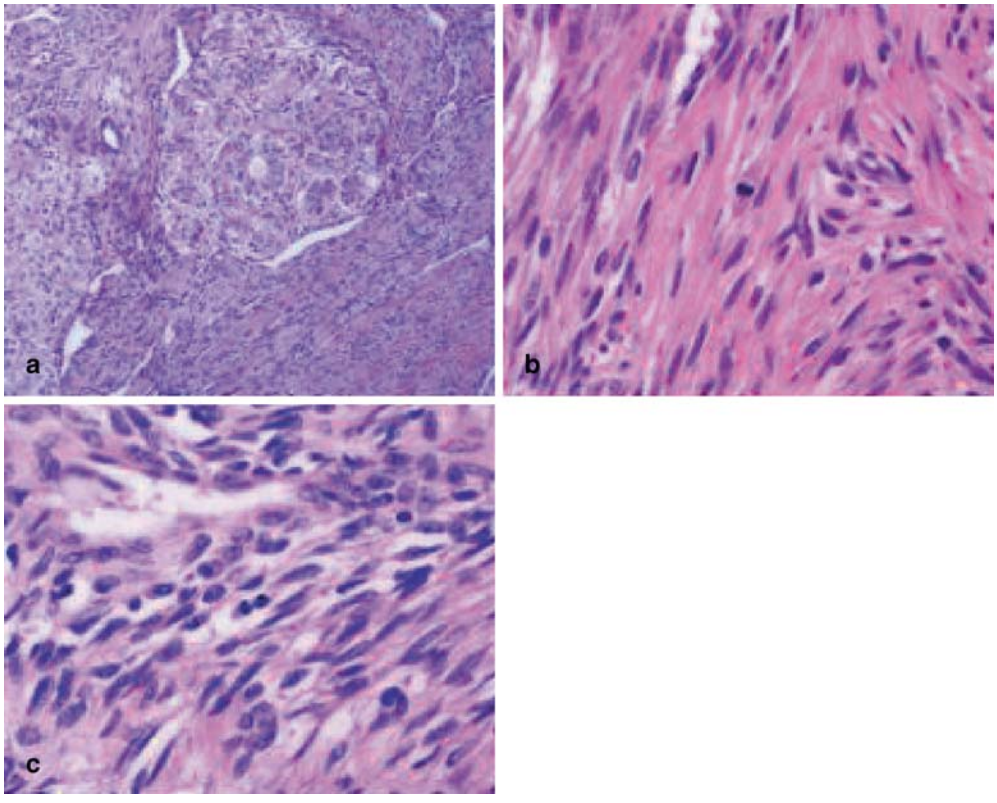



**Fig. 1** Malignant adenomyoepithelioma of the breast. **a** Adjacent glandular and spindle cell components, hematoxylin and eosin (H&E) ×100. **b** Spindle cell component, high power showing mitoses, H&E ×400. **c** Spindle cell metastasis in the liver, high power, showing mitoses, H&E ×400

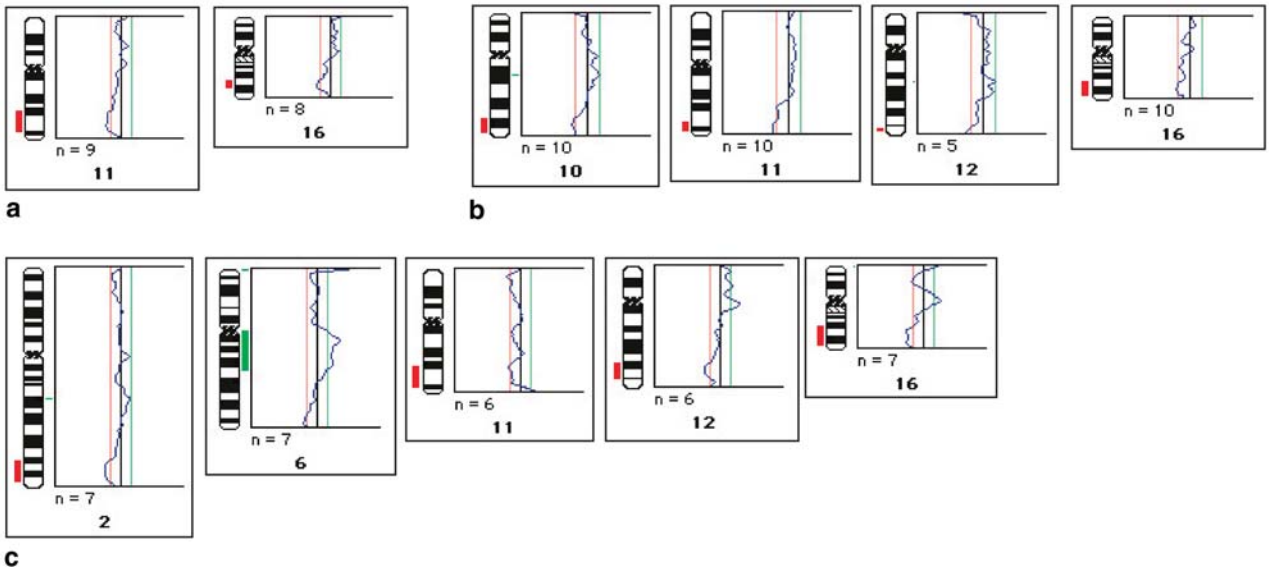



**Fig. 2** **a** Comparative genomic hybridization (CGH) data from adenomyoepithelioma, glandular component, showing losses at 11q23–q24 and 16q22–q23. **b** CGH data from myoepithelial carcinoma, spindle component, showing losses at 10q25, 11q23–q24, 12q24 and 16q22–q23. **c** CGH data from liver metastasis showing loss at 2q35–q37, gain at 6q12–q16, loss at 11q23–q24, loss at 12q24 and loss at 16q22–q24

The breast tumor was a circumscribed mass measuring 3×3×2 cm within 0.5 cm of the inferior line of resection. Microscopically, the tumor showed a mixed glandular and spindle cell morphology. (Fig. 1a). The spindle cell component was extensive in some areas and had increased mitotic activity (up to 4 per 10 high power fields, Fig. 1b) and focal areas of necrosis. Although a diagnosis of an adenomyoepithelioma was made, it was noted that the mitotic activity and necrosis was suggestive of a more aggressive phenotype. No vascular invasion was seen, and staging investigations were negative. At autopsy, multiple tumor deposits were seen in the right lobe of the liver. Microscopically, these were pure spindle cell tumors with a fascicular and focally haemangiopericytomatous pattern, and no evidence of a glandular/epithelial component (Fig. 1c).

**Table 1** Immunohistochemical findings

| Antibody | Primary tumor | | | Metastasis |
|---|---|---|---|---|
| | Glandular areas | | Spindle cells | |
| | Inner cells | Outer cells | | |
| MNF116 | Positive | Negative | Negative | Negative |
| AE1/AE3 | Positive | Negative | Negative | Negative |
| Vimentin | Positive | Positive | Positive | Positive |
| SMA | Negative | Positive | Negative | Negative |
| S100 | Negative | Positive | Negative | Negative |
| SMMHC | Negative | Positive | Negative | Negative |
| GFAP | Negative | Negative | Negative | Negative |
| Desmin | Negative | Negative | Negative | Negative |
| CD34 | Negative | Negative | Negative | Negative |
| Calponin | Negative | Positive | Negative | Negative |
| CK14 | Positive | Positive | Negative | Negative |

The results of immunohistochemical staining of the primary tumor and metastasis against a range of myoepithelial markers are given in Table 1. The inner cells of the glandular component of the primary tumor showed immunopositivity against MNF116, AE1/AE3 and vimentin. This was in contrast to the outer epithelial cells which showed positivity for vimentin, SMA, S100, SMMHC, calponin and CK14, consistent with myoepithelial cells. The solid spindle cell component in the primary tumor was negative for all markers apart from vimentin. The same pattern was seen in the metastatic spindle cell tumors in the liver.

Microdissection, DNA extraction and CGH analysis were carried out as described previously [4]. The data for the CGH analysis of primary tumor and metastasis is shown in Fig. 2. Both the breast and liver tumors showed an overall pattern of genetic alterations by CGH resembling myoepithelial tumors, with few regions of copy number change compared with invasive ductal carcinomas [4]. The glandular component of the primary tumor showed losses at 11q23–q24 and 16q22–q23 (Fig. 2a), while the spindle cell component of the primary tumor showed these losses as well as loss at 10q25 and 12q24 (Fig. 2b). The liver metastasis showed losses at 2q35–q37, 11q23–q24, 12q24 and 16q22–q24, and a gain at 6q12–q16 (Fig. 2c).

## Discussion

Our interpretation of these results is that the losses at chromosomes 11q and 16q indicate a common origin for the two components of the primary adenomyoepithelioma. The undifferentiated spindle cell component then acquired an additional loss at 12q prior to metastasis to the liver, any further genetic alterations occurring subsequent to this event.

As well as adding to the literature on distant metastases of malignant adenomyoepithelioma, this data has implications for the origin of the two components of these biphasic tumors, suggesting a common origin prior to differentiation and metastasis. The spindle cell component, which morphologically resembles a pure myoepithelial cell tumor, also has a molecular cytogenetic profile that is similar to pure myoepithelial carcinomas. Given the clinically aggressive nature of these lesions, it is perhaps not surprising that it is the spindle cell component of the primary tumor that has metastasized to the liver in this patient. In an analogous manner to pure myoepithelial carcinomas, the few genetic alterations exhibited by this tumor may make it an excellent model to study the critical pathogenic events in breast tumorigenesis and metastasis.

**Acknowledgements** Supported in part by Breakthrough Breast Cancer, the Ludwig Institute for Cancer Research and the Sydney and Phyllis Goldberg Memorial Charitable Trust.

## References

1. Bult P, Verwiel JMM, Wobbes T, Kooy-Smits MM, Biert J, Holland R (2000) Malignant adenomyoepithelioma of the breast with metastasis in the thyroid gland 12 years after excision of the primary tumour. Case Report and review of the literature. Virchows Arch 436:158–166
2. Foschini MP, Eusebi V (1998) Carcinomas of the breast showing myoepithelial cell differentiation. Virchows Arch 432:303–310
3. Hamperl H (1970) The myothelia (myoepithelial cells) normal state; regressive changes; hyperplasia; tumors. Curr Top Pathol 53:161–213
4. Jones C, Foschini MP, Chaggar R, Lu Y-J, Wells D, Shipley JM, Eusebi V, Lakhani SR (2000) Comparative genomic hybridization analysis of myoepithelial carcinoma of the breast. Lab Invest 80:831–836
5. Tavassoli FA (1991) Myoepithelial lesions of the breast. Myoepitheliosis, adenomyoepithelioma, and myoepithelial carcinoma. Am J Surg Pathol 15:554–568

Virchows Arch (2003) 442:507–508
DOI 10.1007/s00428-003-0792-4

LETTER TO THE EDITOR

**Isabelle Peyrottes · Antoine Thyss · Georges Maire · Jean-Christophe Machiavello · Agnès Angelozzi · Florence Pedeutour**

# Clonal chromosomal abnormality induced by surgically retained foreign bodies: t(9;17)(q21;p13.3) in a textiloma

Received: 27 December 2002 / Accepted: 7 February 2003 / Published online: 12 April 2003
© Springer-Verlag 2003

Sir,

textilomas are non-neoplastic granulomatous proliferations induced by foreign bodies, such as surgical sponges inadvertently left in operative wounds during visceral or bone surgery. They are composed of cotton matrix surrounded by granulomatous reaction. They may stay asymptomatic for years and be discovered incidentally, or, in contrast, their presence may have a variety of consequences such as pain, occlusion, fistula formation or sepsis [4]. They can also induce the formation of tumors that mimic sarcomas. To the best of our knowledge, there has been no previous karyotypic information concerning textilomas. We have analyzed the case of a cytogenetically abnormal textiloma that involved alterations of chromosomes 9 and 17.

The patient was a 75-year-old woman with a 3-month history of a growing mass in her right thigh. She was otherwise healthy and presented with an unremarkable medical history, except for a fracture of the right femur followed by an osteosynthesis 30 years ago. No loco-regional adenopathy was detected. The tomodensimometric and nuclear magnetic resonance analyses showed a 12-cm well-circumscribed tumor with heterogeneous content. The femoral shaft was not altered. Considering the clinical and radiological features, a diagnosis of sarcoma could not be excluded and a fresh fragment was prepared

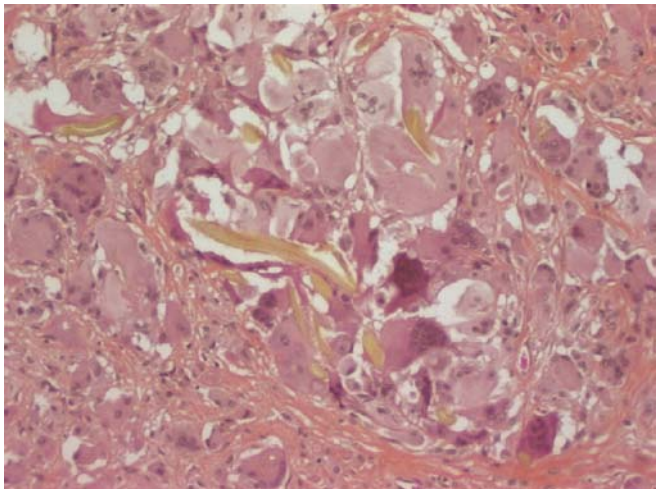


**Fig. 1** Multinucleated giant cell reaction with intracellular foreign bodies in a case of textiloma. Hematoxylin-eosin-safran coloration (magnification ×250)




**Fig. 2** Partial R-banded karyotype showing the t(9;17)(q21;p13.3). The *arrow* indicates the abnormal chromosome 9 and the *arrowhead* indicates the abnormal chromosome 17

I. Peyrottes
Laboratoire d'Anatomie Pathologique,
Centre Antoine Lacassagne,
Nice, France

A. Thyss
Service d'Oncologie,
Centre Antoine Lacassagne,
Nice, France

G. Maire · A. Angelozzi · F. Pedeutour (✉)
Laboratoire de Génétique, Université de Nice–Sophia–Antipolis,
CHU de Nice, Hôpital de l'Archet, BP 3079,
06202 Nice cedex 3, France
e-mail: pedeutou@unice.fr
Tel.: +33-4-92036456
Fax: +33-4-92036465

J.-C. Machiavello
Service de Chirurgie,
Centre Antoine Lacassagne,
Nice, France

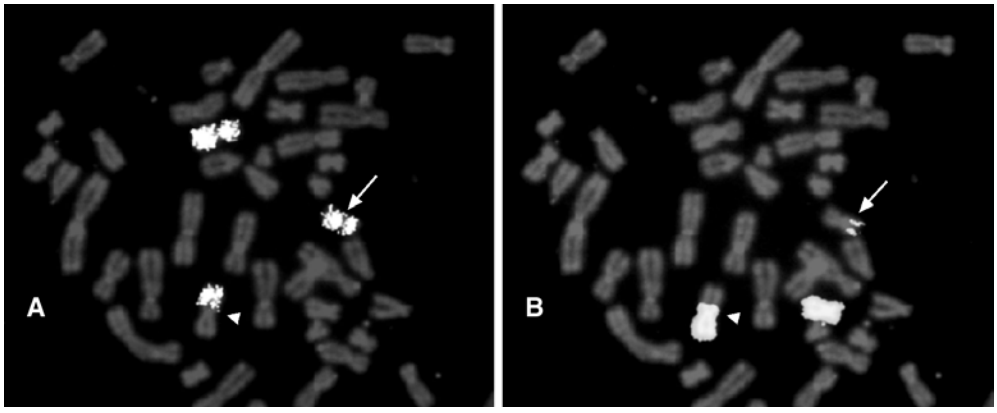



**Fig. 3** Fluorescence in situ hybridization (FISH) analysis on a metaphase cell of the textiloma with whole chromosome painting probes for chromosome 9 (**A**) and 17 (**B**). The *arrow* indicates the abnormal chromosome 9 and the *arrowhead* indicates the abnormal chromosome 17. The chromosomes are counterstained with 4,6,diamidino–2–phenylindole (DAPI)

for cytogenetic analysis simultaneously to the histopathological diagnosis after the surgical complete excision. Polymorphous granulomatous inflammatory alterations and macrophagia of an amorphous material corresponding to the degradation products of a textiloma were observed (Fig. 1). A fresh fragment of the tumor was prepared for cytogenetic analysis. After mechanical and collagenase dissociation of the tumor fragment, the cells were grown in flasks and in chamber slides for 14 days and harvested for chromosomal preparations according to standard procedures [3]. Ten R-banded metaphase cells were studied, and eight of them showed a balanced reciprocal translocation between the long arm of chromosome 9 and the short arm of chromosome 17. The karyotype was: 46,XX,t(9;17)(q21;p13.3)[8]/46,XX[2] (Fig. 2). The rearrangement was confirmed in ten additional cells by fluorescence in situ hybridization (FISH) analysis using whole chromosome painting probes specific for chromosome 9 and 17 (Fig. 3).

Several recent reports have demonstrated the presence of clonal cytogenetic aberrations in other reactive non-neoplastic lesions such as Dupuytren's contracture, gliosis, osteoarthritis, and thyroid and prostate hyperplasia [1, 2]. Numerical aberrations, such as gain of chromosomes 7, 5, 8 and 12 were the most common changes. In a few cases, structural aberrations were also described. Interestingly, the 17p13 region has been shown to be recurrently involved in aneurysmal bone cysts, the nature of which—reactive or neoplastic—is still debated [5].

Our results show that chromosomal anomalies are also observed in textilomas. Whether these clonal chromosomal alterations provide a selective advantage to support the reactive inflammatory mechanisms is a hypothesis that warrants further investigations.

## References

1. Broberg K, Limon J, Palsson E, Lindstrand A, Tokvig–Larsen S, Mandahl N, Mertens F (1997) Clonal chromosome aberrations are present in vivo in synovia and osteophytes from patients with osteoarthritis. Hum Genet 101:295–298
2. Dal Cin P, De Smet L, Sciot R, Van Damme B, Van den Berghe H (1999) Trisomy 7 and trisomy 8 in dividing and non-dividing tumor cells in Dupuytren's disease. Cancer Genet Cytogenet 108:137–140
3. Limon J, Dal Cin P, Sandberg AA (1986) Application of long term collagenase disaggregation for the cytogenetic analysis of human solid tumors. Cancer Genet Cytogenet 23:305–312
4. Le Néel J-C, de Cussac J-B, Dupas B, Letessier E, Borde L, Eloufir M, Armstrong O (1994) Textilomas. A series of 25 cases and a review of the literature. Chirurgie 120:272–276
5. Winnepenninckx V, Debiec-Rychter M, Jorissen M, Bogaerts S, Sciot R (2001) Aneurysmal bone cyst of the nose with 17p13 involvement. Virchows Arch 439:636–639

Virchows Arch (2003) 442:509–510
DOI 10.1007/s00428-003-0788-0

LETTER TO THE EDITOR

**Luca Di Tommaso · Carmine Fortunato · Vincenzo Eusebi**

# Meningothelial hamartoma located in the forehead

Received: 16 December 2002 / Accepted: 7 February 2003 / Published online: 12 April 2003
© Springer-Verlag 2003

Sir,

We report a case of meningothelial hamartoma of the forehead in a 28-year-old man. The lesion manifested as a single, painless nodule that had been present for many years, located in the midline. Its size increased recently and it was removed surgically for esthetical reasons. The patient showed no evidence of intracranial tumors or defect of calvarias at the computed tomography (CT) scan and denied previous trauma of the site. The overall clinical conditions were good; the initial clinical impression was that of a well-circumscribed lesion of the dermis/subcutis without involvement of the epidermis or connection to the underlying skull. Grossly the lesion presented as a 1.5-cm lobulated, soft mass characterized by gray to white tissue on the cut surface. At scanning magnification the lesion was constituted by an admixture of adipose, muscle, and fibrous tissue together with clusters of cuboidal cells with scant eosinophilic cytoplasm and vesicular nuclei. Mitoses were absent, as well as nuclear atypia. Numerous nuclear pseudoinclusions were observed (Fig. 1). Slit-like channels lined by similar cells were seen throughout the lesion. The cells, either lining the channels or arranged in solid clusters, showed strong positivity for epithelial membrane antigen (EMA; Dako; Fig. 2) and vimentin (Dako);

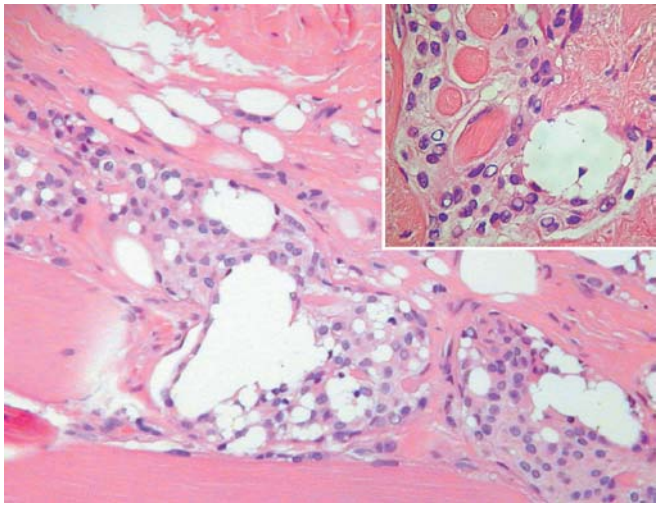


**Fig. 1** Clusters of cuboidal cells with eosinophilic cytoplasm are admixed with fibrous, adipose, and muscular tissue (H&E, ×10). *Inset*: Numerous nuclear pseudoinclusions are evident (H&E, ×40)

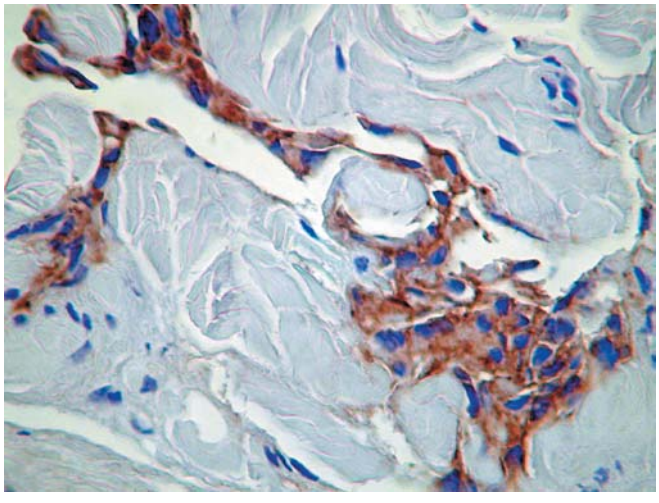


**Fig. 2** Clusters of cuboidal cells and similar cells lining pseudovascular channels are labeled with epithelial membrane antigen (IIC, ×40)

L. Di Tommaso · V. Eusebi
Department of Anatomic Pathology, Bellaria Hospital,
University of Bologna,
Bologna, Italy

C. Fortunato
Servizio di Anatomia Patologica,
Ospedale S. Liberatore,
Atri (Te), Italy

L. Di Tommaso (✉)
Dipartimento di Oncologia, Ospedale Bellaria, Sezione di Anatomia, Istologia e Citologia Patologica "Marcello Malpighi", Università di Bologna,
via Altura 3, 40139 Bologna, Italy
e-mail: luca.ditommaso@ausl.bo.it
Tel.: +39-051-6225523
Fax: +39-051-6225759

cytokeratin (Dako), melanoma antigen recognized by T cells (MART-1; Dako), and thyroid transcription factor 1 (TTF1; Neomarkers) were negative. Rare and scattered cells showed a weak positivity for S-100 (Dako). Clinical, morphological, and immunohistochemical features were consistent with the diagnosis of meningothelial hamartoma; lack of cystic spaces and rudimentary stalk led to the exclusion of type 1 extracranial meningioma, while type 2 extracranial meningioma was excluded, because these lesions should be indistinguishable by ordinary intracranial meningioma [4].

Previously reported meningothelial hamartomas were described exclusively in the scalp region, the most likely explanation for this feature being the presence of displaced, ectopic meningothelial remnants in this site [1, 2, 5]. It has been suggested that these residues may represent rudimentary meningoceles [4]; nevertheless it has been reported recently in a mouse model that meningeal coverings are neural crest-derived structures, thus suggesting that meningothelial rests represent the result of an abortive migration from neural crests [3].

To the best of our knowledge, this is the first case of meningothelial hamartoma located in the forehead. Therefore it seems that the skull is not the only site of origin for these lesions.

## References


1. Gottoschalk J, Jautzke G, Sprung C, Schreiner C, Riebel T (1992). Meningothelial hamartoma of the scalp. A case report with immunohistochemical studies. Zentralbl Pathol 138(5): 355–361
2. Hirakawa E, Kobayashi S, Terasaka K, Ogino T, Terai Y, Ohmori K (1992). Meningeal hamartoma of the scalp. A variant of primary cutaneous meningioma. Acta Pathol Jpn 42(5):353–357
3. Jang X, Iseki S, Maxson RE, Sucov HM, Morriss-Kay GM (2001). Tissue origin and interactions in the mammalian skull vault. Dev Biol 241(1):106–116
4. Lopez DA, Silvers DN, Helwig EB (1974). Cutaneous meningiomas. A clinicopathologic study. Cancer 34:728–744
5. Suster S, Rosai J (1990). Hamartoma of the scalp with ectopic meningothelial elements. A distinctive benign soft tissue lesion that may simulate angiosarcoma. Am J Surg Pathol 14(1):1–11

 © Springer-Verlag 2003

# ANNOUNCEMENTS

6–7 June 2003
**14th Ljudevit Jurak International Symposium on Comparative Pathology**
Zagreb, Croatia

Under the auspices of the European Society of Pathology and Academy of Medical Sciences of Croatia

The aim of this symposium is multidisciplinary approach to human and animal pathology. The main topic of this year' symposium is dermatopathology but all papers regarding other symposium sections (Pathomorphology of human and animal diseases, Iatrogenic, environmental and rheumatological pathology) are also welcome. There will be also slide seminars on histopathology and cytopathology, workshop on nontumor dermatopathology and quiz on pathology. All pathologists are invited to present their work concerning human and animal pathology or both as oral or poster presentations.

*For further information see:*
http://.www.kbsm.hr/Jurak/symposium.htm or contact
Ljudevit Jurak University Department of Pathology,
Sestre milosrdnice University Hospital, Vinogradska 29,
10000 Zagreb, Croatia
E-mail: juraks@kbsm.hr, dtomas@kbsm.hr
Phone: 385 1 3787 909
Phone/fax: 385 1 3787 244

9–11 June 2003
**Multi-Disciplinary Courses on Breast Disease**

Three day course. The first part is multi-disciplinary. Thereafter the different specialties meet to accommodate their own special requirements.

Course Tutors: Dr. I.O. Ellis, Dr. S.E. Pinder, Dr. A.H.S. Lee

| | | |
|---|---|---|
| Course fees: | NHS | £370.00 |
| | Non-NHS | £415.00 |
| | Overseas | £550.00 |

includes refreshments but not accommodation

*For further information please contact:*
Education Administrators
Nottingham International Breast Education Centre,
City Hospital, Hucknall Road, Nottingham NG5 1PB
Tel.: 0115 969 1689; Fax: 0115 962 7707
E-mail: enquiries@nibec.co.uk; www.nibec.co.uk

6 September 2003
**EUROPEAN BOARD OF PATHOLOGY**
**7th EXAMINATION 2003**
Ljubljana, Slovenia

The Seventh Examination of the European Board of Pathology will be held in Ljubljana, Slovenia, Saturday September 6, 2003. This Examination precedes the 19th Congress of the ESP.

*For information about the examination and application forms can be obtained from:*
Prod. Dr. J.G. van den Tweel
(chairman of The Examination Board)
Utrecht University Medical Center
Department of Pathology, H 04.312
P.O. Box 85500
3508 GA Utrecht
Fax: ++31-30-2544990
Tel.: ++31-30-2506565
e-mail: j.vandentweel@lab.azu.nl *or*
W.vanBragt@lab.azu.nl (secretary)
The same information is also available from Internet:
http:www.uems.be/pathol.htm, see index 2 and 3

6–11 September 2003
**19th European Congress of Pathology**
Ljubljana, Slovenia

The largest congress of pathologists in Europe in 2003, covering basic diagnostic standards, update scientific achievements and recent technical advances in all areas of pathology at 4 keynote lectures, 30 symposia, 21 short courses, 21 slide seminars, 14 special presentations, 2 round table discussions and free paper and poster sessions. Internationally recognized invited speakers are from throughout Europe and the USA.

*Updated information on the congress website:* http://www.cd-cc.si

13 October 2003
**Continuing Medical Education**

One day Multi-Disciplinary Update courses

Course fee: £95.00

*For further information please contact:*
Education Administrators
Nottingham International Breast Education Centre
City Hospital, Hucknall Road, Nottingham NG5 1PB
Tel.: 0115 969 1689; Fax: 0115 962 7707
E-mail: enquiries@nibec.co.uk; www.nibec.co.uk

17–19 November 2003
**Multi-Disciplinary Courses on Breast Disease**

Three day course. The first part is multi-disciplinary. Thereafter the different specialties meet to accommodate their own special requirements.

Course Tutors: Dr. I.O. Ellis, Dr. S.E. Pinder, Dr. A.H.S. Lee

| | | |
|---|---|---|
| Course fees: | NHS | £370.00 |
| | Non-NHS | £415.00 |
| | Overseas | £550.00 |

includes refreshments but not accommodation

*For further information please contact:*
Education Administrators
Nottingham International Breast Education Centre,
City Hospital, Hucknall Road, Nottingham NG5 1PB
Tel.: 0115 969 1689; Fax: 0115 962 7707
Email: enquiries@nibec.co.uk; www.nibec.co.uk

Virchows Arch (2003) 442:512–526

# EUROPATH NEWS 2/2003

European Society
of
Pathology

**Editors**
Prof. Niki J. Agnantis
University Department of Pathology
Medical School of Ioannina
GR-45110 Ioannina, Greece
Tel.: +302-651-097795
Fax: +302-651-097858
e-mail: nagnanti@cc.uoi.gr

Dr. Bjørn Risberg
Department of Pathology
The Norwegian Radium Hospital
0310 Oslo, Norway
Tel.: +47-22934174
Fax: +47-22508554
e-mail: brisberg@labmed.uoi.no

**The newsletter of the European Society of Pathology, EUROPATH NEWS, is sponsored by Leica Microsystems Nussloch GmbH**

## *Newsletter of the European Society of Pathology*

Dear Colleagues,

We are very pleased to convey to you the second 2003 issue of our ESP Newsletter.

This issue begins with the Address by the President of the European Society of Pathology, Prof. Gianni Bussolati. It continues with a text "in memoriam" dedicated to the memory of Prof. Dr. Victor Swaen and written by Prof. Dr. U.J.G.M. van Haelst. Also included are announcements of forthcoming conferences, seminars and tutorial courses. Furthermore, information is also provided about the formulated Working Groups. Do not hesitate to provide us with material on the activities of your department and even share with us, through Europath News, your problems. Last but not least, remember that we must increase the number of ESP members. This is a vital matter for the continuity of our Society. You can easily sign up by using the application form for membership (which is included in each issue of the Europath News) or going to our new **website** (whose address is also included). At the same time, you could exert influence on the younger staff in your department to join us.

With warmest thanks and regards,



Prof. Niki J. Agnantis
Chief Editor



Dr. Bjørn Risberg
Assistant Editor

### Address by the President of the European Society of Pathology, Gianni Bussolati

Dear Member,

I do hope you have already planned to come to Ljubljana for our Congress in September 2003 (http://www.cd-cc.si/ecp).

Prof. Dusan Ferluga and other Slovenian colleagues of the Organizing Committee have done their best to produce a very attractive program, providing a good balance of the different areas of interest of our discipline and including a long list of experts and of the best of possible speakers, who will present Keynote Lectures, Symposia, Special Presentations, Round Table Discussions, Short Courses and Slide Seminars. In addition to an update on current diagnostic standards, space will be given to modern techniques and breakthroughs, such as those made real by molecular genetics.

All practising pathologists and scientists are kindly invited to present their scientific achievements and exchange their professional experiences through Free Paper and Poster Sessions. The best Free Papers will be acknowledged by giving the authors the opportunity to present their achievements at the plenary session, at which the authors of the three best Poster Presentations will additionally receive special Awards.

Pre-congress meetings on pulmonary pathology and on non-neoplasic nephropathology have been

arranged, and a three-day Joint Meeting of the European and North American Society of Head and Neck Pathology has also been organized.

In the run-up to its bi-annual meeting, the Society is also heavily involved in a number of other activities.

On 10–13 May, Gavino Faa is organizing the XIIIth EurocellPath Course in Cagliari, Sardinia. The present course is devoted to molecular pathology.

EurocellPath courses are traditionally dedicated to young pathologists wishing to meet experts and to discuss scientific topics. Scientists interested in the molecular mechanisms of carcinogenesis, in genetic disregulations as diagnostic tools in Pathology, and in the molecular pathology of metabolic diseases will find in Sardinia splendid occasions for being mentally stimulated. I would also note that the location is „notorious“ for its very enjoyable character.

EScoP branch courses will be held on 25–28 May in Moscow, on 7–9 June in Ankara and on 14–18 June in Krakow, reproducing courses already successfully completed in Turin on Head and Neck Pathology (course leader: A. Cardesa), Thyroid Pathology (course leader: M. Sobrinho-Simões), and Pulmonary Pathology (course leader: H. Popper).

On 21–24 June, Jahn Nesland will also organize a conference on Tumor Cell Invasion, to be held in Lillehammer, Norway.

As you can see, in our Society you can find many opportunities to open your mind to new areas and to go deeper into topics of your present interest.

Many good reasons to be proud to be a member of the European Society of Pathology.

Yours sincerely,

Gianni Bussolati



Gianni Bussolati
President of the European Society of Pathology

## In Memoriam Prof. Dr. Victor Swaen (1921–2003)



Prof. Dr. Victor Swaen

It is the sad duty of the Executive Committee of the ESP to announce that Prof. Dr. Victor Swaen passed away on 31 January 2003 at the age of 81.

Professor Swaen protected and promoted the financial interests of the Society for 23 years (1964–1987) not only as an enthusiastic member of the first Council/Executive Committee since its inception in 1964 but even more so as its first treasurer. On the occasion of the 11th. European Congress of Pathology in Prague in 1987 he was elected to Honorary Membership of our Society in appreciation of his talents and commitment.

Colleague Swaen enjoyed occupational success as a critical and reliable diagnostic pathologist and research worker at the department of pathology of the medical faculties of Nijmegen, Amsterdam and then Utrecht, first as lector then as full professor. At the age of 63 he was given emeritus status by the Medical Faculty of Maastricht.

During his retirement he remained a man of enterprise: photography, risky and adventurous journeys and trips in the Saharan desert, exploration of prehistoric caves, diving. At home he intensified his eagerness to learn and could not stop himself from pursuing and uncovering the innermost meaning of things left unclear or mysterious.

He was an amiable and truly gentle person with many good friends in all parts of the world, who, in their condolences, expressed their memories of a friendly and cooperative individual of great humanity.

Professor Swaen was a devoted family man and is survived by his wife Irma, and their four children and two grandchildren.

Nijmegen, March 2003

Prof. Dr. U. J.G.M. van Haelst,
Treasurer ESP

## International Workshop on Intestinal Permeability in Health and Disease, 23–24 May 2003, Patras, Greece

**Conference & Cultural Center of the University of Patras**

Invitation

The organizing committee of the International Workshop on Intestinal Permeability in Health and Disease has the great pleasure of inviting you to Patras, Greece, on 23–24 May 2003. Patras, a city with history that can be traced back to prehistoric times, is located on the northern coast of the Peloponnese and has functioned in the last two centuries as Greece's main link to Central Europe. The metropolitan area has a population of over 250,000 people. The city is famous for its Annual Carnival, Venetial Castle and the internationally known wine company of Achaia Claus. The University of Patras was founded in 1964 and is now located on a 600-acre campus just outside the city at the foot of mountain Panachaikos. Its 18 academic departments offer a wide range of undergraduate and graduate courses and degrees. We are looking forward to your participation in what we believe will be an exciting meeting on Intestinal Permeability in Health and Disease, designed to bring together basic and clinical scientists of diverse specialties in an effort to elucidate an emerging and novel field in medicine. See you in Patras in May 2003.

*General Fees:* 75 Euros, Students free

*Congress venue*

The congress will be held at the University of Patras Convention Center, located on the University Campus. Transportation to and from the hotels will be provided.

*Official language*

English

*Social and cultural events*

Reception at the Achaia Claus winery
Visit to Olympia
Visit to Delphi

*The Organizing Committee*

Scopa Chrisoula
Vagianos Constantin
Charonis Aristidis
Skoutelis Athanassios
Kouraklis Gregory

*Important dates*

*Workshop:* 23–24 May 2003

*Deadline for the receipt of abstracts*

15 February 2003

*Scientific program*

The program will consist of half-hour presentations by the invited speakers, a poster session and ample time for discussion of the topics presented.

*Topics include*

- Molecular basis of intestinal permeability
- Interaction between bacterial and intestinal epithelium
- Endocrine and immunological functions of the intestine
- Effect of inflammation on gut barrier function
- Clinical conditions affecting intestinal permeability (jaundice, sepsis, etc.)
- The impact of luminal content on barrier function

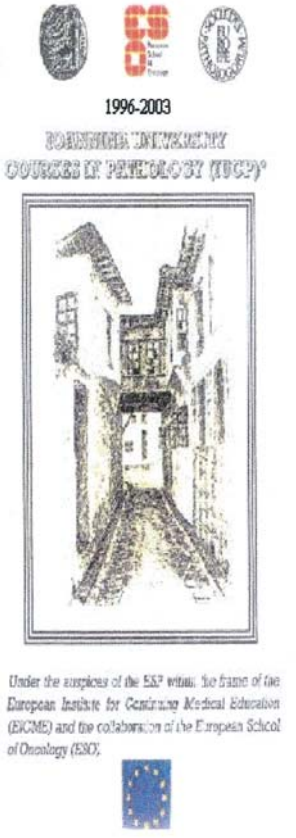
*Invited speakers include*

Alexandridis, T. (Greece)
Anderson, R. (Sweden)
Charonis, A. (Greece)
Deitch, E. (USA)
Filos, K. (Greece)
Jeppson, B. (Sweden)
Kotzabassi, C. (Greece)
Menger, M. (Germany)
Rowlands, B. (England)
Scopa, C. (Greece)
Vagianos, C. (Greece)
Viswanathan, V. (USA)

*Secretariat*

Synedra
Agiou Nikolaou 57
GR-262 21 Patras, Greece
Tel.: +30-610-242999
Fax: +30-610-242997
e-mail: synedra@pat.forthnet.gr




**Ioannina University Courses in Pathology (IUCP)**

**Part one:** Kidneys Pathology-Oncology
27–28 May, 2003
**Part two:** Bladder Pathology-Oncology
29–31 May, 2003

**Faculty**
Alamanos I (Gr)
Briasoulis E (Gr)
Eleftheriades E (Gr)
Kanavaros P (Gr)
Liapis H (USA)
Leontsini M (Gr)
Mairinger T (A)
Mikuz G (A)
Nakopoulou L (Gr)
Pantzaki A (Gr)
Papakostas V (Gr)
Pavlaki K (Gr)
Pentheroudakis G (Gr)
Petraki C (Gr)
Sofikitis N (Gr)
Sotsiou F (Gr)
Tsili A (Gr)

*Registration fees for each part:*
EUROS 400 (200 for residents)
Accommodation (double room, shared)
and full board are included
Account number in EUROS: 359/616930-96
National Bank of Greece, Ioannina, Greece

*Correspondence:*
Prof. Niki J. Agnantis, M.D.,
Institute of Pathology,
University of Ioannina,
Medical School,
University Campus,
45110 Ioannina, Greece
Tel.: +302-651-097795, Fax: +302-651-097858
e-mail: nagnanti@cc.uoi.gr.

For further information please contact
our home page at
http://medlab.cs.uoi.gr/iucp

***(Third announcement)***

**Director-Coordinator: Prof. Niki J. Agnantis**

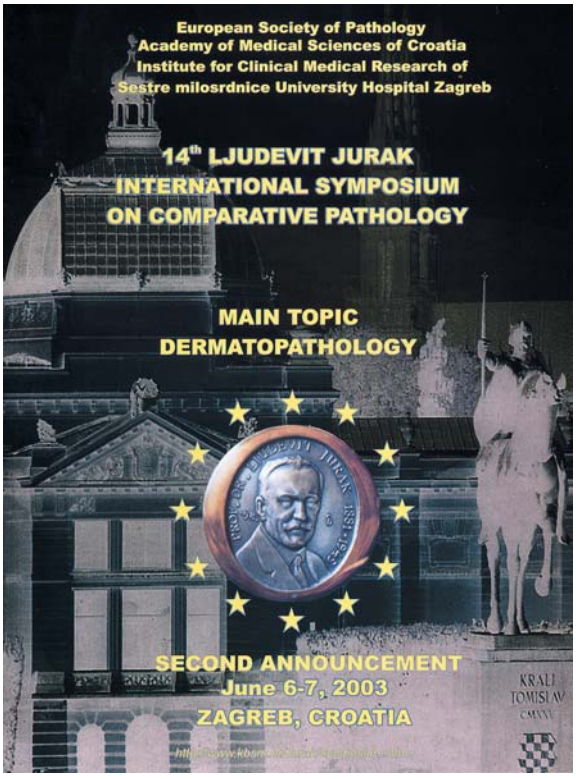
## 14th Ljudevit Jurak International Symposium on Comparative Pathology, Zagreb, Croatia, 6–7 June 2003
*(second announcement)*

### General Information

Zagreb

Welcome to the 14th Ljudevit Jurak International Symposium on Comparative Pathology. The goal of this symposium is to undertake a multidisciplinary approach to human and animal pathology. The main topic of this year's symposium is dermatopathology, but all papers regarding other symposium sections are also welcome. The symposium will be held under the auspices of the European Society of Pathology and Academy of Medical Sciences of Croatia.

Zagreb is the capital of Croatia, one of the oldest of European countries. The city itself is more than 900 years old. A city with a population of 900,000 inhabitants, it has 20 theatres, 40 museums and galleries and many streets that are museums themselves. All participants will have the opportunity to visit the famous and controversial Mimara museum.




*Dates and venue*

The 14th Ljudevit Jurak International Symposium on Comparative Pathology will be held at Sestre milosrdnice University Hospital Multimedial Center in Zagreb, 6–7 June 2003.

*Important dates*

| | |
|---|---|
| 1 April 2003 | Deadline for reduced registration fee and abstracts |
| 1 May 2003 | Notification of acceptance |

*Language*

The official symposium language is English.

*Symposium Organization*

Ljudevit Jurak
Department of Pathology
Sestre milosrdnice University Hospital
Vinogradska 29,
10000 Zagreb, Croatia
Tel.: +385-1-3787909
Tel./Fax: +385-1-3787244
website:
www.kbsm.hr/Jurak/symposium.htm
e-mail: juraks@kbsm.hr

ESCOP
*European School of Pathology*

# Pathology of the Pancreas

**Prof. G. Kloppel, Kiel**

# Pathology of the Liver & Biliary Tract

**Prof. P. Bedossa, Paris**

INSTITUTE FOR SCIENTIFIC INTERCHANGE FOUNDATION

## 2003 courses

**September 19 - 25 Turin, Italy**

### AIM

Post-graduate residential course for young European pathologists based on workshops, slide seminars and few lectures to update and standardise participants' diagnostic ability.

### FEE

- Registration is 300 Euro.
- Full board accomodation (to be paid upon departure) is 75 Euro/day/person.
- A limited number of EScoP scholarships (for ESP Members) is also available upon request

### DATES

**Pancreas Pathology**
**Sept. 19-20, 2003**

**Liver & Biliary Tract Pathology**
**Sept 21-25, 2002**

### PLACE & ORGANIZATION

**Institute for Scientific Interchange (ISI)**
**Villa Gualino,**
**Viale S. Severo 65,**
**10133 Torino, Italy.**

**Phone Office**
**+39 011 6603090**
**Phone Residence**
**+39 011 6603555**
**E-mail: isi@isi36a.isi.it**

### PAST COURSES

1991 Liver & GI path (non neopl)
Ovarian pathology
Breast pathology
1992 Pulmonary pathology
Endocrine pathology
1993 Haematopathology
1994 Haematopathology
Uterine pathology
Breast pathology
1995 Quantitative pathology
Neuropathology
Head & Neck pathology
1996 Uropathology
Dermatopathology (neopl)
1997 Tumors of liver & pancreas
Tumors of GI tract
1998 Soft tissue tumors
Breast pathology
1999 Lung pathology
Cytopathology
2000 Ovarian pathology
GI pathology
2001 Hematopathology
2002 Head & Neck Pathology
Thyroid & parathyroid Path.

### FUTURE COURSES

2004 Pathology of the Uterus
Pathology of the Bladder
Pathology of the Prostate

**APPLY before April 30 to**

**European School of Pathology**
**c/o Dept Pathology, Univ Turin, Via Santena 7,**
**I-10126 Torino Italy** Fax +39 011 6635267
**E-mail mauro.papotti@unito.it**
**Note:** By end June, a letter will confirm or reject the application. Do not send money now, please.

**To EScoP** **RE: Preliminary application**

Surname: ..... Name: ..... Sex: .....
Date & place of birth: ..... Citizenship: .....
Full address.....
.....
Phone: ..... Fax: ..... E-mail: .....

- ☐ application for 2 courses ☐ application for 1 course ☐ Sept. 19-21 ☐ Sept. 21-25
- ☐ I apply for: ☐ EScoP scholarship ☐ EU grant, if available
- ☐ Member of ESP ☐ non member (I apply for 2003 ESP membership)
- ☐ I enclose a brief curriculum vitae stating my experience in pathology

Date..... Signature: .....

# The Montebello Conference 2003

## Tumour Cell Invasion



The Montebello Centre,
Mesnali, Lillehammer, Norway

June 21-24, 2003

http://www.Montebelloconf.org

# Welcome to the Montebello Conference 2003

This years conference is dedicated Tumour Cell Invasion and we invite pathologists, cell biologists and clinicians to attend. Guest speakers will provide "state of the art" lectures and you are invited to present your own work as a free paper or a poster. The conference will take place in The Montebello Centre, Mesnali, Lillehammer during the period June 21.–24. 2003. The centre has a modern auditorium and many recreation facilities. Lillehammer, known for hosting the Winter Olympic Games, offers a peaceful and beautiful natural setting, being situated on the shore of Norway's largest lake, Mjøsa. Combining this with a friendly and open atmosphere, as well as challenging discussions, we believe this will be a rewarding experience

The number of participants is limited to 80. Please register at your first convenience. Registration fee is 330 Euro for non-ESP members and 280 Euro for members of ESP. Accommodation with full boarding (breakfast, lunch, dinner) is 460 Euro in single room and 410 Euro per person in double room for the whole conference.

We invite you to submit an abstract for free presentation and look forward seeing you in Lillehammer.

## The Montebello Conference organizing committee

Raisa Gurvitsj
Wencke Danielsen
Ben Davidson
Elisabeth Emilsen
Jahn M. Nesland

**Correspondence** Jahn M. Nesland
Dept. of Pathology
The Norwegian Radium Hospital
Montebello
NO-0310 Oslo, Norway

**Telephone** 47-22935620 • **Telefax** 47-22730164 • **e-mail**: j.m.nesland@labmed.uio.no

**Registration at the web site**: http://www.Montebelloconf.org

# Preliminary programme

**June 21, Saturday**

| | |
|---|---|
| 16.00 | Transport from Oslo airport, Gardermoen 2 hrs. Arrival in the afternoon. Tea/Coffee – sandwiches |
| 18.00–19.00 | Check in / Registration |
| 19.00–19.15 | Welcome in the Auditorium. *Jahn M. Nesland* |
| 19.15–20.00 | Epithelial – Mesenchymal Transitions in Tumour Progression. *Jean Paul Thiery, Paris* |
| 20.00–20.30 | Sight-seeing The Montebello Centre |
| 20.30 | Dinner |

**June 22, Sunday** 07.30–08.30 Breakfast
**Basement membrane / Stromal modulation**

| | |
|---|---|
| 08.30–09.15 | Basement membrane / Stromal composition. *Giulio Gabbiani, Geneva* |
| 09.15–10.00 | Regulation BM / Stromal degradation. *Fred Bosman, Lausanne* |
| 10.00–10.30 | Break |
| 10.30–11.15 | Dental matrix. A model for stromal modulation. *Ole Petter Lyngstadaas, Oslo* |
| 11.15–11.45 | Cancer initiation and cancer invasion in gastric carcinoma. *Manuel Sobrinho-Simões, Porto* |
| 11.45–12.00 | Break |
| 12.00–12.30 | Squamous cell carcinoma of the upper respiratory tract – development and progression. *Antonio Cardesa, Barcelona* |
| 12.30–13.00 | The role of adhesion molecules and extracellular matrix proteins in the progression of carcinomas of the upper respiratory tract. *Carlo Baroni, Rome* |
| 13.00–13.30 | Regulation of proteolysis in breast carcinomas. *Ben Davidson, Oslo* |
| 13.30–15.30 | Lunch |
| 15.30–17.00 | Free presentations |
| 17.00–17.15 | Break |
| 17.15–18.00 | Tumour lymphangiogenesis. *Kari Alitalo, Helsinki* |
| 20.00 | Dinner |

**June 23, Monday** 07.30–08.30 Breakfast
**Intracellular regulatory mechanisms in tumour cell invasion**

| | |
|---|---|
| 08.30–09.15 | The cadherin / catenin system. *Marc Mareel, Gent* |
| 09.15–10.00 | Intracellular signalling in malignant melanomas. *Vivi Ann Flørenes, Oslo* |
| 10.00–10.30 | Break |
| 10.30–15.30 | Sightseeing |
| 16.00–16.45 | Stromal interactions in malignant lymphomas. *Jan Delabie, Oslo* |
| 16.45–17.30 | Ovarial carcinoma – Regulation of tumour cell invasion. *Reuven Reich, Jerusalem* |
| 17.30–18.15 | Interaction glioblastoma cells and stromal elements. |
| 19.00 | Conference Dinner and Party |

**June 24, Tuesday** 07.30–08.30 Breakfast
**Cell cycle regulation and models for analysing tumour cell invasion**

| | |
|---|---|
| 08.30–09.15 | Cell cycle regulation. *Jiri Bartek, Copenhagen* |
| 09.15–10.00 | Autocrine / paracrine regulation and interaction with growth factor receptor signalling. *Jahn M. Nesland* |
| 10.00–10.45 | Special lecture: Three dimentional models for analysing cancer cell / stromal interaction. *José Costa, Yale* |
| 10.45–11.00 | *Concluding remarks.* *Jahn M. Nesland* |
| 11.00–12.00 | Lunch |
| 12.00 | Bus leaves for Oslo airport, Gardermoen |




**Helmut H. Popper, M.D., Prof. of Pathology**
**Laboratories for Molecular Genetics,**
**Environmental and Respiratory Pathology, Institute of Pathology**
**University of Graz**
**Auenbruggerplatz 25**
**Graz, A-8036, Austria**
**Tel.: +43-316-3804405**
**Fax: +43-316-384329**
**popper@uni-graz.at**

**To the Editors of the ESP Newsletter** **4/8/03**
**Prof. Niki J. Agnantis and Dr. Bjorn Risberg**
**University Department of Pathology**
**Medical School of Ioannnina**
**GR 45110 Ioannina, Greece**

Dear Prof. Agnanti and Dr. Risberg:

First of all I would like to bring to your attention that my fax number has changed to +43-316-384329 and my email and web address to:
popper@uni-graz.at
and
http://www.uni-graz.at/patwww/umweltpat/umweltpat.html, respectively.

Report for the pulmonary pathology working group

From October 2001 until September 2002, the working group was actively engaged in an EU-grant-supported project on rare pulmonary diseases. From all over Europe we collected cases of rare pulmonary and pleura diseases and finally ended up with a collection of over 700 cases. Twenty-four pulmonary pathologists, consisting of members and nonmembers of the working group, gathered in Graz in February and June 2002 to review these cases. In June two clinicians for adult and paediatric pulmonary diseases joined us.

As results we have now a collection set with each of these contributing pathologists (from Turkey to Portugal, from Finland to Italy), which can be used as a source of education and training. A homepage for doctors and patients has been developed, and is being placed on the homepage of all contributing pathologists (details can be viewed at: http://www.uni-graz.at/patwww7umweltpat/rarediseases.html).

The working group was actively incorporated into the program for the upcoming ESP Congress in Ljubljana. A precongress meeting has been arranged with the help of the local organizers of the Congress. This will focus on news and problems in pulmonary and pleural pathology. A postcongress meeting to be held in Golnik, north of Ljubljana, will focus on rare diseases. New entities and cases will be taken up and discussed. During the Congress the group will actively take part in conferences, slide seminars and poster sessions.

The working group has already contributed to the program discussion for the next Intercontinental Meeting to be held in Iguassu, Brazil. A presentation will also be given at the precongress meeting in Rio de Janeiro.

New officers for the working group will be elected in Ljubljana, which should take the responsibility for preparing the ESP Congress in Paris. As its central theme the group has decided on the major impact of interstitial and other nontumorous lung pathology.

With my best regards,
yours sincerely

Helmut H. Popper, M.D.

**Working Group on Molecular Pathology**

Foundation meeting:
Baveno, 20 May 2002

*For further information use the following e-mail addresses:*
For Prof. Dr. Heinz Hofler:
renate.hartmann@lrz.tu-muenchen.de
(his secretary's e-mail address)
For Prof. Generoso Bevilacqua:
g.bevilacqua@med.unipi.it

**Working Group of Pulmonary Pathology**
by Helmut Popper

*Address for information:*
Helmut H. Popper, M.D.,
e-mail: ppopper@kfunigraz.ac.at
Fax: +43–316–380–9636
Laboratories for Molecular Cytogenetics, Environmental and Respiratory Tract Pathology,
Institute of Pathology,
University of Graz

**Working Group on Head and Neck Pathology**
by Antonio Cardesa

*Information address:*
Prof. Antonio Cardesa,
Dept. Anatomic Pathology,
Hospital Clinic, Villarroel 170,
08036 Barcelona, Spain
(Tel: +34 93 227 5450,
Fax: +34 93 227 5717,
e-mail: acardesa@clinic.ub.es)

*New address:*
Prof. Henrik B. Hellquist, Chairman,
Department of Laboratory Medicine and Pathology,
Hamad Hospital, P.O. Box 3050,
Doha, Qatar

**Working Group on Endocrine Pathology**
by Gianni Bussolati

***E.C.E.P***
The European Club of Endocrine Pathology



***The European Club of Endocrine Patholgoy***
***Via Santena 7, Torino 10126, Italy***
***Tel.: +39-11-6706505, Fax: +39-11-6635267***
***e-mail: fassina@uxl.unipd.it***

All infomation, graphics and materials contained in this site are © 1997 by European Club of Endocrine Pathology
Prof. Ambrogio Fassina
© All right reserved

**Important message to all ESP members who want to send material for publication in the *Europath News*, which will appear four times a year (February, May, August, November) incorporated in *Virchows Archiv*: the material should be sent to one of the editors 2 months ahead of time by e-mail:**

**nagnanti@cc.uoi.gr** **brisberg@labmed.vio.no**

**Slide seminar in the Internet**

**Diagnostic histopathology cases presented at the European School of Pathology courses in Turin are going to be shown via Internet.**

**You are kindly invited to visit the site at http://www.isi.it/pathology/index.htm.**

**Working Group of Uropathology**
by Gregor Mikuz

*Addresses for information:*
Gregor Mikuz M.D., FRCPath (Chairman), Institute of Pathology University Innsbruck, Muellerstrasse 44, 6020 Innsbruck, Austria (gregor.mikuz@uibk.ac.at)

Ferran Algaba M.D.(Vice-chairman), Fundacion Puigvert, C/Cartagena 340 –350, 08025 Barcelona, Spain (19612itp@comb.es)

Antonio Lopez-Beltran M.D. (Secretary), Unit of Anatomical Pathology, Faculty of Medicine, 14004 Cordoba, Spain (Em1lobea@uco.es)

Margaret Constance Parkinson BSc, M.D. (Secretary), (HP) Fourth Floor Rockefeller Building, University Street, London WC1E6JJ, UK (Rmkdhmp@ucl.ac.uk)

Rodolfo Montironi M.D., FRCPath (Treasurer), Institute of Pathology, University of Ancona, 60020 Torrette / Ancona, Italy (r.montironi@popcsi.unian.it)

Michael J Mihatsch MD (Nephropathology), Institute of Pathology, University Basel, 4003 Basel, Switzerland (Mihatschmj@uhbs.ch)

**Working Group of Cytopathology**
by Fernando Schmitt

*Address for information:*
Prof Fernando Schmitt, IPATIMUP, Rua Roberto Frias S/N, 4200 Porto, Portugal (e-mail: fernando.schmitt@ipatimup.pt, Fax: +351–225570799)

**A message from the Editors to the Chairpersons of the formulated ESP Working Groups**

**Dear Colleagues,**
**If you are interested in presenting your activities to the EUROPATH NEWS, please send your material by e-mail 2 months ahead of publication.**

**PLEASE NOTE:**
**Due to the restricted number of pages in each issue, texts will appear on a "first come, first served" basis.**

**For information concerning ESP activities, please contact**

**ESP web-site: http://www.Europathology.org**

**Working Group of Gynaecology**
by Manfred Dietel

*Addresses for information:*
e-mail: manfred.dietel@charite.de

**Working Group on Molecular Pathology**

Foundation meeting:
Baveno Monday, 20 May 2002
For further information use the following e-mail addresses:

For Prof. Dr. Heinz Hofler:
renate.hartmann@lrz.tu-muenchen.de
(his secretary's e-mail address)

For Prof. Generoso Bevilacqua:
g.bevilacqua@med.unipi.it

**Electron Microscopy Working Group:**

*Address for information:*
Dr. Brian Eyden (PhD), Head of Diagnostic Electron Microscopy, Christie Hospital NHS Trust, Manchester M20 4BX, United Kingdom
Tel.: +44 161 446 3292
Fax: +44 161 446 3300
e-mail:
Brian.Eyden@christie-tr.nwest.nhs.uk

**ERRATUM**

In Table 1 on p. 193 of Europath News 1/2003 [Virchows Archiv 442(2):193], the following two omissions were noticed: Professor Gunter Kloppel was the organizer of the first EScoP Course in Warsaw (June 1998) on Pancreas Pathology and he was also involved in the first GI and Pancreatic Endocrine Pathology Course in 1992

## The European Society of Pathology

Dear Colleague,

It will surely not have escaped your attention that *Virchows Archiv* is now the Official Journal of the European Society of Pathology.

But did you realise what benefits membership in the society offer you?

- A subscription to the journal *Virchows Archiv* at no extra charge – this is automatically sent to every member every month.
- Access to the journal online (take a look at http://link.springer.de). If you are already a member of ESP but have not yet registered for your free electronic access, you will find the necessary form to complete online here too.
- A discount of 20% on most titles published by Springer. To take advantage of this, simply send your order directly to the publisher, with details of your membership.
- Attendance at the Society's conferences at a reduced fee.

If you have not yet joined the European Society of Pathology, why not do so now? Simply complete and return the form enclosed. If you are already a member, please wait for our renewal letter for 2003.

We look forward to welcoming you as a member in 2003

Yours sincerely

G. Bussolati

President
European Society of Pathology

U. van Haelst

Treasurer
European Society of Pathology

G. Klöppel

Managing Editor
Virchows Archiv




# Application for Membership of the
## EUROPEAN SOCIETY OF PATHOLOGY (E.S.P.)

***Please, type or use block letters to fill in this form!***



FAMILY NAME: .....

First Name(s): .....

Male ❑ Female ❑

Place and date of birth: .....

Title/Present Position: Prof. ❑ Dr. ❑ Resident ❑

Other: .....

*Please, clearly indicate which one of rhe following addresses should be used for subsequent correspondence, mailings, and listing in the Members Handbook*

❑ PRIVATE ADDRESS:

Name: .....

Street: .....

Postcode: .....

City: .....

Country: .....

❑ INSTITUTE / OFFICE ADDRESS:

(This address will be used for subsequent correspondence and listing in Membership Directory)

Name of Institute: .....

Department: .....

Street: .....

Postcode: .....

City: .....

Country: .....

Tel.: .....

Fax: .....

E-mail: .....

FIELDS OF INTEREST: .....

.....

Date: .....

**Signature of Applicant:** .....
**only applicable if sent back by fax.**

---

Please e-mail or fax the completed application form to:

E.S.P. - OFFICE OF THE TREASURER,
Prof. Dr. U. VAN HAELST,
van Cranenborchstraat 6,
NL – 6525 BN Nijmegen
The Netherlands.

Tel: +31-24-3231950
Fax: +31-24-3222304
E-mail: Treasurer.ESP@vanHaelst.100.nl

Your acceptance as a member of E.S.P. will be confirmed in due time.

Membership fee for 2003:

including subscription to the combined printed and electronic version of the Society's journal *Virchows Archiv*: 95.00 EUR

including subscription to the electronic version only of *Virchows Archiv*: 75.00 EUR




# Prefers glass to plastic

**Introducing the new Leica CV5030 Glass Coverslipper**

The Leica CV 5030 automated glass coverslipper provides clear advantages over tape coverslippers, producing slides of superior optical quality and reliable long-term storage. In addition, the CV 5030 is compatible with most common brands and sizes of coverglass and accepts the staining racks of virtually all routine slide stainers

Please ask us for more information on how the Leica CV 5030 can make your laboratory more productive.

**Leica Microsystems. Different to the Rest**

Leica MICROSYSTEMS

Leica Microsystems Nussloch GmbH
Heidelberger Strasse 17-19
D-69226 Nussloch

Phone: (06224) 143-0
Fax: (06224) 143 200
e-mail: histo_info@leica-microsystems.com
www.leica-microsystems.com

Virchows Arch (2003) 442:527–528 © Springer-Verlag 2003

SOCIETY NEWS

# Invitation to the 19th European Congress of Pathology

On behalf of the European Society of Pathology (ESP) and the Organising Committee, we take great pleasure in inviting you to the 19th European Congress of Pathology, which will be held in Ljubljana, Slovenia, 6–11 September 2003.

Slovenia is not a large country, but at the hub of routes of trade and movement from east to west and north to south, it has always played a larger part in European events than its size would suggest. Slovenia is now an independent Central European state, on the sunny side of the Alps, bordering Italy, Austria, Hungary and Croatia. The landscape embraces rolling countryside leading to the Pannonian plain to the east, rugged Karst bordering the Adriatic Sea to the southwest, and the Alps to the north and west. The Slovenian nation of only two million today has survived mainly due to its culture, language and vitality. A bone flute, 30,000 years older than any other known in the world, and Europe's oldest bone needle, testify to the roots of culture here.

Its capital, Ljubljana, has a picturesque unity, composed of an architectural heritage spanning Roman Emona, through Renaissance and Baroque Ljubljana, to Secession Art Nouveau and Modern Ljubljana, so strongly marked by the influence of the world famous Slovenian architect, Jo e Plečnik. Ljubljana is an university city. The roots of the University go back to the seventeenth century with Academia Operosorum, the fourth Academy of Sciences in Europe. A Philharmonic Society dates back three centuries.

Ljubljana's congress tradition began in 1821, when the three emperors of the Holy Alliance met here to discuss the post-Napoleonic fate of Europe. These traditions have been brought together in the new Cultural and Congress Centre Cankarjev dom, with a capacity of 3,600, located in the heart of Ljubljana. Cankarjev dom is well equipped with all modern technical facilities and has an experienced in-house team to ensure the necessary high standards for scientific sessions and exhibitions. All Congress venues, and most hotels, are within walking distance of the centre of the city. Particular attention will be paid to stimulating the participation of trainees and young pathologists by securing as low a registration fee as possible, and inexpensive accommodations.

The European Society of Pathology has been succeeding in establishing its ever more continuous activity and influence. The old idea of a common programme of continuous education of pathologists has been realised through a number of courses organised each year by the European School of Pathology, at its headquarters in Turin and other centres throughout Europe. An increasing number of Working Groups within the European Society of Pathology, devoted to various fields, promote a continuous exchange of professional experiences and other information, the establishment of common diagnostic standards and collaboration on common research projects.

The biannual ESP Congresses retain a major role in fulfilling the main aims of the ESP in pathology education, exchange of the most recent research achievements and, particularly, in keeping together all branches of pathology, that otherwise tend to split according to organ systems, disease processes and the increasing number of techniques. The Congresses also keep together pathologists from the whole of Europe, irrespective of geographical and political borders.

We believe that the 19th European Congress of Pathology will continue the traditional approaches of previous Congresses and will serve to increase both links with European national and international pathology societies and intercontinental links, particularly with the International Academy of Pathology. The framework of the Congress Scientific Programme has been created with the strong impact and assistance of the ESP Working Groups, the ESP Executive/Scientific Committee and the Advisory Council as well as companion Societies. The programme covers all areas of pathology, provides information ranging from current diagnostic standards to recent advances in science and modern techniques, particularly those of molecular genetics, and includes a number of "hot" topics of today and tomorrow, which will be

presented by the best, internationally recognised experts at Keynote Lectures, Symposia, Special Presentations, Round Table Discussions, Short Courses and Slide Seminars. One evening is devoted to ESP Working Group Meetings, both business and scientific. Interesting Satellite Symposia will be organised by supporting companies, two by the main sponsor of the Congress Main Sponsor, Ventana Medical Systems S.A.

Furthermore, all practising pathologists and scientists are kindly invited to present their scientific achievements and exchange their professional experiences through Free Paper and Poster Sessions. The best Free Papers will be acknowledged by giving the authors the opportunity to present their achievements at the plenary session, at which the authors of the three best Poster Presentations will additionally receive special Awards.

All who are coming to Ljubljana are kindly invited to join us at two one-day Pre-Congress Meetings, prior to the Congress Opening Ceremony on Saturday: one on Pulmonary Pathology and the other devoted to non-neoplastic Nephropathology. There will also be a three-day Joint Meeting of the European and North American Society of Head and Neck Pathology. All Pre-Congress Meetings and a whole day Examination by the European Board of Pathology will be organised by using the facilities of the new building of the Faculty of Medicine, University of Ljubljana.

Culture kept the Slovenian national identity alive over the centuries and it still plays an important role in people's lives. The Congress will also highlight the traditional close connection between medicine and art. Some novel events are planned: an exhibition of the work of pathologists/painters and, especially, a Gala Concert on Monday evening in the main Gallus Concert Hall of the Congress Centre in Ljubljana, by pathologists/musicians from all over the world. A social programme is offered which reflects the warmth and hospitality of the Slovenian people.

The Second Millennium we have entered provides major challenges for all biomedical sciences, and the 19th European Congress of Pathology is a challenge for the Organisers. We sincerely hope that attendance at the Ljubljana Congress in 2003 will be a fruitful, enjoyable and memorable experience in every respect for all participants, and will give new impetus to our medical speciality in Slovenia.

We look forward to seeing you in September 2003 in Ljubljana.



Gianni Bussolati
President
European Society
of Pathology



Du an Ferluga
President
19th European Congress
of Pathology

Virchows Arch (2003) 442:529–537
DOI 10.1007/s00428-003-0815-1

ORIGINAL ARTICLE

**A. Gaumann · D. S. Tews · T. Mentzel · P. K. Petrow · E. Mayer · M. Otto · C. J. Kirkpatrick · J. Kriegsmann**

# Expression of drug resistance related proteins in sarcomas of the pulmonary artery and poorly differentiated leiomyosarcomas of other origin

Received: 13 December 2002 / Accepted: 17 March 2003 / Published online: 13 May 2003
© Springer-Verlag 2003

**Abstract** Sarcomas are known to develop resistance to current chemotherapeutic strategies, displaying a multidrug-resistant phenotype. Mechanisms involved in drug resistance include reduced cellular drug accumulation, drug detoxification as well as alterations in drug target specificity. In seven sarcomas of the pulmonary artery (SPA) and ten leiomyosarcomas of other origin, we studied the immunohistochemical expression of P-glycoprotein (P-gp), multidrug-resistance protein (MRP), lung resistance protein (LRP), metallothionein (MT) and topoisomerase II$\alpha$. Upregulation was found in tumour cells for P-gp but not for MRP in SPA and other leiomyosarcomas. Topoisomerase II$\alpha$ was expressed at high levels in tissue of primary tumours as well as recurrent tumours. Both P-gp and topoisomerase II$\alpha$ were present in numerous tumour-associated vessels. LRP was expressed at high levels in SPA but to a lesser extent in the other leiomyosarcomas. MT was expressed at low levels but was markedly present at the border of necrosis. The overall survival and the relapse-free survival did not correlate with the expression of these factors. There was no significant relationship between treated and non-treated patients with respect to the expression of the examined molecules. P-gp, but not MRP, may play a role in the development of drug resistance. P-gp, LRP and topoisomerase II$\alpha$ contribute to drug resistance through expression in tumour-associated vessels. Unique high levels of topisomerase II$\alpha$ reflect the high proliferation rate of these tumours. MT seems to serve as a detoxifying agent of metabolites at the border of necrosis. Our findings underline the fact that multiple factors contribute to chemoresistance and that examination of a spectrum of relevant molecules is probably necessary to plan the best therapy.

**Keywords** Sarcoma of the pulmonary artery · Leiomyosarcoma · Drug resistance

A. Gaumann · M. Otto · C. J. Kirkpatrick · J. Kriegsmann
Institute of Pathology,
University Clinics Mainz,
Langenbeckstrasse 1, 55101 Mainz, Germany

D. S. Tews
Edinger Institute of Neurology,
Deutschordenstrasse 46, 60528 Frankfurt a.M., Germany

E. Mayer
Department of Cardiovascular Surgery,
University Clinics Mainz,
Langenbeckstrasse 1, 55101 Mainz, Germany

P. K. Petrow
University of Jena,
Ziegelmühlenweg 1, 07743 Jena, Germany

T. Mentzel
Institute of Dermatohistopathology,
Siemensstrasse 6/1, 88048 Friedrichshafen, Germany

A. Gaumann (✉)
Max Planck Institute of Physiological and Clinical Research,
W. G. Kerckhoff Institute, Department of Molecular Cellbiology,
Parkstrasse 1, 61231 Bad Nauheim, Germany
e-mail: andreas.gaumann@klinik.uni-regensburg.de
Tel.: +49-941-9446601, Fax: +49-941-9446602

## Introduction

Primary sarcomas arising from major blood vessels (aorta, pulmonary artery, inferior vena cava) are rare and associated with a very poor prognosis. The peak incidence of these neoplasms is during the fifth decade of life [19]. Most cases reported in the literature have been diagnosed at autopsy. However, since diagnostic and surgical procedures, e.g. of chronic pulmonary embolism, have been improved [18], an increasing number of cases of these sarcomas could be successfully treated by surgical resection. Nevertheless, although postoperative polychemotherapy regimens were applied, most patients died early in treatment.

The failure of chemotherapy in general can be attributed to a patient's disease status. However, multiple drug resistance (MDR) has been described in a variety of malignant tumours [9, 13, 34] as being responsible for therapy failure. Some proteins are reported to be related to

MDR. For example, P-glycoprotein (P-gp), a transmembrane protein, encoded by the mdr 1 gene, acts as a efflux transporter system for a variety of organic substances including cytotoxic drugs (e.g. anthracyclines, epipodophyllotoxins). Like P-gp, the multi-drug resistance protein (MRP) is a member of the ABC transporter family and mediates resistance to a similar spectrum of anticancer drugs [3]. Both genes are known to be involved in MDR in different cell lines in vitro. More recently, the major vault protein, called lung resistance protein (LRP), has been identified and was also detected in MDR cell lines [20, 21]. Vaults have been described as small particles located in the cytoplasm and are probably involved in transport processes [17]. LRP is thus believed to contribute to drug resistance by affecting the transport of drugs. Therefore, LRP overexpression is associated with resistance to doxorubicin, vincristin, melphalan and platin agents [15].

Another putative mediator of drug resistance is a low-molecular-weight protein called metallothionein (MT). This cysteine-rich enzyme is able to bind divalent metal ions including copper, cadmium, mercury and platinum. MT is found in normal mammalian tissues such as myoepithelial cells, Sertoli cells, liver, kidney and lung and is therefore a possible mediator of drug resistance in a variety of tumour tissues.

In addition, DNA repair enzymes, e.g. topoisomerases, are reported to be involved in MDR. These enzymes catalyse the interconversion of topologic forms of single and double-stranded DNA, are involved in processes related to cell growth and division and appear to be a structural and functional component of the nucleus. The anthracycline class of cytotoxic drugs specifically targets topisomerase II$\alpha$ [37] by creating a cleavable complex. It is hypothesised that this complex is able to damage DNA, thus causing toxicity, and may induce apoptosis in proliferating cells. It has been reported that overexpression of topoisomerase II$\alpha$ correlates with drug resistance of breast cancer and unfavourable clinical outcome [5].

In order to find out whether the expression of these MDR-related proteins contributes to the poor clinical outcome in patients with sarcomas of the pulmonary artery (SPA) as well as poorly/moderately differentiated leiomyosarcomas of other origin, we studied the expression of the above-mentioned MDR proteins by immunohistochemistry and related them to patients' outcomes.

## Materials and methods

### Patients

Between 1989 and 2001, tissues (two intimal sarcomas, five leiomyosarcomas) from SPAs were obtained from seven patients undergoing surgical tumour resection and pulmonary artery reconstruction because of chronic pulmonary embolism. All tissue samples were provided by the Department of Cardiovascular Surgery of the Johannes Gutenberg University at Mainz. In addition, ten cases of leiomyosarcomas (three cases G2; seven cases G3) were obtained from the Department of General and Abdominal Surgery and four academic hospitals of the University of Mainz between 1982 and 2001. In addition, two leiomyomas from leiomyomatous uteri (one premenopausal, one postmenopausal) obtained from two different academic hospitals were examined as disease controls. Normal control specimens from pulmonary arteries were collected from the archives of the Institute of Pathology and Neuropathology, University of Mainz. Immediately after surgery, tissue samples were fixed in buffered formaldehyde (4%) and embedded in paraffin. Tumours from 15 patients were excised complete and in one case, incomplete. From one patient only a tumour biopsy was performed.

In addition, 11 patients received a regimen of polychemotherapy and/or radiation. For details and clinical data see Table 1.

### DAB immunohistochemical staining

Primary antibodies comprise monoclonal mouse-anti-human P-gp (JSB-1, IgG1, 1:100, Alexis Biomedicals, Grünberg, Germany), MRP (MRPm6, IgG1, 1:20, Alexis Biomedicals), LRP (LRP-56, IgG1, 1:100 Alexis Biomedicals), MT (E9, IgG1, 1:50 Dako Diagnostics Hamburg, Germany) and topoisomerase II$\alpha$ (Ki-S1, IgG2a, 1:50 Roche Diagnostics, Mannheim, Germany).

The tissue sections were dewaxed according to a standard protocol and pre-treated with 2% $H_2O_2$ in methanol for 30 min. Following washing procedures in phosphate buffered saline (PBS), the slides were either placed in 1 M ethylene diamine tetraacetic acid (EDTA) buffer, pH 8.0 (JSB-1) or 10 mM citrate buffer, pH 6.0 (MRPm6, topoisomerase II$\alpha$) and irradiated for 15 min in a microwave oven or incubated with trypsin (1 mg/ml) for 20 min (MT). After washing with PBS, the sections were covered with 2% horse serum (Vector Laboratories) in PBS for 30 min. Then, after another washing step, the primary antibodies were applied and incubated at room temperature (RT) for 1 h. After washing with PBS, secondary anti-mouse antibody (raised in horse, Vector Laboratories, 1:200) was applied to all sections at RT for 30 min. In the third step, the antibody was coupled with the avidin-biotin-peroxidase complex (Vectastatin ABC-Kit, Vector Laboratories) according to the manufacturer's recommendations and incubated at RT for 30 min. Finally, the sections were incubated with the DAB substrate, rinsed for 10 min in running tap water, stained with haematoxylin and mounted in glycerol–gelatin medium. In control sections, the primary antibody was either omitted or substituted with non-specific mouse immunoglobulins. Two lung and kidney carcinomas and glioblastomas known to be positive for the tested molecules, as well as normal pulmonary artery, served as control tissues.

### Quantitative assessment of drug-resistant cells

For quantitative analysis, 20 high-power fields for every sarcoma were defined and the number of positive cells for drug resistance proteins by the presence of the brown reaction product was determined. The respective incidence and the percentage were calculated. Results were classified according to five categories: (–) negative; (+) between 1% and 25% of cells positive; (++) between 26% and 50% of cells positive; (+++) between 51% and 75% of cells positive; and (++++) between 76% and 100% of cells positive. Positivity in cells other than sarcoma cells was not scored.

### Statistics

Statistical analyses and graphic displays were performed using SPSS Scientific Software, SigmaPlot 4.01 (SPSS Scientific Software, Erkrath, Germany) and Graph Pad Prism 3.0. Continuous variables not following the normal distribution were compared between two or more groups using the Mann-Whitney U or Kruskal-Wallis test. A Wilcoxon signed rank test was used to compare related samples. Univariate analyses of time to death due to the sarcoma or time to recurrence (recurrence-free survival) were performed using the product limit procedure (Kaplan-Meier

**Table 1** Clinical and pathological characteristics of the sarcomas. *PT* pulmonary trunk, *PA* pulmonary artery, *RV* right ventricle, *LS* leiomyosarcoma, *IS* intimal sarcoma

| Patient no. | Age | Sex | Relation to vessel, size | Procedure | Histology (grade) | Follow-up | Additional treatment | Recurrence/time after diagnosis |
|---|---|---|---|---|---|---|---|---|
| 1 | 55 | Male | Pulmonary trunk | Pericardium PT resection and reconstruction | LS (G2) | Died 18 months after diagnosis | Radiation | Local, lung/7 months |
| 2 | 49 | Female | Bifurcation right PA branch | Resection PA replacement | LS (G2) | Died 9 months after diagnosis | None | Lung/5 months |
| 3 | 59 | Male | Bifurcation right PA branch | Endarterectomy right pneumonectomy | IS (G3) | Died 7 months after diagnosis | Radiation, doxorubicin/ dacarbacin–5 cycles | Local/7 months |
| 4 | 30 | Male | RV outflow tract | RV outflow resection. Valve/ trunk–reconstruction | LS (G2) | Alive 70 months after diagnosis | Adriamycin–5 cycles | None |
| 5 | 49 | Female | Pulmonary trunk | Resection failed | LS (G2) | Died 18 months after diagnosis | Adriamycin–6 cycles | Local, lung/6 months |
| 6 | 60 | Male | Pulmonary trunk luminal | Endarterectomy failed, left pneumonectomy | IS (G3) | Alive 45 months after diagnosis | Adriamycin/ifosfamide–4 cycles | Lung/5 months |
| 7 | 60 | Male | Pulmonary trunk luminal | PA resection, reconstruction | LS (G2) | Alive 31 months after diagnosis | Adriamycin/ifosfamid–4 cycles | None |
| 8 | 58 | Male | Stomach | Gastrectomy | LS (G2) | Died 35 months after diagnosis | None | Liver/25 months |
| 9 | 72 | Female | Gluteal region/pelvis | Local excision | LS (G3) | Alive 46 months after diagnosis | Radiation–100 Gy | Local/3 months |
| 10 | 51 | Male | Quadriceps femoris | Local excision | LS (G3) | Died 39 months after diagnosis | Adriamycin/ifosfamid–10 cycles | Local, lung/pleura, groin/4 months |
| 11 | 61 | Male | Bladder | Local excision | LS (G2) | Died 43 months after diagnosis | Etoposid/ifosfamid/carboplatin/2 cycles | Local, liver/ 30 months |
| 12 | 70 | Male | Quadriceps | Local excision | LS (G3) | Died 27 months after diagnosis | None | Groin, lung/ 21 months |
| 13 | 48 | Male | Calf | Local excision | LS (G3) | Alive 21 months after diagnosis | None | None |
| 14 | 59 | Female | Uterus | Local excision | LS (G3) | Alive 25 months after diagnosis | Carboplatin/paclitaxel–5 cycles | Liver/25 months |
| 15 | 54 | Female | Upper arm | Local excision | LS (G2) | Alive 40 months after diagnosis | None | None |
| 16 | 67 | Male | Leg | Biopsy | LS (G3) | Died 5 months after diagnosis | Epirubicin–1 cycle | Lung/5 months |
| 17 | 60 | Female | Retroperitoneal | Local excision | LS (G3) | Died 17 months after diagnosis | Etoposide/adriamycin/ifosfamide | Local/7 months |

method) with the date of histological diagnosis at the starting point. Patients who died of other causes were censored at the time of death. Differences between the categories were tested using the univariate log-rank test. All variables with $P \leq 0.05$ were designated as statistically significant.

## Results

### Normal pulmonary artery and leiomyomas

Two pulmonary artery specimens with no obvious morphological disease and two leiomyomas of the uterus were stained using immunohistochemistry with the described antibodies. The results were assessed by light microscopy and analysed with a semi-quantitative score (Table 2). None of the examined molecules displayed a detectable expression in the normal pulmonary artery specimens. In two total hysterectomy specimens with leiomyomas, a moderate positivity for P-gp, topoisomerase II$\alpha$ and MT within the leiomyomas was found. P-gp, topoisomerase and LRP could also be detected in some endothelial cells. LRP was moderately to highly expressed in leiomyomas, but also stained normal smooth muscle cells. MRP and MT were weakly positive or completely absent in these cases.

### Overall survival of pulmonary artery sarcomas versus leiomyosarcomas

Follow-up data of the patients included in this study were retrieved from the medical records (Table 1). The disease-free survival was defined as the time between the diagnosis and the first relapse. The overall survival was defined as the time between the diagnosis and patient's death. In order to find out whether survival differs between SPAs and leiomyosarcomas of other origin we assessed disease and relapse-free survival of both groups. There was a slightly longer overall survival in patients with SPAs, although the difference was not significant ($P$=0.9095). The relapse-free survival did not differ significantly for SPAs relative to the leiomyosarcomas of other origin, as shown in Fig. 1 ($P$=0.9162). Since there was no difference among the groups, we have pooled the data and investigated the influence of the expression of drug-resistant factors on the overall survival in the primary tumours as well as for the relapse-free survival.

### P-gp examination

P-gp was moderately to highly expressed by tumour cells in 50% of the sarcoma specimens (four SPAs; eight leiomyosarcomas of other origin) but was weak or absent in three SPAs and two leiomyosarcomas of other origin

**Table 2** Expression of multi-drug-resistance related proteins in sarcoma cells and tumour-associated vessels. *LS* leiomyosarcoma, *IS* intimal sarcoma, *LM* leiomyoma. (–) negative, (+) between 1% and 25% of tumour cells positive, (++) between 26% and 50% of tumour cells positive, (+++) between 51% and 75% of tumour cells positive, (++++) between 76% and 100% of tumour cells positive, (v) tumour-associated vessels positive, (n) presence of necrosis

| Patient/tumour Clone | P-glycoprotein (JSB–1) | Multi-drug resistance protein-1 (MrPm6) | Lung resistance protein (LRP56) | Topoisomerase II$\alpha$ (Ki–S1) | Metallothionein (E9) |
|---|---|---|---|---|---|
| 1/LS (G2) | ++++,v | – | +,v | ++++,v | +,n |
| 2/LS (G2) | ++++,v | ++ | ++,v | ++++,v | ++,n |
| 3/IS (G3) | +,v | – | ++++,v | ++,v | +,n |
| 4/LS (G2) | +,v | ++++ | +++,v | ++++,v | + |
| 5/LS (G2) | +,v | +++ | +,v | ++++,v | ++,n |
| 6/IS (G3) | ++++,v | + | ++++,v | ++++,v | ++,n |
| 6/Relapse | – | – | +,v | ++,v | +,n |
| 7/LS (G2) | ++++,v | – | ++,v | ++++,v | +,n |
| 8/LS (G3) | ++++,v | ++ | +++,v | ++,v | +,n |
| 8/relapse | ++++,v | +++ | – | ++,v | + |
| 9/LS(G3) | ++,v | – | ++,v | ++++,v | +++,n |
| 10/LS (G3) | +,v | – | +,v | ++++,v | ++ |
| 10/relapse | +++,v | – | +++,v | +++,v | ++ |
| 10/relapse | +++,v | – | +,v | ++++,v | – |
| 11/LS (G2) | ++ | – | +,v | +++,v | + |
| 11/relapse | ++++,v | – | – | +++,v | + |
| 11/relapse | ++++,v | +++ | +,v | ++++,v | –,v |
| 12/LS (G3) | ++,v | – | +,v | +++,v | ++,n |
| 12/relapse | +++,v | – | ++,v | +++,v | + |
| 13/LS (G2) | ++++,v | ++ | +++,v | ++++,v | +++,n |
| 14/LS (G2) | ++++,v | + | ++,v | +++,v | +,n |
| 14/relapse | ++++,v | – | +,v | ++++,v | +,n |
| 15/LS (G2) | ++++,v | – | ++++,v | +++,v | ++,n |
| 16/LS (G3) | ++,v | – | +++,v | ++++,v | ++++,n |
| 17/LS (G3) | ++++,v | – | ++,v | ++++,v | + |
| 18/LM | –,v | – | ++,v | ++,v | + |
| 19/LM | +++,v | – | +++,v | ++,v | – |

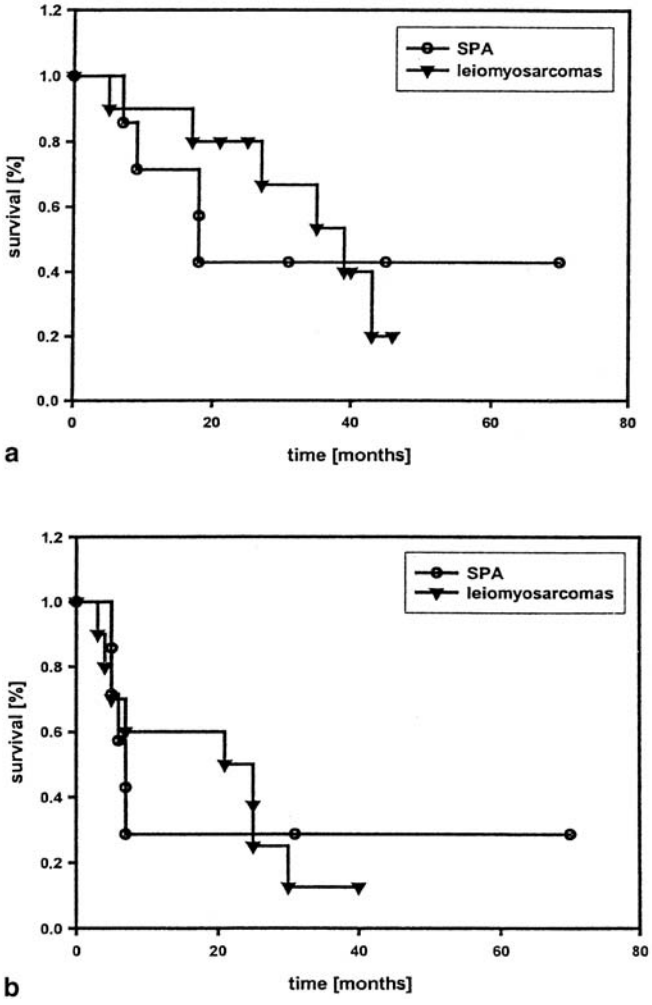



**Fig. 1** **a** Overall survival: sarcomas of the pulmonary artery versus leiomyosarcomas of other origin. **b** Disease-free survival: sarcomas of the pulmonary artery versus leiomyosarcomas of other origin

(Fig. 2a). In addition, varying proportions of tumour-associated vessels showed a distinct expression of this molecule. There was no significantly different expression ($P$=0.818) between primary tumours and their relapses as well as between those cases with or without therapy ($P$=0.106). Of note is that some cases showed an increased expression of P-gp (Table 2, cases 11 and 12) from primary tumours to relapses, whereas others decreased (Table 2, case 6). Concerning the overall and relapse-free survival, no significant difference could be observed when comparing patients who were positive or negative for P-gp ($P$=0.754 and 0.509).

## MRP examination

In contrast to P-gp, MRP was either absent or weakly expressed in nearly all sarcomas and could not be detected in tumour vessels (Fig. 2b). The immunoreactivity for this molecule was usually confined to the cell membrane but sometimes a cytoplasmic staining could also be seen. There was no significant difference observed between primary tumours and relapses ($P$=0.485) as well as between those patients with and without therapy ($P$=0.801). The comparison of the overall and relapse-free survival of patients revealed no significant difference ($P$=0.867 and $P$=0.949).

## LRP examination

LRP displayed a fine granular cytoplasmic expression profile and was present at a moderate to high extent in seven of seven SPAs and was expressed in seven of ten leiomyosarcomas of other origin (Fig. 2c). Numerous tumour-associated vessels stained positively with antibodies against LRP (Table 2). Statistically, no significant difference ($P$=0.31) between primary tumours and relapses could be detected. Similar results were obtained when comparing patients with and without treatment ($P$=0.840). The overall survival was slightly higher in the LRP positive group but was not, however, significant ($P$=0.237). In addition, the relapse-free survival was also not significantly different ($P$=0.081).

## Topoisomerase II$\alpha$ examination

Virtually all tumour cells, as well as numerous tumour-associated mononuclear cells, could be labelled with topisomerase II$\alpha$. The staining pattern for this molecule was mainly restricted to the nucleus (Fig. 2d). Numerous tumour-associated vessels could also be stained with this molecule (Table 2). There were no significant differences in the expression profiles between the primary tumours and their recurrences ($P$=0.485), as well as between the secondary tumours with or without therapy ($P$=0.649). The comparison of the overall and relapse-free survival of patients with or without therapy was not tested because most examined specimens were highly positive.

## MT examination

MT could be detected in all cases of SPAs and in all leiomyosarcomas of other origin. The expression was prominent at the border of necrotic areas (Fig. 2e) but also scattered in other tumour areas (Fig. 2f). The immunoreactivity was mostly confined to the cytoplasm but also simultaneous labelling of the nucleus and the cytoplasm was demonstrated. The MT positive tumour cells were often localised in small clusters (Fig. 2f and Table 2). In addition, numerous non-neoplastic fibroblasts as well as inflammatory cells could be stained with MT. There was no statistical difference between primary tumours and relapses ($P$=0.699) as well as between the groups with and without treatment ($P$=0.65). The overall and relapse-free survival again was not significantly different ($P$=0.709 and $P$=0.248). Regarding individual patients,

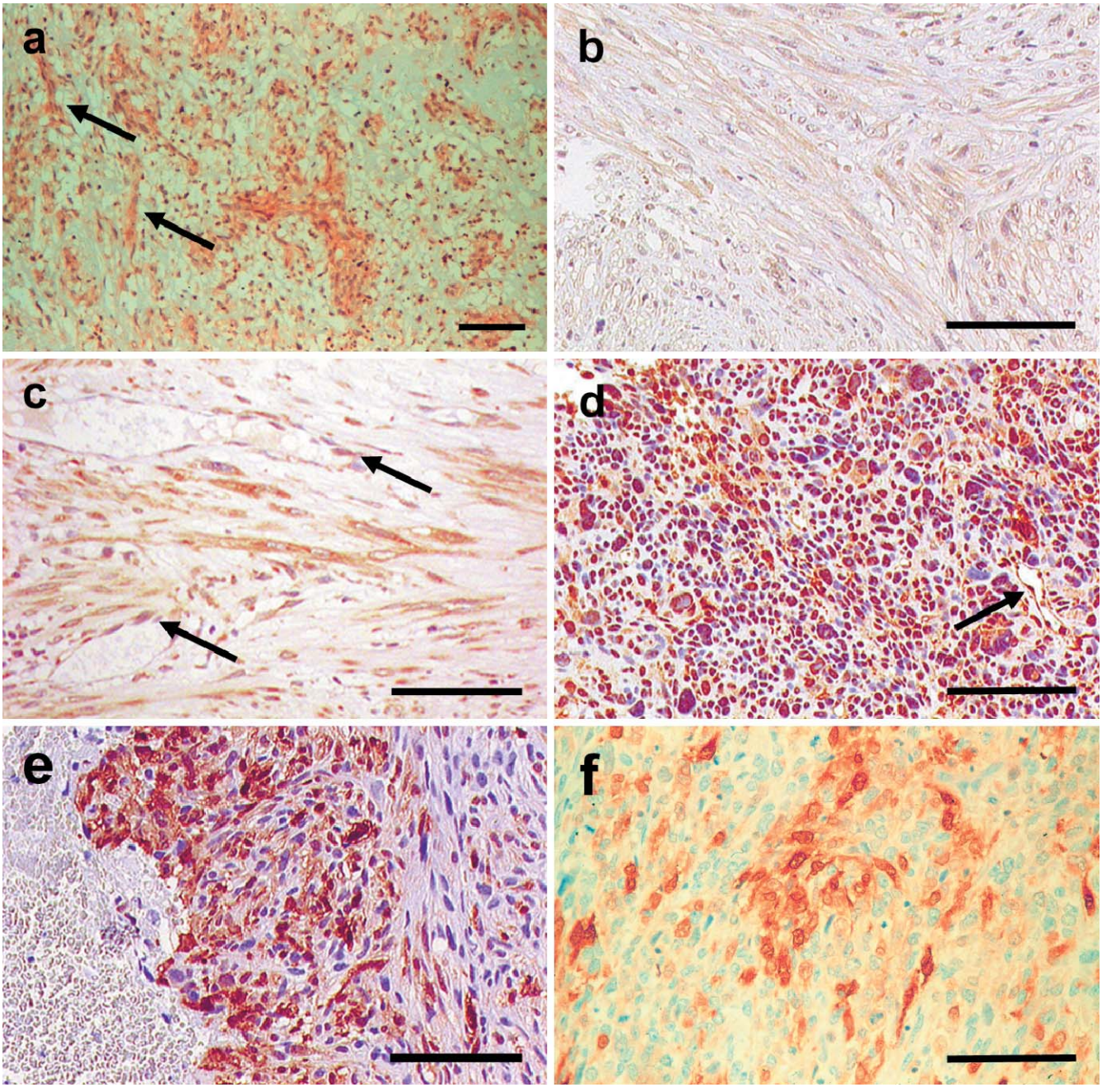



**Fig. 2** **a** P-glycoprotein is moderately expressed in tumour cells and associated vessels (→) case 6 (sarcomas of the pulmonary artery; SPA) (– 100 µm; magnification ×100). **b** Weak expression of multidrug-resistance protein in tumour cells: case 7 (leiomyosarcoma) (– 50 µm; magnification ×400). **c** Scattered positivity for lung resistance protein in sarcoma cells but also in tumour-associated vessels (→): case 14 (leiomyosarcoma) (– 50 µm; magnification ×400). **d** Virtually all cells were positive for topoisomerase II$\alpha$ and also tumour-associated vessels (→): case 16 (leiomyosarcoma) (–100 µm; magnification ×200). **e** Sarcoma cells show enhanced expression of metallothionein at the border of necrosis: case 5 (SPA) (– 100 µm; magnification ×100). **f** Abundant expression of metallothionein in sarcoma cells: case 6 (SPA) (– 50 µm; magnification ×400)

none displayed an intra-individual constant expression pattern among their primary and recurrent tumours.

Taken together, MRPs were differentially upregulated in SPAs as well as in poorly differentiated leiomyosarcomas of other origin. There was no correlation between relapse-free and overall survival and the expression of the MRP examined in this study.

## Discussion

Patients with either SPA or poorly differentiated leiomyosarcoma of other origin are known to have a poor prognosis with short overall survival, despite extensive therapy. A few of different adjuvant chemotherapy regimens exist to eradicate tumour cells. However,

tumour cells frequently develop mechanisms, e.g. drug resistance, that are responsible for relapse, metastasis, and mortality. Thus, we have investigated the influence of some drug resistance factors on tumour development, relapse-free and overall survival. P-gp and MRP contribute to chemoresistance by a transmembrane transport of drugs leading to reduced intracellular drug accumulation [7, 38].

In our study we found in most cases a moderate to strong expression of P-gp but not MRP by the tumour cells. However, we could only observe an increased expression of P-gp in two cases with relapses, while others showed a decrease or stayed at the same levels. This is in line with other reports describing that P-gp gave inconsistent results, ranging from complete absence to constant expression in different tumour entities [4]. In addition, we could not observe a significant influence of P-gp expression in the treated and non-treated groups, as well as the overall survival of the patients in our series. This fact, which has also been described recently by our group for gliomas [30] and meningeomas [31], underlines the fact that many factors are involved in the contribution to a chemoresistant phenotype. Another important observation was the constant expression of P-gp in numerous tumour-associated vessels, which has also been described previously [29, 33]. This underlines that tumour-associated vessels substantially contribute to the drug resistance by an active transport of drugs back to the bloodstream [12, 24].

It has been described that mdr1a knock-out mice, encoding the gene for the P-gp protein, demonstrate an increased sensitivity to P-gp substrate drugs [22]. However, in contrast to non-neoplastic vessels, P-gp was not found in all tumour vessels. This might be explained by the immaturity of newly formed tumour capillaries, presuming that maturity is a prerequisite for the expression of P-gp [2]. LRP is also involved in cytoplasmic drug transport to the nucleus [20] and is thus thought to contribute to a drug-resistant phenotype. We found a moderate to strong cytoplasmic signal for LRP in all SPAs and in most of the leiomyosarcomas of other origin but to a lesser extent. This difference may contribute to the poor response to chemotherapy of SPAs relative to sarcomas in general, but since we could not find any survival difference in our series, the higher levels of LRP in the SPA should have only a low impact on patients' outcomes. It is noteworthy that LRP has been described as a strong prognostic factor for chemotherapy response and outcome in acute myeloid leukaemia and ovarian cancer [20], tumours known to respond well to polychemotherapy. Thus, the investigation of LRP in a larger series of sarcomas might help to define the role of LRP in this entity. In addition, LRP expression was also found in tumour-associated vessels [30, 31]. Our findings confirm the report of Izquidero et al. (1996) who have described a broad distribution of this molecule in normal tissues and tumours [14]. It is likely that an overlapping expression of LRP, P-gp as well as topoisomerase II$\alpha$ in tumour vessels contribute to the multi-drug-resistant phenotype through an altered trans-vascular transport in different compartments of the endothelial cells (cell membrane, cytoplasmic vesicles and nucleus). In addition, we could not detect any influence of LRP expression in the treated and non-treated groups on the overall survival, thereby further enhancing the view that the pathological relevance of LRP is low. DNA topoisomerases are involved in cell growth and division and have therefore attracted major attention as a target for a variety of clinically important anti-cancer drugs [25]. However, the involvement of topoisomerase II$\alpha$ in drug resistance has been the subject of controversial discussions. Topoisomerase II$\alpha$-related resistance is mediated by decreased expression and/or activity of this enzyme in neoplastic cells which may be induced by mutations or altered gene regulation [25]. Thus, for example, topoisomerase II$\alpha$ seems to be necessary to allow doxorubicin and etoposide to intercalate in the double-stranded DNA and to induce stable DNA strand breaks. There is also evidence that shutdown of topoisomerase genes by hypermethylation leads to a downregulation and a reduced activity of this enzyme [28]. In contrast, topoisomerases are related to DNA repair [1, 26] and therefore upregulation of this molecule averts DNA damage and provides neoplastic cells having high topoisomerase expression with a survival advantage [27]. This will not only affect DNA-interacting anticancer drugs but also radiation-induced damage. It was not surprising that we could find a consistently high expression of topoisomerase II$\alpha$ in the SPA since these sarcomas are strongly proliferating lesions, as we have described previously [11].

In a recent report, Wilson et al. (2001) have rejected a role of topoisomerase II$\alpha$ in the development of drug resistance in multiple myelomas, but clearly showed a strong relationship to proliferation as documented by BrdU and Ki-67 labelling [36]. With our data, we cannot definitively answer the question of whether low or high levels of this protein may be responsible for drug resistance. However, one can speculate that drugs inhibiting topoisomerase should allow significant tumour suppression, as has been described for drug-resistant breast cancer. Another known mechanism of drug detoxification is through the action of MTs. Under physiological conditions, MTs contribute to physiological buffering, catalysing redox reactions and collagen metabolism. Thus, we found numerous MT-positive fibroblasts in adjacent normal, non-neoplastic tissue with prominent collagenous extracellular matrix. In cancer, MTs play a protective role against anticancer drugs, such as cisplatin [8, 35]. However, most cases in our series displayed low to moderate levels of this protein, and it is thus unlikely that this molecule plays an important role in this context. In addition, we observed an enhanced expression at the border of necrosis, which has been described before [6]. This observation is in keeping with pathogenetic considerations, since MT is responsible for detoxification of toxic metabolites, usually present at sites of necrosis. The idea that a clonal expansion of tumour cells positive for MT may occur during treatment could

not be substantiated by our findings, as there was no significant increase of MT expression in recurrent tumours relative to primary tumours as well as in treated versus non-treated patients. This is in contrast to a report of Frenzel et al. who described a selection of MT positive clones of murine fibrosarcoma cell lines through repeated exposure to high concentrations of $CdCl_2$ [10] and platin drugs. This contradiction may be explained by the fact that only two patients in our series received platin drugs, e.g. carboplatin. In addition, no correlation between MT expression and previously radiated tumours was found in our patients, although it is known that MT acts as a scavenger for free radicals and thus averts irradiation-induced damage [6, 32]. Thus, it is most likely that MT expression is an epiphenomenon in the drug-resistance context and may only reflect the pathophysiological action of this molecule in the ischaemia-induced micro-environment of the tumour. Notably, Sens and coworkers have recently described the association of the MT isoform 3, which has not been investigated in our series, with poor prognosis in breast cancer [23]. In addition, Joesph et al. have recently shown that MT isoforms 1 and 2 (detected with the same antibody we used) revealed MT expression as an independent predictor of survival in lung cancer [16]. Thus, conflicting results concerning this molecule need to be further investigated in the near future.

In summary, our data indicate that a number of molecules known to be involved in drug resistance were upregulated in human SPAs and leiomyosarcomas of other origin, but did not correlate with absence or presence of chemotherapy and survival. It is obvious that intrinsic sensitivity to drugs is a complex phenomenon and our data suggest that it is highly desirable to provide an individual tumour-specific assessment of various multidrug-resistant factors in order to determine an appropriate individual therapy.

**Acknowledgements** The authors wish to acknowledge the excellent technical support of Sandra Gerecht, Antonietta Rastiello and Claudia Braun.

## References

1. Ali-Osman F, Berger MS, Rajagopal S, Spence A, Livingston RB (1993) Topoisomerase II inhibition and altered kinetics of formation and repair of nitrosourea and cisplatin-induced DNA interstrand cross-links and cytotoxicity in human glioblastoma cells. Cancer Res 53:5663–5668
2. Becker I, Becker KF, Meyermann R, Hollt V (1991) The multidrug-resistance gene MDR1 is expressed in human glial tumors. Acta Neuropathol 82:516–519
3. Cole SP, Sparks KE, Fraser K, Loe DW, Grant CE, Wilson GM, Deeley RG (1994) Pharmacological characterization of multidrug resistant MRP-transfected human tumor cells. Cancer Res 54:5902–5910
4. Cordon-Cardo C, O'Brien JP, Boccia J, Casals D, Bertino JR, Melamed MR (1990) Expression of the multidrug resistance gene product (P-glycoprotein) in human normal and tumor tissues. J Histochem Cytochem 38:1277–1287
5. Depowski PL, Rosenthal SI, Brien TP, Stylos S, Johnson RL, Ross JS (2000) Topoisomerase II alpha expression in breast cancer: correlation with outcome variables. Mod Pathol 13:542–547
6. Ebadi M, Iversen PL (1994) Metallothionein in carcinogenesis and cancer chemotherapy. Gen Pharmacol 25:1297–1310
7. Endicott JA, Ling V (1989) The biochemistry of P-glycoprotein-mediated multidrug resistance. Annu Rev Biochem 58:137–171
8. Endresen L, Bakka A, Rugstad HE (1983) Increased resistance to chlorambucil in cultured cells with a high concentration of cytoplasmic metallothionein. Cancer Res 43:2918–2926
9. Filipits M, Suchomel RW, Zochbauer S, Malayeri R, Pirker R (1996) Clinical relevance of drug resistance genes in malignant disease. Leukemia 10[Suppl 3]:S10–S17
10. Frenzel KR, Saller RM, Kummermehr J, Schultz-Hector S (1995) Quantitative distinction of cisplatin-sensitive and -resistant mouse fibrosarcoma cells grown in multicell tumor spheroids. Cancer Res 55:386–391
11. Gaumann A, Petrow P, Mentzel T, Mayer E, Dahm M, Otto M, Kirkpatrick CJ, Kriegsmann J (2001) Osteopontin expression in primary sarcomas of the pulmonary artery. Virchows Arch 439:668–674
12. Hegmann EJ, Bauer HC, Kerbel RS (1992) Expression and functional activity of P-glycoprotein in cultured cerebral capillary endothelial cells. Cancer Res 52:6969–6975
13. Hofmockel G, Bassukas ID, Wittmann A, Dammrich J (1997) Is the expression of multidrug resistance gene product a prognostic indicator for the clinical outcome of patients with renal cancer? Br J Urol 80:11–17
14. Izquierdo MA, Scheffer GL, Flens MJ, Giaccone G, Broxterman HJ, Meijer CJ, van der Valk P, Scheper RJ (1996) Broad distribution of the multidrug resistance-related vault lung resistance protein in normal human tissues and tumors. Am J Pathol 148:877–887
15. Izquierdo MA, Shoemaker RH, Flens MJ, Scheffer GL, Wu L, Prather TR, Scheper RJ (1996) Overlapping phenotypes of multidrug resistance among panels of human cancer-cell lines. Int J Cancer 65:230–237
16. Joseph MG, Banerjee D, Kocha W, Feld R, Stitt LW, Cherian MG (2001) Metallothionein expression in patients with small cell carcinoma of the lung: correlation with other molecular markers and clinical outcome. Cancer 92:836–842
17. Kedersha NL, Miquel MC, Bittner D, Rome LH (1990) Vaults. II. Ribonucleoprotein structures are highly conserved among higher and lower eukaryotes. J Cell Biol 110:895–901
18. Mayer E, Kriegsmann J, Gaumann A, Kauczor HU, Dahm M, Hake U, Schmid FX, Oelert H (2001) Surgical treatment of pulmonary artery sarcoma. J Thorac Cardiovasc Surg 121:77–82
19. Nonomura A, Kurumaya H, Kono N, Nakanuma Y, Ohta G, Terahata S, Matsubara F, Matsuda T, Asaka T, Nishino T (1988) Primary pulmonary artery sarcoma. Report of two autopsy cases studied by immunohistochemistry and electron microscopy, and review of 110 cases reported in the literature. Acta Pathol Jpn 38:883–896
20. Scheffer GL, Wijngaard PL, Flens MJ, Izquierdo MA, Slovak ML, Pinedo HM, Meijer CJ, Clevers HC, Scheper RJ (1995) The drug resistance-related protein LRP is the human major vault protein. Nat Med 1:578–582
21. Scheper RJ, Broxterman HJ, Scheffer GL, Kaaijk P, Dalton WS, van Heijningen TH, van Kalken CK, Slovak ML, de Vries EG, van der Valk P, et al (1993) Overexpression of a M(r) 110,000 vesicular protein in non-P- glycoprotein-mediated multidrug resistance. Cancer Res 53:1475–1479
22. Schinkel AH, Smit JJ, van Tellingen O, Beijnen JH, Wagenaar E, van Deemter L, Mol CA, van der Valk MA, Robanus-Maandag EC, te Riele HP, et al (1994) Disruption of the mouse mdr1a P-glycoprotein gene leads to a deficiency in the blood-brain barrier and to increased sensitivity to drugs. Cell 77:491–502
23. Sens MA, Somji S, Garrett SH, Beall CL, Sens DA (2001) Metallothionein isoform 3 overexpression is associated with breast cancers having a poor prognosis. Am J Pathol 159:21–26

24. Takamiya Y, Abe Y, Tanaka Y, Tsugu A, Kazuno M, Oshika Y, Maruo K, Ohnishi Y, Sato O, Yamazaki H, Kijima H, Ueyama Y, Tamaoki N, Nakamura M (1997) Murine P-glycoprotein on stromal vessels mediates multidrug resistance in intracerebral human glioma xenografts. Br J Cancer 76:445–450
25. Takano H, Kohno K, Matsuo K, Matsuda T, Kuwano M (1992) DNA topoisomerase-targeting antitumor agents and drug resistance. Anticancer Drugs 3:323–330
26. Taki T, Arita N, Hayakawa T, Ohnishi T, Izumoto S, Yamamoto H, Mogami H (1990) T98G glioma cells have nicks in DNA in quiescent phase. Exp Cell Res 190:212–217
27. Tan KB, Mattern MR, Boyce RA, Schein P (1987) Elevated DNA topoisomerase II activity in nitrogen mustard-resistant human cells. Proc Natl Acad Sci U S A 84:7668–7671
28. Tan KB, Mattern MR, Eng WK, McCabe FL, Johnson RK (1989) Nonproductive rearrangement of DNA topoisomerase I and II genes: correlation with resistance to topoisomerase inhibitors. J Natl Cancer Inst 81:1732–1735
29. Tanaka N, Kita T, Kasai K, Nagano T (1994) The immunocytochemical localization of tumour necrosis factor and leukotriene in the rat heart and lung during endotoxin shock. Virchows Arch 424:273–277
30. Tews DS, Nissen A, Kulgen C, Gaumann AK (2000) Drug resistance-associated factors in primary and secondary glioblastomas and their precursor tumors. J Neurooncol 50:227–237
31. Tews DS, Fleissner C, Tiziani B, Gaumann AK (2001) Intrinsic expression of drug resistance-associated factors in meningiomas. Appl Immunohistochem Mol Morphol 9:242–249
32. Thornalley PJ (1996) Pharmacology of methylglyoxal: formation, modification of proteins and nucleic acids, and enzymatic detoxification—a role in pathogenesis and antiproliferative chemotherapy. Gen Pharmacol 27:565–573
33. Toth K, Vaughan MM, Peress NS, Slocum HK, Rustum YM (1996) MDR1 P-glycoprotein is expressed by endothelial cells of newly formed capillaries in human gliomas but is not expressed in the neovasculature of other primary tumors. Am J Pathol 149:853–858
34. Uozaki H, Horiuchi H, Ishida T, Iijima T, Imamura T, Machinami R (1997) Overexpression of resistance-related proteins (metallothioneins, glutathione-S-transferase pi, heat shock protein 27, and lung resistance-related protein) in osteosarcoma. Relationship with poor prognosis. Cancer 79:2336–2344
35. Welters MJ, Fichtinger-Schepman AM, Baan RA, Flens MJ, Scheper RJ, Braakhuis BJ (1998) Role of glutathione, glutathione S-transferases and multidrug resistance-related proteins in cisplatin sensitivity of head and neck cancer cell lines. Br J Cancer 77:556–561
36. Wilson CS, Medeiros LJ, Lai R, Butch AW, McCourty A, Kelly K, Brynes RK (2001) DNA topoisomerase II alpha in multiple myeloma: a marker of cell proliferation and not drug resistance. Mod Pathol 14:886–891
37. Withoff S, De Jong S, De Vries EG, Mulder NH (1996) Human DNA topoisomerase II: biochemistry and role in chemotherapy resistance (review). Anticancer Res 16:1867–1880
38. Zaman GJ, Flens MJ, van Leusden MR, de Haas M, Mulder HS, Lankelma J, Pinedo HM, Scheper RJ, Baas F, Broxterman HJ, et al (1994) The human multidrug resistance-associated protein MRP is a plasma membrane drug-efflux pump. Proc Natl Acad Sci U S A 91:8822–8826

Virchows Arch (2003) 442:538–547
DOI 10.1007/s00428-003-0809-z

ORIGINAL ARTICLE

**Roman Kodet · Marcela Mrhalová · Lenka Krsková · Jan Soukup · Vít Campr · Tomáš Neškudla · Peter Szépe · Lukáš Plank**

# Mantle cell lymphoma: improved diagnostics using a combined approach of immunohistochemistry and identification of t(11;14)(q13;q32) by polymerase chain reaction and fluorescence in situ hybridization

Received: 29 November 2002 / Accepted: 11 February 2003 / Published online: 1 May 2003
© Springer-Verlag 2003

**Abstract** *Introduction:* Mantle cell lymphoma (MCL) is a clinicopathological entity characterized by an aggressive clinical course, morphological features, and overexpression of cyclin D1 due to juxtaposition of the bcl-1 locus (and CCND1 gene coding for the cyclin D1) to the IgH gene. This phenomenon is caused by t(11;14)(q13;q32). The morphological diagnosis of MCL may pose difficulties. Ancillary methods are available to support the diagnosis. *Patients and methods:* We studied a group of 32 patients with MCL; 24 men and 8 women. The median age at the diagnosis was 64 years. We characterized the investigated group by histology, and to analyze the immunohistochemical (IHC) profile we used a panel of antibodies including anti-cyclin D1. Polymerase chain reaction (PCR) was used to detect the rearrangement of bcl-1/IgH in 26 cases (in 11 patients, the DNA was isolated from frozen tissues or from nucleated cells of bone-marrow aspirate or peripheral blood, in 15 patients we utilized paraffin-embedded material). Dual color fluorescence in situ hybridization (FISH) on interphase nuclei detecting the t(11;14)(q13;q32) was applied in all 32 cases. *Results:* Cyclin D1 IHC was positive in 29 of 30 cases tested (97%). In six, the result was weak and difficult to rely on to support the diagnosis. PCR revealed the fusion gene in 14 of the 26 cases (54%). The best yield was obtained from fresh and frozen samples (8 of 11 positive). Using FISH, we identified the translocation in all 32 patients, the findings being easily interpretable in 29 patients. In three cases, the intensity of red and green signals was weaker and difficult to read though the co-hybridized signals were identified. The classical pattern of the translocation was observed in 26 patients, while in 3 we found variant patterns suggesting a loss of the V segment of the IgH gene (2x) and a shift in the breakpoint region at chromosome 11 (1x). *Conclusion:* The diagnosis of MCL should be supported by a complex laboratory approach. Interphase FISH seems a useful complementary method to morphology and IHC. It is applicable to various tissues and cells prepared as tissue imprints or histological sections.

**Keywords** Mantle cell lymphoma · Laboratory diagnostics · t(11;14)(q13;q32) · PCR · FISH

R. Kodet (✉) · M. Mrhalová · L. Krsková · J. Soukup · V. Campr · T. Neškudla
Department of Pathology and Molecular Medicine,
Charles University,
2nd Medical School and Faculty Hospital in Motol,
V Uvalu 84, 150 06 Prague 5-Motol, Czech Republic
e-mail: Roman.Kodet@lfmotol.cuni.cz
Tel.: +420-2-24435600
Fax: +420-2-24435620

P. Szépe · L. Plank
Department of Pathology,
Jessenius Medical School, Komensky University,
Martin, Slovak Republic

## Introduction

Mantle cell lymphoma (MCL) is a clinicopathological entity with characteristic morphological, immunophenotypic and molecular features [4]. Its recognition is important from the clinical aspect. MCL is more aggressive and refractory to current treatment modalities than other small cell lymphomas [11, 36, 43, 47].

The diagnosis of MCL may not be straightforward without a support of ancillary techniques such as immunohistochemistry (IHC) [15, 24, 29, 37, 39, 51, 56], molecular methods [10, 13, 25, 30, 35, 49], cytogenetics [2, 8, 14, 20, 22, 31, 44], and fluorescence in situ hybridization (FISH) [3, 6, 17, 20, 23, 27, 32, 38, 55]. Some cases of MCL may impose as other well-defined lymphomas. There are cases with focal features of parafollicular/monocytoid B-cell/marginal zone differentiation, cases mimicking hairy cell leukemia, cases

resembling follicular lymphomas, and small cell lymphomas (CLL/SLL) [39, 42]. The problems in diagnosis stand out especially in cases with inadequate material for the morphological investigation or if trephine bone-marrow or peripheral blood specimens are the only samples available.

The diagnostic quandary has been alleviated by a demonstration of cyclin D1 overexpression, a characteristic feature of the disease. It is caused by DNA rearrangement with juxtaposition of the locus bcl-1 along with the gene CCND1 at 11q13 and the joining region of the IgH gene at 14q32 due to translocation t(11;14)(q13;q32).

There are various diagnostic approaches to demonstrate the molecular changes in MCL. At a protein level, the IHC demonstration of cyclin D1 became feasible especially when methods recovering the antigenic epitopes were applied [12, 21]. Alternatively, molecular approach is widely accepted but, due to a large area of breakpoints at the locus bcl-1, the rearrangement is revealed in a variable percentage of cases depending on the method used. The most frequent breakpoints at 11q13 cluster in a region called major translocation cluster (MTC) [25, 34, 37, 49, 50]. Occasional cases are characterized by breakpoints at regions called minor translocation clusters (mTCs) [13, 16, 33]. With application of Southern blot analysis, 55–72% of MCLs reveal the translocation (combining the results of MTC and mTCs analysis); with polymerase chain reaction (PCR) the percentage of a diagnostic result varies between 33% and 56% [16].

Reverse-transcription (RT)-PCR has also been used successfully in detection of the level of cyclin D1 mRNA expression. It is highly sensitive but not entirely specific because other malignant lymphomas express cyclin D1 mRNA. Quantification of the product may be necessary to separate the MCLs with a cyclin D1 mRNA overexpression and lymphomas with a lower level of the cyclin D1 mRNA [9, 40].

Recently, a mixture of double-colored probes detecting the t(11;14)(q13;q32) using FISH on interphase nuclei became available, and their utility in routine diagnostics appears to exceed that of the Southern blot or PCR methods [6, 17, 18, 32].

In the present study, we compared the results of IHC with the DNA diagnostics (PCR) and FISH on interphase nuclei in a series of 32 patients with MCL. For FISH, we utilized sectioned paraffin-embedded tissues in a majority of cases. The aim was to perform a retrospective analysis using a combined laboratory approach—IHC, PCR, and FISH.

## Materials and methods

There were 32 patients with a tentative or definitive diagnosis of MCL in our files (January 1996–March 2002). Paraffin blocks were available in 30 patients; in addition, one also had tissue imprints. In a further two cases, we had a bone-marrow aspirate and cytospin slides of nucleated cells from the peripheral blood (the latter was a patient with a leukemic presentation of the disease). In 11 cases, there was fresh or deep frozen tissue available for the DNA extraction. In a further 15 patients, we isolated the DNA from formalin-fixed, paraffin-embedded tissue.

**Table 1** Primary antibodies used and results of the immunohistochemistry (IHC) performed on 30 cases of mantle cell lymphoma (MCL)

| Antibody | Source, clone | Positive/total investigated |
|---|---|---|
| Cyclin D1 | (DakoCytomation, DCS-6) | 29/30 |
| CD20 | (DakoCytomation, L26) | 30/30 |
| CD3 | (DakoCytomation, rabbit) | 0*/17 |
| CD5 | (DakoCytomation, DK23; CD5/54/F6) | 15*/20 |
| CD43 | (DakoCytomation, DF-T1) | 20/25 |
| bcl-2 | (DakoCytomation, 124) | 27/28 |
| CD23 | (DakoCytomation, MHM6) | 0*/28 |
| CD10 | (Novocastra, 56C6) | 0*/25 |

* Internal control positive

For the IHC investigation, we used a panel of primary antibodies as indicated in Table 1. A LSAB detection kit with diaminobenzidine as a chromogenic substrate (DakoCytomation, Glostrup, Denmark) or a Super Sensitive detection kit with a biotinylated secondary antibody and a complex of streptavidine/alkaline phosphatase (BioGenex, San Ramon, CA) with Fast Red as a chromogenic substrate was used. For detection of cyclin D1, the sections were pretreated by microwave heating (6 min/800 W) in 10 mM citrate buffer (pH 6.0), followed by protein digestion using trypsin (30 s/37°C).

### Polymerase chain reaction

To detect the t(11;14) using PCR, primers covering the MTC at 11q13 and the JH region of the IgH gene at 14q32 were used as described by Luthra et al. in case of DNA isolation from fresh and deep frozen tissues [25]. PCR primers used by Pinyol et al. were adopted for the DNA extracted from formalin-fixed and paraffin-embedded tissues [30].

In case of frozen tissue or fresh samples, the DNA was extracted using Tri-Reagent (Invitrogen Ltd.) according to the manufacturer's instructions. In case of paraffin-embedded tissues, ten sections (5 $\mu$m) were deparaffinized with xylene (two times), followed by washing in absolute ethanol and centrifugation. The pellets were dried and dissolved in 400 $\mu$l of an extraction buffer with proteinase K at a final concentration of 200 $\mu$g/ml. The incubation was performed overnight at 37°C. Proteinase K was inactivated by heating the mix for 10 min at 95°C. Following final centrifugation, the supernatant was used for a salting-out method with 5 M NaCl and absolute ethanol. The DNA was dissolved in 40 $\mu$l sterile $H_2O$ and an aliquot of 3–5 $\mu$l was used as a template for PCR amplification.

*Fresh and frozen tissue procedure.* The PCR mixture contained 1.5 mM $MgCl_2$, 1× concentrated buffer II, 200 $\mu$M of each dNTP, 50 pM of both primers, 1 U *Taq* Gold polymerase (PE-Biosystem), DEPT (diethylpyrocarbonate-treated) $H_2O$ and 0.3 $\mu$g DNA. The reaction was run in an automatic cycler (MJ Research), starting with denaturation at 95°C 10 min, followed by 30 cycles of denaturation at 94°C for 50 s, annealing at 60°C for 75 s, and extension at 72°C for 75 s, followed by the final extension for 10 min at 72°C. The PCR product of an approximate size of 550–650 bp was detected by electrophoresis in a 1.5% agarose gel following ethidium bromide staining. As a control of intact DNA, we used PCR of the N-*myc* gene.

*PCR using DNA extracted from paraffin-embedded tissues.* The PCR mixture contained 2 mM $MgCL_2$, 1× concentrated buffer II, 200 $\mu$M of each dNTP, 50 pM both primers, 1 U *Taq* Gold polymerase. The reaction was carried out with the following temperatures and times. Denaturation 95°C for 10 min, followed by 35 cycles of denaturation at 95°C for 60 s, annealing at 57°C for 60 s, extension at 72°C for 75 s, and final extension at 72°C for 10 min. The expected size of the product was 230 bp for MTC 3/JH primers. As a control of intact DNA, we used PCR of $\beta$-globin gene. The primers used for DNA extracted from the fresh tissue or frozen sections were:

– MTC:5′ CCT CTC TCC AAA TTC CTG
– JH:5′ TGA GGA GAC GGT GAC C

The primers used for DNA extracted from the paraffin-embedded tissues were:

– MTC 3′: GGT TAG ACT GTG ATT AGC
– JH: same sequence as that for the DNA isolated from frozen and fresh tissues

### FISH

For the FISH on interphase nuclei, paraffin sections were cut at 2–3 $\mu$m, deparaffinized in xylene, and dehydrated in absolute ethanol. The slides were then immersed into 0.2 M HCl for 20 min, washed in distilled water, 2× sodium saline citrate (SSC) solution, and incubated in a saturated solution of NaSCN for 30 min at 80°C, washed in distilled water and 2× SSC solution. The sections were trypsin digested for 10 min at 37°C. The enzymatic activity was stopped by washing in 2× SSC solution. The slides were dried at 45°C. Post-fixation in 4% paraformaldehyde was performed for 10 min at 4°C. After washing in 2× SSC, genomic DNA was denatured for 5 min at 72°C in 70% formamide solution (pH 7.2; 2× SSC). The slides were dehydrated in an ascending row of ethanol, and left to dry at 45°C. The probes were denatured (5 min at 73°C) and applied immediately on the sections. The slides were incubated overnight at 37°C in wet chamber. The following day, they were washed in washing solutions (2 min at 72°C in 2× SSC/0.3% NP-40/pH 7.25 and up to 1 min at room temperature in 2× SSC/0.1% NP-40/pH 7.0). Then the slides were left to dry in the dark at room temperature. DAPI (4,6 diamidino-2-fenylindol) in anti-fade solution was used to counterstain the nuclei. In case of tissue imprints and nuclear isolates, the cells were dehydrated and DNA was denatured in 70% formamide for 2 min at 72°C (pH 7.2). The same protocol as in the case of tissue sections was used in the following steps. A fluorescence microscope Olympus AX70 equipped with a triple-band filter to detect SpectrumGreen, SpectrumOrange, and DAPI was employed. In the case of DAPI interference with the intensity of the specific signals, we used a double-band filter omitting the band visualizing DAPI counterstain. The photographs were taken using video camera Sony and Olympus AnalySIS software.

The probes (LSI IgH SpectrumGreen/LSI CCND1 SpectrumOrange, Vysis Inc., IL, USA) hybridize to the locus 14q32 (IgH) and to the locus 11q13 (CCND1). The probes are designed to identify the most common type of the t(11;14), and also variant traslocations with alternative breakpoints at 11q13, and a translocation characterized by a loss of V segment of the IgH gene at 14q32.

The evaluation was adopted according to the manufacturer's instructions (Vysis Inc.). The result was as follows: in the case of both chromosomes intact for the particular regions, two red signals (intact 11q13) and two green signals (intact 14q32) were seen. In the most common type of t(11;14), the two double-marked rearranged chromosomes displayed two co-localized signals (yellow or tightly adjacent green–red, in short "Y"), and one red signal for the intact allele of chromosome 11 and one green signal for the intact allele of chromosome 14 are seen (2Y1R1G). If there was a shift of the breakpoint at chromosome 11q13 (the breakpoint occurs outside the region covered by the probe) the pattern was as follows: one signal of normal chromosome 11 at 11q13 (red), one of chromosome 14 at 14q32 (green), and two signals derived from the translocated chromosomes—one green from the derivative chromosome 11 and one co-localized (yellow) signal from the derivative chromosome 14 (1Y1R2G). Another translocation variant was characterized by a deletion at the "V" segment of the IgH gene. In such a case, one of the regions to which the probe against 14q32 hybridizes was lost. One red signal from the normal chromosome 11, one green signal from the normal chromosome 14, one co-localized signal (yellow) from the derivative chromosome 11 and one red signal from the derivative chromosome 14 were present (1Y2R1G).

Because the interphase FISH on paraffin sections had to be evaluated considering the fact that parts of the nuclei were cut off and the signals were incomplete in some cells, we compared the results of counting the number of signals in a subset of 12 cases of MCL (one hundred cells counted for each case) and in control tissues, in which the yellow fluorescence may have arisen due to an incidental overlapping of the green and red signals (6 hyperplastic lymph nodes, 2 cases of follicular lymphoma grade I, and 5 cases of CLL/SLL involving lymph nodes). All the control cases were cyclin D1 negative by IHC; a weak to moderate endothelial cell positivity served as an internal control of the method. In control tissues, FISH revealed a pattern of two red and two green signals characteristic of non-translocated loci 11q13 and 14q32 in a majority of the cells. Incidental overlapping of signals causing additive (yellow) fluorescence was found in 5–16% of the counted cells (mean 9.5%, median 8.5%), whereas one or two yellow signals were observed in 89–98% of cells in MCLs (mean 93%, median 94%). The result was significant ($t$-test, $P<0.0001$). The most important finding was, however, that in any case of the control group, we observed two yellow signals in one nucleus, whereas the percentage of cells with two yellow signals per a nucleus in the group of MCLs ranged from 45% to 65% (mean 50.67%, median 51%). To establish a high threshold of certainty for diagnosis of the t(11;14), we counted cells with a complete expected pattern of the FISH signals in 100 of the cells in the investigated specimen. In one patient with MCL, we had tissue imprints available and we compared the results of FISH with those obtained from the paraffin section for that case.

## Results

The tumor was identified on the basis of lymph-node histology in 21 cases. Two further patients had simultaneous lymph-node and gastrointestinal tract (GIT) biopsy, and two had small intestine biopsy only (lymphomatoid polyposis). Three patients had a biopsy from the lymphatic tissue of the Waldeyer's ring (palatinal tonsils). In three cases, the diagnosis was established on the basis of bone-marrow investigations (2× trephine biopsy, 1× bone-marrow aspirate), and, in one case—a man with leukemic presentation—the diagnosis was made from samples of the peripheral blood.

### Histology and IHC

In 26 cases of the lymph nodes and palatinal tonsils investigated, MCLs were characterized by a complete or partial effacement of the tissue architecture. Diffuse growth prevailed in 12 patients. In 5, the germinal centers were partially preserved and surrounded by a mantle-type

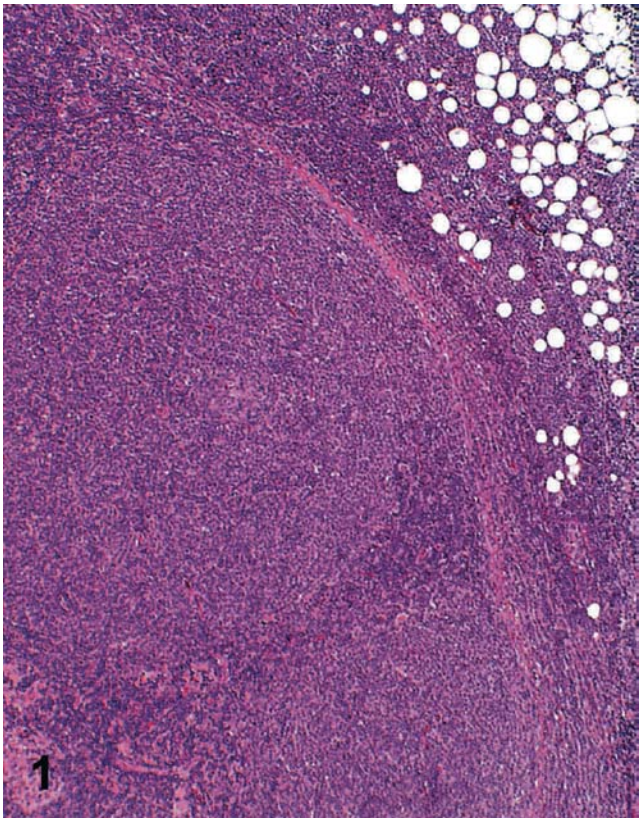



**Fig. 1** A low-power view of the tumor having a nodular pattern; extension of the tumor into the perinodal adipose tissue is seen

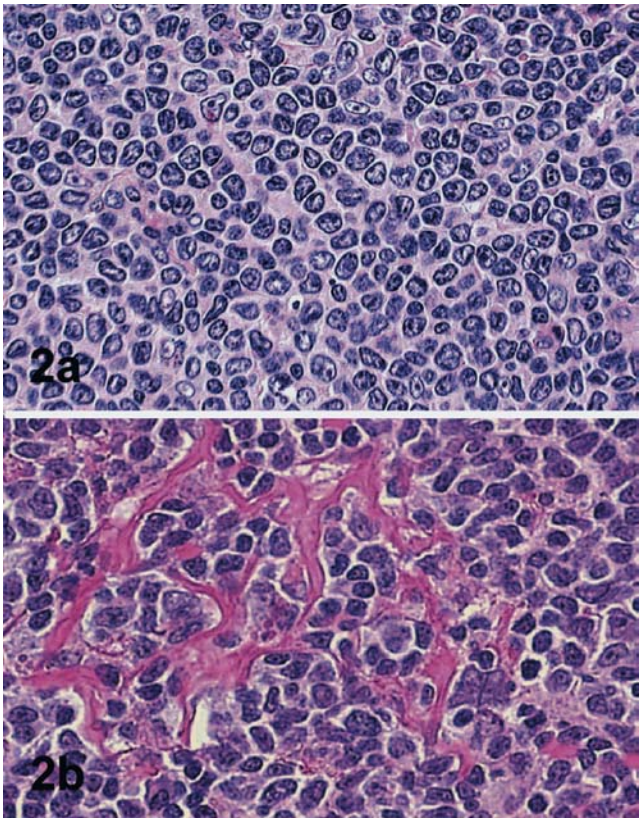



**Fig. 2** **a** The tumor cells of intermediate size and cleaved nuclei can be seen at a higher power view. **b** Hyalinized collagenous trabeculae are present in six cases

growth, and, in 9, the predominant growth pattern was nodular (Fig. 1).

The tumor cells were small to medium sized and had irregular nuclei with nuclear infoldings and a thin rim of cytoplasm (Fig. 2a). In one tumor, the cells had a more abundant clear cytoplasm. In six cases, we observed perivascular irregular bands of hyalinized collagen (Fig. 2b). Epithelioid histiocytes were commonly present, being prominent in two cases. In three patients, the samples from the lymph nodes revealed numerous mitotic figures (>10/10 HPF, objective ×40; 1×HPF=0.145 $mm^2$), and the cells had the appearance consistent with the blastic (lymphoblastoid) variant of the tumor [54]. Consecutive biopsy samples during the follow-up period revealed transformation to the blastic variant in another patient.

In patients with trephine biopsies as the only source of tissue material available for the diagnosis, the infiltration of the bone marrow was diffuse and massive in one; in another it was nodular. The disease presented in a leukemic form in one patient. The peripheral blood samples revealed cells with irregular nuclear outlines, inconspicuous nucleoli and a narrow rim of moderately basophilic cytoplasm.

The results of IHC investigation are summarized in Table 1 and specified in Table 2. Of 30 investigated cases, 29 were positive for cyclin D1 (Fig. 3). The proportion of the positive tumor cell population was difficult to assess but, in all cases, a rough estimate indicated at least 50% of the tumor cell nuclei stained positively with cyclin D1. Residual lymphatic tissue of the lymph nodes and tonsils was negative. Endothelial cells were weakly to moderately positive. The keratinocytes of the tonsilar epithelium were strongly positive, especially in the basal and suprabasal layers. The staining intensity in the tumor cells varied from case to case and also within individual cases. In 7 cases it was strong, in 16 the reaction was considered moderate but easy to interpret, and in 6 cases the staining was weak and difficult to rely on even when compared with the negatively stained areas of the residual tissues uninvolved by the lymphoma. CD5 was evaluated in both frozen and paraffin-embedded tissues: of the total 20 cases investigated, the CD5 was positive in 15 (12 in the paraffin-embedded material). There was a strong CD5 positivity in scattered lymphocytes which were considered reactive T cells (their number roughly corresponded to that of CD3 positive lymphocytes). The CD5 positivity of the tumor cells was markedly weaker. The tumor cells gave a uniformly strong positivity for CD20 and for the bcl-2 protein, and they were also CD43 positive in 20 of 25 cases (Table 1). None of the specimens was CD23 or CD10 positive in the tumor cell population. Remnants of

**Table 2** Summarized results of fluorescence in situ hybridization (FISH), polymerase chain reaction (PCR), and immunohistochemistry (IHC) for cyclin D1 and CD5 in patients with mantle cell lymphoma (MCL). *nd* not done

| No. of cases | FISH t(11;14) | PCR t(11;14) | IHC cyclin D1 | IHC CD5 |
|---|---|---|---|---|
| 8 | Present | Present | 3+, 2+ | + |
| 1 | Present | Present | 3+, 2+ | – |
| 3 | Present* | Absent | 3+, 2+ | + |
| 4 | Present | Absent | 3+, 2+ | nd |
| 3 | Present | nd | 3+, 2+ | nd |
| 1 | Present** | Absent | 3+ | – |
| 1 | Present** | Present | 2+ | + |
| 1 | Present** | Present | 2+ | – |
| 1 | Present | Absent | 2+ | – |
| 1 | Present | Present | 1+ | + |
| 1 | Present | Absent | 1+ | + |
| 1 | Present | Absent | 1+ | nd |
| 1 | Present | nd | 1+ | nd |
| 1 | Present | nd | 1+ | + |
| 1 | Present | nd | 1+ | – |
| 1 | Present | Absent | – | nd |
| 2 | Present | Present | nd*** | nd*** |

*A variant pattern of the t(11;14)
**Two yellow signals were discernible by FISH but the red and green signals were weak and difficult to enumerate
***A sample of peripheral blood and of a bone marrow aspirate

lymphoid follicles were occasionally seen in the lymph nodes infiltrated by the tumor (Fig. 4).

## PCR detection of bcl-1/IgH rearrangement

Eleven patients were investigated on the basis of DNA extraction from frozen or fresh tissue samples. In a further 15 patients, we isolated the DNA from paraffin-embedded tissue, and the yield was of a sufficient amount and quality with a positive control gene ($\beta$-globin) to analyze the samples for the presence of bcl-1/IgH rearrangement. Eight of the eleven patients with the DNA extracted from the frozen tissue revealed the rearrangement indicating t(11;14)(q13;q32) (Fig. 5). The results based on the DNA extracted from the paraffin embedded samples were less fruitful, with 6 of the 15 lymphomas positive for the bcl-1/IgH rearrangement. Altogether 14 cases of the 26 analyzed were identified to harbor the rearranged loci by PCR (54%) (Table 2).

## Fluorescence in-situ hybridization

In all cases, non-neoplastic lymphocytes and histiocytes with the signal pattern typical of non-rearranged cells (2R2G) were present (Fig. 6a). The tumor cells revealed co-hybridized signals (yellow) in all 32 patients (Table 2). The co-hybridized signals were present in a majority of the cells in tissue sections (>85% of the total cell population), although the pattern was incomplete in some cells due to the tissue sectioning. In many tumor cells,

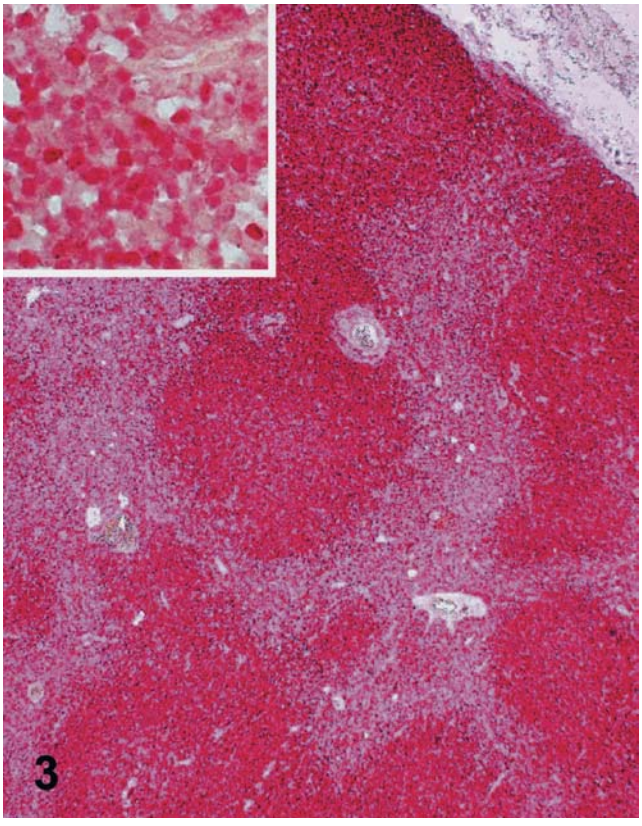



**Fig. 3** Cyclin D1 positivity highlights a nodular pattern of the tumor growth in this example. *Insert* shows a detail of positive cell nuclei in a proportion of the cell population. *IHC* immunohistochemistry of paraffin-embedded tissue section, alkaline phosphatase/Fast Red

however, we observed a complete pattern of signals of the expected appearance—2Y1R1G (average 31.3%; median 32.5%) (Fig. 6b, c). In 29 cases, we identified tumor cells with a complete signal set (27–48 cells in individual lymphomas). In the patient with the cytospin preparation and in the patient for whom we had tissue imprints from a lymph node available we observed a complete pattern of the reciprocal translocation in a majority of the cells present in each sample. The result of the latter case did not differ qualitatively from that of a simultaneously investigated paraffin tissue section. In 19 patients, the pattern was that of two co-localized signals (yellow) for the rearranged loci, one red and one green for the normal alleles of the investigated loci on chromosome 11 and 14, respectively. In three patients, the fusion signals varied from the classical pattern. All counted cells had only one yellow signal for the fusion loci; two patients had the pattern 1Y2R1G indicating a possible loss of the V segment at 14q32 (one with a blastic histology); one had 1Y1R2G suggesting a variation breakpoint at 11q13. All three patients with a variant rearrangement diagnosed by means of FISH also had PCR analysis performed on them, and the result was negative; however, cyclin D1 detected using IHC was positive—in one strongly, and in two the intensity of the reaction was moderate. In seven patients,

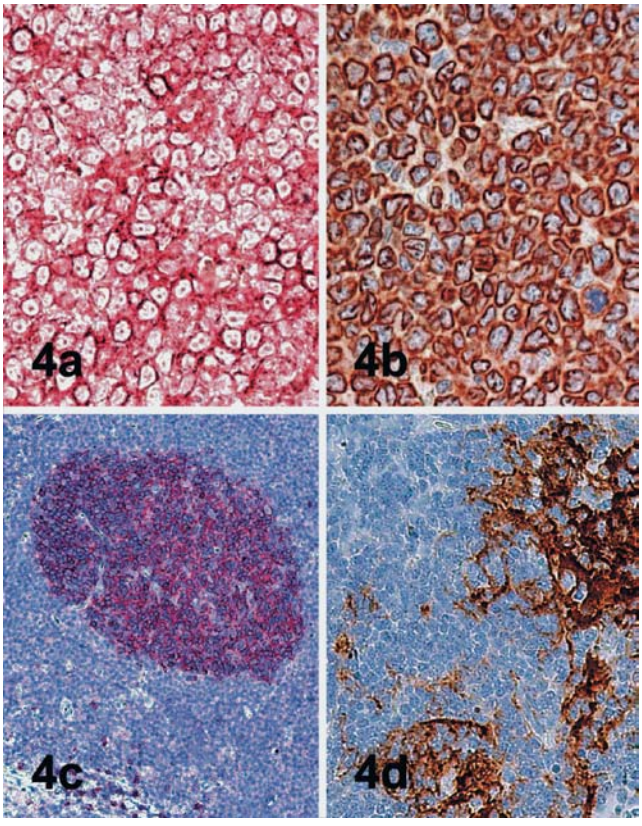



**Fig. 4** **a** CD5 on paraffin sections demonstrates an overall positivity of the tumor. **b** The bcl-2 protein shows a uniformly strong positivity of the tumor cells. **c** Remnants of CD10-positive follicular center cells may be seen in some areas; whereas compartments occupied by the tumor cell population are negative. **d** Residual follicular dendritic cells are highlighted by CD23 positivity. *IHC* immunohistochemistry of paraffin-embedded tissue sections, alkaline phosphatase/Fast Red (**a**, **c**); horseradish peroxidase/diaminobenzidine (**b**, **d**)

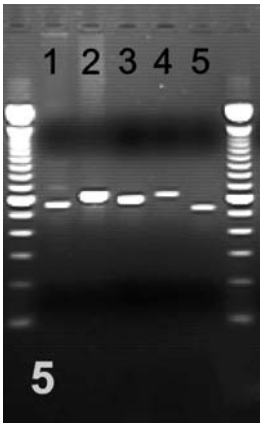



**Fig. 5** Polymerase chain reaction demonstration of the rearranged bcl-1/IgH loci: *lane 1* an 86-year-old man, cervical lymphadenopathy; *lane 2* a 60-year-old man, generalized lymphadenopathy, cervical lymph node; *lane 3* a 72-year-old woman, inguinal lymph node; *lane 4* a 60-year-old woman, bone-marrow isolate; *lane 5* a 70-year-old man, cervical lymph node

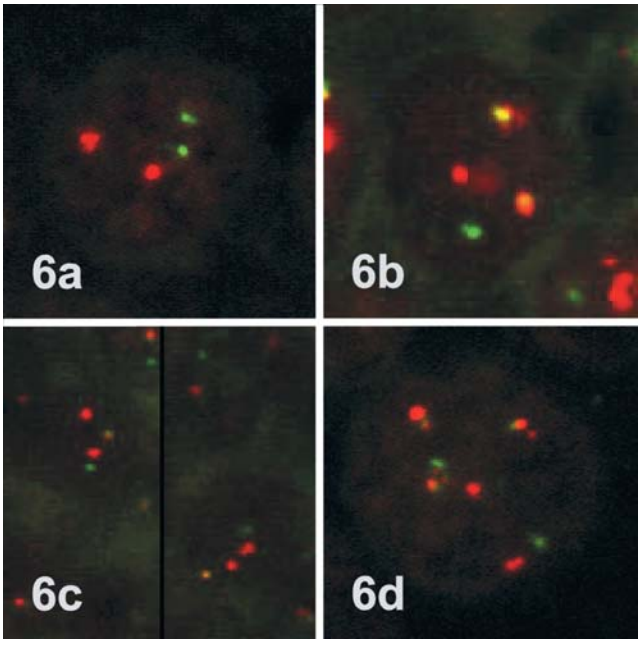



**Fig. 6** Results of fluorescence in situ hybridization. **a** Non-neoplastic cells are characterized by two separate red and green signals for 11q13 and 14q32, respectively (2R2G). **b** Dual fusion pattern of the t(11;14)—two co-localized yellow signals for the translocated loci, one red and one green signal for the intact alleles are present (2Y1R1G). **c** Two cells from a case of MCL with a pattern suggestive of a variant translocation (1Y2R1G). **d** Numerical changes of the locus specific signals—three co-hybridized signals, two red and two green signals are present (3Y2R2G). Dual fusion two color probes (Vysis, Inc), IgH locus—Spectrum Green, bcl-1 locus—Spectrum Orange

there were co-localized signals (in six 2Y, in one 3Y) and a variable number of red or green signals indicating numerical changes of the detected loci suggesting complex numerical changes of chromosome 11 and/or 14 (Fig. 6d). The most frequent pattern in these cases was 2Y2R2G. Two of the seven patients with numerical chromosomal changes had a blastic variant observed by histology and one patient presented with a leukemic form of the disease. In one patient with consecutive biopsies revealing a progression from the classical morphology to the blastic variant of MCL, a classical translocation without numerical changes was seen in the first biopsy; in the sample obtained 4 years later, we observed supernumerary signals for both 11q13 and 14q32 loci. The precise counting of the supernumerary signals was, however, difficult because of the tissue sectioning. For that reason, it appeared that specification of the numerical changes of the loci at chromosomes 11 and 14 is not suitable using tissue sections. All 14 PCR-positive cases were revealed to have the classical pattern of the rearrangement observed using FISH.

In three patients of the 32 investigated, we were able to discern the presence of two fusion signals, but the green and red signals were uncountable due to a weak intensity of fluorescence. Two of these cases were bone-marrow trephine biopsies (decalcified samples); one was an

intestinal biopsy of lymphomatoid polyposis (a consult case). All three samples were positive for cyclin D1.

Thirteen patients were primarily investigated in the years we did not have IHC (for cyclin D1), PCR, and FISH available. The diagnosis of MCL was made in nine; in the remaining four patients, the diagnosis of MCL was on the differential diagnosis list, but we were not certain with the final classification. Most of the diagnostic problems were in differentiating low-grade follicular lymphomas and CLL/SLL. PCR, FISH, and the IHC performed as a part of this study helped to establish the diagnosis retrospectively in these patients.

The average age of the group of 32 patients with the diagnosis of MCL was 64 years, median age was 61 years, range from 47 years to 86 years. There were 24 men and 8 women. The follow-up of 23 of the patients was too short (less than 2 years). Five patients of nine with a follow-up longer than 2 years died, four of the disease progression (27 months to 48 months) and another of ischemic heart disease. The latter patient also had a bulky residual tumor of the lymph nodes, spleen and bone marrow. Four patients are alive, three well without disease progression 2–5 years after the treatment start and one patient has residual disease in the bone marrow.

## Discussion

The diagnosis of MCL may be straightforward using classical histology but in many instances its appearance may be misleading, and the diagnosis should be supported by ancillary methods, in routine diagnosis by IHC [37, 42, 48, 53]. In our series, prior to introduction of newer diagnostic methods, we made a confident diagnosis of MCL in 9 of 13 cases registered in our files by that time on the basis of the lymph node, tonsilar, and intestinal morphology. The final diagnosis of MCL in the remaining 4 cases was made using the tools employed in this study. In some previous retrospective studies, the initial histological diagnosis was reviewed and modified in nearly half of the cases [36]. Of markers used in MCLs, cyclin D1 positivity appears to be pathognomic [15, 19, 39, 41, 51, 52, 53]. The specificity is not absolute because occasional cases of B-CLL/SLL, plasmocytomas, and hairy cell leukemias may show cyclin D1 overexpression [10, 45]. The molecular events in such cases may differ from those involved in MCL [46, 56]. Conversely, not all cases of MCL stain positively for cyclin D1 though being rearranged at the genomic level. Some investigators circumvent the technical problems with IHC demonstration of cyclin D1 using in situ mRNA study for cyclin D1 and showed positive results in almost all cases, including bone-marrow specimens [1]. However, the technical problems of cyclin D1 immunohistochemistry may be overcome by a choice of primary antibodies [29] and methods used in demasking the epitope of the antigen [12, 21]. In this study, the IHC staining for cyclin D1 was shown in 29 of 30 patients investigated. In most cases, the positivity was generally moderate to strong in the tumor cell population, but in six cases it was weak, a result not entirely satisfactory especially when establishing the primary diagnosis of MCL.

Molecular analysis may serve to support the diagnosis of MCL by revealing the CCND1 gene rearrangement, and it is relatively specific [10, 13, 25, 30, 35, 37, 49]. Only rare cases of multiple myeloma have been shown to share the same rearrangement with MCL [46]. However, DNA molecular diagnostics is limited by a large area of bcl-1 locus breakpoints, as was shown by means of Southern blot [10]. In recent years, less laborious PCR techniques are preferred to Southern-blot analysis, and the results of the two methods are similar as for the percentage of positively diagnosed cases [16, 25]. Moreover, using PCR, paraffin-embedded archival material may be successfully utilized [1, 13, 16, 30].

In this study, we investigated a variety of tissue samples—frozen tumor tissue, bone-marrow aspirate, fresh peripheral blood, and formalin-fixed/paraffin-embedded tissues. Of 11 patients with appropriate DNA samples isolated from the fresh or frozen tissues, 8 gave a positive result indicating bcl-1/IgH fusion, and in 6 of 15 cases with the DNA extracted from the paraffin-embedded tissue the translocation was also revealed. Considering the overall efficacy of the PCR, regardless of the type and fixation of the tissue used for the DNA extraction, bcl-1/IgH rearrangement was found in 54% of the patients. Our results thus correspond to those published previously.

FISH on interphase nuclei designed to identify the specific chromosomal changes in MCL has become recently available. Single-color FISH was used initially with a chromosome-11 painting probe [55] and the yeast artificial chromosome spanning the bcl-1 locus [7]. However, the reliability of single-color probes for diagnosis was low relative to two-color probes designed later. Two-color cosmid probes identifying 11q13 were successfully used to detect the breakpoints in leukemic forms of MCL and atypical chronic lymphocytic leukemias [26]. Katz et al. used a mixture of probes identifying the breakpoint at the 11q13 together with a chromosome 11 enumeration probe, which still improves the evaluation of the results [20]. They found breakpoints in all MCLs investigated, whereas other lymphomas had the chromosome 11 intact. Monteil et al. designed a two-color probe model to reveal t(11;14) at the 14+ derivative chromosome and, with use of a cosmid probe Cos17 targeted telomeric to the CCND1 gene and a cosmid probe Ig13, they demonstrated a high diagnostic efficacy of this approach [27]. Because the pattern they rendered (1Y1G1R) is indistinguishable from that caused by incidental overlapping of the investigated loci in normal cells, the use in tissue sections would be limited. Still other probes used in diagnosis of MCL took the advantage in demonstrating the breakpoint at 11q13 by one extra red signal—derived from the splitting of the chromosome (1Y2R1G) while the signal marking the IgH locus at 14q32 was located centromeric to the breakpoint [3, 23]. This pattern proved to be more reliable in distinguishing

the t(11;14)(q13;q32) from the incidental overlapping of the signals. Li et al. first used tissue sections but, because of the small size of the tumor cells in tissue sections and a high density of the cells, they preferred to evaluate nuclei isolated from the paraffin blocks [23].

To further improve the efficacy of FISH, Remstein et al. developed a dual-color, dual-fusion FISH marking the reciprocal translocation to a full extent [32]. It has brought a reliable tool to the investigation of completely preserved nuclei such as tissue imprints or nuclear isolates but, as we have demonstrated, also paraffin sections. Cells with incidental red and green signal overlapping (yellow, indistinguishable from the pattern seen in the translocation) are uncommon according to our experience with investigation of the control cases. In MCLs, the cells displaying co-localized (yellow) signals predominate, and the results are easy to evaluate. At least one co-localized signal was seen in a high percentage of the cells investigated in each sample (>85%), which practically rules out evaluating incidental overlapping of the signals. Moreover, a careful overview of the whole specimen was performed in 12 MCLs and on average in half the cell population counted, we found two co-hybridized signals. In nearly one-third of the cells, a complete expected signal pattern was easily identified. Similar results were obtained in a combined study of MCL, follicular lymphomas and Burkitt's lymphomas [18].

We observed co-localized signals of the rearranged chromosomes in all 32 patients in whom the diagnosis of MCL was made or considered in the differential diagnosis on the basis of histology, IHC and PCR, a finding similar to other observations published on the subject [6, 17]. The efficacy of revealing the translocation by the system designed by Vysis Inc. is high, exceeding 90%; negative findings may be attributable to variant translocations occurring outside the areas covered by the probes [17]. Most importantly, the finding of t(11;14) by FISH confirmed the diagnosis in all six cases with a weak cyclin D1 IHC staining as well as in one case in which cyclin D1 was negative. The most frequent pattern of FISH was that of two fusion signals for the reciprocally translocated chromosomes 11 and 14, and one red and one green signal for the intact allelic chromosomes. Numerical changes of the signals either at 11q13 or at 14q32 were also noted in seven patients, a finding similar to that reported by Katz et al. for chromosome 11 [20]. Numerical chromosomal changes are best revealed by cytogenetics, by comparative genomic hybridization or by more complex FISH studies [2, 5, 8, 14, 28] unavailable to the authors. Still, the information on the numerical chromosomal changes obtained on retrospectively investigated cases with the aid of FISH on paraffin-embedded material may be of some diagnostic value. The patients with complex chromosomal changes are inclined to run a more progressive course [8, 14, 20, 31]. Ott et al. described trisomies of chromosomes 3, 7, and 18 in a fraction of cases, but the most frequent finding was tetraploidy—30% of MCLs. It was most characteristic for the pleomorphic subtype of MCL [28]. In blastoid variant of MCL, Katz et al. found four or more 11q13 signals [20]. Au et al. suggests that MCLs with the involvement of lymph nodes tend to have more complex chromosomal changes than the MCLs presenting as leukemias [2]. Data obtained in the present study are limited but, in general, they are in agreement with these observations. Two patients with blastoid morphology and a high mitotic count diagnosed at the disease onset presented with numerical changes at 11q13 and 14q32. Similarly, the numerical chromosomal changes were observed in a patient with a leukemic form of the disease. One patient had a typical translocation pattern at the first examination, the second biopsy taken with the disease progression 4 years later revealed numerical chromosomal changes. Another case with a blastoid appearance had a variant translocation characterized by a pattern 1Y2R1G (suggestive deletion of the V segment of the IgH gene). However, it has to be stressed that tissue sections did not prove suitable to analyze numerical chromosomal changes along with the translocations because of difficult precise counting of the supernumerary signals.

FISH on interphase nuclei has a major advantage in that it may be used in analyzing histology slides obtained from the paraffin-embedded material. Thus, topographical relationships are maintained, which may help in identifying tumor cell compartments (e.g., in focal bone-marrow infiltrates). Furthermore, consult cases are accessible for the investigation, and a retrospective study on paraffin sections may be performed.

In summary, 32 cases of MCL were diagnosed using a combined morphological, IHC, PCR, and DNA hybridization study. Of the methods employed, FISH on interphase nuclei seems most effective, reliable and specific in identifying the chromosomal rearrangement in MCLs, and it may be added to a panel of investigation methods used in specification of small cell lymphomas, especially in those with weak or ambiguous cyclin D1 immunohistochemistry. In cases with a typical morphology and positive cyclin D1 (IHC), FISH for the t(11;14) may serve to complement the findings, although it does not convey any further information in the diagnostic process. However, a demonstration of numerical chromosomal changes may bring clinically relevant information as they portend a more aggressive course of the disease.

**Acknowledgements** The study was supported by the Internal Grant Agency of the Ministry of Health of the Czech Republic IGA MZ ČR NC/6296–3, by the Research Fund of the Ministry of Education, Youth and Sports of the Czech Republic no. 111 300003, and by VEGA SR no. 1/8152/01. We thank the hematologists and pathologists who submitted individual cases for consultations: Dr. M. Marková (ÚHKT, Prague), Dr. M. Procházka (Dept. of Pathology, Třebíč), Dr. A. Švec (Dept. of Pathology, FNKV, Prague).

## References

1. Athanasiou E, Kotoula V, Hytiroglou P, Kouidou S, Kaloutsi V, Papadimitriou CS (2001) In situ hybridization and reverse transcription-polymerase chain reaction for cyclin D1 mRNA in

the diagnosis of mantle cell lymphoma in paraffin-embedded tissues. Mod Pathol 14:62–71
2. Au WY, Gascoyne RD, Viswanatha DS, Connors JM, Klasa RJ, Horsman DE (2002) Cytogenetic analysis in mantle cell lymphoma: a review of 214 cases. Leuk Lymphoma 43:783–791
3. Avet-Loiseau H, Garand R, Gaillard F, Daviet A, Mellerin MP, Robillard N, Bouyge I, Arcot S, Batzer M, Talmant P, Harousseau JL, Milpied N, Bataille R (1998) Detection of t(11;14) using interphase molecular cytogenetics in mantle cell lymphoma and atypical chronic lymphocytic leukemia. Genes Chromosomes Cancer 23:175–182
4. Banks PM, Chan J, Cleary ML, Delsol G, De Wolf-Peeters C, Gatter K, Grogan TM, Harris NL, Isaacson PC, Jaffe ES, Mason D, Pileri S, Ralfkiaer E, Stein H, Warnke RA (1992) Mantle cell lymphoma: a proposal for unification of morphologic, immunologic, and molecular data. Am J Surg Pathol 16:637–640
5. Bea S, Ribas M, Hernandez JM, Bosch F, Pinyol M, Hernandez L, Garcia JL, Flores T, Gonzalez M, Lopez-Guillermo A, Piris MA, Cardesa A, Montserrat E, Miro R, Campo E (1999) Increased number of chromosomal imbalances and high-level DNA amplifications in mantle cell lymphoma are associated with blastoid variants. Blood 93:4365–4374
6. Belaud-Rotureau MA, Parrens M, Dubus P, Garroste JC, de Mascarel A, Merlio JP (2002) A comparative analysis of FISH, RT-PCR, PCR, and immunohistochemistry for the diagnosis of mantle cell lymphomas. Mod Pathol 15:517–525
7. Bigoni R, Negrini M, Veronese ML, Cuneo A, Castoldi GL, Croce CM (1996) Characterization of t(11;14) translocation in mantle cell lymphoma by fluorescent in situ hybridization. Oncogene 13:797–802
8. Bigoni R, Cuneo A, Milani R, Roberti MG, Bardi A, Rigolin GM, Cavazzini F, Agostini P, Castoldi G (2001) Secondary chromosome changes in mantle cell lymphoma: cytogenetic and fluorescence in situ hybridization studies. Leuk Lymphoma 40:581–590
9. Bijwaard KE, Aguilera NS, Monczak Y, Trudel M, Taubenberger JK, Lichy JH (2001) Quantitative real-time reverse transcription-PCR assay for cyclin D1 expression: utility in the diagnosis of mantle cell lymphoma. Clin Chem 47:195–201
10. Bosch F, Jares P, Campo E, Lopez-Guillermo A, Piris MA, Villamor N, Tassies D, Jaffe ES, Montserrat E, Rozman C, et al (1994) PRAD-1/cyclin D1 gene overexpression in chronic lymphoproliferative disorders: a highly specific marker of mantle cell lymphoma. Blood 84:2726–2732
11. Bosch F, Lopez-Guillermo A, Campo E, Ribera JM, Conde E, Piris MA, Vallespi T, Woessner S, Montserrat E (1998) Mantle cell lymphoma: presenting features, response to therapy, and prognostic factors. Cancer 82:567–575
12. Chan JK, Miller KD, Munson P, Isaacson PG (1999) Immunostaining for cyclin D1 and the diagnosis of mantle cell lymphoma: is there a reliable method? Histopathology 34:266–270
13. Chibbar R, Leung K, McCormick S, Ritzkalla K, Strickler J, Staggs R, Poppema S, Brunning RD, McGlennen RC (1998) bcl-1 gene rearrangements in mantle cell lymphoma: a comprehensive analysis of 118 cases, including B-5-fixed tissue, by polymerase chain reaction and Southern transfer analysis. Mod Pathol 11:1089–1097
14. Cuneo A, Bigoni R, Rigolin GM, Roberti MG, Bardi A, Piva N, Milani R, Bullrich F, Veronese ML, Croce C, Birg F, Dohner H, Hagemeijer A, Castoldi G (1999) Cytogenetic profile of lymphoma of follicle mantle lineage: correlation with clinicobiologic features. Blood 93:1372–1380
15. de Boer CJ, Schuuring E, Dreef E, Peters G, Bartek J, Kluin PM, van Krieken JH (1995) Cyclin D1 protein analysis in the diagnosis of mantle cell lymphoma. Blood 86:2715–2723
16. Fan H, Gulley ML, Gascoyne RD, Horsman DE, Adomat SA, Cho CG (1998) Molecular methods for detecting t(11;14) translocations in mantle-cell lymphomas. Diagn Mol Pathol 7:209–214
17. Frater JL, Tsiftsakis EK, Hsi ED, Pettay J, Tubbs RR (2001) Use of novel t(11;14) and t(14;18) dual-fusion fluorescence in situ hybridization probes in the differential diagnosis of lymphomas of small lymphocytes. Diagn Mol Pathol 10:214–222
18. Haralambieva E, Kleiverda K, Mason DY, Schuuring E, Kluin PM (2002) Detection of three common translocation breakpoints in non-Hodgkin's lymphomas by fluorescence in situ hybridization on routine paraffin- embedded tissue sections. J Pathol 198:163–170
19. Izban KF, Alkan S, Singleton TP, Hsi ED (2000) Multiparameter immunohistochemical analysis of the cell cycle proteins cyclin D1, Ki-67, p21WAF1, p27KIP1, and p53 in mantle cell lymphoma. Arch Pathol Lab Med 124:1457–1462
20. Katz RL, Caraway NP, Gu J, Jiang F, Pasco-Miller LA, Glassman AB, Luthra R, Hayes KJ, Romaguera JE, Cabanillas FF, Medeiros LJ (2000) Detection of chromosome 11q13 breakpoints by interphase fluorescence in situ hybridization. A useful ancillary method for the diagnosis of mantle cell lymphoma. Am J Clin Pathol 114:248–257
21. Korin HW, Schwartz MR, Chirala M, Younes M (2000) Optimized cyclin D1 immunoperoxidase staining in mantle cell lymphoma. Appl Immunohistochem Mol Morphol 8:57–60
22. Leroux D, Le Marc'Hadour F, Gressin R, Jacob MC, Keddari E, Monteil M, Caillot P, Jalbert P, Sotto JJ (1991) Non-Hodgkin's lymphomas with t(11;14)(q13;q32): a subset of mantle zone/intermediate lymphocytic lymphoma? Br J Haematol 77:346–353
23. Li JY, Gaillard F, Moreau A, Harousseau JL, Laboisse C, Milpied N, Bataille R, Avet-Loiseau H (1999) Detection of translocation t(11;14)(q13;q32) in mantle cell lymphoma by fluorescence in situ hybridization. Am J Pathol 154:1449–1452
24. Loyson SAJ, de Boer CJ, Schuuring E, Kluin PM, van Krieken JHJM (1996) Mantle cell lymphoma: a morphological, immunohistochemical and molecular genetic study. Pathol Res Pract 192:781–789
25. Luthra R, Hai S, Pugh WC (1995) Polymerase chain reaction detection of the t(11;14) translocation involving the bcl-1 major translocation cluster in mantle cell lymphoma. Diagn Mol Pathol 4:4–7
26. Matutes E, Carrara P, Coignet L, Brito-Babapulle V, Villamor N, Wotherspoon A, Catovsky D (1999) FISH analysis for BCL-1 rearrangements and trisomy 12 helps the diagnosis of atypical B cell leukaemias. Leukemia 13:1721–1726
27. Monteil M, Callanan M, Dascalescu C, Sotto JJ, Leroux D (1996) Molecular diagnosis of t(11;14) in mantle cell lymphoma using two- colour interphase fluorescence in situ hybridization. Br J Haematol 93:656–660
28. Ott G, Kalla J, Ott MM, Schryen B, Katzenberger T, Muller JG, Muller-Hermelink HK (1997) Blastoid variants of mantle cell lymphoma: frequent bcl-1 rearrangements at the major translocation cluster region and tetraploid chromosome clones. Blood 89:1421–1429
29. Ott MM, Helbing A, Ott G, Bartek J, Fischer L, Durr A, Kreipe H, Muller-Hermelink HK (1996) bcl-1 rearrangement and cyclin D1 protein expression in mantle cell lymphoma. J Pathol 179:238–242
30. Pinyol M, Campo E, Nadal A, Terol MJ, Jares P, Nayach I, Fernandez PL, Piris MA, Montserrat E, Cardesa A (1996) Detection of the bcl-1 rearrangement at the major translocation cluster in frozen and paraffin-embedded tissues of mantle cell lymphomas by polymerase chain reaction. Am J Clin Pathol 105:532–537
31. Pittaluga S, Wlodarska I, Stul MS, Thomas J, Verhoef G, Cassiman JJ, Van den Berghe H, De Wolf-Peeters C (1995) Mantle cell lymphoma: a clinicopathological study of 55 cases. Histopathol 26:17–24
32. Remstein ED, Kurtin PJ, Buno I, Bailey RJ, Proffitt J, Wyatt WA, Hanson CA, Dewald GW (2000) Diagnostic utility of fluorescence in situ hybridization in mantle-cell lymphoma. Br J Haematol 110:856–862

33. Rimokh R, Berger F, Delsol G, Charrin C, Bertheas MF, Ffrench M, Garoscio M, Felman P, Coiffier B, Bryon PA, et al (1993) Rearrangement and overexpression of the BCL-1/PRAD-1 gene in intermediate lymphocytic lymphomas and in t(11q13)-bearing leukemias. Blood 81:3063–3067
34. Rimokh R, Berger F, Delsol G, Digonnet I, Rouault JP, Tigaud JD, Gadoux M, Coiffier B, Bryon PA, Magaud JP (1994) Detection of the chromosomal translocation t(11;14) by polymerase chain reaction in mantle cell lymphomas. Blood 83:1871–1875
35. Rosenberg CL, Wong E, Petty EM, Bale AE, Tsujimoto Y, Harris NL, Arnold A (1991) PRAD1, a candidate BCL1 oncogene: mapping and expression in centrocytic lymphoma. Proc Natl Acad Sci U S A 88:9638–9642
36. Samaha H, Dumontet C, Ketterer N, Moullet I, Thieblemont C, Bouafia F, Callet-Bauchu E, Felman P, Berger F, Salles G, Coiffier B (1998) Mantle cell lymphoma: a retrospective study of 121 cases. Leukemia 12:1281–1287
37. Segal GH, Masih AS, Fox AC, Jorgensen T, Scott M, Braylan RC (1995) CD5-expressing B-cell non-Hodgkin's lymphomas with bcl-1 gene rearrangement have a relatively homogeneous immunophenotype and are associated with an overall poor prognosis. Blood 85:1570–1579
38. Siebert R, Matthiesen P, Harder S, Zhang Y, Borowski A, Zuhlke-Jenisch R, Plendl H, Metzke S, Joos S, Zucca E, Weber-Matthiesen K, Roggero E, Grote W, Schlegelberger B (1998) Application of interphase cytogenetics for the detection of t(11;14)(q13;q32) in mantle cell lymphomas. Ann Oncol 9:519–526
39. Singh N, Wright DH (1997) The value of immunohistochemistry on paraffin wax embedded tissue sections in the differentiation of small lymphocytic and mantle cell lymphomas. J Clin Pathol 50:16–21
40. Suzuki R, Takemura K, Tsutsumi M, Nakamura S, Hamajima N, Seto M (2001) Detection of cyclin D1 overexpression by real-time reverse- transcriptase-mediated quantitative polymerase chain reaction for the diagnosis of mantle cell lymphoma. Am J Pathol 159:425–429
41. Swerdlow SH, Yang WI, Zukerberg LR, Harris NL, Arnold A, Williams ME (1995) Expression of cyclin D1 protein in centrocytic/mantle cell lymphomas with and without rearrangement of the BCL1/cyclin D1 gene. Hum Pathol 26:999–1004
42. Swerdlow SH, Zukerberg LR, Yang WI, Harris NL, Williams ME (1996) The morphologic spectrum of non-Hodgkin's lymphomas with BCL1/cyclin D1 gene rearrangements. Am J Surg Pathol 20:627–640
43. The Non-Hodgkin's Lymphoma Classification Project (1997) A clinical evaluation of the International Lymphoma Study Group classification of non-Hodgkin's lymphoma. Blood 89:3909–3918
44. Vandenberghe E, De Wolf-Peeters C, van den Oord J, Wlodarska I, Delabie J, Stul M, Thomas J, Michaux JL, Mecucci C, Cassiman JJ, et al (1991) Translocation (11;14): a cytogenetic anomaly associated with B-cell lymphomas of non-follicle centre cell lineage. J Pathol 163:13–18
45. Vasef MA, Medeiros J, Koo C, McCourty A, Brynes RK (1997) Cyclin D1 immunohistochemical staining is useful in distinguishing mantle cell lymphoma from other low-grade B-cell neoplasms in bone marrow. Am J Clin Pathol 108:302–307
46. Vasef MA, Medeiros LJ, Yospur LS, Sun NC, McCourty A, Brynes RK (1997) Cyclin D1 protein in multiple myeloma and plasmacytoma: an immunohistochemical study using fixed, paraffin-embedded tissue sections. Mod Pathol 10:927–932
47. Velders GA, Kluin-Nelemans JC, De Boer CJ, Hermans J, Noordijk EM, Schuuring E, Kramer MH, Van Deijk WA, Rahder JB, Kluin PM, Van Krieken JH (1996) Mantle-cell lymphoma: a population-based clinical study. J Clin Oncol 14:1269–1274
48. Watson P, Wood KM, Lodge A, McIntosh GG, Milton I, Piggott NH, Proctor SJ, Taylor PR, Smith S, Jack F, Bell H, Steward M, Anderson JJ, Horne CH, Angus B (2000) Monoclonal antibodies recognizing CD5, CD10 and CD23 in formalin-fixed, paraffin-embedded tissue: production and assessment of their value in the diagnosis of small B-cell lymphoma. Histopathol 36:145–150
49. Williams ME, Swerdlow SH, Rosenberg CL, Arnold A (1992) Characterization of chromosome 11 translocation breakpoints at the bcl- 1 and PRAD1 loci in centrocytic lymphoma. Cancer Res 52:5541s–5544s
50. Williams ME, Swerdlow SH, Meeker TC (1993) Chromosome t(11;14)(q13;q32) breakpoints in centrocytic lymphoma are highly localized at the bcl-1 major translocation cluster. Leukemia 7:1437–1440
51. Yang WI, Zukerberg LR, Motokura T, Arnold A, Harris NL (1994) Cyclin D1 (Bcl-1, PRAD1) protein expression in low-grade B-cell lymphomas and reactive hyperplasia. Am J Pathol 145:86–96
52. Yatabe Y, Nakamura S, Seto M, Kuroda H, Kagami Y, Suzuki R, Ogura M, Kojima M, Koshikawa T, Ueda R, Suchi T (1996) Clinicopathologic study of PRAD1/cyclin D1 overexpressing lymphoma with special reference to mantle cell lymphoma. A distinct molecular pathologic entity. Am J Surg Pathol 20:1110–1122
53. Yatabe Y, Suzuki R, Tobinai K, Matsuno Y, Ichinohasama R, Okamoto M, Yamaguchi M, Tamaru J, Uike N, Hashimoto Y, Morishima Y, Suchi T, Seto M, Nakamura S (2000) Significance of cyclin D1 overexpression for the diagnosis of mantle cell lymphoma: a clinicopathologic comparison of cyclin D1-positive MCL and cyclin D1-negative MCL-like B-cell lymphoma. Blood 95:2253–2261
54. Zucca E, Stein H, Coiffier B (1994) European Lymphoma Task Force (ELTF): report of the workshop on Mantle Cell Lymphoma (MCL). Ann Oncol 5:507–511
55. Zucca E, Soldati G, Schlegelberger B, Booth MJ, Weber-Matthiesen K, Cavalli F, Cotter FE (1995) Detection of chromosome 11 alterations in blood and bone marrow by interphase cytogenetics in mantle cell lymphoma. Br J Haematol 89:665–668
56. Zukerberg LR, Yang WI, Arnold A, Harris NL (1995) Cyclin D1 expression in non-Hodgkin's lymphomas. Detection by immunohistochemistry. Am J Clin Pathol 103:756–760

Virchows Arch (2003) 442:548–554
DOI 10.1007/s00428-003-0808-0

ORIGINAL ARTICLE

**Magali Lacroix-Triki · Eliane Mery · Jean-Jacques Voigt · Luc Istier · Philippe Rochaix**

# Value of cytokeratin 5/6 immunostaining using D5/16 B4 antibody in the spectrum of proliferative intraepithelial lesions of the breast. A comparative study with 34$\beta$E12 antibody

Received: 13 August 2002 / Accepted: 29 January 2003 / Published online: 24 April 2003
© Springer-Verlag 2003

**Abstract** Previous studies have shown that basal-type cytokeratins (CKs) can distinguish usual ductal hyperplasia (UDH) from the spectrum of atypical ductal hyperplasia (ADH), ductal carcinoma in situ (DCIS) and lobular carcinoma in situ (LCIS). Indeed, expression of these CKs is weak or absent in ADH, DCIS and LCIS. However, the diagnostic usefulness of D5/16B4 antibody (anti-CK5/6) has never been compared with that of 34$\beta$E12 antibody (anti-CK1/5/10/14). We performed immunostaining of CK 5/6 and CK1/5/10/14 on 100 breast lesions, including UDH ($n$=31), ADH ($n$=5), DCIS ($n$=54) and LCIS ($n$=10). Abundant immunostaining was observed in all UDH using both antibodies. Four of five of the ADH cases showed less than 5% of CK5/6 stained cells, the remaining case showed 30% of labeled cells. With 34$\beta$E12 antibody, three of five of the ADH cases showed less than 5% labeled cells, while two cases showed more than 30% of stained cells. None of the 54 DCIS or the 10 LCIS was labeled by D5/16B4, while a lack of 34$\beta$E12 immunostaining was observed in only 15 of 54 DCIS and 2 of 10 LCIS. We confirmed that D5/16B4 antibody directed against CK5/6 is useful in distinguishing UDH from the spectrum of ADH/DCIS/LCIS. We also demonstrated that D5/16B4 is far a more specific marker than 34$\beta$E12 antibody.

**Keywords** Cytokeratin 5/6 · Breast · Hyperplasia · Atypical hyperplasia · Ductal and lobular carcinoma in situ

M. Lacroix-Triki · E. Mery · J.-J. Voigt · L. Istier · P. Rochaix (✉)
Laboratoire d'Anatomie et de Cytologie Pathologiques,
Institut Claudius Regaud,
20-24 rue du pont Saint Pierre, 31052 Toulouse Cedex, France
e-mail: rochaix@icr.fnclcc.fr
Tel.: +33-5-61424231
Fax: +33-5-61424602

## Introduction

Epithelial proliferations of the breast encompass a variety of proliferative and neoplastic lesions. Those formed in the terminal ductal-lobular units are categorized as ductal hyperplasia of usual type (UDH) or epitheliosis, atypical ductal hyperplasia (ADH), ductal carcinoma in situ (DCIS) and lobular carcinoma in situ (LCIS). The clinical management of these differs as the related risk of developing an invasive carcinoma is different in each case [1, 8, 18, 20, 26]. Distinction between these lesions is based on cyto-architectural analysis [24]. However, distinction often remains a challenge, as shown by the lack of interobserver reproducibility [17]. Some authors have proposed quantitative data as a useful means in separating ADH from DCIS, but controversies still exist regarding which criterion to apply [25, 26].

Immunohistochemistry may be of useful diagnostic assistance, as the expression of several molecules has been correlated to specific types of epithelial proliferations [22, 27]. Several studies have investigated the value of cytokeratin (CK) expression in such lesions [3, 7, 9, 10, 11, 13, 15].

Normal breast epithelium is complex and known to have three population cells, defined by the CK immunoprofile. The luminal layer is composed of a dual population, one of glandular-type epithelial cells associated with simple-epithelium keratins (CK7, CK8, CK18, CK19), and one of basal-type epithelial cells expressing basal-type keratins (CK5, CK14, CK17) but not smooth muscle actin $\alpha$ (SMA$\alpha$) [2, 3, 9, 11, 14, 28]. The basal layer is composed of myoepithelial cells expressing basal-type keratins (CK5, CK14, CK17) and SMA$\alpha$ [2, 7, 9, 28]. Immunohistochemical studies with anti-CK antibodies have provided evidence for a distinct phenotype between UDH and the spectrum of ADH/DCIS. UDH is composed of a dual population, one associated with simple-epithelium keratins, and one associated with basal-type keratins [3, 7, 11, 13, 14, 15]. In contrast, previous studies have shown that most of ADH/DCIS are composed of a homogeneous population associated with

simple-epithelium keratins [3, 9, 11, 13, 15, 28]. However, the immunohistological distinction between UDH and ADH/DCIS/LCIS is not always clear, as basal-type keratins may sometimes be found in ADH, DCIS and LCIS [3, 9, 13, 15].

Only rare studies of these lesions have investigated the practical value of CK5/6 immunostaining with D5/16 B4, a commercially available anti-basal-type keratin monoclonal antibody (mAb) which does not react with CK14 and which can be routinely used on formalin-fixed, paraffin-embedded specimens [4, 14]. Furthermore, no study has yet compared the CK5/6 immunostaining with the 34$\beta$E12 antibody (anti-CK 1/5/10/14) immunostaining in these lesions. Herein, we report the comparison of CK5/6 and 34$\beta$E12 labelings in 100 breast lesions including UDH, ADH, DCIS and LCIS.

## Materials and methods

### Case selection

All the specimens studied were obtained from the surgical pathology file of the Department of Pathology at the Institut Claudius Regaud, Toulouse, France, during the year 1999. No patient had previously received hormone or cytotoxic therapy. Sections stained with hematoxylin and eosin were reviewed independently by five pathologists (three seniors and two junior residents), and diagnosis discrepancies were resolved during a multi-head microscope session. The sections consisted of 100 consecutive female breast intraepithelial lesions showing either UDH ($n$=31), ADH ($n$=5), DCIS ($n$=54) and LCIS ($n$=10). The lesions were classified according to the criteria of Tavassoli et al. [24, 26]. DCIS cases were classified according to the Van Nuys grading system [21], based on nuclear grade and necrosis. The 54 specimens of DCIS were categorized as follows: 30 cases of grade 1, 12 cases of grade 2 and 12 cases of grade 3.

The tissue samples were fixed in formalin (32 cases) or in ethanol-based Bouin'fluid (Duboscq-Brasil) (68 cases) and paraffin embedded.

### Immunohistochemical techniques

Immunohistochemistry was performed on 4-$\mu$m-thick routinely processed paraffin sections. A prior antigen retrieval based on microwave oven heating in 10 mM citrate buffer, pH 6, was used for all the immunostainings [19]. The primary monoclonal antibodies used were directed against keratins 5 and 6 (clone D5/16 B4; Dako, Glostrup, Denmark; dilution 1:100), and keratins 1, 5, 10 and 14 (clone 34$\beta$E12; Dako, dilution 1:200). The slides were processed using a Techmate Horizon (Dako) slide processor. Antibodies were incubated for 1 h and revealed using a streptavidin-biotin complex reagent (StrepABComplex/HRP Duet, Dako) according to the manufacturer's protocol. The chromogenic substrate was DAB (3,3′-diaminobenzidine). Slides were counterstained with hematoxylin. Staining was cytoplasmic, with or without membrane cell enhancement. Intensity of this staining was graded from weak to strong. Adjacent normal epithelial structures were used as positive (basal and myoepithelial cells) and negative (glandular cells) controls. Non-tumoral peripheral (myoepithelial) cell labeling was not taken into account. The percentage of labeled tumoral cells was reported for each case.

## Results

### Normal breast

All of the 100 specimens had normal breast tissue next to the lesion. Normal tissue showed a slightly different reactivity with CK5/6 and 34$\beta$E12 mAbs: both antibodies stained heterogeneously peripheral myoepithelial cells, but CK5/6 mAb stained a few luminal epithelial cells while 34$\beta$E12 mAb stained most luminal epithelial cells. Intensity of the staining was moderate to strong with both mAbs. Number of epithelial and myoepithelial labeled cells varied greatly from case to case and even within a single case. Columnar cell and apocrine metaplasias showed no reactivity with CK5/6 mAb, whereas a weak immunostaining was observed with 34$\beta$E12 mAb in both metaplasias. The pattern and intensity of the immunostainings were not modified by the fixative used.

### Ductal hyperplasia of usual type

The results of the UDH immunostainings are summarized in Fig. 1. The UDH immunostainings obtained using CK5/6 and 34$\beta$E12 mAbs were very similar. All the cases showed an intense intracytoplasmic staining with cell membrane enhancement of more than 50% of the intraluminal cells with both antibodies (Fig. 2).

### Ductal carcinoma in situ

The results of the DCIS immunostainings are summarized in Fig. 1. All 54 cases of DCIS showed less than 51% of CK5/6 stained cells (Fig. 1). However, the labeled cells seem to be residual normal cells, as they were easily distinguished from tumoral cells according to their different morphological features (Fig. 2). Indeed, labeled cells were flattened and showed no cytological atypia. Moreover, they were often lifted by carcinomatous cells from the basal myoepithelial layer, as in a pagetoid pattern. Therefore, taking these distinctive and previously described features [14, 15] into account, careful microscopic examination showed that no carcinomatous cell was labeled by CK5/6 mAb in all DCIS cases (Fig. 3).

In contrast, in addition to residual cells, a large proportion of carcinomatous cells were stained by 34$\beta$E12 mAb in DCIS cases (Fig. 1 and Fig. 3). These cells were moderately labeled in comparison with the intense staining observed in residual cells. More than 50% of labeled cells were observed in ten cases, and a very strong reaction (more than 70% of stained cells) was observed in four of the cases (Fig. 3). The 34$\beta$E12 immunostaining results did not differ according to the Van Nuys grade (Fig. 4).

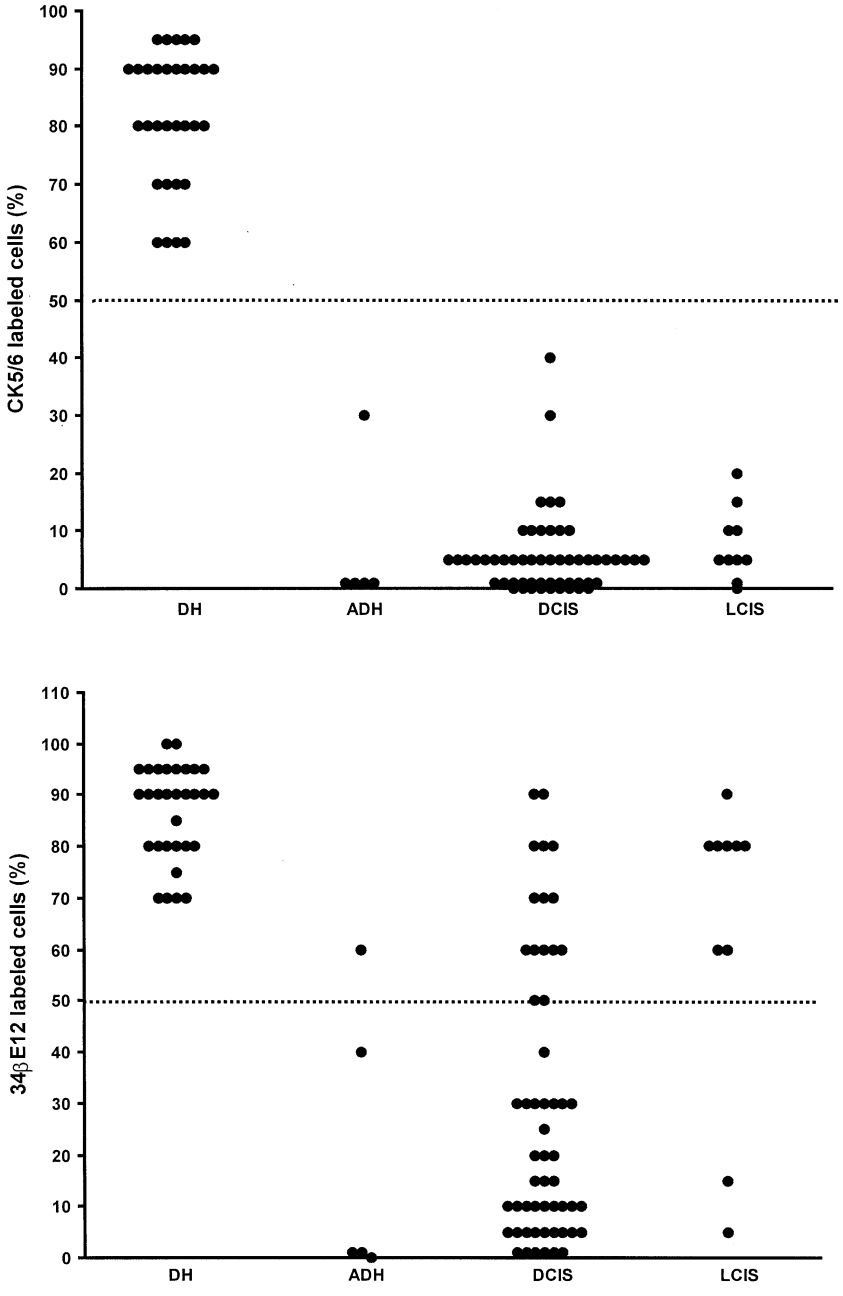



**Fig. 1** Comparative percentage results of CK5/6 and 34$\beta$E12 labeled cells according to the mammary ductal and lobular proliferation type [31 cases of usual ductal hyperplasia (UDH), 5 cases of atypical ductal hyperplasia (ADH), 54 cases of ductal carcinoma in situ (DCIS) and 10 cases of lobular carcinoma in situ (LCIS)]. Peripheral myoepithelial cell labeling was not taken into account

## Atypical ductal hyperplasia

The results of the ADH immunostainings are summarized in Fig. 1. All five cases of ADH showed less than 50% of CK5/6 stained cells. The staining concerned 30% of cells in one case and was very patchy (less than 5% of stained cells) in four cases. Not surprisingly, the labeled cells in these four cases shared the same morphological features as the residual cells in DCIS. They were often isolated and lifted by negative cells (Fig. 2).

Four cases of the ADH showed less than 50% of 34$\beta$E12 stained cells, while more than 50% of labeled cells were observed in one case. These results were similar to those obtained in the DCIS cases.

## Lobular carcinoma in situ

The results of the LCIS immunostainings are summarized in Fig. 1 and Fig. 3. The CK5/6 immunostaining pattern was most often characterized by nonreactive neoplastic cells, sometimes surrounded by immunoreactive nonneoplastic residual cells in the ductal extension of the lesion (Fig. 2). Therefore, none of the LCIS showed CK5/6 immunostaining.

In contrast, 34$\beta$E12 mAb labeled more than 50% of the cells in most of the LCIS (eight) cases. The staining was weak-to-moderate and cytoplasmic in a perinuclear pattern.

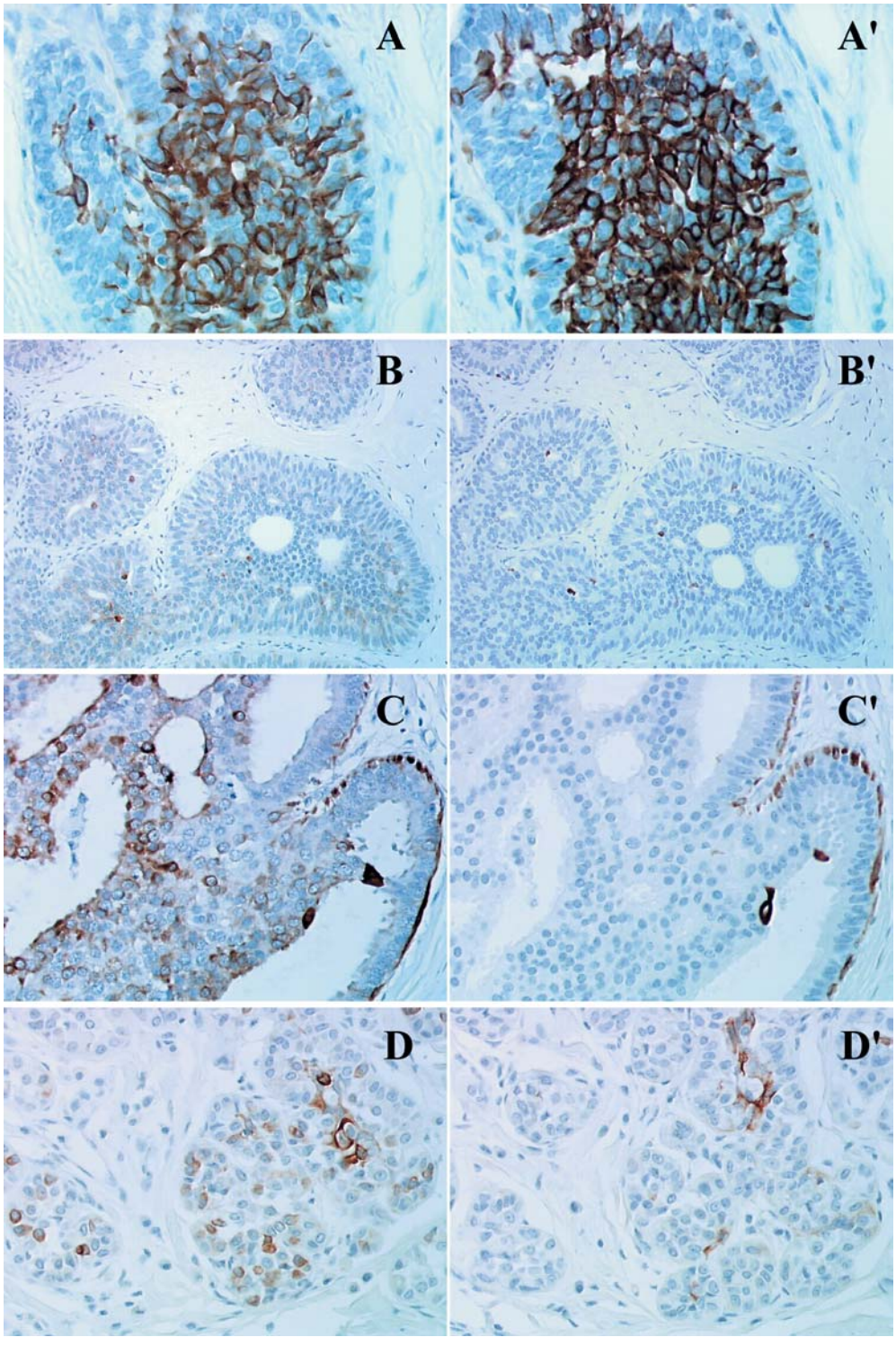



**Fig. 2** Comparative immunostainings with D5/16 B4 (anti CK5/6, *right side*) and 34$\beta$E12 (anti-CK1/5/10/14, *left side*) antibodies. Ductal hyperplasia (**A** and **A'**, ×200): immunostaining of epithelial and myoepithelial cells is quite similar with the two antibodies. Atypical ductal hyperplasia (**B** and **B'**, ×100): some proliferative epithelial cells are weekly stained by 34$\beta$E12 mAb, while only residual normal cells are stained by D5/16B4 mAb. Ductal carcinoma in situ (**C** and **C'**, ×200) and lobular carcinoma in situ (**D** and **D'**, ×200): immunostaining of several carcinomatous cells with 34$\beta$E12 but not with D5/16B4 mAb. Residual entrapped normal cells are strongly marked with both antibodies

## Discussion

Normal breast epithelium is a "mixed" bistratified glandular epithelium composed of three populations of cells, i.e., glandular-type epithelial, basal-type epithelial and myoepithelial cells. Earlier immunohistochemical reports provided evidence that each UDH is composed of a biphasic population, one type associated with simple-epithelium keratins, the other associated with basal-type keratins. In contrast, most DCIS and ADH cases have been reported to be composed of a predominantly or exclusively monophasic population of cells expressing simple-epithelium type keratins; but, in a minority of cases, tumoral cells expressed basal-type CK [3, 9, 11, 13, 14, 15, 28].

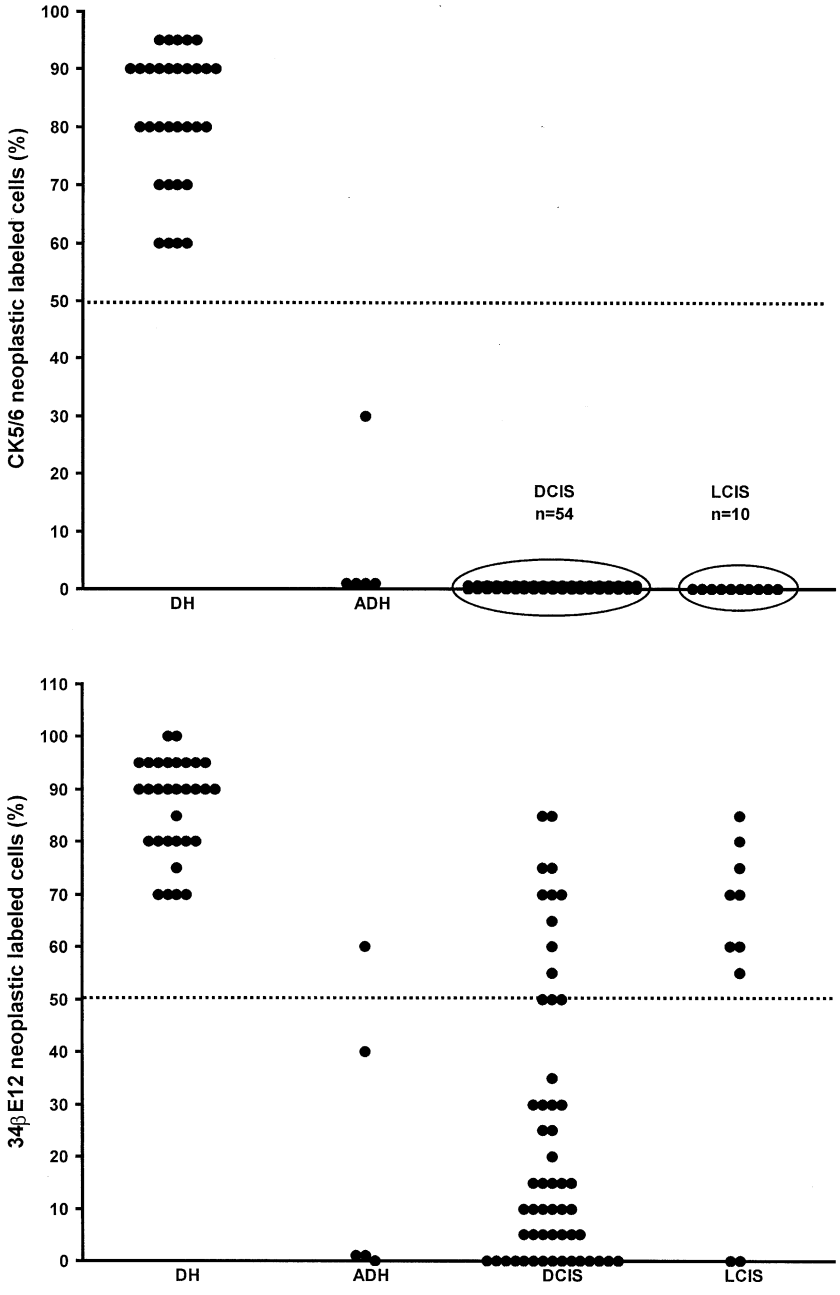



**Fig. 3** Comparative percentage results of CK5/6 and 34$\beta$E12 neoplastic labeled cells according to the mammary ductal and lobular proliferation type [31 cases of usual ductal hyperplasia (UDH), 5 cases of atypical ductal hyperplasia (ADH), 54 cases of ductal carcinoma in situ (DCIS) and 10 cases of lobular carcinoma in situ (LCIS)]. Residual entrapped normal cell labeling was not taken into account

The majority of previous studies of the basal-type CK in in situ breast lesions used antibodies directed against at least the CK14 or CK17 [2, 3, 11, 13, 15, 28]. Antibody directed against CK5 (clone D5/16 B4) without cross reactivity against CK14 or CK17 has been rarely used [14].

The present study is the first to evaluate the practical value of CK5/6 expression in in situ epithelial breast lesions as a comparative study with 34$\beta$E12 mAb. The pattern of reactivity of CK5/6 mAb in normal breast was not exactly the same as that of 34$\beta$E12 mAb. Both antibodies reacted with some epithelial and myoepithelial cells in normal ducts and lobules as previously described for 34$\beta$E12 mAb. However, this later antibody labeled more cells in the inner layer of the ductal epithelium. Therefore, one can hypothesize that CK5/6 mAb is less sensitive for the basal cell detection than 34$\beta$E12 mAb. Another explanation could be that 34$\beta$E12 mAb not only labels basal cells, but also some glandular cells that express CK14 but not CK5/6, leading to this immunostaining discrepancy.

The present results demonstrate that CK5/6 is strongly expressed in all cases of UDH (31 of 31). This result is in agreement with that we obtained with 34$\beta$E12 mAb and those previously reported in the literature [2, 11, 13, 15, 28]. This result also demonstrates that most of the cells in UDH have a true basal-cell immunophenotype, not only due to CK14 but also to CK5 or, less probably, to CK6.

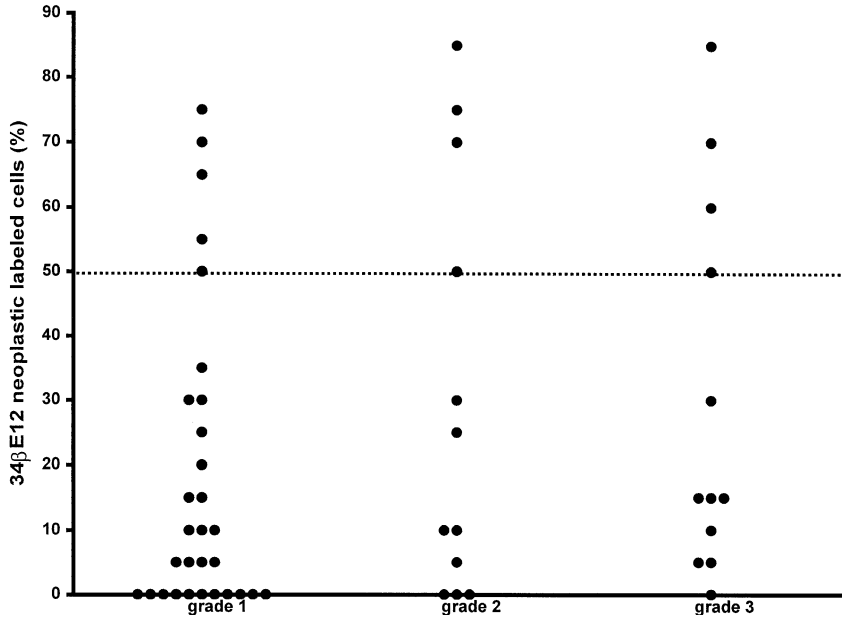



**Fig. 4** Percentage results of 34$\beta$E12 neoplastic labeled cells in the 54 ductal carcinoma in situ (DCIS) cases according to the Van Nuys grade

In contrast, CK5/6 and 34$\beta$E12 immunostainings were significantly different in atypical/malignant in situ lesions. CK5/6 immunostaining was negative, while 34$\beta$E12 mAb labeled more than 50% of cells in 31% of atypical/malignant lesions.

Our results with 34$\beta$E12 mAb in ADH/DCIS appear higher than those of previous studies performed using 34$\beta$E12 mAb [13, 15, 23]. One can attribute this discrepancy to technical parameters such as antibody dilution or the type of fixative used. Indeed, in our study, the staining intensity was most often low in these lesions, even if the percentage of labeled cells was high (Fig. 2). This staining might not have been detected if a higher antibody dilution had been used. The different fixatives used could also partially explain our results, but no modification of the pattern of staining was observed with regard to the fixative used. However, the staining was a specific one, as negative controls were not labeled without background staining.

CK5/6 immunostaining appears to be much more specific than the 34$\beta$E12 immunostaining in distinguishing between UDH and ADH/DCIS/LCIS. Thus, this antibody can be helpful in differential diagnosis between UDH and ADH/DCIS/LCIS when cyto-architectural diagnosis is difficult. CK5/6 use allows for a more simple approach than those used in a recent study to improve 34$\beta$E12 mAb specificity, which combined percentage of labeled cells and staining intensity [13].

ADH lesions share similar CK5/6 and 34$\beta$E12 immunophenotype with DCIS. The diagnosis of ADH was made according to Tavassoli's criteria, i.e., when the lesions displayed cyto-architectural aspects similar to DCIS but were lower than 2 mm in diameter, or when the cells displayed atypia but did not fulfill all the DCIS criteria [26]. The "DCIS-like" immunophenotype of the ADH cells and the loss of the biphasic population suggests a common pathogenetic mechanism with DCIS, leading to basal-type keratin loss and clonal proliferation. In these particularly difficult-to-recognize lesions, CK5/6 immunostaining appears to be a very helpful tool.

For the first time, we report here the immunostaining of LCIS using 34$\beta$E12 and CK5/6 mAbs. The LCIS CK5/6 immunophenotype was close to that of DCIS, implying that CK5/6 mAb cannot be used to distinguish solid variant of low-grade DCIS that mimics LCIS from true LCIS. And yet these lesions, which have overlapping ductal and lobular morphological features, must be separated, as they have different clinical implication. Interestingly, we frequently observed more than 50% of 34$\beta$E12 immunostained cells in LCIS. This important 34$\beta$E12 mAb labeling was much more frequent in LCIS (8 of 10 cases) than in DCIS (24% of the cases). These results are in accordance with those of Bratthauer et al. (2002), which have demonstrated that lobular lesions show cytoplasmic reactivity with 34$\beta$E12 mAb, often in a perinuclear pattern, and lack any immunoreactivity for E-cadherin [5]. Bratthauer et al., therefore, suggested that the combination of 34$\beta$E12 and E-cadherin mAbs could be useful in distinguishing lobular and ductal lesions that have overlapping morphological features [5].

One may infer that the most frequent staining observed with 34$\beta$E12 mAb in DCIS and LCIS lesions is due to CK14 detection. Previous studies that used other antibodies have shown that CK14 expression signifies the worst prognosis in infiltrative carcinomas [6, 12, 16]. Further studies are needed to evaluate the prognostic value of 34$\beta$E12 mAb staining in in situ lesions.

In conclusion, anti-CK5/6 mAb appears to be a new, very sensible and specific tool to assist in the differential diagnosis between benign and malignant in situ epithelial proliferations of the breast—far more specific than the 34$\beta$E12 mAb.

## References


1. Bodian CA, Perzin KH, Lattes R, Hoffman P, Abernathy TG (1993) Prognostic significance of benign proliferative breast disease. Cancer 71:3896–3907
2. Boecker W, Bier B, Freytag G, Brommelkamp B, Jarasch ED, Edel G, Dockhorn-Dworniczak B, Schmid KW (1992) An immunohistochemical study of the breast using antibodies to basal and luminal keratins, alpha-smooth muscle actin, vimentin, collagen IV, and laminin. Part I: normal breast and benign proliferative lesions. Virchows Arch 421:315–322
3. Boecker W, Bier B, Freytag G, Brommelkamp B, Jarasch ED, Edel G, Dockhorn-Dworniczak B, Schmid KW (1992) An immunohistochemical study of the breast using antibodies to basal and luminal keratins, alpha-smooth muscle actin, vimentin, collagen IV, and laminin. Part II: epitheliosis and ductal carcinoma in situ. Virchows Arch 421:323–330
4. Boecker W, Buerger H, Schmitz K, Ellis IA, Van Diest PJ, Sinn HP, Geradts J, Diallo R, Poremba C, Herbst H (2001) Ductal epithelial proliferations of the breast: a biological continuum? Comparative genomic hybridization and high-molecular-weight cytokeratin expression patterns. J Pathol 195:415–421
5. Bratthauer GL, Moinfar F, Stamatakos MD, Mezzetti TP, Shekitka KM, Man YG, Tavassoli FA (2002) Combined E-cadherin and high molecular weight cytokeratin immunoprofile differentiates lobular, ductal, and hybrid mammary intraepithelial neoplasias. Hum Pathol 33:620–627
6. Dairkee SH, Mayall BH, Smith HS, Hackett AJ (1987) Monoclonal marker that predicts early recurrence of breast cancer. Lancet 1:514
7. Dairkee SH, Puett L, Hackett AJ (1988) Expression of basal and luminal epithelium-specific keratins in normal, benign, and malignant breast tissue. J Natl Cancer Inst 80:691–695
8. Dupont WD, Parl FF, Hartmann WH, Brinton LA, Winfield AC, Worrel JA, Schuyler PA, Plummer BS (1993) Breast cancer risk associated with proliferative breast disease and atypical hyperplasia. Cancer 71:1258–1265
9. Guelstein VI, Tchypysheva TA, Ermilova VD, Litvinova LV, Troyanovski SM, Bannikov GA (1988) Monoclonal antibody mapping of keratins 8 and 17 and of vimentin in normal human mammary gland, benign tumors, dysplasias and breast cancer. Int J Cancer 42:147–153
10. Heatley M, Maxwell P, Whiteside C, Toner P (1995) Cytokeratin intermediate filament expression in benign and malignant breast disease. J Clin Pathol 48:26–32
11. Jarasch ED, Nagle RB, Kaufmann M, Maurer C, Böcker WJ (1988) Differential diagnosis of benign epithelial proliferations and carcinomas of the breast using antibodies to cytokeratins. Hum Pathol 19:276–289
12. Malzahn K, Mitze M, Thoenes M, Moll R (1998) Biological and prognostic significance of stratified epithelial cytokeratins in infiltrating ductal breasts carcinomas. Virchows Arch 433:119–129
13. Moinfar F, Man YG, Lininger RA, Bodian C, Tavassoli FA (1999) Use of keratin 34$\beta$E12 as an adjunct in the diagnosis of mammary intraepithelial neoplasia-ductal type benign and malignant intraductal proliferations. Am J Surg Pathol 23:1048–1058
14. Otterbach F, Bànkfalvi A, Bergner S, Decker T, Krech R, Boecker W (2000) Cytokeratin 5/6-immunohistochemistry assists the differential diagnosis of atypical proliferations of the breast. Histopathology 37:232–240
15. Raju U, Crissman JD, Zarbo RJ, Gottlieb C (1990) Epitheliosis of the breast: an immunohistochemical characterization and comparison to malignant intraductal proliferations of the breast. Am J Surg Pathol 14:939–947
16. Santini D, Cecarelli C, Taffurelli M, Pileri S, Marrano D (1996) Differentiation pathways in primary invasive breast carcinoma as suggested by intermediate filament and biopathological marker expression. J Pathol 179:386–391
17. Schnitt SJ, Connoly JL, Tavassoli FA, Fechner RE, Kempson RL, Gelman R, Page DL (1992) Interobserver reproducibility in the diagnosis of ductal proliferative breast lesions using standardized criteria. Am J Surg Pathol 16:1133–1143
18. Schwartz GF, Solin LJ, Olivotto IA, Ernster VL, Pressman PI, and the consensus conference committee (2000) The consensus conference on the treatment of in situ ductal carcinoma of the breast, 22–25 April 1999. Hum Pathol 31:131–138
19. Shi SR, Key ME, Kalra KL (1991) Antigen retrieval in formalin-fixed, paraffin-embedded tissues: an enhancement method for immunohistochemical staining based on microwave oven heating of tissues sections. J Histochem Cytochem 39:741–748
20. Shoker BS, Sloane JP (1999) DCIS grading schemes and clinical implications. Histopathology 35:393–400
21. Silverstein MJ, Poller DN, Waisman JR (1995) Prognostic classification of breast ductal carcinoma in situ. Lancet 345:1154–1157
22. Sloane JP, Ormerod MG (1981) Distribution of epithelial membrane antigen in normal and neoplastic tissues and its value in diagnostic tumor pathology. Cancer 47:1786–1795
23. Soini Y, Miettinen M (1992) Immunohistochemical evaluation of the cytoarchitecture of benign and malignant breast lesions. APMIS 100:901–907
24. Tavassoli FA (1999) Pathology of the breast. Appleton and Lange, Stanford, Connecticut
25. Tavassoli FA, Man Y (1995) Morphofunctional features of intraductal hyperplasia, atypical intraductal hyperplasia and various grades of intraductal carcinoma. Breast J 1:155–162
26. Tavassoli FA, Norris HJ (1990) A comparison of the results of long-term follow-up for atypical intraductal hyperplasia and intraductal hyperplasia of the breast. Cancer 65:518–529
27. Viacava P, Naccarato AG, Bevilacqua G (1999) Different proliferative patterns characterize different preinvasive breast lesions. J Pathol 188:245–251
28. Wetzels RHW, Kuijpers HJH, Lane EB, Leigh IM, Troyanovsky SM, Holland R, van Haelst UJGM, Ramaekers FCS (1991) Basal cell-specific and hyperproliferation-related keratins in human breast cancer. Am J Pathol 138:751–763

Virchows Arch (2003) 442:555–562
DOI 10.1007/s00428-002-0747-1

ORIGINAL ARTICLE

**Claudio Gambini · Massimo Conte · Gabriella Bernini · Paola Angelini · Andrea Pession · Paolo Paolucci · Alberto Donfrancesco · Edvige Veneselli · Katia Mazzocco · Gian Paolo Tonini · Lizzia Raffaghello · Carlo Dominici · Adriana Morando · Francesca Negri · Anna Favre · Bruno De Bernardi · Vito Pistoia**

# Neuroblastic tumors associated with opsoclonus-myoclonus syndrome: histological, immunohistochemical and molecular features of 15 Italian cases

Received: 12 August 2002 / Accepted: 26 November 2002 / Published online: 23 April 2003
© Springer-Verlag 2003

**Abstract** The aim of this study was to investigate the histological, immunohistochemical and molecular features of a series of children with neuroblastic tumors (NTs) and opsoclonus-myoclonus syndrome (OMS). Of 1187 children (age 0–15 years) with previously untreated NTs registered between 1979 and 1995, 15 (1.3%) had OMS at presentation. The majority of patients showed favorable biological characteristics, such as lack of amplification of the neuroblastoma-associated avian myelocytomatosis homolog MYCN oncogene and aneuploid nuclear DNA content. Tumor histology was reviewed according to the International Neuroblastoma Pathology Classification. Histology of the 15 cases of NTs with OMS was ganglioneuroblastoma, intermixed, in 10 patients; ganglioneuroma, maturing, in 1; and neuroblastoma in 4. Of 15 tumors, 12 (10 ganglioneuroblastomas, 2 neuroblastomas) showed abundant interstitial or perivascular lymphoid infiltrates, the latter often organized in secondary lymphoid follicles. The three remaining cases had only minimal infiltrates. A review of 91 cases of age- and stage-matched neuroblastic tumors not associated with OMS tested as controls showed that the degree of lymphoid infiltration was significantly lower than that detected in OMS-related tumors. Furthermore, lymphoid follicles were always present in the latter tumors, whereas they were detected only in a few ganglioneuroma, intermixed tumors from the control group. In conclusion, ganglioneuroblastoma, intermixed subtype, lack of MYCN amplification, aneuploid DNA content and presence of lymphoid infiltrates may contribute to favorable prognosis in NTs associated with OMS.

**Keywords** Neuroblastic tumors · Opsoclonus-myoclonus syndrome · Lymphoid infiltrates

C. Gambini (✉) · A. Morando · F. Negri
Service of Pathology,
Giannina Gaslini Children's Hospital,
Largo Gerolamo Gaslini 5, 16148 Genova, Italy
e-mail: claudiogambini@ospedale-gaslini.ge.it
Fax: +39-010-3742214

M. Conte · P. Angelini · B. De Bernardi
The Department of Hematology-Oncology,
Giannina Gaslini Children's Hospital, Genova, Italy

E. Veneselli
The Division of Neuropsychiatry,
Giannina Gaslini Children's Hospital, Genova, Italy

L. Raffaghello · A. Favre · V. Pistoia
The Laboratory of Oncology,
Giannina Gaslini Children's Hospital, Genova, Italy

A. Donfrancesco · C. Dominici
The Division of Oncology,
Bambino Gesù Children's Hospital, Roma, Italy

K. Mazzocco · G. P. Tonini
Laboratory of Tumor Genetics,
National Institute for Cancer Research, Genova, Italy

P. Paolucci
Division of Pediatrics,
Casa Sollievo della Sofferenza, San Giovanni Rotondo, Italy

A. Pession
Department of Pediatrics, University of Bologna, Italy

G. Bernini
Department of Pediatrics, University of Firenze, Italy

## Introduction

In 1962, Kinsbourne described a novel neurological disorder, named myoclonic encephalopathy or opsoclonus-myoclonus syndrome (OMS), characterized by rapid

and irregular movements of the eyes in all planes, often accompanied by polymyoclonia, ataxia, jerking of the limbs and irritability [24]. OMS may occur at any age, either as a primary disorder or in association with viral infections, degenerative or neoplastic diseases [2, 24, 26]. In childhood, neuroblastic tumors (NTs) are known to associate with OMS, and some cases of OMS-related renal tumors have been reported [16]. Following the first report back to 1968 [5], numerous single case reports and few series of OMS in NTs have thoroughly described these patients, providing detailed information on clinical characteristics, treatment and outcome, including neurological sequelae [1, 4, 11, 23, 25, 28, 29, 31, 35, 41, 42, 44]. It is estimated that 2–3% of NT patients are affected with OMS [35].

The clinical course of OMS in such children is quite variable, ranging from prompt remission following tumor resection to progressive worsening independent of tumor persistence, with one-third of the patients eventually developing severe neurological deficits, such as mental retardation, and motor and/or speech disabilities [1, 25, 28, 33, 35, 36].

Children with NT and OMS have a good probability of cure, possibly because most of them bear favorable clinical features, such as low disease stage and younger age [1, 36]. Some investigators believe, however, that the mechanisms involved in the pathogenesis of the neurological symptoms may account also for a less aggressive tumor behavior.

Here, we have investigated the histological, immunohistochemical and molecular characteristics of 15 NTs associated with OMS, identified retrospectively in the Registry of the Italian Cooperative Group for Neuroblastoma (ICGNB). A part of these results has already been published by our group in preliminary form [11] and confirmed by other investigators [12].

## Patients and methods

### Patients

The clinical records of 1187 children (age 0–15 years) with newly diagnosed NTs registered between January 1979 and December 1995 at the 21 institutions participating in the ICGNB were reviewed with the aim to identify all cases presenting with OMS. Criteria for diagnosis and evaluation of disease extension were reported elsewhere [18]. Diagnosis was based on histological grounds or, in alternative, on bone marrow infiltration by tumor cells, usually associated with elevated urinary catecholamine excretion [45]. Staging criteria of the ICGNB were used until 1989 [18], while the criteria of the International Neuroblastoma Staging System (INSS) [6] have been used thereafter.

### Histological and immunohistochemical studies

A variable number of sections (range 4–25, average 15 per case) were cut from paraffin-embedded tumor specimens, deparaffinized by sequential incubation with decreasing ethanol concentrations (from 100% to 70%) and stained with hematoxylin-eosin (H-E).

The tumor samples studied were from: (a) 15 patients with NTs presenting with OMS and (b) 91 patients affected with NTs but without evidence of OMS (43 of stage-1, 16 of stage-2A, 17 of stage-2B and 15 of stage-3 disease). Slides were reviewed following the International Neuroblastoma Pathology Classification (INPC) criteria [39]. Accordingly, NTs were classified as (a) neuroblastoma (Schwannian stroma-poor), (b) ganglioneuroblastoma, intermixed (Schwannian stroma-rich) or (c) ganglioneuroma, maturing (Schwannian stroma-dominant).

The presence of lymphoid infiltrates was scored in view of the potential role of tumor-infiltrating mononuclear cells (MNCs) in the good outcome of NT patients bearing OMS. In addition, such infiltrates were quantified as follows. Areas of lymphoid infiltration were first selected at low magnification and then carefully inspected at higher magnification (100×). The following score was used to quantify the infiltrates: negative, <1%; ±, 1–10%; +, 11–25%; ++, 25–50%; +++, 50–75%; ++++, >75% cells occupying the microscopic area. The inclusion of each tumor sample in one of these categories was based on the score of the microscopic area containing the highest amount of infiltrating lymphocytes. The presence or absence of follicles was also recorded.

When paraffin blocks and/or frozen specimens were available, immunohistochemical studies were performed using standard immunoperoxidase staining techniques [21]. To characterize infiltrating MNCs, the following murine monoclonal antibodies were used: CD8, CD20, CD21, Myb-1, CD45, CD68, HLA-DR and anti-immunoglobulin (Ig) $\kappa$ and $\lambda$ chains (all produced by Dako, Glostrup, Denmark). CD3 was detected using a polyclonal rabbit antiserum (Dako). The CD4 antiserum was from Novocastra (Newcastle upon Tyne, UK). An anti-HLA class-I monoclonal antibody (TP 25.99) that stains paraffin-embedded tissue sections was kindly donated by Dr. Soldano Ferrone, Department of Immunology, Roswell Park Cancer Institute, Buffalo, NY (USA).

### MYCN gene amplification and chromosome 1p36 deletion

Tumor specimens were evaluated histologically before DNA purification, and only those containing at least 90% tumor cells were processed, in order to allow a clear detection of NT-associated molecular abnormalities. DNA was extracted either from fresh or paraffin-embedded tumor specimens using standard methods [47]. Biological studies included in all cases the assay of MYCN oncogene copy number [40, 43] and the nuclear DNA content (19). MYCN gene was considered amplified when three or more copies were detected [43]. Chromosome 1p36 deletion [32] was evaluated only in four cases.

### Flow cytometric analysis of DNA content

Paraffin-embedded tumor specimens were evaluated histologically, and only those fields containing at least 90% tumor cells were processed. Sections (30 $\mu$m) were cut; thereafter paraffin was removed as detailed above, and tissue sections were re-hydrated and processed as reported [19]. Samples were analyzed with a FACScan flow cytometer (Becton-Dickinson Immunocytometry Systems, San Josè, CA). Sections cut from paraffin-embedded normal lymph nodes were treated as above and run in parallel in the flow cytometry experiments as diploid control [19].

### Statistical analysis

Overall survival was computed as the time from study entry to death or last contact. Event-free survival was computed as the time of registration to relapse, death or last contact. Overall and event-free survival were calculated using the Kaplan-Meier product-limit method [17]. Statistical analysis of lymphoid infiltrates in OMS-associated versus OMS-unrelated tumors was performed using the chi-square test.

## Results

### Patient characteristics

Of 1187 children with newly diagnosed NTs enrolled between January 1979 and December 1995, 15 (1.3%) had clinical evidence of OMS at the time of diagnosis. The main presenting clinical features of these patients are listed in Table 1. Ten patients were male and five were female. The median age was 30 months (range 3–75 months). All but two patients had a localized tumor (stage 1 to 3), which was resected in ten cases and judged unresectable in three. One patient had widespread (stage 4) and one patient had multifocal (stage 4) disease. The primary tumor sites were the abdomen and thorax (seven cases each), followed by pelvis (one case). Patients' neurological symptoms with pertinent investigation at diagnosis, treatment and clinical course are shown in Table 1. In brief, 11 patients had opsoclonus, either alone (4 cases) or associated with ataxia/myoclonia (7 cases), while the remaining 4 presented with ataxia/myoclonia.

Of 15 patients, 13 are presently alive and disease free, three with severe neurological sequelae. The overall survival at 5 years is 84%. The event-free survival is 76%, with a median follow-up of 78 months (range 12–145 months).

### Biological studies of OMS-associated NTs

In no tumor sample was the MYCN gene amplified. Nuclear DNA content was aneuploid in 13 tumors and diploid in 2. One of the diploid cases (case 1) had ganglioneuroblastoma, whereas the other (case 15) had stage-4 neuroblastoma and died 12 months after diagnosis (Table 1). 1p32–36 deletion was not detected in any of the four tumors tested (cases 2, 3, 5 and 11).

### Histological studies of NTs

#### *OMS-associated tumors*

Of the 15 cases, 10 had ganglioneuroblastoma, intermixed, Schwannian stroma-rich, 1 had ganglioneuroma, maturing, Schwannian stroma-dominant, and the remaining 4 had neuroblastoma, Schwannian stroma-poor (Table 1), according to the INPC criteria [38]. All the ganglioneuroblastoma cases and the single ganglioneuroma case were classified as prognostically favorable. Of the four neuroblastoma cases, two had favorable (cases 11 and 14) and two unfavorable (cases 13 and 15) histology [38, 39].

Twelve tumors, ten ganglioneuroblastomas and two neuroblastomas presented marked lymphoid infiltration, with a score ranging from +++ (i.e., 50–75% infiltrating lymphocytes) in eight cases (six ganglioneuroblastomas and two neuroblastomas) to ++++ (i.e., >75%) in four cases (all ganglioneuroblastomas). The remaining three

**Table 1** Main characteristics at diagnosis, treatment and clinical course of 15 children with neuroblastoma and opsoclonus-myoclonus syndrome (OMS). *Adr* adrenal, *RPG* retroperitoneal ganglia, *O* opsoclonus, *A* ataxia, *M* myoclonus, *n* normal, *nd* not done, *a* abnormal, *S* surgery, *CT* chemotherapy, *RT* radiotherapy, *ABMT* autologus bone marrow transplantation, *Ig* immunoglobulins iv, *CR* complete remission, *DOD* dead of disease

| Clinical characteristics | | | | Neurological investigation | | | | Treatment | | Clinical course | |
|---|---|---|---|---|---|---|---|---|---|---|---|
| Sex/age (months) | Stage INSS | Site of primary | Neurological abnormalities | Electro-encephalo-gram | Fundus oculi | Cerebro-spinal fluid | Brain computed tomography | Anti tumor | Anti OMS | Neurological status | Outcome (months) |
| Male,14 | 1 | Thorax | O | n | nd | nd | nd | S | None | Normal | CR, 86+ |
| Male,14 | 1 | Adr. | A, M | n | nd | n | nd | S | Ig+steroid | Persistent ataxia | CR, 17+ |
| Male, 29 | 1 | Adr. | O, A, M | n | n | n | n | S | Ig+steroid | Mental retardation | CR, 12+ |
| Female, 37 | 1 | Thorax | A, M | n | nd | nd | n | S | None | Normal | CR, 64+ |
| Female, 28 | 2A | Adr. | O, A, M | n | n | nd | nd | S | None | Normal | CR, 16+ |
| Male, 40 | 2A | Thorax | A, M | n | nd | nd | n | S | None | Normal | CR,86+ |
| Male, 59 | 2A | Thorax | O, M | n | nd | nd | n | S | ACTH+steroid | Mental retardation | CR,104+ |
| Female, 10 | 2B | Pelvis | O, A, M | nd | nd | n | n | S | ACTH | Normal | CR, 82+ |
| Female, 32 | 2B | Thorax | O, A, M | n | n | nd | n | S | None | Normal | CR,57+ |
| Male, 75 | 2B | Thorax | O | n | nd | nd | nd | S | None | Normal | CR, 73+ |
| Male, 8 | 3 | Thorax | O, A, M | a | n | n | n | S & CT | Ig+steroid | Normal | CR,20+ |
| Male, 12 | 3 | RPG | O, M | n | nd | nd | nd | S & CT | None | Normal | CR, 145+ |
| Male, 50 | 3 | RPG | A, M | a | n | n | n | CT | ACTH | No response | DOD, 18 |
| Female, 3 | 4 s | Adr. | O | n | nd | nd | nd | RT & CT | None | Normal | 2° CR, 76+ |
| Male, 50 | 4 | RPG | O | a | n | nd | n | S & CT & ABMT | ACTH | No response | DOD, 12 |

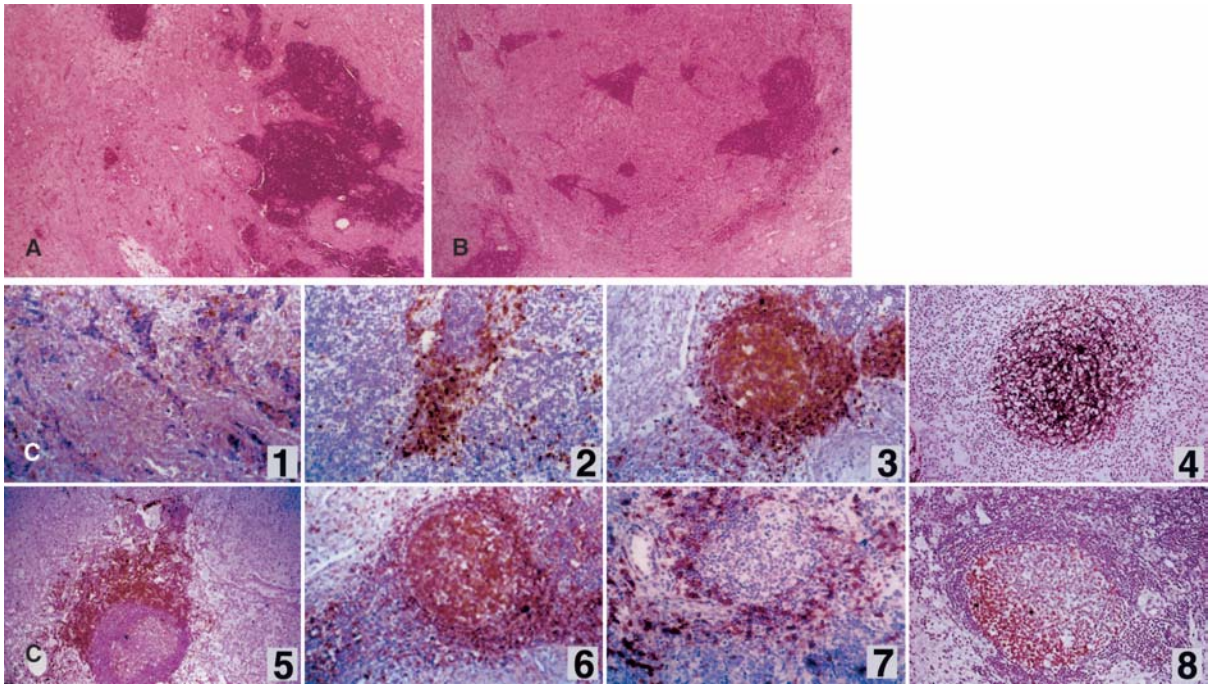



**Fig. 1** Histological and immunohistochemical features of tumor-infiltrating mononuclear cells in patients with neuroblastic tumors and opsoclonus-myoclonus syndrome. **A** Ganglioneuroblastoma intermixed, Schwannian stroma rich. Lymphoid infiltrates appear as thick perivascular cuffs or as single elements disposed in files (see also panels *1* and *2*). Close to the perivascular cuffs, follicular structures are found (see also panels *3–6*) (H-E staining, 40×). **B** Neuroblastoma, Schwannian stroma poor. Lymphoid infiltrates with the appearance of thick perivascular cuffs and occasional follicular organization are detected (see also panels *3–6*) (H-E staining, 40×). **C** Immunohistochemical stainings: *1* Scarce HLA-$DR^+$ cells are visible in the interstitia. *2* CD8 peroxidase staining of interstitial infiltrates (40×). *3* Lymphoid follicle stained with CD20 monoclonal antibody. Positive cells concentrate in the germinal center and in the follicular mantle (peroxidase staining; 20×). *4* Lymphoid follicle stained with CD21 monoclonal antibody. Positive cells concentrate in the germinal center (peroxidase staining; 20×). *5* Lymphoid follicle stained with CD3 antibody (peroxidase staining; 10×). The follicle displays a germinal center area surrounded by a well-developed follicular mantle zone. CD3-positive cells are localized at the periphery of the mantle zone and perifollicularly, with few scattered $CD3^+$ cells in the follicle. *6* Lymphoid follicle stained with anti-HLA-DR monoclonal antibody (peroxidase staining; 20×). The pattern of staining is superimposable to that detected with the CD20 monoclonal antibody (see panel *3*). *7* A small follicle is shown (CD8 peroxidase staining; 20×). A central GC area is surrounded by $CD8^+$ lymphocytes located in the mantle and perifollicular areas. *8* Lymphoid follicle stained with Myb-1 (anti-Ki67) monoclonal antibody. Positive cells concentrate in the basal dark zone of the germinal center (peroxidase staining; 20×)

cases (two neuroblastomas and one ganglioneuroma) had minimal infiltrates, with a score of + (i.e., <25%).

In ganglioneuroblastoma cases, lymphoid infiltration was detected in the form of thick perivascular cuffs or of scattered or single elements disposed in files in the interstitia (Fig. 1A; see also Fig. 1C, panels 1 and 2). In the two neuroblastoma cases, lymphoid infiltrates with the appearance of thick perivascular cuffs were observed (Fig. 1B). Lymphoid follicles were found close to perivascular cuffs in all cases studied, irrespective of the ganglioneuroblastoma or neuroblastoma histology (Fig. 1A and B). Such follicles displayed the typical morphological features of secondary lymphoid follicles, with germinal centers (GCs) surrounded by mantle zone areas (Fig. 1C, panels 3 to 8).

In summary, three major patterns of lymphoid infiltration were identified in NTs associated with OMS, namely (i) perivascular, (ii) interstitial and (iii) follicular.

*Tumors not associated with OMS*

Histological studies carried out with control NT samples showed that 13 of 43 stage-1, 5 of 16 stage-2A, 0 of 17 stage-2B and 2 of 15 stage-3 disease patients had morphologically detectable lymphoid infiltrates. Of the 13 stage-1 specimens displaying infiltrates, 7 had neuroblastoma, 4 had ganglioneuroblastoma, intermixed, and 2 had ganglioneuroma, maturing histology. Of the 5 stage-2A samples with infiltrates, 3 had neuroblastoma and 2 ganglioneuroblastoma, intermixed. No infiltrate was detected in the 17 stage-2B tumors. In the 2 stage-3 cases showing minimal infiltrates, 1 had neuroblastoma and 1 ganglioneuroblastoma, intermixed histology.

When the 20 OMS-unrelated NTs were scored for lymphocytic infiltrates, only 1 case had a +++ score (ganglioneuroblastoma, intermixed), 6 had a ++ score (3 neuroblastomas, 2 ganglioneuroblastomas, intermixed, 1 ganglioneuroma) and 13 received a + score (8 neuroblas-

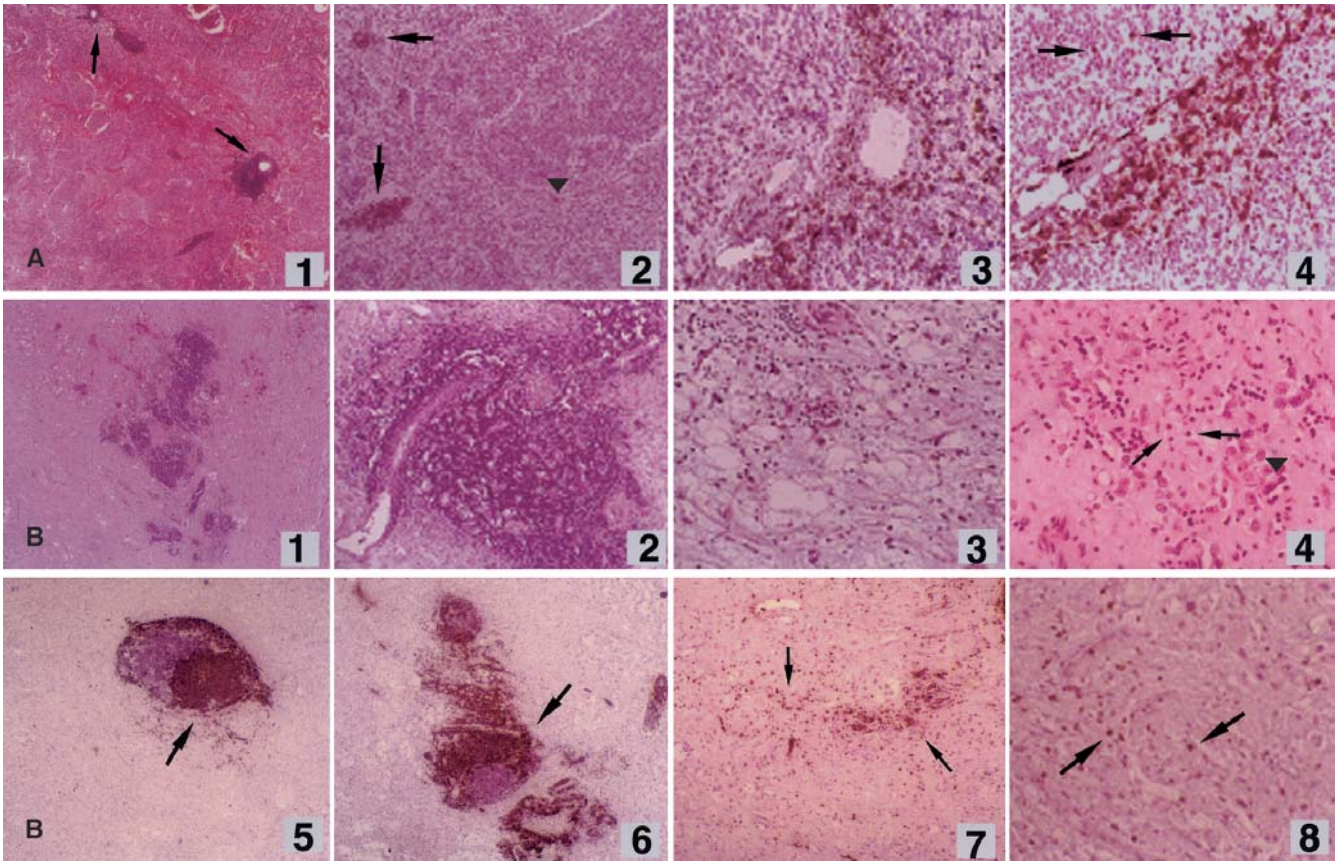



**Fig. 2** Histological and immunohistochemical features of infiltrating mononuclear cells in patients with neuroblastic tumors not associated with the opsoclonus-myoclonus syndrome. **A** Neuroblastoma, Schwannian stroma poor: *1* Scanty perivascular lymphoid aggregates are detectable (*arrow*; H-E staining: 40×). *2* Perivascular lymphoid aggregate stained with a CD45 mAb (*arrows*; peroxidase staining; 40×), indicating the hematopoietic origin of tumor infiltrating cells. Some $CD45^+$ cells are detectable also in the interstitia (*arrowhead*). *3* CD20 staining of perivascular lymphoid cells (peroxidase staining 250×). *4* CD3 staining of infiltrating lymphoid cells (peroxidase staining; 250×). $CD3^+$ cells localize predominantly around small vessels. Some $CD3^+$ cells are found inside the tumor (*arrows*). **B** Ganglioneuroblastoma intermixed: *1* Low magnification area where a lymphoid infiltrate organized in perivascular cuffs and follicles is observed (H-E staining: 40×). *2* Dense perivascular infiltrate organized in follicular structures (*arrow*; H-E staining: 100×). *3* Lymphoid infiltrates in the form of isolated cells or of groups of cells within neurofibromatous stroma (H-E staining, 40×). *4* Lymphoid infiltrates, either sparse (*arrow*) or in close contact with small nests of differentiated neuroblasts (*arrowhead*), are observed (H-E staining, 250×). *5* CD20 staining of a follicular aggregates (*arrow*; peroxidase staining: 40×). *6* CD3 staining of follicular aggregates (peroxidase staining; 40×). Staining is detected predominantly in perifollicular and interfollicular distributions (*arrow*). *7* CD3 staining of lymphoid cells located in the interstitium (*arrows*; peroxidase staining, 40×). *8* CD8 staining of lymphoid cells located in the interstitium (*arrows*; peroxidase staining, 250×)

tomas, 4 ganglioneuroblastomas, intermixed, 1 ganglioneuroma).

Statistical analysis of the amount of tumor infiltrating lymphocytes in OMS-associated versus OMS-unrelated NTs demonstrated that the infiltrates were significantly more abundant in the former than in the latter tumor group ($p<0.0001$).

The distribution of lymphoid infiltrates in neuroblastoma and ganglioneuroblastoma cases, respectively, resembled that observed in OMS-associated cases of corresponding histology. The infiltrates in neuroblastoma samples appeared in the form of perivascular cuffs (Fig. 2A, panel 1), but no follicle was ever detected. In ganglioneuroblastoma cases, the infiltrates appeared as perivascular cuffs (Fig. 2B, panels 1 and 2), or showed an interstitial distribution (Fig. 2B, panels 3 and 4). Follicles were occasionally detected only in ganglioneuroblastoma, intermixed tumors (Fig. 2B, panels 1 and 2).

## Immunohistochemical studies of NTs

The results of these studies are presented without distinction between OMS-related and unrelated-NTs due to the overall immunophenotypic similarities of tumor-infiltrating lymphocytes in the two groups.

Six cases of NTs associated with OMS (five of whom had ganglioneuroblastoma, intermixed, and one had neuroblastoma), as well as the twenty control tumors displaying infiltrates were subjected to immunohistochemical investigations.

The histological studies presented above indicated the consistent presence of lymphoid follicles in OMS-associated NTs, as well as in a minority of OMS-unrelated NTs. To better characterize lymphoid neogenesis in NTs, tissue sections from the six OMS-related tumors were stained with CD21 and Myb-1 (anti-Ki67) mAbs. As shown in Fig. 1, panel C4, CD21 staining disclosed the presence of a rich network of follicular dendritic cells (FDCs) inside the GCs, suggesting that recruitment or in situ maturation of FDCs is a critical factor for GC formation in NTs. Furthermore, scanty CD21 positive cells were detected in some lymphoid infiltrates not yet organized in follicular structures (data not shown).

Figure 1, panel C8, shows that the GCs of follicles in the six OMS-related NTs stained intensely with Myb-1 mAb, which detects actively proliferating cells. In particular, Myb-1 staining was restricted to the basal dark zone, which is enriched for centroblasts in secondary lymphoid tissues, stressing further the analogy between tumor-associated lymphoid follicles and their "classical" counterparts.

The GCs of the follicles, in both OMS-associated and control cases, contained predominantly $CD20^+$ B cells (Fig. 1C, panel 3; Fig. 2B, panel 5) admixed with few $CD68^+$ macrophages (not shown) and rare $CD3^+$ lymphocytes (Fig. 1C, panel 5; Fig. 2B, panel 6). The distribution of HLA-$DR^+$ cells within GCs was superimposable to that of $CD20^+$ B cells (Fig. 1C, panel 6). The mantle zone of the follicles contained $CD20^+$ B lymphocytes (Fig. 1C, panel 3; Fig. 2B, panel 5) admixed with a few $CD3^+$ T lymphocytes (Fig. 1C, panel 5; Fig. 2B, panel 6) and scanty $CD68^+$ macrophages (not shown). The bulk of $CD3^+$ cells were detected in a perifollicular and interfollicular distribution (Fig. 1C, panel 5; Fig. 2B, panel 6). $CD8^+$ cells displayed a similar distribution (Fig. 1C, panel 7). Plasma cells were detected in the interfollicular areas (not shown).

In both OMS-associated and unrelated tumors, the majority of interstitial MNCs were identified as $CD8^+$ lymphocytes (Fig. 1C, panel 2 and Fig. 2B, panel 8), intermingled with a variable but sizable number of $CD68^+$ macrophages and $CD20^+$ B lymphocytes (not shown). CD3 staining (Fig. 2A, panel 4; Fig. 2B, panel 7) showed a pattern similar to that observed in CD8-stained sections, suggesting that most $CD8^+$ cells expressed CD3. In the interstitia, HLA-$DR^+$ cells (Fig. 1C, panel 1) were scarce and displayed a distribution comparable to that of $CD68^+$ and $CD20^+$ cells. $CD4^+$ cells were found to represent a minor, but consistent, component of infiltrating lymphocytes both in the interstitia as well as in the follicular mantle and interfollicular areas (not shown).

A final issue addressed in this study was the expression of HLA class-I molecules on the surface of malignant neuroblasts in the six OMS-related NTs. Staining was performed with a newly developed mAb that works on paraffin-embedded tissue sections. Figure 3 shows the results obtained with one representative case; superimposable results were obtained with the five remaining cases. Neuroblasts were consistently HLA class-I negative, whereas all infiltrating MNCs displayed strong reactivity with the anti-HLA class-I mAb.

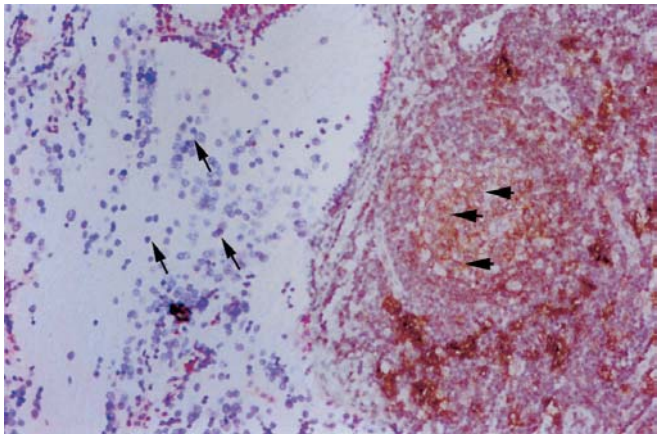


**Fig. 3** HLA-class-I expression in OMS-related neuroblastoma. One representative case of the six studied with identical results is shown. Neuroblasts (*arrows*) do not stain with the anti-HLA class-I monoclonal, whereas infiltrating lymphocytes organized in a huge lymphoid follicle (*arrowheads*) display strong reactivity (peroxidase staining, 20×)

**Table 2** Immunophenotypic characterization of tumor-infiltrating mononuclear cells in opsoclonus-myoclonus syndrome (OMS)-related neuroblastic tumors. Semiquantitative analysis of tumor-infiltrating mononuclear cell populations as assessed by immunohistochemistry according to the following score: –, <1%; ±, 1–10%; +, 11–25%; ++, 25–50%; +++, 50–75%; ++++, >75% cells occupying the microscopic area

| Cases | Surface markers | | | | | |
|---|---|---|---|---|---|---|
| | CD3 | CD4 | CD8 | CD20 | HLA-DR | CD68 |
| 1 | ++ | ± | ++ | + | ++ | + |
| 2 | ++ | ± | ++ | + | + | ± |
| 3 | +++ | ± | +++ | + | + | – |
| 4 | +++ | ± | +++ | + | + | ± |
| 5 | +++ | + | ++ | – | + | + |
| 6 | + | ± | + | +++ | +++ | ± |

Table 2 shows a semiquantitative analysis of tumor-infiltrating MNC populations, as assessed by immunohistochemistry in the six OMS-related NTs. A certain degree of heterogeneity in the composition of tumor infiltrates in the individual cases is apparent.

## Discussion

In this report, we have described the results of an extensive study of 15 children with NTs and OMS, an association which has occurred in 1.3% only of patients of the ICGNB registry. This figure is lower than that reported in other series [35].

The biological features of OMS-related tumors were prognostically favorable. In particular, in no patient was the MYCN gene amplified, while nuclear DNA content was diploid in two patients only, one of whom had

neuroblastoma and died. The rarity of genetic abnormalities in children with NTs and OMS has been reported by others [10, 36] and is thought to contribute significantly to the high cure rate of these patients [1]. Consistent with this assumption, in the only series where the amplified MYCN gene prevailed, the eventual patient outcome was grim [20].

All OMS-associated tumors (ten ganglioneuroblastomas, four neuroblastomas and one ganglioneuroma) contained interstitial, perivascular or follicular lymphoid infiltrates. The lymphoid infiltrate was significantly more abundant in OMS-associated than in OMS-unrelated tumors, and follicles were consistently detected in the former group of tumors, whereas they represented an occasional finding in ganglioneuroblastoma, intermixed tumors from the latter group.

Staining of OMS-related NT tissue sections with CD21 and Myb-1 mAbs demonstrated strong similarities between lymphoid follicles formed de novo inside the tumors and their counterparts in secondary lymphoid tissues. Thus, FDC were detected in the basal dark zone of the GCs, which contains proliferating centroblasts. These results stress the importance of FDCs in the follicular organization of tumor-infiltrating lymphocytes.

The mantle and GC of such follicles contained $CD20^+$ B cells intermingled with a few $CD3^+$ T lymphocytes and $CD68^+$ macrophages. The majority of tumor-infiltrating T lymphocytes were detected close to follicles and in the interstitia, and displayed predominantly a $CD8^+$ immunophenotype.

These latter findings would figure out a cytotoxic cell-mediated attack of the immune system against tumor cells. Although malignant neuroblasts are known to express surface molecules, such as GD2 [9, 37, 46] and neural cell adhesion molecule (NCAM) [30], and embryonal genes of the melanoma antigen gene (MAGE), B antigen gene (BAGE) and G antigen gene (GAGE) families [7, 8, 13, 22], specific cell-mediated responses operated by the host immune system against these antigens have not yet been clearly documented.

However, the huge lymphoid follicles identified in OMS-related tumors may represent the morphological expression of antibody-mediated anti-tumor responses. In this respect, patients with NTs and OMS were found more likely to harbor anti-neuronal antibodies than individuals with NTs in the absence of OMS, but no specific serological marker of OMS was identified [3, 14]. Furthermore, serum antibodies to the HuD onconeural antigen [14] were detected in NT patient sera irrespective of the association with OMS [3, 14], although high titers of such antibodies may be found predominantly in OMS-related tumors.

Previously it was shown that, at variance with OMS-unrelated NTs, neuroblasts from some patients with OMS-related NTs displayed surface expression of HLA class-I molecules [14]. In this study, no HLA class-I expression was detected on tumor cells from six OMS-related NTs. Although the possibility that low amounts of surface HLA class-I molecules—not detected by immunohistochemical techniques—are expressed by neuroblasts cannot be excluded, our results make it unlikely that specific tumor recognition by $CD8^+$ infiltrating T lymphocytes occurred.

It is conceivable that chemokines or other chemoattractants released by neuroblasts or tumor stromal cells are involved in the recruitment of MNCs in the tumor tissue. Infiltrating MNCs, in turn, might produce factors that promote the differentiation of neuroblasts to more mature ganglionic cells. Studies on these topics are now in progress.

In conclusion, favorable prognosis in NTs with OMS may relate to higher incidence of histologically favorable, i.e., GNB intermixed, tumors that lack MYCN amplification, are aneuploid, and show abundant lymphoid infiltrates. Further data are needed to fully support the hypothesis that the host immune response against onconeural antigens may inhibit tumor growth, but also mediate central nervous system damage [15, 27, 34].

**Acknowledgements** We thank Dr. Soldano Ferrone, Department of Immunology, Roswell Park Cancer Institute, Buffalo, NY, for the generous supply of the anti-HLA class-I monoclonal antibody TP 25.99, Marco Ciufferri for the help in tissue handling, and Luca Tedeschi for editing the pictures. This study was supported by grants from Ministero della Sanità, Roma (ICS 070.2/RF99.21) and Associazione Italiana per la Lotta al Neuroblastoma, Genova, Italy.

## References

1. Altman AJ, Baehner RJ (1976) Favourable prognosis for survival in children with coincident opso-myoclonus and neuroblastoma. Cancer 37:846–852
2. Anderson NE, Budde-Steffen C, Rosenblum MK, Graus F, Ford D, Synek BJL, Posner JB (1988) Opsoclonus, myoclonus, ataxia and encephalopathy in adults with cancer: a distinct paraneoplastic syndrome. Medicine 67:100–109
3. Antunes NL, Khakoo Y, Matthay K, Seeger RC, Stram DO, Gerstner E, Abrey LE, Dalmau J (2000) Antineuronal antibodies in patients with neuroblastoma and paraneoplastic opsoclonus-myoclonus. J Pediatr Hematol Oncol 22:315–320
4. Boltshauser E, Deonna TH, Hirt HR (1979) Myoclonic encephalopathy of infants or dancing eyes syndrome. Report of 7 cases with long-term follow up and review of the literature (cases with and without neuroblastoma) Helv Acta 34:119–133
5. Brandt S, Carlsen S, Glenting P, HelwegLarsen J (1974) Encephalophatia myoclonica infantilis (Kinsbourne) and neuroblastoma in children. A report of three cases. Dev Med Child Neurol 16: 286–294
6. Brodeur GM, Seeger RC, Barrett A, D'Angio G, De Bernardi B, Evans AE, Favrot M, Freeman AI, Haase G, Hartmann H, Hayes FA, Helson H, Kemshead J, Lampert F, Ninane J, Ohkawa H, Philip T, Pinkerton CR, Pritchard J, Sawada T, Siegel S, Smith IE, Tsuchida Y, Voute PA (1988) International criteria for diagnosis, staging, and response to treatment in patients with neuroblastoma. J Clin Oncol 6:1874–1881
7. Cheung IY, Cheung NK (1997) Molecular detection of GAGE expression in peripheral blood and bone marrow; utility as a tumor marker for neuroblastoma. Clin Cancer Res 3:821–826
8. Cheung IY, Barber D, Cheung NK (1998) Detection of microscopic neuroblastoma in marrow by histology, immunocytology, and reverse transcription-PCR of multiple molecular markers. Clin Cancer Res 4:2801–2805
9. Cheung NK, Saarinen UM, Neely JE, Landmeier B, Donovan D, Coccia PF (1985) Monoclonal antibodies to a glycolipid

antigen on human neuroblastoma cells. Cancer Res 45:2642–2649
10. Cohn SL, Salwen H, Herst CV, Maurer HS, Nieder ML, Morgan ER, Rosen ST (1988) Single copies of the N-myc oncogene in neuroblastomas from children presenting with the syndrome of opsoclonus-myoclonus. Cancer 62:723–726
11. Conte M, Milanaccio C, Morando A, Favre A, Gambini C, Garaventa A, De Bernardi B, Pistoia V (1999) Characterization of tumor infiltrating lymphocytes in neuroblastoma and opsoclonus myoclonus syndrome (abstract). Scand J Immunol 50:117
12. Cooper R, Khakoo Y, Matthay K, Lukens JN, Seeger RC, Stram DO, Gerbing RB, Nakagawa A, Shimada H (2001) Opsoclonus-myoclonus-ataxia syndrome in neuroblastoma: histopathologic features—a report from the Children's Cancer Group. Med Pediatr Oncol 36:623–629
13. Corrias MV, Scaruffi P, Occhino M, De Bernardi B, Tonini GP, Pistoia V (1996) Expression of MAGE-1, MAGE-3 and MART-1 genes in neuroblastoma. Int J Cancer 69:403–407
14. Dalmau J, Graus F, Cheung N-KV, Rosenblum MK, Ho A, Canete A, Delattre J-Y, Thompson SJ, Posner JB (1995) Major histocompatibility proteins, anti-HU antibodies, and paraneoplastic encephalomyelitis in neuroblastoma and small cell lung cancer. Cancer 75:99–109
15. Darnell RB (1996) Onconeural antigens and the paraneoplastic neurologic disorders: at the intersection of cancer, immunity and the brain. Proc Natl Acad Sci U S A 93:4529–4536
16. De Luca S, Terrone C, Crivellaro S, De Zan A, Polo P, Vigliani MC, Tizzani A (2002) Opsoclonus-myoclonus syndrome as a paraneoplastic manifestation of renal cell carcinoma. A case report and a review of the literature. Urol Int 68:206–208
17. Fleiss JI (ed) (1981) Statistical methods for rates and proportions. Wiley, New York
18. Garaventa A, De Bernardi B, Pianca C, Pession A, Arrighini A, Di Cataldo A, Tamaro P, Iasonni V, Taccone A, Rogers D, Boni L (1993) Localized but unresectable neuroblastoma: treatment and outcome of 145 cases. J Clin Oncol 11:1770–1779
19. Hedley DW, Friedlander ML, Taylor RW (1985) Application of DNA flow cytometry to paraffin-embedded archival material for the study of aneuploidy and its clinical significance. Cytometry 6:327–333
20. Hiyama E, Yokoyama T, Ichikawa T, Hiyama K, Kobayashi M, Tanaka Y, Ueda K, Tanaka Y, Yano H (1994) Poor outcome in patients with advanced stage neuroblastoma and coincident opsomyoclonus syndrome. Cancer 74:1821–1826
21. Hsu SM, Raine L, Fanger H (1981) The use of antiavidin antibody and avidin-biotin-peroxidase complex in immunoperoxidase technics. Am J Clin Pathol 75:816–821
22. Ishida H, Matsumura T, Salgaller ML, Ohmizono Y, Kadono Y, Sawada T (1996) MAGE-1 and MAGE-3 or 6 expression in neuroblastoma-related pediatric solid tumors. Int J Cancer 69:375–380
23. Janss A, Sladky J, Chatten J, Johnson J (1996) Opsoclonus/myoclonus: paraneoplastic syndrome of neuroblastoma. Med Pediatr Oncol 26:272–279
24. Kinsbourne M. (1962) Myoclonic encephalopathy of infants. J Neurol Neurosurg Psychiatry 25:271–276
25. Koh PS, Raffensperger J, Berry S, Larsen MB, Johnstone HS, Chou P, Luck SR, Hammer M, Cohn SL (1994) Long term outcome in children with opsoclonus-myoclonus and ataxia and coincident neuroblastoma. J Pediatr 125:712–716
26. Kuban KC, Ephros MA, Freeman RL (1983) Syndrome of opsoclonus-myoclonus caused by Coxsackie B3 infection. Ann Neurol 13:69–71
27. Lang B, Vincent A (1996) Autoimmunity to ion channels and other proteins in paraneoplastic disorders. Curr Opin Immunol 8:865–871
28. Mitchell WG, Snodgrass SR (1990) Opsoclonus-ataxia due to childhood neural crest tumors: a chronic neurologic syndrome J Child Neurol 5:153–158
29. Nickerson BG, Hutter JJ Jr (1979) Opsomyoclonus and neuroblastoma. Response to ACTH. Clin Pediatr 18:446–448
30. Patel K, Moore SE, Dickson G, Rossell RJ, Beverley PC, Kemshead JT, Walsh, FS (1989) Neural cell adhesion molecule (NCAM) is the antigen recognized by monoclonal antibodies of similar specificity in small-cell lung carcinoma and neuroblastoma. Int J Cancer 44:573–578
31. Petruzzi MJ, De Alarcon PA (1995) Neuroblastoma-associated opsoclonus-myoclonus treated with intravenously administered immunoglobulins G. J Pediatr 127:328–329
32. Pinkel D, Straume T, Gray JW (1986) Cytogenetic analysis using quantitative high sensitivity fluorescence hybridization. Proc Natl Acad Sci U S A 83:2934–2938
33. Pohl KRE, Pritchard J, Wilson J (1996) Neurological sequelae of the dancing eye syndrome. Eur J Pediatr 155:237–244
34. Posner JB, Dalmau J (1997) Paraneoplastic syndromes. Curr Opin Immunol 9:723–729
35. Rudnick E, Khakoo Y, Antunes NL, Seeger RC, Brodeur GM, Shimada H, Gerbing RB, Stram DO, Matthay KK (2001) Opsoclonus-myoclonus-ataxia syndrome in neuroblastoma: clinical outcome and antineuronal antibodies-a report from the Children's Cancer Group Study. Med Pediatr Oncol 36:612–622
36. Russo C, Cohn SL, Petruzzi MJ, De Alarcon PA (1997) Long term neurologic outcome in children with opsoclonus-myoclonus associated with neuroblastoma: a report from the Pediatric Oncology Group. Med Ped Oncol 29:284–288
37. Schulz G, Cheresh DA, Varki NM, Yu A, Staffileno LK, Reisfeld RA (1985) Detection of ganglioside GD2 in tumor tissues and sera of neuroblastoma patients. Cancer Res 44:5914–5920
38. Shimada H, Ambros IM, Dehner LP, Hata J, Yoshi VV, Roald B (1999) Terminology and morphologic criteria of neuroblastic tumors. Cancer 86:349–363
39. Shimada H, Ambros IM, Dehner LP, Hata J, Joshi VV, Roald B, Stram DO, Gerbing RB, Lukens JN, Matthay KM, Castleberry RP (1999) The International Neuroblastoma Pathology Classification (the Shimada System). Cancer 86:364–372
40. Southern EM (1975) Detection of specific sequences among DNA fragments separated by gel electrophoresis J Mol Biol 98:503–517
41. Sugie H, Sugie Y, Akimoto H, Endo K, Shirai M, Ito M (1992) High-dose iv human immunoglobulin in a case with infantile opsoclonus polymyoclonia syndrome. Acta Paediatr 81:371–372
42. Telander RL, Smithson WA, Groover RV (1989) Clinical outcome in children with acute cerebellar encephalopathy and neuroblastoma. J Pediatr Surg 24:11–14
43. Tonini GP, Boni L, Pession A, Rogers D, Iolascon A, Basso G, Cordero di Montezemolo L, Casale F, Pession A, Perri P, Mazzocco K, Scaruffi P, Lo Cunsolo C, Marchese N, Milanaccio C, Conte M, Bruzzi P, De Bernardi B (1997) MYCN oncogene amplification in neuroblastoma is associated with worse prognosis, except in stage 4 s. The Italian experience with 295 children. J Clin Oncol 15:85–93
44. Veneselli E, Conte M, Biancheri R, Acquaviva A, De Bernardi B (1998). Effect of steroid and high-dose immunoglobulin therapy on opsoclonus-myoclonus syndrome occurring in neuroblastoma: a case report. Med Pediatr Oncol 30:15–17
45. Wadman SK, Ketting D, Voute PA (1976) Gas chromatography determination of urinary vanilglycolic acid, vanilacetic acid and vanillactic acid: chemical parameters for the diagnosis of neurogenic tumors and the evaluation of their treatment. Clin Chim Acta 72:49–68
46. Wu ZL, Schwartz E, Seeger R, Ladisch S (1986) Expression of GD2 ganglioside by untreated primary human neuroblastomas. Cancer Res 46:440–443
47. Zhuang Z (1995) A new microdissection technique for archival DNA analysis of specific cell population in lesions less than one millimeter in size. Am J Pathol 146:620–625

Virchows Arch (2003) 442:563–568
DOI 10.1007/s00428-003-0810-6

ORIGINAL ARTICLE

**Jie Zhang · Reiko Ito · Naohide Oue · Xudong Zhu · Yasuhiko Kitadai · Kazuhiro Yoshida · Hirofumi Nakayama · Wataru Yasui**

# Expression of thrombospondin-1 is correlated with microvessel density in gastric carcinoma

Received: 26 November 2002 / Accepted: 18 February 2003 / Published online: 25 April 2003
© Springer-Verlag 2003

**Abstract** Thrombospondin-1 (TSP-1) has been shown to play a role in angiogenesis in a variety of cancers, but some studies indicated a difference in the mechanism of TSP-1 on neovascularization according to organ or histological type. Wild-type p53 protein has been shown to induce TSP-1 expression. We examined the expression of TSP-1 protein in 80 gastric carcinomas using immunohistochemistry and studied the relationship with microvessel counts, p53 expression and clinicopathological factors. We also performed reverse-transcriptase polymerase chain reaction analysis for the TSP-1 mRNA expression in gastric carcinoma cell lines and gastric cancer tissue after laser capture microdissection. Strong expression of TSP-1 protein was detected in 30 (38%) of the 80 cases. Positive staining for TSP-1 was seen in the cytoplasm of the cancer cells. TSP-1 mRNA expression was confirmed in a majority of gastric carcinoma cell lines and carcinoma tissues. Microvessel counts were significantly higher in tumors with strong TSP-1 protein expression than in those without expression or weak expression of TSP-1 ($P$=0.011). No significant correlation was found between TSP-1 expression and p53 staining and clinicopathological factors. Our results support an idea that increased TSP-1 expression may be associated with an angiogenic phenotype in gastric carcinoma and suggest that TSP-1 may play diverse roles in each organ.

**Keywords** Thrombospondin-1 · Gastric carcinoma · Microvessel count · Immunohistochemistry · RT-PCR

J. Zhang · R. Ito · N. Oue · X. Zhu · H. Nakayama · W. Yasui (✉)
Department of Molecular Pathology,
Hiroshima University Graduate School of Biomedical Sciences,
734-8551 Hiroshima, Japan
e-mail: wyasui@hiroshima-u.ac.jp
Tel.: +81-82-2575145
Fax: +81-82-2575149

Y. Kitadai
Department of Medicine and Molecular Science,
Hiroshima University Graduate School of Biomedical Sciences,
734-8551 Hiroshima, Japan

J. Zhang
Department of Pathology,
Shanghai Fifth People's Hospital affiliated to Fudan University,
Shanghai, China

K. Yoshida
Department of Surgery, Research Institute
or Nuclear Medicine and Biology,
Hiroshima University, 734-8551 Hiroshima, Japan

## Introduction

Gastric carcinoma is the second most common cancer in the world [8]. Proliferation and metastasis of cancer involves numerous biological steps—including angiogenesis, which depends on the local balance between molecules that induce and inhibit neovascularization. Various anti-angiogenic factors have been identified, including thrombospondin-1 (TSP-1), TSP-2, angiostatin and vasostatin [21, 23, 28, 31]. TSP-1 is a high-molecular-weight (450 kDa) multifunctional glycoprotein, which was first described as a product of thrombin-stimulated platelets [2]. TSP-1 is synthesized and secreted by various cell types, including endothelial cells, fibroblasts, smooth muscle cells, osteoblasts and neoplastic cells [9, 15, 18, 25]. Presently, the role of TSP-1 in angiogenesis and tumor progression is controversial. The anti-angiogenic effects of TSP-1 have been reported in carcinomas of the urinary bladder, oral cavity, breast, thyroid, lung and prostate [7, 13, 17, 27, 32, 35]. However, TSP-1 has been shown to act as an angiogenic factor in colorectal and pancreatic cancers [11, 33]. Thus, it is possible that TSP-1 plays diverse roles in each organ. Experimental evidence indicates that the expression of TSP-1 is possibly regulated by p53 [5, 36].

The relationship between the expression of TSP-1, p53 and tumor neovascularization in gastric carcinoma has not been well understood. Furthermore, neither have the biological role and expression patterns of TSP-1 been fully characterized. Thus, the purpose of the present study was to analyze the relationship between TSP-1 and p53

expression and tumor neovascularization as well as the clinicopathological characteristics in gastric carcinomas.

## Materials and methods

### Tissue samples

A total of 80 gastric adenocarcinomas (28 female and 52 male) were studied. The median age of patients was 66.0 years (range 24–88 years). For laser capture microdissection (LCM) and RNA extraction, tissue samples obtained at the time of surgery were immediately embedded in O.C.T. compound (Sakura Finetechincal, Tokyo, Japan), frozen in liquid nitrogen, and stored at −80°C until use. For immunohistochemistry, tissues were fixed in 10% buffer-formalin and embedded in paraffin. Histological classification of gastric cancer was made according to the Japanese Classifications of Gastric Cancer [10] as follows: pap, papillary adenocarcinoma; tub1, well-differentiated tubular adenocarcinoma; tub2, moderately differentiated tubular adenocarcinoma; por1, solid-type poorly differentiated adenocarcinoma; por2, non-solid-type poorly differentiated adenocarcinoma; sig, signet-ring cell carcinoma; muc, mucinous adenocarcinoma. We regarded pap, tub1 and tub2 as well-differentiated type and por1, por2, sig and muc as poorly differentiated type. Tumors were staged according to the TNM staging system (39 stage I, 12 stage II, 17 stage III and 12 stage IV). Depth of carcinoma invasion was classified as follows: T1, mucosa and submucosa; T2, muscularis propria and subserosa; T3, serosa exposed and serosa infiltration; T4.

### Cell lines

Eight cell lines derived from human gastric carcinoma were used. Five gastric carcinoma cell lines of the MKN series (MKN-1, adenosquamous carcinoma; MKN-7, MKN-28 and MKN-74, well-differentiated adenocarcinomas; and MKN-45, poorly differentiated adenocarcinoma) were kindly provided by Dr. T. Suzuki (Fukushima Medical University, Fukushima). KATO-III and HSC-39 cell lines, which were established from signet ring cell carcinoma, were kindly provided by Dr. M. Sekiguchi (University of Tokyo, Tokyo) and Dr. K. Yanagihara (National Cancer Center, Tokyo), respectively [34]. TMK-1 cell line was established in our laboratory from poorly differentiated adenocarcinomas [19]. All the cell lines were routinely maintained in RPMI 1640 containing 10% fetal bovine serum in a humidified atmosphere of 5% $CO_2$ and 95% air at 37°C.

### Immunohistochemistry

Consecutive 4-μm tissue sections were prepared from paraffin blocks and immunostained for TSP-1, p53 and CD34. Immunohistochemical staining was performed by means of immunoperoxidase techniques using a Histofine Simple Stain Kit (Nichirei Biosciences, Tokyo, Japan). The sections were respectively incubated with anti-TSP-1 antibody (Ab-4, NeoMarkers, Fremont, CA; dilution 1:50), anti-p53 antibody (DO7, Dako Carpinteria, CA; dilution 1:100) and anti-CD34 antibody (NU-4A1, Nichirei Corp, Tokyo, Japan) for 1 h at 37°C, followed by incubation with the secondary antibody for 30 min. The immunocomplexes were visualized using 3,3′-diaminobenzidine. Sections were then counterstained with hematoxylin.

### Analysis of immunostaining

Two investigators then independently decided the number of positive cells and staining intensity on each slide. TSP-1 immunostaining was divided into three categories based on percentage of stained cells and their staining intensities. The cases were classified as negative (no stained cells present), weak (<30% of the entire population of cells stained weakly or moderately, and >30% of the entire population of cells stained weakly), or strong (>30% of the population stained moderate to strong), as a previously described [25]. Immunohistochemical staining for p53 was considered negative when there was less than 20% and positive with more than 20% reactivity, and only where there was nuclear staining.

### Microvessel density

The microvessel density (MVD) was determined according to CD34-positive tubular structures. To measure intratumoral MVD, the stained sections were screened without any knowledge of the patients data at ×40 magnification to identify the highest vascular area within the tumor. At these hot spots, the individual microvessel count was evaluated at ×200 magnification. The mean MVD obtained from the five fields was used for analysis. All of the CD34-positive structures in the stroma were counted, even if no lumen was presented. Branching structures were counted as a single vessel. This procedure is based on methods previously described by us [12] and others [11, 16, 20, 30]. These reports confirmed that the hot spot is representative of intratumoral neo-vascularization, and microvessel counts there directly correlate with angiogenic factors such as vascular endothelial growth factor (VEGF)-C in a variety of cancers including gastric cancer.

### RNA extraction and reverse-transcription polymerase chain reaction

TSP-1 mRNA expression in gastric carcinoma cell lines and dissected tissues by LCM were analyzed by reverse-transcription polymerase chain reaction (RT-PCR). Total RNA was extracted using the RNeasy Mini Kit (Qiagen, Hilden, Germany) according to the manufacturer's instructions. Total RNA (2 $\mu$g) was converted to cDNA with a first-strand cDNA synthesis kit (Amersham Pharmacia Biotech, Uppsala, Sweden), and PCR was carried out for one cycle of 94°C for 10 min, followed by 34 cycles of 94°C for 2 min, 57°C for 2 min, 72°C for 3 min, and one cycle of 72°C for 10 min. PCR products were revealed on a 1.5% agarose gel. The sequences of the TSP-1 primers are: 5′-CCGACCAGAAGGACTCTGAC-3′ (upper primer), 5′-GGCTGAGACGCCATCGAGAG-3′ (lower primer), and human $\beta$-actin primers were used as an internal control.

### Laser capture microdissection

The frozen tissues of four gastric carcinomas were cut into 5-μm-thick sections using a cryostat (Microm, Waldorf, Germany). The sections were fixed in 70% ethanol containing 5% acetic acid immediately after cutting and counter-stained with hematoxylin shortly thereafter. We used the system of LCM-200, PixCell II. LCM allows isolation of tissue fragments that are as small in diameter as the area that a laser beam focuses at. The laser beam of this LCM system covers a circle of 20-μm diameter. Dissected carcinoma cells (about 200 circles) with minimal contamination of stromal elements were used for RT-PCR.

### Statistical analysis

Statistical analyses were performed using Fisher's exact test. $P$ values less than 0.05 were regarded as statistically significant.

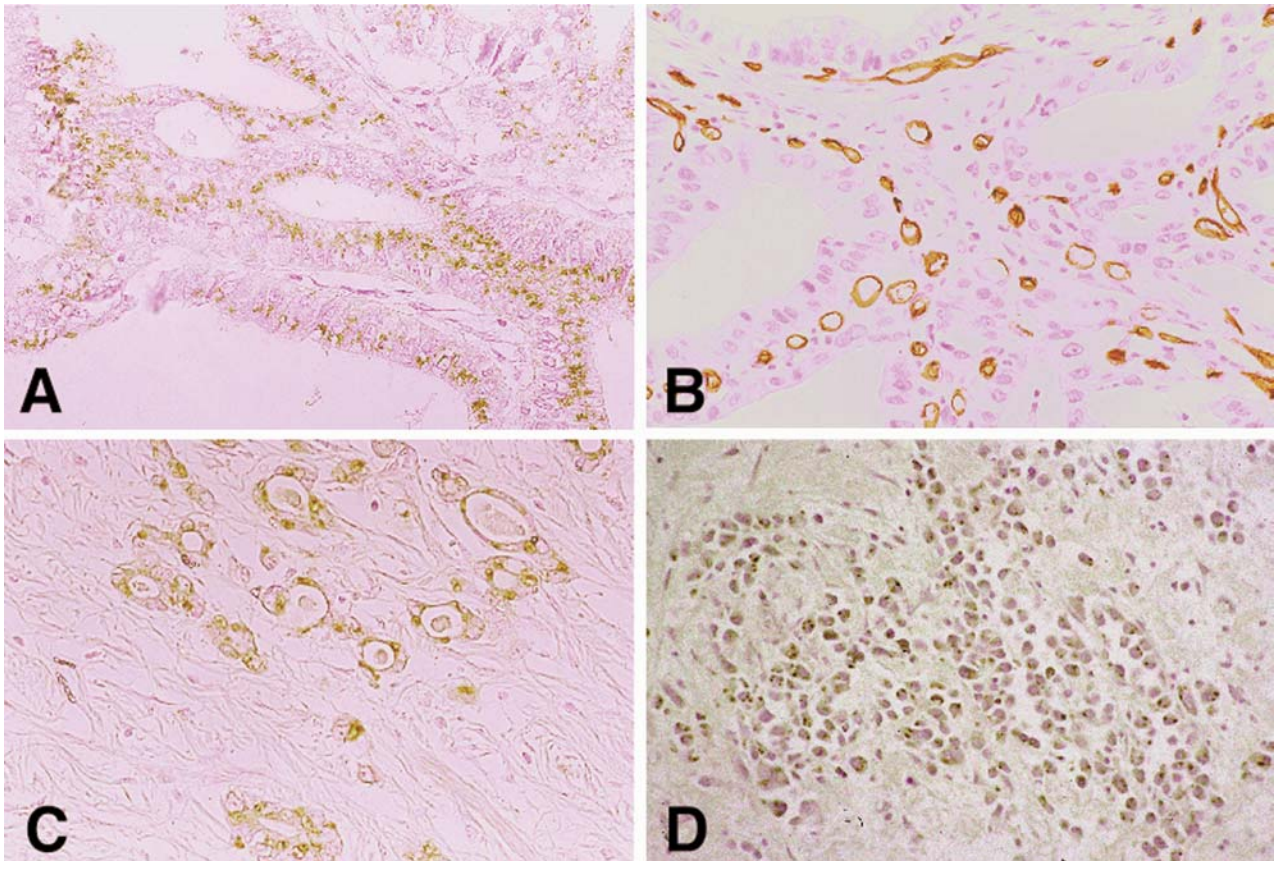



**Fig. 1** Immunohistochemical staining of thrombospondin (TSP)-1. Representative TSP-1 strongly positive cases were shown. **A** TSP-1 immunostaining in a well-differentiated gastric adenocarcinoma, ×400. **B** CD34 staining in well-differentiated adenocarcinoma (the same as in **A**) showing high microvessel counts. TSP-1 immunostaining in a moderately (**C**) and poorly (**D**) differentiated gastric adenocarcinoma ×400

## Results

### TSP-1 protein expression

Positive staining for TSP-1 was seen in the cytoplasm of the cancer cells. Weak staining of TSP-1 was occasionally detected in the endothelial cells of the microvessel and the normal gastric epithelia in some cases. The TSP-1 protein was not found in the extracellular matrix. There were 30 (38%) gastric carcinomas with strong positive staining for TSP-1 (Fig. 1A, C, D), while the other 50 (62%) showed weak or negative staining for TSP-1. While there were two types of patterns in the staining of TSP-1—diffuse immunoreactivity in the cytoplasm (Fig. 1C) and dot-like immunoreactivity in peri-nuclei (Fig. 1D)—these two patterns did not show any difference relative to clinicopathological characteristics.

### TSP-1 protein expression and clinicopathological factors

The relationship between TSP-1 protein expression and clinicopathological features of gastric carcinomas is summarized in Table 1. In a comparison between clinicopathological parameters and immunoreactivity of TSP-1, staining grades "weak and negative" showed an almost similar tendency. Therefore, the grades of TSP-1 expression were classified as "strong" and "weak or negative" when comparing the immunoreactivity of TSP-1 with clinicopathological parameters. TSP-1 immunoreactivity did not correlate with histological type, tumor stage, and depth of tumor invasion and lymph-node metastasis.

### Relationship between TSP-1 and p53

Of the 31 gastric carcinomas with p53 immunoreactivity, 13 (42%) showed strongly positive for TSP-1; whereas, of 49 cases without p53 immunoreactivity, 17 (35%) did so (Table 1). There was no association between TSP-1 and p53 expression ($P$=0.514).

### Correlation between TSP-1 and MVD

MVD was evaluated using CD34-positive structure as an indicator in 80 gastric carcinoma cases (Fig. 1B and

**Table 1** Relationship between expression of thrombospondin (TSP)-1, p53, microvessel density (MVD) and clinicopathological parameters in gastric carcinomas

| | Case no. 80 | TSP-1 expression[a] | | *P* value[d] |
|---|---|---|---|---|
| | | Strong 30 (38%) | Weak or negative 50 (62%) | |
| Histology[b] | | | | |
| Well | 45 | 19 (42%) | 26 (58%) | |
| Poorly | 35 | 11 (31%) | 24 (69%) | 0.322 |
| Stage[b] | | | | |
| I and II | 51 | 19 (37%) | 32 (63%) | |
| III and IV | 29 | 11 (38%) | 18 (62%) | 0.925 |
| Depth of invasion[b] | | | | |
| T1 | 32 | 12 (38%) | 20 (62%) | |
| T2 | 27 | 12 (44%) | 15 (56%) | |
| T3 | 16 | 6 (38%) | 10 (62%) | |
| T4 | 5 | 0 (0%) | 5 (100%) | 0.569 |
| Lymph-node metastasis | | | | |
| Positive | 38 | 16 (42%) | 22 (58%) | |
| Negative | 42 | 14 (33%) | 28 (67%) | 0.418 |
| P53 expression | | | | |
| Positive | 31 | 13 (42%) | 18 (58%) | |
| Negative | 49 | 17 (35%) | 32 (65%) | 0.514 |
| MVD[c] | | | | |
| High | 40 | 21 (51%) | 19 (49%) | |
| Low | 40 | 9 (23%) | 31 (77%) | 0.011 |

[a] Grades of TSP-1 were classified as "strong" and "weak or negative" as in Materials and methods
[b] According to the criteria of TNM classification and the Japanese Classification of Gastric Cancer [10]
[c] Median of MVD for all of the investigated tumors was 61.8, which facilitated to separate the high and the low MVD groups
[d] Correlation was analyzed using the Chi-square for independence test (Fisher's exact), and *P* values were shown. *P* values less than 0.05 were regarded as statistically significant

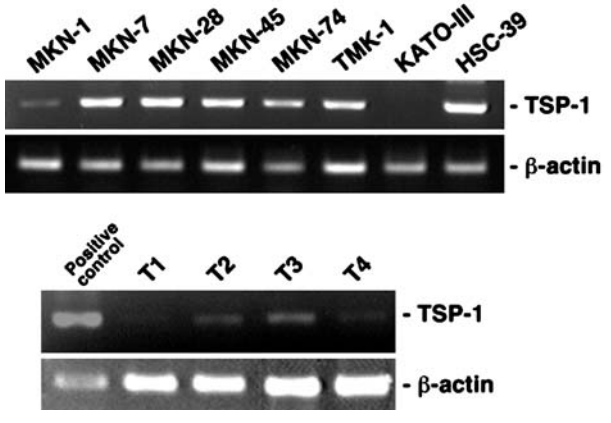



**Fig. 2** mRNA expression of thrombospondin (TSP)-1 in gastric carcinoma cell lines and gastric carcinoma tissues after laser capture microdissection. Seven of eight and all of four gastric carcinoma tissues expressed TSP-1 mRNA at various levels

Table 1). The median value of 61.8 (a range from 26 to 163) facilitated separation of the high MVD and the low MVD groups. Tumors of the high MVD group showed a higher incidence of TSP-1 expression (51%) than those of the low MVD group (23%), the correlation between TSP-1 expression and MVD being statistically significant ($P$=0.011).

RT-PCR analysis

Using RT-PCR, mRNA expression of TSP-1 was examined in eight gastric carcinoma cell lines and four samples of gastric carcinoma after LCM. The mRNA expression of TSP-1 was detected at various levels in seven of eight gastric carcinoma cell lines and in all of four samples of gastric carcinoma (Fig. 2).

## Discussion

Solid tumors require neovascularization for tumor growth, progression and metastasis. Evaluation of angiogenic factors involved in the mediation of neovascularization must be important, because this information could afford novel opportunities for therapeutics. TSP-1 has been shown to play a role in angiogenesis, but, presently, the role of TSP-1 in tumor neovascularization and progression is controversial. It has been proposed that TSP-1 functions as a stimulator or an inhibitor of angiogenesis in an organ-specific manner. In the present study, we investigated the expression and distribution of TSP-1 in gastric carcinomas and found that strong TSP-1 protein expression was detected in 38% of gastric cancers. Furthermore, RT-PCR analysis revealed that TSP-1 mRNA was expressed at various levels in a majority of gastric carcinoma cell lines and carcinoma tissues after

LCM, indicating that gastric cancer cells themselves produce TSP-1. We have performed TSP-1 immunostaining of the two cases (T1 and T2, in Fig. 2) because the paraffin sections of the two were available among four cases examined using RT-PCR. Consistent results were detected between RT-PCR and immunostaining (data not shown). It has been reported that TSP-1 is expressed in cytoplasm of cancer cells of the thyroid, breast and colorectum [4, 14, 27]; whereas, there are some reports indicating TSP-1 expression only in stromal tissues of certain tumors such as bladder cancer, pancreas cancer and prostate cancer [7, 11, 13]. Therefore, pattern of TSP-1 expression in the tumor may differ depending on organs or histological types.

In the present study, we found a positive correlation between TSP-1 expression and intratumoral MVD. Strong expression of TSP-1 was significantly associated with high MVD in gastric carcinoma ($P$=0.011), in contrast to many reports in which TSP-1 expression was inversely correlated with MVD in malignant tumors. However, Bertin et al. [3] reported that mRNA expression of TSP-1 and TSP-2 in invasive breast ductal carcinoma coincided with a high microvessel density. Axelrod et al. [1] showed that elevated TSP-1 expression was positively associated with higher MVD in epithelial ovarian cancer. These findings overall suggest the effects of TSP in tumor angiogenesis may be dependent on tumor type and environmental setting. However, there is growing evidence that the effect of TSP-1 in angiogenesis is concentration dependent. At low concentrations, TSP-1 inhibits angiogenesis; nevertheless, at high concentrations, it stimulates neovascularization [24]. Taraboletti et al. [29] demonstrated the formation of two fragments (25 kDa and 140 kDa) exerting opposing actions on vascular endothelial cells following enzymatic proteolysis of the TSP-1 molecule. The heparin-binding 25-kDa fragment is the angiogenic domain of TSP-1, while the 140-kDa fragment retains the angiosuppressive effect [26, 29].

Previous studies suggested that TSP-1 expression is enhanced by the product of the p53 gene and is downregulated by p53 alteration [5, 6]. In this study, however, we found no significant correlation between TSP expression and p53 status. Recently, we have found that TSP-1 expression is tightly associated with CpG island methylation of the promoter region regardless of p53 gene status [22]. TSP-1 expression is reduced by promoter hypermethylation in 30% of gastric carcinomas. We should examine the expression of TSP-1 methylation status and p53 gene alterations in the same series of gastric carcinomas in the near future.

In conclusion, TSP-1 was strongly expressed in the cytoplasm of gastric carcinomas that were positively associated with neovascularization. This may indicate that increased TSP-1 expression might participate in angiogenic phenotype in gastric carcinoma and also support that TSP-1 might play diverse roles in each organ.

**Acknowledgements** This work was supported, in part, by Grants-in-Aid for Cancer Research from the Ministry of Education, Culture, Science, Sports, and Technology of Japan; and from the Ministry of Health, Labor, and Welfare of Japan. The authors are indebted to Masayoshi Takatani and Mutsumi Ueda for their skillful technical assistance.

## References

1. Axelrod JR, Alvarez A, Bentley R, Rodriguez GC (1999) Regulation of angiogenesis in epithelial ovarian cancer by thrombospondin. Gynecol Oncol 72:472–473
2. Baenziger NL, Brodie GN, Majerus PW (1972) Isolation and properties of a thrombin-sensitive protein of human platelets. J Biol Chem 247:2723–2731
3. Bertin N, Clezardin P, Kubiak R, Frappart L (1997) Thrombospondin-1 and -2 messenger RNA expression in normal, benign, and neoplastic human breast tissues: correlation with prognostic factors, tumor angiogenesis, and fibroblastic desmoplasia. Cancer Res 57:396–399
4. Clezardin P, Frappart L, Clerget M, Pechoux C, Delmas PD (1993) Expression of thrombospondin (TSP1) and its receptors (CD36 and CD51) in normal, hyperplastic, and neoplastic human breast. Cancer Res 53:1421–1430
5. Dameron KM, Volpert OV, Tainsky MA, Bouck N (1994) Control of angiogenesis in fibroblasts by p53 regulation of thrombospondin-1. Science 265:1582–1584
6. Fontanini G, Boldrini L, Calcinai A, Chine S (1999) Thrombospondins I and II messenger RNA expression in lung carcinoma: relationship with p53 alterations, angiogenic growth factors, and vascular density. Clin Cancer Res 5:155–161
7. Grossfeld GD, Ginsberg DA, Stein JP, Bochner BH, Esrig D, Groshen S, Dunn M, Nichols PW, Taylor CR, Skinner DG, Cote RJ (1997) Thrombospondin-1 expression in bladder cancer: association with p53 alternations, tumor angiogenesis, and tumor progression. J Natl Cancer Inst 89:219–227
8. Hamilton SR, Aaltonen LA (2000) Pathology and Genetics. Tumors of the Digestive System. In: World Health Organization Classification of tumors, IARC, Lyon, pp 39
9. Jaffe EA, Ruggiero JT, Leung LK, Doyle MJ, McKeown-Longo PJ, Mosher DF (1983) Cultured human fibroblasts synthesize and secrete thrombospondin and incorporate it into extracellular matrix. Proc Natl Acad Sci U S A 80:998–1002
10. Japanese Research Society for Gastric Cancer (1995) Japanese classification of gastric carcinoma. Kanehara, Co., Tokyo
11. Kasper HU, Ebert M, Malfertheiner P, Roessner A, Kirkpatrick CJ, Wolf HK (2001) Expression of thrombospondin-1 in pancreatic carcinoma: correlation with microvessel density. Virchows Arch 438:116–120
12. Kitadai Y, Amioka T, Haruma K, Tanaka S, Yoshihara M, Sumii K, Matsutani N, Yasui W, Chayama K (2001) Clinicopathological significance of vascular endothelial growth factor (VEGF)-C in human esophageal squamous cell carcinomas. Int J Cancer 93:662–666
13. Kwak C, Jin C, Lee C, Park MS, Lee SE (2002) Thrombospondin-1, vascular endothelial growth factor expression and their relationship with p53 status in prostate cancer and benign prostatic hyperplasia. BJU Int 89:303–309 (http://www.blackwell-synergy.com/servlet/useragent?func=showIssues&code=bju)
14. Maeda K, Nishiguchi Y, Yashiro M, Yamada S, Onoda N, Sawada T, Kang S-M, Hirakawa K (2000) Expression of vascular endothelial growth factor and thrombospondin-1 in colorectal carcinoma. Int J Mol Med 5:373–378
15. Majack RA, Cook SC, Bornstein P (1985) Platelet-derived growth factor and heparin-like glycosaminoglycans regulate thrombospondin synthesis and deposition in the matrix by smooth muscle cells. J Cell Biol 101:1059–1070

16. Martin L, Green B, Renshaw C (1997) Examining the technique of angiogenesis assessment in invasive breast cancer. Br J Cancer 76:1046–1054
17. Morelli D, Lazzerini D, Cazzaniga S, Squicciarini P, Bignami P, Maier JAM, Sfondrini L, Menard S, Colnaghi MI, Balsari A (1998) Evaluation of the balance between angiogenic and antiangiogenic circulating factors in patients with breast and gastrointestinal cancers. Clin Cancer Res 4:1221–1225
18. Mosher DF, Doyle MJ, Jaffe EA (1982) Synthesis and secretion of thrombospondin by cultured human endothelial cells. J Cell Biol 93:343–348
19. Ochiai A, Yasui W, Tahara E (1985) Growth-promoting effect of gastrin on human gastric carcinoma cell line TMK-1. Jpn J Cancer Res 76:1067–1071
20. Okanobu H, Hata J, Haruma K, Matsumura S, Yoshida S, Kitadai Y, Tanaka S, Chayama K (2002) Preoperative assessment of gastric cancer vascularity by flash echo imaging. Scand J Gastroenterol 37:608–612
21. O'Reilly MS, Holmgren L, Shing Y, Chen C, Rosenthal RA, Moses M, Lane WS, Cao Y, Sage EH, Folkman J (1994) Angiostatin: a novel angiogenesis inhibitor that mediates the suppression of metastases by a Lewis lung carcinoma. Cell 79:315–328
22. Oue N, Matsumura S, Nakayama H, Kitadai Y, Taniyama K, Matsusaki K, Yasui W (2003) Reduced expression of the TSP-1 gene and its association with promoter hypermethylation in gastric carcinoma. Oncology (in press)
23. Pike SE, Yao L, Jones KD, Cherney B, Appella E, Sakaguchi K, Nakhasi H, Teruya FJ, Wirth P, Gupta G, Tosato G (1998) Vasostatin a calreticulin fragment inhibits angiogenesis and suppresses tumor growth. J Exp Med 188:2349–2356
24. Qian X, Tuszinski GP (1996) Expression of thrombospondin-1 in cancer: a role in tumor progression. Proc Soc Exp Biol Med 211:199–207
25. Robey PG, Young MF, Fisher LW, McClain TD (1989) Thrombospondin is an osteoblast-derived component of mineralized extracellular matrix. J Cell Biol 108:719–727
26. Sargiannidou I, Zhou J, Tuszynski GP (2001) The role of thrombospondin-1 in tumor progression. Exp Bio Med 8:726–733
27. Tanaka K, Sonoo H, Kurebayashi J, Nomura T, Ohkubo S, Yamamoto Y, Yamamoto S (2002) Inhibition of infiltration and angiogenesis by thrombospondin-1 in papillary thyroid carcinoma. Clin Cancer Res 8:1125–1131
28. Taraboletti G, Roberts D, Liotta L, Giavazzi R (1990) Platelet growth: a potential angiogenesis regulatory factor. J Cell Biol 111:765–772
29. Taraboletti G, Morbidelli L, Donnini S, Parenti A, Granger HJ, Giavazzi R, Ziche M (2000) The heparin binding 25 kDa fragment of thrombospondin-1 promotes angiogenesis and modulates gelatinase and TIMP-2 production in endothelial cells. FASEB J 14:1674–1676
30. Vermeulen PB, Gasparini G, Fox SB, Toi M, Martin L (1996) Quantification of angiogenesis in solid human tumors: an international consensus on the methodology and criteria of evaluation. Eur J Cancer 32:2474–2484
31. Volpert OV, Tolsma SS, Pellerin S, Feige JJ, Chen H, Mosher DF, Bouck N (1995) Inhibition of angiogenesis by thrombospondin-2. Biochem Biophys Res Commun 217:326–332
32. Yamaguchi M, Sugio K, Ondo K, Yano T, Sugimachi K (2002) Reduced expression of thrombospondin-1 correlates with a poor prognosis in patients with non-small cell lung cancer. Lung Cancer 36:143–150
33. Yamashita Y, Kurohiji T, Tuszynski GP, Sakai T, Shirakusa T (1998) Plasma thrombospondin levels in patients with colorectal carcinoma. Cancer 82:632–638
34. Yanagihara K, Seyama T, Tsumuraya M, Kamada N, Yokoro K (1991) Establishment and characterization of human signet ring cell gastric carcinoma cell lines with amplification of the c-myc oncogene. Cancer Res 51:381–386
35. Yao L, Zhao YL, Itoh S, Yue WL, Furuta I (2000) Thrombospondin-1 expression in oral squamous cell carcinomas: correlations with tumor vascularity, clinicopathological features and survival. Oral Oncol 36:539–544
36. Zabrenetzky V, Harris CC, Steeg PS, Roberts DD (1994) Expression of the extracellular matrix molecule thrombospondin inversely correlates with malignant progression in melanoma, lung and breast carcinoma cell lines. Int J Cancer 59:191–197

Virchows Arch (2003) 442:569–576
DOI 10.1007/s00428-003-0811-5

ORIGINAL ARTICLE

**Takahiro Hasebe · Satoshi Sasaki · Masanori Sugitoh · Masato Ono · Norio Saitoh · Atsushi Ochiai**

# Proliferative activities of tumor stromal cells play important roles in tumor thickness and progression of T3 ulcerative-type colorectal cancer

Received: 11 December 2002 / Accepted: 17 February 2003 / Published online: 13 May 2003
© Springer-Verlag 2003

**Abstract** The central depressed area thickness (tumor thickness) of colorectal cancers is an important prognostic parameter for colorectal cancer patients. We examined whether the proliferative activities of tumor and stromal components play important roles in the increase of tumor thickness and the progression of colorectal cancers. Colorectal cancers were classified into thin and thick groups according to tumor thickness. The proliferative activities of fibroblasts and endothelial cells were immunohistochemically evaluated in 157 T3 ulcerative-type colorectal cancers by CD31/MIB-1 (anti-Ki-67 antigen) double staining. The MIB-1 labeling index was estimated as the percentage of fibroblasts with positive nuclei. The CD31-positive microvessels lined by MIB-1-positive endothelial cells were assessed. The proliferative microvessel index was defined as the percentage of proliferative microvessels relative to all microvessels. The fibroblast MIB-1 labeling index was the only parameter significantly associated with tumor thickness ($P$=0.049). High fibroblast MIB-1 labeling indices showed significant correlation with tumor recurrence in the thin group ($P$=0.020). High proliferative microvessel index was a significant parameter of tumor recurrence in the thick group ($P$=0.003) in multivariate analyses. This study strongly suggests that proliferative activities of stromal components are useful parameters of tumor biology and of prognosis for T3 ulcerative-type colorectal cancer patients.

**Keywords** Colorectal cancer · Proliferative activity · Fibroblast · Endothelial cell · Prognosis

T. Hasebe · A. Ochiai (✉)
Pathology Division,
the National Cancer Center Research Institute East,
6–5-1 Kashiwanoha, Kashiwa, 277-8577 Chiba, Japan
e-mail: aochiai@east.ncc.go.jp
Tel.: +81-471-346855, Fax: +81-471-346865

S. Sasaki
Epidemiology and Biostatistics Division,
The National Cancer Center Research Institute East,
Chiba, Japan

M. Sugitoh · M. Ono · N. Saitoh
Department of Surgery,
The National Cancer Center Hospital East,
Chiba, Japan

## Introduction

Since most carcinomas of the colon and rectum are ulcerating tumors with raised averted edges [16], it is important to investigate prognostic predictive factors for patients with ulcerative-type colorectal cancers. We previously reported that the central depressed area (CDA) thickness (tumor thickness) of ulcerative-type colorectal cancers is an important histopathological parameter, predicting tumor metastasis and prognosis in Dukes C colorectal cancer patients [7], and that the degree of stromal fibrosis is closely associated with increasing tumor thickness. We have also clarified that highly proliferative intratumoral fibroblasts play an important role in lymph-node metastasis and distant organ metastasis in cases of invasive ductal carcinoma of the breast and in cases with T3 ulcerative-type of colorectal cancers [8, 9]. In addition to demonstrating the role played by intratumoral fibroblasts, we have also shown that the proliferative activity of intratumoral endothelial cells has a significant effect on outcomes of patients with T3 ulcerative-type of colorectal cancers [9].

The purpose of this study was to examine whether the proliferative activities of fibroblasts and endothelial cells play important roles in the increase of tumor thickness as well as tumor metastasis and death in patients with T3 ulcerative-type colorectal cancer according to CDA thickness. The results demonstrated: (1) the proliferative activity of intratumoral fibroblasts is significantly associated with the degree of the CDA thickness of colorectal cancers and (2) the proliferative activity of intratumoral fibroblasts and that of intratumoral microvessels are independent prognostic parameters for patients with

colorectal cancers of thin CDA and thick CDA, respectively.

## Materials and methods

The study subjects were 157 consecutive patients with T3 ulcerative-type (which has a less elevated surface and is centrally ulcerated [21]) colorectal carcinomas who had undergone curative resection between October 1993 and May 1995 at the National Cancer Center Hospital East. All of the patients were Japanese, and all had a solitary lesion. None of the patients had received radiotherapy or chemotherapy before surgery. There were no cases in which the tumors showed direct invasion of adjacent abdominal organs.

For histological examination, the surgically resected specimens were fixed overnight in 10% formalin at room temperature, and the entire tumor was cut into slices 10 mm in thickness. Several histological sections from each tumor were taken to adequately examine the histological features of the tumor.

Two sections of each tumor were cut from the paraffin blocks. One section was stained with hematoxylin and eosin, and the other was elastica stained to confirm vascular invasion by tumor cells.

The tumor thickness of each T3 ulcerative-type colorectal cancer was measured in the hematoxylin and eosin stained sections (Fig. 1) [7]. Tumors with a thickness of less than 10 mm and greater than 10 mm were classified into the thin and thick groups, respectively. The following histological parameters were examined: (1) tumor size (mm), (2) tumor histology (well, moderately, poorly differentiated), (3) depth of invasion (DI) (DI1: tumors showing minute or moderate invasion of the subserosal or subadventitial layer; DI2: tumors showing marked subserosal or subadventitial invasion, and those showing involvement of the serosa or adventitia), (4) lymphatic invasion and (5) vascular invasion. Histological type was classified according to the guidelines of the World Health Organization [13]. All tumors were classified according to the Dukes classification system [5].

Double CD31/anti-Ki-67 immunohistochemical staining was performed using the diaminobenzidine–cobalt technique [12]. Sections 3-$\mu$m thick on silane-coated glass slides were dewaxed by passing through xylene, and the endogenous peroxidase activity was blocked with 0.3% $H_2O_2$–methanol. The slides were then treated with 0.05% pepsin for 60 min and next were microwaved [22] at 95°C for 20 min to retrieve the immunohistochemical stainings for the Ki-67 antigen (MIB-1, Immunotech, Marseille, France), applied at a 1:50 dilution, and a mouse monoclonal antibody CD31 (platelet/endothelial cell adhesion molecule/PE-CAM, JC/70A, Dako), used at a 1:50 dilution. Anti-CD31 is the most sensitive pan-endothelial marker available that recognizes a greater number of microvessels than other endothelial markers tested for such factor VIII-related antigen or CD34 [10, 19]. Next, the slides were rinsed with phosphate-citrate buffer, pH 7.4, and non-specific antibody binding was reduced by incubating the sections with 10% normal serum in PBS for 30 min. After decanting the excess serum, sections were incubated for 5 h at room temperature with MIB-1 antibody. Then the slides were rinsed with phosphate-citrate buffer, pH 7.4, and incubated with biotinylated horse antimouse IgG for 30 min followed by the avidin-biotin-peroxidase complex (Dako, Glostrup, Denmark) for 30 min. Then peroxidase was visualized with 0.02% 3-3′-diaminobenzidine tetrahydrochloride containing 0.005% $H_2O_2$ and 1% $CoCl_2$ in Tris buffer, pH 7.4. Next, the slides were rinsed with phosphate-citrate buffer, pH 7.4, and were incubated with 10% normal serum in PBS for 30 min. The sections were incubated for 5 h at room temperature with CD31 antibody. Then the slides were rinsed with phosphate-citrate buffer, pH 7.4, and were incubated with biotinylated horse antimouse IgG for 30 min followed by the avidin-biotin-peroxidase complex (Dako) for 30 min. Then peroxidase was visualized with 0.02% 3-3′-diaminobenzidine tetrahydrochloride containing 0.005% $H_2O_2$ in Tris buffer, pH 7.4. After immunostaining, the sections were counterstained with hematoxylin. Sections of colorectal cancers positive for MIB-1 and CD31 were used as positive controls. Normal mouse immunoglobulin was substituted for the primary antibody as the negative control.

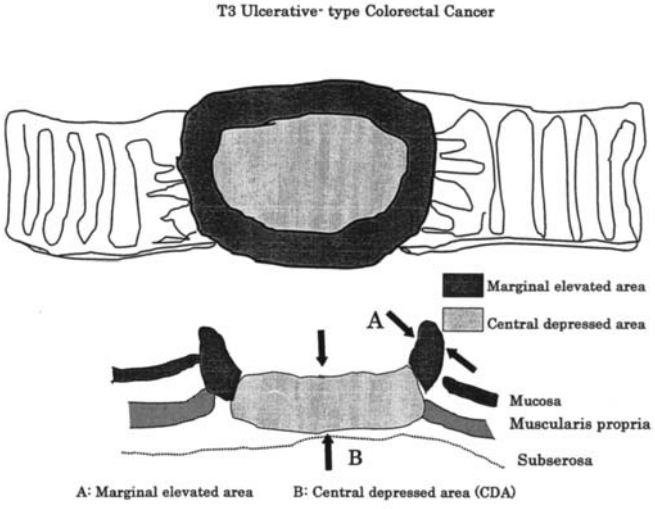



**Fig. 1** Schema of the tumor and non-tumor areas in ulcerative-type colorectal cancer. Central depressed area is marked by *arrows*

Proliferative activity of tumor cells and fibroblasts was assessed by MIB-1. The MIB-1 labeling index was determined as the percentage of tumor cells or fibroblasts showing strongly positive staining of nuclei relative to the total number of tumor cells and fibroblasts counted, respectively. After the fields of the strongest MIB-1 staining area had been identified, at least 1000 tumor cells were counted in the high-power field (×400) of the CDA. A total of 600 fibroblasts were also counted in the high-power fields of the CDA.

The microvessel counts were made under ×200 magnification in fields showing the most prominent neovascularity (×20 objective and ×10 ocular, 0.384 $mm^2$ per field). Results were expressed as the highest number of microvessels in any single ×200-magnified field. Similarly, the area showing the highest number of CD31-positive microvessels lined by MIB-1 positive endothelial cells was assessed in the CDA under a single ×200-magnified field as the proliferative microvessel count. Then the proliferative microvessel index was defined as the percentage of proliferative microvessels relative to the microvessel count in the CDA.

Two of the authors (T.H. and A.O.) investigated the MIB-1 labeling indices of tumor cells and fibroblasts, the microvessel counts and the proliferative microvessel indices. If there were discrepancies in the values of these parameters between the two investigators, the slides were re-examined to reach a consensus.

The patient series in this study was similar to our previous study [9]. Survival was determined by follow-up through December 1999, with a median period of 62 months (range 54–76 months). Among the 157 patients, 87 and 70 were classified into the thin and thick groups, respectively. Eighty-one and seventy-six patients were classified as having Dukes B and C, respectively. One hundred twenty patients were alive and well without tumor recurrence. Tumor recurrence was observed in 37 patients (thin group, 13 cases; thick group, 24 cases), and distant organ metastasis was observed in 26 patients (thin group, 13 cases; thick group, 13 cases). Twenty-three patients died of disease (thin group, 7; thick group, 16). Measurements of disease-free survival, distant organ metastasis-free survival and overall survival began at the time of surgery. Tumor recurrence and distant organ metastasis were confirmed by computed tomography or needle biopsy. Only deaths due to colorectal cancer were considered for the purpose of this study.

Correlations between the mean tumor cell MIB-1 labeling indices, fibroblast MIB-labeling indices, proliferative microvessel indices and microvessel counts were analyzed by Pearson's linear correlation in the thin and thick groups, respectively. We used the *t*-test to examine whether there were any differences in the above parameters between the thin and thick groups. We also used the *t*-test to determine whether there was a significant correlation between stromal fibrosis and the fibroblast MIB-1 labeling indices.

We again examined the prognostic significance of tumor thickness for T3 ulcerative-type colorectal cancer patients. The median values of the tumor cell MIB-1 labeling indices, fibroblast MIB-1 labeling indices, proliferative microvessel indices and microvessel counts in Dukes C colorectal cancer patients with distant organ metastasis were used as the cut-off values for predicting hazard rates (HRs) of disease-free survival, distant organ metastasis or overall survival in this study. The median values or lower were designated "low tumor cell MIB-1labeling index", "low fibroblast MIB-1 labeling index", "low proliferative microvessel index" or "low microvessel count", and values higher than the median were designated "high tumor cell MIB-1 labeling index", "high fibroblast labeling index", "high proliferative microvessel index" or "high microvessel count". The following parameters were examined as potential predictors of disease-free survival, distant organ metastasis and overall survival in the thin and thick groups: (1) tumor size ($\leq$50 vs >50 mm), (2) tumor histology (well/moderately differentiated vs poorly differentiated), (3) DI (DI1 vs DI2), (4) lymphatic invasion (absent vs present), (5) vascular invasion (absent vs present) and (6) tumor location (colon vs rectum). Disease-free survival, distant organ metastasis and overall survival curves were drawn using the Kaplan-Meier method [14], and the differences between the curves were compared using the log-rank test [20]. The parameters that showed a significant correlation in the univariate analysis were entered into the Cox proportional hazard regression model [3], employing the step-down method.

## Results

### Pearson's correlations for the tumor cell MIB-1 labeling indices, fibroblast MIB-1 labeling indices, proliferative microvessel indices and microvessel counts in the thin and thick groups

The tumor cell MIB-1 labeling indices in the thin and thick groups were significantly associated with the fibroblast MIB-1 labeling indices and proliferative microvessel indices, respectively (Fig. 2A, B, D, E). Similarly, the fibroblast MIB-1 labeling indices in the thin and thick groups showed significant correlations with the respective proliferative microvessel indices (Fig. 2C, F).

The tumor cell MIB-1 labeling indices in the thin and thick groups showed significant associations with the microvessel counts ($r$=0.466, $P$<0.001 and $r$=0.421, $P$<0.001, respectively). Although the fibroblast MIB-1 labeling indices in the thin group showed a significant association with the microvessel count ($r$=0.267, $P$=0.012), the association between them was not significant in the thick group ($r$=0.201, $P$=0.095). Proliferative microvessel indices showed no significant associations with microvessel counts in the thin and thick groups ($r$=0.167, $P$=0.121 and $r$=0.139, $P$=0.252).

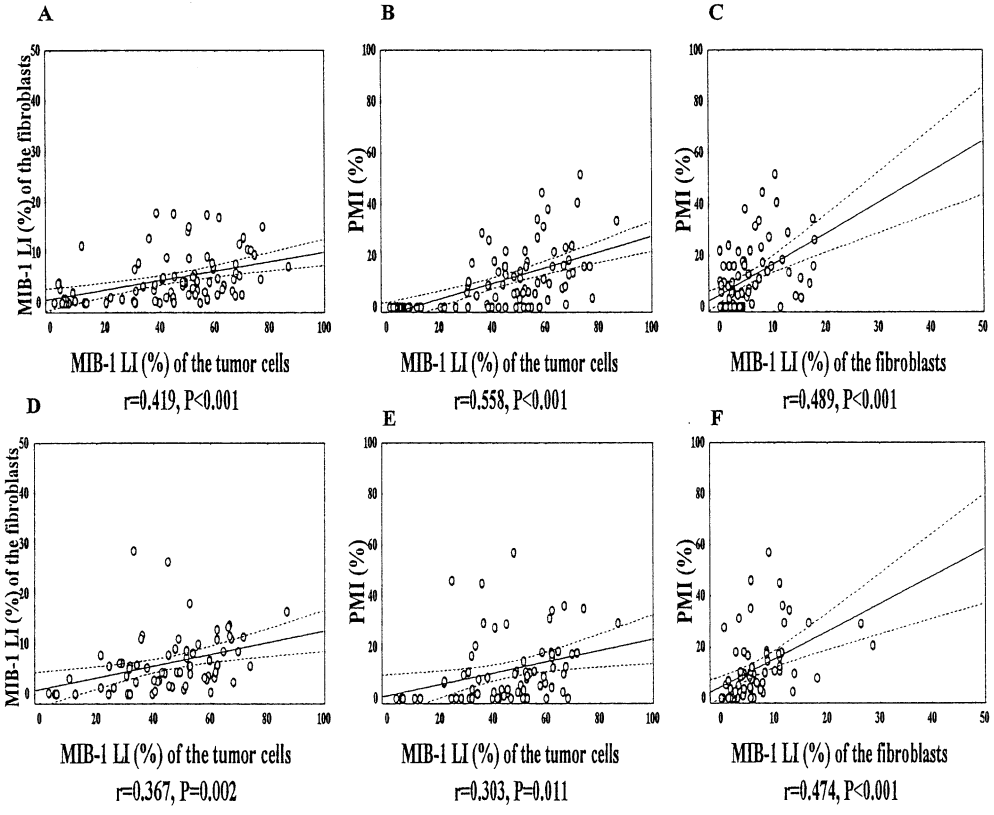



**Fig. 2** Pearson's correlations between the tumor cell MIB-1 labeling indices (TMLIs), fibroblast MIB-1 labeling indices (FMLIs) and proliferative microvessel indices (PMIs) in the thin and thick groups (**A**–**F**). The TMLIs showed significant correlations with the FMLIs and PMIs in both the thin (**A**, **B** $r$=0.419, $P$<0.001 and $r$=0.558, $P$<0.001) and the thick group (**D**, **E** $r$=0.367, $P$=0.002 and $r$=0.303, $P$=0.011). The FMLIs also showed significant correlations with the PMIs in the thin and thick groups (**C**, **F** $r$=0.489, $P$<0.001 and $r$=0.474, $P$<0.001)

**Table 1** The tumor cell MIB-1 labeling indices, fibroblast MIB-1 labeling indices, proliferative microvessel indices and microvessel counts: comparison of thin and thick groups

| | Colorectal cancers | | |
|---|---|---|---|
| | Thin group Mean ± SD (*n*=87) | Thick group Mean ± SD (*n*=70) | Thin vs thick *P* value |
| Fibroblast MIB-1 labeling indices (%) | 4.6±4.6 | 6.2±5.7 | 0.049 |
| Microvessel counts | 61.3±21.6 | 69.5±29.0 | 0.101 |
| Tumor cell MIB-1 labeling indices (%) | 43.6±21.6 | 45.6±17.8 | 0.540 |
| Proliferative microvessel indices (%) | 10.5±11.8 | 11.2±12.9 | 0.717 |

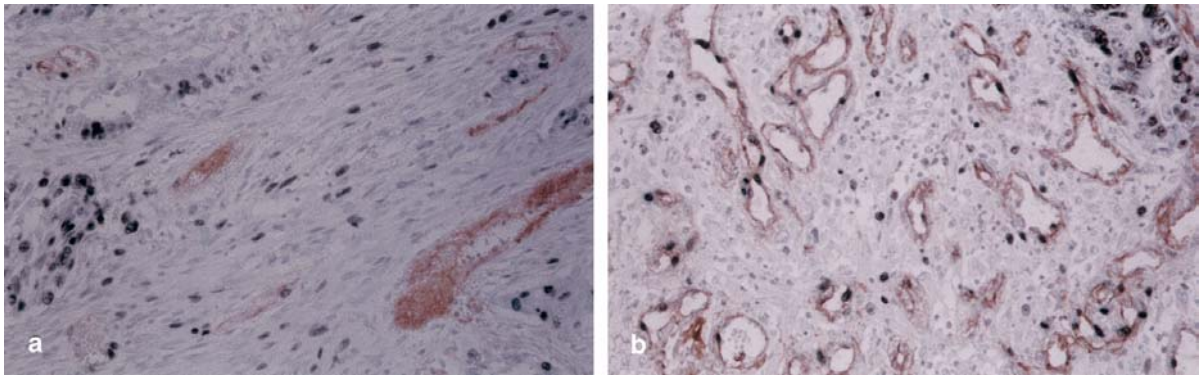



**Fig. 3** Double immunostaining for MIB-1 and CD31 in colorectal cancer. **A** Tumor cells and several fibroblasts show positive nuclear staining for MIB-1. **B** There are many CD31-positive microvessels lined by MIB-1 positive endothelial cells adjacent to the MIB-1-positive tumor cell nests. Occasional MIB-1-positive fibroblasts are also seen

Differences in the tumor cell MIB-1 labeling indices, fibroblast MIB-1 labeling indices, proliferative microvessel indices and microvessel counts in the thin and thick groups

In comparing the thin and thick groups, the fibroblast MIB-1 labeling index was the only parameter significantly higher in the latter than in the former (Table 1, Fig. 3 left).

Stromal fibrosis and the fibroblast MIB-1 labeling indices

The mean ± standard deviation of the fibroblast MIB-1 labeling indices in colorectal cancers without any or only mild stromal fibrosis was 4.2±4.4, while that of the fibroblast MIB-1 labeling indices with moderate to severe stromal fibrosis was significantly higher at 7.1±5.8 (*P*<0.001).

Univariate and multivariate analyses for predictors of disease-free survival, distant organ metastasis and overall survival in the thin and thick groups

The thin group showed a significantly shorter overall survival period than the thick group (*P*=0.012) (Fig. 4). Other histological parameters that were significantly associated with short overall survival period in the univariate analyses included poorly differentiated histology, tumor location, lymphatic invasion and Dukes stage

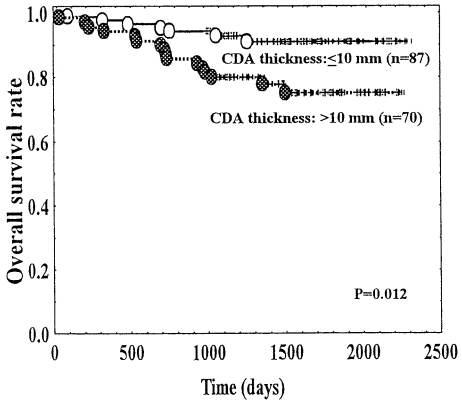



**Fig. 4** Overall survival (OS) curves for the thin and thick groups. The thick group shows a significantly shorter OS than the thin group (*P*=0.012)

classification (*P*<0.001, *P*<0.001, *P*=0.005 and *P*=0.008, respectively). The thick group [HR, 2.8; 95% confidence interval (CI), 1.1–6.6; *P*=0.026], the rectal cancer patients (HR, 6.0; 95% CI, 2.1–17.6; *P*=0.001) and the colorectal cancer patients with lymphatic invasion (HR, 3.4; 95% CI, 1.4–8.4; *P*=0.007) still had significantly increased HRs of overall survival in the multivariate analysis. Dukes stage classification and tumor histology were not associated with significantly increased HRs of overall survival in multivariate analysis. DI, tumor size and vascular invasion had no significant associations with

**Table 2** Univariate and multivariate analyses for tumor recurrence and death in thin and thick groups. Univariate analyses were performed using the log-rank test. Multivariate analysis was performed using the Cox proportional hazard regression model adjusted for parameters showing significantly higher DOMR in the univariate analyses. The step-down method was applied until all remaining factors were significant, at a *P* level below 0.05, in the multivariate analysis. *DFS* disease-free survival, *DOMR* distant organ metastasis rate, *HR* hazard rate, *CI* confidence interval

| Parameters | Univariate analyses | | | Multivariate analysis | | |
|---|---|---|---|---|---|---|
| | Cases | | *P* value | HR | 95% CI | *P* value |
| | | DFSR(%) | | | | |
| Thin group (*n*=87) | | | | | | |
| Fibroblast MIB-1 labeling index (%) | | | | | | |
| Low | 74 | 7 ( 9) | | Referent | | |
| High | 13 | 6 (46) | <0.001 | 4.1 | 1.3–13.1 | 0.020 |
| Dukes stage | | | | | | |
| B | 45 | 3 ( 7) | | Referent | | |
| C | 42 | 10 (24) | 0.026 | – | – | |
| | | DOMR(%) | | | | |
| Fibroblast MIB-1 labeling index (%) | | | | | | |
| Low | 74 | 7 ( 9) | | Referent | | |
| High | 13 | 6 (46) | <0.001 | 6.0 | 2.0–18.2 | 0.001 |
| Vascular invasion | | | | | | |
| Absent | 26 | 1 ( 4) | | Referent | | |
| Present | 61 | 12 (20) | 0.010 | – | – | |
| Thick group (*n*=70) | | | | | | |
| | | DFSR(%) | | | | |
| Dukes stage | | | | | | |
| B | 36 | 5 (14) | | Referent | | |
| C | 34 | 19 (56) | <0.001 | 6.0 | 2.2–16.0 | <0.001 |
| Proliferative microvessel index (%) | | | | | | |
| Low | 49 | 12 (24) | Referent | | | |
| High | 21 | 12 (57) | 0.010 | 3.4 | 1.5–7.5 | 0.003 |
| Vascular invasion | | | | | | |
| Absent | 21 | 3 (14) | | Referent | | |
| Present | 49 | 21 (43) | 0.022 | – | – | |
| | | DOMR(%) | | | | |
| Proliferative microvessel index (%) | | | | | | |
| Low | 49 | 5 (10) | | Referent | | |
| High | 21 | 8 (38) | 0.005 | 5.3 | 1.7–16.2 | 0.004 |
| Dukes stage | | | | | | |
| B | 36 | 3 ( 8) | | Referent | | |
| C | 34 | 10 (29) | 0.026 | 4.7 | 1.3–17.0 | 0.020 |
| Fibroblast MIB-1 labeling index (%) | | | | | | |
| Low | 55 | 7 (13) | | Referent | | |
| High | 15 | 6 (40) | 0.013 | – | – | |
| Vascular invasion | | | | | | |
| Absent | 21 | 1 ( 5) | | Referent | | |
| Present | 49 | 12 (24) | 0.048 | – | – | |

short overall survival periods in the univariate analysis (*P*=0.126, *P*=0.912 and *P*=0.151).

In the thin group, high fibroblast MIB-1 labeling indices and Dukes stage C disease showed significant associations with short disease-free survival periods in the univariate analyses (Table 2, Fig. 5A). The multivariate analysis showed high fibroblast MIB-1 labeling indices to be the only parameter associated with a significantly increased HR of disease-free survival. As for distant organ metastasis, high fibroblast MIB-1 labeling indices and vascular invasion showed significant associations with short distant organ metastasis-free periods in the univariate analyses (Table 2, Fig. 5B), and the former still showed a significant association with a short distant organ metastasis-free period in the multivariate analysis. In addition, high fibroblast MIB-1 labeling index was the only parameter significantly associated with a short overall survival period in the univariate analysis (Fig. 5C). The tumor cell MIB-1 labeling indices, proliferative microvessel indices, microvessel counts, tumor size, tumor histology, DI, lymphatic invasion and tumor location had no significant associations with short disease-free survival, distant organ metastasis-free periods and overall survival periods in the univariate analyses (data not shown).

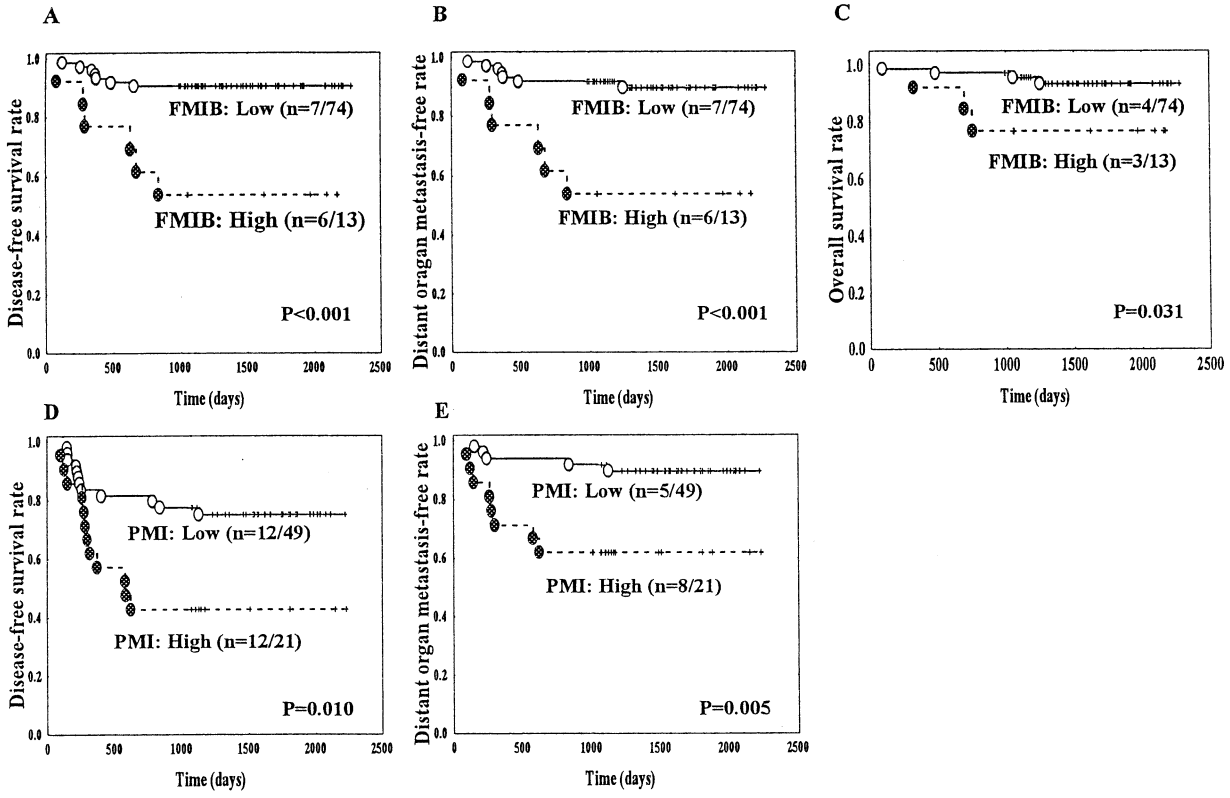



**Fig. 5** Disease-free survival (DFS), distant organ metastasis (DOM) and overall survival (OS) curves for the thin group (**A**–**C**), and DFS and DOM curves for the thick group (**D**–**F**). **A**, **B**, **C** The patients with high fibroblast MIB-1 labeling indices (FMLIs) have significantly shorter DFS, DOM-free periods and OS than those with low MIB-1 LIs of fibroblasts in the same area ($P<0.001$, $P<0.001$ and $P=0.031$, respectively). **D**, **E** The patients with high proliferative microvessel indices (PMIs) have significantly shorter DFS and DOM-free periods than those with low PMIs ($P=0.010$ and $P=0.005$)

In the thick group, Dukes stage C disease, high proliferative microvessel index and vascular invasion showed significant associations with short disease-free survival periods in the univariate analyses (Table 2, Fig. 3 right). Dukes stage C disease and high proliferative microvessel index were still significantly associated with short disease-free survival periods in the multivariate analyses (Fig. 5D), and also with increased HRs of distant organ metastasis in the multivariate analysis (Fig. 5E). As for overall survival, lymphatic invasion, poorly differentiated histology, Dukes stage classification and tumor location correlated significantly with short overall survival periods in the univariate analyses ($P=0.034$, $P=0.039$, $P<0.001$ and $P<0.001$, respectively). Among these parameters, Dukes stage C disease (HR, 7.2; 95% CI, 1.6–31.8; $P=0.010$) and rectal cancer (HR, 6.0; 95% CI, 1.4–26.6; $P=0.018$) still correlated significantly with a short overall survival, while others failed to significantly increase the HRs in the multivariate analysis. Other parameters did not correlate significantly with short disease-free survival period, the distant organ metastasis-free period or overall survival period in the univariate analyses (data not shown).

## Discussion

Significant correlations among the tumor cell MIB-1 labeling indices, fibroblast MIB-1 labeling indices, and proliferative microvessel indices were observed in the thick group as well as in the thin group in this study. This suggests that the tumor thickness of colorectal cancers increases according to the interaction between tumor cells and stromal cells [2, 8, 9, 23]. In addition, since the thick group had significantly higher fibroblast MIB-1 labeling indices than the thin group, the fibroblast MIB-1 labeling index most likely defines tumor thickness, and the degree of intratumoral fibrosis is probably a useful histological parameter predicting the proliferative activity of fibroblasts.

The thin and thick groups are most likely classified into low-risk and high-risk groups. Furthermore, the highly proliferative fibroblasts probably heighten the malignant potential of T3 ulcerative-type colorectal cancers, as the proliferative activity of these fibroblasts was the only parameter that differed significantly between the two groups. Thus, in the thin group, tumors with highly proliferative fibroblasts probably have biological characteristics very similar to those tumors in the thick group. In the thick group, high proliferative microvessel index may be a useful parameter for T3 ulcerative-type

colorectal cancer patients. Since the proliferative activity of fibroblasts in many T3 ulcerative-type of colorectal carcinoma in the thick group is high, T3 ulcerative colorectal carcinoma with the high proliferative microvessel counts in addition to the highly proliferative fibroblasts probably have the highest malignant potential in the thick group. We have clearly shown that the high proliferative activities of intratumoral fibroblasts and endothelial cells show significant associations with tumor recurrence or death of patients with colorectal cancers without nodal metastasis and with nodal metastasis, respectively [9]. Thus, this study strongly suggests that the proliferative activities of intratumoral fibroblasts and endothelial cells are significant prognostic predictors for patients with colorectal cancers independent of the CDA thickness and nodal status of colorectal cancers.

The highly proliferative fibroblasts may secrete larger amounts of proteinases than poorly proliferative fibroblasts [1, 18]. The highly proliferative endothelial cells may secrete larger amounts of growth factors and their receptors or carbohydrate-binding proteins than poorly proliferative endothelial cells [11, 17], and probably support tumor cell migration into microvessels mediated via growth factors and their receptors, or carbohydrate-binding protein. Furthermore, the highly proliferative endothelial cells probably have a greater potential to form anastomosing microvessels or new microvessels, which would enhance the capacity of these tumor cells to migrate into the microvessels, than the poorly proliferative endothelial cells [6, 24]. Thus, next we must clarify which factors—e.g., proteinases, growth factors, secreted by highly proliferative fibroblasts or endothelial cells—play important roles in tumor progression of T3 ulcerative-type colorectal cancers.

In conclusion, this study strongly suggests that the enhanced proliferative activity of fibroblasts and endothelial cells is most likely attributable to tumor and stromal cell interactions. Since tumor thickness in ulcerative-type colorectal cancer can be measured accurately by endosonography [4, 15], tumor thickness can give clinicians an advantage in objectively predicting tumor recurrence or death in colorectal cancer patients. Thus, assessments of proliferative activity of intratumoral fibroblasts and microvessels most likely provide clinicians as well as pathologists additional important information about outcomes of T3 ulcerative-type colorectal cancer patients.

**Acknowledgements** This work was supported in part by a Grant-in-Aid for Cancer Research from the Ministry of Health and Welfare (11–12) and by a Grant-in-Aid for the Second Term Comprehensive 10-year Strategy for Cancer Control from the Ministry of Health and Welfare in Japan. Part of this work was presented at the 90th annual meeting of the Japanese Society of Pathology on 7 April 2001 in Tokyo, Japan.

## References

1. Afzal S, Lalani EN, Poulsom R, et al (1998) MT1-MMP and MMP-2 mRNA expression in human ovarian tumors: possible implications for the role of desmoplastic fibroblasts. Hum Pathol 29:155–165
2. Booth C, Harnden P, Trejdosiewicz LK, et al (1997) Stromal and vascular invasion in a human in vitro bladder cancer model. Lab Invest 76:843–857
3. Cox DR (1972) Regression models and life-tables. J R Stat Soc 34:187–220
4. Dershaw DD, Enker WE, Cohen AM, Sigurdson ER (1990) Transrectal ultrasonography of rectal carcinoma. Cancer 66:2336–2340
5. Dukes CE (1932) The classification of cancer of the rectum. J Pathol Bacteriol 35:323–332
6. Fox SB, Gatter KC, Bicknell R, et al (1993) Relationship of endothelial cell proliferation to tumor vascularity in human breast cancer. Cancer Res 53:4161–4163
7. Hasebe T, Morihiro M, Sasaki S, Shimoda T, Sugitoh M, Moriya Y, Ono M, Arai T, Ochiai A (2000) Tumor thickness is a histopathological predictive parameter of tumor metastasis and prognosis in Dukes C ulcerative-type colorectal cancer patients: two-hospital based study. Cancer 89:35–45
8. Hasebe T, Sasaki S, Imoto S, Ochiai A (2000) Proliferative activity of intratumoral fibroblasts is closely correlated with lymph node and distant organ metastasis of invasive ductal carcinoma of the breast. Am J Pathol 156:1701–1710
9. Hasebe T, Sasaki S, Sugitoh M, Ono M, Saitoh N, Ochiai A (2001) Highly proliferative intratumoral fibroblasts and a high proliferative microvessel index are significant predictor of tumor metastasis in T3 ulcerative-type colorectal cancer. Hum Pathol 32:401–409
10. Horak ER, Leek R, Klenk N, Lejeune S, et al (1992) Angiogenesis, assessed by platelet/endothelial cell adhesion molecule antibodies, as indicator of node metastasis and survival in breast cancer. Lancet 340:1120–1124
11. Hornig C, Barleon B, Ahmad S, et al (2000) Release and complex formation of soluble VEGFR-1 from endothelial cells and biological fluids. Lab Invest 80:443–454
12. Hsu SM, Soban E (1982) Color modification of diaminobenzidine (DAB) precipitation by metallic irons and its application for double immunohistochemistry. J Histochem Cytochem 30:1079–1082
13. Jass JR, Sobin LH (1989) Histological typing of intestinal tumors, 2nd edn. Springer, Berlin Heidelberg New York
14. Kaplan EL, Meier P (1958) Nonparametric estimation from incomplete observations. J Am Stat Assoc 53:457–481
15. Kimmey MB, Martin RW, Haggitt RC, et al (1989) Histologic correlates of gastrointestinal ultrasound images. Gastroenterol 96:433–441
16. Morson BC, Dawson IMP (1990) Morson & Dawson's gastrointestinal pathology, 3rd edn. Blackwell, Oxford, pp 607
17. Nagia-Makker P, Honjo Y, Sarvis R, et al (2000) Galectin-3 induces endothelial cell morphogenesis and angiogenesis. Am J Pathol 156:899–909
18. Noel A, Hajitou A, L'Hoir C, et al (1998) Inhibition of stromal matrix metalloproteases: effects on breast-tumor promotion by fibroblasts. Int J Cancer 76:267–273
19. Parums DV, Cordell JL, Micklem K, et al (1990) JC70: a new monoclonal antibody that detects vascular endothelium associated antigen on routinely processed tissue sections. J Clin Pathol 43:752–757
20. Peto R, Pike MC, Armitage P, Breslow NE, Cox DR, Howard SV (1977) Design and analysis of randomized clinical trials requiring prolonged observation of each patient. II. Analysis and examples. Br J Cancer 35:1–39
21. Rosai J (1996) Surgical pathology, 3rd edn. Mosby, St. Louis, pp 769

22. Shi SR, Key ME, Kalza KL (1991) Antigen retrieval in formalin-fixed, paraffin-embedded tissues: an enhancement method for immunohistochemical staining based on microwave oven heating of tissue sections. J Histochem Cytochem 39:741–746
23. Uría JA, Stahle-Bäckdahl M, Seiki M, et al (1997) Regulation of collagenase-3 expression in human breast carcinomas is mediated by stromal-epithelial cell interactions. Cancer Res 57:4882–4888
24. Vartanian RK, Weidner N (1994) Correlation of intratumoral endothelial cell proliferation with microvessel density (tumor angiogenesis) and tumor cell proliferation in breast carcinoma. Am J Pathol 144:1188–1194

Virchows Arch (2003) 442:577–584
DOI 10.1007/s00428-003-0801-7

ORIGINAL ARTICLE

**Tetsuro Sameshima · Kazuki Nabeshima · Bryan P. Toole · Teruhiko Inoue · Kiyotaka Yokogami · Shinichi Nakano · Takekazu Ohi · Shinichiro Wakisaka**

# Correlation of emmprin expression in vascular endothelial cells with blood–brain-barrier function: a study using magnetic resonance imaging enhanced by Gd-DTPA and immunohistochemistry in brain tumors

Received: 17 September 2002 / Accepted: 4 March 2003 / Published online: 25 April 2003
© Springer-Verlag 2003

**Abstract** In a previous study, we demonstrated that the expression levels in tumor cells of emmprin (CD147) correlated with the grade of astrocytic tumors. Also, we found that emmprin was expressed in vascular endothelial cells of the non-neoplastic brain and hypothesized that emmprin expression could be associated with normal blood–brain-barrier (BBB) function of vascular endothelial cells. In this study, this possibility was examined in non-neoplastic brain, glioma and metastatic carcinoma tissues by comparing emmprin immunohistochemistry with gadolinium diethylenetriaminepentaacetic acid (Gd-DTPA) enhancement of magnetic resonance imaging (MRI), which is a clinical indicator of the BBB function. This study included 10 cases of non-neoplastic brain tissues, 7 of metastatic carcinoma, 7 of diffuse astrocytoma, 4 of anaplastic astrocytoma and 13 of glioblastoma multiforme. In all the cases, MRI with administration of Gd-DTPA was performed. The lesions were resected using the microdissection method with the help of ultrasonography and a neuronavigator. The tissues from Gd-DTPA-enhanced or non-enhanced areas were processed into frozen sections and subjected to immunohistochemistry with anti-emmprin antibody. The expression of emmprin in brain vascular endothelial cells inversely correlated with Gd-DTPA-enhancement of MRI: emmprin was positive in tissues not enhanced by Gd-DTPA and was negative in DTPA-enhanced tissues. Since BBB function presumably remains unimpaired in regions in which MR images are not Gd-DTPA-enhanced, emmprin expression appears to be associated with unimpaired BBB function. This is the first report to demonstrate a possible correlation between emmprin expression and BBB function in humans.

**Keywords** BBB · Emmprin · Glioma · MRI

T. Sameshima · K. Yokogami · S. Nakano · S. Wakisaka
Department of Neurosurgery,
Miyazaki Medical College, Miyazaki, Japan

K. Nabeshima (✉)
Department of Pathology,
Fukuoka University Hospital and School of Medicine,
7-45-1 Nanakuma, Jonan-ku, 814-0180 Fukuoka, Japan
e-mail: kaznabes@fukuoka-u.ac.jp
Tel.: +81-92-8011011
Fax: +81-92-8617300

B. P. Toole
Department of Anatomy and Cellular Biology,
Tufts University School of Medicine, Boston, USA

T. Inoue
Department of Pathology,
Miyazaki Medical College, Miyazaki, Japan

T. Ohi
Department of Neurology, Miyazaki Medical College,
Miyazaki, Japan

## Introduction

Emmprin was discovered by the Biswas laboratory via a functional approach and shown to be a surface molecule on tumor cells that stimulates nearby fibroblasts to produce matrix metalloproteinase (MMP)-1, 2 and 3 [2, 3]. We have recently found that emmprin is also involved in stimulated production of pro-MMP-2 activators, MT1- and MT2-MMP, in co-cultures of glioma cells and fibroblasts [26]. The expression levels of emmprin, as determined by immunohistochemistry and immunoblotting, are upregulated in urinary bladder, breast and lung carcinomas compared with their normal counterparts, and emmprin has been implicated in progression and invasion in these tumors [22, 25]. Additionally, we have demonstrated that expression levels of emmprin mRNA and protein are higher in astrocytic tumors than in non-neoplastic brain tissues, and that within these tumors emmprin expression levels are associated with tumor

progression [27]. Furthermore, interestingly emmprin expression was found not only in tumor cells but also in endothelial cells, especially in endothelial cells of the non-neoplastic brain but not in proliferating endothelial cells of glioblastoma [27]. Thus, we hypothesized that emmprin expression could be associated with normal blood–brain-barrier (BBB) function of vascular endothelial cells.

The cDNA for human emmprin encodes a 269-amino-acid residue polypeptide that includes a signal peptide, an extracellular domain consisting of two regions characteristic of the immunoglobulin (Ig) superfamily, followed by a transmembrane domain and a cytoplasmic domain [3]. The mature emmprin molecule is highly glycosylated and has a molecular mass of ~58 kDa, and this glycosylation is necessary for stimulated production of MMP-1, 2 and 3 [2, 3, 13]. Moreover, the emmprin sequence has been found to be identical to that of human basigin [21] and human leukocyte activation-associated M6 antigen [17], the species homologues of rat OX-47 antigen [9], mouse basigin (gp42) [21], and chicken BBB-associated HT7 molecule, also known as neurothelin [28, 31] or 5A11 [7]; these homologues are now called CD147. Previous studies of these homologues suggest the presence of emmprin functions other than stimulation of MMP production, such as inducing differentiation of neurons and glial cells or maintaining BBB function. However, most of these functions have not been demonstrated in human tissues or cells.

The BBB is a regulatory interface between the blood and the brain for maintenance of homeostasis of the internal environment in the brain [5, 11, 24, 28] In comparison with other organs, the brain requires a more delicate control of import of intravascular substances and of physical and chemical changes in blood circulating through it. Therefore, the BBB severely restricts transfer of substances from blood into the brain, while it possesses several mechanisms for rapid transport of substances needed by the brain. This main function of the BBB is maintained by the endothelial cells of capillaries. Capillary endothelial cells in the brain are characterized structurally by the deficiency of pinocytic vesicles, the lack of fenestrations, and the presence of intercellular tight junctions linking these cells closely [12]. To demonstrate the function of the BBB clinically, imaging techniques such as computed tomography (CT) and magnetic resonance imaging (MRI) are used in conjunction with a contrast medium. Gadolinium diethylenetriaminepentaacetic acid (Gd-DTPA) is the most frequently used contrast medium for MRI [4, 29, 30]. In brain tumors, the enhancement of images by Gd-DTPA indicates an impairment of the BBB. It is generally observed in astrocytic tumors that the more marked the enhancement is, the more malignant tumors are. This is because, in grade-II diffuse astrocytoma, the newly formed capillaries closely resemble normal cerebral capillaries with an intact BBB, while in more malignant tumors, capillaries are fenestrated and show increased pinocytosis. This pathologic alteration of the BBB allows intravascular Gd-DTPA that distributes within the extracellular fluid space to diffuse into and accumulate in brain lesions [29].

In this study, we investigated a correlation between the expression of emmprin and BBB function in humans using emmprin immunohistochemistry and Gd-DTPA-enhancement on MRI. Emmprin expression was found in vascular endothelial cells obtained from non-enhanced portions of non-neoplastic or neoplastic brain, while endothelial cells from Gd-DTPA-enhanced portions lost emmprin expression, suggesting a close association of emmprin expression with BBB function.

## Materials and methods

### Surgical specimens and selection of patients

This study included only the cases, in which tumors were excised en bloc using a microdissection technique with the help of ultrasonography and a neuronavigator (Medtronic Surgical Navigation Technologies, CO, USA), except for one stereotactic biopsy case. Tumor tissues removed en bloc included both Gd-DTPA-enhanced and non-enhanced areas, and all these non-enhanced tissues were taken as a necessary and routine part of standard treatment. Based on the positional information about enhanced portions within resected specimens that was obtained by means of a neuronavigator, tissues were sampled from the portions that definitely corresponded to Gd-DTPA-enhanced or non-enhanced lesions, embedded in OCT compound (Miles, Elkhard, IN), frozen in liquid nitrogen, cut into cryostat sections, and stored at 40°C until used for emmprin immunohistochemistry. Standard light-microscopic evaluation of each section stained with hematoxylin and eosin was performed for histological diagnosis. The histological grading of gliomas was determined according to the World Health Organization (WHO) standards [19].

The glioma cases included in this study were seven diffuse astrocytoma (grade II; 3 males, 4 females; age range 26–72 years, mean=48.1 years), four anaplastic astrocytoma (grade III; 3 males, 1 female; age range 34–65 years, mean=47.5 years), and 13 glioblastoma multiforme (GBM; grade IV; 10 males, 3 females; age range 23–85 years, mean=61.5 years). Ten non-neoplastic brain tissues (6 males, 4 females; age range 16–77 years mean=61.0 years) were obtained from tumor-free edges adherent to the removed tumors in seven metastatic carcinoma (four from lung cancer; one each from breast, colon and thyroid cancer), two lymphoma, and one ganglioneuroblastoma cases. A stereotactic biopsy specimen from a patient with acute disseminated encephalomyelitis (ADEM) was also studied. In this case, a biopsy was performed to rule out malignant lymphoma. All the patients had not undergone any chemotherapy or radiation prior to the brain tumor resection.

Frozen sections were obtained also from tissues outside the central nervous system (CNS), including gastrointestinal tracts, male and female reproductive organs, endocrine organs, lungs, heart, liver, pancreas, kidneys, skin, and lymph nodes. These tissues were taken for intraoperative pathological diagnosis of their lesions.

### MRI

MRI was performed on a 1.5-T system Toshiba MRT-200/RX (Tokyo, Japan). Images were acquired as 5-mm sagittal sections (TR 600 ms/TE 20 ms), followed by T1-weighted axial sections, T2-weighted (TR 2000 ms/TE 90 ms) sections and fluid-attenuated inversion recovery (FLAIR) imaging (TR 8000 ms/TE 120 ms). Subsequently, Gd-DTPA was injected at a rate of 0.1–0.2 ml/kg

(maximum 10–20 ml) followed by axial and/or coronal, sagittal T1-weighted sections.

### Immunohistochemistry

Immunohistochemical staining of frozen sections was performed as described [27]. Briefly, frozen tissue sections were fixed in acetone at 4°C for 5 min. After endogenous peroxidase activity was blocked with 0.5% hydrogen peroxide in methanol for 30 min, sections were incubated with normal rabbit serum (1:5, Dako, Glostrup, Denmark) for 1 h at 37°C. After blocking with normal serum, the sections were incubated with anti-emmprin monoclonal antibody (mAb) (E11F4) [6] overnight at 4°C. The sections were then washed in PBS, and incubated with biotinylated anti-mouse IgG (1:10, Dako) for 10 min at room temperature, followed by streptavidin conjugated to horseradish peroxidase (Dako) for 10 min. The reaction was revealed with metal-3,3′-diaminobenzidine (DAB) (Pierce, Rockford, IL) and counterstained with Mayer's hematoxylin.

The immunohistochemical specificity of the antibody was confirmed by two types of negative controls: substituting mouse nonimmune IgG for the primary antibody and omitting the primary antibody in the staining protocol. Moreover, specificity of this antibody (E11F4) has been determined using immunoblots of whole cell and tissue homogenates and purified emmprin molecule [3, 6, 22, 26].

Vascular endothelial cells, astrocytes and neurons in frozen sections were identified using antibodies against CD34 (Dako), glial fibrillary acidic protein (GFAP, Dako), and neurofilament protein triplet (Signet Lab., Dedham, MA) as primary antibodies, respectively. Staining results were evaluated semi-quantitatively by two independent observers. As described elsewhere [23], immunostaining was considered negative if less than 10% of the endothelial cells failed to stain. In specimens considered positive, staining of the vessels was quantified on a scale from 1 to 4 based on the percentage of blood vessels lined by emmprin-positive endothelial cells. The scale was structured as follows: 1+=10–50%; 2+=50–75%; 3+=75–90%; and 4+$\geq$90%.

Fisher's exact test was used to evaluate the statistical significance of the emmprin protein immunostaining results.

## Results

The case demonstrated in Fig. 1A–D is a 58-year-old Japanese female with metastatic adenocarcinoma (follicular carcinoma) from the thyroid gland. There was an enhanced mass with an irregular contour in the right occipital lobe (Fig. 1A). The non-neoplastic tissue was obtained from the non-enhanced peripheral portion of the resected specimen (asterisk), where almost all vascular endothelial cells showed positive immunoreactivity to emmprin as cytoplasmic and membrane staining (Fig. 1B, arrows). Glial cells and neurons were all negative. The positive emmprin reactivity was not seen in negative controls with non-immune IgG (Fig. 1C, arrows). In contrast, Gd-DTPA-enhanced carcinoma portions showed a loss of emmprin immunoreactivity in vascular endothelial cells (Fig. 1D, arrows).

As in the non-neoplastic brain, emmprin was expressed in most of the vascular endothelial cells in diffuse astrocytomas (Fig. 1G, arrows), MR images of which were not enhanced by Gd-DTPA (Fig. 1E). The tumor boundary was better demonstrated in FLAIR images (Fig. 1F); an arrow indicates the region from which tissue was obtained. Tumor cells were negative for emmprin (Fig. 1G).

In cases of anaplastic astrocytoma, the central portion of the tumor showed Gd-DTPA-enhancement on MR images (Fig. 2A, arrowhead), while its peripheral portion was not enhanced (Fig. 2A, arrow). Some of the vascular endothelial cells in tissues from the enhanced central region lost immunoreactivity to emmprin (Fig. 2B, double arrows), but some others showed positive reactivity (Fig. 2B, arrow). The proportion of emmprin-positive blood vessels varied case by case. The vessels in the non-enhanced peritumoral brain were positive for emmprin (Fig. 2C). In this presented case (34-year-old, Japanese male), most of the tumor cells were negative for emmprin.

Figure 2D–G demonstrates a representative case of GBM in a 74-year-old Japanese female. Gd-DTPA-enhanced T1-weighted MR images showed a ring-enhanced mass in the right temporo-occipital region (Fig. 2D). Tissues obtained from the peripheral non-enhanced portion (Fig. 2D, asterisk) showed emmprin expression in vascular endothelial cells (Fig. 2E). In contrast, the endothelial cells of proliferating blood vessels obtained from the enhanced tumor portion (Fig. 2D, arrow) were all negative for emmprin (Fig. 2G, arrow). Tumor cells showed strong emmprin immunoreactivity in this region. The tissue obtained from the tumor border (Fig. 2D, arrowhead) is shown in Fig. 2F. Proliferating blood vessels within the GBM portion were negative for emmprin (arrowhead), while the blood vessels in the surrounding tissue were positive for emmprin (arrows).

Table 1 summarizes the results of emmprin immunostaining in vascular endothelial cells. Ratios of emmprin-positive blood vessels in non-neoplastic brain, diffuse astrocytoma, and peripheral portions of anaplastic astrocytoma and GBM were all more than 90% (scale 4+). These portions were all non-enhanced by Gd-DTPA on MR images. In contrast, the emmprin-positive ratios in the enhanced portions of GBM were all less than 10% (negative). Tissues obtained from the enhanced portions of anaplastic astrocytoma showed varying positive ratios, scale 1+ to 3+. Metastatic carcinoma portions, which were also enhanced by Gd-DTPA on MR images, showed loss of emmprin expression in a majority of cases (5/7, 71%), and a small positive ratio was seen in the rest of the cases (scale 1+). A loss of emmprin expression in vascular endothelial cells was also observed in a stereotactic biopsy specimen, which was obtained from the Gd-DTPA-enhanced subcortical lesion in a patient with ADEM (data not shown). Altogether, the number of the lesions showing no Gd-DTPA enhancement was 34, and that of the Gd-DTPA-enhanced lesions was 24 (Table 1). High scales of emmprin-positive vessels, 3+ and 4+, were observed in all of the non-enhanced lesions (34/34, 100%) compared with 4.2% (1/24) of the enhanced lesions ($P<0.0001$ by Fisher's exact test).

The vascular endothelial cells outside the CNS were all negative for emmprin as far as we examined, and those in the pituitary gland were also negative (data not shown). In

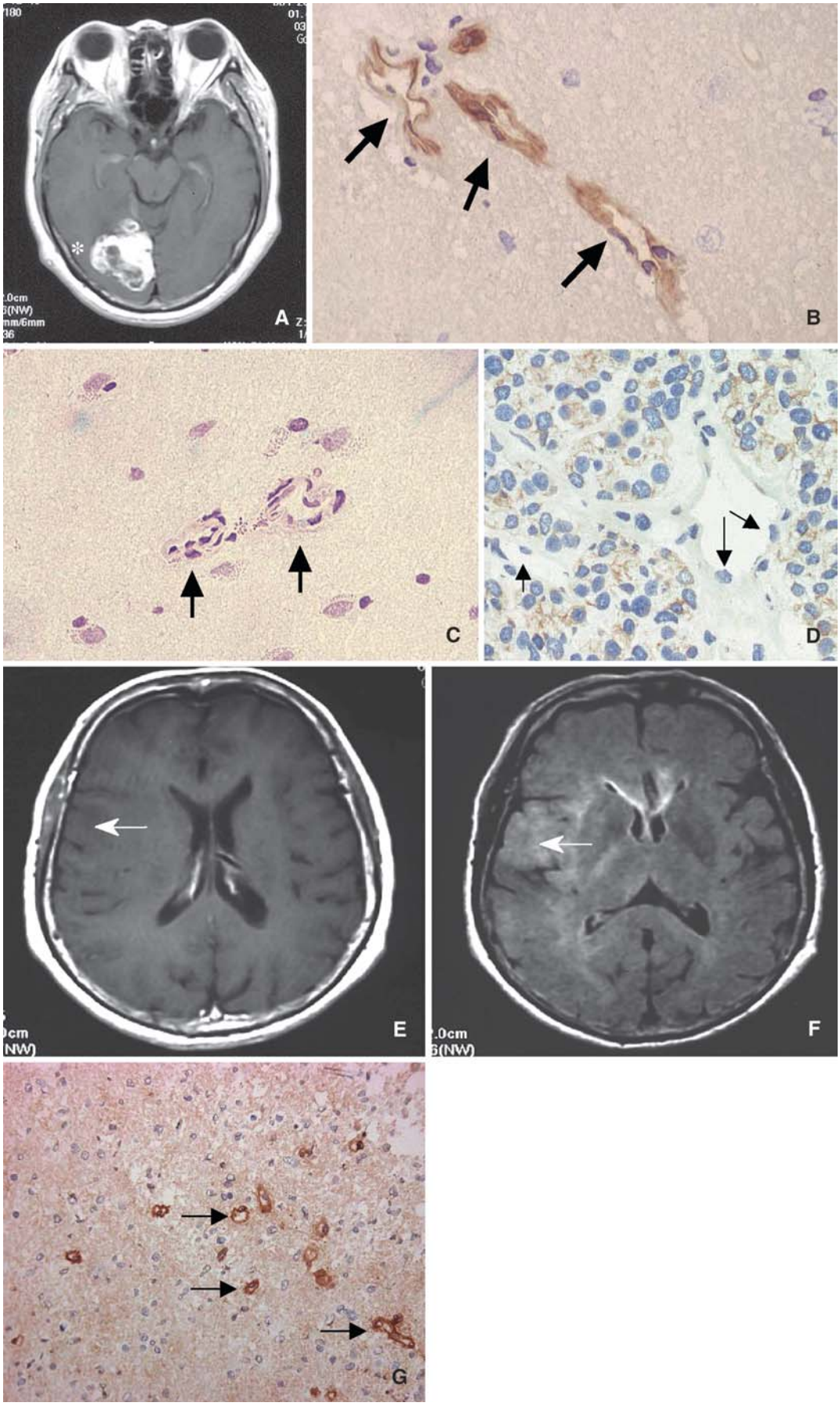

A
B
C
D
E
F
G

**Table 1** Gadolinium diethylenetriaminepentaacetic acid (Gd-DTPA)-enhancement and emmprin expression in vascular endothelial cells. *DA* grade-II diffuse astrocytoma, *AA* anaplastic astrocytoma, *GBM* glioblastoma multiforme

| Tissues[1] | Gd-DTPA enhancement | No. of cases | Scale of emmprin-positive vessels[2] | | | | |
|---|---|---|---|---|---|---|---|
| | | | – | 1+ | 2+ | 3+ | 4+ |
| Non-neoplastic tissue | – | 10 | 0 | 0 | 0 | 0 | 10 |
| DA | – | 7 | 0 | 0 | 0 | 0 | 7 |
| AA | | | | | | | |
| Periphery | – | 4 | 0 | 0 | 0 | 0 | 4 |
| Center | + | 4 | 0 | 1 | 2 | 1 | 0 |
| GBM | | | | | | | |
| Periphery | – | 13 | 0 | 0 | 0 | 0 | 13 |
| Center | + | 13 | 13 | 0 | 0 | 0 | 0 |
| Metastatic carcinoma | + | 7 | 5 | 2 | 0 | 0 | 0 |

[1] Histological diagnosis based on the World Health Organization classification system
[2] Emmprin immunostaining only in vascular endothelial cells is estimated here

contrast, histologically normal brain from several autopsy cases showed positive emmprin staining in vascular endothelial cells [27].

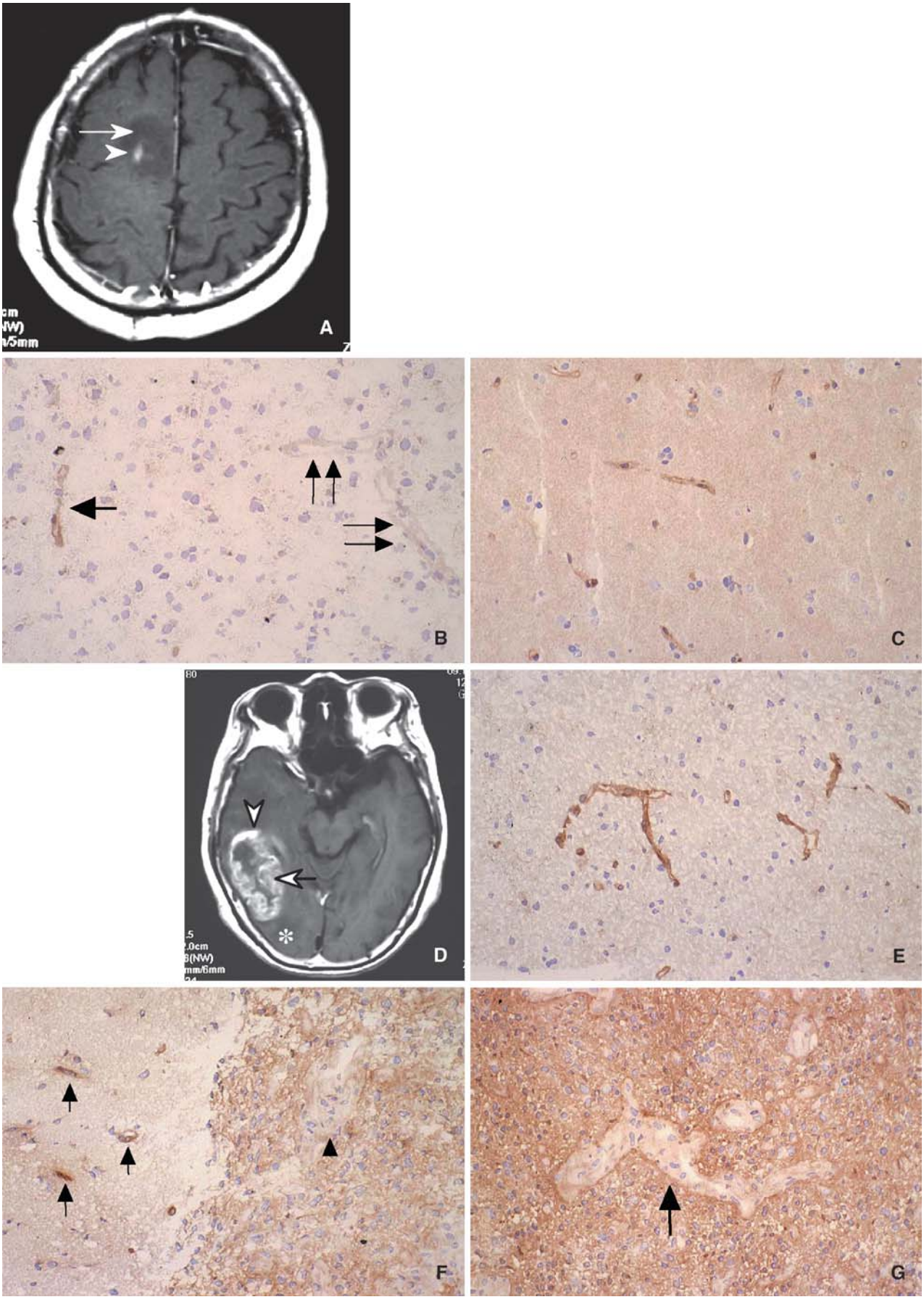
## Discussion

In this work, we have shown a possible correlation between emmprin protein expression and BBB function in the human brain: emmprin was expressed in vascular endothelial cells of the CNS when BBB functioned normally, while it was not when BBB function was impaired. Although the loss of emmprin expression was typically observed in the proliferating blood vessels in the Gd-DTPA-enhanced central portion of GBM, the loss does not seem to be merely the results of cell injuries due to relative hypoxia in the region because the endothelial cells did not show any degenerative changes. The proliferating blood vessels show an abnormal appearance, being surrounded by several layers of endothelial and vascular wall cells. These rapidly proliferating vessels may show altered expression of various antigens. However, normal-appearing blood vessels in the Gd-DTPA-enhanced portion of anaplastic astrocytoma also lost emmprin expression, although the extent of the loss varied case by case. Blood vessels lined by a single layer of endothelium in the Gd-DTPA-enhanced metastatic carcinoma portion also showed a loss of emmprin expression. Moreover, a stereotactic biopsy specimen from the Gd-DTPA-enhanced subcortical lesion in a patient with ADEM, a non-neoplastic, inflammatory disease, also showed a loss of emmprin expression in vascular endothelial cells. Taken together, the loss of emmprin expression does not seem to be merely the result of altered gene expression in proliferating endothelial cells, but may be associated with the BBB dysfunction. However, further studies with more cases, especially non-neoplastic disease cases with BBB dysfunction, are still necessary to confirm our conclusion, and they are now ongoing in our laboratory.

Genetic alterations of the emmprin gene/locus cannot be excluded completely as one of the mechanisms involved in the different distribution pattern of emmprin in the CNS tumors. However, they would be subtle if there are any, because the size of mRNA transcripts was the same as that of the ordinary one [27]. Moreover, we speculate that these genetic alterations are less possible as the primary cause for the loss of emmprin expression in vascular endothelial cells associated with BBB dysfunction, because this loss seems to be secondary due to alterations of endothelial-perivascular microenvironmental interactions caused by neoplastic cell proliferation or inflammation [16, 20].

The immunolocalization and association with BBB function of emmprin in the brain tissue are different between the adult chicken and mouse [1, 15, 28, 31]. HT7/neurothelin, a species homologue of emmprin in the chicken has been demonstrated exclusively in endothelial cells of the CNS but not in neuroglial cells or systemic endothelial cells [28, 31]. Endothelial cells in the circumventricular organs that lack BBB, such as the pituitary, median eminence, subfornical organ, pineal gland and area postrema, are negative for HT7/neurothelin [1]. In comparison, basigin, a species homologue of emmprin in the mouse, is expressed in neurons in addition to some vascular endothelial cells in the brain, and

**Fig. 1** Emmprin immunoreactivity of vascular endothelial cells in non-neoplastic brain tissue, metastatic carcinoma and diffuse astrocytoma. **A** Axial gadolinium diethylenetriaminepentaacetic acid (Gd-DTPA)-enhanced T1-weighted magnetic resonance (MR) image of the brain with metastatic follicular carcinoma from the thyroid gland. Irregular ring-shaped enhancement is seen. **B** The tissue from the non-enhanced portion (*) was subjected to emmprin immunostaining. Vascular endothelial cells (*arrows*) show strong positive staining, while astrocytes stain negatively. **C** Negative control with non-immune mouse IgG, indicating loss of immunostaining of vascular endothelial cells (*arrow*). **D** Metastatic carcinoma cells from the enhanced portion show positive immunostaining for emmprin, whereas intervening vascular endothelial cells are negative (*arrows*). **E**, **F**, **G** A diffuse astrocytoma case of a 72-year-old Japanese female. **E** Axial Gd-DTPA-enhanced T1-weighted MR image. No enhancement of the tumor is seen. **F** FLAIR image. Tumor tissue with high signals are noted in the right fronto-temporal lobe. **G** Vascular endothelial cells are emmprin-positive (*arrows*), while tumor cells are negative. White arrows in (**E**) and (**F**) indicate the portion from which tissues were obtained for immunohistochemistry. **B**, **C**, **D** Original magnification ×132; **G** original magnification ×66


A
B
C
D
E
F
G

functional studies in mice lacking basigin did not reveal changes in BBB function [15]. In this light, we intended to clarify the localization and relationship to BBB function of emmprin in the human brain, especially in vivo with clinical assessment of BBB function using MRI with Gd-DTPA administration. Our observations suggest that the human and chicken share the BBB-specific expression pattern of emmprin (CD147) in the endothelium of the brain. Loss of its expression on systemic endothelial cells outside the CNS is also seen in common in the two species [28].

The way in which emmprin is related to BBB function remains to be investigated. A crucial function of the BBB is to ensure that the microenvironment of neurons is tightly regulated, in order to guarantee unhampered synaptic activity as a means of neuronal conversation [28]. BBB function includes provision of a pure barrier and selective transport of components essential for CNS cell metabolism. The barrier mechanism is mainly based on tight junctions formed between neighboring non-fenestrated endothelial cells. This tight junction-associated BBB function was successfully induced in aortic endothelial cells, which usually do not show such structures or functions, by co-culturing them with astroglial cells [16]. HT7 protein was also induced in vascular endothelial cells of the chick chorioallantoic membrane by incubating with astroglia-conditioned media [20]. The interaction between endothelial cells or between endothelial and astroglial cells via emmprin might be involved in the induction of the tight junctions. This possibility is now under investigation in our laboratory. Furthermore, emmprin may also be associated with selective transport mechanisms in endothelial cells. Rat CD147 expressed in heart cells interacts tightly with lactate transporters, MCT (monocarboxylate transporter)1 and MCT4, and facilitates their cell surface expression and activity [18]. High levels of both MCT1 and CD147 are also found in the rat retinal pigment epithelium, the barrier between the retina, a net producer of lactate, and the choroidal blood supply [8, 10]. In the brain, glucose is usually the major fuel, and the BBB is relatively impermeable to lactate and ketone bodies. However, during conditions such as starvation and diabetes, permeability increases and these monocarboxylates become more important substrates for the provision of energy; MCT1 expressed in the cerebral capillary endothelium is probably responsible for the high rates of lactate and ketone-body transport across the BBB [14].

**Fig. 2** Emmprin immunoreactivity of vascular endothelial cells in anaplastic astrocytoma (**A**, **B**, **C** a case of a 34-year-old Japanese male) and glioblastoma multiforme (GBM; **D**, **E**, **F**, **G** a case of a 74-year-old Japanese female). **A** Axial gadolinium diethylenetriaminepentaacetic acid (Gd-DTPA)-enhanced T1-weighted magnetic resonance (MR) image of anaplastic astrocytoma demonstrating a focal lesion of low signal intensity. Its central portion shows Gd-DTPA-enhancement (*arrowhead*), while the peripheral portion does not (*arrow*). **B** Tissue obtained from the enhanced portion in **A** (indicated by an *arrowhead* in **A**). Some endothelial cells are positive for emmprin (*arrow*), while others are negative (*double arrows*). Tumor cells are negative. **C** Tissue obtained from the non-enhanced portion in **A** (indicated by an arrow in **A**). Vascular endothelial cells are positive for emmprin. **D** Axial Gd-DTPA-enhanced T1-weighted MR image of GBM demonstrating a ring-enhanced mass in the right temporo-occipital lobe. **E** Tissue obtained from the non-enhanced portion in **D** (indicated by an *asterisk* in **D**). Endothelial cells show positive immunoreactivity to emmprin. **F** Tissue obtained from the invasion front (indicated by an *arrowhead* in **D**). Vascular endothelial cells included in the GBM portion (*arrowhead*) are negative for emmprin, while those in the surrounding brain tissue (*arrows*) are positive. **G** Tissue obtained from the enhanced portion in **D** (indicated by an *arrow* in **D**). Proliferating blood vessels (*arrow*) are negative for emmprin, and are surrounded by tumor cells that are emmprin-positive. **B**, **C**, **E**, **F**, **G** original magnification ×66

**Acknowledgements** The authors thank Dr. Y. Nawa, Department of Parasitology, Miyazaki Medical College, for his kind suggestions and discussion, Mr. S. Sato and Ms. K. Narimatsu for their skillful help in immunohistochemistry, and Mr. T. Miyamoto for his help in processing the figures and manuscript. This work was supported in part by a Grant-in-Aid for Encouragement of Young Scientists from the Ministry of Education, Science and Culture of Japan (no. 12770757 to T.S.) and grants from the U.S. Army (DAMD 17-95-1-5017 and 17-99-9413 to B.P.T.).

## References

1. Albrecht U, Seulberger H, Schwarz H, Risau W (1990) Correlation of blood-brain barrier function and HT7 protein distribution in chick brain circumventricular organs. Brain Res 535:49–61
2. Biswas C (1982) Tumor cell stimulation of collagenase production by fibroblasts. Biochem Biophys Res Commun 109:1026–1034
3. Biswas C, Zhang Y, DeCastro R, Guo H, Nakamura T, Kataoka H, Nabeshima K (1995) The human tumor cell-derived collagenase stimulatory factor (renamed EMMPRIN) is a member of the immunoglobulin superfamily. Cancer Res 55:434–439
4. Brant-Zawadzki M, Berry I, Osaki L, Brasch R, Murovic J, Norman D (1986) Gd-DTPA in clinical MR of the brain. I. Intraaxial lesions. Am J Radiol 147:1223–1230
5. Ehrlich P (1885) Das Sauerstoff-Bedurfniss des Organisumus, in Eine Farbenanalytische Studie. Berlin, August Hirschwald, pp 1–67
6. Ellis SM, Nabeshima K, Biswas C (1989) Monoclonal antibody preparation and purification of a tumor cell collagenase-stimulatory factor. Cancer Res 49:3385–3391
7. Fadool JM, Linser PJ (1993) 5A11 antigen is a cell recognition molecule which is involved in neuronal-glial interactions in avian neural retina. Dev Dyn 196:252–262
8. Finnemann SC, Marmorstein AD, Neill JM, Rodriguez-Boulan E (1997) Identification of the retinal pigment epithelium protein RET-PE2 as CE-9/OX-47, a member of the immunoglobulin superfamily. Invest Ophthalmol Vis Sci 38:2366–2374
9. Fossum S, Mallett S, Barclay AN (1991) The MRC OX-47 antigen is a member of the immunoglobulin superfamily with an unusual transmembrane sequence. Eur J Immunol 21:671–679
10. Gerhart DZ, Leino RL, Drewes LR (1999) Distribution of monocarboxylate transporter MCT1 and MCT2 in rat retina. Neuroscience 92:367–375
11. Goldmann EE (1913) Vitalfärbung am Zentralnervensystem. Beitrag zur Physio-Pathologie des Plexus choroideus und der Hirnhäute. Abh. Königl. Preuss Akad. Wiss. Phys-Math. Kl. 1:1–60
12. Goldstein W, Betz AL (1986) The blood-brain barrier. Sci Am 34:70–79

13. Guo H, Zucker S, Gordon MK, Toole BP, Biswas C (1997) Stimulation of matrix metalloproteinase production by recombinant extracellular matrix metalloproteinase inducer from transfected chinese hamster ovary cells. J Biol Chem 272:24–27
14. Halestrap AP, Price NT (1999) The proton-linked monocarboxylate transporter (MCT) family: structure, function and regulation. Biochem J 343:281–299
15. Igakura T, Kadomatsu K, Taguchi O, Muramatsu H, Kaname T, Miyauchi T, Yamamura K, Arimura K, Muramatsu T (1996) Roles of basigin, a member of the immunoglobulin superfamily, in behavior as to an irritating odor, lymphocyte response, and blood-brain barrier. Biochem Biophys Res Commun 224:33–36
16. Isobe I, Watanabe T, Yotsuyanagi T, Hazemoto N, Yamagata K, Ueki T, Nakanishi K, Asai K, Kato T (1996) Astrocytic contributions to blood-brain barrier (BBB) formation by endothelial cells: a possible use of aortic endothelial cell for in vitro BBB model. Neurochem Int 28:523–533
17. Kasinrerk W, Fiebiger E, Stefanova I, Baumruker T, Knapp W, Stockinger H (1992) Human leukocyte activation antigen M6, a member of the Ig superfamily, is the species homologue of rat OX-47, mouse basigin, and chicken HT7 molecule. J Immunol 149:847–854
18. Kirk P, Wilson MC, Heddle C, Brown MH, Barclay AN, Halestrap, AP (2000) CD147 is tightly associated with lactate transporters MCT1 and MCT4 and facilitates their cell surface expression. EMBO J 19:3896–3904
19. Kleihues P, Cavenee WK (2000) Pathology and genetics of tumours of the nervous system. In: World Health Organization Classification of Tumours, IARC press, Lyon, pp 10–39
20. Lobinus JA, Juillerat-Jeanneret L, Darekar P, Schlosshauer B, Janzer RC (1992) Induction of the blood-brain barrier specific HT7 and neurothelin epitopes in endothelial cells of the chick chorioallantoic vessels by a soluble factor derived from astrocytes. Dev Brain Res 70:207–211
21. Miyauchi T, Masuzawa Y, Muramatsu T (1991) The basigin group of the immunoglobulin superfamily: complete conservation of a segment in and around transmembrane domains of human and mouse basigin and chicken HT7 antigen. J Biochem 110:770–774
22. Muraoka K, Nabeshima K, Murayama T, Biswas C, Koono M (1993) Enhanced expression of a tumor-cell-derived collagenase-stimulatory factor in urothelial carcinoma: its usefulness as a tumor marker for bladder cancers. Int J Cancer 55:19–26
23. Nabeshima K, Shimao Y, Sato S, Kataoka H, Moriyama T, Kawano H, Wakisaka S, Koono M (1997) Expression of c-Met correlates with grade of malignancy in human astrocytic tumours: an immunohistochemical study. Histopathology 31:436–443
24. Pardridge WM (1998) Recent advances in blood-brain barrier transport. Ann Rev Pharmacol Toxicol 28:25–39
25. Polette M, Gilles C, Marchand V, Lorenzatio M, Toole BP, Tournier JM, Zucker S, Birembaut P (1997) Tumor collagenase stimulatory factor (TCSF) expression and localization in human lung and breast cancers. J Histochem Cytochem 45:703–709
26. Sameshima T, Nabeshima K, Toole BP, Yokogami K, Okada Y, Goya T, Koono M, Wakisaka S (2000) Glioma cell extracellular matrix metalloproteinase inducer (EMMPRIN) (CD147) stimulates production of membrane-type matrix metalloproteinases and activated gelatinase A in co-cultures with brain-derived fibroblasts. Cancer Lett 157:177–184
27. Sameshima T, Nabeshima K, Toole BP, Yokogami K, Okada Y, Goya T, Koono M, Wakisaka S (2000) Expression of EMMPRIN (CD147), a cell surface inducer of matrix metalloproteinases, in normal human brain and gliomas. Int J Cancer 88:21–27
28. Schlosshauer B, Herzog, KH (1990) Neurothelin: an inducible cell surface glycoprotein of blood–brain barrier-specific endothelial cells and distinct neurons. J Cell Biol 110:1261–1274
29. Schmiedle UP, Kenney J, Maravilla KR (1992) Kinetics of pathologic blood–brain-barrier permeability in an astrocytic glioma using contrast-enhanced MR. Am J Neuroradiol 13:5–14
30. Schoner W, Laniado M, Niendorf HP, Schubert C, Felix R (1986) Time-dependent changes in image contrast in brain tumors after gadolinium-DTPA. Am J Neuroradiol 7:1013–1020
31. Seulberger H, Lottspeich F, Risau W (1990) The inducible blood-brain barrier specific molecule HT7 is a novel immunoglobulin-like cell surface glycoprotein. EMBO J 9:2151–2158

Virchows Arch (2003) 442:585–590
DOI 10.1007/s00428-003-0800-8

ORIGINAL ARTICLE

**Britta Kleist · Micaela Poetsch · Christel Breitsprecher · Godela Düsterbehn · Karl Donath · Gerd Lorenz**

# Epithelial–myoepithelial carcinoma of the parotid gland—evidence of contrasting DNA patterns in two different histological parts

Received: 22 November 2002 / Accepted: 4 March 2003 / Published online: 25 April 2003
© Springer-Verlag 2003

**Abstract** Epithelial–myoepithelial carcinoma (EMC) is a rare neoplasm arising predominantly in the salivary glands, in particular in the parotid gland. We report the morphological features of an epithelial–myoepithelial carcinoma of the parotid gland with one lymph-node metastasis including a molecular genetic study of this tumor. Immunohistochemical and ultrastructural results confirmed the epithelial–myoepithelial dualism of the carcinoma. The loss of heterozygosity (LOH) analysis revealed different LOH results for the solid and the tubular growth pattern of the primary tumor, but showed identical findings for the solid primary tumor component and the lymph node metastasis which had also a solid appearance. LOH could be demonstrated in the whole primary tumor at D13S217 (13q12) and D18S58 (18q21). In three other microsatellite loci [D9S162 (9p22-p21), D10S251 and D10S541 (surrounding the *PTEN/MMAC1* gene on 10q23-q24)], clearly recognizable LOH was found in the solid part and in the metastasis, whereas the tubular component demonstrated only a slight decrease of the same allele. No mutation or methylation of the *p16* gene or alteration of the *PTEN/MMAC1* gene could be found. Nevertheless, our results provoke a discussion, whether these genetic alterations could be considered as determinants of histologically and prognostically divergent types in EMC.

**Keywords** Epithelial–myoepithelial carcinoma · LOH pattern · Parotid gland

B. Kleist (✉) · G. Lorenz
Institute of Pathology, Ernst-Moritz-Arndt-University,
F.-Loeffler-Strasse 23e, 17489 Greifswald, Germany
e-mail: kleist@uni-greifswald.de
Tel.: +49-3834-865718
Fax: +49-3834-865704

M. Poetsch
Institute of Forensic Medicine, Ernst-Moritz-Arndt-University,
Greifswald, Germany

C. Breitsprecher
Department of Oto-Rhino-Laryngology,
Ernst-Moritz-Arndt-University, Greifswald, Germany

G. Düsterbehn
Department of Radiology Greifswald, Germany

K. Donath
Department of Oral Pathology, Rödinghausen, Germany

## Introduction

Epithelial–myoepithelial carcinoma (EMC) is a rare epithelial neoplasm, comprising approximately 1% of all salivary gland tumors [4]. The tumor was first introduced by Donath et al. [3] and is defined as an uncommon epithelial neoplasm composed of variable proportions of ductal and large and clear-staining, myoepithelial differentiated cells. The ratio of clear cells to ductal cells is highly variable, even within the same tumor, and ductal cells have in fact been reported to be nearly absent [4]. This represents a diagnostic challenge and also harbors clinical significance. In particular, previous studies directed their attention to the solid variant of EMC, because it is found to be associated with a more aggressive behavior compared with the other histological types (tubular, papillary, cribriform) [5, 16].

We encountered a case of EMC composed of a well-differentiated tubular pattern and a solid component that showed in comparison more atypia and increased mitotic figures. The varying histological features within this tumor and the additional occurrence of a periparotid lymph node metastasis attracted us beside immunohistochemical and ultrastructural investigations also to search for the genetic background of this certain phenotype of EMC.

## Clinical history

A 78-year-old female presented with a slow-growing left facial tumor having caused facial paralysis for 3 years and local pain for about 2 weeks. Magnetic resonance imaging

documented a circumscribed left parotid gland tumor that measured 8×7×6 cm, grew toward the cervical spine and around the jaw bone. Because of tumor extension and the conjecture of malignancy, a parotidectomy of the left side was performed. Since surgery, the patient has been free of disease until now (22 months).

## Materials and methods

### Histological, immunohistochemical and ultrastructural examination

For light microscopy examination, the tissue was fixed in 4.5% phosphate-buffered formalin (pH 7), routinely processed and embedded in paraffin wax using standard methods. Four-micrometer sections were stained with hematoxylin and eosin and periodic acid-Schiff (PAS). The specimens underwent additional independent histopathologic review (K.D.). Immunohistochemical reactions were carried out on formalin-fixed, paraffin-embedded tissue using the streptavidin-biotin-peroxidase method (Dako LSAB$^{(R)}$2 system) with 3,3′-diaminobenzidine (DAB) as chromogen. The antibodies used included pan-cytokeratin (MNF116), cytokeratins 7, 8, 18, 19, 20, SMA, vimentin, S-100 protein, Ki-67 antigen, and PCNA (all from Dako, Glostrup, Denmark). In addition, a sequential immunohistochemical co-staining with EnVision techniques and DAB and Fast-Red as chromogens was used for pan-cytokeratin and SMA as well as S-100 protein. The clones and dilution are available from the authors on request.

The material for ultrastructural examination was initially formalin fixed. The tissue was processed as described previously [8] and examined in an EM 910 LEO electron microscope (LEO, Oberkochem, Germany).

### DNA isolation

First, hematoxylin and eosin stained slides were carefully inspected under the light microscope to identify areas that carry a sufficient amount (at least 3 $mm^2$) of solid and tubular tumor tissue measured by a scaled optical adjustment. This same area was then identified on the unstained 10-$\mu$m dewaxed, rehydrated and air-dried tissue section, which was fixed in an optical installation allowing the separate isolation of solid and tubular tissue (but not the separation of the myoepithelial and ductal cells of the tubular tissue), predominantly without adherent non-neoplastic structures under microscopic control with a cannula (used for intravenous injections). The DNA isolation of this tissue was performed with the High Pure PCR Template Preparation Kit (Roche Molecular Biochemicals, Mannheim, Germany) according to the manufacturer's instructions with proteinase K digestion overnight.

### Loss of heterozygosity analysis

A panel of 12 fluorochrome (6-FAM, HEX, or TAMRA) labeled polymerase chain reaction (PCR) primer pairs that amplified informative dinucleotide repeat microsatellite loci located on chromosomes 9p22-p21 (D9S162, D9S171), 9q21 (D9S197), 10q23-q24 (D10S185, D10S215, D10S541), 11q25 (D11S910), 13q12-q14 (D13S217, D13S263), 17 (D17S513, D17S786), and 18 (D18S58) were obtained from Genome Data Base (http://gdb-www.gdb.org). The PCR was performed in four multiplex analyses each comprising three different labeled primers in a final volume of 12.5 $\mu$l containing 50–80 ng DNA, 0.3 $\mu$M of each primer, 200 $\mu$M of each dNTP, 1.5 $\mu$M $MgCl_2$, 15 mM Tris/HCl, 50 mM KCl, and 1 U Ampli*Taq* Gold (Applied Biosystems, Weiterstadt, Germany) by denaturing at 95°C for 10 min, followed by 35 cycles of 95°C for 30 s, 55°C for 90 s, 72°C for 120 s, and additional 10 min at 72°C with the Trio Thermocycler (Biometra, Göttingen, Germany). PCR product (1.5 $\mu$l) was mixed with 12 $\mu$l deionized formamide and 0.5 $\mu$l ROX-labeled internal lane standard, denatured at 90°C for 120 s, snap-cooled on ice and electrophoresed with the ABI 310 DNA sequencer (Applied Biosystems). Loss of heterozygosity (LOH) was determined as described by Canzian et al. [2].

### Mutation screening of PTEN/MMAC1 and p16

Mutation analysis of the *PTEN/MMAC1* gene was carried out as described by Steck et al. [14] with slight modifications. We used the FA/RP primers designed by Steck et al. [14] for the exons 1–4 and 6–9, thus allowing the investigation of a greater part of the introns. The DNA of exon 5 was amplified with a shorter version of the FB/RQ primers from Steck et al. [14] (F: 5′CATTTCTAAAGTTACCTA; R: 5′CCATCTGTTTTCCAATAA), since here the FA/RP primer product could not be amplified in DNA from paraffin-embedded tissue due to the shortness of this DNA. Mutation analysis of the *p16* gene was performed as described by Gemma et al. [6] with slight modifications. For exon 1, the published primer pair was used, but exon 2 has to be subdivided into two parts due to the investigation of paraffin-embedded material. It was amplified with the following primer pairs: (2–1) F: 5′TTAGACACCTGGGGCTTGTGTG; R: 5′CCCCGGCCCGGTGCAGCACC (2–2) F: 5′GGCTTCCTGGACACGCTGGT; R: 5′TGGAAGCTCTCAGGGTACAAATTC. The following PCR conditions were used: 50–80 ng template DNA were amplified in a 25-$\mu$l reaction volume containing 200 $\mu$M dNTPs, 1.5 $\mu$M $MgCl_2$, 15 mM Tris/HCl, 50 mM KCl, 0.3 nM primers, and 1 U Ampli*Taq* Gold (Applied Biosystems) by denaturing at 95°C for 10 min, followed by 30 cycles of 95°C for 30 s, 55°C (*PTEN/MMAC1*) or 58°C (*p16*) for 90 s, 72°C for 120 s, and an additional 10 min at 72°C with the Trio Thermocycler (Biometra). For the sequencing PCR, the BigDye Ready Reaction Kit (Applied Biosystems) was used with the same primers as above, according to the manufacturer's instructions with the following PCR conditions: 25 cycles of 95°C for 30 s, 50°C for 5 s, and 60°C for 4 min. The PCR products were sequenced with the ABI 310 DNA sequencer (Applied Biosystems). Sequencing was always carried out in both directions. Each polymorphism or mutation was verified by a second sequencing reaction of an independent amplification product.

### Methylation analysis of p16

The methylation analysis of the *p16* gene was done as described by Herman et al. [7]. Briefly, after a bisulfite modification, a PCR reaction was performed with specific primers for methylated and unmethylated samples. The PCR products were directly loaded onto nondenaturing 6.8% polyacrylamide gels and visualized by a silver staining procedure.

## Results

### Pathological findings

Grossly, the tumor was encapsulated with a small rim of adipose tissue, measured 8×7×6 cm and weighed 180 g. The cut surface was solid, yellowish-gray and had foci of hemorrhage and necrosis. Two lymph nodes measuring 0.5 cm and 0.7 cm were localized in the periparotid adipose tissue.

Microscopically, the tumor showed a multinodular growth pattern with two distinct architectural types: tubular and solid (Fig. 1A). The predominating tubular component was composed of small double-lined ducts, which contained always ductal and myoepithelial cells,

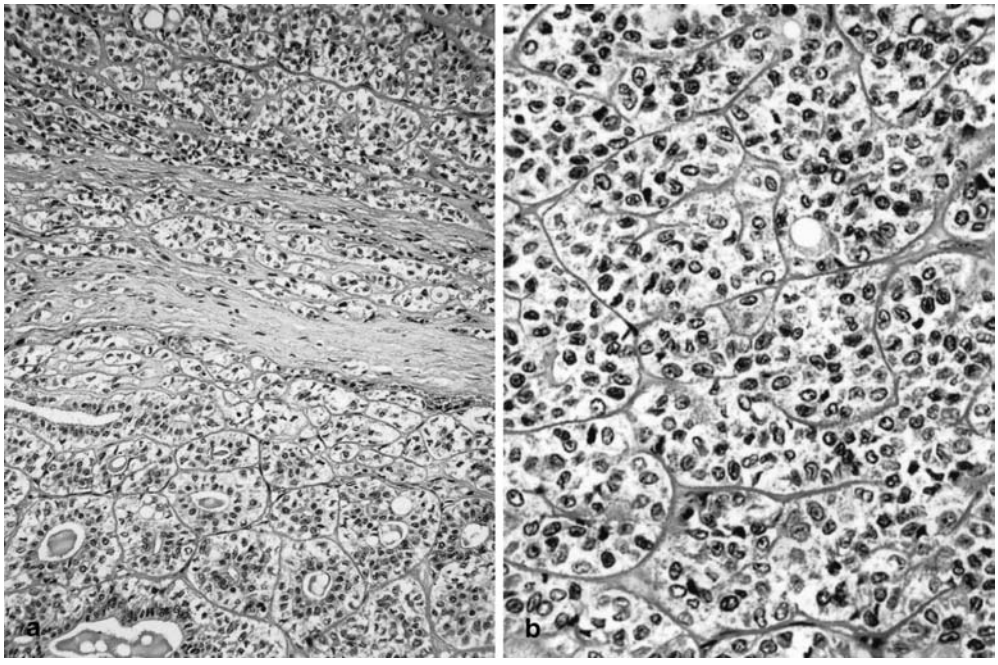



**Fig. 1** Epithelial–myoepithelial carcinoma. **A** A solid tumor component (*above*) composed of sheets of clear cells in the vicinity of a tubular area (*below*) with small ducts lined by dark cuboidal epithelium and surrounded by clear cells. Both patterns were partially separated by fibroconnective tissue. **B** At higher magnification, the clear cells in the solid pattern present more irregular-shaped and -sized nuclei and scattered mitotic figures. Hematoxylin and eosin, **A** ×100, **B** ×300

according to the definition in the literature [4]. The inner layer was made up of cuboidal cells with eosinophilic cytoplasm and round nuclei that presented prominent nucleoli and occupied most of the cytoplasmic compartments. These tumor cells were surrounded by larger cells with clear cytoplasm that presented in the PAS stain glycogen. Nuclear atypia was mild; mitotic figures were rare. In the lumen formed by the inner layer of cells, there was often PAS-positive material. Single ducts were surrounded by a thick hyalinized basement membrane. The solid areas, comprising a minor proportion of the tumor, presented with a predominant clear cell pattern. In this tumor part (Fig. 1B), including additional small foci of ductal differentiation, nuclear atypia was moderate and occurred as well as mitotic figures (2 per HPF) more frequently than in the tubular component. Necrosis and hemorrhage were seen in 10%, predominantly in the solid areas. Focally, solid tumor nests spread beyond the capsule into periparotid fat and had invaded small blood vessels. One of the two lymph nodes prepared in the periparotid adipose tissue showed a metastasis with solid growth pattern.

By immunohistochemistry, the cells of the tubular inner layer were strongly positive to pan-cytokeratin MNF116 (Fig. 2A, B) and to cytokeratins 7, 8, and 18, weakly positive to cytokeratins 19 and 20, focally and sporadically positive to S-100 protein (Fig. 2B). SMA and vimentin proved to be negative. The clear cells in the tubular external layer were strongly positive to SMA (Fig. 2A) and S-100 protein (Fig. 2B), whereas the clear tumor cells in the solid pattern showed focal and sporadic positivity to these two markers. Clear cells of both patterns were found to be negative to pan-cytokeratin and vimentin. Positivity to MIB-1 and PCNA was always strictly nuclear and involved mainly the myoepithelial cells (external tubular layer: 20% and 25%, respectively; solid part: 30% and 35%, respectively), while the epithelial cells (inner tubular layer: 6% and 3%, respectively) hardly ever gave positive results.

Both primary tumor patterns underwent separate ultrastructural examination (results not shown). The cuboidal cells bordering the lumen showed focally atypical microvilli. The round nuclei had evenly dispersed chromatin and nucleoli. Varying quantities of rough endoplasmic reticulum were evident. The cells in the external layer had more flattened nuclei. Densely packed microfilaments could be seen. Pinocytosis vesicles were common. The cells in the solid part presented with round as well as with flattened nuclei and microfilaments.

## Molecular genetic analysis

Of the 12 loci investigated for this tumor, 9 were informative (D9S162, D10S185, D10S215, D10S541, D11S910, D17S513, D18S58, D13S217, and D13S263), whereas the 2 other loci on chromosome 9, and 1 other locus on chromosome 17 were not informative. LOH was found at D13S217 (13q12) and D18S58 (18q21) in all samples of the primary tumor and in the lymph node metastasis (Fig. 3A). In addition, at D9S162 (9p22-p21), D10S251 and D10S541 (10q23-q24), clearly recognizable LOH (an allele decrease of more than 40%) could be demonstrated only in the solid part of the primary tumor and in the lymph node metastasis. At D9S162 and D10S251, the reduction of one allele in the tubular part was only 30–35%, at D10S541 only 20% (Fig. 3B).

All nine exons of the *MMAC1PTEN* gene and both exons of the *p16* gene could be amplified from tumor DNA, but we could not detect any mutations or

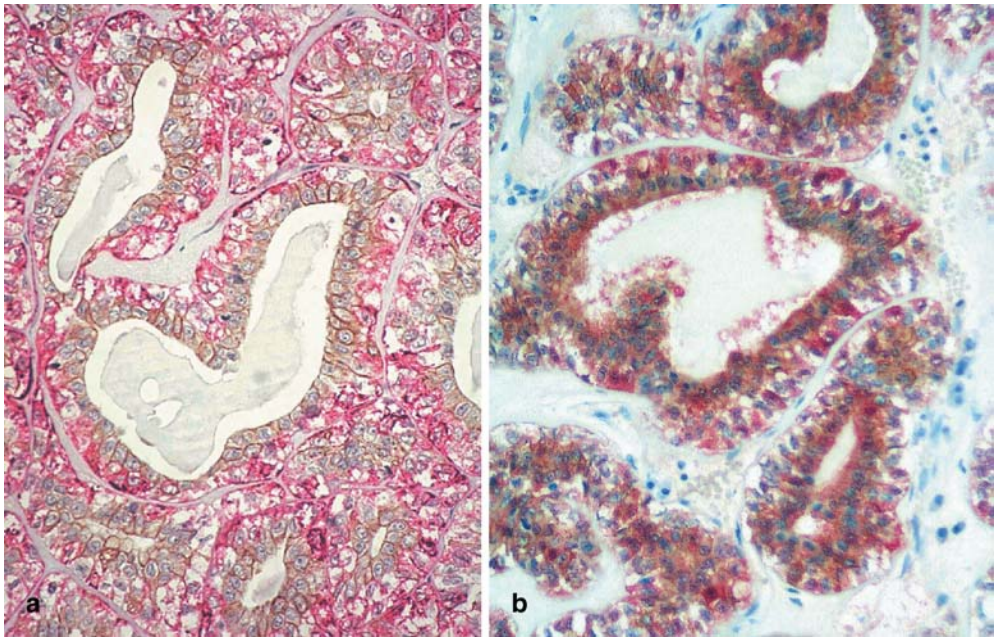



**Fig. 2** Higher magnification of the tubular pattern. Immunoreactivity for MNF116 is exclusively seen in the ductal cells of the inner layer (**A** and **B**, *brown*); immunoreactivity for SMA is exclusively found in the myoepithelial cells of the external layer (**A**, *red*). Immunoreactivity for S-100 protein is displayed in myoepithelial cells and in a few ductal cells as well (**B**, *red*). **A**, **B** ×250

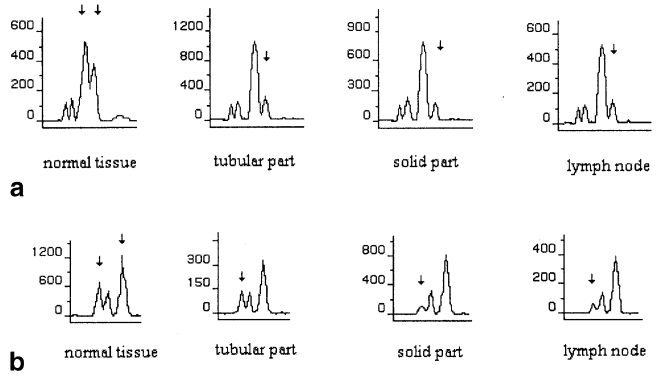



**Fig. 3** Electropherograms of two investigated loci with the Y axis representing the peak height in fluorescence units. The *arrows* mark the lost or decreased allele. **A** Loss of heterozygosity in both parts of the primary tumor and the lymph node metastasis at D18S58. **B** Different amounts of allelic loss in the tubular and the solid part, but nearly identical patterns in the solid component and the lymph node metastasis at D9S162

polymorphism in the exons or the sequenced part of the introns. In addition, we were not able to demonstrate a methylation of the promotor of *p16*.

## Discussion

In the past, detailed studies could define certain immunohistochemical [1, 17] and ultrastructural [10] characteristics of epithelial–myoepithelial carcinoma. Here, we used these well-established techniques to confirm the diagnosis of the present case. EMC has also been investigated by molecular genetic methods [1, 11], but the published data do mainly not reflect the specific biphasic cellular arrangement or different growth patterns of EMC. However, a diagnostic approach to the variable appearances of EMC could be prognostically important, since tumors predominantly composed of clear cells in a solid arrangement are considered to be associated with a more aggressive behavior [5, 16].

This could probably be due to the higher proliferative activity of the solid type than other growth patterns. Our evaluation of the proliferative index measured by MIB-1 and PCNA staining revealed not only more proliferating cells in the solid part compared with the tubular area, but also a clearly higher proliferation activity of the myoepithelial cells compared with the ductal cells. In accordance with other investigations, this result characterizes the myoepithelial cells as the cell population predominantly responsible for the growth of EMC [16]. Probably, for this reason, solid EMCs with prevalence of myoepithelial cells can show accelerated growth and huge size, thus simulating a dedifferentiating or higher malignant other tumor as in our case.

The idea of two cell populations or several growth patterns with different biological behaviors within the same tumor attracted us to perform separate LOH analyses for both architectural types of the primary tumor and the lymph node metastasis. We chose microsatellite markers from chromosomes 9, 10, 11, 13, 17, and 18, because these chromosomal regions and/or corresponding genes (*p16*, *PTEN/MMAC1*, *Rb*, *p53*, *DCC*) displayed alterations in many different tumor types and are therefore likely candidates for genes affecting the tumorigenesis of EMC as well. The results underlined the differences between the two growth patterns revealing additional LOH in the solid component at 9p22 and 10q23–24, and determined the lymph node metastasis to be derived from the solid part of the primary tumor, since it carried exactly the same LOH pattern. These findings point to interesting biological differences within EMC

and could be explained by one of the following two hypotheses. First, the epithelial and myoepithelial cells of the tubular type could harbor the same DNA pattern, which accumulates genetic aberrations during development into the more aggressive solid histological type. Second, the tubular part could be composed of two not only histologically, but also genetically different cell populations with myoepithelial cells being the more genetically unstable and more biologically aggressive cell population thus being responsible for tumor extension and forming metastasis, as in our case. The small decrease of one allele in the tubular component at the loci with clearly recognizable LOH in the solid component (Fig. 3B) can be explained by this hypothesis and could be attributed to a probably diagnostically relevant amount of myoepithelial cells in the tubular component. In addition, the abovementioned clearly higher proliferative activity of the myoepithelial cells compared with the epithelial cells—even in the tubular component—could support this theory. Both hypotheses would be compatible with the occurrence of a tumor component histologically presenting—in comparison with other areas—a higher grade of malignancy with more unfavorable clinical effects as in our case. However, only a separate molecular genetic analysis of epithelial and myoepithelial cells by microdissection techniques would be able to prove definitely the coexistence of two genetically different cell populations in EMC. Further investigations in this field could be worthwhile, because genetic alterations as determinants of histologic subtypes have already been demonstrated in other tumors [9, 13], but, to the best of our knowledge, have not been considered for EMC so far.

Loss of chromosome 10 has already been demonstrated in EMC of the salivary gland [11]. In addition, alterations in the region of the *p16* cell cycle control gene have been described in carcinomas of the parotid gland: LOH at 9p22 and a mutation in the *p16* gene in a primary large-cell neuroendocrine carcinoma of the parotid gland [12] and the complete deletion of the *p16* gene in a carcinoma arising in a pleomorphic adenoma of the parotid gland [15]. These results and our LOH findings prompted us to the sequencing analysis of the *PTEN/MMAC1* gene at 10q23.3 and the *p16* gene and to the investigation of the methylation status of *p16*. Surprisingly, we did not find any mutations in the two genes nor a promotor methylation of *p16* which suggests an involvement of other tumor suppressor genes on chromosomes 9 and 10 in the tumorigenesis or progression of our case.

Regardless of whether the first or second above-named theory for the histogenesis of EMC is true, the LOH patterns found here seem to determine at least two different histological types of EMC with the solid tumor component (compared with the tubular part) being mainly characterized by a higher number of allelic loss, which has been shown to be associated with a worse prognosis in other tumors [18]. Of course, a single case report does not allow generalizing conclusions. Therefore, a greater study with more cases of EMC also distinguishing between the different histological features may reveal a more distinct and prognostic relevant pattern of chromosomal alterations possibly assigning molecular genetic investigations an increasing diagnostic importance.

## References


1. Alos L, Carrillo R, Ramos J, Baez JM, Mallofre C, Fernandez PL, Cardesa A (1999) High-grade carcinoma component in epithelial-myoepithelial carcinoma of salivary glands: clinicopathological, immunohistochemical and flow-cytometric study of three cases. Virchows Arch 434:291–299
2. Canzian F, Salovaara R, Hemminkki A, Kristo P, Chadwick RB, Aaltonen LA, de la Chapelle A (1996) Semiautomated assessment of loss of heterozygosity and replication error in tumors. Cancer Res 56:3331–3337
3. Donath K, Seifert G, Schmitz R (1972) Zur Diagnose und Ultrastruktur des tubulären Speichelgangskarzinoms. Epithelial-myoepitheliales Schaltstückkarzinom. Virchows Arch 356:16–31
4. Ellis GL, Auclair PL (1996) Tumors of the salivary glands. Atlas of tumors pathology, 3rd series, Fascicle 17. Armed Forced Institute of Pathology, Washington, DC, pp 268–281
5. Fonseca I, Soares J (1993) Proliferating cell nuclear antigen immunohistochemistry in epithelial-myoepithelial carcinoma of the salivary glands. Arch Pathol Lab Med 117:993–995
6. Gemma A, Takenoshita S, Hagiwara K, Okamoto A, Spillare EA, McMemamin MG, Hussain SP, Forrester K, Zariwala M, Xiong Y, Harris CC (1996) Molecular analysis of the cyclin-dependent kinase inhibitor genes $p15^{INK4b/MTS2}$, $p16^{INK4/MTS1}$, *p18* and *p19* in human cancer cell lines. Int J Cancer 68:605–611
7. Herman JG, Graff JR, Myöhänen S, Nelkin BD, Baylin SB (1996) Methylation-specific PCR: a novel PCR assay for methylation status of CpG islands. Proc Natl Acad Sci U S A 93:9821–9826
8. Kleist B, Poetsch M, Lang C, Bankau A, Lorenz G, Süess-Fridrich K, Jundt G, Wolf E (2002) Clear cell chondrosarcoma of the larynx. A case report of a rare histologic variant in an uncommon localization. Am J Surg Pathol 26:386–392
9. Ladanyi M, Antonescu CR, Leung DH, Woodruff JM, Kawai A, Healey JH, Brennan MF, Bridge JA, Neff JR, Barr FG, Goldsmith JD, Brooks JS, Goldblum JR, Ali SZ, Shipley J, Cooper CS, Fisher C, Skytting B, Larsson O (2002) Impact of SYT-SSX fusion type on the clinical behavior of synovial sarcoma: a multi-institutional retrospective study of 243 patients. Cancer Res 62:135–140
10. Luna MA, Ordonez NG, Mackay B, Batsakis JG, Guillamondegui O (1985) Salivary epithelial myoepithelial carcinomas of intercalated ducts: a clinical, electron microscopic, and immunocytochemical study. Oral Surg Oral Med Oral Pathol 59:482–490
11. Martins C, Fonseca I, Roque L, Pinto AE, Soares J (1996) Malignant salivary gland neoplasms: a cytogenetic study of 19 cases. Eur J Cancer B Oral Oncol 32:128–132
12. Nagao T, Sugano I, Ishida Y, Tajima Y, Munakata S, Asoh A, Yamazaki K, Muto H, Konno A, Kondo Y, Nagao K (2000) Primary large-cell neuroendocrine carcinoma of the parotid gland: immunohistochemical and molecular analysis of two cases. Mod Pathol 13:554–561
13. Saito T, Oda Y, Sugimachi K, Kawaguchi K, Tamiya S, Tanaka K, Matsuda S, Sakamoto A, Iwamoto Y, Tsuneyoshi M (2001) E-cadherin gene mutations frequently occur in synovial sarcoma as a determinant of histological features. Am J Pathol 159:2117–2124
14. Steck PA, Pershouse MA, Jasser SA, Yung WKA, Lin H, Ligon AH, Langford LA, Baumgard ML, Hattier T, Davis T, Frye C, Hu R, Swedlund B, Teng DHF, Tavtigian SV (1997) Identification of a candidate tumor suppressor gene, *MMAC1*, at

chromosome 10q23.3 that is mutated in multiple advanced cancers. Nat Genet 15:356–362
15. Suzuki H, Fujioka Y (1998) Deletion of the *p16* gene and microsatellite instability in carcinoma arising in pleomorphic adenoma of the parotid gland. Diagn Mol Pathol 7:224–231
16. Tralongo V, Daniele E (1998) Epithelial-myoepithelial carcinoma of the salivary glands: a review of the literature. Anticancer Res 18:603–608
17. Tralongo V, Rodolico V, Nagar C, Mancuso A, Salvato M, Daniele E (1997) Epithelial-myoepithelial carcinoma of the salivary glands: a clinico-pathologic, immunohistochemical and DNA flow cytometric study of three cases. Anticancer Res 17:761–768
18. Vogelstein B, Fearon ER, Kern SE, Hamilton SR, Preisinger AC, Nakamura Y, White R (1989) Allelotype of colorectal carcinomas. Science 244:207–211

Virchows Arch (2003) 442:591–596
DOI 10.1007/s00428-003-0795-1

ORIGINAL ARTICLE

K. C. Lo · J. F. Geddes · R. S. Daniels · J. S. Oxford

# Lack of detection of influenza genes in archived formalin-fixed, paraffin wax-embedded brain samples of encephalitis lethargica patients from 1916 to 1920.

Received: 29 October 2002 / Accepted: 3 February 2003 / Published online: 15 April 2003
© Springer-Verlag 2003

**Abstract** A method was developed for detection of influenza genes in formalin-fixed brains of mice that had been experimentally infected with influenza A/NWS/33 (H1N1) virus. Using this technique, messenger ribonucleic acid (mRNA) of the $\beta$-actin gene was detected in eight clinical brain samples from the 1916–1920 outbreak of encephalitis lethargica, showing preservation of particular mRNAs. However, we did not detect influenza nucleotide sequences of M, NP, and NS genes from these same samples. We conclude either that influenza was not the causative agent of encephalitis lethargica or, possibly, that the virus had a hit-and-run mechanism and was no longer present in the brain at the time of death of the patients.

**Keywords** Encephalitis lethargica (EL) · Influenza · Gene · PCR · Pandemic

## Introduction

The 1918 "Spanish" influenza was the worst infectious pandemic of the last century, infecting half the population of the world and killing 40 million people [12]. Concomitant with the influenza pandemic and extending to the late 1920s, a particular neurological syndrome called Von Economo's disease or encephalitis lethargica (EL) occurred in epidemic proportions. A previous but much smaller epidemic of EL had also coincided with the influenza pandemic of 1889 [5, 6]. On the basis of such epidemiological data, it was suggested that influenza virus was the agent responsible for EL [13].

The polymerase chain reaction (PCR), which allows sequential amplification of a target nucleotide sequence, has revolutionized molecular biology. The sensitivity and specificity of PCR in detecting target sequences has been applied to both fresh and archived formalin-fixed and paraffin wax-embedded tissues [7, 8, 15, 19]. The technique was used to probe eight brain samples, from patients who died of EL between 1916 and 1920, for influenza genes. Our results, which failed to demonstrate the influenza virus genome, cast further doubt on the idea that influenza was the causative agent of encephalitis lethargica.

K. C. Lo · J. S. Oxford (✉)
Academic Virology, Department of Medical Microbiology,
Barts and The London School of Medicine and Dentistry,
Queen Mary, University of London, London, UK
e-mail: j.s.oxford@retroscreen.com
Tel.: +44-20-78827966
Fax: +44-20-78826990

J. F. Geddes
Department of Histopathology and Morbid Anatomy,
Barts and The London School of Medicine and Dentistry,
Queen Mary, University of London,
London, UK

R. S. Daniels
Division of Virology,
National Institute for Medical Research,
The Ridgeway, Mill Hill, London, NW7 1AA, UK

## Materials and methods

### Virus

To provide positive controls for our experiments, mice were infected with a neurovirulent influenza virus, strain A/NWS/33 (H1N1), which should be similar to strains circulating in the 1920s [16]. The virus was grown in eggs and yielded a haemagglutination titre of 196. Ten-fold serial dilutions of virus were made with sterile phosphate-buffered saline A (PBSA) containing penicillin/streptomycin (500 U/ml). For all animal inoculations, fresh dilutions of 1 in $10^3$ and 1 in $10^4$ were made and kept on ice for no more than 1 h prior to infection.

### Inoculation of virus into animals

Three- to four-week-old female Swiss CD1 mice with mean weights of 15–18 g were used in all experiments. All animal inoculations were conducted under light halothane anaesthesia. Each mouse was intracerebrally inoculated in the central frontal region, using a Hamilton syringe and disposable 27-gauge sterile needles, with 20 $\mu$l of the designated virus preparation. Mice

**Table 1** Main features of post-mortem samples from cases of encephalitis lethargica

| Case no. | Year | Sex | Age (years) | Autopsy and cause of death | Histological findings |
|---|---|---|---|---|---|
| 1 | 1916 | M | 3 | Clinically, fulminating EL. Brain swelling | Sections of cerebral cortex, brain stem, thoracic cord normal |
| 2 | 1916 | F | Adult | EL. Clinical diagnosis botulism | Perivascular inflammation in the pons and medulla |
| 3 | 1919 | F | 44 | EL. Brain swelling | Widespread perivascular cuffing, principally in the brain stem and spinal cord |
| 4 | 1920 | M | 17 | EL. Brain swelling | Meningoencephalitis, principally affecting the brain stem and spinal cord |
| 5 | 1920 | F | 37 | EL. Rapid loss of consciousness. Died within 24 h | Cerebral oedema and inflammation in the brain stem |
| 6 | 1920 | M | 41 | Deterioration in conscious level over 1 week. Brain swelling | Inflammation in the upper brain stem |
| 7 | 1920 | M | 0.25 | EL. Admitted unconscious after a 3-day illness. Died same day | Inflammation in the upper brain stem and spinal cord |
| 8 | 1920 | M | 17 | EL. Bronchopneumonia and influenza | Extensive inflammation in the brain stem and upper cervical cord |

forming the control group were similarly inoculated with 20 $\mu$l of sterile PBSA.

### Mouse brain samples

Mice were killed 3 days post-infection by asphyxiation with $CO_2$ according to the UK Home Office guidelines. Each mouse was then immersed in 70% formol saline, the scalp was opened by incision and the brain was removed rapidly using a sterile scalpel and surgical scissors. Brains were chopped finely with scissors and emulsified into sterile plastic universal bottles containing 2 ml of sterile PBSA. Emulsified brain samples were centrifuged at 1,800 rpm for 15 min and RNAs were extracted and stored at −20°C, for use as positive controls in RT-PCR to recover influenza gene fragments.

To ensure good fixation of brains to be wax-embedded, mice were injected with 70% formol saline, which was administered via a tail vein after exposure to carbon dioxide. The formalin-fixed mouse brain was then removed using surgical scissors and placed in a container containing a large volume of 70% formalin prior to paraffin wax embedding 1 week later. Paraffin wax blocks prepared from the brains of mice either infected with A/NWS/33 or inoculated with PBSA were used as positive and negative controls, respectively, for the recovery of influenza gene fragments from human brain samples.

### Human brain samples

Eight cases of EL were identified from the autopsy files at the Royal London Hospital for the years 1916–1920 for which formalin-fixed and paraffin wax-embedded brain samples were available in the archives. Outline details are given in Table 1. A paraffin wax block of brain tissue from a patient who had died of Alzheimer's disease in 1996 was used as a negative control. Ten 5 $\mu$M sections were cut from each human and mouse tissue block, placed in sealed containers and stored at 4°C until used for RNA extraction.

### RNA extraction from tissue sections

Each tissue section was deparaffinized by two extractions with 1 ml *n*-octane on a rotor mixer, with both extractions being performed at room temperature for 60 min. Subsequently, tissues were subjected to two 10-min washes with absolute ethanol, at room temperature, with 2-min centrifugation steps to recover the tissue. Sections were left to air-dry overnight in a fume-hood, with each tube covered by a plastic bag to avoid cross-contamination.

Proteinase K digestion buffer (50 $\mu$l 1 M TRIS pH8.0, 2 $\mu$l 0.5 M EDTA, 5 $\mu$l Tween 20, 20 $\mu$l 10 mg/ml proteinase K and 923 $\mu$l sterile water) was prepared fresh for all tissue digestions and 100 $\mu$l added to each tube containing a deparaffinized tissue section. Tubes were sealed with paraffin film and incubated at either 42°C or 55°C for 3 h, to ascertain the optimal temperature for nucleic acid recovery, then at 99°C for 5 min in a water bath. An empty tube containing only the proteinase K digestion buffer was also processed as a blank/negative control (K1) for each RT-PCR assay. Tubes were centrifuged briefly at the end of the digestion period.

To each digested sample, 225 $\mu$l of lysis solution (0.02 M Tris pH7.5, 0.01 M EDTA, 1% SDS) and 25 $\mu$l 100 mg/ml proteinase K was added and tubes were incubated at 42°C for 30 min. Samples were then extracted with an equal volume of phenol/chloroform/isoamyl alcohol (25:24:1) and twice with equal volumes of chloroform. One-tenth volume of 3 M sodium acetate (pH 5.2) was added to the final aqueous phases with 1 $\mu$l of 10 mg/ml oyster glycogen (Sigma) and 2.5 vol of cold absolute ethanol (stored at −20°C) to precipitate RNA. After 20 min on ice, the precipitated RNA was collected by centrifugation at 13,000 rpm for 20 min at 4°C. The pellets were washed with 70% ethanol, air dried, and resuspended in 4.45 $\mu$l of sterile water ready for complementary DNA (cDNA) synthesis. A clean-water control (X1) was extracted in parallel with the human and mouse samples.

### Oligonucleotide primers

As a test of RNA extraction procedures from human and mouse brains, primers were designed for amplification of $\beta$-actin gene and mRNA sequences. Similarly, primers were selected to allow reverse transcription off three genes of the influenza genome which show good conservation between virus strains: NP/segment 5, M/segment 7, and NS/segment 8. For all genes studied, two sets of primers were designed, allowing nested PCR to be performed. A list of primers used is shown in Table 2.

### Reverse transcription and PCR

cDNA to viral RNA (vRNA/mRNA) and human $\beta$–actin mRNA was synthesized from the RNA extracts using reverse transcriptase (RT, AMV-derived). Reaction mixes (10 $\mu$l) contained 1 $\mu$l 100 mM

**Table 2** Oligonucleotide primers used in RT-PCR gene amplification

| Gene | Primer | Direction[a] | Gene position (nucleotide number) | Sequence (5'→3')[b] | Product size (bp)[c] |
|---|---|---|---|---|---|
| Human $\beta$-actin | BAF 1 | F | 1284–1307 | GAAGAGCTACGAGCTGCCTGACGG | |
| | BAR 1 | R | 1840–1863 | ATACTCCTGCTTGCTGATCCACAT | 373[d] |
| | BAF 2 | F | 1338–1361 | CTGCCCTGAGGCACTCTTCCAGCC | |
| | BAR 2 | R | 1795–1818 | GGCCAGGATGGAGCCGCCGATCCA | 274[d] |
| Influenza M (segment 7) | M/32/1 | F | 32–54 | CTTCTAACCGAGGTCGAAACGTA | |
| | M/273/2 | R | 250–273 | GCATTTTGGACAAAGCGTCTACGC | 242 |
| | M/74/1 | F | 74–96 | TCAGGCCCCCTCAAAGCCGAGAT | |
| | M/190/2 | R | 166–190 | CAGAGGTGACAGGATTGGTCTTGTC | 117 |
| Influenza NP (segment 5) | NP/44/1 | F | 44–68 | TCATGGCGTCyCAAGGCACCAAACG | |
| | NP/326/2 | R | 301–326 | CCTCCAGTyTTCTTxGGrTCyTTCCC | 283 |
| | NP/87/1 | F | 87–110 | ACTGrTGGrGAACGCCAGAATGC | |
| | NP/245/2 | R | 223–245 | ACCATTCTCTCTATTGTkAxGCT | 159 |
| Influenza NS (segment 8) | NS/540/1 | F | 540–562 | GAGGATGTCAAAAATGCAATTGG | |
| | NS/859/2 | R | 835–859 | TAAGCTGAAAxGArAAAGTyCTTAT | 320 |
| | NS/566/1 | F | 566–590 | CCTCATCrrAGGACTTGAATGGAAT | |
| | NS/731/2 | R | 707–731 | CATCTkATyTCTTCrAACTTyTGAC | 166 |

[a] Primers were designed to amplify forward (*F*) to yield positive-sense ssDNA which was back-copied (negative sense) with the reverse (*R*) primer to yield double-stranded DNA
[b] Degeneracy code: y, C/T; k,T/G; r, G/A; w, A/T; x, G/A/T/C
[c] For each gene, two sets of primers were used such that nested PCRs could be performed, the sizes of products using "outer" and "inner" primer pairs are given
[d] The $\beta$-actin primers amplify across an intron in the gene so the amplification products off mRNA are 207 bp shorter than off the gene (DNA) template. Primers used for influenza M gene amplification were designed by Dr. J. S. Robertson (NIBSC)

DTT, 2 $\mu$l 2 mM dNTP mix (0.5 mM for each dNTP), 1.25 $\mu$l RT buffer (0.8 M TRIS pH 8.3 at 42°C, 1.12 M KCl, 80 mM $MgCl_2$), 0.3 $\mu$l ribonuclease inhibitor (1 U; CP Labs) and 0.3 $\mu$l RT (6 U; Advanced Biotechnologies), with 4.15 $\mu$l RNA extract and 1 $\mu$l of either 27 $\mu$M random hexamers or 10 $\mu$M segment-specific primer (for influenza or $\beta$–actin sequences). Tubes were incubated at 42°C for 60 min and then boiled for 2 min. A water-only, negative control (X2) was included.

All products of cDNA synthesis were subjected to two rounds of PCR amplification. Each 50 $\mu$l PCR mix contained 1 $\mu$l cDNA template, 0.25 $\mu$M of each forward and reverse oligonucleotide primer, 16 $\mu$l dNTP mix (1.25 mM each dNTP), 5 $\mu$l reaction buffer (100 mM TRIS pH 8.3, 25 mM $MgCl_2$, 500 mM KCl), and 1 $\mu$l (5 U) amplitaq polymerase (Perkin Elmer). Reaction mixes were overlaid with 50 $\mu$l of mineral oil and subjected to amplification in a DNA thermal cycler (Perkin Elmer). Each nested reaction used 1 $\mu$l of first round PCR product, an inner set of primers and fresh reaction mix. All PCRs were run for 30 cycles of 94°C/30 s, 50°C/1 min, 72°C/1 min. Negative controls, with sterile water as template, were set up in the same manner as the first round and nested PCR (X3 and X4).

First-round and nested PCRs were screened for double-stranded DNA (dsDNA) products by loading 10 $\mu$l of each reaction on 2% agarose gels, electrophoresing at 80 V for 60 min, and subsequent staining in ethidium bromide. Samples were run against 0.5 $\mu$g of a pUC19/Sau 3A digest (Advanced Biotechnologies) to allow sizing of products, which were visualized and photographed on a UV transilluminator.

## Results

### Review of archived tissue samples

The sections of brain from the eight archival cases of EL were reviewed. The principal neuropathological finding in all but one case was a florid lymphocytic rhomboencephalitis, without either necrosis or viral inclusions. In four cases the cervical cord was also affected. The findings are summarized in Table 1. Limited material was available for case 1, a 3-year-old male, and, despite having been diagnosed clinically as having EL, this could not be confirmed neuropathologically on the remaining tissue sections. Nevertheless, the autopsy report strongly suggested the diagnosis.

### Influenza infected mouse brain: detection of $\beta$–actin and influenza gene fragments.

To establish the sensitivity of our technique, we used formalin-fixed brain samples from mice infected with A/NWS/33 (H1N1) [16]. The effects of performing proteinase K digestion at 42°C and 55°C and the use of ribonuclease inhibitor in the RT step were studied.

Following use of random hexamers in the RT step, influenza and $\beta$–actin gene-specific primers were used in the PCR steps. For NP-specific primers, a product of 283 bp was detected in extracts of some sections of a mouse brain digested at 55°C whether or not ribonuclease inhibitor was used in the RT step (Fig. 1a: upper block, lanes 1–10). After nested PCR, products of 159 bp were detected for all ten extracts, five of which had been digested at 42°C (Fig. 1a: lower block, lanes 1–10), confirming the expected increase in sensitivity provided by nested reactions. Similar results were obtained when M- and NS-specific primers were used (not shown). This infers a slight advantage when conducting digestion at 55°C. For $\beta$–actin, fragments of 373 bp were detected in

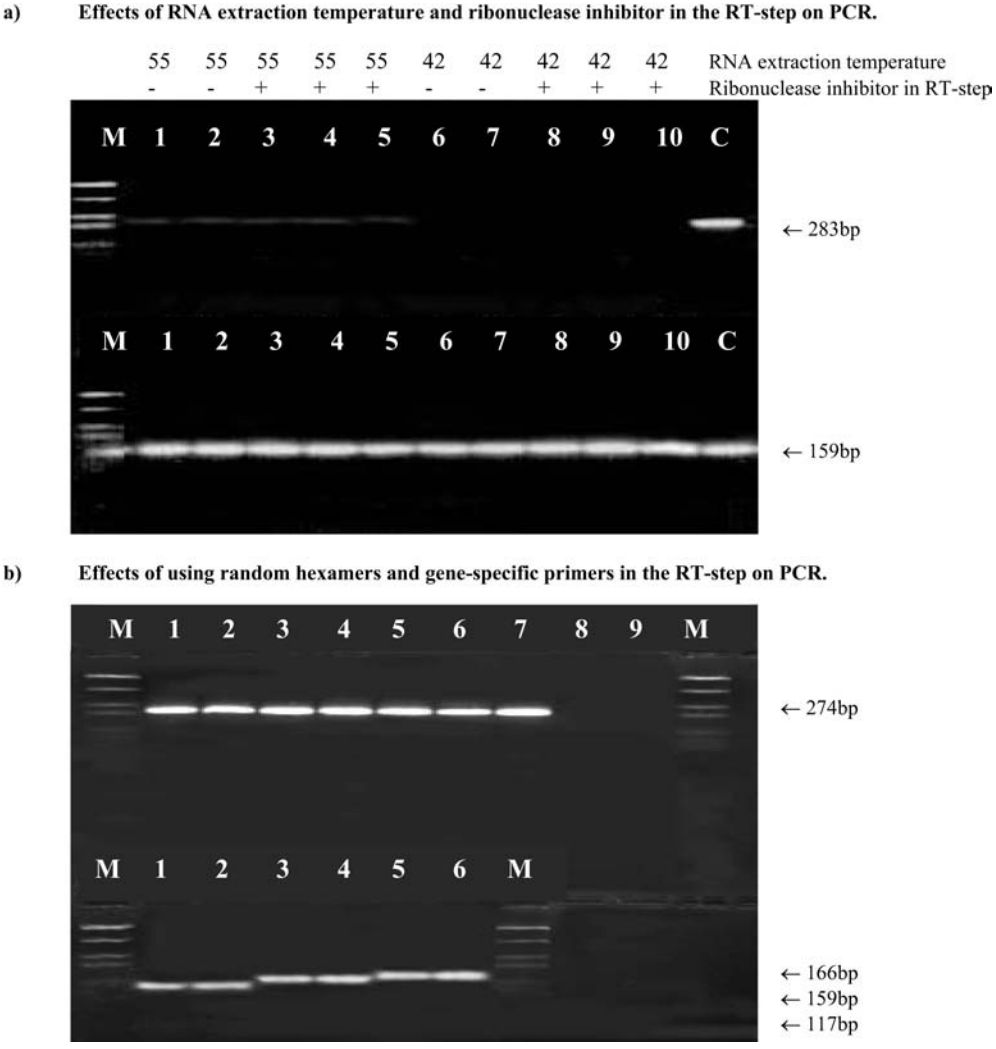



**Fig. 1** Recovery of influenza and $\beta$-actin gene fragments from extracts of A/NWS/33-infected, paraffin wax-embedded mouse brain. *M* indicates marker lanes (pUC19/Sau3A) and shows bands of known size on a DNA ladder. **a** The temperatures used for RNA extraction from sections of wax-embedded mouse brain and the presence (+) of ribonuclease inhibitor in the RT step are indicated *above the lane numbers*. Random hexamers were used for cDNA synthesis. Influenza NP-specific primers were then used in the PCRs. The *upper block* shows analysis of first round PCR products, whilst the lower block shows results for the nested reactions. *C* indicates a positive control for amplification off an extract of a mouse brain infected with A/NWS/33 which had not undergone formalin-fixation and wax-embedding. **b** *Upper block*: Detection of $\beta$-actin gene fragments following use of random hexamers in the RT step. *Lanes 1–6*, six sections of paraffin wax-embedded mouse brain; *lane 7*, a positive PCR control for unfixed influenza virus-infected mouse brain tissue; *lanes 8 and 9*, water negative controls of PCR (*X3, X4*). *Lower block*: Following use of M-, NP- and NS-specific primers in the RT step, extracts of two sections of paraffin wax-embedded infected mouse brain for each, gene-specific nested PCRs were performed. The segment-specific primers used in cDNA synthesis were: M/32/1, lanes 1 and 2; NP/44/1, lanes 3 and 4; NS/540/1, lanes 5 and 6

first-round PCRs (not shown) and 274 bp in the nested reactions (Fig. 1b: upper block, lanes 1–7).

To ascertain whether use of gene specific primers in the RT step might improve the sensitivity of detection, experiments were conducted with influenza gene-specific primers. Again, first-round PCRs were negative (not shown), but nested reactions yielded fragments of 117 bp, 159 bp and 166 bp for M, NP and NS, respectively (Fig. 1b: lower block; lanes 1–6). Overall this indicated no advantage in using gene-specific primers in the RT step, whilst use of random hexamers should provide the opportunity to screen for fragments of different genes in subsequent PCRs. Therefore random hexamers were used for cDNA synthesis in the analyses of extracts of human brain samples.

## RT–PCR analysis of human brain samples for the presence of influenza genes

As for the studies of formalin-fixed, wax-embedded brain samples from mice, the EL-related cases (Table 1) and the 1996 Alzheimer's case were all positive for $\beta$-actin. Ten sections from each wax-embedded sample were screened

and both rounds of PCR were positive for all sections, with defined product sizes of 373 bp and 274 bp, respectively (not shown).

In contrast, when the same RT products were subjected to nested PCR for influenza genes, M, NP and NS, in no instance were products generated of the expected sizes. In the same PCR sets, all positive controls (coming off influenza A/NWS/33 vRNA template in the RT reactions) were positive, and the negative controls, including K1 and X1–4, were negative (not shown). Overall this demonstrates a lack of influenza gene fragments in any of the archived formalin-fixed wax-embedded human brain samples

## Discussion

Here we have assessed the use of RT-PCR in attempting to verify whether or not influenza virus is the causative agent of EL. The mouse model was used as a source of formalin-fixed, wax-embedded brain tissues from control animals and those infected with a neurovirulent strain of influenza, to allow development of a sensitive assay. Using either random hexamers or gene-specific primers in the RT step followed by gene-specific nested PCR, host $\beta$-actin mRNA derived gene fragments of defined size were detected in all tissue sections and in both rounds of PCR. Similarly, when either random hexamers or influenza gene-specific primers (for M, NP and NS genes) were used in the RT step and influenza gene-specific primers in PCR, products of defined size were detected in samples derived from A/NWS/33-infected animals but usually after the second (nested) round of PCR only. The latter result probably indicates a lower level of influenza RNA (vRNA/mRNA) in the tissue extracts compared with that of $\beta$-actin mRNA.

Random hexamer priming of RT followed by gene-specific nested PCR was applied to RNA extracts of eight human brain tissue sections derived from patients who died of encephalitis lethargica between 1916 and 1920 and another who died of Alzheimer's disease in 1996. Again, for all tissue sections, both rounds of PCR yielded products of defined size for $\beta$-actin, but none of the human samples yielded influenza gene-specific products.

A facile explanation for the negative results obtained for the RT-PCR analysis of human archival tissue sections conducted here would be that the influenza gene-specific primers used were incompatible with the infecting influenza. This seems unlikely, as the three genes studied show good sequence conservation between influenza A subtypes. A number of other factors may have contributed to the negative results of the current study.

Firstly, it is possible that the clinical samples either were not infected with influenza virus or that, even if influenza had caused the disease, the mechanism could have been hit-and-run, with only small foci of infection being established. Multiple sections, ten from each human block, were analysed in parallel to minimise false-negative results due to small sample size and possible focal distribution of vRNAs within the tissue block. Secondly, the possibility of RNA degradation during tissue collection and storage may have limited the detection of target sequences. However, we optimized the test by using nested primers which amplified shorter sequences (<180 bp) to increase the sensitivity of detection of target sequences, and $\beta$-actin gene fragments of 373 bp and 274 bp were detected. Thirdly, delays between sample collection and formalin fixation after death of the patient may have resulted in loss of RNA through autolysis. This seems unlikely given the sizes of $\beta$-actin gene fragments recovered and the fact that the human brain contains low levels of ribonucleases and high levels of ribonuclease inhibitors compared with organs such as the lungs [3, 11]. Fourthly, the titre of influenza in human brain might have been extremely low compared with that which was reached in the lung, thereby making detection more difficult with brain samples. In support of the latter point, isolation of influenza gene sequences from formalin-fixed, wax-embedded lung tissue specimens of two US soldiers who died of primary viral pneumonia during the 1918 influenza pandemic has been reported [19, 14]. More recently, the Royal London Hospital archive has yielded formalin-fixed, wax-embedded lung samples from civilian patients who died of pneumonia during the 1918–1919 pandemic that have yielded influenza haemagglutinin gene sequences (Reid AH, Janczewski TA, Greif R, Elliot AJ, Daniels RS, Berry CL, Oxford JS, Taubenberger JK, unpublished work).

The negative molecular analyses presented here are consistent with those of other workers who failed to detect influenza genes in brain specimens of EL victims [9]. The absence of detection of influenza gene fragments in extracts of human brains derived from EL victims does not rule out influenza virus as a contributory factor in the pathology of these cases. Indeed, most epidemiological evidence supports influenza being the most likely candidate virus to cause EL.

The neurovirulent potential of influenza viruses has been demonstrated by infection of mouse brains and led to an understanding of the underlying mechanisms of viral adaptation to allow growth in neural tissues [21]. Further, in developing a mouse model for Reye's syndrome, RT-PCR detection of influenza gene fragments in a variety of tissues including brain has been reported [1]. Whilst studies in humans have been somewhat limited, cases of influenza-related encephalitis have been reported where cerebrospinal fluid (CSF) has proven either RT-PCR- or isolation-positive for influenza [20, 2, 10, 4]. For an autopsied paediatric case of suspected influenza-induced encephalopathy, immunohistochemical staining identified influenza antigen in meningeal and ependymal areas, neurons of the circumventricular regions, the cerebral and cerebellar cortices and zona compacta of the substantia nigra, whilst RT-PCR analysis indicated infection of limited parts of the brain [18]. In many of these studies, the severity of disease and its presentation has been considered inconsistent with the levels of influenza

detected, and it has been suggested that influenza may act in concert with other infectious agents such as human herpesvirus 6 or 7 [17].

If influenza is a causative agent of EL, then influenza pandemic(s) predicted for the twenty-first century should provide further clinical material for molecular investigations. In the meantime, investigation of the current causes of EL, though diagnoses are rare, could shed light on the wider range of potential causative agents and thereby allow directed re-analysis of the valuable but limited archived samples.

**Acknowledgements** We thank Dr. J. S. Robertson, National Institute for Biological Standards and Control, for help in designing the influenza-specific primers used in the present study.

## References

1. Davis LE, Kornfeld M, Daniels RS, Skehel JJ (2000) Experimental influenza causes a non-permissive viral infection of brain, liver and muscle. J Neurovirol 6:529–536
2. Fujimoto S, Kobayashi M, Uemura O, Iwasa M, Ando T, Katoh T, Nakamura C, Maki N, Togari H, Wada Y (1998) PCR on cerebrospinal fluid to show influenza-associated acute encephalopathy or encephalitis. Lancet 352:873–875
3. Futami J, Tsushima Y, Murato Y, Tada H, Sasaki J, Seno M, Yamada H (1997) Tissue-specific expression of pancreatic-type RNases and RNase inhibitor in humans. DNA Cell Biol 16:413–419
4. Hakoda S, Nakatani T (2000) A pregnant woman with influenza A encephalopathy in whom influenza A/Hong Kong virus (H3) was isolated from cerebrospinal fluid. Arch Intern Med 160:1041–1045
5. Hall AJ (1923) Encephalitis lethargica (epidemic encephalitis). Lancet 1:731–740
6. Hall AJ (1924) Epidemic encephalitis (encephalitis lethargica). Wright & Sons, Bristol/Simpkin, Marshall, Hamilton, Kent, London, pp 229
7. Jackson DP, Quirke P, Lewis F, Boylston AW, Sloan JM, Robertson D, Taylor GR (1989) Detection of measles virus RNA in paraffin-embedded tissue. Lancet 1:1391
8. Liebert UG, Baczko K, Budka H, ter Meulen V (1986) Restricted expression of measles virus proteins in brains from cases of subacute sclerosing panencephalitis. J Gen Virol 67:2435–2444
9. McCall S, Henry JM, Reid AH, Taubenberger JK (2001) Influenza RNA not detected in archival brain tissues from acute encephalitis lethargica cases or in postencephalitic Parkinson cases. J Neuropathol Exp Neurol 60:696–704
10. McCullers JA, Facchini S, Chesney PJ, Webster RG (1999) Influenza B virus encephalitis. Clin Infect Dis 28:898–900
11. Nadano D, Yasuda T, Takeshita H, Uchide K, Kishi K (1994) Purification and characterization of human brain ribonuclease inhibitor. Arch Biochem Biophys 312:421–428
12. Oxford JS (2000) Influenza A pandemics of the 20th century with special reference to 1918: virology, pathology and epidemiology. Rev Med Virol 10:119–133
13. Ravenholt RT, Foege WH (1982) 1918 influenza, encephalitis lethargica, parkinsonism. Lancet 2:860–864
14. Reid AH, Fanning TG, Hultin JV, Taubenberger JK (1999) Origin and evolution of the 1918 "Spanish" influenza virus hemagglutinin gene. Proc Natl Acad Sci U S A 96:1651–1656
15. Shibata DK, Arnheim N, Martin WJ (1988) Detection of human papilloma virus in paraffin-embedded tissue using the polymerase chain reaction. J Exp Med 167:225–230
16. Stuart-Harris CH (1939) A neurotropic strain of human influenza virus. Lancet 1:497–499
17. Sugaya N, Yoshikawa T, Miura M, Ishizuka T, Kawakami C, Asano Y (2002) Influenza encephalopathy associated with infection with human herpesvirus 6 and/or human herpesvirus 7. Clin Infect Dis 34:461–466
18. Takahashi M, Yamada T, Nakashita Y, Saikusa H, Deguchi M, Kida H, Tashiro M, Toyoda T (2000) Influenza virus-induced encephalopathy: clinicopathologic study of an autopsied case. Pediatr Int 42:204–214
19. Taubenberger JK, Reid AH, Krafft AE, Bijwaard KE, Fanning TG (1997) Initial genetic characterization of the 1918 "Spanish" influenza virus. Science 275:1793–1796
20. Togashi T, Matsuzono Y, Narita M (2000) Epidemiology of influenza-associated encephalitis-encephalopathy in Hokkaido, the northernmost island of Japan. Pediatr Int 42:192–196
21. Ward AC (1996) Neurovirulence of influenza A virus. J Neurovirol 2:139–151

Virchows Arch (2003) 442:597–600
DOI 10.1007/s00428-003-0814-2

ORIGINAL ARTICLE

**Angela Pucci · Cristina Zanini · Federica Ferrero · Riccardo Arisio · Andrea Valori · Piero Abbruzzese · Marco Forni**

# Misalignment of lung vessels: diagnostic role of conventional histology and immunohistochemistry

Received: 2 October 2002 / Accepted: 1 March 2003 / Published online: 13 May 2003
© Springer-Verlag 2003

**Abstract** Misalignment of lung vessels represents a rare congenital anomaly that may cause respiratory failure in the newborn. It is characterized by abnormal position of pulmonary veins and venules that lie adjacent to arteries and bronchi, and it is usually associated with a decreased number of alveolar capillaries (i.e., alveolar capillary dysplasia), although these two conditions have been separately described. Awareness of this anomaly is required by pathologists because it can be easily overlooked on lung biopsy or autopsy, and because definite diagnosis relies on histology. We report the case of a newborn male baby who developed respiratory distress 18 h after an uncomplicated delivery. The patient died on the 7th day, after high frequency oscillatory ventilation, nitric oxide inhalation and extracorporeal membrane oxygenation were unsuccessful. On autopsy, histology and immunohistochemistry demonstrated diffuse changes, fulfilling diagnostic criteria of misalignment of lung vessels and of alveolar capillary dysplasia in both lungs, with muscularization of very peripheral pulmonary arteries and a prominent interstitial and periadventitial fibrosis. Diffuse distribution of vessel misalignment could explain the rapid onset of respiratory failure, and the presence of diffuse fibrosis might have contributed to irreversible respiratory dysfunction by impairment of lung parenchyma extensibility.

A. Pucci (✉) · C. Zanini · R. Arisio · M. Forni
Department of Pathology,
Servizio di Anatomia ed Istologia Patologica,
Ospedale Infantile Regina Margherita,
Piazza Polonia, 94-10126 Torino, Italy
e-mail: anapatoirm@oirmsantanna.piemonte.it
Tel.: +39-011-3135410, Fax: +39-011-3135412

F. Ferrero
Intensive Care Unit, Pediatric Hospital "Regina Margherita", Italy

A. Valori · P. Abbruzzese
Cardiac Surgery, Pediatric Hospital "Regina Margherita", Italy

R. Arisio
Department of Pathology, S.Anna Hospital, Turin, Italy

**Keywords** Misalignment of lung vessels · Alveolar capillary dysplasia · Neonatal pulmonary hypertension · Immunohistochemistry

## Introduction

In the newborn, persistent pulmonary hypertension is usually secondary to perinatal asphyxia in association with respiratory distress syndrome or with pulmonary hypoplasia [6]. However, in rare cases, it may be caused by the misalignment of lung vessels that is commonly associated with alveolar capillary dysplasia [21]. Misalignment is characterized by pulmonary veins and venules lying in close association with the pulmonary arteries, aside bronchi and bronchioli, whereas alveolar capillary dysplasia is manifested by a decreased number of alveolar capillaries. The vascular anomalies may affect both lungs; however, sometimes there is only one lung or one lobe involved and the patient can survive until 1 year of age and possibly longer [1, 2]. Misalignment is clinically characterized by cyanosis and respiratory distress due to failure of the vascular pulmonary resistance to decrease as it normally occurs on initiation of ventilation, and it is considered a developmental anomaly of capillary formation and migration to the canaliculi [3].

Most reported cases are sporadic [4, 9, 11, 15, 16, 17, 19, 22], but familial occurrence with a possible autosomal recessive gene has been reported [2, 8, 13, 18, 20]. For this condition to be diagnosed or its clinical suspicion to be confirmed, histology is required. The pathologist needs to be aware of this disease as it may be overlooked or misinterpreted on lung biopsy or at autopsy [21].

## Clinical history

A full-term, 3600-g male infant was spontaneously born to healthy, unrelated, white parents in their thirties, after an uneventful pregnancy. He was their first child. At 18 h after delivery, he developed increasing respiratory distress

with bilateral pneumothorax. Echocardiography showed evidence of persistent pulmonary hypertension and a ≤3-mm diameter interventricular septal defect. His respiratory condition deteriorated and high-frequency oscillatory ventilation and inhaled nitric oxide were subsequently administered in order to improve oxygenation, but only a temporary improvement was obtained. The infant underwent extracorporeal membrane oxygenation on the 4th day. The subsequent course was characterized by respiratory deterioration, cerebral hemorrhage and left-sided hemothorax. The patient died on the 7th day.

## Materials and methods

Autopsy was performed and several samples from all organs were formalin fixed, paraffin embedded and investigated by means of conventional histology and immunohistochemistry. For each lung lobe, at least three to four specimens were examined. For histological examination, 4-$\mu$m-thick paraffin sections were stained with hematoxylin and eosin; lung slides were additionally stained with Masson's trichrome and elastic Van Gieson. Immunohistochemical staining was performed on adjacent, serial sections of the paraffin-embedded lung blocks using the Ventana automated immunostainer with a labeled streptavidin-biotin peroxidase detection system. Antigen retrieval was performed by boiling the slides in citrate buffer (0.01 mol/l, pH 6.0) in a microwave oven (2×5 min, 650 W). Antibodies against the following antigens were used in appropriate dilutions: alpha-smooth muscle actin (clone 1A4, Sigma, St Louis, MO, USA), CD34 (clone QBEND 10, Immunotech, Marseilles, France), Von Willebrand factor (Dakopatts, Glostrup, Denmark) and collagen IV (Sigma, St. Louis, USA).

## Results

At autopsy, the most remarkable gross findings were represented by diffuse subarachnoid hemorrhage, cerebral edema, duodenal and jejunal enterorrhagy and mild left hemothorax. Lungs showed a mild diffuse increase of consistency and weighed 69 g (right) and 54 g (left). In

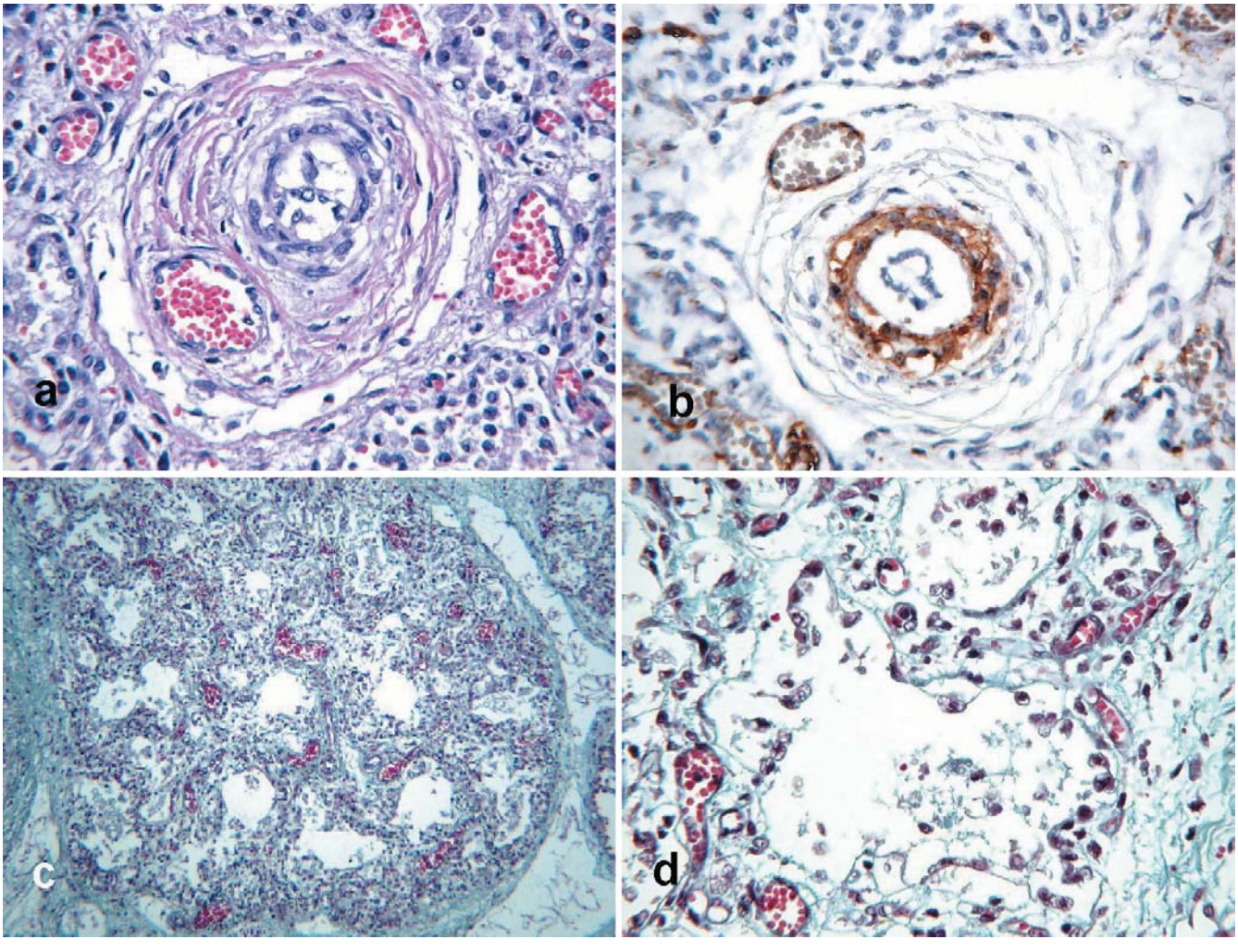



**Fig. 1 a, b** Lung tissue from the right middle lobe showing misalignment of lung vessels: a pulmonary vein lies in close association with a pulmonary artery. The vessels appear to share their adventitia. Hematoxylin and eosin, original magnification ×270 (**a**); $\alpha$-smooth muscle actin stain, original magnification ×270 (**b**). **c**, **d** Thickened alveolar septa (**c**) with reduced number of alveolar capillaries (**d**). Masson's trichrome stain, original magnification ×100 (**c**), ×400 (**d**)

the heart, a small muscular defect was found in the interventricular septum middle part; *foramen ovale* and *ductus arteriosus* were patent. No other abnormal findings were detected in any other organ by macroscopic examination.

On histological examination, both lungs showed similar and diffuse changes represented by prominent muscularized arterioles accompanied by venules, these features also evident at a very peripheral level. Many pulmonary arteries shared their adventitia with thin-walled and widened veins (Fig. 1a, b). Alveolar septa were thickened and alveolar capillaries were reduced in number and total surface extension; septa contained only a few large capillaries and/or venules with wide separation between the vessels and the alveolar lumen (Fig. 1c, d). These features were consistent with alveolar capillary dysplasia, including misalignment of pulmonary veins. In hepatic and renal parenchyma, mild to moderate congestive changes were observed, together with moderate microvacuolization of hepatocytes.

Immunohistochemical actin staining confirmed the diffuse muscularization of peripheral pulmonary arteries in all examined blocks. Collagen-IV immunostaining was intense in the interstitium, particularly in the alveolar septa, and around misaligned lung vessels, either in arteries and thin-walled, widened veins or venules.

## Discussion

Misalignment of lung vessels is characterized by pulmonary veins and venules lying in close association with the pulmonary arteries, that is, next to the bronchi and bronchioli [21]. It was first described in 1981 by Janney et al. [9] and is now considered a congenital anomaly, presenting in an otherwise normal newborn or associated with cardiac, urogenital or phocomelic malformations [14]. It is usually associated with alveolar capillary dysplasia, i.e., thickened, fibrotic alveolar walls and paucity of capillaries [7], as observed in the present case, and the two terms are sometimes used as synonyms [15]. Although very few reports have described capillary dysplasia in the absence of misalignment [7, 14, 17], such a frequent association suggests that misalignment of lung vessels and alveolar capillary dysplasia could represent two manifestations of the same developmental disorder.

The diagnosis of this disease requires histology. The diagnosis should also be considered in neonatal persistent pulmonary hypertension after excluding the more common causes of pulmonary hypertension such as birth asphyxia, meconium aspiration, congenital aspiration pneumonia, diaphragmatic hernia and stenosis of pulmonary veins [6]. Several blocks have to be examined to discover or to rule out misalignment of lung vessels; the paired vein and artery are sometimes difficult to discover and they may have patchy distribution [2, 15]. The immunoreactivity pattern of smooth muscle actin and of collagen IV can be helpful for diagnosis. In the present report, the immunohistochemical stainings demonstrated the increased muscularity of pulmonary arteries (smooth muscle cells were also present in very small intra-acinar arterial branches, normally devoid of muscle) and confirmed the fibrotic changes in the alveolar septa and in misaligned arterioles and veins, which often showed a common fibrous sheath. Type-IV collagen is normally present in alveolar basement membranes and increases in the aging lung [5]: in misalignment of lung vessels, prominent collagenization—together with alveolar capillary dysplasia—could reflect the altered lung development and contribute to respiratory failure by decreasing lung parenchyma extensibility.

In a recent report [22], congenital alveolar proteinosis was associated with misalignment of lung vessels; the reported mutation of surfactant protein B gene was hypothesized to cause misalignment via local vascular growth factor impairment. In fact, both differentiation of the type-II cells (synthesizing surfactant protein B) and vascularization of acinar tubules take place during the canalicular stage of lung development. In the present case, alveolar proteinosis could be excluded on a morphological basis by a thorough histological examination of both lungs. However, misalignment of lung vessels could be the result of different causes, including genetic mutations or fetal infections, with the different ethiopathogenetic mechanisms explaining the variable extension of lung damage.

Only five family occurrences of this disease have been reported to date [2, 8, 13, 18, 20] and an autosomal recessive inheritance has been supposed [20]. The patient of the present report was the son of healthy, unrelated parents with no other children and with no family history of newborn deaths caused by respiratory distress.

Severity of disease correlates with the extension of lung abnormalities [2]. In the present case, diffuse lung vessel anomalies were associated with an early presentation. Patchy histological abnormalities have been described in later onset cases (as late as 5–6 weeks after delivery) [1, 15], with variable phenotypic expression also between siblings in familial cases [2]. Misalignment of lung vessels has an unfavorable outcome, only short-term improvement has been achieved by specific therapies [3, 12]. Lung biopsy has been proposed as the only tool for a definite in vivo diagnosis, particularly in sporadic cases as reported in three patients [19] and in order to avoid further intensive care procedures if lung transplantation is not feasible [10, 14]. However, [15], a sampling error could give false-negative results on biopsy material in the case of a possible patchy distribution.

In conclusion, pathologists must be aware of this rare condition, which has to be taken into consideration in any case presenting with idiopathic persistent neonatal pulmonary hypertension. A thorough histological investigation, with the possible contribution of immunohistochemistry, currently represents the only means for a definite diagnosis.

**Acknowledgements** The authors wish to thank Dr. G.E. Dickey and Dr. T. Stocker for reviewing the case, and Dr. B. Murer for his helpful criticism of the manuscript.

## References

1. Abdallah HI, Karmazin N, Marks LA (1993) Late presentation of misalignment of lung vessels with alveolar capillary dysplasia. Crit Care Med 21:628–630
2. Boggs S, Harris MC, Hoffman DJ, Goel R, McDonald-McGinn D, Langston C, Zackal E, Ruchelli E (1994) Misalignment of pulmonary veins with alveolar capillary dysplasia: affected siblings and variable phenotypic expression. J Pediatr 124:125–128
3. Chelliah B, Brown D, Cohen M, Talleyrand A, Shen-Schwarz S (1995) Alveolar capillary dysplasia- a cause of persistent pulmonary hypertension unresponsive to a second course of extracorporeal membrane oxygenation. Pediatrics 96:1159–1161
4. Cullinane C, Cox PN, Silver MM (1992) Persistent pulmonary hypertension of the newborn due to alveolar capillary dysplasia. Pediatr Pathol 12:499–514
5. D'Errico A, Scarani P, Colosimo E, Spina M, Grigioni WF, Mancini AM (1989) Changes in the alveolar connective tissue of the ageing lung. An immunohistochemical study. Virchows Arch 415:137–144
6. Fox WW, Duara S (1983) Persistent pulmonary hypertension in the neonate: diagnosis and management. J Pediatr 103:505–514
7. Garola RE, Thibeault DW (1998) Alveolar capillary dysplasia, with and without misalignment of pulmonary veins: an association of congenital anomalies. Am J Perinatol 15:103–107
8. Guitierrez C, Rodriguez A, Palenzuela S, Forteza C, Rossello JL (2000) Congenital misalignment of pulmonary veins with alveolar capillary dysplasia causing persistent neonatal pulmonary hypertension: report of two affected siblings. Pediatr Dev Pathol 3:271–276
9. Janney C, Askin F, Kuhn C III (1981) Congenital alveolar capillary dysplasia: an unusual case of respiratory distress in the newborn. Am J Clin Pathol 76:722–727
10. Kane TD, Greenberg JM, Bove KE, Warner BW (1998) Alveolar capillary dysplasia with misalignment of the pulmonary veins: a rare but fatal cause of neonatal respiratory failure. Pediatr Surg Int 14:89–91
11. Khorsand J, Tennant R, Gillies C, Phillipps AF (1985) Congenital alveolar capillary dysplasia: a developmental vascular anomaly causing persistent pulmonary hypertension of the newborn. Pediatr Pathol 3:299–306
12. Kitayama Y, Kamata S, Okuyama H, Usui N, Sawai T, Kobayashi T, Fukui Y, Okada A (1997) Nitric oxide inhalation therapy for an infant with persistent pulmonary hypertension caused by misalignment of pulmonary veins with alveolar capillary dysplasia. J Pediatr Surg 32:99–100
13. Manovrieur Hanu S, Devisme L, Farre I, Hue V, Storme L, Kacet N, Boute-Benejean O, Farriaux JP (1996) Pulmonary hypertension of the newborn and urogenital anomalies in two male siblings: a new family with misalignment of pulmonary vessels. Genet Couns 7:249–255
14. Newman B, Yunis E (1990) Primary alveolar capillary dysplasia. Pediatr Radiol 21:20–22
15. Oldenburg J, Van der Pal HJH, Schrevel LS, Blok APR, Wagenvoort CA (1995) Misalignment of lung vessels and alveolar capillary dysplasia. Histopathology 27:192–194
16. Rehan V, Phillips S, Fajardo C, Seshia MMK (1997) Congenital alveolar capillary dysplasia and misalignment of lung vessels. Arch Pediatr Adolesc Med 151:1163–1164
17. Rutledge JC, Jensen P (1986) Acinar dysplasia: a new form of pulmonary maldevelopment. Human Pathol 17:1290–1293
18. Simonton S, Chrenka B (1993) Familial persistent pulmonary hypertension in two siblings with phocomelia and alveolar capillary dysplasia (ACD): a new syndrome? Mod Pathol 21:629–630
19. Steinhorn RH, Cox PN, Fineman JR, Finer NN, Roesenberg EM, Silver MM, Tyebkhan J, Zwass MS, Morin FC III (1997) Inhaled nitric oxide enhances oxygenation but not survival in infants with alveolar capillary dysplasia. J Pediatr 130:417–422
20. Vassal HB, Malone M, Petros AJ, Winter RM (1998) Familial persistent pulmonary hypertension of the newborn resulting from misalignment of the pulmonary vessels (congenital alveolar dysplasia). J Med Genet 35:58–60
21. Wagenvoort CA (1986) Misalignment of lung vessels: a syndrome causing persistent neonatal pulmonary hypertension. Hum Pathol 17:727–730
22. Wallot M, Wagenvoort C, deMello D, Muller KM, Floros J, Roll C (1999) Congenital alveolar proteinosis caused by a novel mutation of the surfactant protein B gene and misalignment of lung vessels in consanguineous kindred infants. Eur J Pediatr 158:513–518

Virchows Arch (2003) 442:601–604
DOI 10.1007/s00428-003-0805-3

CASE REPORT

**Socorro María Rodríguez-Pinilla · José Luis Rodríguez-Peralto · María Teresa Férnandez-Figueras**

# Transitional cell papilloma of the penis associated with human papilloma virus infection. Report of two cases

Received: 27 December 2002 / Accepted: 6 March 2003 / Published online: 1 May 2003
© Springer-Verlag 2003

**Abstract** Condylomas are one of the most common human papilloma virus (HPV)-related benign lesions of the male genitourinary tract. Although rarely, HPV has also been detected along the urinary tract, using molecular techniques, in transitional cell neoplasms without microscopic signs of koilocytic atypia. When affecting the urethra, condylomas are usually limited to its third distal portion. However, transitional cell neoplasms of the urethra are exceptional and in most of the cases remain limited to its proximal portion. To the best of our knowledge, 12 cases of transitional cell carcinomas and only one case of typical transitional cell papilloma have been described in the anterior urethra. We report two exceptional cases of typical transitional cell papilloma of the glans of the penis near the fossa navicularis which showed microscopic signs of HPV infection.

**Keywords** Transitional cell papilloma · Fossa navicularis · External urethral meatus · Distal urinary tract · HPV infection

## Introduction

Condyloma acuminatum (CA) is a benign lesion caused by human papillomavirus (HPV); types 6 and 11 are the most frequently identified. CA may occur on any moist mucocutaneous surface of the external genitals in either sex. On the penis, these lesions most often affect the coronal sulcus and inner surface of the prepuce, with about 23% of cases occurring in the urethral meatus. Five percent of reported cases involve the urethra, 80% of these affecting the distal 3 cm, while the rest are found in the deeper segment [16]. Other external male genital lesions strongly associated with HPV infection are: Bowen disease, erythroplasia of Queyrat, bowenoid papulosis and squamous cell carcinoma of the penis. In the latter conditions, the most frequent types of HPV are 16 and 18 [11].

While squamous cell papillomas, or condylomas, are common in the anterior urethra, including the fosa navicularis, transitional cell tumors are very rare [16]. Chronic irritation, urethral stricture, urethral diverticule, and chronic infections with sexually transmitted diseases have been considered predisposing factors to either benign or malignant transitional cell neoplasms [8]. HPV has been demonstrated in the neoplastic cells of only a few transitional cell tumors [1, 2, 3, 6, 7, 9]. Bladder cancer is commonly associated with it and more than a few cases reported as urethral carcinoma present secondary involvement by multifocal carcinoma in situ of the bladder [8].

To the best of our knowledge, 12 cases of transitional cell carcinomas [12] and only one case of typical transitional cell papilloma [12] have been described in the anterior urethra. The latter case was remarkable, not only because it emerged from the fossa navicularis but also because it had biological signs of HPV infection without microscopic koilocytic atypia [12].

We report, for the first time, two cases of typical transitional cell papilloma of the glans of the penis near, but not emerging from, the external urethral meatus. Both cases show microscopic features of HPV infection and positivity to HPV types 6 and 11 by means of polymerase chain reaction (PCR). Neither of them had any other lesion in the urinary tract.

S. M. Rodríguez-Pinilla · J. L. Rodríguez-Peralto (✉) · M. T. Férnandez-Figueras
Department of Pathology "12 de Octubre", University Hospital, 28041 Madrid, Spain
e-mail: jrodriguezp.hdoc@salud.madrid.org
Tel.: +34-91-3908710
Fax: +34-91-3908462

S. M. Rodríguez-Pinilla · J. L. Rodríguez-Peralto · M. T. Férnandez-Figueras
"German Trias i Pujol" Hospital, Badalona, Barcelona, Spain

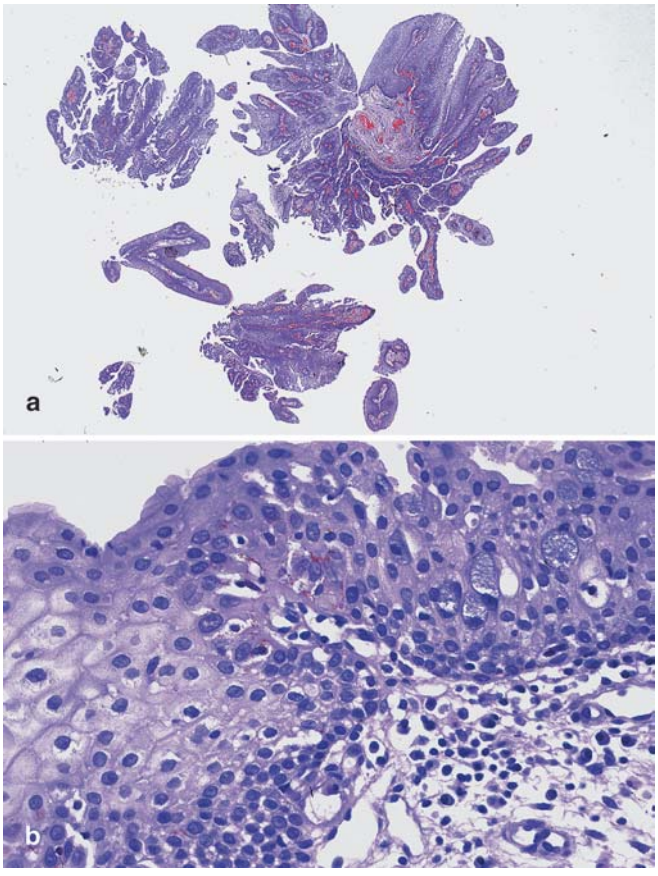



**Fig. 1** **a** Panoramic view of case 1. Note a sessile proliferation formed by the attachment of variable-sized papillae (hematoxylin and eosin ×20). **b** Conjunction zone of transitional cell papillae with mucinous cells and a focus of squamous metaplasia (hematoxylin and eosin ×800)

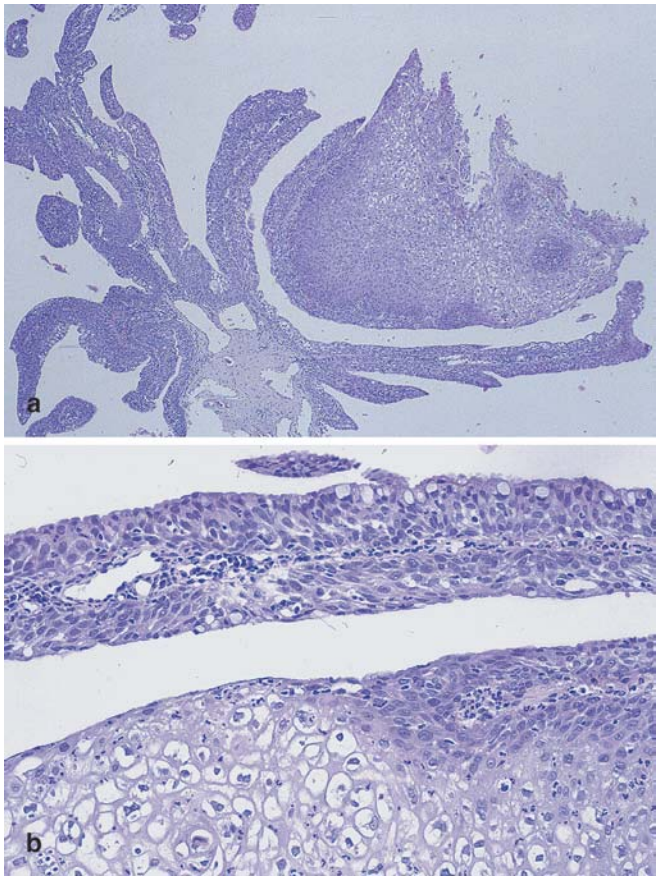



**Fig. 2** **a** Panoramic view of case 2: exophytic proliferation formed by the coalescence of a condyloma and typical transitional cell papilloma-like areas (hematoxylin and eosin ×20). **b** Slender papillae covered by several layers of non-atypical urothelial cells with occasional intercalated mucinous cells. A focus of clear metaplastic cells with perinuclear halo and large, irregular hyperchromatic nuclei (koilocytic atypia) are also seen (hematoxylin and eosin ×800)

## Materials and methods

Specimens received were blocked, fixed in formaldehyde, embedded in paraffin and stained with hematoxylin and eosin. Immunohistochemical studies using the avidin-biotin-peroxidase complex method were also carried out. Tissue sections were incubated with an anti-HPV mouse monoclonal antibody ( K1H8, 1:50 dilution; Dako, USA). PCR amplification of HPV was performed using a commercially available kit ( Master Diagnóstica, Granada, Spain). Appropriate controls were included.

## Case reports

Case 1

A 38-year-old black man from North Africa presented with a reddish verrucous lesion near the penile meatus, which had lasted for many years. He reported having suffered from purulent urethral discharge on many previous occasions. At the time of presentation, he had no other symptoms beyond the verrucous lesion. Genitourinary examination revealed no connection with the urinary tract and no other urinary lesions.

Microscopically, the lesion consisted of a sessile proliferation formed by the attachment of variable-sized papillae (Fig. 1A) composed of slender fibrovascular stalks covered by several layers of slightly enlarged urothelial cells with occasional intercalated mucinous cells (Fig. 1B) and small areas of squamous metaplasia with koilocytic atypia foci without epithelial keratinization.

Case 2

A 53-year-old man presented with a fleshy polypoid tumor on the glans of the penis near the external meatus of 1 month's duration. He had no urinary symptoms or previous medical history. Cystourethroscopy showed no relationship with the meatus and no other urinary tract lesions.

Microscopically, the lesion consisted of a single exophytic proliferation with two different intimately attached architectural growth patterns: a sessile round-bordered papillary structure and a small, slender fibrovascular papillary neoformation (Fig. 2A). The first structure was formed by blunt or fused papillae with acanthosis, epithelial maturation, superficial nuclear atypia with perinuclear halos (koilocytotic atypia) and occasional binucleated forms with minimal nuclear atypia in the lower epithelial layers. The second structure was characterized by slender papillary fronds covered by four to five layers of non-atypical urothelial cells with a relatively complete superficial umbrella cell layer. The papillary cores consisted of loose connective tissue that contained blood vessels and a few mononuclear inflammatory cells (Fig. 2B).

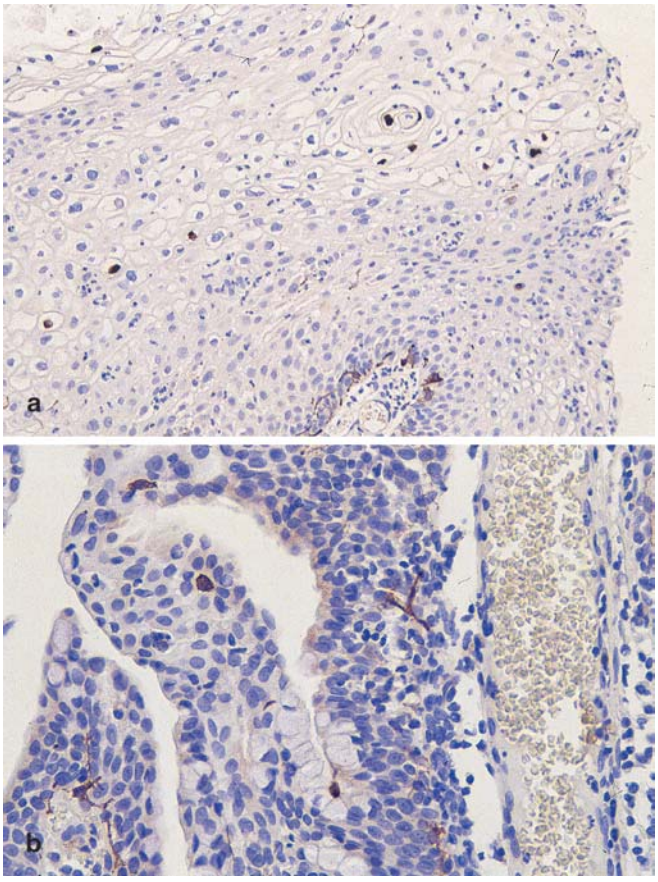



**Fig. 3** **a** Condilomatous area with focal nuclear immunopositivity to human papilloma virus (HPV). **b** Urothelial transitional area with scant nuclear immunopositivity to HPV

Summary

Immunohistochemically, both cases had small foci of nuclear HPV positivity, not only in areas with koilocytic atypia but also in areas of transitional cell epithelial proliferation (Fig. 3A, B). Polymerase chain reaction showed amplification for HPV 6 and 11 in both cases (Fig. 4).

## Discussion

CA of the penis is a venereal disease caused by HPV, most commonly observed between the ages of 20 years and 40 years. It presents as macular, papullar or polypoid lesions in different penis locations, including, in decreasing order of frequency, glans, prepuce, meatus and shaft [11]. CA affects the urethra in 5–25% of men with genital system involvement. The distal urethra is usually the only urethral segment involved, since most lesions affect the urethral meatus. However, extension to the proximal urethra, and rarely to the bladder and ureter, are occasionally observed, even without evidence of external genital lesions [8, 16]. The most common types of HPV found by immunohistochemistry, in situ hybridization, or PCR in both penile and urethral condyloma are 6 and 11 and, less frequently, 16 and 18 [8, 11, 16]. On microscopic examination, there is usually a papillary proliferation of squamous epithelium with hyperkeratosis, koilocytic atypia and a variably prominent inflammatory stromal component [8, 11, 16].

Urethral benign neoplasms of transitional epithelium, as already stated, are extremely rare [8]. Most cases are located in the proximal portion of the urethra, with the exception of fibroepithelial polyps in children, which are usually situated in the distal third of the urethra [8]. Typical transitional cell papilloma of the urethra is exceptional, and only one case has been described [12].

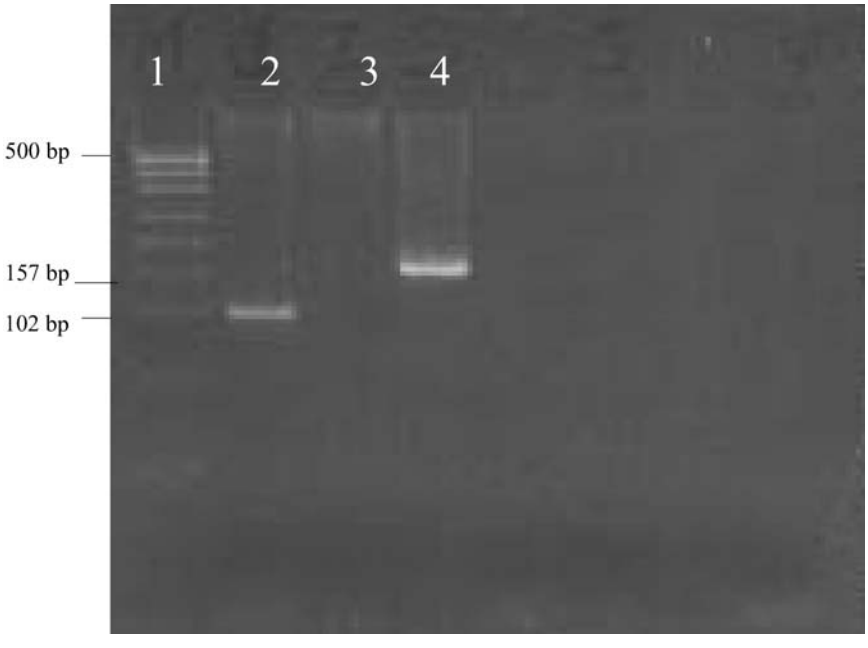



**Fig. 4** Polymerase chain reaction results; *lane 1*: marker; *lane 2*: positive internal control; *lane 3*: negative internal control; *lane 4*: present case, showing positivity to HPV 6/11

Following the criteria of Eble and Young [5], typical transitional cell papilloma is defined as a papillary neoformation composed of layers of polarized non-atypical cells with absence of or very scarce mitotic figures and an intact basement membrane layer on a fibrovascular core. Special attention should be made to distinguish these papillomas from grade-1 papillary transitional cell carcinoma. They have a lower degree of hyperplasia and lack dysplasia [8]. Both our cases fulfilled Eble and Joung criteria to be considered typical transitional cell papillomas.

The only previously reported case of typical transitional cell papilloma [12] occurred in a 48-year-old man who had presented with urethral bloody discharge from the urethral meatus for 3 years. This case was a 3-mm papillomatous lesion in the fossa navicularis arising from the anterior urethra, with no changes in the bladder, posterior urethra, or mucosal glands around the genito-urinary tract. Microscopically, the papillomatous lesion was described as a bladder-tumor-like papilloma with atypia and focus of squamous metaplasia, but without koilocytic dysplasia. Their molecular studies detected HPV type 6 [12].

The present two cases differ from the case reported by Shimiru et al. [12] not only microscopically but also in their location. Our two cases show microscopic features of HPV infection with abundant koilocytic atypical cells, case 1 being a collision lesion formed by the conjunction of a condyloma and a transitional cell papilloma. Moreover, HPV DNA was found by immunohistochemistry in both the transitional and squamous epithelium. Neither of our cases seemed to emerge from the urethral meatus but were located close to it on the glans of the penis. This fact could explain the difference in presentation symptoms: the case reported by Shimiru et al. [12] presented with an intermittent urethral bloody discharge for 3 years, while in both of our cases the patients were asymptomatic.

The association of condyloma of the external or internal genitalia with benign or malignant transitional neoplasms of the urinary tract, although rare, is well known [6, 10]. In situ hybridization and PCR techniques have identified HPV without other microscopic signs of infection in many of these lesions, but the significance of these findings are still unknown. The presence of a transitional cell proliferation associated to koilocytic dysplasia along with demonstration of HPV DNA by immunohistochemical or PCR techniques in both epithelia (transitional and squamous), suggests a similar pathogenetic role for HPV in both lesions. Moreover, the distal urethra, including the fossa navicularis, is usually lined by ciliated stratified columnar or stratified, non-keratinizing squamous epithelia, in continuity with the squamous mucosa of the external meatus. Focal mucous cells are also present within the perimeatal squamous epithelium of the glans [14, 16]. The possible coexistence of both epithelia in the perimeatal area of the glans combined with the presence of lesions due to an HPV infection of the area of epithelial transition, such as the immature papillary metaplasia of the cervix [4, 13, 15], support our suggestion.

In summary, we present for the first time two cases of transitional cell papilloma of the fosa navicularis of the penis with signs of HPV infection.

## References


1. Alonso E, Maróstica A, Roma E, Redín I, Sánchez Mazzaferri F, Toffoni C (1997) Carcinoma transicional papilar de bajo grado, de uretra distal, con diferenciación escamosa focal y asociación con virus papiloma humano, tipos 6–11. Arch Esp Urol 50:875–878
2. Anwar K, Naiki H, Nakakuki K, Inuzuka M (1992) High frequency of human papillomavirus infection in carcinoma of urinary bladder. Cancer 70:1967–1973
3. Boucher NR, Scholefield JH, Anderson JB (1996) The aetiological significance of human papillomavirus in bladder cancer. Br J Urol 78:866–869
4. Crum CP, Egawa K, Fu YS, Lancaster WD, Barron B, Levine RU, Fenoglio CM, Richart RM (1983) Atypical immature metaplasia (AIM). A subset of human papilloma virus infection of the cervix. Cancer 5:2214–2219
5. Eble JN, Young RH (1989) Benign and low-grade papillary lesions of the urinary bladder: a review of the papilloma-papillary carcinoma controversy, and a report of five typical papillomas. Semin Diagn Pathol 6:351–371
6. Grussendorf-Conen EI, Deutz FJ, de Villiers EM (1987) Detection of human papillomavirus-6 in primary carcinoma of the urethra in men. Cancer 60:1832–1835
7. Mevorach RA, Cos LR, di Santägnese PA, Stoler M (1990) Human papillomavirus type 6 in grade I transitional cell carcinoma of the urethra. J Urol 143:126–128
8. Murphy WM, Beckwith JB, Farrow GM (1994) Tumors of the urinary bladder. In: Murphy WM, Beckwith JB, Farrow GM (eds) Atlas of pathology. Tumors of the kidney, bladder, and related urinary structures, third series. AFIP, Washington, pp 193–313
9. Mvula M, Iwasaka T, Iguchi A, Nakamura S, Masaki Z, Sugimori H (1996) Do human papillomaviruses have a role in the pathogenesis of bladder carcinoma? J Urol 155:471–474
10. Olsen S, Marcussen N, Jensen KM, Lindeberg H (1995) Urethral condylomata, due to human papilloma virus (HPV) type 6/11, associated with transitional cell tumors in the bladder and ureter. A case report. Scand J Urol Nephrol Suppl 172:51–55
11. Rosai J (1996) Ackerman's surgical pathology, vol 1. Mosby, St Louis, pp 1059–1318
12. Shimizu N, Ichinose Y, Shimo M, Sano T, Nakajima T, Yamanaka H (1998) Transitional cell papilloma in the fossa navicularis is positive for human papilomavirus. Int J Urol 5:296–298
13. Trivijitsilp P, Mosher R, Sheets EE, Sun D, Crum CP (1998) Papillary immature metaplasia (immature condyloma) of the cervix: a comparison with papillary squamous carcinoma. Hum Pathol 29:641–648
14. Val-Bernal JF, Hernández-Nieto E (2000) Benign mucinous metaplasia of the penis. A lesion resembling extramammary Paget's disease. J Cutan Pathol 27:76–79
15. Ward BE, Saleh AM, Williams JV, Zitz JC, Crum CP (1992) Papillary immature metaplasia of the cervix: a distinct subset of exophytic cervical condyloma associated with HPV-6/11 nucleic acids. Mod Pathol 5:391–395
16. Young RH, Srigley JR, Amin MB, Ulbright TM, Cubilla AL (2000) The male urethra. In: Young RH, Srigley JR, Amin MB, Ulbright TM, Cubilla AL (eds) Atlas of tumor pathology. Tumors of the prostate gland, seminal vesicles, male urethra, and penis, third series. AFIP, Washington, pp 367–489

Virchows Arch (2003) 442:605–610
DOI 10.1007/s00428-003-0807-1

CASE REPORT

**Pellegrino Crafa · Massimo Milione · Cinzia Azzoni · Francesco Paolo Pilato · Silvia Pizzi · Cesare Bordi**

# Pleomorph poorly differentiated endocrine carcinoma of the rectum

Received: 30 October 2002 / Accepted: 12 February 2003 / Published online: 7 May 2003
© Springer-Verlag 2003

**Abstract** We present a case of poorly differentiated endocrine carcinoma (PDEC) of the rectum identified immunohistochemically and characterized by a high degree of cellular pleomorphism, including bizarre giant cells. This case indicates that gastrointestinal PDECs are not restricted to small cell carcinomas. Among the multiple genes investigated, loss of heterozygosity (LOH) of the p53 locus without p53 immohistochemical accumulation, overexpression of c-kit and absent expression of p16 were seen.

**Keywords** Rectum · Poorly differentiated endocrine carcinoma · Pleomorph tumor

## Introduction

In the recently released World Health Organization classification of gastroenteropancreatic (GEP) endocrine tumors [10], poorly differentiated endocrine carcinomas (PDECs) constituted a distinct category—separated from the other two main categories (i.e. well-differentiated endocrine tumors and well-differentiated endocrine carcinomas) because of distinctive histological features and a highly aggressive clinical behavior with poor prognosis (for a recent review of colo–rectal PDECs see [4]). In previous publications, however, PDEC is regarded as a synonym of small-cell carcinoma in every GEP region considered, although occasionally intermediate cells are also mentioned in accordance with the established nomenclature adopted for lung PDEC.

In this report we describe a case of PDEC of the rectum represented by an anaplastic carcinoma with high degree of cellular pleomorphism, including bizarre giant cells. The endocrine phenotype of this tumor, unrecognizable on the basis of conventional histology, was revealed by immunohistochemistry using a panel of neuroendocrine markers. This unexpected observation indicates that PDEC of the GEP system may also include tumors with non-small-cell, pleomorph appearance that were likely unrecognized in the past and classified as non-endocrine carcinomas.

P. Crafa · M. Milione · C. Azzoni · F. P. Pilato · S. Pizzi · C. Bordi (✉)
Department of Pathology and Laboratory Medicine, Section of Anatomic Pathology, University of Parma, 43100 Parma, Italy
e-mail: cesare.bordi@unipr.it
Tel.: +39-0521-290386
Fax: +39-0521-292710

## Clinical history

A 74-year-old male patient presenting with constipation, rectal bleeding and body weight loss of 5 kg in 4 months was admitted to the hospital. Laboratory data were unremarkable except for elevated circulating levels of neuron-specific enolase (28.65 $\mu$g/l; normal value, <13 $\mu$g/l) and serological evidence of hepatitis B virus infection. Endoscopy performed at another institution revealed a stenosing, ulcerated rectal tumor that was diagnosed as adenocarcinoma on biopsy specimens. Revision of the slides did not allow for further characterization because of insufficient material and mechanical artifacts. Multiple metastatic nodules were found in the lung and liver by diagnostic imaging procedures. A preoperative X-ray therapy with a total dose of 40 Gy (250 eGy/day for 4 weeks) was done. A palliative left proctocolectomy was performed. In addition, a liver biopsy showing a metastatic nodule 0.5 cm in size was removed. The patient refused post-operative chemotherapy and was treated with long-acting somatostatin analogues without apparent response. Six months later, after presenting with persistent severe diarrhea and progressively worsening jaundice, the patient died. No autopsy was performed.

## Materials and methods

The surgical specimen included sigmoid colon and rectum. An ulcerated tumor was found at a distance of 0.5 cm from the distal resection margin, which was tumor free. It measured 3.5 cm in its

largest diameter and infiltrated the rectal wall up to the perirectal adipose tissue, in which 19 lymph nodes were isolated. The liver metastasis was also examined.

The tissue was fixed in 10% buffered formalin and embedded in paraffin. Sections were stained with hematoxylin and eosin (H&E) and periodic acid-Schiff stain. The antibodies employed for immunohistochemistry and the relevant working dilutions are reported in Table 1. The immunostaining was visualized using ABC/peroxidase method followed by hematoxylin counterstaining.

As a part of a larger study on gastrointestinal PDEC, loss of heterozygosity (LOH) analysis was performed after DNA extraction from microdissected areas of the patient's formalin-fixed, paraffin-embedded tumor (primary and metastatic), and normal tissue and polymerase chain reaction (PCR) amplification as previously reported [2]. The following polymorphic microsatellite markers were employed: D3S1481 in 3p14.2 (FHIT); D3S1478 in 3p21.3; PYGM, D11S4946, D11S913 in 11q13 (MEN-1); TP53.PCR15 in 17p13.1 (p53); D18S61 in 18q23 (DCC, Smad4/DPC4, Smad2).

## Results

### Histological findings

In H&E preparation, the primary tumor was composed of irregular sheets, clusters or discrete, scattered tumor cells extensively infiltrating the submucosa, the bundles of the muscularis propria and the perirectal adipose tissue. The tumor cells showed a considerable degree of cellular pleomorphism with frequent occurrence of large, bizarre nuclei. They were mostly large with well-represented, polygonal, eosinophilic cytoplasm and round, large, clear nuclei often showing conspicuous nucleoli (Fig. 1A). Interspersed small tumor cells were infrequent and confined to peripheral areas. Focal necrosis was occasionally present. The tumor findings were in no way reminiscent of the established histological features of GEP endocrine neoplasms. Nodal and perinodal metastases were found in 8 of 19 lymph nodes examined. In different nodes, either the same histological features of the primary tumor or a histological pattern characterized by large clusters of poorly differentiated cells of intermediate size with extensive central necrosis (Fig. 2A), more consistent with that usually found in PDEC, were observed. The liver metastasis was composed of clusters and broad trabeculae of large cells similar to those of the primary tumor (Fig. 2B) but pleomorph changes were virtually absent. Several foci of tumor cell necrosis were

**Table 1** Characteristics of the antibodies used in the present study and immunohistochemical results in primary tumor and metastases. *M* monoclonal, *P* polyclonal, *NSE* neurone-specific enolase, *PGP 9.5* protein gene product 9.5, *Map 18* microtubule-associated protein 2a, b, c Ab-3, *Leu 7* human natural killer cell-like, *α-hCG* alpha subunit of human chorionic gonadotropin, *β-hCG* beta subunit of human chorionic gonadotropin, *HMB 45* melanoma cells, *Rb* human retinoblastoma gene product, *FHIT* fragile histidine triad

| Antibodies | | | Results | | |
|---|---|---|---|---|---|
| Antigens (Antibody type) | Source (Code number) | Working Dilution | Primary Tumor | Lymph node Metastasis | Liver Metastasis |
| Chromogranin A (M) | BioGenex (LK2H10) | 1:250 | 1–5% | Neg | Neg |
| Synaptophysin (P) | Dako (1566) | 1:50 | 100% | 100% | 100% |
| NSE (M) | Dako (M0873) | 1:150 | 100% | 100% | 100% |
| PGP 9.5 (M) | Novocastra (10A1) | 1:20 | 10% (focal) | 100% | 100% |
| LEU 7 (M) | Dako (M1014) | 1:50 | Rare cells | Neg | Neg |
| MAP 18 (M) | NeoMarkers (AP18) | 1:50 | 100% | 100% | 100% |
| α-hCG (M) | Prof. S. Ghielmi, Brescia (5E8) | 1:100 | Rare cells | | Neg |
| β-hCG (P) | Dako (A231) | 1:100 | Rare cells | | |
| Cytokeratin 7 (M) | NeoMarkers (K72.7) | 1:15 | Neg | Neg | Neg |
| Cytokeratin 8 (M) | Dako (M0631) | 1:50 | 30% | | 10% |
| Cytokeratin 18 (M) | Dako (M 7010) | 1:25 | 80% | 80% | 80% |
| Cytokeratin 19 (M) | Dako (M 0888) | 1:50 | Neg | Neg | 10% (focal) |
| Cytokeratins AE1\AE3 (M) | Dako (M3515) | 1:50 | 80% | | |
| S-100 (M) | BioGenex (058 M) | 1:400 | Neg | | |
| CD 34 (M) | BioGenex (236 M) | 01:20 | Neg | | |
| HMB45 (M) | Immunotech (1142) | Prediluted | Neg | | |
| p53 (M) | Dako (M7001) | 1:25 | Neg | | Neg |
| p21WAF1(M) | NeoMarkers (DCS602) | 1:10 | 10% (discrete cells) | | |
| p27KIP1(M) | Dako (7203) | 1:50 | 30% | | Neg |
| p16INK4a (M) | NeoMarkers (M7203) | 1:10 | Neg | | Neg |
| Rb (M) | Dako (M7131) | 1:50 | 80% | 80–100% | 40% |
| c-kit / CD117 (P) | Dako (A4502) | 1:100 | 100% | 100% | 100% |
| ki-67 / Mib-1 (M) | Dako (M7240) | 1:50 | 20% | 30–40% | 50% |
| FHIT (P) | Zymed (2R44) | 1:50 | 100% | 100% | 100% |
| Vimentin (M) | Dako (M0725) | 1:50 | 5% (focal) | 5% (focal) | 5% (focal) |
| Desmin (M) | Dako (M0760) | 1:100 | Neg | Neg | Neg |
| Actin (M) | Dako (M0874) | 1:80 | Neg | Neg | Neg |
| Actin smooth muscle (M) | BioGenex (128m) | 01:40 | Neg | Neg | Neg |

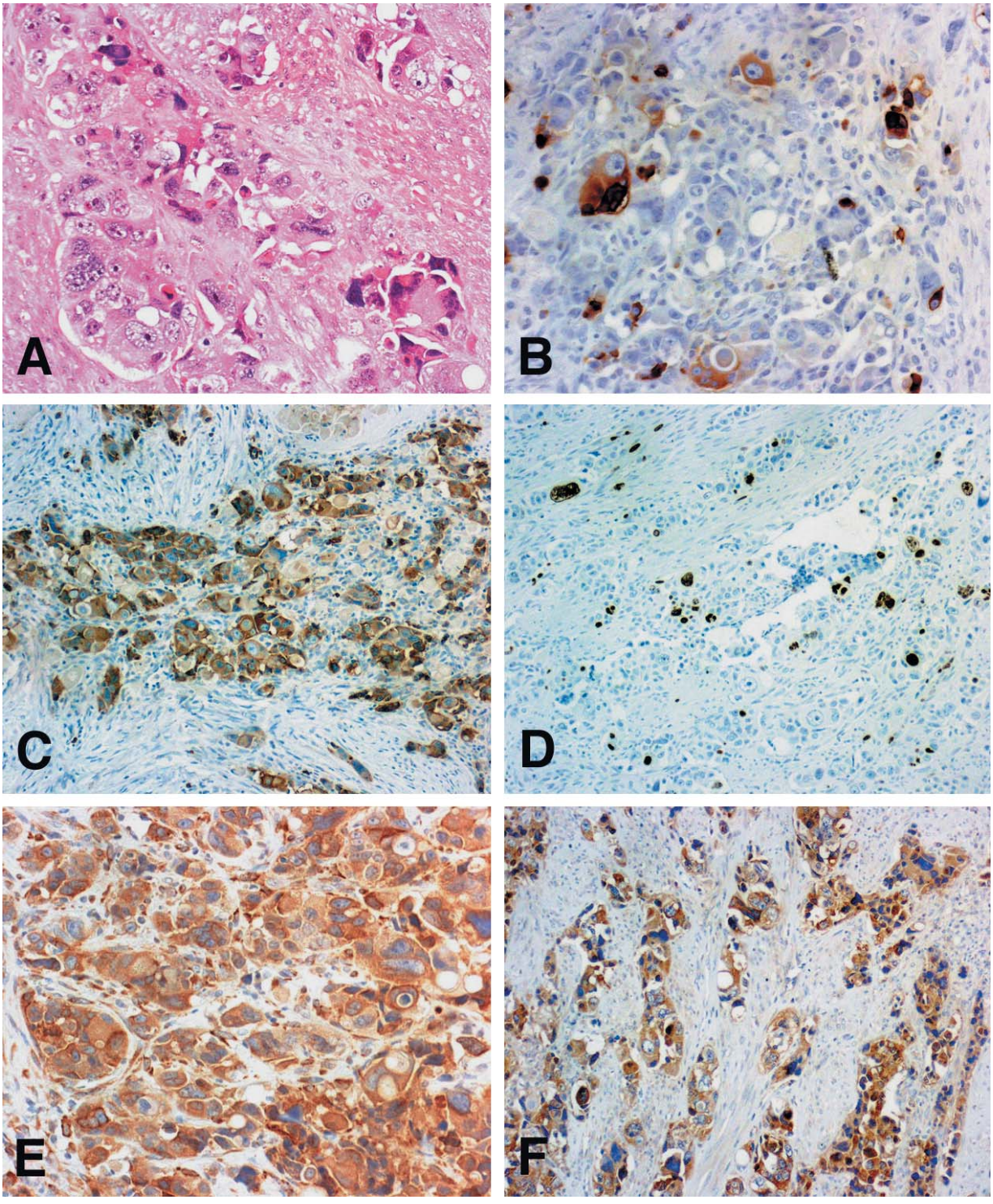



**Fig. 1** Primary tumor. **A** Histological features of the tumor with clusters of large cells with markedly pleomorph nuclei and prominent nucleoli (hematoxylin and eosin). **B** Chromogranin A immunostaining in numerous scattered cells, including the bizarre, pleomorph ones. **C** Diffuse, heavy expression of synaptophysin. **D** Ki 67 immunolabeling of scattered nuclei including those showing pleomorph appearance. **E** Diffuse expression of c-kit showing both membrane and cytoplasmic patterns of immunostaining. **F** Diffuse cytoplasmic immunostaining of tumor cells for the FHIT protein

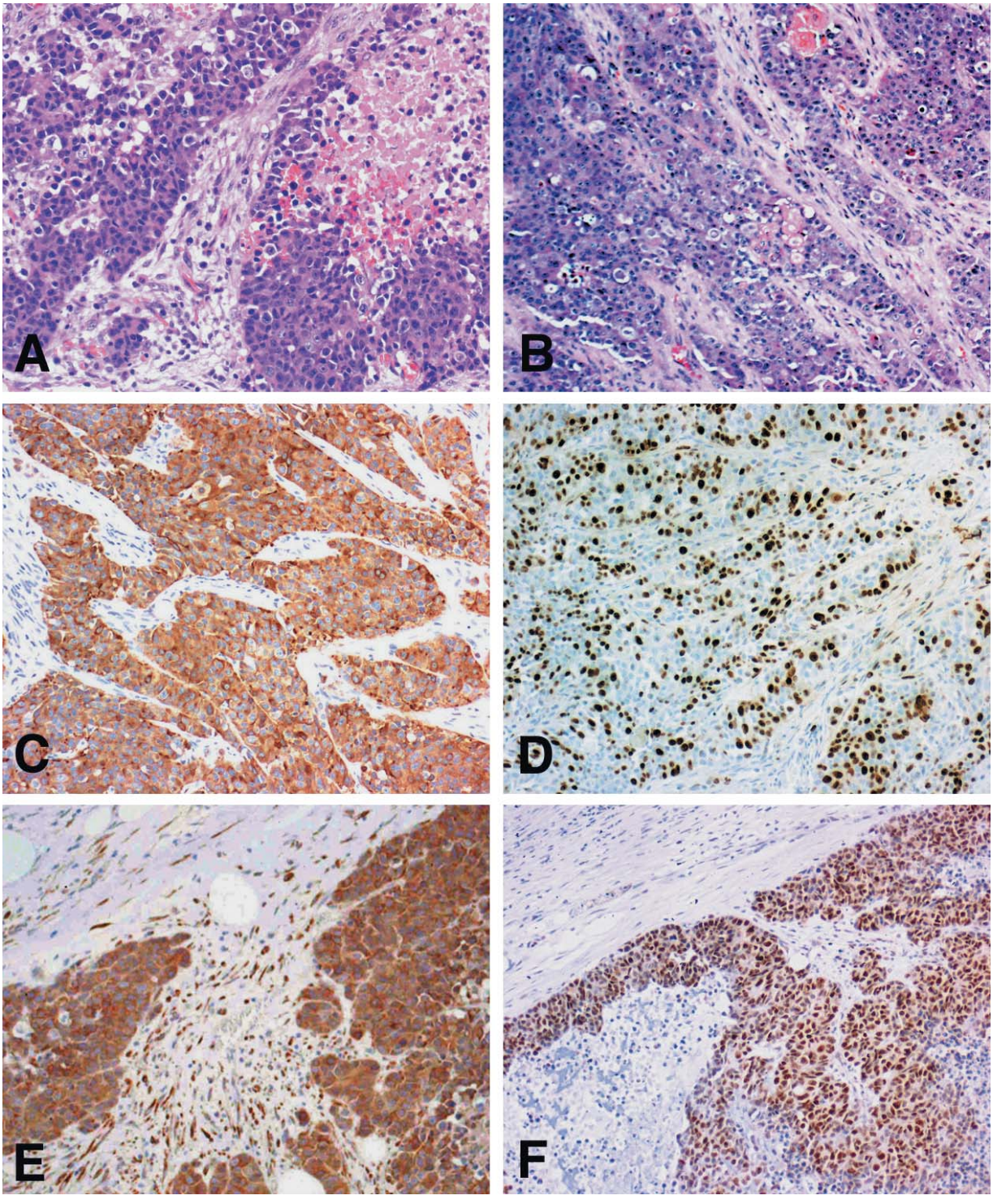



**Fig. 2** **A** Histological appearance of a lymph-node metastasis with large solid clusters of medium-size cells showing extensive central necrosis (hematoxylin and eosin). **B** Histological appearance of a liver metastasis with broad trabeculae of large tumor cells without apparent pleomorphism (hematoxylin and eosin). **C** Pronounced synaptophysin expression by tumor cells of liver metastasis. **D** Extensive Ki67 immunolabeling in liver metastasis. **E** Diffuse c-kit immunoreactivity in cells of a lymph-node metastasis. **F** Intense, diffuse nuclear immunolabeling for the Rb protein in a lymph-node metastasis

found. In both primary and metastatic sites, the tumor appeared to elicit a pronounced stromal proliferation.

### Immunohistochemical findings

The results of the immunohistochemical analyses are reported in Table 1. The epithelial nature of the tumor cells was proved by the cytokeratin immunoreactivity and the negative reaction for all non-epithelial markers investigated except for a minor population of vimentin-expressing cells. Among neuroendocrine markers, chromogranin A was found to be expressed by discrete cells, including the large pleomorph cells, varying from 1% to 5% of tumor cells in different areas of the primary tumor (Fig. 1B). Paradoxically, it was not expressed in the lymph-node metastatic tissue histologically more consistent with an endocrine nature or in liver metastasis. In contrast, synaptophysin (Fig. 1C and Fig. 2C) and Map 18 were expressed by virtually all cells in both primary and metastatic sites. PGP 9.5 was expressed by several focal groups of cells whereas only rare cells were positive for Leu-7, $\alpha$- and $\beta$-human chorionic gonadotrophin (hCG). Both primary and metastatic tumor cells expressed cytokeratins 8 and 18 but not cytokeratin 7, a pattern consistent with that of either ordinary colonic adenocarcinomas or carcinoid tumors [5]. The Ki-67 proliferation index ranged from 20% in the primary tumor (with frequently labeled pleomorph nuclei) (Fig. 1D) to 50% in nodal and liver metastasis (Fig. 2D). Among other proteins tested, it is worth noting the extensive expression of c-kit (Fig. 1E and Fig. 2E), FHIT (Fig. 1F) and Rb (Fig. 2F) and the lack of p53 and of p16 immunoreactivity as well as the lack of expression of muscular antigens.

### LOH analysis

Despite the lack of p53 immunohistochemical expression, LOH was found at the p53 gene locus at 17p13.1. In contrast, no allelic deletions were found at the locus of the MEN-1 gene at 11q13 (including the intragenic marker D11S4946), at 18q23 and at the locus of the FHIT gene in 3p14.2. The latter result is in full agreement with the diffuse expression of FHIT shown immunohistochemically.

## Discussion

This report describes a case of a poorly differentiated epithelial tumor of the rectum composed of large cells with marked cellular pleomorphism. Although such morphological features are at odds with those currently defined as diagnostic for gastrointestinal PDEC [10], a neuroendocrine phenotype was demonstrated immunohistochemically by a panel of neuroendocrine markers. The ominous course of our patient's disease is in full agreement with what is usually presented by PDEC [4].

The novel information provided by our case, therefore, is that gastrointestinal PDECs are not limited to small cell carcinomas and that a marked cellular pleomorphism may be consistent with an endocrine phenotype of the tumor. It is likely that tumors with similar histological features were previously classified as non-endocrine anaplastic carcinomas, thus inferring that the frequency of gastrointestinal PDEC is higher than that reported based on diagnosis using traditional histological criteria.

A case of sarcomatoid carcinoma of the ano-rectal junction with neuroendocrine and rhabdomyoblastic characteristics has been described [7]. Although some morphological features of the latter case, including the appearance of neuroendocrine cells and the occurrence of large bizarre cells, were similar to those of the present case, the tumor cells of our patient did not express the muscular antigens desmin, sarcomeric and smooth muscle actins by means of immunohistochemistry.

The significance of pleomorph changes in the present endocrine tumor remains obscure. Whether they are related to the radiation treatment of the tumor performed before surgery requires confirmation in further cases undergoing the same treatment protocol.

No immunohistochemical expression of p53 was found in tumor cells. Although such expression has been reported as a common feature of gastrointestinal PDECs [10], it has been found to be absent in 4 of 16 PDECs in one study [6] and in 5 of 11 in another [1]. The concomitant demonstration of p53 LOH may, however, indicate altered gene function even in the absence of immunodetectable intranuclear accumulation of the mutated protein.

On the basis of our combined immunohistochemical and LOH approach, no evidence for alterations in genes known to be affected in foregut endocrine tumors (such as MEN-1 gene) [2] or in lung PDEC (such as FHIT or Rb) [9] was found in the present case. In contrast, the altered expression of p16 in our patient is consistent with the findings of lung PDEC [9].

An interesting, unexpected finding of the present case was the diffuse tumor expression of c-kit (CD117) suggesting activation of the KIT tyrosine kinase. c-Kit was found to be expressed in most cells and cell lines of small cell lung cancer [8]. Although expression of c-kit does not necessarily imply tumor cell response [8], it is worth noting that advanced gastrointestinal stromal tumors (GISTs) that express CD117 effectively respond to the treatment with the inhibitor of the KIT tyrosine kinase imatinib mesylate (Glivec) [3].

**Acknowledgements** This work was supported by grants from the Italian Association for Cancer Research (AIRC), Milan and the Italian Ministry for University and Scientific and Technological Research (MURST) (COFIN 2001–2001062472) and the Italian Ministry of Health (grant number ICS060.2/RF00–57).

## References


1. Canavese G, Azzoni C, Pizzi S, Corleto VD, Pasquali C, Davoli C, Crafa P, Delle Fave G, Bordi C (2001) p27: a potential main inhibitor of cell proliferation in digestive endocrine tumors but not a marker of benign behavior. Hum Pathol 32:1094–1101
2. D'Adda T, Pizzi S, Azzoni C, Bottarelli L, Crafa P, Pasquali C, Davoli C, Corleto VD, Delle Fave G, Bordi C (2002) Different patterns of 11q allelic losses in digestive endocrine tumors. Hum Pathol 33:322–329
3. Demetri GD, von Mehren M, Blanke CD, Van den Abbeele AD, Eisenberg B, Roberts PJ, Heinrich MC, Tuveson DA, Singer S, Janicek M, Fletcher JA, Silverman SG, Silberman SL, Capdeville R, Kiese B, Peng B, Dimitrijevic S, Druker BJ, Corless C, Fletcher CDM, Joensuu H (2002) Efficacy and safety of imatinib mesylate in advanced gastrointestinal stromal tumors. N Engl J Med 347:472–480
4. Grabowski P, Schonfelder J, Ahnert Hilger G, Foss HD, Heine B, Schindler I, Stein H, Berger G, Zeitz M, Scherubl H (2002) Expression of neuroendocrine markers: a signature of human undifferentiated carcinoma of the colon and rectum. Virchows Arch 441:256–263
5. Miettinen M (1993) Keratin immunohistochemistry: update of applications and pitfalls. Pathol Annu 28:113–143
6. Rindi G, Azzoni C, La Rosa S, Klersy C, Paolotti D, Rappel S, Stolte M, Capella C, Bordi C, Solcia E (1999) ECL cell tumor and poorly differentiated endocrine carcinoma of the stomach: prognostic evaluation by pathological analysis. Gastroenterology 116:532–542
7. Roncaroli F, Montironi R, Feliciotti F, Losi L, Eusebi V (1995) Sarcomatoid carcinoma of the anorectal junction with neuroendocrine and rhabdomyoblastic features. Am J Surg Pathol 19:217–223
8. Savage DG, Antman KH (2002) Drug therapy: imatinib mesylate—a new oral targeted therapy. N Engl J Med 346:683–693
9. Sekido Y, Fong KM, Minna JD (1998) Progress in understanding the molecular pathogenesis of human lung cancer. Biochim Biophys Acta 1378:F21–F59
10. Solcia E, Klöppel G, Sobin LH (2000) Histological typing of endocrine tumours, 2nd edn. Springer, Berlin Heidelberg New York

Virchows Arch (2003) 442:611–613
DOI 10.1007/s00428-003-0789-z

LETTER TO THE EDITOR

**Akira Ogose · Hajime Umezu · Koji Nikkuni · Takaaki Urakawa · Tetsuo Hotta**

# Anaplastic lymphoma kinase negative sarcomatoid variant of anaplastic large-cell lymphoma presenting as a malignant fibrous histiocytoma

Received: 5 December 2002 / Accepted: 7 February 2003 / Published online: 5 April 2003
© Springer-Verlag 2003

It has been reported that 25–60% of anaplastic large cell lymphomas (ALCL) carry the t(2;5)(p23;q35) translocation that results in the production of a novel chimeric protein anaplastic lymphoma kinase (ALK). Because ALK-positive ALCL has a more favorable prognosis than ALK-negative ALCL, recent investigations have suggested subclassification of ALCL according to ALK expression [1]. The sarcomatoid variant of ALCL is an extremely rare condition, which is easily misdiagnosed as high-grade sarcoma [2]. The ALK expression of sarcomatoid lymphoma has seldom been assessed. We report a case of sarcomatoid ALCL presented as malignant fibrous histiocytoma with evaluation of ALK expression.

A 51-year-old man presented at another hospital with a 2-month history of an enlarging superficial mass in his left groin. The diagnosis based on biopsy results was high-grade sarcoma, probably a myxoid malignant fibrous histiocytoma. The patient was referred to our hospital. Physical examination revealed a soft, ulcerated, infected, immobile tumor which bled easily measuring 23×23 cm in the left groin (Fig. 1). Bacterial cultures of the tumor demonstrated more than ten types of Gram-positive and Gram-negative bacteria. Magnetic resonance imaging



**Fig. 1** Photograph showing a large, soft, easily bleeding tumor of the left groin

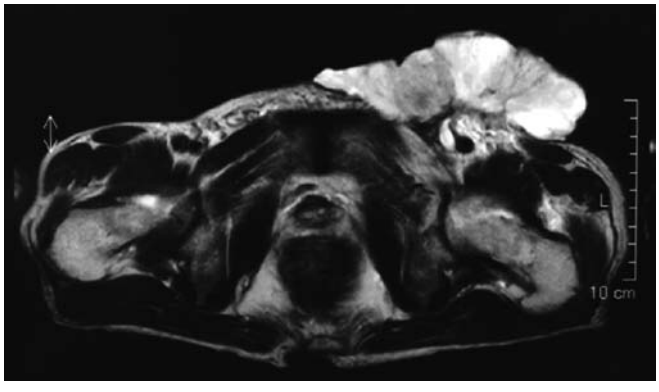



**Fig. 2** T2-weighted magnetic resonance image showing a huge extruded tumoral mass invading the surrounding femoral vessels

A. Ogose (✉) · T. Urakawa · T. Hotta
Division of Orthopedic Surgery,
Graduate School of Medical and Dental Sciences,
Niigata University,
Asahimachi 1-751, 951-8510 Niigata, Japan
e-mail: aogose@med.niigata-u.ac.jp
Tel.: +81-25-2272272
Fax: +81-25-2270782

H. Umezu
Division of Pathology,
Niigata University Hospital,
Niigata, Japan

K. Nikkuni
Division of Hematology,
Graduate School of Medical and Dental Sciences,
Niigata University,
Asahimachi 1-751, 951-8510 Niigata, Japan

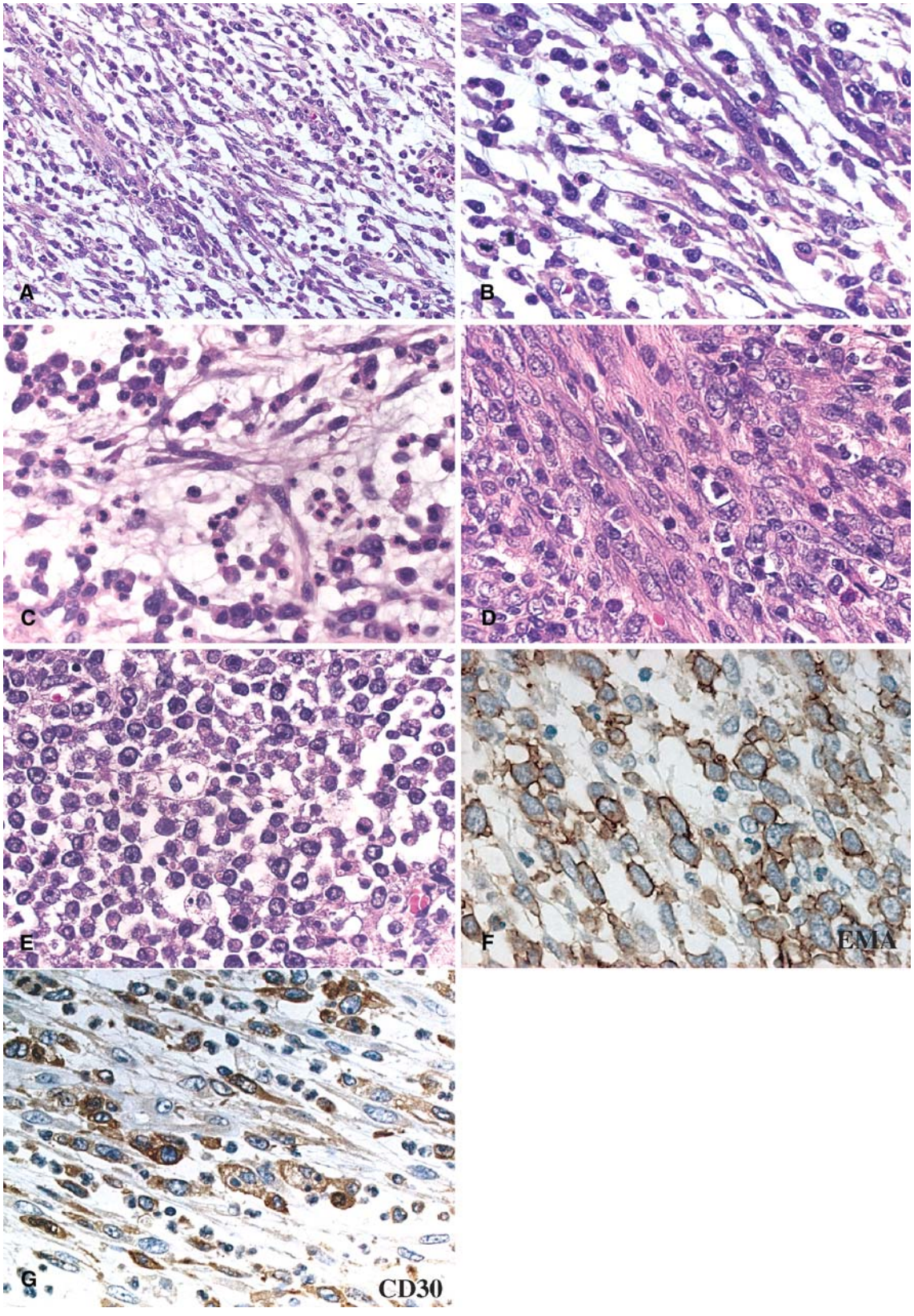



**Fig. 3** Sarcomatoid variant of anaplastic large cell lymphoma. **A** Low-power view of spindle-shaped tumor cells with loose background; ×150. **B** High-power view of elongated tumor cells with loose stroma; ×400. **C** High-power view of oval to spindle-shaped tumor cells with myxoid stroma and numerous inflammatory cells; ×400. **D** High-power view of linear spindle cell arrangement; ×400. **E** High-power view of oval to round tumor cells grew in a patternless fashion; ×400. **F** Membranous immonoreactivity for EMA; ×400. **G** Diffuse immonoreactivity for CD30; ×400

showed a huge extruded tumoral mass invading the surrounding femoral vessels (Fig. 2). No neurological or vascular problems were evident in the left lower extremity. Four days after admission to our hospital the tumor had produced more than 500 ml blood. Tumor resection was performed followed by coverage with the fascia lata myocutaneous flap and mesh skin graft, which preserved the femoral vessels and the nerve.

Histologically, the resected tumor was highly cellular and displayed alternating myxoid and solid patterns. In the myxoid areas the tumor was composed of spindle to stellate shaped cells with myxoid background; additionally, infiltrations of small lymphocytes and granulocytes were observed. A concentration of tumor cells was present around the blood vessels (Fig. 3A–C). In the solid areas, oval-to-round tumor cells grew in a patternless fashion. The tumor cells possessed coarse vesicular chromatin, prominent nucleoli and eosinophilic cytoplasm. Several foci characterized by linear spindle-cell arrangement were apparent (Fig. 3D, E).

Immunohistochemical studies initially revealed diffusely positive reactivity with vimentin and epithelial membrane antigen (EMA; Fig. 3F); additionally, these tests demonstrated negative reactivity with AE1/AE3, CAM 5.2, S100 protein, HMB-45, CD34, CD99, HHF35, Leu7, and L26. Leukocyte common antigen and UCHL-1 were focally positive. Additional immunohistochemical workup indicated that the tumor cells were strongly and diffusely positive for CD30 (Fig. 3G); however, the cells were negative for ALK. The diagnosis was ALCL. Subsequent to pathological diagnosis of ALCL the patient underwent a staging procedure which revealed swelling of the left supraclavicular, paraaortic, right common iliac, left common iliac, and left inguinal lymph nodes. A chemotherapy regimen was implemented including cyclophosphamide, vincristine, bleomycine, etoposide, doxorubicin, and predonisolone. Chemotherapy achieved complete remission; moreover, the patient remains free of disease 14 months after surgery.

ALCL is defined largely immunohistochemically by its expression of CD30 (Ki-1 antigen). The sarcomatoid variant of ALCL is rare; moreover, only several cases have been reported [1, 2, 3, 4, 5]. Due to the presence of myxoid areas and spindle-shaped tumor cells ALCL is frequently misdiagnosed as myxoid sarcoma, i.e., malignant fibrous histiocytoma. Immunohistochemical findings may be a further point of confusion since this tumor can react positively with vimentine, EMA and $\alpha$-smooth muscle actin whereas reactivity may be negative or weak with respect to leukocyte common antigen [1, 2, 3, 4, 5]. Strong CD30 positivity in the majority of the neoplastic cells is the most important diagnostic feature.

It has been suggested to subclassify ALCL according to ALK expression, with distinct clinical and prognostic features between positive and negative cases. ALK-positive cases usually occur within the first three decades of life; moreover, favorable prognosis is observed. ALK-negative cases occur in older individuals; moreover, this situation displays poorer prognosis in comparison to ALK-positive cases [1]. In the sarcomatoid variant of ALCL, an instance of ALK-negative disease was recently described in an elderly woman (similar to the present case) [1]. However, ALK-positive ALCL with sarcomatoid features was recently documented in a 6-year-old girl [5]. Sarcomatoid features may not be correlated with ALK expression. Due to its rarity the prognosis of sarcomatoid ALCL is not well known. We found six examples of sarcomatoid ALCL with available follow-up data in the literature (including the present case) [1, 2, 3, 4, 5]. Among these six cases one received no chemotherapy and died of disease as a consequence of delayed diagnosis; the remaining five patients underwent multidrug chemotherapy. Among the latter five patients complete response and partial response were achieved in three and one case, respectively. Progressive disease was evident in the final patient. This case indicates that ALCL should be considered when a spindle-cell tumor with myxoid stroma arising from a lymph node rich lesion is encountered.

## References


1. Pereira EM, Maeda SA, Reis-Filho JS (2002) Sarcomatoid variant of anaplastic large cell lymphoma mimicking a primary breast cancer. A challenging diagnosis. Arch Pathol Lab Med 126:723–726
2. Chan JKC, Buchanan R, Fletcher CDM (1990) Sarcomatoid variant of anaplastic large-cell Ki-1 lymphoma. Am J Surg Pathol 14:983–988
3. Dusenbery D, Jones DB, Sapp KW, Lemons FM (1993) Cytologic findings in the sarcomatoid variant of large cell anaplastic (Ki-1) lymphoma. A case report. Acta Cytol 37:508–514
4. Buseo-Ramos CE, Pugh WC, Butler JJ (1994) Anaplastic large cell lymphoma presenting as a soft-tissue mass mimicking sarcoma. Mod Pathol 7:497–500
5. Suzuki R, Seto M, Nakamura S, Nakagawa A, Hara K, Takeuchi K (2001) Sarcomatoid variant of anaplastic large cell lymphoma with cytoplasmic ALK and $\alpha$-smooth muscle actin expression: a mimic of inflammatory myofibroblastic tumor. Am J Pathol 159:383–384

Virchows Arch (2003) 442:614–616
DOI 10.1007/s00428-003-0826-y

LETTER TO THE EDITOR

**Takahide Kodama · Kaori Kameyama · Makio Mukai · Hitoshi Sugiura · Tadashi Ikeda · Yasunori Okada**

# Invasive lobular carcinoma arising in phyllodes tumor of the breast

Received: 8 April 2003 / Accepted: 9 April 2003 / Published online: 13 May 2003
© Springer-Verlag 2003

Phyllodes tumor is an uncommon breast tumor that accounts for less than 1% of all breast tumors [10]. The tumors are usually benign, but they may undergo malignant transformation, which usually occurs in the stromal component of the tumors. Although malignant transformation of the epithelial component of phyllodes tumors of the breast is extremely rare, it has been reported in several cases of ductal carcinoma in situ, infiltrating ductal carcinoma, and lobular carcinoma in situ [1, 5, 6, 7, 11]. We report the first case of infiltrating lobular carcinoma arising in phyllodes tumor of the breast.

A 47-year-old Japanese woman was referred to the Keio University Hospital in July 1993 because of a painless mass in her right breast that the patient had first noticed 10 years previously. Her past history was uneventful, and her family history was unremarkable. Ultrasonography of the tumor showed a huge, low-echoic lesion without calcification, and a mammogram revealed a homogeneous, well-circumscribed mass. Physical and radiological examinations of her left breast for neoplastic lesions were unremarkable. Based on these findings, the preoperative diagnosis was benign phyllodes tumor. In August 1995, right subcutaneous mastectomy was performed, and no evidence of recurrence or metastasis has been detected during the 9 years since the operation.

T. Kodama · Y. Okada
Department of Pathology, Keio University School of Medicine, Tokyo, Japan

H. Sugiura
Department of Clinical Pathology and Laboratory Medicine, Kawasaki Municipal Hospital, Kawasaki, Japan

K. Kameyama (✉) · M. Mukai
Division of Diagnostic Pathology, Keio University Hospital, 35 Shinanomachi Shinjuku-ku, 160-8582 Tokyo, Japan
e-mail: kameyama@sc.itc.keio.ac.jp
Tel.: +81-3-53633843, Fax: +81-3-53633644

T. Ikeda
Department of Surgery, Keio University Hospital, Tokyo, Japan

After macroscopic examination of the resected tumor, it was fixed in 10% formalin. Paraffin sections were prepared and stained with hematoxylin and eosin and with Schiff's solution and hematoxylin for periodic acid–Schiff (PAS) staining. Sections were immunostained according to the avidin-biotin peroxidase method with anti-cytokeratin AE1/AE3 antibody (Dako Japan, Tokyo; 1:100 dilution), anti-estrogen receptor antibody (Dako Japan; 1:100 dilution), and anti-progesterone receptor antibody (Dako Japan; 1:50 dilution).

Macroscopic inspection revealed a grayish-white, elastic, firm mass 17×16×8.5 cm in size. The tumor was not encapsulated, but its margin was well defined. The tumor was composed of lobulated nodules of various size and cystic areas (Fig. 1A). No satellite neoplastic lesion was found in the surrounding tissue. Microscopically, the tumor had a very heterogeneous appearance and was characterized by combined proliferation of ductal epithelium and stromal cells. At low magnification, the tumor exhibited a phyllodes pattern, i.e., slit-like ductal structures lined mainly by pseudo-stratified or columnar epithelial cells (Fig. 1B), but some areas of the tumor consisted of fibrous and myxoid stroma, and most of the stromal component exhibited high proliferative activity. Phyllodes tumors must be differentiated from giant fibroadenomas, and these findings indicated that the tumor was not a giant fibroadenoma. The stromal component was composed of collagen fibers and fibroblast-like stromal cells without atypia or mitoses, indicating that the stromal component was benign. The epithelial cells lining the ductal structures also displayed benign features in most areas; however, small epithelial cells with large nuclei were observed in the epithelial component of the lobulated clefts. These atypical cells had formed solid islands of tumor cells, which frequently spread to the ductal epithelium (Pagetoid spread), and thus the lesion was diagnosed as lobular carcinoma in situ (Fig. 1C, D). The carcinoma cells were PAS-positive (data not shown), and, although they were mainly confined to the ducts, they had also invaded the stroma of the tumor (Fig. 1E), where an "Indian-file" pattern was

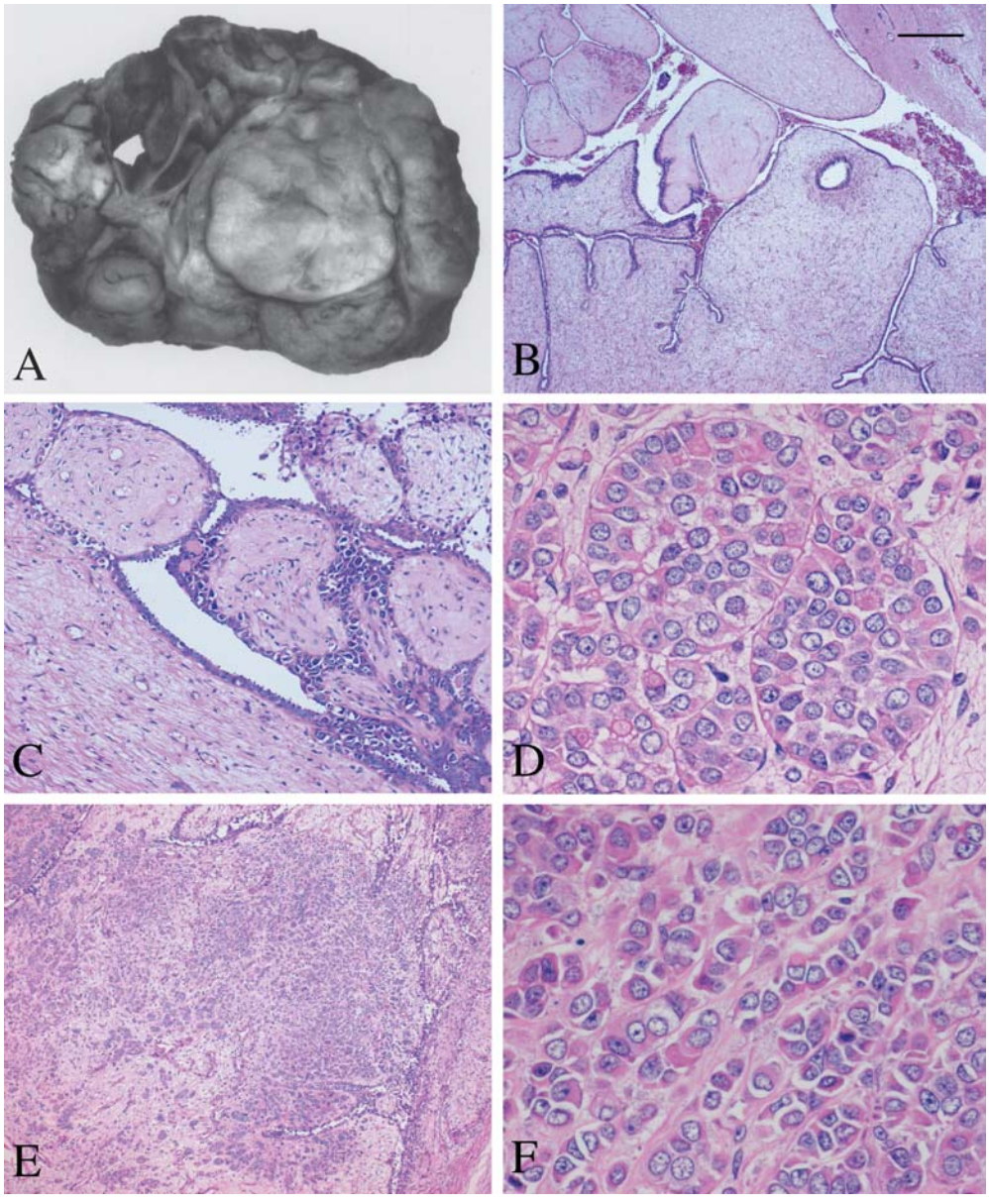



**Fig. 1** **A** Macroscopic appearance. A lobulated tumor shows classical phyllodes architecture, consisting of dense stroma and interlacing clefts. **B** Microscopic appearance of the tumor. The tumor shows foliate structure, and there is little stromal cellularity. **C** Lobular carcinoma in situ showing Pagetoid spread. **D** Lobular carcinoma in situ forming solid islands. **E** Microscopic findings of the invasive lobular carcinoma. Carcinoma cells are seen invading the stroma from the lining layer. **F** High magnification of the invasive carcinoma. The tumor cells exhibit a lack of cohesion and a tendency to form slender strands arranged in a linear "Indian file" fashion. *Bar* 500 $\mu$m in **B**, 50 $\mu$m in **C**, 100 $\mu$m in **E**, and 25 $\mu$m in **D** and **F**

observed (Fig. 1F). Immunohistochemistry showed that both the non-invasive and invasive carcinoma cells were strongly positive for cytokeratin and partially positive for progesterone receptor, but estrogen receptor-negative (Fig. 2A–D).

We have reported the first case of invasive lobular carcinoma arising in a phyllodes tumor. Although the percentages of malignant lesions reported in phyllodes tumors have ranged from 2% to 45%, their frequency in most patients described in this report is more than 20% [7]. However, transformation usually occurs in the stromal component of the tumor, and it is rare in the epithelial component. The incidence of carcinoma in phyllodes tumor is thought to be only 1–2% of all phyllodes tumors [6, 11].

Phyllodes tumors can be discriminated from fibroadenomas by their stromal hypercellularity and characteristic phyllodes pattern. The histological characteristics may explain the more frequent transformation of stromal cells in phyllodes tumors than in fibroadenomas, which seldom show sarcomatous transformation [9]. The epithelial component of phyllodes tumors and fibroadenomas, however, exhibits atypical hyperplasia or in situ carcinoma, although the incidence of carcinoma in phyllodes tumors is rare (1–2%) [6, 11], and it is less than 0.5% in fibroadenomas [8, 11]. Several case reports have referred to the occurrence of ductal carcinoma in situ, infiltrating duct carcinoma, lobular carcinoma in situ, and invasive lobular carcinoma in fibroadenomas [2, 3], and it is noteworthy that more than 50% of carcinomas arising in fibroadenomas are lobular carcinoma in situ lesions [2, 3]. In contrast, no information on the most common carcinoma type arising in phyllodes tumors is available, probably due to its infrequency, although there have been

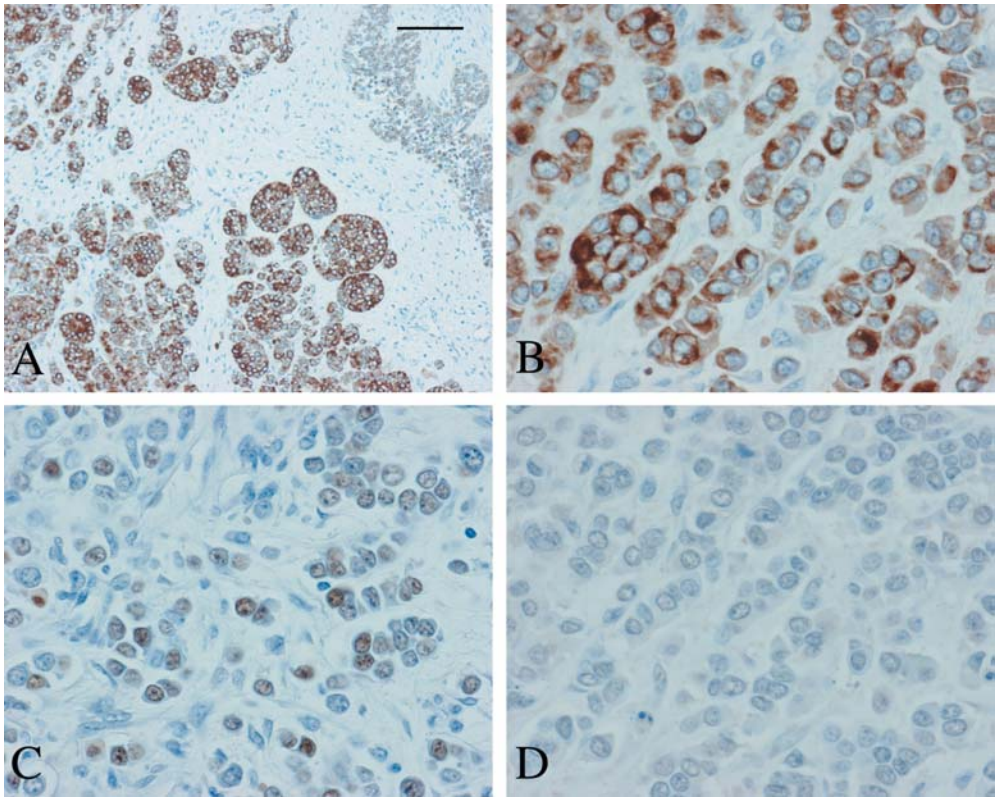



**Fig. 2** Immunohistochemical staining. **A**, **B** Anti-cytokeratin. Epithelial components of both the lobular carcinoma in situ and invasive component are strongly positive for cytokeratin. **C** Anti-progesterone receptor. Carcinoma cells are partially positive. **D** Anti-estrogen receptor. *Bar* 100 $\mu$m in **A** and 25 $\mu$m in **B**, **C**, and **D**

several case reports of lobular carcinoma in situ, ductal carcinoma in situ, and infiltrating duct carcinoma arising in phyllodes tumor [1, 5, 6, 7, 11]. A case of bilateral malignant breast tumor previously reported described the development of a malignant tumor in a patient with a chromosomal abnormality (46,XX/46,XY mosaic) [4]. Our patient, however, did not have any chromosomal abnormality or any family history.

This is the first report of infiltrating lobular carcinoma in a phyllodes tumor. The unique aspect of this case is that the patient neglected the tumor for more than 12 years before resection. Thus, this case supports the general notion that invasive carcinomas can develop in in situ carcinomas during their natural course.

## References

1. Alo PL, Andreano T, Monaco S, Sebastiani V, Eleuteri Serpieri D, Di Tondo U (2001) Malignant phyllodes tumor of the breast with features of intraductal carcinoma. Pathologica 93:124–127
2. Diaz NM, Palmer JO, McDivitt RW (1991) Carcinoma arising within fibroadenomas of the breast. A clinicopathologic study of 105 patients. Am J Clin Pathol 95:614–622
3. Gebrim LH, Bernardes Junior JR, Nazario AC, Kemp C, Lima GR (2000) Malignant phyllodes tumor in the right breast and invasive lobular carcinoma within fibroadenoma in the other: case report. Sao Paulo Med J 118:46–48
4. Kasami M, Yoshida M, Isogaki J, Ogawa H, Shinmura K, Endo Y, Kiyokawa E, Naito Y, Arai T, Kimura T, Inoue R, Sugimura H (1997) Bilateral breast tumors, malignant phyllodes tumor and invasive lobular carcinoma in a 46,XX/46,XY mosaic female with family history of breast cancer. Pathol Int 47:147–154
5. Knudsen PJ, Ostergaard J (1987) Cystosarcoma phyllodes with lobular and ductal carcinoma in situ. Arch Pathol Lab Med 111:873–875
6. Ozzello L, Gump FE (1985) The management of patients with carcinomas in fibroadenomatous tumors of the breast. Surg Gynecol Obstet 160:99–104
7. Parker SJ, Harries SA (2001) Phyllodes tumours. Postgrad Med J 77:428–435
8. Pick PW, Iossifides IA (1984) Occurrence of breast carcinoma within a fibroadenoma. A review. Arch Pathol Lab Med 108:590–594
9. Rosen PP (2001) Unusual clinical presentations. In: Rosen's breast pathology, 2nd edn. Lippincott-Raven, Philadelphia, pp 653–687
10. Rosen PP, Oberman HA (1993) Tumors of the mammary gland. In: Atlas of tumor pathology, 3rd series. Armed Forces Institute of Pathology, Washington, DC, pp 101–114
11. Rosen PP, Urban JA (1975) Coexistent mammary carcinoma and cystsarcoma phyllodes. Breast 1:9–15

 © Springer-Verlag 2003

# ANNOUNCEMENTS

6 September 2003
**EUROPEAN BOARD OF PATHOLOGY**
**7th EXAMINATION 2003**
Ljubljana, Slovenia

The Seventh Examination of the European Board of Pathology will be held in Ljubljana, Slovenia, Saturday September 6, 2003. This Examination precedes the 19th Congress of the ESP.

*For information about the examination and application forms can be obtained from:*
Prod. Dr. J.G. van den Tweel
(chairman of The Examination Board)
Utrecht University Medical Center
Department of Pathology, H 04.312
P.O. Box 85500
3508 GA Utrecht
Fax: ++31-30-2544990
Tel.: ++31-30-2506565
e-mail: j.vandentweel@lab.azu.nl *or*
W.vanBragt@lab.azu.nl (secretary)
The same information is also available from Internet:
http:www.uems.be/pathol.htm, see index 2 and 3

6–11 September 2003
**19th European Congress of Pathology**
Ljubljana, Slovenia

The largest congress of pathologists in Europe in 2003, covering basic diagnostic standards, update scientific achievements and recent technical advances in all areas of pathology at 4 keynote lectures, 30 symposia, 21 short courses, 21 slide seminars, 14 special presentations, 2 round table discussions and free paper and poster sessions. Internationally recognized invited speakers are from throughout Europe and the USA.

*Updated information on the congress website:* http://www.cd-cc.si

10–13 September 2003
**Harvard Dermatopathology Update CME Course**
(Fairmont Copley Plaza Hotel, Boston, MA)

The objective of this year's course is to provide an in-depth review and update on selected topics in dermatopathology focusing on non-neoplastic diseases and melanocytic lesions. The course has been redesigned, and is specifically aimed at practicing pathologists, dermatopathologists, and dermatologists. The program is also suitable for senior residents and fellows preparing for board certification examinations.

*For further information please contact* at
http://www.cme.hms.harvard.edu, at (617) 384-8600
or can be obtained by e-mail at hms-cme@hms.harvard.edu

13 October 2003
**Continuing Medical Education**

One day Multi-Disciplinary Update courses

Course fee: £95.00

*For further information please contact:*
Education Administrators
Nottingham International Breast Education Centre
City Hospital, Hucknall Road, Nottingham NG5 1PB
Tel.: 0115 969 1689; Fax: 0115 962 7707
E-mail: enquiries@nibec.co.uk; www.nibec.co.uk

17–19 November 2003
**Multi-Disciplinary Courses on Breast Disease**

Three day course. The first part is multi-disciplinary. Thereafter the different specialties meet to accommodate their own special requirements.

Course Tutors: Dr. I.O. Ellis, Dr. S.E. Pinder, Dr. A.H.S. Lee

| | | |
|---|---|---|
| Course fees: | NHS | £370.00 |
| | Non-NHS | £415.00 |
| | Overseas | £550.00 |

includes refreshments but not accommodation

*For further information please contact:*
Education Administrators
Nottingham International Breast Education Centre,
City Hospital, Hucknall Road, Nottingham NG5 1PB
Tel.: 0115 969 1689; Fax: 0115 962 7707
Email: enquiries@nibec.co.uk; www.nibec.co.uk